Proceedings of the
Forty-Ninth

INTERNATIONAL
WIRE AND CABLE
SYMPOISUM

NOVEMBER 13 THRU 16, 2000

Sponsored by
International Wire and Cable Symposium, Inc.
(IWCS)
Eatontown, New Jersey
http://www.iwcs.org/iwcs/

With Participation by
US Army Communications-Electronics Command (CECOM)
Fort Monmouth, New Jersey

Supporting Associate
Europacable, Brussels, Belgium

PROCEEDINGS OF
49TH INTERNATIONAL
WIRE AND CABLE
SYMPOSIUM

Sponsored by
International Wire and Cable Symposium, Inc. (IWCS)
Eatontown, New Jersey
Website: www.iwcs.org
Email: admin@iwcs.org

With Participation by
US Army Communications-Electronics Command (CECOM)
Fort Monmouth, New Jersey

Supporting Associate
Europacable, Brussels, Belgium

TRUMP TAJ MAHAL CASINO-RESORT
ATLANTIC CITY, NEW JERSEY
NOVEMBER 13, 14, 15 AND 16, 2000

MISSION

The International Wire and Cable Symposium provides a forum for the exchange of technical information amongst suppliers, manufacturers, and users on technological advancements in materials, processes, and products used for voice, data and video signal transmission systems.

TECHNICAL PRESENTATIONS

Tuesday, November 14, 2000

9:00 am	PLENARY SESSION	Stepping Into The Future – A Vision Of The Communications System Of Tomorrow

Suppliers

12:30 pm	FORUM	I. New Product Presentations

Track 1-- Fiber

1:00 pm	SESSION 1	Fiber Optic Cable Design I
1:00 pm	SESSION 2	Optical Fiber Properties

Track 2 -- Manufacturing, Processing and Materials

1:00 pm	SESSION 3	Manufacturing Process and Control

Track 3 -- Copper

1:00 pm	SESSION 4	Copper Cable Design and Properties

Wednesday, November 15, 2000

Track 1 -- Fiber

8:30 pm	SESSION 5	Fiber Optic Cable Design II
8:30 pm	SESSION 6	Fiber Optic Connectors, Splicing & Closures

Track 2 -- Manufacturing, Processing and Materials

8:30 pm	SESSION 7	Materials I

Track 3 -- Copper

8:30 pm	SESSION 8	DSL – Digital Subscriber Line on Copper Pairs

Suppliers

9:00 am	FORUM	II. New Product Presentations

Track 1 -- Fiber

2:15 pm	SESSION 9	Fiber Optic Cable Design III (LAN)
2:15 pm	SESSION 10	Testing / Field Evaluation I

Track 2 -- Manufacturing, Processing and Materials

2:15 pm	SESSION 11	Materials II

Panel Discussion

2:15 pm	SESSION 12	Wireless Access Systems – An Alternative To Wireline Solutions

4:00 pm	SESSION 13	Poster Papers

Thursday, November 16, 2000

Track 1 -- Fiber

8:30 am	SESSION 14	Aerial Cables I
8:30 am	SESSION 15	Installation / Field Evaluation II
8:30 am	SESSION 16	Fiber Networks & Applications

Track 3 -- Copper

8:30 am	SESSION 17	Home Building Copper Cabling

Track 1 -- Fiber

1:00 pm	SESSION 18	Aerial Cables II / Submarine
1:00 pm	SESSION 19	Testing / Fiber Reliability

Track 3 -- Copper

1:00 pm	SESSION 20	Cables in Wireless Application

PAPERS

PROCEEDINGS/PUBLICATIONS
INTERNATIONAL WIRE AND CABLE SYMPOSIUM (IWCS)

Proceedings - Bound - Available from IWCS

39th IWCS Proceedings - 1990 – $15.00
40th IWCS Proceedings - 1991 – $25.00
44th IWCS Proceedings - 1995 – $40.00

46th IWCS Proceedings - 1997 – $20.00
47th IWCS Proceedings - 1998 – $15.00
48th IWCS Proceedings - 1999 – $15.00
49th IWCS Proceedings - 2000 – $50.00

Copies of original proceedings not listed above can be reproduced for $75.00 per copy plus shipping.
CD's 46th, 47th, 48th & 49th IWCS CD - $10.00
Publications - Bound - Available from IWCS

Index of IWCS Papers (1983-1990); PUB #1001RP-1991 – $15.00
PIC Insulation Testing Field Experience; PUB #1003RP-1992 – $25.00

Extra Copies of the 2000 Proceedings can be obtained for: 1 – $50; 2 – $100; 3 – $150; 4 – $190; 5 – $230; 6 – $270; 7 – $310; 8 – $350; 9 – $390; 10 – $430; 11 and above – $430 plus $30 for each additional copy.

| **Shipping/Handling:**	**Proceedings**	**Publications**	**CDs**
	$8.00 per copy USA only	$4.00 per copy USA Only	$4.00 per copy USA Only
	$20.00 per copy Surface Mail	$10.00 per copy Surface Mail	$7.00 per copy Canada
	(overseas - 4 to 6 weeks)	(overseas - 4 to 6 weeks)	$13.00 per copy Airmail
	$35.00 per copy Airmail (Europe)	$15.00 per copy Airmail	(Europe and Asia)
	$40.00 per copy Airmail (Asia)	(Europe and Asia)	

Payment: Make a check or bank draft payable in U.S. Dollars drawn on a U.S. Bank, to the INTERNATIONAL WIRE & CABLE SYMPOSIUM, INC. or use your VISA/MC/AMEX by providing number and expiration date and forward request to: International Wire and Cable Symposium, Inc., 174 Main St., Eatontown, NJ 07724. Telephone inquiries may be directed to Ms. Pat Hudak +1-732-389-0990 or via email: admin@iwcs.org. Prices are subject to change.

Photocopies are available for complete sets of papers for 1964 through 1999. Information on prices and shipping charges should be requested from the: US Department of Commerce, National Technical Information Service (NTIS), Springfield, Virginia 22161, Telephone: +1-703-487-4650.

Include Title, Year and "AD" Number

13th Annual Wire Cable Symposium (1964)	- AD 787164
15th Annual Wire Cable Symposium (1966)	- AD A006601
16th International Wire Cable Symposium (1967)	- AD 787165
17th International Wire Cable Symposium (1968)	- AD 787166
18th International Wire Cable Symposium (1969)	- AD 787167
19th International Wire Cable Symposium Proceedings 1970	- AD 714985
20th International Wire Cable Symposium Proceedings 1971	- AD 733399
21st International Wire Cable Symposium Proceedings 1972	- AD 752908
22nd International Wire Cable Symposium Proceedings 1973	- AD 772914
23rd International Wire Cable Symposium Proceedings 1974	- AD A003251
24th International Wire Cable Symposium Proceedings 1975	- AD A017787
25th International Wire Cable Symposium Proceedings 1976	- AD A032801
26th International Wire Cable Symposium Proceedings 1977	- AD A047609
27th International Wire Cable Symposium Proceedings 1978	- AD A062322
28th International Wire Cable Symposium Proceedings 1979	- AD A081428
29th International Wire Cable Symposium Proceedings 1980	- AD A096308
30th International Wire Cable Symposium Proceedings 1981	- AD A110859
31st International Wire Cable Symposium Proceedings 1982	- AD A125662
32nd International Wire Cable Symposium Proceedings 1983	- AD A136749
33rd International Wire Cable Symposium Proceedings 1984	- AD A152119
34th International Wire Cable Symposium Proceedings 1985	- AD A164384
35th International Wire Cable Symposium Proceedings 1986	- AD A180828
36th International Wire Cable Symposium Proceedings 1987	- AD A189610
37th International Wire Cable Symposium Proceedings 1988	- AD A200903
38th International Wire Cable Symposium Proceedings 1989	- AD A216023
39th International Wire Cable Symposium Proceedings 1990	- AD A233634
40th International Wire Cable Symposium Proceedings 1991	- AD A244038
41st International Wire Cable Symposium Proceedings 1992	- AD A259235
42nd International Wire Cable Symposium Proceedings 1993	- AD A279242
43rd International Wire Cable Symposium Proceedings 1994	- AD A293473
44th International Wire Cable Symposium Proceedings 1995	- AD A303506
45th International Wire Cable Symposium Proceedings 1996	- AD A324572
46th International Wire Cable Symposium Proceedings 1997	- AD A338941
47th International Wire Cable Symposium Proceedings 1998	- AD A358377
48th International Wire Cable Symposium Proceedings 1999	- AD A373457
Kwic Index of Technical Papers, International Wire Cable Symposium (1952-1982)	- AD A027588

MESSAGE FROM THE CEO, DIRECTOR
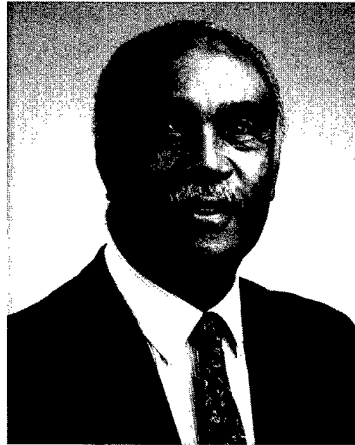
The symposium is approaching the 50th Anniversary, which will take place next year in Orlando, Florida. This will represent quite a milestone. A GALA Celebration is being planned with many festive activities scheduled within Disney World. Family members are being encouraged to attend the symposium and participate in the special activities.

Last year's symposium in Atlantic City did not create the increase in attendance as I had anticipated. I thought a return to Atlantic City would stimulate the interest and nostalgia for revisiting the location that was, for many years, the home of the symposium. In spite of the attendance remaining approximately the same as previous years, the symposium by many was considered an exciting and rewarding experience. The program this year, in addition to its regular features will include for the first time, presentations on new products. During their presentation the presenters will stress the commercial aspects of their product. It should also be noted, that this year's Plenary Session is returning to its original format of multiple speakers. Four outstanding and prominent speakers from different areas of the wire and cable industry will provide a brief insight into their vision of the communication of tomorrow.

One major change has taken place in the organizational makeup of the symposium. The new organization will consist of a Board of Directors and a Symposium Committee. Both groups will work closely together to improve the efficiency of operation, establish long term strategies, direction and goals for the symposium.

Inge Kovacs, Consultant for Polycheck Ltd., is retiring after more than six years on the committee. Inge has been a great worker and strong supporter of the symposium. I extend to her the committee's sincere thanks and appreciation.

The Board of Directors and the Symposium Committee extend to all contributors and attendees their thanks and appreciation for the support they provide the symposium each year.

Elmer F. Godwin
CEO, Director

HIGHLIGHTS OF THE 48TH IWCS
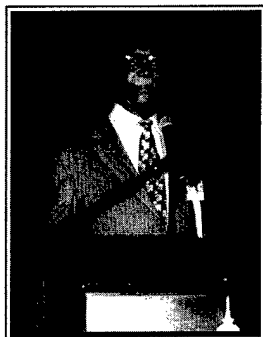## International Wire and Cable Symposium
November 15, 16, 17 and 18, 1999
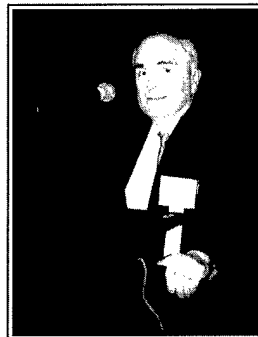### Trump Taj Mahal Casino-Resort, Atlantic City, New Jersey

Announcements/Greetings

Elmer F. Godwin
President/Director, IWCS
Eatontown, NJ

Michel Rousseau
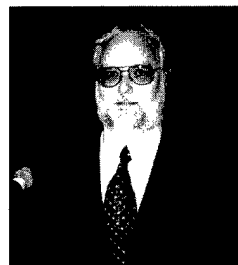IWCS Chairman
Alcatel
Paris, France

Guest Speakers Plenary Session

JOHN SACH
Chairman, Plenary Session
Pirelli Cables & Systems NA
Lexington, SC

MG ROBERT L. NABORS
Commanding General US Army
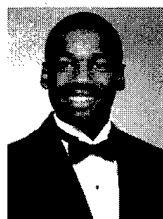Communications-Electronics Command
andFort Monmouth, NJ

STEPHEN R. BAKER
V.P. & Chief, Technology
Officer, Worldwide Fiber Inc.
Vancouver, British Columbia, Canada

Luncheon Speaker
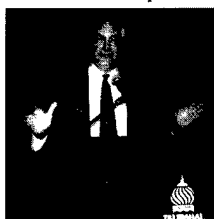
DR. LOWELL CATLETT
Las Cruces, New Mexico

Scholarship Recipients

Twanaze Mitchell
Attending
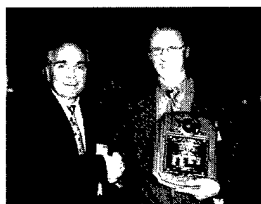Auburn University

Jennifer Gau
Attending
University of Pennsylvania

Jamey J. Brown
Attending
Georgia Institute of Technology

Award Winners

<u>Outstanding Technical</u>
Michel Rosseau of IWCS (on left) making Presentation to
Dr. Bernt-Ake Sultan, , Borealis AB, Stenungsund,
Sweden; (who is also accepting for) **Dr. Thomas
Hjertberg & Karin Ericsson**, Chalmers University of
Technology, Gothenburg Sweden; **Matti Hirvensalo &
Marjo Hanninen**, Borealis Polymers Oy, Porvoo, Finland

<u>Outstanding Poster Paper</u>
Michel Rousseau of IWCS (on left)
making presentationto **Dr. Osman S. Gebizlioglu,
Joe D. Mann and C.R. Kurkjian**
Bellcore, Morristown, NJ

<u>Best Presentation</u>
Michel Rousseau of IWCS(on left)
making presentation to **Dr. Priya L.Tabaddor,**
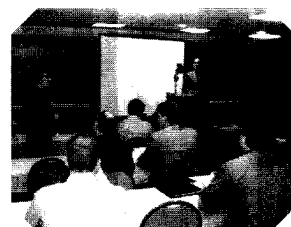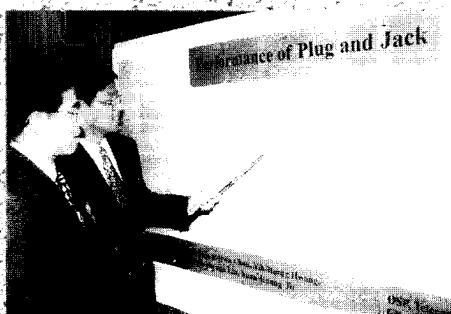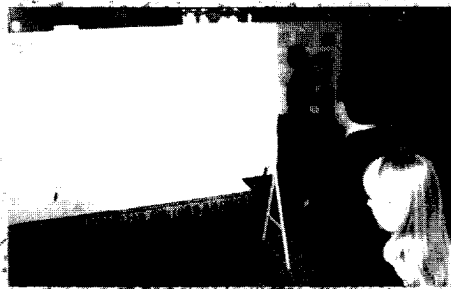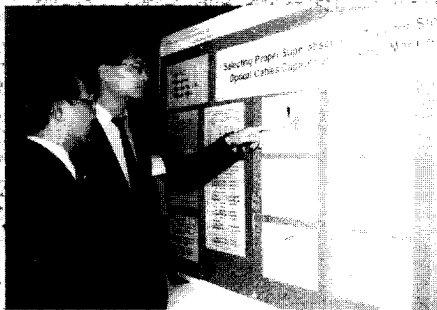Lucent Technologies Inc.,
Norcross, GA

IWCS Retirees

Elmer F. Godwin of IWCS (on left) presenting Retirement
Certificates to **Yasuhiro Kamikura** for **Hirotshi Hondo,** The
Furukawa Electric Co Ltd, Tokyo, Japan; **Fred Narayan,** Phelps
Dodge International Corp, Coral Gables, FL; and **Michel Rousseau,**
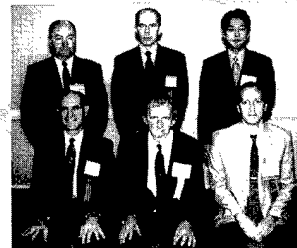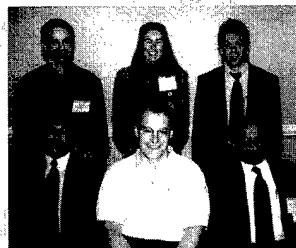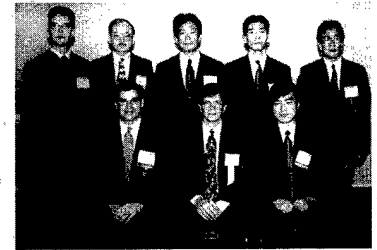Alcatel, Paris, France

Educational

IWCS 1999

Technical
Sessions

Hospitality

Hospitality

TABLE OF CONTENTS

TRACK 1 – FIBER
SESSION 1: FIBER OPTIC DESIGN I
Tuesday Afternoon, Nov. 14, 1:00 - 4:00 PM
Tiara Ballroom A
Chairperson: **Manuel R. Santana,** *Lucent Technologies, Bell Labs.,*
Norcross, GA

TRACK 1 – FIBER
SESSION 2: OPTICAL FIBER PROPERTIES
Tuesday Afternoon, Nov. 14, 1:00 - 4:00 PM
Tiara Ballroom B
Chairperson: **Xavier Mann,** *Fitel Lucent Technologies, Carrollton, GA*

TRACK 2 – MANUFACTURING, PROCESSING & MATERIALS
SESSION 3: MANUFACTURING PROCESS & CONTROL
Tuesday Afternoon, Nov. 14, 1:00 - 4:00 PM
Diamond Ballroom A/B
Chairperson: **James R. Leech,** *Union Carbide Corp., Somerset, NJ*

TABLE OF CONTENTS

TABLE OF CONTENTS

TABLE OF CONTENTS

TABLE OF CONTENTS

TRACK 1 – FIBER
SESSION 14: AERIAL CABLES I
Thursday Morning, Nov. 16, 8:30 - 11:30 AM
Tiara Ballroom A
Chairperson: **Dieter S. Nordmann,** *Alcatel Contracting, Hannover, Germany*

TRACK 1 – FIBER
SESSION 15: INSTALLATION/FIELD EVALUATION II
Thursday Morning, Nov. 16, 8:30 - 11:30 AM
Tiara Ballroom B
Chairperson: **David B. Kiddoo,** *AlphaGary Corp., Sparta, NJ*

TRACK 1 – FIBER
SESSION 16: FIBER NETWORKS & APPLICATIONS
Thursday Morning, Nov. 16, 8:30 - 11:30 AM
Diamond Ballroom A/B
Chairperson: **John R. Sicotte,** *Corning International K. K., Tokyo, Japan*

TRACK 3 – COPPER
SESSION 17: HOME BUILDING COPPER CABLING
Thursday Morning, Nov. 16, 8:30 - 11:30 AM
Diamond Ballroom C/D
Chairperson: **Hans A. Mayer,** *Engineering Consultant, Melbourne, Australia*

TABLE OF CONTENTS

ELMER F. "ACE" GODWIN SCHOLARSHIPS

1999	Twanaze Mitchell, Auburn University, Freshman - Electrical Engineering Jennifer Gau, University of Pennsylvania, Freshman - Computer Science and Engineering James J. Brown, Georgia Institute of Technology, Sophomore - Computer Engineering
1998	Jothan Bowen, Texas A&M University, Freshman - Digital Communications and Computers John D. Taliaferro, Virginia Tech, Junior - Chemical Engineering
1997	Michael Rich, Georgia Institute of Technology, Freshman - Electrical Engineering Major Billy Oates, Georgia Institute of Technology, Senior, Mechanical Engineering and Math Major Janet Armstrong, Rutgers University, Ph.D. Candidate, Ceramic Engineering Major
1996	Anthony Tindall, Cornell University, Freshman - Mechanical Engineering Major John Belle, North Carolina State University, Sophomore - Electrical Engineering Major
1995	Jason Chang, Princeton University, Freshman - Chemistry Major Fionna Murray, Virginia Tech, Junior - Mechanical Engineering Major
1994	Sara Ransom, Massachusetts Institute of Technology, Freshman - Materials Science Engineering Major Jurron Bradley, Vanderbilt University, Senior - Chemical Engineering Major

AWARDS

Year	Outstanding Technical Paper	Outstanding Poster Paper	Best Presentation
1999	Dr. J. Thomas Chapin and Larry L. Bleich – Lucent Technologies; Dr. Pravin Gandhi and Thomas Ebert – Underwriters Laboratories – "The Development and Performance of a Calibration Cable for the NFPA 262/UL 910 Plenum Cable Fire Test"	Shami S. Sodhi, Allen C. Gregory and Gary E. Grogan – Siecor – "Effect of Temperature, Strain and Installation of PMD in High Fiber Count Ribbon Cables"	Eric R. Logan – Siecor – "The Status and Future of High Fiber Count Cable Designs"
1998	Dr. Bernt-Åke Sultan – Borealis AB; Dr. Thomas Hjertberg and Karin Ericsson – Chalmers University of Technology; and Matti Hirvensalo and Marjo Hänninen – Borealis Polymers Oy – "Novel Halogenfree Flame Retardant Polyolefins Intended for Internal Wiring – Properties and Flame Retardant Mechanism"	Dr. Osman S. Gebizlioglu, Joel D. Mann and C. R. Kurkjian – Bellcore – "The Effect of Preparation Conditions on the Strength of Fusion Splices I: Use of AFM Imaging"	Dr. Priya L. Tabaddor – Lucent Technologies Incorporated – "Mechanics of Delamination Resistance Testing"
1997	Debra A. Simoff, Dr. Mark A. Paczkowski, Dr. Daryl Inniss, Dr. Thomas A. Strasser, J. Renee Pedrazzani, Dr. Rolando P. Espindola, Dr. Robert M. Atkins, Katherine T. Nelson, Valerie J. Kuck, John M. Borick and Jennifer Aspell – Lucent Technologies; and Regina Ragan – California Institute of Technology – "Coatings Having Enhanced UV Transparency for the Fabrication of Optical Fiber Gratings"	Katja Lyytikäinen – Nokia – Maillefer Oy – "Numerical Simulation of Optical Fiber Coating Process"	Dr. Neil R. Haigh – BICC Cables Limited – "Applicability of All – Dielectric Self Supporting Cable Systems to Very High Voltage Overhead Power Lines"
1996	Mitsuru Kamikatano and Matsuhiro Miyamoto – Fujikura Limited; and Osamu Ogawa – Tokyo Electric Power Company – "A Time – Varying Optical Fiber Strain Measurement by Using Brillouin Ring Amplifying System"	Jan Björkman – Telia Network Services; and Dr. Torbjörn Svensson – Telia Research AB – " Aging of Fibres and Ribbon in Water and Filling Compound'"	Dr. Priya L. Tabaddor – Lucent Technologies Incorporated, Bell Laboratories – "An Evaluation of Protective Polymer Coatings for Optical Fiber Applications'"
1995	Jean Luc Lang and Jean-Francois Libert – Alcatel Submarine Network; David I. Curtis and Peter Worthington – STC Submarine Systems Ltd. – "Optical Performance of Submarine Cables in Optically Amplified High Bit Rate Systems"	Richard S. Wagman, Gregory A. Lochkovic and Kevin T. White – Siecor Corporation – "Component Optimization for Slotted Core Cables Using 8 – Fiber Ribbons"	Dr. Dan L. Philen – AT&T Bell Laboratories – "Optical Fiber for Amplified Undersea Systems"
1994	Toshio Kurashima, Kazuo Hogari, Satoshi Matsuhashi, Dr. Tsuneo Horiguchi, Dr. Yahei Koyamada and Yutaka Wakui – NTT Access Network Systems Laboratories; and Hiroshi Hirano – NTT Technical Assistance & Support Center – "Measurement of Distributed Strain in Frozen Cables and Its Potential for Use in Predicting Cable Failure"	Dr. Sverker Forsberg – Swedish University of Agricultural Sciences; and Jan Björkman – Telia AB – "Release of Lead from Lead – Sheathed Telecom Cables in Soil"	Barry J. Keon – Telstra – "The Effects of Optical Fiber Coating and Ink Materials on the Corrosion of the Glass Surface"
1993	Dr. Yoshinori Namihira and Toshio Kawazawa – KDD R&D Laboratories; and Naoki Norimatsu – KDD Company, Limited – "PMD Reduction of Optical Fiber Cables for Transoceanic Optical Amplifier Submarine Cable Systems"	Willem Griffioen – PTT Research – "Mechanical Lifetime of Optical Fibers"	Timothy S. Dougherty – AT&T Network Cable Systems – "The Temperature of Aerial Plant and Its Effect Upon Foam – Skin Insulation Life" and Wolfgang Wenski – Kabelmetal Electro GmbH – "First Large Scale FITL Installation: Experience From Opal '93"

1992	Nathan E. Hardwick III and Kris Kathiresan – AT&T Bell Laboratories and J. G. Hartley – Georiga Institute of Technology – "Analysis of Fiber Optic Cable Design Conditions in Vicinity of Steam Lines – Ruptured and Pristine"	Svend Hopland and Albert Klykken – Norwegian Telecom – "Installation of Submarine Fiberoptic Cables in Rugged Coastal Terrain"	Peter Latoszynski – Telecom Australia – "Development of Co – Extruded Polyethylene/Polyamide 12 Insect Resistant Telecommunications Cable"
1991	Shigeru Tomita, Michito Matsumoto, Tetsuro Yabuta and Takuya Uenoya – NTT – "Preliminary Research into Ultra High Density and High Count Optical Fiber Cables"	G. Scott Glaesemann – Corning Inc. – "The Effect of Proof Testing on the Minimum Strength of Optical Fiber"	Sue V. Wolfe – STC Submarine Systems – "Structure and High Voltage DC Behaviour of Submarine Cable Mouldings"
1990	Trevor N. Bowmer, Russell J. Miner, Irene M. Plitz, Joseph N. D'Amico and Lal M. Hore – Bellcore – "Thermal Stability Tests for Polyolefin Insulations"	Steve Lischynsky, Helmut Lukas, Robin McIntyre and Grant Pacey – Bell – Northern Research Ltd. – "New Technology for a Single Mode Mechanical Splice"	Harold W. Friesen – AT&T Bell Laboratories – "An Improved Characteristic Impedance Measurement Technique"
1989	Michel Plasse, Lise Desroches and Paul – Andre Guilbert – Northern Telecom Canada Limited – "High Performance Twisted – Pair Cable for LAN Systems"	Werner Bernard and Susan C. Grant – Siecor Corporation – "Fiber Optic Drop Cables in the Subscriber Loop"	Michel de Vecchis – Les Cables de Lyon – "Results on a Large Scale Installation of a Fibre Optic Distribution Network"
1988	Martin C. Light Jr., James A. Moses, Mark A. Sigmon and Christopher A. Story – Siecor Corp. – "Design and Performance of Telecommunication Cable Optimized for Low Fiber Count"	Dr. R. Raman – Contel Laboratories – "Loss at Dissimilar Fiber Splices"	Janice B. Haber – AT&T Laboratories – "Single – Mode Media and Apparatus for Fiber to the Home"
1987	Stephen B. Pierce – Conel Laboratories – "Digital Transmission on Customer Premises Wiring"	William Wood – Bell Communication Research – "Performance Analysis of Optic Fiber Cleavers"	Richard Rossi – General Cable Company – "Cable Sheathing Design and Performance Criteria"

Year	Outstanding Technical Papers	Best Presentations
1986	Simon D. Dadakarides and Bruce B. Lusignam, Stanford University – "Magnetically Loaded Cables"	Dave Fischer, Superior Cable Corp. – "Progress Towards the Development of Lighting Test for Telecommunication Cables" John C. Chamberlain, Siecor Corp. – "Zero Halogen Fire Retardant Fiber Optic Shipboard Cable"
1985	James A. Krabec and John W. Kincaid, Jr., Belden Technical Research Center – "Advances in the Optimization of Multi – Layer Shield Design"	Stephen Hornung, British Telecom Research Laboratories – "Manufacture and Performance of Fibre Units for Installation by The Viscous Drag of Air"
1984	M. Fujise and Y. Iwamoto, KDD Research & Development Laboratories, Tokyo, Japan – "Self-Core-Alignment Arc-Fusion Splicer Based on a Simple Local Monitoring Method"	William E. Dennis, Dow Corning Corporation, Midland, Michigan– "Hydrogen Evolving Tendencies of Cable Fillers and Optical Fiber Coatings"
1983	V. A. Fentress, Raychem Corp. and D. V. Nelson, Stanford University – "Fracture Mechanics Evaluation of the Static Fatigue Life of Optical Fibers in Bending"	J. R. Bury, Standard Telecommunication Laboratories, Ltd., Hailow, England – "Development of Flame Retardant, Low Aggressivity Cables"
1982	R. H. Whiteley, Raychem Ltd. – "A Comprehensive Small Scale Smoke Test"	A. Yoshizawa, The Furukawa Electric Co., Ltd.– "Structure and Characteristics of Cables for Robots"
1981	C. J. Arroyo, N. J. Cogelia, Bell Laboratories, and B. J. Darsey, Western Electric – "Thermal Behavior of Experimental Plenum Cable Sheaths Determined in a Radiant Heat Chamber"	G. S. Anderson, Belden Corporation – "Installation of Fiber Optic Cable on 457 Meter Tower"
1980	P. Kish and Y. BeBorgne, Northern Telecom Canada Limited, Montreal, Canada – "General Crosstalk Model for Paired Communication Cables"	J. J. Refi, Bell Laboratories – "Mean Power Sum Far – End Crosstalk of PIC Cables as a Function of Average Twist Helix Angle"

1979	S. Masaki, Y. Yamazaki and T. Ideguchi, Nippon Telegraph and Telephone Public Corporation, Japan – "New Aluminum Sheath Cable Used for Electromagnetic Shielding"	I. Wadehra, IBM Corporation – "Performance of Polyvinyl Chloride Communication Cables in Modified Steiner Tunnel Test"
1978	F. Suzuki, S. Sato, A. Mori and Y. Suzuki; Sumitomo Electric Industries, Ltd., Japan – "Microcoaxial Cables Insulated with Highly Expanded Polyethylene By Chemical Blowing Method"	Richard C. Mondello, Bell Labs. – "Design and Manufacture of an Experimental Lightguide Cable for Undersea Transmission Systems"
1977	T. K. McManus, Northern Telecom Canada Ltd. and R. Beveridge, Saskatchewan Telecommunications, Canada – "A New Generation of Filled Core Cable"	William L. Schmacher, AMP Inc. – "Design Considerations for Single Fiber Connector"
1976	N. J. Cogelia, Bell Telephone Laboratories and G. K. Lavoie and J. F. Glahn, US Department of Interior – "Rodent Biting Pressure and Chemical Action and Their Effects on Wire and Cable Sheath"	Michael DeLucia, Naval Ship Research and Development– "Highly Fire – Retardant Navy Shipboard Cable"
1975	T. S. Choo, Dow Chemical U.S.A. – "Corrosion Studies on Shielding Materials for Underground Telephone Cables"	J. E. Wimsey, United States Air Force – "The Bare Base Electrical Systems"
1974	D. Doty, AMP Inc. – "Mass Wire Insulation Displacing Termination of Flat Cable"	G. H. Webster, Bell Laboratories – "Material Savings by Design in Exchange and Trunk Telephone Cable"
1973	Dr. H. Martin, Kabelmetal – "High Power Radio Frequency Coaxial Cables, Their Design and Rating"	R. J. Oakley, Northern Electric Co., Ltd. – "A Study Into Paired Cable Crosstalk"
1972	J. B. Howard, Bell Laboratories – "Stabilization Problems with Low Density Polyethylene Insulations"	S. Kaufman, Bell Laboratories – "Reclamation of Water – Logged Buried PIC Telephone Cable"
1971	R. Lyenger, R. McClean and T. McManus, Bell Northern Research – "An Advanced Multi – Unit Coaxial Cable for Toll PCM Systems"	S. Nordblad, Telefonaktiebolaget L. M. Ericsson – "Multi – Paired Cable of Nonlayer Design for Low Capacitance Unbalance Telecommunications Network" N. Kojima, Nippon Telegraph and Telephone – "New Type Paired Cable for High Speed PCM Transmission"
1970	D. E. Setzer and A. S. Windeler, Bell Laboratories – "A Low Capacitance Cable for the T2 Digital Transmission Line"	Dr. O. Leuchs, Kable and Metalwerke – "A New Self Extinguishing Hydrogen Chloride Binding PVC Jacketing Compound for Cables"
1969	J. P. McCann, R. Sabia and B. Wargotz, Bell Laboratories – "Characterization of Filler and Insulation in Waterproof Cable"	J. D. Kirk, Alberta Government Telephones– "Progress and Pitfalls of Rural Buried Cable"
1968	H. Lubars and J. A. Olszewski, General Cable Corp. – "Analysis of Structural Return Loss in CATV Coaxial Cable"	N. Dean, B.I.C.C.– "The Development of Fully Filled Cables for Distribution Network"

PLENARY SESSION

"Stepping into the Future — A Vision of the Communication System of Tomorrow"
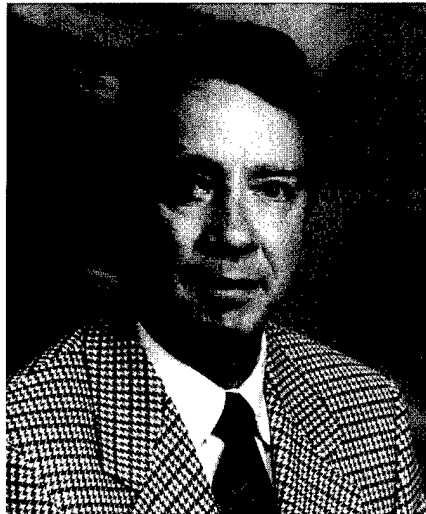
CHAIRMAN

John R. Sach
Pirelli Cables & Systems North America
Lexington, SC
john.sach@us.pirelli.com

John R. Sach is currently the Vice President and Chief Engineer for Pirelli
Cable and Systems NA Communications Division. His responsibilities
include research, development and design of optical fiber cables.

Sach joined Pirelli in 1975 as a Development Engineer working in
high frequency coaxial cables. Subsequently he has worked in
England, Italy and North American for Pirelli holding several position
in the area of Research and Development.

Sach holds a Bachelors degree in Engineering Metallurgy from Imperial
College London University. He is a member of the Optical Society of
America.

PANELISTS

Professor David N. Payne, Director, Optoelectronics Research Centre, University of Southampton,
Southampton, United Kingdom

Professor David J. Farber, Chief Technologist, FCC, University of Pennsylvania, Philadelphia, Pennsylvania

Steven G. Lanning, Vice President of Engineering, Aerie Networks, Inc., Denver, Colorado

PLENARY SESSION SPEAKER

Steven G. Lanning
Vice President of Engineering
Aerie Networks, Inc.
Denver, Colorado
slanning@aerienetworks.com

Steven G. Lanning, Vice President of Engineering, served as Director of Technology Management and Economics Research in the Mathematical Sciences Center at Lucent Bell Laboratories. During his tenure of 14 years, Dr. Lanning's work spanned network optimization, network modeling, economics and marketing science. Lanning has been awarded five patents in the areas of personalization of the telephony network and tracking Internet usage. He was a founder of AT&T's Consumer Lab, where he defined the opportunity for AT&T's first network adjunct for audiotext hosting services, pioneering and defining the AT&T EasyReach® service and consulting to the general manager of AT&T Accessible Communication Services.

Dr. Lanning has served on the advisory board of Rutgers Professional Accounting MBA, the business school faculty at the University of Notre Dame, as advisor to the water polo club and Special Olympics host. He and his wife, Lauren are active in the Juvenile Diabetes Foundation and Children with Diabetes.

Dr. Lanning holds a Ph.D. in economics from Northwestern University and B.S. from the University of California at Riverside.

LUNCHEON SPEAKER

"Humor, Risk & Change"
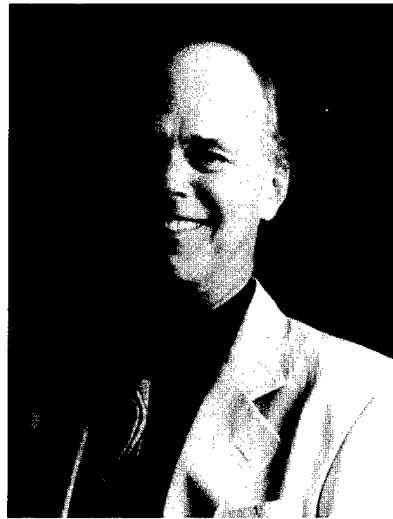
C. W. Metcalf
Fort Collins, Colorado

C. W. Metcalf is a high successful writer and performer. In the Mid-1970's, Metcalf balanced his time between teaching at Florida State University, the University of Michigan and Bennington College, and performing in his own touring theater group. Ultimately Metcalf landed a job in Los Angeles, writing and acting for children's television.

After working in LA for several years and failing to "capture much of Hollywood's imagination or cash," C.W. Metcalf unknowingly changed directions during a visit to the Center for Attitudinal Healing in Tiburon, California. Sent to the center to prepare a script on their revolutionary treatment of terminally ill children, Metcalf was moved by the positive outlook the children possessed.

Soon after his trip to the center, C. W. Metcalf began training as a hospice volunteer. A self-proclaimed cynic afflicted with "terminal seriousness," Metcalf hoped his work with cancer patients would help change his negative outlook on life. After several career changes, and a move to Colorado, C.W. Metcalf began presenting humor and health seminars to local hospice groups in the early 1980's.

After forming C.W. Metcalf & Company with his wife, Roma Felible in 1983, Metcalf began presenting his *Humor, Risk & Change* seminars to corporations around the world. Metcalf's work became popular as economic conditions faltered and companies were forced to downsize or succumb to mergers and takeovers. C.W. Metcalf's work quickly found a niche within high-stress corporate environments.

In 1992, C.W. Metcalf and Roma completed their first book, *Lighten Up – Survival Skills for People Under Pressure.* Metcalf says that *Lighten Up* not only includes information on the value of humor in the workplace, but also offers valuable survival skills for families, children, the terminally ill, alcoholics, and others confronting crisis.

C.W. Metcalf has appeared on the *Today* show, CNN, the Home show and has been featured in the pages of the *Wall Street Journal,* the *New York Times, Reader's Digest,* and *Industry Week.* He is currently developing a television program based on his work for network or syndicated distribution.

A New High-Density Central Cable Core Design

H. Paul Debban, Jr., Luis M. Bocanegra, C. Shawn Davis,
Richard D. Small, Jr., Peter A. Weimann, Manuel R. Santana

Lucent Technologies Inc.
Bell Laboratories
2000 NE Expressway, Norcross, GA 30071

Abstract

The massive deployment of fiber optic cables throughout the telecommunications network requires that new cable designs be fully optimized. New installation conditions such as crowded ducts and high-speed installation demand cables with both high optical density and improved installation characteristics.

To satisfy these demands, a new high-density cable core design has been developed. Central core cables utilizing the new design can be manufactured with fiber densities equaling or exceeding current central core ribbon cable designs. In addition, the core is suitable for use in both dielectric and metallic sheath configurations. The design brings significant advancements in fiber access and handling. As such, it is appropriate for use in a wide range of end-user applications.

Craft friendly features included in the new cable core design include:

- Fiber density equivalent to high-density central core ribbon and fiber bundle cables.
- Improved fiber handling and mid-span entry access.
- Improved fiber routing within splice enclosures.
- Reduced usage of gel filling compounds.

This paper discusses the materials of construction and unique features of the new cable core design. Calculations comparing the fiber packing density of this core design to current core designs are presented. Improvements in fiber access techniques provided by this design are illustrated. Finally, laboratory performance characteristics of cables manufactured using this core design are reviewed.

Keywords

Fiber Optic Cable Core; Cable; Optical Fiber; Fiber Optic Cable; Optical Cable; Ribbon; Easy Entry; Unit Tube;

1. Introduction

The current demand for bandwidth has triggered upgrades to and extensions of worldwide optical fiber backbone networks. It follows that the next phase of optical fiber deployment will be to extend and replace the networks in the customer access network. This application requires a small, rugged cable design of medium fiber count that can be deployed quickly and cheaply.

Current common outside plant cable designs can be divided into three main design groups. Each of these designs has features valued by customers, as shown in Table 1.

Table 1. Traditional Cable Designs

Design Family	Available Fiber Grouping	Features
Loose Tube	• Fiber Tubes • Ribbon tubes (High Fiber Counts)	Fibers and ribbons grouped into color-coded units for identification
Slotted Core	• Ribbons	Fibers grouped by optical circuit for efficient mass fusion splicing and breakout.
Central Tube	• Fiber Bundles • Ribbons	No central strength member, compact, mass fusion splicing with ribbons.

In recent years, a modification of the optical fiber bundle central core design has been introduced. This modification replaces the binding threads used to group fibers in the central core fiber bundle units with low modulus plastic tubes[1][2]. These designs, manufactured under various trade names, combine the compactness and efficiency of older central tube designs with the easy fiber identification of the loose tube design. These cables can be described generically as the Tube-In-Tube (TinT) cable core design, characterized by flexible unit tubes within a central tube cable.

Despite their advantages, recently introduced TinT cable designs have shortcomings that could slow their adoption in the North American market. The tensile strength of these cables is generally less than the *Bellcore GR-20-CORE, Issue 2, 1998* [3] standard of 2670N and the cables are not armored to resist rodent attack. These designs also fail to take advantage of the installation advantages that can be gained through mass fusion splicing of fiber ribbons.

This paper outlines the development of a TinT design, marketed under the trade name *XPressTube™*, which extends the performance of previous TinT cables.

A new unit tube was designed which can be used to group loose fibers, as in traditional loose tube and fiber bundle cables. However, the tube design also can be used to group multiple 4-fiber ribbons. The tube design was optimized for easy fiber access at both cable end and mid-span.

Two alternate cable cores were examined in this work. The first was a soft and flexible cable core that utilizes a bedding compound; the second was a core using established materials. The performance of each core was tested in existing central core cable sheaths.

2. Unit Tube Design

2.1 Fiber Tubes

Figure 1 shows a cross section of a fiber tube. Each tube contains 12 fibers, a ripcord, and a small amount of water blocking cable gel encased in a thin-walled, low-modulus polyolefin tube. The low-modulus material, discussed further in section 2.3, provides a flexible tube that allows for easy routing within closures and distribution frames. The ripcord is provided to facilitate tool-free mid-span tube entry, as discussed in Section 6.3. Each tube is color-coded to allow easy identification. Figure 2 is a photograph of a unit tube, showing the easy ripcord identification.
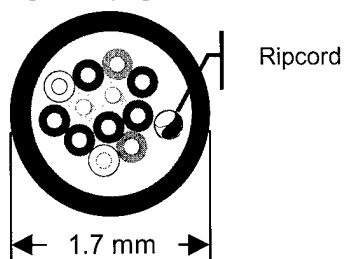
Figure 1. Cross Section of a Twelve-Fiber Unit Tube with Ripcord
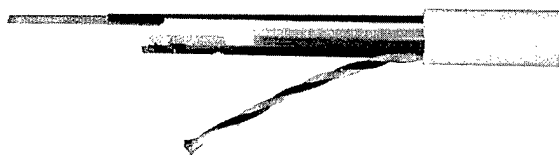
Figure 2. Twelve Fiber Unit with Ripcord

2.2 Ribbon Tubes

Fast fiber deployment is achieved with ribbon cables because of the efficiency of mass fusion splicing. When the ribbon stack height equals the number of fibers per ribbon, central tube ribbon cables achieve the highest packing density of any current cable design[4]. The packing density of traditional ribbon cables can be approached by unitizing the ribbons into round tubes, and packaging the unit tubes within a central core cable.

The 1.7 mm OD tube presented in section 2.1 is sized to package three 4-fiber ribbons into a unit of twelve fibers, as shown in Figure 3.
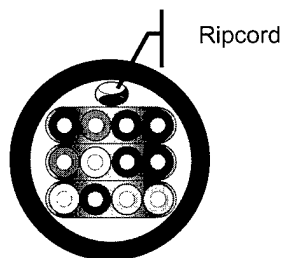
Figure 3. Twelve Fiber Unit Tube with Four Fiber Ribbons

This package maintains the size and flexibility of the twelve-fiber unit, but further groups the fibers for fast circuit breakout and mass fusion splicing.

2.3 Tube Materials

The materials used in loose-tube cable constructions tend to be rigid thermoplastics, such as poly(butylene terephtalate) (PBT) or nucleated impact-modified polypropylene (PP)[3]. These materials have excellent long-term aging stability, and swell minimally when in contact with filling compounds. However, traditional loose tube materials also present some difficulties during cable installation. Access to fibers generally must be provided using tools, and the rigid tubes are often difficult or impossible to route in closures. The ideal material for these tubes must have low stiffness and allow tool-free tube entry, while maintaining the excellent aging performance of conventional loose tube materials.

The low-modulus polyolefin (PO) material selected for this application meets all of these requirements, as confirmed by mechanical property measurements and aging tests. Mechanical tests were performed using a TA Instruments Model 2980 Dynamic Mechanical Analyzer. All tests were performed over a temperature range of –40°C to 70°C, corresponding to the standard service temperature requirements for outside plant cables. In Figure 4, we compare the flexural modulus of the PO material to those of two typical materials used for loose tube applications, a commercial PBT and a commercial nucleated PP. The PO material is much less stiff than either the PP or the PBT over the entire temperature range. As discussed in more detail below, use of this low modulus tube material satisfies the requirements of tool-free entry and enhanced tube flexibility.
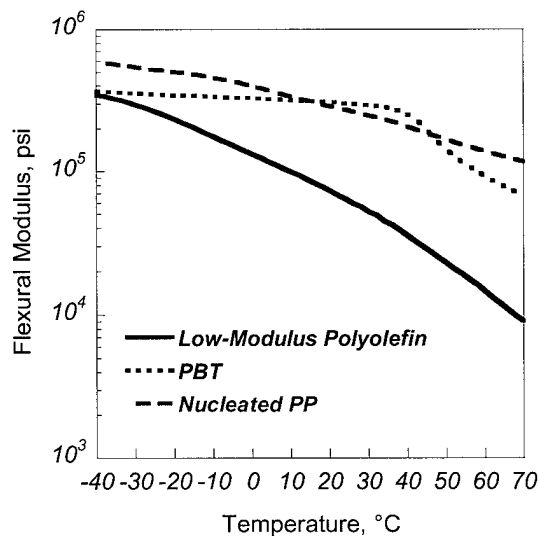
Figure 4. Flexural Modulus vs. Temperature Behavior of Tube Materials

Although this material is much softer than conventional buffer tube materials, its aging performance is similar to that of conventional loose-tube nucleated PP. In order to measure swelling behavior, samples of the PO tube material and the commercial nucleated PP were aged for 29 days at 85°C in a bath of poly(alphaolefin)-based filling compound. As shown in Table 2, the swelling behavior of the PO material is comparable to that of the nucleated PP.

Table 2. Aging and Oxidative Stability Performance of Tube Materials

Property	Low-Modulus PO	Commercial Nucleated PP
Volumetric Swell After Aging‡	2.2%	3.1%
OIT at 200°C (as-received)	> 100 min	> 100 min
OIT at 200°C (after aging‡)	> 100 min	56 min

‡ Samples were aged for 29 days at 85°C in a bath of poly(alphaolefin)-based filling compound.

Oxidative stability of the materials was measured using the Oxidative Induction Time (OIT) method, following the ASTM D 3895 standard. Measurements were made using a DuPont Instruments Model 912 DSC, using aluminum sample pans and a measurement temperature of 200°C. OIT measurements were made for as-received samples of the PO material and a commercial nucleated PP, as well as samples of both materials aged for 29 days at 85°C in poly(alphaolefin)-based filling compound. The stability of the PO material is superior to that of the commercial nucleated PP, as shown by the data in Table 2. The OIT of the PO material is greater than 100 minutes before *and* after aging. Based on our reliability tests, a service lifetime well in excess of 30 years is expected for these tubes in typical outside plant service conditions.

3. Cable Core Design

3.1 Soft Cable Core

In the soft cable core design, Figure 5, the unit tubes are embedded in a layer of low modulus bedding compound. This core is designed to provide the maximum fiber packing density with the 1.7 mm unit tubes. The bedding compound does not adhere to the polyolefin unit tubes. Since it contains no oil, it leaves no residue after removal. The bedding compound can easily be torn or peeled away from the unit tubes without tools. The same thin ripcord used within the unit tubes is used to speed entry into the cable core itself. Superabsorbent materials within the core provide water blocking in the interstices between unit tubes. The soft cable core is surprisingly flexible with little resistance to bending.
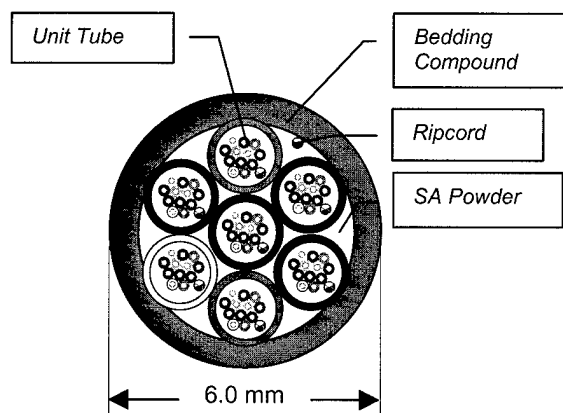
The same thin ripcord used within the unit tubes is used to speed entry into the cable core itself. Super-absorbent powder within the core provides water blocking between the unit tubes.

3.1.1 Function of the Bedding Compound. The bedding compound has the following functions:
- Groups the unit tubes into a compact core that is highly flexible.
- Equalizes stress among the unit tubes
- Provides a heat barrier between the unit tubes and subsequent extrusion operations.
- Captures desired SZ-twist in the unit tubes.
- Can be peeled or removed from the unit tubes with no special tools.

3.1.2 Materials Properties. A variety of thermoplastic materials are available for use as bedding compounds. A suitable bedding compound must have the following materials properties:
- Lower modulus than the unit tube jackets, to provide flexibility and optimum environmental performance.
- Sufficient modulus to provide integrity to the cable core.
- Removable from the unit tubes without tools. (Peel or tear off with fingers.)
- Low processing temperature, to prevent remelt of the unit tubes during application.
- No adhesion to unit tubes.
- Leaves no residue after removal.

3.2 Dry Central Core Tube

The dry central core design, Figure 6, uses a conventional polypropylene core tube. No filling compound is used between the unit tubes to facilitate fiber access and reduce cleaning time. A superabsorbent water blocking tape prevents water penetration within the core, and serves as a heat barrier between the unit tubes and the core tube during manufacture.

The core tube is sized to provide sufficient strain relief for both fiber and ribbon tubes. Excess fiber length control is provided by the same mechanisms used in standard central core ribbon cable. Fiber density is comparable to the fiber bundle cable design. Cable entry is discussed in Section 6.2.2.

Unit Tube | Bedding Compound | Ripcord | SA Powder

◄─── 6.0 mm ───►

Figure 5. Unit Tubes in Soft Cable Cable Core
(84 Fiber)

Unit Tube | SA Tape | PP Tube

◄─── 8.0 mm ───►
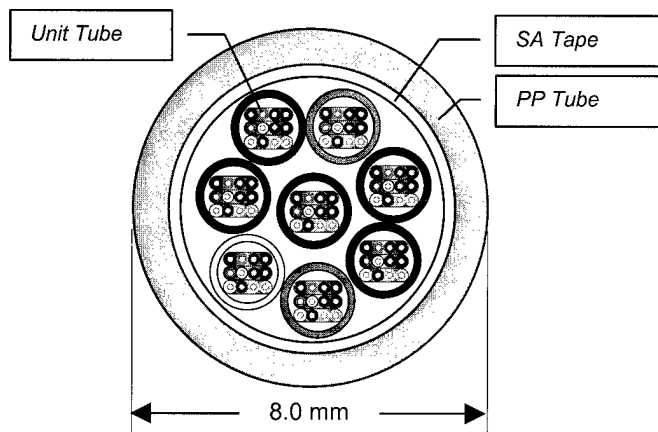
Figure 6. 96 Fibers in Dry Central Core Tube
(4 Fiber Ribbons)

3.3 Fiber Density

Table 3 compares the fiber density of cables with 2700N tensile strength. Cables utilizing the new central core construction are the same diameter in both dielectric and light-armored versions. The central core sheaths used as the basis of this comparison use linear strength members for fast cable entry.

Table 3. Fiber Density Comparison

Cable Core	Fiber Count	Cable Diameter (mm)	Fiber Density (f/mm^2)
Loose Tube 12 Fiber Units, Light Armor	96	16.3	0.46
Filled Central Core 12 Fiber Ribbons	144	15.5	0.76
Filled Central Core 12 Fiber Bundles	96	15.5	0.51
Soft Cable Core 12 Fiber Unit Tubes	144	15.5	0.76
Dry Central Tube 12 Fiber Unit Tubes	96	15.5	0.51
Dry Central Tube 3-4 Fiber Ribbon Unit Tubes	96	15.5	0.51

4. Cable Design

4.1 Performance Requirements

Basic performance parameters for the North American market per *Bellcore GR-20-CORE* are as follows:

Tensile Strength: 2670 N (600 lb.)

Temperature Range:

    Operation: -40°C to 70°C (-40°F to 158°F)

    Installation: -30°C to 60°C (-22°F to 140°F)

    Storage/Shipping: -40°C to 75°C (-40°F to 167°F)

Bending Diameter:

The cable's short-term minimum bending diameter is 20 times the cable diameter in the "No Load" condition and 40 times the cable diameter when "Under Load". The "No Load" condition is defined as up to 30% of the maximum load rating and the "Under Load" condition is defined as any load over 30% of the load rating.

4.2 Cable Sheaths

4.2.1 Metallic Armor Sheath. A schematic of the metallic sheath is pictured in Figure 7. This is a general-purpose cable design suitable for underground conduit, direct buried, or aerial applications. Hundreds of thousands of kilometers of this basic design have been manufactured since the late 1980's, and it has proven its value in both backbone and access networks.

Small modifications were made to this sheath to speed fiber access. The cable is jacketed with a novel high-density polyethylene resin that combines high abrasion resistance and a low coefficient of friction with easy sheath entry. The adhesion between the armor and the polyethylene jacket is controlled to speed jacket entry.
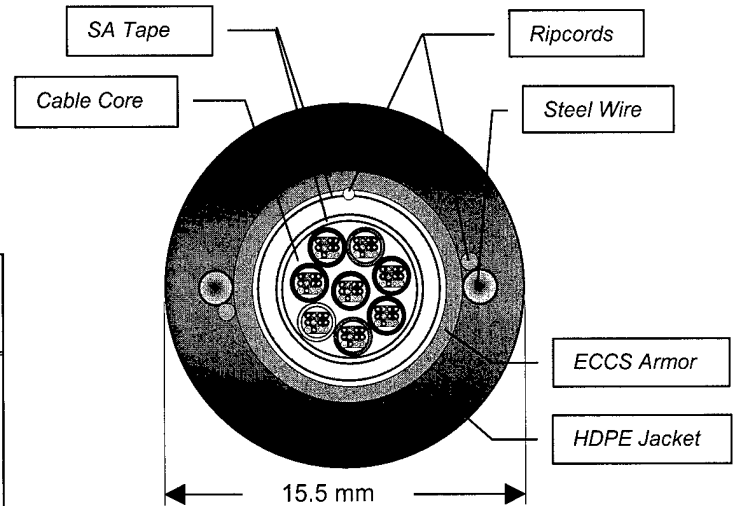
Figure 7. 96 Fiber Armored Cable with Dry Central Core Tube

4.2.2 Dielectric Sheath. The dielectric sheath incorporates two linear dielectric strength members in a HDPE outer jacket. The jacket material is the same as the metallic cable. The cable is a general-purpose sheath with a tensile rating of 2700N[6].

5. Test Results

5.1 Environmental Results

Three test cables were manufactured using dispersion unshifted single mode fibers. The cables were tested according to the *Temperature Cycling and Cable Aging* Tests in *Bellcore GR-20-CORE*. Additional measurements were taken at −30°C. Attenuation results are illustrated in Figure 8 and Table 4.
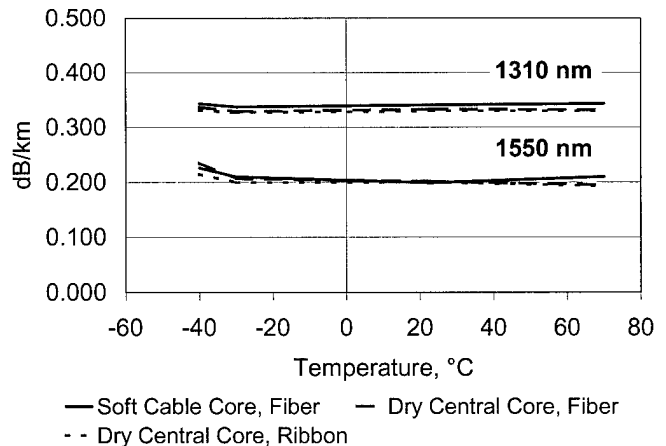
Figure 8. Environmental Performance of New Cable Cores

Table 4. Mean Low Temperature Added Loss at 1550nm

Core Design	Added Loss (dB/km)	
	-30°C	-40°C
Soft Cable Core – fiber tubes	0.011 dB/km	0.03 dB/km
Dry Tube – fiber tubes	0.005 dB/km	0.03 dB/km
Dry Tube – ribbon tubes	-0.001 dB/km	0.02 dB/km

5.2 Mechanical Testing

The metallic dry core cable was tested to the mechanical test requirements of *Bellcore GR-20-CORE*. In all cases, the cable design displays no significant added loss under test conditions. Selected test results are listed in Table 5. The added loss is the maximum observed change in loss observed in any of the 96 fibers. Similar results were observed for a soft cable core test sample with fiber tubes.

Table 5. Mechanical Test Results. 96 Fiber Dry Core in Metallic Sheath

Cable Test	GR-20-CORE		Max Level Tested	
	Test Level	Max Δ Loss‡	Test Level	Max Δ Loss‡
Impact Resistance FOTP 25	4.0 kg	0.01 dB	16.0 kg	0.01 dB
Tensile Loading and Bending FOTP 33	801N (180 lb)	0.02 dB	5338N (1200 lb)	0.07 dB
Compressive Loading FOTP 41	1112N (250 lb.)	0.01 dB	4448N (1000 lb)	0.01 dB
Twist FOTP 85	2m 180°	0.01 dB	0.5m 360°	0.02 dB

‡ Maximum increase in loss in any fiber within the cable.

6. Cable Entry

6.1 Sheath Entry

As discussed in section 4.2.1, the metallic sheath was modified with a new high-density polyethylene jacketing material and the adhesion between the jacket and the armor is controlled to improve sheath entry. The dielectric sheath is equipped with two ripcords that make jacket entry quick and easy.

6.2 Core Entry and Tube Access

6.2.1 Soft Cable Core

The soft cable may be easily opened after the outer sheath is removed. Fingers are used to peel approximately 50 mm of bedding compound to reveal the ripcord. A two-color black/white ripcord is used to slit the dry material. The unit tubes are then easily accessible.

6.2.2 Dry Central Core

Units in the dry cable core may be accessed using standard central core tube entry techniques. The elimination of the filling compound gel in the core tube reduces the time required to clean the fibers.

While the soft cable core cable may be entered without tools, the dry core provides advantages in cable entry. The dry central core cable is fully compatible with existing central core entry techniques. The higher modulus of the PP tube requires less care when extracting the core from the ECCS armor since the PP has a harder surface and is less prone to kinking. In addition, since the unit tubes are free to slide in the core, the sheath can be removed by ring cutting the sheath and the core tube and pulling the protective layers off the unit tubes.

6.3 Unit Tube Entry

One major goal of this design was to allow installers to access the fibers in the unit tubes quickly and easily without the use of special tools. Early in the development cycle, to evaluate fiber accessibility, a cable was manufactured using prototype unit tubes fabricated from a variety of candidate materials. In all cases, tubes could be removed from the fibers by pinching the tube approximately 100mm from the end and pulling the tube off the fiber group. Repeated hand motions were required to access longer lengths of fiber.

Tool free mid-span entry was more complicated. For the initial set of prototype tubes, no suitable method of exposing the mid-span fibers without tools was discovered. In the case of low strength tube materials, only short lengths of tube could be removed at one time. Medium strength materials were too hard to remove by hand and too soft to split open with a tool. Higher strength materials required a tool to split the tube open.

The next set of prototype unit tubes were manufactured using a small ripcord next to the optical fibers. The ripcord significantly improves fiber access. End cable fiber access is easily accomplished with a minimum of hand motions by pulling a short length of tube from the fibers and using the ripcord to slit the tube to the required length. The ripcord is differentiated from the fibers by its two-color black/white construction.

Mid-span entry is easily accomplished with the ripcord. The tube is separated in the middle to expose the ripcord by selecting the entry point, pinching the tube gently with the thumb and index finger of each hand and pulling the jacket in two (see photograph in Figure 9). The tube is then held in one hand while the ripcord is pulled away from the fibers to slit the tube.
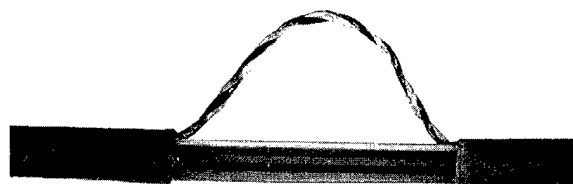
Figure 9. Ripcord Ready for Mid-Span Unit Tube Entry

7. Conclusion

This paper presented two tube-in-tube design options for use with traditional, 2670N tensile strength central core sheaths. The cable core designs presented here combine the best features of central core, loose tube, and slotted core cable designs. The units offer the easy mid-span entry and the compact sheath design of central core cables, and the easy unit identification of traditional loose tube cables is provided with colored unit tubes. The fast splicing and circuit-based fiber grouping of the slotted core cable is available when units containing four-fiber ribbon units are substituted for units containing individual optical fibers. The completed cables comply with *Bellcore GR-20-CORE, Generic Requirements for Optical Fiber and Optical Fiber Cable.*

The soft cable core design provides a compact and flexible platform for fiber optic cables providing excellent mechanical and environmental performance.

The dry core cable design was selected for production. Easier jacket entry and compatibility with existing tools and procedures make this the design the better choice.

The new cable core is packaged in general purpose, rugged sheaths that meet standard North American performance requirements. We believe the efficiencies gained from mass fusion splicing and the ability to group fibers into optical circuits will drive acceptance of ribbons in the low fiber count cable designs.

8. References

[1] P. Jamet and A. Jarlot, "Manufacturing and Field Experimentation of Microsheath Cable for Low Cost Subscriber Loop," *Proceedings of the Forty-Third International Wire and Cable Symposium*, 196-202 (1994)

[2] S. Pastuszka, JP. Bonicel, M.G.S. Emeterio, P. Gaillard, K. Nothofer, and A. Weiss, "A New Type of High Fiber Count, Low Dimension Optical Cable with Simplified Installation Characteristics," *Proceedings of the Forty-Eighth International Wire and Cable Symposium*, 106-111 (1999)

[3] Bellcore GR-20-CORE, *"Generic Requirements for Optical Fiber and Fiber Optic Cable"*, Issue 2, July 1998.

[4] E. R. Logan, "The Status and Future of High Fiber Count Cable Designs," *Proceedings of the Forty-Eighth International Wire and Cable Symposium*, 199-204 (1999)

[5] B. G. Risch, J. Auton, and O. Tatat, "Advanced Impact Polypropylene Buffering Material for Superior Long Term Hydrolytic and Thermo-Oxidative Stability," *Proceedings of the Forty-Seventh International Wire and Cable Symposium*, 698-704 (1998)

[6] R. H. Norris, R. D. Small, and P. A. Weimann, "Development of a Riser Rated Outdoor/Indoor Central Tube Ribbon Cable," *Proceedings of the Forty-Eighth International Wire and Cable Symposium*, 134-140 (1999)
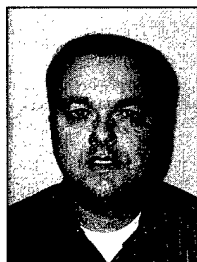
H. Paul Debban is a Distinguished Member of Technical Staff with Lucent Technologies – Bell Laboratories in Norcross, Georgia concentrating on Outside Plant Cable Development. He joined Western Electric in 1980 after graduating from the University of Nebraska – Lincoln in 1980 with a BS in Mechanical Engineering. He joined the outside plant optical cable manufacturing engineering group in 1981 and has worked on a broad range of projects including introduction of filled optical cables, the Lightpack® cable core, the AccuRibbon® cable core, armored cables, and others. He has managed several capital expansion projects and has experience in process control. He joined the optical cable design group in 1999.
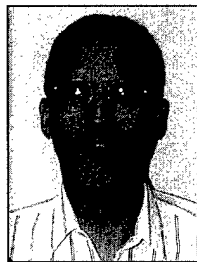
Luis M. Bocanegra is a Member of Technical Staff at Lucent Technologies Outside Plant Cable Development Organization. He joined Lucent Technologies in 1998 after several years of working in academia in Peru and Puerto Rico. Mr. Bocanegra received his Diploma of Mechanical Engineer from the Catholic University of Peru in 1978. He was a Fulbright Scholar from 1984 to 1986 and a United States Pharmacopeia Fellow from 1986 to 1989. He earned MSME and Ph.D. degrees from West Virginia University in 1986 and 1988, respectively. His field of specialization is Thermo-Fluid Sciences. Also, he has participated in Review Panels for the National Science Foundation and has been peer reviewer for ASME and ASEE.
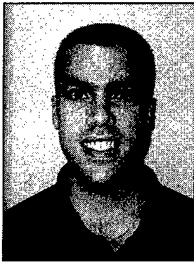
Shawn Davis is a Member of the Technical Staff at Lucent Technologies in the Fiber Optics Outside Plant Cable Development group. His projects focus on cable design, process development, fiber optic cable tool design, and extrusion tool design. Shawn graduated from the Georgia Institute of Technology in 1997 with a Bachelor's degree in Mechanical Engineering, and he is currently working on obtaining his Master's degree at Georgia Tech, specializing in manufacturing.
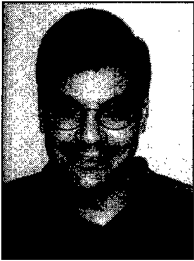
Peter Weimann is a Member of the Technical Staff in the Fiber Optic Materials Technology group at Bell Laboratories, Lucent Technologies, Norcross, GA. His primary focus is materials development for outside plant fiber-optic cable products. Prior to joining Lucent, he received his Ph.D. in Materials Science and Engineering from the University of Minnesota in 1998. His thesis research focused on structure-property relationships in polyolefins. He received a B.S.Eng. in Materials Science and Engineering, as well as a B.S.Econ. in Organizational Management, from the University of Pennsylvania in 1992. He is a member of the American Chemical Society and the Society of Plastics Engineers.
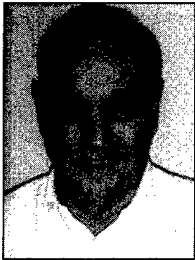
Richard D. Small is a Member of Technical Staff in the Fiber Optics Materials Technology Group at Bell Laboratories, Lucent Technologies, Norcross, GA. His focus is on both material development of fiber optical cable products and material development of fiber optical ribbon products. He received in 1975 from the University of South Florida a Ph.D. in Physical Chemistry. From 1975 until 1978 he was at the University of Notre Dame, doing nanosecond laser flash photolysis organic photochemistry. He joined AT&T in 1978. He has published over 40 outside technical papers in varied technical areas and has 8 patents. He is a member of the American Chemical Society and RadTech.
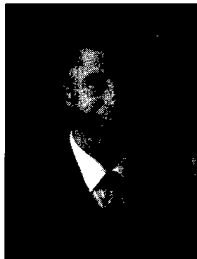
M. R. (Manuel) Santana holds a Bachelor of Science and a Master of Science degrees in Electrical Engineering from the University of Hartford and the Georgia Institute of Technology, respectively. Manuel joined Bell Laboratories in 1970 as a cable designer. He has been involved in fiber-optic cable design since the industry's birth in 1974. Manuel is a technology expert in all areas of fiber-optic cable: design, new processes and manufacturing technology. He is a member of various fiber-optic cable standards boards where he has a leadership position in the area of fiber-optic cable specifications. His career in fiber-optics technology has led to the development of the basic cable products that are the heart of the Optical Fiber Solutions division of Lucent Technologies. These contributions include the Lightpack® and AccuRibbon® core designs, the LXE sheath design, the Tactical military cable and the DuctSaver® high-fiber count cable. Manuel was awarded the 1991 Hispanic Engineer of the Year for Outstanding Technical Contribution and the Alexander M. Nicolson trophy by the Lucent Intellectual Property department for patent commercial value. Manuel was appointed Bell Laboratories Fellow in 1994.

He is a senior member of the IEEE and he has published thirty technical papers in various external publications. He has been granted twelve patents

A New Optical Cable Attachable to Drop Wires

Yukihiro Hamada, Shoji Matsumoto, Fumihiko Shimizu, Hirotaka Tanaka*, Tetsuya Ujie*

Nishi Nippon Electric Wire & Cable Co., Ltd., *Kyushu Electric Power Co.,Inc.

Oita, Japan   *Fukuoka,   Japan

+81-97-537-5568   hamaday@nnd.co.jp

ABSTRACT

We developed a new non-metallic optical fiber unit can be bound to the power drop wires from the aerial lines not only in the factory but also in the field. The results of the tensile performance test of the composite cable using this unit under the maximum permissible tension of the conventional drop wires, showed the excellent with no optical loss changing and than less 0.2% elongation ratio.

Furthermore a new simple and portable binding tool was also developed, which can easily attach the optical fiber unit to the existing installed power drop wires in the field.

We evaluated the new installation method using these optical fiber unit and the binding tool in an actual field test site, the performances were excellent for binding of that 50m optical fiber unit.

KEYWORDS

Optical Fiber; Power Drop Wires; Optical Subscriber Line; Broadband Internet Services; CATV Services; Aramid FRP

INTRODUCTION

The optical subscriber lines are expected to realize the high-capacity data networks such as the broadband Internet services and the CATV services. They are also required to be economically installed, flexible and speedy to answer the various needs of the Internet users.

Generally, optical cables are installed from aerial cables to the users when the each requirement occurs. This method needs high costs of optical cable itself, and the installation that takes a long period. Furthermore, a lot of cables are to be drawn into a house, then the strength up of the common poles becomes necessary.

Therefore, we have been investigating the new method to attach the optical fibers to the power dorp wires, as one of the approaches to solve the above problems.

1 . Composite cable of the optical fiber unit and the power drop wires

1.1 Design conditions

We considered the following conditions in order to unify the developed optical fiber unit to the power dorp wires.

That unit had to be fabricated without any metallic elements to avoid the electromagnetic interference. This unit also needs the enough strength for handling in the cable installation. Therefore, the fiber reinforced plastic (FRP) strength members are unified in this unit.

Considering that the each optical fiber unit may be connected to the various network services, therefore we decided to unify the two single mode fibers in it.

1.2 Optical fiber unit design

Figure 1 shows the cross section of the developed optical fiber unit which consists of a 2-fiber ribbon and two thin aramid FRP strength members both sides of the ribbon.

The selected aramid FRP of the strength members is able to avoid the crush will be caused by the bending when the unit will be fixed to a splice box. We choused the 1.0mm diameter of strength members which can permit a tension of 198N actually measured as the tension force by one hand.

To reduce the manufacturing cost of this unit, it was extruded with the fiber ribbon and the strength members which were coated with the PVC sheath in the lump. This sheath is the same resin of the power drop wires. The unit has two notches on the both sides of the sheath, for separating out the fiber ribbon easily under the installation.

The unit has a diameter of 4.6 mm and a weight of 25 kg/km.
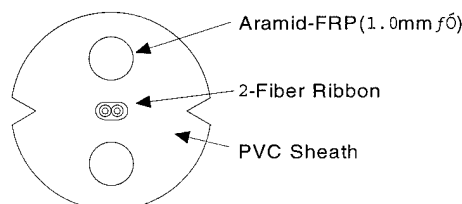
Figure 1 Cross section of the optical fiber unit

1.3 Composite cable design

Figure 2 shows the cross section of composite cable of the developed optical fiber unit described above and the power drop wires.

The composite cable is formed by binding those units and the drop wires each other, in order to achieve the reduction of the manufacturing cost and the wind pressure load. Adapting such composite cable structure, the outer diameter and the weight of it can be almost equal to those of the conventional power drop wires. Furthermore, this composite cable can be separated easily to each other under the installation.

This composite cable has the diameter of 19mm and the weight of 535 kg/km.
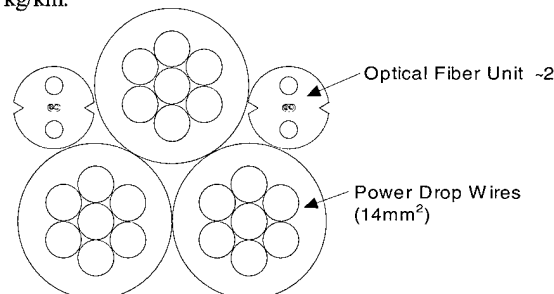
Figure 2 Cross section of the composite cable of the optical fiber units and the power drop wires

1.4 Characteristics of the composite cable

1.4-1 Temperature Characteristic

Figure 3 shows the temperature characteristic of the optical loss changing of the fabricated composite cable in the range of -30 to 60 degrees. The measurement optical wavelength was 1550 nm. The loss changing was excellent with less than 0.01 dB/km.
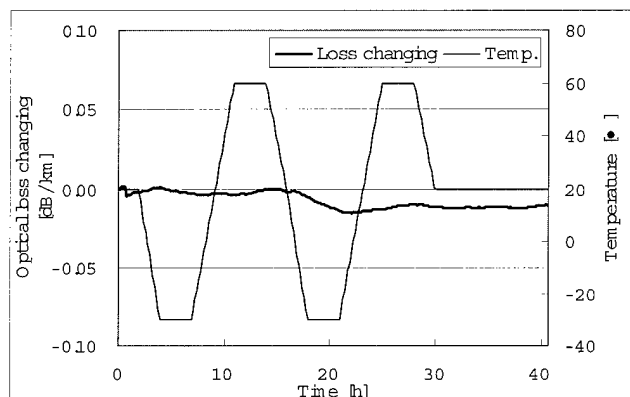
Figure 3 Temperature characteristic of optical loss changing of the composite cable

1.4-2 Tensile test performances

The developed non-metallic optical fiber unit allows attaching to the drop wires which can support the unit instead of the strength member itself by binding each other.
Figure 4 shows the measured tensile performances of the fabricated composite cable, such as the elongation ratio and an optical loss changing with measurement wavelength of 1550 nm. There was no optical loss changing and less than 0.19% elongation ratio equivalents to the fiber strain concerned with its lifetime, under the condition of maximum permissible tension of 5,635 N of the composite cable.
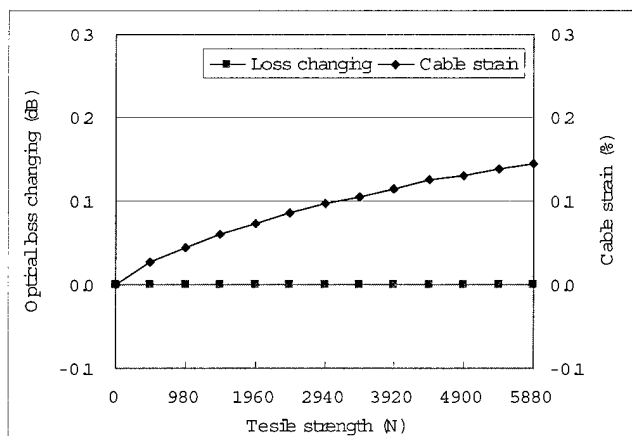
Figure 4 Tensile test results of the composite cable

1.4-3 Other Mechanical Characteristics

Table 1 shows the results of the other mechanical characteristics of the fabricated composite cable. In all examinations, they were excellent results.

Table 1 Test results of the other mechanical characteristics of the composite cable

Test Items	Test Conditions	Loss changing
Lateral Pressure	1470N/50mm	Less than 0.01dB
Bending	300mm diameter ±180deg. 10 times	Less than 0.01dB
Impact	25mm ϕ 500g load 1m drop height	Less than 0.01dB
Torsion	±180deg. 3 turn	Less than 0.01dB
Squeezing	R:250mm wheel 539N 5 turn	Less than 0.01dB

2. Binding tool for the optical fiber unit

2.1 Design conditions

The developed composite cable of the optical fiber unit and power drop wires mentioned before, is suitable for the new installation of optical subscriber. However, the installation cost should be certainly increased if the existing power drop wires is exchanged for the developed composite cable.
Therefore, we intended to develop a new binding method for the optical fiber unit to the existing power drop wires. We considered the following conditions to develop this method and the binding tool.

o   The period for the binding installation of the optical fiber unit is as short as possible.
o   The method and the binding tool can support the various installation conditions.
o   The construction of binding tool is as simple as possible to manufacture with not only the lower cost but also the small size and light weight for operating on a pole.

2.2 Binding tool design

Figure 5 shows the photograph of the developed binding tool for the optical fiber unit.
The binding tool consists of the partial plastic bobbins dividable into the half, can be to attach the existing power drop wires, on which the optical fiber unit can be bound by using a handy electric screwdriver before the binding to that drop wires.
The circumference length of that tool's bobbin was designed to get that the bound optical fiber unit became the same as pitch of the power drop wires.
By pulling the rope with this tool on which the optical fiber unit already was bound, and we can easily unify the unit and the power drop wires. Figure 6 shows the image of the developed installation method of the optical fiber unit.
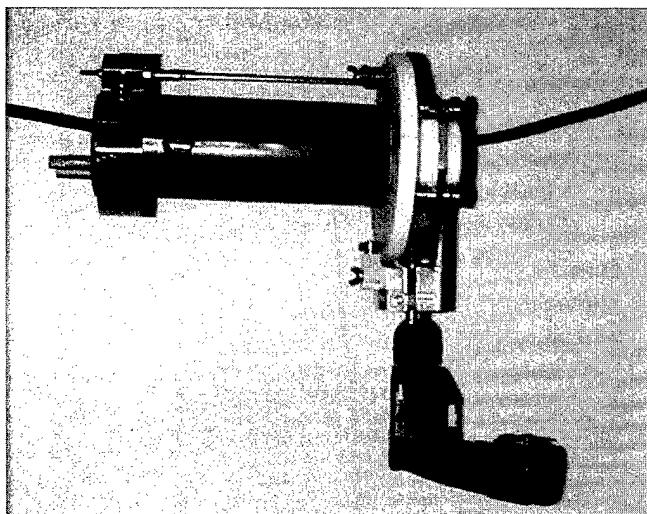
Figure 5 Photograph of the binding tool
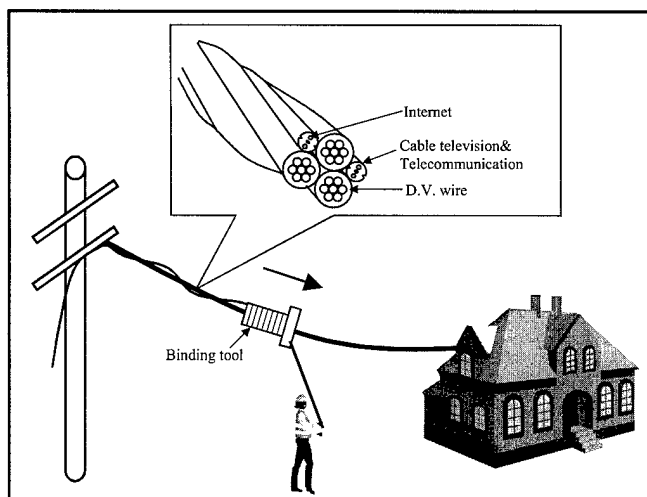
Figure 6 Installation image of the optical fiber unit

2.3 Optical fiber unit design

The optical fiber unit introduced in Chapter 1 can be adopted for this binding tool.

Because we investigated that the developing of the optical fiber unit can be applied for not only the composite cable fabricated in the factory but also the field installation of it by using this tool.

The actually measured tension of the optical fiber unit under binding installation was less than 19.8 N.

Therefore the developed optical fiber unit has the enough strength for installation using this tool as described before.

In addition, the other various excellent performances of this unit were same as the results introduced in Chapter 1.

2. 4 Characteristics of the optical fiber unit

2.4-1 Temperature Characteristic

Figure 7 shows the temperature characteristic of the optical fiber unit loss in the range of -30 to 60 degrees. The measurement optical wavelength was 1550nm.

The changing of optical loss was excellent with less than 0.01dB/km.
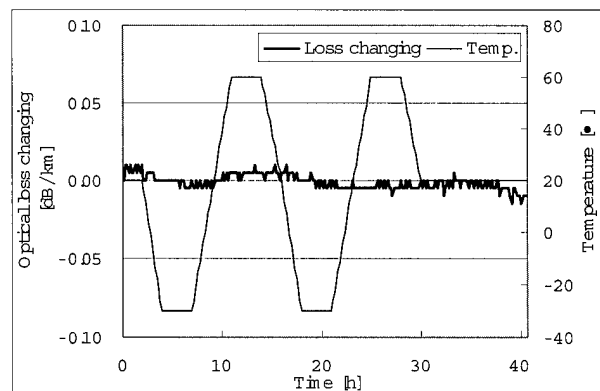
Figure 7 Temperature characteristic of the optical fiber unit

2.4-2 Tensile test performances

Figure 8 shows the unit elongation ratio and a optical loss changing at the 1550nm wavelength under adding tension to the unit.

There was no optical loss changing under the maximum 198N tension, and the cable elongation ratio was less than 0.18%.
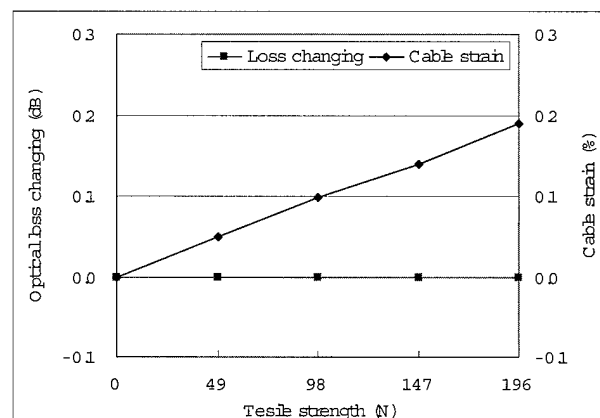
Figure 8 Tensile test results of the optical fiber unit

2. 4-3 Other mechanical characteristic

Table 2 shows the results of the other mechanical characteristics of the optical fiber unit. In all examinations, they were all excellent results.

Table 2 Test results of the other mechanical characteristics of the optical fiber unit

Test Items	Test Conditions	Optical loss changing
Lateral Pressure	1470N/50mm	Less than 0.01dB
Bending	46mm diameter ±180deg. 10 times	Less than 0.01dB
Impact	25mm φ 500g load 1m drop height	Less than 0.01dB
Torsion	±180deg. 3 turn	Less than 0.01dB
Squeezing	R:250mm wheel 196N 5 turn	Less than 0.01dB

2.5 Characteristics of the binding tool

2.5-1 Installation Inspection

The 50m installed power drop wires and the bound optical fiber unit on it are shown in figure 9. The installation period was 7 minutes and 20 seconds, for attaching of the unit using the binding tool.

Figure 10 shows the example of the measured optical loss waveform of that unit after installation by the OTDR. In the other measured data, all results are excellent.

Figure 9 Photograph of the installation sight
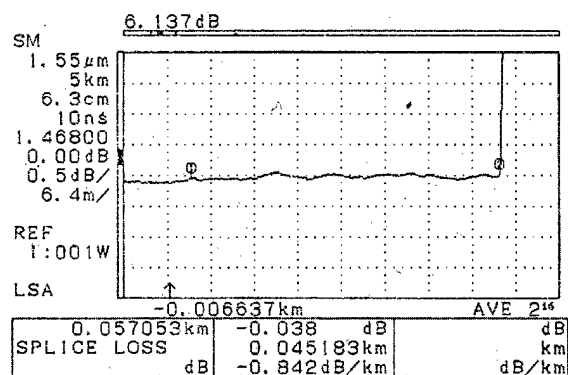
Figure 10 Waveform example of the measured optical loss

2.5-2 Long term reliability examination

Furthermore, we evaluated a long-term optical loss changing after the binding of the unit to confirm the reliability of this new installation method.   Figure 11 shows the measurement results of the optical loss changing in the period of 12 weeks passage from the installation. There is no remarkable loss changing, which means this method has a sufficient reliability.
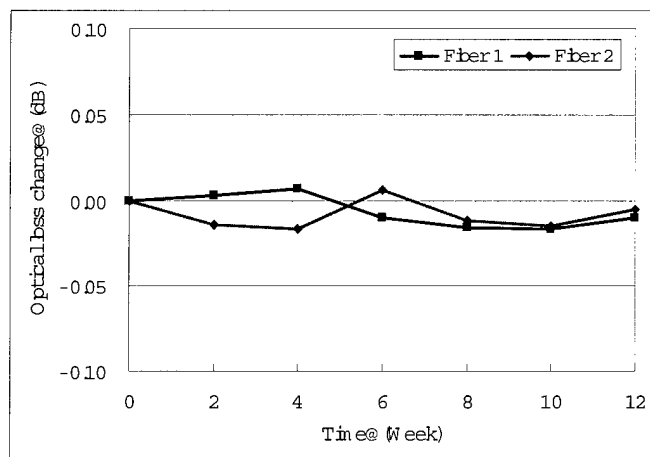
Figure 11 Results of the long term reliability examination

We got the other excellent results in this inspection of the installation for the optical fiber unit by the developed binding tool. The new developed method can realize the effective usage of the optical fiber unit for attaching to the existing power drop wires, and the reducing of the installation period and the numbers of the dropping cables.

CONCLUSION

We developed the new non-metallic optical fiber unit which can be composed with the power drop wires, and the new simple and portable binding tool which can easily attach that optical fiber unit to the existing installed power drop wires in the actual fields.

We evaluated the various performances and characteristics of these new materials described in this paper. The every excellent results of the evaluations indicate that they are suitable for the actual applications.

This new method mentioned before can reduce the cost and the period of installation for the optical fibers. Furthermore, this gives the better view and the lower wind pressure by binding the optical fiber unit and the power drop wires, in comparison with the conventional methods.

Consequently, this method can realize the optical subscriber lines such as the high-capacity data networks which are required to be economically installed, flexible and speedy to answer the various needs of especially the Internet services.

REFERENCES

[1] S. Matsumoto et al., "Development of drop wires with optical fiber cables" IEICE September 1998, B-10-32

[2] Y. Hamada et al., "A study of optical fiber cable attached to the drop wires" IEICE September 1999, B-10-41

AUTHORS

Yukihiro Hamada was born in 1970. He graduated in electric engineering from Oita National College of Technology in 1991. He joined Nishi-Nippon Electric Wire & Cable Co., Ltd. in 1991. He has been engaged in development of optical fiber cable. He is a member of IEICE of Japan.
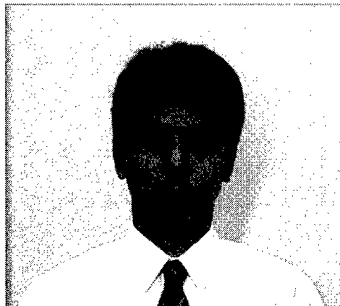
Shoji Matsumoto was born in 1971. He received a M.E. degree in electronic engineering in 1995 from Oita University. He joined Nishi-Nippon Electric Wire & Cable Co., Ltd. in 1995. He has been engaged in development of optical fiber cable. He is a member of IEICE of Japan.
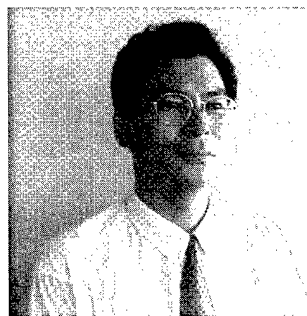
Fumihiko Shimizu was born in 1959. He received a M.E. degree in information engineering in 1984 from Toyohashi University of Technology. He is a manager of Telecommunications Engineering Department, Nishi Nippon Electric Wire & Cable Co., Ltd.. He has been engaged in development of optical fiber cables, optical connectors and their accessories. He is a member of IEICE of Japan.
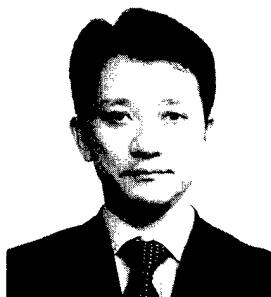
Hirotaka Tanaka was born in 1964. He graduated in electric engineering from Kurume National College in 1985. He joined Kyushu Electric Power Co., Ltd. in 1985. He has been charge of development of Integrated Automatic Distribution System

Tetsuya Ujie was born in 1964. He graduated in electric engineering from Kumamoto University in 1987. He joined Kyushu Electric Power Co., Ltd. in 1987. He has been charge of development of Integrated Automatic Distribution System

Hybrid Cables for Telecommunications and Power Feeding into the Access Network

Marta García, Carlos G. Cortines, Francisco J. Sáez

Alcatel Cable Ibérica
Maliaño, SPAIN
+34-942-250100 · marta.garcia@aci.alcatel.es

Abstract

The introduction of the optical fibers into the access network is, at present, one of the main challenges for the Telecommunications world. Day after day the subscriber is demanding higher technology services (very different from the traditional telephone lines), transporting bigger amounts of information through longer distances and much faster.

The Transport and even the Distribution part of the network are almost 100% covered with optical fiber cables. However, the Access part of the system, the "last mile", still requires a lot investment effort and just a few operators are willing to go for it.

In order to make this FTTH challenge more attractive, we can come up with some ideas combining optical fibers with other services (such as power feeding, copper pairs, coax. etc). Besides all this, the present paper shows one real example of what can be done in this field: one hybrid cable for telecommunications and power transport, to feed the O/E converters of the network, is presented. This cable has been designed and manufactured in Spain and some 400 km of it have already been sold to a Spanish operator, since then.

1. Introduction

The current tendency for the telecommunications business is going to bigger and bigger needs for bandwidth. More and more, the subscriber is demanding services going from the traditional telephone line or the Internet access, to the digital cable TV or video transmission, passing through incoming interactive services, such as PPV, VOD, TV- shopping, TV-bank, and so on. All these services must be provided at a very high speed, including a safe and trustful system easy to upgrade and reliable. Due, among other reasons, to its enormous capacity for information transport (bandwidth), its immunity against interference and its low signal attenuation, the optical fiber seems to be the optimum transmission means to put up with this huge information demand.

The present situation is that the existing systems have a high percentage of fibers. The *Transport network*, connecting the *Head End* (which contains satellite dishes, microwave panels and other devices receiving information form the emitter) with the *Distribution Network* is fully carried through optical fiber. The *Distribution* part of the system, which drives the information from the Transport part, to the subscriber by means of the *Access Network*, is fiber in a high percentage, but not completely. A lot of distribution networks are HFC (hybrid-fiber-coax). However, the existing operators are a little reluctant to design their access networks with optical fibers, since there is a main constrain when they have to get to the receivers: the Opto-Electrical (O/E) conversion.

It is at this point when the need for hybrid cables becomes more important. The installation of mixed cables combining, for instance, copper pairs with some optical fibers (for telephony + future high bandwidth services) allows the operator to put in place the copper pairs he needs at present, together with some optical fibers already installed, for the moment when the technology evolves to the FTTH. This would avoid any extra cable installation, since the fibers will already be there.

On the other hand, the optical networks have really improved since the apparition of the optical amplifiers, *EDFA* (Erbium Doped Fibers Amplifiers), in substitution of the *3R* amplifiers, normally used before, which had, electrically, to "ReShape + ReTime + ReAmplify" the signal. This event allowed the whole connection (the link between the emitter and the receiver) to be purely optical. However, once the signal gets to the receiver, there is still a need for electrical conversion, since the necessary appliances (such as telephone, TV, VCR, computer, etc.) are not optically driven yet. The same problem occurs when, in a HFC network, the operator needs power to feed the O/E converters necessary to pass from the optical fiber to the coaxial cable or even higher power to feed the CATV equipment.

At that point, the need for a solution incorporating to the optical fibers, some copper rods for equipment feeding, is becoming more and more important. This idea would make the operator much more self-sufficient. By integrating the power into the same cable as the information is driven, it will be possible to place the equipment anywhere in the network, with complete autonomy for the operator, to minimize even cost for extra civil works and additional investments in infrastructure.

2. Types of Solutions

Different solutions have been proposed to customers requesting hybrid cables. Among them, we have selected the following, in order to illustrate the applications these cables can achieve.

2.1 Hybrid Drop Cable: Copper Pairs + Fibers

This is a drop cable specially designed to provide both *POTS* (Plain Ordinary Telephony Service) and *Broadband* services. In order to manage that, this fig.-8 cable is made up of an optical and a metallic core (both the same size), kept together by means of a halogen free and flame retardant outer jacket (for indoor applications). Figure 1 shows a picture of this drop hybrid cable.
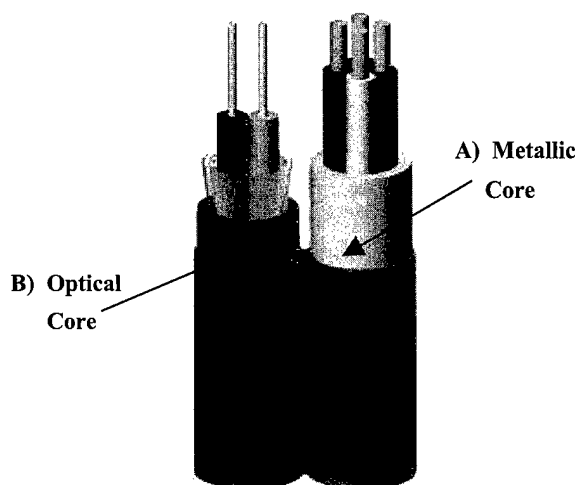
Figure 1. Longitudinal view of a drop hybrid cable

▪ *A) Metallic Core.* This core is made up by four copper wires (or two copper pairs), of 0.51 mm diameter, individually insulated with solid polyethylene (0.22 mm radial thickness). Each two conductors are stranded together making a pair. Around this metallic core, a LSZH flame-retardant jacket is extruded (radial thickness: 0.5 mm), and a ripcord is placed under it to ease the pairs access. The individual outer diameter of the metallic core is 3.15 mm and its weight is around 25 kg/km.

The transmission characteristics requested for a multipair cable are also kept in this design for the *Metallic* core. The main parameters are shown in Table 1

Table 1. Main Transmission Characteristics for the Metallic Core

Parameter	Unit	Value
Ohm Resistance	Ohm/km	≤ 93
Mutual Capacitance	nF/km	52
Attenuation *@ 800 Hz* *@ 3000 Hz* *@ 1 MHz*	dB/km	1.7 2.3 24.0

▪ *B) Optical Core.* The optical part of the cable contains 2 optical fibers inside a loose tube of 1.5 mm OD. A layer of aramid yarns as strength elements are stranded around the tube and a jacket of LSZH flame-retardant material is extruded over it (radial thickness: 0.5 mm). The individual outer diameter of the optical core is 3.15 mm and its weight is around 20 kg/km.

The transmission characteristics for the *Optical* core are those of the fibers included in it. In this case, they are standard single mode fibers (type G.652), even if they could also be other kind, such as multimode (type G.651).

The two cores (copper conductors and fibers), covered by a jacket of LSZH flame-retardant material making a Fig.8 structure, compose the complete Hybrid cable. The radial thickness of this shared outer jacket is 0.5 mm. The final diameter of each sub-cable is 4.15 mm and a nexus of 1-mm length links them together. The final length of the complete hybrid cable is around 9.3 mm and its nominal weight is 45 kg/km. The mechanical and thermal characteristics of the complete cable are:

- Max. Pulling Load: 800 N

- Max. Bending Radius: 80 mm

- Operating Temperature Range: -20; +60 °C

The environmental characteristics, against fire, for this drop Plenum cable are according to IEC, as shown in Table 2

Table 2. Main Characteristics against fire

Property	Test method	Acceptance Criteria
Flame Retardancy	IEC-332-1	s/ IEC-332-1
Halogen Free	IEC-754-1 IEC-754-2	Halogen released < 1% Acidity → pH ≥ 4.2
Low smoke	IEC-1034-1	Transmittance → τ > 50%

This hybrid cable is specially designed for operators providing, at present, telephony services and planning to offer high bandwidth services in the next future.

2.2 Tri-Ways Cable: Coax. + Copper Pairs + Fibers

This is a complete access cable specially designed to provide CATV, *POTS*, and *Broadband* services. In this case, the cable is an uneven fig.-8 design made up of a coax core and a hybrid pairs + fibers core, kept together by means of a halogen free and flame retardant outer jacket (for indoor applications). Figure 2 shows a cross sectional picture of this Tri-Ways cable (Siamese cable including fibers).
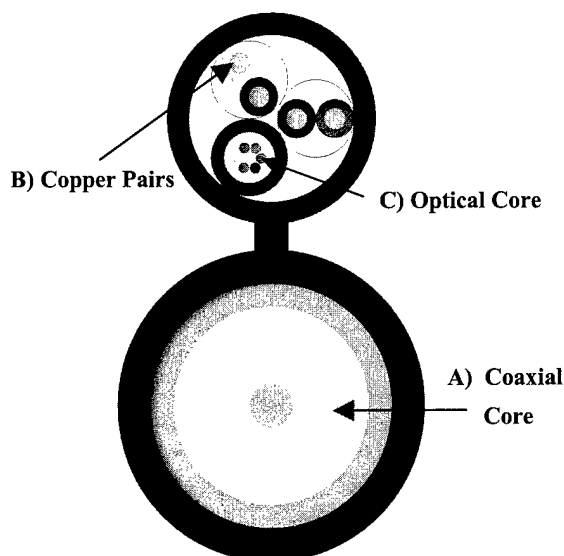
Figure 2. X-sectional view of a Tri-ways hybrid cable

A) Coax. Core: It is an RG-6 Coax. cable including the following elements:

- *Central conductor:* copper clad steel, 1.02 mm OD.

- *Insulation:* foam HDPE, 4.57 mm OD

- *Outer conductor:* it is made of three layers of different materials:

  -. First outer conductor: laminated tape Al + plastic + Al with around 0.12 mm radial thickness

  -. Second outer conductor: aluminum alloy mesh. Radial thickness around 0.6 mm

  -. Third outer conductor: laminated tape Al + plastic + Al with around 0.12 mm radial thickness

The coax core has a final diameter (without jacket) of around 6,2 mm. The electrical and transmission characteristics requested for an RG-6 coax cable must be kept in this design. The main parameters are shown in Table 3

Table 3. Main Transmission Characteristics for the Coaxial Core

Parameter	Unit	Value
Characteristic Impedance	Ohm	75
Mutual Capacitance	nF/km	53
Return Loss (5-1000 MHz)	dB	> 20
Attenuation(max.) @ 5 MHz @ 100 MHz @ 1000 MHz	dB/100 m	1.87 7.20 19.99

In what the mechanical and thermal characteristics of the coax core are concerned, the main are:

- Pulling Load (min.): 450 N

- Bending Radius (max.): 50 mm

▪ **B) Copper Pairs.** The telephony part consists in two copper pairs. The conductors are of 0.51 mm diameter, individually insulated with solid polyethylene (0.22 mm radial thickness). Each two conductors are twisted in a pair and then stranded together with the optical core.

The value of the main transmission characteristics for the copper pairs in this design are shown in Table 4

Table 4. Main Transmission Characteristics for the Copper pairs in the Tri-ways cable

Parameter	Unit	Value
Ohm Resistance	Ohms/km	≤ 93
Mutual Capacitance	nF/km	45
Attenuation(max.) @ 1 kHz @ 100 kHz @ 1000 kHz	dB/km	1.7 9.0 24.0
Impedance @ 1000 kHz	Ohm	100

▪ **C) Optical Core.** The optical part of the cable contains up to 8 optical fibers inside a loose tube of 1.8 mm OD. This tube is then stranded together with the two copper pairs to make the second part of the cable. The final diameter of this stranded core (without jacket) is around 3.4 mm.

The transmission characteristics for the *Optical* core are those of the fibers included in it. In this case, they are standard single mode fibers (type G.652), even if they could also be of other kind, such as multimode (type G.651).

The complete Tri-Ways Hybrid cable is composed by the two uneven cores (coax and copper conductors + fibers), covered by jacket of LSZH flame-retardant material, making a Fig.8 structure. The radial thickness of this jacket is 0.78 mm over the coax core and 0.51 mm over the hybrid (pairs + fibers) core.
The final diameters are:

-. Coax core: 7.2 mm OD

-. Hybrid (Fibers + Pairs) core: 4.4 mm OD

A nexus of 0.6 mm length and 0.4 mm width of the same LSZH material, links both cores together. The final length of the complete Tri-Ways hybrid cable is around 12.8 mm. Its main characteristics against fire are the same as shown in Table 2.

2.3 Optical Fibers + Power Feeding

These cable solutions are specially designed to provide broadband services, together with equipment feeding (for O/E converters, for CATV equipment feeding etc.). Therefore, these designs can be used for any FTTx application, needing power for equipment feeding. We have selected two examples, which have been very welcome among new operators:

2.3.1 FTTB + Feeding. This cable design presents a solution including, together with the fibers, a couple of small copper wires to self-feed the O/E converters in the access network. This design was specially conceived for operators carrying the optical signal through the fibers up to the subscriber's building (FTTB). At that point, the signal has to be converted to electrical, to get to the subscriber by means of copper pairs and/or coax cables. In order to be able to place these O/E converters anywhere around the building, the idea of carrying its feeding within the same cable becomes very attractive. Figure 3 shows a picture of this FTTB + feeding cable, for which the characteristics are mentioned hereafter.
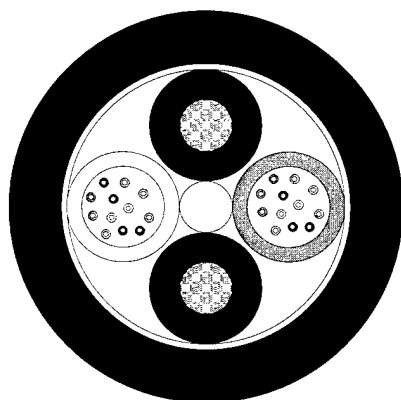
Figure 3- cross-sectional view of a hybrid FTTB + Feeding cable

A) Copper conductors: depending on the tension that has to pass through, the copper conductors can be 1.5 or 2.5 mm² section. The dimensions in every case are as follows:

- *Copper Diameter (flexible copper)*

  -. 1.4 mm OD for the 1.5 mm² section wire

  -. 1.8 mm OD for the 2.5 mm² section wire

- *Copper Insulation (PVC)*

  -. 1.4 mm radial thickness for both cases

- *Wire final diameter (Insulated Copper)*

  -. 3.0 mm OD for the 1.5 mm² section wire

  -. 3.4 mm OD for the 2.5 mm² section wire

B) Fiber Tubes: the two loose tubes, depending again on the copper conductors, will have the following dimensions:

- *Loose tube diameter*

  -. 3.0 mm OD for the cable with 1.5 mm² section wires

  -. 3.4 mm OD for the cable with 2.5 mm² section wires

  In any case, these loose tubes may contain from 2 to 24 optical fibers.

Finally, the four elements are stranded together around a dielectric central strength member (FRP) and an outer jacket of HDPE of 1.4 mm radial thickness is extruded on top of the core. The final dimensions are:

- *Cable Outer diameter*

  -. 10.5 mm OD for the cable with 1.5 mm² section wires

  -. 11.5 mm OD for the cable with 2.5 mm² section wires

The main characteristics for this FTTB + Feeding hybrid cable are shown in Table 5

Table 5. Main Characteristics for the FTTB + Feeding cable

Parameter	Unit	Value	
		1.5 mm²	2.5 mm²
Cable Outer Diameter	mm	10.5	11.5
Cable Weight	Kg/km	75	100
Max. Pulling Load	N	1,000	1,000
Min. Bending Radius	mm	160	170
Ohm Resistance (copper conductors)	Ohm/km	12.1	7.4

The optical characteristics of the cable are those of the optical fibers included in it. In this case, they are standard single mode fibers (type G-652) but they could also be multimode fibers (type G-651) or any other standard type.

Therefore, this FTTB + feeding hybrid cable includes up to 48 optical fibers, together with two copper conductors of 1.5 or 2.5 mm² section for O/E converters feeding (low voltage applications and short distances). In case of needing higher voltage (higher intensity) or going further, another design can be presented:

2.3.2 FTTC + Power. This cable design introduces a solution including, together with the fibers, a couple of bigger copper wires. This is useful in case the operator needs to self-feed equipment through longer distances (i.e. for FTTC) or other devices requesting higher voltage. The proposed solution allows the operator to place the equipment anywhere in the loop, without having to look for a place to plug it in.

Figure 4 shows a picture of this FTTC + power cable, for which the characteristics are mentioned below.
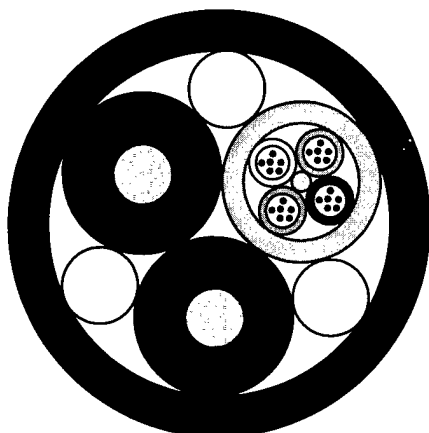
Figure 4. X-sectional view of a hybrid FTTC + Power cable

Depending on the currency that has to pass through the wires and, above all, the distance it has to cover, the copper conductors can be either 10 or 16 mm² nominal section. As usually, we can divide the cable in several parts:

A) Copper conductors: The main dimensions are as follows:

- *Copper Diameter (flexible copper)*

    -.4.1 mm OD for the 10 mm² nom. section wire

    -. 5.1 mm OD for the 16 mm² nom. section wire

- *Copper Insulation (PVC)*

    -. 1.0 mm radial thickness for both cases

- *Wire final diameter (Insulated Copper)*

    -. 6.1 mm OD for the 10 mm² nom. section wire

    -. 7.1 mm OD for the 2.5 mm² nom. section wire

B) Fiber Core: the optical part of the cable consists of 4 loose tubes stranded around a CSM. With the specified dimensions, the cable may contain up to 24 fibers (6 fibers per tube), even if in the present example, the customer requested just 12 fibers so the core was designed with 3 tubes containing four fibers each plus one dummy tube as filler. The dimensions (regardless the section of the copper wires) are as follows:

- *Loose tube diameter:* 2.1 mm OD

- *Filler rod diameter:* 2.1 mm OD

    These four elements are stranded together around a dielectric central strength member (FRP) of 0.9 mm OD, and an outer jacket of PE is extruded on top of the core.

- *Jacket radial thickness (for the optical part)*

    -. 0.5 mm for the 10 mm² nom. section wire

    -. 1.0 mm for the 16 mm² nom. section wire

Then, the three active elements (metallic and optical) are stranded together with three PE dummy rods to fill the core interstices.

- *Outer dummy rods diameter:*

    -. 3.0 mm for the 10 mm² nom. section wire

    -. 3.5 mm for the 16 mm² nom. section wire

Finally, the core is wrapped with a polyester tape and an outer polyethylene jacket of 1.6 mm radial thickness is extruded on top of everything.

The final dimensions for the cable are:

- *Cable Outer diameter*

    -. 17.0 mm OD for the cable with 10 mm² nom. section wires

    -. 19.0 mm OD for the cable with 16 mm² nom. section wires

The main characteristics for this FTTB + Feeding hybrid cable are shown in Table 6

Table 6. Main Characteristics for the FTTC + Power cable

Parameter	Unit	Value	
		10 mm²	16 mm²
Cable Outer Diameter	mm	17.0	19.0
Cable Weight	Kg/km	340	480
Max. Pulling Load	N	2,000	2,000
Max. Compression resist.	N	1,000	1,000
Min. Bending Radius	mm	255	300
Temperature cycling	°C	-20; +70	-20; +70
Ohm Resistance (copper conductors)	Ohm/km	1.9	1.2

The optical characteristics of the cable are those of the optical fibers included. In this case, they are standard single mode fibers (type G-652) but they could also be multimode fibers (type G-651) or any other standard type.

These two cables were manufactured according to the customer requests. The main mechanical and thermal results obtained after testing the 10 mm² wires cable design (which is the most commonly used since them) are shown hereafter:

TENSILE TEST
(IEC 60794-1-E1 / EN 187.000 Method 501)

Cable Length under Test	95 m
Fiber Length under Test	190 m
Initial Load	0 daN
Final Load	200 daN
RESULT	0.03 % max. cable elong. No attenuation change

TENSILE TEST RESULT: **PASS**

CRUSH TEST
(IEC 60794-1-E3 / EN 187.000 Method 504)

Fiber Length under Test	190 m
Dimensions of Plates	100 x 100 mm
Initial Load	0 daN
Final Load	100 daN
RESULT	No cable deformation No attenuation change

CRUSH TEST RESULT: **PASS**

IMPACT TEST
(IEC 60794-1-E4 / EN 187.000 Method 505)

Fiber Length under Test	190 m
Weight Radius	12 mm
Energy	5 J
Number of Impacts	10
RESULT	No cable deformation No attenuation change

IMPACT TEST RESULT: **PASS**

THERMAL CYCLING TEST
(IEC 60794-1-F1 / EN 187.000 Method 601)

Cable Length under Test	1,300 m
Temperature Cycling	-20 ; +70 ºC
Cycle	24 hours / 1 cycle

THERMAL CYCLING RESULT: **PASS** (*see graph)

TEMPERATURE CYCLING (1550 nm)
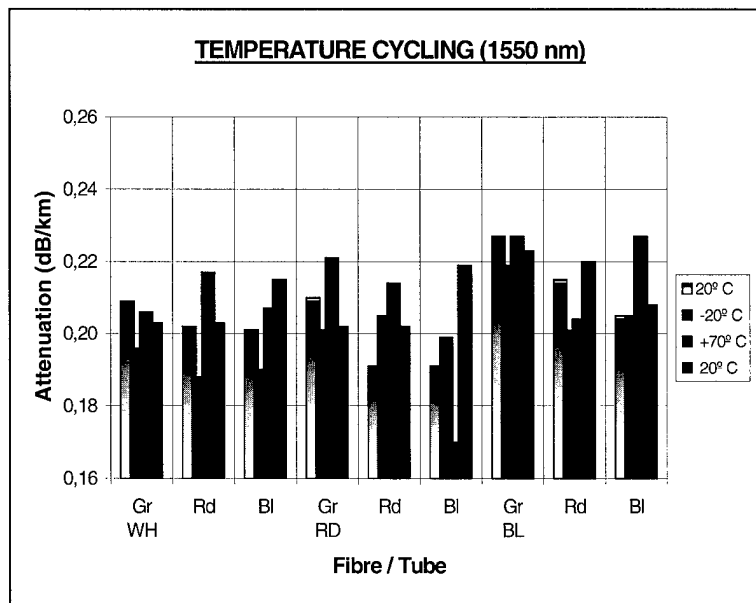
TORSION TEST
(IEC 60794-1-E7 / EN 187.000 Method 508)

Fiber Length under Test	190 m
Cable Length under Test	2 m
Load	10 daN
Angle of Turn	360 º
Number of Cycles	10
RESULT	No cable deformation No attenuation change

TORSION TEST RESULT: **PASS**

REPEATED BENDING TEST
(IEC 60794-1-E6 / EN 187.000 Method 507)

Fiber Length under Test	190 m
Load	10 daN
Pulleys Diameter	300 mm
Number of Cycles	10
RESULT	No cable deformation No attenuation change

REPEATED BENDING TEST RESULT: **PASS**

The FTTC + power hybrid cable, as extracted from the test report shown before, has been manufactured and characterized with good results. In fact, around 400 kilometers of this cable (see Picture 5) have already been installed in Spain.
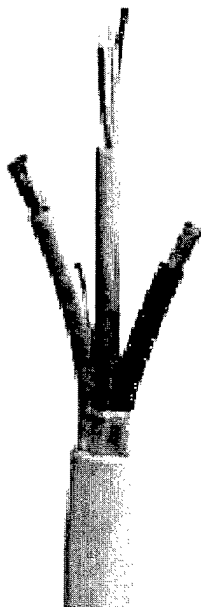
Figure 5. Real Picture of a hybrid FTTC + Power cable

3. Overseen a Real Installation

Taking as an example one of the designs which have more interest for the operator, the FTTC + Power hybrid cable, several pictures are shown hereafter, explaining the installation and applications of this design.

Figure 6

Figure 6 shows a view of the street (FTTC), in where the hybrid cable gets to the left module and takes the feeding from the Power Supply Module (right one in the picture).

Figure 7

Figure 7 shows an internal view of this left module of the street ("splitting-rack"), in where the hybrid cable is divided into its optical and power parts, in order to get the power supply from the module in the right side. This splitting operation is performed in the little box placed at the bottom of the rack in Figure 7.
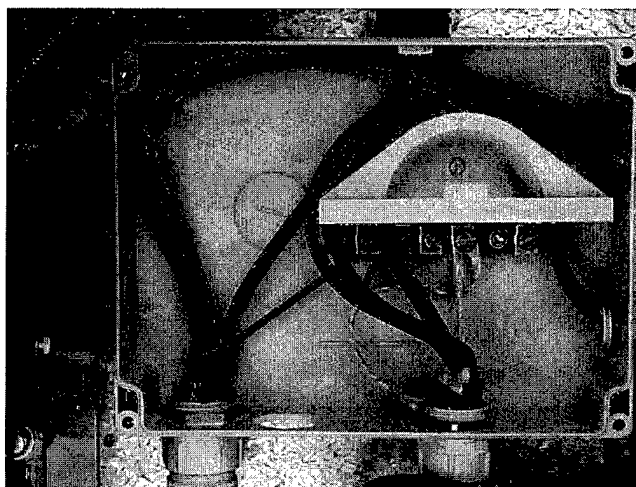
Figure 8

Figure 8 shows a zoom view of this above-mentioned little split-box, for the hybrid cable. As can be seen, the power parts of the two cables getting to the box, go together through a couple of holes in the right side and the optical cores are redirected through a Grey duct, going up to the fiber splicing boxes.

Then, the hybrid cable, carrying both the optical fiber signal and the power supply, gets to the NOE (E/O Module). These converters can be up to 1 km away from the power supply and that's the reason why the power conductors are as big as 10 mm^2 section.
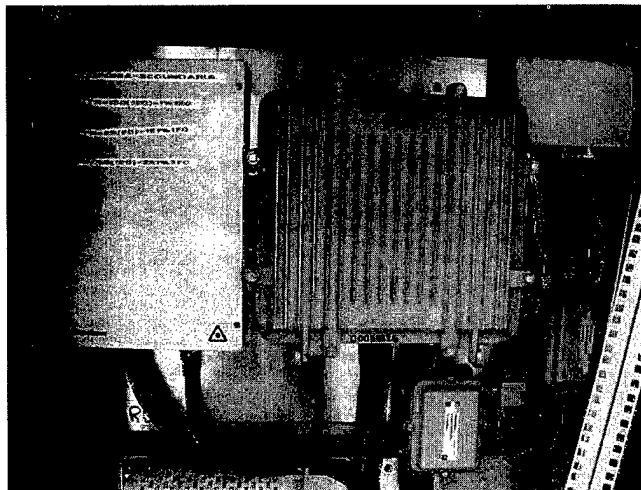
Figure 9

Inside this NOE (see Figure 9), the optical signal is transformed to electrical, thanks to the power conductors and the information that was travelling by the optical fiber so far, is now taken to the subscriber through coax (CATV) and pairs (telephony) cables.

4. Conclusions

This paper has presented several solutions to help the operators to take more advantage of the networks they are deploying. These ideas can be divided in two main groups:

-. Solutions offering basic telephony services for today and broadband applications for the next future (tomorrow). In this case, copper pairs + fiber hybrid cables have been shown, allowing the operator to offer other types of services (high speed Internet, digital cable TV, PPV, TV- shopping, etc.) whenever the subscriber requests it and without having to re-open the ducts or re-installing the cable.

-. Hybrid cables containing fiber and power copper rods, very suitable for operators needing to self-feed their O/E or CATV equipment at the same time they install the optical fiber. This type of hybrid cables provide a compact solution to be able to connect the equipment to the current, anywhere in the access network

One real example of a hybrid Fiber + Power cable installation, in which the converters are placed up to 1 km away from the power supply, has also been presented. Around 400 kms of this cable design have already been installed in Spain

5. Acknowledgments

Authors

Marta Garcia
Alcatel Cable Ibérica
39600 Maliaño- Cantabria
Spain
marta.garcia@aci.alcatel.es

Marta Garcia received her Physics degree with a specialty in Microelectronics in 1992, from the University of Cantabria (Spain). In 1994, she joined Alcatel Cable Iberica, working as a Product Engineer. During 1997 and 1998 she worked in the Alcatel's Optical Fiber Cable Competence Center (OFCCC) in Claremont, NC, working as a project leader for the Design Technology Group. Since then, after going back to Spain, she leads the Product Engineering Group of Alcatel Cable Ibérica.

Carlos G. Cortines
Alcatel Cable Ibérica
39600 Maliaño- Cantabria
Spain
c.cortines@aci.alcatel.es

Carlos G. Cortines is a Physical Engineer. All his professional life, he has been involved in the cable industry, formerly ITT Goup nowadays Alcatel. At present, he is the Technical Manager of Alcatel Cable Iberica, the telecom cable factory located in Spain

Francisco J. Sáez
Alcatel Cable Ibérica
39600 Maliaño- Cantabria
Spain
fj.saez@aci.alcatel.es

Francisco Jose Saez de la Maza was born in 1947. He graduated as a B.S. in 1967 at the Santander Technical University. He jointed ITT Standard Electrica in 1971 and worked at the Materials Development Laboratory. In 1981 he passed to the Optical Fiber Development Group of Alcatel Cable Ibérica, where he is presently the responsible for Optical Fiber Laboratory.

A Dense Multi-Ribbon Cable For Installation in a Harsh Environment at CERN

Bertil Arvidsson[1], Anders Björk[1], Mark Pearce[2], Jan Troska[3], Francois Vasey[4], Alessandro Zanet[5]

[1]Ericsson Cables, Hudiksvall, Sweden, +46-650-36258, bertil.arvidsson@eca.ericsson.se, [2]Royal Institute of Technology, Stockholm, Sweden, [3]Rutherford Appleton Laboratory, Chilton, U.K., [4]CERN, Geneve, Switzerland [5]University of Padova, Padova, Italy

Abstract

The ribbon concept is proposed for a completely new application: an installation in a harsh environment at the European Laboratory for Particle Physics, CERN, in Switzerland. Two major experiments will be installed at the CERN Large Hadron Collider (LHC) called ATLAS and CMS. The experiments are planned to become operational by 2005. Optical links will be required to exchange data between the detector front ends and the control rooms. The ATLAS experiment will use approximately 25000 digital optical links based on 50μm-fiber and 850nm VCSEL emitters while the CMS experiment will operate about 150000 optical links.

A novel ribbon cable with 12-fiber ribbons has been designed and tested. The present study reports on the mechanical properties, radiation tolerance for the entire cable and the individual ribbons.

We also present the inline-technique for processing a 12-fiber ribbon, i.e. coloring and ribbonizing in one step.

1. Introduction

1.1 Particle Physics Experiments and Nuclear Radiation Effects

The European Organisation for Nuclear Research, CERN, is an Intergovernmental Organisation with 19 European member states.

CERN has its seat in the Canton of Geneva (Switzerland) but its laboratories are located on both sides of the Swiss-French border.

CERN is running a number of particle accelerators the largest being the Large Electron Positron Collider (LEP).

The Large Hadron Collider (LHC) project, a large proton-proton collider and superconducting accelerator of 27km in circumference, was approved in 1994. The LHC will be the next major research tool for world particle physics and it is expected to be commissioned in 2005.

Experiments to exploit the new physics expected from high energy proton-proton collisions produced by the Large Hadron Collider (LHC) are currently being prepared.
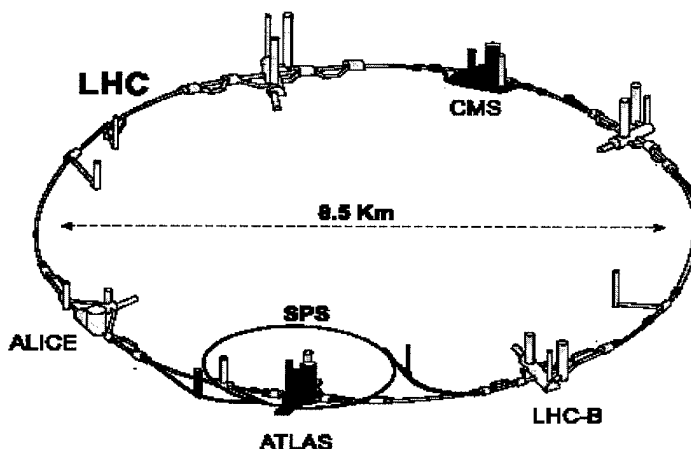
Figure 1. Sketch of the underground part of the Large Hadron Collider at CERN, and its four experiments: Alice, Atlas, LHC-B and CMS.

The main two experiments, ATLAS and CMS, (Fig. 1), will use a large number of optical links to transfer data off the experiments to remote data acquisition electronics, both projects being lead by independent development teams. For example, the ATLAS experiment will use approximately 25,000 digital optical links based on 50/125 multimode fibers and VCSEL emitters operating at 850nm [1].

The inner tracker of the CMS experiment alone has 50,000 analogue optical links using single-mode and edge emitting lasers operating at 1300nm [2-5]. To aid installation the fiber ribbon concept is being studied by both these experiments.

A non-standard feature for the data-links is the radiation environment in which they must operate. The integrated ionizing dose is expected to reach a few 100kGy in the central regions of the experiments after 10 years of running [2].

The CMS experiment has identified a standard un-shifted single-mode fiber, which incurs a loss of 0.04 to 0.06dB/m at such levels of radiation. The ATLAS experiment is studying a fluorine doped 50/60/125 step-index fiber and subsystems further from the central region are hoping to use standard phosphorous-free multimode fiber.

1.2 Ribbon Cable

Since both experiments will use fiber optic cables with similar environment and installation requirements, a new cable has been proposed for indoor use with an 80mm minimum bending radius and an outer diameter of 9mm with HFFR sheath material. Mechanical and environmental tests according to IEC-standards have been performed, as well as additional specific mechanical and radiation tests. The developed cable meets the required specifications, even after exposure to aggressive levels of nuclear and ionising radiation.

2. A Novel Ribbon Cable

A novel ribbon cable with eight 12-fiber ribbons has been designed and tested. The 12-fiber ribbon is of the encapsulated type with a thin outer layer, the ribbon matrix (Fig. 2).
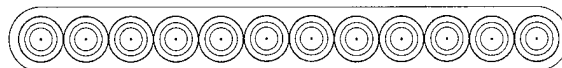
Figure 2. A 12-fiber ribbon

The same ribbon geometry is used for the CMS(single-mode) and ATLAS(multimode) detectors.

The ribbon has been processed with the inline-technique, i.e. coloring and ribbonizing in one step (Fig. 3). The ribbon process is mature and [6] with a professional maintenance program the risk is minimized to obtain a problem in the ribbonizing. It is, however, a complex unit. It is built from different modules (coloring and ribbonizing). It is also possible to extend this further to make ribbons with higher fiber counts or more than one ribbon at the same time.

The cable (Fig. 4) is for indoor use with, as already mentioned, an 80 mm minimum bending radius and an outer diameter of 9 mm with HFFR sheath material.
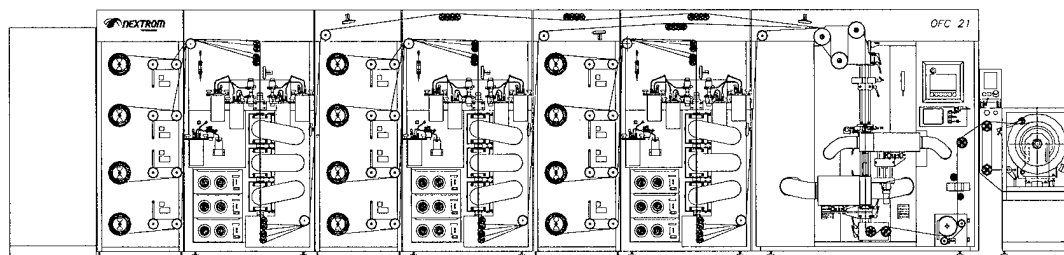
Figure 3. A 12 fiber in-line ribbon machine
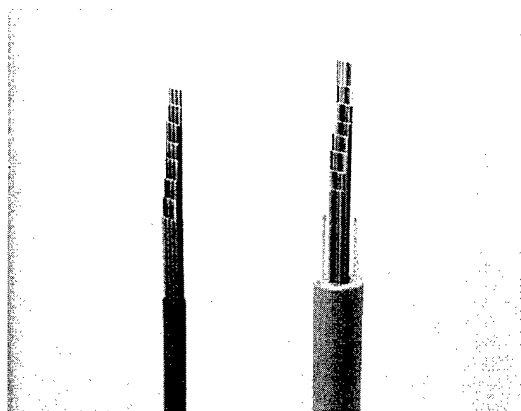
Figure 4. Both the ribbon bundle and the novel ribbon cable are shown above

In addition a simple ribbon bundle with eight 12-fiber ribbons has also been designed for short distances, maximum eight meters.

In Table 1 we give the single-mode ribbon cable characteristics.

Table 1. Cable Characteristics

Fiber Specifications		
Mode field diameter	μm	9.2 ± 0.4
Cladding diameter	μm	125 ± 1
Cladding non-circularity	%	≤ 1
Mode field concentricity error	μm	≤ 0.5
Coating diameter	μm	245 ± 5
Transmission Specifications (λ = 1310nm)		
Attenuation average in the cable	dB/km	≤ 0.37
Attenuation maximum, single fiber	dB/km	≤ 0.40
Zero-dispersion wavelength (dispersion un-shifted)	nm	1300 - 1324
Cut-off wavelength, cable, λ_{cc}	nm	1260
Cable Specifications and Construction		
Sheath diameter	mm	9.5
Bending radius, permanently and during installation (minimum)	mm	80
Tensile force permanent (maximum)	N	80
Pulling force during installation (maximum)	N	800
Crush resistance (maximum)	N	500
Cable net weight	kg/km	75

3. Cable Tests

3.1 Factory Tests

The present study reports on the mechanical properties, radiation tolerance and installation issues for the entire cable and the individual ribbons.

The cable has been tested according to the international standards IEC 60794-1 and EN 187 000.

The main factory test results are presented below.

3.1.1 Transmission performance

The attenuation in all fibers in both test cables was measured in the single fibre and in the completed cable.

The manufacturing process did not significantly change the fiber characteristics.

Fig. 5 shows typical results from the temperature test over the range –40 to +70 °C on the MM-cable.

The cable shows a satisfying behaviour down to –20°C, which is adequate to the functional needs in the detectors. The horizontal axis shows the temperature cycling order.
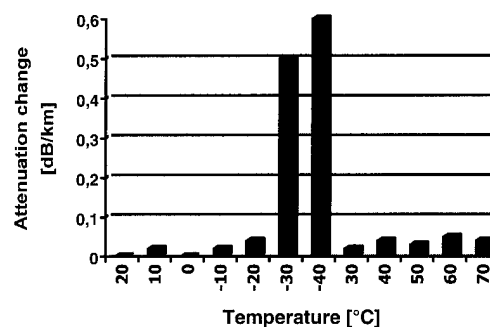
Figure 5. Temperature performance at the wavelength 850nm of the MM-cable to the Atlas project

3.1.2 Tensile performance

The cables were tested up to a tensile load of 2 kN. At this load no significant change in attenuation at neither of the measured wavelengths was noted, see Fig. 6, which shows the test result on the SM-cable.

The fiber strain reaches half of the proof test level at the load 1.1 kN. This is a strain that is commonly used as maximum allowed fiber strain in a cable or during manufacturing of a cable to guarantee the lifetime of the cable. Furthermore, no residual cable elongation was measured after the test.
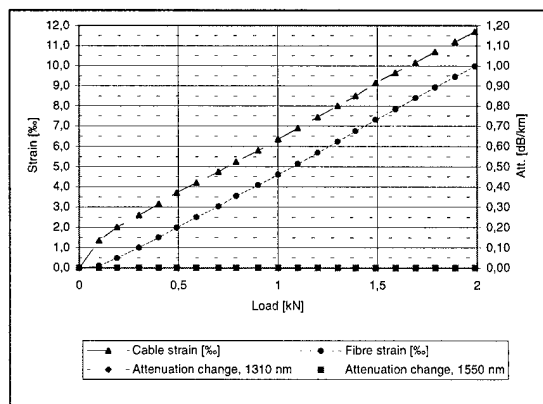
Figure 6. Tensile performance of the SM-cable to the CMS project. Since no attenuation increase can be seen at neither 1310 nor 1550nm, the values for both wavelengths follow the x-axis.

3.1.3 Crush performance

No significant change in attenuation can be seen in the crush test, using a plate with a diameter of 100 mm, when the cable is exposed to compressive loads up to 2 kN. The result from the crush test of the MM-cable is shown in Fig. 7 both 850 and 1300nm.
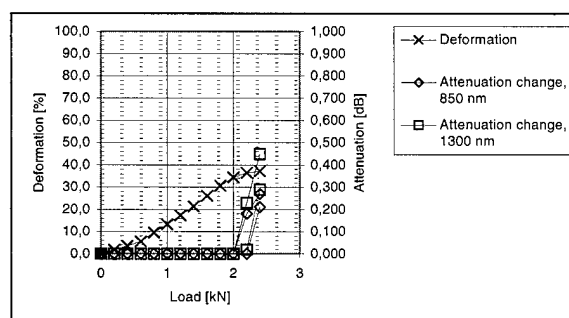
Figure 7. The result from the crush test on the MM-cable for the Atlas project

3.1.4 Flammability test

The test was carried out in accordance with IEC 332-3 category C.

Cable pieces were lashed to a ladder. The ladder was positioned vertically in a test chamber, see Fig. 8.

A flame was applied for 20 minutes. After the test the charred portion was 1.15 meters which means that the cable passed the test and is approved according to the standard.

The standard requires a charred portion less than or equal to 2.5 meters.

3.2 Tests at CERN and other facilities

As mentioned earlier there are two different projects at Cern interested in the 12-fiber ribbon concept. We will treat them here separately. The ATLAS tests will be presented first followed by the CMS-results.

3.2.1 ATLAS cable tests

Two types of experiment were performed:

1. Single and Multiple 360° turn put into cable in bending plane at various radii.

2. Routing of cable under simulated installation conditions within the ATLAS detector

During both types of test the light transmission of the fibers was monitored to assess excess loss caused by the bending of the cable.

Light was injected into the fiber from 840nm VCSEL sources and was monitored using low noise photodiode receivers.

The stability of the injected light was also monitored. The measurement set-up is shown in Fig. 9. An example of a multi-turn test is shown in Fig. 10. Routing along a simulated installed path containing the same number and type of bends as projected for the cable installed in the ATLAS detector is shown in Fig. 11. In addition to being routed inside ATLAS, it is foreseen that some services will require routing in cable chains to allow the end-caps to be withdrawn during assembly and maintenance. For this reason a test of this movement was also carried out as shown in Fig. 12. Qualitative assessment of the handleability of the cable was made during the loss tests.
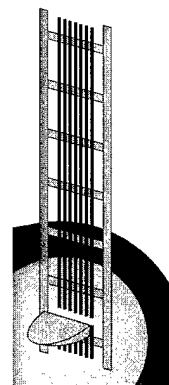
Figure 8. Flammability Test
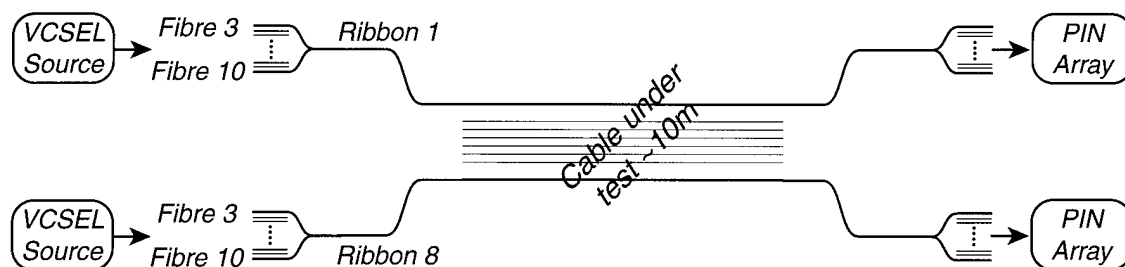
Figure 9. Test set-up
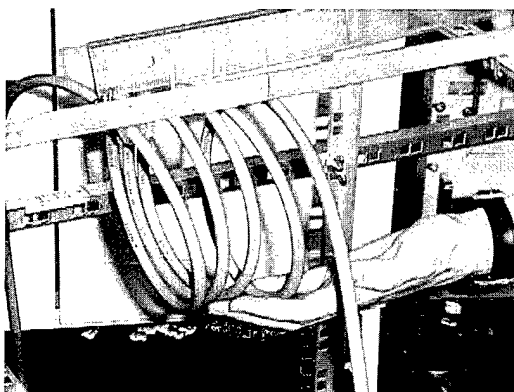
Figure 10. Example of cable bend testing
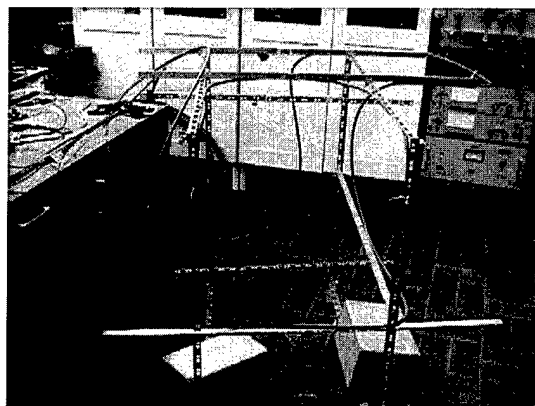
Figure 11. Cable being tested under simulated installed conditions

3.2.1.1 Single and Multiple turns

Complete 360° turns are not realistic in terms of the final installation, but rather provide a worst case for the cable. The results can be summarised for single turns as follows:

◊   No effect on loss if Bend Radius >100 mm

◊   100 mm > Bend Radius > 80 mm: 0.2-0.4 dB loss

◊   Bend Radius < 80mm: 0.5-1.6 dB loss
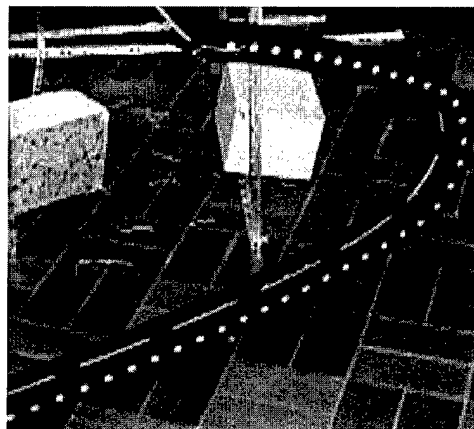
Figure 12. Cable routed in cable chain

Multiple turns caused increased losses:

◊   2-5 turns at Bend Radius = 80mm: up to 4dB loss observed

◊   Over long term (12 hrs), bend radius 85 mm, steady loss @ 1.8dB

No loss was observed for turns <180°, the condition which will be encountered by cables installed within ATLAS.

3.2.1.2 Simulated routing

Mechanical drawings of the proposed cable routing within ATLAS were used to give both the number and nature of the bends foreseen in the current detector layout. This information was used to route the cable around a frame with successive bends in orthogonal planes, spaced more aggressively than the proposed ATLAS cable routing. This route had no bends >90°, and no losses were measured in the fibres. This is in agreement with the bend test results described in the section above. Futhermore, in the cable no losses were observed when the cable was mounted in the cable chain and the cable chain was allowed its full range of movement. Handling the cable for the purposes of these tests did not reveal any special precautions that need to be taken apart from making certain that the ribbon stack exited the cable in the correct orientation. This can be addressed by the proper termination of all ribbons at the cable exit, which will be carried out more carefully in the

final system. No precautions were taken in this regard for these tests.

3.2.2 CMS cable tests

With this set of measurements, we wanted to better understand how the 96-fiber optical cable works under extreme bending conditions. The test set-up is similar to the ATLAS experiment, but we now work with single-mode fibers at 1310 nm. Moreover, the ribbons are spliced together at both ends of the cable under test so that light meanders through all ribbons before being measured.

Two types of experiments were performed. In a first step, the cable attenuation was measured under torsion, and bend conditions. No significant change of attenuation was observed when twisting the cable by as much as 4 turns/m, or winding it (1 turn, 8cm radius). In a second step, the cable was fixed and coiled around a 25cm size wooden cube to simulate successive bends in orthogonal planes. In the test illustrated in Fig. 13, 90° turns (with 8 cm bend radius) were imposed on the cable at neighbouring corners of the cube but on different faces, separated by 9 cm long straight sections where the cable was allowed to twist. The cable attenuation was measured after each quarter of a turn. No significant attenuation increase could be observed even after as many as 25, 90° turns in orthogonal planes.

The SM cable behaviour was thus found to be excellent at 1310nm.

3.2.3 Radiation tests

For the tests reported here the multimode fiber, 50 μm, originates from Plasma Optical Fibres and the un-shifted single-mode fiber from Corning.

It is well established that optical fiber production conditions [7], including the level of phosphorus doping, can strongly affect the radiation tolerance of a given fiber. Pure silica core fibers are generally found to be more radiation tolerant than doped silica examples. The level of optical absorption measured in an optical fiber exposed to radiation depends not only on the total ionising dose (or neutron fluence) but also on the dose rate (or neutron flux). The fiber types used in these tests are not pure silica core, but phosphorus free. The main reason for not using pure silica core in the single-mode case is that transmission is at 1310 nm and the only available pure silica core fiber operates at 1550 nm. Another reason is that the now qualified fiber is the most common one and therefore easy to supply for the CMS-experiment. In the multimode case some links operate at 1.6 Gb/s and therefore require graded-index fiber. For the inner detector links a pure silica core step-index fiber has been chosen. This fiber has not been part of the experiments reported here.

The evaluated multimode fiber exhibits an induced attenuation of ~0.1 dB/m at 800 Gy(Si) and 2×10^{13} n(1 MeV Si)/cm^2 [7]. In the single mode case, induced losses of 0.04 to 0.06 dB/m were measured at 100 kGy(Si) (720 Gy/hr dose rate) [2].
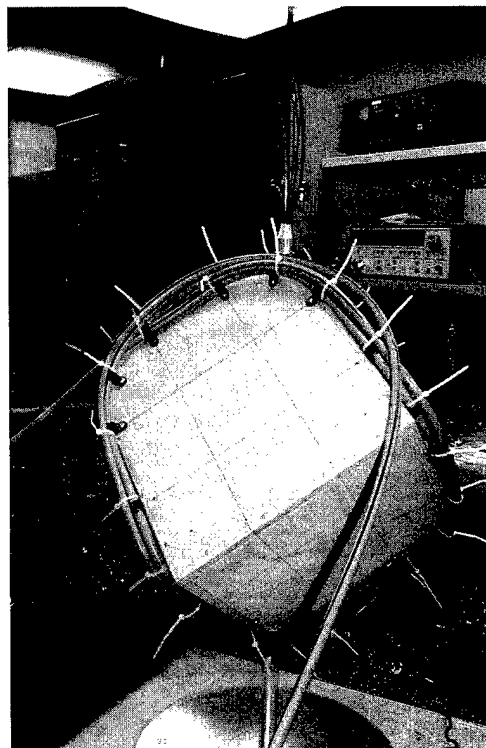
Figure. 13 "Worst case test" with 25 cm cube

The mechanical properties of the cable did not change after neutron and gamma irradiation.

The irradiation facilities have been various institutes and universities in Europe and USA.

4. Conclusion

We have discussed a novel ribbon concept for an application at CERN.

The most important environmental and mechanical properties of the cable:

- Cable diameter, 9.5 mm
- Minimum bending radius, 80mm (90° bend)
- Tensile strength, 1kN
- Fire resistance, according to IEC 332-3 cat 3.
- Radiation resistance

When exposed to standard cable tests and some worst case situations the cable responds well. The design is also very suitable for the extreme installation conditions that will be applicable at CERN.

5. Acknowledgements

6. References

[1] M. Pearce et al., "Surface Emitters Pass Initial Radiation Tests", Opto Laser Europe, Issue 49, 1998.

[2] J. Troska, J. Batten, K. Gill, F. Vasey, "Radiation effects in commercial off-the-shelf single-mode optical fibres," SPIE proceedings Vol. 3440, pp 112-119, 1998.

[3] G. Hall, "Analogue optical data transfer for the CMS tracker", Nuclear Instruments and Methods in Physics Research A, Vol. 386, pp. 138-42, 1997.

[4] F. Vasey, V. Arbet-Engels, J. Batten, G. Cervelli, K. Gill, R. Grabit, C. Mommaert, G. Stefanini, J. Troska, "Development of radiation-hard optical links for the CMS tracker at CERN", IEEE Transactions on Nuclear Science, Vol 45, No 3, 1998, pp 331-337.

[5] F. Vasey, C. Azevedo, G. Cervelli, K. Gill, R. Grabit, F. Jensen, P. Moreira, "Optical links for the CMS-Tracker", Proceedings of the fifth workshop on electronics for LHC experiments, Snowmass, Colorado, September 20-24, 1999, pp 175-9.

[6] B. Arvidsson and J. Tanskanen, "Analysis of the Economics of On-line Colored Ribbon Manufacturing," IWCS 96, Reno, Nevada, USA

[7] G. Mahout et al., "Irradiation studies of multimode optical fibres for use in ATLAS front-end links," Nuclear Instruments and Methods in Physics Research A 446 (2000) pp 426-434.

AUTHORS

Carl Bertil Arvidsson,
Ericsson Cables AB, Technology Division,
S-824 82 Hudiksvall, Sweden

Carl Bertil Arvidsson, manager of fiber optics at Ericsson Cables AB, Technology Division, has been involved in optical fibers for many years. He is active in IEC and CENELEC with the standardization of optical fibers and cables. Prior to joining Ericsson in 1990, he worked as a technical project manager in Sweden, the United States and Switzerland. Before that he was a university lecturer in theoretical physics. He has a doctor degree in Theoretical Physics from Uppsala, Sweden.

Anders Björk,
Ericsson Cables AB,
Technology Division,
S-824 82 Hudiksvall,
Sweden

Anders Björk, manager of optical cables at Ericsson Cables AB, Technology Division. He joined Ericsson Cables in 1989, and first did his technical work for his B.SC. in Computer and Electronics, Gävle-Sandviken, Sweden. Since then he has been working with measuring techniques, type testing and development of fibre optic cables.
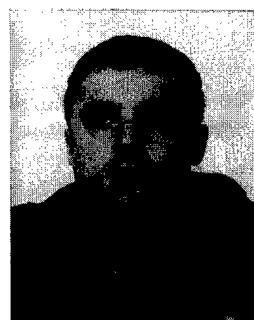
Mark Pearce,
Royal Institute of
Technology,
Stockholm, Sweden

Mark Pearce received his PhD from The University of Birmingham, U.K. in 1996 for studies of the lifetimes of particles containing botton quarks. Upon moving to the Royal Institute of Technology in Stockholm he became involved with the development of radiation tolerant optical links for ATLAS-an activity. He currently shares coordination responsibility within the ATLAS Collaboration.

Jan Troska,
Rutherford
Appleton
Laboratory,
Chilton. U.K.

Jan Troska completed his PhD from Imperial College, London, in 1999 on the subject of radiation-hard optoelectronic data readout for the CMS experiment at CERN, Geneva. Since then he has been conducting research and development at the CLRC Rutherford Appleton Laboratory, UK, on the optoelectronic data readout for the ATLAS experiment also at CERN.

**Francois Vasey,
CERN, Geneve,
Switzerland**

**Alessandro Zanet,
University of
Padova, Padova,
Italy**

Francois Vasey was born in Geneva, Switzerland on Dec. 6, 1961. He received the electronic engineering diploma from the Swiss Federal Institute of Technology ETH-Zürich in 1985 and the Ph. D. degree in physics from the Swiss Federal Institute of Technology EPF-Lausanne in 1992.

In 1985, he joined the Battelle Memorial Institute in Geneva, Switzerland as a research scientist. From 1987 to 1994, he worked on electron beam lithography and diffractive optics, first as a research assistant at the Swiss Federal Institute of Technology EPF-Lausanne, then as a visiting scientist at the IBM Z ürich research laboratory.

Since 1994, Dr. Vasey is working at the European Laboratory for Particle Physics, CERN, in Geneva, Switzerland. His present activity is focused on the development of analog and digital optical links adapted to nuclear environments.

Alessandro Zanet, is an electronic engineer from Padova University in Italy. He is presently employed at CERN in the EP/CMT division. He is involved in several tests over optical cable and connectors to be used in the CMS Tracker Optical Analog Link.

Before that, he worked inside the CERN R&D48 "ROSE" Collaboration in software developing and silicon detectors radiation hardness.

Polyethylene Directly Jacketed Optical Fiber, Used for FTTX Termination

Shinsuke Niiyama, Hiroyasu Hongou, Masayoshi Yamano

Sumitomo Electric Industries, Ltd.
Yokohama 244-8588, Japan
+81-45-853-7220 · niiyama@comm.sei.co.jp

Abstract

This paper summarizes the development of termination cable, which contains few fibers or ribbons.

There will be various methods for the optical fiber termination from feeder cable to subscriber's unit. For example, feeder cable may exist in the aerial, underground or premise. Also subscriber's unit in the outdoor, indoor or individual computer.

So we have manufactured several types of termination cables that suit for each purpose.

These cables commonly have basic structure that thermoplastic elastomer is directly jacketed on the optical fiber.

We had used thermoplastic elastomer such as Silicone/Nylon or polyvinyl chloride for fiber jacketing material conventionally. In this time, we have developed polyethylene or polyolefin jacketed optical fiber because of the following points.

-----------Characteristics of polyethylene jacketed fiber-----------

(1) Stable transmission loss property in the temperature range of –40 to +85℃.

(2) In case of fire, no toxic halogen halide gas generates; also smoke and soot emission is less than Nylon and PVC.

(3) A viewpoint of LCA (Life Cycle Assessment), total CO_2 gas emission can be minimized as compared with conventional cables.

In addition, we investigated and accomplished several requirements, being demanded in cases of various cable installations, such as flame retardant property (from horizontal to vertical flaming condition) etc.

1. Introduction

The construction of optical network in user system, which is provided for each subscriber, is one of the themes for the multimedia era. To accelerate this work, we developed new and low cost termination cables, which permit more efficient installation work, higher network reliability, and less amounts of the pollution emission.

In the points of workability and reliability, it is desirable that optical fiber connection between feeder cable and subscriber's termination unit is constituted by single cable.

To perfect this simple fiber distribution, a cable that can be installed under any conditions is necessary.

This indoor / outdoor compatible termination cable basis Ultra Violet ray curable resin (UV) / Polyethylene (PE) jacketed fiber unit (Fig.1).

It has an excellent temperature performance as shown in Figure 3. In the temperature range of –40 to +85℃, UV / PE jacketed fiber has stable transmission loss property, although conventional Silicone (Si) / Nylon (Ny) jacketed fiber (fig. 2) causes transmission loss increase at –40℃.
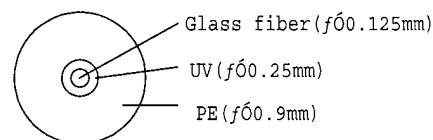
Fig.1 Cross-sectional view of UV/PE Fiber
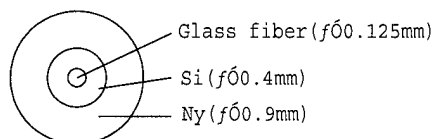
Fig.2 Cross-sectional view of conventional Si/Ny Fiber
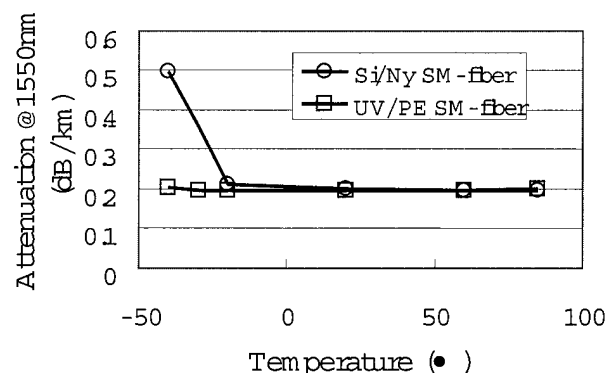
Fig.3 Transmission loss attenuation in Temperature condition

We applied this simple structure to our new termination cables.

Figure 4 and 5 show typical structures of which we developed.

We call the former as tight jacket type and the latter as cord type.

We can access the fiber by tearing the outer cable jacket along the notch.

Shown in table 1, applications with two single fibers or fiber ribbon are also available. Steel strength member can be replaced by dielectric material and jacket can be FRPE also.
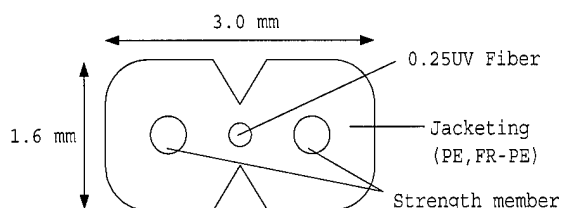
Fig.4 Cross-sectional view of tight jacket type cable
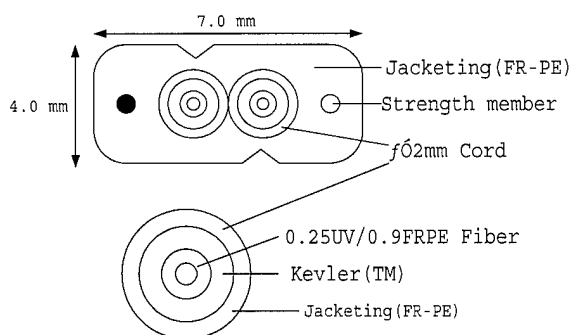
Fig. 5 Cross-sectional view of cord type cable

Table.1 Applicable Components

		Tight jacket type	Cord type
Fiber	One fiber	>	>
	Plural fibers	>	not tested
	Ribbon	>	not tested
Tension member	Steel wire	>	>
	Dielectric	>	>
Jacketing	LDPE	>	not tested
	FRPE	>	>

2. Cable Installation and Design
2.1 Installation Situations
It is necessary to customize the cable individually in obedience to each installing situation.

Figure 6 illustrates cable installation model in user system.
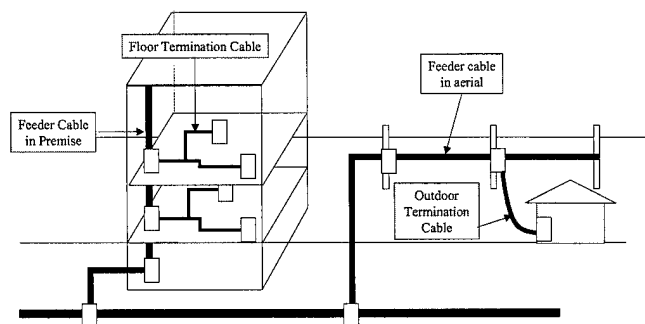
Fig. 6 Cable installation model in user system

In the below, we describe several situations and cables which suits for particular demand.

2.1.1 Floor distribution
Figure 7 illustrates floor distribution model. In this model, we can use both tight jacket cable (Fig. 4) and cord cable (Fig. 5) as floor termination cable.

Termination cables will be laid flat. And considering allowances, we set the test cable by 60-degrees from the horizon level and carried out flame performance test strictly followed by JIS C 3005.
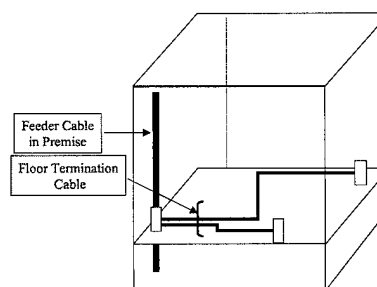
Fig. 7 Floor distribution model

2.1.2 Indoor distribution
Figure 8 illustrates indoor distribution model. Also, both tight jacket cable (Fig. 4) and cord cable (Fig. 5) can be installed.

A cable may be installed vertical direction, attentively. So we designed these cables to meet the vertical grade flame-retardant test, in accordance with JIS C 3521 or UL 1586.
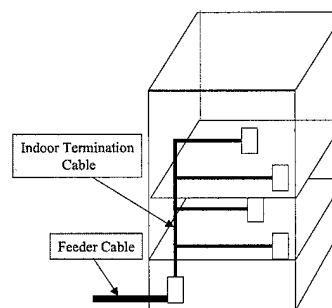
Fig. 8 Indoor distribution model

2.1.3 Outdoor distribution

Figure 9 illustrates outdoor distribution model.

Support wire will be required when the cable is hanged in aerial.

So we designed the outdoor cable to have a self-support wire as shown in figure 10.

Single element cable can be manufactured by jacketing inner members on line.

Multi element cables (2c to 8c) can be manufactured by stranding the elements around the messenger wire.

Cables (or elements) may be placed into subscriber's housing. So we investigated the jacketing material which satisfies both environmental reliability as outdoor cable and flame retardancy as indoor cable.
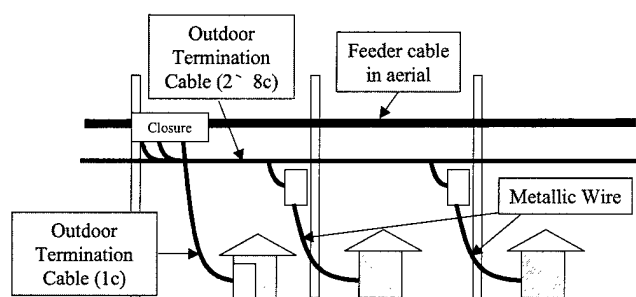
Fig. 9 Outdoor distribution model
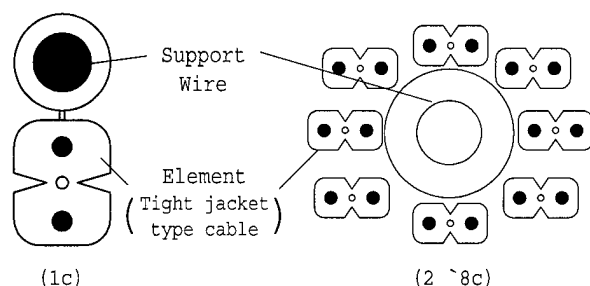
Fig. 10 Self supported cable structure for outdoors

2.2 Jacketing Materials
2.2.1 Material Properties

As described in section 2.1, jacketing material is required several properties listed in table 3. We selected 3 types of polyethylene, and succeeded to satisfy each cable's requirement.

Table. 3 Polyethylene Material Properties

		Metal hydrates filler content	O I	Elongation to break	Elongation change after 6000h SWOM aging	Low temperature brittleness
Require ment	Indoor	Satisfy flame retardant test after cabling		100%	not request	..10 ●
	Outdoor			300%	80%	..30 ●
LDPE		none	not tested	600%	90%	-60 ●
FRPE for Indoor		high	41	150%	not tested	-20 ●
FRPE for Outdoor		low	35	600%	90%	-50 ●

2.2.2 Life Cycle Assessment

We had used polyvinyl chloride (PVC) for these cables jacket conventionally. PVC suits for all requirements referred in the section 2.2.1.

Table. 4 show the reason why we selected the polyethylene cable jacket. It is well known that acid gas, smoke and soot emissions when the cable is burnt can decrease by selecting the halogen free material. We have partly confirmed our flame-retardant cable passed the 3-m cube cable smoke density test (IEC 61034-1,2).

In addition, we calculated the amount of total CO2 gas generation amount in the cable production.

Total CO2 gas emission is calculated from equation (1).

$$CO2total = \Sigma \quad \alpha M + \Sigma \beta W \qquad (1)$$

Where α is an each cabling materials own coefficient that converts unit mass to CO2 gas emission amount.

β is an each cabling processes own coefficient that converts energy to CO2 gas emission amount.

M is a total mass consumption of each cabling material.

W is a total energy consumption of each cabling process.

Calculation model cables are before illustrated figure 4 and 5.

As a result, CO2 gas is cut down 2.8~12.5 percent by selecting LDPE or FRPE instead of PVC.

Table. 4 Assessment of conventional and newly developed cable

		Model Cable	Newly Developed		Conventional
			LDPE	FRPE	PVC
Hazards Emission	Acid Gas	----	none	none	HCl
	Smoke or soot	----	Low	Very Low	High
LCA	total CO2 gas (g/m)	Tight jacket	35	39	40
		Cord	---	140	148

3. Requirements and Test Results
3.1 General

Transmission loss and mechanical properties are commonly required for each cable.

Table 5 and 6 are test results of our trial cables.

All mechanical test methods are based on IEC 60794-1-2.

For each test items, our trial cables indicate good performance.

Table. 5 Transmission loss attenuation

Test cable			Attenuation @1550nm (dB/km)			
				3 times of heat cycle		
Structure	Fiber	Jacketing material	After Cabling	-30 ℃ max	+70 ℃ max	After heat cycle
Tight jacket	2 UV fibers	FRPE	0.21	0.21	0.22	0.22
	2 fiber ribbon	FRPE				
Tight jacket self support	Simplex UV	LDPE				
	Simplex UV	FRPE				
	2 fibers	FRPE				
2-Cords	Simplex UV	FRPE				

Table. 6 Mechanical Properties

Items	Condition		Results
Bending	R30mm ℃80 <		¥Cable
	10 cycles		jackets were
Crush	980N/25mm		not wounded
	after 1 min pressurized		and
Torsion	∮0 < 10cycles		Attenuation
Squeezing	R300mm pulley		change
	0.3% strain loaded		@1550nm
Impact	70N 6cm		were under
	R10mm hard rubber		0.1dB

3.2 Flame Retardant

It is widely accepted that the OI of the FRPE and cross-sectional area of the material greatly influence the flame retardant performance. So we manufactured several types of cables and tested from horizontal to vertical flaming condition.

As a result, we succeed to satisfy every flaming condition by selecting suitable FRPE's OI and cable dimensions (Figure 11).

FRPE's cross sectional area in cable (mm2)
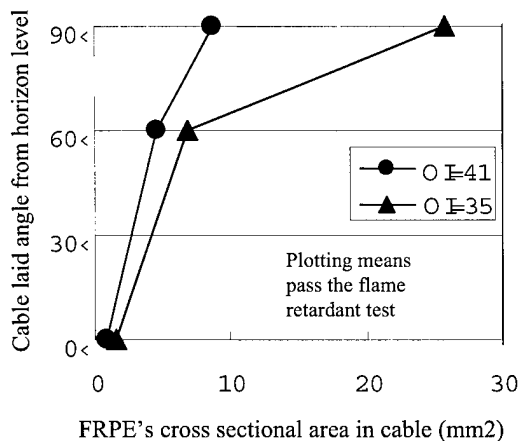
Fig. 11 Flame retardant test results

3.3 Fiber Access in Extreme Condition

Generally speaking, jacket material stiffens in low temperature.

In that condition, conventional cable jacket tearing work to access the fiber becomes difficult.

This problem is solved in newly developed cable, because the modulus of polyethylene is less than PVC in low temperature as shown in table 7.

Table 7 Jacket tearing test result at –30℃

	25% modulus (MPa)		Jacket tearing test	
	20 •	-30 •	20 •	-30 •
PVC	120	2250	good	failed
LDPE	140	720	good	good
FRPE	134	650	good	good

3.4 Marking Durability

For the multi element cables (fig. 10), each element must be identified. So we printed ID number on each element by marking and evaluated its durability.

Test items and results are shown in Table 8.

In this point, polyethylene is inferior to PVC, but we contrived durable ink-jet marking on a polyethylene jacket by suitable ink selection and surface treatment before marking.

Table 8. Marking Durability Test Result

Jacket	Surface treatment	Print ink	Evaluation of Durability	
			Environmental	Mechanical
			SWOM Xe-Lamp 2000h	IEC 60794-1-2 method 2 4.9N/cm ,100cyc
LDPE	none	(A)	good	eliminated
	none	(B)	eliminated	eliminated
	corona discharge	(A)	good	good
PVC	none	(A)	good	good
	none	(B)	good	good

4. Conclusions

We have developed halogen free termination cables, of which basic structure is based Polyethylene Directly Jacketed Optical Fiber and started for sale in July 1999. Those cables meet the general requirements based on IEC 60794-1-2. Also we accomplished to meet the requirements for Indoor/Outdoor installation, respectively.

5. Acknowledgments

6. References

［1］ Yasuji Murakami et al., "Design and Characteristics of Aerial Optical Drop Cable with Electric Power Wires", IEICE TRANS. COMMUN, vol. E83-B, No.1 (January 2000)

［2］ Complete equipment for ecological wire and optical fiber cables database, JECTEC Proceedings (March 2000).

［3］ H. Tanji et al., "Optical fiber cord having stable attenuation characteristics in wide temperature range", IEICE B-1-163 (1988).

7. Authors

Shinsuke Niiyama (niiyama@comm.sei.co.jp)

Shinsuke Niiyama is a member of the Sumitomo Electric Industries in Japan. He received his B.S. degree in physics from Osaka University. And he joined Sumitomo Electric in 1992 as a cable design engineer.

Now he is a manufacturing engineer of optical fiber interconnection device.
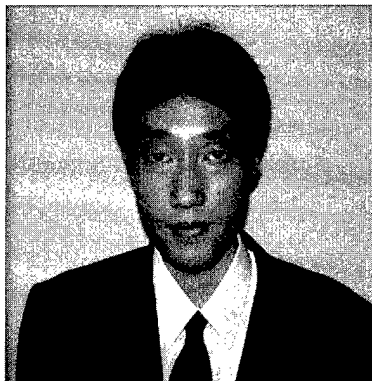
Hiroyasu Hongou (hiro@yklab.sei.co.jp)

Hiroyasu Hongo is a member of the Sumitomo Electric Industries in Japan. He received his M.E. degree in Materials Engineering from Tsukuba University. And he joined Sumitomo Electric in 1986 as an optical fiber production engineer.

Now he is a senior engineer of Optical Fiber R&D Department.
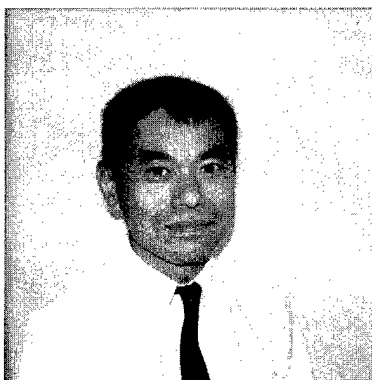
Masayoshi Yamano (yamano@yklab.sei.co.jp)

Masayoshi Yamano is a member of the Sumitomo Electric Industries in Japan. He received his B.E. degree in electrical engineering from Tokyo Metropolitan University. And he joined Sumitomo Electric in 1995 and he has been engaged in research and development of fiber-optic cables.

Now he is a member of Optical Network R&D Department in Yokohama Research Labs.
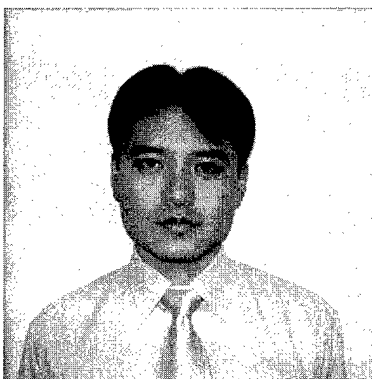
Sorption of Water by Plastic Optical Fibers and Tight Buffers

Ernst Opel, Dieter Heinl and Ilona Schmidt

Corning Cable Systems
Neustadt, Germany
+49 9568 932140 · email address: Ernst.Opel@corning.com

Abstract

The car industry in Germany is going to use Plastic Optical Fibers ("POF") for different applications, e.g. in data links of mobile systems [1]. Due to the harsh environment of mobile systems POF tight buffers have a lot of advantages. Thus we carried out a lot of type appraisal testing on POF tight buffers, which are used to interconnect all network devices inside a car. As an aspect of the available power budget calculation, the long term behavior of POF with special respect to attenuation is under intense investigation. The aging at 85°C with a high humidity has been found as a critical test.

Keywords

Plastic Optical Fiber; aging, automotive applications.

1. Introduction

Plastic Optical Fibers ("POF") may be used in various applications and environments. If the relatively high attenuation compared to glass fiber is acceptable the POF may perform in a lot of areas. One arising field is the use in automotive industry. Plastic Optical Fibers are more and more challenging copper data cables because of lower weight, no electromagnetic interference, and good handling. In a car the POF product must face a lot of different requirements. The product has to serve as long as the expected lifetime of a car, used thousands of miles., no matter what outside temperature, humidity, UV light, vibrations, shocks, will impact the car and its components. Therefore a plastic fiber has to be protected. Several materials are commonly used and some are more suitable for car environment than others. We see Polyethylene, PVC, FRPE, and PA buffered plastic fibers. For a car Polyamide is preferred for several reasons. An inner black sheath may protect the fiber from stray light.

Fiber
PA black
PA yellow

Figure 1. Tight buffer design

The Plastic Optical Fiber consists of a PMMA core surrounded by a Fluoropolymere cladding.

Table 1. Some of available POF products – descriptions:

Category	Buffer material	Jacket Material
Automotive	Polyamide	
Industrial wire	Polyamide	
Industrial Simplex or Duplex cable	Polyamide	Polyurethane
Industrial MIC (stranded)	Polyamide	Polyurethane
Industrial OFNR cable (UL 1651)	PVC	PVC
Commodities	PE or PVC	PVC

2. POF Tight Buffer – Basic Features

Table 2. Comparison of different fiber types

	POF	PCF	MMF 62.5
fiber type	step-index	step-index	graded -index
Ø core/cladding μm	980/1000	200/230	62.5/125
numeric aperture	0.5	0.37	0.275
@ 650 nm	160	10 (*)	-
@ 850 nm		8 (*)	≤ 3.1 (*)
@1300 nm	-	-	≤ 0.8 (*)
@1550 nm	-	-	-
typical wave length	650 ... 670	660/850	850/1300
BW @ 660 nm	10	≥ 17	-
BW @ 850 nm	-	≥ 20	≥ 200
BW @ 1300 nm	-	-	≥ 600

(*) = cabled values

3. Basic Measurement Equipment

3.1 Spectral Attenuation Bench

Due to the big core diameter and the step-index profile a special measurement technique is required for the POF [5]. In principle the cut-back method (JIS C 6863) is used. The launching conditions are controlled by using a fiber optic cross section converter between the monochrometer and the fiber under test. One fiber end is wound on a mode mixer. The other fiber end is fixed in a integrating sphere. The signal is detected by a sensor located at the integrating sphere. With a lock in technique the signal noise level is optimized. The spectral attenuation curve is generated by a PC.

3.2 Insertion Loss Measurement Systems

a. For our first measurements a simple configuration
(LED – Test length – detector) was used.

b. A laser emitting at 657nm is used as a transmitter. A multimode fiber links the laser to the FSMA connector. A mode mixer and pre-length were used to supply a steady state condition for the Plastic Optical Fiber. To measure several fibers parallel a 1/7 coupler with one reference channel is used. For the POF with an NA = 0.5 the detector should be big enough. One detector for each fiber is used.

4. Type Tests for Automotive Applications

a. In appraisal testing we found the following
typical values for a change of attenuation of 0,1 dB

- one 40 mm free bend diameter

- 20 twists per meter

- a tensile force at yield strain (e.g. 60N)

- a crush performance at 1000N/10cm

- a 1000 h resistance against oil

- 100 h resistance against defroster

b. The aging test at 85 °C with high humidity shows a critical behavior, because of the steady increase of attenuation.
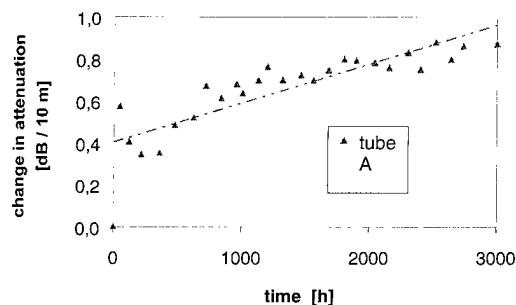
Figure 2. Aging of tube A

5. Aging Mechanism

5.1. Cladding material

Fluoropolymers are typical claddings used for PMMA core fibers. The cladding materials can be divided up in two major classes, namely Polyfluoroolefins and Polyfluoroacrylates. While the first group is limited to applications up to 80°C, the second group allows installations in areas with temperatures up to 105 °C. This seems to be remarkable because the degradation temperatures are expected much higher. The main cause for the loss increase of the Polyfluoroolefins is the morphology of these materials. The olefins are semi-crystalline and therefore sensitive to recrystallization processes. In this case the attenuation loss increases over the complete visible wavelength window. The blue light is more affect than the red one due to scattering effects at the crystalline regions.

Compared to that the acrylates are said to be completely amorphous and therefore robust against recrystallization processes up to 105°C. Because of the thermal requirements (max. = 85°C) Polyfluoroacrylates claddings are in use for automotive applications.

5.2. Core material

Being a polar material with hydrophilic functional groups PMMA shows aging effects due to hydrolysis under high humidity or water soak conditions. Analysis of fission products resulting by storage of PMMA in boiling water for few days shows e.g. Methacrylic acid and Methylalcohol among other degradations products. Due to aging the optical performance between 450 and 500nm is worse than between 640 and 670nm (actual optical window).The aging effects start at a certain temperature and is driven by a relative humidity.

6. Aging Results
6.1. Tests performed at +60°C
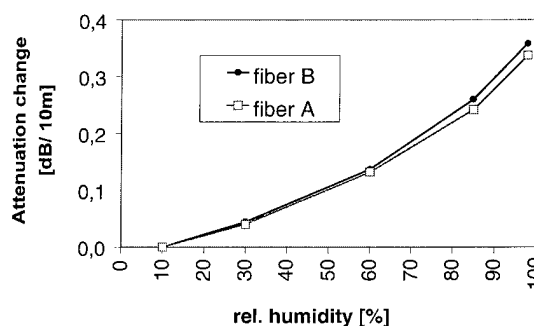
Figure 3. Aging of two fiber types

After storage at high humidity and return to dry air (about 10% r.h.) the attenuation change went back to zero.
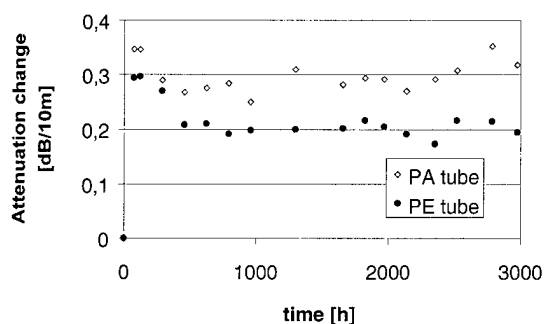
Figure 4. Aging of two tight buffer tubes

6.2. Tests results at 85°C/85% r.h.

The same POF is used for both tight buffer tubes. Within the measurement uncertainty no attenuation slope between 500 h and 3000 h can be seen.

6.3. Tests results for various humidity levels
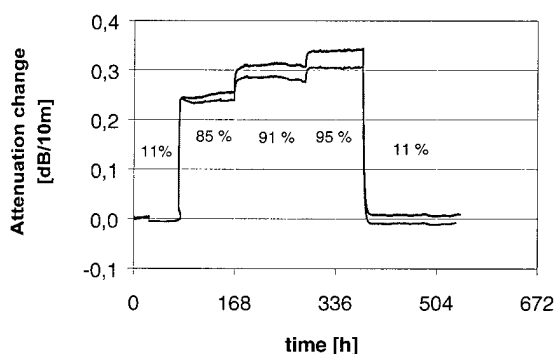
Figure 5. Aging of fiber A at 84°C

After the test no residual attenuation change occurred.
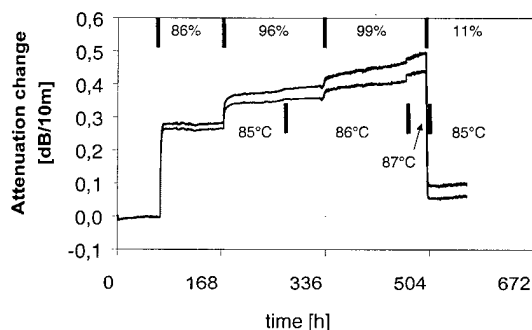
Figure 6. Aging of fiber "A" higher than 84°C

After this test a residual attenuation change at 657nm occurred, therefore a spectral attenuation measurement was performed. We estimate that the aging process starts between 85°C/85% r.h. and 86°C/99% r.h., because of the slope in attenuation change at 86°C and 96% r.h. or higher.
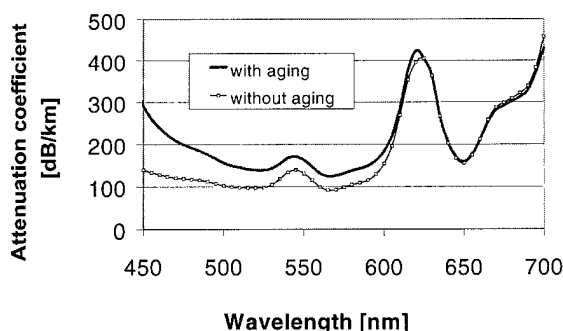
Figure 7. Fiber before and after the test mentioned in figure 6

The residual attenuation change between 450nm and 600nm is much higher than the one at 657nm. The optical window around 650nm seems to be the best for automotive applications.
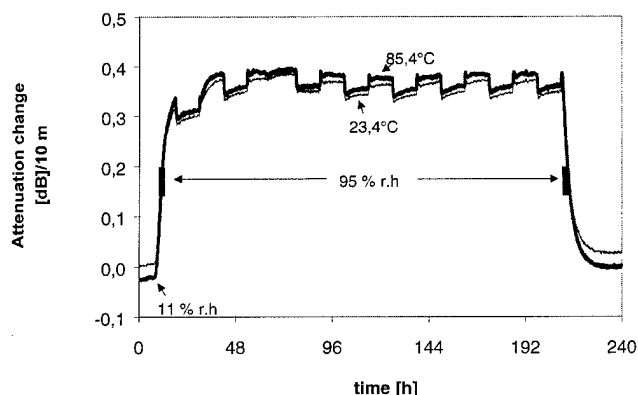
Figure 8. Temperature cycle under certain humidity levels

6.4. Day – Night Shift at a High Humidity Climate

Started with a temperature of 85°C/11% r.h. a temperature cycle with 95% r.h. was performed.

6.5. POF properties under humidity conditions

At a certain point the degradation of the POF core will start. While 85°C/85% r.h. for 3000 h seems to be tolerated. Further statistic investigations are necessary to constrict the critical humidity conditions and to determine the product properties.

7. Conclusions

- The attenuation change measurement in the 650nm window is a good indicator for the degradation of the POF.

- The hydrolysis starts at a certain temperature, depending on the activation energy of the chemical reaction.

- The slope of resulting attenuation curve vs. time strongly depends on aging.

- This slope is a function of relative humidity at $\geq 85°C$.

- The transmission window around 650nm shows the best aging resistance.

8. References

[1] ICPOF, "7th International Plastic Optical Fiber Conference 1998", pp. 205 (Oct, 1998).

[2] G.M. Brauer. and W.T. Sweeney, "Sorption of Water by Polymethyl Methacrylate" *Modern Plastics;* pp. 138 (May, 1959).

[3] O.Ziemann, H.Steinberg, P.E. Zamzow, " CMT – Cable Design for SI – PMMA – POF Applications under highly environment stress " 48th *IWCS ;* pp. 44 (1999).

[4] P. Herbrechtsmeier, " Polymere Lichtwellenleiter" Kunststoffe 79, pp. 1040 (1989).

[5] M.Loch, K.F. Klein, H.P.Poisel and U. Greiner, "Spectral attenuation measurements in POFs with controlled input conditions using different fiber-optic elements", 9th International Plastic Optical Fiber Conference 2000.

Speakers Biography

Ernst A. Opel was born in Völkenreuth in 1959. He received his Dipl.-Ing.(FH) in Feinwerktechnik from the Georg-Simon-Ohm-FH in Nürnberg in 1987. He joined the RD&E group in Neustadt in 1988 and is presently the manager of the Product Evaluation group. He has authored and co-authored several papers.

Email: Ernst.Opel@corning.com

Co- Authors

Dr. Ilona R. Schmidt was born in Munich in 1956. She studied chemistry at the Friedrich-Alexander-University in Erlangen. Starting 1985 she was responsible for materials in several RD&E positions and then manufacturing manager POF. Now she is assigned as the Quality Manager of the plant.

Email: Ilona.Schmidt@corning.com

Dr. Dieter Heinl was born in 1967 and studied Chemistry at the University of Regensburg. From 1996-1999 he was engaged in the Corporate Technology department of Siemens in Erlangen. His main focus was on the development of flame retardant materials. In 1999 he joined the RD&E group in Neustadt and is presently managing the materials group.

Email: Dieter.Heinl@corning.com

Optimized Fiber For Terabit Transmission

Louis-Anne de Montmorillon[1], Alain Bertaina[2], Pierre Sillard[1], Ludovic Fleury[1], Pascale Nouchi[1], Jean-François Chariot[1], Sebastien Bigo[2], Jean-Pierre Hamaide[2]

[1]Alcatel, Conflans Sainte Honorine, France
+33 – 1 – 39 – 19 – 12 – 00 · louis_anne.de_montmorillon@alcatel.fr
[2]Alcatel Corporate Research Centre, Marcoussis, France
+33 – 1 – 69 – 63 – 10 – 42 · alain.bertaina@alcatel.fr

Abstract

Optical fiber with a chromatic dispersion value of 8 ps/nm/km at 1550nm is a good compromise for transmission systems working at Terabit/s rate. Such a value is sufficiently high to avoid Non Zero Dispersion Shifted Fibers (NZDSF) limitations and sufficiently low to avoid Single Mode Fibers (SMF) ones. Moreover, it allows an interesting trade-off between the chromatic dispersion slope and the effective area. Fiber with optimized propagation characteristics has been realized. This fiber, called TeraLight™, has been used in a 1.5 Tb/s system (150 Channel at 10Gb/s in both C and L band with a 50GHz channel interspacing) and in a 1.28 Tb/s system (32 Channel at 40Gb/s). It is adapted for a use in the S wavelength band.

Keywords

Optical Fiber; Guided Propagation; Chromatic Dispersion; Fiber Design.

1. Introduction

Terabit transmission systems through optical fiber are about to become a reality. With an intensive occupancy rate of the C+L bands, between around 1530 and 1610 nm, transmission capacities as high as 3Tb/s have been obtained [1]. Even higher capacities could be reached with the use of enhanced C and L bands and with the opening of a short wavelength band, S, typically between 1450 and 1500 nm.

The choice of the most suitable transmission fiber to meet high capacity and upgradability requirements of Dense Wavelength Division Multiplexed (DWDM) transmissions is one of the main issues in optical transmission systems. Dispersion Shifted Fibre (DSF) exhibits a too low dispersion that enhances the impact of cross-nonlinearities and mainly Four Wave Mixing (FWM). Standard Single Mode Fibre (SMF), with its large 17 ps/nm/km dispersion value in the 1550 nm window, is more suitable for DWDM transmissions as the large dispersion reduces drastically the impact of cross-nonlinearities [2]. Nevertheless, at 10 Gbit/s per channel and above, over terrestrial transmission distances (typically 500 km), such a fiber requires dispersion compensation. Dispersion Compensating Fiber (DCF) can be used for this purpose but it

impacts both on the system cost and, due to its large attenuation, on the Signal-to-Noise Ratio (SNR) at the end of the transmission. There must be a trade-off in terms of chromatic dispersion between DSF and SMF, which will minimize the required amount of dispersion compensation while still providing an efficient cross-nonlinearities reduction. First generation Non Zero Dispersion Shifted Fibers (NZDSF) were expected to meet the requirements, but their local dispersion is still too low and cross non-linear effects are still damaging at the channel spacing considered today [3-4]. A solution to decrease these cross-nonlinear impairments is to increase the effective area of the NZDSF. In fact, such a Large Effective Area NZDSF (LEA-NZDSF) has already shown good transmission performance [5], but this has been done at the expense of a high chromatic dispersion slope.

A new transmission fiber, optimized for present and future needs, seems to be an important challenge. For such an optimization, careful analysis of system requirements as well as a good knowledge of fiber design capabilities is needed. In this paper, we first present a detailed analysis of system requirements for transmission fiber in the case of DWDM high-bit-rate transmission. We then present extensive design results to find best-suited index profiles when system consideration is taken into account.

2. System Requirements

The aim of this part is to focus on the value of the local dispersion of the transmission fiber to find out its optimal value. This is done by numerically varying the dispersion and optimizing in each case the dispersion management. Dispersion management must indeed be carried out carefully considering its critical importance on transmission performance [6].

2.1 Simulation parameters

The simulated transmission link is reported on Fig. 1. At the transmitter side, thirty-two randomly decorrelated channels, 100 GHz spaced, modulated at 10 Gbit/s with a Non-Return to Zero (NRZ) modulation format, are generated with wavelength ranging from 1535.04 nm to 1559.78 nm that fall within the ITU-T recommended grid.

The transmission line consists of five 100 km-long spans of transmission fiber, whose chromatic dispersion is to be optimized, and of 6 dual-stage optical amplifiers. Such an architecture allows to insert dispersion compensation between the two stages with reduced impact on the Noise Figure (NF) of the total amplifier. In our simulations, the power per channel at the output of the amplifiers is set to 5 dBm. Their noise is taken into account by an accurate model that calculates the impact of the internal loss due to the dispersion compensation on the total NF. As an example, when internal loss is set to 0 dB, the NF of the amplifier is 5 dB, and when the loss is 11 dB (which corresponds to the DCF needed to compensate exactly for 100 km of SMF), the NF is 6.5 dB. At the end of the transmission, the receiver power sensitivity is evaluated for a Bit Error Rate (BER) of 10^{-10} and compared to the sensitivity without transmission to obtain the transmission penalty. Characteristics of DCF correspond to commercially available data : dispersion at 1550 nm is -80 ps/nm/km, dispersion slope is -0.12 ps/nm²/km, and attenuation is 0.6dB/km. Concerning the transmission fiber, its zero dispersion wavelength is varied from 1300 nm to 1550 nm, by 50 nm steps, which corresponds to dispersion values at 1550 nm ranging from 0 to 17.5 ps/nm/km by 3.5 ps/nm/km steps. In each case, the dispersion management of the link is optimized by considering in line 90% span dispersion compensation according to [7] and optimizing the amount of pre and post-compensation by 200 ps/nm steps. Then, to only focus on the impact of the dispersion of the transmission fiber, the dispersion slope is set to 0.07 ps/nm²/km and the effective area to a constant 50 µm², whatever the dispersion. To finish, note that the span budget is a large 28 dB to comply with field requirements.
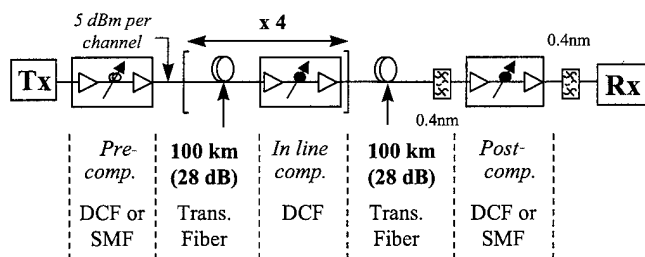
Figure 1. Simulated transmission Setup.

2.2 Results and discussion

Dispersion management is optimized for each chromatic dispersion of the fiber by selecting a value of pre-compensation between -100% and 100% of the cumulated dispersion of one fiber span, and sweeping the value of the post-compensation from -2000 ps/nm to 2000 ps/nm by 200 ps/nm steps. In each case the sensitivity penalties for a 10^{-10} BER are calculated for the 32 channels, as well as the mean penalty and the difference between the best and the worst channel sensitivities. We choose as the best map the one that leads to both the lowest mean penalty and the lowest difference between the best and the worst channel

sensitivities. The results are reported on Fig. 2 for a dispersion of 17.5 (2a), 7 (2b) and 3.5 ps/nm/km (2c). The optimal dispersion map is reported in each case, plotting the cumulated dispersion for channel 1 (dashed) and channel 32 (full) as a function of the distance. The corresponding sensitivity penalties for a BER of 10^{-10} are plotted for each of the 32 channels. Note that when dispersion is zero, error floors are obtained due to the FWM. The mean penalty and the difference between the best and the worst channel sensitivities decrease as dispersion increases, as expected [2], because of the lower impact of cross nonlinear effects.
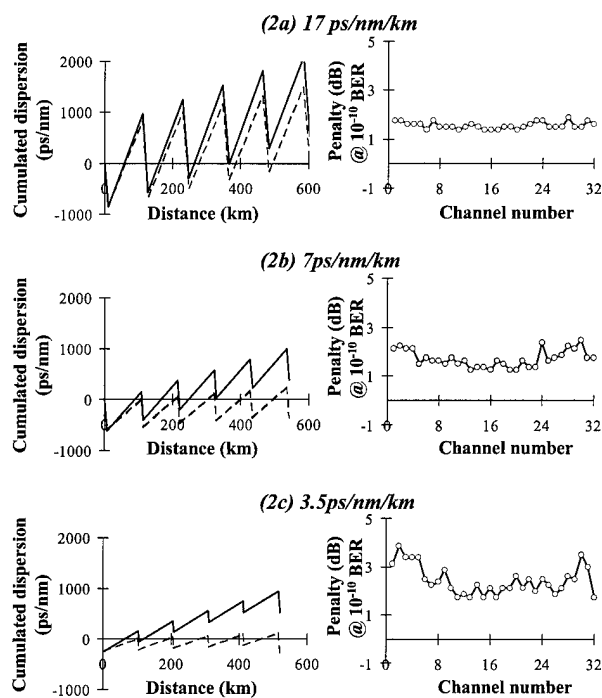
Figure 2. Best maps obtained after dispersion management optimisation and corresponding channel penalties for a 10^{-10} BER, for various values of fibre dispersion at 1550 nm.

To see more clearly the evolution of the penalty as a function of the chromatic dispersion of the fiber, we have plotted on Fig. 3 the best, the worst and the mean penalties for the 32 channels as a function of the fiber dispersion. Once again, the benefic impact of high local dispersion to suppress cross-nonlinear effects can be observed on Fig. 3. If we only consider the mean penalty, we can see on Fig. 3 that a minimum is reached for 14 ps/nm/km and that above this value it increases again because of the SNR degradation due to compensation modules. Nevertheless, a chromatic dispersion of 7 ps/nm/km looks like a threshold value: while worst sensitivity penalties remain below 2.5 dB for dispersion values above 7 ps/nm/km they dramatically increase for dispersion values below 7 ps/nm/km. Consequently, 7 ps/nm/km is the lowest value to guarantee an efficient suppression of cross-nonlinearities. This value

of dispersion is an interesting choice for various reasons. First, the amount of needed DCF is more than twice as low as for SMF, which reduces both the compensation loss and cost. Second, other optical elements such as optical add-and-drop multiplexers can then be inserted inside the dual-stage amplifiers of the link while keeping the inter-stage loss to an acceptable level. Third, the reduced length of DCF also leads to reduced polarization mode dispersion in the link, which is of crucial importance at high bit-rate.
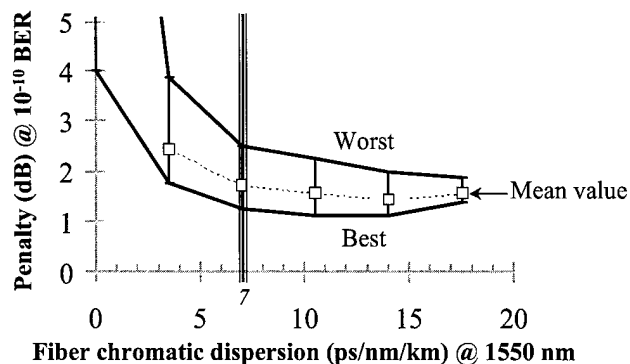
Figure 3. Results obtained as a function of fibre chromatic dispersion. The effective area is a constant 50 μm².

In summary, we demonstrate here that there is a good trade-off around 7-8 ps/nm/km for the chromatic dispersion of the transmission fiber. Such a dispersion guarantees an efficient suppression of cross-nonlinearities in DWDM systems while strongly reducing the DCF length needed in the compensation architecture of the link.

3. Fiber Design

Which fiber propagation characteristics would be obtained for a 8 ps/nm/km chromatic dispersion requirements in the 1550 nm window? We will here study fiber refractive index designs with such a chromatic dispersion value and compare this new family to the preceding ones.

3.1 Key propagation characteristics

Chromatic dispersion is not the only parameter to be considered when designing fiber refractive-index profile. First, the flattest variation of the chromatic dispersion is required. Chromatic dispersion slope at 1.55μm, C', which is the derivative of chromatic dispersion with wavelength needs to be minimized for a more efficient dispersion management over the amplifying bands. The second propagation characteristic (at 1.55μm) to take into account is the Effective Area, A_{eff}. Effective area is a key parameter in describing optical non-linearities and a large effective area is an efficient way to reduce non-linear effects [8]. Fiber refractive-index needs also to ensure good behavior of the fiber in cable. We consider three following parameters at 1.55 μm : bending and microbending losses which need to be minimized and cutoff wavelength which needs to ensure a single

mode behavior of the fiber in the operating channels wavelength. Last but not least, fiber loss needs to be equivalent to preceding generations, that is around 0.2 dB/km in the 1550 nm window.

To compute all these parameters, we use a program that solves the scalar wave equation for arbitrary index profiles and wavelength, using Sellmeier formula for λ-dependence of silica, germanium- and fluorine-doped silica refractive index [9,10]. Once the propagation constant (or effective index) and fundamental mode field distribution is known, we can compute : mode field diameters Petermann 1 and 2 and effective area A_{eff}; chromatic dispersion C and chromatic dispersion slope C'. We can also compute bending loss for any radius using the radiation model of ref. [11] and a microbending sensitivity parameter $S_{\mu c}$ that we defined according to ref. [12]. At last, we also look at the tolerance of propagation characteristics to small fiber-parameter deviations. Small changes in propagation characteristics with changes in core radius and core-cladding refractive index will insure a good control and a good reproducibility of chromatic dispersion during the manufacture process.

3.2 Results and discussion

Optimizing both key parameters, dispersion slope C' and effective area A_{eff} together with low loss, and good cabling behavior is difficult to achieve, as high effective areas are usually associated with high dispersion slope [13].

As a reference, we first studied simple step-index design. As expected, step design is interesting for high chromatic dispersion values and results in too small effective area when chromatic dispersion is below 10 ps/nm/km. We then focused on the well known trapezoid+ring profile shape (Figure 4), which presents more manageable trade-off between effective area and slope values and which presents the technical advantage of a well-controlled process with loss level equivalent to that of SMF.
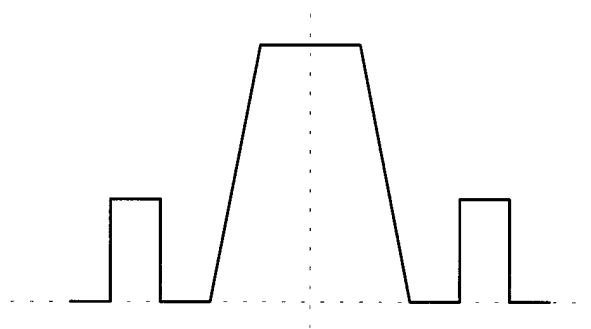
Figure 4. Representation of the trapezoid+ring refractive index profile shape.

This type of profile has 6 adjustable parameters : height of central trapezoid and ring, width and position of ring, trapezoid shape and radius. All these parameters are scanned to find the family of index profiles leading to set chromatic dispersion values C_0, that is 0 to 16 ps/nm/km by 4 ps/nm/km step.

In a given family, we first study the influence of bending loss and cutoff wavelength. These two parameters have a dramatic influence on possible effective area and dispersion slope values. This is illustrated on Fig. 5 for chromatic dispersion C_0 set to 8ps/nm/km. Each curve of Fig. 5 represents the smallest available dispersion slope as a function of effective area but for several given bending loss values. Those curves allow us to follow exactly how the slope changes as effective area and bending loss values are increasing. It is clear that the higher the bending loss level, the smaller the dispersion slopes are. But too large bending loss will lead to poor cablability. The impact of cutoff wavelength is quite similar to that of bending loss, that is the higher the cutoff wavelength, the smaller the slope. But cutoff value is also limited to ensure single mode behavior in cable. So optimum bending loss and cutoff wavelength values have to be carefully chosen to allow the best trade-off between effective area and slope, together with a good behavior in cable.
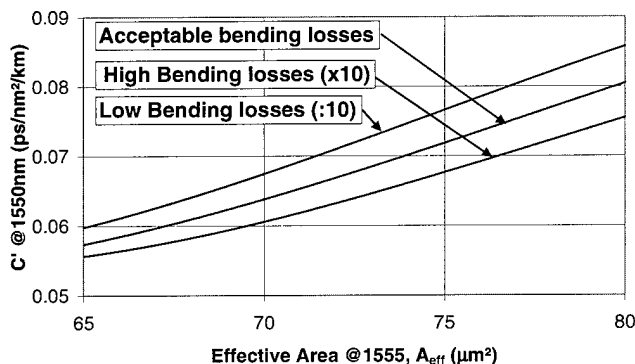
Figure 5. Chromatic dispersion slope as a function of effective area obtained for a chromatic dispersion, C, of 8 ps/nm/km and constant λ_c.

Once optimum bending loss and cut-off wavelength values are chosen to ensure a good behavior in cable, we now study the impact of chromatic dispersion value on the trade-off between effective area and slope. This is illustrated by the curves of Figure 6, which shows how dispersion slope is limited by effective area for different chromatic dispersion values.

The curves of Fig. 6 show several key features. It first appears that increasing the chromatic dispersion values allows a better trade-off between effective area and slope. For example, changing chromatic dispersion from 4 to 8 ps/nm/km allows an effective area increase of about 7 μm^2, when the slope C' is around 0.06 ps/nm²/km. The chromatic dispersion slope also decreases from 0.07 to 0.058ps/nm²/km, when effective area A_{eff} is around 65 μm^2.

The improvement of the trade-off between effective area and slope is noteworthy in the large effective area domain. Indeed, as shown in Fig. 6, the variation of C' with A_{eff} decreases when the chromatic dispersion increases. For an effective area of 80 μm^2,

changing chromatic dispersion from 4 to 8 ps/nm/km allows a chromatic dispersion slope decrease of 0.022 ps/nm²/km, from 0.102 to 0.080 ps/nm²/km. Chromatic dispersion values over 8 ps/nm/km conduct to more interesting trade-off between effective area and slope, but we remind that in this case system design is no longer optimized due to DCF in the compensation architecture of the link.
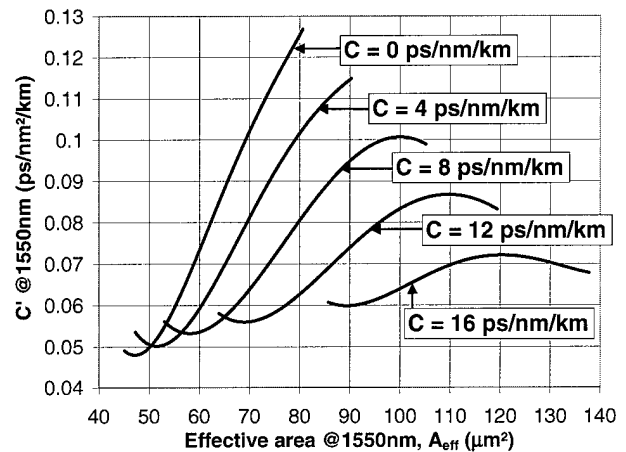
Figure 6. Chromatic dispersion slope as a function of effective area for a set of chromatic dispersion Targets (0, 4, 8, 12 and 16 ps/nm/km), constant λ_c and bending loss @1550 nm (ensuring production of fibers with a good behavior in cable).

We now focus on solutions with an effective area of about 70 μm^2, which is a good trade-off to reduce fiber nonlinearities while maintaining a reasonable chromatic dispersion slope. Figure 7 shows the chromatic dispersion slope as a function of the chromatic dispersion for an effective area of 65 μm^2. It illustrates the huge impact of chromatic dispersion. Indeed, attractive chromatic dispersion slopes lower than 0.06 ps/nm²/km are obtained for chromatic dispersion values over 7 ps/nm/km.

A chromatic dispersion value of 8 ps/nm/km is then a good compromise from a fiber design point of view.

4. Experimental Validation

A novel type of fiber, with local dispersion around 7-8 ps/nm/km and effective area around 65 μm^2, was designed after these numerical results. Fiber results are in very good agreement with our numerical predictions. Microbending loss is comparable to that of standard fibers and cable trials have shown a very good behavior.

The efficient suppression of cross-nonlinear effects was confirmed in a record transmission experiment of 150 channels at 10 Gbit/s over 400 km [14]. BER as low as 10^{-15} have been achieved with channel spacing as low as 50 GHz. A transmission of 32 channels at 40 Gbit/s over 300 km has also been demonstrated [15].
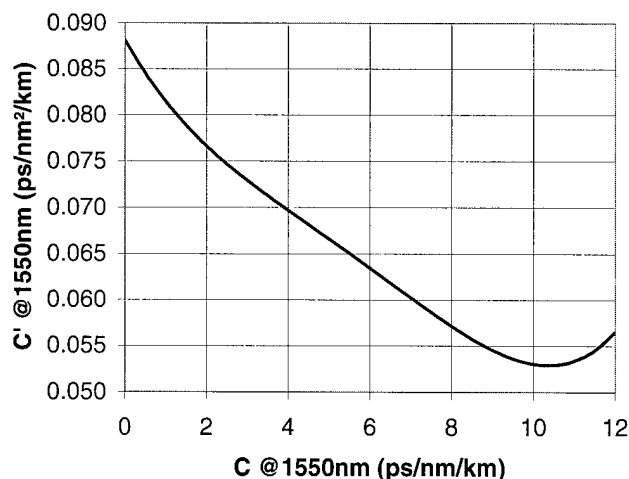
Figure 7. Chromatic dispersion slope as a function of chromatic dispersion for an effective area of 65 μm^2, constant λ_c and bending loss @1550 nm (ensuring production of fibers with a good behavior in cable).

5. Conclusions

To conclude, a chromatic dispersion value of 8 ps/nm/km is a good compromise: it is sufficiently high to avoid NZDSF limitations, sufficiently low to avoid SMF ones, and it allows an interesting trade-off between effective area and slope. Such propagation characteristics have been experimentally validated and conducted to a new fiber, called TeraLight™, with the expected propagation characteristics and cabling behavior. This fiber has been used in a 1.5 Tb/s system (150 Channel at 10 Gb/s in both C and L band with a 50 GHz channel interspacing) and in a 1.28 Tb/s system (32 Channel at 40Gb/s). It is adapted for a use in the S wavelength band.

6. References

[1] T. N. Nielsen et al., "3.28-Tb/s (82x40Gb/s) transmission over 3x100km nonzero-dispersion fiber using dual C- and L-band hybrid Raman/Erbium-doped inline amplifiers", OFC'00, postdeadline paper PD23, Baltimore, Maryland (2000).

[2] S. Bigo et al., "Investigation of cross-phase modulation limitation over various types of fiber infrastructures", Photonics Technol. Lett., Vol.11, No.5, pp. 605-607 (1999).

[3] A. Bertaina et al., "Investigation of the limitations of WDM typical terrestrial transmissions over NZDSF and SMF", Tech. Dig. ECOC'98, paper TuC11, Madrid, Spain (1998).

[4] L. D. Garrett et al., "Experimental comparison of WDM system capacity in conventional and non-zero dispersion shifted fiber", Tech. Dig. OAA'98, paper TuB2, Vail, CO, USA (1998).

[5] S. Tsuda and V. L. da Silva, "Transmission of 40 WDM channels at 10 Gbit/s over 6x100 km of LEAF fiber with dispersion compensation at Tx and Rx terminals", Tech. Dig. ECOC'99, paper MoC2.3, Nice, France (1999).

[6] A. Bertaina et al., "Experimental investigation of dispersion management for an 8 x 10-Gb/s WDM transmission system over nonzero dispersion-shifted fiber", Photonics Technol. Lett., Vol.11, No8, pp. 1045-1047 (1999).

[7] G. Bellotti and S. Bigo, "Cross-phase modulation suppressor for multispan dispersion-managed WDM transmission", Tech. Dig. ECOC'99, paper TuC2.4, Nice, France (1999).

[8] B. Biotteau et al., "Enhancement of soliton system performances by use of new large effective area fibres", Electron. Lett., Vol 31, pp. 2026-2027 (1995).

[9] J. W. Fleming, "Material dispersion in lightguide glasses", Electron. Lett., Vol 14, pp. 326-327 (1978).

[10] S. Kobayashi et al., "Refractive-index dispersion of doped fused silica", IOOC'77, Paper B8-3, p. 309-312 (1977).

[11] A. W. Snyder and J. D. Love, "Optical Waveguide Theory", Chapmann and Hall, New York (1983).

[12] K. Petermann and R. Kuhne, "Upper and lower limits of the microbending loss in arbitrary single mode fibers", Journal of Lightwave Technol., 1986, Vol LT4, pp. 2-9 (1986).

[13] P. Nouchi, "Maximum effective area for non-zero dispersion shifted fiber", OFC'98, Paper ThK3, p. 303-304, San Jose, California (1998).

[14] S. Bigo et al., "1.5 Terabit/s WDM transmission of 150 channels at 10 Gbit/s over 4x100km of TeraLightTM fibre", ECOC'99, postdeadline paper PD2-9, pp 40, Nice, France (1999).

[15] S. Bigo et al., "1.28 Tbit/s WDM Transmission of 32 ETDM Channels at 40 Gbit/s over 3x100 km Distance", ECOC'2000, paper Th10.1.3, Munich, Germany (2000).

Biographies
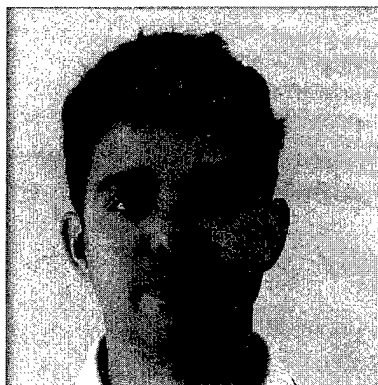
Louis-Anne de Montmorillon received an engineering degree in Optics from the Ecole Supérieure d'Optique in Orsay, France in 1993. He received his Ph. D. degree in Physics from the university of Paris-Sud (France) in 1997 for a work pursued at the Institut Supérieur d'Optique Appliquée, devoted to photorefractive ultrasonic detection. He then joined Alcatel in the Fiber optic R&D unit, Conflans Sainte-Honorine (France).

Alain Bertaina was born in 1973. In 1995, he received an engineering degree in Optics from the Ecole Supérieure d'Optique in Orsay (France). He joined Alcatel in 1997 in the Corporate Research Centre, Marcoussis (France) and received his PhD in Photonics and Optics from the University of Paris XI in 2000 for a work devoted to the impact of the fibre characteristics on the performance of high bit rate transmission systems.
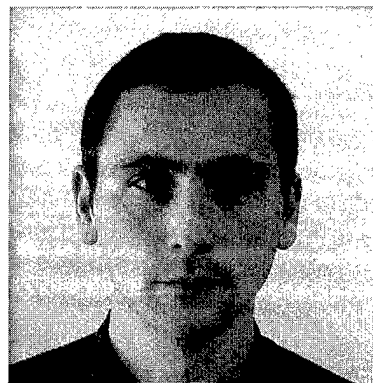
Pierre Sillard received the Engineering Diploma from the Ecole Nationale Supérieure des Télécommunications in Paris, France, in 1994, and the Ph. D. degree from the University of Paris VI in 1998. His thesis work was pursued at the Laboratoire Central de Recherches of Thomson-CSF on the subject of laser resonators with self-pumped phase conjugate mirrors. He then joined Alcatel in the Fiber optic R&D unit, Conflans Sainte-Honorine (France).

Ludovic Fleury received a Physics diploma in 1992 and a Ph. D. degree in optical spectroscopy in 1995 from University of Bordeaux (France) for a work devoted to single molecule spectroscopy in condensed matter. He worked as post-doctorate at Institute of Technology of Chemnitz, Germany, and ETH University of Zürich, Switzerland, from 1995 to 1998. He then joined Alcatel in the Fiber optic R&D unit, Conflans Sainte-Honorine (France).

Pascale Nouchi received an engineering degree in Physics and Chemistry from ESPCI in Paris, France in 1988. She received her Ph. D. degree in Optical Sciences from the University of Southern California in Los Angeles, in 1992. Her work was devoted to photorefractive effects in BSO crystals. She then joined Alcatel in the Fiber Optic Department of the Corporate Research Center, Marcoussis (France). She is since 1996 in the Alcatel Fiber optic R&D unit, Conflans Sainte-Honorine (France).
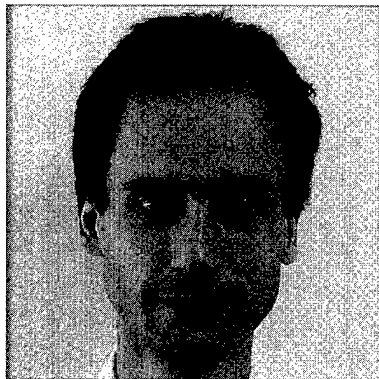
Jean-François Chariot received an engineering degree from Ecole Polytechnique of Palaiseau, France in 1986, and from Ecole des Mines de Paris, France in 1988. He then joined Alcatel in 1988 in the Fiber Optic Production unit, Bezons (France). He is since 1996 in the Alcatel Fiber optic R&D unit, Conflans Sainte-Honorine (France).
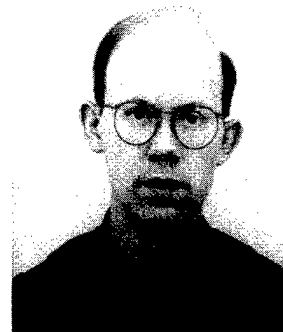
Sébastien Bigo was born in Cagnes-sur-Mer, France, in 1970. In 1992, he graduated from the Ecole Supérieure d'Optique, University of Paris XI. In 1996, he received a ph.D. degree in physics for a work devoted to all-optical processing and soliton transmission. He joined Alcatel in 1993 in the Photonics Networks Unit of the Corporate Research Center, Marcoussis (France), while being a student at the University of Besançon, France. Since 1997, he has worked on high-capacity WDM terrestrial systems. He is now deputy leader of the terrestrial transmission group. He has authored and co-authored more than 50 papers and 20 patents.

Photo not available

Jean-Pierre Hamaide is with Alcatel in the Corporate Research Centre, Marcoussis (France). He his head of terrestrial and submarine transmission groups within the Photonics Networks Unit.

Low Nonlinear Non-Zero Dispersion Shifted Fiber
for Dense WDM Terabit Transmission System

Tomoyuki Nishio[1]   Tomomi Onose[2]   Kengo Kotani[1]   Tsuyoshi Ookubo[2]

1. The 4th Dept. Optoelectronic System Laboratory,Hitachi Cable,Ltd.
2. Optical Fiber Cable Sec. Optical Fiber &Communication Cable Dept.,Hitachi Cable Ltd.
Hitaka-cho,Hitachi-shi,Ibaraki-ken,319-1414 Japan
Phone;+81-294-25-3837· email; nishio@lab.hitachi-cable.co.jp

Abstract

Low Nonlinear Non-zero dispersion shifted single-mode fiber has been developed. The fiber was fabricated by Vapor Phase Axial Deposition (VAD) method. The achieved level of effective area and dispersion slope are 70 – 74 μm^2 and 0.08 - 0.11 $ps/nm^2/km$, respectively. The reliability of fiber with regard loss variation was verified in considering the cable life. Its overall performance in internal trial manufacturing demonstrated the good capabilities of Dense WDM (DWDM) transmission.

1. Introduction

The demand for data communication is growing rapidly due to the increasing popularity of the Internet and other factors. Figure 1 shows the growth in transmission capacity of long haul trunk cables due to progress in transmission system technology. Optical transmission began to be used in trunk cables about 1990, the capacity of those systems was several hundred Mbit/s per fiber. In about 1995 years, the transmission capacity increased to 2.5(5.0) Gbit/s per fiber by optical repeater system using the erbium-doped fiber amplifiers. In about 1998 years, the transmission capacity per fiber increased to 10(20) Gbit/s per wavelength by wavelength Division Multiplexing (WDM) technique[1]. Moreover, in recent system, the overall transmission capacity exceeds 100Gbit/s per fiber by the improvement of the WDM techniques[2]. Usually, these techniques are called Dense WDM (DWDM).

When the number of the signal wavelengths carried in an optical fiber increases, the average transmission power density in optical fibers becomes larger than that in conventional systems. Consequently, optical fiber non-linearities has emerged as a main issue. This non-linearity seriously limits transmission capacity with various non-linear interactions, which are generally categorized as scattering effects and optical signal interactive modulation.

In this paper, we describe a low nonlinear non-zero dispersion shifted single-mode fiber which has an enlarged mode field diameter (MFD).
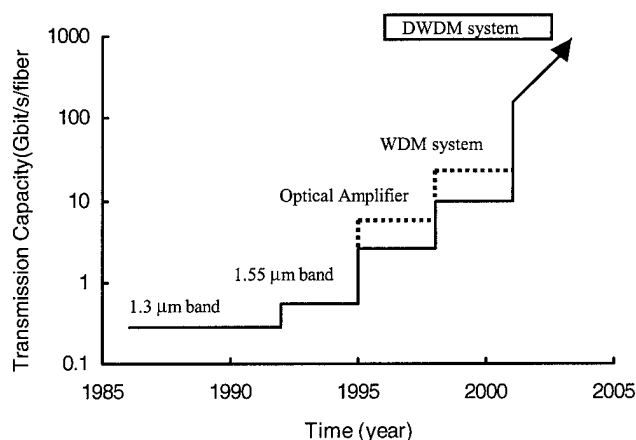
Figure 1. Growth in transmission capacity of trunk cables

2. Requirements for DWDM Fiber

The number of wavelengths in the fibers of DWDM systems is increasing. To use such new optical transmission systems, the DWDM fiber should overcome two transmission-related limitations; optical-fiber non-linearity and dispersion properties.

2.1 Optical non-linearity

Because the signal power density is stronger due to the greater number of channels in DWDM systems, optical-fiber non-linearity limits the number/spacing of channels and the length/ speed of the transmission. In general, the refractive index (n) of optical fibers has a weak dependence on optical intensity (equal to

the signal power (p) per effective area (Aeff) in the fiber):

$$n = n0 + n2\ I$$
$$= n0 + n2(p/Aeff) \qquad (1)$$

where n0 is the ordinary index of the material, n2 is the intensity-dependent refractive index (equal to the non-linear index), and I is optical intensity. Optical-fiber non-linearity arises from modulation of the refractive index caused by changes in the optical intensity of the signal. This causes four-wave mixing (FWM), self-phase modulation (SPM) and cross-phase modulation (XPM). The FWM and SPM distort the signals. Therefore, optical-fiber non-linearity must be reduced. The most practical way to do this is to enlarge Aeff [3]. The relationship between Aeff and MFD can be expressed as

$$Aeff = k\pi(MFD)^2 \qquad (2)$$

Where k is the correction between Aeff and MFD. As a result, enlarging MFD is practical solution for low non-linearity.

2.2 Dispersion properties

The dispersion properties are the dispersion itself and the dispersion slope of the optical fiber. The dispersion value can not be in the zero-value region because FWM occurs interaction between signals (optic channels) in DWDM systems when there is phase matching between the optic channels due to zero dispersion. Therefore, the dispersion value in signal- wavelength region must have the proper non-zero value.

The sign of the dispersion value should be positive for short-distance transmission and the negative for ultra-long-distance transmission[4] because of modulation instability in the positive dispersion in a long link. When the signal wavelength band becomes wider, the difference in the dispersion value at the edges of the wavelength band becomes large. Dispersion compensation thus becomes difficult for long-distance DWDM transmission. To achieve both long-distance and high-speed transmission with easy dispersion compensation for a wide wavelength band, the dispersion slope shall be reduced.

3. Design for DWDM Fiber

Non-zero dispersion-shifted fiber with a conventional design was conducted by enlarging the MFD, with a limitation of 9μm due to the bending loss resistance properties[5].
To enlarge the MFD, we investigated profiles that meet the requirements for the DWDM, considering the ease of fiber fabricating. We used Vapor-phase axial deposition (VAD) to fabricate the fibers because VAD works better in mass production compared with other method, but it is impossible to fabricate a very complex profile by VAD. As a result, we chose the tetra-cladding-type profile for the fibers. The refractive index profile of this type of fiber and its parameters are shown in Figure 2.

b/a: clad1/core
c/a: clad2/core
d/a: clad3/core
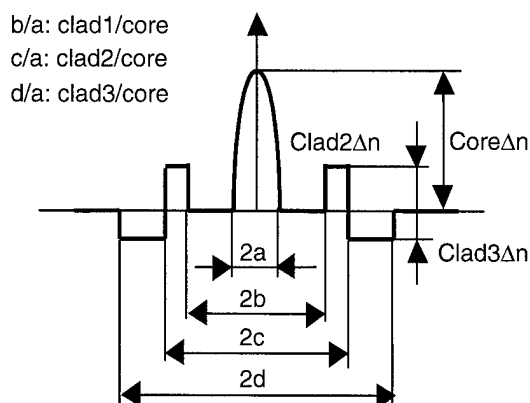
Figure 2. Refractive index profile of tetra-cladding type fiber

4. Experimental Results
4.1 Fiber Performance

We fabricated low non-linear fiber by VAD method. As mentioned above, VAD is the best method for mass producing optical fibers and has low polarization mode dispersion (PMD). This is because we can produce larger and lower-core non-circularity preforms than with other methods, thereby achieving very low birefringence preforms.

The characteristics of the trial fiber are listed in Table 1. The dispersion value was negative, so the fiber is best suited for long-distance DWDM transmission systems. The dispersion slope was computed from the dispersion of linearity rule in the 1550 nm region. It is smaller than that of conventional DSF. The attenuation at a wavelength of 1550 nm with the cable format was very low. The PMD was also very low demonstrating that VAD achieves a lower PMD than other methods. This is because VAD does not include the collapse process which is necessary for other methods. The nonlinear coefficient, n2/Aeff, was measured using the cross-phase modulation method; it was 30% smaller than that for conventional DSF.

Table 1. Typical characteristics of trial fiber

Dispersion	-2.55 ps/nm/km
Dispersion slope	0.089 ps/nm^2 /km
Attenuation	0.199 dB/km
PMD	0.05 ps/km$^{1/2}$
MFD	9.4 μm
Aeff	70.8 μm^2
n2/Aeff	4.1x10^{-18} cm^2/w/nm^2
Macro Bend Loss*	20dB/m

*Bend diameter=20mm

The dispersion slope vs. MFD is shown in Figure 3. The dispersion slope largely depends on the MFD. When the MFD was about 10 μm, the dispersion slope was less than 0.1 ps/nm^2/km. This value is smaller than that with the same type fibers. When the MFD was about 8.3 μm, the dispersion slope was less than 0.06 ps/nm^2/km, which is smaller than that of conventional DSF as well. To increase transmission capacity by increasing the number of wavelengths in the DWDM system, the wavelength bandwidth must be wider. Therefore, the fiber must have a reduced dispersion slope to cover a wider bandwidth. Figure 3 also shows that the fiber we tested can be modified to lower the dispersion slope.
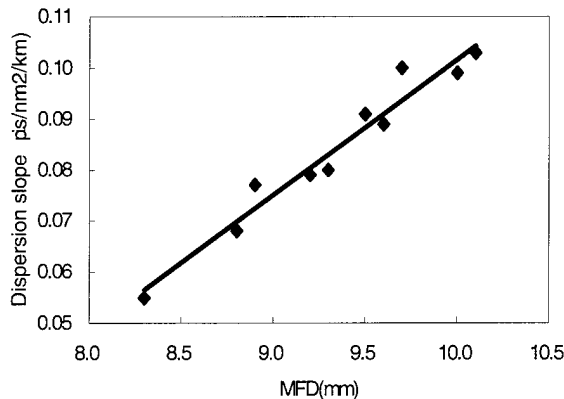
Figure 3. Dispersion slope vs. MFD

4.2 Fiber Reliability

Long-term fiber reliability is an important factor for practical use. We investigated fiber reliability from the point of view of loss variation for various cable-environment parameters: Temperature, Humidity, Radiation etc. Among the factors increasing the loss, the two major factors we investigated were the effects of hydrogen resistance and radiation resistance.[5][6]

4.2.1 Hydrogen Resistance

The loss increase caused by the hydrogen resistance of optical fibers ($\Delta\alpha$) is due to two factors; spectral loss due to hydrogen molecules dissolving into the fiber ($\Delta\alpha H2$) and spectral loss due to hydroxyl groups formation ($\Delta\alpha OH$). The loss increase is expressed as

$$\Delta\alpha = \Delta\alpha H2 + \Delta\alpha OH \; [7] \tag{3}$$

The loss increase at 1550nm was measured experimentally. It is expressed as

$$\Delta\alpha H2 = 0.0152 \exp(9.41 kJ/mol/R/T)P \tag{4}$$

$$\Delta\alpha OH = 3.3 \times 10^3 \exp(-33.3 kJ/mol/R/T)P^{0.5} t^{0.30} \tag{5}$$

where R is the gas constant, T is the temperature in Kelvins, P is the hydrogen partial pressure, and t is time (h).

The universal assumptions for hydrogen pressure and cable temperature in a cable are 0.001atm and three degrees centigrade, respectively. The loss increase of the trial fiber due to the hydrogen effect was estimated using equations (3), (4), and (5), and the results are shown in Figure 4. It was equal to or less than 0.003 (dB/km) for an estimated 25-year lifetime.
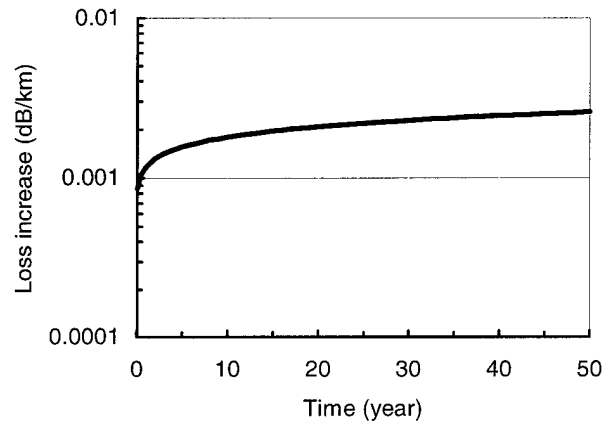
Figure 4. Loss increase caused by the hydrogen diffusion of fiber

4.2.2 Radiation Resistance

The loss increase over the long term due to radiation was estimated by exposing the trial fiber to radiation. We assumed that the total radiation does rate was 0.5 rad/year [8]. After an estimated 25 years, the increase in loss due to radiation was about 0.01 dB/km, as shown in Figure 5.

In summary, the effects of hydrogen and radiation on fiber loss were found to be negligibly small.
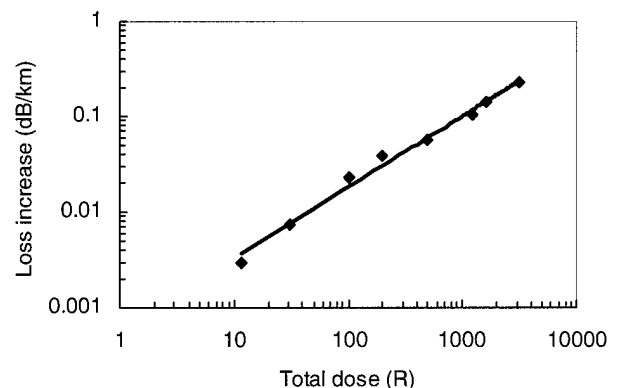
Figure 5. Loss increase due to the radiation of trial fiber at wavelength 1550 nm.

5. Conclusion

We have developed a low non-linear non-zero dispersion shifted single-mode fiber with enlarged MFD by optimizing the design of fiber profile. The non-linear coefficient of trial fiber was 30% smaller than that of conventional DSF. The dispersion value can have a positive or negative value in the signal wavelength area. The dispersion slope is approximately equal to that of conventional DSF, even though the developed fiber has an enlarged MFD. If we design the smaller MFD fiber by using a tetra-clad profile, with an Aeff the same as that of conventional DSF, it will be possible to make the dispersion slope less than that of the trial fiber. Furthermore, we confirmed that the trial fiber has enough hydrogen and radiation resistance to be able to use for the long-term cable life of 25 years.

6. References

[1] G.E.Keiser, Optical Fiber Technol.,vol5, (1999), pp.3-39

[2] Akiba, "Optical Submarine Cable Network", IEICE 00, March 2000

[3] Y.Liu, et al., OFC'96, WK15, 1996

[4] A.Naka, et al., Lightwave Technol., vol.12, No.2, FEBRUARY (1994) pp.280-287

[5] K.Ohsono, et al., IEICE 96, B-965, SEPTEMBER 1997

[6] T.Nishio, et al. IEICE 00, C-3-36, March 2000

[7] K.Noguchi, et at. J. Lightwave Technol., vol. LT-3, No.2, APRIL (1985), pp.236-243

[8] H.J.Schulte, OFC`85,TUQ2(1985)

Author
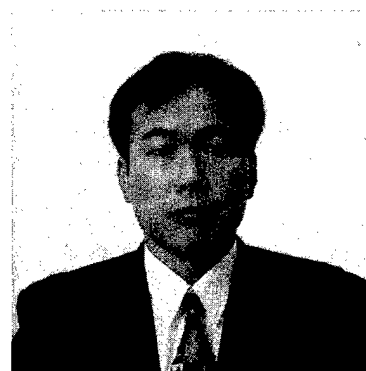
Tomoyuki Nishio

The 4th Dept. Optoelectronic System Laboratory,
Hitachi Cable,Ltd.
Hitaka-cho,Hitachi-shi,Ibaraki-ken,319-1414 Japan
Phone;+81-294-25-3837· email; nishio@lab.hitachi-cable.co.jp

Tomoyuki Nishio received B.E. and M.E degrees in mecanical engineering from Yamagata University in 1988 and 1990, respectively. He joined Hitachi Cable , Ltd. in 1990 and has been engaged in development of optical components and fiber process. He is now a senior resercher in Optoelectronic System Laboratory and a member of the IEICE of Japan.

On-Line Fiber Spinning Monitoring for Low PMD Optical Fibers

F. Cocchini, A. Mazzotti, A. Ricco, and A. Rossi

FOS, Fibre Ottiche Sud
Battipaglia, Italy
+39-0828-675111 · franco.cocchini@pirelli.com

Abstract

A method has been proposed to monitoring the actual spinning of optical fibers during the drawing process. This is an important issue in order to assure the fiber quality. In fact, the apparatus to spin the fiber is usually far from the neck-down region where the torsion is frozen-in. Therefore, an efficiency usually much lower than one comes out between the rotations at the spinning apparatus and those close to the neck-down. In particular, the amount of actual rotations could be not sufficient to reduce the Polarization Mode Dispersion (PMD) of the fiber. The on-line measurement of the actual rotations, on the contrary, allows for a highly reliable forecast of the fiber PMD. The method is based on the Fourier analysis of the side-view diameter of the fiber close to the neck-down.

Keywords

Optical fiber; Spinning; PMD.

1. Introduction

Polarization Mode Dispersion (PMD) is an important parameter in high bit rate telecommunication systems, especially when Optical Amplifiers are used on long distances. PMD is due to birefringence, i.e. the relative propagation delay between the two polarization states of the fundamental mode. This is due to the superposition of core ellipticity, asymmetric lateral stresses and twisting. The application of a frozen-in twist in the fiber (spinning) at a rate of at least 2-10 turns/m is known to substantially reduce PMD [1]. The method is known to be more effective with an alternate rotation [2]. Negligible PMD values, lower than 0.1 ps/km$^{1/2}$, have been currently obtained in spun optical fibers.

The spinning of the fiber is usually obtained by manipulating the coated fiber close to the capstan [1,2] or at the coating applicators [3]. For the sake of illustration, in figure 1, the scheme of a drawing/spinning tower has been reported. The spinning apparatus is able to apply a torque to the fiber, which rotates e.g. by an angle θ_1. The torque is transferred with a delay and attenuated towards the neck-down region, where the fiber rotates by an angle θ_2, while the preform stands still. The time evolution of θ_2 determines the actual frozen-in twist in the fiber, and ultimately the PMD. Unfortunately, the amplitude of θ_2 can be substantially lower than θ_1. This is due to:

i) the long span of fiber between the neck-down region in the furnace and the spinning apparatus,

ii) the viscous drag behavior of the resin in the coating applicators, and

iii) the viscous contribution of the neck-down itself.

Moreover, any sort of slippage of the fiber in the spinning apparatus makes θ_1 itself lower than it should.
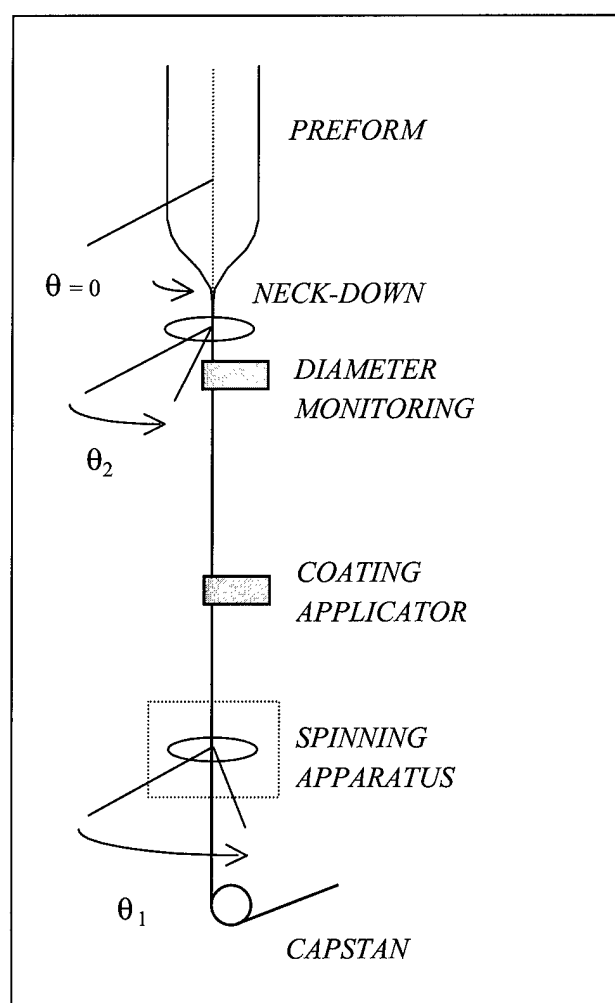
Figure 1 – Scheme of a spinning/drawing tower.

All these make the actual rotations close to the neck-down region highly unpredictable, as can be verified by destructive testing such as visual inspection with a microscope of built-in bubbles in the glass.

We propose a method to measure the actual rotations. It is based on a real-time Fourier analysis of the fiber diameter data as obtained by transverse on-line measurements close to the neck-down. The power spectrum turns out to have several well-resolved peaks, whose frequencies have been correlated to the actual twist of the fiber .

2. Theory

The method relies on the fact that any fiber has a small but not-zero ellipticity. Values ranging from 0.1 to 0.3 are currently typical for a good standard fiber production. The side-view diameter of an elliptical shaped fiber depends on the angle θ of its principal axis with respect to a standing reference (figure 2). It turns out

$$\left(\frac{D_{side-view}}{2}\right)^2 = \frac{a^2 + b^2}{2} + \frac{a^2 - b^2}{2}\cos(2\theta) \qquad (1)$$

where a and b are the larger and smaller semi-axis, respectively.
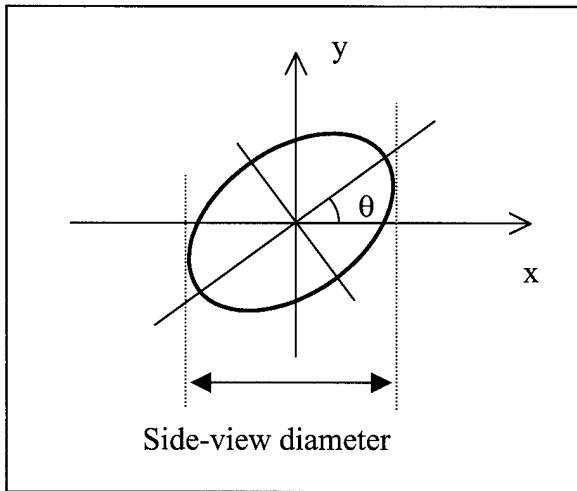
Figure 2 – Side-view diameter of an elliptical fiber.

They are connected to the ellipticity, e, through the following relationship

$$e^2 = 1 - \left(\frac{b}{a}\right)^2 \qquad (2)$$

For the sake of illustration, we can suppose the rotation close to the neck-down described by

$$\theta(t) = \theta_{max}\sin(2\pi vt) \qquad (3)$$

where θ_{max} is the amplitude and v the inversion frequency. While v is univocally determined by the spinning apparatus, θ_{max} is

strongly affected by the drawing tower configuration and process conditions. By sure, it is smaller than the nominal amplitude at the spinning apparatus.

The rotation at the neck-down can be connected to the frozen-in twist, T, according to

$$T = \frac{1}{V_{draw}}\frac{\partial\theta}{\partial t} = T_{max}\cos(2\pi vt) \qquad (4)$$

where V_{draw} is the drawing speed and, from eq.3, the maximum torsion is

$$T_{max} = \frac{2\pi v}{V_{draw}}\theta_{max} \qquad (5)$$

Combining eq. 1 to 3, the apparent diameter variation due to the axial rotation of the fiber turns out

$$\Delta D = \frac{e^2 D}{4}\cos[2\theta_{max}\sin(2\pi vt)] \qquad (6)$$

where D = a + b is the mean diameter (nominal diameter) of the fiber.

The Fourier transform of the signal given in eq. 6 is quite peculiar. The power spectrum has discrete peaks at frequencies $2nv$, with n = 1, 2, 3, ..., which nearly drops down at a maximum frequency given by

$$v_{max} = 2\theta_{max}v \qquad (7)$$

This can be demonstrated by developing the cosine function in eq. 6 in a Taylor series:

$$\Delta D = \frac{e^2 D}{4}\sum_{n=0}^{\infty}\frac{(-1)^n}{(2n)!}[2\theta_{max}\sin(2\pi vt)]^{2n} \qquad (8)$$

Each term in square brackets can be developed according to well-known trigonometric relationships:

$$[\sin(2\pi vt)]^2 = \frac{1 - \cos[2\pi(2v)t]}{2} \qquad (9a)$$

$$[\sin(2\pi vt)]^4 = \frac{3 - 4\cos[2\pi(2v)t] + \cos[2\pi(4v)t]}{8} \qquad (9b)$$

and so on.

Therefore, ΔD can be expressed as a sum of cosine at frequencies $2nv$, with n = 1, 2, 3, ... The spectrum contains infinite terms, but the 1/(2n)! coefficient smears off the contribution of the highest frequencies. The largest significant contribution can be

found by considering that the largest rate of change of the angle θ, i.e. the maximum torsion, is at t = 0 (and at 1/ν, 2/ ν, ….). Therefore, the sine function in eq.6 can now be developed according to

$$\Delta D = \frac{e^2 D}{4} \cos\{2\theta_{max}[(2\pi\nu t) + ...]\} \qquad (10)$$

which is just the contribution at the frequency given in eq. 7.

In figure 3, the spectrum of the signal given in eq. 6 has been reported, in the case of ν = 5 Hz and θ_{max} = 4 π. The Fourier transform has been performed with a discrete FFT over 2048

points at a rate of 500 Hz. In this condition, eq. 7 gives $\nu_{max} \approx 125$ Hz, which nearly corresponds to the actual extent of the spectrum. The spectrum is formed by harmonics spaced by 2×5 Hz, as it should be.

The inversion of the procedure, followed so far, should allow estimating T_{max} from the observed extent of the spectrum:

$$T_{max} = \frac{\pi\nu_{max}}{V_{draw}} \qquad (11)$$
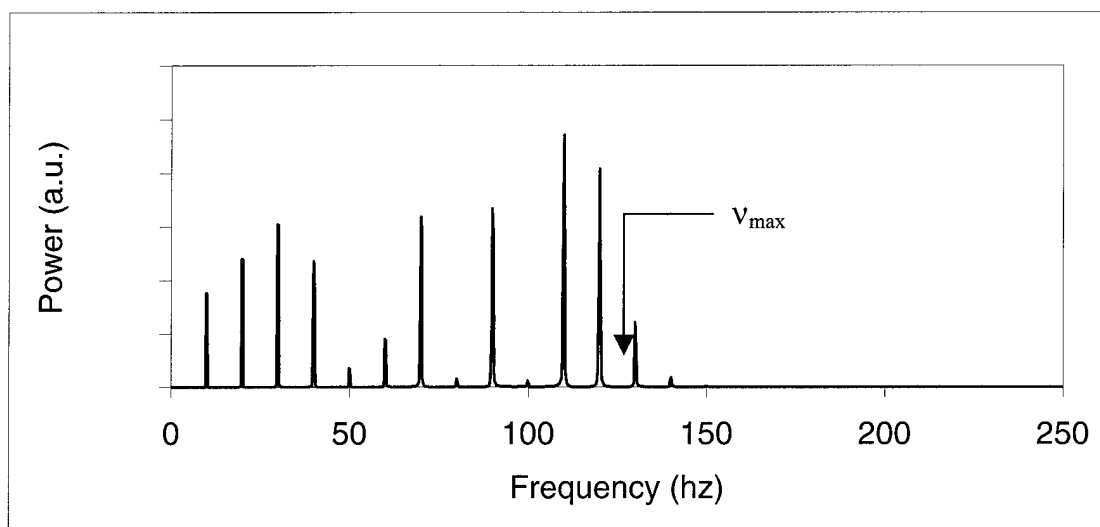
Figure 3 – Simulated spectrum for ν = 5 Hz and θ_{max} = 4 π.

3. Experimental results

In the above section, the ideal spectrum of the side-view diameter variations has been presented. In the real world many sources of noise are expected, e.g.

i) natural variation of the overall diameter;

ii) natural twist of the fiber principal axes;

iii) noise of the diameter measurements;

iv) changes of the θ pattern in the time interval for the Fourier transform.

Nonetheless, it has been found a good resemblance among experimental spectra and the theoretical ones. In figure 4 to 6 we reported experimental spectra obtained with inversion frequency of the spinning apparatus ν = 2.8, 3.8 and 5 Hz, respectively, while maintaining constant the amplitude of the oscillation of the

apparatus. In the first case, the maximum harmonic frequency is at about 130 Hz, in the second at about 180 Hz, and in the latter case the spectrum extends up to nearly 250 Hz, in agreement with eq. 7. An enlarged picture of the first spectrum is presented in figure 7, where the harmonic spacing can be appreciated.

In figure 5, it can be noticed the presence of spurious odd harmonics in the spectra at 3.8 Hz, which is probably due to coupling with lateral vibration of the fiber at the frequency ν and to a little position sensitivity of the diameter monitoring. This however does not seriously affect the estimate of the maximum frequency.

For the sake of comparison, the spectrum of a not intentionally spun fiber is presented in figure 8.
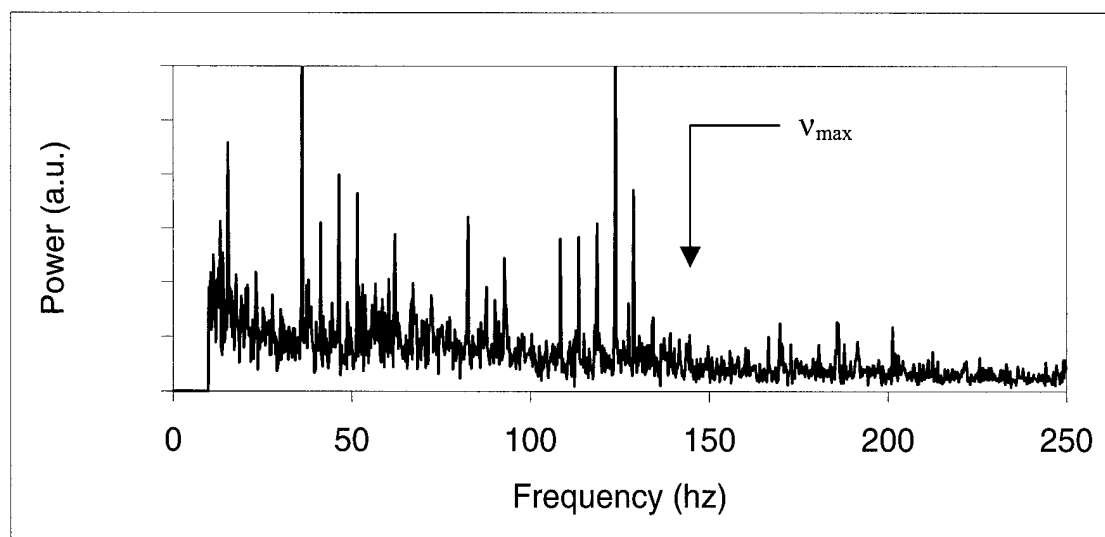
Figure 4 – Experimental spectrum of a spun fiber at an inversion rate of 2.8 Hz.
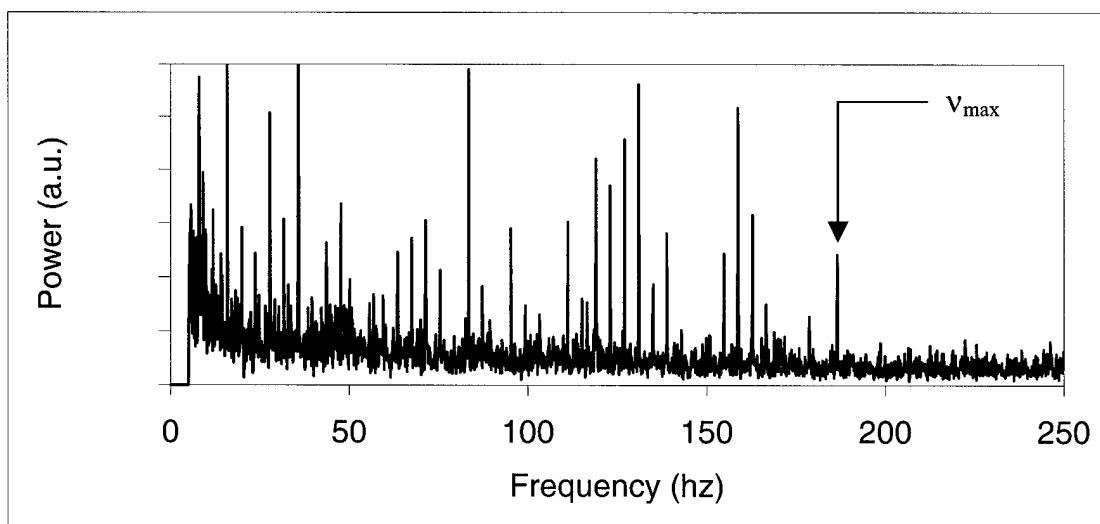
Figure 5 – Experimental spectrum of a spun fiber at an inversion rate of 3.8 Hz.
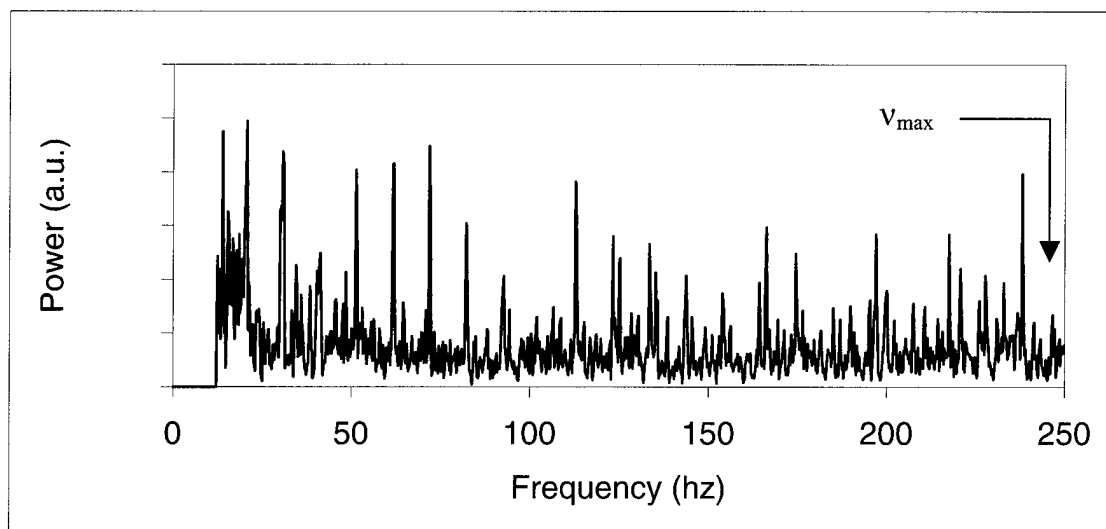
Figure 6 – Experimental spectrum of a spun fiber at an inversion rate of 5 Hz.
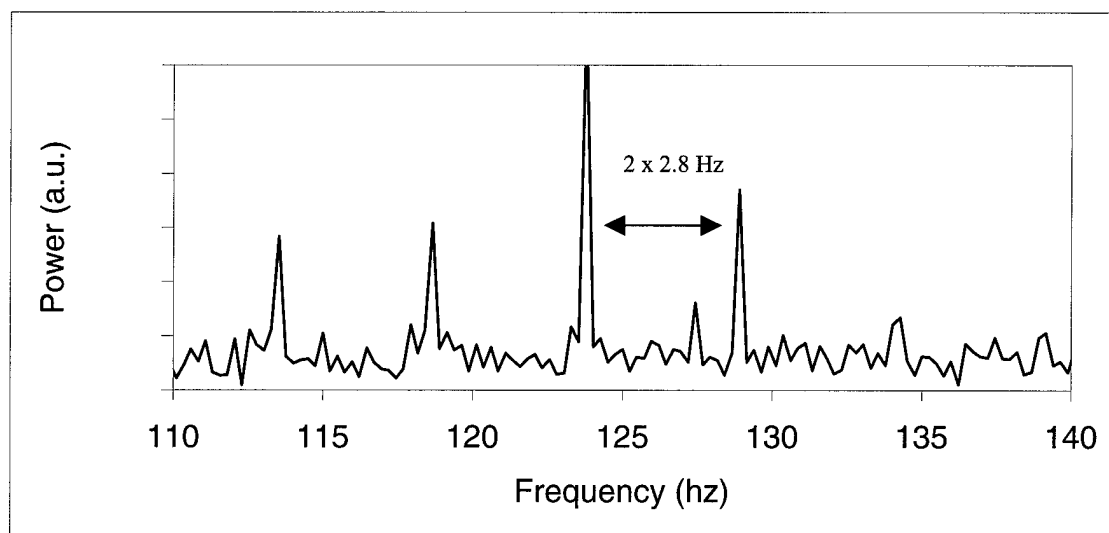
Figure 7 – Same as figure 4 in a reduced frequency interval.
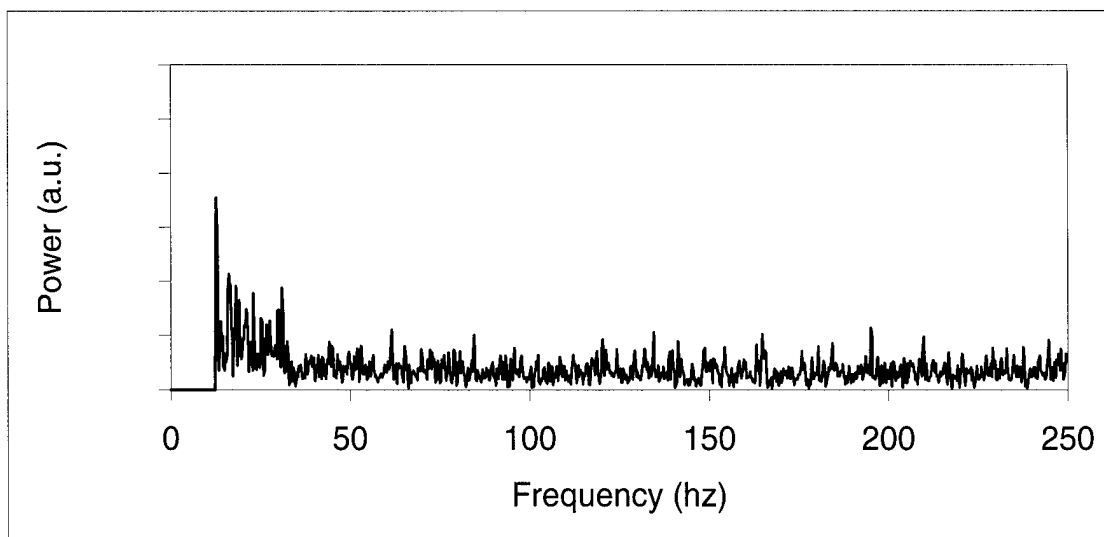
Figure 8 – Experimental spectrum of a not intentionally spun fiber.

The actual torsion frozen-in the fibers of the examples depends on the drawing speed. Good agreement between the on-line method and destructive monitoring at the microscope has been found.

A high confidence on having PMD lower than 0.1 ps/km$^{1/2}$ can be obtained for maximum actual rotations at the neck-down of e.g. 5 turns/meter.

4. Conclusions

We have proposed a method to on-line measure the actual frozen-in spinning rate of optical fibers. The method is based on a real-time Fourier analysis of the fiber diameter data as obtained by side-view measurements close to the neck-down. The power spectrum turns out to have several well-resolved peaks, whose frequencies have been correlated to the actual twist of the fiber. So doing a constant quality of the fibers can be assured, in order to guarantee PMD values lower than 0.1 ps/km$^{1/2}$.

5. Acknowledgments

The assistance of G. DiBenedetto is acknowledged.

6. References

[1] A.J.Barlow, J.J.Ramskov-Hansen, and D.N.Payne, *Applied Optics* **20** (1981) 2962.

[2] A.F.Judy *IWCS 1994 Proc.* (1994) 658.

[3] M.Caiata, F.Cocchini, A.Mazzotti, A.Monetti, and A.Schiaffo *IWCS 1974 Proc.* (1997)

Authors

Franco Cocchini, after graduating in Physics from the University of Pisa in 1983, received a Ph.D. in Solid State Physics from the Scuola Normale Superiore of Pisa. He has worked with EniChem R&D on the rheological and mechanical properties of polymeric materials. He joined FOS in 1991. He is now currently involved in modeling the process for fiber manufacturing and the fiber performances.

Andrea Mazzotti, after graduating in Mechanical Engineering from UNICAL in 1992, joined FOS in 1994, where he dealt with mechanical reliability of optical fibers and coating properties as an active member of COST 246. He is currently involved in technological development of the manufacturing process.

Arturo Ricco graduated from the Technical School on Computer Science "B. Focaccia" in Salerno in 1982. In 1986 he joined FOS, where he is currently involved in Process Control.

Alessandro Rossi, after graduating in Aeronautical Engineering from the University of Naples in 1992, worked at the Mechanical Engineering Dept. of the University of Salerno on surface treatment by cold plasma. He joined FOS in 1996 as researcher in the technological development.

Polarization Mode Dispersion Characteristics of Single Slotted Core Cable by Using NZD Fiber Ribbon

Masakazu Nakano, Makiko Miura, Toshihisa Sato

Lucent Technologies Yazaki Ltd.
1157-106 Hotozawa, Gotemba-city, Shizuoka-Pref., 412-0046, Japan
+81-550-89-7174 · nakano@lt-y.co.jp

Abstract

Recently, Japanese telecommunication service providers have begun using G.655 nonzero dispersion fiber (NZDF) for new network construction. Since long-distance, high-bit rate DWDM transmission requires low polarization mode dispersion (PMD), there has been considerable interest regarding the PMD performance of this type of fiber optic cable. Previous studies have indicated that slotted core ribbon cable might display more PMD than other types of cable. We report on the PMD of representative examples of several different type of NZDF ribbon cables. Our results of measured PMD performance during mechanical and environmental tests designed to simulate field conditions indicate that we can expect good PMD performance. Typical measured PMD coefficient values are approximately 0.05 ps/km$^{1/2}$ in all cable and ribbon configurations. We believe that these results clearly demonstrate that the standard Japanese cable structure will be able to support high bandwidth requirements with NZDF.

Keywords

Polarization mode dispersion; Slotted core cable; Non-zero dispersion

1. Introduction

Japanese service providers have recently begun using DWDM based transmission systems in response to the rapidly increasing needs for bandwidth. Although at present the high bit-rate systems rely on 10 Gb/sec transmissions, it is widely assumed that 40 Gb/sec systems will be commercially deployed in the near future. Since many of the main communication lines exceed 400 km in length, the PMD performance of the cable will be a very important factor affecting the viability of high bit-rate telecommunication. In Japan, the most common cable structure is slotted core ribbon cable. Previously published results have reported that this structure might be have higher PMD than other cable structures such as loose tube [1][2]. At that time however, the maximum transmission bit-rate was 2.5Gb/sec, and 10Gb/sec was considered as a future technology and the PMD performance of the network was not believed to be an important design consideration. Furthermore, the networks were constructed using either G.652 or G.653 fibers. As more carriers begin to adopt high bit rate DWDM transmission equipment, they have begun using G.655 NZDF for new network construction because of its cost saving advantages and its relatively easy upgradability to 40 Gb/sec transmissions. We have earlier reported the initial PMD performance of NZDF cable [3]. However, we believe it is

necessary to evaluate the performance under conditions that approximate field deployment if these cables are intended to support 40Gb/sec transmission.

For a 1dB power penalty, the allowable PMD coefficient can be calculated according to following formula (1)[4].

$$L(km) = \left[\frac{10^3 f}{B(Gb/s) \times PMDC(ps/km^{1/2})} \right]^2 \qquad (1)$$

Where B is the bit-rate, L is the transmission distance, f is the allowed bit-period fraction. Assuming B= 40Gb/sec, f= 0.1 and L = 400 km [5][6] give a maximum acceptable PMD coefficient of 0.125ps/km$^{1/2}$.

2. Cable structure

In this study, we selected a reduced slope NZDF that is optimized for DWDM transmission over a wavelength range from 1530 nm to 1625nm. Because of the importance of low dispersion slope for the performance of a long haul high bit-rate transmission network, this fiber has become the dominant NZDF in Japan. Table 1 shows some of the optical and geometrical characteristics of this fiber. The fiber was drawn using a process that greatly minimizes the PMD.

Table 1. Characteristics of Reduced Slope NZDF

Parameter	Value	Parameter	Value
MFD at 1550nm	8.4+/-0.6 micron	Chromatic dispersion 1530 to 1565nm	2.6 to 6.0 ps/nm-km
Cladding diameter	125+/-1.0 micron	Chromatic dispersion 1565 to 1625nm	4.0 to 8.9 ps/nm-km
Core/Clad Con-centricity error	<=0.6 micron	Dispersion slope at 1550nm	<=0.05 ps/nm²-km
Cladding Non-circularity	<=1.0 %	ITU-T Category	G.655 Example 3

In general, NZDF optical fiber cable is used in trunk lines for long haul network applications. In the case of Japan, the most common trunk line cable structure is a single slotted core containing from 5 to 16 slots, each of which is helically stranded with between 5 and 10 layer stacks of 4 or 8-fiber ribbons. Although the primary application of NZDF is long haul network construction, some Japanese service providers need to collocate the NZDF in the same cables as G.652 fiber used in for the metropolitan area access network. Since it is preferable that these "hybrid" cables have easy mid-span access, they are often SZ stranded. Typically

the NZDF fraction in each cable varies from 10 to 100 percent. Table 2 shows the geometrical parameters of the cable structures evaluated in this work. Figure 1 shows schematics diagrams of these cables.
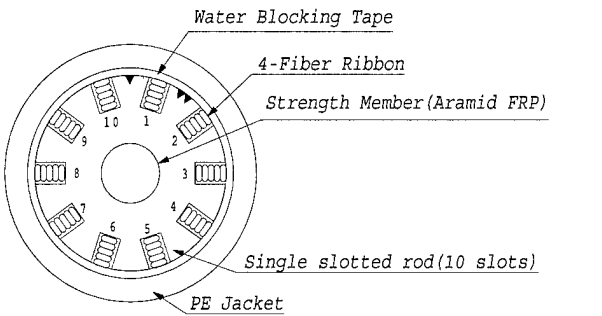
a. 200-fiber cable with 4-fiber ribbon (Cable A)
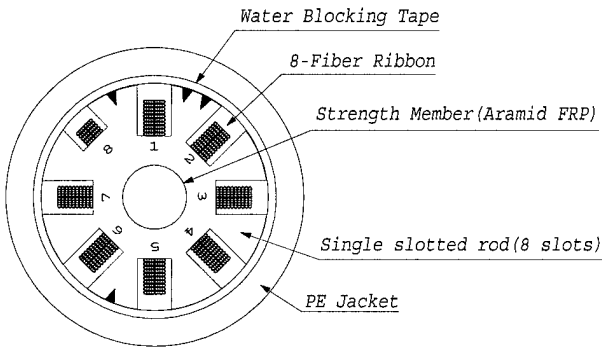
b. 600-fiber cable with 8-fiber ribbon (Cable B)
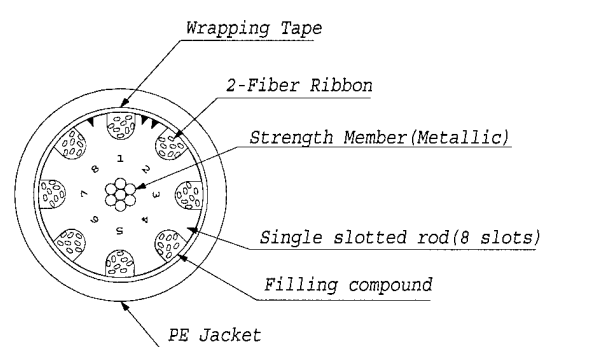
c. 128-fiber cable with 2-fiber ribbon (Cable C)

Figure 1. Detail of Investigation cable structure

Table 2. Cable structure

Parameter	Cable A	Cable B	Cable C
Maximum fiber count	200 fibers	600 fibers	128 fibers
Ribbon type	4-fiber	8-fiber	2-fiber
Ribbon thickness	0.4mm	0.3mm	0.4mm
Ribbon width	1.1mm	2.1mm	0.7mm
Strength member diameter	4.5mm (A-FRP)	4.5mm (A-FRP)	7/1.4mm (Metallic)
Jacket thickness	1.5mm	1.5mm	2.0mm
Cable outer diameter	17mm	22mm	21mm
Stranding method	Helical	Helical	SZ
Water penetration prevention	WB tape	WB tape	Filling compound

3. Optical performance

Table 3 shows the optical transmission characteristics after cabling the NZDF. As can be seen, the optical attenuation was relatively low at 1550nm and 1625nm. In general, the performance of this type of cable under varying environmental and mechanical conditions is usually extremely stable and these samples were no exception. The measured difference in optical attenuation of the different cables is probably not statistically significant.

Table 3. Optical performance of each cable

Items	Wavelength	Cable A	Cable B	Cable C
Optical attenuation of cabled fiber *1) (dB/km)	1550nm	0.203 / 0.005	0.197 / 0.007	0.204 / 0.003
	1625nm	0.209 / 0.006	0.208 / 0.008	0.207 / 0.004
Temperature cycle performance	1550nm	<=0.1dB/km at each wavelength range		
	1625nm	Temperature range: -30 to 70 Celsius		
Mechanical test performance	1550nm	No loss increase and no residual loss		
	1625nm	No residual loss		

*1) Upper number: Average, lower number: σ

4. PMD performance

4.1 Instantaneous PMD characteristics of cabled fiber

Table 4 and Table 5 show the measurement conditions and measured PMD coefficient of each cable. The PMD was measured using the wavelength scanning method from 1169 to 1696nm. Fig 2a-c shows the distribution of PMD values for these cables.

Table 4. PMD measurement conditions

Parameter	Detail
Cable condition	Wound on wooden drum
Cable length	> 1km
Testing temperature	Ambient room temperature

Table 5. PMD coefficient of cabled fiber (ps/km$^{1/2}$)

Parameter	Cable A	Cable B	Cable C
Average	0.0441	0.0450	0.0388
Median	0.0370	0.0370	0.0330
σ	0.0213	0.0236	0.0166
Maximum	0.183	0.159	0.123
Minimum	0.021	0.023	0.019
Fiber count	508	264	528
Average cable length*	1.453km / 0.392km	1.410km / 0.277km	1.474km / 0.288km

*Upper number: Average, lower number: σ
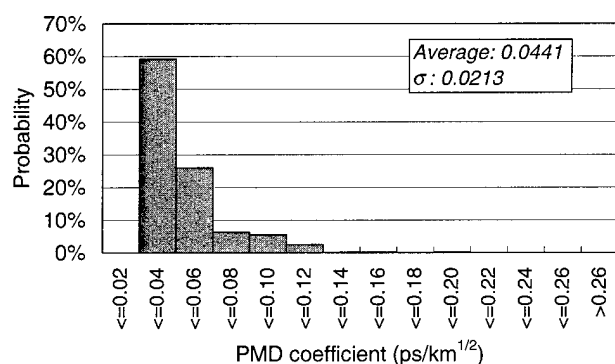
Fig 2a. PMD coefficient of Cable A
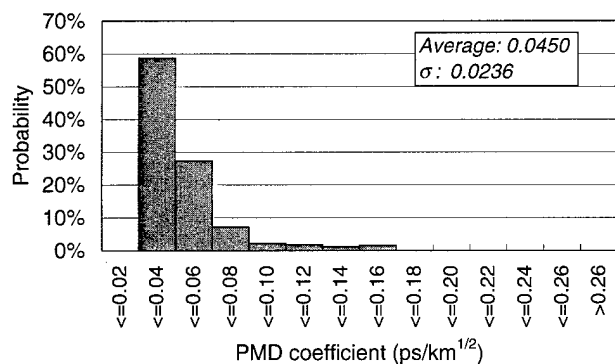
Fig 2b. PMD coefficient of Cable B
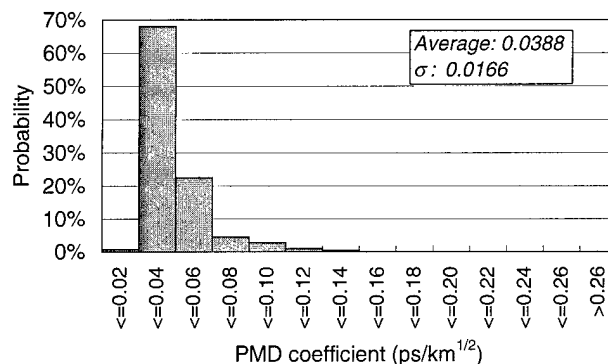
Fig 2c. PMD coefficient of Cable C

Figure 2. Distribution of PMD coefficient of cabled fiber at each cable type

4.2 Calculation of "worst case" PMD performance in the network.

Table 6 shows the simulated "worst case" PMD coefficient we expect in a network link consisting of 20 pieces of concatenated cable. The PMD coefficient was calculated by both Monte Carlo Numeric and model independent methods [5]. The statistical basis of these values was the measured instantaneous PMD of cabled fiber as shown in Table 5 result.

Table 6. Estimated "worst case" PMD coefficient (ps/km$^{1/2}$)

Method	Cable A	Cable B	Cable C
1) Monte Carlo Numeric	0.0802	0.0838	0.0618
2) Model Independent Method	0.0791	0.0850	0.0640

As can be seen in Tables 5 and 6, the instantaneous PMD and "worst case" PMD coefficient are slightly different for each cable type. Cable C showed slightly better PMD performance than Cables A and B. This difference is not surprising in that, among other differences, Cable C has filling compound in each slot. PMD is a complicated function of factors, primarily the fiber birefringence and mode coupling variations along the fiber. We believe it likely that the filling compound altered the stresses on the fiber thereby changing the above factors. Also we can see no statistically significant difference between the calculation methods.

5. Case study of PMD variation

In this section, we evaluated the relationship between some applied lateral pressure and the PMD of both ribbons and cables.

5.1 The PMD characteristics of fiber ribbon

We made three 4-fiber ribbons using three different fibers in order to evaluate the effect of PMD of the location of the fiber in the ribbon. Each ribbon used fiber from the same spool. We also made ribbons of different thickness in order to study the effectiveness of ribbon thickness in buffering changes in lateral pressure. The PMD measurement conditions were as follows:

- Wave scanning method from 1169 to 1696nm

- Ribbon wound on 280mm diameter spools

- 200g winding tension

- 2 km ribbon length

Table 7. Fiber ribbon PMD coefficient (ps/km$^{1/2}$)

Fiber ID		Position 1	Position 2	Position 3	Position 4
Fiber A	0.4mm	0.083	0.222	0.243	0.094
	0.3mm	0.122	0.241	0.273	0.109
Fiber B	0.4mm	0.347	0.259	0.227	0.368
	0.3mm	0.399	0.315	0.324	0.361
Fiber C	0.4mm	0.106	0.149	0.162	0.108
	0.3mm	0.135	0.154	0.134	0.113
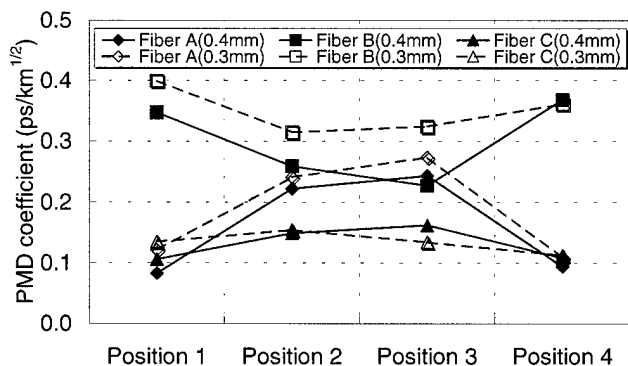
Figure 3. Fiber ribbon PMD coefficient: spool wound, 200g tensions

The results shown in Table 7 and Figure 3 indicate that the PMD performance was affected by the location of the fiber in the ribbon, with a significant difference between the outside fibers (#1 and #4) and the inside fibers (#2 and #3). We also observed a correlation between PMD performance and ribbon thickness. Usually 0.3mm thickness ribbon was more sensitive and had larger PMD than the 0.4mm ribbon.

Each ribbon was subjected to lateral pressure due to the winding tension. This should have resulted in both additional birefringence and mode coupling. The relative significance of these effects varied from fiber to fiber. In some fibers, the PMD increased, indicating that the increased birefringence was more significant than the increased longitudinal mode coupling. On the other hand, the PMD of other fibers decreased, indicating that the effect of longitudinal mode coupling was more important.

5.2 Cabled PMD performance under mechanical testing

In order to simulate installation effects, we evaluated the PMD performance, and the PMD variation in particular as measured by changes in differential group delay (DGD) when the cable was subjected to a lateral load pressure. For this test, the fibers were spliced together to make long loops for measurement. We made two separate loops in Cables A and B using the outside position fibers (loop 1) and the inside position fibers (loop 2). In Cable C, we made a one loop using all fibers in the cable. PMD was measured using wave scanning method from 1384 to 1669nm. Mechanical tests included: a) tensile loading of 1960N on a 6.5m cable segment; b) compressive loading of 1960N/10mm; c) torsion of +/-180 degree/m; d) wrapping 3 times around a 600mm mandrel; e) Flexing, 5 times on a 10m cable segment (similar to IEC-794-1-E8). Table 8 shows the change in DGD during each mechanical test.

Table 8. PMD performance under mechanical test condition (Unit: ps [Change DGD value])

Test	Cable A		Cable B		Cable C
	Outside fiber loop	Inside fiber loop	Outside fiber loop	Inside fiber loop	All fiber loop
Tensile loading	0.01	0.04	0.04	0.02	0.01
Compressive loading	0.03	0.02	0.02	0.01	0.02
Torsion *	0.03 / -0.06	-0.07 / -0.05	0.01 / -0.02	0.05 / 0.01	-0.04 / -0.06
Bending	0.03	-0.05	-0.05	-0.08	0.02
Flexing	0.06	0.00	-0.08	-0.01	0.11

* Upper number: positive torsion, lower number: negative torsion

From these results we see there is no significant PMD variation under normal mechanical testing conditions, nor do we see a relation between PMD performance and fiber location in the ribbon (In Cables A and B).

6. PMD performance of cabled fiber due to variations in environmental conditions

In this section we describe measurements of the PMD during: a) flexing test; b) vibration test; c) temperature cycle test and d) outside environmental temperature test. The effect of flexing and vibration is to load external lateral stress on the cabled fiber. (However, these tests do not significantly add longitudinal stress.) For these measurements we used an interferometric test set with a 1550nm wavelength light source. Rather than the PMD coefficient, we report the changes in DGD. Since most test equipment can not measure the very low PMD of short lengths of fiber, we measured the PMD performance of fiber loops with total PMD ≥ 0.1ps or total fiber length ≥ 10km.

6.1 Flexing test

As mentioned previously, PMD variations are caused by factors related to the fiber, the cable and the fiber/cable interaction. Slotted core type cables generally have more sensitivity to the fiber/cable interaction than other types of cable because of the many points of tangency between the fiber and the core along the cable length. Because the slotted core material is much harder than that of the fiber ribbon, it is very easy to observe the changes in the birefringence and mode coupling distributions along the cable caused by external stresses which occur during flexing, simple vertical vibration, or changes in environmental temperature.

Figure 4 shows the measured variation in PMD during flexing cycles.
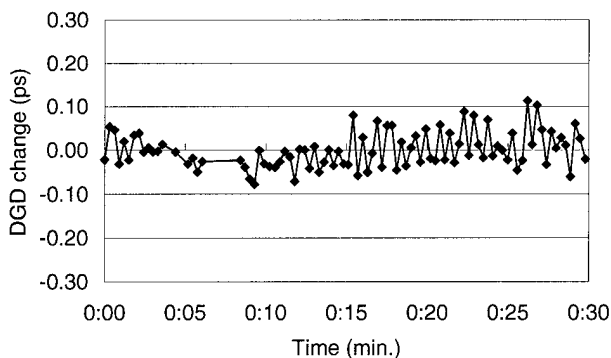
Figure 4. PMD variation during flexing testing
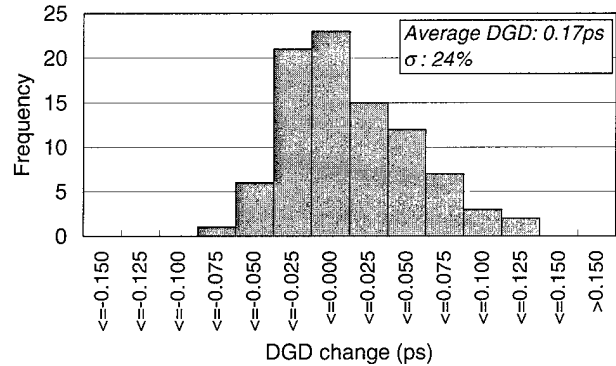
Figure 5. Distribution of PMD variation under flexing test

The flexing test conformed to the method specified in IEC-794-1-E8 method. The load tension was 1960N, the bending diameter was 600mm and the testing time was 30 minutes. This test was performed on Cable C.

The results show roughly 24% variation in PMD (1σ). The distribution of PMD (DGD) is shown in Figure 5. Although there is variation during the actual testing we see no residual effects after testing.

6.2 Vibration test

In this test we investigated the correlation between PMD and vibration in order to estimate the effect of wind induced vibration on cable performance using cable A. We varied the frequency from 5 to 20Hz and the amplitude from ±0.5 to ±10mm at the vibration point. Figure 6 and 7 show the results of this test.
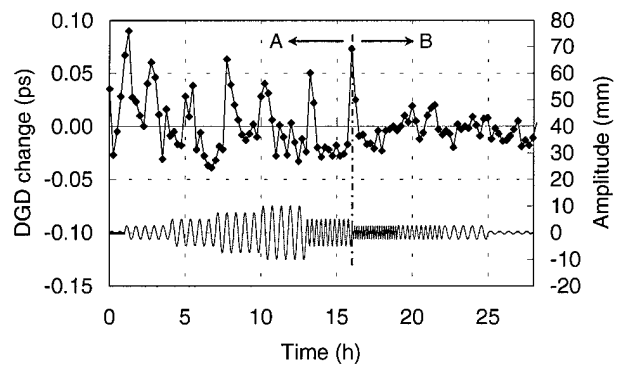
Figure 6. PMD variation during vibration testing
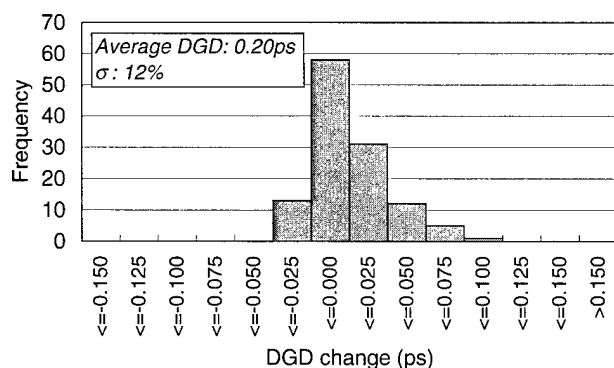
Figure 7. Distribution of PMD variation under vibration test

Figure 6 shows the measured change in DGD during vibration testing. We see the interesting result that changes in vibration frequency had little effect on the PMD (6% variation, 1σ) but changes in amplitude caused brief but significant variation (15%, 1σ) in the PMD. The hold time for each amplitude value was 3 hours. We believe that these results may indicate a potentially larger PMD variation in aerial and railway-bed cables than those in vibration-free location.

6.3 Temperature cycle test

Outside plant fiber optic cable is subject to significant extremes of temperature. In order to evaluate the impact of temperature changes of PMD performance, we performed temperature cycling test. Table 9 shows the various test conditions. Previous studies have reported on the PMD of cabled fiber under temperature cycle tests [1][3][7]. However, the PMD was usually measured under static hold conditions, such as constant 70 Celsius, -30 Celsius, or 20 Celsius environmental temperature. However, the temperature in the field is not static and can chance rapidly and randomly. Therefore, under field conditions the birefringence and mode coupling distribution along the fiber length are constantly and randomly changing, and the time variability of the PMD might be greater than indicated by static temperature tests. In order to study this effect, we measured the PMD at 30 minutes intervals using the wave scanning method from 1386 nm to 1694 nm while we varied the temperature. Figure 8a and 8b show the result of this experiment.

Table 9. Temperature cycle test conditions

Variable	Condition
Cable type	1) Cable A loop1 (Outside fibers loop)
	2) Cable A loop2 (Inside fibers loop)
Cable condition	Wound on a wooden drum
Cable length	Cable A: approx. 1km
	Each loop length was about 47km
Temperature range	-30 to 70 Celsius
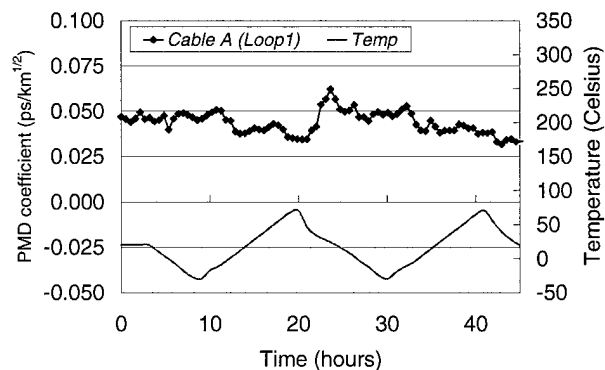
Figure 8a. Correlation between environmental temperature and PMD coefficient (Cable A, loop 1)
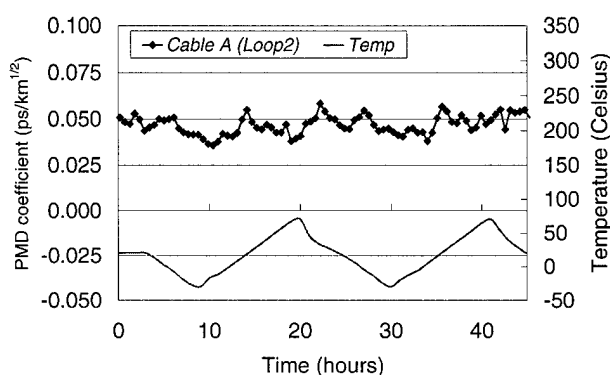
Figure 8b. Correlation between environmental temperature and PMD coefficient (Cable A, loop 2)
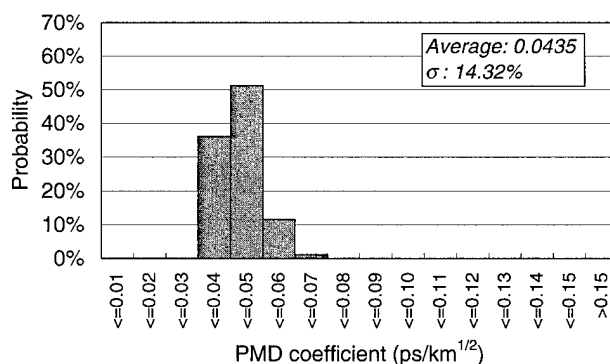
Figure 9a. Distribution of PMD coefficient during changes in ambient temperature (Cable A, loop 1)
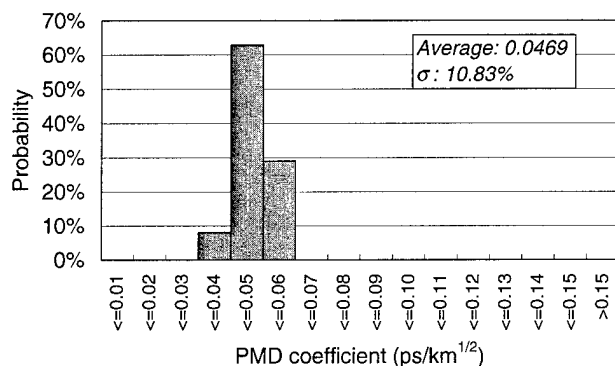
Figure 9b. Distribution of PMD coefficient during changes in ambient temperature (Cable A, loop 2)

As can be seen in Figure 8a and 8b, there is no significant correlation between the PMD coefficients and the environmental temperature. However, we did see a small difference in PMD performance between loop 1 (outer) and loop 2 (inner). The reason for this is most likely that loop 1 consists of the outside fibers which are in close tangential contact with the slotted core of the cable and therefore more likely to be affected by fiber/cable interaction effects than the inner fibers of loop 2, which are somewhat buffered from such effects by the outside fibers. Consequently, loop 1 is subject to greater axial variation in birefringence and mode coupling along the length of the cable. As previously mentioned, the difference in PMD variability between the 2 loops was not very large however: loop 1 was showed 14.3% (1 σ) variation while loop 2 showed 10.8% (1 σ) variation.

6.4 Investigation of actual environmental temperature effects

In order to more clearly understand the performance of the cable under actual field deployment, we performed three additional temperature tests that gradually expanded the range and variability of the ambient temperature. The experimental conditions are shown in Table 10.

Table 10. Additional experimental conditions

Test #	Environmental condition	Sample condition
1	Controlled room temperature	Spooled fiber about 40km
2	Uncontrolled room temperature	Cable length: approx. 1.5km Wound on 1m diameter drum
3	Simulated field conditions	Cable length: approx. 0.5km Installation outside the plant

6.4.1 Controlled room temperature

In this experiment, we measured the PMD of a spooled fiber wound under high tension at room temperature at 30 minutes intervals using an interferometric test set with 1550nm light source. The fiber sample was kept at an extremely well controlled 23 Celsius for 24 hours. As would be expected, the PMD was very stable with almost no variation (2.0%; 1σ). A side benefit of this test was to confirm the stability of the PMD measurement equipment.

6.4.2 PMD variations under uncontrolled room temperature

We wound Cable A on a 1 meter drum and spliced the fibers together to form a loop with a total length of about 60 km. Again we measured the PMD using the interferometric method with 1550nm light source. The sample was placed in our factory storage room where the temperature varies by about +/-3 Celsius. The PMD variation was wider than under the conditions of section 6.4.1. (9.5%; 1σ) during 34 hours of monitoring.

6.4.3 PMD variations under simulated field conditions

We measured the PMD variations of Cable B placed on the ground outside the factory to simulate field conditions. The fibers were spliced together to form a 56 km loop and the cable was exposed to sunshine and ambient temperature variations. Again we measured the PMD variations using the interferometric test set with a 1550nm light source. Monitoring continued for 48 hours from May/26th to 28th 2000. The environment temperature range was about from 13 to 25 Celsius (+/- about 4 Celsius). Figure 10 and 11 show the results of our measurements
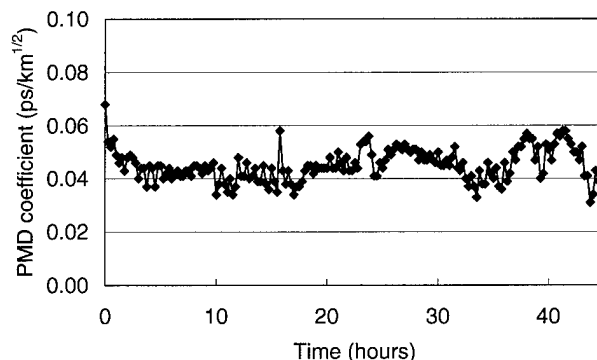
Figure 10. PMD variations under simulated field conditions
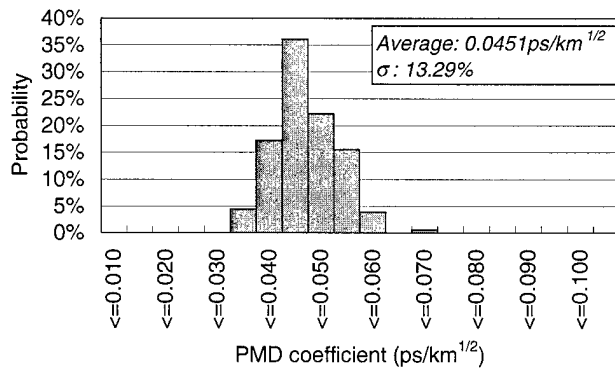
Figure 11. Distribution of PMD under simulated field conditions

From these results, we find that the PMD variation under simulated field conditions was about 13.3% (1 σ). This result is similar to the temperature cycle test result.

7. Simulation of network PMD performance

Based on the results of the above experiments, we estimate that the influence of normal environmental conditions on the PMD characteristics of installed cable is approximately 20%. We estimated the distribution of PMD in a 400km span consisting of concatenated links of each cable type using a Monte Carlo analysis. Generally, for the case of concatenation of individual cable segments, total PMD coefficient can be calculated according to the following formula;

$$X_M = \sqrt{\frac{\sum_{i=1}^{M} x_i^2 l_i}{\sum_{i=1}^{M} l_i}} + \sigma_r \qquad (2)$$

where x_i is the instantaneous PMD coefficient (ps/km$^{1/2}$) of segment i and l_i is the length of cable segment i (km). The distribution of the x_i was based on the statistics underlying the data presented in Table 5. The Monte Carlo selection of l was based on actual records of NZDF cable deployment in Japan. σ_r is a factor representing the influence of environmental conditions. The number of PMD per model was 10,000. Table 11 and Figure 12a, 12b, 12c show the results of these simulations.

Table 11. Simulated PMD for a 400km link (ps/km$^{1/2}$)

Parameter	Cable A	Cable B	Cable C
Average	0.0482	0.0506	0.0420
Median	0.0482	0.0507	0.0421
σ	0.0089	0.0093	0.0078
Maximum	0.080	0.088	0.070
Minimum	0.011	0.016	0.011
Count	10,000	10,000	10,000
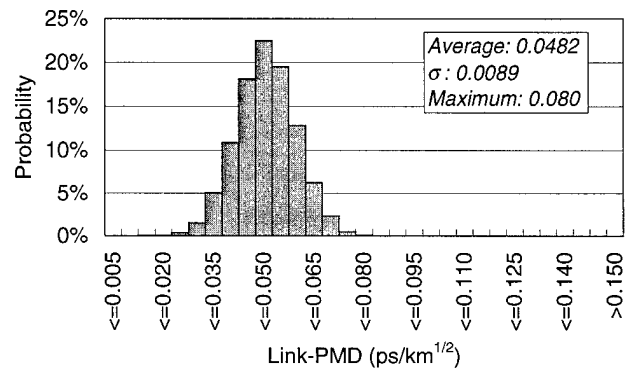
Figure 12a. Simulated PMD of a 400km network constructed with Cable A
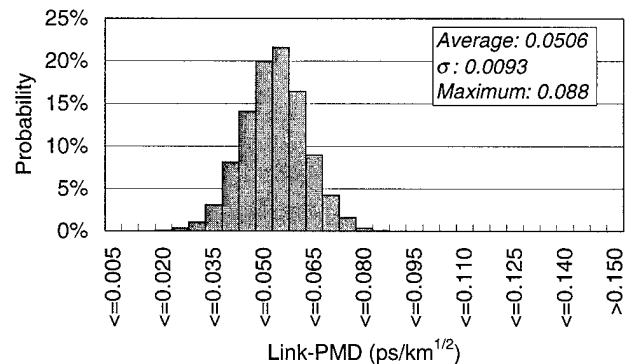
Figure 12b. Simulated PMD of a 400km network constructed with Cable B
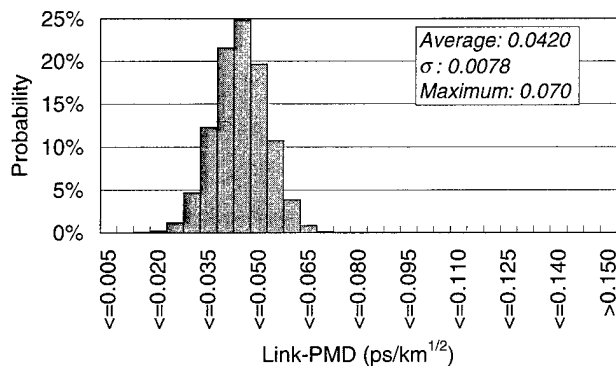
Figure 12c. Simulated PMD of a 400km network constructed with Cable C

From these results and calculations, we can see that the PMD performances of each cable type are quite stable and enough adequate for use with 40Gb/sec transmission.

8. Conclusions

We investigated the PMD performance of 3 different types of reduced slope NZDF cable representing the most commonly used Japanese cable types. On the basis of these results, the most significant factor affecting PMD of installed Japanese spec slotted core cable is environmental temperature variability. The single slotted core cable structure is sensitive to this effect because of the fiber/cable interaction. The instantaneous PMD seems to depend more on the cable design, e.g. filled vs. unfilled, than on the stranding conditions. In addition, our experimental results show that each of the three types of slotted core cable is suitable for use in long haul high bit-rate transmission networks. It is therefore anticipated that the use of this type of terrestrial cable will continue to increase with the further deployment 10 Gb/sec systems and the imminent introduction of 40Gb/sec transmission networks.

9. Acknowledgments

The authors gratefully acknowledge Wayne Lewis, Yosuke Shimozuru and Hideaki Mizuguchi for the work reported in this paper and technical discussions.

10. Reference

[1] Franco Cocchini, Antonio Chiantore, Giovanni Carones^ and Alessandro Ginoccnio, "Cable effects on fiber PMD", 45th IWCS, 13 (1996)

[2] Kim Brising, "Polarisation mode dispersion field measurements -A survey of the swedish national network", 45th IWCS, 18 (1996)

[3] M.Nakano, Makiko Miura, Hideaki Mizuguchi, "Development of slotted core cable using Nonzero-dispersion Shifted Fiber", 48th IWCS, 5 (1999)

[4] Felix P. Kapron, "System considerations for polarization-mode dispersion",

[5] Steve A. Jacobs, James J. Refi, Robert E. Fangmann, "Statistical estimation of the PMD Coefficients of fiber paths", National Fiber Optic Engineers Conference, September 1997

[6] Steve A. Jacobs, James J. Refi, Robert E. Fangmann,"Statistical estimation of PMD Coefficient for system design", Electronics letters, 1997,33,pp.619-621

[7] R. C. Roman, Mark L. Lundergan and Sheila A. Cooper, "Characterization of optical Groundwire's cabled polarization mode dispersion performance as a function of axial strain and temperature: A case study", 45th IWCS, 37 (1996) B. Cerrou, M. Alard, and B. Le Floch, "Coded Orthogonal Frequency-Division Multiplexing," *Proc. User Services*, 81(6), 892-996 (June, 1995).

AUTHORS

Masakazu Nakano

Lucent Technologies Yazaki Ltd.

1157-106, Hotozawa, Gotemba-city, Shizuoka-Pref. 412-0046 JAPAN

M.Nakano received his B.E. degree from Nihon University in 1991. He has been engaging in Research & Development Department and his main work is development of evaluation technology with optical fiber, ribbon and cable.

Makiko Miura

Lucent Technologies Yazaki Ltd.

1157-106, Hotozawa, Gotemba-city, Shizuoka-Pref. 412-0046
JAPAN

Makiko Miura received her B.E. degree from Akita University in
1997. She has been engaging in Research & Development
Department and her main work is development of evaluation
technology with optical fiber, ribbon and cable.
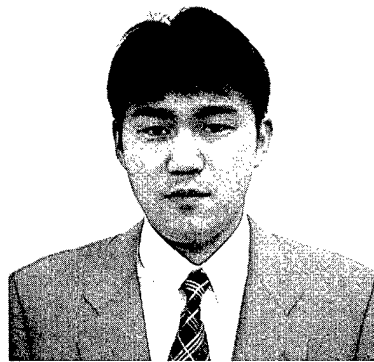
Toshihisa Sato

Lucent Technologies Yazaki Ltd.

1157-106, Hotozawa, Gotemba-city, Shizuoka-Pref. 412-0046
JAPAN

Toshihisa Sato received his M.S. degree from Tokai University in
1995. He has been engaging in Research & Development
Department and his main work is development of evaluation
technology with optical cable.

Gage Capability Analysis for Cable Manufacturing

Helen M. Bush, John E. Hogan, and Buddy C. Martin

Lucent Technologies

Norcross, GA

1 (770) 798-4689 · *hmbush@lucent.com*

Abstract

In this paper, we show the role gage capability studies play in assessing overall process capability and outline the steps to perform the study. We also show the importance of understanding the components of variation in the overall process and how to improve the process based on information from a gage capability analysis. The steps for performing an analysis are illustrated, and an example is given where an optical comparator, a video macroscope, and a machine vision system for measuring cable end samples are compared and evaluated.

Keywords

Gage capability; process capability; repeatability; reproducibility; variance components; cable end sample inspection; optical comparator; video macroscope; machine vision.

1. Introduction

Cable manufacturers rely on the accuracy of their measurements, and customers rely on that accuracy as well. Cable design specifications ensure that cables meeting the specifications will perform well in the field. Cost conscious manufacturers strive to make every cable as close as possible to the specification limit and cannot afford to throw away acceptable cables nor ship unacceptable cables. Therefore measurement accuracy is vital. Measurement devices are calibrated on a strict schedule, yet the variation of the measurements may receive little or no attention, for manufacturers assume that the results from their measurement devices are correct. Consider a cable manufacturing process that has just been evaluated as being *incapable*, that is, its variation is high with respect to its tolerance limits. It has been determined that the only way to make the process capable is to reduce the process variation. Reducing the variation within the product is no easy task and often requires time and money. What if a significant proportion of the process variation was due to the measurement process? Wouldn't that be easier to reduce?

A gage capability study is a useful tool for pinpointing the sources of high variation, whether a source is within the device itself or within the people who are using the device. It can also be used to determine whether or not the measurement error is reasonable with respect to the specification or tolerance limits.

When the error is too high, then the measurement process must be remedied. Gage capability studies are very useful in comparing measurement devices, procedures, working conditions, and training methods. This will ensure that the cable manufacturer is using the best device for the cost. Finally, the studies are also useful as supplementary information to a process capability analysis. If the process variation is too high, a gage capability analysis can help determine whether or not the process variance can be improved by changing the measurement process.

In the following section the components of variation will be presented, and the concepts of *process capability* and *gage capability* will be explained. The third section outlines the procedure for performing a gage capability study, and the fourth section presents an example case of comparing two devices that measure cable end samples.

2. Components of Variation

A manufacturing process is said to be *capable* if a small percentage of manufactured items fail to meet the specifications. Note that the user is allowed to control the definition of *small*. However, for reasons explained below, processes with normally distributed data are generally considered capable if less than 0.27% of the items fall outside the specification limits. Figure 1 below depicts the distribution of three processes with respect to their specification limits. The first process is capable. The second process is not capable because it is off-centered, and the third process is not capable because its variation is too high. USL and LSL are the upper and lower specification limits respectively.

The *natural tolerance limits* of a normally distributed process with mean μ and standard deviation σ are defined as the upper and lower 3σ boundaries. The percentage of the total distribution that exceeds these bounds is 0.27%. Hence, 99.73% of the population falls within a range of width 6σ. Therefore if no more than 0.27% of items from the process fail to meet the specifications, then the process is said to be *capable*. The process capability ratio (denoted *PCR* or *cp* in different texts) is defined as

$$PCR = cp = \frac{USL - LSL}{6\sigma}. \qquad (1)$$
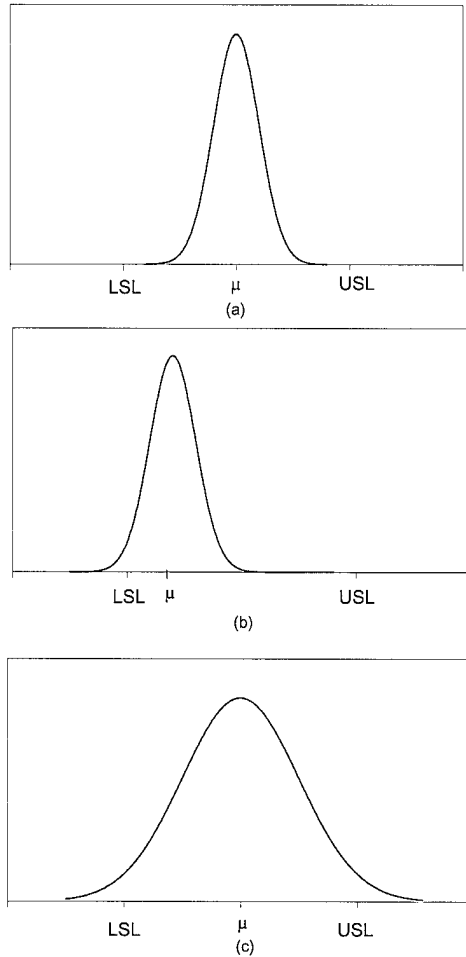
Figure1. Process Distributions of a (a) capable process (b) off-center mean (c) large variance

The process is capable when the ratio is equal to or greater than 1.

For non-centered processes, capability is measured as

$$PCR_k = cp_k = \min\left(\frac{\mu - LSL}{3\sigma}, \frac{USL - \mu}{3\sigma}\right). \quad (2)$$

Note that processes with only one specification limit use the same method for determining capability where

$$PCR_U = cp_U = \frac{USL - \mu}{3\sigma}, \quad (3)$$

and

$$PCR_L = cp_L = \frac{\mu - LSL}{3\sigma}. \quad (4)$$

When the process is not centered between the specification limits, then PCR measures *potential capability*, meaning that this is the best this process can achieve without reducing the process variation.

For example, if a process has a PCR of 1.05, but a PCR$_k$ of 0.85, then it requires a shift in the mean to become capable. Changes in the mean are often easy to control. However, if PCR equals 0.90, then the process will not be capable after an appropriate shift in the mean. This process will require a reduction in process variance in order to become capable.

Any variation between items from the same manufacturing process is understood to be the natural variation of the product. This *observed*, *process* or *total* variation is often referred to as *process noise*. However, this noise has several components. In addition to the *product* variation, there is a variation due to the measurement device, called *gage* or *measurement* variation where

$$\sigma^2_{total} = \sigma^2_{product} + \sigma^2_{gage}. \quad (5)$$

It is important that cable manufacturers know the sources of variation in their measurements so that they can address the appropriate sources in order to reduce the observed variation. When the measurement error is small with respect to the product variation, then a reduction in measurement error will not have a large impact on the total variation, and hence on the process capability. When the measurement error is large, then there is an opportunity to reduce the observed noise without having to change the manufacturing process. The definition of *large* and *small* here is subjective, depending on the particular manufacturing situation. However, there is a standard rule of thumb to comparing the measurement error to the specification limits. Individual measurements are often well characterized by a normal distribution, so measurements can be expected to vary by $\pm 3\sigma_{gage}$. The ratio of $6\sigma_{gage}$ to the range of the specification limits is called the *precision to tolerance* ratio, where

$$\frac{P}{T} = \frac{6\sigma_{gage}}{USL - LSL}. \quad (6)$$

If the precision to tolerance ratio is less than 0.10, then the gage is considered to be capable. Note the difference between process capability and gage capability. Process capability describes the entire process and depends on the distribution of the observed data and the specification limits. It reflects how well the specifications are met and includes gage performance. Gage capability depends on the variance of the gage and the specification limits. It only reflects the adequacy of the measurement process.

The gage variation can have several components itself: *repeatability* variation is the source of variation within the device, and *reproducibility* variation is due to different people using the device, where

$$\sigma^2_{gage} = \sigma^2_{measurement} = \sigma^2_{repeatability} + \sigma^2_{reproducibility} \quad (7)$$

so that

$$\sigma_{total}^2 = \sigma_{product}^2 + \sigma_{repeatability}^2 + \sigma_{reproducibility}^2 . \quad (8)$$

When the measurement variation is too high, it is often the case that only one component is inflated. Reduction of these noise sources requires different approaches. Repeatability error is the error associated with the measurement device itself. Therefore the most obvious approach to reducing repeatability error is to replace the measurement device. However, before changing to a new device, investigate the possibility of changing the standard method of using the device such as settings, instructions for gage usage, sample preparation, and the environment in which measurements are taken. Compare your procedures with the device manufacturer's recommendations.

Reproducibility is the error associated with the differences in the way different operators use the measurement device. This source of variation can be significant when the person is required to make judgments, such as a visual alignment. But other places where the operators can significantly diverge is in sample preparation, test set-up, device settings, and gage usage. Reproducibility can often be improved through standardizing methods and retraining.

3. Repeatability and Reproducibility Studies

The key to estimating measurement error is having multiple measurements on the same item from the same person or persons. An essential requirement is that the measurements be *blind*, meaning that there is no memory of previous measurements. If an operator performs all required measurements of a sample at one time, then it is extremely likely that the measurement error will be dramatically underestimated. The results will be remembered, and the sample set-up will be the same. If each set-up and measurement is performed blind to previous measurements, then the experiment will reflect true measurement variation. Therefore it is recommended that a sufficiently long length of time elapse between each set of measurements, such as one day, and there should be no access to any previous results while measurements are being taken. Additionally, the order in which the samples are measured should be randomized for each set.

There are two main methods of estimating the components of variation in gage capability studies, the range method and the sum of squares method. The range method is described here and is the more traditional and simple method. The sum of squares method is similar to sample standard deviations and is not complicated for one experienced in ANOVA table methodology [1] and is an option in statistical software packages that perform gage capability studies [2]. However it is generally accepted that the range method performs at least as well as the sum of squares method for estimating variance when the number of trials and operators are each less than ten and the data

is normally distributed. In most circumstances, a thorough gage capability study does not require that many observations so the range method of estimation will almost always be appropriate.

It is well known in statistical literature that there is a relationship between the range of a sample from a normally distributed population and the standard deviation [3]. In fact, the ratio of the range to the standard deviation, the *relative range*, has a known distribution. Through this relationship, it is possible to estimate the standard deviation of a population from the range of a sample. This technique is used to create standard $\bar{x}$ and R statistical process control charts where the standard deviation is estimated by

$$\hat{\sigma} = \frac{R}{d_2(h)} , \quad (9)$$

where $d_2(h)$ is the mean of the relative range and is a function of the sample size, h. All quality control textbooks or handbooks should have a table that shows $d_2(h)$.

In order to estimate each of the variation components, repeatability, reproducibility, and product variance, n objects must be measured m times by p operators. For each object and operator, calculate the range of the m measurements

$$R_{ij} = \max(x_{ijk}) - \min(x_{ijk}), \quad (10)$$

for $i = 1,\ldots,p$, $j = 1,\ldots,n$, and $k = 1,\ldots,m$. Then, for each operator calculate the average range.

$$\bar{R}_i = \frac{\sum_{j=1}^{n} R_{ij}}{n} . \quad (11)$$

Next calculate the overall average range

$$\bar{\bar{R}} = \frac{\sum_{i=1}^{p} \bar{R}_i}{p} . \quad (12)$$

The repeatability component is estimated as

$$\hat{\sigma}_{repeatability} = \frac{\bar{\bar{R}}}{d_2(m)} . \quad (13)$$

Note that the sample size used to create each of the ranges is the number of times each item was measured per operator, m.

The reproducibility component is a function of the range of average measurements across all operators. For each object and operator, calculate the average of the m measurements

$$\overline{x}_{ij} = \frac{\sum_{k=1}^{m} x_{ijk}}{m}, \tag{14}$$

and the total average for each operator,

$$\overline{\overline{x}}_i = \frac{\sum_{j=1}^{n} \overline{x}_{ij}}{n}. \tag{15}$$

Finally calculate the range of the p total averages,

$$R_{\overline{\overline{x}}} = \max(\overline{\overline{x}}_i) - \min(\overline{\overline{x}}_i). \tag{16}$$

The reproducibility component is estimated as

$$\hat{\sigma}_{reproducibility} = \frac{R_{\overline{\overline{x}}}}{d_2(p)}. \tag{17}$$

The sample size used for this estimate is the number of operators, p, because $R_{\overline{\overline{x}}}$ is the range of the p operator average measurements.

The measurement error is then

$$\hat{\sigma}_{gage}^2 = \hat{\sigma}_{repeatability}^2 + \hat{\sigma}_{reproducibility}^2. \tag{18}$$

The variation within the product is a function of the range of the average measurement across all trials and operators. Let

$$\overline{x}_j = \frac{\sum_{i=1}^{p} \overline{x}_{ij}}{p}, \tag{19}$$

and

$$R_{parts} = \max(\overline{x}_j) - \min(\overline{x}_j). \tag{20}$$

Therefore

$$\hat{\sigma}_{product} = \frac{R_{parts}}{d_2(n)}. \tag{21}$$

Here, the sample size is n because the range is calculated from the averages of each of the n parts.

The total variation is then

$$\hat{\sigma}_{total}^2 = \hat{\sigma}_{product}^2 + \hat{\sigma}_{gage}^2. \tag{22}$$

Refer to the example in Appendix A for calculation demonstrations. At this point the precision to tolerance ratio can be calculated to assess gage adequacy with respect to the specifications, and the various components can be compared to determine where improvement projects should be focused.

Though the equations for all the calculations are given here, and they are not complicated to follow, most statistical process control software packages will analyze a gage repeatability and reproducibility study automatically and can estimate the variance components with the range method or with the sum of squares method. The packages provide graphs and other features that compliment the basic analysis. Such features will be shown in the next section to demonstrate how a gage repeatability and reproducibility study was used to evaluate three devices used in end sample inspection.

4. Cable End Sample Inspection Example

Cables undergo a rigorous inspection procedure to ensure that outgoing cable quality is high. Part of the inspection process is a verification that the cables meet the dimensional requirements. The verification includes both on-line measurements and cable sampling. Samples cut from the cables are measured, recorded, and tracked through statistical process control techniques.

Traditionally, the end samples are measured using an optical comparator. When we needed new measurement systems, we decided to look at other technologies in addition to existing systems to improve ease of use while maintaining or improving the measurement accuracy and precision. In addition, reducing the measurement time was also desirable. The other systems available for analysis were a video macroscope and a machine vision system.

The optical comparator is an analog device. The device has infinite resolution but poor image clarity. Operators are required to make judgments and alignments during use. The video macroscope is a digital device and operates similarly to the optical comparator in that the operators make the same judgments and alignments. However, the video macroscope has much better image clarity, but poorer resolution. The last option considered is a machine vision system. As with the other devices the operator is required to prepare the sample and place it in the appropriate fixture, but with this system the device makes the measurements. It is also a digital technology, but greater resolution can be achieved by interpolating between pixels, also known as *sub-pixelizing*. While image clarity for the operator is not an issue, sample lighting is the key to reliable and accurate measurements. The machine vision device can make many measurements in a small amount of time, whereas the manual methods take more time. This enables us to take more measurements than we normally would with a human. The main aspects of the three technologies are compared in Table 1 below.

Table 1. Technology Comparison

Optical Comparator	Video Macroscope	Machine Vision
Human	Human	Machine
Analog	Digital	Digital

For simplicity of illustration, the device comparison has been limited to the consideration of three variables. The first variable is the outside cable diameter. The second and third variables are the core tube outside and inside diameters respectively. All variable measurements have undergone a transformation that will not affect the conclusions, but will protect the privacy of the process data.

Appropriate steps were taken to ensure that the measurements were blind. Twenty end samples from twenty cables of the same design were collected. These samples were stored in a divided tray with twenty numbered slots for the samples, so that the samples could be identified without marking the specific sample. For the manual devices, two people were present when measurements were taken. One person took the measurements, and the other person recorded the results and kept track of the samples. Neither person had access to any previous measurements. With the machine vision device, the data was stored as the measurements were made. Needless to say, the device was blind to its own previous measurements.

One distinct advantage of using a software package to analyze the results of such a study is the graphical features available. If a specialized software package is not available, then plots can be made with spreadsheet software. Plots that compare the spread of the measurements and any differences between the operators can be very useful in interpreting the results. For example, suppose the reproducibility component of variance was very high, a graphical representation of the data would show whether or not it was due to a few outliers or if the operators were indeed measuring the samples in different ways.

Several plots generated for the analysis follows. The first set, Figures 2 - 4, compares the variability within the three operators. It shows the range of the three trials for each part and operator. One plot is generated for each measurement device. The scale is not shown, but it is the same for all three graphs.
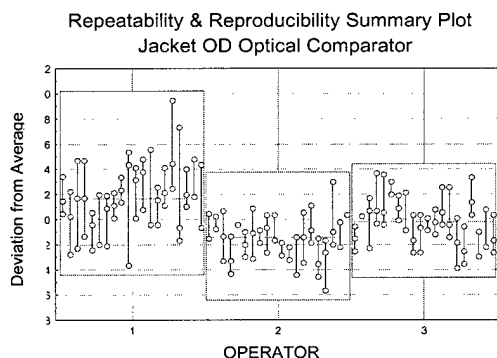
Figure 2. Repeatability and Reproducibility Plot of Jacket Outside Diameter Optical Comparator
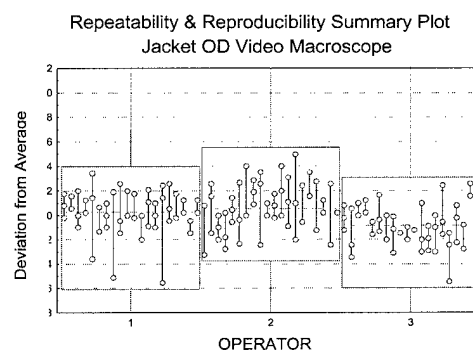
Figure 3. Repeatability and Reproducibility Plot of Jacket Outside Diameter Video Macroscope
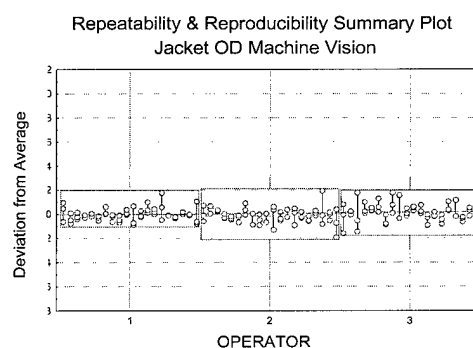
Figure 4. Repeatability and Reproducibility Plot of Jacket Outside Diameter Machine Vision

The next set of plots, Figures 5 – 7, shows the average of the three measurements per part for each operator. It is useful in seeing differences between the operators. Again, the scale is the same for each graph in the set.
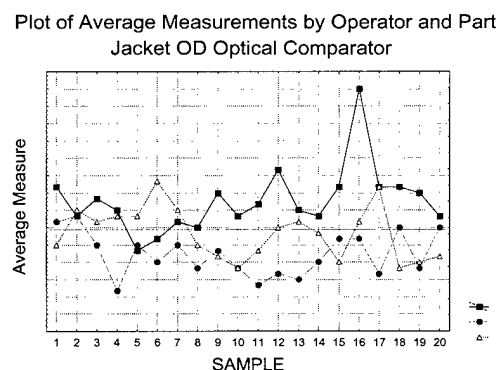
Figure 5. Average Measurement by Operator per Part: Optical Comparator

Plot of Average Measurements by Operator and Part
Jacket OD Video Macroscope
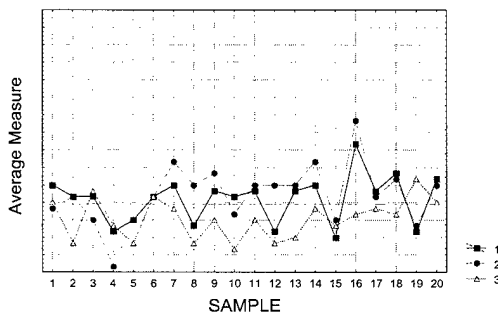
Figure 6. Average Measurement by Operator per Part: Video Macroscope

Plot of Average Measurements by Operator and Part
Jacket OD Machine Vision
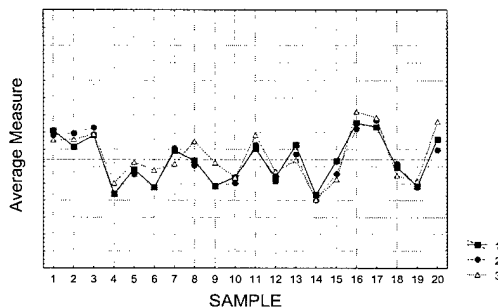
Figure 7. Average Measurement by Operator per Part: Machine Vision

These graphs show several important things. First, the machine vision system has the lowest variance. It is significantly more consistent than the other devices. Figures 2-4 show that the largest deviation from the average value is about one unit for the machine vision, but is closer to five for the optical comparator and four for the video macroscope. Figures 5-7 show that for the machine vision system there is very little difference between the operators, whereas it is apparent that the operators measure the samples differently, or there is a *bias* when using the other devices. For example, with the optical comparator Operator 1 tends to have the highest measurement, and Operator 2 tends to have the lowest. The human-dependent devices require the operators to make the actual measurements, and though they have received the same instruction on measurement methods, it is natural that each has his or her own tendencies. The machine vision system is not subject to the same degree of bias between operators because the operator places the sample in a fixture, and the machine does the rest. Any significant differences between the operators would be in sample preparation and placement. The actual standard deviation estimates are in Tables 2-4 below.

Table 2. Jacket Outside Diameter

	Optical Comparator	Video Macroscope	Machine Vision
$\hat{\sigma}_{repeatability}$	1.93	1.63	0.52
$\hat{\sigma}_{reproducibility}$	1.53	0.71	0.17
$\hat{\sigma}_{product}$	0.87	1.08	1.38
$\hat{\sigma}_{total}$	2.61	2.08	1.48

Table 3. Core Tube Outside Diameter

	Optical Comparator	Video Macroscope	Machine Vision
$\hat{\sigma}_{repeatability}$	4.04	4.47	1.89
$\hat{\sigma}_{reproducibility}$	0.69	0.81	0.13
$\hat{\sigma}_{product}$	2.48	2.64	2.87
$\hat{\sigma}_{total}$	4.79	5.25	3.44

Table 4. Core Tube Inside Diameter

	Optical Comparator	Video Macroscope	Machine Vision
$\hat{\sigma}_{repeatability}$	4.23	4.62	0.96
$\hat{\sigma}_{reproducibility}$	1.54	1.66	0.06
$\hat{\sigma}_{product}$	2.24	2.51	3.11
$\hat{\sigma}_{total}$	5.03	5.52	3.25

For all of the variables, the machine vision system has a drastically reduced measurement error and of course, a more desirable total variance. However, in each case the estimate of the product or part to part variance is higher. Because the same samples were measured repeatedly, the actual product variance can neither decrease nor increase with operator or measurement device. However, much of the variance between the end samples with the other systems was masked by the large measurement error. This is clearly seen in Figures 5-6. When the measurement error is small, the true variance between the end samples is seen and may be captured by the estimate. When the measurement error is large, differences between parts are difficult to detect. Therefore, another important comparison to make is what percent is the measurement error of the total observed error? The results are in Table 5 below. With the optical comparator and the video macroscope the measurement error explains more than 70% of the total variance. With the machine vision system, the measurement error explains 9% to 30% of the total.

Table 5. Measurement Error as a Percent of Total Variation

	Optical Comparator	Video Macroscope	Machine Vision
Jacket OD	89.0	73.1	13.7
Core Tube OD	73.2	74.9	30.3
Core Tube ID	80.1	79.1	8.8

Though not shown here, the precision to tolerance ratio in Equation 6 was calculated for each of the variables, and all were at acceptable levels of less than 0.10 using the machine vision system. This means that the degree of variation that arises from use of the machine vision system is capable with respect to the variable specifications, and that the system would be an acceptable choice.

In this example, the purpose of the study was to select a measurement device to purchase. This should not be done without examining its impact on process capability. A measurement process that reduces the overall variation will have a positive impact on process capability, so it is important to note the improvement in process capability. The results may be helpful in performing a cost/benefit analysis of changing the measurement process. Though our process was already considered capable, Table 6 illustrates the dramatic improvement the machine vision system has on the overall capability of the process.

Table 6. Improvement in Process Capability

	% Improvement
Jacket OD	72
Core Tube OD	107
Core Tube ID	55

5. Conclusion

A gage capability analysis is an important tool in the overall process capability analysis. If the process is not capable and the variance of the process must be reduced, a gage capability analysis is the best next step. It quantifies the components of variance and one can discern whether or not the measurement process is a major contributor to the overall process capability problems. If that is the case, then the analysis also pinpoints whether the problems are operator or measurement device specific. If the task at hand is to select a measurement device or procedure, then a gage capability analysis is useful in making comparisons as shown in the example of cable end sample inspections. In looking to purchase more measurement devices, three technologies were compared, the current method of measurement and two other technologies. The study showed that a machine vision system had the lowest measurement and overall variance and met the requirement of gage capability, leading to improved process capability.

6. Acknowledgments

7. References

[1] George E. P. Box, William B. Hunter, and J. Stuart Hunter, *Statistics for Experimenters*, John Wiley and Sons, New York, (1978).

[2] *Statistica Volume IV: Industrial Statistics*, Statsoft, Tulsa 4171-4174 (1995).

[3] Douglas C. Montgomery, *Introduction to Statistical Quality Control* 2nd ed., John Wiley and Sons, New York, 204, 390 – 396 (1991).

Appendix A
Calculation Example

Part Number	Operator 1 Measurement 1	2	$\overline{x}_{1j}$	R_{1j}	Operator 2 Measurement 1	2	$\overline{x}_{2j}$	R_{2j}	$\overline{x}_j$
1	49	50	49.5	1	50	51	50.5	1	50.0
2	45	44	44.5	1	45	44	44.5	1	44.5
3	54	54	54.0	0	51	51	51.0	0	52.5
4	53	51	52.0	2	53	52	52.5	1	52.3
5	48	49	48.5	1	49	48	48.5	1	48.5
6	49	48	48.5	1	50	49	49.5	1	49.0
7	49	50	49.5	1	49	49	49.0	0	49.3
8	57	57	57.0	0	55	53	54.0	2	55.5
9	52	51	51.5	1	52	50	51.0	2	51.3
10	48	49	48.5	1	48	49	48.5	1	48.5

$$\overline{\overline{x}}_1 = 50.3$$
$$\overline{R}_1 = 0.9$$

$$\overline{\overline{x}}_2 = 49.90$$
$$\overline{R}_2 = 1.0$$

$$\hat{\sigma}_{repeatability} = \frac{\overline{\overline{R}}}{d_2} = \frac{\frac{1}{2}(.9 + 1.0)}{1.128} = .842$$

$d_2(2) = 1.128$. It's based on a sample size of 2 because each operator measured each part twice.

$$\hat{\sigma}_{reproducibility} = \frac{R_{\overline{\overline{x}}}}{d_2} = \frac{(50.35 - 49.90)}{1.128} = .399$$

$d_2(2) = 1.128$. It's based on a sample size of 2 because there are 2 operators ($R_{\overline{\overline{x}}}$ is based on two observations).

$$\hat{\sigma}^2_{gage} = \hat{\sigma}^2_{repeatability} + \hat{\sigma}^2_{reproducibility} = .842^2 + .399^2 = .868$$

$$\hat{\sigma}_{gage} = \sqrt{.868} = .932$$

$$\hat{\sigma}_{product} = \frac{R_{parts}}{d_2} = \frac{55.5 - 44.5}{3.078} = 3.57$$

$d_2(10) = 3.078$. It's based on a sample size of 10 because the averages of 10 parts were used to calculate this range.

$$\hat{\sigma}^2_{total} = \hat{\sigma}^2_{product} + \hat{\sigma}^2_{gage} = 3.57^2 + .868 = 13.64$$

$$\hat{\sigma}_{total} = \sqrt{13.64} = 3.69$$

Helen Bush is a Member of the Technical Staff at Lucent Technologies in the Fiber Optics Outside Plant Cable Manufacturing Engineering group. Her projects focus on process improvement, and her primary responsibilities include designing and executing data analysis, statistical process control, data modeling, design of experiments, root cause analysis, and simulation modeling.

Helen graduated from the Georgia Institute of Technology in 1996 with a Ph.D. in Industrial Engineering specializing in engineering statistics, and her thesis is in nonparametric multivariate quality control. Helen taught several undergraduate courses while she was at Georgia Tech, including *Introduction to Statistical Process Control*, and *Engineering Statistics*. She received her Masters degree from the Georgia Institute of Technology in 1993 in Statistics and her Bachelors degree from Mississippi State University in Industrial Engineering in 1992.

John Hogan is a Member of the Technical Staff at Lucent Technologies in the Fiber Optics Outside Plant Cable Manufacturing Engineering group. His projects focus on process improvement, process control and automation, computer integrated manufacturing, and SAP projects.

John graduated from Georgia Institute of Technology in 1997 with a Ph.D. in Mechanical Engineering specializing in manufacturing automation and robotics. He received his Masters and Bachelors degree in Mechanical Engineering from Georgia Institute of Technology in 1994 and 1992.

Buddy Martin started his career with Western Electric in 1972. He spent the first years working in the copper and fiber optic cable manufacturing areas. In 1986 Buddy became a part of the Training Organization helping to create structured training programs. He has been responsible for development, documentation and administration of training programs for the Fiber Optic Sheathing and Final Packaging area for the Norcross facility. He works with Engineering to develop and design training courses to cover new manufacturing equipment. He is also responsible for coordinating and conducting training for new personnel in the Fiber Optic Sheathing, Final Test, AccuRibbon™ and Final Packaging areas. He performs the certification of more than 185 employees and is responsible for conforming training procedures to ISO 9001 standards. Buddy has coordinated and conducted training for managers and engineers of joint ventures including facilities in Beijing, Thailand and India.

Computer Modeling of Optical Fiber Drawing Process

Jaydeep A. Kulkarni, Srinivas Chippada, Ashwini Kumar, and Eric W. Grald

Fluent Inc.
Evanston, Illinois 60201
+1-847-491-0200 · jak@fluent.com

Abstract

Optical glass fibers are typically formed by heating and drawing under tension a preform of silica glass in a concentric, cylindrical graphite furnace. The primary modes of energy transport are the radiative and the convective heat exchange of the furnace wall with the inert gas inside the heating zone. The main objective of the present work is to simulate the neck-down profile of the fiber as a function of the operating variables such as draw speed and inert gas velocity. The 2-D axi-symmetric, laminar flows of the glass perform/fiber and the inert gas are simulated using the finite element method. The simulation couples heat and momentum transport in the fiber with that in the gas through the boundary conditions on the fiber surface. The diameter of the glass fiber is predicted by employing a deforming mesh free surface approach. Temperature dependence of key material properties of the fiber is taken into account. The commercial computational fluid dynamics (CFD) program, FIDAP (Fluent Inc., Lebanon, NH), is used to obtain the results presented.

Keywords

Optical fiber; glass fiber; fiber drawing; radiation; FIDAP.

Introduction

Krishnan and Glicksman [1] were one of the first researchers to perform analytical and experimental studies to study the transport processes in a heated free jet. They used a pre-specified radially lumped temperature distribution and a two-dimensional velocity distribution with an assumed profile to generate the shape of the jet. Kase and Matsuo [2], and Brown [3] performed one-dimensional analyses of the fiber formation from glass flowing through a nozzle rather than from a preform in the furnace. Since these studies were conducted by treating the glass flow as a jet, they have limited applicability in the present day optical fiber production. Paek and Runk [4] experimentally and numerically investigated the fiber drawing process by assuming a heat flux distribution at the furnace and employing a radiation model to determine the radiative heat input at the glass surface. Employing the Rosseland approximation for an optically thick medium, lumped axial velocity and temperature distributions, and a specified heat transfer coefficient at the fiber surface, they studied the thermal transport in the optical fiber drawing process. Myers [5] concentrated specifically on the disturbances that may occur in the fiber drawing process ignoring inertia, gravity, and surface tension. Both, Peak and Runk [4] and Myers [5] investigated flow only in the glass region excluding that in the gas. Kaminsky [6] was amongst the first researchers to model

the radiative heat transport in the neck-down region without using Rosseland approximation. In her study, she employed the P1 approximation for the radiative transfer in the glass, but her model only considered the upper neck-down region where the diameter is relatively large. In addition, a two-dimensional model was introduced for analyzing the glass and gas flows and radiation. Chaudhury *et. al.* [7] have used the zonal method instead of the Rosseland approximation to model radiation and have studied the conjugate problem involving both glass and the glass. In order to solve the resulting transport equations, they used a false transient scheme coupled with an alternating direction implicit (ADI) approach. In this approach, a radial lumping of the axial velocity is employed for the purposes of simplifying the iterative scheme.

The present work extends the applicability of a deforming mesh free surface approach to relatively high draw ratios. Kaminsky [6] used this approach to simulate a fiber profile for a draw ratio of 100, whereas in this work results are presented for draw ratios of 144 and 576. Furthermore, a systematic procedure to obtain stable solutions for the fiber profile is presented, which is expected to make even higher draw ratios accessible by the deforming mesh approach. The algorithm employed in FIDAP for modeling free surfaces uses an "Arbitrary Lagrangian Eulerian (ALE)" description where the mesh is moved at a velocity different than that of the material. In this approach, no *ad hoc* assumption/approximation is made while updating the free surface location during the solution phase.

The organization of the paper is as follows: First the problem is described in Section 1. Governing equations and boundary conditions are presented in Section 2. The finite element formulation is described briefly in Section 3. Section 4 deals with the solution strategy. Results and discussion are presented in Section 5 and conclusions are drawn in Section 6.

1. Problem Description

The schematic of a typical optical fiber drawing process is shown in Figure 1. As the glass preform is drawn vertically through the furnace, its temperature increases as it gains heat due to the radiative transport and, thus, its viscosity decreases. Under the action of tension, the diameter of the fiber decreases as well. An inert gas is introduced either in a concurrent or a countercurrent direction with respect to the motion of the preform. Among the main quantities of interest are the final fiber diameter resulting from the given processing conditions as well as the temperature distribution in the furnace and within the fiber. Conversely, it is also of interest to

know the tension in the fiber required to obtain the desired fiber diameter.

As shown in Figure 1, R_{in} is the radius of the preform at the entrance of the furnace and R_{out} is the final radius of the fiber at the exit. The preform enters the furnace with a velocity $u_{in,glass}$ and temperature $T_{in,glass}$. The inert gas enters the furnace at a temperature $T_{in,gas}$ with a velocity $u_{in,gas}$. The furnace is assumed to have a parabolic temperature profile with the maximum temperature, $T_{f,max}$, in the center and minimum temperature, $T_{f,min}$, at the entrance and the exit. R_{out} and $u_{out,glass}$ are the radius and the velocity of the fiber at the exit, respectively. Similarly, $u_{out,gas}$ is the velocity of the inert gas at the exit. The geometrical parameters and the boundary conditions are summarized in Table 1.
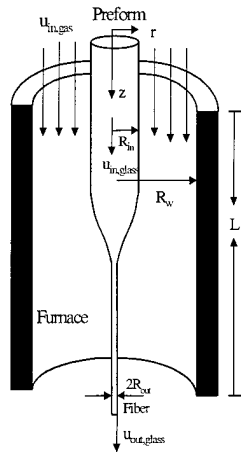
Figure 1. Schematic representation of a typical optical fiber drawing process

Table 1. Geometrical Parameters and Boundary conditions

R_w	0.019 m	$T_{in,glass}$	1900 K
R_{in}	0.006 m	$T_{in,gas}$	1900 K
R_{out}	0.0005 m	k_{glass}	2.68 W/mK
L	0.0254 m	$C_{P,glass}$	1046 J/KgK
ρ_{glass}	2200 kg/m^3	$C_{P,gas}$	5190 J/KgK
ρ_{gas}	0.022 kg/m^3	ε_w	0.75
$U_{in,glass}$	0.01 m/s	n	1.5
$U_{in,gas}$	0.1 m/s	$T_{f,max}$	3000 K
T_{melt}	1900 K	$T_{f,min}$	2300 K
		γ	200 /m

2. Theory
2.1 Governing Equations

In the present work, the flow is studied using a 2-D axi-symmetric geometry. Because the Reynolds number is low in both, gas and glass, flow is considered laminar in both the phases. Furthermore, both the phases are treated as Newtonian and incompressible. Stress-divergence form of the momentum equation is used since it results in a natural boundary condition that can be interpreted as the components of the stress acting on the fluid at the boundary. This interpretation is particularly useful for solving free surface problems involving boundary conditions in terms of stress. Thus, the continuity and the momentum equations in either of the phases can be written as:

$$\nabla \cdot \mathbf{u} = 0 \tag{1}$$

$$\rho\left(\frac{\partial \mathbf{u}}{\partial t} + \mathbf{u} \cdot \nabla \mathbf{u}\right) = -\nabla p + \nabla \cdot \left[\mu\left(\nabla \mathbf{u} + \nabla \mathbf{u}^T\right)\right], \tag{2}$$

where ρ and μ are the density and the viscosity of the phase, respectively. Gravity is ignored since its contribution is expected to be small for a thin filament. The viscosity of glass is taken [5] as

$$\mu(T) = 10^7 \exp\left[32\left(\frac{T_{melt}}{T} - 1\right)\right], \tag{3}$$

where T_{melt} is the melting point of glass. The inert gas is assumed to be Helium and the temperature dependence of its viscosity [8] is given in Table 2.

Table 2. Viscosity of Helium

T(K)	μ (Ns/m^2) x 10^{-6}	T(K)	μ (Ns/m^2) x 10^{-6}
1800	65.7	2200	74.2
1900	67.9	2300	76.3
2000	70.0	2400	78.3
2100	72.2	2500	80.2

Those material properties that are assumed to be constant are summarized in Table 1. The two phases are considered to be non-participating for the radiative heat transport and hence there is no heat generation in the two phases due to radiation. Since the viscosity of glass is very strongly dependent upon the temperature and as such has strong gradients in the neck-down region, viscous dissipation cannot be neglected. Thus, the energy equation in each phase becomes:

$$\rho C_p\left(\frac{\partial T}{\partial t} + \mathbf{u} \cdot \nabla T\right) = k\nabla^2 T + 2\mu\mathbf{s}:\mathbf{s}, \tag{4}$$

where C_p and k are the specific heat and the conductivity of the phase and $\mathbf{s}$ is the rate of strain tensor defined as

$$\mathbf{s} = \frac{1}{2}\left(\nabla \mathbf{u} + \nabla \mathbf{u}^T\right). \tag{5}$$

The specific heats of the two phases are assumed to be constant. Rosseland diffusion approximation is used to model the radiative heat transport within glass. Hence, the effective thermal conductivity of glass can be written as

$$k = k_c + k_r, \tag{6}$$

where k_c is the molecular conductivity and k_r is the radiative conductivity which can be modeled as [4,5]:

$$k_r = \frac{16n^2\sigma T^3}{3\gamma}. \tag{7}$$

Here, n and γ are the refractive index and the absorption coefficient of glass and σ is the Stefan-Boltzmann constant. Thermal conductivity of Helium is assumed to be temperature dependent and is given in Table 3.

Table 4. Thermal Conductivity of Helium

T(K)	k (W/mK)	T(K)	k (W/mK)
1800	0.570	2200	0.669
1900	0.596	2300	0.693
2000	0.620	2400	0.716
2100	0.644	2500	0.739

In order to model the radiative heat transfer between the glass surface and the furnace wall, it is assumed that the fiber surface and the wall furnace are gray and diffuse. A closed enclosure is constructed consisting of four bounding surfaces – the fiber surface, gas inlet, furnace wall and the gas outlet. Each one of these faces is divided into many, constant radiosity zones. In the present study, each zone corresponds with the respective face (i.e., an edge in the axi-symmetric analysis) of a finite element used in the finite element analysis. View factors among all the surface zones are computed by the FACET algorithm [9] employing an area integration technique. It should be noted that, for each zone i,

$$\sum_{j=1}^{N} F_{ij} = 1, \tag{8}$$

where F_{ij} is the view factor between zones i and j and N is the total number of zones. The resulting heat exchange between the zone i and the other radiating zones is given by

$$\sum_{j=1}^{N}\left(\frac{\delta_{ij}}{e_j} - F_{ij}\frac{1-e_j}{e_j}\right)\mathbf{q}_r^j = \sum_{j=1}^{N}\left(\delta_{ij} - F_{ij}\right)\sigma T_j^4, \tag{9}$$

where e is the emissivity and $\mathbf{q}_r^j$ is the radiative heat flux. δ_{ij} is the Kronecker delta defined as

$$\delta_{ij} = \begin{cases} 1...\text{when } i = j \\ 0...\text{when } i \neq j \end{cases} \tag{10}$$

2.2 Boundary Conditions
The boundary conditions are as follows:

$$u_r = 0, u_z = u_{in,glass}, T = T_{in,glass} \qquad \text{at } z = 0, 0 \leq r \leq R_{in} \tag{11}$$

$$u_r = 0, u_z = u_{in,gas}, T = T_{in,gas} \qquad \text{at } z = 0, R_{in} < r < R_w \tag{12}$$

$$u_r = u_z = 0, T = \text{parabolic profile}\left(T_{f,min} - T_{f,max}\right) \\ \text{at } 0 \leq z \leq L, r = R_w \tag{13}$$

$$\frac{\partial u_z}{\partial r} = 0, u_r = 0, \frac{\partial T}{\partial r} = 0 \qquad \text{at } r = 0, 0 \leq z \leq L \tag{14}$$

$$u_z = u_{out,glass}, u_r = 0, \frac{\partial T}{\partial z} = 0 \qquad \text{at } z = L, 0 \leq r \leq R_{out} \tag{15}$$

$$\sigma_{zz} = 0, \frac{\partial T}{\partial z} = 0 \qquad \text{at } z = L, R_{out} < r < R_w \tag{16}$$

Following boundary conditions hold at the free surface which is the interface between the fiber and the inert gas:

$$\mathbf{u} \cdot \mathbf{n}\big|_{glass} = \mathbf{u} \cdot \mathbf{n}\big|_{gas}, \mathbf{u} \cdot \mathbf{t}\big|_{glass} = \mathbf{u} \cdot \mathbf{t}\big|_{gas} \tag{17}$$

$$T_{glass} = T_{gas} \tag{18}$$

$$-k\nabla T \cdot \mathbf{n}\big|_{glass} = -k\nabla T \cdot \mathbf{n}\big|_{gas} + \mathbf{q}_r \cdot \mathbf{n} \tag{19}$$

$$\sigma \cdot \mathbf{t}\big|_{glass} = \sigma \cdot \mathbf{t}\big|_{gas} \tag{20}$$

$$\sigma \cdot \mathbf{n}\big|_{glass} - \sigma \cdot \mathbf{n}\big|_{gas} = 2\gamma H\mathbf{n} = 0 \ (\because \text{surface tension is neglected}) \tag{21}$$

Surface tension is neglected in the present analysis since its contribution in determining the free surface shape is expected to be small for highly viscous flows.

3. Finite Element Formulation
A structured mesh consisting of quadratic (9-noded) quadrilateral elements is used for the present analysis. 9-noded elements were found to give more accurate and stable results as compared to linear (4-noded) quads due to large gradients in pressure arising from rapid changes in the viscosity of glass. The mesh consists of 20 elements in the r direction, 10 in each one of the two phases, and 100 in the z direction. Grading is applied closer to the furnace wall to capture the velocity and thermal gradients and also in the vicinity of the free surface to accurately track its movement.

The governing equations are solved using a commercial CFD code, FIDAP (Fluent Inc., Lebanon, NH), which is based on the Galerkin finite element method. FIDAP has a fully coupled numerical method in which all degrees of freedom are solved simultaneously using a Newton-Raphson type technique. It also

has a segregated method in which all degrees of freedom are solved in a sequential manner including the pressure degree of freedom which is decoupled from velocities. The fiber shape is not known *a priori* and is computed using the moving mesh free surface technique. The free surface method is based on the arbitrary Lagrangian-Eulerian (ALE) approach in which the mesh nodes are moved (remeshed) in a manner independent of the material velocity. Several remeshing techniques are available in FIDAP. In the present study, the spines technique, in which the nodes are constrained to move along predefined straight spines, is used.

4. Solution Strategy

The overall problem is severely non-linear and coupled due to the presence of radiation and a free surface, and also due to rapidly changing physical properties. Hence, it is important to provide a good initial guess to ensure stability of the solution. With this objective in mind, the simulation is divided into the following sequential steps:

1. Isothermal run: The material properties of glass and the gas are set at their values corresponding to the temperatures of 1900 K and 2300 K, respectively. Then, the velocity field is calculated with an assumed shape of the glass-gas interface and in the absence of radiation. In the present study, a cosinusoidal shape is used as a guess for the interface shape. A fully coupled solver (Newton Raphson) is used.

2. Radiation run: Using the velocity field from the isothermal run, the new flow and temperature fields are computed in the presence of radiation. As mentioned earlier, the two phases are considered non-participating. An enclosure analysis is employed to account for the surface to surface internal radiative heat exchange. All the surfaces are assumed to be gray and diffuse. The emissivity of the gas inlet and outlet boundaries is set equal to 1. The emissivity of the fiber surface is assumed to be a function of fiber diameter [5] and its value varies from that of 0.6 in the preform region to 0.1 in the fiber region. View factor calculation is done only once at the beginning of the simulation by properly accounting for the obstruction posed by the fiber in the axi-symmetric configuration. A fully coupled solver (Newton-Raphson) is used.

3. Free surface run (transient) : The segregated solver is used in conjunction with kinematic updating in order to solve for the free surface shape subject to the flow and boundary conditions. Since the effect of surface tension is ignored, the capillary number is infinite and the kinematic update is found to be the correct choice. Here, the normal and tangential stress balance conditions are imposed as boundary conditions in the momentum equation and the following kinematic condition is used to update the location of the free surface:

$$\frac{\partial S}{\partial t} + \mathbf{u} \cdot \nabla S = 0 \qquad (22)$$

where S is the location of the free surface. In the spirit of the ALE approach, the momentum equation for a transient simulation is modified as follows to take into account the movement of the mesh:

$$\rho\left(\frac{\partial \mathbf{u}}{\partial t} + (\mathbf{u} - \mathbf{u}') \cdot \nabla \mathbf{u} \right) = -\nabla p + \nabla \cdot \left[\mu \left(\nabla \mathbf{u} + \nabla \mathbf{u}^T \right) \right] \qquad (23)$$

where $\mathbf{u}'$ is the mesh velocity. The method of spines is used to move the nodes on the free surface and those interior to the two phases. The transient free surface run offers additional stability to the solution through the control of the time step size. The same view factors as those calculated in the previous step are used throughout the solution procedure. This is because it was found to be prohibitively expensive to calculate them on the fly as the free surface location is updated in every time step. Instead, the view factors are recomputed after a fully converged free surface is obtained (next step) and the free surface calculation is repeated. Also, it should be noted that the free surface need not be converged with a tight convergence criterion in this step as it will be followed by a steady state run where such a criterion is implemented.

4. Free surface run (steady state): Finally, fully converged flow and temperature fields as well as free surface location are obtained by performing a steady state simulation after reading in the solution variables from the previous run. At this stage, new view factors are computed and the steady-state computation of the free surface is repeated until it is observed that the free surface shape no longer changes. It was found that usually only one repetition was needed to obtain a converged free surface.

5. Results and Discussion

Results for the base case are presented first where a draw ratio of 144 was chosen. The desired draw ratio is imposed by specifying the inlet velocity and the inlet diameter of the preform, and also the outlet velocity of the fiber. The corresponding fiber profile along with initial guess is shown in Figure 2.

The final converged flow and temperature fields and the free surface profile satisfy the following convergence criteria:

$$\left\| \frac{\mathbf{U}_i - \mathbf{U}_{i-1}}{\mathbf{U}_i} \right\| \leq 0.0001 \quad \text{(velocity and temperature)}$$
$$\leq 0.001 \quad \text{(surface)} \qquad (24)$$

Here, $\mathbf{U}_i$ is the solution vector at the i'th iteration and the norm is a root mean square norm summed over all the equations for the model. The CPU times for the four steps mentioned in the previous section are as follows: Isothermal run – 103 s, radiation run – 640 s, transient free surface run – 3102 s, and the steady-

state free surface run – 3.2 hrs. The simulation was performed on a single processor HP C3000 machine. The temperature contours in the fiber are shown in Figure 3 and the temperature along the axis of the fiber is shown in Figure 4. It is seen that the temperature in glass varies by about 600 K and that changes the viscosity of glass by about 4 orders of magnitude.
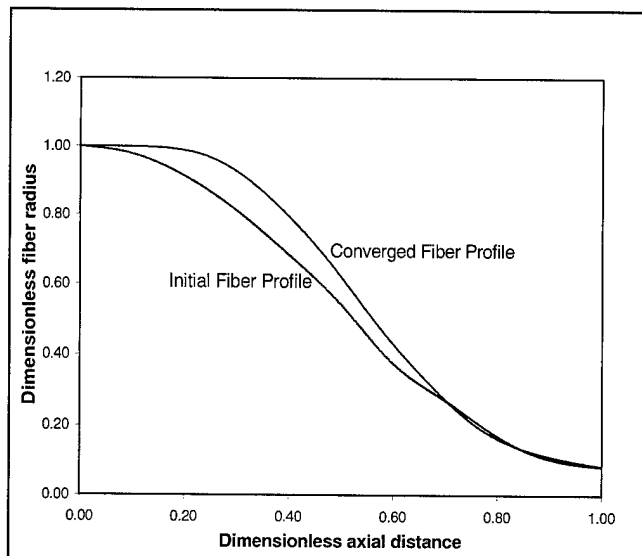
Figure 2. Dimensionless fiber radius as a function of the dimensionless axial coordinate for a draw ratio of 144
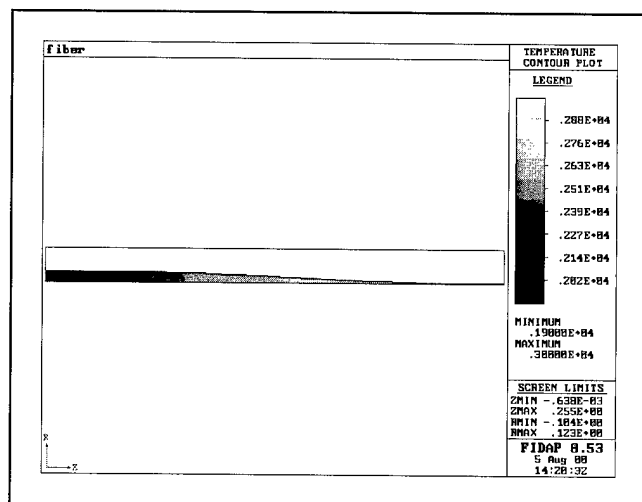
Figure 3. Temperature contours in the fiber

The variation of effective thermal conductivity of glass along the axis is shown in Figure 5. As can be clearly seen, radiation plays a dominant part and the radiative component of thermal conductivity dominates the molecular one.
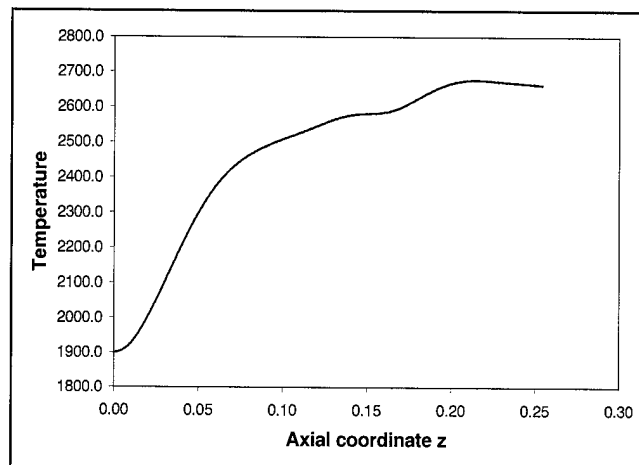
Figure 4. Temperature along the axis of the fiber
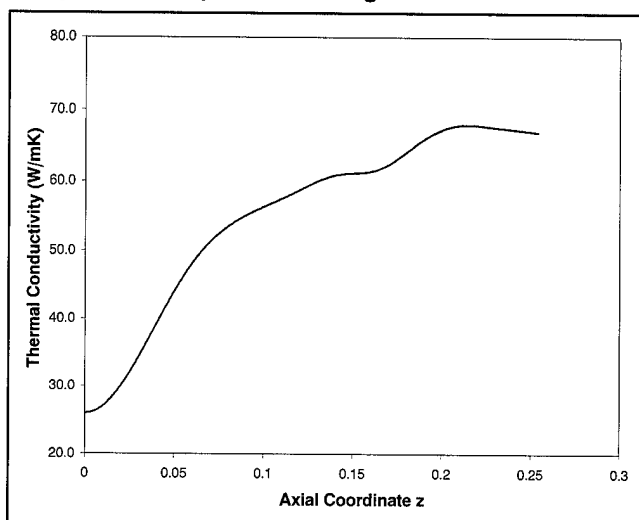
Figure 5. Thermal conductivity along the axis of the fiber

The temperature distribution in the furnace is shown in Figure 6. The temperature is maximum in the center and decreases away from it due to the corresponding parabolic temperature distribution that is applied at the furnace wall. The z component of the velocity in the two phases at the furnace exit is shown in Figure 7. u_z is constant in the fiber and is equal to its value specified through the boundary condition (1.44 m/s for the draw ratio of 144). As can be seen, the no-slip condition at the fiber surface results in a substantial gas velocity in the vicinity of the glass-gas interface.

All the results presented above are for a draw ratio of 144. A simulation was performed with a draw ratio of 576. The draw ratio was imposed by imposing u_z = 5.76 m/s at the fiber exit. The corresponding fiber profile is shown in Figure 8.
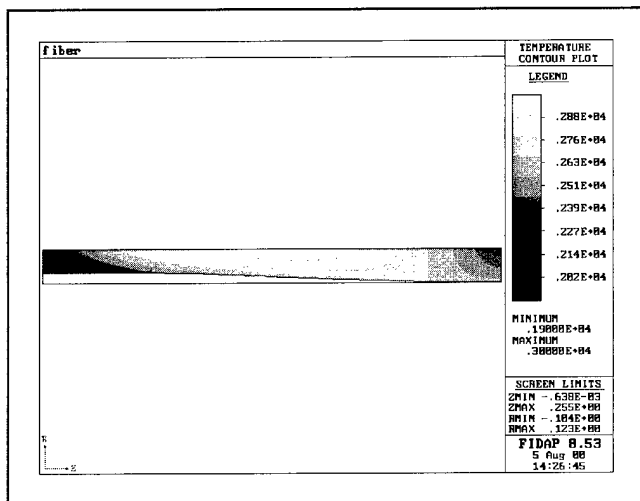
Figure 6. Temperature contours in the furnace
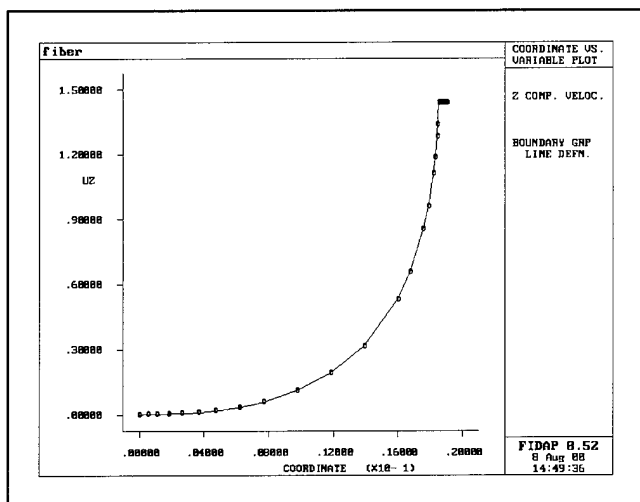
Figure 7. z component of the velocity at the exit of the furnace. The coordinate increases radially inwards from the furnace wall where the gas velocity is zero. u$_z$ is constant in the fiber and is equal to its specified value (1.44 m/s).

For the simulation shown in Figure 8, the same guess for the initial fiber profile that was used for the draw ratio of 144 is used. It was found that this was satisfactory, but for higher draw ratios it may be necessary to adjust the initial guess to the expected fiber diameter at the exit of the furnace.

6. Conclusions

A computer modeling of the optical fiber drawing process is presented.. The conjugate problem involving flows in both glass and gas are solved using a finite element method. The fiber surface is modeled as a free surface whose location is determined by a deforming mesh approach. It is shown that the temperature and flow fields in the two phases as well as the shape of the fiber surface can be accurately predicted. The draw ratios presented in this work (144

and 576) are rather small as compared those found in industrial fiber drawing (about 10000). Hence, direct comparison with experimental results is not possible at this juncture. However, it has been verified that the predicted fiber profiles match qualitatively with the numerical results presented elsewhere [7]. It is seen that radiation plays an important part and should be properly accounted for. In this model, an enclosure analysis is used to model surface-to-surface radiation in the furnace. The Rosseland approximation is used to model radiation in glass. This model is strictly valid only for optically thick media and could introduce inaccuracy downstream of the draw-down region where the fiber diameter is small. Currently, work is underway to introduce participating media radiation using P-1 approximation which is expected to alleviate this limitation. The improved radiation model and higher draw ratios will form a subject of a future publication.
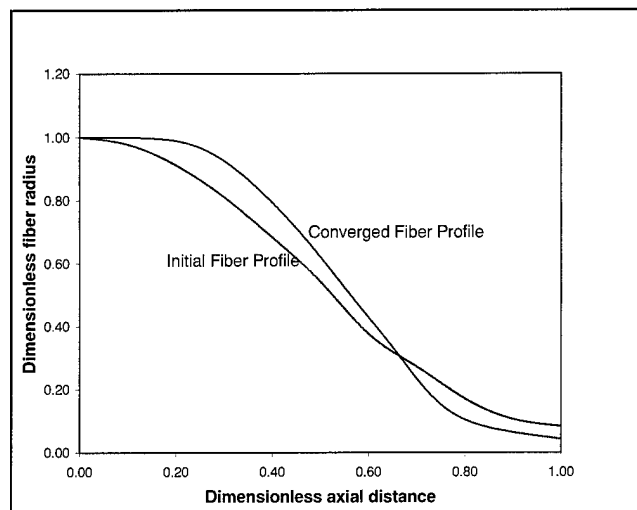
Figure 8. Dimensionless fiber radius vs. the dimensionless axial coordinate for draw ratio of 576

7. References

[1] S. Krishnan and L. R. Glicksman, "A Two-Dimensional Analysis of a Heated Free Jet at Low Reynolds Numbers," *Journal of Basic Engineering*, 93, 355-364 (1971).

[2] S. Kase and T. Matsuo, "Studies on Melt Spinning: I. Fundamental Equations on the Dynamics of Melt Spinning," *Journal of Polymer Science*, 11, 251-287 (1967).

[3] G. A. Brown (ed. by B. Bendow and S. S. Mitra), *Fiber Optics: Advances in Research and Development*, Plenum Press, p. 55 (1979).

[4] U. C. Paek and R. B. Runk, "Physical Behavior of the Neck-Down Region during Furnace Drawing of Silica Fibers," *Journal of Applied Physics*, 49(8), 4417-4422 (1978).

[5] M. R. Myers, "A Model for Unsteady Analysis of Preform Drawing," *AICHE Journal*, 35(4), 592-602 (1989).

[6] Z. Xiao and D. A. Kaminsky, "Flow, Heat Transfer, and Free Surface Shape During the Optical Fiber Drawing Process,"

National Heat Transfer Conference, ASME, 9, 219-229 (1997).

[7] S. R. Chaudhury, Y. Jaluria, and Steve H.-K. Lee, "A computational Method for Generating the Free-Surface Neck-Down Profile for Glass Flow in Optical Fiber Drawing," *Numerical Heat Transfer, Part* A, 35(1), 1-24 (1999).

[8] Y. S. Touloukian et al., *Thermophysical Properties of Matter*, Plenum publishing.

[9] A. B. Shapiro, "FACET- A Radiation View Factor Computer Code for Axi-symmetric, 2-D Planar, and 3-D Geometries with Shadowing," *An Informal Lawrence Livermore Laboratory Report.*

Jaydeep Kulkarni was born in Pune, India. He did his B.S. in Chemical Engineering from the Indian Institute of Technology, Bombay in 1995 and went to the University of Delaware for graduate studies. He finished his Ph.D. in 2000 and since then is working for Fluent Inc.

Understanding and Extracting Measurement Error in Non Destruct and Destruct Measurement Systems

Douglas B. Relyea

Quality Principle Associates
Norwich, CT
1-860-889-0754 qualityprinciple@aol.com

ABSTRACT

This paper will provide an in depth discussion of the importance of understanding the measurement system in terms of accuracy, precision and discrimination.

The need to identify the repeatability (precision) of a measurement system with respect to the particular product to be measured will be presented in context of wire and cable examples.

A mathematical model will be provided that will develop a single metric (discrimination ratio) that will serve to identify if a particular measurement system is adequate for process improvement purposes or must be limited to a go/no go function.

A second model will be offered that will provide an understanding of the actual amount of product variation (intraclass correlation coefficient) being experienced. This will be accomplished by mathematically separating the amount of measurement system variation from the total variation of measurement observations.

The paper will deal with all of the above topics of non-destruct as well as destruct measurement systems.

INTRODUCTION

The global market place has redefined quality. No longer is it satisfactory to make product that merely falls within specification. Customers are demanding and receiving product and services that demonstrate a minimum amount of variation about a target.

In addition to satisfying customer demands for reduced variation about a specific target, manufacturers are discovering the competitive benefit of manufacturing product with reduced variation. Consider the potential that exists in conservation of raw material when wall thickness variation is reduced. This enables the average wall thickness to be moved closer to the customer's lower requirement.

The concept of the 1.33 Capability Index (Cpk) introduced to American industry by the automotive companies is aimed at minimizing product variation about a target. By minimizing variation about a target, processes can absorb minor process average shifts without producing objectionable product.

Some companies will not deal with a supplier that cannot demonstrate a minimum 1.33 Cpk. Motorola requires certified suppliers to adhere to their Six Sigma requirement which is equivalent to a 2.0 Cpk.

Quality has become synonymous with minimizing variation. It stands to reason, then that truly competitive companies will expend resources to understand how much variation is normal to their processes and strive to reduce the variation as much as economically possible.

The classic method of determining the degree of variation that is normal for a given process is to perform a process capability study. This entails allowing the process to produce product for a given amount of time without human interference; that is allowing the process to run normally, without introducing unwarranted adjustments. Random samples are selected and measurements are recorded. The measurements are then analyzed using simple statistical techniques and the amount of normal variation is determined.

Unfortunately, many process capability studies are performed and conclusions reached without taking into consideration the amount of variation due to the measurement system.

Taking a measurement involves the same components as making product. Both include people, raw material, equipment and methods, and measurement processes fall into two general categories -- non-destruct and destruct.

The German mathematician and philosopher Hiesenberg stated that the very act of measuring changes that which is being measured. Although non-destruct measurement systems might somewhat change the sample that is being measured, the sample is not destroyed. A micrometer used to measure the diameter of insulated wire certainly may alter the diameter as a function of taking the measurement but does not totally destroy the sample. On the other hand testing insulation for elongation or tensile, in fact changes the sample to the point of destruction; that is, the same sample cannot be measured again.

Variation due to the act of measuring is introduced into the final results regardless of which type of measurement system is employed.

When the variation of recorded measurements is analyzed, it must be remembered that this observed variation is comprised of the variation of the product plus the variation of the measurement system.

The Challenge

The challenge to understanding the actual amount of product variation lies in being able to remove from the variation of the observations that variation realized due to the normal variation inherent in the people, raw material, equipment and methods employed in taking the measurements.

It is conceivable that the degree of variation of the recorded observations when compared to the customer specification might result in a Cpk lower than the industry wide accepted minimum Cpk of 1.33.

Figure 1 graphically represents a relationship of total specification to total variation that would result in a Cpk value of .88. The calculation that results in the Cpk value of .88 is found below Figure 1.

Remember - the total amount of variation of six sigma, equal to .0048, represents the variation of the observations. The variation of the observations consists of the variation of the product plus the variation due to the measurement system.

In order to determine a more accurate Cpk, it is necessary to remove the amount of measurement variation from the total variation of the observations. To accomplish this task it is necessary to understand several fundamentals of measurement process and the terms used to describe them.

$1\sigma = .0008$

.4578   .4580   .4582
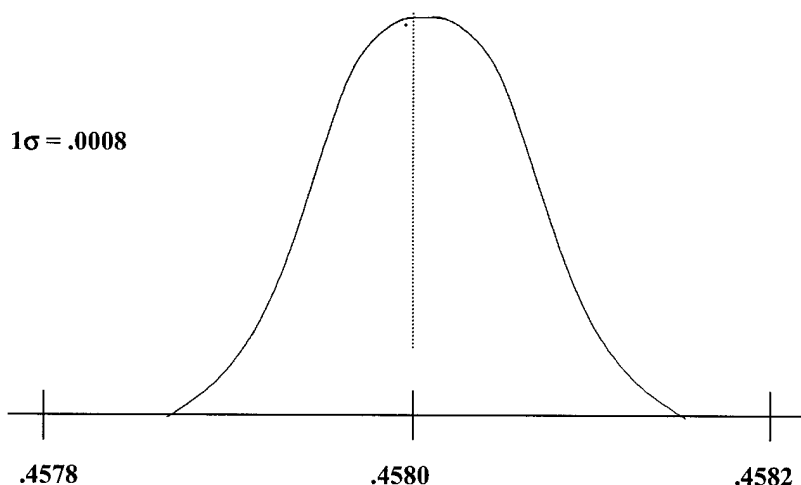
Figure 1

$$Cpk = \frac{\text{Total Specification}}{\text{Total Variation}}$$

When the process average is centered at nominal

$$Cpk = \frac{.004}{.0048} = .83$$

Accuracy

When we compare a measurement device such as a micrometer to a known standard such as a gage block we are determining the accuracy of the equipment. Calibration programs in the modern and competitive manufacturing organization address the concern of

measurement equipment accuracy quite well through calibration efforts.

Precision

Precision refers to the ability of a measurement process to repeat the same measurement when the same sample is measured more than once.

Everything in nature varies and measurement systems are no exception. If several people were to measure the same sample, in the same area, using the same equipment, it is very likely they would not record identical measurements. Most everyone in manufacturing has encountered the situation wherein an operator has recorded a measurement that differs significantly from the inspector's reading. The differences that exist between measurements recorded by individuals is quite probably due to the natural variation between people, how they hold or stage the sample and individual technique in using the measurement device as well as possible deformation of the sample that results from the measurement.

The characteristic of the sample being measured has a great deal of impact on the precision of the measurement process. A perfectly calibrated micrometer in the hands of two different experienced operators measuring the diameter of steel wire will often result in slight differences of perhaps .0001 to .0005. On the other hand the same operators using the same micrometer will record differences of .002 or greater when measuring the diameter of compressible insulted conductor.

It is the lack of precision that must be understood and removed from the variation of the overall observations.

In broad terms, the precision of a measurement process, in terms of standard deviation, is determined by requiring several experienced people to measure several samples of the same product a number of times. The range of each sample measured by the same individual is calculated and the average range of all measurements is divided by a constant in order to determine the measurement error (σ_e).

Figure 2 represents micrometer measurements of copper wire diameter. An average and a range are developed for each subgroup. Each subgroup consists of the same sample being measured by the same person using the same instrument. Below Figure 2 is the calculation that develops a σ_e of **.00064**, a metric that describes the measurement process imprecision.

Discrimination

The success of statistical process control, design of experiment technologies, ANOVA and other statistical techniques so important to improving manufacturing processes is largely dependent upon the ability of the measurement process to determine normal variation.

Discrimination or the ability of the measurement system to distinguish between samples made during periods of normal manufacturing process variation is the third element that needs to be considered when qualifying a measurement system.

The ability of a measurement process to discriminate between samples made during periods of normal manufacturing process variation is dependent upon two relationships.

The first of these relationships is that of the gage resolution – the smallest unit of measurement – and the standard deviation of the manufactured product in question.

A micrometer that measures to three places (.001) might very well have adequate discrimination when measuring the diameter of rolled steel rod. The same micrometer however would not have the same degree of discrimination when measuring drawn copper wire. Although the resolution of the measurement device remains the same when measuring either steel rod or copper wire, the standard deviation of the steel rod would very likely be an order of magnitude larger than .001 and the normal variation of the rod could be detected using the micrometer. On the other hand, the standard deviation of the copper wire would be an order of magnitude smaller than .001 and the normal variation of the copper wire would be lost in the relative coarse resolution of the three-place micrometer.

The second of the two relationships that determines the ability of the measurement system to adequately discriminate is the Discrimination Ratio (D_R). D_R is the ratio of the product variation σ_p to the variation of the measurement process σ_e.

The formula to determine discrimination ratio follows –

$$D_R = \sqrt{\frac{2\sigma_p}{\sigma_e} - 1}$$

A discrimination ratio equal to or greater than 4 is required before a measurement process can be considered adequate for purposes of statistical process control, design of experiments, etc.

Components of Variation

In order to determine the discrimination ratio, it is necessary to identify the measurement error σ_e and the actual degree of product variation σ_p.

In order to extract the amount of σ_p from the total variation of the observations σ_o, it is helpful to think of the relationship of the variation of all the observations σ_o, to the measurement error σ_e and the product variation σ_p in terms of a right triangle.

Consider the hypotenuse of the right triangle to represent the variation of the observations σ_o, the leg as the measurement error σ_e and the base as the product variation σ_p.
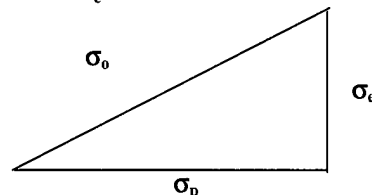
The Pythagorean theorem provides us with the following relationship.

$$\sigma_o^2 = \sigma_e^2 + \sigma_p^2$$
$$\sigma_p^2 = \sigma_o^2 - \sigma_e^2$$

This simple calculation provides us not only with an estimate of the actual amount of product variation, but also the ability to determine the discrimination ratio.

Extraction

It is a simple matter to extract the amount of product variation from the overall variation of the observations, once we have estimated the variation of the measurement process.

$$\sigma_o^2 = \sigma_e^2 + \sigma_p^2$$
$$\sigma_p^2 = \sigma_o^2 - \sigma_e^2$$
$$\sigma_p^2 = 5.6^{10-7} - 4.1^{10-7}$$
$$\sigma_p = .0004$$

Applying the corrected value of the true product variation to the Cpk formula we develop a more accurate understanding of the actual capability of the manufacturing process.

$$Cpk = \frac{.004}{.0024} = 1.67$$

Measurement system analysis for non-destructive test

Sample size:	5
# repetitions:	4
# operators:	4

	Operator 1					Operator 2				
	Sample 1	Sample 2	Sample 3	Sample 4	Sample 5	Sample 1	Sample 2	Sample 3	Sample 4	Sample 5
Rep. 1	0.4582	0.4575	0.4550	0.4558	0.4570	0.4566	0.4569	0.4562	0.4561	0.4563
Rep. 2	0.4566	0.4565	0.4555	0.4566	0.4556	0.4579	0.4564	0.4564	0.4559	0.4561
Rep. 3	0.4565	0.4568	0.4569	0.4564	0.4564	0.4568	0.4564	0.4550	0.4559	0.4556
Rep. 4										
Rep. 5										

Average	0.343	0.343	0.342	0.342	0.342	0.343	0.342	0.342	0.342	0.342
Range	0.0017	0.001	0.0019	0.0008	0.0014	0.0013	0.0005	0.0014	0.000154	0.0007

	Operator 3					Operator 4				
	Sample 1	Sample 2	Sample 3	Sample 4	Sample 5	Sample 1	Sample 2	Sample 3	Sample 4	Sample 5
Rep. 1	0.4563	0.4584	0.4562	0.4559	0.4567	0.4565	0.4585	0.4565	0.4566	0.4570
Rep. 2	0.4567	0.4563	0.4562	0.4559	0.4563	0.4580	0.4565	0.4566	0.4560	0.4566
Rep. 3	0.4566	0.4562	0.4567	0.4567	0.4557	0.4567	0.4566	0.4562	0.4558	0.4558
Rep. 4										
Rep. 5										

Average	0.342388	0.342713	0.342263	0.3421	0.34215	0.3428	0.3429	0.342325	0.3421	0.34235
Range	0.0004	0.00215	0.00055	0.0008	0.00105	0.0015	0.002	0.0004	0.0008	0.0012

Figure 2

$$\sigma_e = \text{Average Range} / d_2$$
$$\sigma_e = .00108 / 1.693$$
$$\sigma_e = .00064$$

Session for the Non-destructive Measurement System Analys,

Variation components	Std. Dev.	Variance
Variation of the measurement system	0.00064098	0.00000041
Variation of the product	0.00042455	0.00000018
Variation of the observations	0.00074623	0.00000056
Variation of the operators	0.00015084	0.00000002

Figure 3

	Std. Dev.	Variance	%Contribution
Gage R&R	0.00065849	0.00000043	70.64%
Repeatability	0.00064098	0.00000041	66.93%
Reproducibility	0.00015084	0.00000002	3.71%
Part to part	0.00042455	0.00000018	29.36%
Total variation	0.00078349	0.00000061	100.00%

Discrimination ratio (DR)	1

Figure 3 represents an analysis of the discrimination ratio and a breakdown of the components of variation for the copper wire diameter / micrometer measurement study.

The preceding has been offered as an example of estimating the actual amount of product variation by arithmetically removing the imprecision of the measurement process. This is, at times, necessary in order to identify the true manufacturing process capability, in terms of Cpk, without having the Cpk calculation artificially inflated by measurement error. This method should be considered as a means to understand the actual amount of product variation when further improvements to the precision of the measurement system are either not possible or not economically justified. As North American manufacturers continue to improve product quality by means of reducing measurement variation, the benefits of expending resources to further reduce measurement process imprecision will become more difficult to justify.

Destruct Measurement Processes

It is often necessary in the manufacture of wire and cable, to rely upon destruct measurement systems such as elongation testing, tensile testing, burn chamber tests, etc. A destruct measurement process is, of course, a measurement that destroys the sample as a result of performing the test.

Understanding the imprecision and discrimination of the destruct measurement processes also relies upon the requirement of the same people measuring the same samples with the same equipment just as is in the case of analyzing non destruct measurements.

The difficulty, of course, is the impossibility of measuring more than once a sample that has been destroyed.

To overcome this reality it is necessary to make an assumption that continuous product manufactured in a very brief period of time is essentially homogenous.

If a single elongation measurement requires a test sample to be six inches long, and the material is manufactured at a rate of 100 fpm, two contiguous six-inch samples will be manufactured in approximately .6 seconds. It is reasonable to assume that very little normal product variation will be realized between these two contiguous samples. It is also reasonable to assume that when these two contiguous samples are measured the majority of the difference recorded in elongation will be due to the imprecision of the measurement process.

Figure 4 represents the raw data for an analysis of an elongation measurement process.

Figure 5 represents the arithmetic reduction of the sources of variation.

Figure 6 represents a graphical representation of the sources of variation.

It is apparent that this measurement process is contributing almost 42% of the total variation of the observations. Repeatability or imprecision accounts for 37.44%; Reproducibility or differences due to operator technique accounts for the balance. The portion of total variation due to the product is approximately 58%.

The discrimination ratio of 2 indicates that this measurement process cannot effectively identify the elongation variation between samples of this material. Any one single elongation measurement recorded as a result of using this elongation measurement process can be overstated or understated by as much as +/- 3 standard deviation (σ_e) of the measurement error or +/- 38.4%.

Measurement system analysis for destructive test

Sample size:	5
# repetitions:	2
# operators:	4

	Operator 1					Operator 2				
	Sample 1	Sample 2	Sample 3	Sample 4	Sample 5	Sample 1	Sample 2	Sample 3	Sample 4	Sample 5
Rep. 1	190	180	160	160	185	165	175	160	175	150
Rep. 2	200	175	125	170	180	170	175	140	205	170

Average	195.000	177.500	142.500	165.000	182.500	167.500	175.000	150.000	190.000	160.000
Range	10	5	35	10	5	5	0	20	30	20
Moving Range	17.500	35.000	22.500	17.500	15.000	7.500	25.000	40.000	30.000	20.000

	Operator 3					Operator 4				
	Sample 1	Sample 2	Sample 3	Sample 4	Sample 5	Sample 1	Sample 2	Sample 3	Sample 4	Sample 5
Rep. 1	170	180	140	170	170	185	180	155	180	160
Rep. 2	190	170	130	160	190	205	195	140	200	170

Average	180.000	175.000	135.000	165.000	180.000	195.0000	187.500	147.500	190.000	165.000
Range	20	10	10	10	20	20	15	15	20	10
Moving Range	5.000	40.000	30.000	15.000	15.000	7.500	40.000	42.500	25.000	

Figure 4

Session for the Destructive Measurement System Analysis

Variation components	Std. Dev.	Variance
Variation of the measurement system	12.8546	165.2410
Variation of the product	16.0017	256.0547
Variation of the observations	20.0160	400.6406
Variation of the operators	4.4814	20.0833

	Std. Dev.	Variance	%Contribution
Gage R&R	13.6134	185.3243	41.99%
Repeatability	12.8546	165.2410	37.44%
Reproducibility	4.4814	20.0833	4.55%
Part to part	16.0017	256.0547	58.01%
Total variation	21.0090	441.3790	100.00%

Discrimination ratio (DR)	2

Figure 5

Variation Components
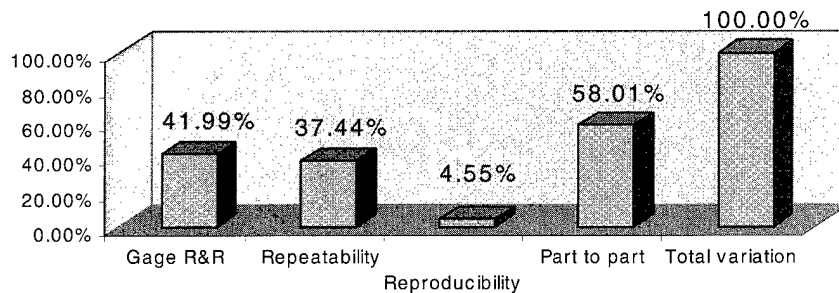
Figure 6

Probable Error

It is impossible to identify the actual elongation value of any one particular sample due to the imprecision of the measurement system. However, it is possible to make pass/fail decisions for individual samples with a certain degree of statistical confidence using the concept of probable error.

As long as the measurement system is stable, we can consider the error to be normally distributed. As such, 50% of the measurements will fall within +/- .67σ_e of the actual elongation value.

With this concept in mind, we can modify the specification by bracketing the upper and lower requirements with +/- .67σ_e. Any single value falling between the nominal and the lower spec plus .67σ_e or the nominal and the upper spec minus .67σ_e should be considered to be acceptable. On the other hand, any single value falling outside of the upper spec plus .67σ_e or outside the lower spec minus .67σ_e should be considered to be rejected.

Values that fall between the upper specification plus .67σ_e or between the lower specification minus .67σ_e require further investigation. When this eventuality occurs, several contiguous samples should be measured and the average of the several measurements should be used to determine disposition of the material.

Figure 7 is a graphical representation of the concept of using Probable Error to make determinations based on single measurements.

CONCLUSION

Problem solving and process improvements in manufacturing can only be realized through prudent data collection and analysis.

This paper is a compilation resulting from first hand knowledge of problem solving and process improvement efforts that were less than successful because data was collected with measurement systems that were unstable, imprecise or unable to distinguish between samples.

As companies strive towards a Six Sigma goal, or some other measure of competitiveness based upon the reduction of variation, it becomes necessary to utilize analytical tools such as statistical process control (SPC),designed experiments (DOE), ANOVA, etc. The successful application of these statistically based analytical tools invariably requires an accurate estimate of normal product variation. If an inadequate measurement system is employed for any type of process improvement based upon the use of SPC, DOE, ANOVA, etc. false conclusions will result because of inappropriate estimates of normal product variation.

Biography of Douglas B. Relyea
Quality Principle Associates
7 Stony Ridge Rd,
Norwich, CT 06360

Mr. Relyea founded Quality Principle Associates in 1987 after a successful career of over 20 years in industry. Mr. Relyea has authored a number of articles and books including The Practical Application of SPC in the Wire & Cable Industry.

Reference: Understanding Measurement Systems
Dr. Donald Wheeler
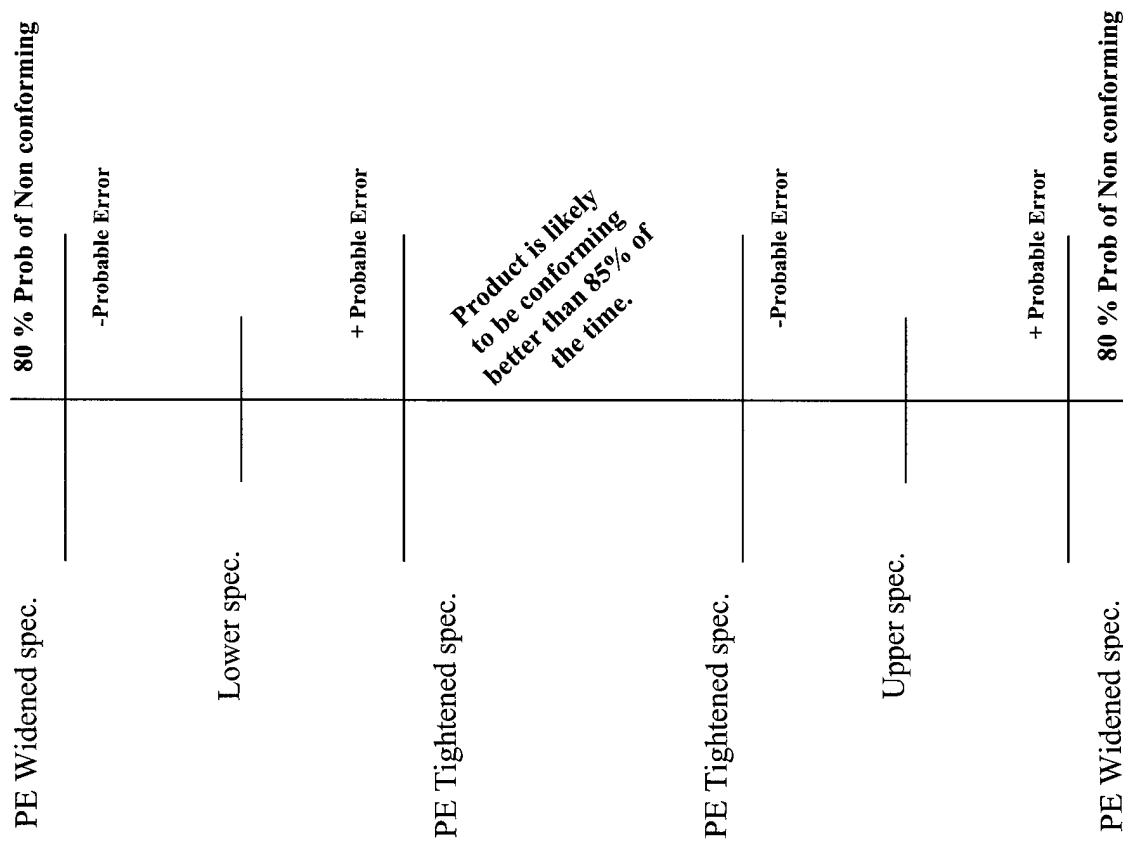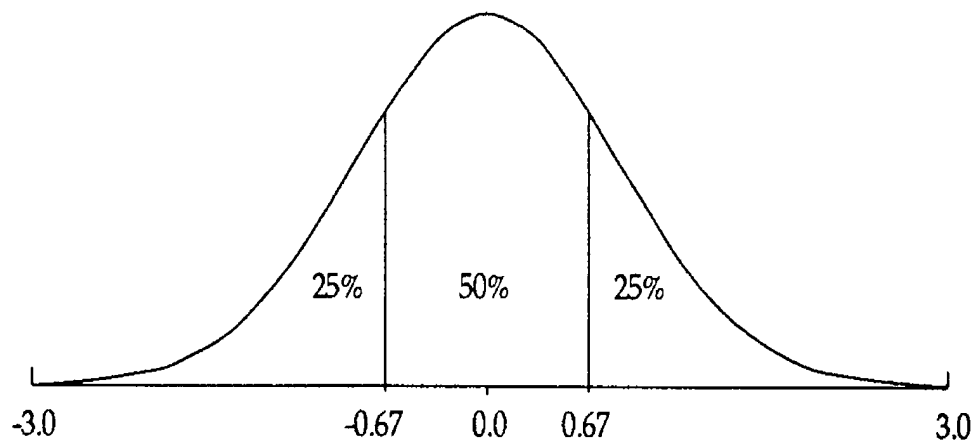
Figure 7

CFD Simulation of Optical Fiber Coating Flows

Costas D. Dimitropoulos*, Srinivas Chippada*, Eric W. Grald # and Jaydeep A. Kulkarni*

*Fluent Inc.,
Evanston, Illinois
+1-847-491-0200 · cdd@fluent.com

#Fluent Inc.,
Lebanon, New Hampshire
+1-603-643-2600 · ewg@fluent.com

Abstract

In this work, we examine the process of optical fiber coating through computational fluid dynamics (CFD) simulations. FIDAP, a commercially available finite-element (FEM) package was used. The FEM method is preferred because it is particularly well-suited for free-surface flows. This work focuses on simulation of the flow within a pressurized coating die at high fiber coating speeds. The effect of different fiber coating speeds and inlet pressure boundary conditions is considered for a modern die design. The maximum fiber speed examined was 20 m/sec. The magnitude of the applied pressure at the inlet of the coating reservoir, was of the order of 1 MPa for viscosity of 1 Pa*sec and density of 1100 Kg/m^3. Results demonstrating the effect of the flow conditions on the shape of the upstream and downstream menisci are presented motivating the advantages of detailed CFD predictions in die design.

Keywords

Optical Fiber; FEM; High-Speed Coating; FIDAP; Pressurized coating reservoir; Primary Coating; Biconic die; Meniscus Stability.

1. Introduction

Optical fiber coating is an important process that prevents flaws from forming on the fiber surface (for example, adhesion of airborne particles), shields the fibers from surface abrasion and also increases the fibers' tensile strength [1, 2, 3]. Optical fiber coating is usually a "wet" process involving drawing a fiber through a reservoir of coating material (typically a polymer) and subsequently curing the resulting coating in order to harden it [1, 2]. In most cases, a dual layer of coating materials is applied. The first coating layer corresponds to relatively soft material, such as a silicone resin, whereas the second coating layer corresponds to a higher modulus polymer that is curable, and is primarily responsible for higher strength and resistance to abrasion [1, 2]. In such dual coating processes these two coatings can be applied in tandem or simultaneously within the same coating applicator. In the tandem arrangement the first layer is applied and cured and then the same is performed for the second layer. In the simultaneous arrangement both layers are applied before the curing process [1]. During the coating process it is common to observe defects due to entrainment of air bubbles between the fiber and the coating layers. These bubbles can create to a variety of problems such as poor signal transmission and inhomogeneous mechanical properties [1]. This is due to an instability of the upstream interface between the air and the coating material, which occurs as the fiber speed increases [4].

Given the explosion in the growth of the telecommunications industry, the demand for large quantities of high-quality optical fibers at low cost is becoming increasingly large [2, 3]. This necessitates high production rates at coating speeds that can presently reach in excess of 20 m/sec and will increase in the near future [1, 3]. It is therefore a natural consequence that increasing emphasis has been given to design coating applicators that can be used at high coating speeds without the formation of defects due to instabilities [1, 4]. One of the main developments was the use of pressurized dies in order to achieve higher coating velocities. These devices which have replaced open-cup applicators are characterized by having the coating material contained in a high-pressure reservoir [1, 2]. Operation at high pressure has two main advantages. It helps minimize slip between the coating material and the fiber surface, which enables the liquid to actually coat the fiber at high velocities, and also prevents air to enter in the coating applicator and entrain in the form of bubbles between the fiber and the coating layers [1, 4].

Modeling such a process to study the effect of operating conditions on the flow within the coating applicator emerges as an important design tool. In addition, to predicting the range of operability of a particular device and to optimize a die design, CFD simulations can be instrumental in achieving precise control of the coating process in order to minimize variations in the coating thickness and to provide a concentric coating. In this work we focus on using CFD to visualize the flow field within a high-pressure coating applicator where a single layer of coating is applied. In contrast to previous work, we focus primarily on the computation of the position of the upstream and downstream free-surfaces that are formed. Previous work has focused on including heat effects, computing centering forces and computing flow with only the downstream meniscus free to move or after fixing both free-surfaces. In addition, there is still a need to research the fluid mechanics of optical fiber coaters under high pressure conditions (see [1, 3, 5] and references therein). The scope of this work is to provide a framework upon which more detailed studies that can include non-Newtonian rheology, heat transfer effects and fluid-structure interaction.

This paper is organized as follows. In Section 2 the geometry, properties and boundary conditions of problem under study are described along with the nondimensionalization of the model equations. Section 3 includes a brief description of modeling strategies for coating flows using the FEM method, as well as a description of the FIDAP model that has been used. Section 4

consists of the major results of this work and a discussion of their implications and importance. Our final conclusions are presented in Section 5.

2. Problem Description

2.1 Geometry and Governing Equations

We consider the die design in Figure 1. This corresponds roughly to the biconic die apparatus presented in a recent patent [1]. The geometry under consideration in this work is the primary coating die and is axisymmetric (r is the radial and z is the axial direction). The bulk flow is governed by the steady-state Navier-Stokes (1) and continuity (2) equations. The fluid velocity is denoted by $\underset{\rightarrow}{u}$, the stress tensor by $\underset{=}{\tau}$ and Re is the Reynolds number. The flow is driven by a normal stress at the inlet of the coating reservoir (3) and

by the fiber that is moving through the coating die with a velocity $\underset{\rightarrow}{u}_f$ (the subscript f refers to a quantity related to the fiber). For a fully developed flow the normal-stress at the inlet is equal to the pressure, p, of the fluid. We neglect here the effects of gravity and variable viscosity (temperature or deformation dependent). After entering through the opening of the pressurized coating reservoir, the fiber continues through a biconic centering and sizing die. In addition, it is assumed that the fiber is centered along the axis of symmetry. This is due to the fact that the focus of this work is on the change of the flow-field without any feedback on the structure. FIDAP can also accommodate deflection studies [6] and fully coupled fluid-structure interaction calculations are an exciting future extension of this work.
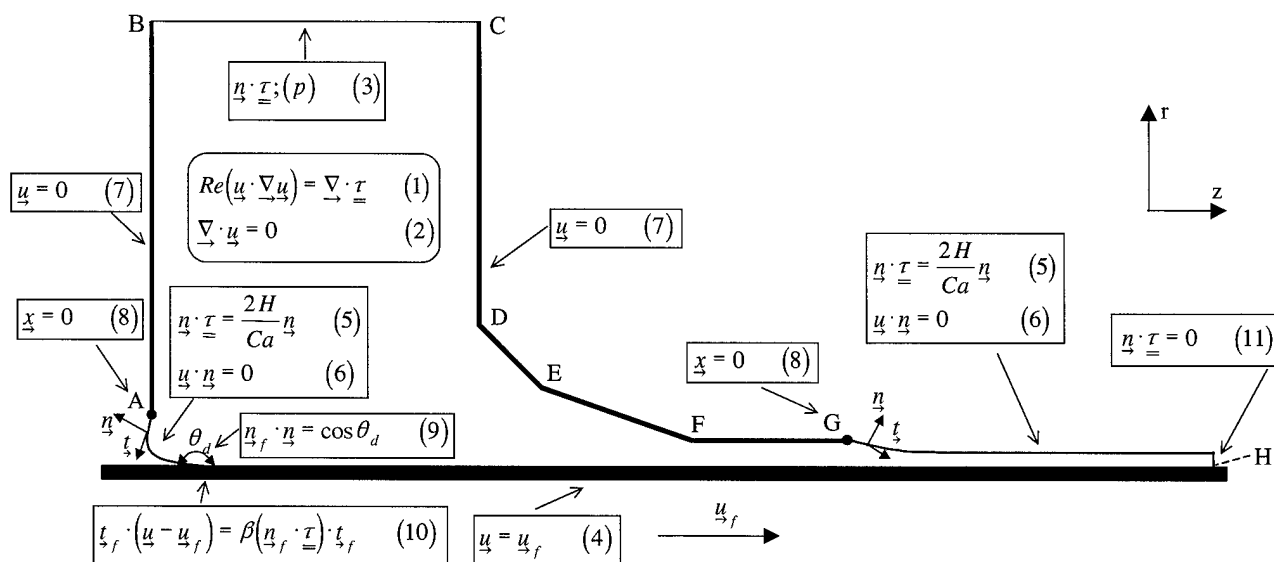
Figure 1. Governing equations and boundary conditions for optical fiber coating flow

There are two free-surfaces that are formed during the coating process. At these locations, one needs to apply boundary conditions for the normal and tangential stress (5) as well as the steady-state kinematic condition (6). The mean curvature of the free-surface is denoted by H and Ca is the capillary number. The normal and tangential vectors are represented by $\underset{\rightarrow}{n}$ and $\underset{\rightarrow}{t}$, respectively. It is important to note that for this type of coating flow there is no vacuum applied to the upstream free-surface. No-slip conditions are applied on the surface of the fiber (4) and on the walls of the coating applicator (7). At the point of contact between the fiber and the upstream free-surface there is need to apply a value for the dynamic contact angle, θ_d, (9), which is a parameter that is correlated primarily with experimental observations. At this region around the dynamic contact point with the fiber surface a condition such as Navier-slip (10) should be applied in order to remove the non-integrable stress-singularity [4, 7, 8]; β represents the dimensionless

slip coefficient, which is essentially an empirical parameter. We assume that the upstream free surface is pinned at the top lip of the die entrance and that the downstream free-surface is pinned ($\underset{\rightarrow}{x}$ represents the position vector) at the exit of the die (8). Finally, at the outflow boundary zero normal and tangential stress conditions are imposed (11).

2.2 Nondimensionalization of Equations

The problem is solved in dimensionless form. The characteristic velocity scale is the magnitude of the fiber velocity, u_f. The characteristic length scale is taken to be equal to the difference between the radius of the die-exit and the radius of the fiber and is denoted by L^*. The Navier-Stokes equation (1) is solved with viscous scaling for the pressure (or equivalently the stress). Thus the Reynolds number is defined as

$$Re = \frac{\rho \; u_f \; L^*}{\mu}, \qquad (12)$$

where ρ is the density and μ is the viscosity of the fluid. The pressure scale, p^*, is equal to

$$p^* = \frac{\mu \; u_f}{L^*}. \qquad (13)$$

The capillary number is defined as

$$Ca = \frac{\mu \; u_f}{\gamma}, \qquad (14)$$

where γ is the surface tension.

Typical values of the physical properties were chosen in order to calculate realistic flows [3, 5]. Specifically, the density was taken to be 1100 Kg/m^3, the viscosity 1 Pa*s and the surface tension was equal to 0.03 N/m.

The dimensions of the geometry under consideration are also of importance. A fiber with radius equal to 63.50 µm is considered. The coordinates of the points that are denoted in Figure 1 are listed below in Table 1. Note that Figure 1 is not to scale.

Table 1. Physical dimensions of coater geometry

Point	z (µm)	r (µm)
A	0	114.30
B	0	1371.60
C	800	1371.60
D	800	459.57
E	901.70	342.90
F	1988.82	114.30
G	2387.52	114.30
H	3500	63.50

As a result, L^* is equal to 50.80 µm, the Reynolds numbers considered here vary according to the relationship

$$Re = 5.588*10^{-2}*u_f \qquad (15)$$

and the capillary numbers vary as

$$Ca = (100/3)*u_f. \qquad (16)$$

The set of conditions defining the problem becomes complete by specifying the dynamic contact angle, the slip coefficient, the fiber velocity and the normal-stress at the inlet of the coating reservoir. The dynamic contact angle is taken to be equal to 135° and the dimensionless slip coefficient is equal to 10^{-2}. In this work, we did not study the effect of these parameters extensively. We simply report the amount of slip that is induced (which as will be seen is very small) and perform an indicative sensitivity test. Numerous flow configurations were computed through different combinations of the fiber velocity and the inlet normal-stress condition. The

velocity ranged from 10 to 20 m/s and the inlet pressure was as high as of the order of 10 atm (1 MPa).

From this point and in the following sections we will be referring to the inlet pressure for convenience, even though an inlet normal-stress is actually imposed. It is important to note that for the cases that will be presented here the flow is not strictly fully developed at the inlet of the coating reservoir. The selected location for this inlet is a little shorter than necessary and the inlet velocity profile is affected by the recirculation in the coating reservoir. Thus the pressure at the inlet is actually different than the normal-stress, but not more than 5% in the most extreme cases.

3. Numerical Method
3.1 FEM Simulation of Coating Flows
Many industrially important coating flows have been studied through numerical simulations in recent years [4]. CFD simulation has provided insight on coating flow stability to small disturbances, operability in different parameter ranges and sensitivity under transient flow conditions. The FEM method has been a research workhorse in the field of coating flows. In this numerical approach, the governing model equations are discretized in weak form in a grid corresponding to the physical flow domain [9]. This mesh is free to move to accommodate the change in the geometry due to the movement of the free-surface boundaries. The steady state or transient flow is then solved within this changing domain. This approach has a great advantage that the imposition of free-surface boundary conditions is greatly simplified. Numerical methods with such boundary-conforming discretization approaches are often referred to as arbitrary Lagrangian-Eulerian (ALE) methods. This is because the mesh does not correspond to a fixed Eulerian frame and does not necessarily follow the motion of fluid particles in a Lagrangian sense [4]. For ALE methods it is necessary for transient problems to account for the relative motion between the deforming mesh and the flow. This corresponds to being consistent in accounting for a time-dependent coordinate system [10].

FEM methods are characterized by that the grid consists of a set of elements. In free-surface flows the free-surfaces or internal interfaces coincide with element boundaries and any changes in the shape of the free-boundary triggers a deformation of the mesh to account for the change in the topology. There are generally three classes of mesh adaptation techniques used in ALE simulation of free-surface flows. The first is what is referred to as algebraic mesh generation where the mesh deforms according to a user-defined parametrization of the free-surface nodes. The most widely-used approach is the method of spines where a set of generator lines guides the movement of the free-surface in such a way that only the nodes belonging to these spines are moved so that their initial aspect ratio of their position is retained [11]. Another important approach is the mapped approach, where the new free-surface location is computed as a displacement along the local normal. The free-surface is then moved to its new location in a prescribed way, accompanied by remeshing the associated interior domain by recreating a mapped mesh in a defined region below the free-surface [11].

The second remeshing class is elliptic mesh generation, where the new mesh is computed by solving a system of differential equations for the mapping of the computational domain to the physical domain [12]. Therefore, computations can be performed on the fixed rectangular grid of the computational domain. Such curvilinear coordinate systems can be very advantageous since they greatly simplify the application of boundary conditions. Other advantages are that the resulting mesh is smoother and the mesh properties are better controlled locally. Elliptic mesh generation can result in conformal, pseudoconformal, orthogonal and non-orthogonal meshes [10, 12, 13, 14]. The last category is the most widely used for coating flow computations where special stretching functions are used to generate high quality nearly orthogonal meshes [4].

Finally, the third class of remeshing techniques corresponds to what is referred to elastic remeshing, where the mesh is computed from the equations governing the displacements of a deforming elastic solid. The driving force for the deformation is the free-surface displacements corresponding to the kinematic condition. The grid is assumed to correspond to a pseudo-solid and the free-surface boundary conditions are satisfied when the elastodynamics problem is also satisfied [6]. The main advantage of this approach is that in contrast to the other two classes of remeshing, it is not necessary to use structured grids. Fully unstructured grids can be readily employed, allowing for efficient refinement near points of singularity (such as contact lines) and boundary layers, as well as allowing for additional control of the local mesh quality for capturing large free-surface deformations [6].

3.2 FEM Modeling with FIDAP

FIDAP provides with multiple options for simulating free-surface flows [11]. Briefly, remeshing can be accomplished through three approaches. The first way is to use the method of spines, through both the coupled and the segregated solver. The remaining two approaches, namely the mapped and the elastic remeshing can be used only with the segregated solver. For a fully coupled solver, the Newton-Raphson approach is used, where all degrees of freedom are solved simultaneously. This approach typically needs a good initial guess since it has a small radius of converges and converges rapidly (it exhibits quadratic convergence behavior). The main drawback is that efficiency suffers for large problems due to the coupled solution approach and that currently only the spine remeshing technique can be used. The segregated solver solves all the degrees of freedom separately and successively till convergence is achieved [15]. After the flow problem is solved by satisfying all the boundary conditions for the momentum and scalar transport equations, the remaining boundary condition (typically the kinematic condition) is used to update the free-surface. This process is repeated iteratively till convergence is obtained. The segregated solver has a larger radius of convergence, but convergence is not as fast as for fully coupled solvers due to the reduced coupling between the free-surface and flow solutions. More importantly though, the segregated solver becomes much more efficient than the Newton solver as the problem size increases. For both types of solver, running the problem initially

as transient helps achieve more stable convergence behavior since the solution at each time-step is naturally an excellent initial guess for the next. This strategy is typically used to provide a better initial guess. In addition, FIDAP has flexibility in the way the boundary condition that updates the position of the free-surface is handled. Specifically, in the case of the segregated solver for small capillary numbers, the normal component of the interfacial stress boundary condition is used to update the interface position, whereas the kinematic equation is used in its place as a boundary condition for the momentum equation. Optical fiber coating flows are typically large capillary number flows and the traditional approach of applying the kinematic condition to update the free-surface is used here.

The simulations presented in this work are based on the segregated solver using the mapped remeshing technique. The reason for this selection was that the mapped remeshing approach provided with more flexibility for representing the movement of the nodes in the remeshed regions of the computational domain, especially close to the upstream meniscus. Specifically, mapped remeshing could account for movement of the nodes not just along one direction (as would the case be for spines) decreasing the possibility for severe mesh distortions near the dynamic contact line that would require excessive remeshing to be resolved. In comparison to the elastic remeshing approach it required fewer computational resources for this problem and exhibited better behavior in retaining the initial element apsect-ratio close to the dynamic contact point. The elastic remeshing technique even though it is more flexible needs more customization in some cases. The mapped meshing approach was a natural fit for this type of problem.
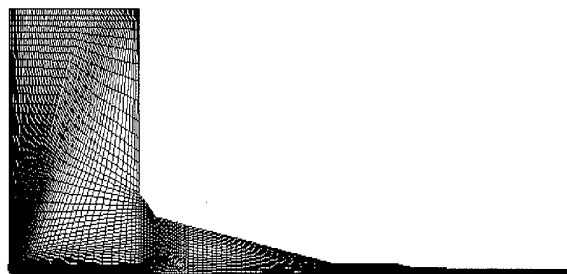
Figure 2. FEM mesh used in present simulations

The mesh used for the results presented here consisted of 6352 elements and 6106 nodes. It is shown in Figure 2 and as can be seen is mapped in its majority. Only one part near the biconic constriction is meshed with the tri-primitive approach [16] in order to refrain from using an excessive amount of mesh elements downstream. Linear elements are used for the velocity and the discontinuous approach for the pressure is employed. The current mesh configuration is capable of resolving well the flow structures that develop in the cases examined in this work. We solve the equations described in section 2 up to a tolerance of 10^{-5}. The main results of our study are presented in the next section.

4. Results and Discussion

We performed runs for velocities equal to 10, 15 and 20 m/s. These values result in small (less than 1) Reynolds number flows as equation (15) shows. In addition, we can see from equation (16) that the capillary numbers that result are very large (more than 100). Therefore, viscous forces will dominate over both inertia and surface tension in these flows. The selected nondimensionalization scheme forces a dimensionless velocity of 1 for the fiber, but also uses a dimensionless pressure that is inversely proportional to the velocity scale. In this work we will distinguish between the various cases by referring to the dimensional value of the velocity and the dimensionless pressure. This is because these values facilitate distinguishing between cases. The reader should note that for the present scale selection the dimensional pressure is proportional to the velocity ratio when the velocity changes.
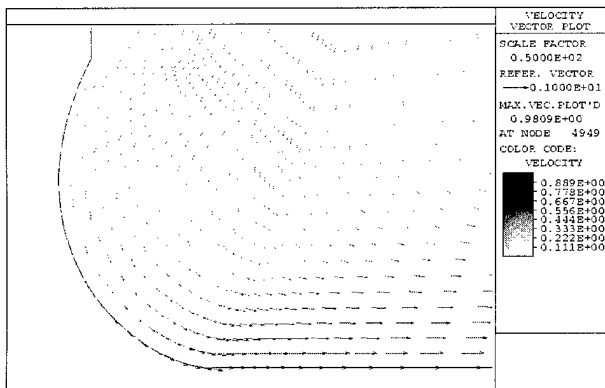
Figure 3. Dimensionless velocity field at upstream meniscus for u_f = 20 m/s and p_{inlet} = 2.5 (gage)

We simulated coating flows with the dimensionless gage pressure at the inlet of the coating reservoir ranging from 1.0 to 5.0 above the ambient value, which was taken to be equal to zero. For the current set-up of boundary conditions the convergent results were in the range between 1.5 and 4.5. In order to simulate successfully flows at lower pressure values, it is necessary to reconstruct the mesh in order to improve the quality of the elements that in the initial mesh had deformed excessively. This was regarded as being outside the scope of the present work, which is to examine the feasibility of optical fiber coating simulations and provide preliminary results. This also applies to the case of the higher pressure values where it is necessary to examine the validity of the assumption that the upstream meniscus is pinned at the top lip of the entrance of the coating die. The results presented here indicate that at the higher pressure values clearly indicate that the coating fluid tends to wet the entrance die leading to the coating reservoir.

Figure 3 provides a snapshot of the dimensionless velocity field in the vicinity of the upstream meniscus for an indicative case (20 m/s and p=2.5). The maximum velocity is on the fiber, a little further away from the dynamic contact point due to the Navier slip condition. Figure 4 shows a streamline contour plot for the same case where it is clear that the recirculation region within the coating reservoir is the dominating flow structure. The location of the

recircurlation is such that it interacts with the biconic constriction of the coater. This constriction is clearly seen to act in such a way that the recirculation is contained within the coating reservoir. The length of this constriction is definitely adequate. Figure 5 which shows the velocity field in the beginning of the downstream free surface, clearly demonstrates that the flow in this region where the coating is formed is not affected by the recirculation caused by the large fiber velocity and is essentially simple shear. Given the large viscosity of the liquid the downstream free-surface levels quite quickly and this is also seen from figure 5. In fact, the downstream free-surface modeled here is longer than necessary.
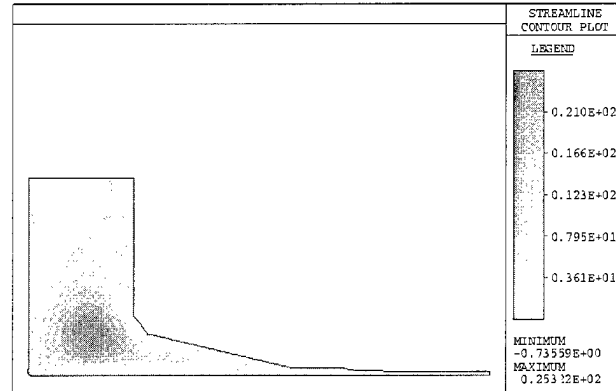
Figure 4. Contours of dimensionless streamlines for u_f = 20 m/s and p_{inlet} = 2.5 (gage)

Figure 6 shows a comparison between two simulations of the same case when the slip coefficient is changed from 10^{-2} to 10^{-3}. The results are very close, predicting a difference of the locations of the dynamic contact point of 1 μm. In addition, it was observed for the smaller slip coefficient that the velocity on the area of the fiber declared as slip is 97.7% of the fiber velocity at the dynamic contact point and increases to the full value after a few nodes as we proceed downstream. For the slip coefficient used for the rest of the results presented here the value at the dynamic contact point is 90.5% smaller. Given these relatively small differences it is safe to assume that the choice of parameters is adequate to demonstrate some of the basic physics of this type of flow.
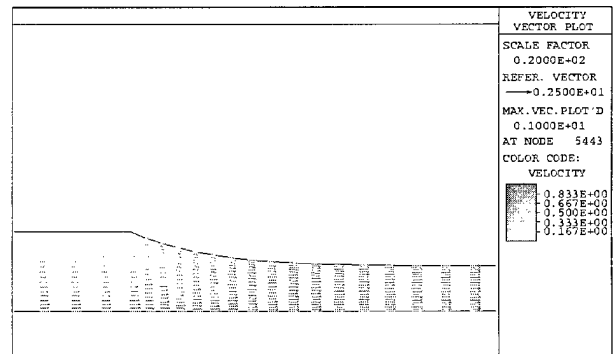
Figure 5. Vectors of dimensionless velocity at the origin of the downstream meniscus for u_f = 20 m/s and p_{inlet} = 2.5 (gage)

to these studies, it is important to study the effects of heat-transfer, as well as that of non-Newtonian or viscoelastic fluid rheology. These are consequences or the large shear rates and the polymeric nature of the coating materials. The nature of the fiber and the manner in which the coating process operates motivate the study of the interaction of the flow with the structure of the fiber. Computational modeling provides with tools for computing deflections from the desired positions as well the forces that cause them. Finally, one can extend this work to the study of simultaneous multi-layer coating. In general, extending coating simulations to predict the characteristics of the final product is still an active research subject and advances that can refine the current modeling capabilities are continuously becoming available.

6. References

[1] F.V. DiMarcello, A.C. Hart, R.G. Huff, K.S. Kranz, L.M. Larsen-Moss, "Biconic Coating Die for Making Optical Fibers," *United States Patent,* No. 6,030,664 (2000).

[2] T. Izawa and S. Sudo, *Optical Fibers: Materials and Fabrication*, KTK Scientific Publishers, Tokyo, p. 71 (1987).

[3] K. Rattan and Y. Jaluria, "Simulation of Flow in Die and Applicator for Optical Fiber Manufacture," *Proc. 48th IWCS,* 700-707 (November, 1999).

[4] K.N. Christodoulou, S.F. Kistler and P.R. Schunk, "Advances in Computational Methods for Free-Surface Flows", in *Liquid Film Coating* (S.F.Kistler and P.M. Schweizer eds.), Chapman & Hall, London, p. 297 (1997).

[5] J.S. Abbott and D.C. Francis, "Analysis of the Optical Fiber Coating Process Using FIDAP: Flow, Heat Trannsfer, and 3-D Calculation of Centering Forces," Proc. 3rd FIDAP Users Conference (September, 1989).

[6] FIDAP 8.5 Update Manual, Fluent Inc., p. 4-1 (1999)

[7] C. Huh and L.E. Scriven, "Hydrodynamic Model of Steady Movement of a Solid/Liquid/Fluid Contact Line, " *J. Colloid Int. Sci.* 35(1): 85-101 (1971).

[8] E. B. Dussan V., "On the Spreading of Liquids on Solid Surfaces: Static and Dynamic Contact Lines," *Ann. Rev. Fluid Mech.* 11: 371-400 (1979).

[9] P.M. Gresho and R.L. Sani, *Incompressible Flow and the Finite-Element Method, vols. 1& 2*, John Wiley & Sons, New York (1998).

[10] C.D. Dimitropoulos, B.J. Edwards, K-S. Chae and A.N. Beris, "Efficient Pseudospectral Flow Simulations in Moderately Complex Geometries," *J. Comput. Phys.* 144: 517-549 (1998).

[11] FIDAP 8, Volume 5: Theory Manual, Fluent Inc., p. 9-1 (1998)

[12] J.F. Thomson, Z.U.A. Warsi and W.C. Mastin, "Boundary-Fitted Coordinate systems for Numerical Solution of Partial Differential Equations – A Review," *J. Comput. Phys.* 47: 1-108 (1982).

[13] K.N. Christodoulou and L.E. Scriven, "Discretization of Free Surface Flows and Other Moving boundary Problems," *J. Comput. Phys.* 99: 39-55 (1992).

[14] G. Ryskin and L.G. Leal, "Orthogonal Mapping," *J. Comput. Phys.* 50: 71-100 (1983).

[15] V.H. Haroutunian, M.S. Engelman and I. Hasbani, "Segregated Finite Element Algorithms for the Numerical Solution of Large-Scale Incompressible Flow Problems," *Int. J. Numer. Meth. Fluids* 11: 323-348 (1993).

[16] GAMBIT 1 Modeling Guide, Fluent Inc., p. 3-73 (1998)

AUTHOR

Costas D. Dimitropoulos

Fluent, Inc.
500 Davis Street, Suite 600
Evanston, IL 60201
cdd@fluent.com

Costas D. Dimitropoulos received his Ph.D. in Chemical Engineering from the University of Delaware in 1999. He is the FIDAP Product Support Specialist at Fluent Inc. He is located in Fluent's Evanston office and his interests focus primarily on free-surface flows, turbulent flows, biological/biomedical flows and fluid-structure interaction.

Minimization of the Secondary Coating Setting Times by Using an Advanced Fiber Pay-Off and Cutter System

Mikko Pfäffli

BL Fiber Optics, Nextrom Oy
Finland
Tel. +358-9-5025 3135 · mikko.pfaffli@nextrom.com

Abstract

The setting times in connection with a change of loose tube production batch should be rendered as short as possible. The total line down time can be quite long if several batches have to be made during a day. The setting times can easily be calculated for color changing, fiber launching, ramping up and down the line, and threading new fibers. A typical problem in loose tube production is that the excess fiber length is changing as a function of line speed during ramping. The daily amount of fiber under ramping will be very high. In the stranded loose tube cable construction, such loose tubes have also shown increased attenuation.

Nextrom has analyzed the line productivity, and in order to improve it, has introduced a new technology for fiber launching and cutting where no ramping is needed. By combining full speed fiber cutting and full speed fiber launching, it is possible to cut scrap costs drastically down.

1. Introduction

1.1. Loose Tube Cable Construction

"Stranded loose tube type cable construction" is based on plastic tubes extruded around 1 to 12 fibers. The plastic tube protect the fibers from lateral forces and the fibers have some space, excess fiber length, to move inside the tube when the cable length is changed. The tubes are filled with jelly to prevent water penetration into the tube, stranded around a strength member and sheathed to give the typical "Stranded loose tube type cable construction" shown in Figure 1.

It is important that length of the fiber and the tube are the same at operating temperature in the stranded loose tube cable construction. The fibers are on the average in the center of the tube (Figure 1). When the cable is elongated the fiber will move towards the cable core.

When the temperature decreases, the cable shrinks and the fiber moves outwards from the center.

When the cable has reached the allowed maximum shrinkage or elongation, the fiber will touch the tube wall causing increased attenuation.
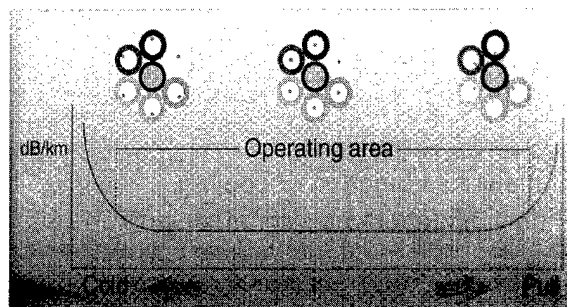
Figure 1. "Cross-section of an ADSS construction". The number of fibers is six. The construction is designed to give free space for the fiber movement in the tube under the given load of 10 kN and in the temperature range of +70 to –60C taking ice and wind loading into account

1.2. Production Parameters for Loose Tube Production

In the Secondary Coating Line (Figure 4) **the key parameters** in controlling the excess fiber length and loose tube post shrinkage are:

-Fiber tension
-Jelly viscosity (temperature),
-Cooling water temperature.
-Line tension between mid-capstan and end-caterpillar
-Take up tension
-Line speed:
- High line speed decreases the crystallization rate (Figure 2), and thus resulting in high post shrinkage and in high excess fiber length (Figure 3). In high line speed the plastic has less time to stay at the optimized crystallization temperature. For polybutylene terephthalate the temperature giving the highest crystallization rate is 210 °C
- Cooling water friction will be increased at high line speed. Higher line tension is needed to pull the loose tube through the water baths and the tube will be crystallized under tension, and thus resulting in high post shrinkage and also in high excess fiber length.

produce 500 m more loose tube in the same time than with "One set of pneumatic pay-off and Fiber Quick Cutter" because one set of pneumatic pay-off and Fiber Quick Cutter can be under pre-loading while the other is under production, and there is no time needed for threading of new fibers between runs.

In the same manner in Figure 9. there is compared production lengths for 25000 m production length.

It can be found that the production length increase from conventional "counter weight dancer type" of set-ups to new type is for 25000 m production length lower due to the fact that the fibers are usually run empty from the reels and no ramp down is needed.

In Figure 10. there is compared the improved productivity percentages for conventional "counter weight dancer type" with new type of pneumatic pay-off and Fiber Quick Cutter set-ups for 6 and 25 km batch lengths.

Table 2. A typical process situation for conventional "counter weight dancer type" system compared with new type of pay-off and Fiber Quick Cutter systems"
*) Line preparation comprises when needed such activities as: color change, threading the loose tube and scap reel change.

3.0/2.0 MM LOOSE TUBE, 12FIBERS, 25 KM FIBER REELS, COLOR BATCH 6 KM (24 MIN), LINE SPEED 250 M/MIN	Conventional "counter weight dancer type" system (in which it is impossible to launch or cut the fibers at higher speed than the jogging speed)	Pneumatic pay-off 12 f + Fiber Quick Cutter	Two sets of pneumatic pay-off 12 f + Fiber Quick Cutter. As one set of pneumatic pay-offs with Fiber Quick Cutters is under pre-loading, the other one is already under production.
Line preparation*)	3 min	3 min	3 min
Launching	1 min	1 min	1 min
Ramping	ramping up **2 min** ramping down **2 min**	NO RAMPING NEEDED	NO RAMPING NEEDED
Threading new fibers	every 4 run 10 min <=> every run 10/4 min=**2.5 min**	every 4 run 10 min <=> every run 10/4 min=**2.5 min**	No need
Change-overs	(24 + 10.5) min=34.5 min =>**41.7 Change-overs/24 h**	(24 + 6.5)min=30.5 min=>**47.2 Change-overs/24 h**	(24+ 4)min=30 min=> **48 Change-overs/24 h**
Change over time tot.	10.5 min	6.5 min	4 min
Line NOT in production	41 times 10,5 min=>**430.5 min/24 h**	47 times 6.5 min=>**305.5 min/24 h**	48 times 4 min=>**192 min/24 h**
Line in production	70 %	78 %	86 %
Improved production	NO	70%->78%=>**11.4%**	70%->86%=>**22.9%**
Fiber loss (unstable EFL) due ramping	41 times 4 min => **246 km/24 h**	**No fiber loss** due pneumatic pay-off + Fiber Quick Cutter	**No fiber loss** due pneumatic pay-off + Fiber Quick Cutter

Production length 6000 m
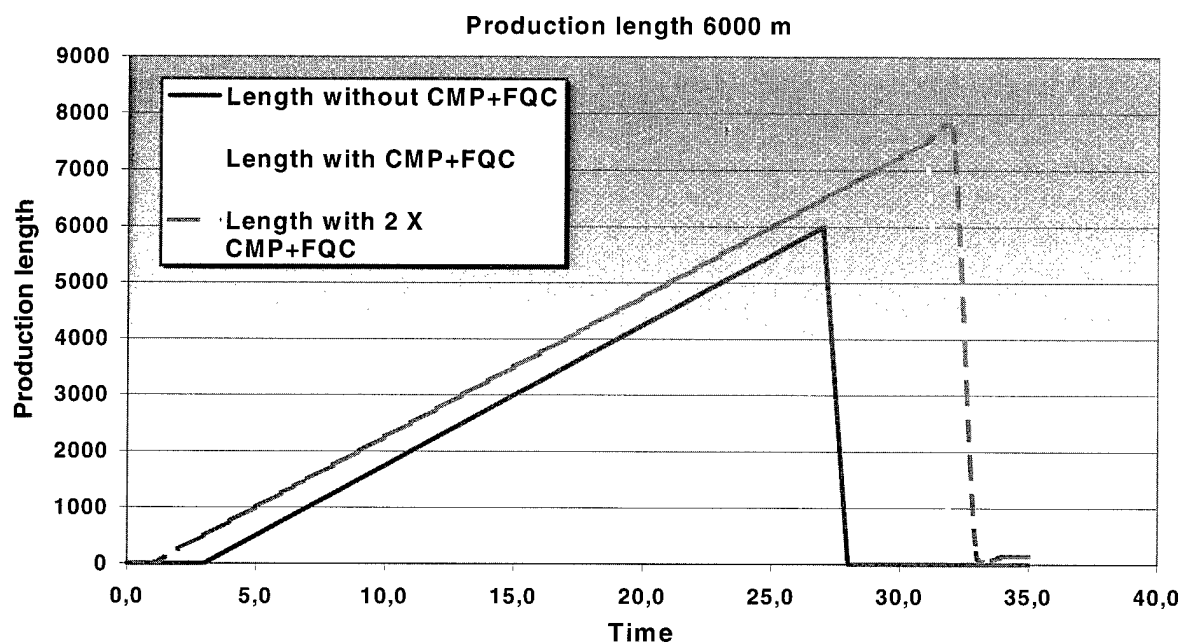
Figure 8. Production time and length for conventional "counter weight dancer type", one set of pneumatic pay-off and Quick Cutter and two sets of pneumatic pay-offs and Fiber Quick Cutters when having 6000 m batch length.

Production length 25000 m
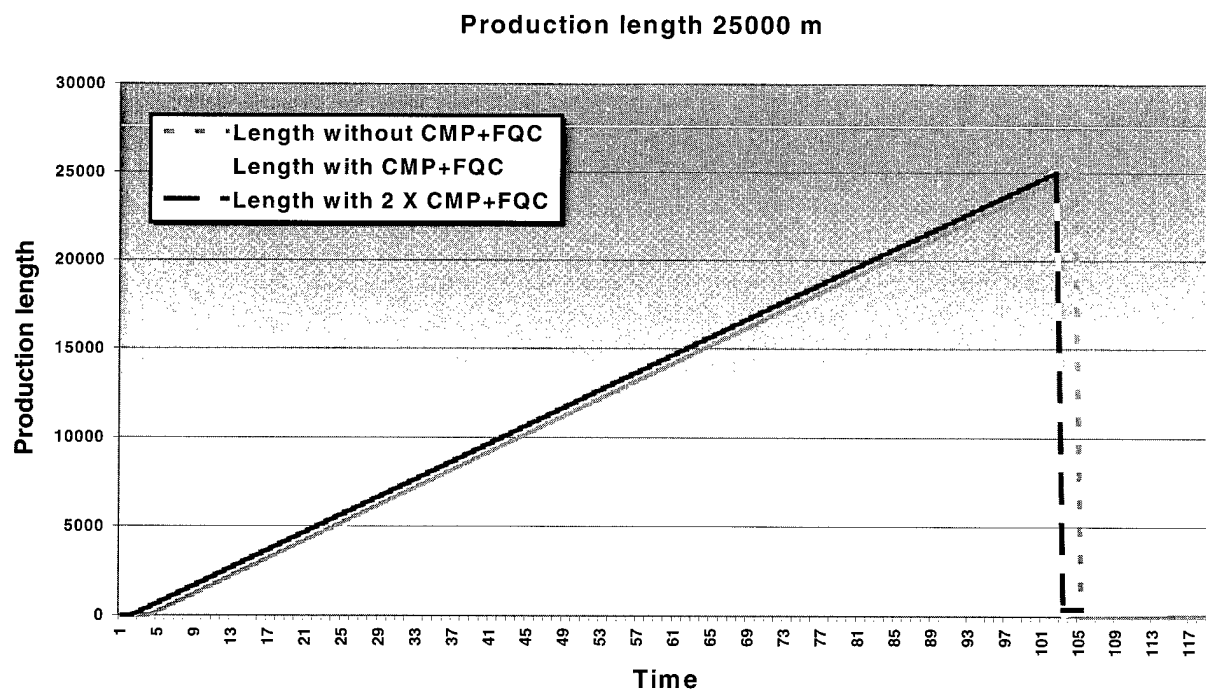
Figure 9. Production time and length for conventional "counter weight dancer type", one set of pneumatic pay-off and Fiber Quick Cutter and two sets of pneumatic pay-offs and Fiber Quick Cutters when having 25000 m batch length.

Improved production
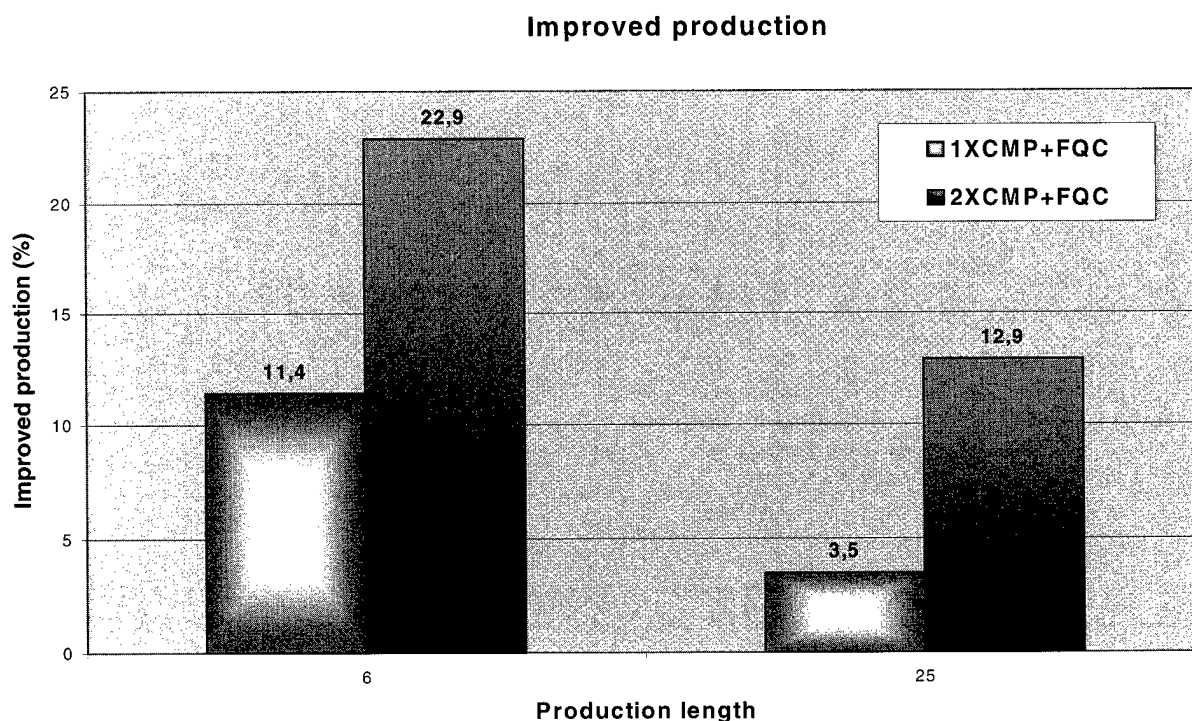
Figure 10. Improved productivity for 6 and 25 km batch lengths.

3. Conclusions

In loose tube production, it is now possible to drastically reduce scrap costs by combining full speed fiber cutting and full speed fiber launching. Scrap costs can especially be reduced if several product changes have to be made during the day. A well-known fact is that the excess fiber length changes as a function of line speed during ramping the loose tube production. The excess fiber length change can be avoided when using full speed fiber cutting and full speed fiber launching. In the stranded loose tube cable construction the tubes manufactured during ramping have shown increased attenuation risk. The typical fiber length under ramping when having 25-km color batches will be 72 km per day for a loose tube of 12 fibers. Depending on the batch lengths this new approach will increase the productivity between 3.5 and 22 %.

4. References

K. Junkyung, M. E. Nichols, R. E. Robertson
J. Polym. Sci., Part B, Polym. Phys.
32, 887-889, 1994

Author
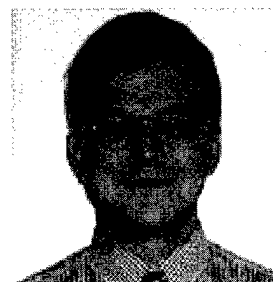
Mikko Pfäffli, MSc. graduated in 1993 with degree in Chemical engineering at Åbo University of Technology. During his studies he worked at Nokia Cables as a research chemist. Since graduation he has been working as R&D engineer at Teknos paint factory, and in 1996 joined Nokia-Maillefer (recent Nextrom) where he is working as Product Manager responsible for Secondary Coating lines.

Mikko Pfäffli, Nextrom Oy, P.O. Box 44, FIN-01511 Vantaa, FINLAND

Measurement Methods of UV Radiation as Applied to Fiber Process Industries

Andrew W. Ridyard

4D Controls Ltd. – Solatell, Redruth, Cornwall, UK

+44-1209-214400 . andrew-r@solatell.com

Abstract

This paper describes some recent advances in UV spectroradiometry as required by the fiber manufacturing industry. The demands from fiber process engineers have presented some severe challenges in developing accurate and reliable UV measuring instruments. Such instruments are now available to provide both intensity and wavelength data in the form of UV spectral distribution analysis and monitoring in an easy to understand form.

Three approaches can be used with state-of-the-art UV spectroradiometers for these process industries: -

- Off-line, without fiber, for UV lamp system performance benchmarking inside the quartz tube

- On-line, with fiber, for UV lamp manual performance checks and problem diagnosis

- On-line, with fiber, automatic data collection and UV watchdog monitoring.

These different approaches are described, and the practical benefits and drawbacks of each approach discussed. Some real examples of lamp system performance during lamp starting, run up and longer term effects are presented from some typical fiber coloring lines.

Keywords

UV; measurement; spectrum; calibration of UV measurement; fiber processes; UV cured formulation; on-line monitoring; process control.

1 Introduction

High intensity Ultra Violet radiation is a critical ingredient in the manufacturing process for quartz fiber and cable in the following four areas:
1. fiber draw,
2. fiber coloring,
3. fiber ribbon matrix,
4. fiber cable non-ferrous strength member.

In fact, the absolute intensity and wavelength distribution of the UV reaching the process during manufacture can be a critical limiting factor on process speed. However, fiber draw process speeds in excess of 20m/sec are not uncommon. If it is not taken into account, inadequate UV irradiation during the manufacturing process may lead to inadequate cure, which if not detected can lead to in-service problems, premature failure, or loss of performance of the fiber once installed.

But how can one know that the UV radiation reaching the fiber is adequate, or is being sustained at an adequate level during manufacture? Only by the accurate measurement of the UV itself, both from a quantitative and also from a qualitative standpoint, can we progress towards this desire. The essence of good quality control in any of the application areas mentioned therefore is to be able to measure and compare meaningful UV spectral measurements of the photon flux causing the radiation curing of the formulation being applied in the process.

2 The UV cure zone

Quartz fiber optic cable is a remarkable product; a very highly developed and demanding process at the forefront of UV curing. Process engineers are continually pushing the envelope of speed of cure, mechanical handling, and process machine performance. Naturally, to keep the process in control, many parameters are monitored to very exacting standards. Recently, spectral monitoring has also been made possible for the UV radiation, which is such a critical part of the process.
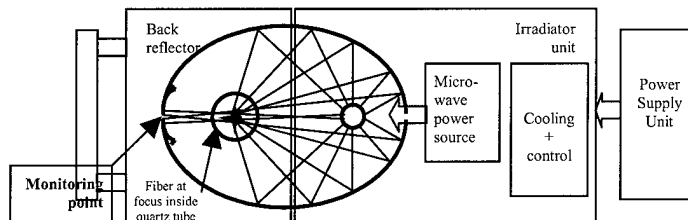
Figure 1. Microwave excited lamp systems commonly used in fiber processes

Generally, the lamp used in the fiber process industries is of the form shown in figure 1. Here we have a very highly focused, microwave excited UV lamp with the bulb positioned at one focus of an elliptical reflector, and the fiber product running through the second focus of the ellipse. The fiber product in Figure 1 is running perpendicular to the page, and the curing zone of the lamp is typically 250mm long i.e. the fiber product is exposed to UV for 250mm of its passage through the quartz tube of one lamp. Often many lamps are arranged vertically, one above the other with the fiber running through one long tube, or several quartz tubes carefully aligned vertically. Sometimes more conventional mercury arc lamps are used instead of the 250mm microwave excited lamps, but although these are longer in length, they cannot reach the extremely high intensity tight focus the microwave lamp can offer due to its smaller bulb diameter.

The microwave lamp comprises essentially three different components; a) The **irradiator**, which contains the microwave sources and cavity, the bulb, half of the elliptical reflector and the

cooling and control system for the lamp, b) the demountable **back reflector**, which completes the other half of the elliptical reflector, holds the quartz tube containing the fiber and nitrogen inerted atmosphere, and provides UV monitoring access points, and c) the **power supply**, which is either switchable between low and high power or is continuously variable between typically 25 and 100%.

The other parameter which can be altered is the type of bulb fill used. The most common two types of bulb are referred to as 'D' and 'H' and are contrasted in Figure 2 (spectral data are measured using an instrument type described later in this paper).

The D bulb, while having lower peaks in the longer wavelength region, has a higher total integrated power than the H bulb in the region 320 to 400nm. Whereas the H bulb, for the same input power, emits a higher total power in the short wavelength region, shown here as 240 to 280nm.
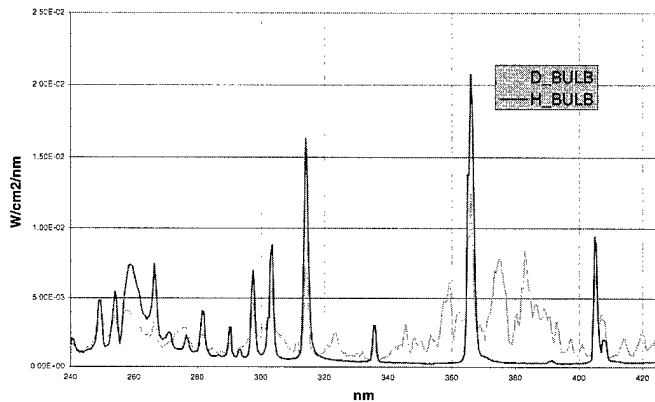
Figure 2. Typical fiber curing lamp spectral charts

2.1 Process types

In the fiber cable manufacturing industry, we can look at the four distinct areas where high intensity UV is used as part of the manufacturing process

i)   **fiber draw** – the initial manufacturing stage where quartz fiber is drawn from a preform, then coated with a UV cured functional coating;

ii)   **fiber coloring** – where the quartz, coated fiber from stage i) is colored for identification purposes using a dyed, UV-cured lacquer (sometimes stages 1 and 2 are combined into one process);

iii)   **fiber ribbon matrix** – where typically 10 or 12 colored fibers are combined into a flat ribbon, for construction into a cable

iv)   fiber cable non-ferrous **strength member** – the final cable has many fibers contained within it (often in the form of many ribbons); the cable is given longitudinal strength by the addition of a central spine, or strength member. This strength member is increasingly made of a composite material which is UV cured.

In each of the above processes, the type of UV lamp used is often of the microwave excited type as shown in Figure 1. In order for cure to occur in each process, the UV formulation is applied wet, then the product is passed through one, or more usually, several UV curing lamps inside a quartz tube which has nitrogen gas continually supplied into it. The reason for the nitrogen is to render the curing atmosphere inert, more specifically to remove

oxygen which would otherwise inhibit the curing process. During each of these processes, temperature will also play an important role in the speed of the process and the fullness of cure.

3 UV requirements to cure a fiber process formulation

As fiber processes increase in speed, there is demand for just a straightforward increase in the W/cm (or W/inch) output from the lamp. This is a traditional way of specifying UV lamp systems e.g. 600W/inch, but is somewhat misleading because it says nothing about the actual power seen at the process. It does not take into account the effect of the reflector geometry, or distance from the lamp system, nor does it say anything about the spectral distribution of the UV irradiance which is so critical to the process. As we know from 'the cure zone' section 2, we can select a bulb type for its higher short (H) or longer (D) wavelength UV output performance. Some fiber processes use a combination of H and D bulbs in series for their better suitability to surface cure, or adhesion (through cure) properties respectively. However the formulation often is specified as simply needing UV in one or two peak areas e.g. '...at 254 and 365nm', which obviously correspond to the actual mercury vapor naturally occurring peaks, but say little about the matching of real bulb output (see Figure 2) to the absorption spectra of the UV formulation. Some experimentation is often required to determine the best lamp number, spectrum and power combination to achieve a specific cure rate.

The reason multiple lamps are often required is partly due to the speed at which the fiber passes through the cure zone. A UV lamp does not have a completely stable 'dc' output, but rather fluctuates with the utility supply frequency. Such is the speed of the fiber that if the UV lamp output is going through a minimum as the fiber passes through the cure zone in one specific lamp then inadequate UV dose would be achieved with only one lamp. Two or more lamps overcome this phenomenon.

Added to this is the almost universal need to exclude oxygen from the curing process area as mentioned in the previous section. The temperature of the fiber as it passes through the cure zone can also play a significant role in the overall cure rate.

Once the UV lamp number + spectrum + power and process speed formula are settled upon, it is necessary to ensure that this lamp array continues to deliver the required power and spectra for a sustained period, and to have the ability to diagnose problems if they occur.

4 Effects of inadequate cure on fiber processes

What are the dangers associated with inadequate cure, and how can it occur? Break outs (quartz fiber breaking out of coating during handling), in-system failures, or loss of performance of the installed fiber are the main problems. Also mechanical problems can become evident with the preparation of the fiber during installation whereby the buffer coating cannot be stripped reliably, thus making the fiber difficult to use.

With colored fiber, the actual dye color can have a major bearing on the effectiveness of cure, with some colors e.g. orange, being more difficult to cure reliably with a greater tendency for break outs. Better matching of UV emission spectra to absorption

spectra of colored UV coatings can help here, as well as process speed modification.

As already mentioned, the fiber process is a complex one with many elements contributing to a successful and reliable result. However we will concentrate on the UV radiation necessary for cure, which is clearly a critical element with different parts of the spectrum being generally associated with different effects.

Figure 3 shows the effect of different portions of the UV spectrum. For convenience the diagram depicts the effect of short (UVC), medium (UVB) and long (UVA) wavelengths where it is generally understood that the shortest wavelengths are absorbed near the surface of the coating, so are associated with surface cure effects, while the longer wavelengths penetrate further and are associated with depth of cure, or adhesion between the coating and the fiber.
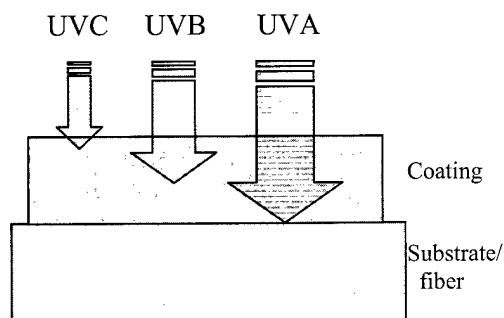
Figure 3. Penetration dependence on UV wavelength

5 What can go wrong?
In providing UV radiation to the fiber process we have a high power optical system. Although the lamp systems are generally very reliable there are nevertheless factors in the process itself which can contribute to the deterioration of the optical surfaces involved, some of which are briefly reviewed below.

5.1 Quartz tube fogging
The most common problem is the so-called 'fogging' of the quartz tube used in the lamp system shown in Figure 1. In severe cases during run up, a quartz tube can become quite dark due to a little uncured coating or dye becoming deposited on the inside surface, then becoming 'baked on'. This darkening can have a dramatic effect in the UV reaching the process. Fortunately, the monitoring points shown in Figure 1 allow a UV measuring probe to be positioned to see the effect of two thickness of quartz in front of the bulb, so this problem can be detected fairly easily with the manual or automatic monitoring systems described later.

5.2 Bulb overheating
The cooling airflow provided to the bulb when the lamp system is turned on must be maintained above a certain level. If the airflow is inadequate then the bulb can overheat. The effects of this can be the bulb output spectrum changing, or the bulb actually expanding so effecting focus. Some increase in bulb output may be obtained over a shortened period, as we will see later, but the consequence will ultimately be the bulb failing prematurely.

5.3 Wrong bulb
It is relatively straightforward to check that the correct bulb type is being put in the lamp system by checking its marking during routine maintenance. However, once in service, it is not easy to check the bulb type without disassembly of the lamp. A quick check on the bulb's spectrum in operation verifies the correct type is fitted.

5.4 Low power setting
The spectrum of a D bulb will look quite different – more like that of an H bulb – if it is operated at low power (see figure 2). Not only is the output of the bulb a lot lower, the spectral matching of the bulb output to the chemistry of the UV formulation is no longer optimized. Experience shows that power settings in multiple lamp systems may not always be set correctly. The output power and spectral distribution 'signature' of the lamp can reveal whether it is operating correctly, by comparison with previously recorded spectra.

5.5 Lamp maintenance requirement
Normally a UV lamp system will give thousands of hours of trouble free use if it is looked after properly. As we have described above, if the lamp system has, for example, a poor airflow, the bulb will behave abnormally and can fail after only hundreds of hours.

The lamp system is complex, and whilst essentially very reliable, may develop in-service operation issues affecting its output. While these issues are normally avoided by routine maintenance, it can happen that the maintenance itself can create an operational abnormality if the lamp is not reassembled quite correctly.

Magnetrons are used to generate the necessary microwave energy to power up the bulb shown in Figure 1. These magnetrons have a finite life, and usually there are two. If one half of the bulb has lower output than the other then it may suggest one magnetron is nearing the end of its service life before the other.

6 UV measurement for fiber industries
6.1 Industry needs
The primary requirements for UV monitoring in the fiber process industries are firstly, consistency of measurement. It is very desirable to be able to provide reliable specifications for the UV being delivered and methods of comparing measurements between different machines and different sites. If measurements are consistent and reliable and have absolute calibration traceability [1] across a broad spectrum, then the end user and UV coating formulator are able to speak the same language, and it is possible to 'close the loop' on formulation development and end user requirements for process performance and UV quality control.

6.2 Generic types of measuring device
It is outside the scope of this article to exhaustively compare different methods of UV measurement, but essentially there are two types of physical devices most commonly used for UV measurement [1], where the signal conditioning and amplification electronics are attached to some form of display device, viz. a viz.

a) Radiometers or b) Spectroradiometers. The essential differences are summarized in Table 1.

Table 1. The differences between radiometers & spectroradiometers

Radiometers	Spectroradiometers
Low to Medium cost	Medium to High cost
Broad band devices, comprising photodiode and optical filter combinations	Narrow wavelength discrimination, hence irradiance units in W/cm²/nm (1 nm resolution)
Intensity information in pass band of filter	Intensity and wavelength information, and calibration across wide spectrum
No precise wavelength information	Precise intensity vs. wavelength plot
Only calibrated for one type of light source spectrum, specified at time of ordering	General calibration 'flat response'; purpose is to show calibrated differences in spectra
Gives a **number** as an irradiant Power (P) in W/cm²	Gives a **Graph** – a picture of spectral distribution, with calibrated units as :- X axis = nanometers (nm) Y axis = W/cm²/nm Irradiant power can be calculated by 'integrating under the curve' of the spectral distribution over programmable ranges.

As mentioned in the table, radiometers comprise an optical band-pass filter, and a photodiode, both of which are subject to manufacturing tolerances. The optical filter can also suffer from temperature effects and its characteristics can change with time as the filter deteriorates, or 'solarises', in the presence of high intensity UV radiation. The radiometer's combined effect of the filter and diode in series cannot actually be known at the time of manufacture (unless each radiometer is painstakingly characterized nanometer by nanometer, using a spectroradiometer as a reference measuring instrument). The normal procedure to overcome this difficulty in not knowing the combined response, is for the radiometer to be calibrated in front of a particular light source of known power and spectral distribution against a reference radiometer calibrated by a standards institution (e.g. the NIST in the USA, NPL in UK, or PTB in Germany).

The result of this process is that the calibration of the radiometer can only be relied upon for one type of light source, that which it was calibrated against. If the spectral distribution of the light source to be measured differs substantially from the calibrating light source then the radiometer readings are effectively uncalibrated and can only be used as relative readings. Indeed, it will often be found that one radiometer reading cannot be compared against another radiometer because of the unknown nature of the combined response effect of the filter and diode mentioned in the previous paragraph. The radiometer is however useful as a relative measuring device when these considerations are taken into account.

By contrast, the higher cost spectroradiometer is designed to be able to judge the relative height, or contribution of one part of the spectrum against another part with equal weight (or indeed with an absorption spectra applied to provide 'effective irradiance' measurements). The whole point of the spectroradiometer is that it can be calibrated to give absolute measurements across a wide spectral range, from a wide range of UV lamps, and then can display the spectral distribution faithfully in absolute units.

The spectroradiometer can then be relied upon to give both quantitative and qualitative checks, to allow the user to make judgments about the state of the UV lamp system e.g. whether the spectrum is correct, whether the short wavelength UV has deteriorated – possibly as a result of contamination on one of the optical surfaces – or whether the overall power level in one installation matches another in absolute units.

So there are clear advantages to using a spectroradiometer if absolute UV measurement accuracy is required.

6.3   The ideal?

What are the factors which can have a significant effect on UV measurements for high power lamp systems? They can be summarized as follows: -

- Position – is the probe + spectroradiometer combination being accurately and repeatably placed?
- Probe effects – has the attenuation of any optics been taken into account?
- Spatial response – the angular response effects
- Calibration – is the instrument properly calibrated?
- Scan time – is the time to make a measurement too short / too long?
- Stray light – what out of band radiation effects could affect the measurement?
- Temperature – could effect the electronics or the optics performance

In order to make accurate and meaningful UV spectral measurements in a high power curing process, first of all we need to be able to insert our measuring instrument entrance as close as possible to a representative position, or positions, seen by the process. To do this, it is convenient to use a probe of some type capable of withstanding the high temperatures and extreme UV intensity normally found from a lamp system (bulb + reflector combination). In the case of the lamp configuration in Figure 1, we are unable to position our probe in exactly the same position as the fiber while the process is running, so next best is at a defined position which will take into account most of the contributing factors to the lamps system's performance. Indeed, some lamp manufacturers have provided this type of monitoring points at strategic positions exactly for this purpose.

6.4   Robust miniature UV Spectroradiometers

Since their introduction to the radiation curing industry less than 5 years ago, the development of robust miniature battery operated UV spectroradiometers has been continuing. These devices are based on a miniature, monolithic, single diffraction grating spectrograph, optimized for UV spectroradiometry [1]. They comprise a self-scanned UV enhanced array of typically 512 photodiodes, mounted on focal plane of the spectrograph. A wide range of wavelengths in the UV can be collected in one (or a few)

rapid scan(s), with typically a 1nm bandwidth; so that spectral lines of typically 2nm spacing can be resolved.
Current wavelength ranges from such instruments range down to the short wavelength UVC (below 240nm), to well into the near visible, stopping at typically 470nm.

Such UV spectral intensity measurement devices are available as hand-held, battery-operated instruments with a graphical display able to show UV lamp spectra, and with color display versions to compare one spectrum with another directly.

More recently, simpler, lower cost devices, based on the same type of core UV spectrograph technology, have come along in the guise of 'programmable UV-near-visible radiometers' with the purpose of being used in a production environment as a simple go/no go check on the output from a UV lamp system on, for example, a fiber optic cable draw tower. Such devices are able to store a complete UV reference spectra, and to allow comparison of this with the latest reading to establish whether a lamp may have lost power in part of its output spectra e.g. due to a contaminated quartz tube. A simple traffic light arrangement can tell an unskilled operator in seconds the condition of his lamp system.

All of the above types of instrument are usually used in radiation curing measurement application with a UV probe, capable of withstanding the high temperatures and UV intensities found in such applications. As already mentioned, there is a requirement to position the probe in the same position every time a measurement is taken, so accurate location methods providing very good repeatability have needed to be developed, and are available for the types of microwave excited lamps used in the fiber optic industry, shown in Figure 1.

Such small Spectroradiometers have also been successfully applied to providing complete system for on-line monitoring of UV spectra with, for example up to 16 channels monitored [3].

6.5   Probes

An example of a typical, elevated temperature (to 250°C) withstanding UV measurement probe is shown in the photograph Figure 4.
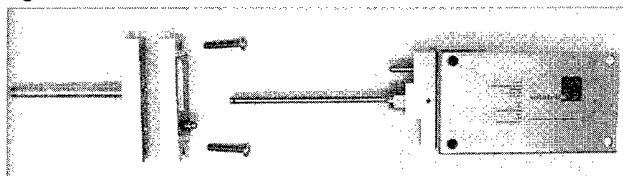
Figure 4. The original UV probe and precision location system

It has only a 1 mm entrance aperture so can be very accurately positioned in the irradiant field of the UV lamp system. On the left of the photo is a locating mechanism for the probe. This is normally mounted on the machine or UV lamp system and provides accurate (to within 0.5mm) and very repeatable positioning of the UV probe for taking measurements. A sprung loaded flap on the locator ensures that UV light is not allowed to escape from the locator when the probe is not inserted.
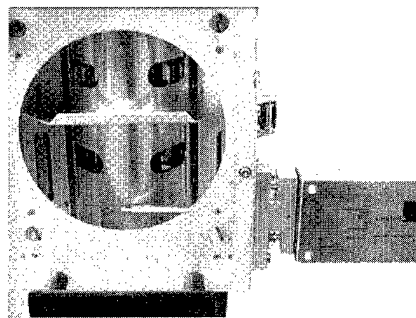
Figure 5. The probe of Figure 4 in position in a microwave excited lamp's back reflector

Other larger diameter probes capable of being operated at temperatures up to 350°C have been successfully manufactured with a built in diffuser in order to extend the spatial response of such probes to an approximation to a cosine response which can actually be used inside the quartz tube off-line with no fiber running through.

6.6   Monitoring approaches for fiber industries

Various approaches have become available for the fiber process industries to allow a range of choices for both checking and monitoring the operation of the UV lamps' capability to deliver the expected spectral distribution and power levels necessary to achieve cure at the required process speed. These approaches are briefly described below.

6.6.1   Off-line, without fiber, for UV lamp system performance benchmarking

The first approach allows the UV lamp system to have measurements made directly inside the usual quartz tube, as shown in Figure 6.

Figure 6.   Measuring off-line inside quartz tube

Here the operator is able to use, for short periods, a specially designed quartz probe protected inside a thick stainless steel tube which can be inserted inside the quartz tube of the secondary 'back reflector', illustrated in Figure 1. Once inserted inside the tube with the lamp on at full power, the quartz probe is designed to be able to 'look' sideways, at 90°, either directly at the bulb, or at the reflector to be able to judge the condition and operation of the various system components, from the spectral distribution observed, depending on the rotation of the probe. Also, by observing differences at one part of the tube compared to the

another, it is possible to judge whether there is an even spectral power distribution along the length of the bulb. If there is a marked difference from one end to another, then it is possible that a magnetron may need attention.
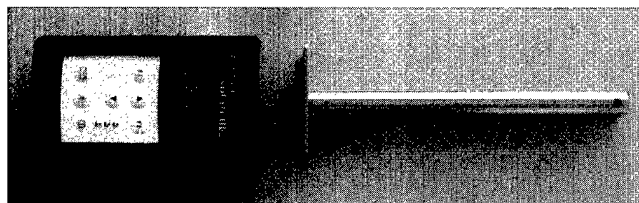
Figure 7. Compact spectroradiometer based checking device, with high temperature probe for use inside quartz tube.

A recent self-contained hand held instrument with detachable probe for use inside the quartz tube is shown in Figure 7. Both instruments in Figures 6 and 7 can provide valuable lamp system diagnoses when the lamp is demounted from the machine, for example, in a maintenance department. The UV output of the lamp can be thoroughly checked before being brought back in to service after being maintained.

Because it is used right inside the quartz tube, this measuring option gets very close to measuring what the fiber actually 'sees' while passing through the quartz tube. However, it has the disadvantage that it cannot be used for checking the lamp during fiber manufacture, so is described as 'off-line'.

6.6.2 On-line manual, with fiber, for UV lamp performance checks and problem diagnosis

As we have seen in Figures 4 and 5, probe locators can be fitted to the lamp to take advantage of the monitoring points provided by the lamp manufacturer to allow measurements to be taken 'on-line', either before or during a fiber manufacturing run.
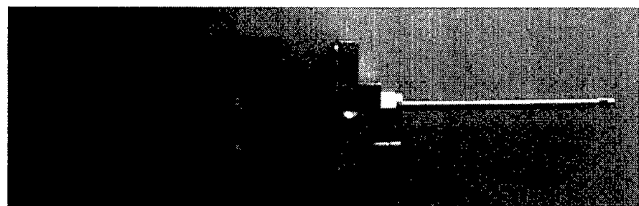
Figure 8. New compact spectroradiometer based sensor with fine probe for use with probe locator on lamp system

Figure 8 shows a more recent sensor with the same type of probe illustrated in Figures 4 and 5 for allowing measurements to be taken at the monitoring points shown in Figure 1 while fiber is running through the process. This system provides absolute calibrated measurements at an exact point in the lamp system which is defined mechanically with very precise positional accuracy. This type of probe can be manually moved from monitoring point to monitoring point to take and compare measurements easily. It can also be left 'in-situ' to allow permanent on-line monitoring measurements to be taken, with several sensors arranged in a digital network, feeding UV spectral data back to a host PC or PLC.

The probes and sensors of Figure 7 and Figure 8 are interchangeable and each contains their own calibration data to take the probe characteristics into account. The probe should always be calibrated on the sensor it is intended to be used with.

6.6.3 On-line automatic, with fiber, for data collection and UV watchdog monitoring.

The UV measurements systems so far described are essentially manually operated where an operator or engineer must physically take the measurement, and store the data (though the networking possibilities of the system in 6.6.2 allow this possibility now). Complete, multichannel on-line UV spectral monitoring systems are also available, as shown in Figure 13 [3]. The electro-mechanically operated shuttered probe is connected by a UV transmitting quartz fiber back to the control unit. The probe can be fitted in exactly the same position on the microwave lamp back reflector as the probe locator shown in Figures 4 and 5. Inside the control unit is a single spectroradiometer sensor which is mechanically indexed to look at one of up to 16 UV fibers in sequence to be able to detect relatively slow changes in lamp output caused by optical surface deterioration, or other factors described in Section 5. The reader should refer to Reference 3 for a more detailed description of this system.
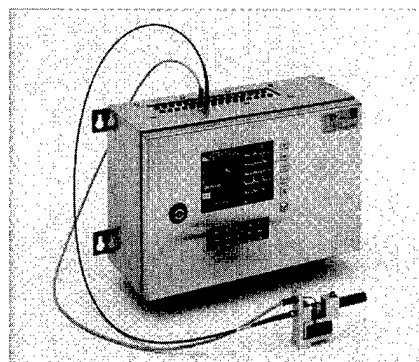
Figure 9. Complete, 16 channel on-line UV spectrum monitoring system

The system is relatively low cost, but can only provide relative measurements because of the unknown effect of the optical interfaces. It can be connected to a PLC or PC to provide monitoring and control of one, or several fiber process machines. The advantage is that it provides completely automatic monitoring of the UV lamps, and can be programmed to provide warning and alarms of UV lamps operating outside defined limits in any part of the UV spectrum from 240 to 425nm.

6.7 Calibration

All of the UV spectroradiometer systems described are calibrated according to the same methods. Although at the time of writing there are no international standard methods of calibrating UV Spectroradiometers (neither is there for UV radiometers) the steps used by the author can be summarized as: -

1. Define geometry of light sources and the collection optics to be involved in the calibration and field measurement
2. Perform wavelength calibration using Mercury and other 'pen-ray' lamps

3. Perform system response 'shape' characteristics calibration using special smooth continuum lamps (especially Deuterium & tungsten lamps) traceable to national standards
4. Set final overall level, at representative power level e.g. Curing Lamp (undoped Mercury medium/high pressure preferred) – for industrial applications

There is a growing body of work [1][2] in the international arena to move towards standardization of UV measurements, particularly with the use of spectroradiometers which do not suffer from the disadvantages of radiometers outlined in Section 6.2

7 Practical application of spectroradiometers in a production environment

The above described spectroradiometer instruments and high temperature probes have been in use in the various applications in the UV radiation curing industry for several years. During that time ways have needed to be found to make measurements as easy and error free as possible, but with such instruments, UV probes, and probe locators it is possible to: -

- Collect UV spectral data regularly with date and time stamping
- Position spectroradiometer / probe combination in the same place each time a reading is to be taken
- Compare calibrated readings
- Compare intensity with pre-established baseline data
- Check lamp spectra are correct
- Check short/long wavelength ratios – *see Figure 7.*

By following this discipline it is possible to diagnose a situation where a UV process is failing to cure, and decide if there is a lamp issue, or whether one needs to look somewhere else for the cause of the problem.
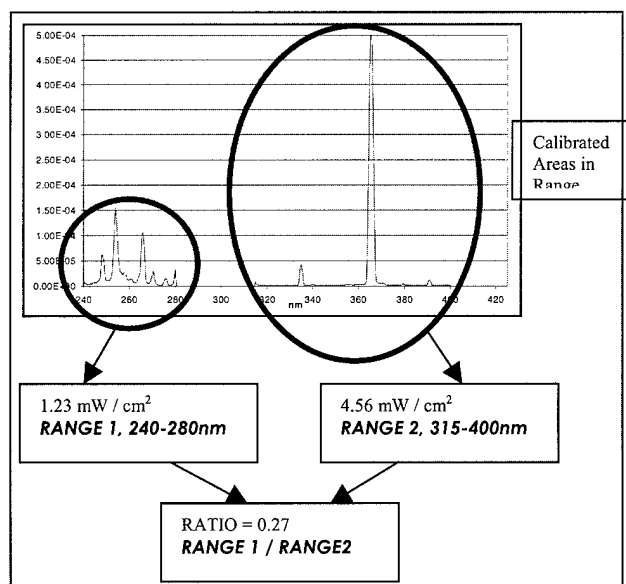
Figure 10. Using a spectroradiometer to integrate power in two specified ranges

Figure 10 shows how different parts of a typical UV spectrum from a curing lamp can be compared as a ratio between short wavelength and long wavelength data to form a ratio between the two. Should the short wavelength power fall off as a ratio of the long wavelength power then the bulb may be nearing the end of its life (particularly if it is an arc lamp), may be dirty, may have a dirty reflector or contaminated quartz tube.

In addition to lamp diagnostics, it is possible by following the rigorous calibration process with UV Spectroradiometers [1] to allow valid comparisons using absolute power measurements (over specified wave ranges) to be made between lamps, between different lamp systems or machines, between different processes and between different plant locations. Such absolute calibration ability also points the way for new and better methods of process specification.

8 Examples

There now follow some examples of data collected from real UV lamp systems used in the fiber process industries. The typical application is in fiber coloring. In each case we are monitoring 'D' type bulb (as shown in Figure 2). As described above, we can integrate using a UV spectroradiometer over a defined special range. We have defined two spectral ranges 300 to 425nm (A1), 280 to 320nm (A2), and also have plotted the behavior of one specific Mercury line, that at 313nm. The traces have been normalized to show their behavior one against another.
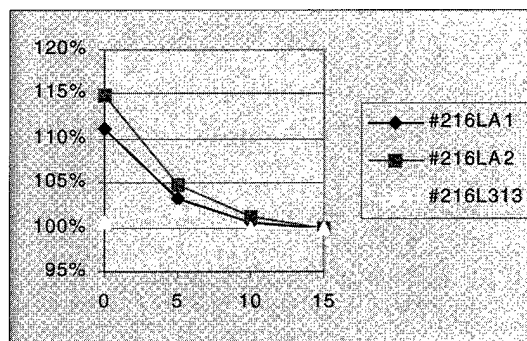
Figure 11. Typical D bulb cold start-up

Figure 11 shows a typical lamp startup recorded automatically every 5 minutes. The 100% normalization level has been set at 15 minutes since the lamp is turned on from cold. It is interesting to note that the total UV spectral output in A1 and A2 start at a higher level, approximately 10 to 15% above their settled level, and take about 10 to 15 minutes to settle to steady state. The 313nm spectral line, being derived from pure mercury settles to its 100% level much faster. This phenomenon can be explained by the different behavior of the pure mercury and the additives in the D bulb which modify the spectral distribution of the bulb output. The D bulb is more input power and envelope temperature dependant than a straightforward mercury H bulb, as we noted above.
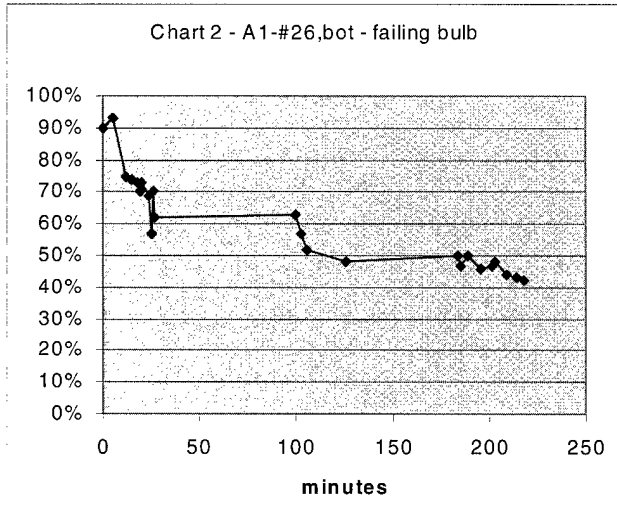
Figure 12. Failing bulb due to overheating (inadequate airflow)

If we have a faulty bulb – in this case due to lack of airflow – the bulb overheats and fails quite rapidly. In this case we can see with three successive coloring runs that the bulb deteriorates each time it is used, falling to below 50% of its original power level when monitoring started.

After this was noticed, the bulb was changed for a new one, the lamp system serviced and then run again, and checked more frequently, as shown in Figure 13.
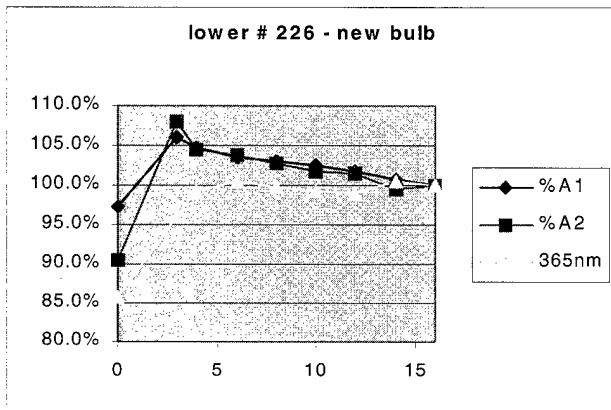
Figure 13. New D bulb start up

Figure 13 has sampling points collected more frequently (every 2 minutes) and shows more clearly the different behavior of the mercury and additive performance after start up. The initial sample point is taken almost immediately after turn on so the microwave lamp's very rapid turn on behaviors is exhibited very well.

9   Conclusions

Such UV spectral measurement instrumentation as described in this paper is increasingly being used throughout the fiber process industries to reduce uncertainty about the quality of the UV power being delivered to the process during manufacture. Regular, accurate manual UV spectral measurements, and automatic on-line monitoring have shown themselves to be worthwhile activities across many manufacturing sites, and during process development.

10   References

1. 'Accurate, High Power UV Spectral Measurement'– Andrew Ridyard, 4D Controls Ltd. RadTech USA 2000 (Baltimore) proceedings.

2. 'Reliable Spectroradiometry' - Henry J. Kostkowski, published 1997 by Spectroradiometry Consulting, MD, USA. ISBN 0-9657713-0-X

3. 'A UV lamp spectral measuring multi-point on-line monitoring system for Radiation Cured processes' – Andrew Ridyard, 4D Controls Ltd. RadTech USA 98 (Chicago) proceedings.
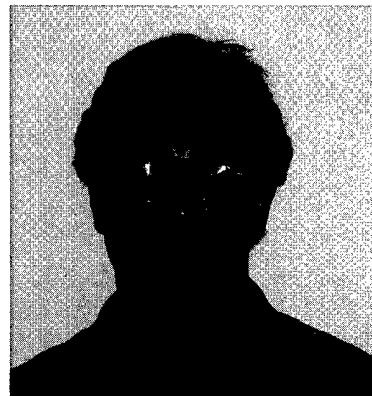
The author is managing and technical director of 4D Controls Ltd. After a 4-year student apprenticeship with GEC in the UK, he achieved a First Class Honours degree in Electrical and Electronic Engineering from the University of Bath. He worked for 4 years for Eurotherm International as an industrial instrumentation and control electronics design engineer. He then traveled and worked in Australia and the USA before returning to the UK in 1986 to start 4D Controls Ltd., to design, develop and manufacture a range of industrial measurement, control and automation products. He is a Chartered Engineer and a Fellow of the Institution of Electrical Engineers. He is the inventor of the patented Solatell® technology for UV radiation spectral distribution measurements, and chief designer of UV spectral instrumentation for 4D Controls Ltd. He has presented numerous conference papers in the UK, Europe, the USA and Japan.

Twisted Pair Cable Design Analysis and Simulation

Mohammed M Al-Asadi[¹], Alistair P Duffy[¹], Kenneth G Hodge[*] and Arthur J Willis[*]

[¹]Department of Engineering and Technology, De
Montfort University. Leicester, LE1 9BH UK.

Brand-Rex Ltd., Glenrothes, Fife, KY6 2RS, Scotland,
UK.

Principle Contact: email alasadi@dmu.ac.uk

Abstract

In this paper, a family of equations has been developed to describe the behaviour of twisted pair cables as functions of cable dimensions, basic material parameters and frequency of operation. These equations allow the prediction of secondary parameters without the need to extrapolate from measurements. Further a simulation method has been developed which requires dimensions, materials and frequency only and enables investigation of the behaviour of the cable under the influence of periodic, sporadic or random deformities, such as those arising through poor installation practice or production process variability. Both analytical and simulation approaches complement the more historical approach of iterative development and practical extrapolation. The set of equation derived and the simulation approach were then used to predict the performance of a twisted pair cable where the dimensions and the materials are known. The results obtained were then validated against measurements. Excellent agreement is in all cases demonstrated.

1. Introduction

Data communication is of increasing importance to society, with the information revolution showing no sign of slowing. Applications such as the Internet and mobile communications are becoming an integral part of everyday life. A common component in all the applications is the communication channel. This may be transmission line and cable, optical fibre, wave-guide, 'free space' propagation, etc. This paper is concerned with twisted pair cables.

Twisted pair cables have been in use for a long time. Early telephone signals were sent over twisted pair cable and now virtually all networked buildings use twisted pair cable for telephone and computer communication signals. Despite the fact that coaxial cables and optical fibre cables were developed to handle higher frequency signals with minimal interference, twisted pair cables have been developed so that they can carry increasingly higher frequency signals; The proposed category 8 cable will be specified to 1.2 *GHz*.

Different varieties of twisted pair cables are available for different needs and applications. First is the basic telephone cable, which is known as direct-inside wire (DIW), is still in use in some countries. Developments over the years, such as improvements in the individual wire sheaths and variations in the twist have led to the development of standard-compliant Category 3 UTP cables specified for frequencies up to 16 *MHz*. Further improvement led to the development of Category 4 for specifications up to 20 *MHz* and Category 5 for specifications up to 100 *MHz*. The next generations of Category 6 and Category 7 cables are now emerging in the open market. The specifications of those Categories reach 200 *MHz* and 600 *MHz* respectively. Category 6 cable can be, and Category 7 cable is, shielded.

With the emergence of new technologies in high frequency communication system, the employment of multi-conductor twisted pair cable has increased. The primary parameters, R, L, G and C, for a such cables at high frequencies, are not difficult to calculate [1]. The calculation of the secondary parameters, such as attenuation constant α, the phase constant β, the propagation constant γ, and the characteristic impedance Z_o, relies on the calculation of the primary parameters [1,2].

Cable manufacturers and design engineers are keen to understand the behaviour of communication cables, specifically twisted pair cables, at high frequencies. They need to understand the effects of changing the dimensions of the cable and the material, particularly the dielectric, on cable performance at the frequency of operation. Therefore there is a need for a set of design equations to relate all the secondary parameters to the zeroth order parameters: cable dimensions, material parameters and the frequency of operation. Hence, the first aim of this paper is to develop a family of equations to describe the behaviour of twisted pair cables as function of cable dimensions, basic material parameters and frequency of operation.

For a regular communication channel, where the cable is uniform and the matching between the communication channel components is perfect, the calculation of secondary parameters can be obtained using the developed set of equations. But what will happen when the cable used suffers an irregularity ? And what would be the way of measuring or calculating the secondary parameters of cable affected by such variations along itself or by miss-handling the cable properly? This paper addresses cable irregularities and the calculation of secondary parameters. The answer could be difficult to find using measurements at higher frequencies [3]. Hence, the need for further analytical development and the development of a modelling technique, capable of tackling the problems arising in testing cables at very high frequencies.

The second approach illustrated in this paper is the development of a computer-modelling tool, using the Transmission Line Matrix, TLM, method [4], capable of simulating the behaviour of both regular and irregular twisted pair cables. The model is able to incorporate other parameters of the communication channel, such as connectors and different termination, to analyse their contribution to the performance of the communication channel. The next section includes the derivation of the secondary parameter equations of a twisted pair cable.

2. Secondary Parameters Derivation

This section presents the derivation of equation for the calculation of attenuation constant, phase constant and hence propagation constant for unshielded twisted pair cable (UTP). It also presents the derivation of an equation for the calculation of the attenuation constant of a shielded twisted pair cable (STP). Equations for the calculation of both amplitude and phase of the characteristic impedance of UTP cables are also derived and presented in this section.

2.1 UTP Cables Attenuation Constant Calculation

The attenuation constant (α_u), can be obtained by calculating the real part of the propagation constant (γ), where γ is given by [1]:

$$\gamma = \alpha_u + j\beta_u \tag{1}$$

and β_u is the phase constant. Letter u is used to differentiate between the unshielded formula and the shielded formula presented later (where letter s is used). The propagation constant is also given as:

$$\gamma = \sqrt{(R + j\omega L)(G + j\omega C)} \tag{2}$$

Where R, L, G and C are the distributed primary parameters per unit length of one segment of a single pair cable and given as [4]:

$$R = \frac{2R_s}{\pi\ d}\left[\frac{D/d}{\sqrt{(D/d)^2 - 1}}\right] \quad (\Omega/\text{m}) \tag{3}$$

$$L = \frac{\mu d}{\pi}\cosh^{-1}\left(\frac{D}{d}\right) \quad (\text{H/m}) \tag{4}$$

$$G = \frac{\pi\ \sigma_d}{\cosh^{-1}\left(\frac{D}{d}\right)} \quad (\text{S/m}) \tag{5}$$

$$C = \frac{\pi\varepsilon}{\cosh^{-1}\left(\frac{D}{d}\right)} \quad (\text{F/m}) \tag{6}$$

where D is the distance between the centres of the two conductors of the cable, d is the diameter of each conductor and R_s is the surface resistance of the conductor. For low loss cables at relatively high frequency, it can be assumed that $R << \omega L$. Using the binomial expansion of [5]:

$$(1 + b)^{\pm\frac{1}{2}} = 1 \pm \frac{b}{2} \qquad \text{For} \qquad b<<1$$

Equation .2 can be simplified to the following form:

$$\gamma = \frac{1}{2}\left(R\sqrt{\frac{C}{L}} + G\sqrt{\frac{L}{C}}\right) + j\left(\omega\sqrt{LC} - \frac{RG}{4\omega\sqrt{LC}}\right) \tag{7}$$

Comparing the above equation with equation 1, the attenuation constant can be given as:

$$\alpha = \frac{1}{2}\left(R\sqrt{\frac{C}{L}} + G\sqrt{\frac{L}{C}}\right) \tag{8}$$

Substituting the values of the primary parameters given in equations 3→ 6 in the last equation with some mathematical simplifications gives:

$$\alpha = \frac{1}{2}\left[\frac{2R_s}{\pi d} \times \left(\frac{D/d}{\sqrt{(D/d)^2 - 1}}\right) \times \frac{\pi}{\cosh^{-1}(D/d)}\sqrt{\frac{\varepsilon}{\mu_d}} + \sigma_d\sqrt{\frac{\mu d}{\varepsilon}}\right] \tag{9}$$

The surface resistivity for any material can be given as ($R_s = R_k \cdot f^{1/2}$), where R_k is a constant related to the conductivity of the conductor material, σ, and the skin depth, δ. For example, for copper conductors, the constant R_k is given in reference [1] as 2.61×10^{-7}. Substituting R_s into equation 9, and further simplifying, gives:

$$\alpha = \frac{R_k f^{1/2}}{d\cosh^{-1}(D/d)}\left(\frac{D/d}{\sqrt{(D/d)^2 - 1}}\right)\sqrt{\frac{\varepsilon}{\mu_d}} + \frac{\sigma_d}{2}\sqrt{\frac{\mu_d}{\varepsilon}} \tag{10}$$

It is easier to visualise 'cause and effect' if the equation is a function of the dielectric thickness around each conductor and the conductor diameter. Therefore, if τ is the thickness of the dielectric then, for the two-wire cable, $D = 2\tau + d$. Hence, the term (D/d) in the last equation can be written in terms of the dielectric thickness and the conductor's diameter as ($D/d = 2\tau/d + 1$) Meanwhile, the conductivity of the dielectric can be given as [1] ($\sigma_d = \omega\varepsilon = 2\pi f\varepsilon$). To obtain the attenuation constant in decibels, the last equation should be multiplied in 8.686 [1]. Hence equation 10 can be further simplified to:

$$\alpha_u = \left\{\frac{8.686R_k}{d\cosh^{-1}\left(\frac{2\tau}{d} + 1\right)}\left(\frac{\left(\frac{2\tau}{d} + 1\right)}{\sqrt{\left(\frac{2\tau}{d} + 1\right)^2 - 1}}\right)\sqrt{\frac{\varepsilon}{\mu_d}}\right\}f^{1/2}$$
$$+ \left\{8.686\pi\varepsilon''\sqrt{\frac{\mu_d}{\varepsilon}}\right\}f \tag{11}$$

Assuming that:

$$\alpha_{ua} = \left\{\frac{8.686R_k}{d\cosh^{-1}\left(\frac{2\tau}{d} + 1\right)}\left(\frac{\left(\frac{2\tau}{d} + 1\right)}{\sqrt{\left(\frac{2\tau}{d} + 1\right)^2 - 1}}\right)\sqrt{\frac{\varepsilon}{\mu_d}}\right\} \tag{12}$$

and

$$\alpha_{ub} = \left\{8.686\pi\varepsilon''\sqrt{\frac{\mu_d}{\varepsilon}}\right\} \tag{13}$$

The attenuation can be written in a simple form as:

$$\alpha_u = \alpha_{ua} f^{1/2} + \alpha_{ub} f \tag{14}$$

It is clear that α_{ua} is mostly a dimension dependant factor while α_{ub} is a material dependant factor. For a copper cable where $D = 0.94$ mm and $d = 0.53$ mm, and attenuation is in $dB/100m$ and frequency is in MHz, both factors given in equations 13 and 14, are calculated and found as; $\alpha_{ua} = 1.7259$, $\alpha_{ub} = 0.01453$. Equation 14 is similar to the equation commonly used by manufacturers, which is in the following form [6]:

$$\alpha_u = af^{1/2} + bf + cf^{-1/2} \tag{15}$$

The terms a, b and c of equation 15 are reported as [6]; $a = 1.967$, $b = 0.023$ and $c = 0.1$. It can be seen that for the high frequencies, the 3rd term of equation 15 will be very small and can be ignored. However, it does not appear in equation 14, which was obtained through direct analysis (using high frequency assumption).

2.2 UTP Cables Phase Constant Calculation

Following the same procedure, comparing equations 1 and 7, the phase constant of the UTP cable can be obtained as:

$$\beta = \left[\omega\sqrt{LC} - \frac{RG}{4\omega\sqrt{LC}} \right] \tag{16}$$

For a low loss cable, the phase constant may be represented by the 1st term of the above equation; this is common practice [1]. But, for accurate calculations, for any cable and over a large range of frequencies. It is more appropriate to use equation 16. Again, substituting equations $3 \rightarrow 6$ in equation 16 and with some mathematical simplification the phase constant can be obtained as:

$$\beta = \beta_a f^{1/2} + \beta_b f \tag{17}$$

where:

$$\beta_a = \frac{-R_k \varepsilon''}{2d\sqrt{\mu_d \varepsilon}\, \cosh^{-1}\!\left(\frac{2\tau}{d}+1\right)} \left[\frac{\frac{2\tau}{d}+1}{\sqrt{\left(\frac{2\tau}{d}+1\right)^2 - 1}} \right] \tag{18}$$

and

$$\beta_b = 2\pi\sqrt{\mu_d \varepsilon} \tag{19}$$

It is clear that equation 17 is obtained in a similar form to that of equation 14 as a function of cable dimensions, material properties and frequency

2.3 UTP Cables Propagation constant calculation

For the unshielded twisted pair cable, substituting equations 14 and 17 in equation 1, a simple formula for the propagation constant can be obtained as:

$$\gamma = (\alpha_a + j\beta_a) f^{1/2} + (\alpha_b + j\beta_b) f \tag{20}$$

which can again be rewritten as:

$$\gamma = \gamma_a f^{1/2} + \gamma_b f \tag{21}$$

where,

$$\gamma_a = \alpha_a + j\beta_a \tag{22}$$

and

$$\gamma_a = \alpha_b + j\beta_b \tag{23}$$

It can be seen that as both attenuation and phase constants are functions of cable dimensions, material properties and frequency, subsequently, the propagation constant is also obtained as a function of the cable dimensions, materials properties and frequency. The next secondary parameter discussed is the characteristic impedance of the cable that is analysed in the following sub-section.

2.4 UTP Cables Characteritic Impedance calculation

It is well known that the characteristic impedance, Z_o can be given as [1]:

$$Z_o = \sqrt{\frac{R + j\omega L}{G + j\omega C}} \tag{24}$$

As it is a complex quantity, both impedance amplitude and phase are derived as functions of cable dimensions, materials properties and frequency of operation.

2.4.1 *Amplitude Calculations:* Squaring both sides of equation 24 and taking the magnitude gives:

$$\left| Z_o^2 \right| = \left(\frac{R^2 + \omega^2 L^2}{G^2 + \omega^2 C^2} \right)^{0.5} \tag{25}$$

Therefore the magnitude of the characteristic impedance Z_o can be given as:

$$\left| Z_o \right| = \left(\frac{R^2 + \omega^2 L^2}{G^2 + \omega^2 C^2} \right)^{0.25} \tag{26}$$

Using equations $3 \rightarrow 6$, and replacing σ_d by ($\sigma_d = \omega\varepsilon'' = 2\pi f\varepsilon''$), the above equation can be mathematically simplified as a function of cable dimensions, material properties and frequency to:

$$\left| Z_o \right| = \frac{\sqrt{\left(\cosh^{-1}\!\left(1 + \frac{2\tau}{d}\right) \right)}}{\pi} \cdot \left[\frac{\frac{(2.61 \times 10^{-7})^2 (2\tau + d)^2}{4\pi^2 d^2 f^{1.75} \tau\ (\tau + d)} + \mu^2 \left(\cosh^{-1}\!\left(1 + \frac{2\tau}{d}\right) \right)^2}{\left(\varepsilon''^2 + \varepsilon^2 \right)} \right]^{0.25} \tag{27}$$

To enhance clarity equation 27 can be rearranged in the form:

$$|Z_o| = a \left(\frac{b+c}{e} \right)^{0.25} \qquad (28)$$

where:

$a = \dfrac{\sqrt{\left(\cosh^{-1}\left(1 + 2\tau/d \right) \right)}}{\pi}$ is a function of dimensions,

$b = \dfrac{\left(2.61 \times 10^{-7} \right)^2 (2\tau + d)^2}{4\pi^2 d^2 f^{1.75} \tau \ (\tau + d)}$ is a function of dimensions and frequency, but note the 10^{-14} term,

$c = \mu^2 \left(\cosh^{-1}\left(1 + 2\tau/d \right) \right)^2$ is a function of materials and dimensions, and

$e = \left(\varepsilon''^2 + \varepsilon^2 \right)$ is a function of material properties only.

At high frequencies, assuming that $b \ll c$ and $\varepsilon'' \ll \varepsilon$ then equation 27 can be simplified as:

$$|Z_o| = \frac{\sqrt{\left(\cosh^{-1}\left(1 + 2\tau/d \right) \right)}}{\pi} \left(\frac{\mu^2 \left(\cosh^{-1}\left(1 + 2\tau/d \right) \right)^2}{\varepsilon^2} \right)^{0.25}$$

$$= \frac{\sqrt{\left(\cosh^{-1}\left(1 + 2\tau/d \right) \right)}}{\pi} \sqrt{\frac{\mu \left(\cosh^{-1}\left(1 + 2\tau/d \right) \right)}{\varepsilon}}$$

Hence, at high frequencies, the magnitude of the characteristic impedance of the cable may be simplified to the following form:

$$|Z_o| = \frac{\cosh^{-1}\left(1 + 2\tau/d \right)}{\pi} \sqrt{\frac{\mu}{\varepsilon}} \qquad (29)$$

Equation 29 is similar to the equation reported by [1] at high frequencies.

2.4.2   Phase Calculations: Again, squaring both sides of equation 24 and taking the phase gives:

$$\angle Z_o^2 = \tan^{-1}\left(\frac{\omega L}{R} \right) - \tan^{-1}\left(\frac{\omega C}{G} \right) \qquad (30)$$

Using de Moivre's theorem [5], the phase constant of the characteristic impedance, Z_o, is given as:

$$\angle Z_o = \frac{1}{2} \left(\tan^{-1}\left(\frac{\omega L}{R} \right) - \tan^{-1}\left(\frac{\omega C}{G} \right) \right) \qquad (31)$$

which can be rearranged to [5]:

$$\angle Z_o = \frac{1}{2} \left(\tan^{-1}\left(\frac{\omega L}{R} \right) + \tan^{-1}\left(-\frac{\omega C}{G} \right) \right) \qquad (32)$$

Since [5]:

$$\tan^{-1}(\phi) + \tan^{-1}(\vartheta) = \left(\tan^{-1}\left(\frac{\phi + \vartheta}{1 - \phi\vartheta} \right) \right) + \theta$$

where:

$$\theta = \begin{cases} \pi, & \phi\vartheta > 1, \phi > 0 \\ 0, & \phi\vartheta < 1 \\ -\pi, & \phi\vartheta > 1, \phi < 0 \end{cases}$$

Therefore equation 32 can be rewritten as:

$$\angle Z_o = \frac{1}{2} \left(\tan^{-1}\left(\frac{\dfrac{\omega L}{R} - \dfrac{\omega C}{G}}{1 + \dfrac{\omega L}{R} \cdot \dfrac{\omega C}{G}} \right) + \theta \right)$$

Since

$$\frac{\omega L}{R} - \frac{\omega C}{G} < 1$$

Therefore θ of the above equation goes to zero and hence, the phase of the characteristic impedance can be simplified to:

$$\angle Z_o = \frac{1}{2} \left(\tan^{-1}\left(\frac{\omega LG - \omega RC}{RG + \omega^2 LC} \right) \right)$$

Once again, substituting equations 3→6 in the above equation, the phase constant of the characteristic impedance will be given in terms of cable dimensions, materials and frequency, after some mathematical simplifications, in the following form:

$$\angle Z_o = \frac{1}{2} \tan^{-1}\left(\frac{a_\theta \varepsilon'' f^{1/2} - b_\theta \varepsilon}{a_\theta \varepsilon \ f^{1/2} + b_\theta \varepsilon''} \right) \qquad (33)$$

where:

$$a_\theta = \pi \mu_d \qquad (34)$$

And

$$b_\theta = \frac{2.61 \times 10^{-7}}{d \cosh^{1/2}(1 + 2\tau/d)} \left(\frac{\left(1 + 2\tau/d \right)}{\sqrt{4\tau/d \left(1 + \tau/d \right)}} \right) \qquad (35)$$

Equations 34 and 35 demonstrate that a_θ is a function of the cable materials and b_θ is a function of its dimensions, therefore equation 33 is a function of materials, dimension and frequency as required

At this stage, the only secondary parameter that is not discussed here is the return loss. This is investigated in detail in an associated paper [7]. The next subsection illustrates the derivation of a similar

equation for the calculation of the attenuation constant of a shielded twisted pair cable (STP).

2.5 STP Cables Attenuation Constant Calculation

For this analysis, it will be assumed that the shield is a perfect cylinder. In this case, the inner diameter of the shield D_S, is twice the distance between the centres of the conductors, (i.e. $D_S = 2D$). The attenuation constant due to the conductors and the shielding material, α_c, is given by [1] as:

$$\alpha_c = \frac{R}{2Z_O} \tag{36}$$

R, in the above equation, is the resistance per unit length, Ω/m, and is given as [1]:

$$R = \frac{2R_{S2}}{\pi d}\left[1 + \frac{1+2p^2}{4p^4}\left(1 - 4q^2\right)\right] + \frac{8R_{S1}}{\pi D_S}q^2\left[1 + q^2 - \frac{1+4p^2}{8p^4}\right] \tag{37}$$

where $p = D/d$ and $q = D/D_S$. As $D = d+2\tau$, p and q can be written as:

$$p = \frac{d + 2\tau}{d} = 1 + \frac{2\tau}{d} \tag{38}$$

$$q = \frac{D}{D_S} = \frac{D}{2D} = 0.5 \tag{39}$$

For a copper conductor, the surface resistivity is $R_{S2} = 2.61 \times 10^{-7}$ $f^{1/2}$, and for an Aluminium shield, the surface resistivity is $R_{S1} = 3.26 \times 10^{-7}$ $f^{1/2}$. However, to make the design equations more general, the surface resistivity for the conductors is taken as $R_{S2} = R_{k2}f^{1/2}$, and for the shield as $R_{S1} = R_{k1}f^{1/2}$. R_{k1} and R_{k2} are constants related to the conductivity, σ, and the skin depth, δ, of both the conductors and the shield respectively. Substituting equations 38 and 39 in equation 37, the resistance R will be given as a function of the conductor diameter d, the dielectric thickness τ, and the frequency of operation f. Equation 37 may now be further simplified to the following form:

$$R = \frac{2}{\pi}\left[\frac{R_{k2}}{d} + \frac{R_{k1}}{2(d+2\tau)}\left(1.25 - \frac{1+4\left(1+\frac{2\tau}{d}\right)^2}{8\left(1+\frac{2\tau}{d}\right)^4}\right)\right]f^{1/2} \tag{40}$$

The characteristic impedance Z_o, of equation 36 is given as [1]:

$$Z_O = \frac{\eta}{\pi}\left[\ln\left\{2p\left(\frac{1-q^2}{1+q^2}\right)\right\} - \frac{1+4p^2}{16p^4}\left(1 - 4q^2\right)\right] \tag{41}$$

Using the dielectric factor $\eta = \sqrt{\mu d / \varepsilon}$ and equations 38 and 39, equation 41 can be further simplified to:

$$Z_O = \frac{1}{\pi}\sqrt{\frac{\mu d}{\varepsilon}}\left[\ln\left\{1.2\left(1+\frac{2\tau}{d}\right)\right\}\right] \tag{42}$$

Using the values of R and Z_o, given in equations 40 and 42 respectively, the attenuation due to the conductor given in equation 36, can then be written as:

$$\alpha_c = \frac{\frac{2}{\pi}\left[\frac{R_{k2}}{d} + \frac{R_{k1}}{2(d+2\tau)}\left(1.25 - \frac{1+4\left(1+\frac{2\tau}{d}\right)^2}{8\left(1+\frac{2\tau}{d}\right)^4}\right)\right]f^{1/2}}{\frac{2}{\pi}\sqrt{\frac{\mu d}{\varepsilon}}\left[\ln\left\{1.2\left(1+\frac{2\tau}{d}\right)\right\}\right]} \tag{43}$$

which can be simplified to the following form:

$$\alpha_c = \frac{\left[\frac{R_{k2}}{d} + \frac{R_{k1}}{2(d+2\tau)}\left(1.25 - \frac{1+4\left(1+\frac{2\tau}{d}\right)^2}{8\left(1+\frac{2\tau}{d}\right)^4}\right)\right]}{\left[\ln\left\{1.2\left(1+\frac{2\tau}{d}\right)\right\}\right]}\sqrt{\frac{\varepsilon}{\mu d}}f^{1/2} \tag{44}$$

The attenuation due to the dielectric α_d, is also given by [1] as:

$$\alpha_d = \frac{\sigma\eta}{2}$$

Substituting both σ and η, by their values, the last equation can be simplified to the following form:

$$\alpha_d = \frac{\varepsilon''\omega}{2}\sqrt{\frac{\mu d}{\varepsilon}} = \pi\varepsilon''\sqrt{\frac{\mu d}{\varepsilon}}f \tag{45}$$

Using equations 44 and 45 and simplifying, the total attenuation α_s in dB/m can be given as:

$$\alpha_s = 8.686\left\{\frac{\left[\frac{R_{k2}}{d} + \frac{R_{k1}}{2(d+2\tau)}\left(1.25 - \frac{1+4\left(1+\frac{2\tau}{d}\right)^2}{8\left(1+\frac{2\tau}{d}\right)^4}\right)\right]}{\left[\ln\left\{1.2\left(1+\frac{2\tau}{d}\right)\right\}\right]}\sqrt{\frac{\varepsilon}{\mu d}}f^{1/2}\right\}$$
$$+ \left\{8.686\pi\varepsilon''\sqrt{\frac{\mu d}{\varepsilon}}\right\}f \tag{46}$$

Given that:

$$\alpha_{sa} = 8.686 \left\{ \frac{\left[\frac{R_{k2}}{d} + \frac{R_{k1}}{2(d+2\tau)} \right] \left[1.25 - \frac{1+4\left(1+\frac{2\tau}{d}\right)^2}{8\left(1+\frac{2\tau}{d}\right)^4} \right]}{\left[\ln\left\{ 1.2\left(1+\frac{2\tau}{d}\right) \right\} \right]} \right\} \sqrt{\frac{\varepsilon}{\mu d}}$$

(47)

and

$$\alpha_{sb} = \left\{ 8.686 \, \pi\varepsilon^{''} \sqrt{\frac{\mu d}{\varepsilon}} \right\}$$ (48)

Equation 46 can now be simplified and written in the following form:

$$\alpha_s = \alpha_{sa} f^{1/2} + \alpha_{sb} f$$ (49)

This is similar to equation 14 developed earlier for the calculation of the attenuation constant for unshielded twisted pair cable. It should be noted that the f term α_{sb} is exactly equivalent to the f term of a UTP cable in equation 14. The only variation will arise from different effective permittivity due to presence of the shield. In here, an equation for the calculation of the attenuation constant of a shielded cable has been developed. A set of similar design equations for the calculations of the rest of the secondary parameters can also be developed in.

The next section of this paper illustrates the development of a modelling approach for the simulation of both regular and irregular twisted pair cables (UTP), which can incorporate other communication channel components such as connectors into the model. The modelling method used is the Transmission Line Matrix (TLM) modelling method.

3. TLM Model of a UTP cable

The Transmission Line Matrix (TLM) modelling method is a time domain numerical analysis technique that was originally developed at Nottingham University in the early 1970s [8]. It is based on the representation of the modelled physical phenomena by a network of transmission lines. Any model developed using a TLM approach consists of many transmission-line segments connected together [4]. For the purpose of this paper, TLM may be understood via a description of a twisted pair cable model. One elemental section (of length Δl) of a lossy, single pair cable is shown in figure 1.

As described in [9] and [10], the combination of L and C can be replaced by a link line of impedance $(Z_o=(L/C)^{1/2})$, and the time step for a wave to propagate one TLM node is $(\Delta t=(L.C)^{1/2})$. R and G, as they are not time dependent parameters, are left in the TLM model without change. For a regular cable, Z_o would replace the LC combination at every segment along the cable. If the cable is not regular, then L and C are not the same along the cable, hence to keep a constant time step, Δt, for iterative TLM method, the minimum inductance, L_{min} and minimum capacitance C_{min} are

computed and combined in a link line of impedance $(Z_{min}=(L_{min}/C_{min})^{1/2})$.The remaining parts of both L and C at each node are calculated and replaced by stub transmission line models, having their impedances as in [9,10]. The time step in this case is calculated as $(\Delta t_{min}=(L_{min}.C_{min})^{1/2})$.
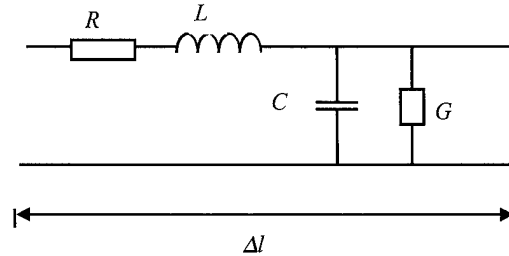
Figure 1. One segment of transmission line showing its primary parameters

The TLM model of two neighbouring segments can then be obtained and their Thevenin equivalent circuit as in figure 2.
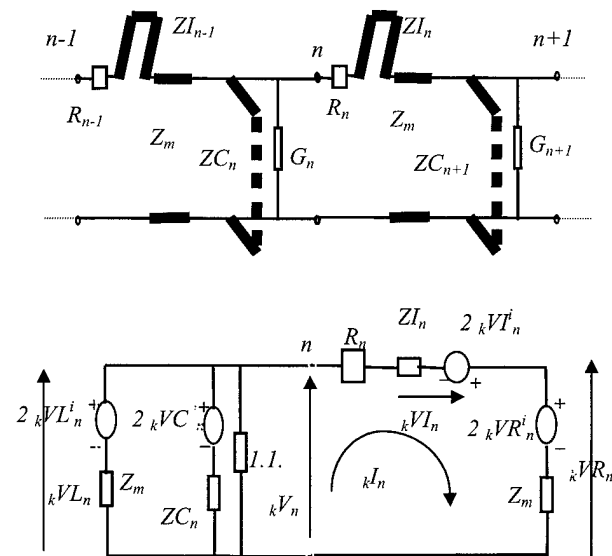
Figure 2. TLM model of two segments of the cable and its Thevenin equivalent circuit.

The variation of both L and C may come about due to regular or random variations in the distance between the centres of the conductors (changing the thickness of the dielectric or dielectric non-uniformity). The benefit of the developed TLM approach is that the stubs may be ignored in the case of modelling a regular cable. This process reduces the overall computing time required to run the TLM program. Hence the same TLM model can actually be used for the simulation of both regular (uniform) and irregular (non-uniform) twisted pair cables. It should be mentioned that the twist length is taken into account by calculating the actual length

of the cable to be used for the calculation of the number of the TLM nodes (segments) that represent the whole cable.

Using the parallel generator theory, the nodal voltage of the above circuit can be obtained as:

$$_kV_n = \frac{\dfrac{2_kVL_n^i}{Z_m} + \dfrac{2_kVC_n^i}{ZC_n} + \dfrac{2_kVR_n^i - 2_kVI_n^i}{R + Z_m + ZI_n}}{\dfrac{1}{Z_m} + \dfrac{1}{ZC_n} + \dfrac{1}{R + Z_m + ZI_n} + G_n} \quad (50)$$

Using the process described in [8,9], incident and reflected voltages on, and from, the stubs and the TLM links can be computed and used in the iterative solution of the wave propagation along the cable. Further details about the TLM method can be obtained from [4] and about the twisted pair cable model from [9,10].

In order to compute the secondary parameters of the cable, namely attenuation and return loss, S-parameters of the cable should be obtained. Knowing both near and far end incident and reflected voltages of the TLM model of the cable in the time domain, their values in the frequency domain and at the frequency of operation can be obtained with the use of a Fourier Analysis program.

4. Implementation and Results

The first sub-section validates both approaches against measurements. And the second sub-section is to report the implementation of the TLM model for the calculation of secondary parameters, under different working conditions of the cable.

4.1 Validation

In order to validate the analysis and modelling approaches, the attenuation constant of UTP cable is calculated using equation 14 and computed using the TLM approach where the dimensions of the cable are: $D = 0.94$ mm, $d = 0.53$ mm and the lay length $ll = 20$ mm.
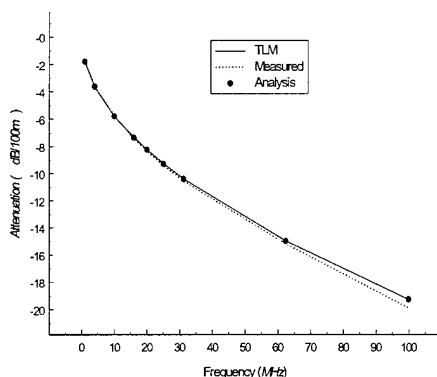
Figure 3. Calculated, modelled and measured attenuation for 100m cable.

Then results obtained using both approaches were plotted along with the measured data for the same cable as function of the frequency as in figure 3.

For the same cable, both phase and propagation constants were calculated using equations 17 and 23 respectively. Both sets of results were validated against standards equations obtained from [1] and plotted as in figures 4 and 5 respectively.
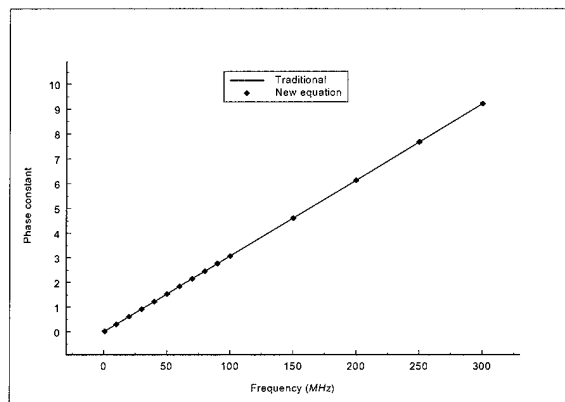
Figure 4. Calculated phase constant as a function of the frequency.
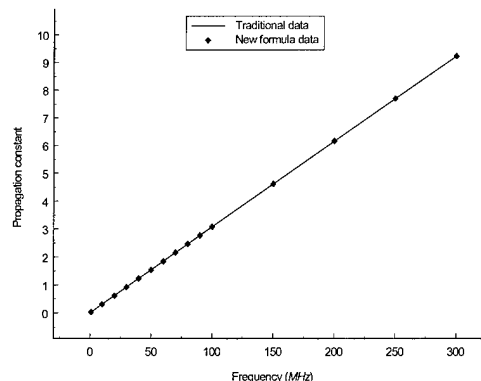
Figure 5. Calculated propagation constant as a function of frequency.

For the same cable, the amplitude of the characteristic impedance is calculated using equation 28 and plotted along with results obtained using the standard equation 24 and plotted as a function of the frequency as in figure 6.

For a shielded twisted pair cable where the cable dimensions are:

$D = 1.52$ mm. $\qquad d = 0.574$ mm. $\qquad ll = 20$ mm

The screen tape thickness was 0.062 mm. It consisted of 2 layers. The outside layer was of 0.05 mm aluminium alloy and the inner side layer was of 0.12 mm polyester. Equation 49 was used for the calculation of the attenuation constant. Results are plotted along with the measured data as illustrated in figure 7.
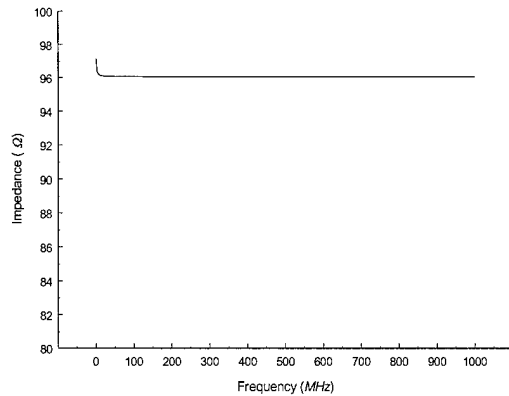
Figure 6. Calculated amplitude of Z_o as a function of frequency.

Figure 8. Calculated and measured attenuation for a deformed cable.

The return loss of the cable is also computed for both cases of regular cable and a deformed cable. Both sets of results are plotted in figure 9.
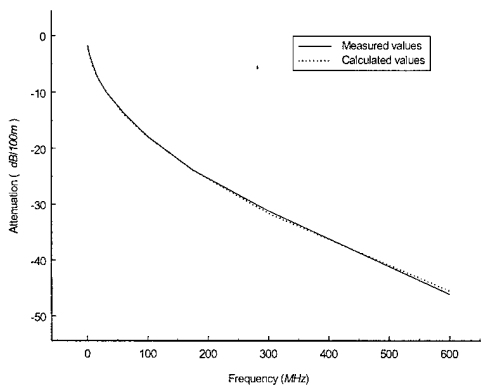
Figure 7. Calculated and measured attenuation constant for STP cable

4.2 TLM model applications

The TLM model described earlier is used for the calculation of both attenuation constant and return loss for the UTP cable investigated in this paper. Results for the attenuation of a regular cable were reported earlier along with those obtained using the design equations for validation purposes. Results for the return loss of a 1m link terminated with a matched load at the far end are illustrated with those obtained for irregular cable for comparison purposes in the following sub-sections. The TLM model is then used to investigate the irregularity effects on both time domain and frequency domain responses of the cable.

4.2.1 Handling effects: For the same category 5 UTP cable investigated here, exhibiting a cyclical variation in the separation of individual wires of the pair by ±100 microns, with five such cycles per meter length. A voltage source of a step wave are applied and the serial resistance of the source is 10 mΩ, the attenuation constant is calculated and plotted as a function of frequency along with the regular cable results as illustrated in figure 8.

Figure 9. Calculated and measured return loss for a deformed cable.

4.2.2 Pig-tailing effects: Again, both ends of the same cable were connected between a source and a load via a pig-tail connection illustrated in figure 10.
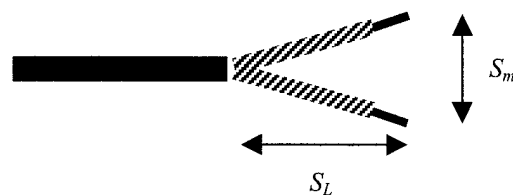
Figure 10. Illustration of pigtail connection.

For a 1m length of cable where $S_m = 2.5$ *mm* and $S_L = 10$ *mm*, the attenuation constant was calculated and is plotted as a function of the frequency along with the "no pig-tailing" case. Results are illustrated in figure 11.
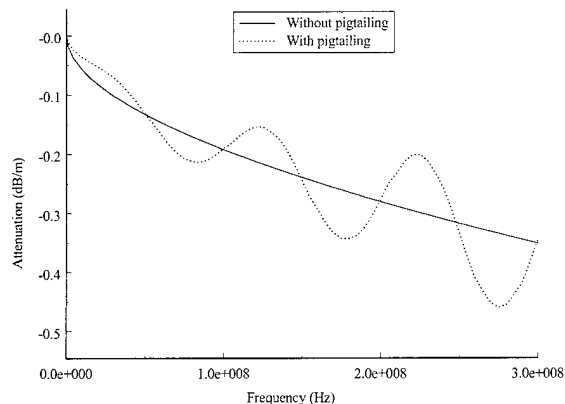
Figure 11.Attenuation computed for a pigtailed and uniform case.

While return loss for both cases are also computed and plotted as illustrated in figure 12
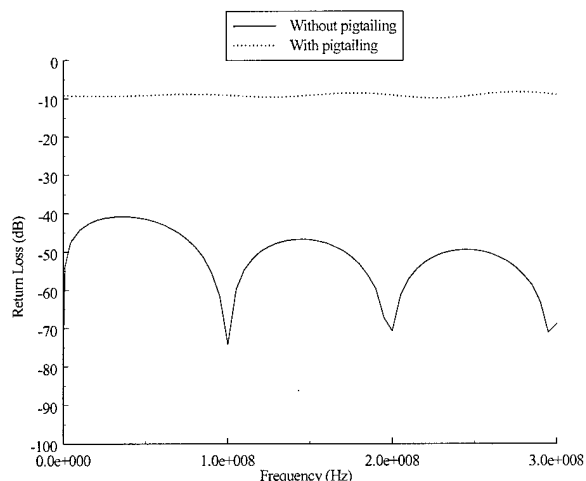
Figure 12.Return loss computed for a pigtailed and uniform case.

5. Conclusions

A family of design equations has been developed to describe the behaviour of twisted pair cables as functions of cable dimensions, materials properties, and frequency of operation. They are validated against measurements and an excellent agreement between both measured and calculated data have been demonstrated.

A TLM model for a twisted pair cable is developed. The model is capable of simulating both regular and irregular cables. It also incorporates the modelling of various communication channels elements, such as connectors. This provides a unique tool for the investigation of the performance of twisted pair channels under different working conditions.

Results obtained for a regular cable, using the TLM model show a very good agreement with both analytical and measured sets of data. The model is then used for the investigation of defected cable performance. Defects represented by changing the distance between the centres of the wires in some places, which provides an impedance discontinuity along the cable. Analytical solutions for such cable performance prediction are very difficult if not impossible to obtain. Results are plotted for both attenuation and return loss along with those for a regular cable. They illustrate the irregularity effects on the obtained results.

Another reason for impedance discontinuity is the 'pig-tailing' connection between both ends of cable and connectors at both source end and load end. Such conditions provide variable impedance values between the nominal impedance of the cable and may be 4 times its value. Again, attenuation and return loss calculations illustrate the fact that a good attention and care should be taken when installing short communication links.

The paper provides a simple set of secondary parameter equations that rely directly on the physical parameters of the cable and hence make them suitable to be used as a reference for future cable developments. It also provides a fast, flexible and accurate approach that can be used for the investigation of cable performance under different working conditions.

6. References

[1] S. Ramo, J. R. Whinnery and T. Van Douzer, *Fields and waves in communication electronics*, 2nd ed., Wiley, New york (1984).

[2] IEC/TC 46C, project number: IEC 61156-1 titled, "Test procedures for determining characteristic impedance (Zo) and return loss (RL)," (March 1996) and its amendment, (October 1997).

[3] Ke Lu, "An efficient method for analysis of arbitrary non-uniform transmission lines," IEEE Transaction on MTT, 45(1), 9-14, (January 1997).

[4] C. Christopoulos, *The Transmission Line Modelling method TLM,* IEEE Press, New York, (1995).

[5] L. Rade and B. Weestergren, *Mathematics Handbook for Science and Engineering,* 3rd edition, studentlitterature, (1995).

[6] Yin-Ying, "UTP cable attenuation constant", an article on a virtual textbook used in EE35 'Telecommunication' posted on the WWW, (14th February 1996), Worcester Polytechnic Institute, Worcester, Massachusetts.

[7] Mohammed M Al-Asadi, Alistair P Duffy, Keeneth G Hodge and Arthur J Willis, "Return Loss Prediction for Cascaded Systems", paper no. 17-04, IWCS 49th, (November 2000).

[8] P. B. Johns and R. L. Beurle, "Numerical solution of 2-dimensional scattering problems using a transmission line matrix", Proc. 118(9), 1203-1208, IEE, (September 1971).

[9] M. M. Al-Asadi, A. J. Willis, K. Hodge and A. P. Duffy, "Modelling as a tool for analysing handling effects in structured wire cabling", 10th IEE Int. Conf. on EMC, 131-136, (September 1997).

[10] M. M. Al-Asadi, A. P. Dufy, A. J. Willis and K. Hodge, "Analysing Link Performance in High Frequency Transmission Systems", 13th In. Symp. On EMC, Zurich 117-120, (February 1999).

Authors Biographies

Mohammed M. Al-Asadi, Alistair P. Duffy, Kenneth G. Hodge and Arthur J. Willis. For photos and biographies see "Return Loss Prediction For Cascaded Systems", paper 17-04 in these proceedings.

Electromagnetic Modeling of Twisted Pair Cables

Juliusz Poltz

OptEM Engineering Inc.,
100 Discovery Place
3553 - 31st Street N.W.
Calgary, AB Canada T2L 2K7
+1-403-289-0499
jpoltz@optem.com

Dietmar Gleich, Mats Josefsson, Marcus Lindström

Ericsson Cables AB Network Technologies
SE-824 82 Hudiksvall, Sweden
+46-650-360-00
dietmar.gleich@eca.ericsson.se,
mats.josefsson@eca.ericsson.se, marcus.lindstrom@eca.ericsson.se

Abstract

In this paper, a methodology of electromagnetic modeling of twisted pair cables is discussed. First, a brief description of the cable design environment is provided. This environment is used for entering cable design data including materials, plating, stranding, twisting, and wire naming. The geometrical information is then processed in order to calculate a realistic model of a twisted pair cable. The resulting model of the cable is subsequently analyzed numerically using a combination of finite element and boundary element methods. The skin depth parameter is used for optimal meshing. Unit (L,R,C,G) parameters, are verified against analytical and measurement results. Propagation parameters which are calculated for selected frequencies, are then used to build frequency dependent circuit models of twisted pair cables. Finally, a circuit simulation environment is introduced and TDR simulation results are presented.

1. Introduction

There is strong pressure to rapidly design and implement new systems operating at continuously increasing speeds. When prototyping is too expensive and too slow, computer modeling may offer a cost effective solution. However, digital systems now utilize frequencies into the GHz range. At these frequencies cable attenuation, dispersion and cross-talk affect the signal quality and system performance in a significant way. Modeling has proven its ability to predict these effects with high accuracy.

Despite its relatively simple geometrical structure, a twisted pair cable is difficult to model accurately. With the increase in operating frequencies, the secondary effects that were originally neglected in theoretical studies of cables [1] gained importance. It is now necessary to include twisting of wires and pairs, stranding [2] and plating when building cable models. It is impossible to build an accurate model without considering skin and proximity effects in wires, eddy currents in cable shields, and dielectric losses in insulation. The skin effect causes reduction of the interconnect inductance and a rapid increase of the interconnect equivalent resistance. Since conductor and shield losses were analyzed numerically much earlier for power cables [3,4,5,6], a similar technique was adopted in the development of OptEM

Cable Designer [7] in order to calculate unit parameters of high frequency cables. Once the current distribution is considered the losses and frequency dependence of unit parameters can be calculated. These values are then to be included in cable circuit models, which is also a difficult task.

2. Cable Design Environment

Despite its simple geometrical structure, twisted pair cable design offers challenges for numerical modeling and electromagnetic simulation. Since results of numerical simulations cannot be more accurate than the geometrical models representing the cable, it is essential to specify the cable geometry as accurately as possible. To achieve this goal we introduced a two stage process which allows detailed specification of the cable design parameters like wire and insulation dimensions, materials, stranding, and lay length using a graphical interface (Figure 1) and a three step procedure of collapsing the geometrical data described in the next section - Modeling Realistic Cable Geometry.

The graphical user interface provides a hierarchical environment in which the user can draw a wire, and assign parameters which include conductor details like plating and stranding and its insulation. The wire can be subsequently saved as an independent design which can be used at the next level as a building block for a pair. The pair can then be used a number of times as a building block for a bundle etc. The entire process of assembling a real cable can be replicated in this multistage process of specifying instances and levels. Proper assignment of instance names (Figure 1) also allows an automated (hierarchical) naming of wires in the extracted circuit model of the entire cable.

The graphical environment also allows the user to specify and assign different twisting parameters to any instance that is defined during the design process. The cable is assembled at specific locations (cross-sectional points). All instances can be individually placed and rotated at any level in order to produce a realistic geometrical structure at a particular location. In addition, each instance carries information related to its lay length which allows the program to automatically generate cross-sectional information at any location of the cable or to assemble a three dimensional model of any section of the cable.
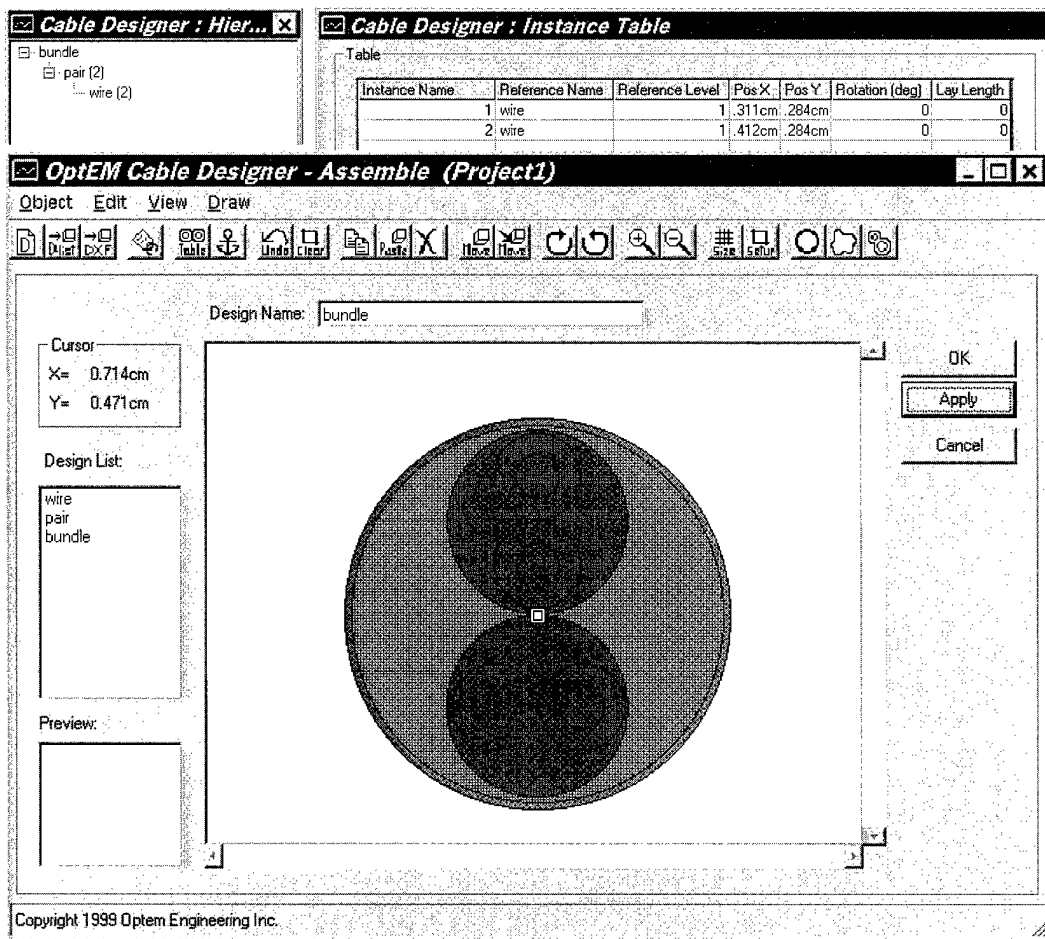
Figure 1. Graphical interface for cable design parameters like wire and insulation dimensions, materials, stranding, and lay length offers a hierarchical environment in which the user can draw a wire, which is used at the next level as a building block of a pair, which subsequently is used as a building block of a bundle etc.

3. Modeling Realistic Cable Geometry

A realistic geometrical model of a cable must consider the collapsing of the cable's initial geometry under the pressure of external insulation and shield and in the presence of core twisting. Since the wires, pairs and other building blocks of the cable cannot maintain a spatial separation in the presence of the external collapsing force, a three step procedure of post processing the

geometrical data was introduced. This process must be performed before the electromagnetic analysis of the cable can start.

First the cable building blocks are collapsed in the sequence they are assembled, starting from pairs or quads and their insulation. Then the bundles are pressed together followed by the collapsing of the cable enclosure (Figure 2).

| Start position | Collapsing of quads | Collapsing of quad insulation | Collapsing of the bundle | Collapsing of the cable enclosure |
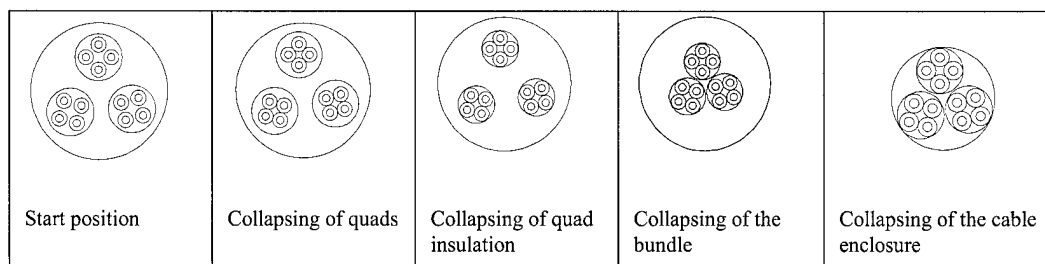
Figure 2. The first stage of collapsing the cable geometry removes redundant space between pairs, quads, their enclosures

The second stage of collapsing is related to individual movements of instances in specific cross sections. As pairs are rotated additional space may be available between wires. Since this additional space results from the fact that a twisted pair does not have a circular cross section, it is important to include information about pair twisting when collapsing space between pairs. This collapsing can be performed by assigning a tolerance to a helical path of a pair and allowing the pair to deviate from the path only by a certain amount, which is dependent on positions of the pair before and after the cross section that is investigated (Figure 3). The user has to provide the distance between cross sections to be linked and the acceptable level of deformation of the helical radius of the weight center of the pair. This process is repeated for every three consecutive cross sections until the entire segment of the cable is analysed.
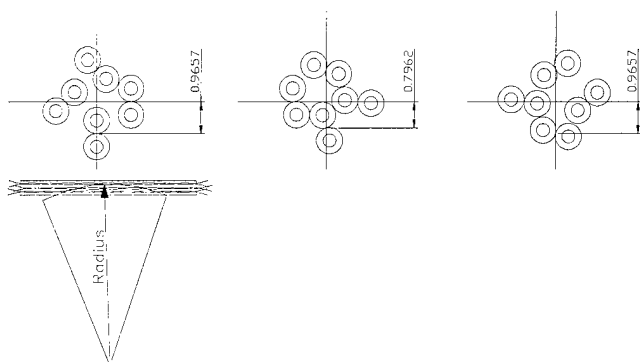
Figure 3. The second stage of geometry collapsing links consecutive cross sections along the cable length. Pairs are moved towards the centre of a bundle. The difference of the pair position is calculated for three consecutive cross sections and the process is stopped when the deformation of the radius of the helical path surpasses the tolerance level assigned by the user

The final stage of cable collapsing is related to deformation of external insulation and shield which is stretched over the concave assembly of wires (Figure 4). The deformation is dependent on mechanical properties of the enclosure and must be selected by the user. The user simply specifies an allowable deformation parameter (0% ≤ x ≤ 100%) which is used to calculate a min and max allowable radius of the enclosure based on the circular radius of the original shape. It is assumed that the enclosure follows a convex path and that 0% deformation means that the shield maintains its original circular shape. The min and max allowable radius of the enclosure curvature is calculated from the following equations:

$$min = radius \cdot \frac{100 - x}{100} \quad max = radius \cdot \frac{100}{100 - x} \quad (1)$$

4. Numerical Analysis

Despite the small dimensions of wires in today's high frequency cables the skin and proximity effects are well developed and cause the current to follow generally in a non-uniform path in wire cross sections. This frequency dependent behavior of the current has a predominant influence on the selection of the analysis method to determine unit propagation parameters of the cable. Since electromagnetic field distribution and losses in power cables were analyzed numerically much earlier [3-6], a similar technique was adopted in the development of OptEM Cable Designer [7] in order to calculate unit parameters of high frequency cables.

X = 0   x = 50   x = 100
min = 1.77   min = 0.89   min = 0
max = 1.77   max = 3.54   max = infinity
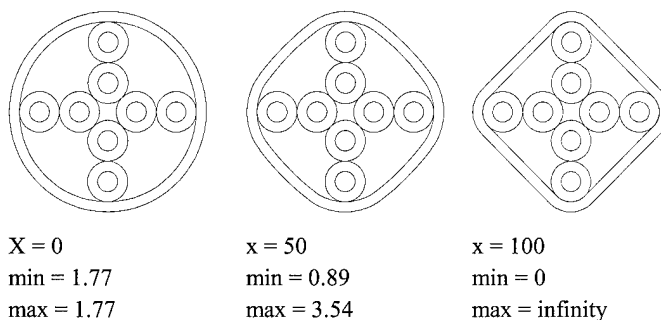
Figure 4. By increasing the value of the deformation parameter (0% ≤ x ≤ 100%), the user can control the final shape of the cable enclosure

Most currently available commercial field solvers solve static equations which do not allow the calculation of current distribution inside conductors. However, the field solver used in the OptEM Cable Designer software does numerically calculate current density (J) in the conductor cross-sections. Theoretically, a second order partial differential equation known as the Helmholtz equation can be used to calculate current distribution in conductors [1,3,8]:

$$\Delta \vec{\underline{J}} = j\omega\mu\gamma\underline{J} \qquad (2)$$

where: ω - circular frequency, μ - permeability, γ - conductivity.

However, there are some obvious advantages in adopting the equivalent representation of the Helmholtz equation known as the Fredholm integral equation of the second kind, for calculating unit parameters of cables[3,4,8]. In two-dimensional space (cross-section of the transmission system) the longitudinal component of the current density can be calculated from the following integral equation [3,8]:

$$\underline{J}(M) = -\frac{j\omega\mu\gamma}{2\pi}\int_S \underline{J}(P)\ln\frac{1}{r(M,P)}dS_P - j\omega\gamma\underline{A}(M) \qquad (3)$$

where: $\underline{A}(M)$ - represents external (source) field. **P** and **M** represent points in the cross-section.

OptEM Cable Designer calculates current distribution by solving equation (3) using a combination of Finite Element Method (FEM) and Boundary Element Method (BEM).

Bulky conductors are divided into finite elements, whereas ground and power planes are modeled as multilayer boundaries (as shown in Figure 5). Although difficult at the programming stage this method is the most efficient technique of solving the Helmholtz equation for practical interconnect applications.
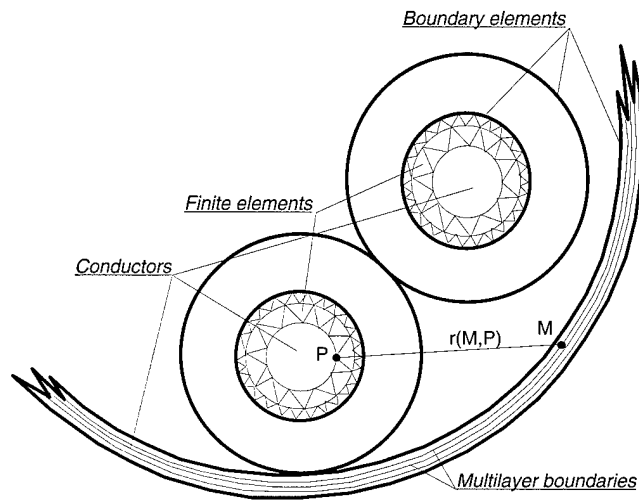
Figure 5. Calculation of L,R values using a combination of BEM and FEM

Numerical solution of the integral equation (3) requires selection of an approximation technique and the generation of linear constrains in the form of algebraic equations. The approximation technique was based on a generated mesh of finite elements and boundary layers (Figure 5). It was found that the current distribution within bulky conductors can be well represented by quadratic elements whereas currents in thin and wide planes (like ground and power layers) are represented by cubic splines based on boundary layers. This combination of finite and boundary elements offers numerical stability and accuracy.

A combination of different approximation techniques requires an adequate procedure for building linear algebraic equations. After analyzing different variational methods (including simple collocation) the Galerkin method was selected as the only one offering correlation between the approximation accuracy and the numerical effort in setting up and solving algebraic equations.

To allow the calculation of unit propagation parameters of cables the complex, frequency-dependent current distribution must be calculated for a set of independent source currents. The inductance and resistance matrices are calculated together as the imaginary and real parts of the impedance matrix. They are both related to the distribution of currents.

For a set of conductors the current is calculated from the current density for each conductor as:

$$\underline{I}_i = \int_{S_i} \underline{J}(M)dS_M \qquad (4)$$

We repeat the current calculation procedure for different (orthogonal) voltage conditions, $\left[\underline{V}\right] = j\omega\gamma[\underline{A}]$. In matrix notation:

$$\left[R + j\omega L\right][\underline{I}] = [\underline{V}] \qquad (5)$$

In practice matrix $\left[\underline{V}\right]$ can be selected as the diagonal unit matrix, therefore the unit inductance and resistance matrices can be calculated by separating the real and imaginary parts of the inverse current matrix:

$$[R] + j\omega[L] = [\underline{I}]^{-1} \qquad (6)$$

Since the current distribution is frequency dependent, the resulting [L] and [R] matrices may be strongly affected by the selection of frequency. Typical behavior of the wire inductance (measured against the cable shield) is presented in Figure 6. One can observe the gradual reduction of inductance with the increase of frequency and the distance to the shield. Percentage wise, conductors located close to the shield vary their frequency-dependent inductance more than conductors located far away from the shield. By solving the Helmholtz equation, OptEM Cable Designer automatically includes eddy-current and proximity effects when calculating unit parameters (L,R) of the cable.

Losses associated with a conductor include dc loss (due to material resistivity), skin effect loss (due to non-uniform distribution of currents in the conductor cross section), and eddy-current loss in neighboring wires (due to proximity effect). Eddy-current losses constitute "mutual" resistance values.

Similarly for the current distribution, the charge distribution on the dielectric interface and conductor surface can be calculated from the Fredholm integral equation. In two-dimensional space (a cross-section of the transmission system):

$$\underline{V}(M) = \frac{1}{2\pi\underline{\varepsilon}} \int_l \underline{\sigma}_c(P) \ln\frac{1}{r(M,P)} dl_P + \underline{C} \qquad (7)$$

Additional constraints are applied to the dielectric interface. Finally, a condition for the total charge is used to calculate the
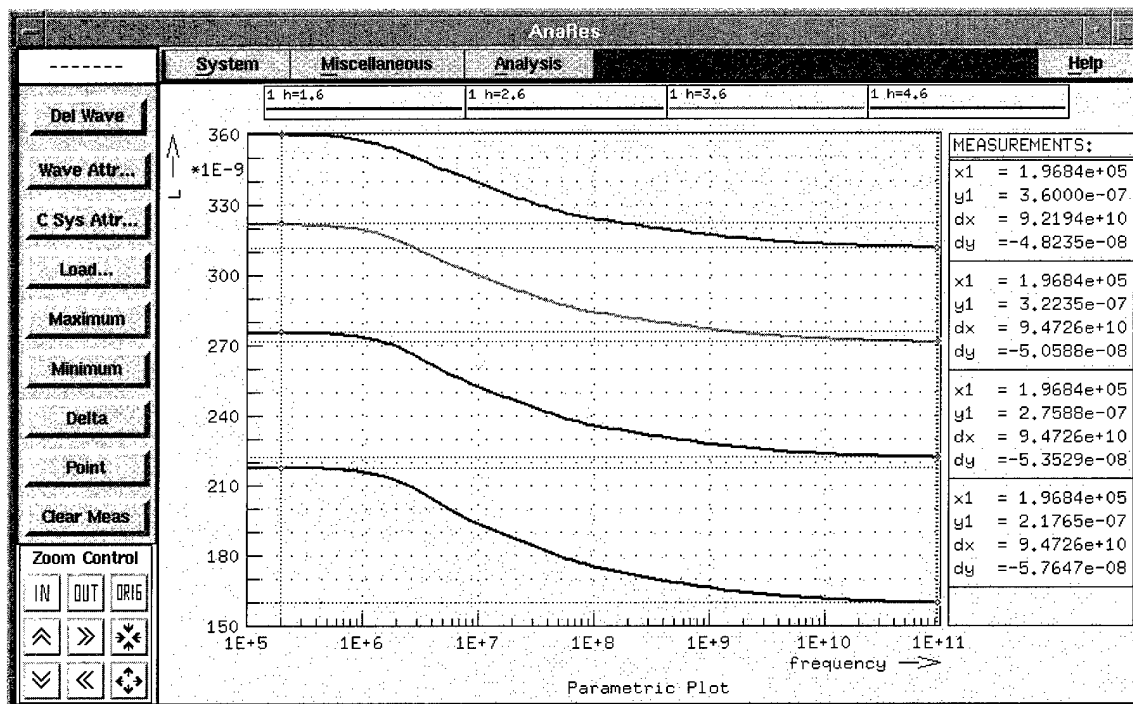
Figure 6. Calculated inductance of a single wire (return path in the shield) as a function of frequency for four different values of the distance between the wire and the screen

constant $\underline{C}$:

$$\int_1 \underline{\sigma}_c \, dl = 0 \qquad (8)$$

where:

$\underline{\sigma}_c$ - charge density,

l - conductor (and dielectric interface) boundaries.

For the individual conductors the charge on the surface is calculated as:

$$\underline{Q}_i = \int_{cond_i} \underline{\sigma}_i \, dl \qquad (9)$$

We must repeat the charge calculations for different voltage boundary conditions $\left[\underline{V}\right]$. $\underline{Q}$ and $\underline{V}$ are complex for lossy dielectrics, and when in a matrix notation:

$$\left[\underline{Q}\right] = \left[C - j\frac{G}{\omega}\right]\left[\underline{V}\right] \qquad (10)$$

Similarly for the magnetic field calculation, the matrix $\left[\underline{V}\right]$ can be selected as the diagonal unit matrix and therefore the unit capacitance and conductance matrices can be calculated separating the real and imaginary parts of the complex charge matrix as:

$$[C] - \frac{j}{\omega}[G] = \left[\underline{Q}\right]. \qquad (11)$$

A complex charge distribution in the form of cubic splines is used to represent sources of the electric field for lossy dielectrics. The C and G values are calculated from charge distributed on the surface of the conductors.

5. Unit Parameters of Twisted Pair Cables

The numerical method was verified against laboratory testing and analytical formulae available for a simple – single pair configuration [1]. Comparison of calculated and simulated unit parameters is included (Table 1).

We also performed detailed analysis of twisted pair cables. As expected the unit parameters measured against the cable shield oscillate with a period proportional to the pair lay length (Figure 7). These oscillations are substantially reduced when differential pair parameters are extracted, nevertheless even for differential pair resistance and capacitance values are strongly influence by twisting. Of course our ability to measure these oscillations of unit parameters depends strongly on the frequency spectrum of the signals used. For low frequency applications, with the wave length extending over the twisting period, the circuit model remains valid based on the average parameters. However, the twisting of wires leads to changes in the net (average) capacitance, resistance, inductance, and leakage of the interconnection line.

Table 1. Comparison of analytical, measurement and simulation results

Method	Frequency	Z	Zphase	Att	Phase	R	L	C	Velocity	Delay
	MHz	Ohm	Deg	dB/100m	rad/100m	Ohm/100m	uH/100m	nF/100	% Co	ns/m
Kaden [1]	1.0	103.0	-7.6	4.1	3.5	96.7	57	5.52	0.59	5.6
Measured	1.0	100.5	-8.0	4.3	3.5	98.4	54	5.63	0.60	5.6
Simulation	1.0	99.6	-9.4	5.0	3.5	115	53	5.69	0.60	5.6
Kaden [1]	10.0	94.0	-1.9	9.2	32.6	198	49	5.52	0.64	5.2
Measured	10.0	90.0	-2.2	11.4	31.7	230	45	5.63	0.66	5.1
Simulation	10.0	88.6	-2.4	11.6	31.6	237	44	5.69	0.66	5.0
Simulation	100.0	86.9	-0.63	29.3	310	583	43	5.69	0.67	4.9

And the correct unit parameters must be calculated in order to build a valid low frequency model.

The oscillation of unit parameters resulting from twisting can significantly impact the performance of the transmission line at very high frequencies. We are convinced that for very high frequencies the variation of unit parameters due to wire twisting must be included in the model.

6. Circuit Models and Circuit Simulation

The calculation of L, R, C, and G matrices for selected cross sections allows equivalent circuit models to be built for uniform and non-uniform lossy multiconductor transmission lines. One has to use very efficient modeling and simulation techniques to analyze a substantial portion of a twisted pair cable. A practical approach offering high accuracy and reasonable computational time was selected here. The proposed method uses three-types of modeling: - the two dimensional analysis of uniform, lossy, and coupled multiconductor cross-sections of the cable, an interpolation and extrapolation technique for non-uniform

multiconductor sections, and very limited three-dimensional analysis of selected discontinuities like end connectors etc. Segments of wires which are not included in the uniform transmission lines are not ignored but are automatically interpolated between uniform sections or extrapolated to connection points.

Electrically short transmission lines, like short segments of cables, can be modeled accurately with lumped circuits. Due to twisting of wires the ladder model, which is based on the applied geometrical segmentation, typically consists of LRCG lumped sections with various characteristics. To minimize the number of components one can combine segments by integrating their unit parameters along the wire path. However, the length of a ladder section must be carefully calculated to prevent a filtering effect of higher frequencies which may be included in the spectrum of the analyzed signals. The optimal interconnect model consists of lumped sections with a similar cutoff frequency.

The numerical value of the cutoff frequency f_c of a low-pass filter
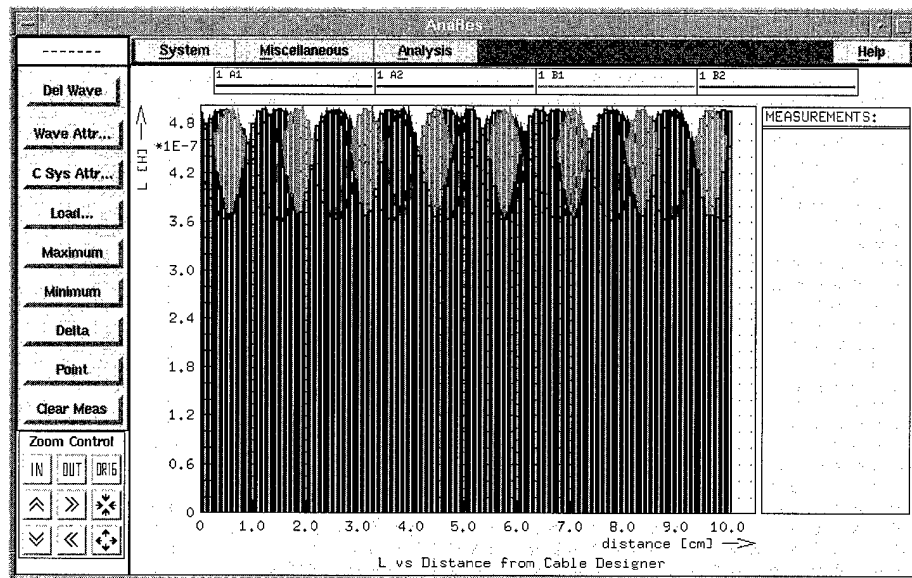
Figure 7. Simulated unit inductance of wires against cables shield

- representing Δx section of the cable - can be calculated from the following formula:

$$f_c < \frac{1}{\pi \sqrt{(L_{max}\Delta x)(C_{max}\Delta x)}}$$ (12)

The highest frequency f_h for which this model is valid must be lower than the cutoff frequency. Therefore, the ladder section length in this analysis is calculated using:

$$\Delta x < \frac{1}{\pi f_h \sqrt{L_{max}C_{max}}}$$ (13)

where:

$L_{max}C_{max}$ - maximum diagonal terms of the inductance and capacitance matrices.

Using this modeling technique may be very expensive numerically for high frequency cables. The number of required components in the model grows proportionally to the increase of the signal frequency and cable length. In addition, substantially larger circuits are required to model frequency dependent characteristics of the cables. To reduce model size and offer frequency dependent response, a truly frequency-dependent model can be assembled using the concept of modal propagation. Comparison of TDR responses simulated for a number of different models is presented in Figure 8.

One can observe the influence of the model on the simulated circuit response. Models which are built using unit parameters calculated for a single frequency either underestimate the losses for the fast changing transients or overestimate the losses for steady states. Only truly frequency-dependent models (highlighted response in Figure 8) can provide realistic waveforms for long sections of twisted pair cables.

The extracted SPICE cable models can be used in any circuit simulator to predict propagation delays, attenuation, distortions and cross-talk. The results of frequency domain simulation can also be presented in the form of S-parameters.

7. Conclusions and Future Directions

There are five major contributions of the research work described in this paper:

o graphical design environment for twisted pair cables was build,

o a system for post processing geometrical information was designed,

o a frequency dependent electromagnetic solver was built and initially verified,

o some frequency dependent models of twisted pair cables were developed,

o TDR environment for simulating twisted pair cables was built.

While working on the project we discovered that:

o Wires of high frequency twisted pair cables have cross sectional dimensions within the skin depth range, and an accurate solution of the Helmholtz equation is required. The Helmholtz equation allows for the analysis of eddy-currents, and proximity and skin effects for quasi-TEM propagation.

o Calculation of losses in modeling twisted pair cables allows the prediction of attenuation and dispersion and
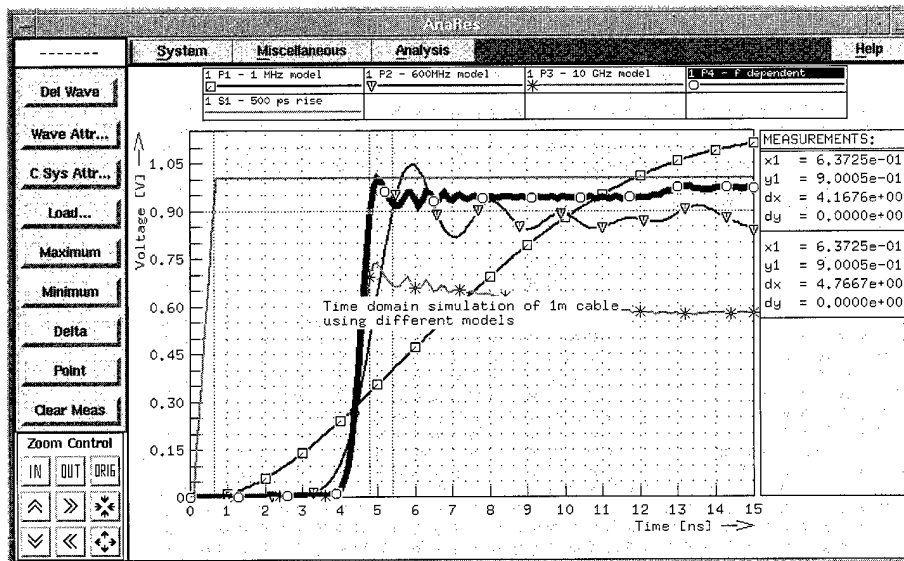
Figure 8. TDR simulation results

very good correlation with experimental results for a wide frequency range.

o Inclusion of twisting in modeling twisted pair cables is essential for prediction of cross talk parameters.

o A combination of Finite Element Method (FEM) and Boundary Element Method (BEM) offer an accurate and efficient method for analyzing twisted pair cables.

o Conductor and dielectric losses represented by the resistance and conductance matrices can be efficiently calculated together with inductance and capacitance matrices and included in optimized twisted pair cable models.

o If a model is built based on simulation results at a single low frequency, the subsequent discrepancies with wave front modeling may occur and time delay values can be incorrect. If a model is built and assembled for a single high frequency, the losses are overestimated for lower harmonics, and waveforms cannot reach proper steady state values.

o For predicting waveforms (time domain simulation) it is necessary to build frequency dependent models of twisted pair cables.

In continuation of this study we plan to:

o Perform additional verification of the simulation procedures against measured results.

o Verify stranding and braiding models.

o Verify dielectric loss calculation against measurement.

o Optimize frequency dependent models for long sections of twisted pair cables.

o Perform statistical analysis including material and manufacturing tolerances

8. References

[1] H. Kaden, *"Wirbelstrome und Schirmung in der Nachrichtentechnik"*, Springer-Verlag, Germany (1959).

[2] J. Poltz and S. Grzybowski, "Magnetic Field Outside the Three-Core Cable Considering the Cable Stranding", *IEEE Transactions on Power Apparatus and Systems*, Vol. PAS-98, No. 4, p. 1142, (July/August 1979).

[3] E. Kuffel and J. Poltz, "AC Losses in Crossbonded and Bonded at Both Ends High Voltage Cables", *IEEE Transactions on Power Apparatus and Systems*, Vol. PAS-100, No. 1, pp. 369-374, (January 1981).

[4] J. Poltz, E. Kuffel, S. Grzybowski, and M.R. Raghuveer, "Models Adopted for the Calculation of Eddy-Current Losses in Pipe-Type Cables", *IEEE Transactions on Magnetics*, Vol. MAG-17, No. 6, P. 2592-2594, (1981).

[5] J. Poltz, E. Kuffel, S. Grzybowski and M.R. Raghuveer, "Eddy-Current Losses in Pipe-Type Cable Systems", *IEEE Transactions on Power Apparatus and Systems*, Vol. PAS-101, No. 4, pp. 825-832, (April 1982).

[6] J. Poltz and E. Kuffel, "A Simple and Accurate Evaluation of Eddy-Current Loss in Magnetic Pipe of a Cable", *IEEE Transactions on Power Apparatus and Systems*, Vol. PAS-104, No. 8, pp. 1951-1957, (August 1985).

[7] "*OptEM Cable Designer User's Manual,*" Version 4.5, OptEM Engineering Inc., Calgary, Alberta, (May 2000).

[8] J. Poltz, "On Eddy Currents in Thin Plates," *Archif fur Electrotechnik*, Springer-Verlag, Germany, Vol. 66 (4), pp. 225-229 (1983).

Cross - Talk Measurements with Random Noise Sources

J.- H. Walling* and R. Pederian**

*Consultant, Beaconsfield, Quebec, Canada

1-(514)-695-8220 E-mail: jo.walling@sympatico.ca

**NORTEL Networks, Montreal, Quebec, Canada

1-(514)-818-2551 E-mail: pederian@nortelnetworks.com

Abstract

We show that it is feasible to use random noise source for the measurements of cross talk. In fact, both the pair to pair cross talk as well as the power sum cross talk - we call it the integral power sum cross talk - can be measured. For the latter we use power splitters. We compare the measurements with those, which are obtained using the traditional method with sinusoidal disturbing signals and a network analyzer in conjunction with an S-parameter test set.

We develop a method, which should allow, to measure alien cross talk in installed cabling systems of local area networks, using hand held testers. By using random noise sources to energize over baluns and power splitters as many cables as deemed necessary, it is possible to assess the alien cross talk susceptibility of an installed base, cable by cable.

Keywords

Alien cross talk; channel; NEXT; FEXT; random noise; hand held tester.

1. Background

Cross talk is traditionally measured, using sinusoidal signals. Originally cross talk was measured at specific discrete frequencies. However, in the last two decades, it became more and more common to use "swept frequency" measurements. This is basically the same measurement method at discrete frequency measurements, the only difference being that the frequency point density has been substantially increased.

With the increased advent of digital transmission for telecommunications, it has been conjectured, that digital cross talk may have a somewhat different behavior than cross talk measurements with sinusoidal signals.

Thus cross talk measurements have been made with randomly selected signal patterns within the considered coding scheme. However, the obtained results confirmed the validity of the assumption, that the cross talk performance can be correctly assessed, using sinusoidal signals.

Our objective here is to indicate a way to obtain a signal, which can be used in the field, to assess alien cross talk of installed cabling systems. To achieve this we use random white noise generators to energize either the disturbing pair or all disturbing pairs within one cable over a power splitter simultaneously. Our goal is to demonstrate the feasibility of using broadband random

white noise generators, based upon random noise diodes, to measure the cross talk with a spectrum analyzer.

The objective is to explore the possibility to use power splitters in conjunction with random noise generators and an amplifier, to energize pairs within an installed cabling system, which are not under direct measurement, but which generate due to their proximity an alien cross talk in the cable under measurement. For this reason we limit our measurements on 90 m of cable, and for easier comparison we do not consider the connecting hardware. However, it should be mentioned, that the connecting hardware has also an influence on the cross talk performance.

In this way, several circuits of an installed cabling system can be powered with random noise, whereas the cable under measurement is energized on the disturbing pair or pairs, while measuring the cross talk or the alien cross talk alone on the disturbing pair.

2. Introduction

We limit our reporting to 4 pair cables only, each having a length of 90 m. For our test we use a Noise/Com amplified noise module NC 1109A, which has a flat random noise power output in the frequency range from 100 Hz to 1 GHz. The output of the random noise generator is amplified with a broadband amplifier, in order to obtain a sufficiently high power level. We use furthermore a passive power splitter M/A-Com DS-4-4.

We use baluns from BH Electronics, having an operating frequency range from 3 MHz to 350 MHz. We use these baluns only for their ease of utilization in conjunction with the power splitters, having both SMA-connectors. Additionally they simplify our task of connecting the pairs to the baluns.

The method for the pair to pair cross talk measurement, using the network analyzer is straight forward and does not require any schematics. In case of the pair to pair measurements with the random noise generator the output of the amplifier is directly connected over a 3 dB attenuator to the balun, which is connected to the disturbing pair.

For the measurement of the integral power sum NEXT we use the set-up shown in Fig. 1, whereas for the integral power sum IO-FEXT we use the set-up according to Fig. 2.

For termination of the pairs we use resistors supplied by JC Electronics Corp, which are especially designed for testing at higher frequencies.

The common mode port of all the baluns used is terminated with a 50 Ohm resistor.

For all our measurements we use an HP-4195A Spectrum/Network analyzer. The HP-4195A instrument allows both, the measurement of the S-parameters and the power spectrum measurement

3. Methodology

3.1 Normal pair to pair and power sum cross talk measurements

The measurements of pair to pair cross talk, using the network analyzer in conjunction with an S-parameter test set are straight forward: The loss of the baluns used for the measurements is determined, and is subtracted from the measured values of cross talk, which include the loss of the baluns.
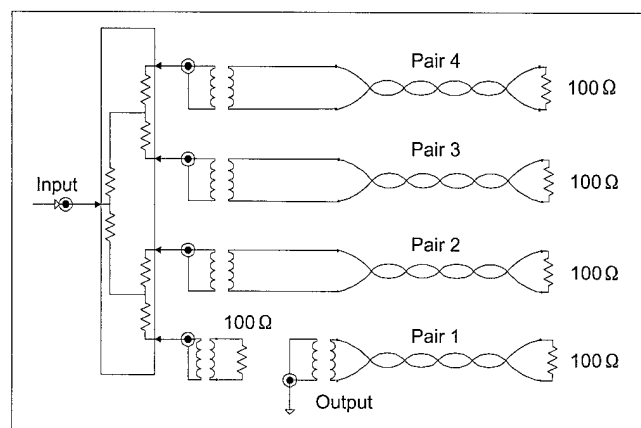
Fig. 1 : Set-up of Power splitter for measuring power sum NEXT for pair # 1
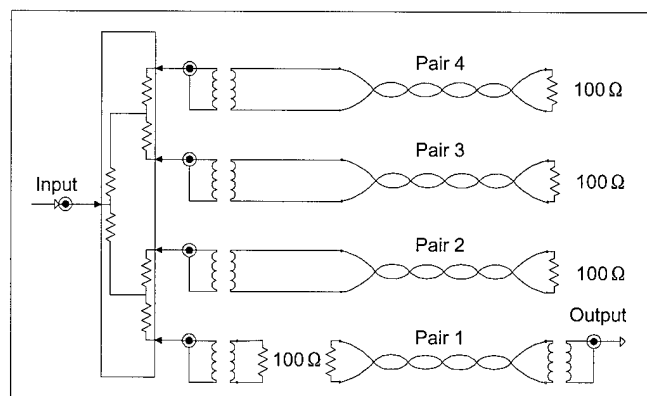
Fig. 2: Set-up of Power splitter for measuring power sum IO-FEXT for pair # 1

For the direct power sum cross talk measurement we use a power splitter. Though we are loosing some information on the S-parameters through the use of the power splitters, we can devise different ways to calibrate the set-up shown in the Fig. 1 and Fig. 2 [see also 1]. We indicate these in the following.

- We can calibrate the network analyzer with the S-parameter test set just prior to the power splitter. The losses for each path must to be measured. Both losses, i.e. the loss of the pair position on which the integral power sum is being measured and

the power sum loss for the remaining positions, where the disturbing pairs are being connected, must to be subtracted from the result obtained.

- Alternatively we can terminate all the baluns of the disturbing pairs with a 100 Ohm termination, and calibrate on the path for the disturbed pair. In this case only the power sum of the remaining position will have to be subtracted from the obtained result.

We explored both alternatives, and compared the results obtained with the power sums calculated from pair-to-pair measurements, which are taken directly, using two baluns on the network analyzer/S-parameter test-set.

We generally measure between 3 and 350 MHz with linear frequency division of this interval. We use 1601 points per sweep.

3.2 Pair to pair and power sum cross talk measurements with random noise sources

For the measurements, using the broadband random noise generator, we proceed as follows:

For pair to pair cross talk measurements we terminate the pairs not under measurement on both sides in 100 Ohm. The disturbing pair is connected, via a balun at its near end to the random noise generator, whereas the far end is terminated in 100 Ohm. For NEXT measurements, the disturbed pair is connected, again via a balun to the input of the spectrum analyzer, whereas the far end is terminated with a 100 Ohm resistor. The measurements of the IO-FEXT are done correspondingly.

For the measurement of power sum NEXT and IO-FEXT the power splitter is connected via baluns to the disturbing pairs, whereas the disturbed pair is connected over a balun to the spectrum analyzer. The connections are done as well following the schematics as given in Fig. 1 and Fig. 2.

The calibration is done, using by measuring the power at each balun output. This power level serves as a reference power input. We use the same frequency window for the spectrum analyzer, which is used for of the network analyzer measurements. Thus the LF frequency of the network analyzer is equal to the frequency window for the spectrum measurement.

We limit, to save measurement time, the frequency range of the measurements from 10 to 350 MHz. For lower frequencies the window for the spectrum analyzer measurements will have to be decreased and this will also substantially increase the measurement time.

To obtain the ELFEXT from the IO-FEXT we measured the attenuation, both as the power decrease over the channel length and as the insertion loss, using the network analyzer.

4. Results

In the Figures 3, 5, 7 and 9 is shown the directly measured PS - NEXT for the four pairs, using a spectrum analyzer. In this case the integral power sum has been measured, using the power splitter. As a comparison, there are given in the same graphs also the traces of the measurements obtained using the power splitter in conjunction with a network analyzer.

The Figures 4, 6, 8 and 10 finally show the results of the power sum NEXT calculated from the pair to pair measurements. Here the results obtained with the spectrum analyzer for each pair combination and the same results using the network analyzer are shown, to allow a comparison.

In the Figure 11, we have the attenuation of one pair, measured with the random noise generator. The trace is relatively rough, such that for useful attenuation a curve fitting would be required. However, for the purposes pursued here, i.e. for the calculation of EL FEXT from IO-FEXT, the obtained results are sufficient.
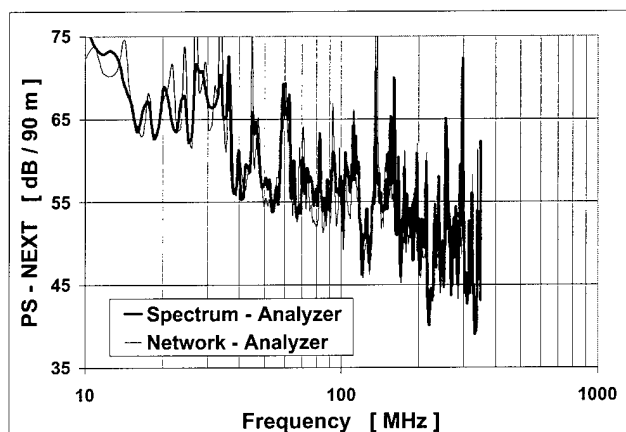
Fig. 3 : PS - NEXT for pair 1, measured directly with direct powering of all disturbing pairs over a power splitter.
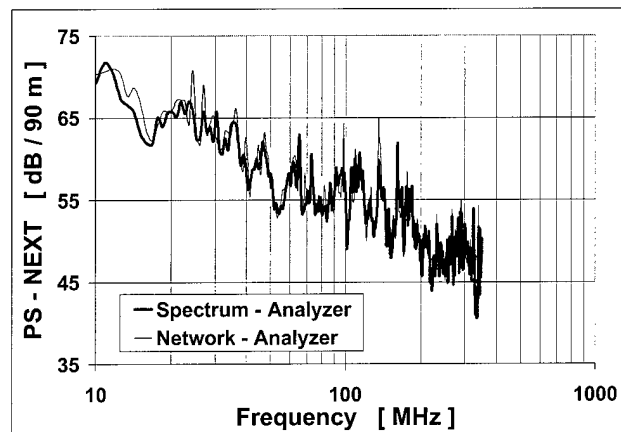
Fig. 4 : PS - NEXT for pair 1, calculated from pair to pair measurements.
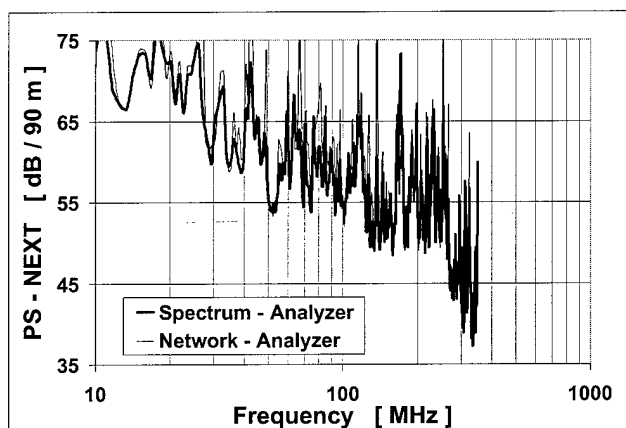
Fig. 5 : PS - NEXT for pair 2, measured directly with direct powering of all disturbing pairs over a power splitter.
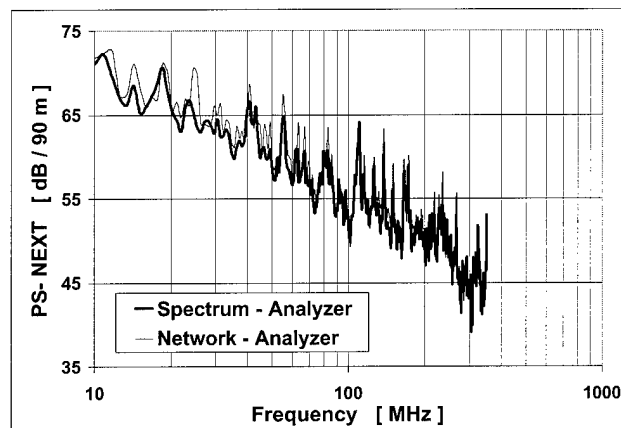
Fig. 6 : PS - NEXT for pair 2, calculated from pair to pair measurements.
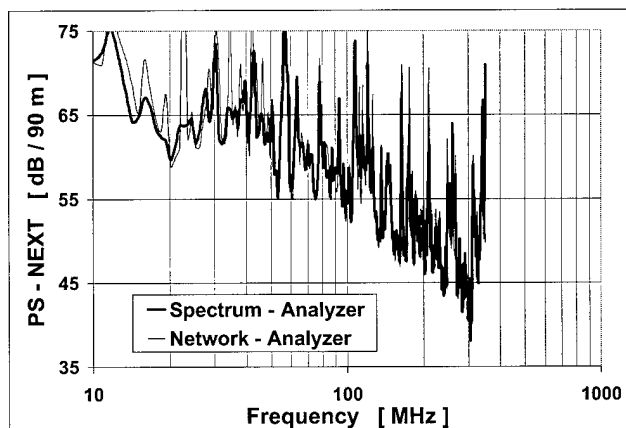
Fig. 7 : PS - NEXT for pair 3, measured directly with direct powering of all disturbing pairs over a power splitter.
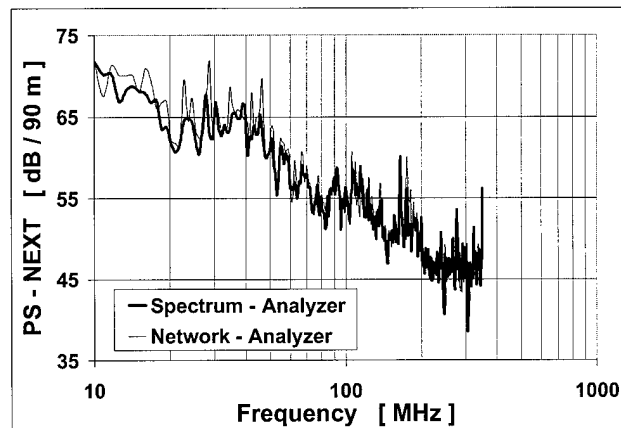
Fig. 8 : PS - NEXT for pair 3, calculated from pair to pair measurements.

The Figures 12, 14, 16 and 18 as well as Figures 13, 15, 17 and 19 finally show for the four pairs of the cable the measurements of the integral Power sum EL FEXT and for the calculated power sum EL FEXT, based upon pair to pair measurements. In each case there is given the result obtained with the spectrum analyzer and with the network analyzer.
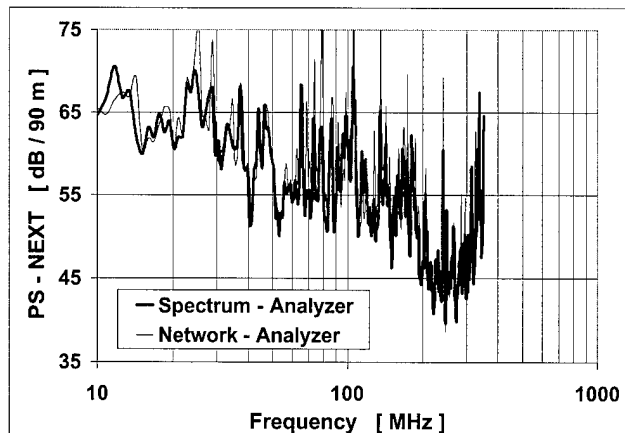
Fig. 9 : PS - NEXT for pair 4, measured directly with direct powering of all disturbing pairs over a power splitter.
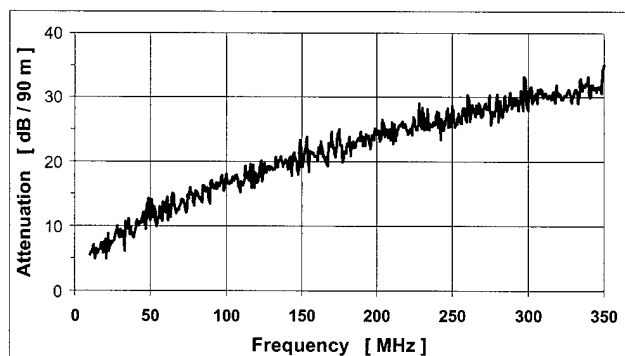
Fig. 11 : Attenuation of one pair, measured with the random noise generator.
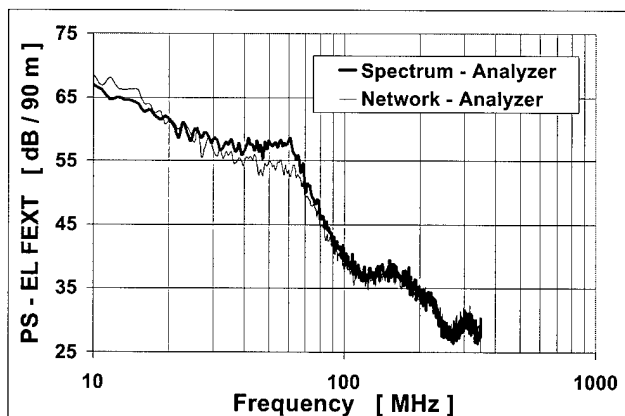
Fig. 12 : PS - EL FEXT for pair 1, measured directly with direct powering of all disturbing pairs over a power splitter.

5. Discussion of Results

The integral power sum NEXT measurements, using the power splitter, yield, in comparison to the results obtained under the same conditions, with the network analyzer absolutely comparable results. In fact, the deviations are so small, that they can be neglected. (see Fig. 3, 5, 7 and 9)
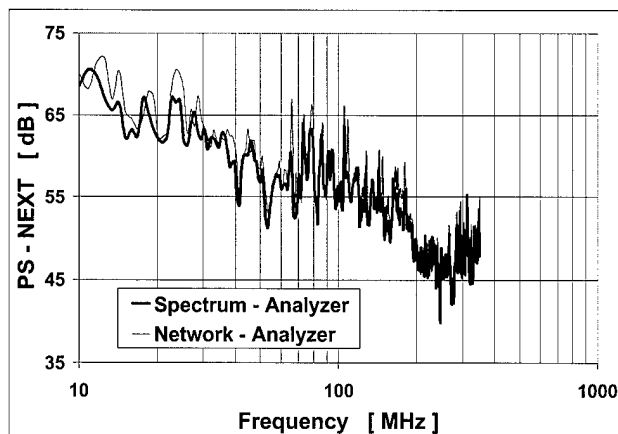
Fig. 10 : PS - NEXT for pair 4, calculated from pair to pair measurements.

The same is also true for the calculated power sum NEXT measurements, which are based upon individual pair to pair measurements. (see Fig. 4, 6, 8 and 10) The measurements, using the network analyzer, can be used as reference measurement results. The results obtained with the random noise generator yield absolutely comparable results to the reference results.

However, there are differences when comparing the Fig. 3 and 4, 5 and 6, 7 and 8 and finally Fig. 9 and 10. The results, using the power splitter and the pair to pair measurements are significantly different. This difference has to be attributed either to the power splitter itself or to the used error correction method. As in a previous study, the use of power splitters for power sum cross talk measurements has been already validated [1], it seems, that
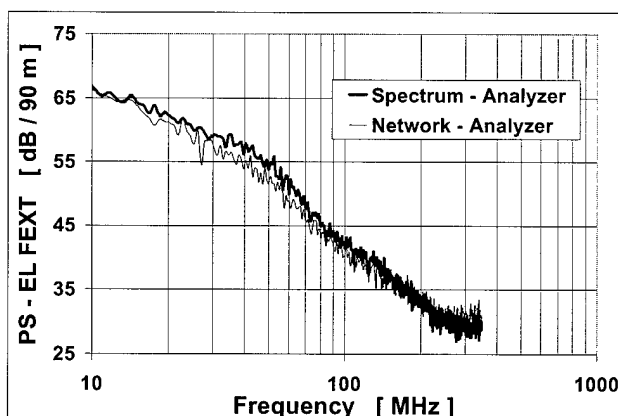
Fig. 13 : PS - EL FEXT for pair 1, calculated from pair to pair measurements.

these deviations have to be attributed to the specific power splitter used.

The Fig. 11 shows, as already mentioned the attenuation trace of one pair, using the random noise source and a spectrum analyzer. Here the spectral power of the noise sources at the input balun to the twisted pair is measured, and compared to the spectral power at the end of the same pair. The obtained trace is relatively

rough. It should be mentioned that these measurements are not intended to measure the attenuation of the pairs. Therefore, the roughness of the results is of relatively low importance in the context of our investigation.
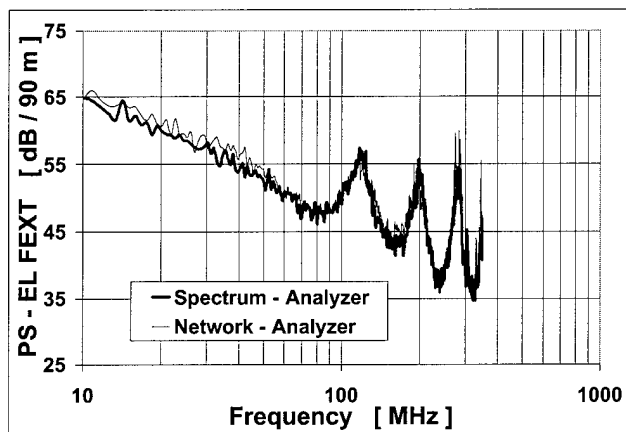
Fig. 14 : PS - EL FEXT for pair 2, measured directly with direct powering of all disturbing pairs over a power splitter.
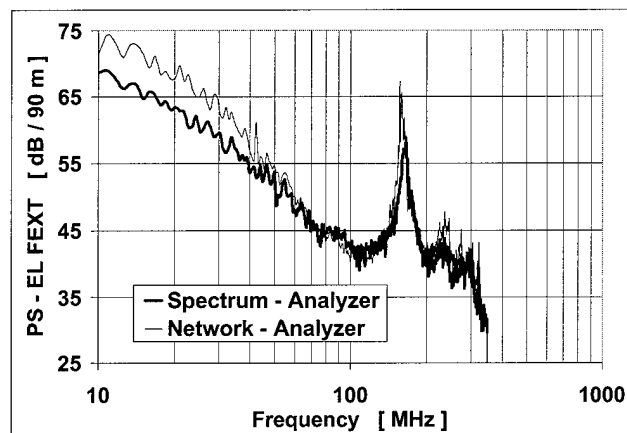
Fig. 15 : PS - EL FEXT for pair 2, calculated from pair to pair measurements.
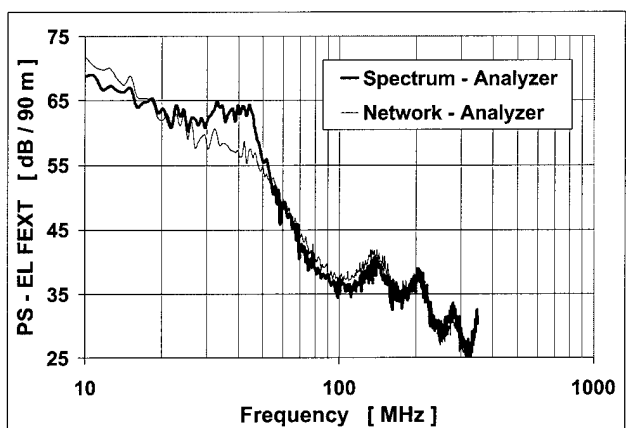
Fig. 16 : PS - EL FEXT for pair 3, measured directly with direct powering of all disturbing pairs over a power splitter.
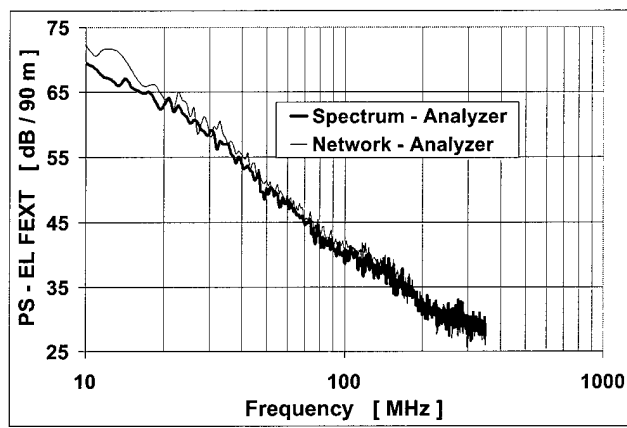
Fig. 17 : PS - EL FEXT for pair 3, calculated from pair to pair measurements.
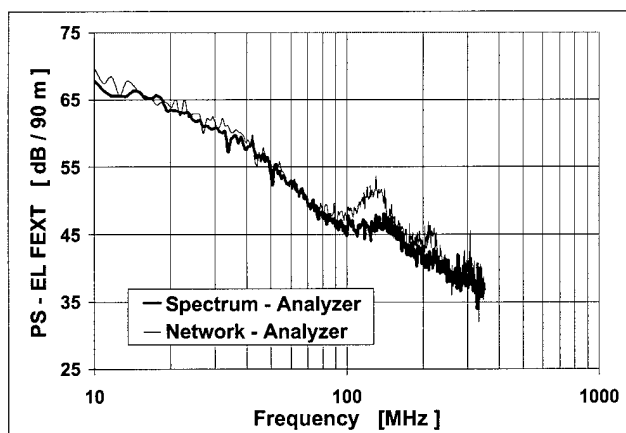
Fig. 18 : PS - EL FEXT for pair 4, measured directly with direct powering of all disturbing pairs over a power splitter.
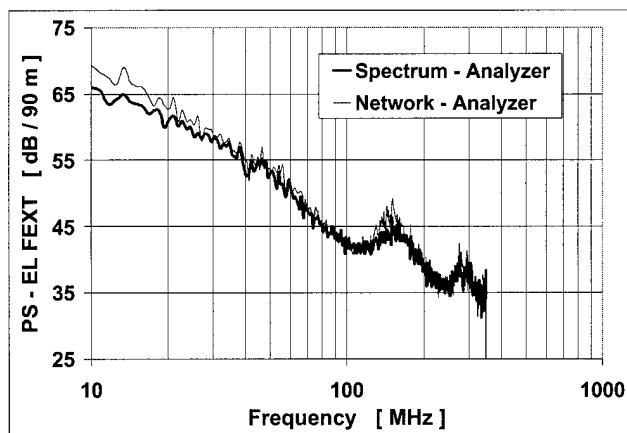
Fig. 19 : PS - EL FEXT for pair 4, calculated from pair to pair measurements.

Our main objective is to verify, if it is feasible to measure the alien cross talk induced in one cable by adjacent and neighboring cables. It is not the intention to use the proposed method to replace existing measurement methods.

Hence, the precision of the attenuation measurement, and the resultant roughness, using the random noise generator is not essential. They are here used only for completeness. In practical applications, a multitude of cables is energized, using random noise generators, either with or without power splitters. For the actual cable under measurement the parameters, including the attenuation are known, thus that the PS-EL FEXT can be directly determined from the PS-IO-FEXT.

The attenuation, using random noise generators, if ever used, would require a curve fitting of the data to obtain useful and meaningful results.

Here, the attenuation measurements are used exclusively to calculate from the IO-FEXT measurements the EL FEXT.

Again, our measurements are very comparable between the results obtained with the spectrum analyzer and the network analyzer. (see Fig. 12 to 19) The results obtained for the pair to pair measurements are nearly identical for those obtained with the spectrum and network analyzer. (see Fig. 13, 15, 17 and 19).

However, comparing the results to those of the integral power sum EL FEXT (see Fig. 12, 14, 16 and 18) there are similar differences occurring as between the power sum NEXT results.

We can clearly state, that the measurement of cross talk, using random noise sources yields absolutely comparable results to those obtained, using sinusoidal signals, as used in a network analyzer. This is convincingly confirmed by the fact, that the results, obtained using a power splitter to energize all disturbing pairs simultaneously, are also absolutely comparable. In this case the results with the random noise generator and those obtained with a network analyzer yield very comparable results.

6. Conclusion

We show convincingly, that cross talk measurements using random white noise sources yield absolutely comparable results to those obtained in the classical way, using sinusoidal disturbing sources.

This renders the utilization of random noise sources feasible for alien cross talk measurements. Towards this purpose, it is proposed to energize in an installed system as many channels as deemed required, using random noise sources on one side, and terminations on the other side. This allows the evaluation of the impact of alien cross talk, on the channel or cable under test. The random noise sources may be easily realized, using commercially available random noise diodes.

7. References

[1] M. Belanger et al: Power Sum, Integral Power Sum and Vector Sum - Crosstalk.

47th IWCS (1998) p. 768-775

8. Authors
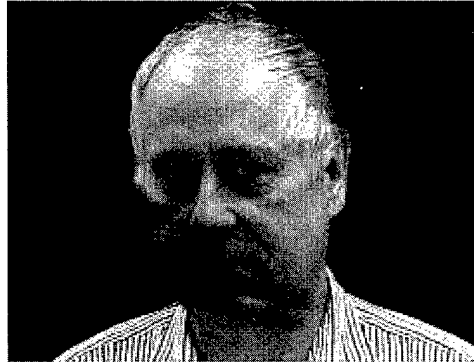
Jörg-Hein (Jo) Walling received his diploma in Mechanical Engineering in 1966 at the Technical University of Berlin. In 1974 he obtained a Doctor's degree (Dr.-Ing.) at the same University. In 1974 he joined Northern Telecom in the Research and Development department. Since 1976 he has been senior engineer at the NORTEL, Lachine Cable Plant. Later on he continued to work at the NORDX/CDT facilities, responsible for the design of Outside Plant and Data Grade Wires and Cables. Since 1999 he is an independent consultant for cables, standards and machinery.

Raffi Pederian holds a Bachelor's degree in Electrical Engineering with a specialization in Telecommunications from l'École Polytechnique de Montreal (1996). He started his career at Nordx/CDT, where he worked in the Research and Development group as a Structured Cabling Systems Engineer. His main line of work consisted in the evaluation of transmission characteristics of data grade cables and their corresponding connecting hardware. Since April 2000, he is working for Nortel Networks and his current position is in Systems Engineering for IP/Data network management solutions for Service Providers and Carriers.

Screening Attenuation of Long Cables

Carl W. Dole, John W. Kincaid

Belden Electronics Division
Richmond, Indiana
+1-765-983-5884 · cdole@globalsite.net   +1-765-983-5332 · jkbelden@globalsite.net

Abstract

The characteristics of a triaxial test fixture which has been developed for screening attenuation measurements on long shielded cables are described. Screening attenuation performance of a selection of coaxial CATV cable braid and multi-foil/braid shield designs are presented. Measured screening attenuation results for 30 meter long cables covering the frequency range 1-100 MHz are compared with results from measurements on 1.5 meter long cables that were measured over the frequency range 1-1000 MHz. The comparison shows that the estimation or deduction of long length, low frequency performance from high frequency performance can have significant error. The paper concludes that worse case or minimum screening attenuation performance should be assessed for cable lengths and frequencies pertinent to usage of the cable.

Keywords

Attenuation; braid; CATV; coaxial; effectiveness; foil; IEC; screen; SCTE; shield; test

1. Introduction

Screening attenuation is a practical shield effectiveness parameter and the test method is being standardized in IEC 61196-1 [1], prEN 50289-6 and SCTE test method IPS-TP-403B2 [2]. The test was originally developed for short length copper coaxial cables involving a resonant triaxial test fixture length of 1-2 meters [3] and the frequency range of interest was 100 MHz to 3 GHz. The minimum screening attenuation corresponds to the condition of maximum power transfer that occurs at resonant frequencies within the test fixture. With a 1.5 meter long fixture the lowest resonant frequency is at about 100 MHz. The frequency range is primarily determined by fixture length and the fixture TEM mode cut-off frequency. A complete test system is available commercially [4] and test fixture implementations involving standard commercially available components for fixture lengths of 1.5 and 6.7 meters have been reported [5,6]. Preliminary results obtained with a 30 meter long fixture have also been reported [7].

Applications such as CATV return path and data I/O have stimulated interest in screening attenuation performance where cable lengths are tens of meters long and the frequency may be as low as 5 MHz. However the chief obstacle to implementing the screening attenuation test at these frequencies is the required fixture length. A 6.7 meter length is limited to about 20 MHz and a 30 meter length is required to arrive at about 4 MHz which

corresponds to about ½ wavelength electrical length in the sample under test.

Section 2 of this paper presents the mechanical, electrical and installation aspects of the triaxial fixture. Sections 3 and 4 cover the test procedure and the test program including samples tested and results. The conclusions are given in section 5.

2. Triaxial Test Fixture

2.1 Overview

The triaxial test fixture is sketched in Figure 1. The main components are five sections of six meter length, 76.5 mm diameter rigid transmission line segments (without center conductor and end disc supports) which are cascaded together with gas tight coupling flanges. The segment joints are fitted with metallic spacer rings to maintain 50 Ohm impedance across the joint. A continuous length of low loss dielectric tubing material is used to support the sample under test from end to end. The tubing is centered with disc spacers which are randomly located along the 30 meter length. An end plate closes the housing at one end and an end cap transition encloses the other. A feed-through connector is mounted in the center of the end plate.

The end cap is fitted with a 50-ohm type N jack connector. The center pin of the N jack connects to an anchor connector socket. The sample termination shield is made from a split anchor connector that is mated to the end cap anchor connector socket. One side of the split anchor connector is fitted with a feed-through connector and the mated pair encloses and shields the cable sample termination. This arrangement provides for terminating the cable sample under test with a shielded resistive load and for connecting the shield to the center pin of the N connector. The cable sample under test is fitted with a plug type connector at each end and is connected between the feed-through connectors respectively located in the end plate and the split anchor connector.

2.2 Electrical Characteristics

The shield of the cable under test (CUT) defines the boundary between the two electrical regions within the fixture. As shown in Figure 2, these are (1) the resonant region, which is located between the rigid metallic cylindrical housing and the cable sample shield, and (2) the cable sample (CUT). The diameter ratio of the housing and sample shield diameters is important for determining the impedance and percent velocity of the resonant region, which are approximately 150 Ω and 90 % respectively.
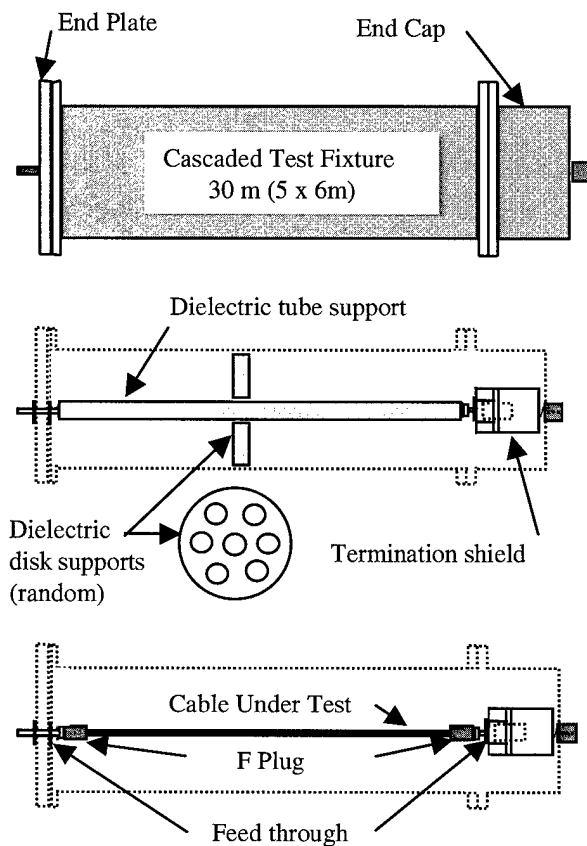
Figure 1. Triaxial test fixture overview
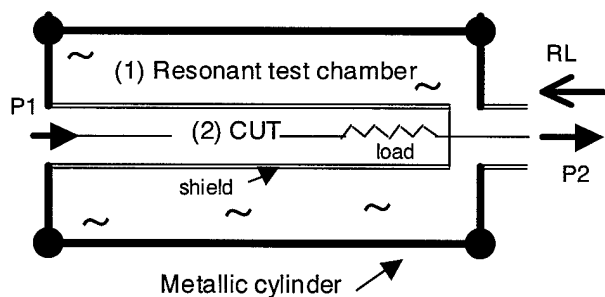
Figure 2. Electrical regions of triaxial test fixture
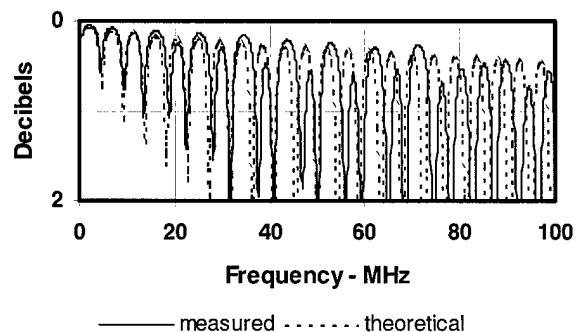
Figure 3. RL of test chamber:
measured and theoretical

In the resonant region of the test chamber the termination at the end plate (left hand side in Figure 2) is a short circuit while at the end cap (right hand side in Figure 2) the termination is a 50 Ohm coaxial interconnect. Thus the chamber is mismatched at both ends with respect to 150 Ohms. The return loss, RL, measured at the end cap (shown in Figure 3) is a result of the termination mismatches and the uniformity of the 30 meter long coaxial test chamber. Here the center conductor is the shield of the sample under test and the dielectric is made up of the sample jacket as well as the dielectric support material and air. The measured RL is in close agreement with the theoretical values shown in Figure 3.
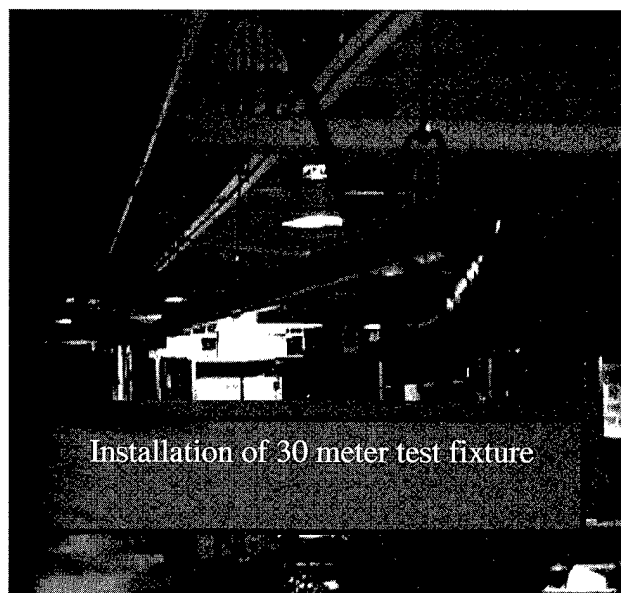
Figure 4. Open corridor installation of 30 meter test
fixture

2.3 Installation

The fixture was installed as shown in Figure 4 above an open corridor that was located on a mezzanine in the Belden Engineering Center. Individual transmission line segments were suspended 2.2 meters above the floor and aligned with commercial "Clevis" hangars. This arrangement provided relatively easy access to both ends of the fixture; nonetheless it was necessary to run approximately 35 meters of low loss 50 Ohm coax to provide the input power P1 at the end plate. The network analyzer, amplifier and data acquisition equipment were located at the far end in Figure 4. This provided for direct connection of the low level power output P2 to either a preamplifier or the network analyzer input.

3. Test Procedure

3.1 Equipment setup

The equipment setup is given in Figure 5 and the equipment used is listed in Table 1.

30 m Test Fixture (5 x 6m)
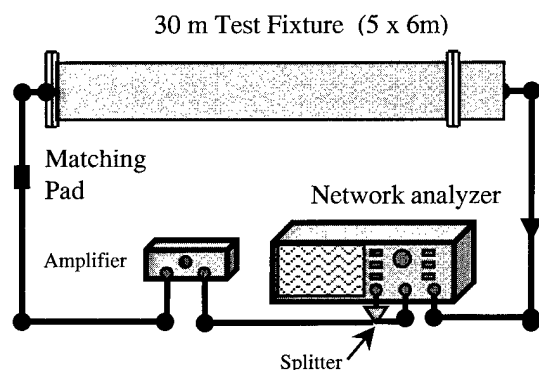
Figure 5. Equipment setup for screening attenuation measurement

Table 1. Test equipment

Network Analyzer:
HP8753ES, +10dBm, 10 Hz res. bandwidth
Power Splitter:
HP11850C, 9.5 dB loss nominal, DC-3 GHz
Matching Pad:
HP11852B, 5.7 dB loss nominal, DC-3 GHz
Power Amplifier:
HP8347A, 25 dB gain nominal, 100 kHz-3 GHz
Resistive Termination on sample under test:
75Ω type F for CATV applications

3.2 Normalization

Screening attenuation is derived from the difference in power levels (insertion loss) between the end plate P1, (energized sample input) and the end cap P2, (test chamber output). The measured power ratio is normalized [1] with the following formula. The screening attenuation curve is then obtained by drawing the envelope (not shown) formed by connecting the resonant peaks in the power ratio versus frequency plot.

$$a_n = |a_{meas}| + 10\log_{10}\left|\frac{2Z_S}{Z_1}\right| + 20\log_{10}\left(\sqrt{2}\,\frac{\left|1 - \sqrt{\dfrac{\varepsilon_2}{\varepsilon_1}}\right|}{\left|1 - \dfrac{\varepsilon_3}{\varepsilon_1}\right|}\right)$$

Where:

a_n = normalized screening attenuation (decibels).

a_{meas} = measured screening attenuation of sample in normalized and calibrated setup (decibels).

Z_1 = impedance of cable under test (ohms).

Z_S = normalized impedance of screening attenuation fixture (150 ohms).

ε_1 = relative dielectric permittivity of cable under test.

ε_2 = relative dielectric permittivity of the environment of the cable.

ε_3 = relative dielectric permittivity of screening attenuation fixture outer circuit with respect to a 10% velocity difference.

4. Test program

4.1 Samples tested

Several constructions of RG-6 type and RG-59 type coaxial cable were tested and are designated #'s 1-4. (#1 is RG-59 type and #'s 2-4 are RG-6 type cables). The details are given in Tables 2 and 3.

Table 2. Cable shield design data

#	Foil (inner)	Braid/ Angle (inner)	Foil (outer)	Braid Angle (outer)	Shield DCR mΩ/m
1	–	95% b. c. /23°	–	–	9
2	a	60% Al 27°	–	–	31
3	a	80% Al /27°	b	–	15
4	a	60% Al /27°	a	40% Al /20°	17

Table 3. Shielding tape design data

	Layer Thickness (mm)			
Foil Type	Al Foil	Polyester	Al Foil	Width (mm)
a	.00889	.02286	.00889	19.05
b	.0254	.02286		25.4

4.2 1.5 meter fixture test results

Test results are plotted versus frequency in Figures 6 and 7 for the 100-1000 MHz and 1-100 MHz frequency ranges respectively. The test program involved testing multiple samples of the designs given above. However only single sample results are shown for clarity. The statistical characteristics of screening attenuation are beyond the scope of this paper.

In Figure 6 the lowest frequency resonance peak (not shown) is just below 100 MHz. Resonance peaks out to 1000 MHz are connected by envelopes, as shown. The 1.5 meter fixture length is long enough to produce response peaks which correspond to maximum power transfer as well as minimum screening attenuation performance at specific frequencies. The exact frequency location of the peaks will vary as the length is varied, but the peak amplitude will follow the envelope. Envelopes for designs #1 and #3 are approximately flat whereas envelopes for designs #2 and #4 show an upward slope. At these frequencies the cable length under test is electrically long.
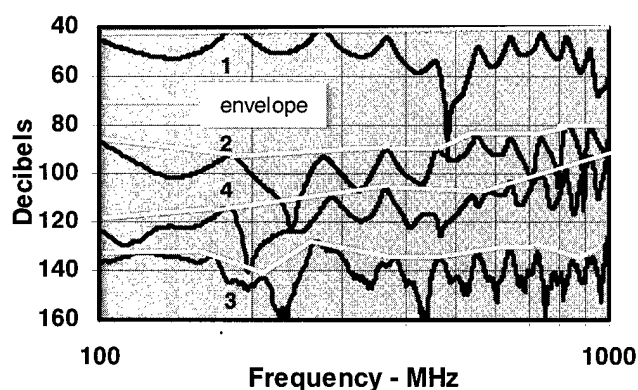
Figure 6. Screening attenuation versus frequency

In Figure 7 only one resonance peak is shown at about 95 MHz. The fixture length of 1.5 meters is too short to allow resonance to occur at lower frequencies. Therefore, power transfer does not reach a maximum and the measured screening attenuation performance is consequently not minimal. Designs #1-#4 show a tendency to converge below 1 MHz. At these frequencies the cable length under test is electrically short.
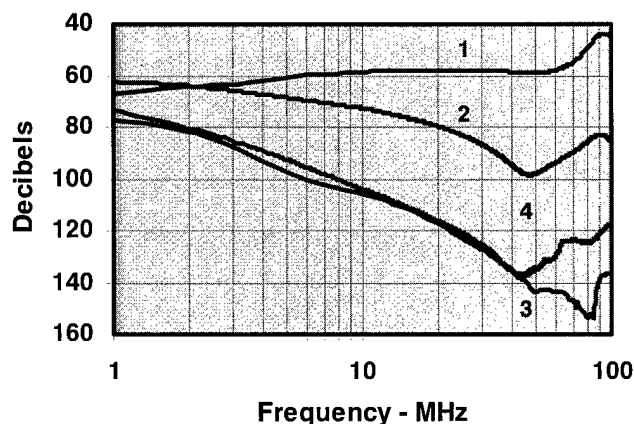
Figure 7. Screening attenuation versus frequency

4.3 30 meter fixture test results

Figures 8-11 present screening attenuation results for 30 meter lengths of designs #1-#4 respectively. 1.5 meter results are also shown.
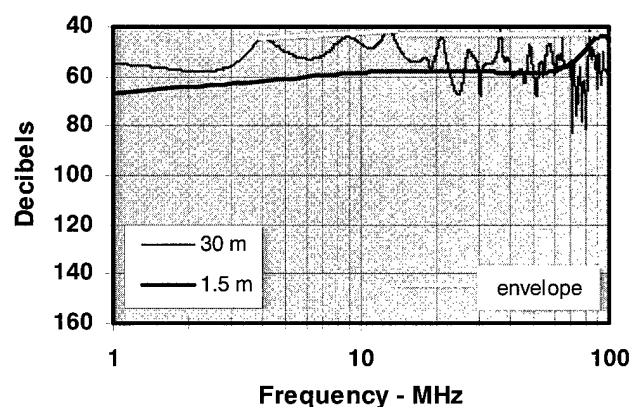
Figure 8. Screening attenuation versus frequency – Design #1
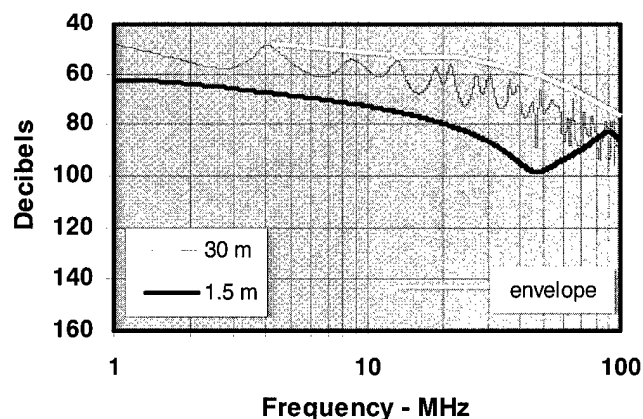
Figure 9. Screening attenuation versus frequency – Design #2
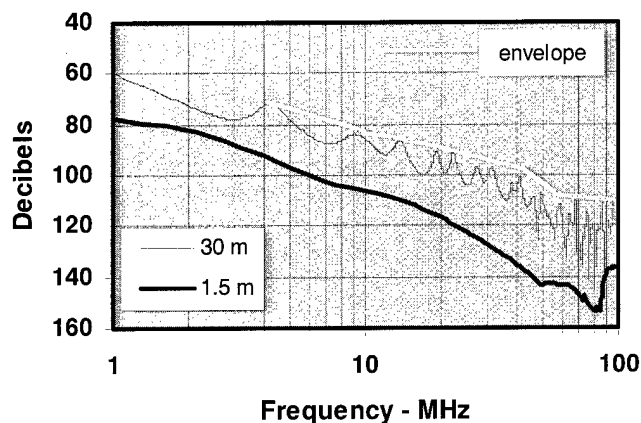
Figure 10. Screening attenuation versus frequency – Design #3
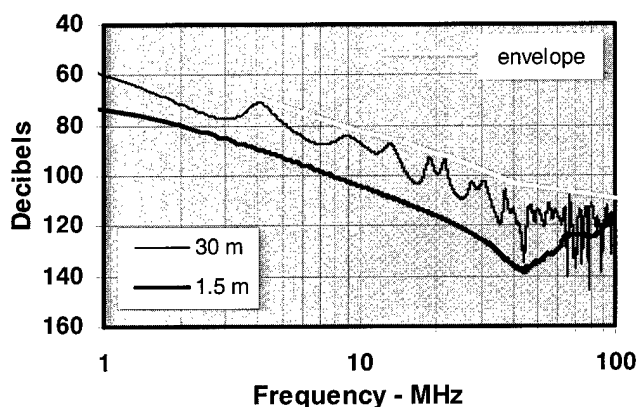
Figure 11. Screening attenuation versus frequency – Design #4

Table 4. Screening attenuation estimates versus test length

Design #	dB at 10 MHz		dB at 100MHz
	1.5 meter	30 meter	1.5 meter
1	60	41	41
2	73	52	82
3	106	82	135
4	104	82	120

For each design the 30 meter length produces minimal screening attenuation as shown by the envelope curve.

Table 4 summarizes the relationship between 1.5 meter and 30 meter lengths for 10 MHz and 100 MHz results. For example, there is approximately a 20 decibel difference in performance at 10 MHz between the 1.5 meter and 30 meter sample lengths.

Alternatively, it can be seen that the difference in performance (error) is approximately 40 decibels (designs #3 and #4) if it is assumed the 30 meter performance at 10 MHz should be approximately equal to that of the 1.5 meter performance at 100 MHz. For design #1 the 30 meter performance at 10 MHz is about the same as the 1.5 meter performance at 100 MHz. For design #2 the difference is about 30 decibels.

5. Conclusions

The paper has described a test methodology that is in the process of being standardized internationally. The test has been applied to 30 meter and 1.5 meter long cable samples and a comparison of the measured screening attenuation performance of a selection of braid and multi-foil/braid shield designs has been presented. The performance of 30 meter and 1.5 meter long samples has been compared and differences as high as 40 decibels were noted depending on frequency.

The worse case or minimum screening attenuation performance of a particular shield design can depend on the length of the cable as well as the frequencies involved. In this work the test fixture has been normalized to 150 Ω and 90 %VP, but in actual usage the electrical environment around the cable can also influence the actual screening attenuation performance.

Cable specifiers and system designers should be sure to specify screening attenuation requirements which take into account the frequency band of operation as well as the cable lengths utilized.

6. Acknowledgements

The authors are grateful to the Belden Electronics Division for the support extended to develop screening attenuation measurement technology. Thanks to Benjamin Willett for assistance with the laboratory measurements.

7. References

[1] 61196-1 Amendment 1 Radio-Frequency Cables – Part 1: Generic Specification – General, definitions, requirements and test methods.

[2] SCTE (Society of Cable Telecommunications Engineers, Inc.) IPS-TP-403B2 (preliminary-2/18/2000), Test Method for Shield Effectiveness: Screening Attenuation of Coaxial Cable.

[3] O. Breitenbach, T. Hähner, and B. Mund, "Screening of Cables in the MHz to GHz Frequency Range Extended Application of a Simple Measuring Method", *IEE Colloquium on Screening Effectiveness Measurements*, Savoy Place, London, May 6, 1998.

[4] bedea/Rosenberger, CoMeT Coupling Measuring Tube. bedea BERKENHOFF & DREBES GMBH, Herborner Straße 100 • 35614 Aßlar • Germany

[5] J. Kincaid, and C. Dole, "Test Fixture Design and Shielded Screening Attenuation Performance of CATV Coaxial Cable", *IEE Colloquium on Screening Effectiveness Measurements*, Savoy Place, London, May 6, 1998.

[6] J. Kincaid, and C. Dole, "Implementation of IEC 61196-1 Shielded Screening Attenuation Test Method", *International Wire and Cable Symposium*, Philadelphia, Pennsylvania, November 19, 1998.

[7] J. Kincaid, and C. Dole, " Shielded Screening Attenuation Test Method Down to 5 MHz", *International Wroclaw Symposium and Exhibition on Electromagnetic Compatibility*, Wroclaw, Poland, June 27, 2000.

Carl Dole

John Kincaid

Carl is an Associate Product Engineer and has been at the Belden Engineering Center for ten years. He will be graduating "With Highest Distinction" in December 2000 with a BS degree in Electrical Engineering Technology from Purdue University. Prior to joining Belden, Carl worked 10 years in television broadcast engineering and has a FCC General Class Radiotelephone License. Presently he is working on developing improved electrical test methodologies as well as new product developments. He is a member of IEEE, SMPTE, and SBE.
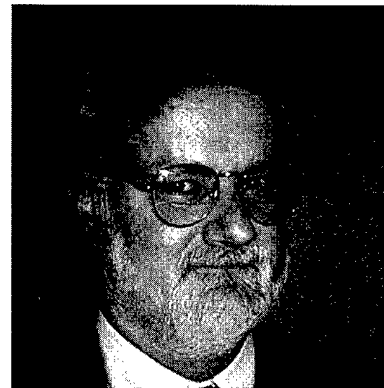
John is a Senior Product Engineer at the Belden Engineering Center. He holds BSEE and MSEE degrees from the University of Oklahoma and has over 25 years experience with Belden. His experience encompasses engineering management and product development positions in the USA as well as in Europe. He holds nine patents. John is a member of the IEEE and is active in IEC and TIA cable standardization activities. He is the US Technical Advisor to IEC SC 46A on coaxial cables, and is Convenor of IEC SC 46A/WG3 on data and CATV cable. He is also an expert on working groups 5 and 7 dealing with shielding and premises cabling issues.

The Effect of Powering on Corrosion in CATV Drop Cable

Alan J. Amato

Director of Engineering

Times Fiber Communications, Inc.
Wallingford, CT 06492
+1-203-265-8612 · alanamato@compuserve.com

Abstract

Corrosion is a process that is continually occurring all around us. Last season a New York Yankees game was postponed and Yankee Stadium closed because atmospheric corrosion had weakened a 75 year old, 600 lb. support girder to the extent that the girder could not support its own weight and failed. Televised visits to the Titanic dramatically illustrate the effects of aqueous corrosion on that ships massive and once pristine structure. Coastal cable television (CATV) operators are, unfortunately, all to familiar with the degrading effect of salt-water spray on exposed connectors, amplifiers and other metallic system elements.

Times Fiber Communications, Inc. (TFC®) has undertaken an Engineering study to answer the question: "Is the corrosion of CATV drop cable accelerated when power is carried over the drop system?" It is hoped that the results presented here will further the industry's understanding of the corrosion process as it relates to drop cables carrying limited amounts of power.

1. Introduction

The importance of maintaining corrosion free CATV drop cable cannot be overemphasized. The corrosion process, by definition, is the process causing deterioration of a material, usually metal, and its properties. Deterioration of aluminum in CATV drop cable results in loss of shield isolation capability and an increase in DC loop resistance. In the most severe cases of corrosion all of the metallic shield and connector may be lost to the corrosion process. This will allow interfering signal ingress and transmitted signal egress.

Other papers have demonstrated how AC and DC voltages affect the corrosion of cables from a physical standpoint. This paper investigates the effect on CATV cables from both a physical and degradation of shielding standpoint.

The CATV industry does not have any established procedure for corrosion testing of cables. TFC® has chosen to expose cables to a corrosive medium by a) emersing the test cables in baths of a mildly corrosive liquid and b) actual installation in an underground setting.

The general procedure for testing prepares the various samples and collects *initial* transfer impedance data. This information is gathered in a 401 data point sweep from 1 MHz to 1 GHz utilizing TFC®'s Terminated Triaxial Test Fixture. Samples are then conditioned (if required by the test plan) in a corrosive medium consisting of ASTM corrosive water for 90 days. In the underground portion of the study, environmental exposure is for one year in either Seymour, CT or Chatham, VA as applicable.

Conditioned samples are then tested to determine the after aging transfer impedance.

Finally, the shield and connector (if applicable) visual corrosion rating is determined using the system in Appendix B. The rating system has a scale from 0 to 10 with 10 being no indication of corrosion and 0 being electrical discontinuity due to corrosion.

2. Test Program & Conditions

Three different 6 Series, *Standard Shield TFC® Drop cable configurations were chosen. They are:

Standard Cable - 6 Series, Standard Shield, PVC Jacket

Underground Cable - 6 Series, Standard Shield, polybutylene flooded, PE Jacket

lifeTime® Cable - 6 Series, Standard Shield, lifeTime® flooded, PVC Jacket.

Note: lifeTime® is a TFC® registered trademark for a non-drip corrosion protecting floodant.

*Note: Standard Shield cable is defined as an aluminum-polypropylene-aluminum (APA) laminated tape, sealed to the dielectric core with an adhesive and a 60% optical coverage of aluminum alloy braid wires.

The cables were presented to the various corrosive medium either as unaltered cable, cable with a known defect (¼", 0.6 cm) ring cut in the jacket to allow simulation of damage during cable installation or damage by gophers or other rodents.) or with two connectors and a splice (F81 barrel) installed.

Three different manufacturers connectors were used the study. In order to maintain the focus of this paper on the effect of powering on drop cable, the connectors will be referred to only as Connector A, B, & C.

Four different powering situations were used:

Unpowered (control),

60 Volts, DC (negative ground) @ 1.5 amperes,

60 Volts, AC @ 1.5 amperes and

90 Volts, AC @ 1.5 amperes.

The test utilized ASTM corrosive water bath (refer to ASTM D2570) and direct burial in underground sites at both Seymour, CT and Chatham, VA as the corrosive medium. Soil samples were obtained from the Seymour and Chatham sites (See Appendix C) to determine factors relevant to the corrosion process such as pH, dissolved metals and salts in the soil, organic content and soil resistivity.

3. Mechanical Results

In all cases of unaltered cable, the visual corrosion rating was excellent (Unaffected – no indication of corrosion). Both PVC and PE jacketing materials protected the dielectric core and shield from the corrosive environment resulting in excellent mechanical performance in the corrosion test

The visual corrosion rating for the AC test cables with known defects in the jackets, whether in ASTM corrosive water or directly buried, ranged from excellent (superficial etching on the surface) to very good (Uniform metal attack and/or localized pitting). Similar results, relative to the visual corrosion rating, were noted on cables with connectors installed.

Cables exposed to DC voltages with known defects in the jackets bathed in ASTM corrosive water were very substantially affected. The visual corrosion rating in every instance was very poor (Severe corrosion, shield is electrically discontinuous due to dissipation of metal by corrosion.)

Cables with connectors installed and exposed to DC voltages in ASTM corrosive water were also affected. The visual corrosion rating ranged from excellent (superficial etching on the surface) to very poor (Severe corrosion, shield/connector is electrically discontinuous due to dissipation of metal by corrosion.)

4. Degradation of Shielding Results

4.1 General

Transfer impedance was chosen as the base method of evaluating the shielding characteristics of drop cable. The results that follow, however, are not presented in the typical milliohm per meter (mΩ/m) transfer impedance format. The mΩ/m data collected was first converted to *degradation factor*. Degradation factor (DF), as used in this paper, is defined as the after aging average of three sets of data divided by the before aging average of three sets of data. Therefore any DF above one (1) represents a decrease in shielding effectiveness and similarly, any DF below one (1) represents an increase in shielding effectiveness relative to the cables initial transfer impedance. Finally, in an effort to present the data in the more familiar dB format, the calculated DF is converted to *change in shielding effectiveness* (ΔSE) using

$$\Delta SE = 20 Log(1/DF), \qquad (1)$$

where ΔSE is expressed in dB. For example, if the ΔSE is equal to -5 dB this indicates a 5 dB reduction in shielding effectiveness.

A convenient way to present the large amount of data collected in this study is in tabular form, such as that located in Appendix A and titled, Table 1, ASTM Corrosive Water, or Table 2, Directly Buried Installation.

4.2 Unaltered Jackets

Tests on cables with unaltered jackets indicated ΔSE values between -1.6 dB and –9.2 dB. This includes all powering situations and cable types (See Figure 1).

Figure 1

ASTM Corrosive Water
Unaltered Cable
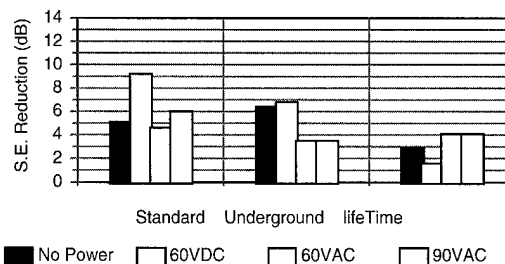
The degrading effect of power on cables, when considered as an averaged group, indicates that 60 VDC is the most severe on shielding performance with an averaged ΔSE of –5.8 dB.

Unpowered cables degraded an average of –4.8 dB with 60 VAC and 90 VAC degrading cables by –4.0 and –4.5 dB respectively.

The unpowered cables in ASTM corrosive water for 90 days degraded approximately as much as the cables installed underground in Seymour, CT for one year (See Figure 2).

Figure 2

Underground Installation
Unaltered Cable
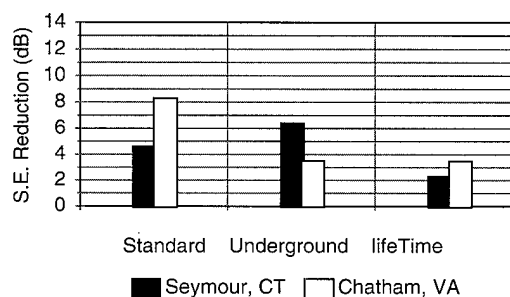
4.3 Known Defects in Jacket

Cable exposed to DC voltages with known defects (windows) in the jacket and bathed in ASTM corrosive water were very substantially affected from a shielding standpoint. Typical ΔSE for these cables confirmed that which had been noted in the visual examination, complete loss of shielding capability ranging from –84.6 dB to –93.1 dB (See Figure 3, note scale change).

Figure 3

ASTM Corrosive Water
Cable with Windows

Figure 3 — ASTM Corrosive Water, Cable with Windows (60VDC)

4.4 Cables with Connectors

As was discussed previously, the ΔSE charts compare *performance* before and after *aging*. Therefore, it is necessary to point out that the following Figures *do not* illustrate or include the ΔSE due to the installation of connectors. Test results gathered in this study indicate that installing connectors will have little influence on shielding effectiveness in the area of 10 Mhz. The ΔSE noted by installing connectors was approximately –5 dB at 100 MHz region and –15 dB in the 1,000 MHz region after connector installation.

Similar to that noted in the cable only tests, 90 VAC cable/connectors performed as well as or better than the 60VAC cable with connectors and the unpowered cable with connector.

When compared to the 60VDC non-connectorized cables (ref. Figure 3), it is interesting to note that the cable with connector samples performed quite well in the 60VDC test (See Figure 6, 7 & 8 on following page).

Installation of the connector manufacturer's recommended boot for underground installations showed mixed results. Figures 12 & 13 in comparison with Figures 6 & 8 show that about half of the time boots improved performance and the other half of the time performance was degraded. Note: Boots were not available for connector B.

Cables in ASTM corrosive water with known defects in the jackets, *excluding* the DC tests, indicated ΔSE's between –1.6 dB and –13.1 dB (See Figure 4, note scale change). Unpowered cables with windows in the jacket degraded an average of –7.7 dB. 60 VAC and 90 VAC exposed cables degraded by an average of –5.2 and –4.2 dB respectively.

Cables with windows and installed underground in the Seymour and Chatham sites for one year performed identically with the exception of the standard cables. (See Figure 5)

Figure 4

ASTM Corrosive Water
Cable with Windows

Figure 4 — ASTM Corrosive Water, Cable with Windows (No Power, 60VAC, 90VAC)

Figure 6

ASTM Corrosive Water
Cable with Connector A

Figure 6 — ASTM Corrosive Water, Cable with Connector A (No Power, 60VDC, 60VAC, 90VAC)

Figure 5

Underground Installation
Cable with windows

Figure 5 — Underground Installation, Cable with windows (Seymour, CT; Chatham, VA)

Figure 7

ASTM Corrosive Water
Cable with Connector B

Figure 7 — ASTM Corrosive Water, Cable with Connector B (No Power, 60VDC, 60VAC, 90VAC)

Figure 8

ASTM Corrosive Water
Cable with Connector C

Legend: ■ No Power, □ 60VDC, □ 60VAC, □ 90VAC
Categories: Standard, Underground, lifeTime
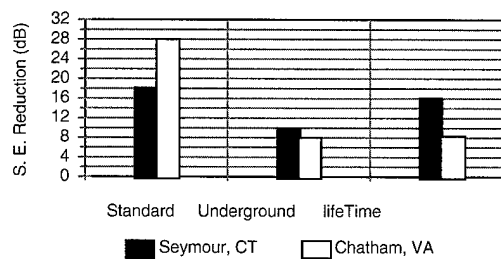
Similar to that noted in the unaltered cable and cable with window tests the Chatham, VA installation was more detrimental to shielding effectiveness than the Seymour, CT site.

Figure 9

Underground Installation
Cable with Connector A

Legend: ■ Seymour, CT, □ Chatham, VA
Categories: Standard, Underground, lifeTime

Figure 10

Underground Installation
Cable with Connector B

Legend: ■ Seymour, CT, □ Chatham, VA
Categories: Standard, Underground, lifeTime
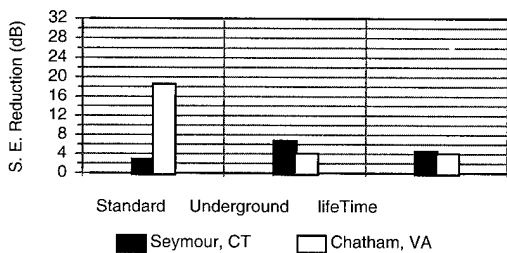
4.   Discussion

The core of the test cables was selected to be the widely used 6-Series cable with a shield consisting of an APA tape and 60% aluminum braid coverage. Differences existed in the cable constructions as far as the flooding compound (polybutene and lifeTime®) and jacket materials (PE and PVC).

Figure 11

Underground Installation
Cable with Connector C

Legend: ■ Seymour, CT, □ Chatham, VA
Categories: Standard, Underground, lifeTime

Figure 12

ASTM Corrosive Water
Cable with Connector A & Boots

Legend: □ 60VDC, □ 60VAC, □ 90VAC
Categories: Standard, Underground, lifeTime

Figure 13

ASTM Corrosive Water
Cable with Connector C & Boots

Legend: □ 60VDC, □ 60VAC, □ 90VAC
Categories: Standard, Underground, lifeTime

Typical characteristic ΔSE curves indicate little degradation due to corrosion from 1 MHz to 15 MHz and increasing degradation from 10 MHz to 1,000 MHz.

The underground flooding compound was found to seal small jacket punctures and minimize moisture migration into the sample; ultimately resulting in reduced shield degradation. It was also observed in connectorized samples that occasionally the underground floodant flows into the connector/F81 interface.

lifeTime® flooded cables indicate the best overall performance in the studied corrosive environments. lifeTime® stops moisture migration at the damaged area and has superior qualities over underground

floodant in protecting the exposed shield from corrosion. lifeTime® flooding compound did not demonstrate the characteristic of flowing into the connector/F81 interface.

The 60-Volt DC cable installation, with windows in the cable, caused rapid and catastrophic degradation of cable shielding. Examination of the vastly larger ΔSE numbers in DC testing, as compared to the AC tests, indicate that the corrosive mechanism at work is electrolytic corrosion, sometime called stray current corrosion.

Stray currents are defined as those direct currents that follow paths other than their intended circuit. Stray currents leave their intended path because of poor electrical connections within the circuit or imperfect electrical insulation or jacketing around the intended conductive (center or outer conductor) material. These type of corrosion problems occur on underground metallic structures as a result of the operation of direct current equipment such as electric railways, welders, cranes or plating equipment in the area of the structures.

The 90-Volt AC and 60-Volt AC performance results were similar to, or *better* than unpowered cables. The time varying nature of alternating current has minimized stray current corrosion in the 60 and 90-Volt AC installations. The corrosive processes at work in the unpowered and AC tests are a combination of pitting corrosion and galvanic corrosion. In addition, the power present (I^2R) has *protected* the cable from the corrosion process. This type of protection occurs when heat created in current carrying conductors, prevent or minimize the migration of moisture into the area of the cable shield. A similar phenomenon is well known in the power cable industry. That is, cable with power will have substantially less moisture content in the dielectric than an unpowered cable.

From visual inspection of the connector interfaces all three connectors performed equally well with very little change in surface appearance. All three connectors showed about the same surface degradation in ASTM corrosive water with no power.

After visual examination of the connectors, it was found that failure of the connector occurred by the migration of moisture along threads of the connector/F81 barrel and into the shield/dielectric area. Rubber boots from the connector manufacturers were tested on the connector interface to see if this would stop moisture migration into the connectors. The boots are placed over the threads of the barrel and when the connectors are installed they compress the boot creating a seal. The performance of these boots was mixed and generally unreliable; a large percentage of the boots allowed moisture to migrate into the connectors. In addition, this type of boot did not protect the surface of the connector from corrosion.

The underground testing, while not powered, provides some interesting areas of discussion. The Seymour, CT site was found to be slightly less detrimental to the cable shield in comparison to Chatham, VA. The pH value of the soil at each site was measured and found to be almost identical and nearly neutral. The Chatham site contained substantially more chloride than Seymour, and aggressive anion which probably, more than any other factor, accelerated the corrosion in Chatham relative to the Seymour site.

Other significant factors in underground corrosion are soil resistivity and drainage characteristics of the soil. For example, a soil that drains rapidly will be relatively non-corrosive regardless of its resistivity. However, a soil that drains slowly and then remains from 50 to 95% saturated with water for extended periods will be corrosive, particularly if its resistivity is low. This may be another contributing factor in the slightly accelerated corrosion noted in the Chatham test cables.

5. Conclusions
DC powering, when used in the drop system, is detrimental to the metallic components of the system. Higher levels of corrosion should be expected in the area of railroads, welding shops and plating businesses.

The materials used in cable today perform well in both network powered broadband cable as well as conventional unpowered CATV drops.

Overall, the conclusion of this paper is an endorsement of powering over the drop cable. However, it has been demonstrated that the fundamental enemy of CATV drop cables is moisture. Moisture may migrate into a cable construction through breaks in the jacket, unprotected paths through the cable/connector junction or migration through the jacket materials. Flooding compound placed between the cable outer conductor and cable jacket is the answer to preventing moisture migration into the cable construction. While flowing type flooding compounds have demonstrated cable-protecting qualities, non-flowing flooding compounds, like TFC®'s lifeTime®, have been proven to be most effective over time.

6. Acknowledgments
Special thanks to TFC for their support during the term of this testing and to Randall Simpkins for his dedication to the project.

7. References
[1] Baboian R., Hessler G., Bow K., Haynes G., The Effect of Alternating Current On Corrosion of Cable Shielding Materials In Soils

[2] Husock B., Causes of Underground Corrosion, Plant Engineering, April 15, 1982

[3] Baboian R., Pohlman S., Galvanic Corrosion, Metals Handbook, Ninth Edition, Volume 13, Corrosion.

[4] Pohlman S., Stray-Current Corrosion, Metals Handbook, Ninth Edition, Volume 13, Corrosion.

[5] Hollingsworth E., Hunsicker H., Corrosion of Aluminum Alloys, Metals Handbook, Ninth Edition, Volume 13, Corrosion.

[6] Schick G., Corrosion in Telephone Cable Plants, Metals Handbook, Ninth Edition, Volume 13, Corrosion.

Author
Alan J. Amato received his B. S. Degree in Electrical Engineering from the University of New Haven, West Haven, CT.

In 1994 he joined Times Fiber Communications, Inc. and is currently Director of Engineering.

He has been involved with cable engineering since 1978 and is a Senior Member of the Society of Cable Telecommunications Engineers (SCTE).

Appendix A, Table 1
Cable Performance Comparisons Installed in ASTM Corrosive Water

(Change in Shielding Factor in dB (ΔSF) from 1 MHz to 1 GHz)

Cable	No Power	60 VDC	60 VAC	90 VAC	Average
Standard Cable	-5.1 (10)	-9.2 (10)	-4.6 (10)	-6.0 (10)	**-6.2**
Standard W/Windows	-13.1 (8)	-84.6 (0)	-4.1 (8)	-6.4 (8)	***-7.9**
Standard Conn. A	-9.8 (9)	-3.5 (8)	-8.9 (8)	-4.6 (8)	**-6.7**
Standard A & Boots	N/A	-17.0 (8)	-6.8 (8)	-13.1 (8)	**-12.3**
Standard Conn. B	-10.9 (9)	-2.3 (7)	-8.3 (8)	-6.0 (8)	**-6.9**
Standard Conn. C	-30.4 (9)	-10.9 (8)	-25.6 (8)	-8.3 (8)	**-18.8**
Standard C & Boots	N/A	-28.0 (0)	-10.9 (9)	-4.1 (9)	**-14.3**
Standard Cable Average	**-13.9**	***-11.8**	**-9.9**	**-6.9**	
Underground Cable	-6.4 (10)	-6.8 (10)	-3.5 (10)	-3.5 (10)	**-5.1**
Underground W/Windows	-7.2 (8)	-93.1 (0)	-7.6 (9)	-4.6 (9)	***-6.5**
Underground Conn. A	-8.9 (9)	-10.9 (8)	-4.1 (8)	-3.5 (8)	**-6.9**
Underground A & Boots	N/A	-3.5 (8)	-2.3 (8)	-2.9 (8)	**-2.9**
Underground Conn. B	-9.8 (9)	-6.0 (4)	-4.1 (8)	-4.1 (8)	**-6.0**
Underground Conn. C	-12.0 (9)	-5.6 (9)	-6.8 (8)	-6.0 (8)	**-7.6**
Underground C & Boots	N/A	-20.8 (0)	-8.0 (9)	-16.1 (9)	**-15.0**
Underground Cable Average	**-8.9**	***-8.9**	**-5.2**	**-5.8**	
LifeTime® Cable	-2.9 (10)	-1.6 (10)	-4.1 (10)	-4.1 (10)	**-3.2**
LifeTime® W/Windows	-2.9 (9)	-88.6 (0)	-4.1 (9)	-1.6 (9)	***-2.9**
Lifetime® Conn. A	-7.2 (10)	-6.0 (8)	-5.1 (8)	-4.1 (8)	**-5.6**
lifeTime® A & Boots	N/A	-4.6 (6)	-2.9 (8)	-4.1 (8)	**-3.9**
Lifetime® Conn. B	-7.2 (9)	-1.6 (9)	-4.6 (8)	-2.9 (8)	**-4.1**
Lifetime® Conn. C	-15.4 (9)	-5.1 (9)	-14.0 (8)	-8.0 (8)	**-10.6**
lifeTime® C & Boots	N/A	-10.9 (8)	-5.1 (9)	-9.2 (8)	**-8.4**
Lifetime® Cable Average	**-7.1**	***-5.0**	**-5.7**	**-4.9**	
Overall Average	**-10.0**	***-8.6**	**-6.9**	**-5.9**	

Note: 1) Asterisk * values indicate that the 60 VDC, W/Window, ΔSF values have been excluded.

                      2) Parenthetical () values indicate visual corrosion rating (see Appendix B)

Appendix A, Table 2
Cable Performance Comparisons Installed Underground

(Change in Shielding Factor in dB (ΔSF) from 1 MHz to 1 GHz)

Cable	Seymour, CT	Chatham, VA	Average
Standard Cable	-4.6 (10)	-8.3 (10)	**-6.5**
Standard W/Windows	-5.1 (10)	-8.3 (10)	**-6.7**
Standard Conn. A	-4.1 (9)	-16.8 (9)	**-10.5**
Standard A & Boots	N/A	N/A	**N/A**
Standard Conn. B	-2.9 (9)	-18.6 (9)	**-10.8**
Standard Conn. C	-18.1 (9)	-28.0 (8)	**-23.1**
Standard C & Boots	N/A	N/A	**N/A**
Standard Cable Average	**-7.0**	**-16.0**	**-11.5**
Underground Cable	-6.4 (10)	-3.5 (10)	**-5.0**
Underground W/Windows	-4.1 (10)	-4.1 (10)	**-4.1**
Underground Conn. A	-5.1 (9)	-7.6 (9)	**-6.4**
Underground A & Boots	N/A	N/A	**N/A**
Underground Conn. B	-6.8 (9)	-4.1 (9)	**-5.5**
Underground Conn. C	-9.8 (9)	-8.0 (8)	**-8.9**
Underground C & Boots	N/A	N/A	**N/A**
Underground Cable Average	**-6.4**	**-5.5**	**-6.0**
lifeTime®	-2.3 (10)	-3.5 (10)	**-2.9**
lifeTime® W/Windows	-1.6 (10)	-1.6 (10)	**-1.6**
lifeTime® Conn. A	-2.9 (9)	-6.0 (9)	**-4.5**
lifeTime® A & Boots	N/A	N/A	**N/A**
lifeTime® Conn. B	-4.6 (9)	-4.1 (9)	**-4.4**
lifeTime® Conn. C	-16.0 (9)	-8.3 (9)	**-12.2**
lifeTime® C & Boots	N/A	N/A	**N/A**
lifeTime® Cable Average	**-5.5**	**-4.7**	**-5.1**
Overall Average	**-6.3**	**-8.7**	**-7.5**

Note:　　1) Asterisk * values indicate that the 60 VDC, W/Window, ΔSF values have been excluded.

2) Parenthetical () values indicate visual corrosion rating (see Appendix B)

Appendix B
Visual Corrosion Rating System

Rating	Performance	Degree of Corrosion
10	Excellent	Unaffected - no indication of corrosion.
9	Excellent	Superficial rust or etching on the surface.
8	Good	Uniform metal attack, rust, and/or slight localized pitting.
7	Good	Appreciable pitting over the surface, but no perforations through metal shield. Some minor delamination or dissipation of metallurgically or plastic-bonded metals leaving cathodic metal intact.
6+	Good	Localized pitting: only one perforation in the shield by pitting.
6	Good	Localized pitting: 2 to 5 perforations in the shield by pitting.
5	Fair	Many localized pits causing perforations of shield <5% of the shield dissipated by corrosion; extensive delamination of metallurgically bonded metals.
4	Poor	Severe corrosion: pitting to perforation of shield; 5 to 10% of shield dissipated by corrosion; severe corrosion of anodic part of metallurgically bonded metals.
3	Poor	Severe corrosion: pitting to perforation of shield; 10 to 25% of shield dissipated by corrosion.
2	Very Poor	Severe corrosion: more than 25% of shield dissipated by corrosion; shield stick has electrical continuity along the cable.
1	Very Poor	Severe corrosion: shield is close to electrical discontinuity (ELD) due to perforation in shield and dissipation of metal by corrosion.
0	Very Poor	Severe corrosion: shield is electrically discontinuous (ELD) due to dissipation of metal by corrosion.

Appendix C
Soil Analysis Chatham, Virginia and Seymour, Connecticut

	Seymour, CT	Chatham, VA
Corrosion Indicators: (at 10% slurry)		
pH (SU)	6.24	6.21
Specific Conductance (µmhos)	15.60	14.80
Alkalinity (mg/L)	4.80	2.90
Calcium (mg/L)	3.30	0.87
Constituent Analysis: (Results in mg/Kg unless otherwise noted)		
Total Metals:		
Sodium	392.2	1072.0
Magnesium	3351.0	2537.0
Calcium	1382.0	328.6
Potassium	1492.0	2037.0
Iron (% w/w)	1.54	4.27
Chloride	nd<1.0	48.0
Nitrate	13.0	11.0
Sulfate	nd<10.0	nd<10.0
Insoluble Material	87.90	77.81
Soil Resistivity (Ω-cm):	73,890	24,247

Note: Soil resistivity testing was conducted by TFC® Engineering. Environmental Monitoring Laboratory, Inc., Wallingford, CT, conducted all other soil analysis.

Copper LAN Cable: Combined Improvement of Various Manufacturing Steps

J. Altmayr
Rosendahl Maschinen GmbH*, Austria

P. Letout
Pourtier France, Chelles Cedex*, France

Abstract

The increasing demand for LAN cable with higher transmission rates and enhanced flame resistance had led to develop new technologies for wire drawing, core extrusion, twinning and jacketing.

Existing process have reached their limits, and it clearly appeared that each manufacturing step has to be enhanced. Considering also that each step strongly influences the result of the next, a common approach has to be led.

The group of Companies has therefore focused their combined research and development on:

FEP foaming with improvement on extruders, screws, crosshead and gas-dosing system.

Triple twist twinning with increasing output and improved electrical performances of pair.

Jacketing with flame retardant materials and improved tension control to keep the quality of triple twisted pairs.

The specific evaluation of the results shows that the methods which have been developed, and will be continued, give superior improvements for Category cables, with possible application on further development in copper LAN cable production, and other types of data cable using copper conductors.

Core Insulation for Twisted Pair LAN Cables

Twisted Pair Cable Market

The Information age linking phones, computers, printers, scanners, etc. has increased the wiring of office buildings markedly during the last decades and now starts to expand even inside our homes.

New applications as well as the rapidly increasing performance of hardware effects the demand for better quality and capacity of e.g. the Local Area Networks (LANs).

Latest marketing analyses speak about market for installation of LAN Cat. 5 for office buildings having passed the big boom and being rather stagnating now (especially western communities). The big increase may be expected in leading-edge technologies for wiring the homes, plants, locomotion, support of media-on-demand and other next generation applications, e-commerce, shared periphery, new interface technologies (IEEE 1394 USB, firewire, i-link, etc.), new networks (Gigabit Ethernet, etc.), and therefore new cable and new cabling design standards.

Upcoming Twisted Pair Cable Standards (Table 1)

Regarding the fact that Networks are generally built to fit at least for a period of 15 years and the costs for the cable itself is about less then 10% of the average network installation costs only, the usage of the new high performance cables will get it's way into all newly installed LANs very soon. Appropriate specifications and standards for the cabling systems are already released or at least in development. (e.g. Anixter Level 5, 6, 7 or TIA/EIA 568-A Cat .5e, Cat. 6, Cat .7, DIN44312-5 etc.).

Upcoming Twisted Pair Cable Designs

World wide, a variety of UTP and STP constructions are in development or already in use to meet this requirements. Cables based on the Category 6 specifications are likely to be tightly wounded and prevented from unravelling and pair-to-pair interactions. The proposed Category 7 recommendations call for a cable that is capable of 600-MHz transmission speeds. Initial Category 7 cable are likely to be shielded both, the individual pairs and the whole strand (SSTP) to achieve the 600-MHz data rate. In addition to the demanding electrical properties, plenum rated cables have to meet most stringent flame and smoke spread specifications. In this respect, national regulations are still different from North America to Europe and Asia.

Foamed FEP

Several testing results shows clearly that structure (2 pairs, 4 pairs, multiple pairs, UTP, S-UTP, STP, S-STP,...) and materials must harmonize perfectly to meet all electrical, mechanical, smoke and fire retardant, and last but not least economical requirements.

If electrical properties only were the criteria, PE would be the material of choice for insulation. It is featuring a very low dielectric constant, inexpensive, free of halogens and during production easy to process at very high speeds. In combination with a jacket of flame retardant PVC or polyolefin it is mainly utilized for non-plenum risers and vertical tray cables. PE is used for solid, foam-skin and skin-foam-skin design.

To pass the hard smoke and flame tests (UL, ITS, CSA) for plenum cables installed in USA and Canada, designs with FEP insulation and low smoke PVC jacketing usually have been used. Some cables have been developed that utilize PE, FRPE and FEP in combination with LSPVC or FEP jacketing providing excellent electrical performance and correspond to the fire regulations.

---

* Both companies are part of the Knill Gruppe, Austria.

Cabling Standards

	CAT 5e	CAT 6 *draft 6* (class E)	CAT 7 *draft* (class F)	Level 5	Level 6	Level 7
Frequency	100 MHz	250 MHz	600 MHz	250 MHz	350 MHz	400 MHz
Design	STP, UTP	STP, UTP	STP	UTP, STP	UTP, STP	UTP, STP
Attenuation	22db	19,8 (19,9) db	19 db	22 db	22 db	19.9 db
NEXT	35.3	44.3	72,2	35.3	38.3	44.3
ACR	-	24.1 (24,4)	53,4	13.3	16.3	24.3
NEXT PS	32,3	42.3	*Not specified jet*	32.3	34.3	43.3
ACR PS	-	22.5 (22,4)	*Not specified jet*	10.3	12.3	23.4
ELFEXT	23.8	27.8	*Not specified jet*	23.8	25.8	27.8
ELFEXT PS	20.8	24.8	*Not specified jet*	20.8	22.8	25.8
Return Loss	17.1	20,1 (17,1)	*Not specified jet*	20.1	20.1	20.1

(Table 1: Passive testing of cables 100m at 100 MHz; Electrical Requirements as specified in TIA/EIA standards (resp. ISO/IEC 11801) and Anixter Levels)

Rheological properties

	FEP	PE
Meltingpoint	507°F (264°C)	375°F (132°C)
Processing temperature	603-633°F (360-390°C)	413 – 234°F (170–210 °C)
Viscosity	8000 Pa s	1300 Pa s
Critical Shear Rate	15-25	1000 -2000

(Table 2: Comparison of rheological properties of examples of gasified FEP and PE resins used for insulation of foamed primariesfor twisted pairs at an avaerage processing temeperature)

Extrudersettings

	FEP	PE
Feeding	605 °F	199°F
Transition	614°F	453°F
Metering	635°F	433°F
Adapter	635°F	433°F
Head	635°F	433°F
Die	635°F	453°F

(Table 3: Comparison of guidelines for temperature settings of extruders for physical foaming)

For future cable designs of next generation cabling solutions, thin wall application of foamed FEP has become of central interest. The foaming of the dielectricum results in better performing cable with faster velocity of propagation and less delay. Besides the economic aspects of saving FEP material, the cable becomes more flexible, thinner and lighter than a comparable cable of solid design. Foamed FEP is also utilized for the insulation of mini coaxial cables.

Processing of foamed FEP for thin wall application

Apart from meeting the same fire regulation demands the application of foamed PE and FEP for dielectricum of twisted pair communication cables for high data transmission rates is very similar. However, processing of the two materials is most unequal. This results of the different rheological properties of PE and FEP (Tables 2 and 3).

Low viscosity, low processing temperature and low shear sensitivity allows processing of foamed PE with bigger dimensioned extruders at high processing speeds up to 9000fpm. Processing speed for foamed FEP is limited by the properties of the material. Without reduction of the molecular weight of the material (degradation) or decrease of the insulation quality (melt break, high excentricity) production speeds far above 2200 fpm can't be expected.

Efficient Processing equipment for thin-wall insulation of cores

To value the productivity of an extrusion unit all components of the system have to be considered. Each single element influencing the production process has a certain impact on expenditure, running costs, maintenance needs, yield, endurance, loss of value and last but not least space requirements.

Because of the unequal rheological properties of gasified PE and FEP the economic utilizing of the same equipment for both is limited but advisable in some cases.

With an appropriate line concept, the special design of extruder, screw and crosshead and the corresponding conversion kit, a certain compatibility for both FEP and PE is feasible. Restrictions in terms of quality respectively quantity of the production have to be considered.

Over the last two years limits of efficiency for lines designed to process foamed PE and FEP have clearly shown up. Processing of PE does not loose any of its advantages regarding the high foaming degree, constant diameter, roundness and perfect centricity up to 9000ft/min production speed. Only, abrasion is higher due to the softer material used for fluor-resistant components.

Though limited by the material properties the production speed at processing FEP is still high at about 300m/min. Nevertheless, the line components geared for high speed production are fairly oversized.

The key for highest efficiency of the extrusion equipment is to optimize all components of the system to process either PE or FEP. Special designed extrusion equipment and an enhanced monitoring and control system allows to fully utilize the specific properties of each of the materials. The main difference for designing the extrusion equipment is the size and L/D Ratio of the extruders, screw geometry and especially the layout of crosshead and dies.

The use of a 45mm single-screw extruder with LD ratio 36 and the special designed FEP foaming screw has a lot of advantages. Without going beyond the critical shear rate the melt can ideal be mixed, gasified and homogenized at moderate temperature. This results in fine and uniform cell structure of the insulation.

Any dead-spots inside the double layer crosshead extend the dwell-time of parts of the FEP melt and would cause degradation of the material and thus cause major irregularities of the core insulation. With FEM (Finite Elements Method) continuos flow and proper distribution of the melt can be verified during design of the crosshead.

Dies for tube-extrusion show the best results for processing of FEP. For this reason, the perfect homogenized melt and fine structure is of utmost importance for thin-wall application. Premature expansion and cooling of the melt has to be prevented, otherwise melt fracture and cone-break causes a rough surface.

The heating of the entire crosshead including adapters and the conductor guiding thorn helps to keep the best environment for the melt right to the preferred point of expansion. The appropriate draw-down ratio for the melt cone is depending on the viscosity of the melt between the outlet of the die and the point of contact with the conductor . Thus, also final line speed is depending on the properties of the gasified FEP melt.

For PE, compression dies are used, which makes the foaming process much easier to handle.

If now all of the special designed and selected line components (tandem drawing with annealer and preheater, measuring equipment, cooling section and take up) besides the processing equipment are tuned precisely, nothing can hold efficient production anymore. This kind of high quality cores (low excentricity, exact diameter and smooth surface) is the basis for better twisted pairs (Table 4).

Twinning Pair for LAN Cables

Regarding production of high frequency copper cables, such as LAN cables cat.5, cat 5+, cat.6, cat.7, the key point remains good quality of the primary copper conductor itself :copper core quality((material,quality, diameter consistency, elongation, surface quality) is very important.Type and quality of insulation is similarly very important (talking for example about PE insulation, : solid, foam skin, skin foam skin, and foaming rate or percentage of air or other type of insulation such as FEP).Most important of all however being concentricity between copper core and insulation material.

Twinning Process has also its importance, specially as far as accuracy of pair laylength is concerned. The necessary accuracy has to be obtained in order to meet the required cable performance.

The laylength accuracy generally required, and obtained, is less than +/- 1% when measured for example over 20 consecutive lays.

It is interesting however to note that even this parameter (accuracy of lay length) is being influenced by the quality of copper core itself (mainly by elongation ratio and annealing factor).

The above-mentionned parameters being very well mastered, focus has been put on increasing productivity when pairing the copper conductors for LAN cable.

✔ For instance, one single pair for LAN cat.6, with short laylength 10 mm, would be produced today, with conventionnal method, at following speed :

0.010 m (laylength in meter) x 4000 twists/mn (conventional pairing speed) = 40 m/mn

✔ The proposed method would allow :

0.010 m (laylength in meter) x 6000 twists/mn = 60 m/mn

which represents a significant increase of production speed.

Processing equipment

	FEP (PE utilization <20%)	PE (FEP utilization <20%)
Mainextruder (Type)	Horizontal extruder RE 1.45.36*Fluor resistant*	Horizontal extruder RE 1.60.30*Fluor resistant* (*Expansion*>68%: additional 6D Extension)
L/D Ratio	36	30 (+6 for extension)
Inner skin extruder	- (PE kit: Vertical extruder 1.30.24) -	Vertical extruder 1.30.24
Outer skin extruder (Type, L/D Ratio)	Co-extruder RE 1.30.24 CO *F*	Co-extruder RE 1.45.24 CO *F*
Screw Inner Skin Extruder	- (PE kit: Universal barrier screw 30.24 RB2)	Universal barrier screw 30.24 RB2
Screw Outer Skin Extruder	Barrier screw 30.24 3*F*	(FEP kit: Barrier screw FEP 45.24 3F)
Screw Mainextruder	Barrier screw 45.36*F*; hardsurfaced flights (PE kit: Barrier screw 45.36 ionitrated; hardsurfaced flights)	Barrier screw 60.30 C5*L* (barrier screw 60.36 C6.2*L* for *Ex*>68%) hardsurfaced flights (FEP kit: barrier screw 60.30 3F)
Flange	Heated	heated
Crosshead	Double layer X-head Fluor: shear retardant (PE kit: Triple layer X-head)	Triple layer X-head (FEP kit: Double Layer Fluor: shear retardant)
Die	Tube extrusion dies; thorn heated; balanced for FEP PE kit: compression dies	Compression dies (FEP kit: tube extrusion dies; thorn heated;
Vacuum pump	Yes	(FEP kit: yes)
Gas dosing&injection	RSD (up to 800 bar)	RSD (up to 800 bar)
Max. Linespeed	600 – 2200 fpm	9000 fpm (FEP: 600 – 2200 fpm)
Foaming degree	20 – 60% (PE: up to 73%)	Up to 73% (FEP: 20 - 60%)
Control&Monitoring	RIO enhanced	RIO enhanced

Table 4: Comparison of optimized processing equipment for foamed thin-wall insulation of FEP/PE foam cores diameter over insulation)advised by Rosendahl Maschinen GmbH. The necessity to process to a certain percentage both of the materials on one line has been taken into consideration. Also, with an additional kit the equipment can be adapted to solid insulationwith increased linespeed.

Fig. 1

Fig. 2
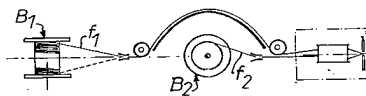
New Twinning process

The new twinning process includes:

1/ Backtwister unit :

A backtwister unit (as shown in Fig.1) is producing one pair under the following process :

-wire f1, coming from from a stationary pay-off (B1) is backtwisted when going through the bow which rotates around B2 (at speed 2000 RPM)

-wire f2 is coming from stationary pay-off (B2).

-The 2 wires f1 & f2 are then twinned at speed upto 2000 twists/mn corresponding to to the bow rotation speed.

At this point, the pair is formed with full backtwist (100%) on each wire.

This system is well known to the cable makers and has long been used for various production in the cable industry.

It is a single twist process with full backtwist.

2/ Double twit take-up :

The pair which has been formed previously on the backtwister unit is then twisted again on conventionnal double twist take-up unit (buncher) as shown on Fig.2

The buncher provides a double twisting wich is added to the twist already made.

This kind of buncher is generally giving 4000 twists/mn s
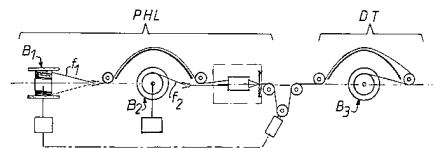
The combination of the backtwister unit and double twist take-up is resulting in a triple torsion giving :

2000 tw/mn + 4000 tw/mn = 6000 tw/mn

This performance is of course surpassing all existing process.

The main point is that it also improves the electrical performance of the twisted pair by giving a certain percentage of backtwisting for each wire.

This percentage depends upon the respective speed of each bow, as shown on Fig.3.
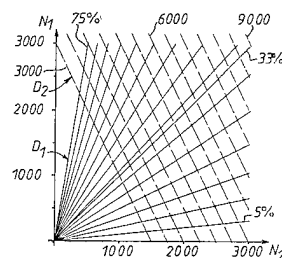
Fig. 3

On the diagram shown on Fig.3:

-N1 is the rotating speed of backtwister bow in RPM.

-N2 is the rotating speed of the buncher bow in RPM.

The backtwist ratio can be calculated with the following formula :

$$BTR = 1 - 2 \times N2/(N1 + 2 \times N2)$$

The backtwisting effect given naturally by the new process is generally 33% and contributes to improve electrical performance of the pair by randomising the defects of the copper conductor.

Advantages of new Twinning Process

Substantial increase of productivity in copper pair production (+ 50%)

Introduction of natural bactwist effect adjustable between 0 and 100% for better electrical performance of the pair.

Can be applied to a complete new line or can consist in up-grading an existing line, using conventionnal bunchers, by addition of the bactwister unit described in paragraph1/.

In USA, a series of evaluation of Triple Torsion payoff was carried on and compared to a classical backtwist payoff.

On the triple torsion line the trials were run with an additional 50% of productivity, but it could have been possible to increase it even more. Thousands feet of cable were produced on both payoffs to compare the input impedance uniformity, near-end crosstalk headroom margin and margin uniformity in order to determine the quality of the cable.

DATA ANALYSIS

The main means of analysis lay in input impedance standard deviation and mean crosstalk headroom margins and standard deviation. For near and-end cross talk, the decision was make to analyze the worst-pair combination margin at each individual point, since most cable specifications are stated as worst-pair values. The worst-value for each point (every 0.5 MHz roughly) was found, and we used all data points from the samples lengths for statistical purposes.

Graphical representations of average input impedance data show little differences between the two payoffs. This indicates that the singles experienced similar stresses during the twinning process. Visual inspection of the pairs that were twisted with the Triple torsion unit showed no visible crushing at the twist lay contact points.

With the specific FEP wire that was used during this trial we obtain an increase in crosstalk margin of 0.5 dB.

Near-end crosstalk in the cables produced using the Triple Torsion payoff outperformed that of the classical machine by approximately 0.5 dB for CAT 5 E and by 3 dB for CAT 6 of headroom margin. Standard deviations of headroom margins over the tested frequency spectrum were 0.5 to 1 dB, with this trend holding at higher frequencies as well.

Based on the experimental data shown in this evaluation and the previous trials, the concept of Triple Torsion is extremely promising for the LAN cables industry all over the world and especially in north America.

Literature:

Websites:
Cat. 6: Myth or Serious Standard?
Frank Dickman, Anixter Inc: Cabling Installation and
Maintenance magazine; June 2000
Evolution of cabling design standards
Alan Flatma, Lan Technologies; Congleton, UK

Market trends
Frank Murawski, FTM Consulting; Hummelstown, PA

Bandwidth at issue at cable assemblies
Gina Roos, CMP Media EET S0061; Plymouth, MASS

Sorting Out Cabling Standards
Joel Conover, CMP Media NCW S0024,

Codes and Standards at a glance
Du Pont, Product Information; Le Grand Saconnex, CH

Next Generation Loose Tube Cables: Reduce the Size, Not the Performance

Matthew G. Soltis, Ray G. Lovie, Dean J. Rattazzi

Alcatel Telecommunications Cable, OFCCC
Claremont, NC 28610
+1-828-459-8222 · matt.soltis@cable.alcatel.com

Abstract

The loose tube design is the workhorse of the fiber optic cable industry. For years it has provided the mechanical, thermal, and environmental robustness needed to ensure optical performance in rugged aerial and underground applications. A strong customer desire, however, is to reduce the size and weight of these cables to get more fiber density in conduit systems, install cable further, and reduce support strength needed for aerial application. To accomplish this goal, without surrendering cable resilience, requires advanced technologies, including Finite Element Analysis, statistical design optimization, material science advancements, and a tightly controlled manufacturing process.

This paper discusses the various design considerations and the different steps of development that led to a reduced size loose tube cable family with performance comparable to the current, larger, designs. Benchmarking test results are presented to support this conclusion.

Keywords

Cable; loose tube; size; performance; FEA; modeling

1. Introduction

As fiber demand increases, carriers are continually striving to get more bandwidth out of their rights-of-way, while remaining economically competitive. For duct and aerial-lashed applications of fiber optic cable, it is advantageous to have a smaller and lighter cable for a given fiber count. The increased fiber-density can allow more cables in a duct, and the lighter weight can result in lower pull force or less loading on an aerial messenger. The basis of reducing the size and weight of a loose tube cable is to reduce the size of the buffer tube housing the fibers. This, in turn, leads to a smaller central member and outer sheath diameter, thus achieving a higher fiber density. One of the immediate benefits includes the capability of manufacturing longer cable lengths without having to modify existing reels, thus lowering shipping costs. In addition, the product performance benefits of a smaller tube / cable include more storage length in manholes and enclosures, smaller bend radii, and increased flexibility.

Reducing the cable size challenges designers and manufacturers to employ advanced analysis techniques, tighter tolerances, and increased process control.

2. Advancements in Technology

Analogous to computer chip development, making a product smaller often necessitates advancements in technology. Simply "scaling" dimensions of the current product could lead to disastrous results if the design, material, and manufacturing control are not enhanced in pace. Understanding what advancements would be necessary for developing a reduced-size loose tube cable began with a categorization of the general cable performance characteristics, followed by identification of those that may be affected by reducing the cable size. The list below is a subset of the performance attributes of loose tube fiber optic cables:

- Optical performance under compressive loads
- Fiber strain under tensile loads
- Optical performance at extreme temperatures
- Viscous flow of filling compounds at elevated temperature
- Optical and mechanical performance under bending conditions at temperature extremes
- Optical and mechanical performance under torsional loads
- Optical and mechanical performance under impact loading
- Prevention of water penetration through cable elements
- Compatibility and integrity of cable with termination closures under temperature extremes

Of these, it was felt that compression, tensile, and thermal performance deserved detailed analysis before prototype cables were manufactured. To study the resistance to compression, it was determined that a more sophisticated technique, such as finite element analysis, was necessary since the interaction between cable elements and materials is too complex to predict performance using simple analytical approaches. To characterize the tensile and thermal performance, which are linked to the helical fiber "window" in a loose tube cable, statistical techniques were developed for a more accurate prediction based on normal manufacturing / material variation. Thus, the development process of this new product included the creation of several analytical and finite-element models which were then validated through experimentation. The culmination of these efforts was a family of reduced-size loose tube qualification cables that were manufactured and tested. A summary of the findings will be presented in the section of results.

2.1 Compression Resistance

The resistance to compression of a loose tube cable is dependent on dimensions and/or materials used in three main components; the buffer tube, the stranded core, and the protective sheath. This composite structure of viscoelastic components requires advanced analysis techniques, such as Finite Element Analysis (FEA), to simulate the deformation behavior under compressive loading conditions. FEA makes it possible to analyze the compression response of a reduced size loose tube cable design, and more importantly, allows for the evaluation of systematic changes to geometry and materials. Besides helping to achieve an optimized design, FEA can greatly reduce the design cycle time by allowing iterations to occur on the computer instead of the prototype lines.

In order to perform a finite element analysis, a model representing the cable structure must be developed. A solid geometric model of a length of cable is constructed by considering tube dimensions, stranding pitch, jacket thickness, etc. Figure 1 shows the solid model for a five-position loose tube cable.
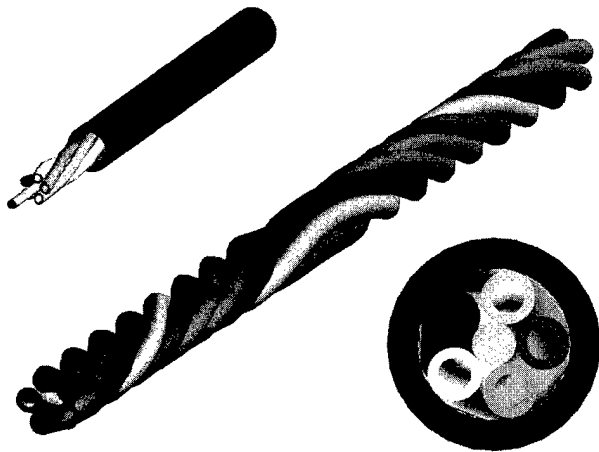
Figure 1. Solid Model of Loose Tube Cable

The solid geometry model must be broken up into many small pieces called finite elements. The elements provide a means for a computer code to track the behavior of the entire structure under loads, and allow material properties to be assigned to various parts of the model. The finite element mesh created for the cable model is shown in Figure 2.

The compressive loading on the cable can be modeled by using rigid plates that are driven by a prescribed force or velocity. All the model data is used as input to a finite element analysis code that solves a set of equations simultaneously for all the elements in the model. The results generated from the solution, typically displacement, strain, and stress, can be analyzed and visualized graphically through the use of a post processing software package. A more detailed description of finite element analysis with application to cable compression modeling can be found in a 1998 IWCS paper on the subject[1].
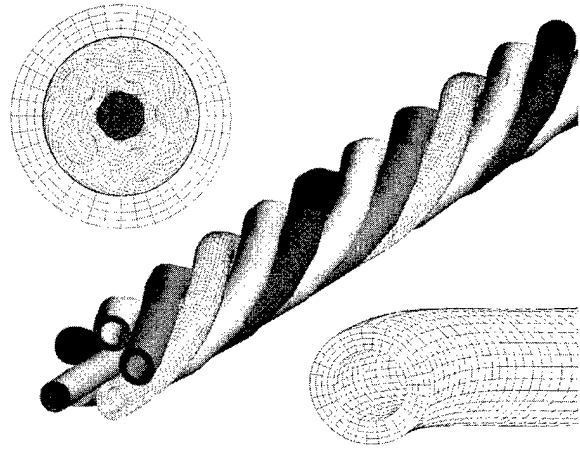
Figure 2. Finite Element Mesh of Cable

A finite element analysis was performed that simulated the compressive loading of the current product design, and the results were compared to data from an actual compression test. Figure 3 shows a comparison of the load versus deflection data obtained from the FEA model and an experimental sample. Since the finite element model makes assumptions regarding the fiber gel-filling within the buffer tubes, it is reasonable to expect that the experiment would show an increasingly stiffer response as the load increases. In the operational loading region of a cable, however, the FEA correlates well with the experimental data.

Figure 4 shows cross sectional views of the deformed configuration obtained from FEA and a sample under load. Though this snapshot is of a cable under a load well beyond the operational necessity, the good correlation between model and experiment validates the model, and makes it suitable for use in design studies.
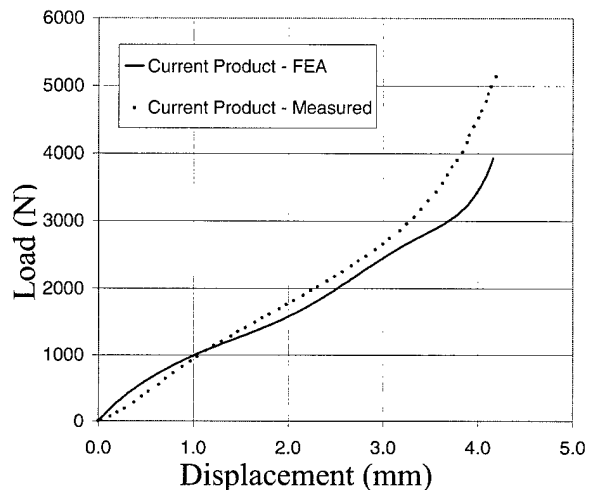
Figure 3. Comparison of Compressive Cable Response for FEA Model and Experimental Sample
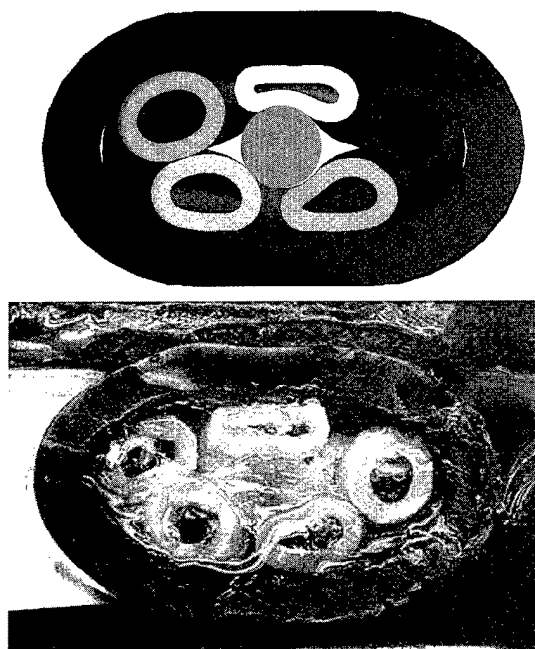
Figure 4. Deformed Configuration, at Extreme Load, Obtained from FEA and Experiment

The stranding parameters for the 1st-iteration of the new product design were chosen to satisfy tensile and thermal performance, but the jacket material and thickness were initially kept the same as the current product. Figure 5 shows a comparison of compressive load versus deflection for the current product and the 1st–iteration of the new product design obtained from FEA.
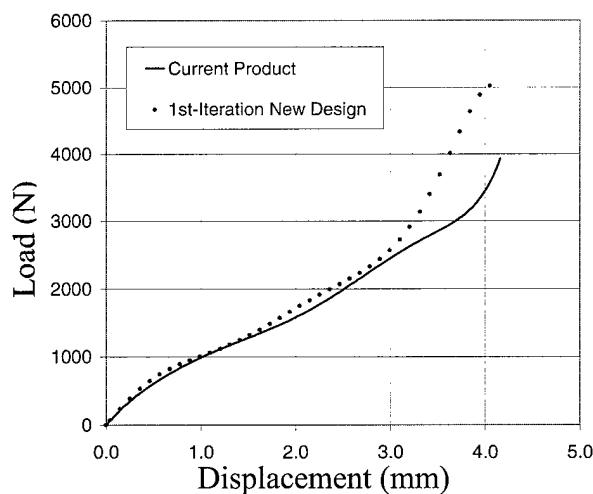
Figure 5. FEA Comparison of the Compression Response for Current and 1st-Iteration Designs

The response of the two cables is essentially the same, which would seem to indicate the choice of jacket thickness and material is satisfactory. However, since the new product design has smaller buffer tubes, there is less space available for the fibers, and it is possible that the fibers could get pinched at lower loads. Therefore,

an additional indicator is necessary to judge the performance of the new design.

The test criteria for acceptable compression performance is typically an increase in fiber attenuation, which is a result of the fibers being pinched between the walls of the buffer tube. Without considering the fibers in the finite element model, a reasonable approximation to the onset of fiber pinch would be the load required to exhaust the available free space around the fibers within the buffer tube. The cross sectional view of the deformed cable in Figure 4 shows that the top buffer tube is being pinched the most severely. Since the tubes are stranded around the center member, the pinch point will occur periodically in all the tubes along the length of crushed cable. However, considering a single pinch location in one of the buffer tubes is sufficient due to symmetry. Also, the pinched section of a tube is localized enough that a cross sectional area at that point is an adequate characterization of the available free space for the fibers.

The cross sectional area of the buffer tube at a pinch location was computed over a range of compressive loads for the current product and the 1st-iteration of the new product design. An effective fiber bundle area was subtracted from the buffer tube area to give an indication as to when the empty space is exhausted.

The fibers tend to spread out when the buffer tube deforms, so an effective area of a deformed bundle was used. Figure 6 shows the remaining buffer tube area curves for the two cable designs. The curves show that the area is exhausted at a lower load for the 1st-Iteration new product cable design, which suggests that this cable may not perform as well as the current product under compressive loading.
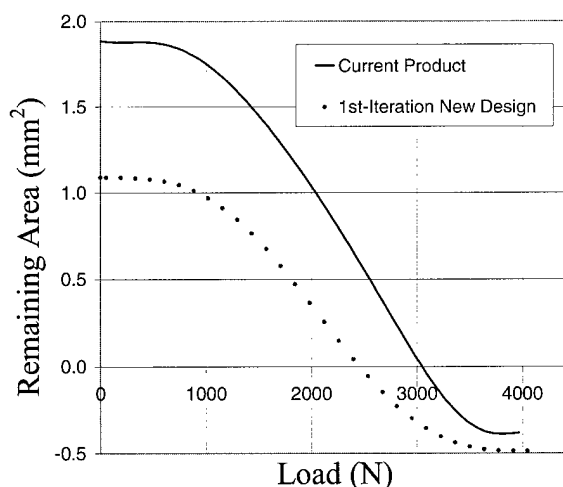
Figure 6. FEA Comparison of Remaining Area under Load for Current and 1st-Iteration Design

For the 2nd-iteration of the new cable design, a jacket material with a higher modulus was chosen to help reduce the effect of the compressive load on the remaining buffer tube area. The curve for remaining area versus load is shown for the 2nd-iteration design in

Figure 7. This option helps to offset the critical load for diminished area, and maintains the compact dimensions of the cables. It does not however, produce an optimized design when comparing compression performance to the current product.
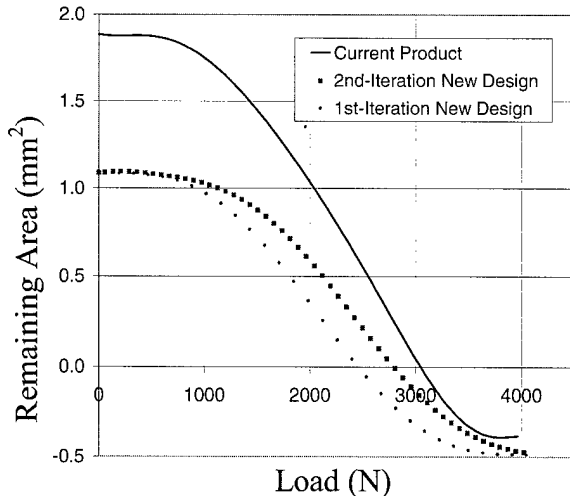
Figure 7. FEA Comparison of Remaining Area under Load for Current and 2nd-Iteration Design
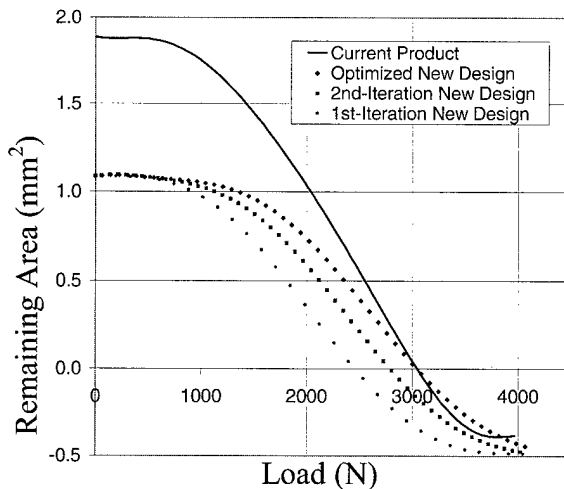
Figure 8. FEA Comparison of Remaining Area under Load for Current and Optimized Designs

A study of the influence of jacket wall thickness on the remaining area showed that a slight increase in thickness results in better performance. Figure 8 shows the remaining area curve for the optimized new product design. The optimized design provides comparable performance and still meets the objective of reducing the size of the cable components, thereby reducing the overall cable diameter.

During subsequent cable testing, it was found that the simple power monitoring at a given load was not sensitive enough to show differences between small design changes and did not provide all of the data required to validate the models. Therefore, an ultra-fast (50 Hz) dual wavelength power monitoring system (UPM) was employed which, when integrated with the load frame (Instron), allowed for continuous power measurements for multiple fibers while also recording compressive load and deflection values. Figure 9 shows a typical output of this measurement equipment. Note that this example shows attenuation beginning near the same compressive loading as predicted by the FEA modeling shown in Figure 8.
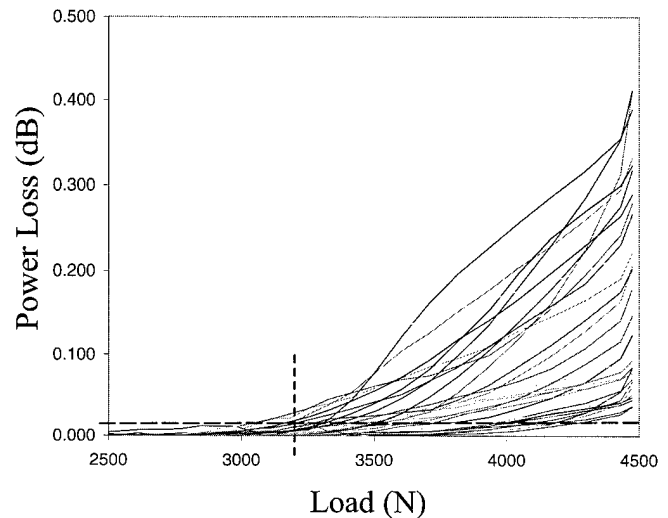
Figure 9. Attenuation Monitoring During Compressive Loading

2.2 Design Tolerances

As with any design for manufacturing, the tolerances assigned to critical dimensions, as well as material properties, must be accounted for to ensure that cable performance remains acceptable for all products manufactured within these limits. Two approaches were adopted in the design of the reduced size loose tube cable; a statistical evaluation of tolerances on cable performance and tightening of the currently accepted manufacturing variations to handle the advanced design.

The concept of statistical evaluation of dimensional and material properties can be clarified by an example of a rod and a plate with a hole. If the objective is to have a rod that just fits inside the hole, one must take into account the tolerance in the diameters of the rod and the hole. If the tolerances are stacked, one might mistakenly design around the worst case - minimum hole diameter and the maximum rod diameter. If, however, the statistical distributions of the rod and hole diameters are obtained, then a more realistic prediction of a "no-fit" situation can be determined - to any confidence level.

This concept was extended to the much more complex situation of loose tube cable design, where parameters such as center member diameter, tube dimensions, jacket thickness, and stranding geometry have known statistical variations from the nominal, based on

Table 1. Comparison of Statistical and Stacked Design Tolerancing

	MINIMUM	MAXIMUM
	(From Nominal)	
stacked tolerances tensile window	-36%	+46%
statistical tolerancing	-12%	+12%
stacked tolerances contraction window	-38%	+50%
statistical tolerancing	-13%	+13%
stacked tolerances fiber bend radius [mm]	-13%	+14%
statistical tolerancing	-6%	+6%
stacked tolerances buffer tube gap [mm]	-170%	+171%
statistical tolerancing	-69%	+69%
stacked tolerances cable elongation under load	-11%	+13%
statistical tolerancing	-4%	+4%

empirical process control data. The raw materials themselves have properties that can be characterized by a distribution, including density, modulus, and thermal expansion coefficient. Mathematical analysis can then determine both the nominal and predicted distribution of cable performance, based on these underlying variations. This process is used to predict critical cable performance characteristics such as tensile and contraction windows, buffer tube gap, fiber bend radius, and cable elongation under load. Table 1 shows an example of calculations that illustrate this statistical concept.

2.3 Process Control

The beauty of loose tube cable designs is that the helical or SZ stranding of the tubes creates an automatic overlength of fiber compared to the cable length. Under increasing tensile load the fibers move radially inward (toward the CSM), without any measurable fiber strain, until they contact the tube wall. Similarly, during low temperature cable contraction, the fibers can move outward, freely. If the fibers contact the tube wall, the induced buckling will eventually lead to an increase in attenuation.

The most critical parameter that affects the tensile and contraction windows is the position of the fiber bundle within the tube after cabling. If the radial position of the bundle deviates from the designed position, the cable may show excessive strain under tensile load or excessive attenuation at cold temperature. Therefore, correct bundle placement in a cable with a smaller tube requires advancement in control techniques. It is important to decrease this variation both from cable to cable and along the length of any one

cable. It was found that the winding process of buffering could cause a significant variation in bundle position along the length of the stranded cable. On the other hand, changes in core geometry (5@1, 8@1, etc...) can produce different dynamics under the same typical stranding process setpoints. This has the possibility to cause cable to cable variation unless design-specific controls are employed.

2.3.1 Buffering. Starting with the buffering process, the parameter to control was the excess fiber length (EFL) that would later come off a wound reel at stranding. After an extruded buffer tube leaves the cooling water troughs, there are still significant mechanical and thermal conditions that can affect the EFL. These include the mechanical stress distribution created simply by the winding itself, and the amplifying and permanent effects of stress relaxation, thermal contraction, and post-extrusion shrinkage.

Analytical and FEA models were created to simulate these post-process effects on a buffer tube. The accuracy of the models was verified by measuring the EFL along the length of experimental tubes. Numerical simulations were then performed to find an industrial solution through modification of the input processing conditions. This proved successful, and culminated with the manufacture and stranding of tubes that had minimal variation in EFL along their length.

Figure 10 shows a sample of these results, which prove the viability of advanced EFL control in these aggressive designs.
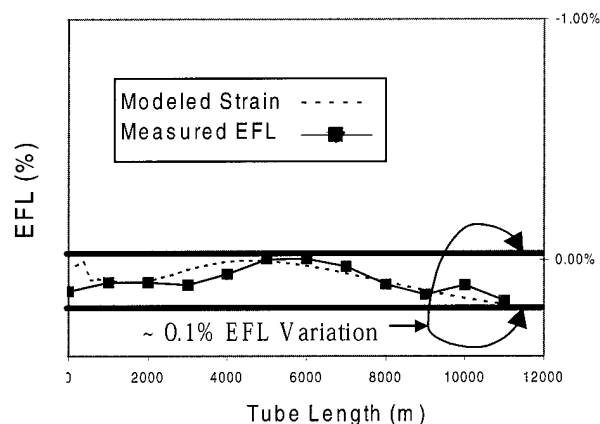
Figure 10. Control of the Strain Distribution and EFL of a Wound Buffer Tube

2.3.2 Stranding. Assuming nearly constant EFL within the buffer tubes, the stranding process will not significantly vary the position of the fiber bundle along the length of any one cable. The challenge, however, is that identical process setpoints can affect different core designs (5@1, 8@1, etc...) differently. For any given tube and CSM strains, along with the stranding geometry (laylength, number of turns, etc...), the twist imparted to the underlying CSM will vary with the number of tubes stranded and the radius at which they are applied to the CSM. Since the longitudinal and torsional strains all shift the radial position of the fiber bundle in the finished cable, the

proper combination must be optimized for each core design and its stranding geometry.

An analytical model was developed to account for these shifts to find the optimum stranding setpoints for each design. The first challenge of validating this theory was to understand the actual tube tension seen at the stranding, or closing, point. During the SZ stranding process, turns are accumulated prior to the closing point to control the reversal from "S" to "Z". This accumulation naturally increases the tension of the tube compared to the initial payoff tension, yet is not normally measured during production.

Therefore, a full-factorial Design of Experiment (DoE) was executed, in which four stranding parameters were varied. A load-cell was placed inline to measure the tube tension at the closing point while the strander was operating. It was found that this tension increase was most affected by the number of turns and by the initial payoff tension. This empirical data was used to create a relationship between the tube payoff and stranding tensions which was incorporated into the complete stranding model. Unfortunately, the experiments also showed that this tension "multiplier" depended, as well, on the type and brand of stranding equipment used – making for strander-specific optimization. Figure 11 shows some results from these experiments compared to the resulting model predictions.
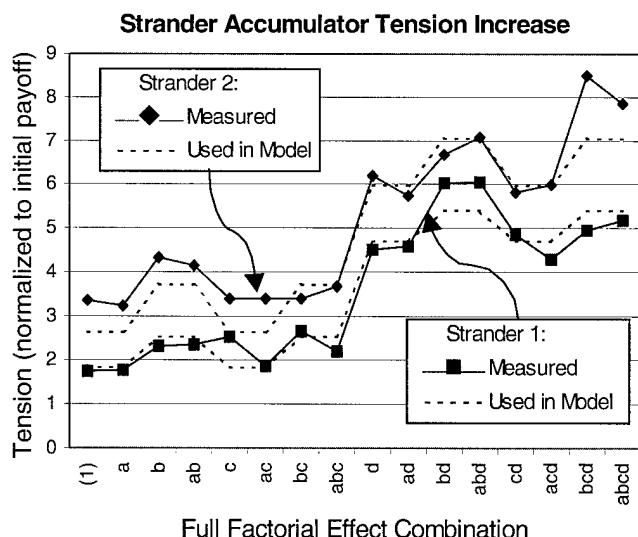
Figure 11. Tube Tension Designed Experiment Measurements and Resulting Model

The resulting stranding model was validated through both tensile and thermal testing of prototype cables. The prediction of fiber bundle position, thus window, was validated by close correlation of the measured and predicted fiber strains during a tensile test. An example of this correlation is shown in the results section.

Low temperature attenuation data, however, is more difficult to correlate directly to the initial position of the fiber bundle. This is because any attenuation increase is a function of both the bundle position and the amount of cable contraction. To help with this analysis, a custom "CTE bench" was designed, which enabled the measurement of cable contraction and elongation throughout a wide temperature range. These contraction measurements provided the empirical data necessary to then correlate attenuation to bundle position.
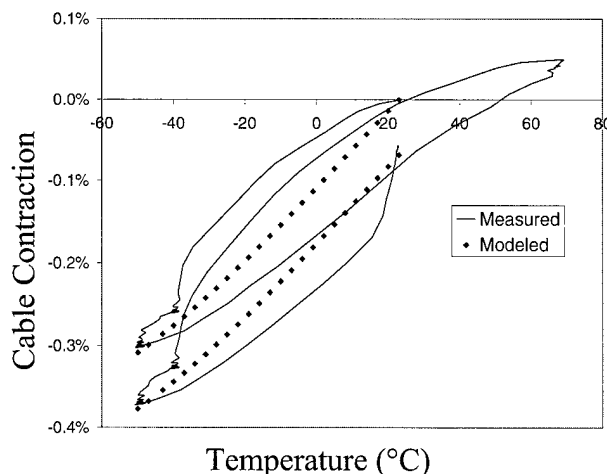
Figure 12. Model and Measurements of Cable Contraction at Varying Temperatures.

In addition, the CTE bench measurements provided empirical data to substantiate the design calculations used to predict the thermal properties of composite structures (Rule of Mixtures). Figure 12 shows a typical loose tube cable response during thermal cycling within the CTE bench, along with the corresponding prediction.

In summary, the design- and line-specific advanced control of the critical stranding process parameters, including tensions and twist, combined with the buffering EFL solution, made possible the manufacture of a cable family with predictable and repeatable tensile and thermal performance.

3. Results

Using the newly developed design and process modeling tools, and with the material and geometry changes suggested by the FEA, the development proceeded with the design of a family of reduced-diameter cables. All cables were subjected to a full series of qualification and characterization testing according to the prevailing industry specifications and standards.

Table 2 shows a typical set of test results, demonstrating full compliance to all requirements relative to anticipated installation and operating conditions.

In addition to specification compliance, there was much interest in the extent to which cable performance matched the theoretical design and process models. For tensile performance, the key parameter to check was the fiber strain at, and beyond, installation load. Figure 13 shows the range of statistically predicted fiber

Table 2. Industry Test Results[2]

Reduced Diameter Loose Tube Cable Qualification Test Summary GR-20 Issue 2	CABLE DESCRIPTION:	60 FIBER DIELECTRIC	
		RESULT	MAXIMUM VALUE
Finished Cable Attenuation		PASS	0.35/0.22
Qualification Tests			
Compound Flow	6.3.3	PASS 10/10	NO DRIP
Low and High Temperature Bend	6.5.3	PASS	0.014 dB
Impact Resistance	6.5.4	PASS 4/4	0.004 dB
Compressive Strength	6.5.5	PASS 5/5	0.012 dB
Tensile Strength of Cable	6.5.6		
Fiber Strain at Installation Load		PASS	0.374%
Fiber Strain at Residual Load		PASS	0.006%
Fiber Strain at No Load		PASS	0.002%
Attenuation at Residual Load		PASS	0.003 dB
Attenuation at No Load		PASS	0.002 dB
Cable Twist	6.5.7	PASS	0.003 dB
Cable Cyclic Flexing	6.5.8	PASS	0.003 dB
Cable Termination	6.5.9	PASS	0.039 dB
Temperature Cycling	6.6.3	PASS	0.031 dB/km
Cable Aging	6.6.4	PASS	0.024 dB/km
Cable Freezing	6.6.5	PASS	0.020 dB
Water Penetration	6.6.7	PASS 5/5	305 mm

strains (taking into account the assigned tolerances), which compare favorably to the measured fiber strains.

For compression and impact resistance, it was felt that the industry-specified tests were not rigorous enough to critically compare designs. Therefore, tests-to-failure were conducted in order to ensure the product robustness and functionality up to the failure point.

During compression testing, each cable was subjected to a continuously increasing compressive load. Attenuation was continuously monitored on multiple fibers, using the optical monitoring system (UPM). The load at which the first six fibers showed a measurable attenuation increase (failure point) was recorded.

Current Design
min 3137 N
max 3831 N
median 3488 N
average 3511 N

Reduced Diameter Design
min 2830 N
max 3928 N
median 3564 N
average 3525 N

Test each design 5 times
Record the load at which the first 6 fibers show
measurable attenuation increase

Construction

Figure 14. Compressive Load to Failure Results

Figure 14 shows the summarized result of this testing. The reduced diameter cable demonstrates a compressive resistance that compares favorably to the current product. Note that the failure point was designated as attenuation increase just above the measurement noise, which is much more restrictive than the industry compression criteria[2]. Even with this aggressive standard, the minimum load for either design was at least 125% of the industry maximum loading.

The cables were also subjected to impact testing. Using the same continuous monitoring technology, the impact count at failure (under different impact energies) was recorded. As shown in Figure 15, the new and current products perform quite similarly, with initial indications that the new design outperforms the current product. Further study is scheduled to "zoom in" on the impact energy around the failure point to better resolve any differences.

Tensile Load (N)

Figure 13. Measured Strains Compared to Statistical Prediction

Impact Energy (N•m)
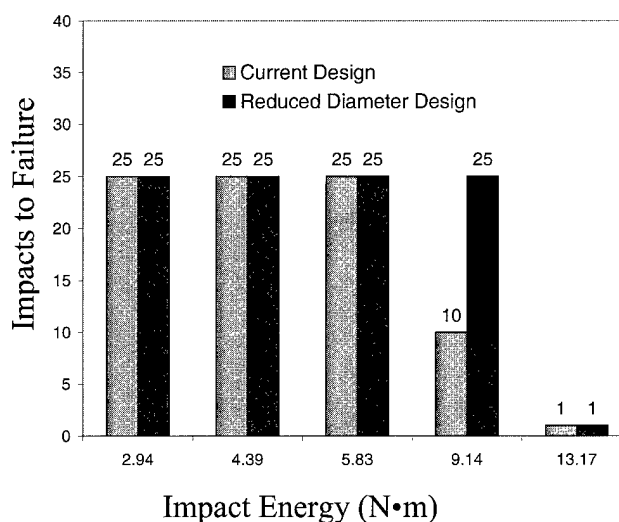
Figure 15. Impact Test-to-Failure

Now that specification compliance and robustness have been demonstrated, it is time to go back to the original objective of offering the customer a loose tube cable with operational advantages. Figure 16 and Table 3 show that, in fact, a reduced-size design provides significant rewards for the end user.

Current 72f Dielectric
Diameter: 12.4 mm
Weight: 111 kg/km
Fiber Density: 0.60/mm2

New 72f Dielectric Cable
Diameter: 10.4 mm
Weight: 82 kg/km
Fiber Density: 0.81/mm2
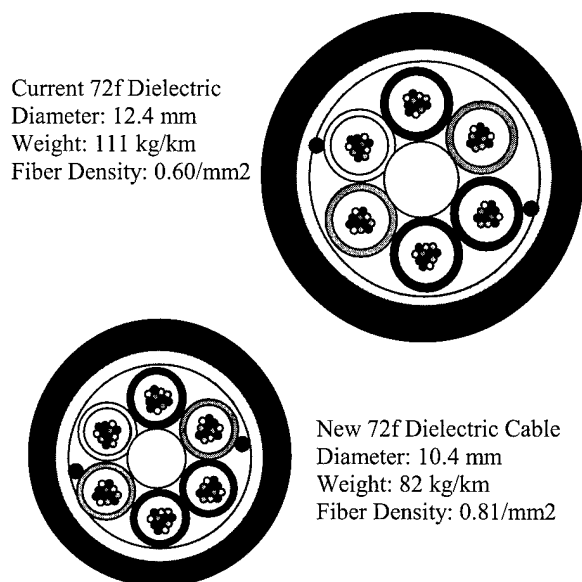
Figure 16. Current and New Cable Products

Cable diameters and weights have been reduced significantly. Fiber density has increased, and storage length per unit volume (for example, space available on a reel) has improved. The new cable has a reduced flexural stiffness, and the required installation pulling tension[3] (for the same route) has decreased.

Table 3. Product Comparison

		Standard	Reduced	Difference
Cable Diameter	[mm]	12.40	10.67	-14%
Cable Weight	[kg/km]	111.1	86.4	-22%
Fiber Density	[f / mm²]	0.60	0.81	35%
No Load Bend Radius (10X)	[mm]	124	107	-14%
Storage (length / unit volume)	[km/m³]	1.18	1.38	17%
Cable Flexural Stiffness (E*I)	[N*m²]	1.10	0.79	-28%
Pulling Tension	[N]	1376	1070	-22%

4. Conclusions

Over the years, the loose tube cable design has earned a rugged reputation for providing the necessary mechanical, thermal, and environmental robustness to the fiber optic cable industry. Now, the challenge is to reduce the size and weight of these cables without sacrificing the esteemed performance. The solution requires developing and employing advancements in technology in both the cable design and manufacturing process.

The result was the successful design, manufacture and testing of a family of fiber optic loose tube cables, incorporating a reduced buffer-tube size. Full compliance to specification requirements has been verified, and, although the free space within the tube has been significantly reduced, the mechanical and thermal robustness has not been sacrificed when compared to cables that are currently available.

These cables are up to 15% smaller, 20% lighter, and nearly 30% more flexible, proving that you can reduce the size without reducing the performance

5. Acknowledgements

This paper would not have been possible had it not been for Bob Stulpin and Mike Rossi, the process engineers within Alcatel's R&D who conducted the cable process experiments.

Also, the efforts of Nicholas Nechitailo are appreciated, for providing the theory behind the stress and strain distribution within a wound structure.

Finally, special thanks to the test and measurements groups for helping develop, execute, and analyze the cable tests.

6. References

[1] J. Boyet Stevens et al., "Finite Element Modeling of Fiber Cable Crush Performance", 47th IWCS Proceedings, pgs. 25-33 (November 1998)

[2] Bellcore (Telcordia) GR-20-CORE, "Generic Requirements for Optical Fiber and Optical Fiber Cable", Issue 2 (July 1998)

[3] IEC 60794-1-1, "Generic Specification for Optical Fibre Cables", Draft 86A/565/CDV

7. Authors
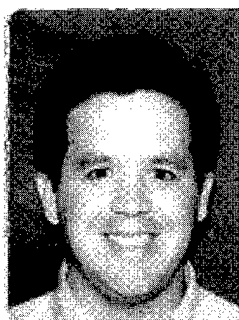
Matt Soltis is the Design Technology Manager for Alcatel's global R&D center for fiber optic cable. He received his B.S. in Aerospace Engineering from the U.S. Naval Academy in 1989. Prior to joining Alcatel, Matt served as an officer and aviator in the U.S. Marine Corps, specializing in aircraft accident analysis, radar theory, and the kinematics of air-to-air combat.

Ray Lovie is a Senior Cable Development Engineer in the Optical Fiber Cable Competence Center at Alcatel Telecommunications Cable in Claremont, NC. He holds a B.SC. (ME) degree from the University of Manitoba, and has 15 years' experience in the wire and cable industry.

Dean Rattazzi is a Design Engineer in the Optical Fiber Cable Competence Center at Alcatel Telecommunications Cable in Claremont, North Carolina. He holds a BA degree in Physics, and a BS degree in Mechanical Engineering from Binghamton University, and an MS degree in Engineering Mechanics from Virginia Tech. His area of research includes the application of finite element modeling to the design and development of fiber optic cables.

Development of New Dry Tube Cable with Water Blocking Laminated Tape

Naoki Okada, Yoshiyasu Sato, Hirohito Watanabe,

Koichiro Watanabe, Matsuhiro Miyamoto

Reseach and development department, Telecommunication cable division

1440, Mutsuzaki, Sakura-shi, Chiba, Japan

+81-43-484-3945 · naookada@s.fujikura.co.jp

Abstract

We have designed and developed the new dry tube cable with the specially designed water blocking laminated tape. This cable makes mid span access easily, then the networks for distributed customers can be constructed economically. In case of aerial application, this cable can be adapted for the self-supporting structure with cable slack.

We have manufactured several prototype cables composing 250micron coated fibers, 2-fiber ribbons, 4-fiber ribbons, 8-fiber ribbons and 16-fiber ribbons, and have evaluated its cable performance. The fiber counts composed in these cables are from 2 to 80 fibers. All cables shows good transmission characteristics and easy mid span access operations.

Keywords

Optical cable, fiber ribbon, dry tube, mid span access

1. Introduction

In recent years, a large number of optical cables have being installed to construct the access networks and the FTTH networks. In order to construct these networks economically, it will be necessary to reduce both the cost of components and the cost of constructing the networks. From the view point of optical cable design, reduction of the cabling cost must be demanded, and the cable structure should be designed considering branch of the fibers to the other cables or the optical drop wires. Especially, mid span access capability of the optical cable for the access networks will be more important[1]. In this paper, we describe about the new dry tube cable with the specially designed water blocking laminated tape.

2. Cable design concepts

We have designed and developed the new optical cables based on following concepts.

2.1 Reduction of cabling cost

The new cable must be manufactured with single process to reduce the cabling cost

2.2 Water blocking performance with dry structure

In order to get the easy handling, the water blocking performance should be achieved with dry structure using water swellable material. We have developed the new dry tube cable with the water blocking laminated tape.

2.3 Prevention of fiber movement

The fiber movement in cable may be critical problem on the dry tube structure. Therefore, any restrictive means to fiber movement may be needed.

2.4 Mid span access capability

Mid span access from the installed cables is very important to construct the distributed access networks economically. Therefore, the cable structure should be designed considering easy sheath entry operation.

2.5 Feasibility composing any fiber structure

The cable should be able to compose any type of fiber, for example, SM, MM and NZ-DSF, single fiber and ribbon fiber, and so on. Because, the optimized fibers are demanded for each applications. The unified cable structure may be effective not only reduction of cabling cost but also simplifying the cable accessories and the operations for installing and jointing.

2.6 Self-supporting structure for aerial application

In case of aerial application, the cable can be adapted for the self-supporting structure with cable slack. This structure is effective to get easy mid span access operation under aerial condition.

2.7 Fire retardant structure for indoor application

The fire retardant performance is demanded for the indoor application. The fire retardant polyethylene may be used for the sheath material. Dry structure without jelly compound is suitable to get high resistance to the fire.

3. Cable design

3.1 Cable structure

Based on these requirements, we introduce the new cable structure as shown in Figure 1. The specially designed water blocking laminated tape is used for the dry core tube. The fibers are inserted into the dry tube, and the special resin is put in the tube intermediately in order to fix the fibers in the cable. This special resin is enough soft to maintain good transmission characteristics and can be removed easily from the fibers without special tools or solvent. This newly developed cable is composed of single layer polyethylene sheath with the dual ripcords, in order to remove the sheath easily. This cable can be manufactured with single process.
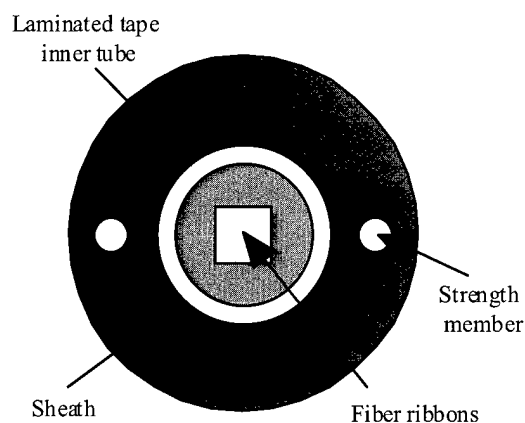
Figure 1. Laminated tape inner tube cable

3.2 Excess fiber length and inner diameter of a tube

In order to get good transmission characteristics, the excess fiber length in a tube is one of the most important parameters.

The excess fiber is packed in a tube as shown in Figure 2. In order to avoid loss increase, the inner diameter of a tube should be designed considering allowable fiber curvature radius in a tube. The minimum fiber curvature radius "rmin" can be expressed in terms of the amplitude of sinuous fiber "a" and the excess fiber length ratio "e", as shown in equation (1).

$$rmin = a / 4e \qquad (1)$$

The inner diameter of a tube should be determined considering the excess fiber length, the liner expansion coefficient of a cable and the allowable fiber curvature radius in a tube. Figure 3 shows a calculated result of the relationship between these three parameters. The excess fiber length and the inner diameter of a tube are designed considering this result.
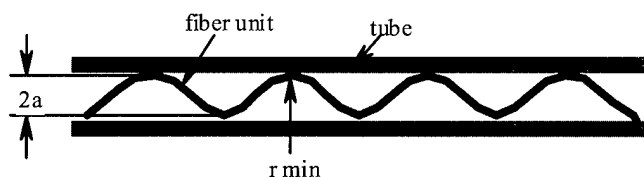
Figure 2. Sinusoidal fiber in a tube

Moreover, the fiber slack can be obtained by this excess fiber at the mid span access point as shown in Figure 4. We investigated the relationship between the fiber slack and the excess fiber length theoretically. Figure 5 shows the calculated result.
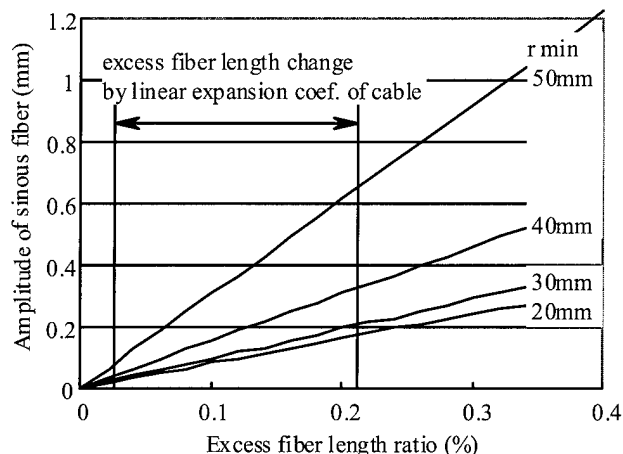
Figure 3. Relationship between excess fiber length, amplitude of sinous fiber and fiber curvature radius
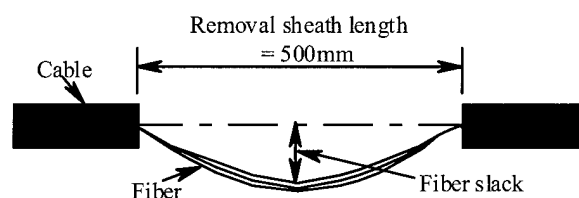
Figure 4. Fiber slack at mid span access point
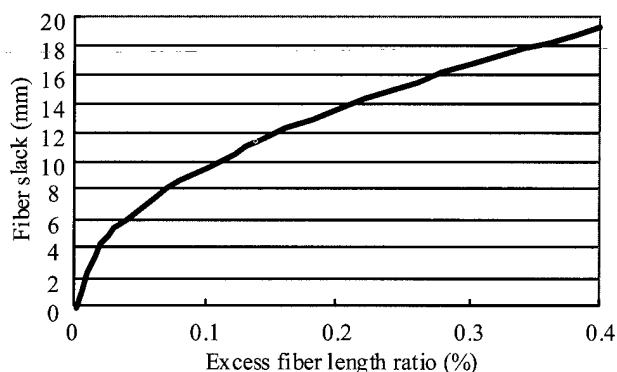
Figure 5. Relationship between excess fiber length and fiber slack at mid span access point

3.3 Mechanical strength

It is necessary to get the enough mechanical strength by the polyethylene tube sheath. Mechanical strength is influenced by the outer diameter and the thickness of the tube. The cable deformation characteristics under lateral load had been reported [2]. The mechanical strength of the polyethylene tube sheath could be expected by this method. In elastic region, the resistance to lateral pressure can be assumed by equation (2). Here, "ro" and "rs" are

outer and inner radius of a tube, and "t" is thickness of a tube and "c" is constant.

$$d = c \, ((\, ro + ri \,) / 2t \,)3 \qquad (2)$$

We prepared some tubes which have different inner and outer radius, and investigated its lateral pressure characteristics. The results are shown in Figure 6, then it was confirmed that the equation (2) may be usefull for estimating strength of a tube. Based on this analysis, the prototype cables were designed in order to get the enough mechanical strength.
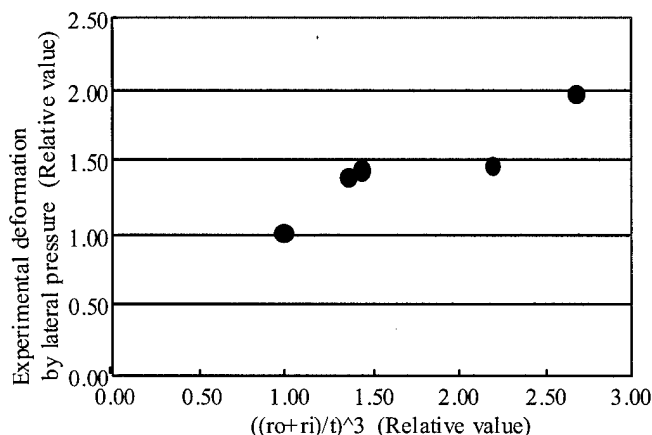
Figure 6. Lateral pressure test results of several tubes

4. Trial cables

We designed and manufactured several prototype cables and evaluated these cable performances.

4.1 Trial cable structures

We designed and manufactured several prototype cables with various fiber structures as follows.

1) 24-fiber cable with 250 micron coated fibers

2) 24-fiber cable with 2-fiber ribbons

3) 24-fiber and 40-fiber cable with 4-fiber ribbons

4) 40-fiber cable with 8-fiber ribbons

5) 48-fiber cable with 12-fiber ribbons

6) 80-fiber cable with 16-fiber ribbons

The structural parameters are listed in Table 1. In case of aerial application, the self-supporting structure with cable slack as shown in Figure 7 can be applied [3]. Moreover, we tried to design and manufacture more smaller fiber count cable, which may be used for drop cable. 2-fiber and 4-fiber drop cable could be achieved using 2-fiber ribbons.

Table 1. Structural parameters of prototype cables

Fiber	Fiber count	Cable diameter	Cable weight
250 micron fibers	24	7.0mm	0.06kg/m
2-fiber ribbons	24	7.0mm	0.06kg/m
4-fiber ribbons	24	9.5mm	0.08kg/m
8-fiber ribbons	40	9.5mm	0.08kg/m
12-fiber ribbon	48	9.5mm	0.08kg/m
16-fiber ribbons	80	14.6mm	0.16kg/m

Fiber slack at mid span access point
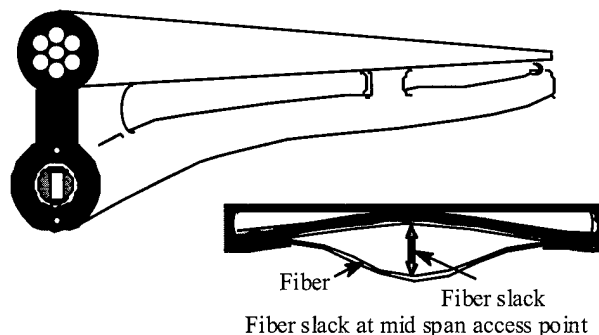
Figure 7. Self-supporting structure with cable slack

4.2 Cable performance

These trial cables are investigated its performance. The evaluated results are listed in Table 2. These results show that this newly designed structure have comparable performance like the conventional slotted core cables. And the water blocking characteristic have been confirmed also.

Table 2. Cable performance

Item	Test condition	Results
Attenuation	1310nm	< 0.35dB/km
	1550nm	< 0.25dB/km
Temperature	-30 ...70 deg.	< 0.10dB/km
Tensile	0.3% elongation	No loss change
Squeezing	250mmR	No loss change
Bending	160mmR	No loss change
Lateral pressure	2000N/100mm	No loss change
Twisting	90 deg./m	No loss change
Impact	9.8N/m	No loss change
Water blocking	3m	No water leakage

4.3 Mid span access operation

We tried the mid span access on the trial cables. The operating processes of mid span access are following. At first, the sheath is cut with the dual ripcords, and the cable is divided to two pieces. Then, the fibers can be picked out from the divided cable easily and the sheath can be removed safety.

We measured the operational time and the optical loss change during mid span access operation. The operational time is shown in Figure 8, compared with that of a conventional SZ-slotted core cable. As results, the newly designed cable has easy handling for

mid span access, and the optical loss change at 1.55 micron was not observed.
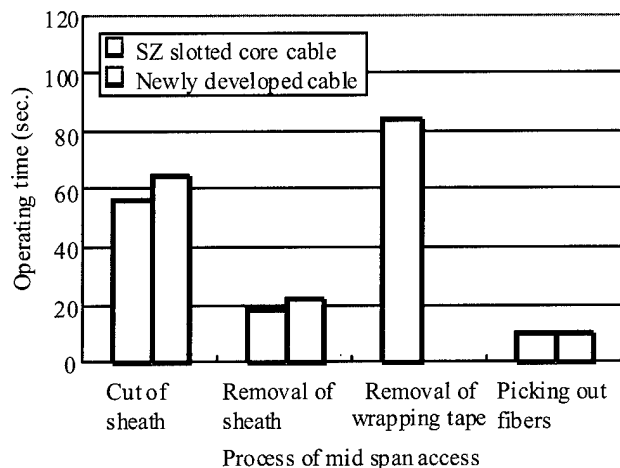
Figure 8. Operating time for mid span access

5. Conclusions

We have designed and developed the new dry tube cable with the specially designed water blocking laminated tape. This cable makes mid span access easily, then the networks for distributed customers can be constructed economically. We have manufactured several prototype cables composing various kind of fibers, and have evaluated its cable performance. It was confirmed that all cables shows good transmission characteristics and easy mid span access operations.

6. References

[1] H. Iwata, M. Okada, S. Tomita, N. Kashima, T. Hoshijima, M. Kama and K. Nishizawa, "Design of aerial optical fiber cable system suitable for easy brabching", 1997 IWCS Proceeding, pp.4-10

[2] Y. Mitsunaga, Y. Katsuyama and Y. Ishida, "Optical cable deformation characteristics under lateral load", IEIEC Vol.J64-B No.2, 1981

[3] N. Okada, M. Yamanaka, Y. Sato, H. Watanabe and O. Koyasu, M. Miyamoto, "Study of the SZ-slotted rod type optical cable with 4-fiber ribbons for aerial applications", 1997 IWCS Proceeding, pp.785-792

Authors
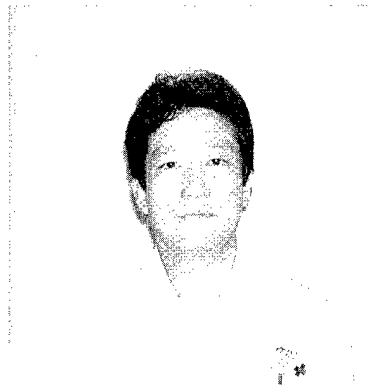
Naoki Okada

Reseach and development department

Telecommunication cable division

Fujikura Ltd.

1440, Mutsuzaki, Sakura-shi, Chiba, 285, Japan

Naoki Okada was born in 1964. He joined Fujikura Ltd. after his graduation from Chiba University with a B.E. degree in 1986 and has been engaged in research and development of optical fiber cables. He is now an engineer in the Telecommunication Cable Department and a member of the IEICE of Japan.
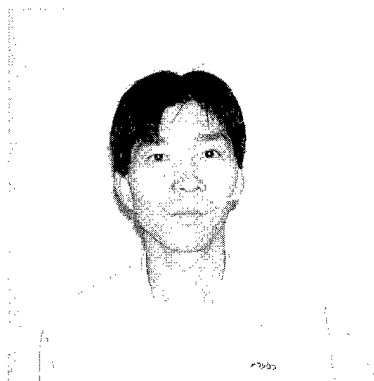
Yoshiyasu Sato

Reseach and development department

Telecommunication cable division

Fujikura Ltd.

1440, Mutsuzaki, Sakura-shi, Chiba, 285, Japan

Yoshiyasu Sato was born in 1969. He joined Fujikura Ltd. after his graduation from Tokyo Institute of Technology with a M.E. degree in 1995 and has been engaged in research and development of optical fiber cables. He is now an engineer in the Telecommunication Cable Department and a member of the IEICE of Japan.
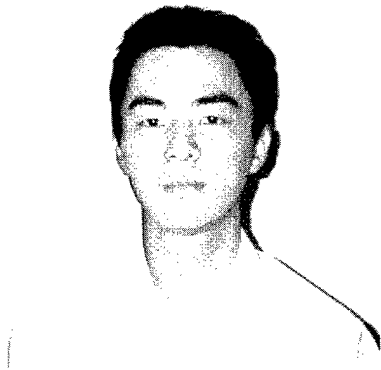
Hirohito Watanabe

Reseach and development department

Telecommunication cable division

Fujikura Ltd.

1440, Mutsuzaki, Sakura-shi, Chiba, 285, Japan

Hirohito Watanabe was born in 1971. He joined Fujikura Ltd. after his graduation from Yokohama National University with a M.E. degree in 1996 and has been engaged in research and development of optical fiber cables. He is now an engineer in the Telecommunication Cable Department and a member of the IEICE of Japan.
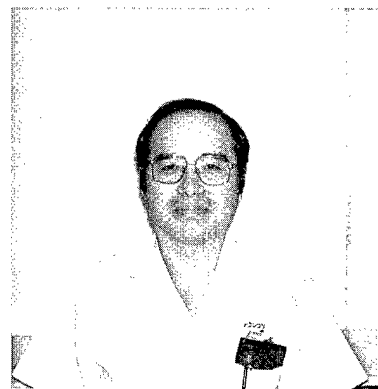
Matsuhiro Miyamoto

Reseach and development department

Telecommunication cable division

Fujikura Ltd.

1440, Mutsuzaki, Sakura-shi, Chiba, 285, Japan

Matsuhiro Miyamoto was born in 1953. He graduated from Nagoya Institute of Technology with a B.E. degree of electrical engineering. He joined Fujikura Ltd. after his graduation from Tokyo Institute of Technology with a M.S. degree in 1978 and has been engaged in research and development of optical fiber and optical fiber cables. He is now a manager of the Telecommunication Cable Department and a member of IEICE in Japan.

Kohichiro Watanabe

Reseach and development department

Telecommunication cable division

Fujikura Ltd.

1440, Mutsuzaki, Sakura-shi, Chiba, 285, Japan

Kohichiro Watanabe was born in 1959. He received a B.E. degree in electrical engineering from Tohoku University in 1982. Since joining Fujikura, Ltd. in 1988, he has worked on the development of optical fiber cables. He is currently employed in the Telecommunications Cable Section of the Opto-electronics laboratory.

Development of a new Optical Fiber Cable to be Installed by Blowing Method

Marcos Antonio Nunes, Alexandre M. Simião, Marcos Aurélio Caetano, Cleber Brunhara, Antonio Carlos Silva, Leonardo Silvério

Furukawa Industrial S.A. Produtos Elétricos, Curitiba, Paraná, Brazil

Phone: +55 41 341-4088, Fax: 55 41 341-4141, E-mail: nunes@furukawa.com.br

Abstract

Among several method used to install cable in long distance routes, blowing method is higher recommended due to the lower cost, short time and low tension. In order to take advantage of this method, it is well known that cable design shall be optimized. In this paper we present the development of new cable to be installed by using this technique. The structural design of this cable was investigated and based on this results, the cable was installed and its performance was compared with a conventional cable for used in ducts.

Keywords

Optical Fiber Cable; Blow Method; Blowing Installation.

1. Introduction

Recently the installation of optical fiber cables by blowing method in Brazil has been used in long distance routes. For this reason, it is requested fast network implementation with high productivity and obviously lower cost. In the same way, it is important to use an optical cable with sufficient performance to attend these necessities.

In this work we present a new cable to be installed through blowing technique. We evaluated several types of cables with different outer sheath materials as well as many kind of surfaces of the cable to reach a minimal friction coefficient and a maximum blowing force. The use of duct routes is the most common installation method. Subducts are also much used, in which individual cables can be pulled without interfering with the other cables (see Figure 1). This is an advantage to minimize the initial cost of the route because you can install the amount of optical fiber according to the necessity.
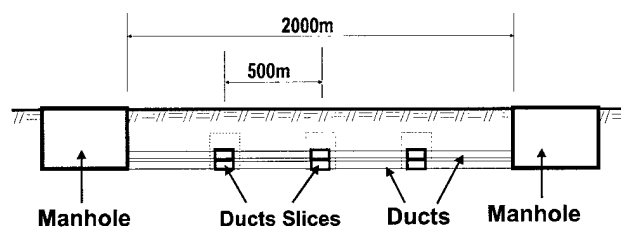
Figure 1. Blowing Method Configuration

The method to install optical cable by blowing consists in the injection of pressurized air along the duct and pushing the cable into the duct (see Figure 2). When a high-speed airflow is forced along the cable, a distributed force is exerted on this cable. The total blowing-force is an order of magnitude lower than the forces that appear when the pulling technique is used, reducing the risk of damaging the cable. The airflow makes a blowing force on the cable, and the driving wheels push the cable into the duct.
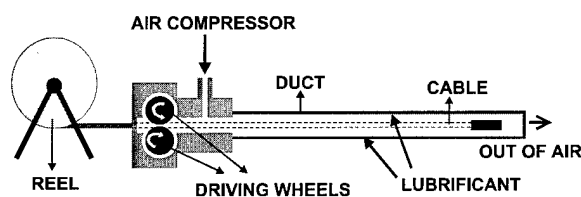
Figure 2. Blowing Technique System

1.1 Components of Blowing Method

- **Air compressor:** provides air to the system

- **Driving Wheels:** It has double function, pushing or breaking the cable into the duct.

- **Lubricant:** leaves the inner duct surface with a layer that decrease the friction cable-duct.

- **Ducts:** must have to support the maximum pressure that the air compressor can provides. The internal duct surfaces also can help to minimize the friction between cable-duct.

- **Cable:** It must present characteristics that help to reach the larger length in a short time.

1.2 Variables of Blowing Technique

In order to understand how the variables influence in the Blowing System, this math simple model to the Blowing Method was developed.
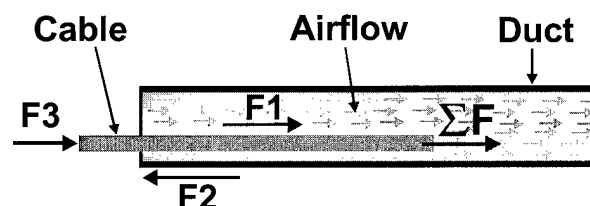
Figure 3. Blowing Technique Forces

This is a dynamic problem with three forces that can be written this form;

$$\Sigma F = F1 + F2 + F3$$

where:

F1 – Is the blowing force caused by viscosity airflow on the cable surface

$$F1 = \tau . \pi . dl$$

Where;

τ - Is the shear stress average on the surface of the cable.

F2 – Is the friction force between cable and duct. This force is against to movement of the cable.

$$F2 = - fa . \omega . l$$

Where;

fa – Is the friction coefficient cable-duct
ω - Is the cable specific weight

F3 – Is the force provided by driving wheels, it can present values negative or positive.

$$F3 = \pm F$$

ΣFext – Resultant of forces that moves the cable into the duct.

$$\Sigma Fext = \tau . \pi . dl - fa . \omega . l \pm F$$

Where each term is mainly influenced by variables describe below:

The term τ (shear stress) depends mainly on:
- In Pressure.
- Internal diameter duct.
- External diameter cable.
- Cable weight.
- Internal surface duct.
- External surface cable.

The term **fa** (friction coefficient cable-duct) depends on
- Internal surface duct
- External surface cable
- Material of duct and cable.

The ω (specific weight) depend on:
- Cable diameter.
- Cable weight.

2. Development of New Cable

In order to get the best performance, the cable was projected take into account the following characteristics:
- Small Weight
- Small Specific Weight
- Small Friction Coefficient.
- Large Stiffness.
- Large drag force.

A loose tube dry core cable was used to reach a minimal cable diameter and weight. We had also applied a outer jacket material with dimensional variation along the cable length in order to

decrease the friction between cable-duct and improve the drag force and cable stiffness.

A schematic drawing of the cable design is shown in Figure 4.
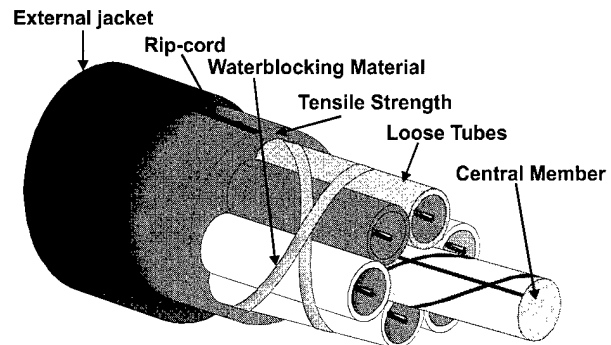
Figure 4. Design of the New Cable to be Installed by Blowing Method.

2.1 Comparative Analysis.

In order to know the real improve of performance of the NC (New Cable), it was compared with the more usual cable in Brazil, the DD-G (Cable with filled jelly core to install in ducts).

2.1.1 Dimensional.

The next graphs shows the dimensional differences between the NC and DD-G in several configurations.
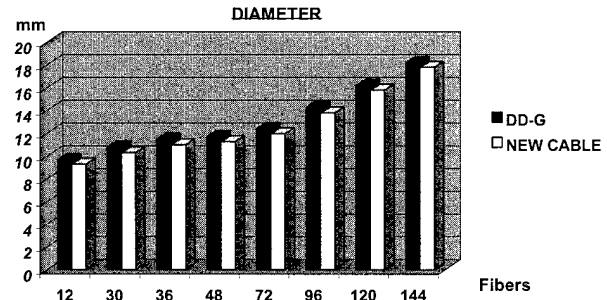
Figure 5. Comparative diameters values between DD-G and NC.
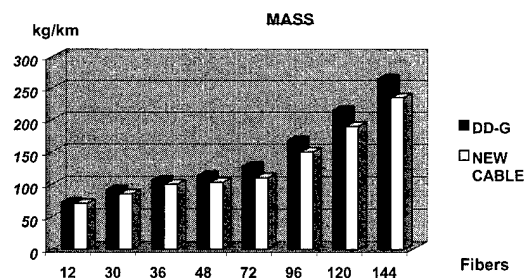
Figure 6. Comparative mass values between DD-G and NC.

2.1.2 Stiffness

When the cable is crossing a duct can occur loss speed because of the curves or pressure variation. In this moment the cable suffer compress forces that buckle it. When it occurs, the cable is pressed against the duct wall, raising the friction cable-ducts. The cable stiffness must be sufficient to avoid this effect.

For this reason it was compared the stiffness of NC with DD-G in the same configuration (72 fibers). In order to make this comparison it was used method that sag a clamped cable, according to IEC 60794-1-2 / 1999, see the Figure 7.
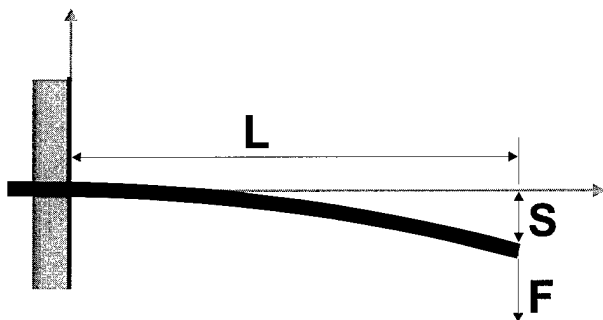
Figure 7. Basic scheme to meter the stiffness.

The stiffness is calculated by this expression:

$$B = F . L^3 / 3 . S$$

Where,

- **B**: Stiffness of the cable.
- **F**: Applied force.
- **S**: Sag of the cable.

2.1.3 Friction.

It is the most important factor that influence the installations. The NC was tested according to BELLCORE TR NWT 000356 standard that define the friction between cable-duct. Figure 8 shows the scheme used in friction test according to Bellcore standard.
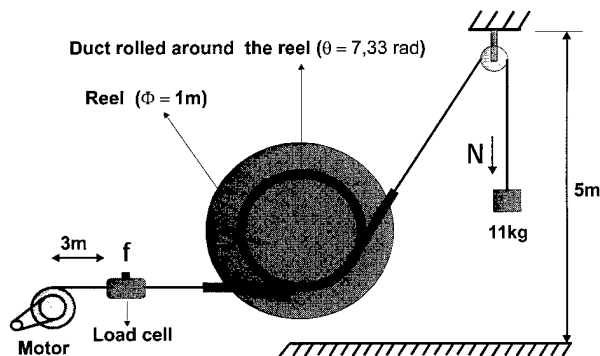
Figure 8. Friction scheme test.

The coefficient of friction is calculated by this expression:

$$\mu = Ln (F / N) / \theta$$

where,

- μ: Friction coefficient.
- F: Load of pulling
- N: Mass that must be pulled
- θ : Angle of duct around reel

3 Field Tests

The NC was tested in several conditions, always comparing with a usually cable, the DD-G. The ducts used in these tests were: 40mm of external diameter, 34mm of internal diameter and corrugated internal surface. The air compressor used was with 10bar (1 MPa).

3.1 Circuit 1

The Figure 9 shows the circuit draw where there are several curves.
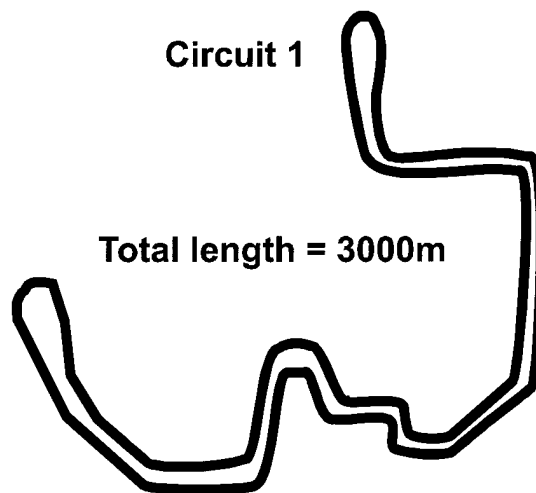
Figure 9. Test Circuit 1

The Figure 10 shows the slopes of circuit 1.
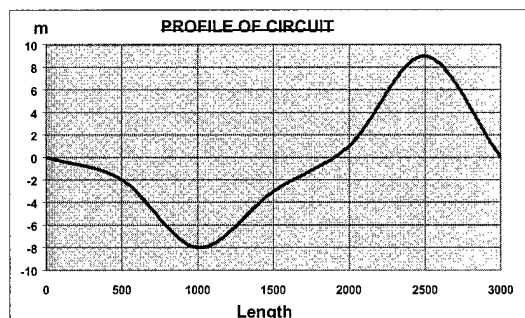
Figure 10. Circuit 1 profile.

The Photo 1 shows the place where was made the tests.
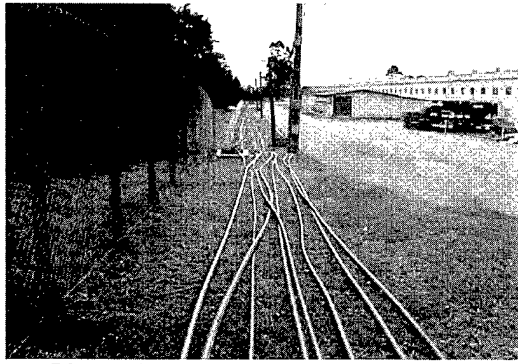
Photo 1. Local Picture of the tests

In this circuit were performed it was made the tests with different lengths of the ducts; 2000m, 2500m and 3000m.

3.2 Circuit 2
This test was performed in a circuit according to Figure 11. 7 laps were rolled up with a total duct length of 3000m.
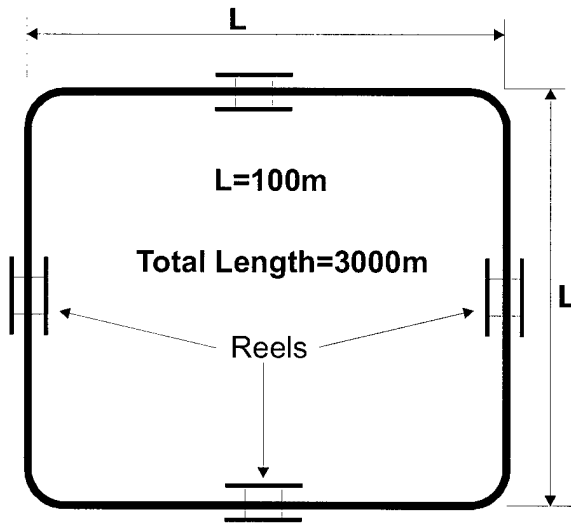
Figure 11. Scheme of Circuit 1

In each middle of side was put a reel about 1,5m of height to simulate slope a long of circuit, it was used to see the effects of the slopes in the installation(see Photo 2)
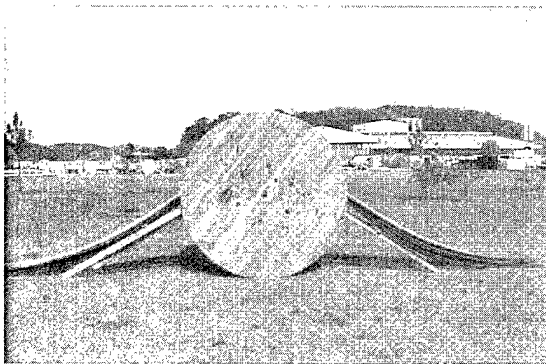
Photo 2. Detail of the Reel in the Circuit 2

The Figure 12 shows the profile for each 400m.
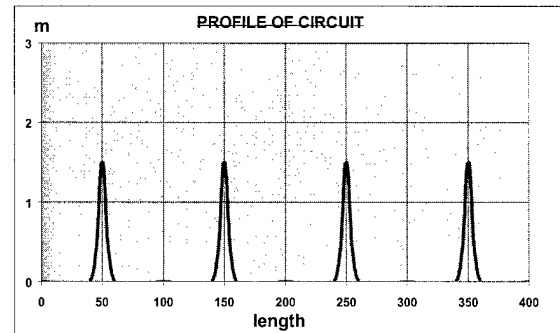
Figure 12. Profile for each 400m.

The Photo 3 shows a detail of corner.
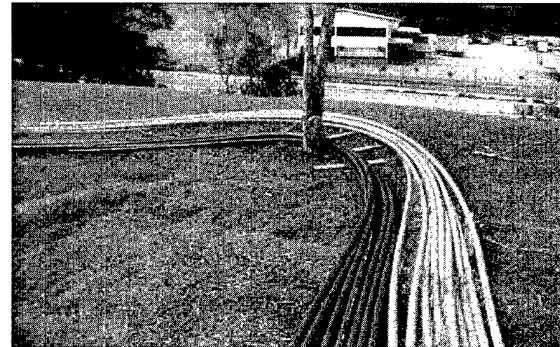
Photo 3. Detail of corner in circuit 2.

4. Results and Discussions.
The results of the field experiments showed a superior performance of the NC when compared with DD-G. This better performance is associated with a optimized design, low friction coefficient and high stuffiness, as showed in table 1.

Table 1. Results of Comparative Analysis

Characteristic	DD-G 72F	NC 72F
Diameter(mm)	12.4	12
Weight (kg/km)	128	110
Stiffness (N.m^2)	2.56	2.86
Coefficient Friction	0.20	0.16

Table 2. Results of Circuit 1

	DD-G 72F	NC 72F
Average Speed (m/min)	-	25(0.42m/s)
Max. Length (3000m)	150	3000

	DD-G 72F	NC 72F
Average Speed (m/min)	30(0.50m/s)	40(0.67m/s)
Max. Length (2500m)	1500	2500

	DD-G 72F	NC 72F
Average Speed (m/min)	45(0.75m/s)	50(0.83m/s)
Max. Length (2000m)	2000	2000

Table 3. Results of Circuit 2

	DD-G 72F	NC 72F
Average Speed (m/min)	9.32(0.15m/s)	28.95(0.48m/s)
Max. Length (3000m)	466	3000

The results for circuit test given in table 2 showed that the NC reach the maximum lengths in all situation. For DD-G , the results showed that above 2000 m max length, the performance decrease significantly. The better installation speed for NC was observed due mainly smaller dimensional values of NC. With 2000m, the new cable maintains an average speed near of the maximum, 50m/min (0.83m/s).

The results of the circuit 1 and 2 showed that for maximum. length between 2500 and 3000 m, DD-G cable present poor performance associated with a low blowing force, low cable stiffness and high coefficient friction.

5. Conclusion.

We noted that the cable stiffness and the cable density were important to reach a maximum installation speed and length. We installed these cables and made some laboratory tests in order to define the best design of the cable's surface to increase the blowing force. The cable stiffness was also evaluated because of its importance of the pushing force caused by driving wheels at inlet of duct. The installation of the cable in real conditions was made by landing ducts over the ground. Along the circuit the ducts were exposed to many windings and different levels of terrain. In this paper we showed in the results of tests the different performances between NC in relation to DD-G cable. This better performance reflect directly in the configuration of system, for the NC allows to construct larger distances between splices.

Other benefits that NC provide in a blowing installation are:

- Larger productivity.
- Smaller time in splice services
- Smaller costs to implantation.

6. Acknowledgements

Special thanks to Marco Aurélio Caetano, Cleber Brunhara, and all people that helped in this work.

7.References

[1] IEC 60794-1-2, Ed1999, "Basic Optical Cable Test Procedures"

[2] Bellcore TR NTW 000356, "Generic Requirements for Optical Cable Innerduct"

[3] W. Griffioen, "Installation of Optical Cables in Ducts", Plumettaz, 1993,

[4] Sakabe, Y. kitamura, W. Katsurashima, G. Morikawa "A Theoretical Study on the Cable Design for blowing installation in consideration pushing force at duct inlet" IWCS, 1999, 88 45 7164

[5] 4W. Griffioen, "The Installation of conventional Fiber-Optic cables in Conduits Using the viscous Flow of Air ", Journal of Ligthwave Technology , vol.7 no 2, Feb. 1989.

8. Biography

Marcos Antonio Nunes - Furukawa Industrial S.A.
R. Hasdrubal Bellegard, 820 CIC 81450-140
Curitiba – Parana - Brazil

Marcos Antonio Nunes joined Furukawa Industrial S.A. in 1997 after receiving his B.S. degree as an Electrical Engineer from Federal Center of Technological Education (CEFET)" . He has been involved in the optical fiber cables design and Installation techniques . He is currently Product Engineering .

Alexandre M. Simião - Furukawa Industrial S.A.
R. Hasdrubal Bellegard, 820 CIC 81450-140
Curitiba – Parana - Brazil

Alexandre M. Simião received a B.S. degree in Chemical Engineering in 1996 from Federal University of Parana (UFPR)". He joined "Furukawa Industrial S.A." in 1997. He has worked with a variety of design and development projects in cables, materials and testing. Mr. Simião currently serves as a Product Development Engineer in the Cable Development Engineering Department.

Antonio Carlos Silva - Furukawa Industrial S.A.
R. Hasdrubal Bellegard, 820 CIC 81450-140
Curitiba – Parana - Brazil

Antonio Carlos Silva joined Furukawa Industrial S.A. in 1977 after receiving his B.S. degree as an Mathematics from PUC PR" . He has been involved in optical and metallic cables design and Installation techniques . He is currently working in Product Engineering .

Leonardo Silvério - Furukawa Industrial S.A.
R. Hasdrubal Bellegard, 820 CIC 81450-140
Curitiba – Parana - Brazil

Leonardo Silvério joined Furukawa Industrial S.A. in 1984 after receining his B.S. degree as an Electrical Engineer from Federal Center of Technological Education (CEFET)" . He has been involved in the optical fiber cables design and development. He is currently Marketing Manager.

Development of Premise Cables for MTRJ Connector

Kazunaga Kobayashi, Masahiro Kusakari, Yoshio Hashimoto, Matsuhiro Miyamoto

Fujikura Ltd.

Telecommunication Cable Dept., Fujikura Ltd. 1440 Mutsuzaki, Sakura-shi, Chiba-ken, Japan

+81-43-484-3945· kkobayashi@s.fujikura.co.jp

Abstract

We have newly developed premise cables for MTRJ connector. First, we developed floor cables and patch cord with 0.75 mm pitch 2-fiber ribbon. As for floor cables, two thin steel wires are arranged in this cable in consideration of pulling tension when it is installed. We prepared two types of floor cables, one of these is cable with 2-fiber ribbon, and the other is cable with 2-fiber ribbon cord. All of the cables we developed have excellent optical transmission characteristics and mechanical characteristics.

Next, we developed backbone cables with 0.75 mm pitch 2-fiber ribbons. The cables are slotted rod structure. Maximum of 25 2-fiber ribbons can be stacked in the slots. In consideration of the installation to and removal from congested places, the cable has special low-friction sheath material. The cables have excellent optical transmission characteristics and mechanical characteristics.

These cables are suitable for MTRJ connector. Simple and inexpensive premise networks can be constructed by using these cables and MTRJ connector.

Keywords

Optical fiber cable; optical fiber cord; optical fiber ribbon; Premise cable

1. Introduction

Recently, the requirement of high speed LAN with optical fiber is increasing. As for conventional optical premises system, simplex cord with single fiber and SC (or ST) connector is usually used. However, as for such systems, two simplex cords (one for the transmitting side and the other for the receiving side) have to be necessary for one computer terminal. From the viewpoint of compactness and economics, we developed cables with 0.75 mm pitch 2-fiber ribbons. These cables are suitable for MTRJ connector. Therefore, simple, inexpensive, and downsized premise networks can be constructed by using these cables.

2. 0.75mm pitch 2-fiber ribbon

First we developed 0.75 mm pitch 2-fiber ribbon. Figure 1 shows the cross section of the 2-fiber ribbon. The width is 1.1 mm and the thickness is 0.4mm, which is almost the same dimension of conventional 4-fiber ribbon. We made three types of ribbons, SM type, 50/125 GI type and 62.5/125 GI type.

The ribbon has special structure whose two 0.25 mm coated fibers does not contact with each other. So, we did mechanical test and

heat cycling test to confirm the eligibility of this ribbon. Table 1 shows the mechanical characteristics of the ribbon, such as lateral pressure, bending and twisting. Figure 2 shows the result of the heat cycling test. These results show that the newly developed 0.75 mm pitch 2-fiber ribbon has almost the same characteristics as conventional 0.25 mm pitch 2-fiber ribbon.
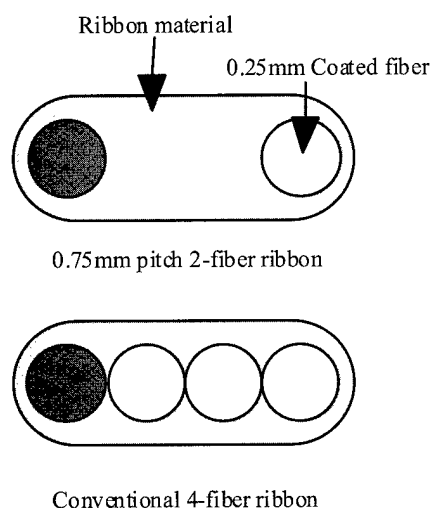
Fig.1 Optical fiber ribbon

Table1. Mechanical characteristics of the 2-fiber ribbon

Test Item	Condition	Test Result	
		0.75mm Pitch 2-fiber Ribbon	Conventional 4-fiber Ribbon
Lateral Pressure	490N/100mm	<0.05dB	<0.05dB
		No mechanical damage	No mechanical damage
Bending Test	R=10mm, 10times	<0.05dB	<0.05dB
		No mechanical damage	No mechanical damage
Twisting Test	Pitch=20mm, 10times	No mechanical damage	No mechanical damage
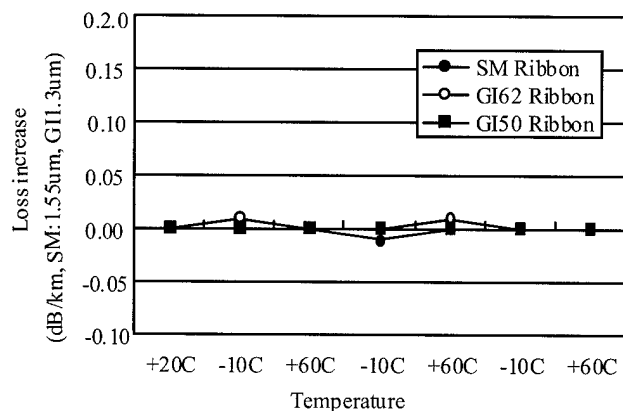
Figure 2. Result of the heat cycling test

We then examined strippability of the ribbon. The ribbon could be easily stripped into two glass fibers by using a conventional ribbon jacket stripper. Figure 3 shows the side view of the ribbon after the jacket was stripped. There is no residue of the coating material on the glass fibers, and the ribbon coating is cut completely in the position where the edge was inserted.
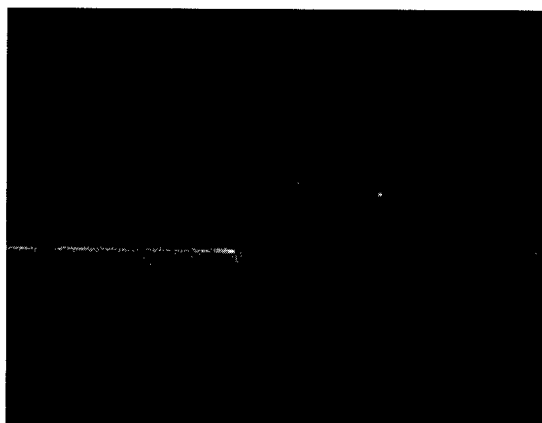
Figure 3. The side view of the ribbon after the jacket stripped

3. Premise cables for MTRJ connector

3.1 Patch cord

We then developed patch cord with the 0.75mm pitch 2-fiber ribbon for MTRJ connector. Figure 4 shows the cross section of the patch cord. The outer diameter is 2.8 mm. The patch cord is used for inside the patch panel and used as interconnection cable from outlet to desk. As for the jacket material, we can use either PVC or halogen-free material for the sheath of the cord. In this development, we adopted halogen-free material for them from the viewpoint of environmental protection.
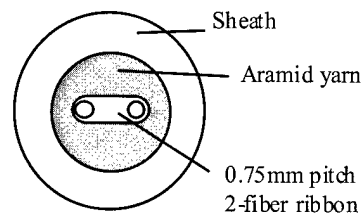
Figure 4. Patch cord structure

Table 2 summarizes the mechanical characteristics of the patch cord. Almost no loss increase is observed at the tensile strength of 100N. As for compression characteristics, almost no loss increase is observed at the load of 490N/100 mm. Therefore, the cord has almost the same mechanical characteristics as the conventional 2.8 mm cord with 0.9 mm coated fiber. Besides, the cord has passed the JIS-C 3005 horizontal flame test.

Table 2. Mechanical characteristics of the patch cord

Test Item	Condition	Test Result
Tensile Test	100N	<0.05dB No mechanical damage
Lateral Pressure	490N/100mm	<0.05dB No mechanical damage
Frame Test	JIS C3005 Horizontal	Pass

3.2 Floor cables

3-2-1. Cable structure

We prepared two types of floor cables, one of these is a cable with 2-fiber ribbon, and the other is a cable with 2-fiber ribbon cord. Figure 5 shows the cross section of the floor cables. These floor cables have two steel wires are arranged in the sheath in consideration of pulling tension when the cable is installed to conduit or floor duct.

3-2-1-1. Floor cable with 2-fiber ribbon

The former type cable is less expensive structure than the later, but the application is limited to the place where the connector's tensile strength is not so required. Therefore, the floor cable with 2-fiber ribbon is suitably used as interconnection cable from the patch panel to the outlet where the connectors are seldom plugged in and out.

Figure 5-1 shows the cross section of the 2-fiber ribbon type cable. The cable has very thin diameter. The width is about 3.8 mm, and the thickness is about 1.8 mm. The cable also has halogen-free flame retardant material. The 2-fiber ribbon can be taken out from the cable easily by tearing the sheath.

3-2-1-2. Floor cable with 2-fiber ribbon cord

The floor cable with 2-fiber ribbon cord is suitable for direct connection cable from the patch panel to the desk. We prepared two types of 2-fiber ribbon cord cables, one is encapsulated type cable, and the other is edge-bonded type cable.

A) Encapsulated type cable

Figure 5-2 shows the cross section of encapsulated type cable. Optical cord with the 0.75 mm pitch 2-fiber ribbon and two thin steel wires are arranged and sheathed with jacket material. The width is about 6.5 mm, and the thickness is about 4.0mm. The cable also has halogen-free flame retardant material. The optical cord can be taken out from the cable easily by tearing the sheath.

B) Edge-bonded type cable

Figure 5-3 shows the cross section of edge-bonded type cable. Optical cord part with the 0.75 mm pitch 2-fiber ribbon and two coated steel wire parts are bonded with bridges. The width is about 6.4 mm, and the thickness is about 2.8 mm. The cable also has halogen-free flame retardant material. The cord part can be easily separated from the cable.
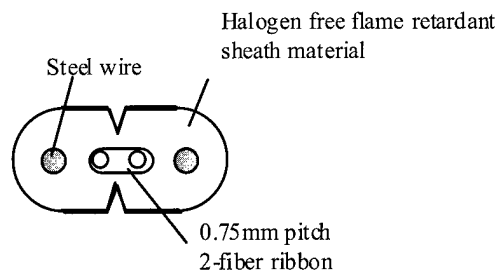
Figure 5-1 Floor cable with 2-fiber ribbon
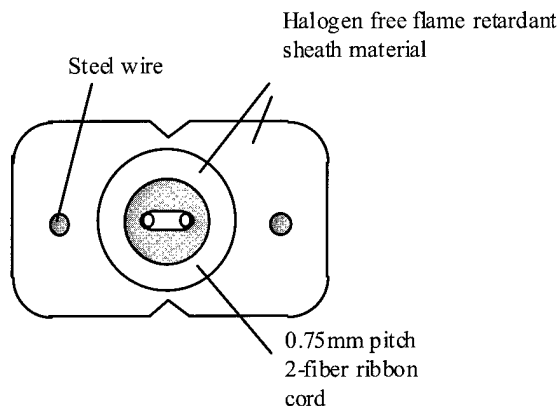
Figure 5-2 Floor cable with 2-fiber ribbon cord
(Encapsulated type)
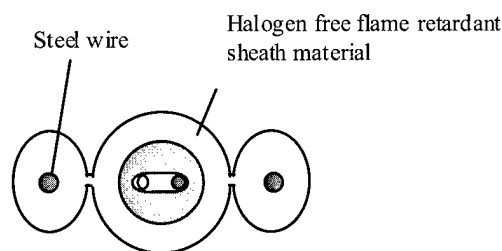
Figure 5-3 Floor cable with 2-fiber ribbon cord
(Edge-bonded type)

Figure 5. Floor cables

3-2-2. Lateral pressure characteristics of the edge-bonded type cable

Because of its simple structure, the edge-bonded type cable is less expensive than the encapsulated one. However, it is obvious that the edge-bonded type cable is inferior to the encapsulated type cable in mechanical characteristics, especially in lateral pressure. So, we investigated the cable structure to improve the lateral pressure characteristics.

the duct is 14 mm. The duct has 4 bends with 140 mm radius. The cables are squeezed in a mock duct and monitored the optical loss change. Then the cables are exposed to high and low temperature. Figure 8 shows the changes in optical losses of the cables during the test. Almost no loss increase was observed over the test. These results indicate that the cables are suitable for installation to floor duct or conduit.

Figure 6. Relationship between the lateral force and the loss increases of Floor cables

We prepared four kinds of cables. The size of the coated steel wire part is varies in these cables. Figure 6 shows the relationship between the lateral force and the loss increases of these cables. The lateral pressure characteristics strongly depend on the height of the coated steel wire part. The test result indicates that the lateral pressure characteristics of the edge-bonded type cable can stand comparison with that of the encapsulated type cable, by optimizing the steel wire part dimension.

3-2-3 Installation characteristics of the floor cables

As mentioned above, these floor cables have two steel wires in the jacket. So, it is expected that these cables have sufficient strength for the pulling or squeezing stress in cable installation. Table 3 shows the result of the cable tensile test. The fiber strain is under 0.3% at the tensile strength of 200N, and no loss increase was observed. We then investigated the cable squeezing test. That is modeled after the cable installation into bending duct. Figure 7 shows the test method of the squeezing test. The inner diameter of

Table 3. Tensile characteristics of the floor cables

	Floor cable with 2-fiber ribbon	Floor cable with 2-fiber ribbon cord	
		Encapsulated type	Edge-bonded type
Condition	200N	200N	200N
Loss Increase	< 0.05dB	< 0.05dB	< 0.05dB
Fiber Strain	< 0.3%	< 0.3%	< 0.3%
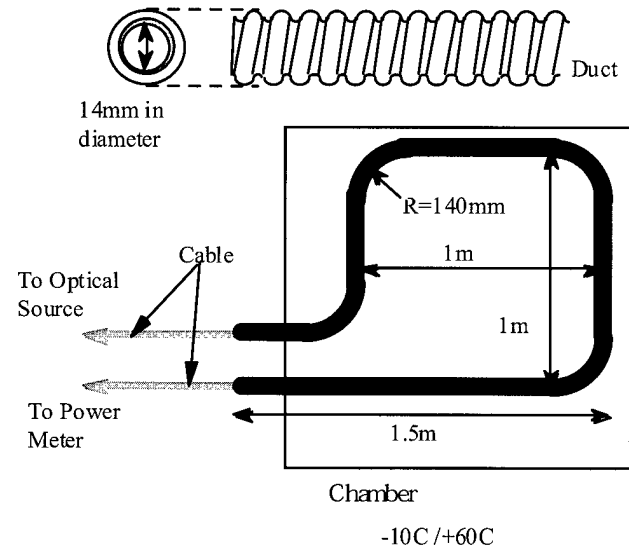
Figure 7. The test method of the squeezing test
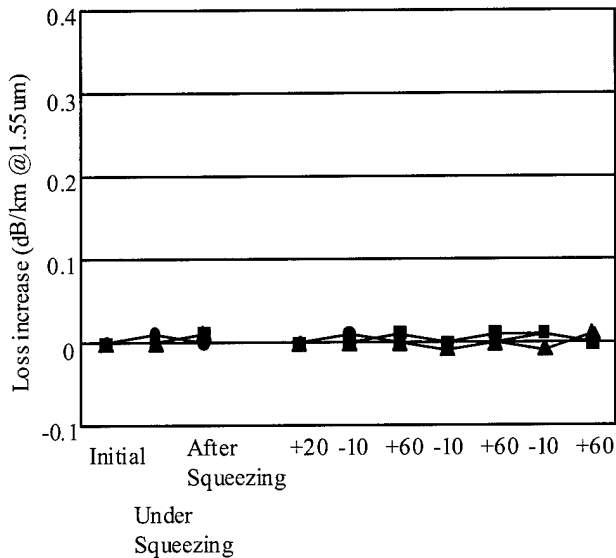
Figuer 8. The changes in optical losses of the cables during the test

3-2-4. Mechanical and transmission characteristics of these floor cables

Table 4 summarized the other mechanical characteristics such as impact, twisting, and bending test, and temperature characteristics. The cables we developed have excellent optical transmission characteristics and mechanical characteristics. Besides, the cord has passed the JIS C3005 inclined flame test.

Table 4. Mecanical characteristics of the floor cables ·

Table 4-1 Floor cable with 2-fiber ribbon

Test Item	Condition	Test Result	
		SM	GI 50/125 GI 62/125
Initial Transmission Loss		<0.30 dB/km @1.55um	<1.0dB/km @1.3um
Impact Test	Load : 1 kg Height : 0.3 m	Loss <0.1 dB	Loss <0.1 dB
Twisting Test	Length: 1m, 90 Degree	Loss <0.1 dB	Loss <0.1 dB
Bending Test	R=30mm, 10 times	Loss <0.1 dB	Loss <0.1 dB
Temperature Characteristics	-10C/+60C	Loss increase <0.1dB/km	Loss increase <0.3dB/km

Table 4-2 Floor cable with 2-fiber ribbon cord

Test Item	Condition	Test Result	
		SM	GI 50/125 GI 62/125
Initial Transmission Loss		<0.30dB/km @1.55um	<1.0dB/km @1.3um
Impact Test	Load : 1kg Height : 0.3m	Loss <0.1 dB	Loss <0.1 dB
Twisting Test	Length: 1m, 90 Degree	Loss <0.1 dB	Loss <0.1 dB
Bending Test	R=30mm, 10 times	Loss <0.1 dB	Loss <0.1 dB
Temperature Characteristics	-10C/+60C	Loss increase <0.1dB/km	Loss increase <0.3dB/km

3-3 Backbone cable

3-3-1 Cable structure

We also developed backbone cables with 0.75mm pitch 2-fiber ribbons. Figure 9 shows the cross section of the cable. The cable is slotted rod structure where conventional slotted rod for 4-fiber ribbon is used, and 0.75 mm pitch 2-fiber ribbons are stacked in the slots. Maximum of 25 2-fiber ribbons can be stacked in the slots. The cable sheath is halogen-free flame retardant material.
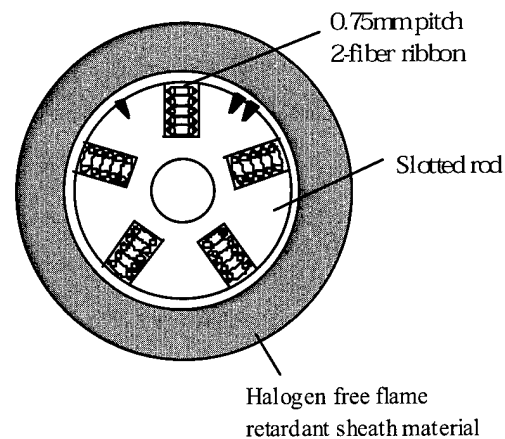
Figure 9. Cross section of the backbone cable

3-3-2 Characteristics of the backbone cable

Table 5 summarizes the mechanical characteristics of the backbone cables. As for tensile test, almost no loss increases are observed and the fiber elongations are under 0.2% at the tensile strength of 1470 N. Concerning compression characteristics, no loss increases are observed at the load of 980 N/100 mm. Therefore, the cables have equal mechanical characteristics as the conventional slotted rod cables with 4-fiber ribbon. Besides, the cables have passed the IEC332-3 flame test.

Table 5.   Mecanical test results of the backbone cables

Test Item	Condition	Test Result	
		SM	GI 50/125 GI 62/125
Initial Transmission Loss		<0.30dB/km @1.55um	<1dB/km @1.3um
Tensile Test	1470N	Loss <0.1dB	Loss <0.1dB
		Strain <0.2%	
Lateral Pressure	1960N/100mm	Loss <0.1dB	Loss <0.1dB
Impact Test	Load : 1kg Height : 1m	Loss <0.1dB	Loss <0.1dB
Twisting Test	Length: 1m, 90 Degree	Loss <0.1dB	Loss <0.1dB
Bending Test	R=80mm, 10times	Loss <0.1dB	Loss <0.1dB
Temperature Characteristics	-10C/+60C	Loss increase <0.1dB/km	Loss increase <0.3dB/km

4. The application to premises network

Figure 10 shows an example of premises network by using these cables. The patch cord is used for inside the patch panel and used as interconnection cable from outlet to desk. The floor cable with 2-fiber ribbon is suitably used as interconnection cable from the patch panel to the outlet. The floor cable with 2-fiber ribbon cord is suitable for direct connection cable from the patch panel to the desk.

These cables bring about many advantages in premises network by using MTRJ connector and compact optical transceiver module. In the horizontal networks, only one cable is necessary for one computer terminal. In the vertical networks, the cable can be easily attached to the field installable 2-fiber connector at the floor distributor in each floor. So, only one kind of connector will be necessary through the whole of the network. Therefore, simple, inexpensive, and downsized premise networks can be constructed by using these cables.
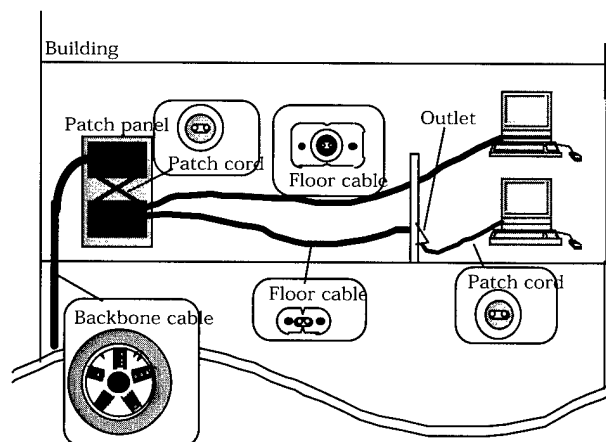
Figure 10.   An example of premises network by using these cables

5. Conclusions

We newly developed premise cables with 0.75 mm pitch 2-fiber ribbons for MTRJ connector. All of the cables we developed have excellent optical transmission characteristics and mechanical characteristics. The newly developed cables are useful for design of simple and inexpensive premise networks.

6. References

[1]   K. Takizawa et al, "MTRJ optical connector,"48th IWCS, p. 324-331 (Nov, 1999).

[2]   M. Takaya et al, "Design and performance of modular jack type Mini-MT connectors, 48th IWCS, p. 332-339 (Nov, 1999).

[3]   K. Kusakari et al, "Development of the halogen free flame retardant 2-fiber ribbon cables," EuroCable '98, p. 105-111 (1998).

Telecommunication Cable Department and a member of the IEICE of Japan.
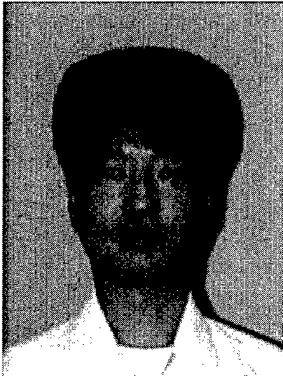
Kazunaga Kobayashi was born in 1961. He joined Fujikura Ltd. after his graduation from Gunma University with a M.E. degree in 1985 and has been engaged in research and development of optical fiber cables. He is now an engineer in the Telecommunication Cable Department and a member of the IEICE of Japan.
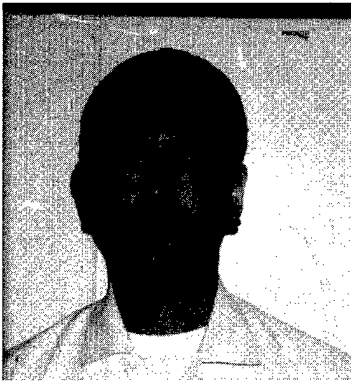
Masahiro Kusakari was born in 1965. He joined Fujikura Ltd. after his graduation from Nagasaki University with a B.E. degree in 1990 and has been engaged in research and development of optical fiber cables. He is now an engineer in the

Yoshio Hashimoto was born in 1973. He joined Fujikura Ltd. after his graduation from Ibaraki University with a M.E. degree in 1998 and has been engaged in research and development of optical fiber cables. He is now an engineer in the Telecommunication Cable Department and a member of the IEICE of Japan.
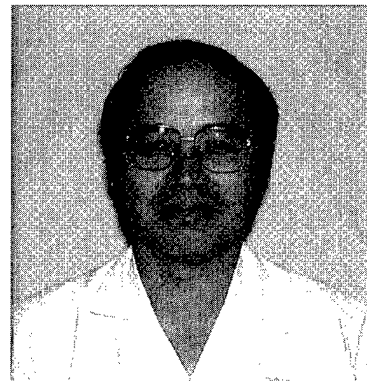
Matsuhiro Miyamoto was born in 1953. He joined Fujikura Ltd. after his graduation from Tokyo Institute of Technology with a M.E. degree in 1978 and has been engaged in research and development of optical fiber cables. He is now an engineer in the Telecommunication Cable Department and a member of the IEICE of Japan.

Development of Optical Fiber Cable with Halogen Free Flame Retardant Jacket

Osamu Kato, Akira Murata, Keiji Oohashi, and Matsuhiro Miyamoto

Fujikura Ltd.,
Sakura-City Chiba, JAPAN
+81-43-484-3946 kato@s.fujikura.co.jp

Abstract

Using halogen-free flame-retardant polyolefin as a jacketing material, we created prototypes of indoor cables and aerial drop cables, which are used for subscriber-line fiber-optic cables. We then assessed the performance of these prototypes. These evaluations, which included combustion tests, tests of optical loss and its heat cycle characteristic, mechanical properties, and workability such as the adhesion of tension members, provided positive results.

Cable materials require a fine balance of flame-retardancy and mechanical durability. For aerial drop cables, the weather-resistant property is also important. The prototype cables demonstrated excellent characteristics, meeting these requirements.

Keywords

Halogen Free, Flame Retardant Jacket

Introduction

The demand for fiber-optic cables (indoor cables, aerial drop cables) is expected to increase significantly, due in part to projects such as the fiber-to-the home (FTTH) project, with the demand for cable materials expected to keep pace. While PVC is currently in wide use in the manufacture of cable jackets, other materials are being sought that are both flame-resistant and environment-friendly, given the increasing use of cables in residential environments.

For this reason, we investigated the use of halogen-free flame-retardant material in cable jackets as a replacement for conventional resins. Because its major component is a hydrate of a light metal, the additive in the halogen-free flame- retardant resin offers a high degree of flame-retardancy and also presents no health hazards. It is ecologically-friendly, producing no poisonous gases during combustion and leaching no hazardous materials into ground water when buried underground.

1. Structure of cable

Figure 1. shows the structures of the prototype indoor cables and aerial drop cables.

(1) Indoor cable

This cable features a structure in which a φ0.25mm SM-type optical fiber and two φ0.4mm tension member steel wires are integrated in a jacket of halogen-free flame-retardant resin (polyolefin-based resin; the flame-resistant agent is a magnesium hydrate).

(2) Aerial Drop cable

This cable is composed of a φ0.25mm SM-type optical fiber, two φ0.4mm tension member steel wires, and a φ1.2mm steel wire that serves as a support wire. Those component wires are integrated in a jacket made of halogen-free flame-resistant resin.

φ 0.4mm steel wire

φ0.25mm SM optical fiber

HFFR resin

\<Indoor cable\>

Support wire (φ1.2mm steel wire)

HFFR resin

φ0.25mm SM optical fiber

φ 0.4mm steel wire

\< Aerial Drop cable \>
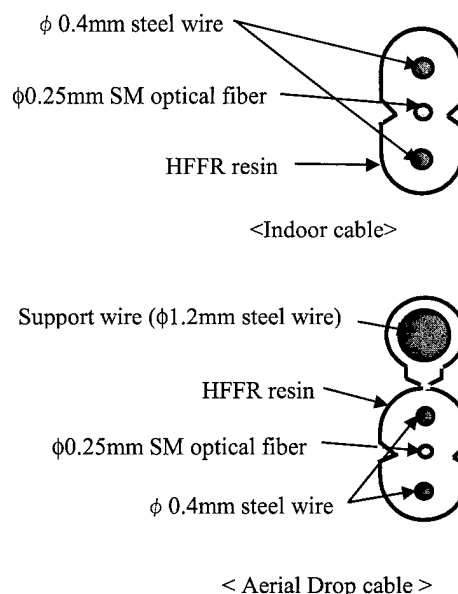
Figure 1.   Structure of Cables

2. Design of the jacketing material

Used as the jacket material in the current investigation, halogen-free flame retardant polyolefin has a high concentration of a non-organic component that serves as a flame-resistant agent. To avoid significant reductions in tensile strength, the composition of this material needs to be carefully balanced to provide both adequate mechanical properties and flame-resistance.

We selected two types of halogen-free flame-resistant resins of different composition for each aerial drop cable and indoor cable prototype.

Keeping in mind the need for weather-resistance, we selected a highly durable Ethylene Ethyl Acrylate(EEA)-based material, to which carbon black was added. For indoor cables, we chose an Ethylene Vinyl Acetate(EVA)-based material, placing a priority on flame-resistance.

Flame-retardancy

Flame-retardancy was evaluated with Oxygen Index(OI) and a cone calorimeter. Cone calorimeters are used to measure the rate of heat generation and the amount of heat generated when a specimen of 10cm x 10cm, 3mm-thick sheet is burned in a cone-shaped heater (shown in Figure 2). This is a highly useful measure of the combustion properties of a specimen. Figure 3 and Table 1 summarize the rate of heat generation, peak-top amount of generated heat and the start time of combustion. The test results indicate that even specimens of the same OI value and base material exhibit different combustion phenomena. Specimens A and C demonstrated long combustion times and low heat generation speed, while B and D exhibited significant combustion heat and rapid combustion. We made prototype cables using materials A-D for the cable jackets, then performed an inclined combustion test at 60°, based on JIS C 3005 (for a description of the test method, see Figure 10.). Then the combustion of specimens A and C stopped voluntarily within one minute, while that of specimens B and D failed to stop. These test results indicate that heat propagates quickly in cables that have higher rates of heat generation leading to more extensive flame damage. The behavior observed in the cone calorimeter tests agrees well with the actual combustion behavior of cables. The cone calorimeter differentiates between actual combustion characteristics among cables of the same OI value. Based on the test results, we decided to use as jacket material A for the aerial drop cable and C for the indoor cable. A detailed description of the combustion tests of the cables will be described later.

Temperature measurement
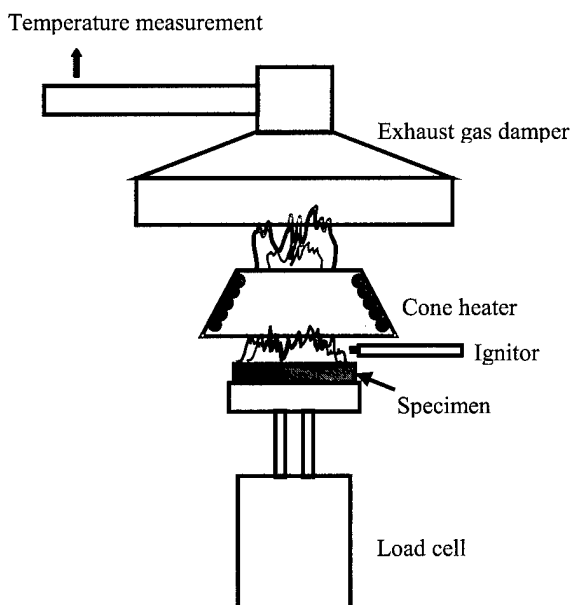
Figure 2. Schematic structure of cone calorimeter

Table 1. Cone calorimeter test results for each jacketing material for cables

Cable	Aerial Drop Cable		@ Indoor Cable	
Jacketing Material	A	B	C	D
Base resin	EEA	EEA	EVA	EVA
OI	31	35	43	41
Peak top value of generated heat(kW/m^2)	162	274	175	312
Total heat generation(MJ/m^2)	59	76	65	67
Combustion start time (seconds)	46	69	41	60
Residual weight after combustion (%)	34.8	36.6	36.6	44.8
Cable combustion test (JIS C 3005)	pass	fail	pass	fail
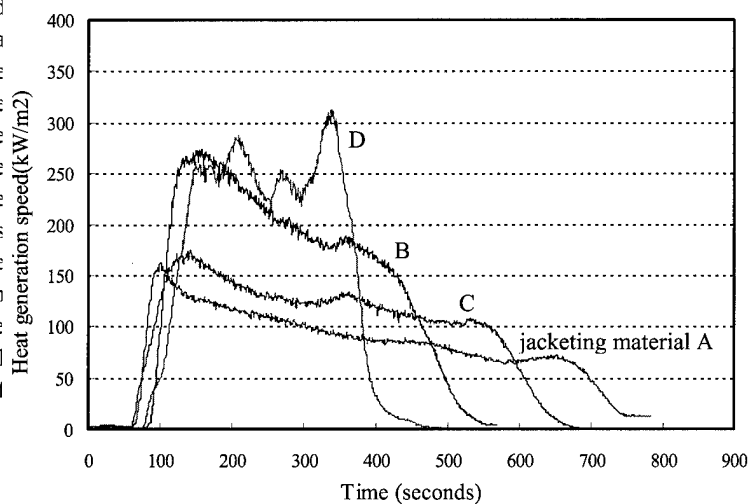
Figure 3. Heat generation speed for each jacketing material for cables

Mechanical performance

We conducted tensile and stiffness tests on specimens A and C. Table 2 provides the test results. The jacketing material A for the aerial drop cable demonstrated excellent mechanical performance, with an initial breaking strength of at least 10Mpa, a breaking elongation of at least 500%, and a stiffness temperature of -40°C. The jacketing material C contains a lot of inorganic material. Using an inorganic material increases flame-retardancy, although the inorganic material can lower mechanical strength. Therefore, it is necessary to balance between mechanical properties and flame-retardancy. Nevertheless, the material C showed a breaking strength of at least 10MPa, a breaking elongation of at least 160% and the stiffness temperature was -15°C. The materials demonstrated an excellent balance between flame-retardancy and mechanical strength.

Table 2. Initial performance of each jacketing material

	@@@@Value Measured	
Jacketing material	A(For Aerial Drop Use)	C(For Indoor Use)
Yield Point Strength(MPa)	7.4	11.5
Breaking Strength(MPa)	10.7	11.5
Breaking Elongation(%)	556	160
Stiffening Temperature(•)	-40	-15
O.I(Oxygen Index/ASTM D 2863)	31	43
Fuming Properties (Smoke Density Ds/ASTM E 622)	97	100
pH of Gases Generated (IEC 754-2)	4.0	9.1

Reliability

The mechanical properties of the aerial drop cable jacket are subject to degradation, since they are used outdoors and are subject to the full range of weather conditions. We examined the resistance of the material to attack by chemical agents such as acids, alkali, and oil. Its weather resistance was evaluated by a one-year outdoor exposure test and a 4000-hour degradation acceleration test using an sunshine weather-o-meter. The test results are provided in Table 3. The jacket demonstrated excellent chemical resistance and weather resistance, retaining full tensile strength in all tests.

Table 3. Chemical and weather resistance of jacket material (A) for the aerial drop cable

Item	Retention of Breaking Elongation after attack (%)
Temperature attack: 100• ×48hrs.	95
Acid attack: 10% HCl 50• ×50days	102
Alkali attack: 3% NaOH 50• ×50days	98
Insulation oil attack: 50• ×50days	96
Sunshine weather-o-meter 4000hrs.	92
One-year outdoor exposure	100

3. Evaluation of prototype cables

Optical loss properties

Table. 4 shows the results of the evaluation test of the prototype cables. Both the aerial drop cable and the indoor cable demonstrated excellent performance in the initial optical loss test. No increase in optical loss was observed, even after the cables were subjected to three heat-cycles ranging from -30°C to 70°C.

Optical loss after mounting simulation test

The temperature dependence of this performance was further investigated in another heat-cycle test. As shown in Figure 4. and 5, the aerial drop cable and the indoor cable were fixed to plates with cleats and staples, respectively, as they would be in actual use, then subjected to two heat-cycles ranging from -30°C to 70°C. Figure 6. shows the optical loss of the cables, along with the patterns of temperature change. No significant change in the magnitude of optical loss was observed.
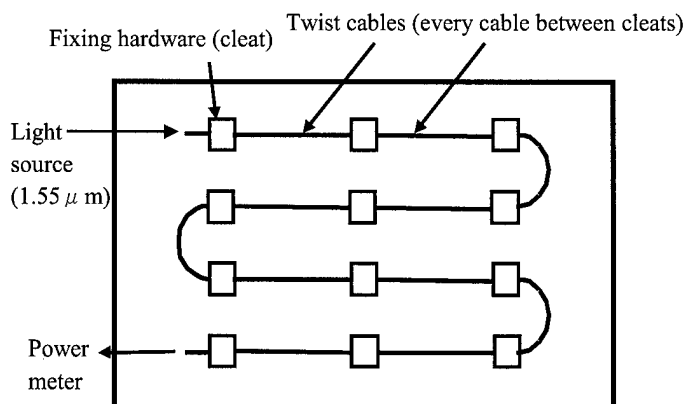
Figure 4. Mounting simulation test for the aerial drop cable
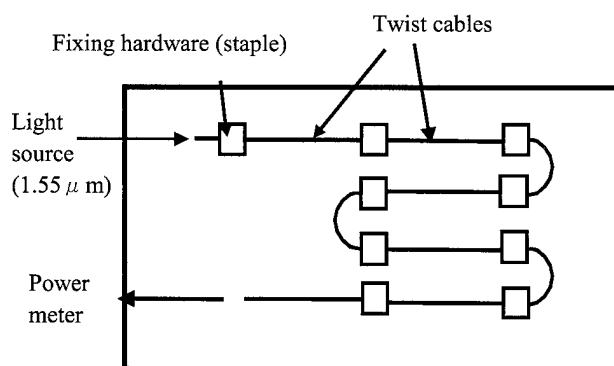
Figure 5. Mounting simulation test for the indoor cable
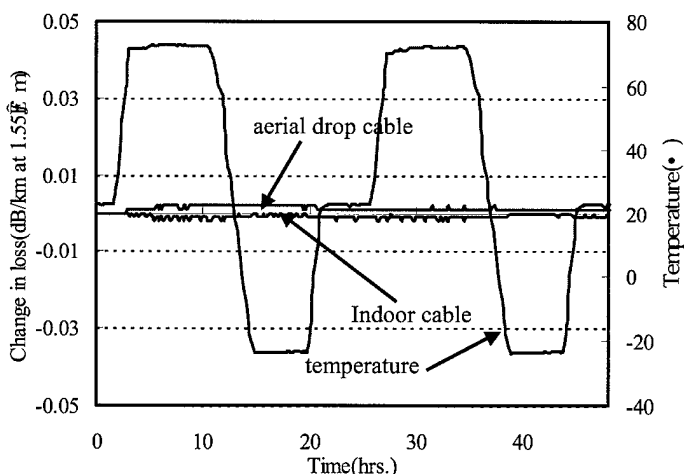
Figure 6. Temperature dependence of optical loss in mounting simulation test

Adhesion of tension member

The adhesion between the tension member (ϕ0.4mm steel wires) and the jacket, which is represented by a steel wire drawing force, must fall within a proper range related to reliability and workability. Figure 7. shows the measurement method. If the drawing force is no more than 5N/cm, the fluctuations in optical loss may pose problems. On the other hand, a drawing force equal to or greater than 30N/cm impedes any stripping of the tension member. Adhesion measurements were 26N/cm for the aerial drop cable and 19N/cm for the indoor cable, both falling within the appropriate range.
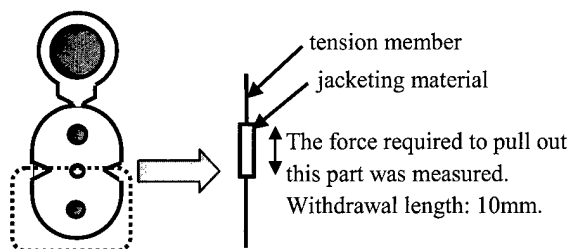
Figure 7. Measurement of tension member adhesion

Long-term reliability of adhesion of tension member (for aerial drop cables)

We evaluated the long-term reliability and weather resistance of the aerial drop cable. The cable was first exposed to outdoor conditions for a predetermined duration, then the change in adhesion between the tension member and jacket was measured. The test results are shown in Figure 8.

he cable was found to be highly weather-resistant, retaining approximately 95% of its initial adhesion traits after an exposure of one year. We also performed an acceleration test conducted at high temperature and humidity (70°C, 95%RH) to assess the adhesion between the tension member and jacket. The test results are shown in Figure 9. The cable retained approximately 85% of its initial adhesive qualities following a three-month exposure, again demonstrating good weather-resistant properties.
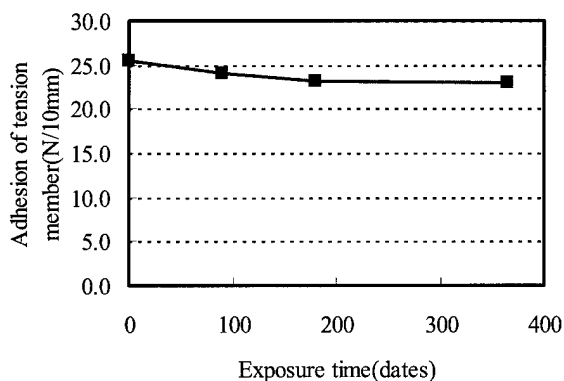
Figure 8. Exposure test for tension member
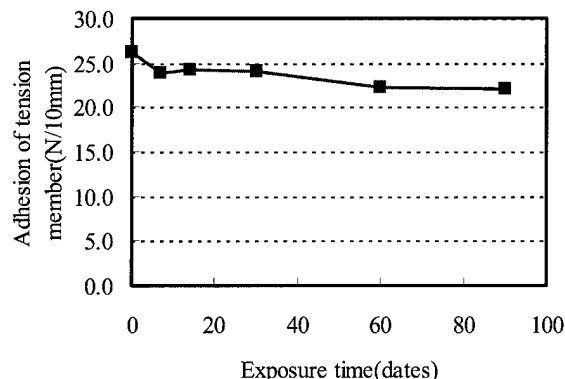
Figure 9. High temperature and high humidity test for tension member adhesion

Flame-retardancy

The flame-resistance of the prototype cables was measured by the JIS C 3005 inclined 60° combustion test. Figure 10. shows the measurement setup. In the test, the combustion time and combustion duration after ignition were measured. For both the aerial drop cable and the indoor cable, the fires expired without intervention within one minute, demonstrating excellent flame-resistance.

In addition, the UL 1581 VW-1 test was conducted on the aerial drop cable. The test results are shown in Table 4. Again, the fire expired without intervention, confirming the cable's excellent flame-resistance.
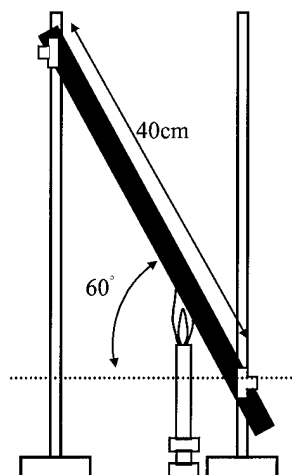
Figure 10. JIS C 3005 60° inclined combustion

Long-term reliability of adhesion of flame-retardancy (for aerial drop cables)

We performed the JIS C 3005 inclined 60° combustion test and UL 1581VW-1 combustion test on cables that had been exposed for one year. Fires expired without intervention in both combustion tests, demonstrating adequate flame-resistance following exposure.

Table 4. Performance characteristics of prototype cables

	Evaluation Conditions	Test Results	
		Aerial Drop Cable	Indoor Cable
Transmission Loss	OTDR	0.34dB/km (1.31f m̂) 0.20dB/km (1.55f m̂)	0.34dB/km (1.31f m̂) 0.21dB/km (1.55f m̂)
Heat Cycle Characteristics	Temperature Range ₧30 • 70 Number of cycles ₧0cycles Left at respevtive temperatures for 6 hours each	Change of Loss ₧.03dB/km or lower (1.31f m̂) Change of Loss ₧.03dB/km or lower (1.55f m̂)	Change of Loss ₧.03dB/km or lower (1.31f m̂) Change of Loss ₧.03dB/km or lower (1.55f m̂)
Heat Cycle Characteristics in mounting simulation test	Temperature Range ₧30 • 70 Number of cycles ₧cycles	Change of Loss ₧.03dB/km or lower (1.31f m̂) Change of Loss ₧.03dB/km or lower (1.55f m̂)	Change of Loss ₧.03dB/km or lower (1.31f m̂) Change of Loss ₧.03dB/km or lower (1.55f m̂)
Strength Member Adhering Properties	Length Covered ₧cm	26N/cm	19N/cm
Bending Properties (IEC 794-1 Repeated bend)	Bending Radius ₧0mm Angle ₧80ß Number of Cycles ₧0cycles	Change of Loss ₧.01dB or lower (1.55f m̂)	Change of Loss ₧.01dB or lower(1.55f m̂)
Lateral Pressure Properties (IEC 794-1 Crush)	Added Weight ₧200N/25mm Time ₧min.	Change of Loss ₧.01dB or lower (1.55f m̂)	Change of Loss ₧.01dB or lower (1.55f m̂)
Impact Properties (IEC 794-1 Impact)	Falling Weight ₧.9N Height ₧m	Change of Loss ₧.02dB or lower (1.55f m̂)	Change of Loss ₧.02dB or lower (1.55f m̂)
To,¦"‰₧Properties (IEC 794-1 Torsion)	Sample length ₧m Torsion Condition : ± 90ß ₧cycle	Change of Loss ₧.01dB or lower (1.55f m̂)	Change of Loss ₧.01dB or lower (1.55f m̂)
Working Properties in the Cable Installation	Cut to a depth of 10mm with scissors and tear with hands.	Good	Good
Flame Retardant Properties		Self-extinguishing (UL 1581 VW-1 and JIS C 3005)	Self-extinguishing (JIS , ₧3005)

Mechanical properties

We measured the mechanical properties of the prototype cables using a side-stress test, repeated bending test, shock test, and twist test. Table 4 summarizes the test conditions and results. The results of all tests were excellent.

Conclusions

We developed aerial drop cables and indoor cables with jackets composed of halogen-free flame-resistant polyolefin. These jackets demonstrated excellent flame- and weather-resistant properties. Excellent mechanical performance was obtained by optimizing the composition of the jacket materials, including the resin, and flame-resistant agent.

References

[1] Kusakari et al., 1997 Proc. IEICE Soc. Conf., B-10-22.

[2] Ando et al., 1999 Proc. IEICE Gen. Conf., B-10-3.
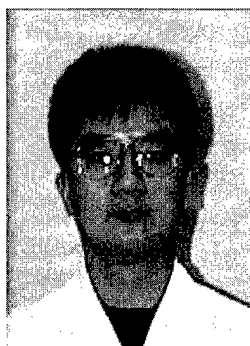
Osamu Kato

R&D Dept.
Telecommunication
Cable Division
Fujikura LTD.

1440 Mutsuzaki,
Sakura, Chiba,
285-8550, JAPAN

Osamu Kato graduated from Nagoya Institute of Technology with a B.E. degree in 1990. After six years of work as an engineer for material analysis, he has been engaged in research and development of optical fibers. He is now an engineer in the Telecommunication Cable Material Section and a member of the IEICE of Japan.

Development of Two-Dimensional Array MT Connector

Tatsuya Ohta, Kazuhiro Takizawa, Akito Nishimura, Toru Arikawa, and Yasuhiro Tamaki

Cable Network Components Division, Fujikura Ltd.
1440 Mutsuzaki, Sakura, Chiba 285-8550 JAPAN
Phone: +81-43-484-3948

Abstract

Advances in high dense fiber systems such as parallel optical interconnection technologies and high capacity ATM switches have led to the development of a high fiber count MT type connector[1] with two-dimensional (2-D) fiber arrangement in a connector. Fiber count for this 2-D array MT connector increases in multiples of 12 or 8 up to a maximum of 60. The average insertion loss of the 60-fiber (12c x 5r) MT connector[2] is 0.33dB for single-mode fibers and 0.04dB for multi-mode fibers. Return loss values are higher than 40dB and 30dB for the respective fiber types. The 16- and 24-fiber (8c x 2r, 12c x 2r respectively) connectors have the same performance. In environmental tests such as temperature cycling, thermal aging, and humidity aging test , loss changes are less than 0.2dB for single-mode fibers and 0.05dB for multi-mode fibers. In fact, optical performance is the same as conventional MT connector. The 2-D array MT can be adapted for other MT configurations such as the multi-fiber push-on/pull-off (MPO) [3] and back-plane type connectors. The 24-fiber MPO connector was developed with an average insertion loss of 0.25 dB and minimum return loss of 50 dB for single-mode fibers.

Keywords

MT connector; MPO connector; High density connection; Optical and environmental characteristics.

1. Introduction

The escalating demand for more bandwidth in the optical subscriber networks to support increasing types of services has led to the development of very high fiber count and dense optical fiber distribution cables that require an economic and quick way of connecting the individual fibers. These cables commonly employ fiber ribbons because of their high packing density and the best way to connect them would be to use MT connectors. Also, there has been a great deal of interest and research in parallel optical interconnection for use in huge throughput systems such as high capacity switching systems and massive parallel computers[4]. The MT connector can be employed to connect multiple fibers economically and reliably.

Foreseeing the need for higher fiber counts and connection density for such optical interconnect applications, we have developed a high fiber count MT type connector with two dimensional fiber arrangement in a connector that has many times the connection density of conventional MT connectors.

Maximum fiber count of as high as 60 is possible with this 2-D array MT connector. In this paper, we first describe the structure of the MT connector, followed by the structure and connection density of the 2-D array MT. Next, the method of production is described followed by results of optical and reliability testing. The structure and performance of the 24-fiber MPO connector are then reported before presenting the conclusion.

2. Structure of MT Connector
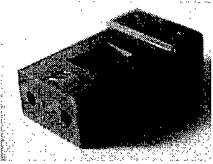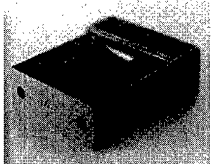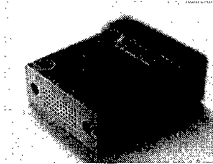
Figure 1 shows the structure of the MT connector. The MT connector is molded from composite plastics and has standard dimensions for accommodating up to a maximum of 12 optical fibers arranged in a linear array. Alignment of the connecting fiber arrays is provided by a pair of precision diameter metal guide pins that fit into accurately molded guide pin holes in the connector. The connection is then completed by securing the mated connectors with a metal clip which serves to keep the fibers in stable contact.
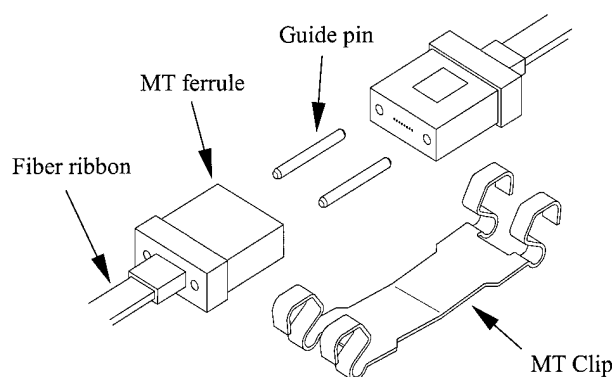
Figure 1. Structure of MT Connector

Table 1 shows various variants of MT connector ferrules that were developed from the original design. The mini-MT ferrule is a miniaturized version of the MT and can accommodate up to 4 fibers within an end face dimension of 4.4 x 2.5 (mm). It is developed specifically for premises optical cabling applications where high density duplex connections are required. The MT-RJ small form factor connector[5] uses the mini-MT ferrule to achieve compact size for high density duplex connection with a pitch of 0.75mm between fibers.

Table 1. Types of MT connector ferrule

Ferrule types	Mini-MT	MT (IEC 60874-16)	2-D array MT
Appearance			
Fiber count	1, 2, 4	2, 4, 8, 12	16, 24, 60
End face dimensions (mm x mm)	4.4 x 2.5	6.4 x 2.5	
Application connector types	Mini-MT Mini-MPO MT-RJ	MT MPO(MTP)/MPX MT-BP	

3. 2-D Array MT Connector

3.1 Structure

To increase fiber counts, we have developed the 2-D array MT ferrule which can terminate up to 60 fibers while retaining the dimensions of the original MT connector ferrule. Instead of restricting to a single row across the ferrule endface, the fibers are arranged in 2-D fashion with a pitch of 0.25mm such that a maximum fiber count of 60, with limit of 12 fibers in a row (between guide pin holes) and 5 in a column, is possible. Also, by retaining the dimensions of the original MT, the 2-D array MT ferrule can be used in connector designs based on the original MT such as the multi-fiber push-on/ pull-off (MPO/MPX) and back-plane type connectors.

The conventional MT connector has fiber guiding grooves molded into the connector to allow easy insertion of fiber ribbon into the fiber holes. In order to facilitate the insertion of multiple fiber ribbons, the guiding grooves are arranged in a step-like fashion so that the fiber insertion process is visible from the ferrule window.

Until now, the following configuration of 2-D array MT connectors assembled on 8- and 12-fiber ribbons were successfully developed and tested. The fiber arrangements are shown in Table 2 looking from the connector end-face.

(1) 16MT : 8 columns by 2 rows ; 0.25mm pitch between rows and columns.

(2) 24MT : 12 columns by 2 rows ; 0.25mm pitch between columns and 0.5mm pitch between rows.

(3) 60MT : 12 columns by 5 rows ; 0.25mm pitch between rows and columns.

3.2 Connection Density

The 2-D array MT has a connection density that is many times higher than that of single array MT connectors besides having greater fiber count per connector. This important characteristics of the 2-D array MT reduces the space requirements for fiber dense interconnection. Table 2 compares the fiber count and connection density of the various types of MT connector ferrules. The connection density of the 60MT is 5 times that of five 12MT packed together.

Table 2. Fiber count and connection density

Connector types	Mini-2MT	12MT	2-D array MT		
Fiber count	2	12	16	24	60
End-face appearance					
End face dimensions W x H (mm²)	4.4 x 2.5	6.4 x 2.5			
Connection density (fiber count/cm²)	18	75	100	150	375

4. Method of Production

The 2-D array MT ferrule is manufactured by transfer molding from thermoset resin. Figure 2 shows the transfer molding process flow. First, the heated upper and lower mold dies are clamped together. Next, pre-heated resin is dropped into the mold die. After the plunger has pushed the resin to fill the mold cavity, pressure is maintained at high temperature to solidify the resin. Finally after a period of time, the mold is opened and the molded parts are ready.
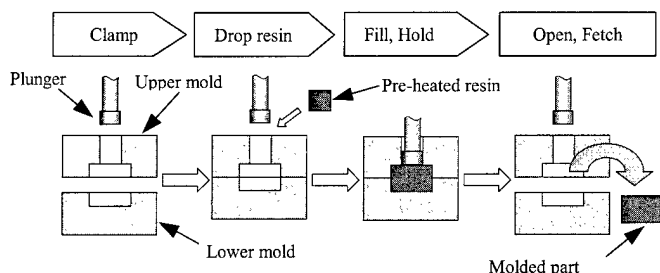
Figure 2. Transfer molding process

Figure 3-1 shows the essential structure of the mold design used to produce the original single array MT connector. The MT fiber holes and guide pin holes are formed by the core pins which are placed on the V-grooves in the lower mold plate. However, this mold design is applicable only for single array MT. In order to produce the 2-D array MT, we modified the mold design by replacing the V-grooves with a placement-hole structure for positioning the core pins. Figure 3-2 shows the placement-hole type mold design. The micro-holes in this structure are precision drilled to within a positional error of less than 0.25μm in order to accurately position the core pins. This mold design is much more versatile than the V-groove method for placing the core pins because it allows multiple rows of core pins to be placed vertically. The molded connector will then have a 2-D arrangement of fiber holes. Moreover, the hole pitch can be easily designed as either 0.25mm or 0.5mm or any other values.
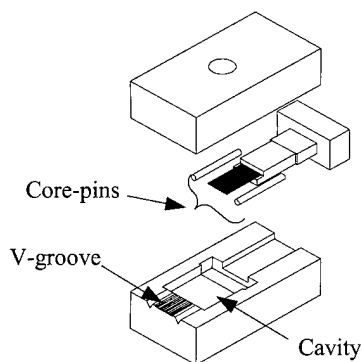
Figure 3-1. V-groove type mold
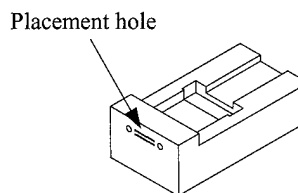
Figure 3-2. Placement hole type mold

5. Performance

2-D array MT connectors were evaluated for optical and environmental performance. The results are summarized in Table 3. Detailed tests and results are discussed in the sections that follow.

Table 3. Summary of test results for 2-D array MT connector

Tests	Methods and Conditions		Loss / Loss dev.	
			SM	MM
Insertion Loss	Random mating (avg.)	16 MT	0.23dB	0.03dB
		24 MT	0.23dB	0.04dB
		60 MT	0.33dB	0.04dB
Return Loss	Random mating	16 MT 24 MT 60 MT	≥40dB	≥30dB
Durability	500 cycles	16 MT 24 MT 60 MT	≤0.20dB	≤0.08dB
Temperature Cycling	Range : -40 to +75 °C Duration: 10 cycles	16 MT 24 MT 60 MT	≤0.15dB	≤0.05dB
Thermal Aging	Temperature : +85 °C Duration : 240 hr	16 MT 24 MT 60 MT	≤0.15dB	≤0.05dB
Thermal Aging	Temperature : -40 °C Duration : 240 hr	16 MT 24 MT 60 MT	≤0.15dB	≤0.05dB
Humidity	60 °C @95%RH Duration : 14 days	16 MT 24 MT 60 MT	≤0.20dB	≤0.08dB

5.1 Insertion Loss and Return Loss

The insertion and return loss of the 2-D array MT connector samples were measured at a wavelength of 1.31μm through random mating. Index matching material was used at the connection point. Average insertion losses of less than 0.33dB is achieved for single-mode fibers and less than 0.04dB for multi-mode fibers. Figure 4 and 5 shows the insertion loss histogram of
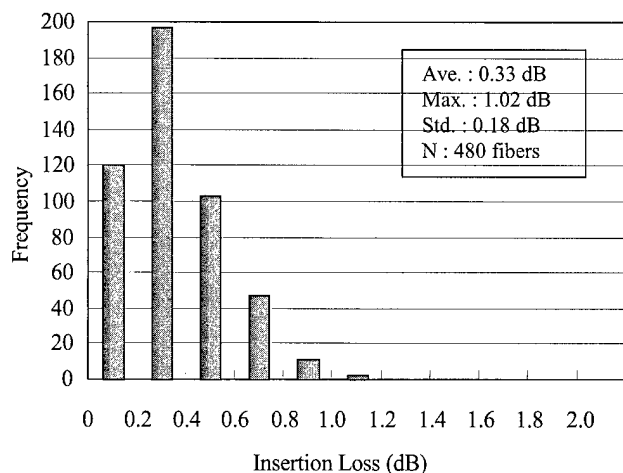
Figure 4. Insertion loss of 60MT connector for single-mode fiber
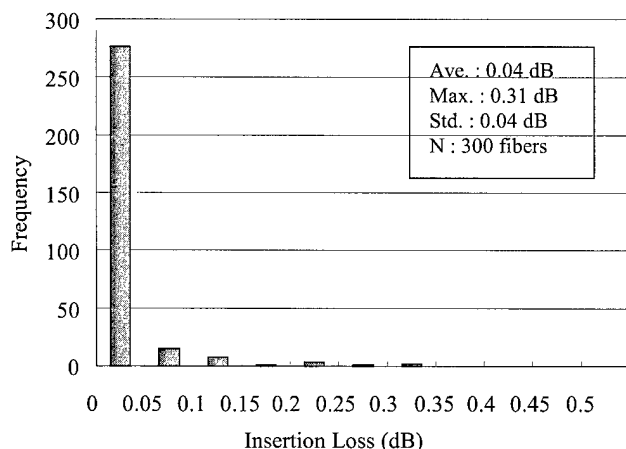
Figure 5. Insertion loss of 60MT connector for multi-mode fiber

the 60MT connector for 10/125 μm single-mode and 62.5/125μm multi-mode fibers. Result of the return loss measurements shows the 2-D array MT to have an average return loss of about 40dB for single-mode fibers.

5.2 Temperature Cycling Test

Samples of 60MT connectors were placed in a continuously varying temperature environment to determine performance over a specified operating range. The insertion loss changes for 12 out of the 60 fibers were measured every ten minutes for a total of 10 cycles of temperature variation from -40 to 70 degrees. Figure 6 shows the result for single-mode samples. The loss changes during the test were well within 0.2 dB.
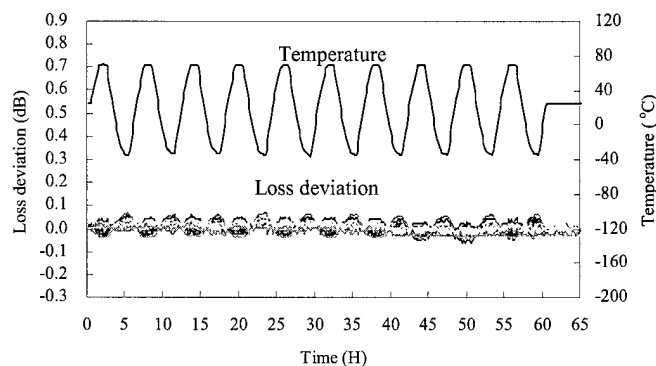
Figure 6. Temperature cycling characteristics of 60MT connector

6. 2-D array 24-Fiber MPO Connector

The 2-D array MPO connector was developed for low return loss performance and enable simple and fast connection without using index matching material. Based on angle polishing technology, we have succeeded in developing the 2-D array 24-fiber MPO connector.

6.1 Structure

Figure 7 shows the structure of the 24-fiber MPO connector (hereafter referred to as 24MPO) . It has the same structure as conventional MPO connector that houses the MT ferrule. The connectors are aligned by 2 guide-pins, and are mated through an adapter. The springs within the connector housings produce compression forces which hold the connector end-faces mated tightly against each other.

The end-face is angle polished at 8 degrees with fibers protruding from ferrule end-face. Angled end-face prevent light signals from reflecting back into the transmitting fiber. Fiber protrusion prevent air gap between fibers when the connectors are mated. This physical contact (PC) between fibers allows low loss connection to be realized without index matching material.
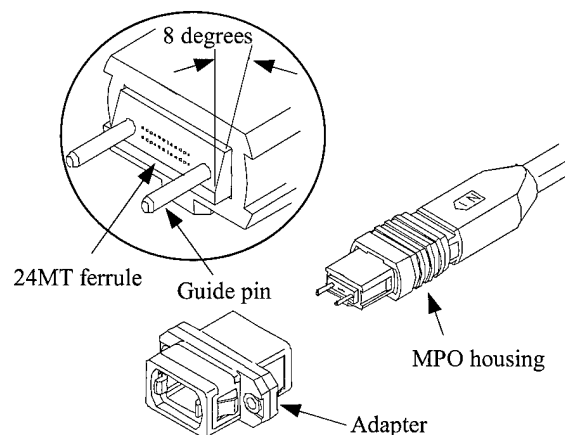
Figure 7. Structure of 2-D array MPO connector

6.2 Performance

6.2.1 Insertion loss

We measured the insertion loss of the 24MPO connector for single-mode fiber through random mating. The measurement was conducted at a wavelength of 1.31μm without the use of index matching material. Figure 8 shows the loss histogram for the 24MPO. The average insertion loss is 0.25dB.
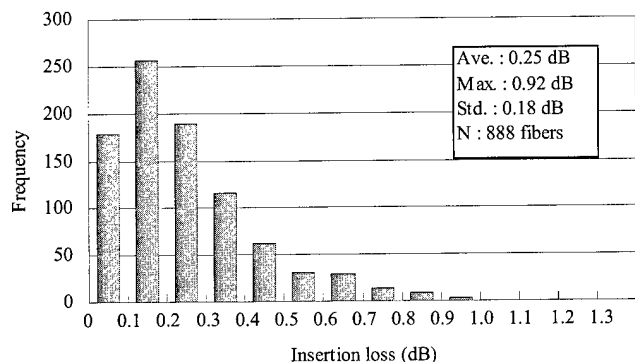
Figure 8. Insertion of 24MPO connector

6.2.2 Return loss

Figure 9 shows the result of return loss of the 24MPO connector for single-mode fibers measured without the use of index matching materials. The return loss values are higher than 50dB. These values are typical of PC connectors with angle-polished ferrule end-face. The fiber to fiber contact significantly reduces the back reflection at the connection interface due to Fresnel reflection caused by the presence of an air gap.
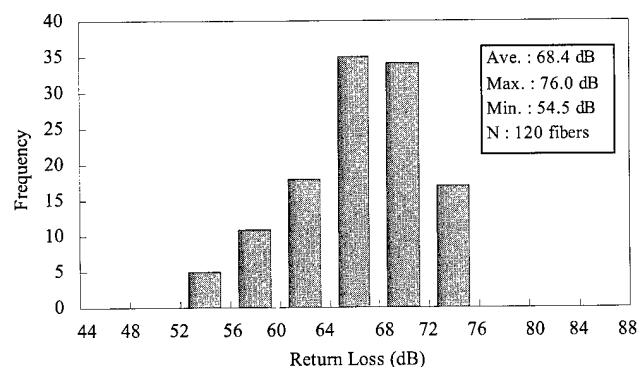
Figure 9. Return loss of 24MPO connector

6.2.3 Durability Test

Samples of 24MPO connector were subjected to continuous connect-disconnect cycles and the insertion loss changes were measured every 25 cycles for a total of about 500 cycles. Figure 10 shows the result of the loss changes to be less than 0.2dB for single-mode fiber. No damage was observed at the mating surface. This result shows good repeatability characteristics for the 24MPO connector and that the guide-pin holes are reasonably wear resistance to allow long term usage.
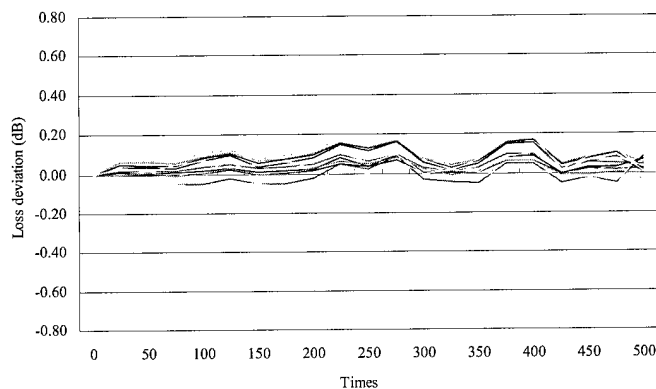
Figure 10. Repeated mating loss characteristics of 24MPO connector

6.2.4 Environmental test

Three environmental test were performed in series on the 24MPO connector for single-mode fibers. The thermal aging test (85 °C, 336h) , the humidity test (65°C, 95%RH, 336h) and the temperature cycling test (-40 to +75 °C, 42 cycles). Figure 11 shows the results. The loss changes were less than 0.3dB during the tests.
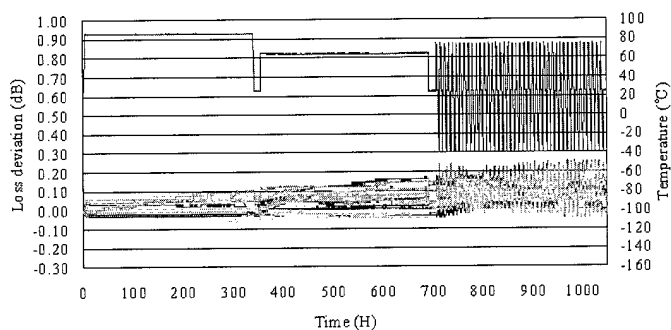
Figure 11. Environmental test result of 24MPO connector

7. Conclusion

A high fiber count MT type connector with 2-D fiber arrangement was successfully developed. This 2-D array MT connector features a maximum fiber count as high as 60, providing a connection density many times that of the original MT connector. Results of optical loss measurements and reliability tests for the 2-D array MT connector matches that of conventional single array MT in delivering good optical performance and connector reliability, besides enabling more throughput per connector. In addition, we have developed the 24-fiber MPO connector that has good optical and environmental characteristics. Thereby confirming the successful application of the 2-D array MT ferrule in the 2-D array MPO connector without using index matching materials.

Applications for the 2-D array MT connector includes connecting high fiber count optical cables as well as parallel optical interconnection and other high dense fiber systems.

8. References

[1] S. Nagasawa, et al. : Mechanically transferable single-mode multifiber connectors, IOOC'89, 21C2-1, pp.48-49 (1989)

[2] M. Takaya, et al. : Design and performance of very high-density multifiber connectors employing monolithic 60-fiber ferrule, IEEE Photo. Tech. Lett., Vol.11, No.11, pp.1446-1448 (November,1999)

[3] S. Nagasawa, et al. : A high-performance single-mode multifiber connector using oblique and direct endface contact between multiple fibers arranged in a plastic ferrule, IEEE Photo. Tech. Lett., vol.3, No.10, pp.937-939 (1991)

[4] Y. Ando: Trends in optical interconnection technologies and their impact on next-generation equipment packaging, NTT R&D Vol.48, No.3, pp.271-280 (1999)

[5] K. Takizawa, et al. : MT-RJ optical connector, 48th IWCS, pp.324-331 (1999)

Authors

Tatsuya Ohta
Fujikura Ltd.
1440, Mutsuzaki, Sakura, Chiba 285-8550, Japan

Tatsuya Ohta received his B.E. and M.E. degrees in mechanical engineering from Shinsyu University in 1994 and 1996. He joined Fujikura Ltd. in 1996, and has been engaged in the design and development of optical fiber connector. He is now a research and development engineer in Cable Network Components Division.

Kazuhiro Takizawa
Fujikura Ltd.
1440, Mutsuzaki, Sakura, Chiba 285-8550, Japan

Kazuhiro Takizawa was born in 1968. He graduated from Yokohama National University with an M.E. degree in 1993. He joined Fujikura Ltd., and has been engaged in the research and development in the Cable Network Components Division. He is a member of the IEICE of Japan.
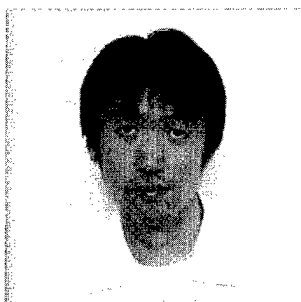
Akito Nishimura
Fujikura Ltd.
1440, Mutsuzaki, Sakura, Chiba 285-8550, Japan

Akito Nishimura was born in 1967. He joined Fujikura Ltd. after his graduation from Ibaraki University with an M.E. degree in 1992. He has been engaged in the research and development in the Cable Network Components Division. He is a member of the IEICE of Japan.
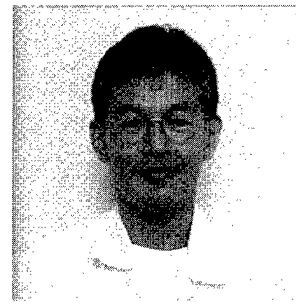
Toru Arikawa
Fujikura Ltd.
1440, Mutsuzaki, Sakura, Chiba 285-8550, Japan

Toru Arikawa is a manager of Research and Development Department in the Cable Network Components Division. He received B.E. and M.E. degrees in image science engineering from Chiba University in 1982 and 1984, respectively. He joined Fujikura Ltd. after his graduation.

Yasuhiro Tamaki
Fujikura Ltd.
1440, Mutsuzaki, Sakura, Chiba 285-8550, Japan

Yasuhiro Tamaki was born in 1955. He received a B.E. degree in mechanical engineering in 1977 from Saitama University. He joined Fujikura Ltd. in 1982. He is now a general manager in Research and Development Department in the Cable Network Components Division and a member of the IEICE of Japan.

An Analysis of Optimization of Mass Fusion Splicing of
Non-zero Dispersion Fiber Ribbon

Makiko Miura, Masakazu Nakano, Keiji Mitsumori
Lucent Technologies Yazaki Ltd.
1157-106 Hotozawa, Gotemba-city, Shizuoka-Pref., 412-0046, Japan
+81-550-89-7174 · miura@lt-y.co.jp

Abstract

In the Japanese fiber optic network, the splicing density is very high because the typical cable segment is very short. This means that low average splice loss is important for constructing long haul networks, and carriers have considerable interest in minimizing fiber splice loss, especially for non-zero dispersion fiber (NZDF) because Japanese telecommunications carriers have recently begun installing NZDF cable for their new long haul network construction. Since the most commonly used cable structure in Japan is either a 2, 4, or 8-fiber ribbon slotted core cable, the cable segments are almost always joined using mass fusion splicing. One of the factors affecting splice loss is the mode field diameter (MFD) at the splice point following fusion. By analyzing measurements of the MFD at the splice point we optimized the mass fusion splicing program for fiber and obtained splicing performance to be similar to that of G.652 fiber ribbon.

Keywords

Mass fusion splicing program; Non-zero dispersion fiber; Fiber geometry.

1. Background

Although still lagging behind the U.S. and most of Europe, there has nevertheless been a rapid growth of bandwidth requirements in Japan. In order to support this need for bandwidth Japanese carriers have begun installing DWDM transmission equipment. Although both G.652 and G.655 (and to a very limited extent G.653) fibers can be used with the current generation of commercial DWDM transmission equipment, a general consensus has arisen in Japan that for 10 Gb/sec and the next generation of 40 Gb/sec systems, reduced slope G.655 fiber is the superior choice of fiber for new installation. The advantages of G.655 fiber are primarily due to its chromatic dispersion characteristics. However, these characteristics are created by somewhat more complicated index of refraction profiles than that of standard matched clad G.652 fiber. Also, the MFD of most G.655 fibers are slightly smaller than G.652 fiber. Consequently, there has been some concern that the NZDF fusion splice loss might be significantly higher than for G.652 fiber. Further exacerbating the concern is the unfortunate (from the point of view of optical attenuation) fact that in Japan, the typical fiber optic cable segment is very short (1km to 1.5km) resulting in a large number of splices

relative to what is typically seen in North America. This is the reason why splice loss reduction is particularly important.

The standard cable structure in Japan for fiber counts up to 1000 fibers is a single slotted core structure with 4 or 8-fiber ribbons. Consequently mass fusion splice is almost always used for joining cable segments during field installation, although occasionally cable segments are joined with multifiber connectors. Because it is readily available and provides generally acceptable splice loss, the splicing program for dispersion shifted G.653 (DSF) fiber (standard DSF mode) is usually used for NZDF ribbon splicing. The authors have previously reported an average mass fusion splice loss of 0.055 dB at 1550nm using standard DSF mode in the laboratory [1].

In this paper we report on the optimization of mass fusion splice condition for NZDF ribbon by analyzing the fiber geometric parameters and we show that the splice loss of reduced slope NZDF can be made comparable to that of standard G.652 fiber.

2. NZD-Fiber characteristics and ribbon geometry
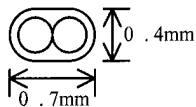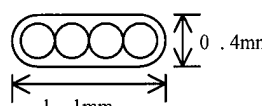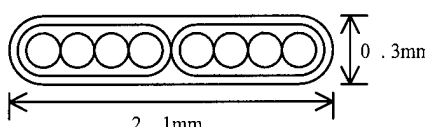
Table 1 shows the optical and geometric characteristics of our chosen NZDF. We chose to study this fiber because it is currently the most widely deployed type of NZDF, not only in Japan, but worldwide. Table 2 shows the geometry of typical encapsulated ribbon used in Japan.

Table 1. Reduced slope NZD-fiber characteristics

Parameter	Value
MFD at 1550nm	8.4+/-0.6 µm
Cladding diameter	125+/-1.0 µm
Core/clad concentricity error	≤ 0.6 µm
Cladding Non-circularity	≤1.0 %
Chromatic dispersion (C-band)	2.6 to 6.0 ps/nm-km
Chromatic dispersion (L-band)	4.0 to 8.9 ps/nm-km
Dispersion slope at 1550nm	≤ 0.05 ps/nm²-km
Typical attenuation at 1550nm*	0.202 dB/km
Typical attenuation at 1625nm*	0.208 dB/km
ITU-T Category	G.655 Example 3

*Typical attenuation after cabling

Table 2. Fiber ribbon geometry

Ribbon type	Ribbon dimensions
2-fiber ribbon	0.4mm 0.7mm
4-fiber ribbon	0.4mm 1.1mm
8-fiber ribbon	0.3mm 2.1mm

3. Analysis of the relationship between splice loss and fiber geometry following fusion splicing

The fiber geometric parameters most influential for fusion splice loss is the difference in MFD between the 2 fibers (ΔMFD) and the mode field eccentricity. A simple relationship between MFD mismatch and single-mode fiber splice loss can be expressed as: [1]

$$Loss_w[dB] = -10\log\left[\frac{4w_T^2 w_R^2}{[w_T^2 + w_R^2]^2}\right] \qquad (1)$$

Where W_T is the mode field radius of transmitting fiber and W_R is the mode field radius of receiving fiber.

This theoretical relationship is based on the fiber geometry before splicing and assumes that the splicing process causes minimal perturbations to the index profile of the fiber. While this formula has been shown to apply to non-dispersion shifted single mode fiber (G.652) as will be shown later, it cannot be simply applied to NZDF which has a more complex index profile (i.e. dopant concentration profile) and is more susceptible to mode field perturbations during splicing. Given the difficulties inherent in deriving a theoretical relation between initial MFD mismatch and splice loss for mass fusion splicing of NZDF, we first investigated this relationship for single fiber splices.

3.1 Analysis of splicing with single NZDF

In mass fusion splicing, it is especially difficult to control some aspects of the process, such as the end face condition of the individual fibers, the angle of the fiber end face and the distance between the spliced fibers. Accordingly, we decide to study single

fiber splicing with NZDF in order to investigate the relationship between splice loss and fiber geometry after fusion splicing.

We first studied the effect of the splicing process on MFD and mode field eccentricity. We cleaved and respliced, at the cleave point and with the same orientation, fibers with three different values of MFD in order to exclude the effect of initial MFD mismatch and misalignment. We then cut the fiber at the splice point and measured the fiber geometry and mode field characteristics at the fiber end face using the far field scanning method. The splice loss was also measured using bidirectional OTDR.

Table 3. Variation range of splicing parameters

Parameter	Value
Arc duration	4 to 16 sec
Arc power	13 to 28
Pre-arc duration	0 to 0.1 sec
Gap between fibers *	11 to 34 μm
Z push distance	12 to 30 μm
Over lap distance	-10 to 30 μm
Time before pull	1 to 5 sec

*Actual value

As a result of this examination, we observed a change in the MFD and eccentricity following. The induced change in MFD at 1550nm varied with changes in fusion arc power and fusion arc duration, ranging from −0.09 to +3.38 μm. Also, the change was asymmetrical with respect to the left and right side of the spliced fiber. The eccentricity after splicing was observed to change −0.3 to +1.2 μm as compared to the eccentricity before splicing. We attribute these changes to the splicing process itself, because we spliced between the same fibers with the same orientation.

Figures 1, 2 and 3 show the relationship between the splice loss at 1550nm and mode field geometry imperfections following fusion splicing, such as ΔMFD, maximum eccentricity at the splice point (Eccentricity) and the MFD expansion ratio MFDe, where

$$\Delta MFD = \frac{MFD}{MFD_{Ave}} \qquad (2)$$

$$MFDe = \frac{MFD_A - MFD_B}{MFD_B} \qquad (3)$$

Where MFD_{ave} is average of mode field diameter of the transmitting fiber and the receiving fiber, MFD_A is the mode field diameter after splicing and MFD_B is MFD before splicing.
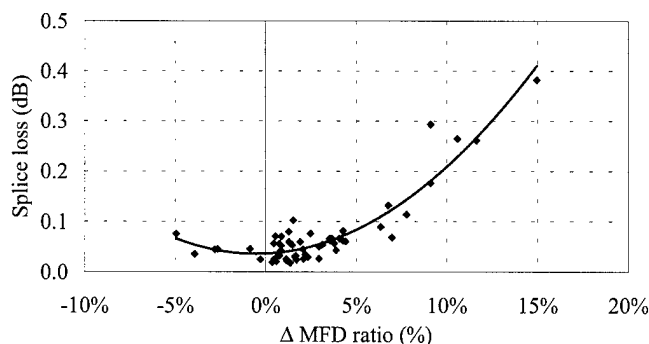
Figure 1. Correlation between ΔMFD ratio and splice loss at 1550nm
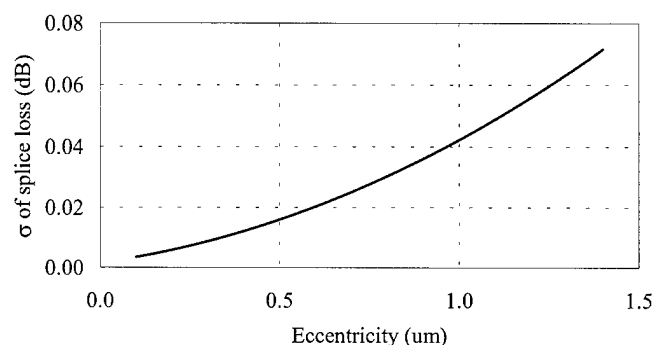
Figure 2. Estimated standard deviation of splice loss at 1550nm
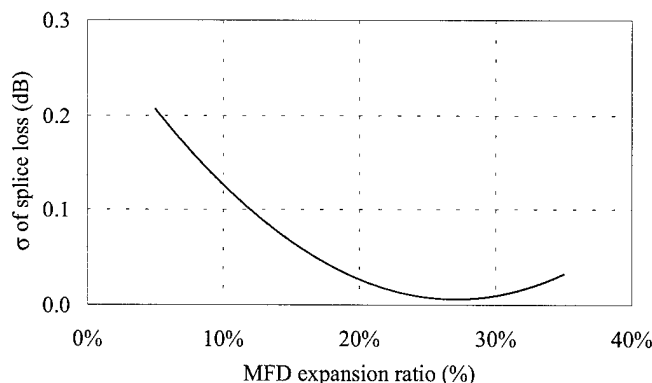
Figure 3. Estimated standard deviation of splice loss at 1550nm

As the result of our analysis, we see there is a correlation between ΔMFD ratio and the average of splice loss, while the eccentricity and MFD expansion ratio are correlated with the standard deviation of splice loss.

Although formula (1) provides reasonably accurate values for the splice loss in G.652 fiber, we find that it does not adequately

represent the splice losses in NZDF. In this case we need to develop a more accurate formula by combining equation (1) with a linear fit to the actual splice loss vs. theoretical loss, as shown in Figure 4.

$$Loss_w[dB] = 3.9\left\{-10\log\left[\frac{4w_T^2 w_R^2}{\left[w_T^2 + w_R^2\right]^2}\right]\right\} + 0.038 \qquad (4)$$
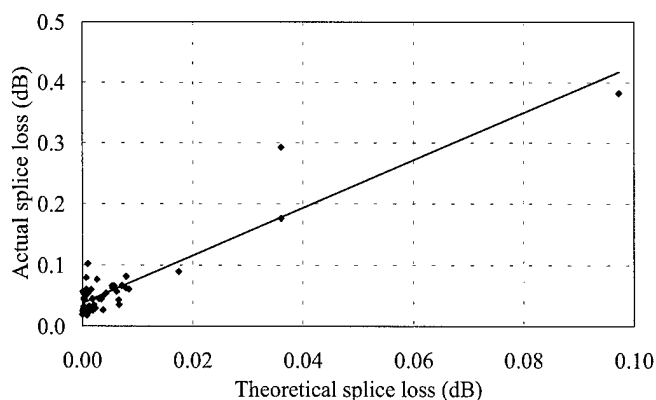
Figure 4. Correlation between actual and theoretical splice loss at 1550 nm.

We see from equation (4) that in order to obtain an actual splice loss at 1550nm of ≤0.1dB, the permissible range of ΔMFD ratio is ±6%. For a splice loss of ≤0.2dB, the permissible range of ΔMFD ratio is ±10%.

Table 4. Target values for low splice loss

Parameter	Specification
ΔMFD ratio at 1550nm	+/- 6%
Eccentricity	≤ 0.8μm
MFD expansion ratio at 1550nm	20 to 35 %

3.2 Optimization of the fusion splice conditions for single NZDF splicing

From the above results, we see that it is possible to reduce the splicing loss by controlling the fiber geometry parameters after fusion splicing to the ranges shown in Table 4. Table 5 shows the permissible range of each splicing parameter required to obtain the level of performance shown in Table 4. It is interesting to note that the final over lap distance and pre-arc duration showed no correlation between with the geometric parameters of the splice. In principle, this means it is possible to choose any value within the range, such as −10 to 30 μm in the final over lap and 0 to 0.1 seconds in the pre-arc duration.

Table 5. Summary of optimized conditions for Single NZDF splicing

Control factor	Optimized range	Total range
Arc duration (sec)	11 to 13	4 to 16
Arc power	20 to 27	13 to 28
Pre-arc duration (sec)	0 to 0.1	0 to 0.1
Gap between fibers (μm)*	27 to 34	11 to 34
Z push distance (μm)	12 to 30	12 to 30
Over lap distance (μm)	-10 to 30	-10 to 30
Time before pull (sec)	2 to 4	1 to 5

*Actual value

The most important splicing parameters were arc power and arc duration, both of which show a strong correlation with MFD expansion ratio. This is not surprising in that the fusion arc causes the diffusion of dopant elements in the core, such as Germanium etc. Figures 5 and 6 show this relationship.
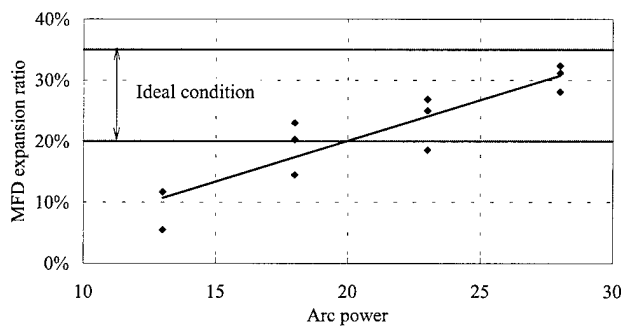
Figure 5. Correlation between arc power and MFD expansion ratio
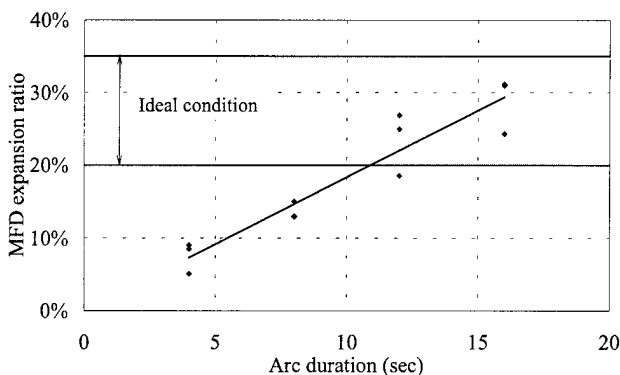
Figure 6. Correlation between arc duration and MFD expansion ratio

4. Mass fusion splicing

There are several factors contributing to the difference in performance seen between single fiber splicing and mass fusion splicing [4]. Among the more important factors are the end face gap variation and MFD expansion ratio caused by the variation in arc characteristics at each fiber position in a ribbon. One reason for this variation is that the outside fibers are closer to the fusion arc rod. Therefore, we expect more perturbation of the MFD in the outside fibers than inside fibers. However, the difference of MFD expansion ratio between the outside fibers and the inside fibers should be subject to modification by adjustments to the fusion arc power and duration. Figure 7 shows the correlation between fusion arc conditions and the difference ratio between the fiber location in the 4-fiber ribbon. In order to study these phenomena, we measured the geometrical parameters after fusion splicing each fiber in a 4-fiber ribbon. For this study we used 4-fiber ribbons containing the same fiber in each location. We have already seen from the results presented in Table 4 that it is important to control the MFD expansion ratio within a range of 20 to 35% in order to obtain low splice loss.
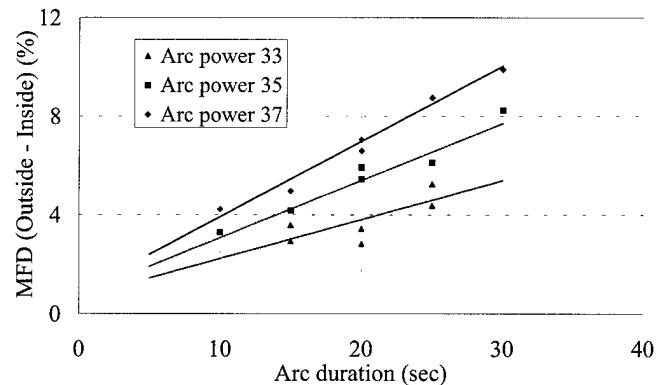
Figure 7. MFD difference of fiber position of 4-fiber ribbon

Next we investigated the relationships between the fiber geometric parameters after splicing and the fusion splice loss, and between the fusion splice conditions and fusion splice loss. We compared the results to the case of single fiber splice. Table 6 shows the splice condition we varied for this experiment. As mentioned before, these 4-fiber ribbons use the same fiber in each position in order to eliminate any initial MFD mismatch effect.

Table 6. Variation range of mass fusion NZDF splicing

Parameter	Value
Arc power	33 to 37
Arc duration	10 to 20 sec
Gap between fibers*	16 to 42 μm
Z push distance	15 to 25 μm
Final overlap distance	0 to 10 μm
Post arc duration	0 to 10 sec
Z push speed	150 to 350 μm /sec
Z Pull speed	150 to 350 μm /sec

*Actual value

A comparison of the theoretical curves shown in Figures 1, 2 and 3 with the actual splice loss of 4-fiber ribbon is shown in Figures 8, 9 and 10. The theoretical curves in these figures are calculated from the single splicing results. Figure 8 shows all the data for the case of Δ MFD ratio within +/-6%. It is impossible to find any significant relation between ΔMFD ratio and splice loss because the range of variation of the experimental conditions is too small. For the other geometric parameters, we obtained similar relationships as we did in the case of the single fiber splice analysis (Figures 9 and 10).
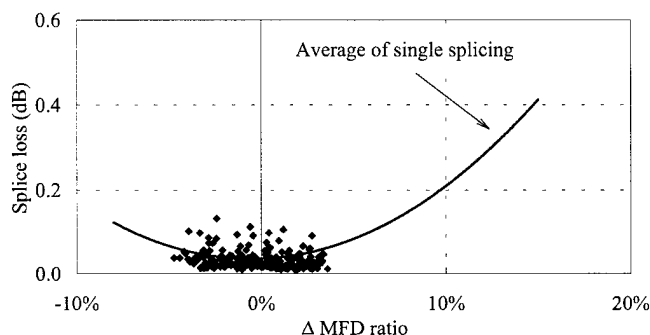
Figure 8 Correlation between splice loss at 1550nm and Δ MFD ratio
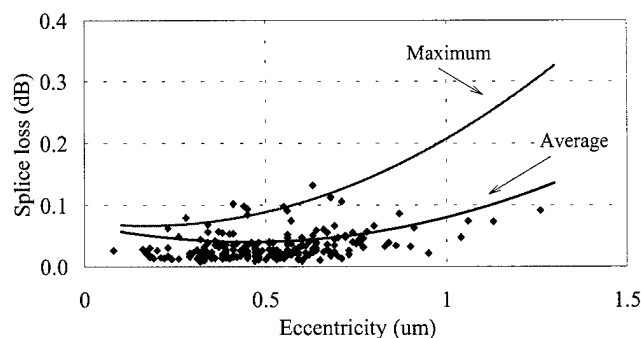
Figure 9. Correlation between splice loss at 1550nm and Eccentricity
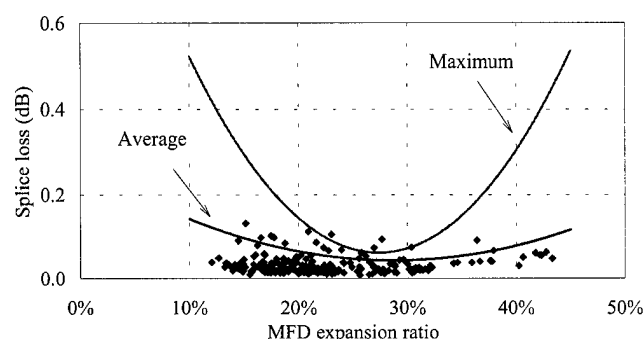
Figure 10. Correlation between splice loss at 1550nm and MFD expansion ratio

From Figures 8, 9 and 10, we see that the choices of arc power and duration need to be decided based on the number of fibers being spliced and their positions. Figure 11 shows the relationship between the fusion arc conditions and the MFD expansion ratio for the case of 4-fiber ribbon splicing. From the single splice results we saw that 20-35% is a permissible range for the MFD expansion ratio. From the mass fusion splicing results, we see that it is possible to choose an arc power from 34 to 40 with an arc duration of 20 seconds, and from 33 to 39 for an arc duration of 25 seconds and still meet the above criteria for MFD expansion range. In consideration of these results, we chose an arc power of 36 and an arc duration 25 seconds, close to the middle of the acceptable range of these parameters. Table 7 shows the results of the same analysis for other splicing parameters. Each splicing parameter was within the permissible range of optimizing for single NZDF splicing except arc power and arc duration. In the same way and by MFD expansion ratio base, we investigated the optimum arc condition for 2-fiber ribbon and 8-fiber ribbon. As the result, arc power 29 and arc time 22 seconds was suitable for 2-fiber ribbon and arc power 48 and arc time 20 seconds was suitable for 8-fiber ribbon.
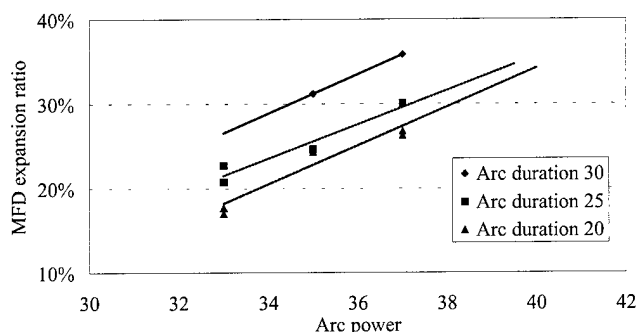
Figure 11. Correlation between arc power and MFD expansion ratio

Table 7. Summary of optimized condition

Splicing parameter	Ribbon splice			Single splice
	4-fiber	2-fiber	8-fiber	
Arc duration (sec)	25	22	20	11 to 13
Arc power	36	29	48	20 to 27
Pre-arc duration (sec)	0.1			0 to 0.1
Gap between fibers (μm)*	35			11 to 34
Z push distance (μm)	22			12 to 30
Over lap distance (μm)	0			-10 to 30
Time before pull (sec)	3			2 to 4
Z push speed (μm/sec)	150			
Z pull speed (μm/sec)	350			

*Actual value

5. Experimental evaluation of splicing program parameter optimization

5.1 Confirmation of performance improvements

To verify that an improvement in performance could be obtained with the optimized splicing program parameters, we performed completely random splicing of actual factory manufactured cable using both the optimized program and the standard DSF mode splicing program. Results are shown in Tables 8 and 9, and Figures 12, 13 and 14. As can be seen, we have significantly reduced both the actual splice loss and the standard deviation of splice loss for all ribbon types. In addition, we measured the 4-fiber ribbon splice loss

at 1625 nm and again found that the optimized program is significantly better than the standard DSF mode.

It should be emphasized that these results represent the results of a random selection of fibers whose MFD distribution is the same as that of the parent fiber distribution. We confirmed a statistically significant difference at a level of 99.996% of the two populations of splices (optimized condition and standard DSF mode) using the F-test method.

Table 8. Random splicing of 4-fiber ribbon (dB)

Splice program	Optimized program		Standard DSF mode	
Wavelength	1550nm	1625nm	1550nm	1625nm
Average	0.0418	0.0468	0.0638	0.0690
Median	0.0370	0.0420	0.0588	0.0615
σ	0.0302	0.0333	0.0457	0.0425
Maximum	0.155	0.154	0.345	0.366
Minimum	0.000	0.000	0.003	0.020
Fiber Count	96	96	96	96
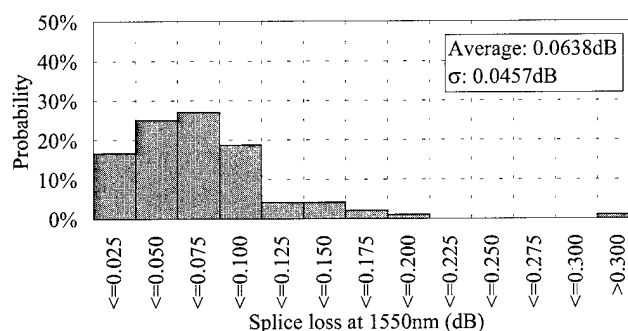
Figure 12. Standard DSF mode at 1550nm
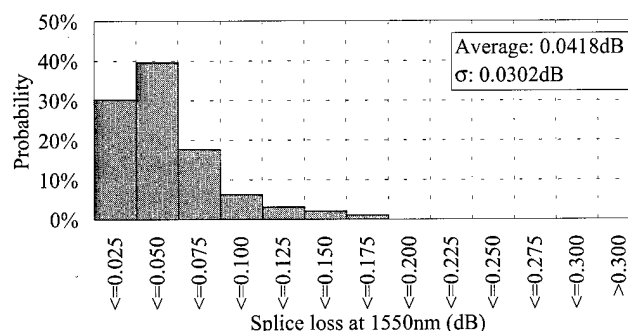
Figure 13. Optimized program at 1550nm
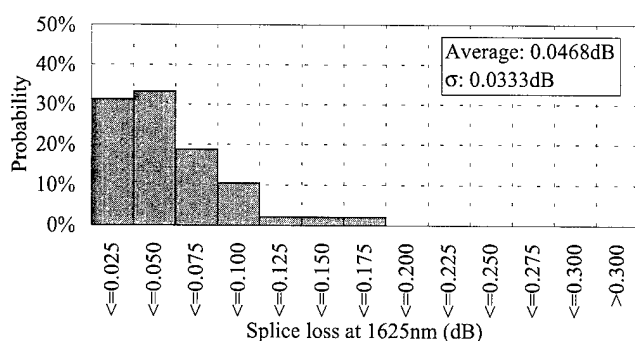
Figure 14. Optimized program at 1625nm

Table 9. Random splicing of 2 and 8 fiber ribbon at 1550nm (dB)

Splice program	Optimized program		Standard DSF mode	
Ribbon type	2-fiber	8-fiber	2-fiber	8-fiber
Average	0.0408	0.0585	0.0525	0.0772
Median	0.0340	0.0480	0.0463	0.0630
σ	0.0227	0.0347	0.0269	0.0525
Maximum	0.116	0.164	0.214	0.351
Minimum	0.014	0.013	0.014	0.031
Fiber Count	96	80	96	160

5.2 Simulation of total transmission loss performance of the network

Table 10 and Figure 15 show the results of a Monte Carlo simulations comparing network performance between the standard DSF mode and the optimized splicing program for an assumed span of 400km for 4-fiber ribbon. Results indicate a potential improvement of 6.5dB at 1550nm using optimized splicing program. In addition, the total loss at 1625nm using optimized program is lower than standard DSF mode performance at 1550nm.

Table 10. Estimate total loss of 400km span (dB)

Splice program	Optimized program		Standard DSF mode	
Wavelength (nm)	1550	1625	1550	1625
Average loss	92.940	97.091	99.363	102.915
Median loss	92.939	97.088	99.355	102.919
σ	0.506	0.560	0.735	0.735
Maximum	94.86	99.34	102.14	105.71
Minimum	90.97	94.98	96.82	100.04
Simulated points	10,000	10,000	10,000	10,000
Splice density (%) Ave.	12.940	14.062	18.569	18.923
Splice density (%) σ	0.445	0.470	0.586	0.562
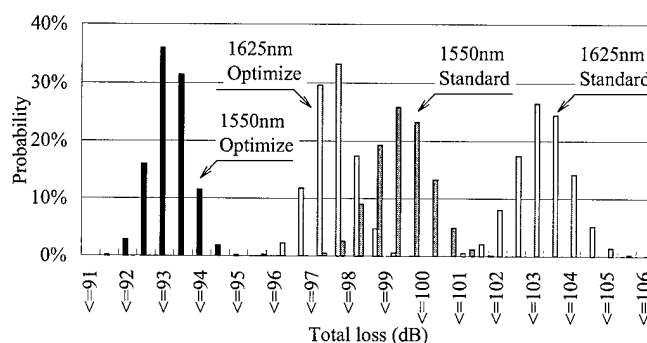
Figure 15. Simulated result of total loss of 400km span

5.3 Confirmation of simulation results

Table 11 shows the result of cut-back method measurements of transmission loss using actual factory manufactured cable. Splice spacing is less than 1 km. This result is consistent with the Monte Carlo simulation results.

Table 11. Total measured loss of sample cable

Wavelength		1550nm	1625nm	1310nm
Standard DSF mode	25km	7.08	7.13	11.43
	50km	13.90	13.90	21.90
	100km	27.50	27.50	43.70
Optimized program	25km	6.23	6.50	10.15
	50km	12.35	12.90	20.15
	100km	24.10	25.10	39.50

6. Conclusions

We studied the optimization of the splicing program for NZDF ribbon based on and analysis of fiber geometric parameters following splicing. We also investigated the relationship between the splice loss and both MFD imperfections and eccentricity introduced by the splicing process. Although the standard DSF mode provides acceptable splices with splice loss well within accepted Japanese and international standards, it is nonetheless possible to further reduce splice loss by controlling the ΔMFD ratio, eccentricity and MFD expansion ratio. The estimated difference in total network splice loss between the optimized splicing conditions and standard DSF mode splicing conditions is about 6.5dB at 1550nm. It needs to be emphasized that these results are from controlled laboratory conditions, and there is of course no certainty that these performance differences can be realized during field installation. In this we have presented results obtained using only one splice machine. However, we are able to improve the splicing condition from analysis fiber geometry after splicing for all current splice machines.

7. Acknowledgments

The authors are thankful to Wayne Lewis, Hideaki Mizuguchi and Yosuke Shimozuru for discussion and suggestion of technical issue.

8. References

[1] Masakazu Nakano, Makiko Miura, Hideaki Mizuguchi, "Development of slotted core cable using Nonzero-dispersion Shifted Fiber", 48th IWCS, 5 (1999)

[2] Stephen C. Mettler, "Monte-Carlo Analysis of the Effect of Mode Field Diameter Mismatch on Single-mode Fiber Splices", NFOEC (1992)

[3] Tomomi Sano, Tsutomu Watanabe, Keiji Osaka, "Analysis of Mass Fusion Splice Loss", 44th IWCS, 245 (1995)

[4] Stephen C. Mettler, Neil W. Sollenberger, Ken W. Jackson, "ADVANCES IN MASS FUSION SPLICE LOSS INCREASE OPTICAL FIBER CABLE INSTALLATION PRODUCTIVITY",45th IWCS, 221(1996)

AUTHORS
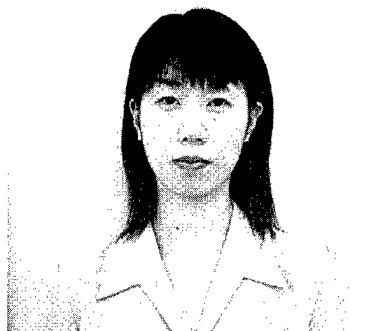
Makiko Miura

Lucent Technologies Yazaki Ltd.

1157-106, Hotozawa, Gotemba-city, Shizuoka-Pref. 412-0046 JAPAN

Makiko Miura received her B.E. degree from Akita University in 1997. She has been engaging in Research & Development Department and her main work is development of evaluation technology with optical fiber, ribbon and cable.

Masakazu Nakano

Lucent Technologies Yazaki Ltd.

1157-106, Hotozawa, Gotemba-city, Shizuoka-Pref. 412-0046 JAPAN

M.Nakano received his B.E. degree from Nihon University in 1991. He has been engaging in Research & Development Department and his main work is development of evaluation technology with optical fiber, ribbon and cable.

Keiji Mitsumori

Lucent Technologies Yazaki Ltd.

1157-106, Hotozawa, Gotemba-city, Shizuoka-Pref. 412-0046
JAPAN

K.Mitsumori received his B.E degree from Ehime University in
1993. He has been engaging in Research & Development
Department and his main work is design of optical cable.

Development of 24-Fiber Mass Fusion Splicer

Hiroshi Sugawara, Hiroshi Sato

Takeshi Sato, Shonosuke Yaguchi

Precision Instruments Research & Development Dept., Fujikura Ltd.
1440 Mutsuzaki, Sakura, Chiba, 285-8550, JAPAN
+81 43 484 3963 · hsugawar@opt.fujikura.co.jp

Abstract
Cables with 24-fiber ribbon have become common. Up to now, a mass fusion splicer could only splice 12-fiber ribbon simultaneously. To meet the demand of high fiber count cables with 24-fiber ribbon a new splicer must be developed. There are two major technical problems to overcome when developing a 24-fiber ribbon mass fusion splicer. First, the air gap distance between electrodes is very large. The arc produced creates an uneven distribution of temperature across all fibers. The results are "hot" and "cold" regions resulting in poor splice loss distribution. Secondly, difficulty of designing a compact and reliable 24-fiber ribbon observation system. If the splicer has the same optical magnification as present mass fusion splicers for accurate image processing, a field mechanism would be required to view all the fibers. The splicer's size would be larger due to the additional field mechanism assembly. Also, adding such an assembly would add an extra motor and more moving parts, thus reducing reliability. The newly developed 24-fiber ribbon mass fusion splicer provides the solution of these two problems.

1. Introduction
In recent years, the demand for high fiber count cables has increased substantially. To meet these needs, and in order to make cables simple and compact, cables using 24-fiber ribbon have become common [1]. Initially, these cables contained up to 432 fibers, but recently, 864 fiber count cables have been deployed [2]. Present mass fusion splicers can splice a maximum of 12 fibers [3]. Therefore, it was necessary to separate 24-fiber ribbons into 12-fiber sub-units [4]. This practice is inconvenient, time consuming, and requires storage for twice as many mass fusion splices in the splice closure. As the cable fiber counts have increased to 864, this situation has become progressively less acceptable. Today's field conditions still require a mass splicer that is small, fast, robust. It is also expected to work in less than perfect field conditions. Accordingly, we have developed a new mass fusion splicer capable of providing low loss splicing of 24-fiber ribbons with compact and reliable design for the field use.

2. Arc Discharge Surroundings

2.1 Design for 24-Fiber Ribbon Splice
When splicing 24 fibers simultaneously with low splice loss, it is necessary to distribute adequate heat across the entire 24-fiber array. A 24-fiber ribbon requires a much larger electrode gap than that of the present mass fusion splicer for 12-fiber ribbon. Unfortunately, this alternation causes three problems. One problem is that the present high-voltage arc discharge unit lacks sufficient output power to provide enough heat. Therefore, we have developed a new high-voltage arc discharge unit that produces twice the amount of power as the discharge unit used in a 12-fiber splicer. This has been accomplished in a production package the same size as the arc discharge unit used in the 12-fiber ribbon splicer. This small arc generation circuit meets one of the requirements that allow the creation of a compact and practical 24-fiber splicer.

The second problem that arises from the wide electrode gap is the heating distribution imbalance in the discharge area across 24-fibers. Figure 1 illustrates the various isothermal regions produced from the wider electrode gap. As shown, the proper isothermal region is insufficient in length to support 24-fiber splicing. Hence, the wider electrode gap results in a heating imbalance across the 24-fibers even with careful selection of the electrode position relative to the fibers is made. In order to solve this problem, the shape of the plasma arc has been deliberately curved and expanded by altering materials and components that are in proximity to the plasma field. By positioning the proper materials within the plasma field, it is possible to achieve the correct isothermal heat distribution across the entire 24-fiber array, as shown in Figure 2.

The third problem with the wider electrode gap is potential instability of the shape of the arc discharge. As the gap between the electrodes increases, the plasma arc shape becomes more sensitive to external factors. The route or shape of the plasma field of ionized air can more easily be disturbed by factors such as wind or electrode contamination. The new splicer has features

to neutralize these factors. For example, the splicer has an advanced wind protector design to eliminate the influence of external air movement, even in the presence of high wind. In addition, special fiber V-groove clamps are utilized which fix the shape of the arc to avoid the effects of other adverse influences.
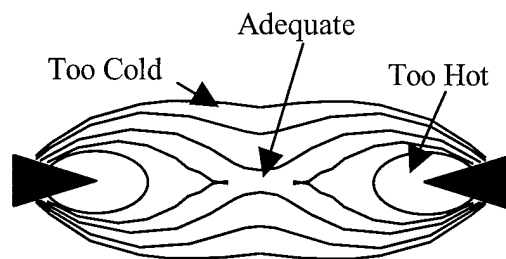
Figure 1. Straight Arc Discharge with Wide Gap
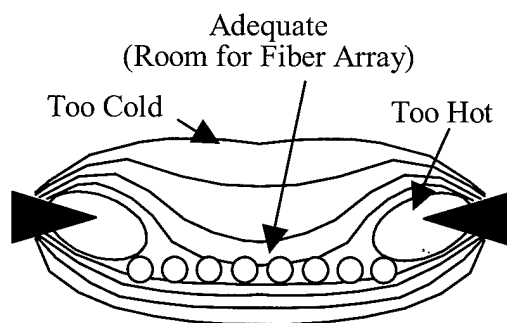
Figure 2. Curved Arc Discharge with Wide Gap

Figure 3. Melt Back Measurement
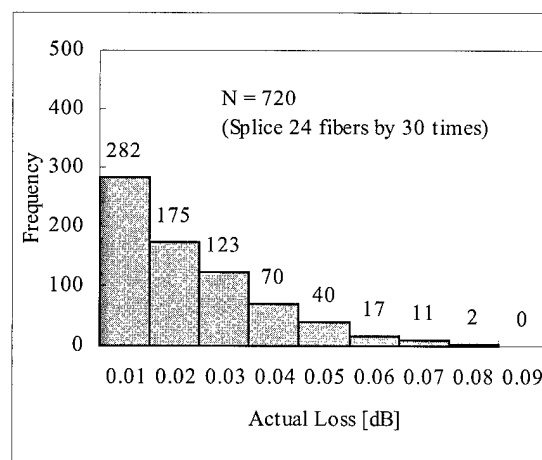
Figure 4. Splice Loss Results (SMF-SMF)

3. Observation System

3.1 Requirement
In order to build a small splicer with very good reliability in harsh field conditions the observation system should be small with no moving parts. Therefore, the splicer should observe 24 fibers simultaneously. The most desirable observation system would incorporate as much magnification as possible. However, available CCD image sensors are small and there pixel density is limited, therefore they cannot observe 24 fibers simultaneously if the optical magnification is high. Linking two CCD cameras together in each observation axis creates a complex and large optical system. Hence, in order to achieve a small observation

2.2 Performance of 24-Fiber Ribbon Splice
The temperature distribution across the 24-fiber array can be analyzed by measuring the melt back amount of the fibers. Figure 3 shows the fiber image that is produce after a melt back test is performed. The melt back test results with the new 24-fiber splicer are within the acceptable melt back range established for splicing 12-fiber ribbon. As a result of establishing the correct isothermal region, it is possible to achieve splice losses consistently below 0.08dB as shown in Figure 4.

system in a compact splicer, the optical magnification must be slightly less than optimal. The advantages of selecting a one per axis CCD system are its compact size, durability, and processing speed.

3.2 Design

In order to observe the fibers precisely without high magnification, minimal distortion of the fiber image is required. If the distortion is low, image-processing software can use the wide area image as valid and accurate data. There are two major causes of fiber image distortion that should be considered. One is a lack of precision in the lens elements. The second source of image distortion is uneven strength or direction of the illumination light. This is important because the image processing software can only use the gradation of the fiber image light-intensity profile as data. Due to the wide observation area of the 24-fibers (which is roughly 4 times the size of the 12-fiber image area), it is necessary to develop an improved light source to provide even distribution of light over the entire fiber array. The light source consists of a LED and a large diameter lens. The observation system structure is shown in Figure 5. As the result of this development, precise observation of all 24 fibers is achieved with a simple and compact observation system.
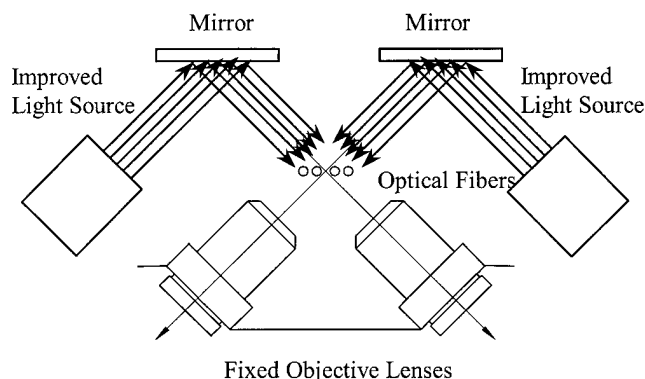
Figure 5. Observation System Design

3.3 Splice Loss Estimation Result

The estimation algorithm in the 24-fiber splicer uses cladding axis offset to determine loss estimations. Poor core/clad eccentricity in the past was the major reason for estimation inaccuracies. Today, telecommunication grade optical fiber is produced with minimal core/cladding eccentricity. With improvements in core/clad eccentricity, loss estimation using cladding axis offset becomes feasible and accurate. The second major contributor to poor estimation accuracy is core deformation. Luckily, core deformation trouble can be avoided with warnings before splice, such as cleaved angle alarm or large fiber axis offset alarm.

Figure 6 shows the difference between estimated and actual splice loss resulting from the new optical system when splicing SMF-SMF. In this test, axis offsets of left and right fibers before splice were increased to check the estimation performance of the splicer.
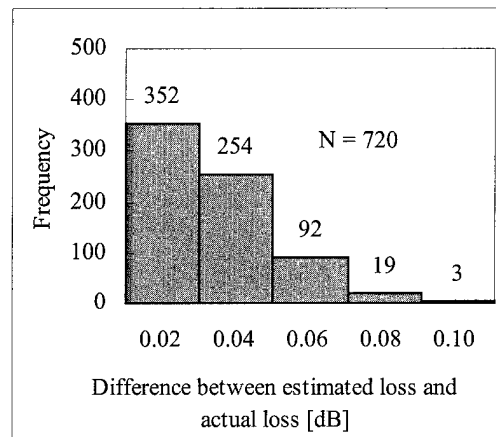
Figure 6. Estimated vs. Actual Loss (SMF-SMF)

4. Conclusions

We have developed a new mass fusion splicer capable of splicing 24 fibers with low loss. The compact arc circuit and the observation system allow the splicer to be lightweight and small, which is ideal for field use. The simultaneous observation of all 24-fibers provides very fast splicing time. Productivity for field splicing is also enhanced by the elimination of the need to separate 24-fiber ribbons into 12-fiber sub-units. This also allows for increased splice storage density in splice closures. As fiber counts in optical cables continue to increase, the use of 24-fiber ribbons will come into even greater use. Therefore, the productivity benefits of 24-fiber splicing will be increasingly valued. This new mass fusion splicer meets these challenges.

5. References

[1] David Gibson, Howard Kemp, Kris Kathiresan, Ruben Travieso, Greg Karl, George Mackie, "Field Deployment and Test Results for High Fiber Count Cables", Proc. of NFOEC '97, Volume 1, pp. 333-341.

[2] K.W. Jackson, N.E. Hardwick, M.D. Kinard, M.R. Santana, R. Travieso, "Optimal Design Strategies for Central Tube Ribbon Cables Comprising 864 Fibers and Beyond", Proc. of IWCS '99, pp. 118-126

[3] T. Kusayanagi, et al, "New Mass Fiber Fusion Splicer FSM-30R", Fujikura Technical Review, No.27, pp. 13-16.

[4] K. Konstadinidis, et al, "Optimization of Fiber Ribbon Sub-Unit Robustness by Means of a Lateral Matrix-To-Matrix Adhesion Gradient", Proc. of IWCS '99, pp. 66-71

Biography

Hiroshi Sugawara

Precision Instruments R&D Dept.

Fujikura Ltd.

1440 Mutsuzaki, Sakura, Chiba, 285-8550, JAPAN

hsugawar@opt.fujikura.co.jp

Hiroshi Sugawara received his M.E. degree in Electrical Engineering from Chiba University in 1995. He joined Fujikura Ltd. in 1995 and has been engaged in the research and development of optical fiber fusion splicers.

Shonosuke Yaguchi

Precision Instruments R&D Dept.

Fujikura Ltd.

1440 Mutsuzaki, Sakura, Chiba, 285-8550, JAPAN

syaguchi@opt.fujikura.co.jp

Shonosuke Yaguchi was born in 1955. He graduated in mechanical engineering from Keio University in 1979.

He joined Fujikura Ltd. in 1979 and has been engaged in the Plant Engineering Section for 12 years and currently is a general manager of the Precision Instruments R&D department.

Takeshi Sato

Precision Instruments R&D Dept.

Fujikura Ltd.

1440 Mutsuzaki, Sakura, Chiba, 285-8550, JAPAN

tsatoh@opt.fujikura.co.jp

He graduated in mechanical engineering from Chiba University in 1984.

He joined Fujikura Ltd. in 1984 and currently is an assistant manager of the Precision Instruments R&D department.

Hiroshi Sato

Precision Instruments R&D Dept.

Fujikura Ltd.

1440 Mutsuzaki, Sakura, Chiba, 285-8550, JAPAN

hsato@opt.fujikura.co.jp

Hiroshi Sato received his M.M. degree in Mechanical Engineering from Gunma University in 1993. He joined Fujikura Ltd. in 1993 and has been engaged in the research and development of optical fiber fusion splicers.

New High Durability Electrodes with Arc Stabilizers for Extended Service Cycles and Increased Performance

Bert Zamzow, Rainer Kossat
Corning Cable Systems, SCC SED
Munich, Germany
+49 89 722 - 35729 · bert.zamzow@corning.com

Marty Anderson
Corning Cable Systems
Hickory NC
+1 828 323 - 6808 · marty.anderson@corning.com

Abstract

Fusion splicing is used to join optical fibers with low splice loss, low reflection and long-term stability. One main quality criterion for splicing machines is the splice loss, which means that both the average loss and the deviation of all loss values have to be as low as possible.

One crucial point to achieve a constant splice performance is a stable fiber heating during the fusion process. Most common splicing machines use an electric arc discharge between two electrodes as a heat source. As the number of splices increases during operation, contaminants deposit on the electrode tips. This causes the fiber heating to become unstable with the time, resulting in a significant degradation of splice quality.

To achieve low losses constantly, regular electrode maintenance intervals are obligatory. However this is time consuming and decreases the splicing machine's effectiveness significantly.

This paper introduces a new type of electrodes with integrated arc stabilizers that guarantee constant fiber heating without any maintenance. These arc stabilized electrodes allow to extend maintenance intervals from about 500 to over 5000 splices, while ensuring constant low loss splice performance over the whole time.

Keywords

fiber; splice; loss; fusion; electrode; arc; stabilize; maintenance; heat

1. Introduction

The process of making a fusion splice consists of several steps. Except for the first and final steps, which are fiber preparation and splice protection, all other steps are performed by common automatic splicing machines without any operator interaction. After inserting the prepared fiber ends, the machine first aligns the fibers cores. When perfect alignment for an optimum light transmission through the splice is reached, the fiber heating process starts. After reaching the best temperature, the splicing machine applies an appropriate feed to the fibers [1] and melts them together. When the splice is finished, the heat is turned off and the splice loss is evaluated to make sure that the splicing process was successful [2].

The main criterion to consider a splice to be good is its loss. First of all a splicing machine should produce splices with a low average loss. This is the basic prerequisite that enables the machine to fulfill today's acceptance criterions for splice losses in optical transmission lines. But also the deviation of all splice losses has to be considered.

In addition to a low average loss a small deviation ensures that only a very few of all splices exceed the given acceptance criterion. So a small deviation level makes the splicing machine more efficient, because only very few splices need to be repeated.

Every commercial available splicing machine is designed for a certain range of applications. For the corresponding purposes nearly all machines deliver low losses and small loss deviations when they are brand new. But as the number of splices increases, the average loss and also the deviation of the loss values increase. In the next section this is investigated in more detail.

2. Change of Splice Loss with Operation

Figure 1 shows an example for the change of the splice loss distribution if a common fusion splicing machine is operated without any service procedure in between. Every 500 splices the splice losses of a set of 30 splices were measured by an OTDR. The resulting loss distributions after 500, 1000 and 1500 splices are shown in Figure 1.
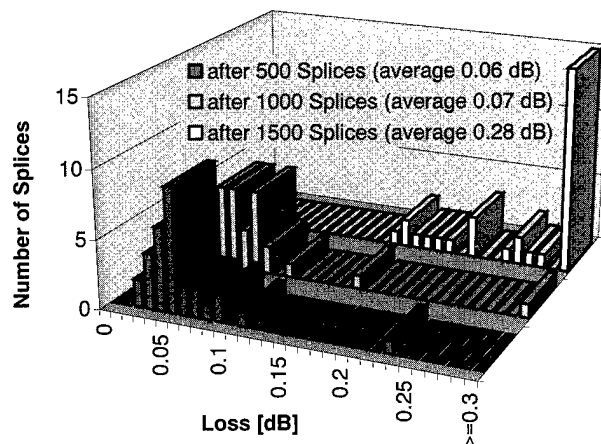
Figure 1: Change of Splice Loss Distribution

The average loss increases from 0.06 dB after 500 splices to 0.07 dB after 1000 splices. Together with the increase in deviation (standard deviation rises from 0.04 to 0.05 dB) this marks the beginning of splice quality degradation. After 1500 splices the average loss has already reached 0.28 dB together with a standard deviation of 0.08 dB. These values clearly show that the machine needs service immediately to continue operation in a reasonable way.

It is necessary to consider that the transition from an average of 0.07 dB after 1000 splices up to 0.28 dB after 1500 splices happens slowly and is overlapped by the increased variation of the single loss values. This means, the decision to service the machine if the splice results turn bad is dangerous, because this point is often recognized far beyond the point the losses get bad in average. Therefore it is essential to follow the recommended service cycles.

3. Reason for Splice Loss Degradation

To evaluate the reason for the growing splice loss in connection with an increasing number of splices it is necessary to have a closer look at the electric arc used by common splicing machines to heat the fibers. During the heating phase the arc burns between two electrodes. Figure 2 shows two pictures of one single electrode tip. The electrode has been used for more than 500 splices.
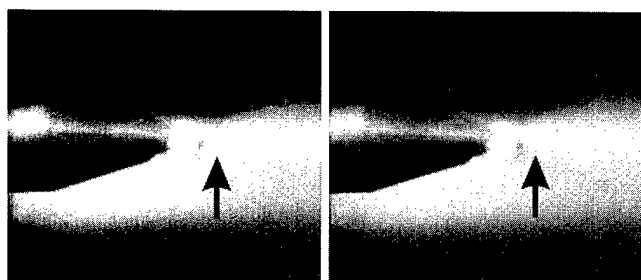
Figure 2: Spontaneous Change of Arc Emission

Both pictures show the electrode tip during fiber heating. The picture on the right was taken 80 ms after the left picture. The brightly glowing arc emission zone on the electrode tip is visible. The difference between the two pictures is that the location of the arc emission zone is shifted from the center of the tip to a position slightly above the tip. Such a position shift happens spontaneously and only with electrodes that have been used for a number of splices.
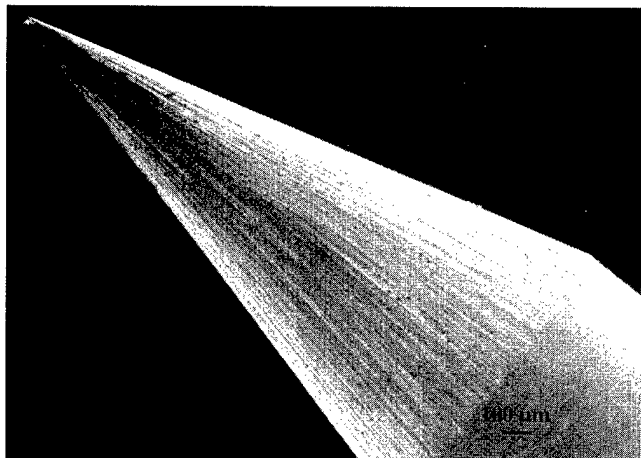
Figure 3: SEM-Image of unused Electrode

The changed location of the arc emission zone influences the whole fusion arc. The arc location varies slightly and as well does the arc intensity. Therefore the portion of the splice heated and its temperature are unstable during the splicing process. This instability

prevents the fibers from melting together in the desired optimum way. The final result is an increased splice loss as shown in Figure 1.

The reason for the spontaneous changes of the arc emission zone position are contaminants that deposit on the electrode tip with each splice. With an increasing number of splices, these contaminants begin to form a layer which covers the electrode tip surface. Figure 3 shows a scanning electron microscope image of an electrode tip that never had been used for splicing. The clean electrode surface structure without any deposits is clearly visible.
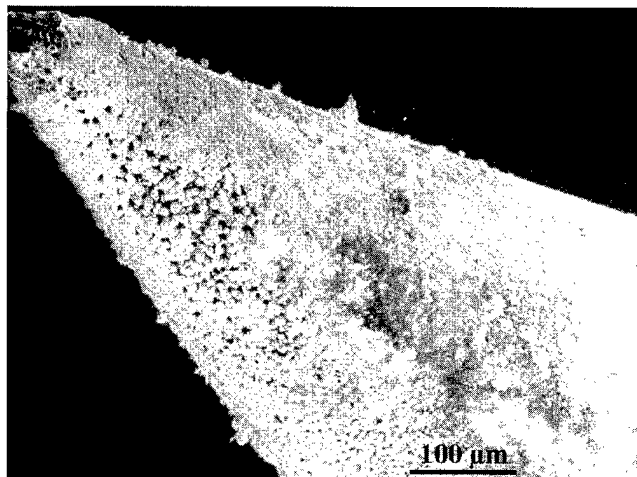
Figure 4: SEM-Image of Contamination Layer on Electrode

In contrast to that Figure 4 shows the tip of an electrode that was used for 200 splices. The surface is now covered by a porous contamination layer. It consists of small spheres that adhere to the electrode's surface.
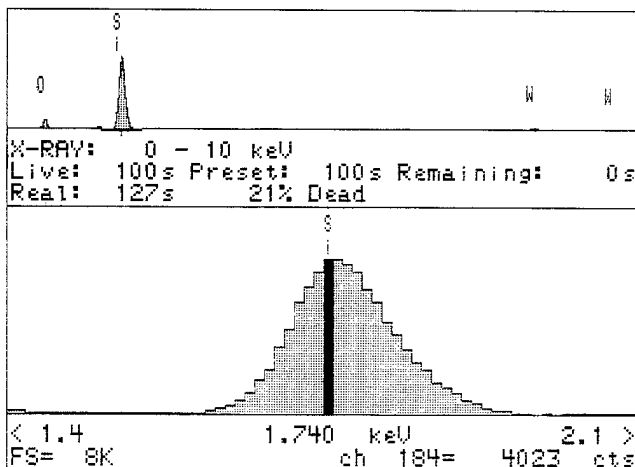
Figure 5: EDX Analysis of Electrode Contamination Layer

To find out the origin of this contamination layer its ingredients were examined by an energy dispersion x-ray analysis. The results are shown in Figure 5. The silicon and oxygen peaks identify silica

as the main component of the contamination layer. The small wolfram peaks are caused by the original electrode material.

This result suggests the following explanation for the origin of the contamination layer on the electrodes: The high temperature during the fusion process evaporates silica from the fiber surface. A part of this silica deposits on the electrode tips and forms a layer as the number of splices increases.

The silica deposit acts as an insulator, leading to randomly spaced low conducting regions on the electrode surface. Now the arc prefers the remaining high conductivity regions for emission. Because these regions are randomly spaced, very slight changes in arc emission conditions cause the arc to choose a more appropriate location to emit from. This results in the spontaneous variations of the arc emission location, as shown in Figure 2, with the consequences described earlier.

4. Avoiding Splice Loss Degradation

Up to now the only way to avoid splice loss degradation as shown in Figure 1 was to clean the electrodes on a regular basis. Before cleaning, the electrodes have to be removed from the splicing machine and afterwards they need to be reinstalled. Due to the time required, electrode maintenance decreases the machine's productivity.
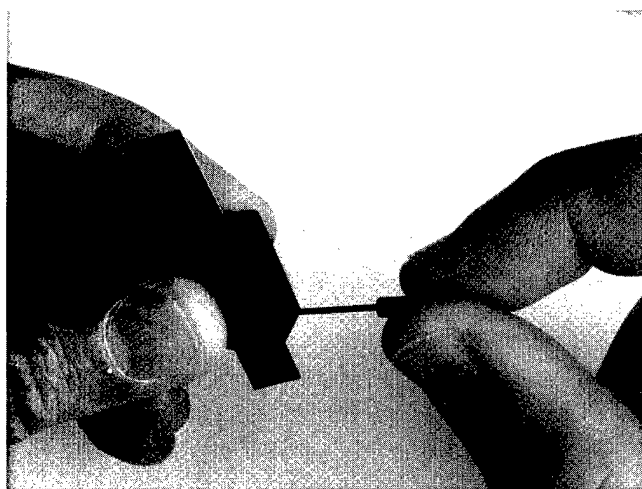
Figure 6: Common Electrode Cleaning Procedure

An additional point to be considered is that this maintenance operation is a manual process. Although various cleaning tools are available (see Figure 6), this means that the splicing machine operator needs training for removal, reinstallation, and cleaning of the electrodes. But even the best training can not prevent errors like insufficient cleaning, damage or pollution of the tips by bad handling, or incorrect reinstallation of the electrodes after cleaning. All this can lead to splicing results even worse than before the cleaning attempt.

This paper introduces a new electrode type for fusion splicers that eliminates the need for electrode maintenance and will solve all the problems related with it. The idea was to attach the fusion arc to a

fixed position by something that is far more insensitive to contaminant deposits than the electrode surface. The realization of this idea is shown in Figure 7.
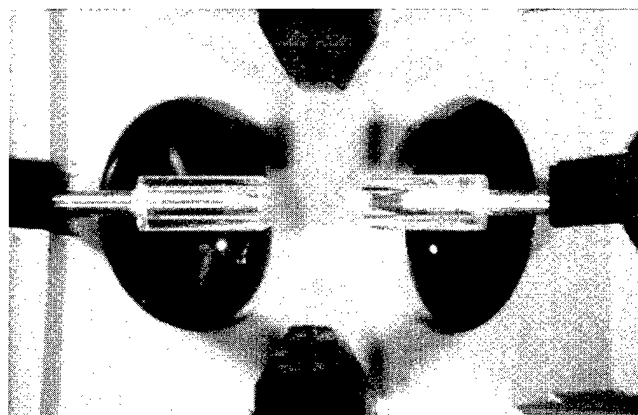
Figure 7: Electrodes Equipped with Arc Stabilizers

Figure 7 shows the arcing area of a commercial available fusion splicer. On the top and bottom of the picture a part of the v-grooves for holding the fibers is visible. In the center of the picture, in horizontal direction the electrodes are visible with the two lenses for fiber positioning behind them.

In contrast to normal fusion splicers, these electrodes are equipped with tubes on their tips. The well defined circular opening of each tube forces the emitting arc to stay in its desired position independently of any contaminant deposition on the electrode itself. So with the arc forced to stay in place also the fiber heating becomes stable and finally also losses become constantly low.

5. Arc Stabilization Effect

The arc stabilizing effect can be measured directly by the setup shown in Figure 8.
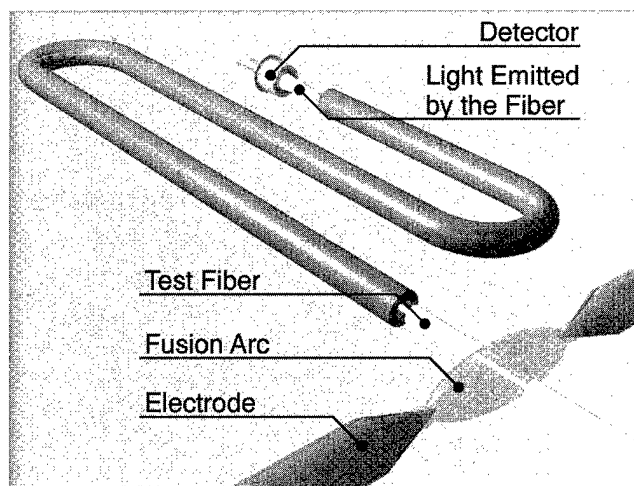
Figure 8: Light Emission Measurement Setup

A test fiber is heated by the fusion arc in exactly the same way as for normal splicing. Due to the high fiber temperature the fiber is beginning to glow and starts to emit light. A fraction of this light is

coupled into the fiber core and propagates along the fiber. This fraction of light can be measured by a detector diode at the end of the test fiber. The emitted light directly corresponds to the fiber temperature within the interesting range. Therefore the power level measured at the fiber end also directly corresponds to the fiber temperature. So this is a very easy method for monitoring the fiber temperature directly during the splicing process.

By this method the effect of the arc stabilizers was investigated. The measurement was repeated several times and the results are shown in Figure 9.
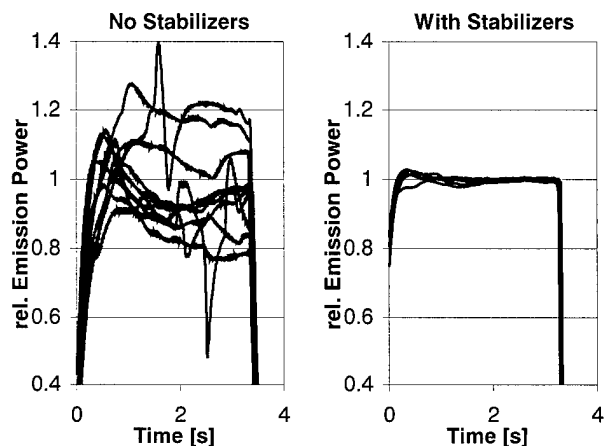
Figure 9: Arc Stabilization Measurement Results

The relative power variation of the emitted light is shown over the fusion time. On the left half of Figure 9 the results for worn standard electrodes are shown. It is obvious that there is a huge variation of the fiber temperature between the different repetitions of the measurement. Even during each single fusion process the temperature varies across a wide range. This reflects the unstable arc conditions that cause the high, varying loss values shown in Figure 1.

The right side of Figure 9 shows the test results for used stabilized electrodes. It is clearly visible that the temperature during each fusion process is nearly constant compared to standard electrodes. Also the temperature variation between all the fusion processes was significantly reduced. This shows already the positive effect of the arc stabilizers on temperature stability. But to make sure that this stable temperature will also lead to constant low splice loss results, more than 5000 splices with and without arc stabilizers were made and the results are compared in the next section.

6. Splice Test Results

6.1 Test Conditions
The main focus for this test was on how fiber heating stability influences the splice loss. Splicing of high eccentric fibers is exceptionally sensitive to unstable fiber heating, because when such fibers are fused together the surface tension tends to destroy the core to core alignment that was established prior to the fusion process. Normally the fusion process is tuned to minimize the consequences

of this self centering effect. But this compensation is only successful if the fiber temperature is very close to its desired value. Otherwise the compensation fails, the cores are unaligned and the splice loss significantly increases.

When splicing two eccentric fibers, the effective eccentricity depends on the coincidental orientation of the concentricity errors of both fibers. So to have a very strong sensitivity to fiber heating variations, the fibers for the tests were rotated to have a core offset of at least 1.3 µm.

After 500 and then after every 1000 splices the loss was measured for sets of 30 splices each. The splices were measured bidirectionally by an OTDR to obtain reliable results.

6.2 Test Results
The first set of splices was measured after 500 Splices. The recommended electrode cleaning service was ignored to investigate the influence of the contamination layer on the electrode tips. The corresponding results are shown in Figure 10.
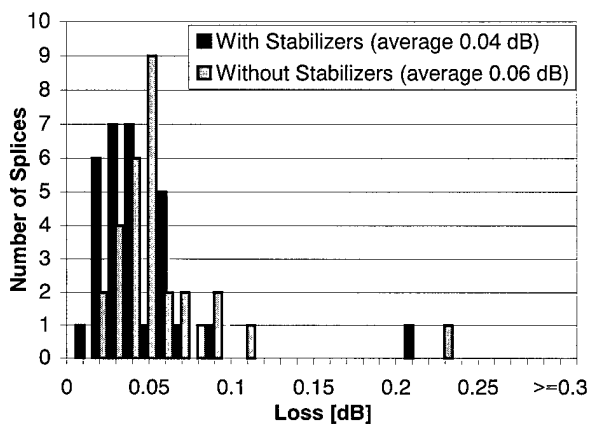
Figure 10: Splice Loss after 500 Splices

With standard electrodes the average loss of 0.06 dB was slightly higher compared to arc stabilized electrodes (0.04 dB). The standard deviation of the loss values did not differ significantly, it was 0.04 dB for both electrode types.

After 1500 splices without cleaning, the situation had changed completely as shown in Figure 11. Now the average loss for standard electrodes was 0.28 dB. Not one of the 30 splices was able to meet a reasonable acceptance criterion like for example 0.10 dB. This means that long before a number of 1500 splices is reached it does not make sense to continue splicing with such a set of electrodes.

However, with arc stabilized electrodes the situation looked completely different. Without any cleaning the average splice loss had only decreased slightly from 0.04 to 0.06 dB. The standard deviation had not changed at all and remains at 0.04 dB. The larger average loss was caused by the fact that 10 % of the 30 splices failed

to meet the 0.10 dB acceptance criterion. It will be explained later in this section how these bad splices are eliminated.

Figure 11: Splice Loss after 1500 Splices

Originally, it was planned not to clean the electrodes at all during the whole test. But after 1500 splices the operation of the standard electrodes was so poor (see Figure 11) that continuation of the test in this way would not have delivered any reasonable results for standard electrodes.

As a result the recommended electrode cleaning procedure was performed from then on. That means that after every 500 splices and also before the set of splices was measured the standard electrodes were cleaned as shown in Figure 6.

Additional tests have shown that the splice loss performance of the arc stabilized electrodes can be enhanced by the application of a cleaning arc every 500 splices. The obvious effect of this conditioning is the elimination of all splices that exceed 0.10 dB. The application of the cleaning arc can easily be integrated in the automatic fusion process control of common splicing machines and will be performed automatically without any user interaction. For the following tests the cleaning arc was applied every 500 splices and therefore also just before the set of splices was measured.

The results after 2500 splices with the appropriate cleaning procedures are shown in Figure 12. First of all the success of cleaning the standard electrodes is clearly visible. The average loss was reduced significantly and brought the splice losses back into a reasonable range. However the average loss of 0.08 dB is still twice as high as with arc stabilized electrodes. Also the standard loss deviation of 0.05 dB is significantly higher than that for arc stabilized electrodes (0.02 dB).

For the arc stabilized electrodes the positive effect of the cleaning arc is also visible in Figure 12. First, the average loss was reduced from 0.06 down to 0.04 dB. Second, splices exceeding the acceptance criterion of 0.10 dB were completely eliminated when the cleaning arc was used, as compared to Figure 11, when no cleaning arc was used.

Figure 12: Splice Loss after 2500 Splices

This performance is now maintained for up to 5000 splices as shown in Figure 13 to Figure 15.

Figure 13: Splice Loss after 3500 Splices

Figure 14: Splice Loss after 4500 Splices

Figure 15: Splice Loss after 5000 Splices

The Results in Figure 13 to Figure 15 show that the average loss for standard electrodes was slightly higher than for arc stabilized electrodes. The main reason for this was that approximately 13 % of all the splices failed to meet an acceptance criterion of 0.10 dB. For the arc stabilized electrodes only one of all measured splices failed the acceptance criterion, with 0.11 dB after 5000 splices. The standard deviation for standard electrodes fell into the range between 0.06 and 0.08 dB. With arc stabilized electrodes the small standard deviation of about 0.02 dB was reached.

Finally Figure 16 shows the splice performance over all measured splice losses. Only the measured set of the 30 splices for uncleaned standard electrodes after 1500 splices was ignored, because of their extremely poor performance.
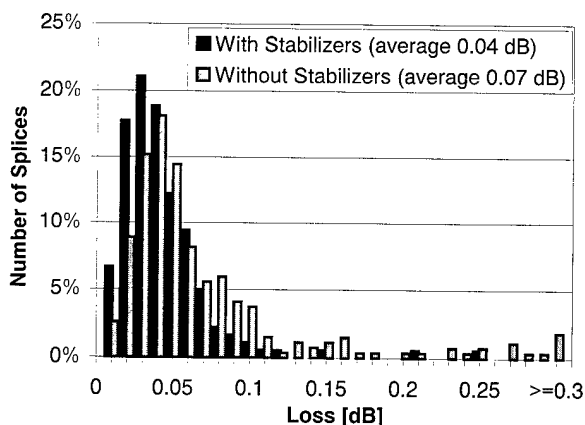
Figure 16: Splice Loss over all Splices

The average loss of 0.07 dB for standard electrodes was nearly twice as high as for arc stabilized electrodes (0.04 dB). The same is valid for the standard deviation which is 0.07 dB for standard and 0.03 dB for arc stabilized electrodes.

All the significant data for the measured splice losses is summarized in Table 1.

Table 1: Summary of All Splicing Results

Splices	Average Loss [dB]		Standard Deviation [dB]	
	Standard	Stabilized	Standard	Stabilized
500	0.06	0.04	0.04	0.04
1500	0.28	0.06	0.08	0.04
2500	0.08	0.04	0.05	0.02
3500	0.10	0.04	0.08	0.02
4500	0.08	0.03	0.06	0.02
5000	0.07	0.04	0.08	0.03
overall	0.07	0.04	0.07	0.03

7. Conclusions

This paper has introduced a new type of fusion splicer electrodes with integrated arc stabilizers. The results presented demonstrate that these electrodes provide a better splicing quality. They reduce by 50 % the average splice loss and also the standard deviation compared to standard electrodes.

Further, the results showed that standard electrodes need to be cleaned within the recommended cleaning cycles. Otherwise the splice performance decreases beyond reasonable limits. Due to the fact that electrode cleaning is a manual procedure the resulting cleaning quality is highly operator dependent. In addition it should be considered that the necessary electrode maintenance is omitted by some operators in an effort to achieve higher efficiency. The results also showed that this is a fallacy, because the increasing number of splices that fail the acceptance criteria due to contaminated electrodes will drive down efficiency even more.

In contrast to mechanically cleaning electrodes, the new arc stabilized electrodes are maintenance free. A cleaning arc, which is applied by the splicing machine automatically, is sufficient to ensure continued low loss splicing for over 5000 arcs. Because no operator interaction is necessary, the operator does not need training for electrode maintenance anymore.

8. References

[1] B. Zamzow, G. Ruegenberg, M. Anderson, H. Krupp, "High Quality Fiber Optic Splices and Significantly Improved Splice Loss Measurement Accuracy", *Proceedings of the Forty-Seventh International Wire and Cable Symposium*, pp. 854-863 (1998)

[2] B. Zamzow, G. Ruegenberg, M. Anderson, W. Knop, "Numerical Simulation of High Quality Fiber Optic Splices for High Precision Loss Evaluation", *Proceedings of the Forty-Eighth International Wire and Cable Symposium*, pp. 621-628 (1999)

Bert Zamzow graduated as an engineer of telecommunications. He received his degree as Diplom-Ingenieur from the Technische Universität Hamburg-Harburg. He joined the splicing machines development department at Corning Cable Systems (former Siemens Nachrichtenkabelnetze) in 1996. He is currently working as a project manager on next generation fusion splicers. Further on he is responsible for managing the software development process for splicing machines.

Rainer Kossat received his diploma in electrical engineering from the Fachhochschule in Munich in 1984. For a period of two years he was employed at the Department of Telecommunication at the Fachhochschule in Munich. Starting in 1986, he worked at Siemens AG on the design of fiber optic test equipment and optical CATV systems. Since 1991 he has been working on the development of fusion splicers. He is responsible for the development of new methods in arc fusion splice technology and optical measurement systems.

Marty Anderson received his Electrical Engineering degree from North Carolina State University in 1990. He joined Corning Cable Systems as a field engineer installing fiber systems in many applications. He has been in the Splice Equipment Product Line Management group for 5 years where he is currently manager for North and South American operations.

High Density Termination Cabinet for Optical Fiber Cable

Kansei Shindo, Hiroshi Furukawa, Yoshikazu Nomura, and *Makoto Saikawa

Cable Network Components Division, Fujikura Ltd.
1440 Mutsuzaki, Sakura, Chiba 285-8550 JAPAN
Phone: +81-43-484-3953
*Engineering Research and Development Division, Tokyo Electric Power Company
4-1, Egasaki-Cho, Tsurumi-Ku, Yokohama, 230-8510 Japan
Phone: +81-45-585-8853

Abstract

The termination cabinet for optical fiber cable has been developed with high density, compact, low cost, and high performance functions. We have developed a high density type termination cabinet for optical fiber cable capable of storing 2,500 fibers maximum within a dimension of 780 x 2300 x 350 mm (W x H x D) which allows maintenance on one side. The connection points in the optical module have an average insertion loss of 0.10 dB and a return loss of more than 45 dB. We have also developed optical splitter module connected to optical module through the optical patch cord. 8-branching type has an insertion loss of less than 11.7dB and a return loss of more than 40dB. 4-branching type has an insertion loss of less than 7.6dB and a return loss of more than 40dB. An important feature of the termination cabinet for optical fiber cable is that it can be customized for different types of optical fiber cable and network system. With this feature, fiber routing can be done efficiently within an optimum space.

Keywords

Optical Termination cabinet; Optical module; Optical splitter module; High density accommodation; Optical and environmental characteristics.

1. Introduction

Recent years have seen the rapid deployment of optical fibers in communication access and subscriber networks. Fiber interconnection and maintenance have become important issues in these networks. In such a situation, the termination cabinet for optical fiber cable has become indispensable for housing large numbers of optical fiber access points interfaced with optical connectors. To design a high density termination cabinet for optical fiber cable, it is necessary to develop a small accommodating area for the connecting fibers. These units provide modular storage for small number of fibers. In complex optical networks, it is possible to provide routing flexibility and efficiency using suitable optical module for different types of optical fiber cable and network system. A cabinet with optimum size can be designed easily to fit the various floors in a transfer office. In this paper, we describe the high density termination cabinet for optical fiber cable which allows maintenance on one side, followed by the structure and performance of optical module and storage unit for optical modules.

2. Design of Termination Cabinet for Optical Fiber Cable

We have successfully developed a termination cabinet capable of storing 2,500 fibers maximum within a dimension of 780 x 2300 x 350 mm(W x H x D). It is possible to add units of the optical module or units of the storage unit for optical modules. Height dimension of the termination cabinet for optical fiber cable depends on the number of storage units for optical modules. In this way, it becomes easy to design for optimal dimension according to each floor in the transfer office. Figure 1 shows the structure of the termination cabinet for optical fiber cable. Table 1 shows the specifications of standard types of termination cabinet.

(2400 Fibers Type)
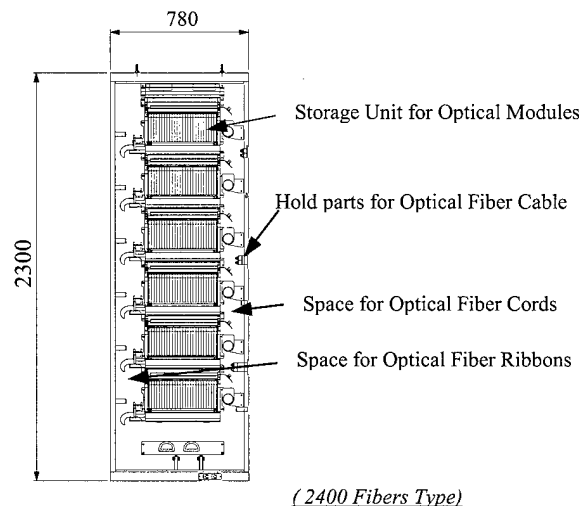
Figure 1. Structure of Termination Cabinet for Optical Fiber Cable

To realize high-density housing, optical fiber cables and the optical connectors needs to be packed tightly together. At the same time, sufficient space for routing the optical fiber cable must also be considered. Therefore it is important to reduce size of the optical module and manage the wiring route around the optical module to satisfy the above requirements. Details of the optical module and the storage unit for optical modules will be discussed further.

Table 1. Specification of High-Density Termination Cabinet

Item	Type for 2400 fibers	Type for 1200 fibers	Type for 800 fibers
Fiber capacity	2496 fibers	1248 fibers	832 fibers
Connector Type	SC2 connector	SC2 connector	SC2 connector
Optical modules capacity	156	78	56
Capacity of storage unit for optical modules	{ 26 modules) unit} 416 fibers		
Number of optical fiber cables	24	12	8
Optical fiber cord diameter	1.5mm	1.5mm	1.5mm
Size	Width 780mm Height 2,300mm Depth 350mm	Width 780mm Height 1,400mm Depth 350mm	Width 780mm Height 900mm Depth 350mm
Maintenance side	One side (Front only)	One side (Front only)	One side (Front only)

3. Structure of Optical Module

We have developed the optical module which is optimized for one side maintenance in the optical termination cabinet. The optical module is part of storage area for the connection part of the optical fiber cable and the optical fiber connector, and it may also store passive optical components.

Inside the optical module, there are 3 (three) parallel-divided storage areas, for the optical connectors, for fiber connection points and for a slide length of excess fiber.

The storage area for the optical connectors stores optical connector adapters and fiber ribbons with connectors.

The storage area for the fiber connection points stores the fusion splice points of optical fiber cables and optical modules.

The storage area for the slide length of excess fiber is a space for managing and storing slide length of excess fiber when the optical module is drawn in front during connection of optical fiber cords.
Installers can confirm the wiring condition inside the optical module, because it is divided with a semitransparent sheet between storage areas for fiber connection points and a slide length of excess fiber. Also, we have developed a cap for the optical connector adapter that can be handled by hand or a tool when the circuit is not in use.
There are 2 types of optical module, 16 fibers type and 20 fibers type. The 16 fibers type applies to 2 or 8 fiber ribbon optical fiber cable and the 20 fibers type applies to 4 fiber ribbon optical fiber cable. Therefore it is possible to accommodate different types of fiber ribbons in the slot structure of the optical fiber cable.
The standard optical module has SPC(Super PC polished) connectors for $10/125\,\mu$ single-mode fibers.
Figure 2 shows the structure of optical module.
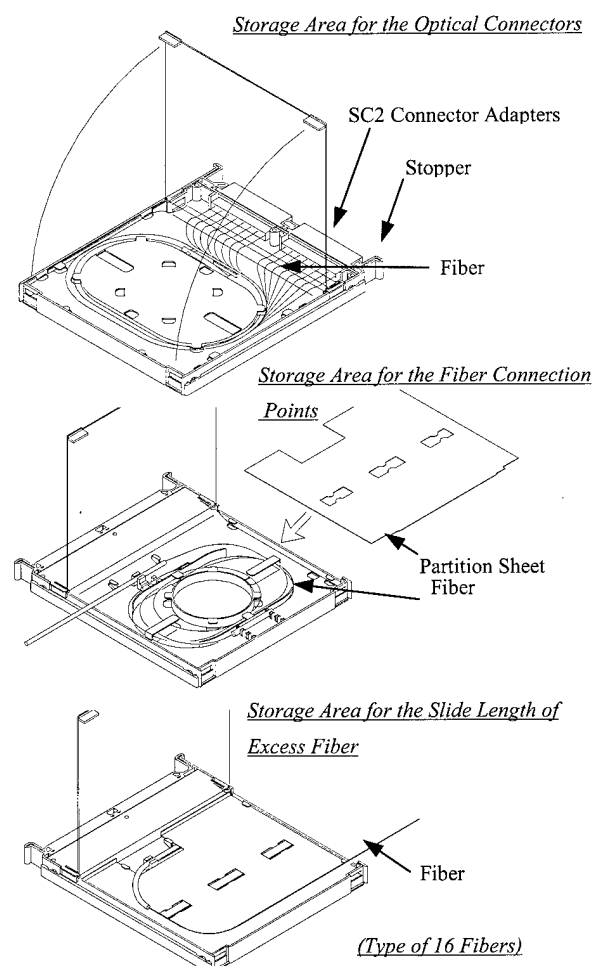
Figure 2. Structure of Optical Module

4. Structure of Storage Unit for Optical Modules

The optical modules are fitted vertically in storage units which are vertically stacked in the termination cabinet. Fiber ribbons from the distribution cable drop in from above into each module and are branched out at the front ends of the modules into connectorised fiber cords. Figure 3 shows the structure of the storage unit for optical modules.

An important feature of the storage unit for optical modules is the slide length method for managing excess fibers. The excess fiber length from above can slide automatically in or out of the slide length partition, when the optical module is push in or pulled out. The slide length is about 40 cm long. The storage unit for optical modules has a stopper, which can hold an optical module to a stand-by position, which can be re-engaged later. Using this structure, it is possible to do maintenance using the tool in a position fairly ahead from the storage unit. This advantage not only allows easy maintenance and working with optical fibers and connections, but provides high–level of circuit protection as well. The circuits in the other modules are not affected. Also, it is easy to take out individual optical fiber cord during maintenance because the wiring area of optical fiber cords has a structure that can be opened downward.

5. Performance and Reliability of Optical Module

We performed optical and environmental tests on the optical module. The results are summarized below.

5.1 Insertion Loss and Return Loss

Figure 4 and 5 shows the insertion loss result and return loss result of the optical module. The optical module samples were measured at a wavelength of 1.31 μ m. The module has an insertion loss of less than 0.30dB and a return loss of more than 45dB.
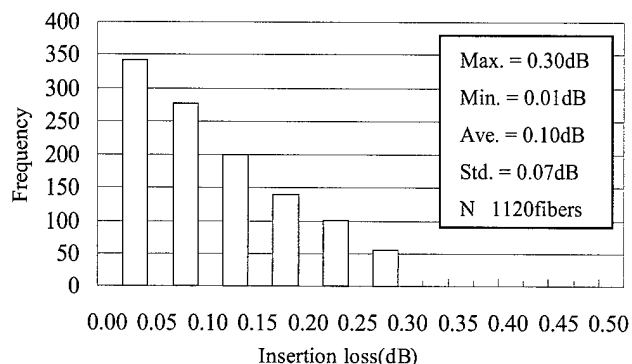
Figure 4. Insertion loss of Optical Module
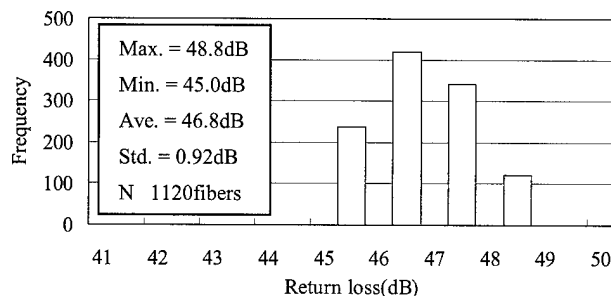
Figure 5. Return loss of Optical Module

Figure 3. Structure of Storage Unit for Optical Modules

5.2 Temperature cycling test

Figure 6 shows the result of the temperature cycling test. The insertion loss changes for optical module were measured every 20 minutes during a total of 3 cycles of temperature variation from –20 to 60 degrees. The optical module samples was measured at a wavelength of 1.31 μ m and 1.55 μ m. The loss changes during the test were well within 0.2dB.

Figure 6. Temperature cycling characteristics of optical Module

The Body of the Optical the Optical Splitter Modules

SC2 Connectors

Outside Cover

Inside Cover

Body

Contact Junction

Outside Cover

(2(1x8) Type)
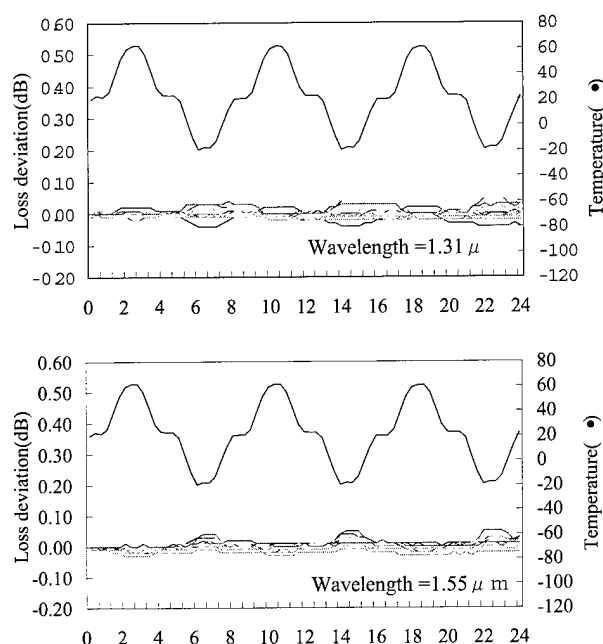
Figure 7. Structure of Optical splitter Module

6. Optical Splitter Module

We have developed the optical splitter module that is able to fit in the termination cabinet for optical fiber cable. The optical splitter module includes optical splitters and optical couplers, and is connected to the optical modules through optical patch cords.

6.1 Structure

Figure 7 shows the structure of the optical splitter module. The optical splitter module features an expandable body by stacking multiple segments to achieve the required number of splitters and connector ports. There are contact junctions between the individual segments to allow fiber linkage. Hence, the number of splitters required can be flexibly adjusted. The thickness of the module will depend on the required configuration and increases in steps of the thickness for each segment. The standard optical module has SPC(Super PC polished) connectors for $10/125\,\mu$ m single-mode fibers. Table 3 shows the types of optical splitter module.

6.2 Performance

We performed optical and environmental tests on the optical splitter module. The results are summarized below.

6.2.1 Insertion loss and Return loss

The optical splitter module samples was measured at a wavelength of $1.31\,\mu$ m. 8-branching type has an insertion loss of less than

Table 3. Various Types of Optical Splitter Module

Branchings	8		4	
Types of Splitter Module	$2(1\times 8)$	$4(1\times 8)$	$2(1\times 4)$	$4(1\times 4)$
Number of Input ports	2	4	2	4
Number of output ports	16	32	8	16
Module Thickness (No. of segment)	2	3	1	2

11.7dB and a return loss of more than 40dB. 4-branching type has an insertion loss of less than 7.6dB and a return loss of more than 40dB.
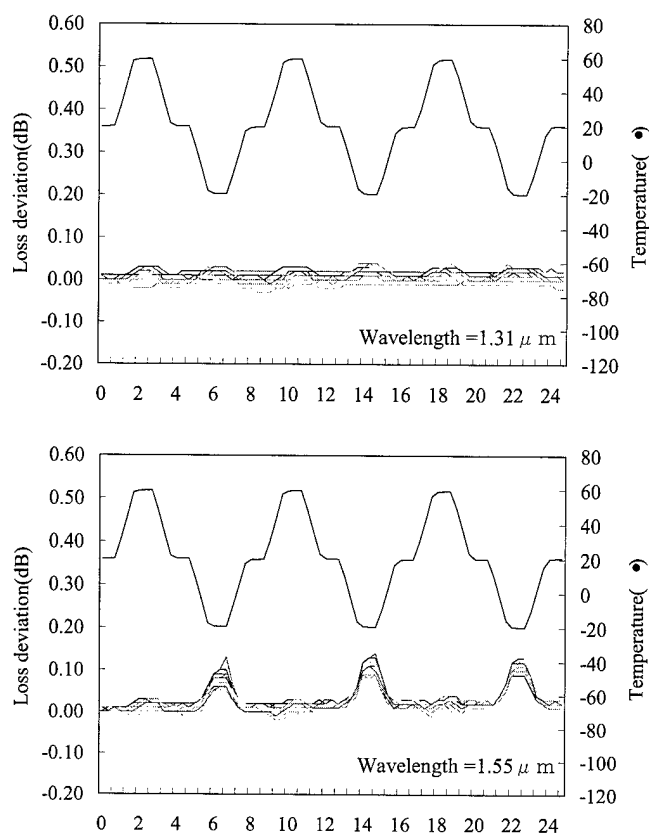
Figure 8. Temperature cycling characteristics of Optical Splitter Module

6.2.2 Temperature cycling test

Figure 8 shows the result of the temperature cycling test. The insertion loss changes for optical module were measured every 20 minutes during a total of 3 cycles of temperature variation from –20 to 60 degrees. The optical module samples was measured at a wavelength of 1.31 μ m and 1.55 μ m. The loss changes during the test were well within 0.2dB.

7. Conclusion

We have successfully developed the high density termination cabinet for optical fiber cable which allows maintenance on one side. The optical module has the characteristics incorporating compact, high density as well as wide working space when slid forward during maintenance of connecting optical fiber cable and optical fiber cords. Using this structure, we not only can achieve easy maintenance, but high-level of circuit protection as well. The circuits in the other modules are not affected.

Presently, we are developing various types of termination cabinets for optical fiber cable based on the structure of this optical module.

8. References

[1] Y. Ando: Trends in optical interconnection technologies and their impact on next-generation equipment packaging, NTT R&D Vol.48 No.3,pp.271-280(1999)

[2] K. Takizawa, et al. : MT-RJ optical connector, 48th IWCS, pp.324-331(1999)

Authors
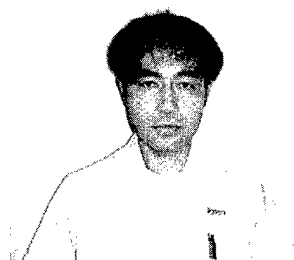
Kansei Shindo

Fujikura Ltd.

1440 Mutsuzaki, Sakura, Chiba, 285-8550, Japan

Kansei Shindo was born in 1969. He received the B.E.degee in mechanical engineering in 1992 from Tokyo University of Agriculture and Technology. He joined Fujikura Ltd. In 1992 and has been engaged in the research and development of telecommunication cable and accessories. He is now an engineer in the Cable Network Components Division
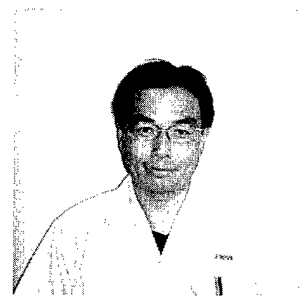
Hiroshi Furukawa

Fujikura Ltd.

1440 Mutsuzaki, Sakura, Chiba 285-8550 Japan

Hiroshi Furukawa was born in 1959. He received the B.E.degee in mechanical engineering in 1984 from Chiba University.

He joined Fujikura Ltd. In 1984 and has been engaged in the research and development of telecommunication cable and accessories. He is now a manager in the Cable Network Components Division.

Yoshikazu Nomura

Fujikura Ltd.

1440 Mutsuzaki, Sakura, Chiba 285-8550 Japan

Yoshikazu Nomura was born in 1951. He received the B.E.degee in mechanical engineering in 1975 from Shinsyu University.

He joined Fujikura Ltd. In 1975 and has been engaged in the research and development of telecommunication cable and accessories. He is now a general manager in the Cable Network Components Division.
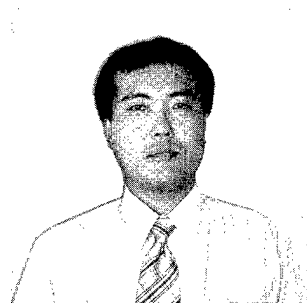
Makoto Saikawa

Tokyo Electric Power Company

4-1, Egasaki-Cho, Tsurumi-Ku, Yokohama, 230-8510 Japan

Makoto Saikawa was born in 1967. He received the M.E.degree in Physical Electronics in 1993 from Tokyo Institute of Technology.

He joined Tokyo Electric Power Company in 1993 and has been engaged in the research and development of telecommunications engineering. He is now an engineering staff of the Optical/Radio Waves and Electronic Technology Group in the Computer and Communications R&D center.

Improving the Abrasion Resistance of Insulated Wire Using Co-extrustion Technology

Ndiba Dioh and Jeff Borke

Equistar Chemicals, LP
Cincinnati, OH
+1-513-530-4313 · ndiba.dioh@equistarchem.com

Abstract

An experimental analysis is presented which shows that poor needle abrasion performance of thin wall insulated cables is largely due to a tearing mechanism which ultimately results in rapid wear. The data presented indicates that prolonging the onset of the tearing mechanism using co-extrusion technology leads to significant improvement in abrasion performance. This is because of the superior fatigue crack growth performance of the skin layer. Even though the present study deals primarily with a high density polyethylene (HDPE) skin over a crosslinked polyethylene (XLPE) insulation, the co-extrusion technology developed here is applicable to other wire and cable systems which exhibit poor abrasion performance.

An analysis is also described which demonstrates that needle abrasion performance and hence the mode of failure can be predicted from measurements of the compliance, tensile stress and fracture toughness of the resins. These parameters influence the size of the damage zone that results from contact between the test needle, the insulation and the wire.

1. Introduction

Many studies have been conducted on wire and cable abrasion, especially in the automotive and offshore oil industries. In the offshore industry, cables must resist damage from inspection tools as these are lowered into wells. In the automotive industry, resistance to abrasion is required mainly for handling purposes while cables are being installed or assembled into harnesses. In order to design against failure that directly or indirectly results from abrasion damage to wire insulation, it is important to understand the abrasion mechanism involved in each specific system. This normally involves various mechanical tests which attempt to simulate field conditions such as scraping of the cable against sharp objects. Two tests used for this are the needle and sandpaper abrasion tests.

Standard wire dimensions used in automotive under the hood applications consist of a 22 AWG wire with an XLPE insulation thickness of 16 mils (0.41 mm). Constructions such as these satisfy all the necessary United States automotive specifications where they have been successfully used for over 20 years. These specifications include sandpaper abrasion tests, where XLPE constructions meet all the required specifications. However, for certain foreign markets, abrasion performance is determined by use of the needle abrasion test, the requirements of which are not always satisfied by XLPE constructions.

In the present paper we are concerned with developing a system which satisfies needle abrasion requirements for an under the hood automotive application. While the needle abrasion performance of any given wire and cable system can be improved by increasing the insulation thickness, cost, weight and space limitations usually prevent such an approach. In the present paper, a study of needle abrasion mechanisms for XLPE and HDPE wires has been carried out in order to explore the possibility of developing a co-extruded system which offers improved needle abrasion performance for a given insulation thickness without sacrificing performance.

A procedure is also presented which can be used to predict the abrasion performance of cables made from any given polymeric material so long as some basic mechanical properties of the material are known.

2. Experimental

The generic materials involved in the present study are shown in Table 1. Both resins shown in the table are produced by Equistar Chemicals, LP and variations of these are used in telecommunications and automotive wire and cable applications. Sample A is a high density polyethylene resin, with low shrink back characteristics, developed for use as primary insulation for telephone singles. Sample B is a non-halogenated flame retardant crosslinked polyethylene compound formulated for use as insulation in low voltage automotive wire and cable. The XLPE sample contains an in-organic non halogenated flame retardant filler. Both resins can be processed using conventional extruders, however, for Sample B, a continuous vulcanization tube is required. For Samples A and B, processing melt temperatures should be approximately 253 °C and 122 °C respectively.

Needle abrasion tests are carried out on a Tocksfors Verstads AB (TVAB) needle abrader with a needle diameter of 45 mils (1.14 mm), Figure 1. As shown in Figure 1, the longitudinal axis of the needle is perpendicular to that of the test wire. Testing is carried out by first clamping the test wire down, after which the needle oscillates back and forth over the insulation at a frequency of 60 Hz and an amplitude of 25.4 mm. The piano wire applies a 7 N load on the insulation as shown in Figure 1. The wire's resistance to abrasion is determined be the number of strokes that are needed before the wire insulation has been worn away. The equipment stops in this position automatically as there will be an electrical short circuit between the needle and the wire's conductor.

Current requirements for the needle abrasion test call for greater than 200 strokes prior to failure.

Table 1. Mechanical properties of resins used in the present study.

Property	Resin	
	Sample A	Sample B
Density, g/cm3	0.943	1.4
Tensile Strength, MPa (psi)	21.7 (3150)	20.7 (3000)
Elongation, %	660	220
Stiffness, MPa (psi)	593 (86000)	218 (31600)
Compliance, MPa^{-1} (psi^{-1})	1.68×10^{-3} (1.16×10^{-5})	4.59×10^{-3} (3.16×10^{-5})
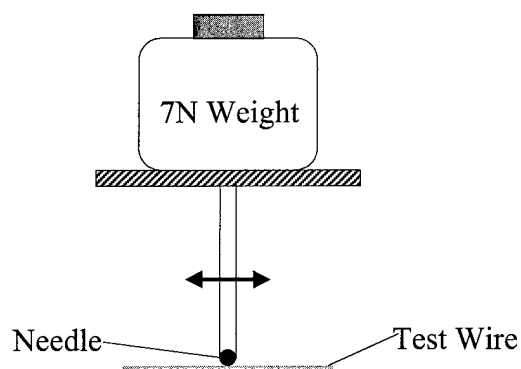
Figure 1. Schematic diagram of TVAB needle abrader.

All wires used in the current study were produced at lines speeds of 1800 fpm on a commercial wire line. For the co-extruded sample, a two step process was used which first involved running a 10 mil (0.25 mm) thick 22 AWG single layer XLPE construction on a continuous vulcanization line. The XLPE wire was then reeled and subsequently re-run in a second step where the 3 mil (0.08 mm) thick HDPE layer was extruded over it.

3. Results and discussion

Needle abrasion results for wire samples made from XLPE, HDPE and a co-extruded construction of both are shown in Figure

2. The following interesting observations can be made from the results presented in Figure 2:

a) The 16 mil (0.41 mm) thick HDPE sample fails after 1363 strokes, far exceeding the requirement of 200 strokes. Therefore, for the same insulation thickness, HDPE exhibits far superior needle abrasion performance than the corresponding XLPE sample.

b) The co-extruded construction of 13 mil (0.33) overall insulation thickness fails after 843 strokes, satisfying the 200 stroke requirement; and in fact does so at a smaller insulation thickness. As mentioned in Section 2, the multi-layer construction consists of a 10 mil (0.25 mm) XLPE inner layer and a 3 mil (0.08 mm) thick HDPE outer layer. It is worth noting that a 10 mil (0.25 mm) thick XLPE sample fails after 45 strokes and a 3 mil (0.08 mm) HDPE sample fails after only 5 strokes. The combined system is therefore more effective than each of the individual constructions on their own.

c) As expected, abrasion performance depends on insulation thickness, with the thinner wall thicknesses exhibiting inferior performance.
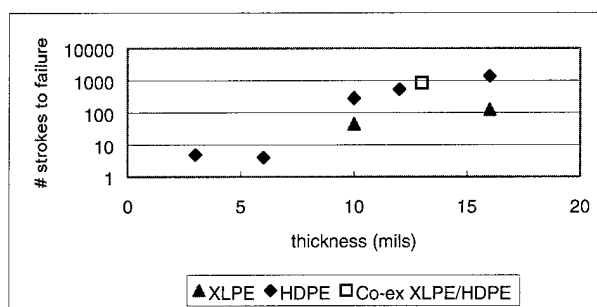
Figure 2. Needle abrasion performance of XLPE, HDPE and co-extruded XLPE/HDPE insulated wires.

An explanation for the superior performance of the 16 mil (0.41 mm) HDPE construction over the XLPE construction of the same insulation thickness in part lies in the difference in compliance between the two resins. As shown in Table 1, the HDPE resin is of lower compliance, suggesting that during testing, the needle penetrates further into the XLPE insulation since both are subjected to the same normal force of 7 N. Therefore, as the needle oscillates back and forth, it causes more damage in the insulation made from XLPE. By this token, using a needle of smaller diameter should exacerbate the resulting damage and speed up the rate of abrasion. Since the normal force will be the same for both needles, the higher stresses on the insulation from the thinner needle causes higher levels of strain, higher penetration into the insulation and therefore more damage. Data obtained for a thinner needle, showing the higher rate of abrasion are shown in Figure 3. The compliance of the wire therefore plays a significant role in the abrasion mechanism.
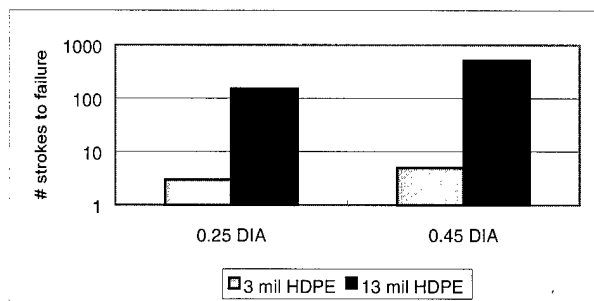
Figure 3. HDPE abrasion data for 0.25 (0.00635) and 0.45 (0.114) mil (mm) diameter needles

A further explanation for the superior performance of the HDPE insulation over that made from XLPE is evident from the abrasion mechanism associated with both. Scanning electron microscopy (SEM) photomicrographs of the abraded surfaces of a 16 mil (0.41 mm) XLPE sample and a HDPE sample of the same insulation thickness are shown in Figures 4 and 5.

The photomicrographs shown in Figures 4 and 5 are taken after 5 strokes in the needle abrasion test. As seen, both wires exhibit the typical ridge pattern associated with severe wear conditions in polymeric materials [1]. This is characterized by a series of ridges that develop at right angles to the sliding direction. As the needle oscillates back and forth over the insulation, abrasion proceeds mainly by crack propagation that occurs at the base of the ridge. During this process, fracture processes on the scale of microns take place, involving the detachment of relatively large particles from the ridge edges. In highly filled compounds, the detached particles tend to cause further wear by virtue of their abrasive characteristics [2].

Therefore materials that possess good resistance to crack propagation are likely to exhibit good needle abrasion. As a result, even though both XLPE and HDPE exhibit similar abrasion patterns (at least in the initial stages of the test), the superior fatigue crack growth performance of HDPE over the highly filled XLPE leads to the better needle abrasion performance.

SEM photomicrographs of the co-extruded sample is shown in Figure 6 after 5 strokes. Unlike the single layer constructions, the co-extruded sample exhibits no evident surface damage after 5 strokes. The use of the HDPE skin over the XLPE insulation therefore prolongs the onset of surface damage to the insulation leading to the observed improvement in abrasion performance. Although the mechanism that exists in the multi-layer constructions is not fully understood, it is thought to be related to the damage zone that exists at the outer and inner surfaces of the insulation [3].
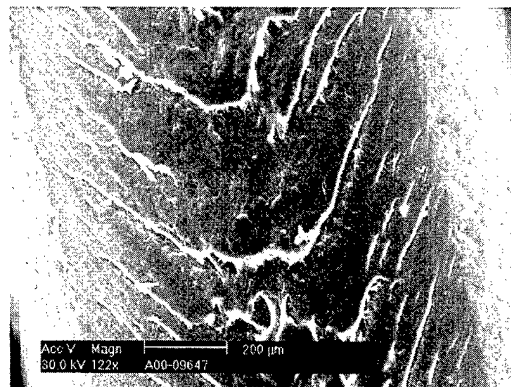
Figure 4. SEM photomicrograph of a 16 mil (0.41 mm) thick XLPE 22 AWG wire after 5 strokes in the needle abrasion test.
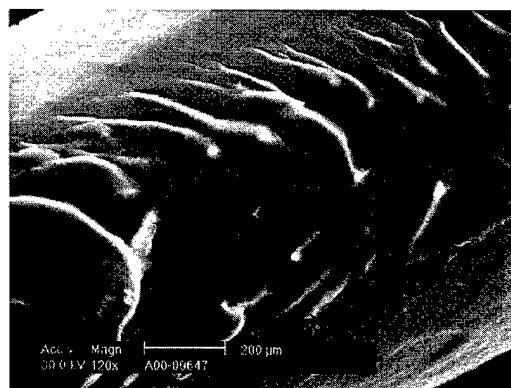
Figure 5. SEM photomicrograph of a 16 mil (0.41 mm) thick HDPE 22 AWG wire after 5 strokes in the needle abrasion test.
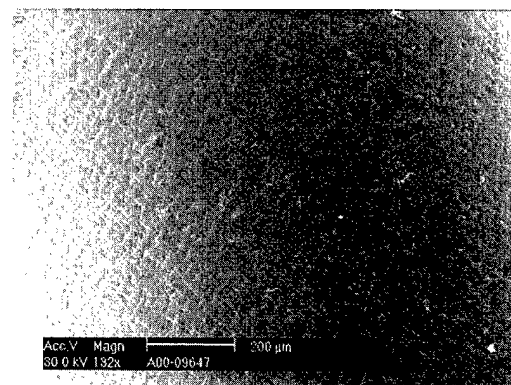
Figure 6. SEM photomicrograph of a 13 mil (0.33 mm) thick XLPE/HDPE 22 AWG co-extruded wire after 5 strokes in the needle abrasion test.

During needle abrasion tests, the normal force imposed on the insulation creates a damage zone of yielded material at the needle/insulation interface. This normal force also creates a

second damage zone at the interface between the wire conductor and the inner surface of the insulation (Figure 7). As the thickness of the insulation is reduced, the inner and outer damage zones overlap. As a result the bulk of material between the conductor and test wire is past its yield point suggesting a much lower modulus and therefore a much higher compliance. This results in deeper penetration of the needle into the insulation which leads to more severe damage. Clearly, for insulation thicknesses up to a certain value, the inner and outer damage zones will overlap, resulting in severe abrasion damage and subsequently high abrasion rates. This is confirmed by the data shown in Figure 8, where the thinner samples investigated in the present work exhibit abrasion rates at least an order of magnitude higher than the thicker samples. It is interesting to note that by extruding a HDPE skin over XLPE, the abrasion rate of the co-extruded construction is similar to that of a single layer HDPE construction of comparable thickness.
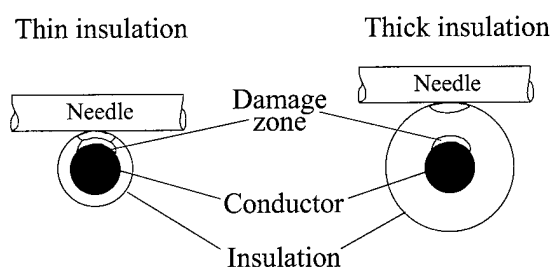
Figure 7. Damage zone on insulation of two different thicknesses.
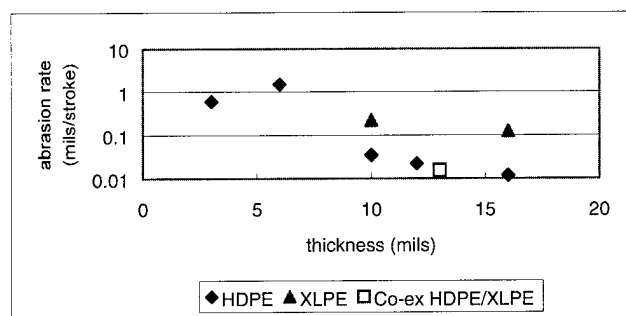
Figure 8. Abrasion rate of XLPE, HDPE and co-extruded XLPE/HDPE insulated wires.

A precise calculation of the size of the damage zone in the needle abrasion test configuration is difficult and requires numerical finite element or finite volume techniques. However, for comparing the relative performance of materials, the plastic zone size serves as an indication of the damage zone size. The plastic zone, defined as the region around the tip of a crack where the material has undergone yielding can be predicted from [3]:

$$R_p = \frac{1}{2\pi}\left(\frac{EG_c}{\sigma_y^2}\right) \tag{1}$$

In Equation (1), R_p is the plastic zone size and E, G_c and σ_y are the Young's modulus, energy release rate and yield stress of the material respectively. The energy release rate is a measure of the fracture toughness of the material. The parameter, R_p, therefore lumps into a single numerical value the compliance of the material, its toughness and its yield stress. The combined effect of these mechanical properties on needle abrasion can therefore be investigated by simply studying the effect of plastic zone size on needle abrasion performance.

Needle abrasion data has been obtained for a range of commonly available polymers for which literature values for E, G_c and σ_y are readily available [4]. Figure 9 shows the calculated plastic zone size for the polymers investigated and Figure 10 shows the corresponding needle abrasion results for 10 mil (0.25 mm) thick insulation over 22 AWG wire. It is clear that polymers such as PVC, polypropylene and nylon, with the smallest plastic zone sizes exhibit the best needle abrasion performance. It therefore appears that needle abrasion performance can be predicted by a single parameter, R_p, which takes into account the compliance of the material, its toughness and its yield stress. This is in agreement with the results obtained in the present work which suggest that material compliance and toughness do influence the needle abrasion performance of wires insulated with XLPE and HDPE.

Results such as those presented in Figures 9 and 10 have been generated for each of the mechanical properties listed above and attempts have been made to relate each of these to needle abrasion. The results indicate that a relationship between needle abrasion and each individual mechanical property does exist. However, it appears that the best correlation is obtained when all of the above mechanical properties are lumped into the plastic zone term.
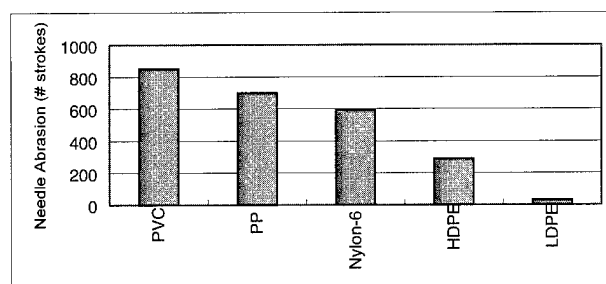
Figure 9. Needle abrasion performance of some common polymers.
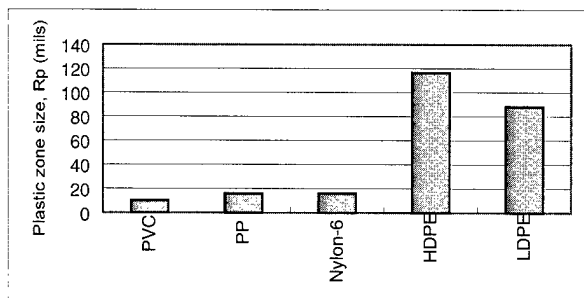
Figure 10. Corresponding plastic zone sizes for resins presented in Figure 9.

4. Conclusions

Data is presented which shows that deficiencies in the needle abrasion performance of XLPE insulated wires can be overcome by extruding a HDPE skin over a single layer XLPE wire construction. This improvement in needle abrasion is attributed to a temporary suppression of the tearing mechanism which is otherwise responsible for rapid wear. In addition, it is shown that the rate of abrasion for wires insulated with polymers is highly thickness dependent with smaller insulation thickness exhibiting much higher rates of abrasion. Finally, results are shown which suggest that a single parameter such as plastic zone size, which depends on the stiffness, toughness and yield stress of the insulation material, can be used to predict the needle abrasion performance.

5. Acknowledgments

6. References

[1] E. H. Andrews, eds, *Developments in Polymer Fracture-1*, Applied Science Publishers Ltd, London, p. 173 (1979).

[2] N. Symonds and B. G. Mellor, "Polymeric coatings for impact and wear resistance I: Wear," *Wear* 225-229 p. 111 (1999).

[3] A. J. Kinloch and R. J. Young. *Fracture behavior of polymers*, Applied Science Publishers, London p. 91 (1983).

[4] A. M. Howatson, P. G. Lund and J. D. Todd, *Engineering tables and data.* 2nd ed. Chapman and Hall, London, (1991).

Lifetime Prediction of the Additive for Rodent Repellent Fiber Optic Cable

Cristina Y. Kuniyoshi, Janúncio A. M. Neto, João M. Furtado, Leonardo Silvério

Furukawa Industrial S.A. Prod. Elétricos

Curitiba, Paraná, Brazil

++ 55 41 341 4092 - cristina@furukawa.com.br

Abstract

In this paper we present the lifetime evaluation of the capsaicin additive used in optical cables polyethylene sheath to provide an anti-rodent cable by repellent effect. The lifetime prediction of the capsaicin additive was obtained from different accelerated aging conditions. The experimental results from accelerated aging study were than extrapolated to actual in-service environment using Arrhenius model. With degradation curve estimated for various application temperatures it is possible to predict the initial dosage of capsaicin required in the sheath to guarantee the rodent repellent efficiency during the optical cable lifetime.

Keywords

Anti-rodent cables; capsaicin; lifetime prediction; Arrhenius equation.

1. Introduction

It is known that the long term reliability of optical cables can be seriously affected if the cable is submitted to the attack of rodents. In order to provide protection against this type of damage, one of the solutions is the use of microencapsulated synthetic capsaicin in the optical cables sheath as additive repellent against rodents. This is mainly convenient for the situations in which it is desired a cable with small diameter and lightweight properties[1]. The use of microencapsulated synthetic capsaicin as rodent repellent additive has been showing efficient against rodent attack. Since the optical cables require long-term functionality, the chemical stability of the capsaicin in the sheath during the optical cable lifetime must be assessed. As optical cables are continuously submitted to different temperature and the degradation rate of the capsaicin additive will depend fundamentally on the environment temperature where the optical cable is installed, it is necessary to study the effects of the temperature on the stability of the additive in order to predict the long term functionality of this chemical product.

2. Statistical Prediction of Capsaicin Stability in the Cable Sheath

2.1 Theory

The prediction of the chemical stability of capsaicin in the cable sheath can be made by submitting samples at different accelerated aging environment and by using Arrhenius equation.

This approach involves firstly the determination of a correct order of degradation reaction to describe the functional relationship between the capsaicin additive (CA) content versus time and temperature. The equations for zero, first and second-order degradation reactions can be summarized in a simplified way as[3]:

$$C = C_0 - k \times t \tag{1}$$

$$C = C_0 \exp(-k \times t) \tag{2}$$

$$1/C - 1/C_0 = k \times t \tag{3}$$

where k is the rate of degradation reaction, and C_0 and C are the contents of CA at time zero and time t, respectively. The equation for the first-order reaction can also be expressed in a linearized form:

$$LnC = LnCo - k \times t \tag{4}$$

The k parameter can be defined using Arrhenius equation (5 and 6) as:

$$k = A \times \exp\frac{-Ea}{R \times T} \tag{5}$$

$$Logk = LogA - \frac{Ea}{R \times T} \tag{6}$$

where R is the gas constant, Ea the activation energy, A is a constant and T is the absolute temperature in Kelvin. By using equations 6 e 2 the half-life of CA can be obtained.

2.2 Experiment and Statistical Analysis

In order to determine the rate of degradation reaction (k), samples of polyethylene (PE) suitable for use in the sheath containing 0.38, 0.66 and 0.95 % of CA (before aging) were prepared. The samples were conditioned in an oven for 40 days at 100°C. After aging, the concentration of CA in the samples was measured by using HPLC (High Performance Liquid Chromatography) analysis method previously extracted with toluene and methanol from polyethylene. The results are presented in Table 1.

Table 1- Remaining percentage of CA after aging for 40 days at 100°C

CA content in PE		Remaining Percentage
Before aging	After 40 days at 100°C	
0.38 %	0.24 %	37%
0.66 %	0.42 %	36%
0.95 %	0.62 %	35%

From the results showed in Table 1, the remaining percentages were equivalent for the three different concentrations of CA in PE. As the degradation rate was proportional to the CA content, the reaction can be expressed by equation 2 (or 4).

The stability of CA was evaluated using a 10 mm diameter of conventional optical cable as described in Figure 4, sheathed with PE which was added 0.49% of the additive. Pieces of cable samples were aged for a specific time and temperatures of 50, 80, 100 and 120°C. After each aging condition, the CA content in the sheath was measured. The results are presented in Table 2.

Table 2 – Effects of aging on CA content

Temperature		Aging period versus CA concentration				
50°C	Days	0	30	60	90	180
	% CA	0.41	0.40	0.39	0.38	0.37
80°C	Days	0	10	30	80	--
	% CA	0.41	0.37	0.31	0.24	--
100°C	Days	0	7	14	40	--
	% CA	0.41	0.32	0.27	0.16	--
120°C	Days	0	1	5	7	--
	% CA	0.41	0.34	0.19	0.17	--
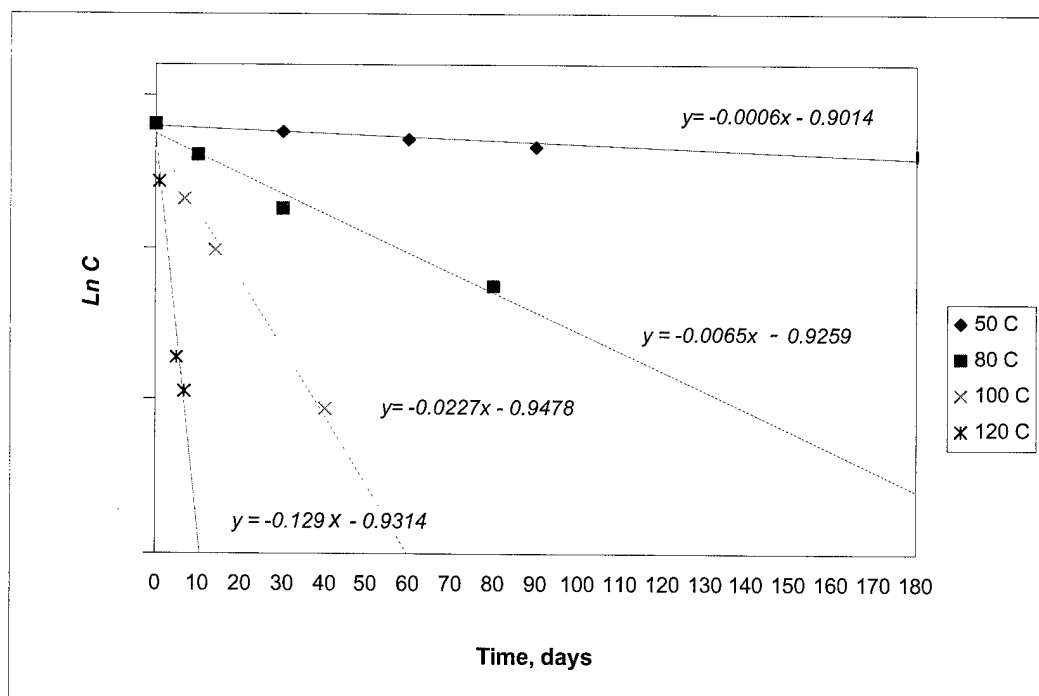
Figure 1- CA degradation

The Figure 1 shows the plot of CA content versus aging time period, using the experimental data form Table 2. By using linear regression analysis, the rate of reaction k and correlation coefficient were estimated. The results are given in Table 3.

The Figure 2 shows the plot of Log k versus the reciprocal of absolute temperature (1/T). By linear regression, the best fit for the experimental Arrhenius plot is given by:

$$Log\, k = 9.549 - 4136 \times \frac{1}{T} \qquad (7)$$

Table 3 – Rate of degradation reaction k

Temperature		Rate of reaction k	Log k
Celsius	Kelvin		
50°C	323	0.0006	-3.2218
80° C	353	0.0065	-2.1871
100°C	373	0.0227	-1.6440
120° C	393	0.1290	-0.8894
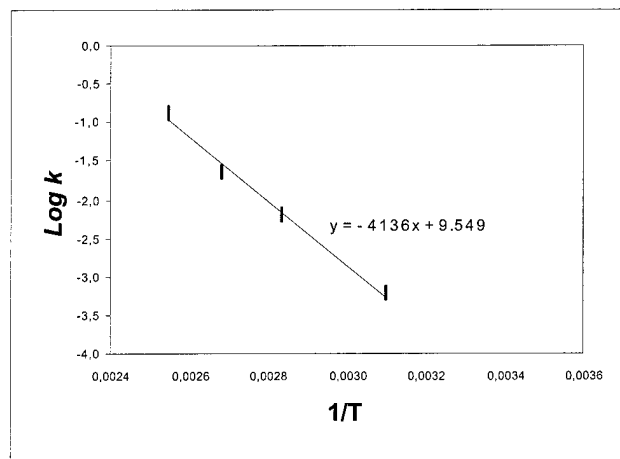
Figure 2 – Arrhenius plot

2.3 Prediction of CA Concentration Reduction in the Cable Sheath.

By using the equation 7, the k values were calculated taking into account the temperatures which the cable would be submitted when in an in-service environment and with the equation 2, the period of elapsed time when the content of CA (residual) is in 75, 50 and 25% in relation to the initial, for each k value. The calculated k and elapsed time are presented in Table 4 and the degradation curve is shown in Figure 3.

Table 4 – The degradation rate k and elapsed time prediction

°C	k	Elapsed time, years		
		75%	50%	25%
25	4.68E-05	16.9	40.6	81.2
30	7.92E-05	9.9	24.0	47.9
35	1.32E-04	6.0	14.4	28.8
40	2.16E-04	3.6	8.8	17.6
50	5.55E-04	1.4	3.4	6.8
60	1.34E-03	0.6	1.4	2.8
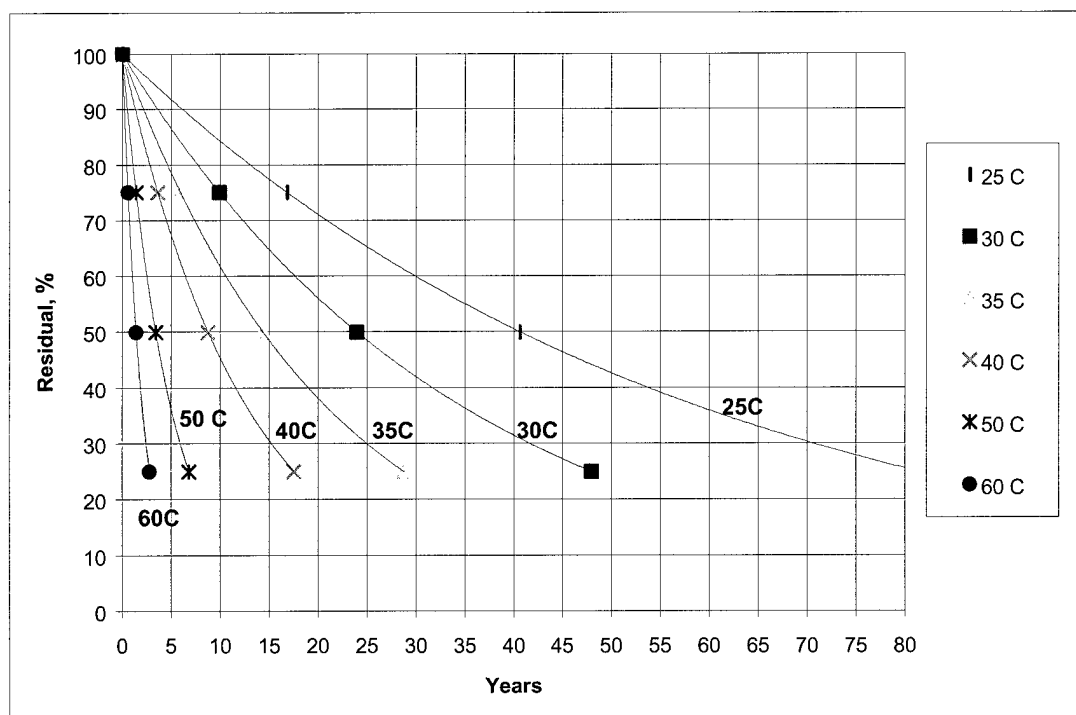
Figure 3 – Degradation curve of CA in the cable sheath

3. Rodent Repellent Cable Evaluation

3.1 Cable Design and Additive Concentration

The Figure 4 shows the rodent repellent optical cable used in this study. The cable consists of a conventional optical cable, which was added 0.40 and 0.86% of capsaicin to the polyethylene jacket. Although capsaicin is a very friendly substance to the environment and non-toxic, it is known that it can cause irritation to human being during cable handling. Therefore, in order to avoid this problem, we have adopted 0.2mm thickness of skin application to guarantee safety during handling operation.
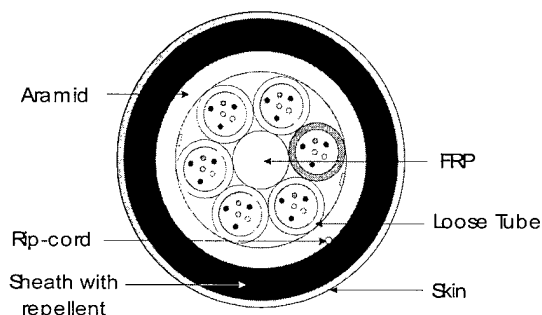
Figure 4 – Rodent Repellent Fiber Optic Cable

3.2. Rodent Attack Test

Being a destructive animal pest found in and around town sewers and buildings, the common brown rat, *Rattus norvegicus* also called Norway rat or sewer rat from wild and laboratory (domestic), was used for the rodent attack test. An optical cable in accordance with Figure 4 with 0.40% and 0.86% capsaicin dosage measured in the inner sheath, with more than 60% in microencapsulated form was submitted to test attack as follow:

Test description:
Pair of cable pieces, 20cm length, 10mm diameter, one cable sheath containing additive and other without additive, were placed in a cage where three rats, 68 weeks old, 516g weight and with 25cm body length were housed. Free access to drinking water and food was allowed throughout the evaluation. The cable pieces were taken out after leaving for 4 days. The test was replicated five times.

The following criteria was used for evaluation:
0: Jacket not scratched
1: Jacket scratched but not penetrated
2: Jacket penetrated with no damage to the core cable
3: Jacket penetrated with damage to the core cable and optical fiber
4: Highly destroyed, close to cable cut

The results are presented in Table 5 and 6 with their respective Photos 1 and 2 after the rodent attack test.

Table 5 – Cable damage for 0.40% additive

| Cage No | Optical Cable Sample | |
	With additive	Without additive
1	1	2
2	1	2
3	0	4
4	0	3
5	1	2
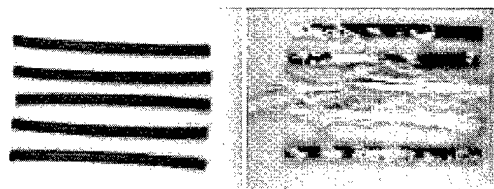
Photo 1 – Optical cable with 0.40% additive and without additive

Table 6 – Cable damage for 0.86% additive

| Cage No | Optical Cable Sample | |
	With additive	Without additive
1	0	4
2	0	4
3	0	2
4	0	3
5	0	4
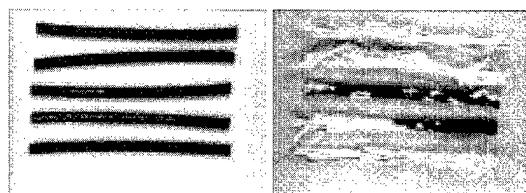
Photo 2 – Optical cable with 0.86% additive and without additive

4. Discussion

The degradation study of the capsaicin in the PE sheath showed that the repellent efficiency will depend strongly on the temperature which the cable will be submitted when in-service environment. The Figure 3 shows that for temperature above 35°C, the concentration of CA in the cable sheath will present a significant reduction along the time. Thus, in order to guarantee the efficiency of the repellent during the cable lifetime it would be necessary to predict an additional amount of CA to compensate the degradation.

The rodent tests have confirmed the repellent effect over sewer or brown rat. The optical cable samples with 0.40% and 0.86% of additive were very efficient to stop the rodent attack. Samples with 0.4% of additive showed satisfactory resistance level since the rats start gnawing the cable and stopped when they reached the inner jacket with capsaicin additive.

In a rodent attack test with *Thrichomys apereoides* also called punaré or rabudo[4][5] conducted in a similar way as described for the test with *Rattus norvegicus* the optical cable samples were totally destroyed by the rodent even in high concentration. The *Thrichomys apereoides* rodents inhabit the open areas that go from the southeast to the northeast of Brazil embracing the whole center-west and live in rocky blooming, building nests in logs or holes in the ground. Therefore, for cables installed in areas where these rodents are found, the use of capsaicin additive in the cable sheath to avoid rodent attack is not applicable.

The repellent effect is caused by hot stimulus of capsaicin, which is sensed as heat stimulus at palate nerves. The hot stimulus is sensed more intensely in the end part of tongue where lot of nerves is distributed. Differently to the *Rattus norvegicus* in which such effect happens, to the *Thrichomys apereoides* there is not the repellent effect, being probably due to non occurrence of the contact between the additive and palate when this gnaws.

5. Conclusion

With the degradation curve of the capsaicin additive in the cable sheath it was possible to evaluate statistically the stability of the additive for a long period, which will depend strongly on the environment temperature where the cable is installed. The more accurate the knowledge of the application temperature the better the prediction of initial additive concentration needed to compensate the degradation and thus guarantee the repellent effect against the rodents.
In a rodent attack test, the optical cables with 0.4% of additive in the sheath showed satisfactory resistance level to the sewer or brown rat.

6. References

[1] H. Miyano, M. Katayama and H. Tanji, "Anti-Rodent Type Portable Fiber Optic Cable for Safety Operation", *International Wire & Cable Symposium Proceedings*, p597 (1998).

[2] D. R. Parris and Zhan Gao, "Determination of the Real Lifetime of Polymeric Cable Materials", *International Wire & Cable Symposium Proceedings*, p122 (1997).

[3] O. Levenspiel, "Chemical Reaction Engineering", John Wiley & Sons Inc., (1972).

[4] P. Curado, C. Pitombo et al "Study and Analyses of Rodent Attacks in Optical Fiber Cables", *International Wire and Cable Symposium Proceedings*, p711 (1996).

[5] H. Durigan, L. Silvério, R. F. Cruz, M. A. B. Caetano "The Development of Rodent Protected All-Dielectric Optical Cables", *International Wire and Cable Symposium Proceedings*, p819 (1997).

Biographies

Cristina Y. Kuniyoshi has received her B.S. degree in Chemical Engineering from Federal University of Parana (UFPR) and her M.S. degree in Economic Engineering from Catholic University of Administration and Economy (FAE/CDE). She joined Furukawa Industrial S.A. in 1990 as Materials R&D Engineer and currently is responsible for Materials Engineering Department.
e-mail: cristina@furukawa.com.br

Janúncio A. Medeiros Neto received his B.S degree from Federal University of Rio Grande do Norte (UFRN) and M.S. and PhD in Physics from University of Campinas (UNICAMP) in 1991. After post-doctoral appointment at ORC-University of Southampton – England, he joined UNICAMP as research associated. In 1998, he joined Federal Center of Technological Education (CEFET-PR) as research fellow and Furukawa Industrial S.A. as consultant. He has worked in various areas of glass science such as non-oxide glass for optical fiber amplifiers. He is currently working in the area of optical fiber and component reliability.
e-mail: januncio@furukawa.com.br

João Mauricio Furtado has received his B.S. degree as a Chemical Engineer from Federal University of Parana (UFPR) and a M.S. degree in Administration from Catholic University of Administration and Economy (FAE/CDE). He joined Furukawa Industrial S.A. in 1992 as Materials R&D Engineer and currently is responsible for the Cable Development Engineering Department.
e-mail: jfurtado@furukawa.com.br

Leonardo Silvério joined Furukawa Industrial S.A. in 1984 after receiving his B.S. degree as Electrical Engineer from Federal Center of Technological Education (CEFET-PR). He has been involved in the optical fiber cables design and development. He is currently Product Engineering Manager.
e-mail: leosilve@furukawa.com.br

Combustion Atmosphere Toxicity of Polymeric Materials intended for Internal Cables

Bernt-Åke Sultan, Filip Samson
Borealis AB, Stenungsund, Sweden
James Robinson
Borealis N.V. Antwerpen, Belgium

Abstract

There is no doubt that the inhalation of toxic products formed during the combustion process is the major cause of fatalities that occur during fire catastrophes. There is however considerable dispute as to the best means to mitigate these hazards. Essentially two approaches are currently adopted – the American and the European. In summary the US approach is that heat release is all important. Toxicity is directly linked to carbon monoxide, which in flashover fires is proportional to heat release. In Europe, the fire hazard model is different. Fire deaths are believed due to a two stage process - incapacitation followed by carbon monoxide poisoning. Therefore the focus is on controlling the smoke and irritant gases which cause incapacitation.

In spite of the obvious concerns most cable specifications do not take toxicity/irritancy into account. A few, such as BS 7211, VDE 0250 pt 214 and 215, limit the acidity (irritancy) by a simple restriction of the halogen content of the combustion fumes (IEC60754-2). Consideration of the more general toxicity/irritancy problem is much more difficult. Animal testing is probably the most reliable approach but is very difficult to justify on moral grounds. The alternative is to identify and quantify critical components of the combustion fumes (NES 713, IMO MSC 41(64)). Toxicity is then estimated by assuming that the overall hazard is the sum of the component parts. The resulting parameter is known as the Fractional Effective Dose. A similar approach may be adopted in considering irritancy. ISO 130571 is a draft specification aimed at incorporating this type of analysis into a system of building hazard assessment.

The purpose of this paper is to give an overview of the toxicity/irritancy of the main combustion products formed during the combustion of materials used in three types of data cable. The key difference to the methods cited above is the use of GC/MS, which ensures consideration of all components of the combustion process.

Introduction

The life cycle of plastic materials covers 3 phases - manufacture, use and end of life disposal. Combustion behaviour is important both in the case of accidental burning during normal use and in the more controlled end of life disposal by incineration. Although this paper is primarily concerned with safety in the case of accidental combustion, the incidence of this occurrence is trivial in comparison to the volume of material subject to disposal by incineration.

The literature is full of conflicting claims and counter claims regarding the relative safety of combustion fumes arising from the burning of plastic materials. The problem is complex. Fume composition varies with the nature of the fire, providing obvious scope for identifying specific cases of products giving superior or inferior performance. This unsatisfactory situation has been addressed by ISO TR 9122 which attempts to identify the principle phases which occur during a fire, table 1. This should form the starting point of any fire hazard assessment.

Table 1. Fire Classification Scheme (revised ISO)

Fire Stage of Type	Temperature °C		Fire Effluent		
	Fire	Hot Layer	Oxygen to fire %	Oxygen from fire %	CO_2/CO V/v
1. Non-flaming					
a. Self sustaining.	450 - 600	RT	21	>20	1 - 5
b. Oxidative pyrolysis from externally applied radiation.	300 - 600	<50	0	>20	1 - 5
c. Non-oxidative pyrolysis from non externally applied radiation.	300 - 600	<50	0	0	<5
2. Well ventilated flaming					
Where fire is small wrt compartment size, flames are below the base of hot gas layer and fire size is fuel controlled.	>700	RT to 500	>15	5 - 21	>20*
3. Low ventilated flaming					
Where fire is small wrt compartment size, flames are partly above the base of hot gas layer and fire sizes is ventilation controlled.					
a. Small vitiated fire in closed compartment	>700	RT to 500	>15	0 - 12	2 - 20
b. Post-flashover fires in large or open compartment	>700	RT to 1000	>15	0 - 12	2 - 20

*Note may be lower for materials containing FR additives, to determine whether fire is type 2 or 3, use non FR, efficient burning material.

Having identified the fire scenario the next phase is to test for hazardous combustion products which may be either gaseous or particulate in nature. Most test protocols involve the quantification of specific products which may or may not coincide with those evolved by the product under investigation. This is especially true for the so called "super toxins" with critical FED of the order of a few ppm. A further concern is that the analytical technique must not itself modify the products being analysed - an issue which will be addressed later.

The purpose of this paper is to give an overview of the toxicological properties of fumes arising from the combustion of 3 different types of data cable. The basis is a mass balance - being the only way to ensure the consideration of all components.

Experimental

Materials
In this work the polymers described in table 2 have been investigated.

Table 2. Description of polymer samples investigated

Polymer sample	Description
PVC	Standard PVC jacketing compound. Comprising approx. 20% Plasticiser (DOP), 23% chalk calcium/zinc stabilisers and titanium dioxide.
FR-PVC	Flame retardant PVC compound typically used for plenum cable jacketing. Comprising phosphorus containing plasticiser, 35% aluminium hydroxide, antimony trioxide, zink borate, titanium dioxide, and lead stabiliser. Unknown calcium and silica containing substance identified.
Casico (FR4804)	Casico flame retardant technology and its physical, electrical and burning characteristics, as well as its flame retardant mechanism, were presented at IWCS –98[1] . FR4804 is a general purpose jacketing compound consisting of an ethylene butyl acrylate copolymer, 30% chalk, 5% high molecular weight silicon elastomer and 0.2% phenolic antioxidant
FEP	Fluorinated ethylene propylene copolymer typically used as plenum insulation

Burning characteristics of three category 5 unscreened twisted pairs (UTP) data cables (4 pairs, 0.5 mm copper conductor) utilising the above described jackets have been additionally studied. These cables are described in table 2.

Table 3 Cable samples

Cable sample	Description
PVC	Standard PVC jacket (0,49mm). Solid polyethylene (ME6032) insulation free from flame retardants. Outer diameter 0.89 mm.
Casico	FR4804 jacket (0.52 mm). Solid polyethylene (ME6032) insulation free from flame retardants. Outer diameter 0.89 mm.
Plenum	FRPVC jacket (0.4mm), FEP insulation. Outer diameter 0.82 mm

Fire tests
Cone calorimeter (Stanton tests were performed according to ASTM E 1354-90, on the UTP cables. The cables were cut into lengths of 10 cm, end sealed with Teflon tape and placed in the sample holder.

Corrosiveness of combustion fumes
The analysis was performed in accordance with IEC 60754-2. The cable samples, as well as pure FEP, were decomposed in a tube furnace at 950°C for 30 min. The fire gases were absorbed in water and the acidity measured using a pH meter.

Thermogravimetry
Thermogravimetric analysis (TGA) was made on both the polymer jackets and the FEP insulation using a Mettler Toledo TGA 850. 10 mg samples were decomposed in air as well as in a pure nitrogen atmosphere (50ml/min) at a heating rate of 10°C/min and also isothermally.

Identification of combustion fumes
The polymeric samples (0.3-1g) were decomposed for 15 minutes in a tube furnace similar to that described in IEC60754-2. The furnace temperature was 575°C and the airflow rate 2 litres per minute. The air contained 2000 ppm water. Different techniques were used to collect the various species of fire effluent for subsequent analysis. Fire gases were collected in Tedlar bags and carbon monoxide (CO) and carbon dioxide (CO_2) levels determined by non-dispersive infrared analysers; for nitrogen oxides chemical reagent tubes were used. Hydrocarbons, halogenated hydrocarbons and aldehydes were determined using a gas chromatograph/mass spectrometer (GC/MS). In this case the fire gases were transferred from the Tedlar bags and adsorbed onto various sorbents (Tenax, Charcoal and XAD-2) within 1-2 hours to stabilise the gases. The gases on the tubes were then desorbed into the GC/MS for analysis. Hydrogen chloride (HCl) and hydrogen fluoride (HF) were determined by absorbing the fire gases in 0.1M aqueous solution of sodium hydroxide prior to quantification by ion-chromatography. The mass of airborne particles retained on a 1 micron filter was measured for the FEP sample. For the PVC and Casico the 1 mm filter caused an excessive back pressure and a 1.6 micron filter was used for these tests.

Results

Cone calorimeter
The cone calorimeter results for the different data cables are presented in table 4. Examples of the rate of heat release, smoke and carbon monoxide production as a function of time are presented in Figure 1a-c.

Table 4. Cone calorimeter results for the three different data cables

	PVC/PE			Casico/PE			FRPVC/FEP			
Heat Flux, kW/m²	30	40	50	30	40	50	30	40	50	70
Ignition Time, s	42	26	9	143	85	45	80	37	11	7
Burning Time, s	210	190	181	170	150	160	110	158	234	223
Mass loss, %	30	30	30	30	30	31	14	19	36	42
Heat release (max), kW/m	1.4	1.6	2.0	3.7	3.9	4.4	0.46	0.48	0.7	0.56
Heat release (ave), kW/m	1.1	1.2	1.3	2.2	2.4	2.3	0.21	0.23	0.28	0.3
Heat of Combustion, kJ/m	240	230	230	380	370	380	35	43	66	70
Smoke (SEA), m²/m	8.2	12	13	7.3	8.3	6.8	0.9	2.4	2.1	4.3
CO, g/m	0.44	0.45	0.52	0.23	0.25	0.25	0.21	0.31	0.82	1.5
CO₂, g/m	15	15	15	25	24	25	2.3	2.8	4.2	5
CO₂/CO ratio	34	33	29	109	96	100	11	9	5.1	3.3
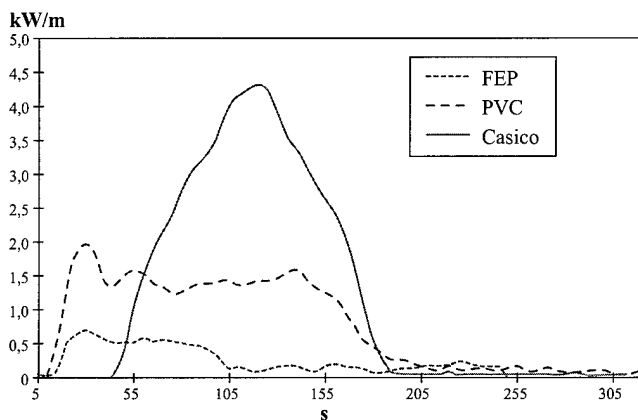
Figure 1a. Heat release
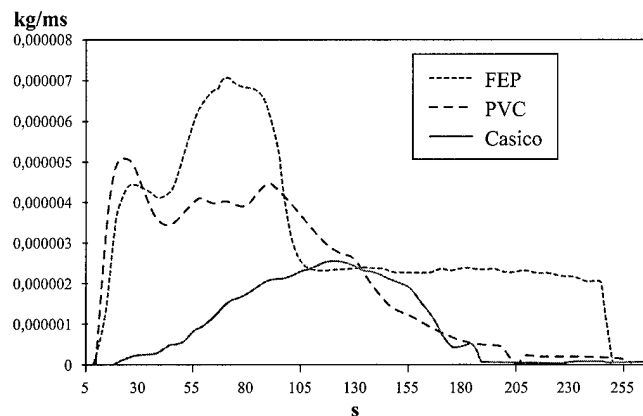
Figure 1c. Carbon monoxide
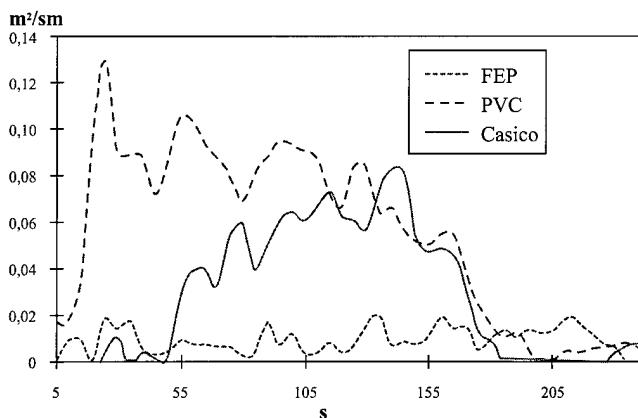
Figure 1b. Smoke (SEA)

Figure 1a-c. Cone calorimeter results at a heat flux of 50 kW/m²

The nature of the combustion is generally described by the ratio CO_2/CO. In a well ventilated fire, such as in a cone calorimeter, a hydrocarbon based compound like Casico will burn with a CO_2/CO ratio of the order of 100. It should be noted that even in the well ventilated cone calorimeter, the FEP sample burns as if in an extreme oxygen depleted environment.

The plenum rated cable shows a low carbon dioxide formation and accordingly the lowest heat release. The cable gives a smoke with good visibility. Carbon monoxide formation is extensive at the higher heat fluxes. Due to the high density of FEP, the cable shows a higher weight loss at the higher heat fluxes than the other cables. It is first at a heat flux of 70kW/m² that all polymeric material is decomposed. Both the other cables show complete decomposition at 30kW/m², giving a weight loss of 30%.

The LSZH cable has by far the longest ignition time and the lowest carbon monoxide formation. Carbon dioxide formation and heat release is comparably high. As can be seen from figure 1 the peak heat release and peak smoke obscuration occurs much later with the LSZH cable than the halogenated ones. In a fire situation this should provide enough visibility and time for escape before flash over.

The standard PVC cable quickly ignites and peak heat release, CO and smoke obscuration is already achieved after about 20 seconds at a heat release of 50 kW/m² (see figure 1). The FEP cable displays similar behaviour with the exception of its effect on visibility.

Acidity of fire gases

Strong acids are highly corrosive, irritant and reactive substances. They adversely affect the chances of escaping a fire due their irritant action on the eyes, upper respiratory tract and lungs. Pulmonary oedema and subsequent death often follow exposure to high concentrations, usually 6 to 48 hours after exposure[2].

The results of the IEC 60754-2 test for the different data cables are presented in table 5. In standards such as DIN VDE 0266 part 3 cables giving a pH below 4.3 are considered corrosive and are not fulfilling the requirement.

Table 5. Acidity of combustion fumes

Jacket/insulation	pH	Pass/Fail DIN VDE 0266 part 3
PVC/PE	2.9	Fail
Casico/PE	5.4	Pass
FRPVC/FEP	2.6	Fail
FEP insulated core	2.9	Fail

The only cable giving neutral combustion fumes is the Casico/PE cable. The PVC containing cables produce highly acidic combustion fumes. The FEP insulated cable core was tested separately. Resulting in an acidity similar to that of the PVCs.

Thermal stability

Combustion reactions and the resulting decomposition products are highly dependant on the molecular structure of the polymer, oxygen concentration and temperature. In order to study the decomposition pattern for the polymers involved, TGA studies have been performed both in air and in the complete absence of oxygen.

Weight losses of the different compounds heated in air at a heating rate of 10ºC/min are presented in Figure 2.
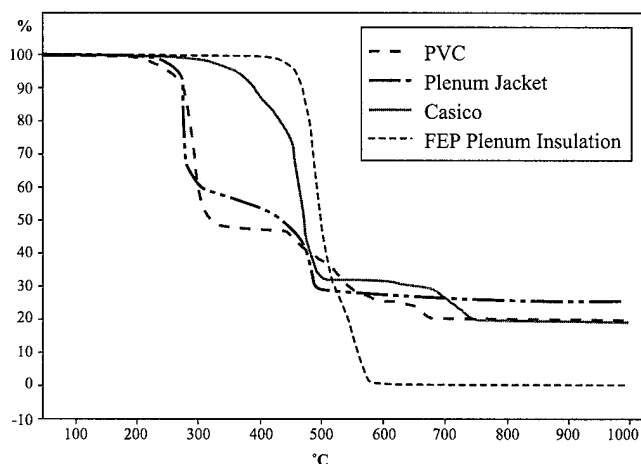
Figure 2. Weight losses in air as a function of temperature. Heating rate 10°C/min

Under these conditions, weight loss for both PVCs is visible at about 200°C. Between 200-300°C the more highly flame retardant PVC loses 40% of its weight and for the less highly filled standard type a loss of about 50% is observed. In this temperature range the volatilisation of the plasticisers takes place and the aluminium hydroxide added to the FR-PVC starts to decompose. For both PVC's a rapid dehydrochlorination take place i.e. the formation of volatile HCl and a more stable polymeric hydrocarbon residue consisting of conjugated unsaturations (see below). At about 500°C the decomposition of this residue is more or less complete. Finally, the decomposition of chalk ($CaCO_3$) take place leaving a stable residue of calcium oxide at about 750-800°C.

For the polyethylene based Casico formulation, weight loss is observed at about 400°C and at about 500°C the decomposition of the hydrocarbon chain is complete. A residue of chalk and silicon oxide remains[1] . Finally, the chalk starts to decompose at 700°C.

For FEP the decomposition takes place between 500-600°C. The FEP sample contains no filler and as expected, no residue over 600°C is observed.

In figure 3a-c the decompositions in air are compared to those occurring in a nitrogen atmosphere. As expected the dehydrochlorination of the PVCs are not affected by the change in atmosphere. The decomposition of the remaining hydrocarbon chain goes, however, much more slowly in nitrogen. Even at 1000°C the hydrocarbon chain does not completely decompose in nitrogen. This indicates that highly stable aromatic structures are formed. FEP and the polyethylene based compounds are more quickly degraded in air, but no difference in the residual amount is noticed at temperatures over 600°C.
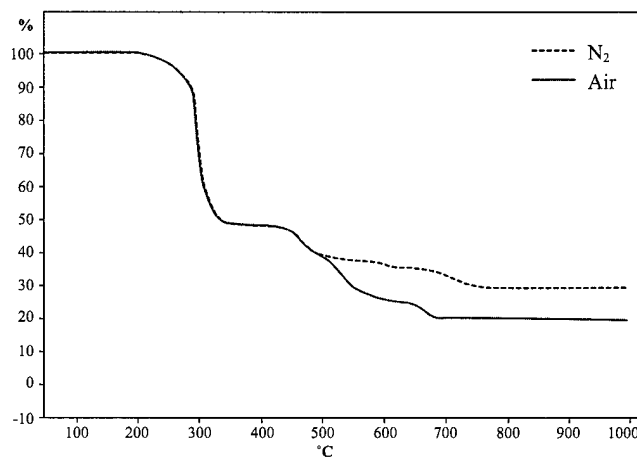
Figure 3a. PVC
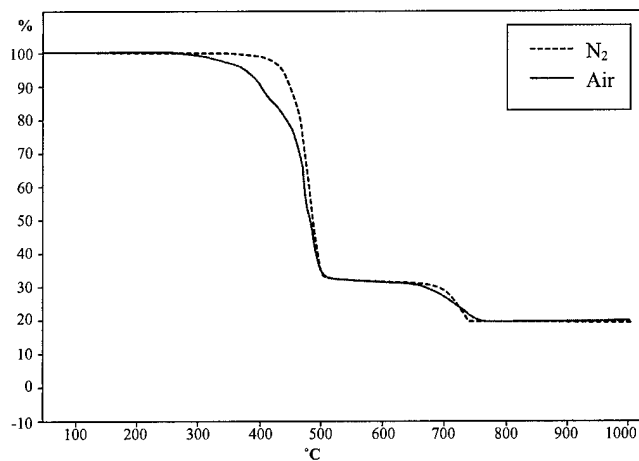
Figure 3b. Casico
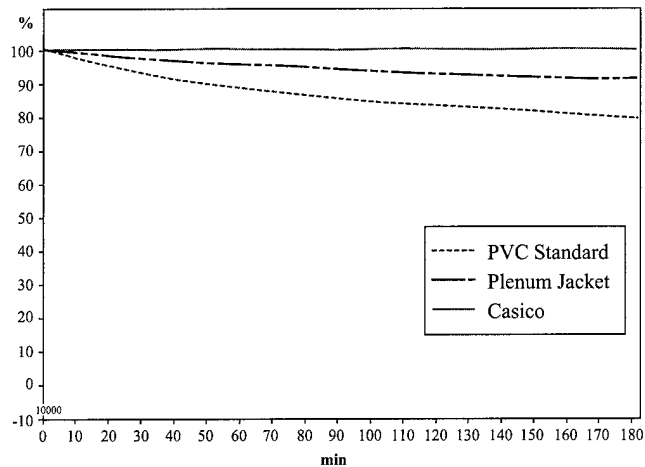
Figure 4a. 200°C
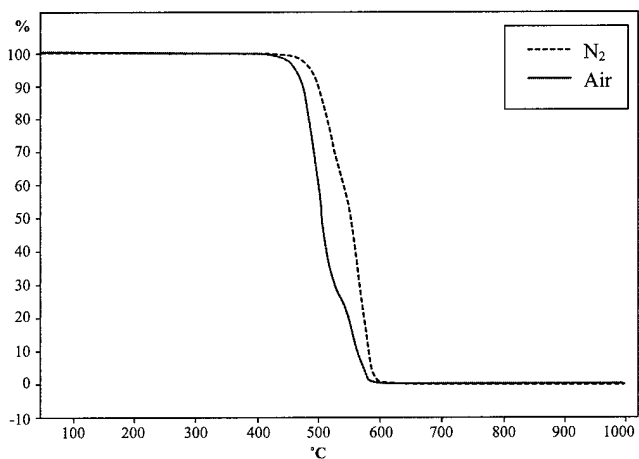
Figure 3c. FEP
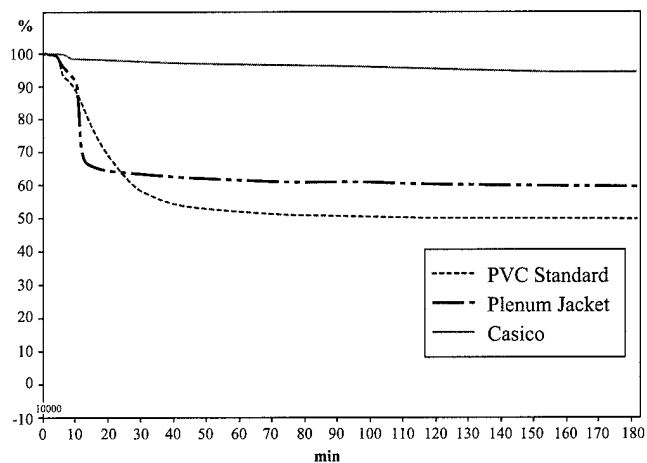
Figure 4b. 250°C

Figure 3a-c Comparative studies of weight losses in air and nitrogen. Heating rate 10°C/min.

Isothermal investigations in air show that the volatilisation of plasticiser and dehydrochlorination is rapid at temperatures as low as 200°C. A slow decomposition of Casico is observed at 300°C and for FEP at 400°C. At 500°C all polymers are rapidly volatilised, fig 4.
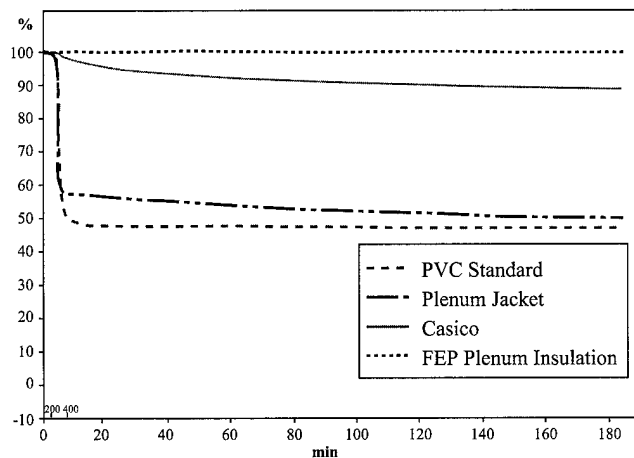
Figure 4c. 300°C
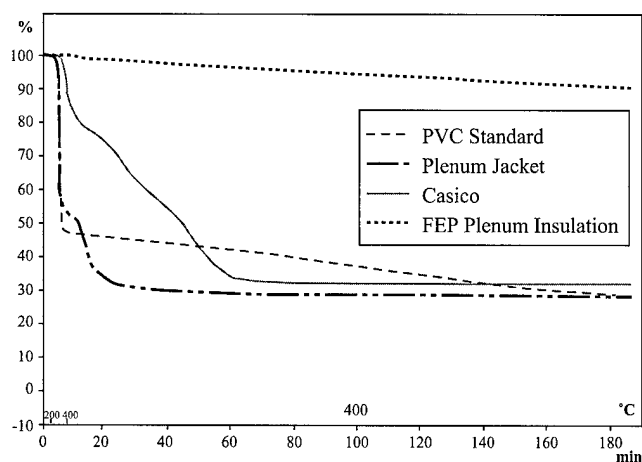
Figure 4d. 400°C
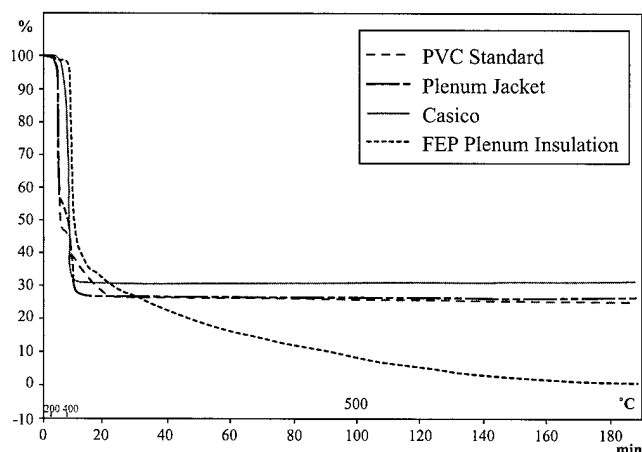
Figure 4e. 500°C

Figure 4a-e Isothermal degradation in air

Identification of combustion products

As in the TGA study, the polymers were dismantled from the cables and conductors and degraded separately. FRPVC has not been included in this test. For the others, decomposition took place at 575°C for 15 minutes and the fire gases were collected in Tedlar bags prior to analysis. The gas stream was passed through a filter in which airborne particles were collected. The amount of airborne particles trapped in the filter was measured. Results of the main decomposition products have been quantified. The results are presented in Table 6.

Table 6 Quantification of major decomposition products and airborne particles expressed as gram gas per gram initial polymer

	PVC	Casico	FEP
Mass loss, %	70	69	100
Carbon dioxide (CO_2), g/g	0.56	0.98	0.49
Carbon monoxide (CO), g/g	0.042	0.065	0.034
Hydrogen Fluoride (HF), g/g	0	0	0.49
Hydrogen chloride (HCl), g/g	0.15	0	0
Airborne particles, g/g	0.041	0.028	0.009

The results explain the high acidity of the combustion fumes of the PVC and the plenum rated cable observed above. Both HF and HCl are very strong acids. 50% of the initial weight of the FEP polymer is decomposed as HF and 15% of the PVC as HCl. The PVC compound contains approx. 30% chlorine. The results indicate that only half of this amount turns into HCl after its degradation. This is surprising since the TGA analysis indicates a rapid and complete dehydrochlorination even at rather low temperatures (see fig 2 - 4). HCl is, however, very reactive and as will be seen below most of the "missing" chlorine ends up as chlorinated hydrocarbons.

As in the cone calorimeter experiment, the Casico material produces far higher amounts of non-toxic CO_2 compared with the halogenated materials. The carbon monoxide level however differs remarkably from the cone calorimeter results in which the Casico cable showed significantly lower CO levels than the other materials. In these test the opposite is observed. The explanation is that the cone calorimeter shows what happens in a well-ventilated fire. The air flow chosen in this experiment shows what happens in a non-ventilated fire. In the tube furnace experiment, the oxygen concentration was reduced to about 10% giving a CO_2/CO ratio of approximately 15 for all materials.

In order to quantify the other decomposition products formed from the compounds, a mass balance is presented in table 7. The oxygen in CO_2 and CO is taken up from the air and the hydrogen present in HF from moisture in the air. In table 7 the weight contribution from these atoms has been withdrawn, making it possible to calculate how much of the initial polymer has ended up in other decomposition products. The result shows that for all three polymers about 35% of the polymer has ended up in other more heavier decomposition products.

Table 7 Mass balance

	PVC	Casico	FEP
Residue, %	30	31	0
CO_2 as C, %	15	27	13
CO as C, %	1.8	2.8	1.5
HF	0	0	47
HCl; %	15	0	0
Airborne particles, %	4.1	2.8	0.9
Totally identified, %	65.9	63.8	62.4
"Missing", %	34.1	36.2	37.6

In order to identify the "missing" substances, GC/MS analysis was performed on the gases collected in the Tedlar bags. The major "missing" decomposition products identified by GC/MS are summarised in order of peak area size for the respective polymers in table 8.

Table 8. Major "missing" decomposition products in order of peak are size

PVC	Casico	FEP
Benzene	Heptane	Perfluoropentane
Toluene	Benzene	Trifluoroacetic acid
Naphthalene	Toluene	Perfluoroethyl methyl ester?
Chlorobenzene	Phenol	Mixture of perfluorohexane, heptane and octane
Dichlorobenzene	Styrene	Perfluoroundecane
Phenol	Naphthalene	Perfluoro-oligomers higher than dodecane
Butenone	Hexene	Perfluorodecane
Phenylethyne	Cyclopentadiene	Perfluorododecane
Styrene	Heptene	Perfluorononane
Chlorooctadecane	Ethylbenzene	Perfluoropropene and other fluorinated C3 substances
Chlorophenol	Octene	Heptafluorobutanoic acid
Benzene dicarboxylic acid	Butadiene	Perfluorobutane and other fluorinated C4 substances
Benzaldehyde	Xylene	Perfluoroheptene
Oleic acid	Undecane	Perfluorocyclopentane
Chlorohexadecane	Phenylethyne	

The identified substances have been divided into different classes. For PVC 45 different substances were identified. These can be divided into six classes (see table 9). For Casico, 28 different substances representing three different classes were identified. For FEP, the 15 different compounds identified were either perfluoroaliphatics or fluoro-oxygenated decomposition products.

Table 9 GC/MS results expressed in area-% of the major types of decomposition products identified from the different compounds

	PVC, area-%	Casico, area-%	FEP, area-%
Aliphatic hydrocarbons	9.4	46	
Aromatic hydrocarbons	46	40	
Oxygenated hydrocarbons	19	14	
Chloro-aliphatic compounds	11		
Chloro-aromatic compounds	10		
Chloro-oxygenated compounds	4.6		
Perfluoro-aliphatic compounds			62
Fluoro-oxygenated compounds			38

In these non-ventilated fire conditions, PVC decomposes primarily to aromatic hydrocarbons. Large amounts of both aliphatic and aromatic chlorinated hydrocarbons are formed in addition. With Casico, aliphatic and aromatic hydrocarbons are predominantly formed. Fully fluorinated chain fragments are mainly formed with FEP, but large amounts of oxygenated compounds also occur, primarily trifluoroacetic acid. Surprisingly only trace amounts of carbonyl fluo-

ride were identified. In earlier investigations of the decomposition products from a similar polymer, polytetrafluoroethylene, carbonyl difluoride was the major decomposition product[3,4].

Discussion

Background
In an earlier publication the composition of combustion fumes from a similar set of cables has been reported[5] using the classical methods described in IMO MSC 41(64) using the NBS smoke chamber and the IEC 606695-7-50 draft using the Purser furnace. In both these tests, quantification of a chosen number of gases are performed by Fourier Transformed Infrared (FTIR) gas detection. This earlier work raised concerns that the techniques employed failed to consider a significant part of the decomposition products. The current work addresses these issues by means of a mass balance.

Polyvinyl chloride (PVC)
This investigation shows that cables using standard PVC compounds ignite easily and very quickly form dense black smoke and high hydrogen chloride and carbon monoxide levels, even in well-ventilated fires. Peak heat release is quickly reached. The results confirm what has been found in full-scale fire experiments[6].

The addition of a chlorine atom to a hydrocarbon chain has a great influence on the polymer's thermal stability and its combustion reactions. The carbon-chlorine bond is weak leading to the formation of HCl even at compounding conditions i.e. at temperatures below 200°C, Fig. 4a via a dehydrochlorimation[7];

$$\underset{\underset{H}{|}}{\overset{\overset{H}{|}}{\sim C}}-\underset{\underset{Cl}{|}}{\overset{\overset{H}{|}}{C}}\sim \longrightarrow \underset{}{\overset{\overset{H}{|}}{\sim C}}=\underset{}{\overset{\overset{H}{|}}{C}}\sim \ + HCl$$
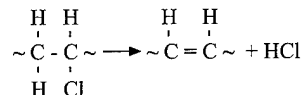
Non-filled PVC contains 57% chlorine by weight. In a typical cable compound in which plasticiser, chalk etc. is added the typical chlorine content is reduced to about 25-35%. Fig 2-4 shows that the evaporation of plasticiser (normally about 20% added) and a complete dehydrochlorination, giving a weight loss of about 40-50%, occurs quickly at temperatures over 200°C. The polymer residue consisting of a hydrocarbon chain with conjugated unsaturations starts to decompose at temperatures similar to that of polyolefins. As can be seen from the GC/MS results presented in table 8 and 9, the conjugated double bonds favour, not surprisingly, the formation of benzene and other aromatic structures. This, together with the mode of chlorine as a flame retardant, is the explanation for the severe smoke formation observed when burning standard PVC.

The GC/MS results show that PVC degraded at 575°C gives an HCl level of approx. 15% (table 6). This is only about half of the theoretical level, and what the TGA study indicates. HCl is a very reactive compound and the large number of chlorinated hydrocarbons identified (table 8 and 9) indicates that the remaining 15% ends up in these substances. Table 10 summarises the decomposition products found from PVC in this investigation. The quantification of the heavier aromatic and aliphatic substances is made indirectly from the mass balance and relative peak area sizes. It should be noted that this gives only an approximate indication of the amount.

Table 10 Quantification of the major decomposition products from PVC in non-ventilated fires (575°C)

	g/g initial polymer
Carbon dioxide (CO2), g/g	0.6
Carbon monoxide (CO), g/g	0.04
Hydrogen chloride (HCl), g/g	0.15
Aromatic hydrocarbons	0.16 estimated
Oxygenated hydrocarbons	0.07 estimated
Chlorinated aliphatics	0.04 estimated
Chlorinated aromatics	0.03 estimated
Aliphatic hydrocarbons	0.03 estimated
Chloro-oxygenated hydrocarbons	0.02 estimated
Airborne particles, g/g	0.04
Residue (mostly chalk), g/g	0.30
Total	1.44

The degradation of the sample in the tube furnace at an airflow of 2 litres/minutes resulted in rather low oxygen concentrations - between 8-10% for all polymers. Accordingly, the degradation was performed under "non-ventilated fire conditions". A low oxygen concentration favours the formation of aromatics and aliphatics. The combustion reactions for PVC under different fire conditions are summarised in figure 5.
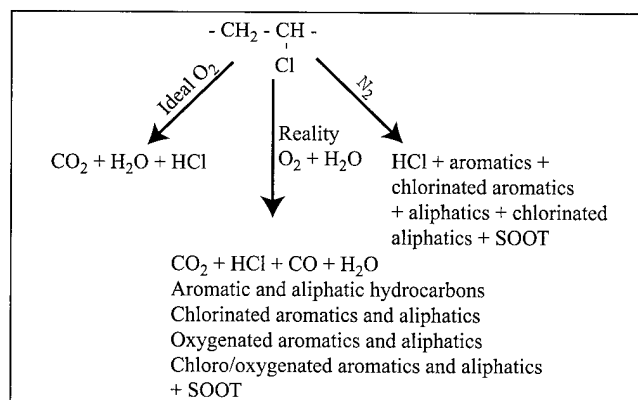
Figure 5 Combustion reactions of PVC under different fire conditions

Halogen acids are the source of the corrosive effects of burning PVC and are cited as the cause of serious pulmonary illnesses observed in fire victims and fire fighters.

Several authors however, have observed that the irritancy of the smoke from PVC is more than can be explained by the formed levels of CO and HCl alone[8,9,10]. It has been long known that many halogenated hydrocarbons are carcinogenic and toxic on inhalation[11]. However, no studies covering the influence of such substances on escape from fires have been found. In table 11 some of the available toxicity and irritancy data in the literature have been collected. The data is expressed as Lethal concentration 50% (LC50) i.e. the concentration statistically calculated to cause deaths of half of the test animals (mice) exposed to a toxicant for a specified time. The irritancy of the substances is expressed as its Respiratory Depression 50% (RD50) value i.e. the statistically calculated con-

centration of an irritant required to reduce the breathing rate of laboratory rodents by 50% after 10 minutes exposure[12].

Table 11 LC50 and RD50 values of potential fire gases

Polymer/Decomposition producta	LC50 (30 minutes exposure) in rats, mg/l polymer	ppm	RD50 (10 minutes exposure), ppm
Wood (DIN) Well ventilated	24-48		
Polyethylene			10-100 (XLPE, brominated)[6]
PVC	10[9]		100-1000[8]
PTFE	0.05-2.9 [13]		
Carbon/oxygen containing compounds;			
Carbon dioxide		90 000	
Carbon monoxide	3.79	3250[13], 3500[14], 4600[15]	1100[14]
Acetone			77516[6]
Ethanol			27314[8]
Formaldehyde	0.92	825[13]	3.13[8]
Acetaldehyde		50[15]	
Acrolein	0.32	135[13,15]	1.68[8]
Aromatics;			
Xylene			500[8]
Styrene			980[8]
Methyl styrene			800[8]
Ethyl styrene			800[8]
Chlorine containing compounds;			
Chlorine	0.3	100[13]	
Hydrogen chloride	5.8	3800[13], 2000-4000[15]	309[8], 200[6]
Phosgene (Carbonyl chloride)	0.32	75[13]	
Alpha-chloroacetophenone			0.96[8]
Chloromethane			9000[8]
Hexachloropropene		425[16]	
Fluorine containing compounds;			
Fluorine	0.58	370[13]	
Hydrogen fluoride	1.88	2250[13]	120[6]
Carbonyl fluoride	1.96	720[13]	
Perfluoroisobutylene	0.047	0.5 ppm Approximate lethal concentration 4 hours (ALC)[17]	
2-fluoroethyl fluoroacetate	0.02	5.7[13]	
Others;			
Oxygen	Min.	67000[14]	-
Hydrogen cyanide	0.23	200[13], 110[15]	63[14]
Hydrogen bromine		3800	200[6]
Sulphur dioxide		400[6]	117[8], 30[6]
Nitrogen dioxide	0.3	155[13]	25[6]

These data show that aromatics such as xylene and styrene show some irritant effects but a chlorinated aromatic, chloroacetophenone, is highly irritant.

Carbon monoxide is claimed to be present at lethal levels in 50% of fatalities in fire victims[18] and is probably the major cause of fire death other than burns[19]. Carbon monoxide has a similar LC50 value as HCl, but HCl is a much more irritant and corrosive substance. HCl is also formed in much larger amounts than carbon monoxide from a PVC fire (table 10). Accordingly HCl is the most critical component in the fire gases from PVC for humans as well as for equipment. The influence of the large amounts of chlorinated hydrocarbons formed during combustion of PVC on the chances of escape from a fire is not yet understood. Many of these substances are highly carcinogenic and areas exposed to these fire gases have to be carefully cleansed by protected personal prior to reuse.

The Beverly Hills Supper Club fire was one of the largest PVC wire insulation fires of the 1970s and its consequences have been well documented[20]. In that fire, 161 people died without being in direct contact with flames and long before the carbon monoxide had reached a concentration which affected the rescuers.

One of the survivors gave the following description of the effect of being exposed to PVC fire fumes; "The reservationist of the Supper Club noticed white-to-grey wispy smoke whirling down from the ceiling of the Zebra room. When she entered that room, it wound about her head, and she stumbled out of the room immediately. Her eyes were so irritated and watery that she could not see, and her nasopharyngeal area burned and filled with fluid. Her finger nail polish reacted with the smoke, and her fingernails were eaten through. She developed second-degree burns wherever the wispy, grey-white smoke touched her". About one third (239 out of 700) of the fire fighters who attended the fire required medical attention. Many of these suffered adverse effects to health, most commonly linked to their respiratory function, for years afterwards.

Casico
Compared with halogenated materials cables sheathed with Casico have long ignition times and form low amounts of carbon monoxide in well ventilated fires. They do however attain higher heat releases. Peak levels of heat release and smoke occur late in the combustion process.

The TGA investigations show that the polyolefin base copolymer is rather stable. Decomposition is noticeable at about 300°C in air and 400°C in nitrogen.

Table 12 summarises the decomposition products found from Casico in non-ventilated fire conditions at 575°C.

Table 12. Quantification of the major decomposition products from Casico in non-ventilated fires (575°C)

	g/g initial polymer
Carbon dioxide (CO2)	0.98
Carbon monoxide (CO)	0.065
Aliphatic hydrocarbons	0.16 estimated
Aromatic hydrocarbons	0.14 estimated
Oxygenated hydrocarbons	0.05 estimated
Airborne particles	0.028
Residue (Chalk with traces of silicone oxide)	31
Total	1.89

Compared with PVC, the absence of conjugated unsaturations in polyolefins favours the formation of rather harmless aliphatic hydrocarbons. Accordingly it results in a reduced formation of soot and polyaromatics. Carbon monoxide is the main critical component in the fire gases from polyolefins. In well ventilated fires the carbon monoxide formation is much lower than for halogenated polymers. In non-ventilated fires somewhat higher levels are reached. Aromatic hydrocarbons show a slight irritant effect and seem to be the main irritants in the fire gases from polyolefins, table 11. Combustion reactions of halogen free polyolefins is summarised in figure 6.
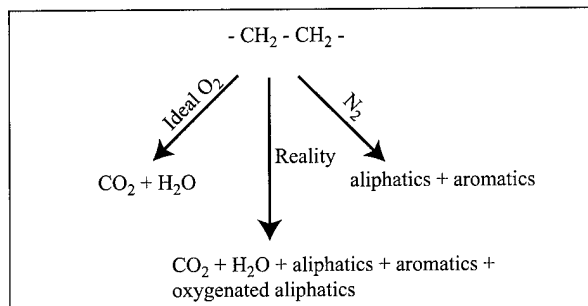
Figure 6 combustion reactions of halogen free polyolefins under different fire conditions.

Fluorinated Ethylene Propylene Copolymer (FEP)
FEP is a copolymer of tetrafluoroethylene and hexafluoropropylene. It has most of the desirable properties of the original fluoropolymer, polytetrafluoroethylene (PTFE). Copolymerisation with hexafluoropropylene results, however, in a side branch which decreases its melting point, making it possible to process FEP by conventional extrusion techniques. Accordingly, both have a similar chemical structure and are fully fluorinated polymers consisting of 76% fluorine by weight.

Having a limited oxygen index of 95%, FEP is highly flame retardant. Cone calorimetry shows that the FEP insulated plenum cable burns with a low heat release and forms a thin white smoke giving good visibility. The cable shows, however, low ignition times and high carbon monoxide levels especially at heat fluxes over 40kW/m².

The TGA investigation show that FEP starts to decomposes at approx. 400°C in air. In nitrogen the decomposition temperature is increased by about 40°C. The C-F bond strength is approx. 115kcal/mol compared with less than 100 kcal/mol for the C-H bond in a hydrocarbon[21]. This accounts for the high thermal stability of the polymer.

GC/MS study of the fire gases of FEP is summarised in table 13.

Table 13. Quantification of the major fire gases from FEP at non-ventilated fire conditions at 575°C

	g/g initial polymer
Carbon dioxide (CO2)	0.49
Carbon monoxide	0.034
Hydrogen fluoride	0.49
Perfluoro aliphatics	0.23 estimated
Fluoro-oxygenated compounds	0.14 estimated
Airborne particles	0.009
Residue	0
Total	1.393

A large amount of hydrogen fluoride was identified. About half of the original polymer ended up as HF, which is three times as much as the HCl content from the PVC sample. Like hydrogen chloride, hydrogen fluoride a strongly irritant acid. It is said to be highly irritant at a level of 120 ppm compared with 200 ppm for HCl[6]. It has a somewhat lower LC50 value, 2250 ppm, than that which is commonly reported for HCl (table11). Carbon monoxide was in the same range as for the other polymers and comparably lower than in the well ventilated cone calorimeter experiment. Large amounts of fully fluorinated aliphatics and fluoro-oxygenated compounds, especially trifluoroacetic acid, were also observed.

An unsaturated perfluoroaliphatic like perfluoroisobutylene (PFIB) is reported to be very toxic having an Approximate Lethal Concentration of only 0.5 ppm after 6 hours exposure to rats i.e. six times as toxic as phosgene[17]. On the other hand substances such as tetrafluoroethylene and hexafluoropropene are harmless, with ALC values of 40,000 and 2650 ppm after six hours exposure to rats[22]. PFIB has not been specifically sought in this investigation. In most published works on the decomposition of PTFE it is however reported to be present[4, 9, 22]. Fluoro-oxygenated compounds such as carbonyl fluoride have a relatively low LC50/30 min value of 720 ppm while a substance like 2-fluoroehtylfluoroacetate is very toxic having a LC50/30 min value of 5.7 ppm[13]. Trifluoroacetic acid is a highly corrosive substance. Its vapour mist is very irritating and can be destructive to the eyes and respiratory system[23]. Some workers have reported carbonyl difluoride to be the major decomposition product of PTFE and FEP[3, 24]. In our investigation, where the continuous air flow contained 2000 ppm water, only trace amounts of carbonyl difluoride were found. If water is present carbonyl difluoride is quickly hydrolysed to carbon dioxide and water:

$$F\text{-}\overset{\overset{\text{O}}{\|}}{C}\text{-}F + H_2O \longrightarrow 2HF + CO_2$$
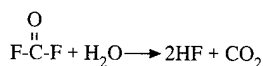
Our recently reported work[5] including testing of a FEP containing plenum cable according to IMO MSC.41 (64), a test in which the hazard is assessed by virtue of the individual concentration of a number of specified gases. Including HF but **not carbonyl difluoride**. Only a small amount of HF was identified. This test is performed in a closed chamber, which probably results in so small an amount of water that carbonyl fluoride will be the main toxic component in these conditions.

The main decomposition reactions of FEP are outlined in Figure 7.
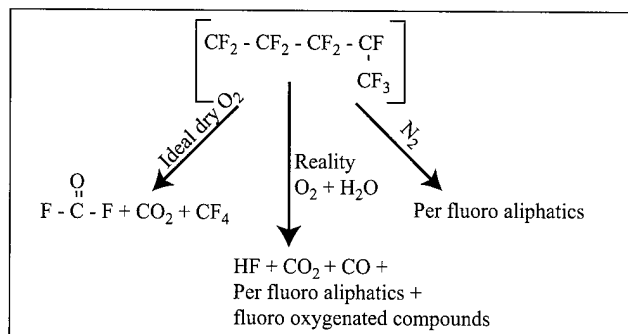
Figure 7. Decomposition reactions of FEP under different fire conditions

The current investigation shows that FEP produces a comparatively low amounts of airborne particles. However, under certain fire conditions it has been found that such particles from FEP/PTFE can be "super toxic"[3, 13, 17, 22]. The particulate consists of FEP/PTFE chain fragments with molecular weights in the 2000-4000 range, and a number of particles in the 0.01-0.15um diameter range[13]. When small pieces of PTFE/FEP are decomposed in such way as to produce extreme toxicity, the normal decomposition products (HF, carbonyl difluoride, PFIB etc) are present at concentrations too low to have any toxic effect. Rats exposed to these conditions do not show signs of sensory irritation, but at some time during a 30 minute exposure they develop a pattern of rapid shallow breathing indicative of irritation of the deep lung. The rats usually die within a few hours following exposure and the pathological signs are those of severe pulmonary oedema and congestion[13]. Mice surviving exposure to the particulate show irreversible damage to the lung[25].

The highest toxicity occurs when perfluoropolymers are decomposed under non-flaming conditions across a temperature range of 400-650°C, and when the primary decomposition products are subjected to continuous secondary heating[13]. Under these conditions PTFE achieves an LC50 value of 0.05mg/l (mass loss), approximately 1000 times as toxic as wood and most other materials. When the polymer is decomposed under such conditions that the super toxic particles are not formed the LC50 value is typically 2.9mg/l, approximately ten times as toxic as wood and other materials. Toxicity in this case is due to upper respiratory tract and airway irritation and is consistent with the known effects of hydrogen fluoride and carbonyl fluoride[13].

It is also reported that the decomposition products of perfluoro polymers may cause an influenza-like illness, "polymer fume fever" when heated above 300°C in an oven, an extruder, or even by friction of a tool edge against the polymer in high speed machines[25]. The symptoms normally occur a few hours after exposure with a gradual increase in temperature, pulse and possibly respiration rate, followed in most cases by episodes of shivering and sweating and a rapid consequent recovery[26].

Conclusions

1. A mass balance has demonstrated potential to quantify all products of decomposition.
2. GC/MS has been shown to be a procedure amenable to this study.
3. The chemical structure of the polymer is the main parameter deciding fume composition and hence its irritancy and toxicity.
4. The model fire conditions strongly influence CO_2/CO and aromatic/aliphatic ratios.
5. The GC/MS study revealed the combustion fumes to contain (in order of mass);

   PVC

   CO_2, aromatic hydrocarbons, HCl, oxygenated hydrocarbons, airborne particles, CO, chloro-aromatics, aliphatic hydrocarbons. The principal hazard is the extreme irritancy of the HCl/CO combination and the short and long term toxicity of the halogenated hydrocarbons.

   LSZH

   CO_2, aliphatic hydrocarbons, aromatic hydrocarbons, CO, oxygenated hydrocarbons and airborne particles. The principal hazard is CO.

   FEP

   HF, CO_2, perfluoroaliphatics, fluoro-oxygenated hydrocarbons, CO and airborne particles. The principal hazard is the massive formation of corrosive and irritant HF and, under certain fire conditions, the formation of very toxic airborne particles. Dependant on the fire conditions, the decomposition products of fully fluorinated polymers are reported to be 10-1000 times more toxic than most other polymers[13].

6. It should be noted that in some previously reported studies involving FEP, large amounts of carbonyl difluoride have been identified, a substance somewhat more toxic than HF. It is believed that under the more humid conditions chosen in this work, with an air (2000ppm water) flow of 2 litres per minute, carbonyl difluoride is hydrolysed to HF and CO_2.
7. A large number of chlorinated and fluorinated substances of unknown effects on humans are formed from FEP and PVC.

Acknowledgement

References

1. Sultan, B-Å., Ericsson, K., Hirvensalo, M., Hjertberg, T., and Häninen, M., "Novel Halogenfree Flame Retardant Polyolefins Intended for Internal Wiring – Properties and Flame retardant Mechanism", International Wire and Cable Symposium, Philadelphia, USA, 1998.
2. Hartzell, G.E., Packham, S.C., Grand, A.F. and Switzer, W.G., "Modelling of Toxicological Effects of Fire Gases part III, J. Fire Sciences, Vol. 3, May/June, 33-40, 1985.
3. Coleman, W. E., Scheel L. D, Kupel, R. E., and Larkin R. L., "The Identification of Toxic Compounds in the Pyrolysis Products of Polyterafluoroethylene (PTFE)", American Industrial Hygiene Assoc. J. Jan-Feb., 1968.
4. Fardell, P. J., "UK Studies of the Toxic Potency of PTFE in Fire", 257-271, Interflam, UK, 1990.
5. Robinson, J. E., Samson, F., and Sultan, B-Å., "Cable Fire Smoke and Toxicity", Eurocable 2000, Stuttgart, Germany, 2000.
6. Fagrell, O. and Robinson, J.E., "Low Cost Building Wire in a Large Scale Fire", Plastics in Telecommunication VIII Procedings, London, Sept 1998.
7. Palma, G., and Carenza M., J. Appl. Polym. Sci. A, 2, 3505, 3515, 1964.
8. Hirchler, M.A., Purser, D. A., "Irritancy of the Smoke (Non-flaming Mode) from materials Used for Coating Wire and Cable Products, both in the presence and Absence of Halogens in their Chemical Composition", Fire and Materials, Vol 17, 7-20, 1993.
9. Hartzell, G. E., Grand, A. F., and Switzer, W. G. "Modelling of Toxicological Effects of Fire Gases part IV", J. Fire Sciences Vol. 5, Nov./Dec., 368-391, 1987.
10. Barrow, C. S., Alaire, Y., and Stock, M., F., "Sensory Irritation Evoked by the Thermal Decomposition Products Of Plasticized Poly(vinyl chloride)", Fire and Materials, Vol. 1, 147-153, 1976.
11. Lester, D., and Greenberg, L.A. Arch. Industr. Hyg. 2, 335, 1950
12. Klimisch, H. J., Doe, J. E., Hartzell, G. E., Packham, S. C., Pauluhn, J., and Purser, D. A., "Bioassay Procedures for Fire Effluents: Basic Principles, Criteria and Methodology", J. Fire Sciences, Vol. 5, March/April, 73-104, 1987.
13. Purser, D. A., "Recent Developments in Understanding the Toxicity of PTFE Thermal Decomposition Products", Fire and Materials, Vol. 16, 67-75, 1992.
14. Matijak-Schaper, M., and Alaire, Y., "Toxicity of Carbon Monoxide Hydrogen Cyanide and Low Oxygen, J. Combustion Technology, Vol. 9 21-61, 1982.
15. Sasse, H. R., Einbrodt, H. J., and Prager, F., H., "Development of a Safety Concept for Assessment of the Toxicity of Combustion Products", J. Fire Sciences, Vol. 6, Jan./Feb., 43-60, 1988.
16. Alexeff, G. A., and Packham, S. C, "Evaluation of Smoke Toxicity Using Concentration-Time Products", J. Fire Sciences, Vol. 2, Sep./Oct., 362-379, 1984.
17. Zapp, J. A., Jr., Limperos, G., and Brinker, K. C., "Toxicity of Pyrolysis Products from Teflon Tetra fluoroethylene Resin", Amer. Inust. Hyg. Assoc., Annual Meeting May 1955.
18. Harland, W. A., and Anderson, R. A., "Causes of Death in Fires", Confernece on Smoke and Toxic Gases from Burning Plastics, London, 6-7 January 1982, P15/1-15/19, London: QMC Industrial Research Ltd.
19. Purser, D. A., and Berill, K. R., "Effects of Carbon Monoxide on Behaviour in Monkeys in Relation to Human Fire Hazard, Archives of Environmental Health, Vol. 38, No 5, Sep./Oct., 308-315, 1983.
20. Wallace, D. N., "Dangers of PVC Wire Insulation Decomposition. I. Studies of Fire Fighters of the 1975 New York Telephone Fire and of Survivors of the1977 Beverly Hills Supper Club Fire", J Combustion Toxicology, Vol. 8, Nov., 205-232, 1981.

21. Gilbert, A. G. (Chairman), "Flammability, Smoke, Toxicity, and Corrosive Gases of Electric Cable Materials", Nationals Material Advisory Board, National Academy of Sciences, p. 73, Washington D. C., Publication No NMAB.342, 1978

22. Waritz, R. S., and Kwon, B. K., "The Inhalation Toxicity of Pyrolysis Products of Polytetrafluoroethylene Heated Below 500 Degrees Centigrade", American Ind. Hygiene Assoc. J. Jan.-Feb., 1968.

23. Laboratory safety http://www.qrc.com/hhmi/science/labsafe /icss/icss86.htm

24. Kupel, R. E., Nolan, M., Keenan R. G., Hite, K., and Scheel, L. D., "Mass Spectrometric Identification of Decomposition Products Polytetrafluoroethylene and Polytetrafluoro-ethylenepropylene", Anal. Chemistry, Vol. 36, No. 2, 386-389, February 1964.

25. Scheel, L. D., Lane, W. C., and Coleman, W. E. "The Toxicity of Polytetrafluoroethylene Pyrolysis Products-Including Carbonyl Fluoride and a Reaction product, Silicon Tetrafluoride", Amer. Ind. Hygiene Assoc. J., Jan-/Feb., 41-48, 1968.

26. Harris D.K., "Polymer Fume Fever", The Lancet, Dec. 1, 1009-1011, 1951.

Biographies

Bernt-Åke Sultan (bernt-ake.sultan@borealisgroup.com) is managing Borealis' marketing and development group for low voltage and internal cables. He graduated with a M.Sc degree in Chemical engineering in 1981 and obtained later a Ph.D., from Chalmers University of Technology Gothenburg, Sweden. His thesis covered studies of the thermal degradation behaviour of ethylene copolymers. Since 1984 he has been working with development of Borealis products intended for cable applications. His contribution to IWCS 1998 was chosen as the "most outstanding technical paper".

James Robinson (james.robinson @borealisgroup.com) completed his Msc (Imperial College, London) in 1973. He has since held numerous posts involving development and technical service of polyolefins for use in cable applications. He is currently responsible for the marketing and development of cable products for building applications within the Borealis W&C Business Unit

Filip Samson (filip.samson@ borealisgroup.com) completed his studies ("gegradueerde Chemie", HTI St Lieven, Ghent) in 1985. He has worked in the W&C department of Borealis Antwerp since 1992. Currently he holds the post of Development Engineer, in the Stenungsund laboratory of Borealis. Special interests include the analysis and toxicologic properties of combustion fumes.

Polyethylene Based Black Jacketing Compounds: Structure-Compounding-Performance Relations

Chun D. Lee and Tim S. Schloemer
Equistar Chemicals, LP. Cincinnati, OH 45249
Chun.lee@equistarchem.com

Abstract

Polyethylene (PE) black cable jacketing compounds containing 2.35 - 2.85 wt% carbon black (CB) have been widely used in the wire and cable industries. These cable jacket materials offer excellent performance and properties, such as processability, environmental stress crack resistance (ESCR), tensile strength, low temperature properties, shrinkage, moisture resistance and ultraviolet (UV) stability. These performance characteristics are attributed to the resin morphology and structure of the resin such as the molecular weight (Mw), molecular weight distribution (MWD), short-chain branching, and CB filler dispersion.

Jacketing compounds were produced with several PE resins and black master batches (MB) using both commercial batch and continuous mixers. The compounds produced by the continuous mixer exhibited significant change in melt index (MI), melt viscosity, and elasticity number, compared to those compounds prepared by the batch mixer. The change derives from the development of long chain branching (LCB) coupled with the degradation processes. The compound with higher LCB level shows poorer ESCR, higher shrinkage, and higher extrusion head pressure than that with lower LCB. For a given resin formulation, the change in structure was related to the thermo-mechanical stability of the CB master batches (CB MB).

A new commercial CB MB has been developed to minimize this change and yield performance enhancements compared to traditional MBs. The enhanced performance is the result of an improved thermo-mechanical stability with excellent CB dispersion.

Introduction

PE based jacketing compounds containing 2.35 to 2.85wt% carbon black (CB) have been used for telecommunication, fiber optics, coaxial, and power cables in the wire and cable industries. This wide range of jacketing end-uses can be attributed to the unique combination of excellent mechanical properties, long-term weatherability, processability, and performance characteristics for cable design and applications [1-4]. Telecom applications require excellent environmental stress crack, processability, and low temperature brittleness whereas power cables need excellent high temperature resistance. Fiber optic cables construction requires not only excellent mechanical strength but also superior environmental stress crack resistance and minimum jacket shrinkage. Thus, the selection of suitable jacketing material for a specific application is critical to provide a good balance in all properties of importance.

There are several ways of compounding jacketing materials commercially. Two of the most common type of equipment in jacket compounding are continuous mixers such as a Farrel Continuous Mixer (FCM) and batch type mixers such as a Banbury Mixer (BM). Each mixer has its advantage and

disadvantage for commercial use and the selection of suitable compounding equipment depends on a) equipment price, b) machine capabilities, c) flexibility of operation, d) machine quality and reliability, e) technical assistance, and f) others. In general, a FCM provides better productivity than a BM. However, a high shear mixing process for FCM sometimes leads to product quality problem resulting from a degradation process present during the compounding process.

We produced several commercial jacketing compounds with ranges of MI (0.2 to 0.9 g/10 minutes) and densities (0.930 to 0.950 g/cc). It was found that the FCM compounds produced significant change in structure compared to those from the BM. We investigated the nature and origin of such a structural change and the effect of the structural change on the performance of compounds. It is also our aim to explore the way of minimizing such a structural change occurring during the jacket compounding process or during end-use applications.

Experimental

Materials

Jacketing compounds were produced with 2.4 to 2.6 wt% CB content from the CB MB "A" and "B" using the commercial BM and FCM. All compounds contain suitable antioxidant packages.

Methods

A Rheometrics ARES equipped with parallel plates was used to determine the complex viscosity as a function of frequency at 190 $^\circ$ C for base PE resins and compounds. We also estimated the melt elasticity number (ER) from the G'(storage modulus) and G"(loss modulus) curves from the dynamic data [5]. A TA Instruments 2910 DSC was used to determine melting and crystallization of compounds. Tensile properties were determined by ASTM D-638. ESCR was determined by ASTM NCTL D5397 which is a stress cracking under a constant tensile load (30% of yield stress) condition and an accelerated environmental condition in 10% Igepal.

Thermo-mechanical stability tests were carried out using a Haake Rheomex 90 at 80 RPM and 230 $^\circ$ C for the master batches. The master batch was let down into a LDPE (1.0 MI, 0.920 density) with 5.2wt% CB. We monitor a torque rise as a function of mixing time. The torque rise was used as a measure of stability and confirmed later from the rheological testing from the stability tested samples.

Wire extrusion runs were carried out on a 64 mm Davis-Standard line using a double angle die and 24 AWG Cu at 180 m/minute to prepare cable insulation for shrinkage tests and to determine processibility. Shrinkage tests were conducted on 10 specimens of 15 cm long insulation (with removal of wire) by aging at 100 $^\circ$ C for 24 hours.

Results and discussion

Table 1 shows MI and densities of the PE base resins, PE-A and PE-B and the jacketing compounds. As expected, addition of CB reduces MI and raises density as compared the base resin to the compound. We observed more dramatic change in MI between the FCM and the BM compounds. The FCM compound acts like higher molecular weight (Mw) material than the BM (based on an inverse relation of MI to Mw). Since each compound in the group has the identical formulation, lowering MI for the FCM compound resulted from the experence of chain extension or cross-linking reaction coupled with a degradation process during the high shear compounding process. An enhanced viscosity at the low frequency region (Figure 1) supports a presence of a degradation process leading to a development of higher viscous compound.

Table 1. Basic data for the compounds

Compound [1]	Mixing [2] equipment	Master [3] batch	MI	Density
PE-A	-	-	0.70	0.920
A-1	BM	A	0.66	0.931
A-2	FCM	A	0.60	0.930
PE-B	-	-	0.73	0.931
B-1	BM	B	0.72	0.941
B-2	FCM	B	0.48	0.941
C-1	BM	A	0.18	0.946
C-2	FCM	A	0.13	0.947
D-1	BM	A	0.28	0.949
D-2	FCM	A	0.20	0.949

1) PE-A and PE-B are the PE base resins of the compounds in Groups A & B

2) BM stands for Banbury Mixer and FCM = Farrel Continuous Mixer

3) A and B are 31% CB master batches based on LDPE and MDPE.

Figure 1. Dynamic rheological data for the compounds
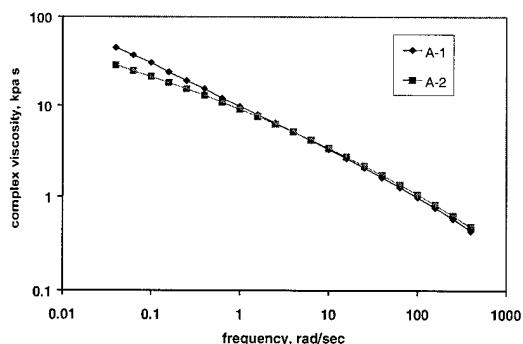
As shown in Table 2, a change in MI shows little effect on the crystallization behavior such as crystalline melting (Tm), crystallization (Tc), and heat of fusion (a measure of crystallinity). Such a very similar crystallization behavior for the compounds in each group leads to similar tensile properties of the compounds such as yield strength, elongation at break, and tensile strength (Table 3). An increase in yield strength going from group A to D results from increase in density (crystallinity).

Table 2. DSC data for the compounds

Compound	Tm °C	Tc °C	Heat of Fusion J/g
A-1	118	108	106
A-2	118	108	105
B-1	123	112	146
B-2	124	111	143
C-1	126	116	161
C-2	126	116	160
D-1	128	117	197
D-2	128	116	193

Table 3. Tensile data for the compounds

Compound	Yield Strength Mpa	Elongation %	Tensile Strength Mpa
A-1	10.1	910	21.5
A-2	10.6	830	21
B-1	17.7	890	27
B-2	17.0	920	28.1
C-1	20.2	890	31.1
C-2	20.3	910	31
D-1	22.6	580	22.7
D-2	23.3	750	23.3

Table 4 shows the melt viscosity, melt elasticity parameter (ER), extrusion data, and shrinkage of the base resins and compounds. For a given linear PE, ER is associated with the level of long chain branching (LCB)[5]. The addition of CB into PE base resin raises both melt viscosity and ER as compared to the base PE resin to the compound such as PE-A to A-1 or A-2 and PE-B to B-1 or B-2. Addition of fine solid particles into liquid enhances viscosity of mixture due to a volumetric effect of solid particles with large surface area. In general, an addition of inorganic filler reduces melt elasticity such as die swell [6]. Also, addition of CB into the PE matrix with 2.4 to 2.6% does not contributes the formation of any levels of LCB. However, increase in ER on adding CB results from a certain extent of LCB addition in the PE matrix phase. We believe that an increase in ER is due to the presence of chain extension or cross-linking reaction coupled with a degradation of the high shear FCM process. A presence of CB appears to be promoting degradation process, leading to the dramatic enhancement in viscosity as well as elasticity. We will show more evidence to support this observation. Such a viscoelastic enhancement of the FCM compounds results in increased extrusion head pressure. Higher shrinkage shown by the FCM compound appears to be due to more residual stress associated with the slower relaxation behavior of higher LCB, compared to the BM.

Table 4. Melt viscosity, elasticity number (ER), extrusion head pressure, and shrinkage data for the compounds

Compound	viscosity [1] kPa s	ER	Head Pressure Mpa	Shrinkage %
PE-A	20.2	3.0	-	-
A-1	21.3	3.3	16.0	5.2
A-2	30.5	4.1	18.2	6.0
PE-B	20	3.6	-	-
B-1	20.2	4.0	17.4	5.3
B-2	25.7	5.2	19.5	7.8
C-1	49.1	4.5	25.0	6.6
C-2	58.7	6.7	27.5	7.4
D-1	40.9	5.6	21.6	4.5
D-2	51.4	7.4	23.5	6.3

1) Taken at 0.1 rad/sec

It is interesting to note some correlation between structure and ESCR. In general, higher Mw (lower MI) in linear PE resins shows better ESCR, when other structural parameters such as MWD, density, and comonomer type remains similar. This is based on the fact that the longer the polymer chains and random coil length, increases the population of tie chains [7,8]. Consequently, the ESCR goes up with Mw. Theoretical calculations predict a maximum in the tie chains probability versus density at about 0.935 [9]. For higher density than 0.935, lamella thickness is large which reduces the number of effective tie chains due to folding of chains on the same lamellae. Thus, for density above 0.935, it is expected that ESCR will decrease with an increase in density provided the other molecular structure variables such as Mw, MWD, and comonomer type remains same.

Table 5 shows ESCR data of the PE base resin and compounds in relation to MI, density, and ER. We observed the followings: 1). PE base resin shows better ESCR than the compound, 2) ESCR decreases with an increase in density, 3) lower MI reduces ESCR, 4) For a given density (> 0.935), higher ER reduces ESCR. Interestingly, compounds A-1 and A-2 showed little change in ESCR in spite of dramatic change in MI, viscosity, and elasticity. This might be due to the nature of such a lower density for the compounds. Basically, the reduction in MI results from an increase in not Mw but LCB. An evidence for this statement will be given in the later section.

Table 5. NCTL ESCR data for the compounds

Compound	ESCR, hr [1]
PE-A	>1300
A-1	>1300
A-2	>1300
PE-B	88.7
B-1	75.4
B-2	50.2
C-1	63.4
C-2	50.4
D-1	6.8
D-2	3.3

1) Standard deviations for the data were less than 6% for all test samples.

The reduction in ESCR for the higher density (> 0.935) compound with a higher level of LCB appears to be resulting from the combined effects: 1) higher LCB relatively reduces the population of tie molecules and 2) slower relaxation process leads to more build-up of residual stress during the cooling stage. More work is needed to confirm this observation. The significant effect of residual stress on the reduction of ESCR has been discussed in the literature [10].

A. Root cause of enhanced melt viscosity and elasticity

In order to understand higher viscosity and ER from the FCM compound compared to the BM, we treated the base PE-B (without CB addition) using the Haake mixer at 230 ° C for 10 minutes (referred to sample-I) and 30 minutes (sample-II). longer treatment produces more degradation than shorter. As shown in Figure 2, sample-II showed much higher viscosity at the low frequency range (< 0.1 rad/sec) than sample-I. Sample-II also showed much higher ER (= 8.2) than sample-I (ER= 6.0). Untreated PE pellets showed a ER of 5.2. This rheological data indicate that sample-II acts like a higher Mw (lower MI) material than sample-I. Such an enhancement in viscosity and ER for sample-II resulted from a presence of more of the degradation process developed by the longer thermo-mechanical treatment. This viscosity and ER variation between sample-I and –II is similar to that between the BM and FCM compounds.

Figure 2. Dynamic rheological data for the stability tested PE resins: sample-I (10 minutes treated) and sample-II (30 minutes)
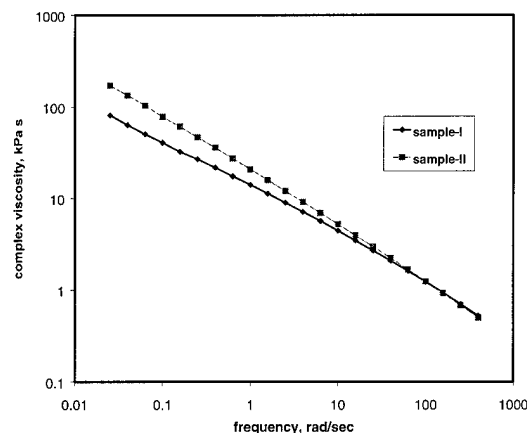
Such a dramatic difference in viscosity should show a Mw difference in the GPC data. Figure 3 shows the GPC curves of sample-I and sample–II. There is little difference in the curves of Mw species between sample-I and sample–II. Tabulated numbers also indicates little difference in Mw and MWD (= Mw/Mn) for two samples. A presence of a small amount of LCB in linear PE polymers does not affect the GPC curves but significant in the rheological data [11,12]. We observed a very similar behavior for sample-I and –II. This leads to a conclusion that the dramatic increase in viscosity and ER for the FCM compound originates from a presence of higher level of LCB. This observation is in line with the previous statement of LCB based on the reference [5]. The mechanism of LCB formation via the hydrogen abstraction process during the degradation process has been also published in literature [13].

Figure 3. GPC data for the stability tested PE resins (the same samples in Fig. 2)
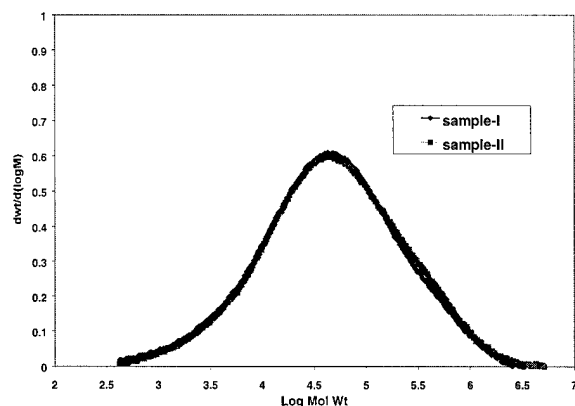
It is also well known that the presence of CB in molten compound accelerates the degradation process during compounding process. The extent of acceleration depends on the stabilization and compounding process. Figure 4 shows the result of stability test for the blend of the LDPE (0.920 density, 1 MI) with the black MB "A", compared to that of the base LDPE resin. We observed more torque rise as a function of mixing time for the black compound compared to the base PE resin. More torque rise for the compound indicates a presence of more chain extension, leading to the development of more LCB with the mixing time.

Figure 4.Stability test results for the PE base resin and PE+ MB "A"
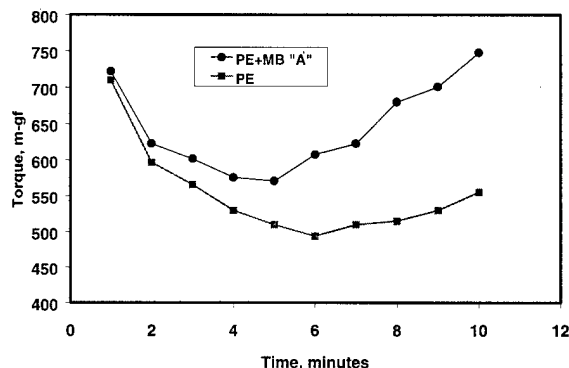
This leads to the conclusion that the FCM compounding process promotes more degradation (as compared to BM) leading to the creation of more LCB in the finished jacketing compounds. This is due to the higher shear FCM compounding process with a higher temperature in the presence of CB.

B. Improved jacketing compounds

We developed a new commercial 40% CB MB (termed MB"C") to eliminate or to minimize a problem associated with the compounding process and to enhance the performance of the finished jacketing compound. Table 6 shows a summary of basic data and performance for compounds A-1 (as a control for comparison purpose) vs. A-new (produced by MB "C") and B-1

(control) vs. B-new (by MB "C") with the same BM process. The compounds with the new MB showed enhanced MI, reduced viscosity, reduced ER, reduced shrinkage and improved ESCR compared to corresponding compounds produced by MB "A" and "B". The improvement by the use of MB "C" resulted from minimized degradation during the compounding process. The stability test for the MB "A" vs. "C" (Figure 5) indicates that the use of the more thermo-mechanically stable MB "C" (as indicated by little change in torque with mixing time in the figure) minimizes the formation of LCB in the final jacketing compound leading to enhanced performance.

Table 6. Basic data for the new compounds, A-new & B-new from the MB "C", compared to those control compounds A-1 & B-1 made from MB "A" and "B"

Compound	MI	Viscosity, kPa s	ER	Shrinkage %	ESCR Hrs.
A-1	0.66	21.3	3.3	5.2	> 1300
A-New	0.92	17.8	2.9	3.5	> 1300
B-1	0.72	20.2	4.0	5.3	75.4
B-New	0.89	15.9	3.6	3.8	83.4

Figure 5.Stability test results for PE+ MB "A" and PE+ MB "C"
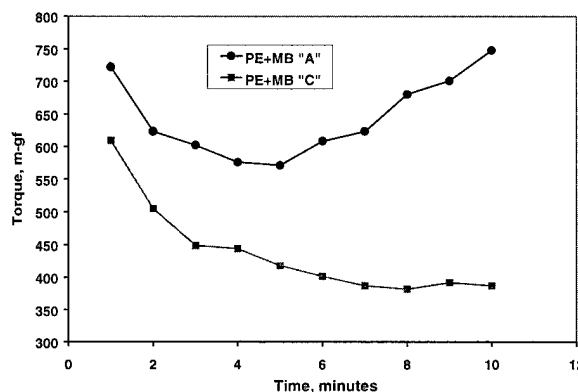
We further investigated a concept to have an improved economic jacketing composition without deteriorating the performance. One way is to use a direct dry blend of the MB "C" with resin pellets for producing a final jacketing cable product. In order to simulate the jacketing process, the dry pellet blend of PE-A with MB "C" (2.6wt% CB content) was extruded through a Davis-Standard single screw extruder and pelletized for evaluations. Rheological data indicates little change in viscosity and ER for stability tested sample (even for 30 minutes mixing) and the ESCR of the product was similar to or better than the corresponding BM compounds (see Table 6). CB dispersion data (as a courtesy of Cabot Corporation for Figure 6) indicates that the Davis-Standard product (Fig. 6 (B)) shows an excellent CB dispersion compared to the commercial A-1 compound (Fig. 6 (A)) produced by the BM. Therefore, we concluded that the use of a thermo-mechanically stable black MB is the most desirable to producing a jacketing compound with acceptable performance regardless of the compounding process.

Figure 6. CB dispersion data: (A) for the compound A-1 , (B) for David-Standard product
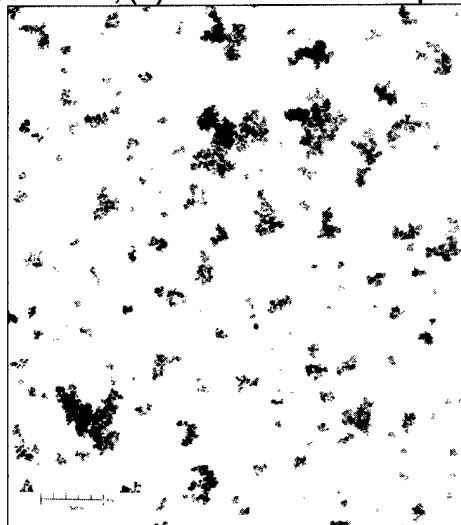
(A)
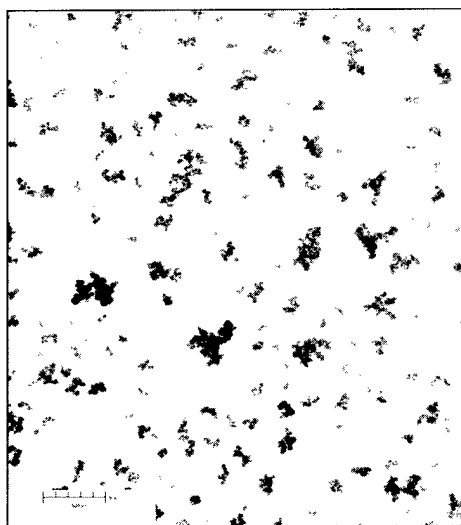
(B)

CONCLUSIONS

The FCM produces a jacketing compound with lower MI, higher viscosity, elasticity number than the BM. This rheological change results from the development of a higher level of LCB associated with the degradation process occurring during the higher shear compounding process. It was found that such a rheological change imparts little change to tensile mechanical properties due to little change in the compound crystallinity. However, the rheological change affects some properties as well as performance such as shrinkage, extrusion head pressure, and ESCR. The extent of variation in the ESCR data appears to be dependent of the density range of the compounds.

The use of thermo-mechanically stable master batches minimizes or eliminates such a rheological change regardless of compounding process. Thus the compound produced by the stable MB shows better performance than that with the less stable MB.

References

1. Yamacuchi, K., & Kishi, H., International Wire & Cable Symposium, P272 (1976)
2. Kale, L.T. and Bow, K.E., SPE ANTEC., **96**, P1647 (1996)
3. Rogestedt, L. and Martinsson, H.B., International Wire and cable Symposium, P126 (1997)
4. Chun, D and Leech, J.R., Imternational Wire and Cable Symposium, P807, (1999)
5. Shroff, R. and Mavridis, H., J. Appl. Polym. Sci., **57**, P1605 (1995)
6. Khanna, Y. P. and Slusarz, K.R., Polym. Eng. Sci., **33**, P122 (1993)
7. Chrissman, J. M., Polym. Eng. Sci., **29**, P1598 (1989)
8. Duvall, D.E. and Broutman, L.J., SPE ANTEC, P140 (1992)
9. Hosoda, S and Umera, A., Polym. J., **24**, P939 (1992)
10. Huang, Y.L. and Brown, N., J. Mat. Sci., **23**, P3648 (1988)
11. Shroff, R. and Lee, C., Equistar Imternal Report (199
12. Shroff, R., Prasad A., & Lee C., J. Polym. Sci. Phys ed. 34, 2317 (1996)
13. Rideal, G. R. and Padget, J.C., Polym. Eng. Sci., **57**, 1 (1976)

Authors
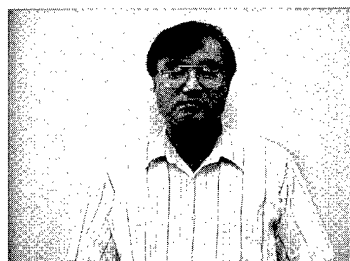
Chun D. Lee
Equistar Chemicals, LP
Equistar Technology Center, Cincinnati, OH 45249

Chun Lee received his Ph. D. degree in Polymer Science and Engineering from the Case Western Reserve U. in 1984. Chun joined the company in 1984 and is currently in the Product Development group within the Wire and Cable Group focusing on the Communications Market segment.

Tim S. Schloemer
Equistar Chemicals, LP
Equistar Technology Center, Cincinnati, OH 45249

Tim Schloemer received his Bachelor of Science degree in Materials Engineering from the University of Cincinnati in 1994. Tim joined the company in 1992 and is currently the Applications Specialist for the Wire and Cable Group providing technical support to the Communications Market segment.

Analysis Techniques for
Loop Qualification and Spectrum Management

David L. Waring
Stefano Galli
Kenneth Kerpez
John Lamb
Craig F. Valenti

Telcordia Technologies, Inc.©
Morristown, New Jersey
+1 973 829-2000

Abstract

The telecommunications industry has worked for over a decade to develop digital subscriber line (DSL) technologies to revitalize the embedded copper plant. Now the industry is on the threshold of reaping the benefits of this effort, bringing megabit-per-second connectivity to offices and homes. However, network providers must properly manage the introduction and application of these systems to the local network. Accurate engineering is critical to avoid incompatibilities and failed provisioning that would otherwise create customer disappointment, delay and higher costs.

An understanding of subscriber loop make-ups, including length, wire gauge and location of bridged taps, is key to the proper engineering of DSL systems. While some loop records exist, they may be inaccurate or out of date. Knowing the types of systems that are transmitting in a given cable is also critical, because of the resultant crosstalk and the potential need for spectrum management. In this paper, we describe techniques for obtaining precise loop make-ups, and for determining the current crosstalk profile in the loop plant.

1. Achieving the Full Potential of DSL Technology

Among the new techniques being used to upgrade the public network are access technologies that use embedded copper plant to support higher bandwidth services. These technologies include ISDN, HDSL, ADSL and others for which carriers have announced aggressive deployment plans.

The new DSL technologies have the potential to become strategically important to an operator's business plans. While they have proven robust in trials, any new technology, no matter how powerful and reliable, must be properly applied. This involves several engineering tasks, the two most important of which are:

- Loop qualification - knowing what type of DSL system and what bit-rate can be successfully and reliably provisioned on a given customer's loop.

- Spectrum management - an engineering process that allows an operator to place new DSL systems into the plant in compliance with spectral compatibility guidelines and standards, and to troubleshoot field problems suspected of being caused by crosstalk from other systems.

Maintaining accurate records of the loop plant is important to many aspects of an operator's business. Beyond supporting traditional voice services, even more accurate and detailed loop records are needed when deploying DSL-based services. These technologies are typically engineered to operate over a class of subscriber loops, such as Revised Resistance Design (RRD) loops (up to 18 kilofeet), or Carrier Service Area (CSA) loops (up to 12 kilofeet). In fact, the need to be able to qualify a loop for use with one of these technologies is becoming critical as the technologies emerge and deployment begins. The ability to easily and accurately qualify loops will allow operators to offer a range of new services. Conversely, problems and high expenses associated with qualifying loops could inhibit deployment, thus lowering or eliminating associated new revenues.

Several approaches and tools are being developed to facilitate loop qualification. The most common is mining existing data in loop databases, checking it for accuracy, and then bulk-provisioning loops that are candidates for DSL-based service. Sometimes a combination of loop records and engineering information about feeder route topology is used to obtain an estimate of loop length. Another technique uses loop loss measurements from traditional POTS loop testing systems to estimate loop length.

These approaches use good engineering judgement and result in large populations of loops that are likely candidates to support advanced services. However, a typical approach is to minimize customer disappointment by biasing the techniques toward low probabilities of false-positive results. This is done at the expense of increasing the probability of false-negative results. In other words, the approaches are conservative, and some loops that might support DSL service remain unused.

Other loop qualification methods use the adaptation settings of a modem operating over the subscriber loop of interest. For example, if a DSL system is operational, the adaptive filter settings contain useful information about the loop. This approach has the decided disadvantage that a DSL system must first be in operation on the loop which one hopes to qualify. Yet another technique called the Sapphyre^{SM} technique uses standard dial-up modems that operate over any subscriber loop to glean voice-band information about the loop, in order to predict performance at higher frequencies of interest to DSL.

It would be desirable to have a technique that could identify and qualify all nonloaded subscriber loops in a mechanized and highly accurate manner without the need for special equipment or intervention at the subscriber's location. In the following section, such a system is introduced.

Historically, local exchange carriers have carefully controlled systems that they place in the distribution network. T-carrier, used to support digital loop carrier remote terminals and private line services, is a highly engineered transmission system with carefully controlled power levels and pulse templates. ISDN Basic Rate Access and 2B1Q-based HDSL were carefully engineered for spectral compatibility assuming worst case scenarios of long loops with bridged tap and high binder group fills. A similar philosophy was initially proposed for ADSL. However, ADSL standards deliberations were more vendor-driven, and more aggressive. In particular, the option to use a historically high transmit power level was allowed. Simulations show that, under certain conditions, such systems could result in spectral incompatibilities, wherein crosstalk from one type of system interferes with another type of system.

Part of the rationale used to approve more aggressive ADSL standards was that local telephone companies could pick and choose among technologies and set power levels via software provisioning to control the spectral environment. However, several issues now complicate an operator's ability to deal with the situation. First, multiple technologies are being developed by equipment manufacturers, including DMT, CAP and QAM. Second, these systems run at multiple bit rates. Finally, and perhaps most importantly, the Telecommunications Act of 1996 includes loop unbundling provisions that make it possible for competing operators, often referred to as Competitive Local Exchange Carriers (CLECs), to gain access to

---

^{SM} Sapphyre is a service mark of Telcordia Technologies, Inc.

individual loops. This activity was initially POTS-focused, but several operators are already offering ADSL-based unbundled services. This trend has been tremendously accelerated by the November 1999 FCC "line sharing" ruling, under which a CLEC can return the POTS connection and service to the incumbent, and retain the DSL bandwidth to offer only data services, such as high-speed Internet access.

Over time, the competitive local environment may lead to several providers gaining access to the copper distribution plant, with each having a significant customer base. The customer base will be randomly dispersed in an area, driven by marketing forces and consumer choice. The competitive environment is expected to yield churn rates significantly higher than current churn rates for POTS. All this means that the spectral environment in a cable will be difficult to predict, and will be constantly changing.

In recognition of the importance of spectral compatibility in the loop plant, American National Standards Institute (ANSI) Working Group T1E1.4 initiated a project in 1998 to develop relevant standards. The group has been responsible for DSL standards on ISDN Basic Access, HDSL and ADSL, and is an excellent forum in which to foster industry consensus on spectral compatibility requirements.[1]

The deliberations have been well attended by industry players, including new equipment manufacturers and operators focused on market niches. This has led to a number of proposals for new DSL systems, for example the class of symmetric DSLs (SDSL). Unfortunately, this creativity complicates the problem of spectrum management, as is apparent from Table 1 which shows the currently agreed classes of DSL systems.

Table 1. Spectrum Management Classes

Spectrum Management (SM) Class	Deployment Guideline, max loop length EWL 26 gauge kft	Included DSL Technologies
Class 1	all nonloaded loops	ISDN SDSL ≤ 300 kbps 2-line & 4-line DAML
Class 2	11.5 kft	SDSL ≤ 512 kbps
Class 3	9 kft	HDSL and 784 kbps SDSL
Class 4	10.5 kft	HDSL2 (single-pair HDSL)
Class 5	all nonloaded loops	ADSL, CAP/QAM RADSL, G.lite (partial-overlapped)
Class 6	Not defined	VDSL
Class 7	6.5 kft	SDSL ≤ 1568 kbps
Class 8	7.5 kft	SDSL ≤ 1168 kbps
Class 9	13.5 kft	Overlapped, echo-canceled ADSL

Figure 1 shows currently proposed power spectral density (PSD) templates for each of these spectrum management classes. There are several ways to comply with the standard, the simplest being that the PSD of the signal transmitted by a piece of equipment fall under the template at all frequencies. This will generally be verified during manufacture, but if problems arise in the field the local operator will need to resolve incompatibilities and complaints, possibly including identification of systems that are transmitting in violation of the standard.
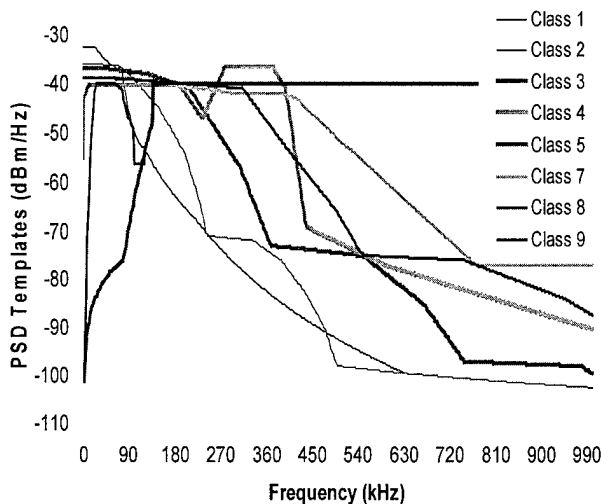
Figure 1. Spectrum Management Class PSDs

It would be desirable to have a technique that could characterize the crosstalk environment on a loop-by-loop basis, in a mechanized and highly accurate manner without the need for special equipment or intervention at the subscriber's location. In the following section, the same system used to identify and qualify loops will be extended to support spectrum management.

2. The Broadband Test Head

The mainstay of the telephone company local network is the local loop plant. Nearly all residential customers and many business customers are served by metallic twisted pair cables connected from a local switch in the central office (CO) to the subscriber's telephones. When customers request service, request a change in service or drop service, these facilities must be appropriately connected or rearranged in the outside plant by specially-trained craft dedicated full-time to this task. Obviously, an operator must understand its subscriber loops and know where they are connected, where the flexibility points such as junction boxes are, etc. Loop make-up records have been kept on paper and, more recently, have been manually entered into a computer database. Whether on paper or stored in computer memory, there have been questions about the accuracy and currency of these records.

One way to improve existing records is to examine and update them manually if they are missing or inaccurate.

This method is expensive and time consuming. Furthermore, new technologies such as DSL require additional information that was not previously kept for voice services, so new information must be added to the existing records. Test set manufacturers offer measurement devices that can greatly facilitate this process, but this typically requires a remote craft dispatch and two-ended testing.

A highly mechanized, highly efficient and almost universally deployed loop testing system already exists. Originally developed by the Bell System, one of the most important elements of this system is the Mechanized Loop Testing (MLT) system that was retained by (now) Lucent Technologies at divestiture. This system uses a metallic test bus and full-splitting metallic access relays on line card electronics. By these means, a given subscriber loop can be taken out of service and metallically connected to a centralized test head where single-ended measurements can be made on the customer's loop. The test head runs a battery of tests aimed at maintaining and diagnosing the customer's narrowband (4 kHz) voice service.

Telcordia has invented key technology to upgrade this infrastructure. The intent is to replace the narrowband test head with a new, broadband test head. This test head would be able to interface with a switch to connect to a specified loop, apply a set of test pulses to that loop and record the response of the loop. The results would then be analyzed using sophisticated signal processing algorithms to determine the complete loop make-up. This approach has many uses. First, it can be used to check existing records; the loop make-ups can be methodically obtained and compared with existing database records. Because we expect the information to be more accurate and detailed than the existing records, the new data will often replace existing data and populate the database. Thus, through an entirely mechanized process, an operator can completely update its loop records.

The updated loop make-ups can be used by another system to calculate and qualify the ability of a given loop to support advanced DSL services. A computer system will take the loop make-ups, models of the various DSL systems and standards for spectral compatibility, and determine very precisely what service the customer's loop can support. Such determination should be achievable in real-time, for example in response to a service agent query while on a different phone line with a customer.

In addition to determining the loop make-up, additional information can be determined regarding the noise environment a particular loop is exposed to. By means of additional spectrum analysis algorithms this noise may be identified, further facilitating the service provisioning process, identifying noise sources exceeding spectral compatibility requirements, and generally facilitating maintenance and administration.

3. An Example of Loop Identification

Most solutions for qualifying a loop for DSL services do so without unveiling the exact make-up of the loop. Recent work has demonstrated the feasibility of a technique that can achieve precise loop make-up identification via single ended measurements. The availability of the exact make-up of the loops in the local plant will not only solve the problem of qualifying loops for DSL-based services, but will also support other important loop plant engineering functions.

The approach used for determining the loop make-up is in the time-domain. Special probing pulses are launched onto the loop via the local metallic test bus. If a discontinuity is present (gauge change, bridged tap, end of loop), a signal (echo) travels back to the CO corresponding to the discontinuity. Such echoes are collected in the CO and are then processed. The solution employs a combination of advanced reflectometry and signal processing techniques. The advanced reflectometry allows the detection of very weak echoes generated at the ends of long loops, while additional signal processing is necessary to resolve overlapping echoes and identify discontinuities.

Several problems have to be solved in order to achieve the capability of exact loop make-up identification, especially those related to the limitations of current Time Domain Reflectometers (TDRs). First of all, today's TDRs have an effective range of some number of kilofeet (kft) and are not sufficient to allow detection of echoes generated by far discontinuities. Secondly, today no commercial TDR has the capability of detecting echoes generated by gauge changes. Moreover, even when all echoes can be detected it is not trivial to resolve them. In fact, the available observations consist of an unknown number of echoes, some overlapping in time and frequency, some not, some *real* and some *spurious*[1], that exhibit unknown amplitude, unknown time of arrival and unknown shape. The problem of resolving the above observations on the basis of a *single-sensor experiment* is a very complex problem that is seldom addressed in the literature.

An example of a TDR trace is given in Fig. 2, for the case of a 12 kft AWG-24 cable with a 1 kft bridged tap located either at 1 kft (Case A) or at 10 kft (Case B). The typical negative-positive sequence characterizing a bridged tap is manifest for Case A, but not for Case B where there is no sign of the presence of an echo. However, by using special signal processing on the waveform of Case B, it is now possible to see the negative positive echoes of the bridged tap (Case B + Processing).

Figure 2: Effectiveness of signal processing on a TDR trace (bridged tap case)

With the use of special signal processing techniques, it is also possible to see gauge changes. The fact is that the echoes generated by a gauge change cannot normally be seen, not because they are too weak to be detected, but because they are hidden. An example is given in Fig. 3, where the TDR trace of a 3 kft AWG-26 cable spliced to a 12 kft AWG-24 cable is shown. The normal trace of a TDR does not reveal the presence of any echo, but the processed trace clearly shows a negative echo that indicates the transition from a medium with higher characteristic impedance to a medium with a lower one.

Finally, very good results have been obtained with a newly developed algorithm that uses sophisticated signal processing to perform loop make-up identification. Preliminary tests indicate that the algorithm is able to precisely identify loop make-ups, whatever topology they may have.

---

[1] We define "spurious" echoes as echoes resulting from multiple back-and-forth reflections, as opposed to the "real" echoes that are the echoes that immediately return to the CO when generated by a discontinuity in the cable. The presence of spurious echoes is due to the fact that each discontinuity generates both a reflected and a refracted signal, so that a part of the signal travels back and forth on the line, bouncing between discontinuities, before it ultimately arrives at the CO.

Figure 3: Effectiveness of signal processing on a TDR trace (gauge change case)

4. An Example of Crosstalk Identification

Spectral compatibility is the property whereby crosstalk among different systems transmitting on different pairs in the same twisted-pair cable does not cause significant degradation to the performance of any of the systems. Spectrum management is the process of deploying DSLs in the loop plant in a manner that ensures spectral compatibility. Figure 4 below depicts crosstalk in a typical loop environment, including near-end crosstalk (NEXT) and far-end crosstalk (FEXT).
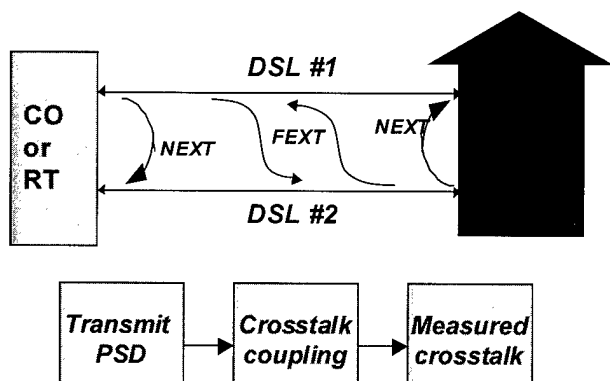
Figure 4. Crosstalk: transmitted signal, coupling, and received crosstalk

Current techniques for spectrum management apply relatively rigid rules uniformly across the entire loop plant, as embodied in the draft spectrum management standard currently under development by ANSI committee T1E1.4. These rules do not take into account the individual types of crosstalk sources or crosstalk couplings related to a particular pair in a cable, which may be considerably different than the near worst-case couplings that are assumed in the draft standard. Thus, a system that can characterize crosstalk on a loop-by-loop basis has the potential to yield a much more granular crosstalk characterization of the plant. This data, entered into a new loop spectrum management database, in turn has the potential to be mined, correlated and exploited to provide more optimal performances for individual subscriber loops.

To see how such a database might be created, we give the following example in which the crosstalk noise on a given pair is analyzed and characterized. NEXT from an upstream ADSL source is measured for a number of pair-to-pair combinations. These NEXT PSDs are correlated with the PSD crosstalk templates of some known sources. As can be seen from the calculated results in Table 2, each measured NEXT is highly correlated with the template NEXT from upstream ADSL. The unknown NEXT source is correctly identified.

Table 2. Correlations of measured NEXT from unknown source with known crosstalk templates

Measured NEXT	BRI NEXT	HDSL NEXT	T1 NEXT	ADSL Down NEXT	ADSL Up NEXT
5 -> 4	0.218	0.790	-0.276	-0.221	0.975
6 -> 15	0.194	0.798	-0.269	-0.215	0.992
11 -> 20	0.183	0.792	-0.269	-0.214	0.957
10 -> 21	0.153	0.808	-0.258	-0.204	0.994
4 -> 25	0.201	0.784	-0.267	-0.214	0.983
3 -> 12	0.071	0.768	-0.223	-0.174	0.938
13 -> 15	0.088	0.770	-0.227	-0.179	0.952
9 -> 20	0.230	0.791	-0.279	-0.223	0.962
14 -> 24	0.213	0.806	-0.276	-0.220	0.983
8 -> 18	0.120	0.802	-0.246	-0.194	0.976
2 -> 22	0.106	0.771	-0.233	-0.184	0.969
12 -> 4	0.085	0.735	-0.216	-0.171	0.935
1 -> 5	0.130	0.798	-0.247	-0.195	0.975
7 -> 18	0.066	0.790	-0.231	-0.177	0.896

5. An Advanced Loop Provisioning and Maintenance System

Let us consider a system that analyzes the responses of subscriber loops to probing signals to perform loop identification, and measures crosstalk and identifies the types of systems that are the sources for that crosstalk. The data is collected and used by a provisioning and maintenance system to enable more efficient engineering, provisioning, spectrum management, and maintenance of the copper loop plant.
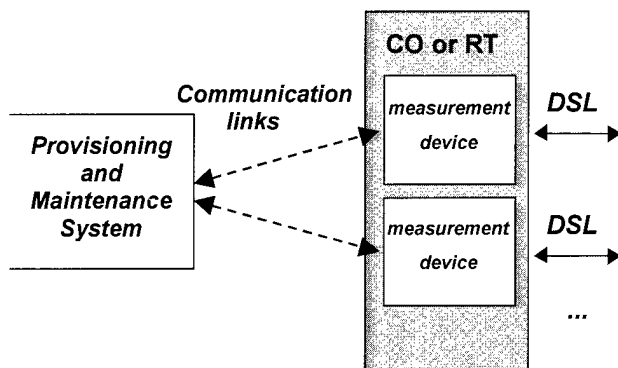
Figure 5. An advanced DSL Operations Support System

The loop make-ups, and types and numbers of crosstalkers in a cable can be measured, recorded, and tracked. This database can be coordinated with a DSL provisioning system to allow the highest possible service rates while ensuring spectral compatibility. Rather than using broad-brush loop estimates and spectrum management rules based on worst-case assumptions, precise loop make-ups and accurate noise characterization along with the actual powers of DSLs transmitting in the cable can be coordinated by the system.

This system is useful for network monitoring and maintenance. A DSL may experience significant degradation when signal to noise ratios (SNRs) are inadequate, perhaps when another source transmits a PSD that is too high. The system can isolate the causes of failures such as long loops or bridged taps, identify crosstalk sources, and help mitigate problems by techniques such as power back-off or lowering transmitted bit-rates. The system can also determine if an unbundled loop is receiving crosstalk levels that are within specifications.

6. Conclusions

We have introduced techniques for determining loop make-ups and for obtaining a spectrum analysis on a loop-by-loop basis. These techniques are not the only methods for obtaining such information, but they have the advantage of being applied in a mechanized, single-ended fashion from the central office. Thus, a new "broadband test head" can be installed in the office that will automatically and routinely provide current information on loop make-ups and crosstalk. Using sophisticated signal processing and analysis approaches, we hope to be able to precisely determine loop make-ups for the entire nonloaded loop plant, including section lengths and bridged tap composition. The same approach can be used to gather and characterize crosstalk information for each of the loops.

This information can be input to a provisioning and maintenance system that will retain and correlate the records. This database can in turn be used for a number of important functions, such as loop plant engineering, loop qualification and provisioning of DSL-based services, spectrum management, and maintenance of the loop plant. We believe that such a capability is required to fully exploit the power of emerging DSL technologies, and to effectively deal with the increasingly complex and dynamic unregulated local loop environment.

References

[1] Draft proposed American National Standard, Spectrum Management for Loop Transmission Systems, Committee T1 – Telecommunications, Working Group T1E1.4, T1E1.4/2000-002R3, Vancouver, Canada, August 14, 2000

Authors

Stefano Galli received the Ph.D. in "Information Theory and Communications" from the University of Rome "La Sapienza" (Italy) in 1998. Stefano's main research efforts are devoted to the problem of automatic loop qualification and, more recently, to the analysis and performance assessment of wireless home networks and power line carrier systems. His research interests also include detection and estimation, channel equalization and coding, personal wireless communications and, more recently, DSL system and crosstalk modeling. Dr. Galli is a Member of the IEEE and has authored over 30 technical papers.

Dr. Kerpez received his Ph.D. in Electrical Engineering from Cornell University in 1989. He has analyzed, invented, and helped standardize new transmission systems, modulation techniques, codes, equalizers, multiplexing and networking techniques for digital local access telecommunications systems. Dr. Kerpez worked extensively on high-bit-rate digital subscriber lines (HDSL), and he was instrumental in the invention and subsequent definition of asymmetric digital subscriber lines (ADSL). He has been active in the T1E1.4 DSL standards committee since 1989. He has authored over 100 technical papers. Dr. Kerpez is a Senior Member of the IEEE.

John Lamb received a Master of Electrical Engineering degree from Stevens Institute of Technology in 1982. He began his career at Bell Laboratories designing integrated circuits for telephone systems. At Telcordia, he has been responsible for many phases of conformance testing for various types of DSL hardware, including test system design, test plan development and physical layer testing. He has authored over 50 analysis reports on DSL equipment ranging from chip sets to routers to line cards for switches and digital loop carrier systems.

Dr. Valenti received a Ph.D. in Physics from the City University of New York in 1977. He has contributed to the development of physical layer requirements for digital subscriber line (DSL) and Fiber in the Loop (FITL) systems. Much of Dr. Valenti's recent work has focused on the measurement and characterization of crosstalk, impulse and background noise in the copper loop access network. He has provided leadership for many years within the ANSI T1E1.4 Working Group where he is currently serving as Editor of the Spectrum Management standard.

David L. Waring received a Master of Science degree in Electrical Engineering from Georgia Tech in 1978. He began his career at Bell Laboratories designing subscriber loop electronics. He moved to Bellcore at its inception in 1984, where he worked on a number of projects including early Metropolitan Area Network field trials. He led teams that proposed requirements for HDSL and ADSL. He was project manager of several industry-leading interactive digital video trials. Dave currently leads research into "last mile" broadband local access and customer premises networks. Dave is a Senior Member of the IEEE.

Copper Access Network Transmission Characteristics

Arne Ernbo
Telia AB, Carrier & Networks
Farsta, Stockholm Sweden
+46-8-713-3799 · arne.l.ernbo@telia.se

Anna Lindgren
Telia AB, Carrier & Networks
Farsta, Stockholm Sweden
+46-8-713-3134 · anna.s.lindgren@telia.se

Abstract

A database of measurements on the copper access network in Sweden has been compiled during 1999. The measurements comprise attenuation, balance, noise levels and characteristic impedance in the frequency range of 10 kHz to 15 MHz. The database is used to evaluate the network with respect to xDSL, to compare the network to international standards used by the transmission system providers, and to foresee possible problems when new systems are to be implemented.

Keywords

Copper; access; attenuation; noise; NEXT; xDSL.

1. Introduction

1.1 Transmission System Development

In the mid-90ties new equipment for traffic with more capacity for the access copper network began to emerge. The specifications were made from standardized models of the copper network. The systems were tested in a laboratory environment to comply with the standards and demonstrated to operate correctly on test cables. But would they work in the real network? The question became still more urgent when starting the planning of ADSL introduction.

The local loop normally consists of different types of cables, paper insulated at the beginning, filled or unfilled plastic insulated in the middle and unfilled and sometimes untwisted pairs at the customer end, all with different transmission characteristics. Because of this a mathematical treatment would involve the use of chain matrix parameter computing. Such work has been done in the past. However, additional complications like unknown lengths of cable and splicing positions make it hard to calculate standardized parameters. The only way to answer the question is to make actual measurements in the real network.

The main parameters affecting xDSL performance are:

- Attenuation – Length and gauge dependent

- Noise – Crosstalk from other systems, impulse Noise and EMC

- Variation of impedance – Reflections due to changes of cable types, unbalance of hybrids (echo)

- Balance, LCL – Radiation problems, splitter performance

1.2 Network History

The present copper access network in Sweden has been built mainly during the last 50 years. It contains a multitude of different cable designs, wire dimensions and materials, an overview of which will be given below. The operating quality of the cables also varies due to moisture, maintenance methods, and the like.

To collect more information on the access network a measurement program was started in 1999. Measurements were made all the way from the main distribution frame at the central office to the subscriber network termination point. The pairs were selected to cover all relevant combinations of copper cables in use today. The measurements were also spread geographically since the installation methods may vary from north to south.

During 1999 around 400 lines in the copper access network were measured, 200 of them in both directions, from the central office to the customer and from the customer to the central office. The measurements were collected in a database to make the evaluation more convenient. The database also contains various data for the measured line, types of cables, dimensions, lengths etc.

The purposes of the measurements were to find out

- how many of the customers can be offered new services like xDSL, and at what bitrate

- if existing quality levels, working methods and maintenance methods are sufficient

- whether the access network complies with the internationally standardized models.

2. Network Design

The access network consists of three parts: the primary, the secondary and the distribution network. The interfaces between the parts consist of cabinets and pedestals respectively in buried network parts and corresponding material in aerial networks.

2.1 Primary Network

From the central office large pair count cables are used to connect with cabinets. Normally a single cable connects with several cabinets, which is the reason for the large pair count of these cables. For the same reason it pays off to pressurize the cables to simplify maintenance in those areas where unfilled cables are used. The cabinet contains two sets of terminals for the primary cables and the secondary cables respectively. The two sets of terminals are connected with cross-connect-wires. The pair count of the cables in the primary network is normally between 100 and 1800.

2.2 Secondary Network

From the cabinets smaller cables are used to connect with a large number of distribution points which are often geographically spread out over a fairly large area. For this reason the cables used normally

contain 10-300 pairs. Pressurization is normally not applied in the secondary network, even with unfilled cable.

2.3 Distribution Network

From the pedestal to the network termination point in single-family homes 2- to 5-pair cables are used, in older installations self-supporting dropwire or even open-wire lines were used. In large apartment buildings another structure is used, with indoor cables connecting the basement with distribution points on each floor, where single- or two-pair cables carry further into the apartments.
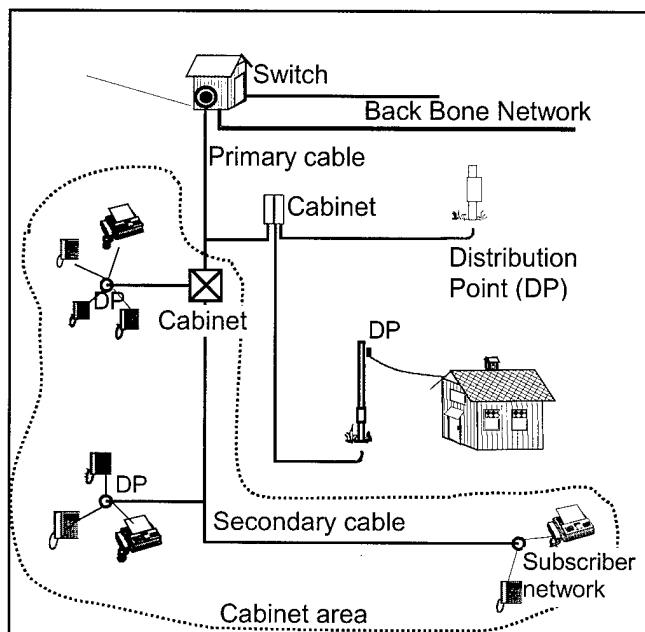
Figure 1. Summary of the copper access network

3. Cable design

3.1 Primary and Secondary Network

The large pair count cables used in the access network have two different lay-ups. The old paper-insulated cables are mostly of the layer type, whereas polyethylene-insulated cables are of unit type with subunits of 10 pairs and main units of 50 or 100 pairs. The conductor diameter is 0,4 to 0,7 mm. The mutual capacitance of the PE-cables is standardized to 42 nF/km. Buried cables are jelly-filled, using foam-skin or cellular insulation. Aerial cables are unfilled, using solid insulation.

Layer-type cables were normally spliced randomly, i.e. deliberately ignoring the pair numbering completely. Present-day unit-type cables, on the other hand, are fully color-coded and spliced in such a way as to maintain the pair numbering across the splice. Since no more paper-insulated cables are bought extensions and maintenance of the primary and secondary network is carried out using unit-type polyethylene cables. A consequence of this is that in splices between old and new cables a layer-type cable can meet a unit-type one. Apart from difficulties and extra workload during splicing to find out which pair is which this will also influence the attenuation and

crosstalk values of the line. Up till now, this has had no significant influence on the performance of the network, being used mainly for voice-frequency traffic, but may become increasingly important when large numbers of ISDN, HDSL and ADSL systems are installed.

In the access network all cables are strictly pair-type. Star quad cables have not been used in this part of the network. In the old long-distance network, on the other hand, DM quads were used extensively to enable exploitation of phantom circuits together with loading coils.

3.2 Distribution Network

In the distribution network 2- and 5-pair cables are used. The 2-pair cables are designed as a star quad, the 5-pair cable contains normally stranded pairs. The conductor diameter is 0,5 or 0,6 mm, the mutual capacitance between 35 and 45 nF/km. Both aerial and buried versions exist. Large amounts of single-pair self-supporting dropwire with 0,9 mm-diameter copper-clad steel conductors are also present in aerial distribution networks. Such dropwire is no longer used for new installations and is gradually replaced with 2- or 5-pair cables both because present-day installation standards prescribe at least two pairs and because the single-pair dropwire has been found to be inadequate for broadband systems.

3.3 Central-Office Cables

The cables between the cable entry in the basement and the MDF can consist of two cable types, with very different characteristics. In older installations a PVC-insulated cable with a mutual capacitance of 85-100 nF/km was often used. In newer installations a PE insulated version with the same mutual capacitance as the outdoor cables, i.e. 42 nF/km, is preferred.

Between the MDF and the switching equipment the same types of cables can be used, in many cases a nylon-insulated cable with 100 nF/km is also utilized.

4. Measurements

4.1 Measuring Equipment

The instrument used was a spectrum analyzer from Hewlett Packard with an s-parameter test kit. The lines where terminated at both ends with a balun (except during the impedance measurement). For the measurement of attenuation a Sweep generator from Hewlett Packard where used.

To comply with all makes of xDLS equipment, the measurements were made in the frequency range of 10 kHz to 15 MHz. For most of the measurements the total frequency range was split into two subranges, 10 kHz to 1,5 MHz and 1,5 MHz to 15 MHz, in order to obtain satisfactory resolution.
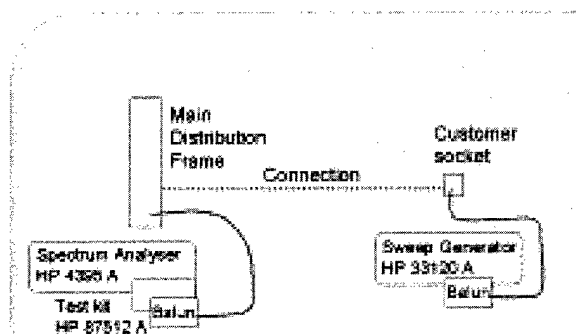
Figure 2: The setup used for the measurements

4.2 Measurement Planning

The measurements were spread geographically all over Sweden and included all types of combination of cables that are installed in the access network. The lengths were limited to 6 km and there are no lengths shorter than 400m. Lengths outside these limits were considered to be of no interest: shorter lengths will not be a problem and longer lengths are not useful because of too high attenuation.

5. Results

5.1 Noise Levels

For tests of ADSL systems noise levels have been defined in ETSI A (-49,4dBm) and ETSI B (-43dBm). From figures 3 and 4 below we see that 94% of the results are below ETSI A and 96% below ETSI B. In reality the results will probably be still better since a few doubtful results should be removed.

The evaluation of the noise at the subscriber side indicated that the noise is affected by crosstalk from existing digital systems. In the future we can consequently expect a different noise situation when the penetration of xDSL increases.
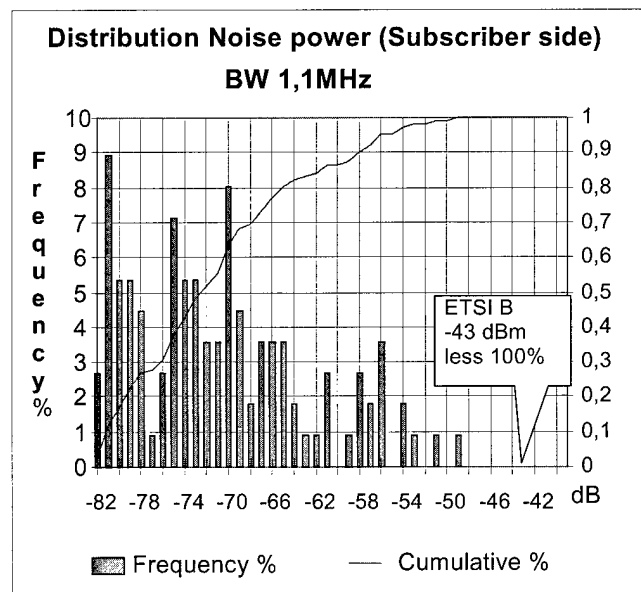
Figure 3: Noise at the subscriber side
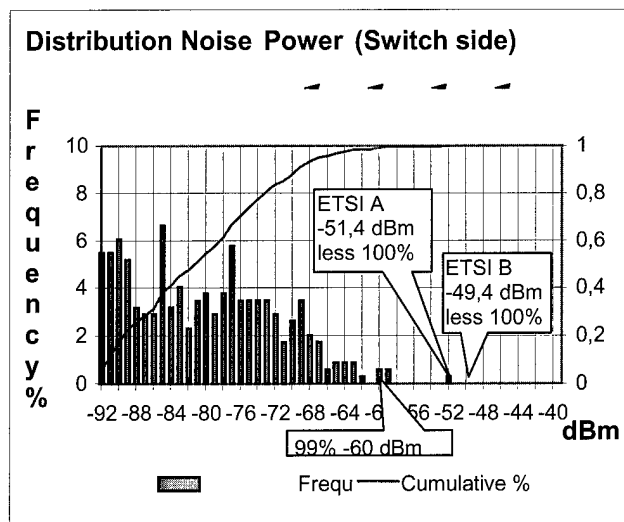
Figure 4: Noise at the switch side.

5.2 Longitudinal Conversion Loss

The balance of the line was measured as Longitudinal Conversion Loss (LCL) at 1,5 MHz. The values obtained have a median of 58 dB. The minimum value requirement for ADSL systems is 40 dB, which is fulfilled for 99% of the lines.
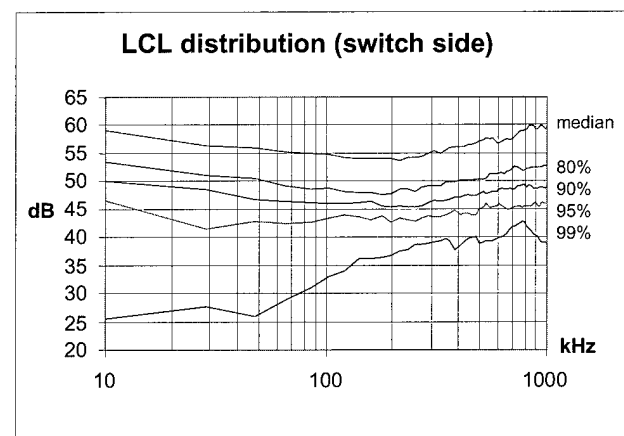
Figure 5: CO side Longitudinal Conversion Loss
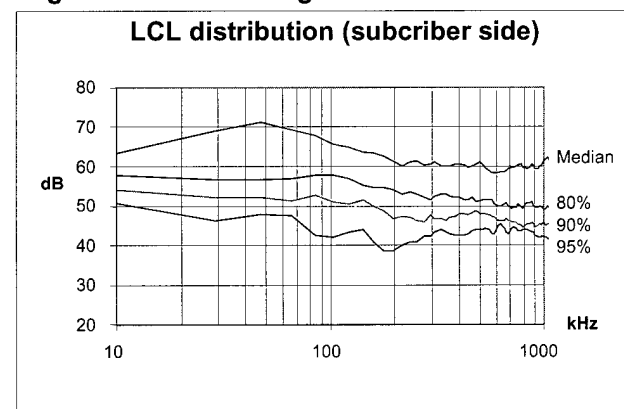
Figure 6: Subscriber side LCL

5.3 Attenuation

The attenuation was measured directly as the level difference between the sending and the receiving end, using a sweep generator (HP33120A) and a spectrum analyzer (HP4396A), but was also calculated from the short circuit - open circuit input impedance measurements in the database. The short circuit - open circuit measurements showed less accuracy than the direct level measurements, which could be expected from the long lengths of cable measured.

Distribution relative attenuation 0.5mm
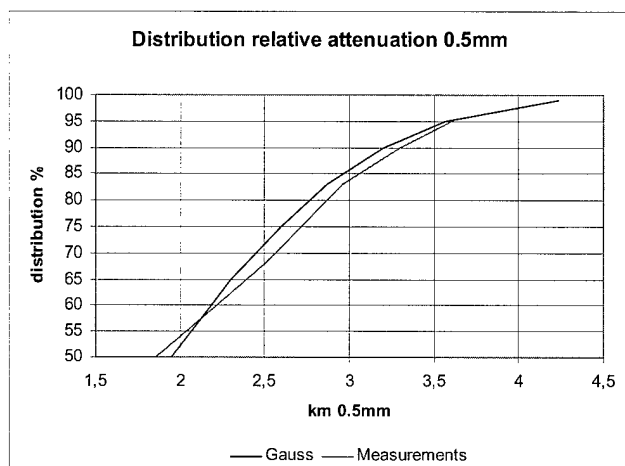
Figure 7: Total attenuation from MDF to NTP

The attenuation, independent of the length, was compared with a gauss distribution and as seen above are the divergences small. The attenuation in our Network from the switch side, can accordingly be considered an 0,5 mm normal frequency distribution with an average value of 1,9 km with standard deviation of about 1 km.

Attenuation normalized with the length. The database consists of lengths both measured (i.e. pulse echometer, resistance, capacitance measurement) and manual (maps). The values are similar and the attenuation per km does not alter much depending on the type of length that are used.

Attenuation/km (Switch side)
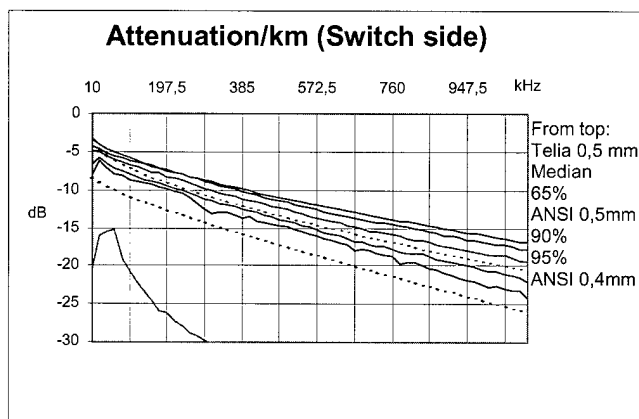
Figure 8: Attenuation per unit length

5.4 Characteristic Impedance

The characteristic impedance of the lines at 1 MHz was determined by measuring the input impedance of the near end with the far end open and shorted. From the two measured complex input impedances the magnitude and phase angle of the characteristic impedance are calculated. The propagation constant (attenuation and phase shift) can also be calculated.
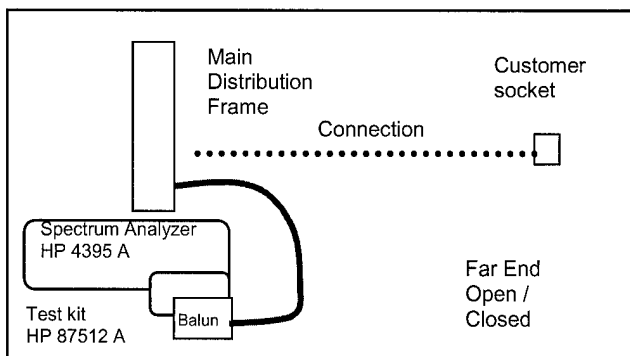
Figure 9: Measuring setup used for impedance tests

70% of the values fall between 130 and 145 ohms, well above the design value of 120 ohms for the cables in the primary and secondary networks. This may be due to the low mutual capacitance (35 nF/km) and consequent high impedance of the dropwire at the customer end, where the measurements were performed. The impedance on the subscriber side varies more then the impedance on the switch side. The variation also increases with the frequency.

Z distribution (switch side)
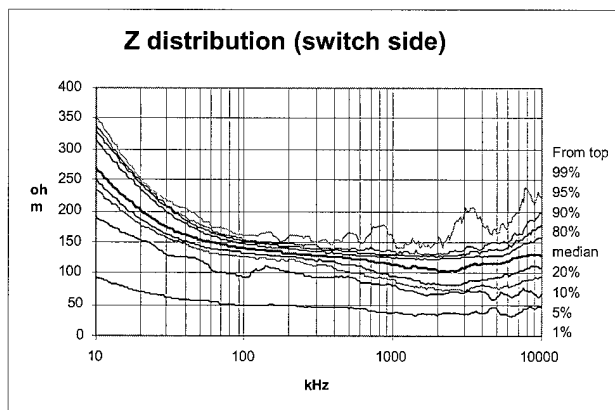
Figure 10: Input impedance measured from CO

Z distribution (subcriber side)
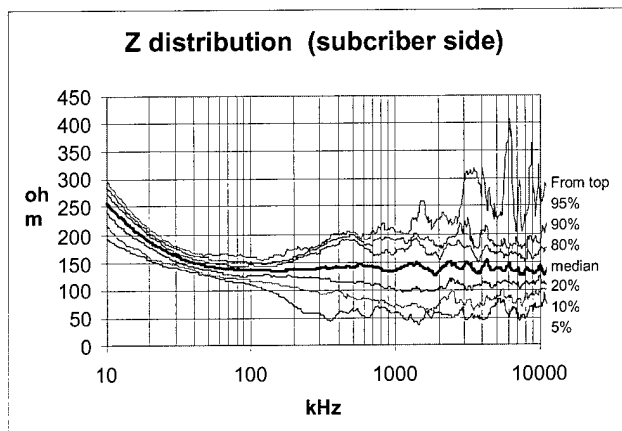
Figure 11: Input impedance measured from customer side

5.5 Near-end Crosstalk

Because of the inconveniences of measuring NEXT in a network with working traffic, an older database was converted and evaluated. The measurement where only made from switch to distribution point and did not include the distribution network. But the NEXT measurement where estimated to be sufficiently reliable. The NEXT measurements were compared with the result of the balance and noise measurements.

** NEXT model used
measured 99±1%
—— measured 50%
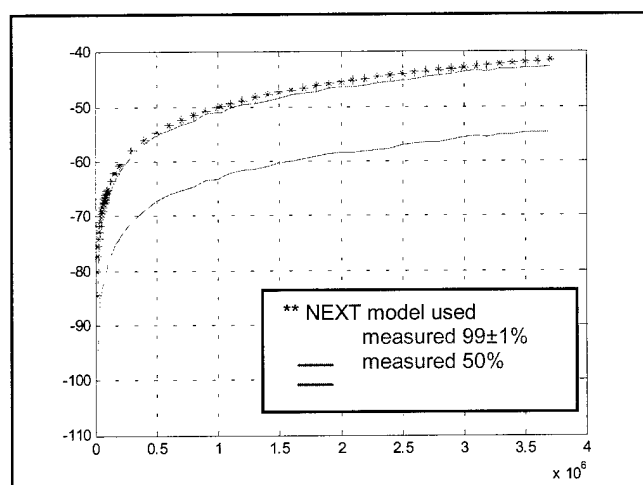
Figure 12: NEXT limits

6. Evaluation

The evaluation was made to meet demands from the ADSL introduction. The composite access network was found to be slightly better than the ANSI standard for 0.5-mm conductor diameter with respect to attenuation. This seems reasonable since most of the access network consists of 0,5 mm cables and the nominal mutual capacitance of the cables is a low 42 nF/km.

The measurement results stored in the database have been used for calculations of the background noise in the cables resulting from the deployment of ADSL, PCM, HDSL and ISDN systems. In this case, an equivalent noise level in accordance with methods developed by ETSI TM6 and adapted to the actual conditions prevailing in the network has been used to represent the system mix. The crosstalk level between the pairs of the cable has also been taken into account in accordance with ETSI standards.

The results from the noise calculations have been used to determine the number of different systems that can be applied simultaneously to each part of the network. This has served as a basis for the network planning necessary for Local Loop Unbundling. The results obtained are well in line with existing and proposed ETSI standards.

7. Discussion

The fact that the network is stable with respect to resistance has probably contributed to the good results. Another contributing factor is the absence from bridge taps. On the other hand we have also observed a detrimental influence from high-capacitance switchboard cables sometimes present in too long lengths in old central offices. A similar degradation of system performance may be expected, and has actually been observed in some cases, from the use of unsuitable cable at the customer end, e.g. unscreened cables, or untwisted dropwire in areas with elevated electromagnetic interference. The copper-clad steel conductor dropwire is no longer used in new installations for this reason. On the other hand we have not encountered any problems arising from changes in conductor diameter, e.g. 0,4 mm to 0,5 or 0,7 mm, in splices.

From the MDF to the NTP at the customer the network is known (even if from time to time it is repaired) so that the model developed from the measurements can be applied. The customer, on the other hand, owns the premises network, and it is his responsibility to build it in accordance with established standards. Failure of the xDSL system to operate may well be caused by non-compliant premises wiring.

The total number of measured lines is around 400. This will give a statistical confidence of about 5%. Even if this may seem unsatisfactory, it must be remembered that an increased confidence level, e.g. 0,5% would require about 1000 measured lines.

All measured pairs complied with the electrical quality levels i.e. no faulty pairs were measured. Such pairs would have been repaired anyhow before applying xDSL to them. Also, one of the purposes of the work was to find out whether pairs compliant to the existing quality standards could be used for xDSL without further measurements or improvement of the line.

Local Loop Electrical Quality Levels	
Insulation resistance	> 1 Mohm
Pair-to-ground capacitance unbalance	<2-3 %
Disturbing Voltage Conductor to ground	<10 V AC/DC
Idem, between conductors in a pair	<8mV

8. Conclusions

- 90% of the local loops have a length below 3,2 km of 0,5 mm ANSI

- The average attenuation of the loops corresponds to 1,9km of 0,5mm ANSI-line.

- The attenuation of 85% of the lines is below the ANSI standard for 0,5mm conductors.

- Noise levels are far below ETSI references. However, these value are expected to increase with a higher penetration of xDSL in the access network

9. Acknowledgements

The authors wish to thank Björn Kolmbäck and Kjell Holm of Telia Carrier & Networks, and Tomas Stefansson, Hans Lundberg, Daniel Bengtsson, Joachim Johansson and Sivert Håkansson, all of Telia Research AB, as well as Thomas Wallin of Telia Prosoft, for their valuable contributions to this paper.

10. Authors

Anna Lindgren graduated from Technical College in 1985. After that she attended an extensive In-house Telia Course for engineers. She works in Telia Carrier & Networks, Technology section with methods and instructions for maintenance and installation on copper cables and with evaluations, field trials and specifications on new instruments to be used on copper cables.
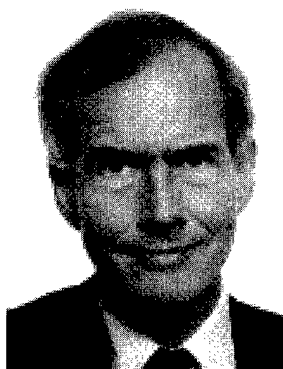
Arne Ernbo received his M.Sc.E.E. and Ph.D. (Electrical Measure-ments) in 1973 from Lund Institute of Technology, Lund, Sweden. He joined Telia in 1990 where he works with copper cable specifications, development and procurement at Telia Carrier & Networks, Outside Plant section. He is also engaged in copper cable standardization, being chairman of the Swedish National Committee of the IEC Technical Committee N° 46: Cables, Wires, Waveguides, R.F. Connectors, and Accessories for Communication and Signalling, and the corresponding Cenelec body

DSL Deployment Issues - DSL Demons and Critical Points

Ernie Gallo

Telcordia Technologies, Inc.
Ph. (973) 829 4638 • egallo@telcordia.com

Introduction

This article will discuss DSL (Digital Subscriber Line) deployment issues that carriers will face as we move to mass deployment. DSL "demons" are those issues that will hinder the successful mass deployment of DSL, and DSL critical points are those issues that can prevent DSL mass deployment from reaching its full potential. At the present time service providers are provisioning lines with some success, but what will deployment look like when DSL is fully marketed to the public and a single central office and outside plant work center are faced with provisioning 200 lines a day. Today ILECs are provisioning 500 to 1000 lines company-wide.

Voice Over DSL

Adding voice over DSL (VoDSL) provides an attractive telecommunications solution for small businesses (up to 50 employees) and SOHOs (Small Office/Home Office). VoDSL will be able to support up to 16 voice lines over a single copper pair with the only customer equipment required being a Integrated Access Device (IAD) for both the voice and data. One pair should be connected directly from the NID (-48Vdc) to the station set bypassing the IAD so that lifeline POTs can be provided in the event of loss of power. With the cost of leasing copper pairs becoming more and more expensive, a CLEC can provide more services and potentially get more revenue from a single copper pair through DSL technologies. The promise of such business applications will dramatically increase DSL deployment and recycle copper pairs into higher value circuits with minimal investment in new physical plant. For DSL to be successful it needs to support business applications that require at least 500Kbps in the downstream direction.

However, there are some down sides. Systems like SDSL will not support Plain Old Telephone Service (POTS). Digital Added Main Lines (DAMLs) that are added to increase capacity is

areas where there is plant exhaustion cannot be used with DSL and will have to be removed if a pair is converted to DSL, which will further tighten plant availability. However, VoDSL can be used to provide "pair-gain" as a replacement for DAMLs. There are two types of VoDSL; circuit switched and packet switched although the economics comparing the two has yet to be determined.

Other advantages of VoDSL is that after the initial installation, the provisioning of additional voice lines without requiring additional pairs and associated dispatch. It improves the cut-thru rate by reducing the need to "steal" non-working cut-thru loops. So VoDSL reduces the number of required physical working loops, and reduces the technician activity because of reduced installation and repair dispatches, thus reducing technician created troubles.

Line Sharing and DSL Capabilities

The recent FCC ruling on line sharing will allow a data CLEC to use the high frequency (data) spectrum part of the line to offer data through DSL, while the ILEC can use the low frequency (voice) spectrum to provide voice services. Figure 1 shows the DSL line coding that would implement the FCC's contemplated line sharing. It is now more critical for ILECs to focus on DSL. If not, they risk becoming access providers, and will lose revenues from enhanced services. Line sharing will speed up CLEC deployment of service since they won't have to order new lines from the ILEC. Since line sharing uses an existing line, versus the present method of implementing DSL on a new line, a CLEC could cut the time needed to provide service from 2 to 4 weeks to 1 to 2 weeks. In addition, DSL service can displace data traffic off the PSTN and thereby ease network congestion.
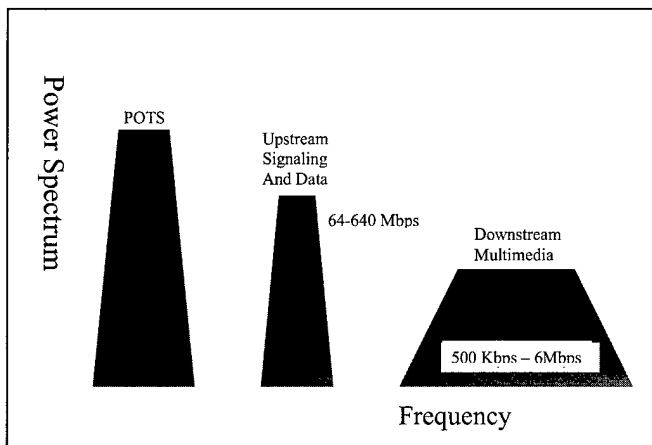
FIGURE 1. DSL CODING
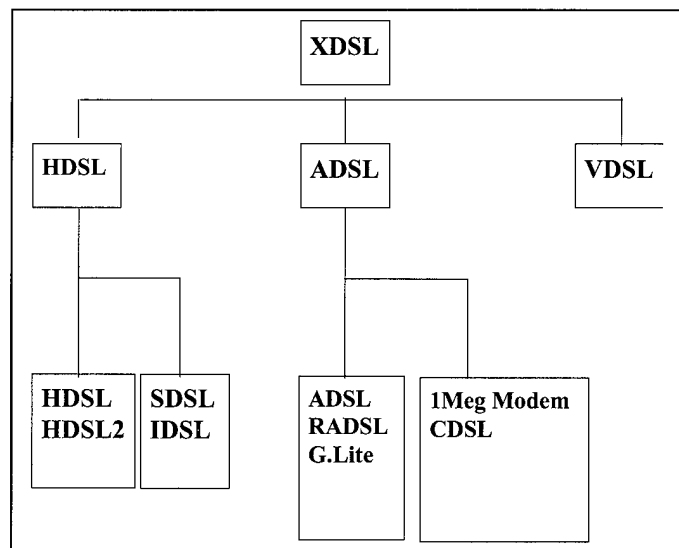
FIGURE 2.   DSL FAMILY TREE

FIGURE 3. DSL OVERVIEW				
Service	CO to Subscriber	Subscriber to CO	Maximum Design Rule Distance	Remarks
ADSL	0.5 – 8 Mbps	64 – 64- Kbps	12 – 18 kft	ADSL-3 provides 1 ~ 4 MPEG unidirectional video channels
"ADSL Lite"	1 Mbps	128 Kbps	12 – 18 kft	Doesn't require a "splitter
HDSL	1.544 Mbps 2.048 Mbps	1.544 Mbps 2.048 Mbps	12 kft on 2-pairs 12 kft on 3-pairs	Dual-duplex, repeaterless T1 or E1 equivalent
HDSL2	1.544 Mbps	1.544 Mbps	12 kft on 1-pairs	Symmetric T1 rate on a single-pair
IDSL	128 Kbps	128 Kbps	18 kft	ISDN equivalent used for long distance serving areas
RADSL	Variable up to 12 Mbps	Variable up to 1 Mbps	18 – 25 kft	Rate adaptive with CO DSLAM to obtain the highest data rates
SDSL	From 12 Kbps to 1.024 Mbps, (typically provisioned at 768 Kbps)	From 12 Kbps to 1.024 Mbps, (typically provisioned at 768 Kbps)	11.5 – 22 kft (depending on data rate)	Symmetrical rates Originally provided as a ½ DS1 rate service
UDSL	2 Mbps	2 Mbps	12 kft	Symmetric rates
VDSL	Rates (Mbps) of 6.5, 13, 26 or 52	Rates (Mbps) of 6.5, 13, 26 or 52	1 – 4.5 kft	Multimedia applications, short metallic loop, uses ATM protocol, connected to a FITL ONU feeder.

FIGURE 4. TRANSMISSION SPEED OVERVIEW FOR DSL (Approximate Time in Seconds Required to Transmit 125 Kbyte Digitized Photo)		
Transmission System	Sending Data CO → Subscriber	Receiving Data CO ← Subscriber
28.8 Kbps Modem	45	45
ADSL	0.2	2
ADSL Lite	1	8
HDSL	1	1
IDSL	8	8
RADSL	Variable	Variable
SDSL	1	1
UDSL	0.5	0.5
VDSL	0.02	0.04

There are technical and operation issues that need to be addressed, particularly in OSS systems, if line sharing is to work. A big issue is who is the customer going to call first for solutions and who is going to fix the problems on shared lines. Also, in this new telecommunications landscape, the conditioning and maintenance of the underlying copper may become a key factor for success.

Figures 2 and 3 provide an overview of the DSL family tree and the capabilities and characteristics of the different flavors of DSL available.

The Competition and DSL Advantages

There are diverse sources of broadband transport. One can compare DSL services (ILECs and CLECs are on the same team) with other high-speed data alternatives such as cable modems and wireless media. Presently, cable modems have about a 5 to 1 lead over DSL in installed base. Once a customer decides to go with a cable modem it is unlikely that they will switch from a cable modem to DSL; even if financial incentives of lower monthly service charges are offered. The customer will already have an investment in the cable modem, home wiring, installed software, familiarity with the cable's ISP, and so forth. The Multiple System Operators (MSO's = *the cable guys*) can deliver video, data, voice both local and long distance, and cable TV in an attractively bundled services package. Although cable modems can operate as high as 10Mbps (10base T), their more realistic performance is in the 1.5Mbps regime. The price for a cable modem of about $300 coupled with a the monthly fee of about $40/month is roughly equivalent to DSL.

Cable Modems that use Data Over Cable Service Interface Specifications (DOCSIS) certified by Cable Labs will be interoperable which may not be the case with all DSL modems. Cable modems do have their own operational and reliability issues such as the need to implement two-way plant. Traditional CATV systems were designed to send video from the headend to the customer, so they tend to operate well only in the downward

FIGURE 5. ACCESS MEDIA COMPARISON

MEDIUM	COSTS Monthly Service/Installation	SPEED RANGES: Downstream/Upstream	ASSESSMENT
Dial-Up	$20 / $35	56 kbps/33.6 Kbps	Advantage: Only need phone line and modem Disadvantage: Slow
ISDN	$70 /$150	128 Kbps/128 Kbps (most common)	Advantage: Twice as fast as dial-up Disadvantage: Per-minute charges are expensive, service not always-on
Satellite	$50 per 100 hours/ $900	400 Kbps/33.6 Kbps	Advantage: Fast downstream speed Disadvantage: Upstream uses dial-up, complex and expensive installation
Cable Modem	$30-$65/ $300	1.5 Mbps/2.5 Mbps	Advantage: High-speed connection Disadvantage: Not a dedicated line
DSL	$40-$1,200/ $300-$1,500	144-8 Mbps/64-8 Mbps	Advantage: Always-on, dedicated line service
VDSL		13-55Mbps/ 1.5-55Mbps	Disadvantage: Limited by plant conditions
Frame Relay T1, T3	$300 - $3,000/ ???	56-45 Mps/56-45 Mbps	Advantage: Reliable Disadvantage: Expensive
LMDS	?	50 Mbps	Advantage: Bypassed local loop Disadvantage: Wireless line of sight needed

direction. With pay per view and other services such as voice and data, CATV companies are investing billions of dollars upgrading their plant. Figure 6 presents the basic CATV network architecture to deliver these broadband services. Cable modems operate on a shared system similar to a LAN, so as more users connect to the network, the system will slow down. Some industry analysts have raised security issues and service quality concerns that the cable industry is currently addressing.
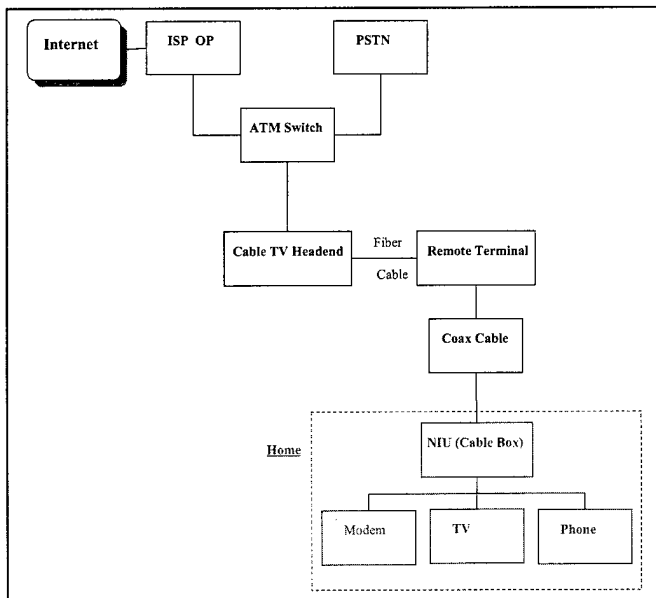
FIGURE 6. CATV ARCHITECTURE

A major alternative to DSL in the business applications market is wireless LMDS (Local Multiport Distribution) which can operate in the 28GHz frequency range and deliver data at up to 50Mbps. The use of wireless, minimizes local loop issues. It offers high speed service that bypasses all the local loop issues.

As broadband services expand into mass market deployment, it is expected that consumer report rankings will emerge similar to the widely quoted JD Power survey for telephony service. Such rankings would allow direct comparisons for consumers for various data alternatives and use criteria such as percent availability, average upstream and downstream transmission rates, grading of technical support, and quality of content provided. Informal rating are starting to spring up on the WEB as customers share their "broadband experience".

In addition to the potential revenue enhancement advantages, DSL service also brings other benefits to an ILEC. For example, the use of DSL will get data traffic off the PSTN which will ease network congestion. The average voice call is 4-6 minutes long while the average for data is 1-2 hours and is increasing, while and SOHO users are on for many hours at a time. The old CCS calculations that guided telephone engineers for many years no longer apply. DSL is designed to be always on with a dedicated line (some companies are using a shared DSL modem pool to provide a lower monthly cost), so there is no need to spend 5 minutes in a dial up procedure just to check football scores or local movie schedules. However, if system is down, it will get noticed immediately by the customers. So the old 99.99 percent (53 minutes of downtime per year) availability will not have the same meaning to every customer; including the FCC.

FIGURE 7. DSL ARCHITECTURE
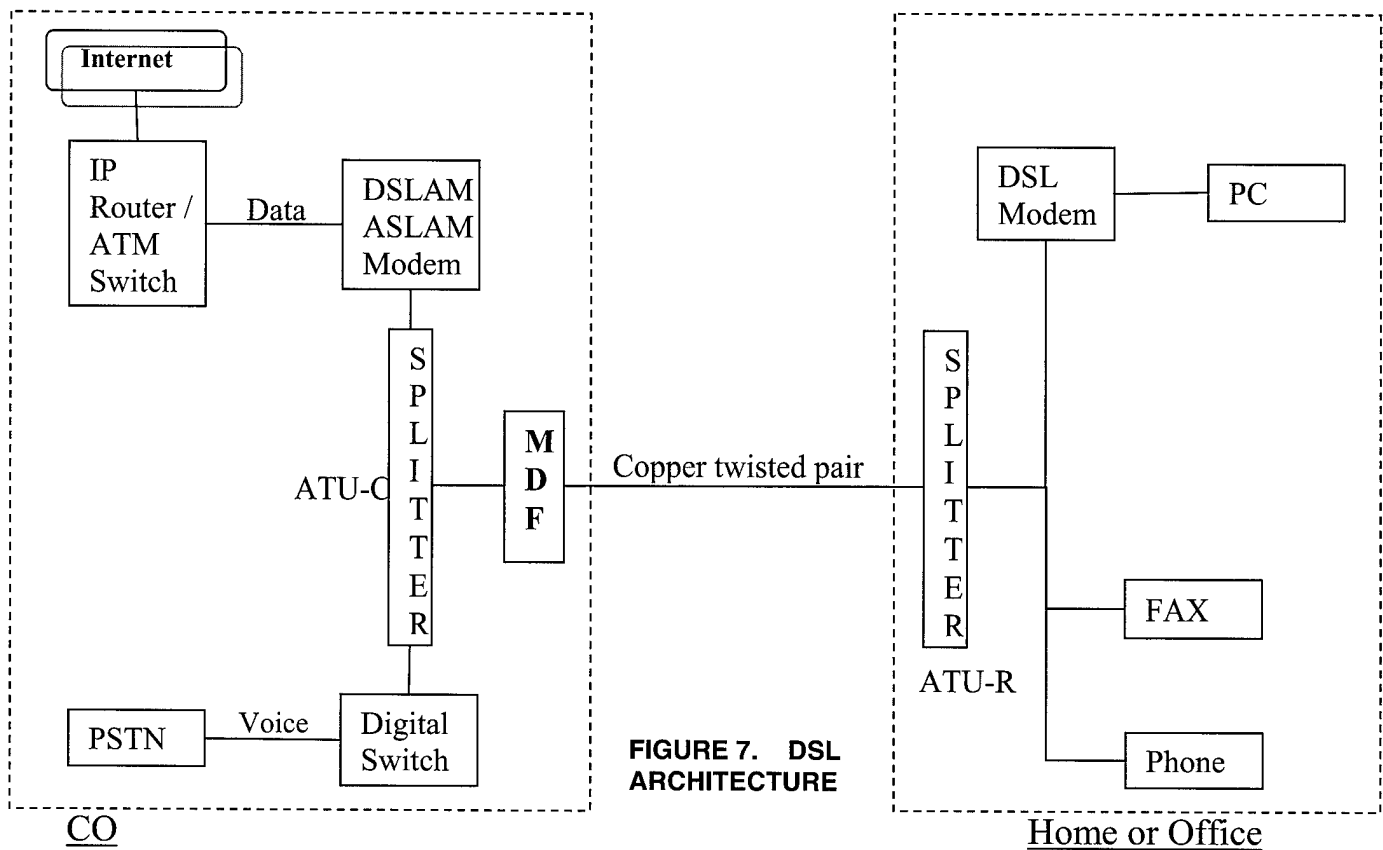
DSLAM Digital Subscriber Line Access Multiplexer.

ASLAM ATM Subscriber Access Multiplexer.

ATU-R Device also called ADSL Network Termination (ANT). Terminates ADSL access network at the customer PC. Modem uses Discrete Multitone (DMT).

ATU-C Central Office ATU–R.

FIGURE 8. VDSL ARCHITECTURE
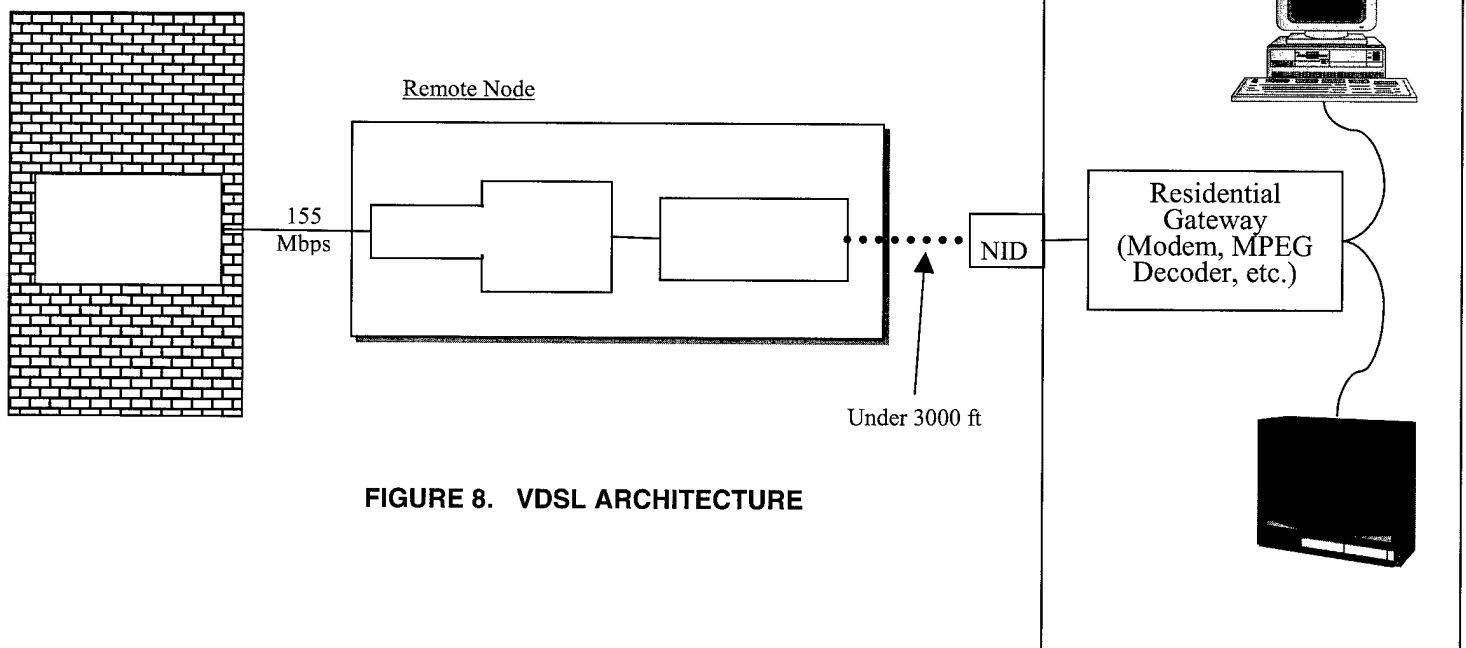
In a voice world if the phone system is down, but I am not on the phone, it does not mean that much to me. In a DSL data world customers will know when the network is down because they will loss their DSL connections and have to re-log in. If ADSL fails to POTS so lifeline service is preserved which may not be the case with voice over cable or other DSL systems like HDSL. So customers will know when there DSL system is down. This DSL demon will result in increased trouble reports and their associated expenses. Some DSL services like HDSL could hurt revenue since they provide similar service as a T1 line but at a fraction of the monthly fee. VDSL is the "mother" of all DSLs and can provide voice, data, and full video services. For services like video conferencing 300Kbps is required, but to provide MPEG quality video 3Mbps would be required and VDSL is needed. Reviews are under way to determine if VDSL can support more than HDTV in a home.

DSL Issues

The fundamental network architectures for DSL delivery shown in Figures 7 and 8 can be visualized as pipelines to the customer. There are several areas where these pipelines can "spring a leak" reducing DSL's value to the customer and reducing shareholder return to the service provider (Figure 9 below). Each one of these points is a network operations area that needs to be analyzed, repaired and maintained. If only one or two "leaks" are plugged, the increased pressure along the rest of the pipe will cause more "leaking" at other susceptible points. Below we will discuss these critical points that exist in the DSL network.

What happens when DSL service fails after the COs are declared ready with DSLAMs in place, and the customers have their NIC cards, modems, and software installed and ready? Ultimately in such a case, the blame for the broken or leaking DSL service will be placed on the shoulders of the people with responsibility for outside plant.

Process Flow

To repair and maintain this DSL pipeline, a diverse collection of technical, management and marketing individuals and groups have to work together for a successful DSL deployment. Figure 10 below illustrates the complex interplay of groups that need to communicate to provide efficient and reliable DSL broadband service.

Central Office Issues

One of the first possible critical points is the central office (CO). DSLAMs need to be installed properly and a certification process should be in place to help ensure that the DSLAMs are ready for service. In our review of central offices, we have found issues that impede DSLAM installation. In one case, no signal or response was found during our remote testing back to a central office that was listed as having a DSLAM installed and working. Further investigation determined that the DSLAM was at the CO, but still sitting crated on the receiving dock. Unfortunately, according to the process flow records, this situation constituted a DSL ready central office. We have also found installed DSLAMs that could not communicate to the ATM switch, and others that had incorrect IP addresses so that the software handshake with the IP Router was not possible.

In visits to COs with working DSLAMs, we saw large commercial floor fans pointed directly at the equipment that were needed to cool the equipment and keep it running. There was no apparent plan to redesign either the building A/C or the DSLAM equipment to provide for heat dissipation. While the fans may cool the system, they were clearly blowing dust and other particulate contaminants directly on the equipment that may shorten its life.

As more and more customers sign up for DSL, the backbone needed for connections to the ISPs will become overloaded, so additional fiber capacity will be needed. Some ISPs are being fed with DS1 lines, but it looks like at least a fiber optic OC-3 should be provided to reduce network congestion.

To address spectrum management and interference issues in COs, some folks are using expensive shielded cable, which adds significant expense. Much of this CO information on actual deployment problems of the DSLAM switch and local environmental (heat) problems remains limited to the local management level. These issues only come to the surface after a number of major congestion problems, increased trouble reports or escalating held line orders are reported.

Standards

Interoperability of DSL equipment needs to be established and maintained. In one instance we saw modems that could not talk to their intended DSLAM without being reconfigured. If DSL is to flourish, interoperability is key. There are many industry efforts underway in this area. The following is a reference to some of the industry documents that are available on DSL.
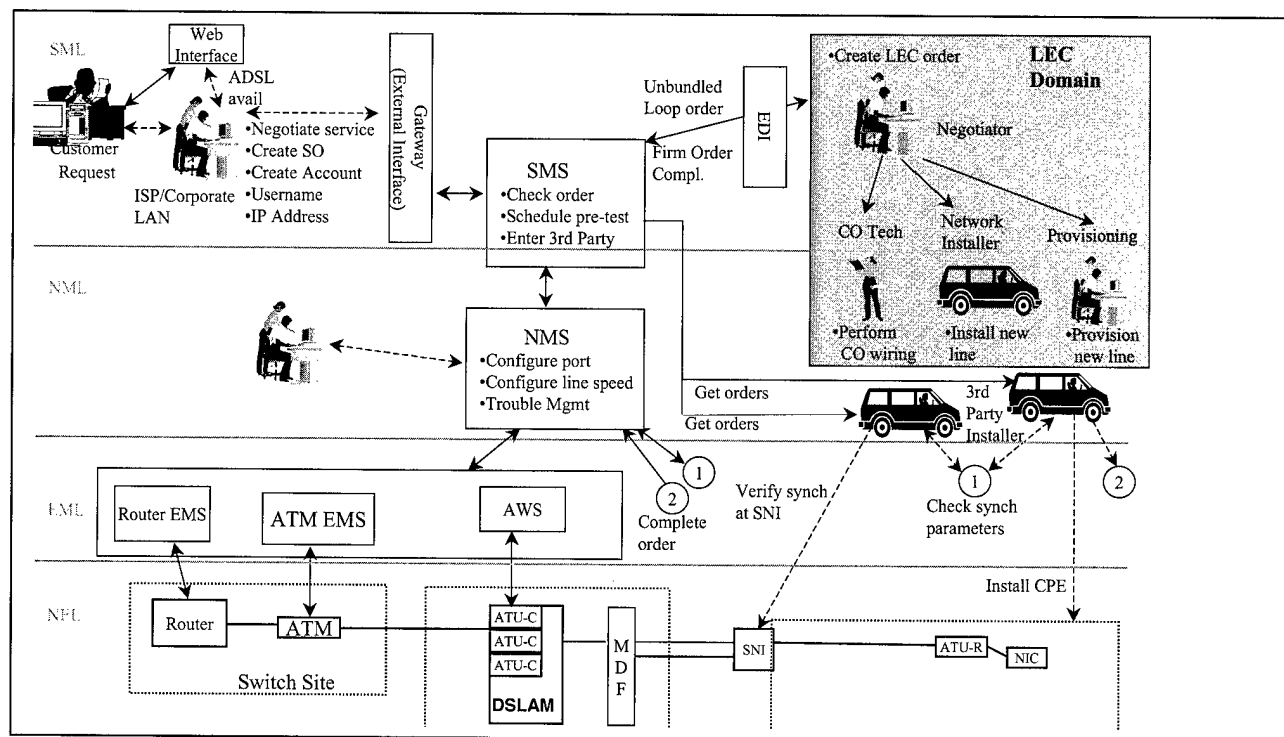
FIGURE 10. DSL END USER SERVICE ACTIVATION FMO PROCESS

FIGURE 11. DSL STANDARDS		
Study Area	**Status**	**Title**
ADSL	G.992.1 Determined (10/98)	Asymmetric Digital Subscriber Line (ADSL) Transceivers
ADSL	G.992.2 Determined (10/98)	Splitterless Asymmetric Digital Subscriber Line (ADSL) Transceivers.
XDSL (generic)	G.996.1 Determined (10/98)	Test Procedures for Digital Subscriber Line (DSL) Transceivers.
ADSL	G.997.1 Determined (10/98)	Physical layer Management for Digital Subscriber Line (DSL) Transceivers.
XDSL (generic)	G.994.1 Determined (10/98)	Handshake Procedures for Digital Subscriber Line (DSL) Transceivers.
S(H)DSL	G.991.2	Single Pair High Speed Digital Subscriber Line (SHDSL) Transceivers.
VDSL	G.993	Very High Speed Digital Subscriber Line (VDSL) Transceivers.
XDSL (generic)	G.995.1 Determined (10/98)	Overview of Digital Subscriber Line (DSL) Recommendations.

Loop Qualification

The next critical point is duing loop qualification and circuit conditioning. Telcordia offers a DSL loop qualification service to address loop qualification issues. To avoid a false positives and high numbers of held line orders, many carriers are taking a very conservative approach in who they qualify for DSL service. So who are the chosen ones? Well, a qualified customer

- needs to have DSLAM installed in their local central office,

- must be within the serving loop distance guidelines

  (e.g., the Carrier Service Area (CSA) Guidelines are

  9Kft for 26 AWG wire loop and 12kft for 24 AWG wire loop),

- needs all the load coils removed, and

- minimal bridge taps on their circuit loop

So what customer base does that leave? The USA has about 160 million access lines with approximately 60% residential within the 12kft average loop length. About 20% have load coils. Bridge taps and mixed wire gauges are *ubiquitous* throughout the network. The average loop has 20 splices that can corrode, attenuate and reflect signals.

At the present time in order to reduce the number of false positives (telling customers they can get DSL, when they really can't) service providers have been very conservative in indicating who they can provide service to. As we move to mass DSL deployment the rules will lessen and we will extent the offer reach from 12Kft to 15 or even 18Kft. As we move further in the network, the DSL transmission signal will weaken and be more susceptible to plant conditions, noise and other spectrum issues.

Outside Plant Issues

Load coils were intended to counteract capacitance and increase POTS service reach. Since these load coils block the passage of DSL signals, they must be removed to provide DSL service. We have not seen companies with a plan for widespread removal of load coils. The end result is that technicians are going into a manhole and removing one load coil today knowing full well that they will be back to remove more coils on the following day or the next week. Circumstances have occurred where customers that were turned away by an ILEC because the ILEC was not willing to provision the plant (too costly to condition the circuit). The customer would then call the competing CLEC, who in turn called the ILEC who is then required to provision the plant by removing load coils and bridge taps for that single circuit. While the ILEC may be compensated by the CLEC to provision the plant in such circumstances, it may be losing a DSL customer. Changing plant configuration to supply a single DSL circuit is inefficient for engineering groups, installation technicians and can lead to future field problems if plant records are not routinely updated.

Bridge taps (intended to make it easier to add and drop customers) add attenuation and reflection, and crosstalk to DSL signals. The number or length of these bridge taps must be minimized. We have found that the negative effects on DSL service performance were much worse if the bridge tap is closer

(<1000 ft.) to the customer. Therefore, the decision as to which bridge taps to remove is critical to the time and expense needed to provision a line. Again, the folks responsible for DSL in the outside plant need to have the same detailed and thought-out methods and procedures for DSL that they now enjoy for POTS.

The next outside plant issue to address is that those customers served by Digital Loop Carrier (DLC), and Next Generation Digital Loop Carrier (NGDLC) that cannot get DSL unless equipment (MiniRAMS) are installed. Depending on location DSL concentration ranges from 15% to 70%. Installation of remote equipment is expensive and can create heat dissipation and space limitation issues when installed in a HUT, CEV or cabinet. Real Estate and right of way issues necessitate that remote DSL equipment must take up as little room as possible. What does the future hold? Possibly co-location requirements currently employed inside the central office will be applied analogously in some manner to that outside plant.

Further possible critical points are the physical components of the network itself and their associated impairments. There is a fundamental design gap in the outside plant used for DSL. The Voice Public Switched Telephone Network (PSTN) was designed for 4Khz, while DSL operates at least at 400Khz, and in the 1.1Mhz range depending on line conditions. This approach of using for digital data, a network designed, built and maintained for analog voice service, is not unexplored territory. The past experience and issues addressed with ISDN and Caller ID involve basically the same basic problem -- putting digital signals on a network that was designed for analog traffic.

The situation becomes further complicated if work is performed in the outside plant to remove load coils and bridge taps. Trouble rates may increase and customers not ordering DSL may have trouble with their phones.

During our field work, the F2 plant records (the last mile of the loop) were often of questionable reliability which makes provisioning and trouble shooting difficult. We know that splices and different wire gauges (reflections) raises issues, but inaccurate F2 records makes it extremely difficult to trace pairs and determine root causes of problems that are experienced. One such interesting DSL "demon" was traced to mid-span drop splices. The drop wire will bend and flex in the wind, which can cause a change in wire characteristics that will create "digital" problems that will be hard to trouble shoot. Such continual flexing can reduce wire cross-section and therefore reduce the effective gauge as well as cause fatigue fractures. It took two weeks to identify this particular trouble on one job because it was intermittent. *So please no mid-span drop splices.*

Dampness in cable and induced AC (hum) can adversely affect the speed and quality of DSL transmission. For voice service wires, merely making physical contact was adequate. This is not true for digital service. Some of the old demons that mildly interfere with POTS service such as DC faults, series resistance faults, opens, crossed battery, and circuit unbalance will cause major problems for DSL service. The transmission demands for digital service are more demanding than for simple voice analog service. We have all experienced these problems with today's digital equipment, faxes, caller ID and so forth.

Network components such as MTUs, RFI Filters, electrical protection devices with high capacitance, high resistance heat coils can be an issue particularly with high
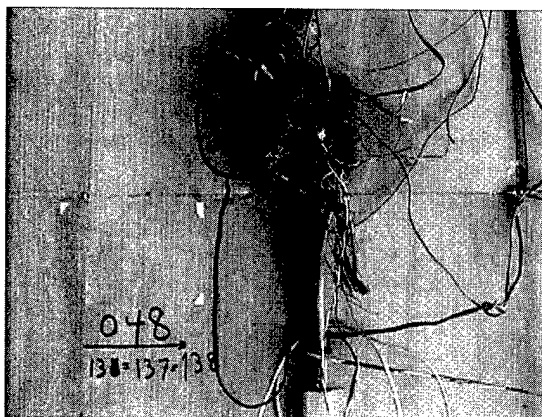
FIGURE 12. PHYSICAL NETWORK IMPAIRMENTS

frequency services like VDSL. Corrosion and poorly maintained plant will be even more of an issue with DSL. To compensate for poor plant conditions, companies are using ISDL, which is ISDN based, and can reach longer distances, and RDSL which is Rate Adaptive DSL will adjust data rate based on plant conditions. The following photographs illustrate plant conditions that we have found that POTS service still worked over, but DSL would be impossible.

Proactive Maintenance as a DSL Solution

One approach followed by various companies is to complete a close review of their proactive maintenance plans to promote cost-effective and reliable DSL deployment. We all know that proactive maintenance is a real winner for POTS by increasing service quality levels and reducing trouble report and repeat rates, but if done right proactive maintenance can also extend the reach of DSL, lead to faster data rates, and increased quality of service.

Spectrum Management Issues

An additional critical point is the complex area of spectrum management issues. As you can see from Figure 12, some DSL services do not "play nice" together. Crosstalk and signal interference can reduce data transmission rates, increase bit-error-rates or even cause service disconnection.

There can also be noise on the line from sources such as
- lightning,
- induced AC from electrical transmission as well as
- from building electrical equipment rooms and closets,
- transformers, and

other similar sources that can interfere with DSL service. We even have trouble incidents that we traced to a household light dimmer switch interfering with transmissions rates. Radio (RFI) particularly from high powered AM radio station will also be an issue. So areas that have "music on the line" will also have problems with certain flavors of DSL. Since ADSL uses relatively low signal power levels and low frequencies, it is unlikely to radiate to interfere with other services. ADSL is

more likely to be a victim of, not a cause of, RFI interference problems. VDSL also has low signal power, but high frequency, so the balance of the cables with the shorter wavelength (due to high frequency) can make an efficient antenna.

Looking at conducted emissions, other DSL signals in the same cable bundle with overlaps in spectrum will cause interference. Non-linear components in telephone sets (zener diodes) result in inter-modulation with products from the upstream signal which will cause interference. Even simple on hook/off hook operations may lead to interference. FEXT for HDSL and repeated T1 can interfere with ADSL if in the same cable bundle or even simply co-located in the same cable conduit/tray.

Many of the spectrum issues will be at the customer's location. What type of wiring is required, and should the existing wiring be replaced? Initial studies indicate that Category 3 wire as defined by TIA 568A may be sufficient for most DSL applications. We have all heard about DSL issues in the last mile, well most of our big issues may occur in the last 100 feet. We can provide DSL to the network interface of a multiple tenant unit such as an apartment building, mall, college dormitory, but the digital signals still must travel over the building's or complex's private copper network.
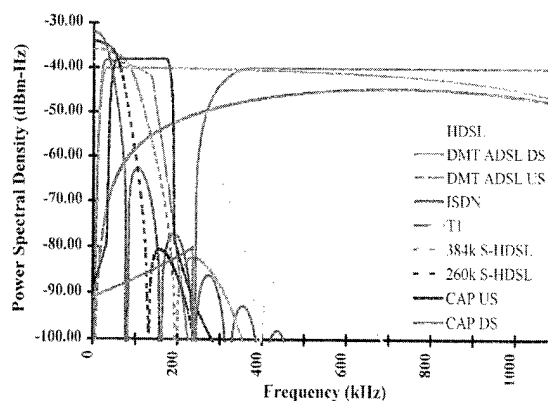
FIGURE 13. DSL SPECTRUM MANAGEMENT

At the Customer

One of the more persistent critical points will be provisioning at the customer location. If a splitter is required a truck roll is needed to place the splitter in the NID. It would be beneficial if at that point the technician checked to see if DSL was available

CO

NEXT (Near End Cross Talk)

FEXT (Far End Cross Talk)
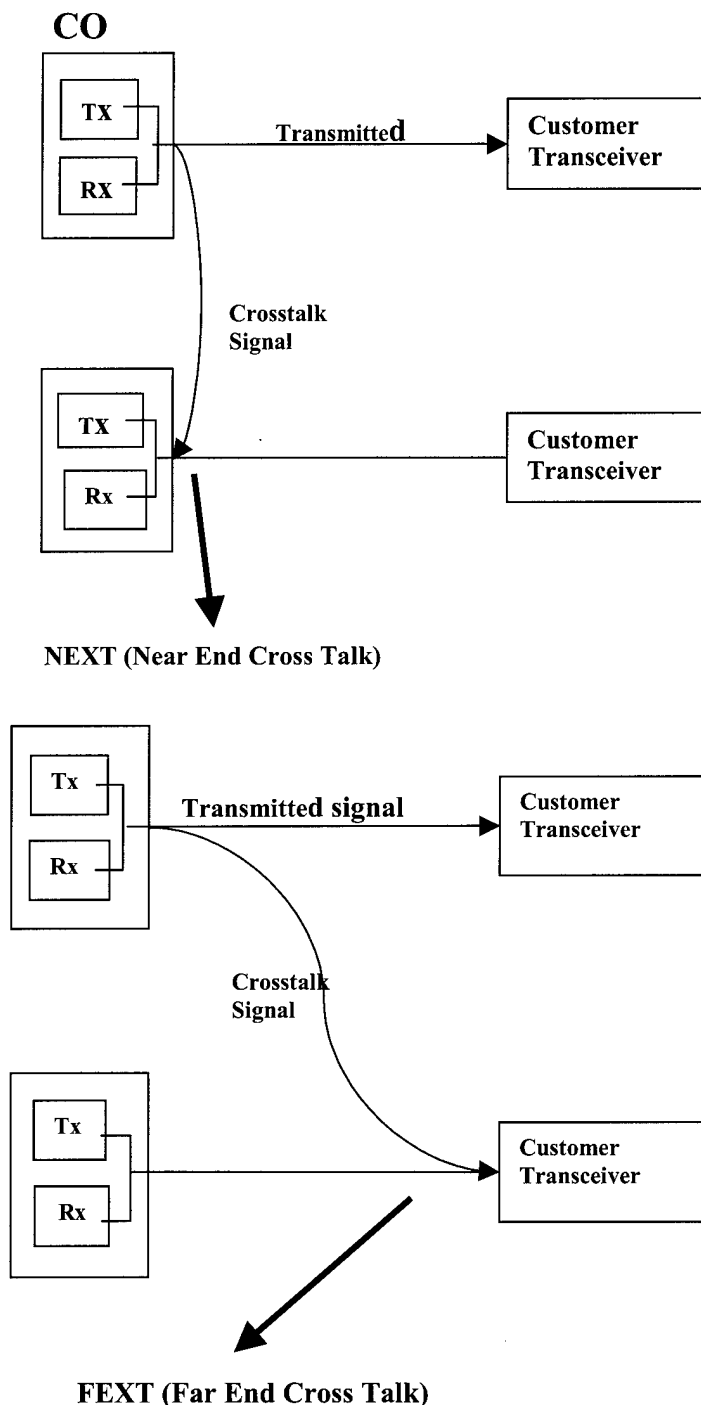
FIGURE 14. SPECTRUM MANAGEMENT - FEXT AND NEXT

at the NID before the third party installer visits to install the Network Interface Card (NIC) in the computer with software, and modem or if the customer will do the installation. Many companies are using G-Lite (splitterless), and the customer can do the complete installation. We have seen crosstalk and interference issues with the use of G-Lite and FAX machines and caller ID boxes.

As DSL moves past the "early adopter phase" to mass deployment, can customers do installations? To date we have seen a high rate of initial troubles with customer installations, with as much as a 70% initial trouble rate. Also, with self-installs it may be difficult for the service provider to accurately determine if their service commitments have been met and the data throughput that the customer is getting. And, as discussed above, another installation issue is the customer inside wiring.

Testing and Trouble Shooting and the Technician

So let's assume we have the CO, outside plant, and customer end all provisioned. How do we effectively plan to test and trouble shoot DSL? How will DSL troubles be coded to determine if the trouble is in the DSLAM, the outside plant or at the customers end? If you can't track where and what the problems are, you can't study the issues and put proper plans in place.

For traditional POTS, the MLT has proved effective, but MLT will not give the complete picture for DSL, so a remote testing solution is needed. In addition, new trouble codes may be needed so that DSL troubles can be easily identified. The overall load on the technicians will increase with mass DSL deployment, which may cause other jobs, like proactive maintenance to suffer, which will lead to ever-increasing troubles. If the trouble rate is high, and resources are limited we usually focus on resolving the troubles, and not on proactive maintenance. Since we would not be focused on proactive maintenance, the plant degrades and we get more troubles, which leads to less proactive maintenance, which leads to more troubles and so on in a feedback loop that wastes technician's time and a company's money. Proper test tools and trouble ticket data mining are necessary to establish a path for proper maintenance of broadband services.

Technicians and operational managers need the knowledge to install, provision and trouble-shoot DSL. Intelligent use of a TDR (not just looking for a physical connection anymore) is needed to maximize the information on plant condition, trouble location and root cause that can be deduced from a TDR profile.

Since various DSL services require higher working voltages than POTs lines, technicians *MUST* follow safety rules. With the unbundling of network elements, the technicians may not know what services are providing in a loop that they are working with. The causes safety concerns, and spectrum management issues. It is important to note that outside plant technicians and their managers must be well trained. Most customer interaction is with the technician, and customers will gauge their view of the service provider based on the knowledge and professionalism of the technician. The customer does not see all the equipment in the CO, care about the OSP conditions, or care about the internal company processes. All they care about is that they get the service they are paying for. If it is broken then they expect a

technician who is knowledgeable and really cares about solving their problem, who arrives promptly at their door. All customer-facing personnel are critical to the growth of DSL services and revenues; i.e., installers, repair technicians and service representative.

To maximize DSL deployment and broadband revenues, service providers will need analyst angels to identify DSL "demons" and eliminate critical points in the network outside plant, marketing, provisioning and quality assurance processes. The conditioning, repair, and maintenance of the physical components in the network will be a critical component in closing the gap between the potential of DSL the realized service quality, performance and revenues.

Cabling Systems for XDSL Services in Both Residential and Business Buildings

E. Cressan, O. Bouffant, P. Guillas, H. Le Cozic, P. Mercier, M. Lissillour
FRANCE TELECOM - BD/FTR&D/DTD/IBL
Technopole Anticipa
2, avenue Pierre Marzin
22307 LANNION Cedex, France

Abstract
This paper presents the cabling systems defined by France Télécom for offering xDSL services in residential and business environments.

The first part of the paper will describe the residential aspects with the definition of a new cabling system for new buildings, able to offer several narrowband and broadband interfaces to users in apartments, creating a lasting installation and significant mobility. The second part deals with broadband services to business customers. High performance cabling systems have to be defined with regard to access technology (such as ADSL) and the bit rate supplied (several dozen Mbits/s) to the existing customer LAN.

Keywords
Customer premises network; home network; cabling system; copper cable; optical cable; xDSL systems;

1. Introduction
France Télécom is currently deploying ADSL technology in several towns in France and testing other technologies (like VDSL) in field trials.

These techniques allow high bit rates (from 500 Kbits/s for residential to several Mbits/s for business) for the delivery of broadband services such as high speed Internet access, networking, etc.

The aim of telecommunications operators is to distribute all these services to the Customer Premises Network (CPN), to the home of the residential customer as well as the Local Area Network (LAN) of the business customer.

The residential approach takes into account two important points, the re-use of existing cabling and the realization of new cabling systems. The business approach describes cabling systems in terms of building backbone and horizontal cabling systems taking into account existing cabling and the evolution of cabling systems for the performance of field trials.

2. Residential approach
2.1 Introduction
For the residential customer, 2 scenarios will be considered for bringing narrowband and broadband services into the house: re-use of the existing cabling system and the creation of a new cabling system.

The two approaches differ completely. In the first scenario, the customer premises network (CPN) is re-used without any work required inside the house or the apartment, which is very much appreciated in the residential environment.

The second situation concerns new buildings or the restoration of older buildings. It consists in the creation of a new cabling system able to deliver all home services to all rooms in the house, allowing significant mobility for the customer and a long lifespan for the CPN infrastructure.

Firstly we shall describe the existing CPN, showing how it is re-used for the multiservices CPN and ADSL architectures. Then, we shall define the new cabling systems designed to bring multimedia services into the home network.

2.2 Existing cabling system
2.2.1 Existing CPN
The existing CPN for residential customer is described in figure 1. Since the 1970s, to deliver POTS services France Télécom has deployed an Unshielded Twisted-Pair (UTP) cable with a capacity of 2 or 4 pairs and a transmission quality equal to category 3 (UTP-3). The cable is put on a bus or Y (two branches) architecture with "T" connectors. The point of France Télécom services delivery is called the Network Interface Device (NID). The home network is of average quality but is sufficient for POTS service transmission, for which it was created.
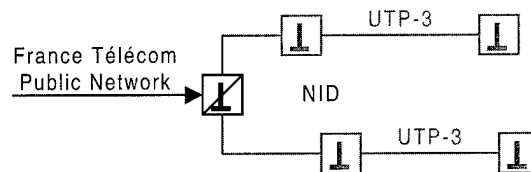
Figure 1: Existing CPN for residential customer

2.2.2 Multiservices CPN
The more current 4 pair UTP-3 cable (about 80 %), is used in existing CPNs as shown in the following table:

Pairs/services	POTS	ISDN	ADSL
No. 1	line1	U access	ADSL + line 1
No. 2	line 2	line 1	line 2

This applies to the "Plug & Phone or Play" solution where the active equipment is placed on one dedicated outlet on the CPN. With ISDN, the network line ("U access") is brought up to the dedicated outlet to connect the ISDN Network Termination (NT). ADSL needs only one pair (see the description in the next section). This ADSL solution is called "distributed filter."

The use of an existing CPN with the active equipment placed at the entrance of the house (at the NID) is described in the following table:

Pairs/services	POTS	ISDN	ADSL
No. 1	Line 1	Line 1	Line 1
No. 2	-	S Bus (R)	-
No. 3	Line 2	Line 2	Line 2
No. 4	-	S Bus (E)	ADSL

Here, with the active equipment placed at the entrance, before the CPN, several outlets can be used for broadband services. With ISDN, the user interface, called "S bus", using 2 pairs, is distributed to all rooms and allows the connection of ISDN terminals in all outlets via adapters. The ADSL solution, called "master filter", is described in the next section.

2.2.3   ADSL architectures

As mentioned above, two solutions exist for the distribution of ADSL services to existing CPNs: the "distributed filters" solution and the "master filter" solution.

With the "distributed filters" solution, no changes to the existing CPN are required (see figure 2). Both ADSL and POTS signals are transmitted on the same pair inside the rooms on all outlets. The low-pass filters (LPF) are distributed on the "T" outlets connected to analog phones. On the outlet dedicated to the ADSL signal, the ADSL modem is connected via an adapter. The PC terminal is connected to its ATM or Ethernet interface.
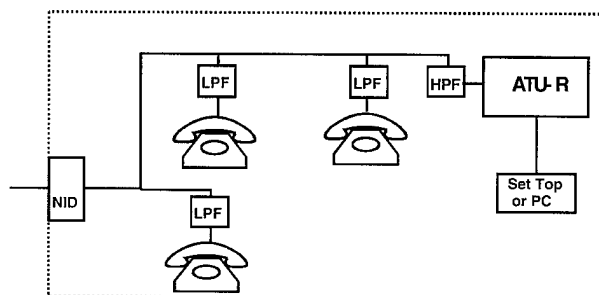
Figure 2: The "distributed filters" solution

When the "distributed filters" solution is not possible (because of CPN complexity or long lines), the "master filter" solution is used (see figure 3). The filter is placed at the entrance to the NID point (end of public network). The POTS signal is re-injected on pair no. 1 of all the CPN branches. The ADSL signal is injected on a free pair. A modification is made to the existing CPN.

These two scenarios only allow one PC terminal to be used. The current objective is to make it possible for the customer to install a mini-LAN (Local Area Network) to use several PC terminals and to create a network.
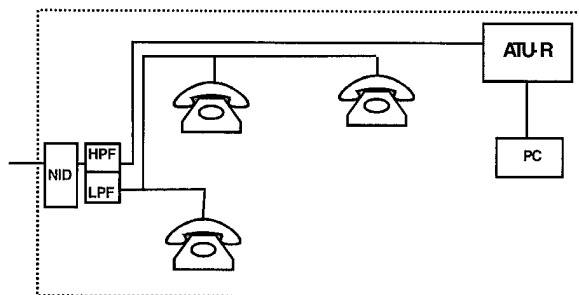
Figure 3: "Master filter" solution

2.3 Multimedia cabling system for home network
2.3.1   Residential CPN stakes
Today residential customers are using an increasing number of electronic devices in the home, such as TV sets, phones, faxes, PCs, printers, camcorders, etc., and their wish to connect these devices together is also increasing. Furthermore, new communication functions are appearing for existing devices such as refrigerators, washing machines, coffee machines, heaters and anything that comes within the field of "home automation". Against the background of this expanding, increasingly popular area of home services, the major concern of telecommunications operators is to forge partnerships with service providers and then keep their customers by improving their home services offer.

2.3.2   Different architectures: gateways and private and collective networks
For the convergence of all these services, with inter-operability between different terminals, the notion of "gateway" has been created for networking home resources. There are major domains here, such as audio-video and data. The most important forums working today on the definition of a "residential gateway" are "HAVI" (Home Audio Video Interoperability) and OSGI (Open Service Gateway Initiative).

Several different architectures and technologies are being studied in relation to the evolution of the residential CPN to deliver all the services to the customer. For a private apartment, the services will converge to a private residential gateway (see figure 4).
For collective apartments, two gateways can be combined: one collective gateway and one private gateway (see figure 5).
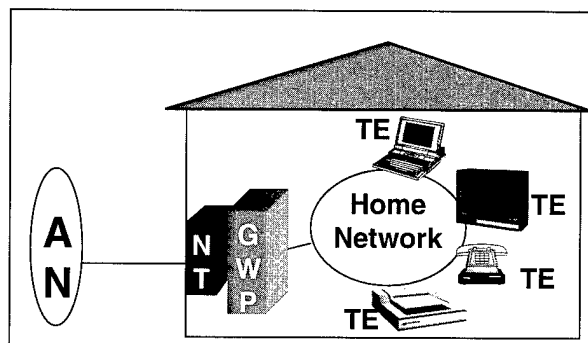
Figure 4: Private "gateway"
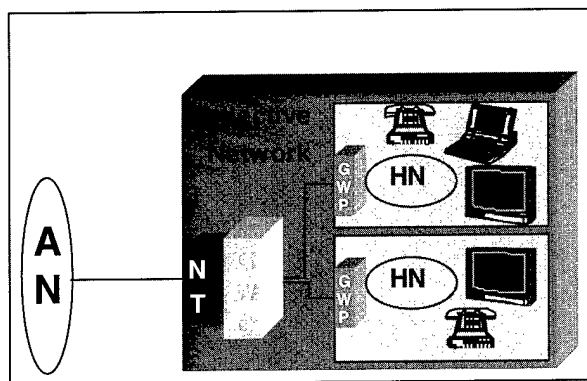
Figure 5: Private and collective "gateways"

2.3.3 Networks Convergence: several transmission systems

For the convergence of the different home networks and inter-operability between communications terminals, several transmission systems can be used. These systems use the two previous types of cabling systems: re-use of existing cabling and the creation of new cabling. For the re-use of existing cabling (also called "no new wire"), the techniques used involve the "phoneline" reusing the POTS network and the "powerline" reusing the existing low voltage network. The existing coaxial cable network can also be re-used.

Another way to avoid changing the existing networks is to use wireless techniques such as "infra-red" or "radio", with systems like "DECT, Bluetooth, IEEE802.11, etc.". "Phoneline" technology is based on the Home PNA specifications. The principle is that one pair is re-used on the phone cable to connect 2 PC terminals equipped with Home PNA cards to share high bit rate Internet access such as ADSL (see figure 6).
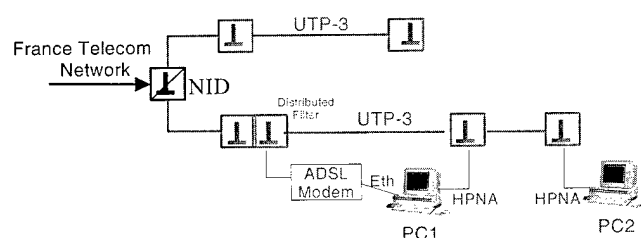
Figure 6: Connection of 2 PCs with "Home PNA" interface

The principle of "powerline" technology is also to share a high bit rate network link between several home devices connected to the same low voltage network, via a specific "powerline" interface (see figure 7). The first investigations of France Télécom in this domain are described in another paper of this symposium [1].

Another technology used for the creation of new cabling systems inside the house (or for new houses) is called "IEEE1394" bus. This "IEEE1394" network allows the connection of all types of equipment with the IEEE1394 interface creating the home network.
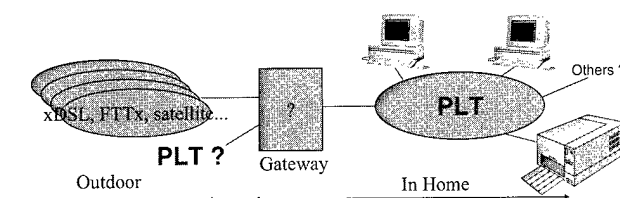
Figure 7: Principle of multi-terminal connection with Powerline

New specifications allow attractive distances for home networks (up to 100 meters) on media such as copper (cat. 5) and optical fiber (glass and plastic). The following table sums up the specifications in relation to the bit rates.

Media/bit rate (Mbits/s)	S100	S200	S400	S800	S1600
Twisted Pair cat. 5	ISO/IEC 11801 **max. 100 m**				
Plastic Optical Fiber	Core = 1000 um **max. 50 m**				
Hard Plastic Clad Fiber	Core = 225 um **max. 100 m**				
Glass Optical Fiber	Core = 50 um **max. 100 m**				

Another technique for creating a mini-LAN in residential homes is to use the definition of the business network with category 5 cables and a class D link, for example.
The details of these networks are developed in the following paragraph.

2.3.4 Cabling reference for buildings complex

The infrastructures described below are defined and produced for new buildings. This field trial, performed near Paris, concerns a large buildings complex with about 1000 apartments in quite small buildings, spread over about 12 hectares (see figure 8).
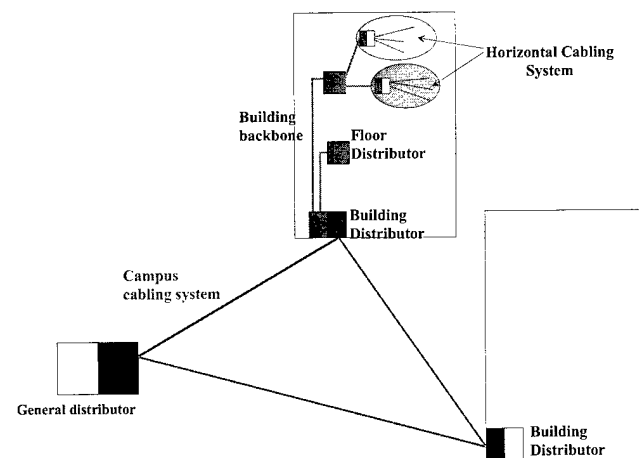
Figure 8: Schematic of buildings complex cabling system principle

The objective is to enhance the reputation of the property developer and the service providers, to propose alternative solutions allowing for the future integration of broadband transmission systems and to perpetuate investments while reducing costs.

The infrastructures described in figures 9 and 10 take into account the different types of access network such as xDSL (ADSL, VDSL, SDSL, etc.) and FTTx currently deployed or used in field trials at France Télécom.

This infrastructure covers a high number of services to customers in both private and collective areas, taking into account individual services (POTS, audiovisuals, IP, etc.) and collective services (remote meter reading, Intranet, cyber-spaces, etc.).
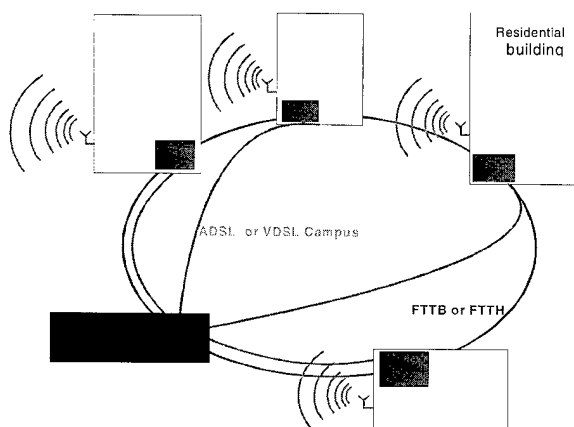
Figure 9: Campus cabling system infrastructure

The campus cabling system consists of two networks: one xDSL copper point to point network (made of classical cables used in the France Télécom public network) and one FTTx network (made of optical loops connecting the buildings). Outdoor radio cover is provided to offer proximity services such as self-surveillance, etc.
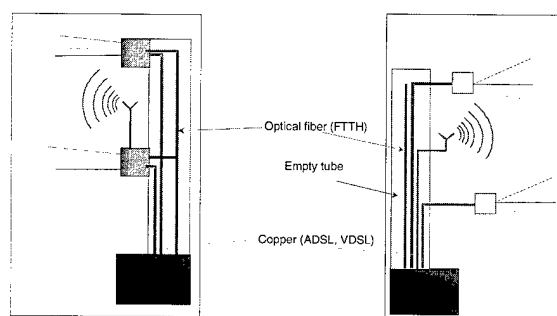
Figure 10: Building backbone infrastructure

The building backbone cabling system also consists of two networks: one with copper cables (xDSL services) and the other with optical cables (FTTx services). Empty tubes are installed in order to be able to install optical cables and offer further services later on. Radio terminals can be used for internal building communications (Intranet, etc.).

The principle for horizontal cabling system inside the apartment described in figure 11 is to equip each apartment with 2 complementary wiring networks (plus the coaxial cable network used for CATV services): one classical POTS network (as described in section 2.2.1 using cat.5 cables) and one second network with a star topology cabling system. This cabling system begins at the entrance (NID) of the apartment and each branch of the network is dedicated to one outlet for the transmission of broadband services using cat. 5 cables and cat. 5 "RJ45" outlets.
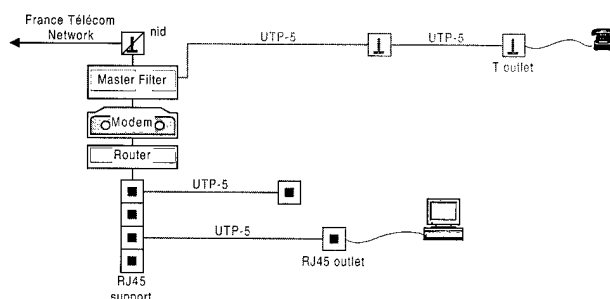
Figure 11: Schematic of housing cabling system principle

2.4 Conclusion

For residential customers the two approaches (re-use of cabling and new cabling systems) are advantageous. The first scenario allows for optimization of the use of existing cables inside the house with lots of services for the customer. Nevertheless, some parameters are limited, such as the number of terminal devices used.

This limitation is lower with the use of technologies currently being studied such as "phoneline" or "powerline" and does not exist anymore with the creation of a new cabling system. In this scenario, technologies using IEEE1394 bus or business LAN cabling systems are very promising.

3. Business approach

3.1 Introduction

Due to the explosion of Internet services, cabling systems for business buildings are having to support an increasingly high bit rate. In this context, xDSL techniques have the advantage of meeting demand without any major investment by using the existing network. Another important parameter for this type of customer is the necessity of having a very high quality of service: low disconnection time and reconnection time, for example.

Cabling systems for buildings can be divided into two parts:

1. The building backbone cabling subsystem that extends from the building distributor to the floor distributor. This mostly uses the copper cabling system, but optical cabling systems are being increasingly deployed to answer the increase in bit rate and to protect the network by providing double cabling. Another alternative is to install empty micro tubes initially and then fill them with optical micro cables when requested.

2. The horizontal cabling subsystem that extends from the floor distributor to the telecommunication outlet. This is generally made with category 5 copper materials in accordance with the ISO 11801 standard [2]. To respond to the increase in bit

rate, many solutions can be deployed: copper cabling systems with category 6 or 7 materials, empty microtubes which will be filled with fibers on request, optical cabling systems with the possibility of using converters at the ends to make the most of existing copper-based equipment.

The second part of this paper, after making a brief presentation of the existing cabling systems, presents various alternatives tested in our laboratory for lasting cabling systems.
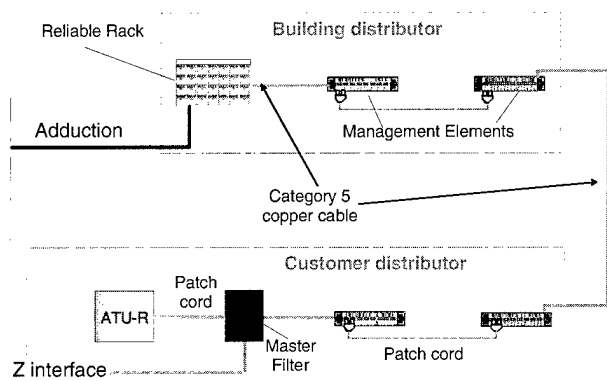
Figure 12: Typical architecture for ADSL techniques

3.2 Existing cabling system

3.2.1 Backbone cabling subsystem

The building backbone cabling subsystem for business buildings is traditionally made with copper cables, whether the access network uses copper or optical cables.

Figure 12 shows the typical architecture for delivery of services based on ADSL techniques.
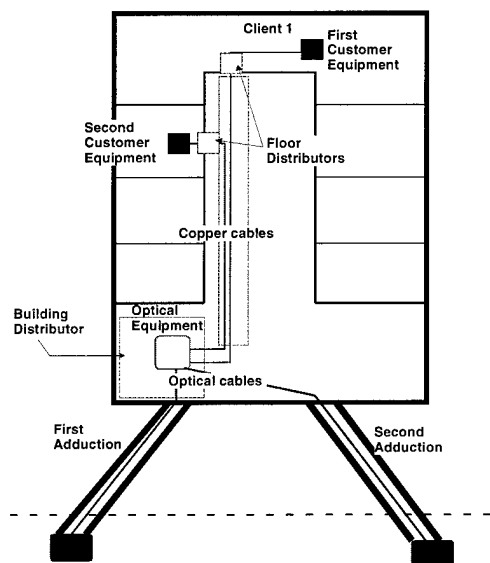
Figure 13: Typical architecture for shared equipment

For a higher bit rate, optical cables are commonly used with the STM system. If the optical equipment is common to all the customers of the building, the backbone cabling is made with copper cable and if the optical equipment is dedicated to each customer the backbone cabling is made with optical materials. Figure 13 and 14 describe the typical architecture for these two cases.
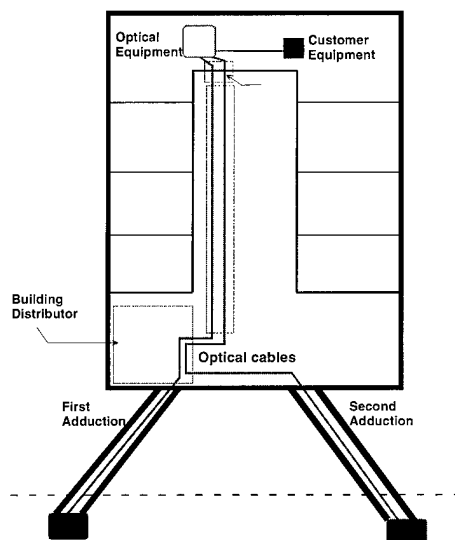
Figure 14: Typical architecture for unshared equipment

3.2.2 Horizontal cabling subsystem

The horizontal cabling subsystem is usually class D cabling, produced according to the ISO 11801[2] standard with category 5 materials. Figure 15 represents the typical architecture with the requested values in terms of distances.

A+D max 5 m (7,5 m électric)
B max 5 m (7,5 m électric)
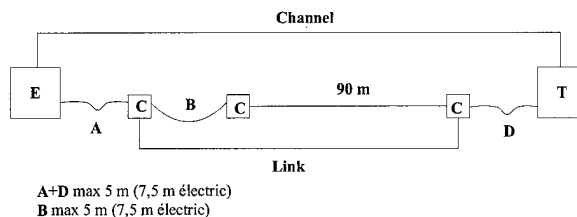
Figure 15: Horizontal cabling architecture

3.3 Cabling system evolution

3.3.1 Backbone cabling subsystem

With bit rates becoming increasingly important for business customers, the backbone cabling subsystem is commonly created with optical cables. To assure a good quality of service and particularly to continue to provide services in the event of an incident in the cabling, various options are offered to protect the network. Different levels are proposed: doubling of the backbone cables, doubling of the distributors or a double link with the central exchange. Figure 16 represents the typical architecture for the higher level of guaranty.

Multicostumer building
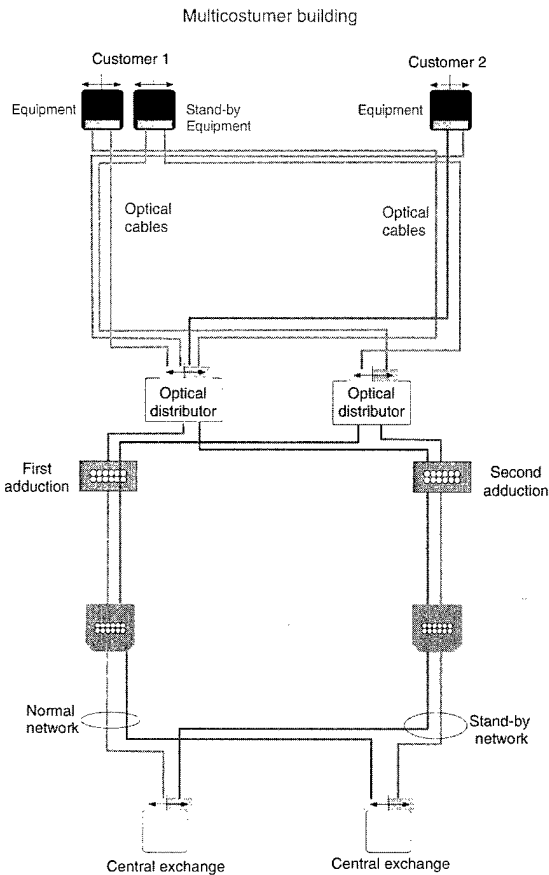
Figure 16: Typical architecture for the higher level of guaranty

Figure 17: Attenuation measurements
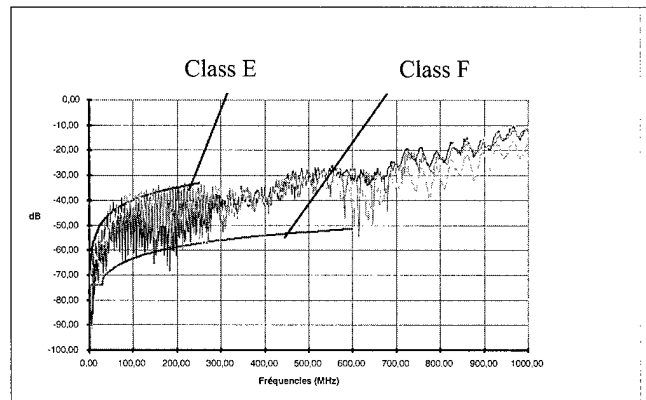
Figure 18: NEXT measurements

Engineering rules have been established to propose different solutions to produce this type of cabling: cabling or precabling with the point to point technique or the loop technique and extraction of useful fibers.

An alternative solution is to install an empty microtubes network in parallel, which will be filled, on request, with optical microcables. This is an attractive solution, which allows for limited investment.

3.3.2 Horizontal cabling subsystem
3.3.2.1 Copper cabling system
To respond to the requirements of increasing bit rates taken to the workplace, copper solutions have been found: category 6 for frequencies of up to 250 MHz and category 7 for frequency of up to 600 MHz. These solutions are discussed in standardization bodies.

A cabling system made with category 6 cables and connectors has been tested. Figures 17 and 18 represent the two main characteristics: attenuation and near-end crosstalk loss (NEXT).

These solutions appear very promising, but the main disadvantage is that they are owner solutions even during discussions in standardization bodies. Another disadvantage is that there are delicate operations to be performed in the field.

3.3.2.2 Optical cabling system
Another solution for delivering higher bit rates is to lay optical fibers up to the outlet. In parallel, using converters means that the most can be made of existing copper-based equipment.
A field trial is currently being conducted inside our company building to study different methods of bringing fibers up to the outlet. The purpose of the experiment is to define not only the best technical choice, but also the most economical one[3]. Four types of optical cabling system are being tested:

- First zone: "traditional" optical cabling in existing pathways where 900 µm fiber cables are put in raceways partly occupied by copper cable.
- Second zone: "optimized" optical cabling in dedicated "steel wire" raceways where compact and light cables (micromodule type) are installed.
- Third zone: also "optimized" optical cabling, but with the use of ribbon cables.
- Fourth zone: microtube laying where tubes with specific characteristics are installed and microcables are put inside on request with blowing techniques.

The cabling laid supplies optical fibers to fifty offices. Each office has two access points that contain four outlets, two multimode (62.5/125 μm) and two single mode. Figure 19 shows the access point used for the field trial. In this paper only the results of the first and second cabling types will be presented, as the others are planned for the end of this year.
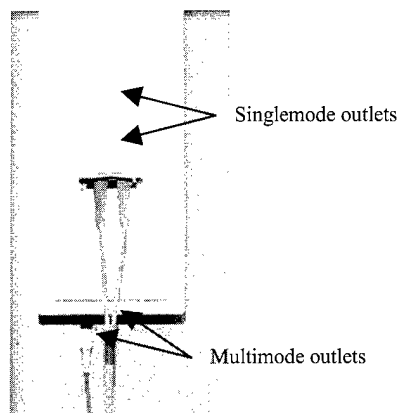
Figure 19: Access point structure

The first phase of the field trial provides information used to aid the search for the most effective way of taking fibre up to the outlet.

The "steel wire" raceway seems particularly well adapted to the laying of optical cables, where EMC aspects are not to be taken into consideration. Cables, which have a micromodular structure present clear economic benefits both for laying and end setting. The OPTOCLIP®II connector (push-pull type) has a slightly shorter installation time than the VF-15™ connector (small factor form type), but this depends on the cable used (due to the facility of access to the 250 μm coating) and one of the advantages of the latter is its duplex configuration that makes cabling management more attractive for the work area.

Two types of rack have been tested: a classical 19 inch rack and a "wheel concept" system [4]. The results show equivalent installation time. The main advantages of the "wheel concept" system are that its high capacity could provide savings in floor space and that its management is simplified with the use of only one length of lead.

3.3.2.3 Microtube laying system
This solution consists in laying microtubes in which microcables are installed inside later with the blowing-pulling method[5]. Tubes and cables with specific properties are required. An adapted apparatus named Microjet® is used and provides additional pushing, enhancing installation performance.

An experiment concerned horizontal cabling based on the tubing method combined with the blowing-pulling technique has been conducted in FTR&D buildings. Tubes supply about four hundred offices with one tube for each office. Due to their low weight and small friction coefficient, tubes are laid twice as fast as conventional building cables. Several tubes are pulled through a guide simultaneously (figure 20).

In the distributor, tubes are connected to distribution closures adapted to a 19 inch rack (figure 21). This is convenient for

producing cabling on demand because there is permanent access to the tube and fibre management is easy. In the office, the outlet and connectors are assembled when the cable is blown. The blowing-pulling performance achieved with the Microjet® tool allows cable installation in a complete horizontal distribution infrastructure. The building presents cabling lengths of less than one hundred meters with about 10 or 15 bends of 90°.
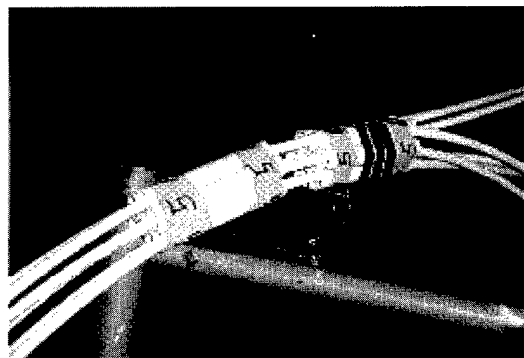
Figure 20: Tube installation
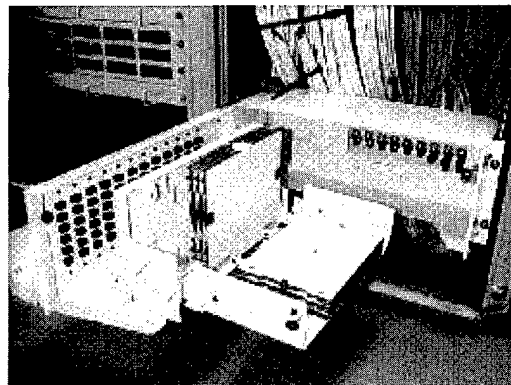
Figure 21: The distribution enclosure in the cabinet

3.4 Conclusion
All the different cabling systems presented in this part of the paper show that there are many solutions to respond to customer requests. The economic advantage of these solutions varies, depending on the customer type and the durability desired for the cabling.

The increase in bit rate for business customers implies that the installation of optical media is becoming an increasing reality. One interesting alternative, which needs a lower initial investment than optical cabling systems, is to lay empty microtubes and fill them on request with optical microcable.

4. Conclusion
For the distribution of narrowband and broadband services to both residential and business customers, there are many solutions which are of interest. In the case of residential users, the re-use of existing cabling systems such as phoneline or powerline is useful for the connection of several terminals and for networking.

For new buildings, new cabling systems are created based on LAN cabling systems or technologies such as IEEE1394 bus. In

the business approach, different copper and optical cabling system solutions exist to respond to the increase of bit rate in the customer LAN. Economically, the advantage of these solutions varies depending on different parameters such as customer type, initial investment, number of outlets needed, etc., but the installation of optical media is becoming an increasing reality. In both residential and business approaches, solutions are being tested and validation in field trials is in progress to define cabling systems for France Télécom customers.

5. References

[1] IWCS 2000 session 17 track 3 « power line telecommunications for residential home network » O. Bouffant et al., France Télécom R&D / DTD

[2] ISO 11801 standard

[3] Optical Fibre Deployment until the Outlet – E.Cressan et al. – EC'2000

[4] Density Cross-Connect Mainframe – H.Aoustin et al – EC'99

[5] An economical optical cabling method for building networks – AC.Réau et al – EC'2000

6. Authors

Emmanuelle Cressan received the title of Docteur of the University of Rennes (Physics and Chemistry of Materials) in 1994. She joined the France Telecom R&D center in 1994 to work on optical cables (writing specifications, performing tests, European standardization, implementation of cables in field trials). Since 1998, working in the Access Network Infrastructure laboratory, she has been charge of studies relating to cabling systems for business customers.

Olivier Bouffant graduated from the University of Toulon in Electronics in 1992. He joined the France Telecom R&D center in 1994. Working in the Access Network Infrastructure Laboratory, he is the project manager for in-house Networks for residential and business customers

Pierrick Guillas began his career with France Telecom R&D in 1976. After six years in Research and development at the Computer Center in Paris, he joined the Access Network Infrastructure laboratory in 1982. Working on standardization for data cables, he is an expert on copper cables, for outside and inside use, writing specifications and test methods.

Hervé Le Cozic began his career with France Telecom R&D in 1981. After six years in a Physical-Chemical Laboratory, he joined the Access Network Infrastructure Laboratory in 1987. Working on standardization for data cables, he is in charge of telecom cables, connectors and home wiring tests.

Philippe Mercier began his career with France Telecom R&D in 1980. After five years in the LAN (Physical layer) group, he joined the Access Network Infrastructure Laboratory. Working on business cabling systems, he is in charge of connectors and field trials.

Michel Lissillour began his career with France Telecom R&D in 1967. He worked in the Test Laboratory for computers from 1967 to 1989. After four years managing the LAN (Physical Layer) group, he joined the Access Network Infrastructure Laboratory to manage the Optical and Copper Cables group working on specifications, performing tests and implementation of cables and cabling in Field Trials. Since 1998, he has been the manager of the Architecture and Copper Cables group working on copper cables and new high bit rate applications on Customer premises Cabling Systems.

Performance of a New Multipair Copper Cable Design Optimized for Evolving xDSL Applications

S.Cámara, C.G.Cortines, J.C. Robredo, O. Vaquero

ALCATEL Cable Ibérica

Maliaño, Cantabria, Spain

+34-942-250100 · susana.camara@aci.alcatel.es

Abstract

Due to the close connection between transmission bit rates and distances of xDSL systems, many limitations exist concerning maximum speeds. Both systems used nowadays, ADSL and VDSL, can reach up to 2.5 km and 300 m respectively over standard telephone lines. It is very important to consider that all these systems are continually evolving. In fact, a new term has come out to solve the existing confusion, xDSL. Under this term we can group all the DSL technologies, which can include all these variants (symmetric and asymmetric): ADSL, HDSL, iDSL, RADSL, BDSL, SDSL, VADSL and VDSL.

In this environment it is very easy to come to the conclusion that copper lines must also evolve as the demand for new broadband services increases. The aim is to obtain cables optimised for the xDSL technologies.

The optimum parameters needed in xDSL systems have been determined and, further to the values obtained, different designs of cable prototypes have been specified with pair count ranging from 12 up to 200 and with different core structures, fillings and materials. Representative prototypes of the cable have been manufactured and a complete characterization of every cable prototype, up to 100 MHz, has been done measuring all pairs of the final cable prototypes.

1. Introduction

A new copper pairs cable has been developed with a high precision symmetric pairs manufacturing process. The result is a cable that combines optimized transmission parameters for xDSL systems, characterized up to 100 MHz, with an unknown pair count/performance, up to 200 pairs. The optimum parameters needed in xDSL systems have been determined and, further to the values obtained, different designs of cable prototypes have been specified with pair count ranging from 12 up to 200 and with different core structures, fillings and materials. Representative prototypes of the cable have been manufactured and a complete characterization of every cable prototype, up to 100 MHz, has been done measuring all pairs of the final cable prototypes.

Electrical and transmission parameters have been processed and compared with standard conventional copper pair cables and with the specified values in the cable design. In all cases the results obtained have been optimum levels of Attenuation, Return Losses, Impedance Stability, NEXT and FEXT, compared to conventional copper pair cables. All the measurements of these parameters have been used to make a complete simulation of the cable over an A/VDSL system in order to determine the performance of this cable in terms of maximum transmission speed and distance over DSL systems.

Transmission characteristics and loop reach over A/VDSL systems have been compared to international standards and conventional cables. The result is a high length and pair counts cable, capable of supporting current and future DSL technologies with the maximum performance in speed and distance and a superior performance compared to conventional copper pairs cables.

Table1. Non-POTS modem evolution

Year	DESCRIPTION	DISTANCE
1985	U-IC 160 Kbps Duplex	8 - 10 km
1990	HDSL 2 Mbps Duplex	2.4 – 4.9 km
1995	ADSL 1.5 - 6 Mbps downstream 16-640 Kbps upstream	1 – 5.4 km
1997	VDSL 55 Mbps downstream 1.6 – 2.3 Mbps upstream	200 - 500 m

2. xDSL Concept
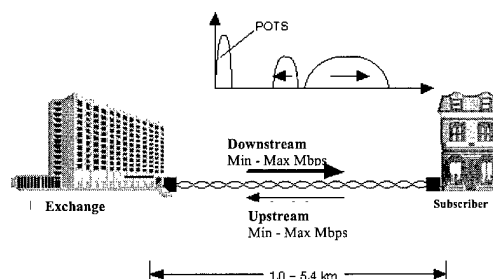
Figure 1-ADSL channels (Down and Upstream)

As it was mentioned before, the appearance of xDSL systems is based on the use of the existing spectrum of standard telephone subscriber lines, further from the telephone channel bandwidth.

The philosophy of these systems is to offer, through the standard telephone twisted pair, an additional bandwidth to transmit the everyday much more requested services (High Speed Internet, Interactive TV …).

To the traditional telephone channel a new possibility is added, as we can see in Figure 1.

Nowadays, downstream channels and upstream channels are in the range of 1 MHz or 30 MHz of bandwidth, for ADSL and VDSL respectively.

With the systems development higher bandwidths will be needed. The problem is with the standard copper cables, because their transmission parameters degrade directly with the increase in frequency and distance.

The cable developed has been fully tested up to 100 MHz, so it not only supports the present systems up to 30 MHz, but also, its design foresees future developments.

At present, two methods of managing upstream and downstream channels are used, FDM (Frequency Division Multiplexing) and EC (Echo Cancellation).

Each one of these two methods present different undesired crosstalk effects over the signal (Self-NEXT, Self_FEXT, etc). The cable can guarantee that with both systems, because of its excellent FEXT and NEXT levels, together with a suitable attenuation and interference protection, the future xDSL will be possible.

2.1 Real Time Speeds

One of the main features of this type of codification is the possibility to continually adapt to the conditions of the line.

Initially, xDSL protocol information frames are exchanged between the Local Exchange transmitter and the Subscriber receiver to test the Signal to Noise levels in the line to the different frequencies. Once these values are known, the maximum number of Bits/Tone that can be sent in every carrier inside the bandwidth of the signal is determined.

The previous process is continually repeated and that is why it can be considered that this type of system is constantly adapting to the conditions of the line. The following illustration (figure 2) shows this process.
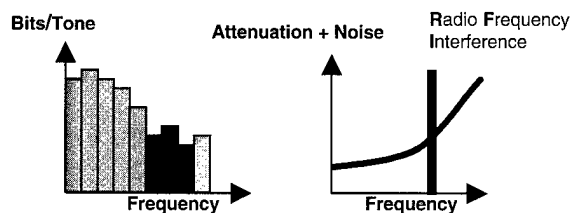
Figure 2.- Effect of attenuation and interference over transmission in xDSL systems

To the frequency where the interference is significant (Crosstalk, White Noise, Gaussian Noise, etc) xDSL system considerably reduces the Bits/Tone rate. It can also be noticed that attenuation significantly contributes to the degrading effects over the system bit rate.

So far, standard copper cables have been used just for low frequencies (Telephone channel), and only ISDN services have needed a little more bandwidth, therefore, requirements of these cables have been little restrictive and even non-existents to higher frequencies.

In the cable, parameters obtained have been optimized to achieve the maximum performance in a band even higher than the actual xDSL requirements. The effect over a xDSL system is shown in the picture below (figure 3).
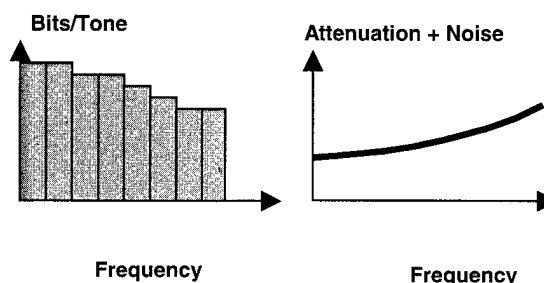
Figure 3.- Effect of attenuation and interference over transmission in xDSL systems with the new cable

The parameters present a very steady behavior all through the band, and that allows a bigger S/N level and consequently higher bit rates and distances, allowing xDSL systems to achieve the maximum of their possibilities in every carrier.

To provide suitable protection for outdoor applications and in order to avoid interferences and accomplish EMC requirements, the cable core is sheathed with a laminated aluminum tape and an outer PE jacket.

2.2 Structure

Table 2.- Components description

COMPONENT	NATURE
Conductors	0.51 mm annealed copper (24 AWG) IEC Publication 28
Insulation	Polythene (ASTM D-1248 type 3, cat. 4)
Watertightness	Option 1.- Fully Filled (BT M 142) Option 2.- Dry Core Cable
Tape & Binder	Non-hygroscope & dielectric material
Screen	Corrugated Laminated Aluminium Tape both side PE longitudinally applied and thermobonded
Outer Sheath	Black PE (ASTM D-1248 type 3), and optionally HFFR or PVC compound

Copperplus family construction is based on 12 and 13 pairs sub-units or in 25 pairs units (figures 4 & 5).
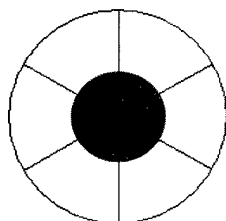
Fig.4 –100 pairs core structure (central 25 pairs unit + 12/13 subunits)
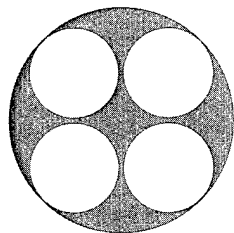
Fig.5– 50 pairs core structure (12/13 subunits)

3. Cable Performance

3.1 Electrical Characteristics

Main electrical parameters obtained in **ALCATEL** cables are shown in table 3.

Table 3.- Main electrical parameter values

PARAMETER	VALUE
Conductor resistance max	93 ç/Km
Resistance unbalance max	2 %
Dielectric strength min (3 s)	5 KV d.c. or 3.5 KV a.c.
Insulation resistance, min.	5,000 Mç· Km
Capacitance unbalance: pair-screen, max.	1,000 pF/Km
Propagation delay: max, at 10 MHz	5.7 ns/m

3.2 Transmission Parameters

3.2.1 Impedance

Cables have been specified to achieve the maximum stability in impedance for the entire design band. A typical curve is shown in figure 6.

Cables with 100 ç and 120 ç have been designed.
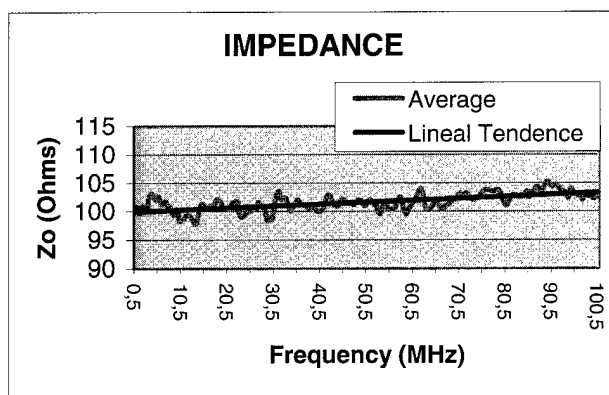
Figure 6.- Average Impedance of a 50 pairs cable

3.2.2 Attenuation

Attenuation results, shown in table 4 and in figures 7 and 8, comply with the expected design values. Attenuation was measured up to 100 MHz in a cable test length of 200 m.

Table 4.- Attenuation values

FREQUENCY (MHz)	Average Values (dB/100m)
0,5	1,3
2	2,7
10	6,1
20	8,5
25	10,5
40	12,2
60	15
80	17,4
100	18,9
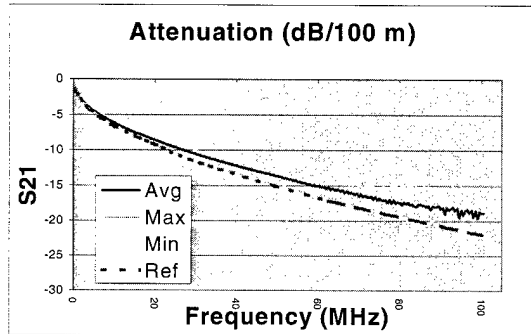
Figure 7.- Attenuation of a 50 pairs *CopperPlus*™ cable

To understand better the real deviation to high frequencies of the attenuation regarding the reference graph, the following statistical table of attenuation of 50 pairs to 100 MHz is presented.
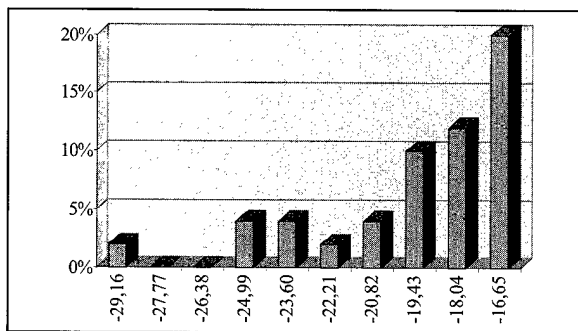
Figure 8.- Statistical graph of attenuation to 100 MHz of a 50 pairs cable

3.2.3 Crosstalk – NEXT and FEXT

In NEXT and FEXT results it can be noticed that the new cables widely satisfy the crosstalk levels necessary to achieve the maximum Bit Rate vs. Distance requirements in actual and future xDSL systems. (Figures 9 & 10)
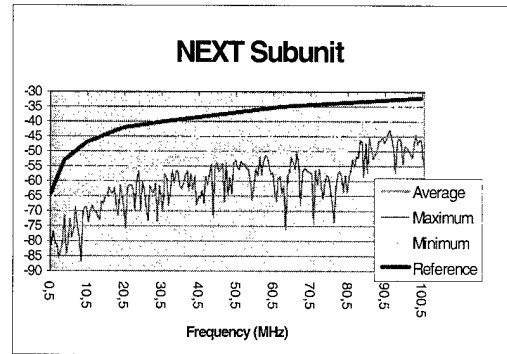
Figure 9.- NEXT of a 50 pairs cable
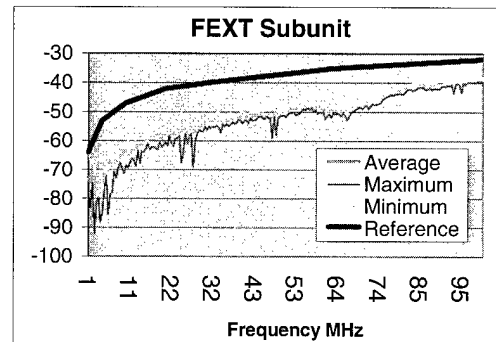
Figure 10.- FEXT of a 50 pairs cable

3.2.4 Return Loss

In table 5, typical average values of a cable at different frequencies are shown.

Table 5.- Return Loss values

Frequency (MHz)	SRL (dB)
15	25,7
30	28,2
50	30
70	24,5
80	24
100	23,1

4. Performance of xDSL Systems (Simulation Results)

The theoretical capacity of a transceiver can be computed based on the SNR measured at the input of the receiver and the bandwidth occupied by the systems. For transmission over the metallic access network, the SNR at the receiver is influenced by the insertion of the loop and the Xtalk environment in which the system operates.

ADSL (G.992.1) was designed against an objective of coverage over all copper loops without load coils conforming to Revised Resistance Design (RRD) rules. ADSL can transport rates between 1 and 8 Mbps downstream and 32 to 800 kbps upstream over loops of a few kilometers. Performance tests have been specified in G.996.1 based on a reference set of noise models and cable types (G.test).

For VDSL (G.VDSL), there currently exists no test specification. The system requirements documents developed in the different regional standardization bodies (ANSI-T1E1.4, ETSI-TM6) have projected loop reach performances based on noise models and cable models developed and agreed upon in these bodies. It should be recognized that these models are representative for the noise environment in the network of the operator and the cable types currently used in the access network.

In this document, the performance of xDSL services (A/VDSL) is assessed under the assumption that the "Copper plus" cable type is used instead of the cable types specified in the standard documents for ADSL and VDSL. Loop reaches for the different service types are simulated based on insertion loss measurements of the cable, FEXT and NEXT xtalk measurements in a binder filled with this enhanced copper cable.

Based on the results of measurements of the cable, the parameters equivalent to the ones specifying in the standard models were derived.

These parameters are compared to those described in the ETSI and ANSI standards.

The results show that the cable developed will have performances close to that ANSI Cat.5 cables, as far as Xtalk is concerned. The FEXT coupling is about 16 dB lower as compared to the standard models. The NEXT coupling is about 20 dB lower as compared to the standard models. As a consequence the spectral efficiency will be improved by over 3 bits/Hz (as long as NEXT and FEXT are the dominating noise at the receiver). In case of using this cable, the loop reach performances would be increased substantially as compared to the use of the standard cable types.

4.1 Insertion loss of the Copper plus cable

The insertion loss of a twisted pair cable can be modeled as

$$\text{Attn (in dB)} = 10.\log_{10}\left(|H(f)|^2\right) =$$
$$10.\log_{10}\left(\exp\left(-d/d_0.\left(k_1\sqrt{f/f_0} + k_2 f/f_0\right)\right)\right)$$

with d the distance in meter and $d_0 = 1\text{m}$; and f the frequency in MHz, $f_0 = 1\text{MHz}$. The value of the $k1$ and $k2$ parameters depends on the cable type. For the copper plus cable, the results for the mean of the cable and for the maximum and minimum cables are summarized in the following tables.

	Mean	Min	Max
K_1	2.22e-3	2.11e-3	2.29e-3
K_2	-1.56e-6	-3.36e-6	1.01e-5

Attenuation
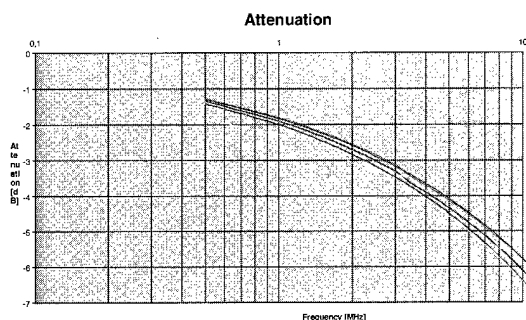
4.2 FEXT in a Copper plus binder

A typical FEXT model, computed as the power sum due to 20 twisted pairs in the binder, can be expressed as follows:

$$FEXT(f) = K_{FEXT,20}.(d/d_0).(f/f_0)^2.|H(f)|^2$$

where d is the distance in m, $d_0 = 1\text{m}$; f is the frequency in MHz, $f_0 = 1\text{MHz}$; and $H(f)$ is the channel transfer function. For the enhanced cable, FEXT (f) is the power sum on the 20 measured pairs and H (f) is the fitted mean transfer function. The results compared to the standard value are summarized in the table below.

	CABLE	ETSI	ANSI	ANSI Cat.5
K_{fext} (in dB)	-83.76	-67.00	-68.14	-93.30

FEXT
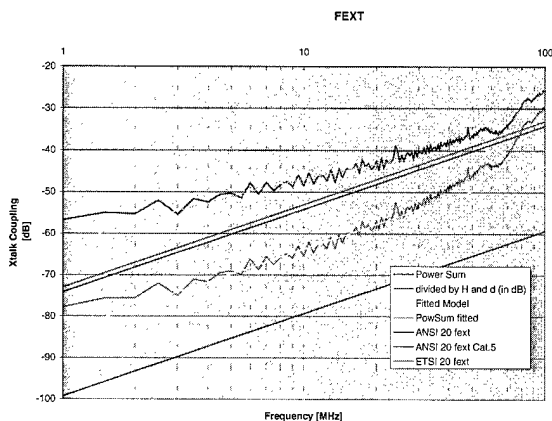
Frequency [MHz]

4.3 NEXT in a Copper plus Binder

A typical NEXT model, computed as the power sum due to 20 twisted pairs in the binder, can be expressed as follows:

$$NEXT(f) = K_{NEXT,20} \cdot (f / f_0)^{1.5}$$

where f is the frequency in MHz, f_0 =1MHz. For this cable, $NEXT(f)$ is the power sum on the 20 measured pairs. The results compared to the standard value are summarized in the table.

	CABLE	ETSI	ANSI	ANSI Cat.5
K_{next} (in dB)	-62.92	-42.00	-42.88	-67.15

NEXT Coupling

Coupling [dB]

Frequency [MHz]
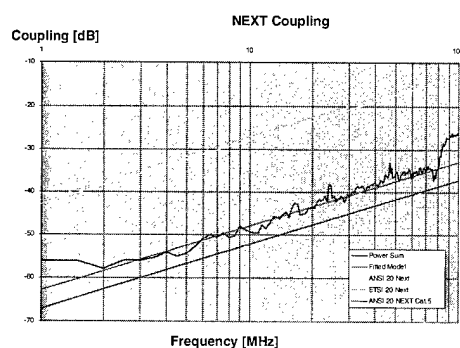
5. Conclusions

Due to the close connection between Transmission Bit Rates and Distances of this kind of systems, many limitations will exist concerning maximum speeds. Both systems being used nowadays, ADSL and VDSL, can reach up to 2,5 Km and 300 m respectively, over standard telephone lines.

The developed cable, due to its optimized parameters can increase distances to which these systems can work to the maximum bit rates.

It is very important to consider that all these systems are continually evolving. In fact, a new term has come out to solve the existing confusion, xDSL. Under this term we can group all the DSL technologies, which can include all these variants (asymmetric and symmetric): ADSL, HDSL, iDSL, RADSL, SDSL, BDSL, VADSL and VDSL.

In this environment it is very easy to come to the conclusion that copper lines must also evolve as the demand for new broadband services increases. **ALCATEL** has anticipated the future by developing a new cable, manufactured with high precision symmetric pairs, that provide optimized parameters to face the requirements for the current and future technologies.

6. Acknowledgement

We would like to thank our colleagues Thierry Pollet and Jacques van Remortel from Alcatel Telecom in Belgium for their support in the analysis of the performance of xDSL systems (ADSL and VDSL) in binders filled with Copper plus cables.

7. References

[1] ETSI-TM6, Transmission multiplexing TM; Access transmission systems on metallic access cables; Very high speed digital subscriber line (VDSL); Part 1: functional requirements, TS 101 270-1 (1999-08).

[2] ANSI-T1E1.4, Very-high-speed Digital Subscriber Lines – System Requirements, T1E1.4/98-043R8.

Authors

Susana Cámara
Alcatel Cable Ibérica
39600 Maliaño – Cantabria
Spain
e-mail: susana.camara@aci.alcatel.es

She reached her degree in Chemical Engineering in 1983 from Oviedo University, in Spain. She joined Alcatel Cable Ibérica (Maliaño - Spain) as Material Development Chief in 1987. Since 1993 up to now, she is responsible of Product Marketing dealing with new developments in optical and copper telecom cables.

C.G.Cortines
Alcatel Cable Ibérica
39600 Maliaño - Cantabria
Spain
e-mail: c.cortines@aci.alcatel.es

He is a Physical Engineer. All his professional life has gone by cable industry, formerly in ITT group, nowadays Alcatel.

Currently, he is the Technical Manager of Alcatel Cable Iberica, the Alcatel telecom cable factory located in Spain.
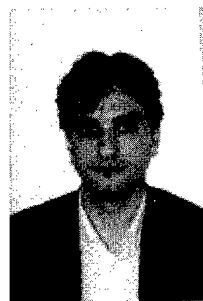
Julio Robredo
Alcatel Cable Ibérica
39600 Maliaño – Cantabria
Spain
e-mail: j.robredo@aci.alcatel.es

Born in Caracas, Venezuela, in 1971. He reached his degree in Telecommunications Engineering in 1996 at Cantabria University, in Spain. He was enrolled in an Alcatel Cable Facility (Maliaño - Spain) as a Quality Assistant by the end of 1996. Since 1997 up to now, he is responsible of Quality Engineering Area dealing activities of final testing automation, instrumentation advisory and prototype follow up.

Orlando Vaquero
Alcatel Cable Ibérica
39600 Maliaño – Cantabria
Spain
e-mail: orlando.vaquero@aci.alcatel.es

Born in September 1972 in Santander (SPAIN). He obtained his Telecommunication Technical Engineering degree in the University of Cantabria in 1.995 (Project: Comparison Study of Different Attenuation Models for Indoor Mobile Applications) and his Telecommunication Engineering Degree in 1997 (Project: Coverage Prediction Method for Broadcasting Services in Radio and TV in VHF and UHF Bands).

Melt Filament Reinforcement "MFR" for Shrink Free Fiber Optic Cable

Reiner Schneider and Helmut Nowsch

Corning Cable Systems, Corning Inc.
96465 Neustadt, Germany
+49-9568-93-2686, reiner.schneider@corning.com
+49-9568-93-2543, helmut.nowsch@corning.com

Abstract

Longitudinal stability is one of the most important properties of buffer tubes as well as cables. Polyolefins, frequently used materials for jackets and buffer tubes, have high shrinkage rates and high coefficients of elongation. Therefore, fiber optic cables have to be reinforced by anti buckling elements. This paper describes a method to produce anti buckling elements by co-extrusion of thermoplastic filaments with buffering and jacketing (Melt Filament Reinforcement: MFR). A number of material combinations were tested. An excellent anti buckling behavior was achieved with co-extruded filaments made of LCP (Liquid Crystal Polymer), closely packed in Polyethylene based LSZH compound. MFR elements show no length change even after several temperature cycles. There is no length limitation for those online extruded reinforcement filaments and they can be produced in any size and any number, tailor made for the product.

Keywords

Reinforcement; LCP; Co-extrusion; Buffertube; Jacket;

1. Introduction

A cable should be designed to prevent all stresses from the optical fiber. Longitudinal stability is one of the most prominent requirements. Both, contraction, e.g. caused by shrinkage of the materials, as well as elongation may lead to macro or micro bending of the optical fibers and thus to an increase of the attenuation. Another problem is pistoning. Let's assume the cable is fixed in a closure and/or the buffer tubes are terminated by connectors. When the cable tube shrinks then the fibers or the ribbons move out of the shrinking cable/tube, and most likely get bent which may lead to increased bend stress and in extreme cases to fiber breaks.

Polyethylene is the mostly used material for cable jackets.

Polypropylene and Polyester are common materials for buffer tubes. All semi crystalline resins have high shrinkage rates, therefore the optical cables have to be reinforced by rigid elements. GRP rods or steel wires are the mostly used anti buckling elements for fiber optic cables. Particularly in

small cables and in buffer tubes it is not easy to place GRP rods or steel wires in the optimum position. We developed a technology to produce thermoplastic reinforcement filaments in co-extrusion with the buffer tube or the cable jacket. Extrusion cross head and tools were designed by our company. By combination of different materials for filaments and the matrix, it is possible to generate special product properties. The 1st part of this paper discusses MFR buffer tubes, the 2nd part shrink free cable jacket for ribbon cable. Of course, this technology may also be used for different other products like tubes for fluids and other extruded profiles.

2. MFR Buffer Tube Design

The following objectives should be fulfilled by the buffer tubes:

- low shrinkage
- low temperature coefficient
- high crush resistance
- good chemical resistance
- easy to manufacture
- reasonable costs
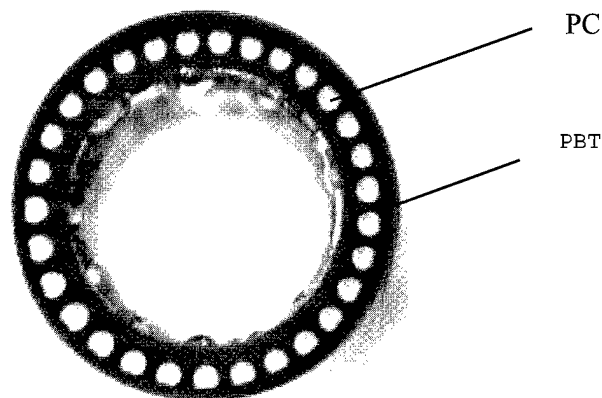
Photo 1: Cross section of an MFR Buffer Tube

Tube-diameter (ID/OD) 1,7 / 2,5 mm

MFR buffer tubes were produced with different materials and in different dimensions:

Table 1.Tested MFR Buffer Tubes

No	Dimensions (nominal)		Material	
	Inner diameter	Outer diameter	Matrix	Filament
1	1.75	2.50	PBT Typ 1	PC
2	1.75	2.80	PBT Typ 1	PC
3	1.75	2.80	PP X301	PC
4	1.45	2.40	PBT Typ 2	PC
5	1.90	3.00	PBT Typ 2	PC
6	1.75	2.80	PBT Typ 1	LCP Vectra

3. Results for MFR Buffer Tubes

Test results are not completed for all MFR tubes

We had to consider different shrinking effects: One is the material contraction as a result of temperature reduction in the cooling trough.The second part is the post shrinkage due to relaxation and post crystallization which depends not only on material characteristics but also on processing.

3.1. Shrinkage During Processing

To draw conclusions from material contraction during processing, as a result of temperature reduction in the cooling trough, we measured fiber excess length (EFL) in the buffer tubes, immediately after buffer tube manufacturing. Although this EFL measurement provides no absolute contraction figures, it is very helpful for comparison.

Table 2. Excess Fiber Length " EFL" immediately after extrusion

Tube Type	Material	Matrix / Filaments in %	EFL in mm
homogen	PP	100	0.154
MFR	PP / PC	90 / 10	0.036
homogen	PBT	100	0.111
MFR	PBT / PC	80 / 20	0.026
MFR	PBT / PC	95 / 05	- 0.002

3.2 Post Shrinkage

Post shrinkage was defined by length change of the buffer tube, stored without any stress at room temperature (see Figure 1).Test samples where taken as soon as possible after manufacturing. Measurement started 5 to 10 minutes after extrusion.
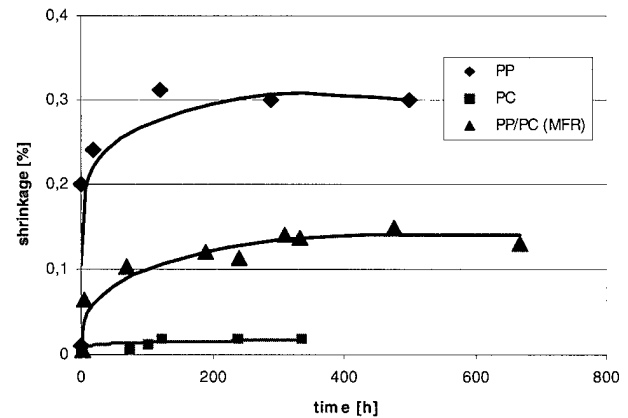
Figure 1. Comparison of post shrinkage with different buffer tube materials

3.3 Shrinkage by Aging

PBT shrinks spontaneously at temperatures around 70 °C, therefore aging test was done at 50 °C for 30 days.

Table 3. Shrinking by Aging
Comparison between homogeneous PBT- and MFR tubes

Buffer tube	Material	EFL(mean value) Production day	EFL(mean value) 30 d / 50°C
1-Layer homogeneous	PBT	0,111 %	0,213 %
MFR 80% / 20 %	PBT / PC	0,026 %	0,046 %
MFR 95% / 5%	PBT / LCP	- 0.002%	- 0.003 %

3.4 Length Change in Temperature Cycling
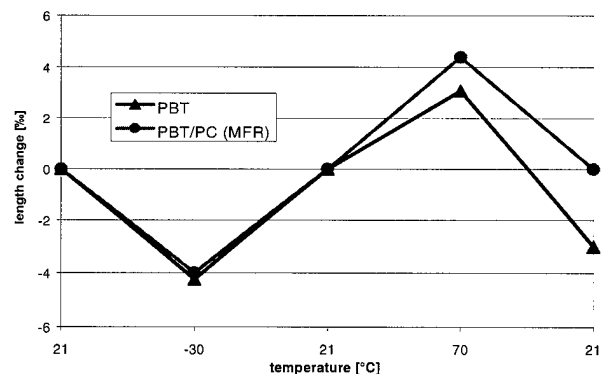
Figure 2. Temperature cycling

This test indicates the temperature coefficient and also the shrinkage of PBT, when the temperature comes to the range of 70°C. After passing only one temperature cycle +21 –30 +70 +21 °C

the homogeneous PBT tube was 0.3 % shorter. The MFR tubes had no length change after this test.

3.5 Discussion

In all shrinkage tests, MFR tubes behaved as good or better than homogeneous tubes. If buffer tubes were reinforced by with at least 5% LCP, there were no shrinkage in any test.

MFR reduces the shrinkage

- during processing

- during storage at room temperature,

- during aging

- and after temperature cycling

Crush resistance:

There is no mentionable difference between MFR and homogeneous buffer tube with identical dimensions.

Chemical performance:

More freedom in choosing buffer tube material, for the postulated chemical resistance, because the length stabilization is warranted by the filaments of the MFR tubes.

Manufacturing

The extrusion crosshead is more difficult than a standard one layer head. But the buffer tube production process is in some case more stable. Polycarbonate filaments, which have a high melt strength, stabilizes the draw down cone.

Cost factor

If PC is used for the filaments with a 20% rate, there is no significant cost difference to homogeneous PBT buffer tubes. If LCP is used for the filaments, with a rate of 5%, the material cost for the buffer tube increases more than 50 % Because of this cost increase, we did not continue buffer tube reinforcement trials with LCP.

4. Design for a Shrink free Cable Jacket
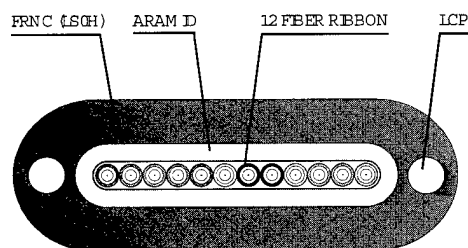
Figure 3 cross section (drawing) of a12 fiber ribbon cable with LCP reinforced LSZH jacket

Flame retardance, zero halogen (LSZH) and very low shrinkage were the main objectives for the cable jacket.

A similar cable design with a PVC jacket without any anti buckling elements operates well. When we changed from PVC to LSZH jacket material, what is usually requested in Europe, we got problems with pistoning. We solved this problem by melt filament reinforcement. Two filaments of liquid crystal polymere (LCP) with a total volume share of 6% (to 94 % LSZH material) are enough to make a LSZH cable jacket practically shrink free.

For co-extrusion of LCP together with LSZH compound, we selected material types which are producible with not to much difference in extrusion temperature.
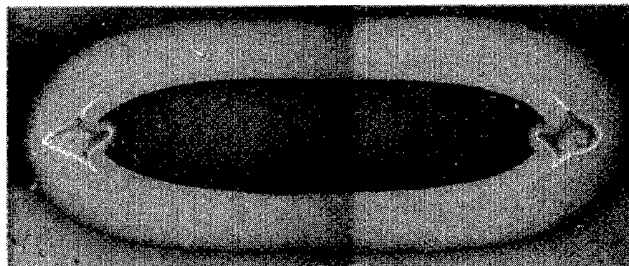
Photo 2 Cross section of a MFR jacket with 2 filaments in opposite position (a)
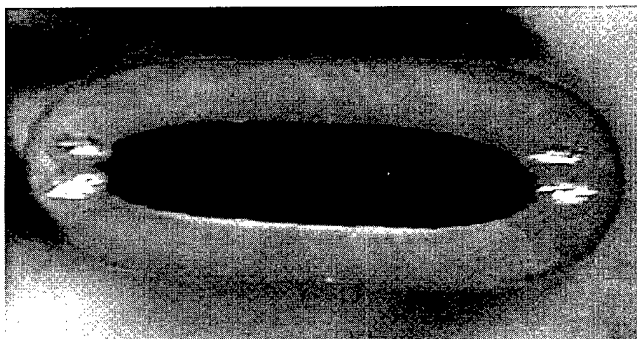
Photo 3 Cross section of a MFR jacket with 2 x 2 filaments in opposite position (b)
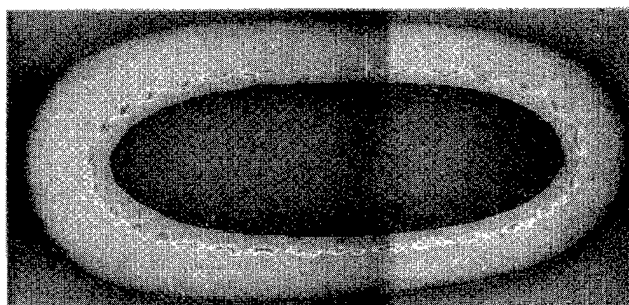
Photo 4 Cross section of a MFR jacket with 30 filaments distributed along the circumference (c)
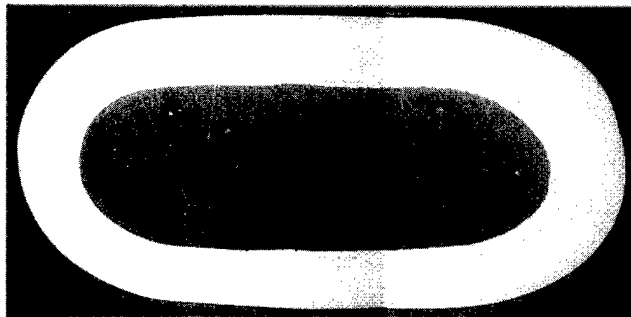
Photo 5 Cross section of a LSZH jacket without filaments

(d)

5. Results for MFR LSZH Cable Jacket

5.1 Shrinkage Measurement in Temperature Tube

Test according to:	Internal test procedure
Equipment:	Vertical temperature tube;
Uncertainty (2s)	2°C (temperature); dΔL ≤ 2 mm
Procedure:	Test temperature (time)
	23 °C (> 6h); +60C (24h) +70°C(24h);
	23°C (>12h);
	Active sample length (L) of about 5 m
Requirement:	Length change of the cable jacket due to temp. change

Table 4. Linear thermal expansion

Temperature °C	LSZH /LCP (a) mm	LSZH /LCP (b) mm	LSZH /LCP (c) mm	LSZH (d) mm
23	initial	initial	initial	initial
+ 60	0	0	0	0
+ 70	0	0	0	-6
23	0	0	0	-21

5.2 Elongation of the Cable due to Temperature Changes

Test according to:	Internal test procedure
Equipment:	Horizontal temperature chamber;
Uncertainty (2s)	2°C (temperature);
	Active sample length (L) between clamps:
	1,27 ... 1,35 m
	dL = 6 cm (due to clamps and coupling);
	ε(T) = ΔL\L;
Procedure:	Test temperature (time)
	a. 23 °C (6h); -30C (10h); -40°C (6h);
	23°C (6h); 60°C (8h); 23°C (6h); 70°C
	(8h); 23°C (12h);
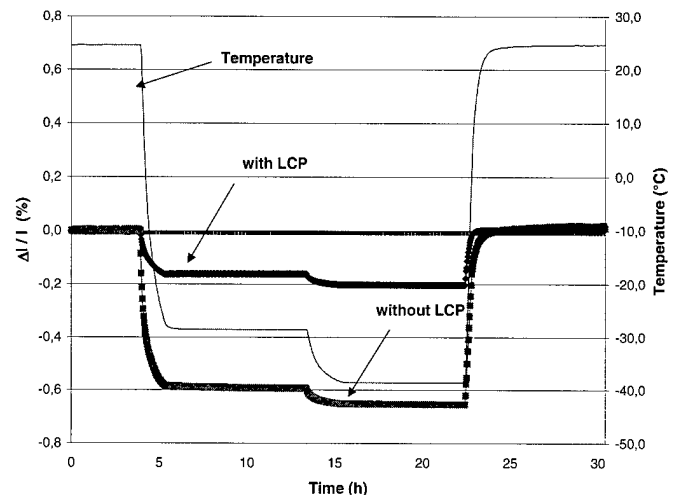
Figure 3. Thermal expansion at low temperature

5.3 Shrinkage Measurement in Horizontal Temperature Tube

Test according to:	Internal test procedure
Equipment:	Temperature horizontal tube;
Uncertainty (2s)	2°C (temperature); dΔL ≤ 2 mm
Procedure:	Test temperature (time)
	23 °C (12h); -30C (24h); 23°C (12h);
	Active sample length (L) of about 23m
Requirement:	Length change of the cable jacket due to temperature change

Table 5. Linear thermal expansion in horizontal tube

Temperature °C	LSZH/LCP (a) mm	LSZH/LCP (b) mm	LSZH/LCP (c) mm	LSZH (d) mm
23	initial	Initial	initial	initial
-30	-3	-2	-13	-118
23	-2	-1	-10	-76

5.4 Force Strain at Different Temperatures

Table 6. Force at 1 % strain

Temperature °C	LSZH/LCP (a) N	LSZH/LCP (b) N	LSZH/LCP (c) N	LSZH without LCP N
23	122	105	96	13
-30		216		125
60	38	50	38	3
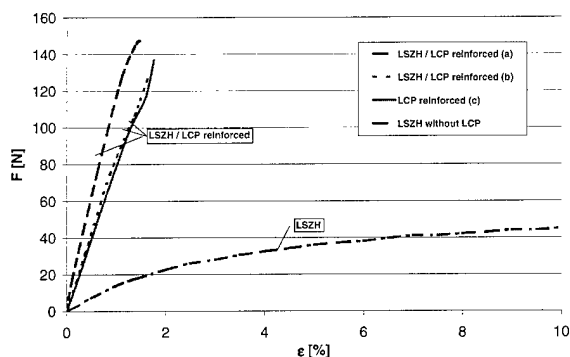
Figure 4. Force strain curves at 23 °C
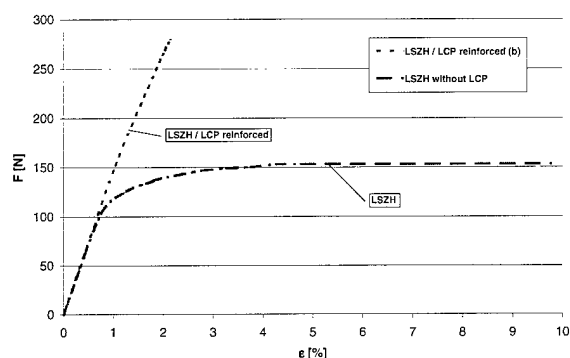
Figure 5. Force strain curves at - 30 °C
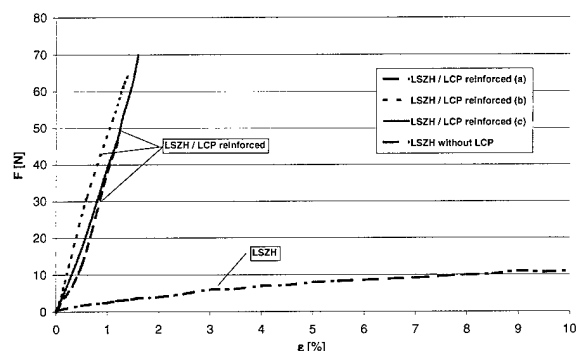
Figure 6. Force strain curves at 60 °C

Every LSZH-jacketed sample had a cross-sectional area of about 6 mm² and a LCP cross-sectional area of about 0,30 to 0,35 mm² From the strain curves we can calculate tensile strength and tensile modulus for the LCP filaments.

All LCP reinforced samples show almost linear curves up to break.

Table 7. Tensile Strength and Tensile Modulus for Sample (b)

Tempera-ture °C	Tensile strength MPa	Tensile modulus MPa	Elongation at Break %
23	310	18.230	1,7
-30	430	20.000	2,15
60	190	14.156	1,3

5.5 Flame Retardance

Cables with LCP MFR (see photo 2) and without LCP (see photo 5) were tested according to the specification IEC 60332

The test results of this two cables where completely congruent. Both cables fulfill the requirements of the specification IEC 60332.

6. Conclusions

Melt filament reinforcement can protect buffer tubes and cable jackets against shrinkage. MFR with about 5% of LCP makes a buffer tube or a cable jacket shrink free over a wide temperature range. MFR buffer tubes with 20 % PC filaments have also a better longitudinal stability than not reinforced tubes of PBT or PP. All other properties are similar. Regarding longitudinal stability LCP was the best choice for MFR tubes. The high tensile strength and the high tensile modulus of the co-extruded LCP indicate, that the LCP-filaments have a very high ratio of anisotropy. Because of the high tensile modulus, LCP MFR technology can replace traditional reinforcement elements like GRP rods for some special applications. The MFR filaments can be co-extruded in any size, in different shapes and in unlimited length. The filaments can be put in the optimal position of an extrusion profile.

7. Acknowledgments

The authors would like to thank the people who contributed to this development program. Special thanks to Oliver Buechner, and Frank Koschwitz.

7.1 Pictures of Authors
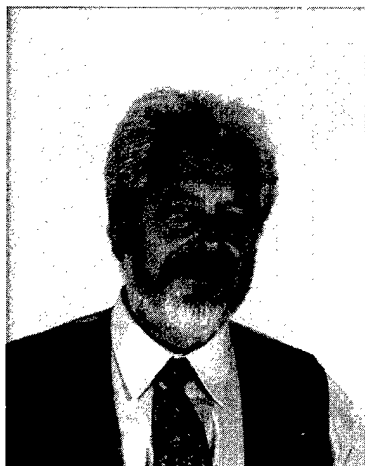
Reiner Schneider

Corning Cable Systems
SCC Special Communication Cables GmbH & Co. KG
Austrasse 101
D-96465 Neustadt bei Coburg
Germany

Reiner Schneider was born in 1942. He studied mechanical engineering. In 1967 he joined Siemens for telephone cable development. Since 1989 he has been involved in fiber optic cable development. He is responsible for development of cable design and production technology for fiber optic cable.

Helmut Nowsch

Corning Cable Systems
Special Communication Cables GmbH & Co. KG
Austrasse 101
D-96465 Neustadt bei Coburg
Germany

Helmut Nowsch was born in 1956. In 1988 he completed his studies in electrical engineering and information science at the Technical University of Dresden. Afterwards he got the responsibility for a development group for computer calculation projects of an energy industry company in Berlin. He joined Siemens in 1990 for fiber optic cable development. Since 1997 he has been responsible for development of indoor cable design for optical fiber network solutions.

Novel Optical Fiber Cable for Feeder and Distribution Use in Access Networks

Junichi Kawataka, Hideyuki Iwata, Kazuo Hogari and Kiminori Sato

NTT Access Network Service Systems Laboratories
Hanabatake, Tsukuba, Ibaraki , 305-0805 JAPAN
Phone +81(298)52-2522
Fax   +81(298)60-6130
E-mail address kawataka@ansl.ntt.co.jp

Abstract

We have successfully developed new optical fiber cables for feeder and distribution use in access networks. These cables have great advantages in terms of cost and installation workability that will enable us to realize fiber to the home (FTTH). In this paper, we describe the requirements for termination, feeder and distribution cables. We designed and fabricated the cables based on these requirements and confirmed the stability of their mechanical and thermal characteristics for practical use.

Keywords

Access network; optical fiber cable; feeder cable; termination cable; distribution cable;

1. Introduction

Progress on multimedia technology has led to the active development of many kinds of services using the telecommunication network. It is important for us to realize high speed and broad-band networks to provide such services economically. In order to provide these services in a timely way, it is important to construct optical access networks, economically, immediately and efficiently. Therefore, to make optical access networks more economical, we must reduce the cost, not only of the cable itself, but also of installation, maintenance and operation. However, conventional cables are too expensive for FTTH and several of their features need to be redesigned. To achieve this, we have developed new cables based on our requirements and here we describe their design and performance. Our developments as regards feeder and distribution cable considered mainly of reducing their diameter and weight. For the termination cable, we added a new function to the termination end. We fabricated these cables and measured their characteristics to confirm their performance levels.

2. Access network configuration

Figure 1 shows the optical access network configuration. An optical access network consists of 4 areas; the central office, feeder system, distribution system and user system areas. The feeder system extends from a fiber termination module (FTM) in central office to a distribution point. The termination cable is used to terminate fibers at an FTM situated in a central office and the feeder cable is
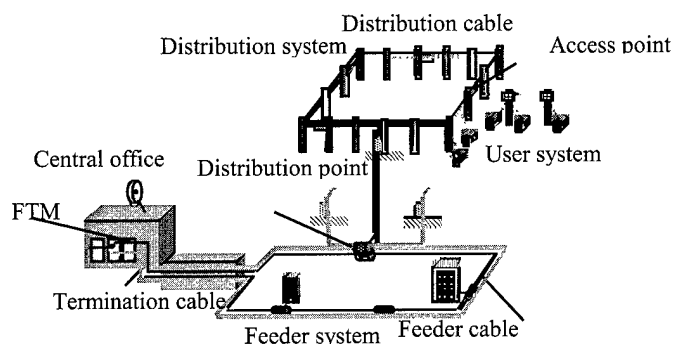
Figure 1. Optical access network Configuration

installed in cable tunnels and /or ducts. In the distribution system, aerial cable is connected with feeder cable at a distribution point, and led to an access point via telecommunication poles. In this paper, we describe an overall cost reduction, including reductions in installation and operation costs, in feeder and distribution system areas.

3. Requirement for feeder, termination and aerial cable

Some of the main requirements for feeder, termination and aerial cable are shown in Table 1. The loss change in cables must be as small as possible under harsh environmental and mechanical conditions including temperature change, and the bending and squeezing of the cable. Moreover, all types of cable require good workability and high reliability.

3.1 Feeder cable

400- and 1000-fiber cables are shown in Fig.2 as the examples of feeder cable. The cables consist of ten 8-fiber ribbons stacked in the slots of a slotted rod covered with a PE sheath. With feeder cable, it is important that the cable diameter be reduced to allow ducts to be used more effectively. In addition, a reduction in cable weight would improve workability.

Table 1. Requirements for termination, feeder and distribution cable

		Item	Requirement
Feeder	Feeder cable	Diameter, weight	Smaller and lighter
		Thermal stabilization	No loss increment
		Mechanical strength	No loss increment and no damage
		Workability	Easy installation and handling
		Reliability	Long term stability of transmission loss
		Cost	Reduction in cable and installation cost
	Termination cable	Diameter	Possible to install through ducts and pipes
		Length of the end	Shorter
		Mechanical strength	No loss increment and no damage
		Maximum allowed tension	1470 N
		Water blocking characteristics	No water penetration into the termination end
		Cost	Reduction of cable and installation cost
Distribution	Distribution cable	Fiber ribbon	Separable 4 fiber ribbons
		Diameter, weight	Smaller and lighter
		Thermal stabilization	No loss increment and no damage (Temperature -30 ℃　70 ℃)
		Mechanical strength	No loss increment and no damage
		Workability	Easy branching Installation without machine (For small count fiber cable)
		Reliability	Long term stability of transmission loss
		Cost	Reduction in cable and installation cost

8 fiber ribbons
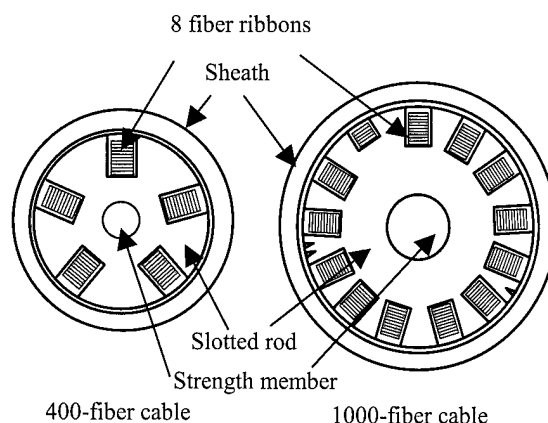
Figure 2. Optical fiber feeder cable

400-fiber cable　　　　1000-fiber cable
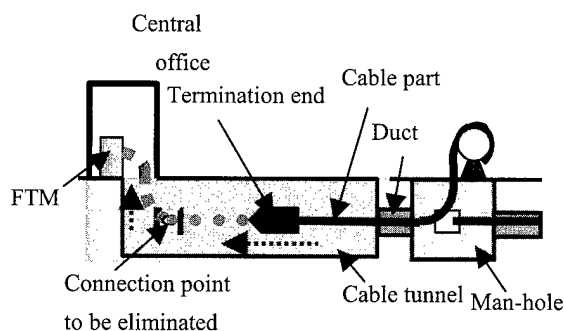
Figure 3. Installation of termination optical fiber cable

Therefore, we focused mainly on reducing of the cable weight and diameter in order to reduce the cable and installation costs.

3.2 Termination cable

When conventional termination cable is installed, the cable drum is placed near an FTM in a central office and the cable is pulled from the central office to the cable tunnel and /or duct, because the termination end is not protected from the various forces that occur during installation. Therefore, the installation cable is about 100m shorter than it could be because of the restriction imposed on the drum size as regards bringing it into a central office and the construction cost increases due to increase in the number of fiber connection point. To overcome these inefficient installations condition, we added a pulling function to the termination end. This function enables us to install a termination cable from a cable tunnel or a man-hole outside of the central office and connect it to the FTM as shown Fig.3. The design problems that we had to solve with this cable were the resistance for pulling force and the size reduction

Table 2. Diameter and weight of feeder cable

		New	Conventional
400-fiber cable	Diameter	19 m	24 mm
	Weight	0.27 kg/m	0.57 kg/m
1000-fiber cable	Diameter	29 mm	30 mm
	Weight	0.61 kg/m	0.85 kg/m

needed to enable us to apply the installation method between a cable tunnel or duct, and a central office.

3.3 Distribution cable

In a distribution system which extends from a distribution point to an access point, it is hard to share the facilities because of its widespread needs. To provide services flexibly, we need an aerial cable with a structure that allows mid-span access. Therefore, SZ slotted rod cable has been used in distribution systems [1]. In addition to mid-span access, SZ slotted rod cable has advantages as regards weight and diameter for cable of more than 100 fibers. By contract, we need to improve the installation workability for cable with a small fiber count of 40 fibers or less by achieving further size and weight reduction. Moreover, relatively low fiber count cables are also expected to be used frequently. Therefore, we concentrated mainly on reducing the cable weight and diameter to reduce the cable and installation costs.

4. Optical fiber cable technologies

4.1 Feeder cable

We changed the cable design so that we could develop a structure that satisfied our two main requirement; reduction of cable weight and diameter. To reduce the cable weight, we tried to reduce the diameter of the strength member by changing two items in the cable design. The first involved redesigning the maximum elongation strain of the cable by increasing fiber proof level. The second involved decreasing the maximum applied tensile strain. We investigated the cable installation method and this revealed that the maximum tensile strength was less than 1960N for 400-fiber cable. This enabled us to decrease the tensile strength to a quarter of its conventional value (7840N). For 1000-fiber cable the strength was reduced to almost a half. These changes in cable design made it possible to reduce the diameter of the tensile strength member, which directly contributed to a reduction in the cable weight.

Table 3. Performance of feeder cable (400-fiber cable)

Item	Performance
Attenuation Wavelength : 1550 nm	Less than 0.25 dB / km
Heat cycling Wavelength : 1550 nm, Temperature : -30 ℃～70 ℃	Less than 0.05 dB/km
Bending : radius 240 mm	No loss increase
Lateral pressure : 1960N/10 mm	No loss increase
Squeeze : radius 600 mm	No loss increase
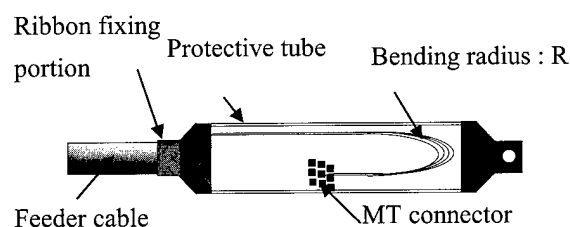
Figure 4. Termination end structure

Table 4. Performance of termination end

Item	Performance
Outer diameter	73 mm
Length	2450 mm
Squeezing	Less than 0.01dB/fiber, No damages
Bending	Less than 0.02 dB/fiber, No damages
Termination end decomposition time	About 20 minutes (MT connector cover removal time included)

To reduce the cable diameter, we changed the structure of slotted rod because some of slotted rod cable includes an empty slot.

Table 2 shows the diameter and weight of our newly developed cables compared with 400- and 1000-fiber cables. Specifically, we reduced the weight of the 400-fiber cable, to about a half and its diameter to about 80% of the conventional cable, thus achieving our goal of developing lighter and smaller cable. Moreover, we from confirmed that mechanical performance and thermal stability were sufficient for practical use, as shown in Table 3.

This lightweight cable means we can reduce the number of the cable-pulling machine used for installing cable in ducts, and decrease the installation cost.

4.2 Termination cable

We focused on tree main items when developing the termination cable. The first involved designing a structure to resist the maximum allowable pulling force. The second was the diameter of the cable passing through the duct. The third was the length of the termination end. For the first and second items, we adopted a protective tube to resist the pulling force, in order to secure enough space to accommodate many fiber ribbons with an MT connector. In terms of the third item, the fiber ribbons were turned back on themselves in the protective tube. Therefore, we had to determine the allowable bending radius in the protective tube to maintain long-term ribbon reliability. Therefore, we estimated the minimum allowable bending radius by taking the fiber failure rate into account, and found it to be 20 mm.

The structure of the termination end is shown in Fig. 4. This end is composed of fiber ribbons with an MT connector, a ribbon-fixing portion that prevents fiber ribbons in the tube from being pulled into the cable during installation, a protective tube, and a pulling portion. The termination end has an outer diameter of less than 73 mm to allow it to pass through the duct, and an allowable pulling tension of 1470 N. The performance of our prototype termination end is shown in Table 4. From this result, we can confirm that the performance is sufficient for practical use.

4.3 Aerial cable

As mentioned in 3.3, we need small lightweight distribution cable with good handling characteristics. We, therefore, developed a new cable without a slotted rod as shown in Fig. 5. In terms of reducing the cable size, the diameter of the cable part must be reduced. This is because the cable part occupied about 60% of the total cable height, as shown in Fig. 6. Therefore, we use a simple structure without a slotted rod.

By contract, as regard reducing the cable weight, we considered the adoption of a structure with no slotted rod and a smaller messenger wire. The rod free structure enables us to eliminate the not inconsiderable weight of the slotted rod. Moreover, in order to achieve further weight reduction, we designed a smaller messenger wire, because it accounted for about 50% of the total cable weight,
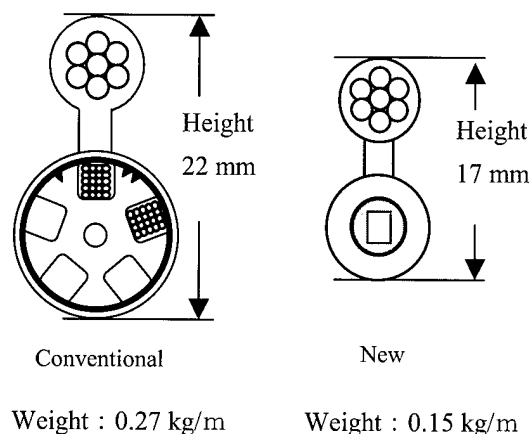
Figure 5. Distribution cable structure
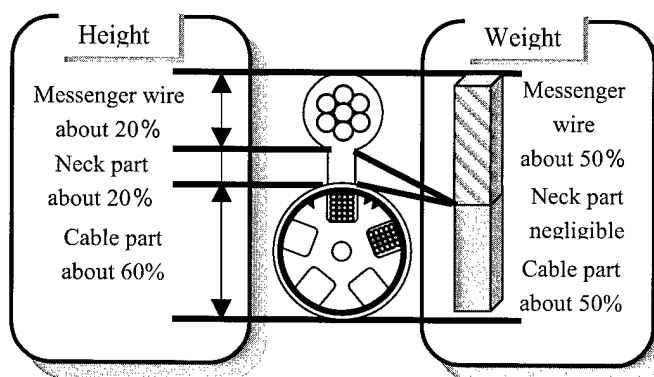
Figure 6. Size and weight of 40-fiber cable

Table 5. Performance of distribution cable

Item	Performance
Attenuation Wavelength : 1550 nm	Less than 0.25 dB / km
Heat cycling Wavelength : 1550 nm, Temperature : -30 ℃～70 ℃	Less than 0.06 dB / km
Lateral pressure : 1960N/10 mm	No loss Increase
Bending : radius 160 mm	No loss Increase

a : Cutting combined part
b : Extracting rip cord from sheath
c : Cutting and removing sheath
d : Extracting fiber ribbons out
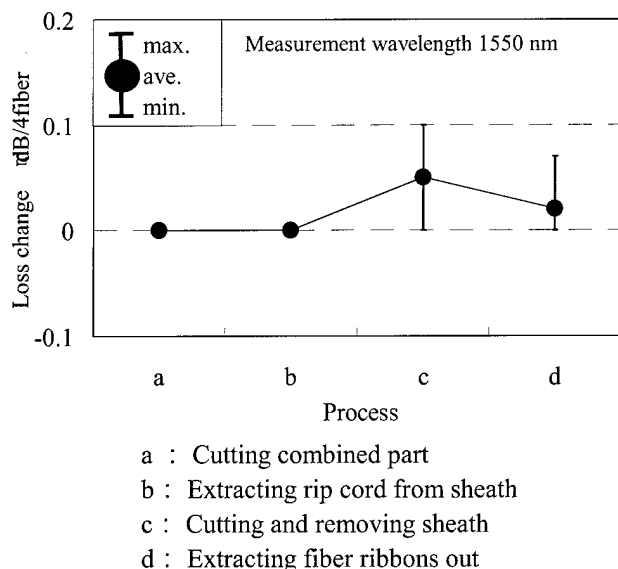
Figure 7.   Mid-span access loss characteristics

as shown in Fig. 6. In designing, we did this by taking decrease of wind pressure which is main factor of the load applied to the messenger wire into account since the smaller cable height leads to a decrease in wind pressure [2].

If the size and weight of the cable are similar to those of cluster type drop cable [3], we can expect to use the simple manual installation method used for cluster type drop cable and drawing cable for aerial cable, resulting in installation cost reduction.

We fabricated the prototype cable based on the above consideration. The structure of our newly developed 40-fiber cable is shown in Fig.5 in comparison with the conventional one. This new cable is 50% lighter and 20% smaller than the conventional cable. The mechanical and thermal characteristics shown in Table 5 reveal its good performance. The experimentally obtained mid-span access loss change, which is one of the most important test items, is shown in Fig. 7. From the first process of dividing the messenger wire and cable part to the last process of fiber ribbon identification, the maximum loss is 0.1 dB/4 fiber, which is small enough in relation to the allowable loss of 1.0 dB [4]. Moreover, these processes take about 7 min which is almost same as for the conventional cable and we confirmed good workability for practical use. Furthermore, the installation length for the new cable with our simple installation method can be extended to 380 m which is about 85% longer than for conventional cable. In distribution systems most cable installation lengths are less than 300 m. Therefore, this cable can be installed by a simple installation method resulting in cost reduction.

5. Conclusions

To allow us to construct optical access networks, economically, immediately and efficiently we studied the structures of the feeder, termination and distribution cables that are main components of access networks. We also examined their performance based on our requirements by taking workability into account. Our main targets for both feeder and distribution cable were to reduce cable weight and size. We also investigated ways of improving the structure of the termination and that enables the termination cable to be pulled towards a central office. As a result, we successfully developed a relatively low cost optical fiber cable with good performance for practical use.

Acknowledgments

References

[1] H.Iwata et al, "Design of aerial optical fiber cable system suitable for easy branching", 46th IWCS, pp.4-11(1997)

[2] H.Iwata et al, "Novel optical fiber cable for distribution use in access network", 48th IWCS, pp.20-24(1999)

[3] K.Hogari et al., "Optical fiber cables for residential and business premises", Journal of Lightwave Technology, Vol.16, No.2, pp.207-213(1998)

[4] K.Suto et al., "Optical receiver design considering fiber loss fluctuation for subscriber loops", Trans.IEICE, vol.E74, No.3, pp.547-554(1991)

Author
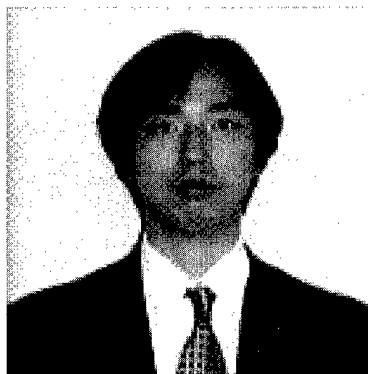
NTT Access Network
    Service Systems
    Laboratories

Tsukuba, Ibaraki

305-0805, JAPAN

E-mail address

kawataka@ansl.ntt.co.jp

Junichi Kawataka is a research engineer. He was born in 1973 and received B.E. and M.E. degrees in electrical and electronic engineering from Muroran Institute of Technology in 1996 and 1998, respectively. He joined NTT in 1998 and started research and development on design of optical fiber cable.

Premises Optical Network System Providing Almost the Same Workability as a Conventional Metallic System

Eiji Araki, Masaaki Takaya, Kimio Andou, Sadaaki Takano and Shinji Nagasawa

NTT Access Network Service Systems Laboratories
1-7-1 Hanabatake, Tsukuba, Ibaraki, 305-0805 JAPAN
+81-298-52-2625 · email address: e-araki@ansl.ntt.co.jp

Abstract

We examine a premises network system with single-mode (SM) optical fiber cables that provides almost the same workability as a conventional metallic system. This paper describes the design and performance of low bending loss fiber cable and an easy to handle enhanced MT-RJ (e-MTRJ) connector for this premises network system. The low bending loss fiber can be stored in a conventional electric flush type outlet, and the e-MTRJ connector enables us to realize metal-like handling, high density packaging and reliable joints.

We have confirmed that these techniques are highly effective for constructing high-speed and broadband premises optical network systems.

Keywords

Cable; Optical; Fiber; Connector; MT-RJ; Cabinet; Premises

1. Introduction

It is important to develop optical fiber distribution systems to provide business buildings with multimedia services. These systems must be flexible, efficient and economical. Recently, single-mode (SM) optical fiber cables have been introduced in access networks as the medium for high-speed and broadband services. By contrast, grated index (GI) optical fiber cables, coaxial cables or metal cables have been mainly used for the systems in premises networks such as local area networks. However, if we consider compatibility with main access lines and potential demand for further high speed and broadband services, premises networks will require more compact and simpler distribution cabling, using SM optical fiber cables. We proposed a SM optical fiber premises optical network system designed to meet this requirement.

2. Outline of Premises Optical Network System

Figure 1 shows an image of our premises optical network distribution system, in which we take fiber to the desktop (FTTD)

into consideration. The characteristics of this optical distribution system are described below.
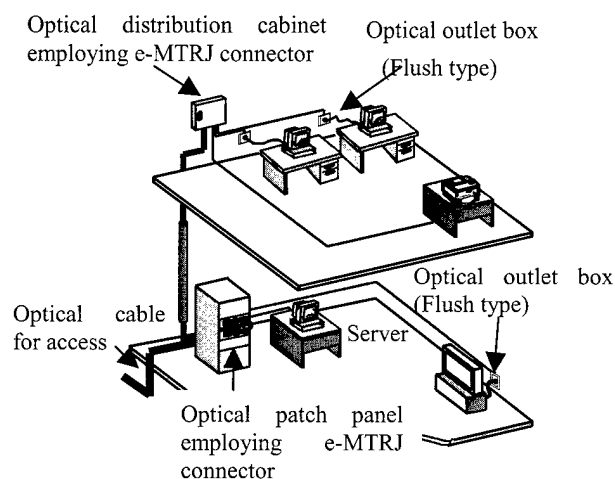
Fig. 1 Premises optical network system using SM optical fiber

1) The cable installation workability is improved by using indoor cable, under-carpet cable and termination-cable with low bending loss optical fiber.

2) An e-MTRJ connector is employed with a termination cabinet, a patch-panel, a distribution cabinet and an outlet in the premises network. As the e-MTRJ connector is provides the same workability as a metallic modular jack connector, it is easy to connect and disconnect the plugs, and the e-MTRJ connector enables us to realize high density packaging and reliable joints.

3) It is possible to reduce the size of the cabinet and outlet by using the low bending loss fiber cable and a high density e-MTRJ connector.

3. Low Bending Loss Fiber

Today, metallic cable, coaxial cable, optical fiber (GI type or SM type) cable and plastic fiber cable are used for premises optical network systems according to the transmission bandwidth and cable length. We have studied SM optical fiber cable. Since we consider it is important to become compatible with main access lines and meet the potential demand for further high speed and broadband services. However, there is a problem that must be solved as regards their workability when we install them in a premises optical network. SM type optical fiber cable is more difficult to install than metallic cable due to its bending radius specification. So we investigated the contours of optical fiber parameters exhibiting low bending loss to obtain almost the same workability as that of a conventional metallic system.

3.1 Fiber for Premises Optical Network System

SM type optical fiber falls broadly into two categories; single-mode fiber (SMF) and dispersion shifted fiber (DSF). SMF is used as the optical cable for access lines and DSF is use for trunk lines. We examined the bending loss of SMF.

A permissible bending radius target for low bending loss fiber is 15 mm or less. This is because this value allows us to store fiber in an outlet box of the same size as a metal outlet box. And when fiber is installed in an outlet box, the permissible bending loss is 0.2 dB/m or less. We measured the fiber bending loss for bending radius from 10 to 20 mm. Figure 2 shows the bending loss versus bending radius. In terms of SMF, the bending loss to meet the value required for the fiber parameters at a bending radius of 15 mm.

If we select the SMF parameters, we can use SMF with a bending radius of 15 mm. Figure 3 shows a comparison of measured bending losses and calculated values reported by Marcuse. Based on the results, we calculated the relationship between fiber parameters and bending radius to obtain a low bending loss. The contours of the optical fiber parameters with calculated numerical expressions of bending loss are shown in Fig.4. The contours provide a more severe specification than the fiber parameters currently in use, but it is possible to employ them in a premises optical network system.
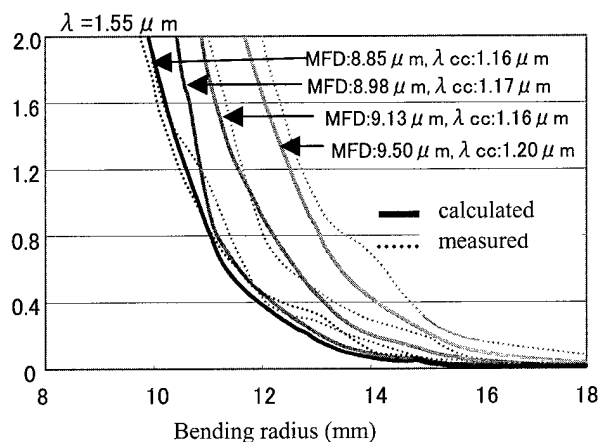
Fig. 3 Correlation between measured bending losses and calculated values

Fig. 2 Bending loss versus bending radius of SMF
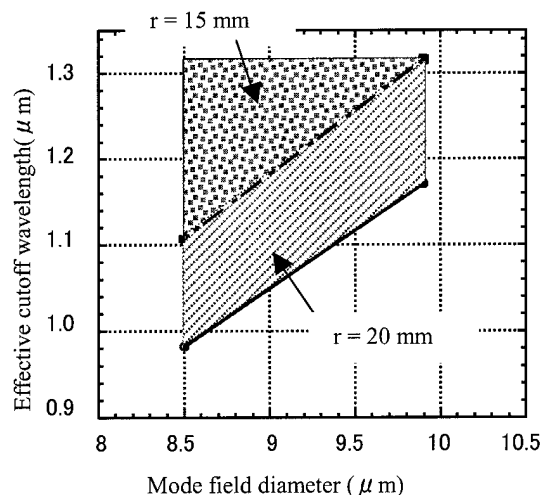
Fig. 4 Contours of optical fiber parameters exhibiting a low bending loss of 0.2 dB/m at a 1.55 μ m wavelength

4. Enhanced MTRJ Connector

As a connector for the joining points in premises networks, we designed and fabricated a modular jack type 2-fiber mini-MT connector (e-MTRJ connector). This connector provides us with both metal-like handling and a reliable joint with a locking key, and offers twice the density of the SC-type duplex connector. We confirmed that the optical characteristics are almost the same as these of the SC type connector. Figure 5 shows the structure of the e-MTRJ connector. The connector plug must be assembled on the customer's premises, but the assembly processes for conventional connectors are too complicated because there is adhesive to harden and plug end-faces to polish. It must be possible to assemble the connectors easily and quickly and so we have developed the field installable e-MTRJ connector.

Fig. 6 Structure of mechanical splice type e-MTRJ connector

We measured the insertion loss of the connector at a wavelength of 1.3 μm using an LED. The average insertion loss was 0.20 dB with a maximum value of 0.37 dB. The field installable e-MTRJ is compatible with the conventional MT-RJ connector and can be assembled very easily and quickly on the customer's premises.

Fig. 5 Outline of e-MTRJ connector

5. Cabinet and Outlet

It is difficult to reduce the size of the cabinet and outlet in a premises optical network because of the cable bending radius and the optical connector size. A conventional optical outlet, for example, is large (120 mm(w) •115 mm(h)), as shown in Fig.7.

Figure 6 shows the structure of the connector plug, which includes a ferrule component in the housing. This component is composed of a MT ferrule part and a mechanical splicing part. The optical fibers are housed internally between the connector ferrule end-face and the middle of the mechanical splicing part. The ferrule end-face is polished in the factory. When the connector is assembled, the fibers are inserted in the ferrule component and joined with internal fibers housed in the component at the mechanical splicing part. The mechanical splicing part consists of a V-groove substrate, coupling plates, and a clamp spring. When the connector is assembled, first we form a gap between the substrate and the coupling plate by inserting a wedge into slots formed in the side of the mechanical splicing part. Next, we insert fibers into the mechanical splicing part. We then remove the wedge after confirming that the fiber end-faces are touching the internal fibers. Moreover, the fiber connection region of the mechanical splice has index matching material to reduce the Fresnel reflection. This process eliminates the need for heating the adhesive and polishing the ferrule end-face. The plug assembly time is about 5 minutes.

Fig. 7 External appearance of conventional optical outlet box

We made a small experimental cabinet and outlet using both low bending loss fiber (r=15 mm) and a high density e-MTRJ connector thus confirming that we can reduce their sizes. We made both flush and protruding type outlets, as shown in Fig.8. The flush type outlet is the same size as a metal outlet box (54 mm(w) •109 mm(h)).
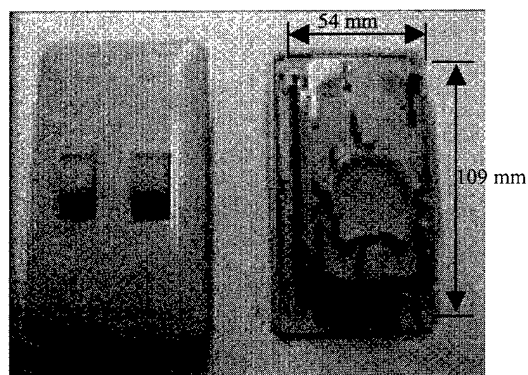
(a) Flush type
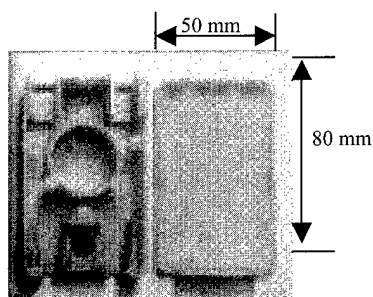
(b)Protruding type

Fig. 8 **Appearance of experimental optical outlets**

We also stored low bending loss fiber in a fabricated outlet box and measured the bending losses. As a result, the losses satisfied a target value of <0.2dB/m, as shown in Fig.9.
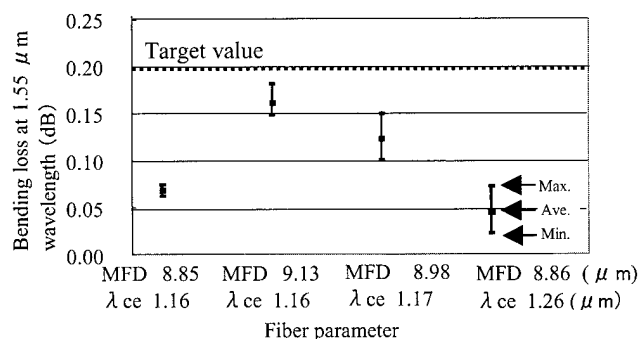
Fig. 9 **Bending loss of fibers stored in fabricated flush type outlet box**

5. Conclusions

We have developed low bending loss fiber cable and an easy to handle enhanced MTRJ connector which are basic components for realizing premises optical distribution systems with metal-like handling. Moreover, we were able to reduce the size of the cabinet and outlet by using these basic components. We expect these developments contribute to the expansion of optical fiber use in premises and users' networks.

6. References

[1] D. Msrcuse, "Loss Analysis of Single-Mode Fiber Splices", Bell syst. Tech.. May-June pp.703-718 (1977)

[2] Katuyama,Y., Tokuda,M., Uchida,N. and Nakahara, M.: "New method for measuring V-value of a single mode optical fiber ", Electron.Lett., 12, 25, PP. 669-670 (1976).

[3] M.Takaya, S.Nagasawa, Y.Murakami and S.Hatanao, "Design and Performance of Modular Jack Type Mini-MT Connectors", IWCS., '99 PP.332-339 (1999)

[4] R.K.Selli, S. Berglund, "Novel V-groobe –based Interconnect Technoligy," Optical Engineering, vol.37, No.12, PP3134-3142

[5] I.Sankawa at. el: "Development of Optical Fiber Distribution System for Office Buildings." OECC '97, PP.530-532 (1997)

Speakers Biography

Eiji ARAKI
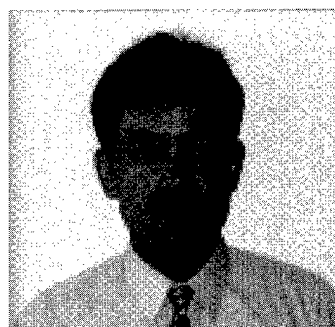
NTT
Access Network
Service systems
Labratories
1-7-1, Hanabatake,
Tsukuba, Ibaraki,
305-0805
JAPAN

Eiji ARAKI is a research engineer at NTT Access Network Service Systems Laboratories. He joined NTT in 1986. He has been engaged in the research and development of customer service system since 1998. He is a member of IEICE of Japan.

Flexible Detection System Using Portable Remote Fiber Testing System (RFTS) for Damaged Optical Cable Networks

Mamoru Hyodo*1, Kazuhiro Namikawa*2, Naoki Nakao*1, Toshinao Kokubun*1
(*1) NTT Access Service Systems Laboratories, Makuhari, Chiba, JAPAN
(*2) NTT-EAST Research and Development Center, Makuhari, Chiba, JAPAN
+81-43-211-3337   email : hyodo@ansl.ntt.co.jp

Abstract

Nippon Telegraph and Telephone Corporation (NTT) has been constructing optical cable networks for various multimedia services. Maintenance of these networks is obviously important as service increases. We describe a way of recovering optical cable networks after a disaster like the Great Hanshin Earthquake that occurred in Kobe in 1995.

This paper details the features of a mini-test equipment module (mini-TEM), a portable remote fiber testing system (RFTS) designed to make testing of optical cable networks more efficient. It describes the functions of a new flexible detection system, its configuration, work flow, and general purpose functions. This system will be introduced in all service areas of NTT.

Keywords

RFTS; Disaster; Damaged optical cable networks; Macro detection; Micro detection

1. Introduction

Up to now, a variety of outside facilities such as manholes and telegraph poles that can withstand disasters have been developed and introduced. When the Great Hanshin Earthquake (Fig. 1) occurred, however, we were not immediately able to assess how much damage had been caused to cable networks. We were also not able to see how many lines were interrupted in each area. Thus cable networks could not immediately be recovered, and this of course caused problems for the customers. Therefore | the Maintenance and Service Operation Department at NTT set a number of objectives for itself. It was decided that damaged areas needed to be located within half a day, and that damaged fibers and their locations needed to be identified within four days of a disaster. This information is needed to quickly recover damaged cable networks.

A flexible detection system for damaged metallic cable networks was quickly developed and introduced smoothly. This system was made up of existing testing equipment, which had already been introduced at all remote offices. However, as the existing RFTS, an automatic optical fiber operation system (AURORA) [1], did not have the scalability or portability needed when optical cable networks were suddenly damaged. Therefore, we decided to develop a compact and portable RFTS mini-TEM [2][3] that can test damaged networks in detail.

Fig. 1 Disastrous scene of the Great Hanshin Earthquake

2. Development of The mini-TEM

2.1. Configuration of The mini-TEM

The mini-TEM consists of control and measurement equipment and a portable optical-fiber selector (Fig. 2). All this equipment is compact and light enough to carry around as needed.
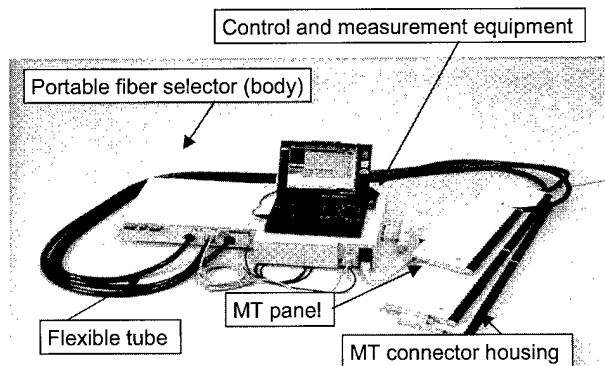
Fig. 2 Configuration of the mini-TEM

2.2. Functions of The mini-TEM

The mini-TEM has 3 main functions. There is a 3-wavelength (1.31, 1.55, and 1.65 μm) optical time domain reflectometer (OTDR) function, a remote control function, and a data management function.

Up to now, a portable testing tool with 3-wavelength OTDR function has not been available. Therefore, we developed the mini-TEM with 3-wavelength OTDR for portable use. Moreover, the 3-wavelength optical fiber identifier (ID tester) function is provided in it. Thus, portable 3-wavelength OTDR testing, loss testing, and fiber identification testing become possible.

The remote control function makes remote testing easier for an operator. Once the mini-TEM is set up in the office, fibers can be tested from the remote work site, such as in manholes or on telegraph poles, with a cellular phone and a handheld PC.

Using the data management function, an operator can create reports on testing and manage data at the office. The current manual operation means that it takes a lot of time to create reports by manual pasting, and it is difficult to manage data because some data is not systematically managed.

These functions make the mini-TEM very useful for various optical fiber testings. Since March 1999, about 80 mini-TEMs have been put into use in Japan.

2.3. Features of The mini-TEM

2.3.1. Flexible Set Up in Fiber Termination Module (FTM).
The mini-TEM can be set up in almost all kinds of FTMs (Fig. 3). Appropriate attachment devices are designed to fit the mini-TEM in all kinds of FTMs. Moreover, a mechanical transferal (MT) panel can be separated from the optical fiber selector body and set up in the FTM flexibly. A flexible tube that accommodates optical fiber ribbons connects the MT panel to the optical fiber selector body (Fig. 2).
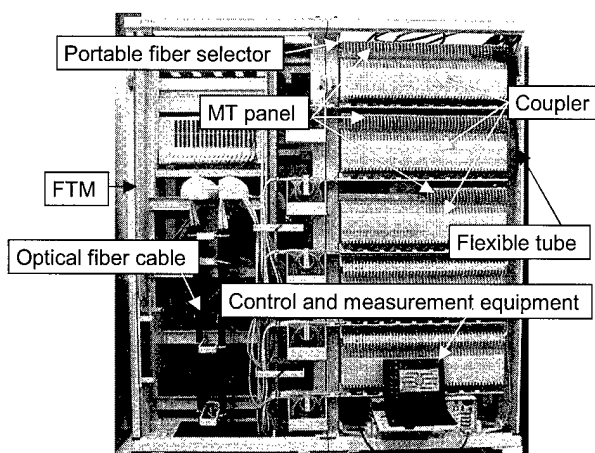
Fig. 3 Example of setting up the mini-TEM in an FTM

2.3.2. Easy MT Connecting Function.
The mini-TEM is connected to the optical fiber cables and optical couplers. Using a connecting tool, the 8- or a 4-MT connector of an optical fiber cable and an optical coupler are easily connected to the MT connector housing of the MT panel (Fig. 4) [4]. The MT connector housing contains an 8-MT connector, two guide-pins, and a connecting hook. This new connection significantly shortens the connection time compared with the conventional manual connection using only the guide-pins and the clamp spring.
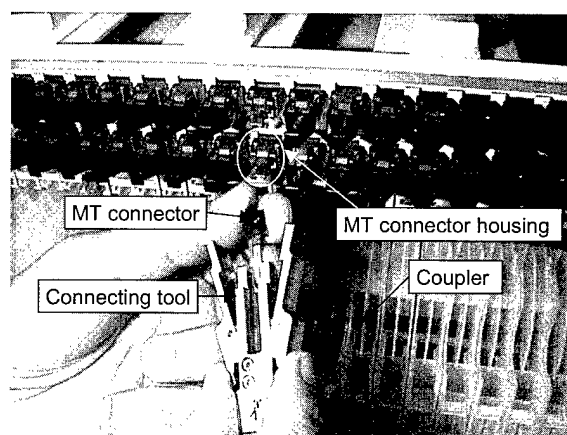
Fig. 4 Simple connection of MT connector to the MT connector housing

2.3.3. Special Testing Control Application of The mini-TEM.

The mini-TEM reduces the time taken for the following operations: connecting optical fibers, testing, analyzing, diagnosing defects, and creating reports. These operations without AURORA have until now been executed manually at remote offices. A special testing control application that can test with a semi-automated work flow was developed. This application makes it possible to test 2,000 optical fibers continuously. The application software runs on the Windows 95/98 operating systems. Therefore, this application is very easy to handle. It is easy to install and some result data can be used with applications such as Microsoft Excel. In addition, using an interface converter and dynamic link library (DLL) software, the mini-TEM can control the optical fiber selector of the AURORA. In this way, the mini-TEM can test many fibers using with AURORA in a short time.
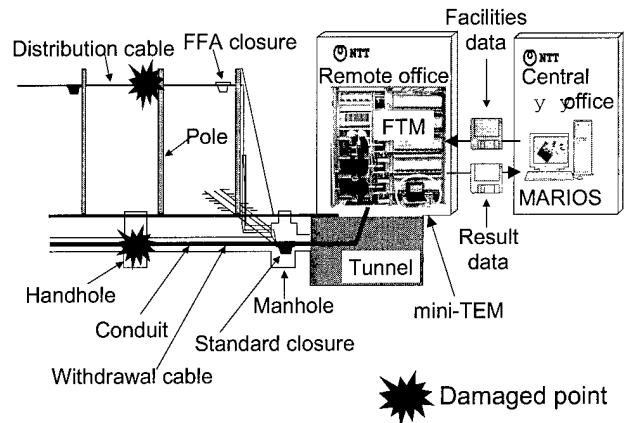
3. Flexible Detection System For Damaged Optical Cable Networks

3.1. Functions of The New Flexible Detection System

This system has two functions for detecting damage and making a recovery plan for optical cable networks. These are the macro and micro detection functions.

3.1.1. Macro Detection.
The macro detection locates affected areas within half a day of the disaster occurring by testing the main fibers deployed in identified optical cable network areas. The macro detection is used for planning the efficient micro detection.

3.1.2. Micro Detection.
The micro detection identifies damaged fibers and their locations within four days by testing all the fibers deployed in that area. The micro detection is used in advance for making an effective recovery plan. Both the macro and micro detections are very important to make an efficient recovery plan.

3.2. System Configuration

This system is composed of the mini-TEM and a management support system for access task reengineering innovation objects (MARIOS) (Fig. 5) [5] [6]. MARIOS, which is a planning system [7] in the access network domain, has a lot of facilities data, such as the number of optical fibers, optical cables, telegraph poles, and manholes. It provides an enhanced end-user computing environment based on object-oriented programming technologies.

Fig. 5 System configuration

3.3. Features of The New System

The disaster recovery work needs a lot of operators nationwide, and naturally different from ordinary operations. We have therefore developed a new mini-TEM application that optimizes the work flow in the testing operations, and two applications operated by MARIOS that can make facilities data for testing optical cables using the mini-TEM and display detailed results of testing clearly on screen.

3.3.1. The New mini-TEM Application.
The new mini-TEM application optimizes the work flow in the testing operations. In addition, it automates the conventional manual tasks, such as setting facilities data, setting OTDR parameters, and analyzing and diagnosing defects. Using the facilities data entry function, an operator can enter the latest facilities data easily, because the facilities data outputted from MARIOS is always the latest and it is imported to the mini-TEM by floppy disk. Moreover, using the automated testing function, the testing time is considerably reduced compared to that of the conventional application. The new application makes testing optical fibers very easy work for all operators.

3.3.2. Display of MARIOS.
With result data, MARIOS can display the color-coded damaged areas and their area number at the macro detection (Fig. 6), the locations of damaged fibers found along the cable routes (Fig. 7), and the damaged areas gradated by amount of damage in order to show how badly the areas are damaged at the micro detection (Fig. 8).
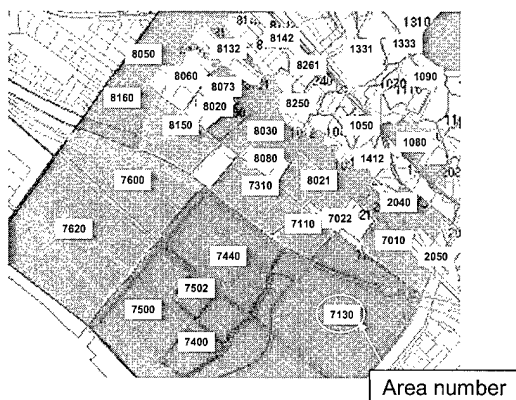
Fig. 6 Display of MARIOS (macro detection)
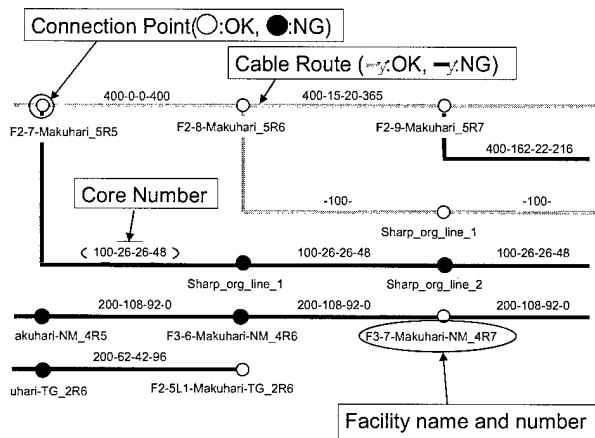
**Fig. 7 Display of MARIOS
(micro detection: damaged fibers locations)**
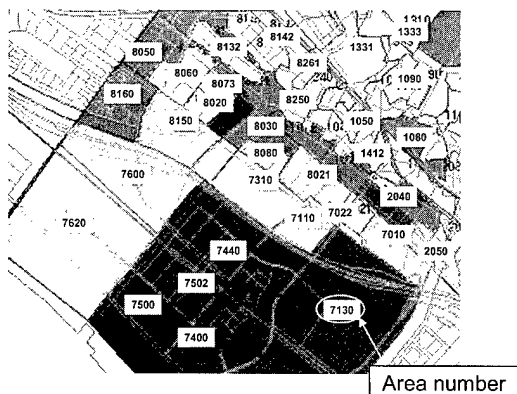
**Fig. 8 Display of MARIOS
(micro detection: damaged areas)**

3.4. Work Flow of Operation

If a disaster occurs, an operator goes to the remote office from the central office with a mini-TEM and the facilities data outputted from MARIOS as soon as possible. Then, the mini-TEM is set up in the FTM and the testing of fibers for macro detection is started. After testing the fibers, the operator goes back to the central office with the result data and puts it into MARIOS to locate the affected areas. Using the results of the macro detection, the plan for micro detection is then made to decide which area is to be tested first. Next, the same work for micro detection is carried out. Then, the recovery plan is scheduled using the results of the micro detection. Finally, the priority for restoring the damaged areas and how workers are to be dispatched are decided.

3.5. Effect of System Introduction

Table 1 compares the operation time in the case of manual operation, the mini-TEM using an existing application, and the new system. Each operation time is normalized as 100 by the manual operation time.

Using only the mini-TEM, the setting time is reduced by 90% compared with the manual operation, thanks to the easy MT connection. The testing time is reduced by 40% thanks to semi-automated work flow of the existing mini-TEM application. However, this is a manual detection method, so it is not effective at reducing detection time.

Using this system, the setting time is reduced from 90% to 95% thanks to the facilities data entry function. The testing time is reduced from 40% to 75% thanks to the automated testing function of the new mini-TEM application. Moreover, the detection time is reduced from 20% to 90% thanks to the MARIOS. This system reduces by 80% the total time compared with the manual operation. Thus, we can do the micro detection and the macro detection immediately.

Table 1. Effect of the new flexible detection system.

	Setting (*1)	Testing	Detection	Total
Manual operation	100(*2)	100(*2)	100(*2)	100(*2)
Only the mini-TEM	10	60	80	60
The new system	5	25	10	20

(*1) Includes cable connecting time.
(*2) Each operation time is normalized as 100 by the manual operation time.

3.6. General Purpose Use of The New System

The occurrence of disasters cannot be predicted. Therefore, this system has some functions for general purpose use. It has an outside facilities data entry function, an automated testing function, and a data management function. These functions are applied for the regular monitoring of optical cable networks at night and maintenance without intensive work during busy times. They are also used in a large scale of optical cable network construction.

3.6.1. The Facilities Data Input Function. The facilities data outputted by MARIOS is formatted in comma separated value format (CSV). Therefore, it can be edited using Microsoft Excel, for example. Facilities data is imputed to the mini-TEM by floppy disk without on-line data transmission, because in a great disaster, telecommunication lines may not be available.

3.6.2. The Automated Testing Function. Setting the OTDR parameter is difficult for an inexperienced worker. Testing with manual setting of the OTDR parameter might be not possible to test well. Therefore, a worker may change parameters and test again many times. The best testing can be done anytime by the automated testing function.

3.6.3. The Data Management Function. As already described, using this function, some result data can be used with applications on the market such as Microsoft Excel. Moreover, the result data can be easily referred by a variety of key words such as the office name where the test was executed, the testing date, and the facilities name.

4. Conclusions

The new flexible detection system has a portable and compact fiber testing module (the mini-TEM) with data management and display functions using MARIOS. The visual display of the test results is very useful for making disaster recovery plans for optical cable networks that are used as lifelines. This system reduces by 80% the total operation time compared with that in manual operation. Moreover, this system can be used not only in disasters but also in ordinary maintenance operations by general purpose functions.

5. Acknowledgments

6. References

[1] K. Tomita, K. Yoshioka, N. Nakao, and N. Tomita, "Optical fiber distribution in central offices and testing methods for commercial FTTH system", 47th *IWCS, pp.808-814,* (1998).

[2] M. Hyodo, T. Inoue, and N. Nakao, "Development of mini-test equipment module which supports efficiently optical fiber testing", *Raisers, pp. 38-40,* (August, 1998).

[3] H. Katayose, K. Sakuma, K. Yasuhara, and Y. Nomura "Remote and automatic 4,000-fiber optical testing system", 47th *IWCS, page 517 Session 13: Poster papers,* (1998).

[4] T. Murakami, T. Komiya, K. Saito, and H. Maki, "Development of MT receptor", *IEICE, B-10-18,* (September, 1998).

[5] Y. Mitsunaga and M. Nakagawa "Development of management support system for access task reengineering innovation objects (MARIOS)", *NTT Technical Journal vol.6, no.8, p. 92,* (1994).

[6] T. Itoh, et al. "Management for deployment of optical access network", 45th *IWCS, pp.260-264,* (1998).

[7] T. Kokubun, T. Abe, Y. Mitsunaga, and M. Gencho, "Integrated operation systems for access cable networks: OPTOS", *GLOBECOM, pp.282-287,* (1998).

7. Authors
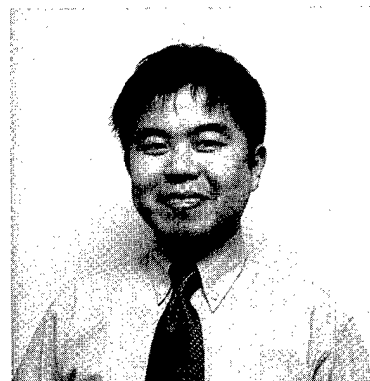
Mamoru HYODO

NTT Access Service Systems Laboratories.
NTT-Makuhari Building 1-6 Nakase Mihama-ku Chiba-shi, Chiba 261-0023 Japan
Tel: +81-43-211-3337
e-mail: hyodo@amsl.ntt.co.jp

Mamoru Hyodo received his Bachelor's degree and Master's degree in naval architecture and ocean engineering from Hiroshima University in 1995 and 1997, respectively.

After joining NTT in 1997, he engaged in the development of the mini-TEM. He is currently a technical staff member of the Access Service Systems Laboratories, and is engaged in the development of operation systems for optical access networks.

Kazuhiro NAMIKAWA

NTT-EAST Research and Development Center.
NTT-Makuhari Building 1-6 Nakase Mihama-ku Chiba-shi, Chiba 261-0023 Japan
Tel: +81-43-211-3408
e-mail: k.namikawa@rdc.east.ntt.co.jp

Kazuhiro Namikawa graduated from Choshi high school in 1985.

After joining NTT in 1985, he engaged in constructing outside telecommunication plants. He is currently a technical staff member of the NTT-EAST Research and Development Center, and is engaged in the development of operation systems for optical access networks.

Naoki NAKAO

NTT Access Service Systems Laboratories.
NTT-Makuhari Building 1-6 Nakase Mihama-ku Chiba-shi, Chiba 261-0023 Japan
Tel: +81-43-211-3204
e-mail: nakao@amsl.ntt.co.jp

Naoki Nakao received his Bachelor's degree and Master's degree in electrical engineering from Okayama University in 1985 and 1987, respectively.

After joining NTT in 1987, he engaged in the development of splicers for copper pairs. He is currently a Senior Research Engineer in the Access Service Systems Laboratories, and is engaged in the development of operation systems for optical access networks.

Toshinao KOKUBUN

NTT Access Service Systems Laboratories.
NTT-Makuhari Building 1-6 Nakase Mihama-ku Chiba-shi, Chiba 261-0023 Japan
Tel: +81-43-211-3307
e-mail: bun@amsl.ntt.co.jp

Toshinao Kokubun received his Bachelor's degree and Master's degree in electrical engineering from Ibaraki University in 1980 and 1982, respectively and a Ph.D. degree from Osaka University, Japan, in 1992.

He joined NTT in 1982. He has been engaged in the research and developmental work on the design and characterization of optical-fiber cables for subscriber loops and high-speed optical transmission systems. He is presently engaged in research on access network operation systems in Access Service Systems Laboratories, Makuhari, Japan.

Impact Resistance Requirements for Traditional and Multi-Environment Fiber Optic Cables

Richard D. Beggs

+1-770-798-3813 · rbeggs@lucent.com

Paul E. Neveux, Jr.

+1-770-798-5314 · pneveux@lucent.com

Premises Fiber Optic Cable Development
Lucent Technologies, Inc.
Norcross, Georgia, USA

Lisa A. Dixon

+1-770-798-3787 · lad13@lucent.com

Michael D. Kinard

+1-770-798-2109 · mkinard@lucent.com

Outside Plant Fiber Optic Cable Development
Lucent Technologies, Inc.
Norcross, Georgia, USA

Abstract

The rapidly growing, highly competitive telecommunications market has pushed fiber optic cable manufacturers to develop the highest performing, yet most cost effective cable designs. Toward that goal, industry standards groups have been re-evaluating existing cable performance standards to ensure that there are no ill-defined standards that would inhibit the acceptance of the most user-friendly and robust products. As a consequence, standards are being revised to provide requirements more narrowly tailored to each cable application. In the case of impact resistance, specifying requirements based on cable applications -- Premises versus Outside Plant -- has been proposed. But, this approach has uncovered the potential vulnerability of the new multi-environment cables (Outdoor/Indoor and Indoor/Outdoor cables) to impact. Operating in both Outside Plant and Premises environments, multi-environment cables *ideally* should meet all the typical requirements of *both* environments. However, the limited scope of available materials and acceptable costs forces a compromise - a compromise that can sacrifice impact resistance. This paper discusses the implications of the current standard and its proposed revision for the specification of all cable types, but particularly for those designed for multiple environments.

Keywords

Fiber optic cable; impact resistance; standards; multi-environment applications; Indoor/Outdoor; Outdoor/Indoor.

1. Introduction

The rapidly growing, highly competitive telecommunications market has pushed fiber optic cable manufacturers to develop the highest performing, yet most cost effective cable designs. A truly cost effective cable design is one that is light and compact, while still able to survive the rigors of installation and service life -- nothing more, but nothing less. Toward that goal, industry standards groups have been re-evaluating existing cable

performance standards to ensure that there are no ill-defined standards that would inhibit the acceptance of the most user-friendly and robust products. As a result, standards are being revised to provide requirements more specifically tailored to each cable application. For impact resistance, a standard product performance attribute, significant changes have been proposed. Separate requirements for military, Outside Plant, Riser, Plenum and Interconnect cables — in both energy levels and numbers of cycles — are being considered. These changes represent a positive step forward for design efficiency, but may have key implications for cables which operate in more than one of these application environments, specifically the new Outdoor/Indoor and Indoor/Outdoor cables. This paper examines the evolution and function of the impact standard in specifying quality cable designs.

To begin, the following section presents the recent evolution of impact standards for fiber optic cables, and Section 3 follows with a discussion of the potential consequence of specifying impact resistance based only on the predominant, existing standard -- including its proposed revisions. Section 4 describes a selection of cables types that are currently produced for multi-environment applications, and Section 5 outlines the test scenarios used to evaluate the impact resistance of these types of cables. Sections 6 and 7 present and discuss the results of impact tests on these cables, respectively. Section 8 summarizes the work to date and makes recommendations for future experimental work and standards development.

2. Background
2.1 Evolution of Impact Standards for Fiber Optic Cables

Impact Resistance has been a standard performance attribute for telecommunications cables for many years. Under current standards for optical fiber cables, acceptable impact performance includes resistance to physical damage both to the sheath (cracking or splitting) and to the optical fibers (breaking),

or permanent sheath deformation resulting in unacceptable fiber attenuation increases. The impact test, TIA/EIA-455-25B, FOTP-25, currently a U.S. National Standard, is becoming the predominant international Standard for specifying test procedures and recommending performance levels for impact performance. ICEA's Standards 640 and 596 and Telcordia's GR-20 and GR-409 all reference this Standard in their requirements for Fiber Optic Outside Plant and Premises cables, respectively. In this test, a cable is subjected to a repeated impact load, simulated by a mass dropping from a fixed height of 150 mm. The current standard for non-military cables requires 25 impacts on the cable. The requirement for military cables is 50 impacts. The mass used, unless otherwise specified, is dependent of the cable's diameter.

All of the requirements outlined in FOTP-25 were originally based on those used in military standards. Meeting military-level requirements meant that a cable could survive very brutal installation and lifecycle environments. With the advent of fiber optics, ensuring that the fragile, brittle fibers could survive a severe environment was a concern, especially for Outside Plant cables, so the Military model was adopted. However, over the last decade, the market has pushed fiber optic cable manufacturers to develop even more cost effective cable designs. A truly cost effective cable design is able to survive the standard rigors of commercial installation and service life but is as light and compact as possible. Cables that are "over-designed" to meet unrealistic standards can be expected to be bigger, heavier, stiffer and more costly -- characteristics that are disadvantageous to customers *and* manufacturers. To allow designs to be optimized, designers have re-evaluated the performance requirements that define the types of designs that will be acceptable to non-military customers. The goal of these revisions, obviously, has been to make the standards more reflective of only the *true* performance level that a cable must have to survive in the field, nothing less, *but* nothing more.

One way to eliminate unrealistic or unnecessary cable requirements is to create less general specifications. For cables, this can be done with performance specifications that are unique to an application environment. The original FOTP-25 was modified previously in this manner (1996) to provide the separate, less stringent performance requirements for all non-military cables. As mentioned, the recent market push to develop even more installation-friendly, cost-effective cables has once again led to a debate on what impact requirements approximate the actual cable environment. The proposed revisions to FOTP-25 to make its requirements more accurate for cables used for different applications. The latest changes would further reduce the requirements for many of the non-military OSP and Premises cables. The details of those proposed revisions are discussed in the next section.

2.2 Latest Revisions to Impact Standard FOTP-25

The two major proposed changes to the FOTP-25 standard are both aimed at making the test more accurate in screening cables for adequate, mainstream impact performance.

First, the number of impacts imparted during the test is to be reduced to two from twenty-five. This change is seen as a move toward realism, as a field scenario involving the repeated hammering of the cable is very unlikely, while one or two impacts from dropped tools or falling rocks (in backfill for buried OSP cables) are normal occurrences. At the same time, these two impacts are to be applied at three different sites along the cable. Second, five categories of non-military cable applications are proposed for determining the energy level to be used in the test. These categories are a switch from the approach used currently (and still to be used for military cables), which identifies the impact level for the test based on the cable's diameter (see Table 1) [1]. There are currently nine diameter ranges, while the new proposal includes the following five application categories: Outside Plant (OSP), Riser, Plenum, Drop Cable and Interconnect [2]. These new categories allow designers to better optimize cables for each type of application, the assumption being that cables in each application area are expected to encounter successively lower levels of impact (See Table 2). Figure 1 shows a schematic comparison of the current requirements for impact resistance for optical cables, depending on application (military and non-military, shown with solid-line ovals), and the newly proposed values for Outside Plant and the Premises applications (shown with dashed-line ovals). One additional energy level is also included (filled oval). This single value, 9.8 N·m, has been a common performance measure for OSP cables specified by international customers.[1]

In general, the change to specifying impact energy based on application rather than cable diameter has reduced the maximum impact that a cable must survive in testing. Table 2 summarizes the new proposed values for non-military cables. In the United States, Telcordia specification GR-409 (for Premises cables) had already prescribed the lower values for Plenum and Interconnect cables (see Table 3), but the new value for Riser cables represents a 50% reduction in impact energy (down to 2.94 from 5.88 N·m) [3]. For OSP cables, the current *median* energy level, 4.41 N·m, is proposed as the new *maximum* value (current maximum is 7.35 N·m). The current revisions of the ICEA Standards follow the lead of the FOTP revision.

Unfortunately, these new values in the revisions are not based on any scientific analysis, but on anecdotal information on the kinds of the impacts that do and do not occur in the field, and on capability testing of existing cables. If cable designs are

---

[1] Impact values have traditionally not been specified in international standards. However, several parts of IEC 60794, *Optical Fibre Cables*, currently under active ballot propose methodology and impact energy values similar to those proposed for FOTP-25.

modified based on these lesser requirements, the appropriateness of the reduced energy levels can only be validated by successful time in the field. This lack of scientific soundness has been adequate in the past -- impact failures appear to few and far between -- and may continue to be so for some cable applications. However, the next section discusses the cases in which the current and proposed standards may be inadequate.
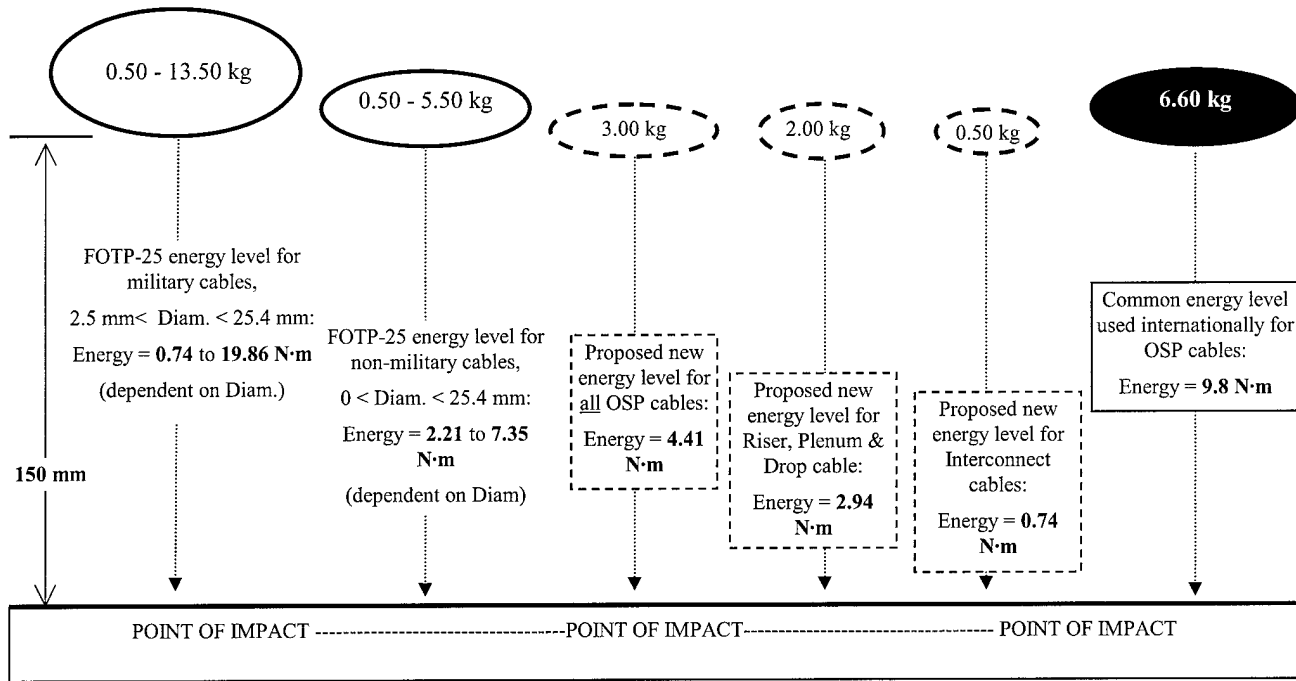
Figure 1. Impact Resistance Requirements - The impact that a cable must survive is generated by a weight falling from a given height. In this approach, the impact energy is approximated as the potential energy of the suspended mass. The potential energy converts to kinetic energy as the weight falls, and the assumption is that the cable absorbs all of this kinetic energy in resisting the impact. Therefore, the energy of impact is equivalent to the potential energy of the suspended mass (*potential energy = height * weight ≈ impact energy, e.g., impact energy = 0.150 m * 13.50 kg * 9.8 m/s² = 19.86 N•m*). Note: The common international impact level is usually generated using a 1 kg mass dropped from a height of 1 meter, but the height of 150 mm is used here to simplify comparisons to tests specified by FOTP-25.

Table 1 - Drop hammer mass/test impact energy in current impact standard, FOTP-25 [1]

Cable Diameter		Hammer Mass		Impact Energy	
mm	(inches)	kg	(lb)	N•m	(lb•ft)
0 < D ≤ 3.8	(0 < D ≤ 0.10)	0.5	(1.10)	0.74	(0.55)
3.8 < D ≤ 5.3	(0.10 < D ≤ 0.25)	1.00	(2.20)	1.47	(1.08)
5.3 < D ≤ 7.5	(0.25 < D ≤ 0.50)	1.50	(3.31)	2.21	(1.63)
7.5 < D ≤ 13.0	(0.50 < D ≤ 0.55)	2.00	(4.41)	2.94	(2.17)
13.0 < D ≤ 15.0	(0.55 < D ≤ 0.59)	3.00	(6.61)	4.41	(3.25)
15.0 < D ≤ 16.6	(0.59 < D ≤ 0.70)	3.50	(7.72)	5.15	(3.80)
16.6 < D ≤ 18.9	0.70 < D ≤ 0.79	4.00	(8.82)	5.88	(4.34)
18.9 < D ≤ 21.4	(0.79 < D ≤ 0.90)	4.50	(9.92)	6.62	(4.88)
21.4 < D	(0.90 < D)	5.00	(11.02)	7.35	(5.42)

Table 2 - Drop hammer mass/test impact energy in proposed revision of FOTP-25 [2]

Cable	Hammer Mass		Impact Energy	
Application	kg	(lb)	N•m	(lb•ft)
Outside Plant	3.0	(6.6)	4.41	(3.35)
Riser	2.0	(4.4)	2.94	(2.17)
Plenum	2.0	(4.4)	2.94	(2.17)
Drop Cable	2.0	(4.4)	2.94	(2.17)
Interconnect	0.5	(1.1)	0.74	(0.55)

Note: 1 N•m = 1 Joule.

3. Effect of Proposed FOTP-25 Revisions

3.1 Impact Resistance of Traditional Outside Plant and Premises Cables

As mentioned previously, impact requirements currently implemented for OSP cables have been more stringent than those for Premises cables. The proposed revisions continue this trend, incorporating the majority of the values used in GR-409 (Table 3). This difference in performance requirements has most likely evolved for two reasons: 1) operating environment, and 2) mechanical limits of fire retardant jacket materials. The environment in which OSP cables are expected to operate successfully generally is accepted as much more hazardous during installation and in field-life. Whether it be from falling tools or rocks, OSP cables are designed to resist significant impacts. Conversely, Premises cables are installed in much friendlier environments, with stray knocks from tools or slaps against spools or reels being the most likely impact scenarios. As a result, Premises cables are not expected to be as rugged as OSP cables. Added to this, some dominant requirements for Premises cables are those related to fire codes (flame retardant, low smoke generation, etc.). The polyethylene materials used in OSP products burn like fuel, so materials selected to meet fire codes do not include PEs but PVCs and heavily filled EVAs. PVCs can be very brittle in impact. Filled materials generally have reduced moduli (very soft) which increases the potential for jacket splitting, especially when jacketing layers are thin. Thus, lesser impact requirements for Premises cables have become acceptable in favor of better fire resistance characteristics.

Unlike Premises cables, the impact capabilities of most OSP cables *significantly* exceed - by double or more - even their own current requirements. Still, the proposed revision to the standard significantly reduces the impact requirements for many OSP cables (for all those with an OD of 15 mm (0.60") or larger). This lowering of standards might be of greater concern, but the other requirements -- including crush resistance, cyclic flex performance, cold temperature bend -- which govern the design of OSP cables are most likely to generate cables that maintain the current level of impact resistance.

However, cables designed to operate in both OSP and Premises environments may be of concern. The issues related to multi-environment cables are discussed in the next section.

Table 3 - Drop hammer mass/test impact energy in Telcordia GR-409 [3]

Cable	Hammer Mass		Impact Energy	
Application	kg	(lb)	N•m	(lb•ft)
Riser Cable	4.00	(8.82)	5.88	(4.34)
Plenum & General Purpose Cable	2.00	(4.4)	2.94	(2.17)
General Purpose Interconnect Cables	0.50	(1.10)	0.74	(0.54)
General Purpose Undercarpet Cables	16.00	(35.20)	23.5	(17.3)

3.2 Issues with Impact Standards and New Multi-Environment Cables

The concern with new multi-environment cables is that neither the current nor revised standard will identify impact problems at *low temperatures*. Historically, impact (and other) testing at low temperatures directly has not been required for OSP cables, although other cable properties are tested at temperatures as low as -40 °C. This practice has been "safe" because OSP cables are designed to meet enough other requirements (UV and environmental aging, crush and tensile strength) that promote the choice of materials (e.g., polyethylene) and design structures that behave very well in impact, even at low temperatures. In fact, standard, polyethylene-jacketed OSP cables can pass the FOTP-25 test at -40 °C with no problem.

In contrast, the dominating requirements for Premises cables are those related to fire codes, as discussed in the last section. OSP's polyethylene burns like fuel, so PVCs and filled EVAs are chosen as Premises jacket materials instead. Low temperature performance in bending is only considered down to --20 °C, at the very lowest, and most other mechanical tests — including impact —are performed at ambient temperature. But, as mentioned, PVCs can be very brittle in impact, *even* at room temperature. Highly filled materials can also have problems at low temperatures unless an appropriate base resin is selected. As a result, multi-environment cables inherit the weaknesses of Premises cables in impact scenarios, yet these Premises-biased products must also perform adequately at low temperatures. As cables are not currently tested for cold temperature impact, this vulnerability may remain uncovered until field problems occur.

The next section looks at some current multi-environment cables.

4. Current Multi-Environment Cables

Over the last couple of years, multi-environment cables have been introduced in two contexts, those using the tight buffered fibers of Premises cables and those using non-buffered or ribbonized fibers of OSP cables. The first type is referred to in this paper as Indoor/Outdoor - indoor or Premises products that are also capable of being used in an outdoor environment. Conversely, Outdoor/Indoor cables are OSP cables that are fire-rated for the indoor environment. Thus, either type can be installed building-to-building or building-to-OSP node without special termination or use requirements in either environment.

4.1 Indoor/Outdoor Cables - Plenum and Riser Rated

Both plenum and riser-rated Indoor/Outdoor cables have been introduced in the market place. Of those, some use PVC-type jacketing materials, while others use EVA materials heavily filled with fire-retarding $Mg(OH)_2$ (magnesium hydroxide) or ATH (aluminum trihydrate). An example of an EVA jacketed cable is shown in Figure 2. Of the two fire ratings for cables, plenum rated cables have more stringent fire requirements. As a result, LSPVC (low smoke PVC) or PVDF (polyvinylidenefluoride) are the preferred materials.

PVDF, as opposed to LSPVC, is best suited for plenum rated indoor/outdoor or outdoor/indoor cables. The high amount of plasticizer required to keep the PVC flexible at low temperatures can cause additional smoke generation in the UL910 Steiner Tunnel test. In contrast, with PVDF, there are co- and terpolymer grades that not only provide fire retardancy and low smoke generation, but also produce a highly weatherizable, tough, and crack resistance jacket, even at low temperatures.

4.2 Outdoor/Indoor Cables - Plenum and Riser Rated

Several Outdoor/Indoor cables are on the market, two of which were presented in papers in the proceedings of IWCS 99. One of these was a Outdoor/Plenum cable with a loose tube construction [4] and the other was a Riser-rated, OSP central core ribbon cable [5]. The riser-rated cable design is shown in Figures 3. This cable also uses the highly filled EVA jacket material.

Using the cables pictured in Figures 2 and 3, as well as other commercial cables, the next section will discuss a series of impact test scenarios that can be used to highlight the issues associated with the impact performance of multi-environment cables. The test data presented is intended as a reference for future standard developments and revisions.

5. Impact Testing of Multi-Environment Cables

As discussed in Sections 2 and 3, the evolution of the impact standards to date may leave multi-environment cables vulnerable to

impact. In essence, this vulnerability may not be because the cables are poor performers under the existing or revised FOTP-25 requirements, but because this FOTP-25 is no longer adequate to screen for all realistic impact failures -- most notably, cold impact failures. Therefore, data (where available) from three test scenarios are used to evaluate the adequacy of current and proposed impact resistance standards: 1) cable performance under the current standard, 2) cable performance under the proposed standard and 3) cable performance in cold impact. The current and proposed requirements are shown in Tables 1 and 2, respectively. The cold impact testing was done with the impact values used in the proposed FOTP revision (Table 2), but at a series of temperatures lower than the standard room temperature requirement (see Table 4). These sub-ambient temperature impact tests were completed from *inside* the environmental chamber.
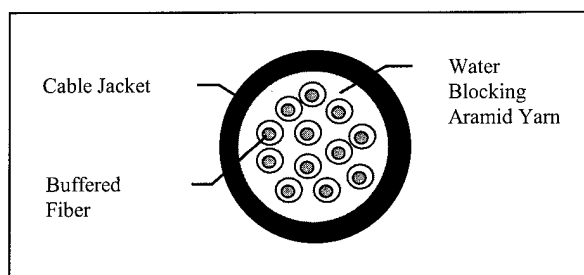
Figure 2. Lucent Indoor/Outdoor Cable
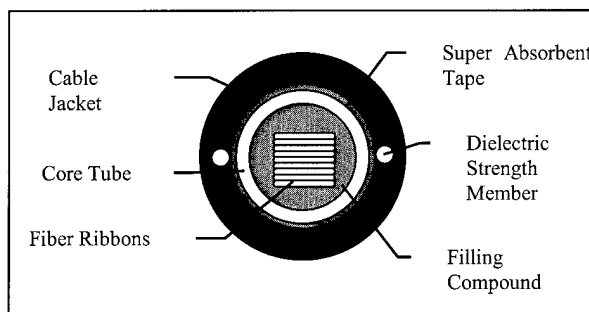
Figure 3. Lucent Outdoor/Indoor Cable

6. Test Data

The collection of test data from the assortment of Indoor/Outdoor and Outdoor/Indoor cables tested is shown in Table 4. The cables are grouped by application type (OSP, O/I, I/O and Premises). Cables 1 and 9 are included as benchmarks of normal OSP and Premises cable performance, respectively. The data shown in the table were collected either from in-house testing or public documents published by the cable manufacturer [4, 5].

The first test scenario of concern is defined by the appropriate requirements from GR-20 and GR-409 (Tables 1 and 3) and ambient temperature. Pass/fail data from this scenario is available

Table 4 - Data from impact tests conducted at various operating temperatures

Cable No.	Cable Type	Jacket Material Type	Test Masses, kg, GR-409/GR-20 (highest mass in revised FOTP-25)	Temperature at Impact (°C) (sub-ambient tests used newly proposed test masses)						
				Ambient Temp*	10	0	-10	-20	-30	-40
OSP CABLE										
1	Lucent **OSP** Cables	HDPE and MDPE with 2.5% carbon black	**4.00** *(OSP, 3 kg)*	**pass**	**pass**	**pass**	**pass**	**pass**	**pass**	**pass**
O/I CABLE										
2	**O/I Cable -** Plenum Rated (12 fiber) [4]	Plenum flame retardant and UV resistant mat'l	**2.00/1.50** *(OSP, 3 kg)*	**pass/pass**	*NR*	*NR*	*NR*	*NR*	*NR*	*NR*
3	**O/I Cable -** Plenum Rated (72 fiber) [4]	Plenum flame retardant and UV resistant mat'l	**2.00/2.00** *(OSP, 3 kg)*	**pass/pass**	*NR*	*NR*	*NR*	*NR*	*NR*	*NR*
4	Lucent **O/ I Cable** - Riser Rated [5]	Highly filled EVA	**4.00/4.00** *(OSP, 3 kg)*	**pass/pass**	*TBT*	*TBT*	*TBT*	*TBT*	*TBT*	*TBT*
5	**O/I Cable A -** Riser Rated (12-fiber)	PVC-type	**4.00/3.00** *(OSP, 3 kg)*	**pass/pass**	*TBT*	*TBT*	**FAIL**	**FAIL**	**FAIL**	*TBT*
6	**O/I Cable B -** Riser Rated (12-fiber)	PVC-type	**4.00/2.00** *(OSP, 3 kg)*	**pass/pass**	*TBT*	*TBT*	**FAIL**	**FAIL**	**FAIL**	*TBT*
I/O CABLE										
7	**I/O Cable A -** Riser Rated (12-fiber)	PVC-type	**4.00/1.50** *(OSP, 3 kg)*	**FAIL/ pass**	*TBT*	*TBT*	**FAIL**	**FAIL**	**FAIL**	*TBT*
8	Lucent **I/O Cable** - Riser Rated (12-fiber)	Highly filled EVA	**4.00/1.50** *(OSP = 3 kg)*	**pass/pass**	*TBT*	*TBT*	**pass**	**pass**	**pass**	*TBT*
PREMISES CABLE										
9	Lucent **Premises** Cable -Riser-Rated	PVC	**4.00** *(Riser, 2 kg)*	**pass**	*TBT*	**FAIL**	**FAIL**	**FAIL**	*TBT*	*TBT*

* Cables were tested at ambient temperature, which is 23 °C ± 5 °C.

Note: *NR* = No data reported by product manufacturer.

   TBT = To be tested. (Data planned for presentation at IWCS 2000.)

for all cables. The expectations of Cables 1 and 9 are governed by GR-20 and GR-409, respectively, and perform successfully. Being multi-environment cables, Cables 2 through 8 are subject to the requirements of both standards and in all but one instance meet both sets of requirements (the test masses of these multiple requirements are listed in the fourth column of Table 4). The exception among those evaluated at ambient temperature was Cable 7. It was a smaller diameter cable and passed the

diameter-dependent requirement for OSP cables, which uses a 1.5 kg mass. However, the Premises Riser requirement uses a 4 kg mass, regardless of diameter, and caused one of the fibers in this cable to break. The second test scenario of concern is cable performance at ambient temperature based on the proposed revision to the FOTP-25. For all but three cables, the current requirements equal or exceed the new requirements. However, the performance of Cables 2, 3, and 7 is unknown under the new requirements as the proposed generic test mass for OSP cables (3 kg) would exceed that for either of the current OSP or Premises tests. Additional testing is ongoing

Shifting to the cold impact testing and the third test scenario, tests were completed inside an environmental chamber using the masses included in the proposed FOTP-25 revision. As expected, the cable designed primarily for an outdoor environment (Cable 1) performed well at low temperatures. The basic Premises cable (Cable 9) did poorly, also as expected. The potential for vulnerability in cold impact for other Premises-like cables was demonstrated by Cables 5, 6, 7, and 9. However, the success of Cable 8 shows that suitable jacket materials are available for multi-environment cables.

Spurred by the data presented in Table 4, additional testing is ongoing to generate a more complete set of data. A more comprehensive set of data will identify the transitional temperatures for each material, and thereby identify which materials are suitable only for a Premises environment and which can survive in an OSP environment as well.

It is worth particular mention that the cold impact tests were carried out with one key procedure: the test apparatus was set up inside the environmental chamber. It was found that even the short amount of time needed to remove a cable sample from a cooling chamber and place it in a room-temperature test set was enough to allow the cable sample to warm significantly -- significantly enough for some cables to "pass" the test when they failed a test that was completed inside the environmental chamber.

Also of note is the discovery that at low impact loads the commonly-used impact test apparatus designs have shown sufficient parasitic losses to render the results invalid. In the current apparatus, the test mass slides down a post to the sample. When a relatively heavy mass is used, the frictional energy losses caused by the guide shaft are not an issue. In contrast, friction can greatly reduce the effective impact on the sample when smaller masses are used. Further, these discrepancies in effective impact can go undetected because no calibration method is recommended. However, there are a number of ways that an apparatus could be calibrated, including using a calibrated spring to measure actual deflection under impact, and thereby the actual energy of impact. Therefore, it is recommended that methods for calibration be included in a future revision of the standard. For now, the currently proposed

revision to FOTP-25 contains language cautioning users on the effect of parasitic losses.

7. Conclusions

The impact test data presented in this paper clearly indicates that cold impact performance is poor for multi-environment cables. However, the testing also identifies that some good choices for multi-environment jacket materials are available and have been used -- knowingly or not.

So, with the advent of cable products designed to cross the boundaries between traditional OSP and Premises application areas, the authors believe the time has come to introduce standard low temperature impact test requirements for multi-environment cables—and Premises cables. The specific values would reflect the actual performance of cables that have demonstrated acceptable performance in service. If nothing else, the test would serve as a defense for cables that traditionally have been expected to perform poorly in colder environments. Proposals to introduce cold impact standards have been made and are being debated in Industry standards working groups. The data and notes on test procedure included in this paper should provide useful information for the development of this proposed test standard.

8. Acknowledgments
The authors thank Sherrie Gentry, Joe Edmondson, Ernest Swann, and Rick Norris for their assistance in cable testing and data collection.

9. References
[1] TIA/EIA-455-25B, *Repeated Impact Testing of Fiber Optic Cables and Cable Assemblies*, September 1996.

[2] TIA PN-4600, Committee Letter Ballot of proposed revision TIA/EIA-455-25C, *Repeated Impact Testing of Fiber Optic Cables and Cable Assemblies.*

[3] Telcordia GR-409-CORE, Issue 1, *Generic Requirements for Fiber Optic Cable,* 1994.

[4] D.A. Keller, et. al., "Continued Development of The Plenum-Outdoor Totally Dry Optical Fiber Cable Designs," *Proceedings of the 48th International Wire & Cable Symposium,* 1999, pp. 409-415.

[5] R.H. Norris, et. al., "Development of a Riser Rated Outdoor/Indoor Central Tube Ribbon Cable," *Proceedings of the 48th International Wire & Cable Symposium,* 1999, pp. 134-140.

Authors
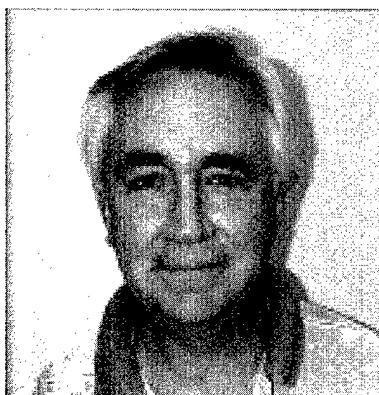
Richard D. Beggs, Lucent Technologies, Inc.
2000 NE Expressway, 1D-51, Norcross, GA 30071

Richard D. Beggs is a Member of Technical Staff with Lucent Technologies, Inc. Bell Laboratories, Norcross, GA. He holds a BSME from Iowa State University. He has worked in cable design and development for more than twenty years and holds a number of patents in product design.

Michael D. Kinard, Lucent Technologies, Inc.
2000 NE Expressway, F050, Norcross, GA 30071

Michael D. Kinard is a Senior Development Engineer and Distinguished Member of Technical Staff with Lucent Technologies, Inc. Bell Laboratories, Norcross, GA. He holds a BSME from Old Dominion University and an MSME from Georgia Institute of Technology. He was worked in cable design and development for more than twenty years. He holds a number patents in the cable design and processing area.

Lisa A. Dixon, Lucent Technologies, Inc.
2000 NE Expressway, 1E-47, Norcross, GA 30071

Lisa A. Dixon is a Member of Technical Staff with Lucent Technologies, Inc. Bell Laboratories, Norcross, Georgia. Dr. Dixon joined Lucent Technologies in 1997 in the capacity of Development Engineer. She received her B.S. degree in Engineering Science from Trinity University, an International Diploma from Imperial College, London, UK, and M.S. and Ph.D. degrees in Mechanical Engineering from Georgia Institute of Technology. She is currently working in the area of Outside Plant Cable design and development.

Paul E. Neveux, Jr., Lucent Technologies, Inc.
2000 NE Expressway, 2G-02, Norcross, GA 30071

Paul E. Neveux, Jr. obtained his Ph.D. in Chemistry from the University of North Carolina at Chapel Hill. After a post-doctoral fellowship at Duke University, he was a Senior Design Engineer and Materials Laboratory Supervisor at Sumitomo Electric Lightwave Corp in Research Triangle Park, NC from 1986 to 1997 working on optical fiber outside plant cable materials. Currently, Paul works in the Premises Cable Materials Group of Bell Labs in Norcross, GA, focusing on the use of fluoropolymers for both optical and copper LAN cables.

Flexural Rigidity Analysis of Optical Fiber Cable

Bradley J. Blazer
Research, Development & Engineering, Corning Cable Systems
Hickory, NC
+1-828-323-6239 · bradley.blazer@corning.com

Abstract

The ability to measure and predict the flexural rigidity or stiffness of various cable designs is an important consideration when seeking to improve installation efficiency. Since cable stiffness is also a variable required by some installation modeling software, it can be expected that customers will demand accurate stiffness data as cable system designers seek to maximize pull lengths. Several measurement methods were studied and a procedure based on the 3-point apparatus was selected. Test results from various cables and their components were used for comparison and as an aid in predicting the stiffness of future cables. The effects of temperature and bending rate on cable stiffness were also investigated and found to be very significant. Field trials confirmed the major effect that cable stiffness has on duct installation.

Keywords

Flexural rigidity, flexure, stiffness, moment, inertia, modulus, bending, duct installation

1. Introduction

Bending theory, material properties and practicality were considered in evaluating and selecting a test procedure for cable stiffness. A method of stiffness prediction was also developed which provided useful insight for cable design considerations. Real world installation conditions were considered when evaluating cable stiffness and its effects on the end user.

2. Mechanics of Bending

2.1 Bending Theory

When a cable is bent, the region on the outside of the bend experiences tensile strain and the region on the inside of the bend experiences compressive strain. The boundary between the tensile region and the compressive region is called the neutral axis. The strain at any point is proportional to the curvature of the bend and the distance from the neutral axis. The stiffness contribution of any element is proportional to modulus, amount of strain, cross-sectional area and distance from the neutral axis (note that for a simple round rod radius will be raised to the fourth power.) For the cable to be in equilibrium, the stiffness of the tensile and compressive regions must be equal. Since most cables are symmetrical about their center the neutral axis will pass through the center of the cable. Some materials such as aramid reinforced plastic have a tensile modulus that is significantly higher than their compressive modulus. As a result the neutral axis will shift in the direction of higher modulus to

achieve equilibrium. A cable with a preferential bend has a minimum stiffness along one axis and a maximum stiffness along the orthogonal axis. Following a preferential bend will minimize the distance between high strength elements and the neutral axis.
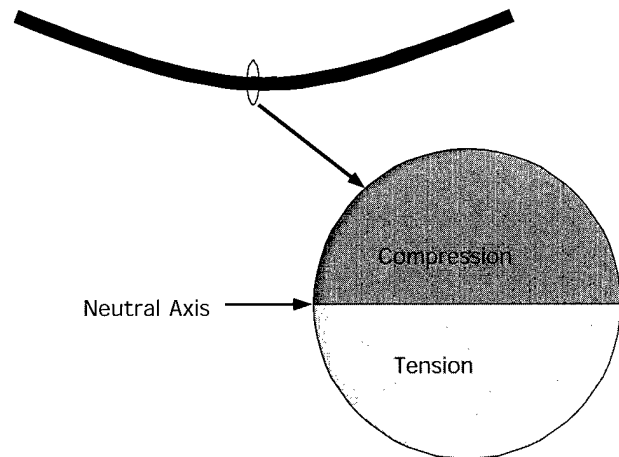
Figure 1 Bending stresses

2.2 Stiffness Calculations

2.2.1 Equations Following is a list of equations required for most stiffness calculations[1,2]:

$$\text{Stiffness}: \quad B = EI \qquad (1)$$

Where B = Stiffness, E = Young's modulus and I = moment of inertia.

$$\text{Moment of Inertia}: \quad I = \int_A y^2 dA \qquad (2)$$

Where y = distance from neutral axis and A = cross-sectional area.

For a cylinder:

$$I = \frac{\pi D^4}{64} \qquad (3)$$

For a hollow cylinder: $\quad I = \dfrac{\pi(D_o^4 - D_i^4)}{64} \qquad (4)$

For a sub-element with some distance y from its neutral axis to the neutral axis of the cable:

$$I = I_0 + Ay^2 \qquad (5)$$

2.2.2 Assumptions A typical fiber optic cable composed of tensile/anti-buckling strength elements, plastic fiber protecting elements and a protective outer sheath acts as a composite structure in bending. Good stiffness predictions were obtained were by assuming that all solid elements act as a unit and by neglecting the contributions of loose elements such as fiber or yarns. A special case is the stranded steel wire used as a tensile/anti-buckling element in some cable designs. The stiffness of such elements is a function of partial coupling due to stranding and plastic up-jacketing.

2.3 Modulus in Bending

Elastic elements such as solid steel wire are very predictable in bending. The properties are well known and they perform predictably. The properties of plastics are not as well defined. Performance data can be hard to find or incomplete especially in light of the large variations in modulus when the bending rate or the temperature changes. An effective method of finding the right modulus value for a plastic or any new material is to test the stiffness of one or more simple elements and back-calculate the modulus. For complex elements such as the stranded wire mentioned above, which occur in various sizes but with the same geometry, it is convenient to assign an effective bending modulus.

3. Test Apparatus

There are several styles of test apparatus appropriate for testing outdoor cables. IEC 60794-1-2[1] describes 3-point and cantilever tests. ASTM D790-98[3] also describes a 4-point test. The 3-point and cantilever tests were chosen for evaluation. Evaluation criteria included precision and accuracy, simplicity and ease of use.

3.1 3-Point Test

The 3-point test apparatus is strong in simplicity and accuracy. Some simple modifications to the apparatus make it the top choice in precision and ease of use also. The cable sample is placed between two end supports and a central loading nose (connected to a load frame) is used to deflect the sample. The load frame then provides force vs. deflection (F/y) data. Stiffness is calculated from this data using the equation[1]:

$$B = \frac{L^3 F}{48y}$$ (6)

3.1.1 3-point Apparatus Details The accuracy advantage of the 3-point apparatus comes from the constant bending moment reference length for bending moment provided by the fixed distance between the end supports and the loading nose. A penalty for this is the sliding friction between the cable and the end supports. Furniture polish was applied to the cable sheath for initial trials and bearings were subsequently added to the end supports to allow them to roll freely. A shallow v-profile was machined into the cylindrical loading nose and end supports to aid in sample alignment. This self-aligning feature also made it possible to test cable samples by bending either with or against

pre-existing curvature. There was no discernable difference in measured stiffness based on amount or direction of pre-existing curvature within reasonable limits.

End Support Detai l
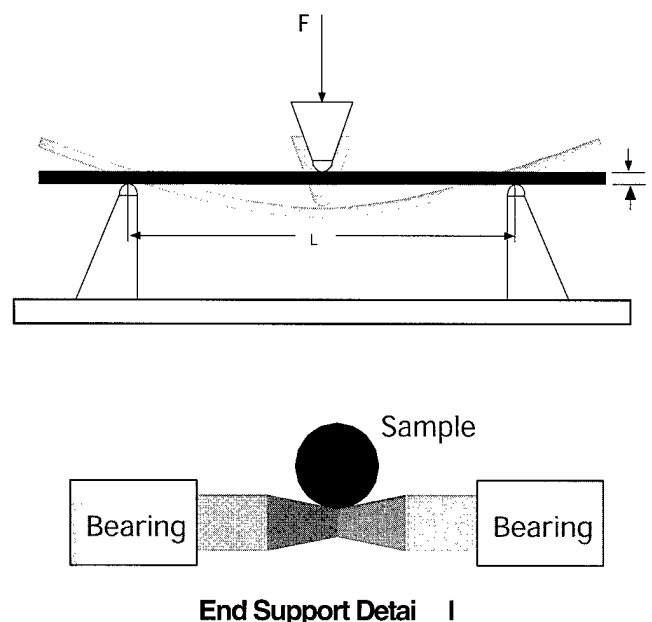
Figure 2. Apparatus for 3-point test

3.2 Cantilever Test

The cantilever test apparatus produces a bending geometry similar to half of the 3-point geometry. The sample is clamped at one end and a load is applied at the other end. The equation[1] for stiffness from the cantilever test results reflects the fact that measured force and length are cut in half compared to the 3-point test:

$$B = \frac{L^3 F}{3y}$$ (7)

3.2.1 Cantilever Details This apparatus initially appeared promising with respect to shorter required sample length, the stability provided by the clamp and the ability to eliminate frictional effects by using a pivoting link to apply the load. The major disadvantage came to light when investigating the effects of pre-existing cable curvature: Stiffness results when bending against the pre-existing curvature were lower than results obtained when bending with the pre-existing curvature. The cause becomes apparent when one considers that the path of the point of application of force was actually an arc. The effective moment-arm length changed along this path and affected the result. A rolling support on the loading nose such as that described for the 3-point end supports may alleviate this problem. Test setup was another disadvantage of the cantilever apparatus since each cable size required a different clamp insert and alignment with respect to pre-existing curvature was critical to avoiding torsion effects.
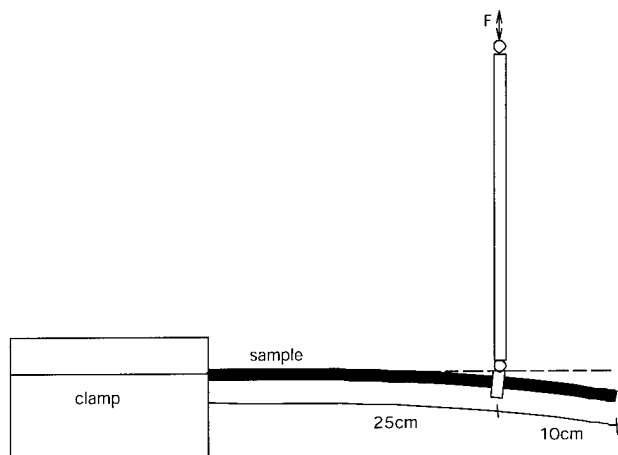
Figure 3. Apparatus for cantilever test

very significant effect on measured stiffness. The logarithmic curve fit is typical of viscoelastic behavior. An observed advantage of testing at high bending rates was a reduction in standard deviation of the test results. The plastic materials appeared to behave in a more linearly elastic, predictable manner as rate was increased.

Rate Variatioı
30mm SCR cak

$y = 0.7982Ln(x) + 5.0$
$R^2 = 0.9964$

Displacement Rate (mm/ı

• Measured Stiffness N•sq.ɪɐ Log. (Measured Stiffness N•s
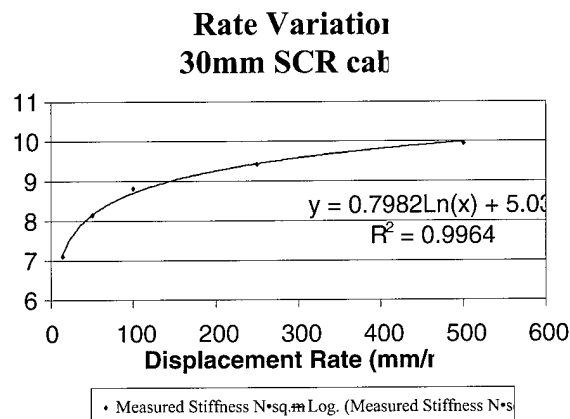
Figure 5. Bending rate variation

3.3 4-point Apparatus.

No testing was conducted using a 4-point apparatus but it does warrant discussion. The configuration is similar to the 3-point apparatus but with two loading noses equidistant from the center. Advantages are lower sidewall pressure at the loading noses and a center region that, except for error caused by friction, experiences pure bending (no shear stress). A caveat to the pure bending region is that no direct measurement of deflection occurs there.

Figure 4. Apparatus for 4-point test

4. Test Parameters

4.1 Test Rate

The primary purpose of the stiffness testing that was conducted was to predict cable behavior during installation. Since bending rates during a typical cable pull far exceed the capacity of most load frames the highest practical rate was selected. At the highest test speeds a flying start may be required to allow the machine to accelerate to full speed before contacting the test sample. The variation of stiffness with bending rate is a function of the properties of the plastics incorporated in the cable and their contribution to the overall cable stiffness. As shown in the graph, test rate can have a

Although strain rate also varies with radius within the cable, the effect on modulus is accounted for in the moment of inertia calculation when predicting stiffness. As a result, all cables tested at a given *bending* rate can use the same set of modulus values regardless of cable diameter. For this reason it is not appropriate to adjust the test rate to achieve a standard maximum strain rate such as the 1%/min described in ASTM D 790-98[3] and other standards for material testing.

4.2 Sample Length

The span length of the sample under test can have two significant effects. The bending rate is inversely proportional to sample length therefore the length must be limited to achieve a bending rate similar to that seen in the field. On the other hand the ratio of length over diameter must be large enough to eliminate excessive shear deflection during the test. The 16:1 ratio described in ASTM D790-98[3] for the 3-point test (equivalent to 8:1 in the cantilever test) is a good guideline for the largest cable diameters in a given category. Smaller cables within the same category should be tested with the same sample length to maintain a standard bending rate.

4.3 Temperature Effects

When comparing cable designs, it is useful and reasonable to observe stiffness at standard temperature. Actual field conditions, however, may vary considerably with typical recommended installation temperatures of –20°C to +50°C. The limiting condition will most likely be the lower end of the temperature range where stiffness can be 2-3x larger than at room temperature. A 1000F SCR cable was tested over a range of temperatures to investigate the effects of temperature on cable stiffness. The change in stiffness vs. temperature was also calculated based on secant modulus vs. temperature data from the resin supplier[4]. In this prediction the supplier data was used to estimate the

fractional change in modulus vs. temperature with a room temperature modulus derived from experimental data. It should be noted that sample conditioning at the test temperature is a requirement for repeatable results.

Stiffness vs. Temperature
1000F SCR Cable
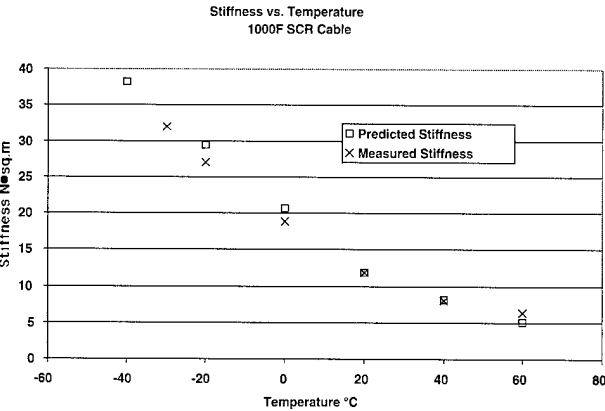
Figure 6. Temperature effects

5. Test Results

A variety of cables were tested and the measured stiffness was compared to the predicted values. The initial, most nearly linear portion of the load vs. deflection data was used in the calculation of measured stiffness. Final testing was conducted using the 3-point apparatus. Sample length was 300mm for low fiber count cables and 500mm for high fiber count cables. The test rate was 250mm/min for all samples. All predicted stiffness calculations in figure 7 were found using same empirical modulus values by changing only the cable dimensions.
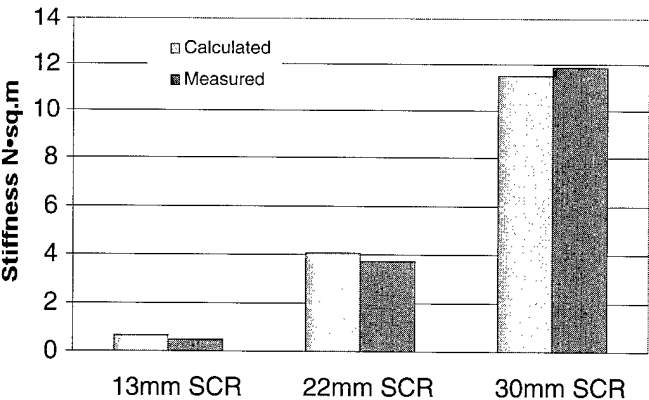
Figure 7. Calculated and measured stiffness

One of the more interesting aspects of the investigation was the relative stiffness contribution of each cable component. .In nearly every cable design, the jacket is the biggest contributor to stiffness. This should be no surprise considering that stiffness is proportional to the fourth power of diameter. The calculated stiffness against the preferential bend of the single tube designs is a factor of ten larger than the minimum stiffness that is reported.
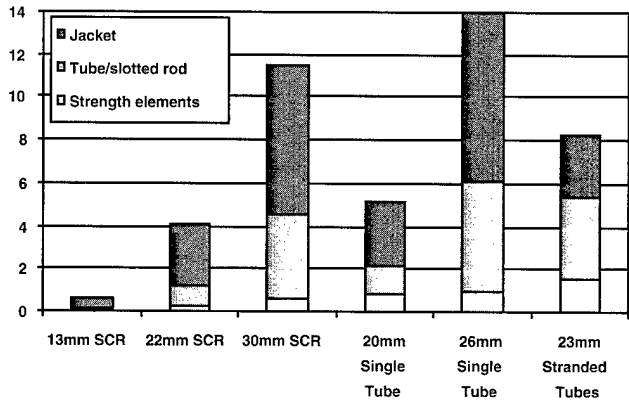
Figure 8. Stiffness contributors

6. Field Comparisons

In field studies presented by Lail and Logan[5] that examined the effect of stiffness on pulling force, single tube cables were manufactured with and without steel armor to produce a 30-50% variation in measured stiffness with the same outer diameter. The samples were then installed in a variety of duct cable routes utilizing conventional winches and air-assisted installation. The results showed that the cable property of stiffness was second only to diameter in its effect on pulling force. The change in pulling force due to stiffness closely matched the predicted values (see figure 9). This data underscores the importance of accurate stiffness data when predicting maximum installation lengths.

Pulling Forces - Inner Duct

Relative Cable Stiffness	Actual Difference lbs(kg)	Pred.Diff. Eqns 1/2 lbs(kg)	Pred.Diff. Eqns 1/2/3 lbs(kg)
10/15	100(45)	40(18)	100(45)
15/20	140(64)	60(27)	140(64)

Figure 9. Pulling force comparison from presentation by Lail and Logan[5] which demonstrates the effect of stiffness on pulling force predictions.

Weight/Frictional Forces

Equation #1

$$F_w = fWL + F_B$$
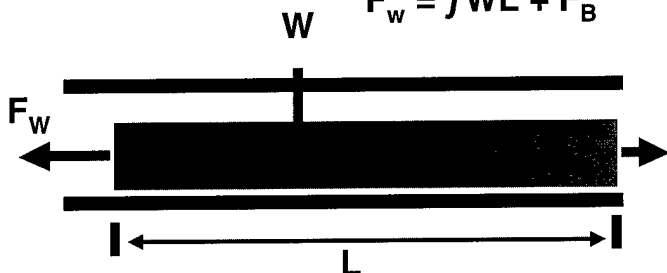
Bending Forces (High Tension)

Equation #2

$$F_{HTB} = F_B e^{f\theta}$$
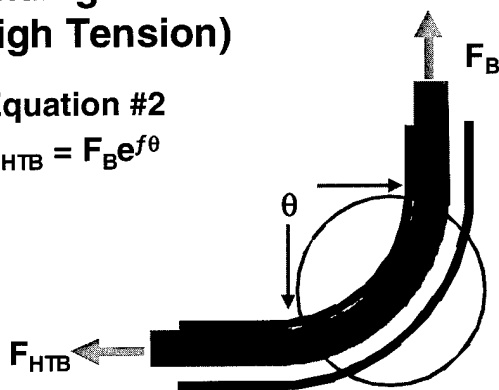
Bending Forces (Low Tension Bend)

Equation #3

$$F_{LTB} = \frac{2Bf}{(6*(D_d-D_c)R_B^3)^{0.5}} + F_B$$
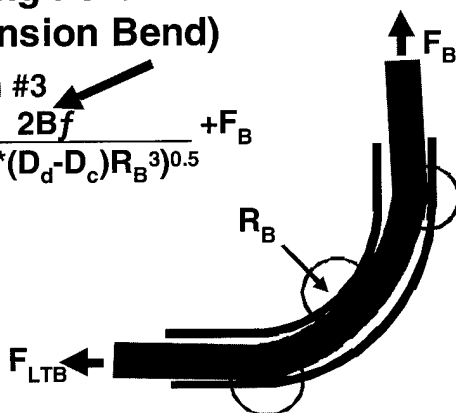
Figure 10. Equations presented by Lail and Logan depicting theory of duct pulling calculations.

7. Conclusions

Historically, cable flexural rigidity or stiffness has frequently been an ignored or unreported cable property. Today as installation costs are receiving more scrutiny, stiffness is emerging as an important factor to consider.

- In this investigation, the 3-point apparatus was found to provide the most elegant method of obtaining accurate, repeatable and predictable test results. Bending rate and temperature were found to be the biggest factors affecting test results. The significant effect of temperature on stiffness is also an important consideration for planning and methods of cold weather installation.

- When predicting cable stiffness, bending modulus for plastic components is best obtained through actual bending tests but published properties can be very useful in assigning relative values. When designing cables to minimize stiffness, the relative contribution of each component must be considered, especially for the outer layers.

- Cable stiffness is a major factor affecting ease of installation in ducts. Accurate stiffness values are a requirement when estimating duct-pulling requirements. Accurate estimates of duct pulling requirements can help to save material and installation costs while ensuring the reliability of installed cables.

8. Acknowledgements

NTT Japan is acknowledged for guidance and coordination in evaluating supplier input and establishing a detailed test specification for cable stiffness.

Special thanks to Eric Caldwell of Corning Cable Systems for his testing services and test method evaluation.

9. References

[1] IEC60794-1-2, "Optical Fiber Cables-Part 1-2: Generic Specification – Basic Optical Cable Test Procedures" International Electrotechnical Commission, 1999, pp. 91-99

[2] J. Gere and S. Timoshenko, *Mechanics of Materials,* 2nd ed., PWS-Kent, Boston, pp.740, 761, 771, (1990)

[3] ASTM D790-98,"Standard Test Methods for Flexural Properties of Unreinforced and Reinforced Plastics and Electrical Insulating Materials", American Society for Testing and Materials, 1999

[4] "DHDA-8864 Black 9865" Union Carbide Corporation, 1997

[5] J. Lail and E. Logan, "Maximizing Fiber Count in 31.8mm (1.25inch) Duct*" NFOEC Technical Proceedings,* Volume 1 p.169-180 (2000)

Presenting Author

Bradley J. Blazer is a Development engineer in the Japan cable group at Corning Cable Systems RD&E in Hickory, NC. His responsibilities include product and process development of slotted core ribbon cables. He received a B.S.M.E. degree from North Carolina State University in 1992. He was an Instructor at the US Navy Nuclear Power School from 1992 to 1996. He joined Siecor, now Corning Cable Systems in 1991 as a field engineer where he led several installation projects and taught numerous hands-on installation courses. Since moving to RD&E in 1999, Bradley has worked on product and test procedure development. He is currently working on process and product development for SZ-SCR cables.

Static and Kinematic of High Fiber Count Ribbon Cables

Andreas Stingl
CCS RD&E 4
Neustadt / Coburg, Germany
+49-9568-93-2494 · Andreas.Stingl@Corning.com

Abstract

In fiber optic cables, fiber strains and fiber compression, as well as lateral contact pressure are the dominant reasons for attenuation increase. Furthermore high fiber strains reduce the fiber lifetime and the reliability of the system. Considering ribbon cables, due to stranding, temperature or bending load, a complex stress strain distribution may occur. Especially the ribbon geometry depicting both, axis of high and low bending stiffness, causes peak strain values at the corner fibers. To reduce the maximum stress each ribbon tries to take the position of minimum potential energy, i.e. each ribbon tends to relax. Whereas this relaxation is important for the function of the cable, the negative side effects are ribbon to ribbon and ribbon to slot interactions, which cause macro- and microbending. To investigate both effects separately two finite element (FE)- models have been developed. An implicit [1] model representing the static strains and an explicit [2] model representing the full kinematic relaxation behavior.

Keywords

finite elements, implicit, explicit, stress, strain, relaxation, macrobending, microbending.

1. Introduction

The goal of the modelling is to achieve the full static stress-strain-distribution of the ribbons as well as the full relaxation behavior, as a function of the major geometric ribbon and cable parameters, f.i. ribbon width, stranding radius, laylength or slot cross-section. The objective is to find a general, flexible and easy to use model to investigate all kind of ribbon cables, f.i. SST, SCR or SZ cable. To achieve maximum flexibility the modelling is based on FE-methods, using analytical functions to describe the stranding geometry. To analyze the static stress-strain-distribution, an implicit large deflection FE-modell, considering just one ribbon has been developed. To investigate the relaxations of the ribbons and their interactions the way is to model a representative portion of the whole cable with the entire set of degrees of freedom (DOF), i.e. without constraining the ribbon DOF in the slot. As all instabilities may occur it is useless to try implicit methods. The way to handle the structural nonlinearities is modelling on the basis of explicit methods [1].

2. FE Modelling
2.1 Basic Idea
The basic idea of Finite Element (FE)-Modelling is to divide the structure of interest into certain portions, the so-called elements.

These elements are connected by nodes. Each node has several degrees of freedom, i.e. displacements and rotations. In the displacement method the node displacements and rotations are introduced as unknowns. The solution is derived from the equilibrium conditions for all nodes, taking into account an appropriate interpolation function for the node displacements and a proper material law for the structure under test.

3. FE Model of a single ribbon
3.1 Ribbon discretization with shell elements
From the structural point of view the ribbon is a composite of different materials, i.e silica glass and polymer matrix material. Therefore a straight forward approach would be a full discretization via brick elements. As the ribbon is a detailed structure, flexible and long the usage of brick elements consumes an enormous amount of elements and CPU time. To achieve a small and flexible model with a minimum CPU time, the ribbon is discretisized with shell elements, i.e the ribbon cross section is reduced to three nodes, independent of the amount of fibers in the ribbon.

Physical ribbon   FE-ribbon
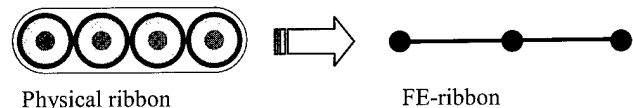
Figure 1. Reduction of a 4 fiber ribbon to 3 nodes

The information about the ribbon width is represented by the maximum distance of the nodes. The ribbon thickness is considered via a parameter d in each node. The youngs modulus E_m is approximated by the moduli E_i and areas A_i of the composite materials via:

$$E_m = \frac{\sum_i E_i \cdot A_i}{\sum_i A_i}$$

From a perspective point of view the ribbon appears like a lattice.

$$N_i = \begin{bmatrix} x_i \\ y_i \\ z_i \\ rotx_i \\ roty_i \\ rotz_i \end{bmatrix}$$
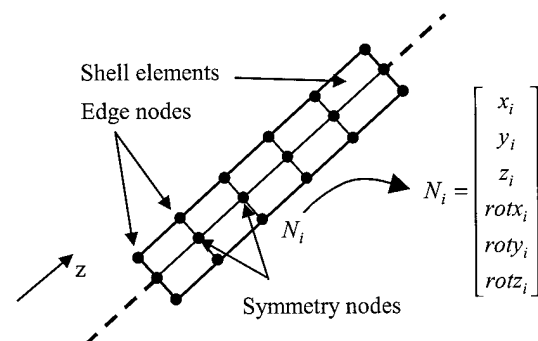
Figure 2. Part of the ribbon modell

The length of the model is about 1000mm, the width of the model is defined by the width of the ribbon. Each node N_i has 6 degrees of freedom, i.e. 3 displacements and 3 rotations. Some of these DOF, especially of the nodes defining the symmetry axis of the ribbon, are used to apply the displacements, derived from the stranding geometry of the cable under test. The residual DOF are unknowns and free to move to the positions of the minimum potential energy consistent with the stranding geometry.

3.2 Modelling an SZ-stranded ribbon

The ribbon model is used, f.i. to investigate the stress and strain distribution of an SZ-stranded ribbon. The stranding geometry of the SZ-cable with sinusoidal profile can be derived via a basic cylindric and cartesian coordinate system:
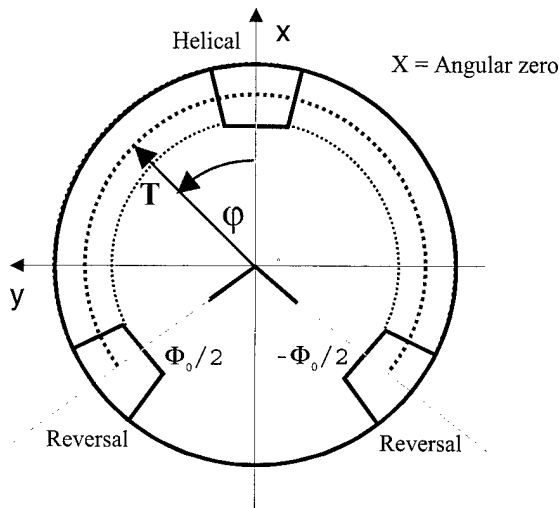
Figure 3. Coordinate system for parametrization of an SZ-layprofile

Fig. 3 depicts a general coordinate system for the parametrization of an SZ stranded layprofile. The z-axis is coincident with the cable axis, x and y-axis are orthogonal to the z axis. The sketch shows the projection of 1 distance between reversals (dbr), 2 reversal and one helical range onto the cable cross section. The orientation of the x-axis (= angular zero) is from the cable center through the midst of the helical. The layprofile is described by a vector T of constant length r_0, swinging around the cables z-axis, describing a line through all middle points of each slot cross section. The maximum angular offsett between reversals is 275.5°, the optimum reversal angle Φ_0.

$$T(z) = \begin{pmatrix} r_0 \\ \dfrac{\Phi_0}{2} \cdot \cos\left(\dfrac{z}{S} \cdot 2\pi\right) \\ z \end{pmatrix} \xrightarrow[y=r\cdot\sin(\varphi)]{x=r\cdot\cos(\varphi)} \begin{pmatrix} r_0 \cdot \cos\left(\dfrac{\Phi_0}{2} \cdot \cos\left(\dfrac{z}{S} \cdot 2\pi\right)\right) \\ r_0 \cdot \sin\left(\dfrac{\Phi_0}{2} \cdot \cos\left(\dfrac{z}{S} \cdot 2\pi\right)\right) \\ z \end{pmatrix}$$

$$\underbrace{}_{\text{Cylindric } T(z)_{r,\varphi}} \qquad \underbrace{}_{\text{Cartesian } T(z)_{x,y}}$$

R_0: Stranding radius   S: Laylength

For a fundamental static investigation it is assumed, that the parametric cartesian coordinates $T(z)_{x,y}$ can be used as displacement boundary conditions to constrain the DOF of the symmetry nodes throughout the whole ribbon model.
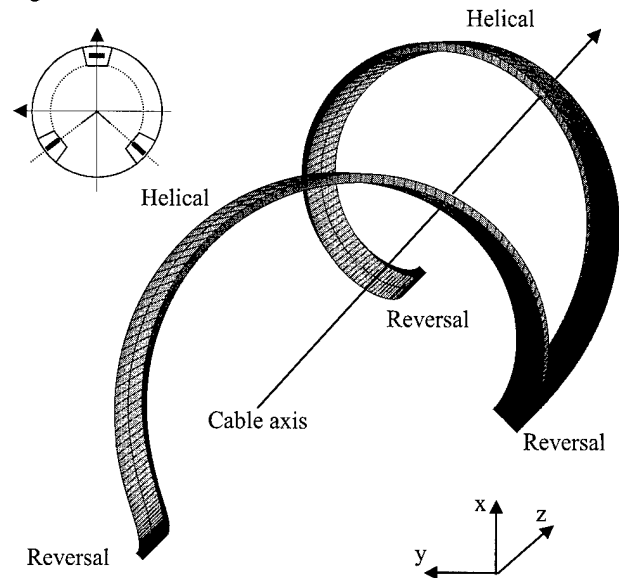
Figure 4. SZ stranded ribbon model

Figure 4 shows an SZ-stranded ribbon model. The original length of the model is 4 DBR, the picture shows 2 dbr. The perspective view is similar to Fig. 3, but for the sake of presentation the model is rotated 1 degree about the x and y axis, either. To minimize shear and torsional forces the natural behavior of the ribbon is backtwist, i.e. in the FE- model the ribbon rotates in the z degree of freedom around the symmetry nodes. A value of interest are the edge fiber strains. These values are derived from the equilibrium position of the corner nodes via:.

$$\varepsilon(z_i) = \frac{D(n_{i+1}/n_i)_f - D(n_{i+1}/n_i)_0}{D(n_{i+1}/n_i)_0}$$

$D(n_{i+1}/n_i)_{f,\,0}$ denotes the distance of adjacent nodes before and after stranding. The value is derived for all nodes as a function of z.
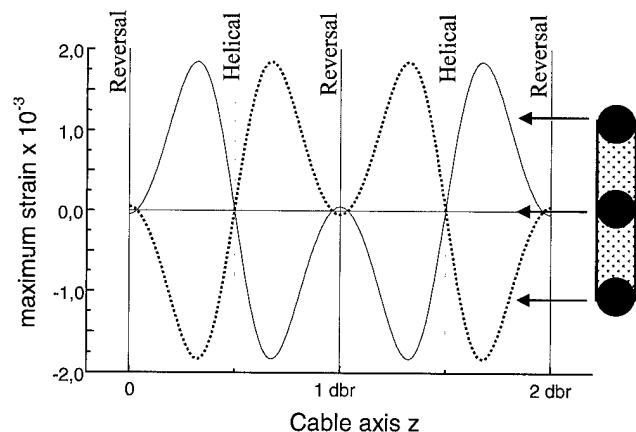
Figure 5. Calculated fiber strain (2 dbr)

Fig. 5 shows the calculated strain distribution of the corner fibers, as well as of the symmetry axis of the ribbon. The strain distribution is symmetric to the ribbon axis. The maximum strain due to bending and torsion appears in between the helical and the reversal points. The values in Fig. 5 are derived for typical cable dimensions. The maximum strain is close to 0.2 percent which is assumed to be the lifetime strain limit. Therefore the strain distribution is used to vary the cable parameters to keep maximum strain low.

Another interesting result derived from this modelling is the reaction force distribution as a function of the cable z-axis. As the stranding function is applied on the symmetry nodes via cartesian displacements, each constrained node n_i has two corresponding reaction force components fx_i. and fy_i. The total reaction force f_{tot} is derived straight forward from these components using the relation:

$$f(z)_{tot} = \sqrt{fx_i^2 + fy_i^2}$$

This force function f(z) is closely related to the contact pressure between ribbon and slot.
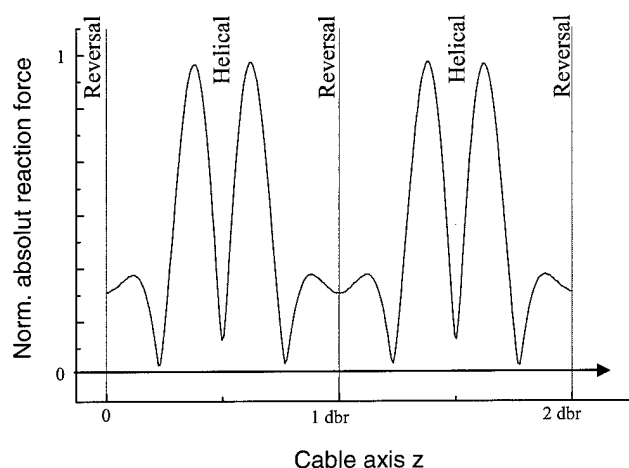
Figure 6. Calculated reaction force (2 dbr)

Fig. 6 shows the calculated reaction force f(z) for 2 dbr. The reaction force shows a maximum value between helicals and reversals. Therefore this range is the distance where the maximum contact pressure between ribbon and slot is to be expected.

3.3 Discussion of the ribbon model
The ribbon modell is based on the assumption, that the stranding function could be generated via static boundary conditions applied directly to the ribbon. The advantage of this method is, that it is sufficient to consider just one ribbon. Therefore the model is very small, consuming few CPU time. This is a big advantage considering parameter studies on a large scale. The disadvantage of just considering one ribbon is neglecting ribbon to ribbon as well as ribbon to slot interactions.

Another disadvantage is the necessity of applying boundary conditions directly to the ribbon, which means to constrain part of the relaxation behaviour. To investigate the full relaxation behavior of a ribbon-cable under stranding, bending, temperature or crush load, a full 3d modell has to be generated containing the whole set of ribbons, describing all their degrees of freedoms within the slot-cross-section.

4. Full kinematic 3d cable modelling
To investigate the relaxation behavior is to consider long, flexible structures, interacting with each other, showing the whole set of structural nonlinearities, i.e geometric, structural and material nonlinear behavior [1]. Implicit FE-methods are not the promising tool to control all these nonlinearities. The remedy is quasistatic explicit dynamics with a minimum kinetic energy control.

4.1 Structure of the model
A typical ribbon cable of interest for modelling is the SCR Cable.
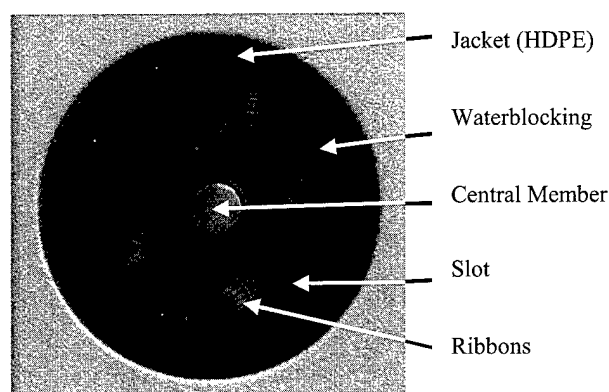
The FE-model consists of brick [1] , shell and contact [1] elements.
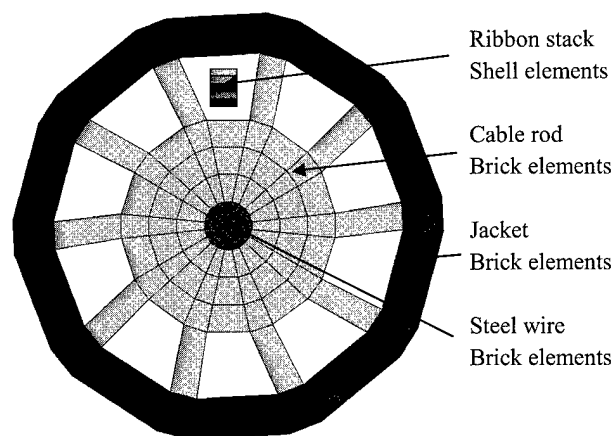
Figure 7. Physical cable and FE-model

Fig. 7 shows the physical cable cross-section as well as the corresponding FE mesh. Just one slot is under consideration, i.e. filled with ribbbons. The ribbons are modelled via shell elements, each shell ribbon structure loose in the slot.

The slot and the rest of the cable consist of brick elements. The model is discontinuous, i.e. the ribbons and the rod are not connected by structural elements. The interactions like contact pressure are considered by contact elements. The cross-section of the model is about 20mm. The length is, dependent of the stranding geometry under consideration, about 1000mm.

Excess ribbon length

1000 mm

Rod / jacket brick elements
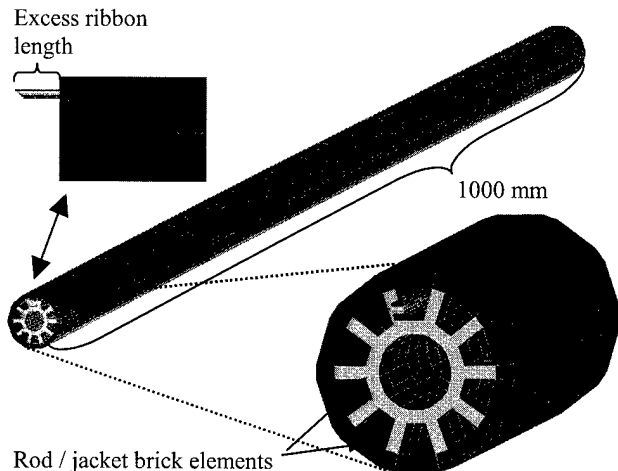
Figure 8. Perspective view of the model

Fig. 8 shows a perspective view of the model, treating two laylength, for minimizing the influence of the model's ends. As the model is to represent any portion of the cable, proper boundary conditions for the open model ends have to be found. The excess ribbon length distribution is calculated according to the stranding geometry under consideration and added to each ribbon-shell-element-structure.

4.2 Relaxation Modelling

Stranding and bending are modelled by applying displacements and rotations to the rod's and jacket's brick element nodes. These displacements are transferred to the ribbons via contact elements. Each ribbon is totally unconstrained within the slot cross-section, to take the minimum potential energy position. Therefore a distinct decrease of strain, compared to the static ribbon model is observed.

Static ribbon model

Kinematic ribbon model
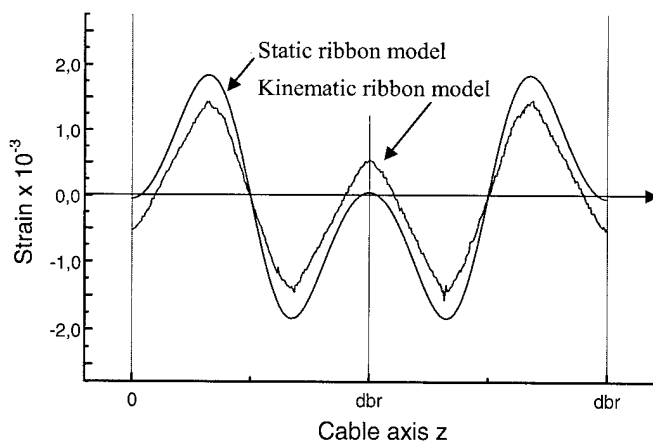
Figure 9. Strain relaxation

Fig. 9 compares the edge fiber strain of the static model to the strain results of the kinematic model. Under consideration is the straight SZ-profile, described in Fig. 3.

Due to ribbon relaxation within the slot dimensions, the maximum fiber strain between reversal and helical is reduced by approx. 25%.

In this case the results can be compared easily, as a straight, symmetric stranded cable is under consideration. If the cable f.i. is bent, the strain distribution is much more complex, depending on the position of the slot relatively to the bending axis. To get an easy to understand output from the modelling it is assumed, that the total potential energy E_{tot} of the ribbons is a good indicator for the ribbons' mechanical load. This energy consists of shear deflection energy values E_s and the normal deflection energy values E_n.

$$E_{tot} = E_s + E_n$$

Therefore the response of each ribbon is a 1-dimensional energy function of the external load, which is typically a bending load.

4.3 Typical Examples

Investigating the ribbon bending and relaxation behavior of an SZ-SCR cable, due to the ribbon backtwist, each slot has two distinct bending axis with different bending behavior. One bending axis is the symmetry axis x of Fig. 3, the second is the orthogonal y axis. The bending process starts with infinite diameter, i.e. the straight cable and ends with 250mm minimum bending radius.
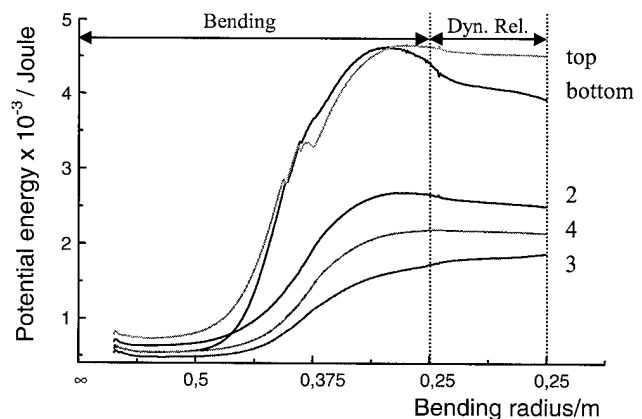
Figure 10. Bending about y axis

Fig. 10 shows 5 potential energy traces as a function of bending radius, each line representing one ribbon. The simulation consists of the real bending process and a dynamic relaxation process. Whereas during bending the abszissa values range from infinity to 0.25m minimum, in the dynamic relaxation the radius is constant 0.25m, this gives the ribbons some extra time to relax after bending is completed. The ribbon relaxation is perfect, when the energy traces are parallel to the abszissa. To save CPU time the calculation is stopped, when the slope of each trace is smaller than a certain criterium.

For optimum cable behavior the lines should be close together at a low potential energy value, which means the ribbons are equally low mechanical loaded. In Fig. 10 the ribbons bottom and top have a problem at small bending radii, i.e. high strains resulting in high energy values, causing attenuation.

To avoid this the cable parameters have to be changed. Another remedy could be constraining the bending specifications to radii smaller than 0.5m, which seems to be a critical point for the configuration under test, i.e. the traces start to diverge.
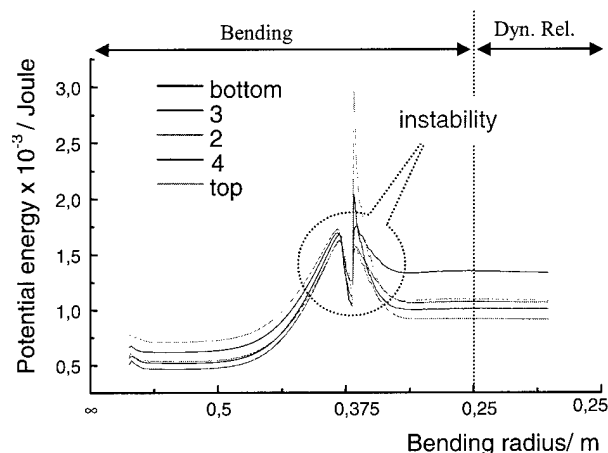
Figure 11. Bending about x axis

Fig. 11 shows the potential energy bending traces for bending the cable about the slot x-axis. The energy response function shows a distinct energy peak at bending radii about 0.38m. This peak denotes an instability. It is caused by ribbon flip, due to bending load on the ribbons' stiff bending axis. To minimize this load, the whole ribbon stack tends to tilt. This is critical for the integrity of the ribbon stack as well as for the attenuation values. Again the remedy is to avoid small bending radii, in this case smaller than 0.38m.

5. Conclusions

To investigate the static load on ribbons and their kinematic relaxation behavior two FE-models have been developed. The modelling is common for ribbon cables, some special problems are illustrated with the SZ-SCR stranding geometry.

The modelling gives insight in the stress-strain and bending radii distribution of the ribbons due to stranding, temperature, crush or bending load, considering contact forces and friction. It helps to understand the ribbon relaxation behavior indicating critical loads, where high fiber strains or ribbon instabilities occur.

6. References

[1] K.J. Bathe "Finite Element Methods": *Spinger Verlag*, Berlin (1990).

[2] A.H. Stingl "Statik und Kinemtaik hochfaseriger Bändchen-kabel" *Dissertation Universität Bayreuth* Bayreuth (2000)

Author

Andreas Stingl
Corning Cable Systems
96465 Neustadt Coburg
Germany

Andreas Stingl was born 05.11.1970. He joined Siemens RD&E in 1996, he received his physics degree from the university of Bayreuth in 1997. He has been working on his PHD, considering numerical models for cable simulation from Jun. 1997 until Feb 2000. He is now responsible for FE simulations at RD&E Corning Cable Systems, Neustadt / Coburg.

Optical Loss Stability of Access Cables in 1600 nm Range

Seiichirou Takahashi (1), Takeo Kusumoto (2), Ryuji Takaoka (1), Ichirou Kobayashi (1)

(1) FITEL PHOTONICS Laboratory, The Furukawa Electlic Co., Ltd.
6 Yawatakaigan-dori, Ichihara, Chiba, Japan, +81-436-42-1771 staka@ch.furukawa.co.jp
(2) The Tokyo Electlic Power Co., Inc., 1-3 Uchisaiwai-cho 1-chome,Chiyoda-ku, Tokyo, Japan

Abstract

In order to confirm the applicability of the WDM system to access networks, we investigated the optical characteristics in 1600nm-wavelength range of various types of optical access cables with SMF. Optical loss change in wavelength range up to 1640nm was investigated during temperature change, mid-span branching and mechanical change, which are expected as factors to affect the optical characteristics after and during cable installation. From the test results, it was confirmed that these types of cables have stable characteristics at each wavelength in 1600nm range enough for the WDM transmission system to be applied to access networks. Moreover, we compared the wavelength dependence of loss increase caused by temperature change with that of macro- and micro-bending loss. Then we deduced the cause for the loss increase, which depends on cable structure and fiber position in a cable cross section.

Keywords

Optical access cable; 1600nm range; WDM; SMF.

1. Introduction

To meet the recent demands for increase in transmission capacity, the WDM transmission system has been applied mainly to the long-haul telecommunication. For more rapidly increasing demands, the WDM transmission system is beginning to extend to access networks. A model of access network is shown in figure 1. Access network is composed of feeder cable portion and distribution cable portion. The feeder cables accommodate high fiber count up to 1000 and are mainly installed underground. On the other hand, distribution cables are mostly aerial in Japan, spreading over the wide area of the access network.

To apply the WDM system to access network, it is necessary to confirm the goodness of the optical characteristics in the underground feeder cables and aerial distribution cables in 1600nm-wavelength range used in WDM system. Therefore, we investigated optical loss change in 1600nm range during temperature change and mid-span branching, which are expected as factors to affect the optical characteristics after cable installation. In addition, we investigated optical loss change in 1600nm range during mechanical change, which is expected as a factor to affect the optical characteristics during cable installation. Moreover, we examined the wavelength dependence of macro- and micro-bending loss. Then we discussed the mechanism of loss increase caused by temperature change, by means of comparing the wavelength dependence of this loss increase with that of macro- and micro-bending loss.
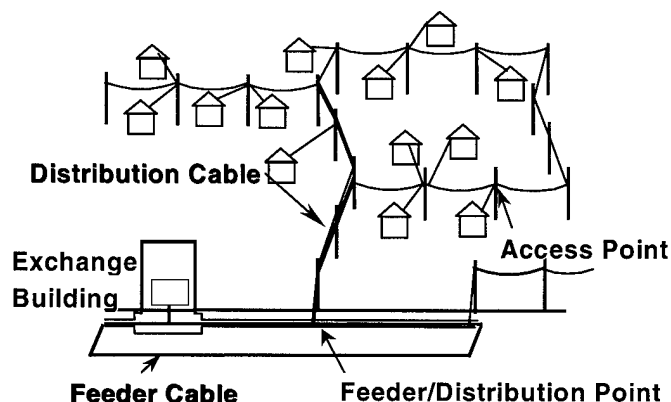
Figure 1. Model of access network

2. Cable structure

Figure 2 shows the cross sections of the cables of which we investigated optical characteristics. SMF 's are used in these cables.

2.1 [Type A] Stranded loose tube cable

Six tubes are stranded around a central strength member and each tube contains six 0.25mm diameter fibers. This cable type is used worldwide.

2.2 [Type B] Single tube cable with 4-fiber ribbon

Several 4-fiber ribbons are stacked and accommodated in a central tube. This cable has self-supporting cable structure with excess cable length relative to suspension member, and is used as an aerial distribution cable. This cable would be used widely in the potion of aerial distribution cable because of its down sized simple structure.

2.3 [Type C] S-slotted core cable with 8-fiber ribbons

Ten 8-fiber ribbons are accommodated in each helical slot. This cable type is widely used as an underground feeder cable.

2.4 [Type D] SZ-slotted core cable with 4-fiber ribbons

Five 4-fiber ribbons are stacked and accommodated in each slot of SZ-slotted rod. Since each slot changes its direction periodically, fiber ribbons can be easily extracted from slotted rod. Self-supporting cable structure with excess cable length relative to suspension member is also adopted and this cable is used widely in Japan as an aerial distribution cable.
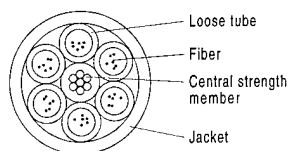
Type A : Stranded loose tube cable
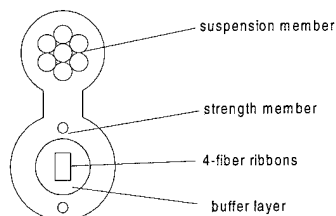
Type B : Single tube cable with 4-fiber ribbon
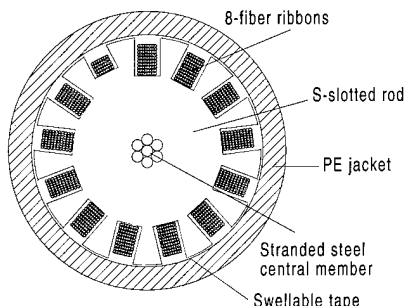
Type C : S-slotted core cable with 8-fiber ribbon
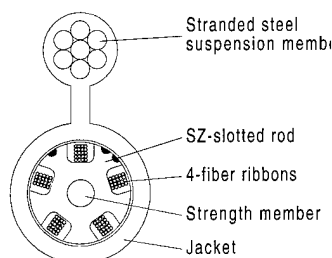
Type D : SZ-slotted core cable with 4-fiber

Figure 2. Cross sections of investigated optical access cables
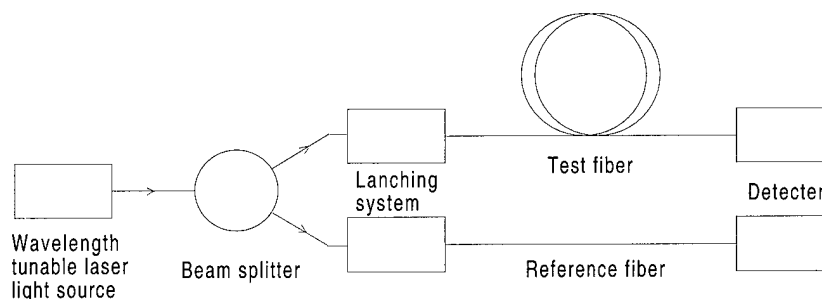
Figure 3. Schematic diagram of measurement set-up

3. Characteristics of optical loss change

3.1 Measurement method

Optical loss Change was measured by the method of IEC 60793-A-C10A – Transmitted power monitoring (see figure 3). This method has an advantage of keeping the measurement accuracy during long time test such as temperature characteristics examination, since change of light source power can be corrected. Wavelength tunable laser was used for light source.

3.2 Temperature characteristics

Optical loss changes at 70 and –30°C from at 20°C, were measured at 1530, 1550, 1600, 1625 and 1640nm wavelengths on type A to D

cables wound around drums. Measured fibers in each cable were selected mainly from the fibers that are expected to show large loss increase owing to their positions in cable cross section.

Measurement results in each cable are shown in figure from 4 to 7. For each cable, the results were good since loss increase at both 70 and –30°C were less than 0.1dB/km. Accordingly, it was confirmed that each cable has temperature characteristics satisfactory for practical purposes in the wavelength range from 1530 to 1640nm. However, a small amount of loss increase was observed in some of the cable types and the fibers. We will discuss these in detail later (see chapter 5).

3.3 Mid-span branching characteristics

Mid-span branching characteristics were examined on type B, C, and D cables.

The loss changes in removing the jacket and extracting the ribbons were measured at 1550, 1600 and 1640nm wavelength.

Results are shown in table 1. In each cable, loss increase greater than 0.05 dB was not observed. Accordingly, it was confirmed that each cable has mid-span branching characteristics satisfactory for practical purposes in the wavelength range up to 1640nm. With regard to the wavelength dependence of loss increase, it could not be observed in these three wavelengths at this measurement.

Table 1. Results of mid-span branching tests

Procedure	Loss change								
	Type B			Type C			Type D		
	1550 nm	1600 nm	1640 nm	1550 nm	1600 nm	1640 nm	1550 nm	1600 nm	1640 nm
Separating suspension member	< 0.05 dB			—			< 0.05 dB		
Removing the jacket				< 0.05 dB					
Removing the wrapping tape									
Extracting the ribbons									

3.4 Mechanical characteristics

Mechanical tests were performed on type B, C, and D cables at 1550, 1600 and 1640nm wavelength. Results are shown in table 2. In each cable, loss increase greater than 0.05 dB was not observed. Accordingly, it was confirmed that each cable has mechanical characteristics satisfactory for practical purposes in the wavelength range up to 1640nm. With regard to the wavelength dependence of loss increase, it could not be observed in these three wavelengths at this measurement.

Table 2. Results of mechanical tests

Item	Method	Loss change								
		Type B			Type C			Type D		
		1550 nm	1600 nm	1640 nm	1550 nm	1600 nm	1640 nm	1550 nm	1600 nm	1640 nm
Reapeted bending (Cycle:10) (R=160mm for typeB,D) (R=240mm for type C)	IEC 60794 -1	< 0.05 dB			< 0.05 dB			< 0.05 dB		
Crush (1960N/100mm)										
Torsion (±90°/1m)										
Impact (1kg×1m) (Impact surface diameter : 10mm)										

4. Optical loss caused by macro- and micro-bending

In the temperature characteristics shown in figure from 4 to 7, a small amount of loss increase was observed in some cases of the
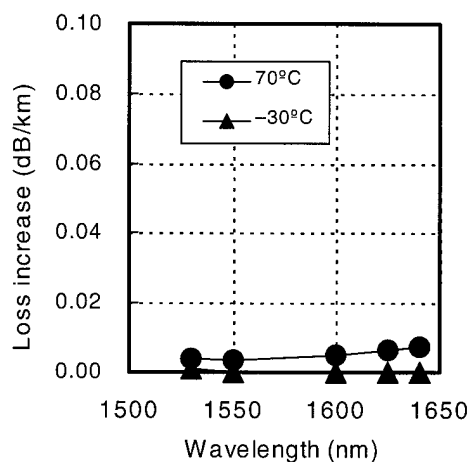
Figure 4. Temperature characteristics of loss increase on type A
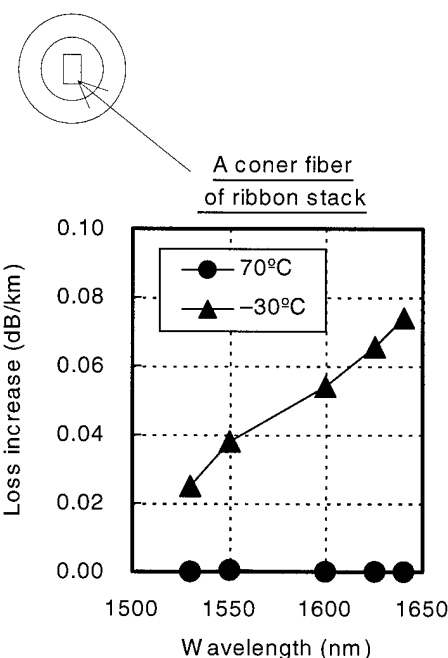
Figure 5. Temperature characteristics of loss increase on type B

results. Moreover, these loss increases do not always show the same wavelength dependence. Therefore, we examined the wavelength dependence of macro- and micro-bending loss, which is expected to be the cause of the loss increase. Then the wavelength dependence of the macro- and micro-bending loss will be compared with that of temperature characteristics, in chapter 5.

4.1 Fiber parameters

For two types of fiber shown in table 3, the wavelength dependence of macro- and micro-bending loss was examined. Type 1 fiber has a relatively high sensitivity to macro-bending and type 2 fiber has an average sensitivity to macro-bending.
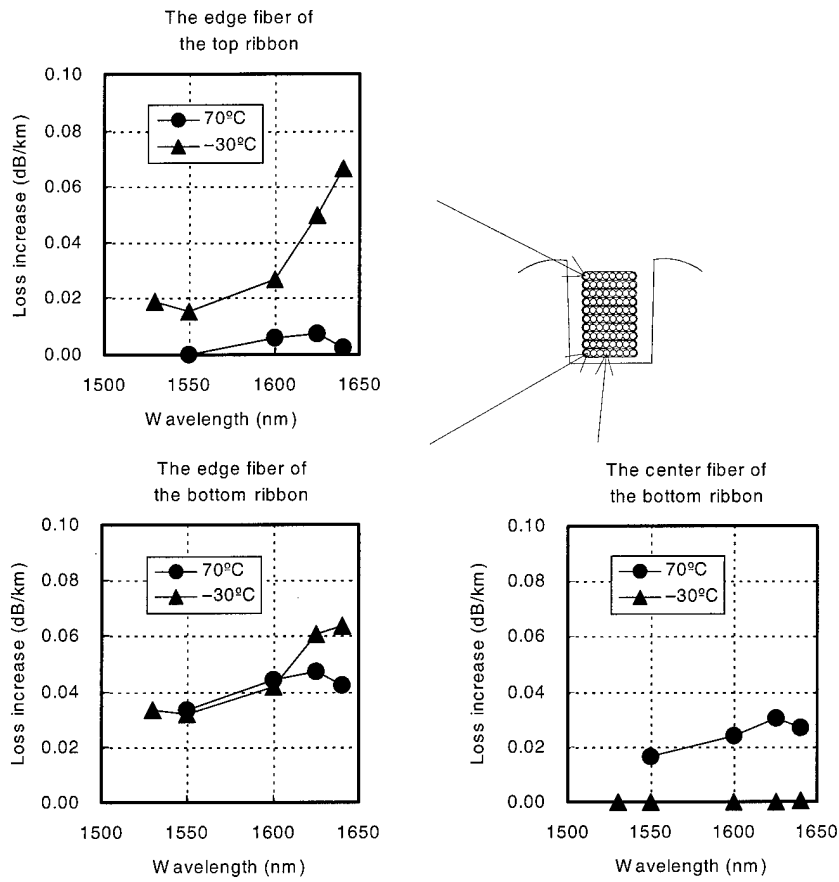
Figure 6. Temperature characteristics of loss increase on type C
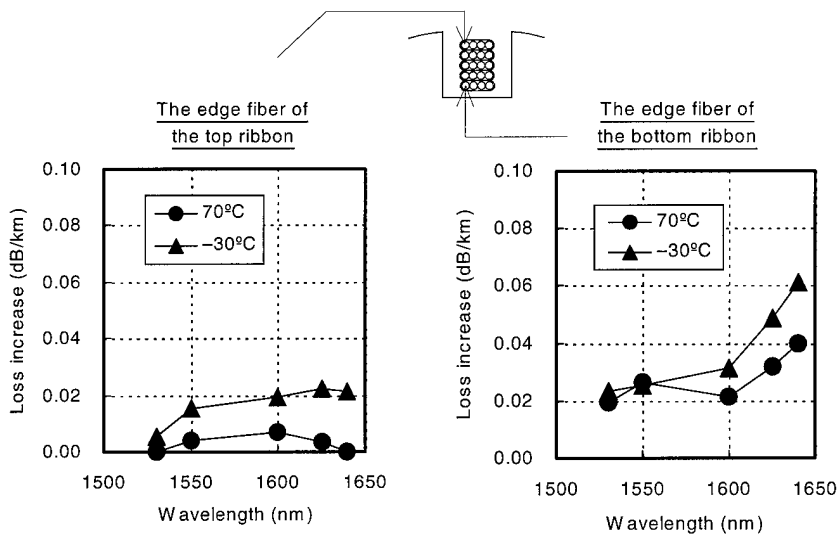
Figure 7. Temperature characteristics of loss increase on type D
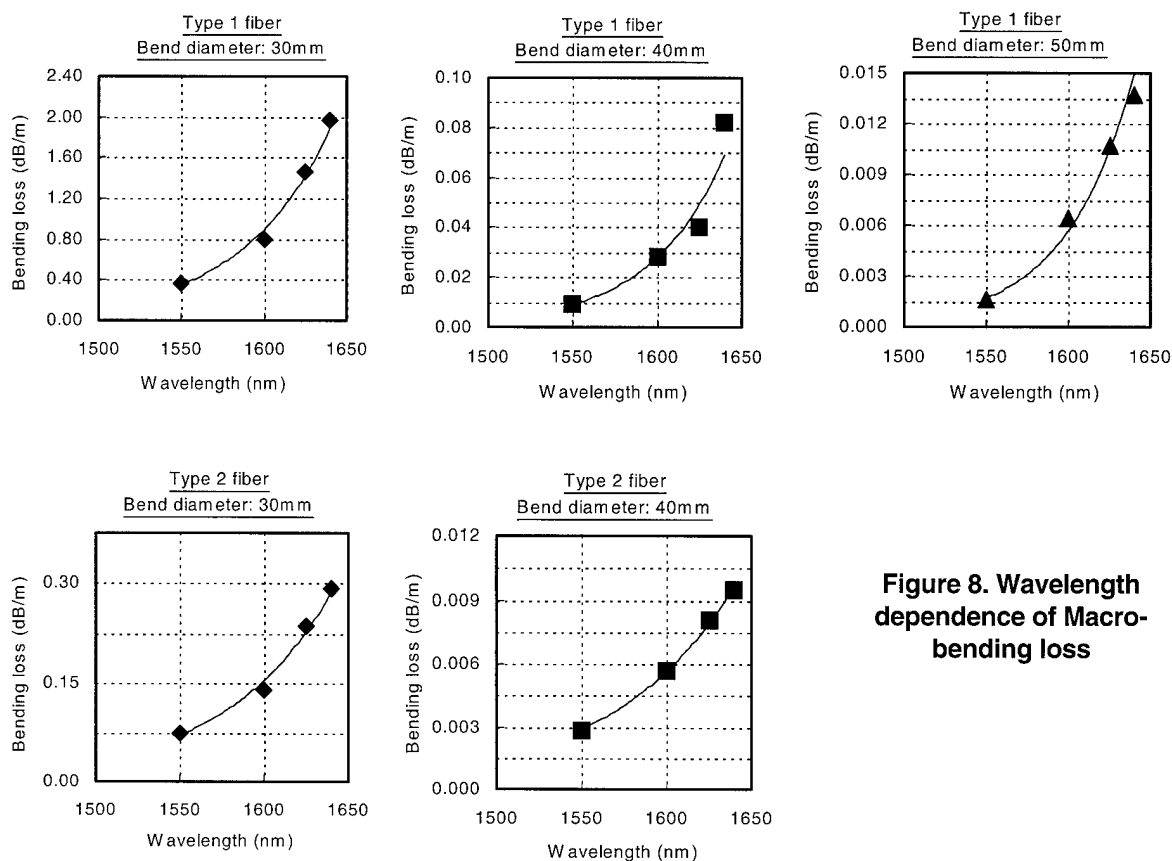
Figure 8. Wavelength dependence of Macro-bending loss

Table 3. Parameters of test fibers

Type	Cut-off (nm)	MFD (μm)	
1	1260	@1550nm	10.6
		@1600nm	10.9
2	1330	@1550nm	10.5
		@1600nm	10.7

Table 4. Conditions of wire mesh microbending test

Length of fiber under test		300 mm
Load Increment		1 kg
Mesh specification	Woven	
	Wire diameter	0.22 mm
	Wire pitch	0.62 mm

4.2 Macro-bending loss

Macro-bending loss was measured by method in accordance with IEC 60793-1-C11. Bend diameters were 30, 40, and 50mm.

Measurement results are shown in figure 8. Since type 1 fiber is more sensitive to macro-bending than type 2 fiber, loss increase of type 1 is lager than that of type 2. Moreover, two types of fiber differ in the wavelength dependence of macro-bending loss. For example, if we take the ratio of loss increase at 1640nm to at 1550nm, it is from 5 to 9 for type 1 and from 3 to 4 for type 2. These results show that fiber which is more sensitive to macro-bending has larger wavelength dependence of macro-bending loss in this wavelength range.

The macro-bending characteristics of fibers used in the test cables were nearly equivalent to that of type 2 fiber, owing to their fiber parameters. Therefore, also the wavelength dependence of macro-bending loss of these fibers is considered nearly equivalent to that of

type 2 fiber. That is to say, the ratios of their macro-bending loss at 1640nm to at 1550nm are thought to be approximately from 3 to 4.

4.3 Micro-bending loss

Micro-bending loss was measured by method in accordance with IEC 60793-1-C3C–wire mesh microbending test method. Measurement conditions are shown in table 4.

Measurement results are shown in figure 9. These results show that the loss increase and its wavelength dependence are relatively insensitive to fiber types. Moreover, the slope of loss increase versus wavelength is flatter than that of macro-bending loss. The ratio of loss increase at 1640nm to at 1550nm, for instance, is a little less than 2.

4.4 Comparison of macro- and micro-bending loss

The above results show that the wavelength dependence of macro-bending loss is steeper than that of micro-bending loss in this long

By wire mesh method
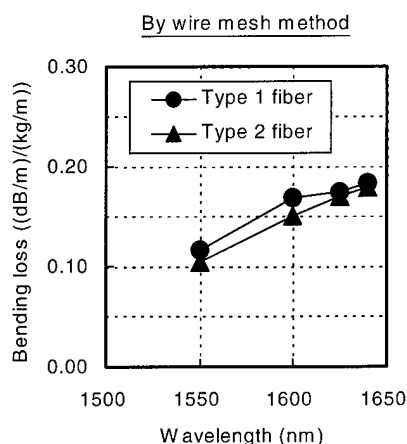
**Figure 9. Wavelength dependence
of Micro-bending loss**

wavelength range. For two types of fiber used in this experiment, the ratio of loss increase at 1640nm to at 1550nm is more than 3 for macro-bending and a little less than 2 for micro-bending (see table 5).

**Table 5. Wavelength dependence of bending
loss**

(Ratio of loss increase at 1640nm to at 1550nm)

Type	Macro-	Micro-
1	5 ~ 9	< 2
2	3 ~ 4	< 2

5. Causes of temperature characteristics

As described above, macro- and micro-bending loss shows different wavelength dependence. Therefor, by examining the wavelength dependence of temperature characteristics of each cable, we can deduce which type of bending (macro- or micro-) mainly caused the loss increase.

5.1 Temperature characteristics of type B

5.1.1 Wavelength dependence

In this cable, a corner fiber of 4-fiber ribbon stack was measured. The result is shown in fig.5. The result was that loss increase was observed at –30°C, whereas at 70°C it was not observed. At –30°C, loss increase at 1640nm is about twice as large as that at 1550nm. This wavelength dependence is more similar to that of micro-bending loss than macro-bending loss. Accordingly, it can be assumed that the principal factor of this loss increase was micro-bending rather than macro-bending.

5.1.2 Consideration of low temperature characteristics

The reason for the occurrence of micro-bending loss at low temperature may be assumed as follows:

Since the tube contracts in the longitudinal direction at low temperature, ribbon stack undulates in the tube. At this point, the ribbons would be pressed against the inner wall of the tube. It is assumed that this lateral pressure caused the micro-bending loss, especially in corner fibers of the ribbon stack.

5.2 Temperature characteristics of type C

5.2.1 Wavelength dependence

In this cable, ten 8-fiber ribbons are stacked in each slot. Three fibers in a slot were measured. These are the edge fiber of the top ribbon, the edge fiber of the bottom ribbon and the center fiber of the bottom ribbon. These results are shown in figure 6. The wavelength dependence, which is expressed as the ratio of loss increase at 1640nm to at 1550nm, is shown in table 6. As before, the wavelength dependence of these results was compared with that of macro- and micro-bending loss. Then the principal factor of loss increase was deduced. The deduction is shown in table 7.

Table 6. Wavelength dependence of type C

(Ratio of loss increase at 1640nm to at 1550nm)

Temperature	Top ribbon	Bottom ribbon	
	Edge fiber	Edge fiber	Center fiber
70°C	Not increase	< 1.5	< 2
-30°C	About 4	About 2	Not increase

**Table 7. Deduction of principal factor of
loss increase on type C**

Temperature	Top ribbon	Bottom ribbon	
	Edge fiber	Edge fiber	Center fiber
70°C	Not increase	Micro-	Micro-
-30°C	Macro-	Micro-	Not increase

The reason for occurrence of these deferent types of bending loss may be assumed as follows:

5.2.2 Consideration of high temperature characteristics

Owing to the cable elongation in the longitudinal direction at 70°C, ribbon stack in a slot is strained. In order to reduce the tension, ribbon stack moves toward the bottom of the slot. Consequently, ribbon stack would be pressed against the bottom wall of the slot. It is assumed that this lateral pressure caused the micro-bending loss in the fibers of the bottom ribbon.

On the other hand, because the top ribbon does not directly touch the bottom wall of the slot, micro-bending loss was not caused.

5.2.3 Consideration of low temperature characteristics

At -30°C, owing to the cable contraction in the longitudinal direction, excess of ribbons relative to the slot increases. At this point, since there is a small amount of clearance between the top ribbon and the wrapping tape, it is assumed that macro-bending was induced in the top ribbon. In contrast to this, in the ribbons positioned below the top ribbon, especially in the bottom ribbon,

movements toward up and down are suppressed. Therefore, the macro-bending is hard to be induced. But the edge fiber of the bottom ribbon is liable to be pressed against the upper ribbon or the bottom or the side walls of the slot. Owing to this lateral pressure, it is assumed that micro-bending loss was induced in the edge fiber of the bottom ribbon.

On the other hand, it seems that the center fiber of the bottom ribbon is not pressed against the bottom wall of the slot at the low temperature. Nor does center fiber contact directly with the side walls of the slot. For these reasons, it is assumed that micro-bending loss due to lateral pressure was not induced in the center fiber of the bottom ribbon.

5.3 Temperature characteristics of type D

5.3.1 Wavelength dependence
In this cable, stacked five 4-fiber ribbons are inserted in each SZ-slot. Two fibers in a slot were measured. One was the edge fiber of the top ribbon, the other was the edge fiber of the bottom ribbon. These results are shown in figure 7. The wavelength dependence, which is expressed as the ratio of loss increase at 1640nm to at 1550nm, is shown in table 8. As before, from comparing the wavelength dependencies of these results with that of macro- and micro-bending loss, the principal factor of loss increase was deduced as shown in table 9.

Table 8. Wavelength dependence of type D
(Ratio of loss increase at 1640nm to at 1550nm)

Temperature	Top ribbon	Bottom ribbon
	Edge fiber	Edge fiber
70°C	Not increase	About 2
-30°C	< 1.5	About 3

Table 9. Deduction of principal factor of loss increase on type D

Temperature	Top ribbon	Bottom ribbon
	Edge fiber	Edge fiber
70°C	Not increase	Micro-
-30°C	Micro-	Macro-

The reason for the occurrence of these deferent types of bending loss may be assumed as follows:

5.3.2 Consideration of low temperature characteristics
In SZ-slotted rod cable, the friction force between ribbons and a slot is larger than in S-slotted rod cable. In addition, the dimension of slot is designed large, so there is a lager amount of clearance between ribbons and a slot. For these reasons, it is assumed that macro-bending was induced in the bottom ribbon at –30°C, when excess of ribbons relative to the slot increased owing to the cable contraction in the longitudinal direction.

On the other hand, in the top ribbon, it is dubious why the loss increase caused by macro-bending was not observed. But, in the edge fiber of the top ribbon, loss increase caused by micro-bending was observed. The reason for this may be assumed as follows:

When excess of ribbons relative to the slot increase, the ribbons undulate in the slot. At this point, the edge fibers would be easy to be pressed against the bottom or the side walls, as described in figure 10. Therefor, it is assumed that this lateral pressure caused the micro-bending in the edge fiber of the top ribbon.

5.3.3 Consideration of high temperature characteristics
As cable elongates in high temperature, the stacked ribbons in a slot are strained and they move toward the bottom of the slot as a whole. Consequently, the edge fiber of the bottom ribbon would be easy to be pressed against the bottom or the side walls of the slot, as figure 10. This lateral pressure is assumed to have caused micro-bending loss.
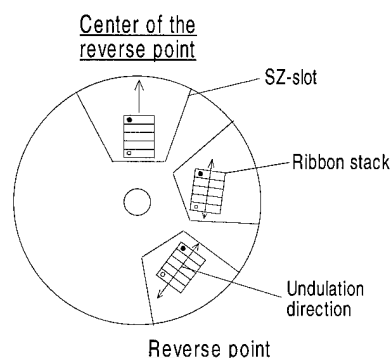
Figure 10. Ribbon stack in SZ-slot

6. Conclusion

For various types of optical access cables with SMF, temperature characteristics, mid-span branching characteristics and mechanical characteristics were investigated in the wavelength range up to 1640nm. These are important characteristics for optical cables used in access network.

In each mechanical test, no remarkable loss increase was observed in each cable. From this result, it is considered that the damage that causes loss increase in the long wavelength range would not be caused by cable installation operation.

In mid-span branching test, no remarkable loss increase was caused in each cable. Consequently, it is confirmed that each cable is suitable as an access cable from the viewpoint of mid-span branching.

In temperature characteristics test, the difference of the wavelength dependence of loss increase was observed, due to cable structure and fiber position. However, the loss increase was less than 0.1 dB/km in each case, so that the practicability of each cable was confirmed in the wavelength range up to 1640nm.

As a conclusion, it was confirmed that the various types of preset access cables with SMF can be applied to the WDM system.

7. References

[1] IEC 60793-1 Optical fibers Part1: Generic specification.

[2] IEC 60794-1 Optical fiber cable — Part 1: Generic specification.

[3] H.Iwata et al., "Novel Optical Fiber Cable for Distribution Use in Access Network" 48th IWCS, pp.20-24 (1999)

[4] T.Aihara et al., "Novel Optical Fiber Cable for Distribution Use in Access Network" Proceedings of the EuroCable Conference 2000, pp.79-86 (2000)

[5] H.Iwata et al., "Pre-connectorized 1000-fiber Single Slotted Core Cable" 44th IWCS, pp.627-634 (1995)

[6] H.Iwata et al., "Design of Aerial Optical Fiber Cable System Suitable for Easy Branching" 46th IWCS, pp.4-11 (1997)

[7] S.Hopland, "Investigation of 1625nm loss performance of fibre optic cables intended for use at 1550nm" 48th IWCS, pp.780-788 (1999).

[8] E.Jauhiainen and R.Pulliainen, "Loss behaviour of optical fiber cable network for future WDM" 48th IWCS, pp.789-794 (1999)

[9] JF.Libert, JL.Lang, and J.Chesnoy, "The new 160 gigabit WDM challenge for submarine cable system" 47th IWCS, pp.375-384 (1998)

[10] D.Iwakura et al., "Development of new aerial self-supporting cable with excess fiber ribbon length in SZ-slot" 48th IWCS, pp.578-584 (1999).

Authors

Seiichirou Takahashi
The Furukawa Electric Co., Ltd.
6 Yawatakaigan-dori, Ichihara, Chiba, Japan
staka@ch.furukawa.co.jp

Seiichirou Takahasi received his B.E. degree in physics from Tsukuba University in 1991. He joined The Furukawa Electric co., ltd. in 1991 and has been engaged in research and development of optical fiber cables. He is now a research engineer of FITEL PHOTONICS Laboratory.
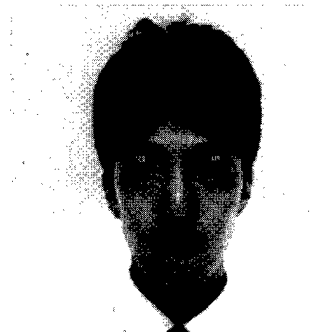
Takeo Kusumoto
The Tokyo Electric Power Co., Inc.
1-3 Uchisaiwai-cho 1-choume, Chiyoda-ku, Tokyo, Japan

t0725390@pmail.tepco.co.jp

Takeo Kusumoto received his M.E. degree in Electric Engineering from Keio University in 1991. He joined The Tokyo Electric Power co., Inc. in 1991 and has been engaged in development of optical transmission system.

Ryuji Takaoka
The Furukawa Electric Co., Ltd.
6 Yawatakaigan-dori, Ichihara, Chiba, Japan
ryuji@ch.furukawa.co.jp

Ryuji Takaoka recievedhis M.E. degree in Mechanical Engineering from Keio University in 1996. He joined The Furukawa Electric co., ltd. in 1996 and has been engaged in research and development of optical fiber cables. He is now a research engineer of FITEL PHOTONICS Laboratory.

Ichiro Kobayashi
The Furukawa Electric Co., Ltd.
6 Yawatakaigan-dori, Ichihara, Chiba, Japan
Ichiro@ch.furukawa.co.jp

Ichiro Kobayashi received his B.S. degree in Physics from Chuou University in 1986. He joined The Furukawa Electric co., ltd. in 1986 and has been engaged in research and development of optical fiber cables. He is now a manager of FITEL PHOTONICS Laboratory.

High Voltage ADSS Reliability Modeling: Environmental and Climatological Effects on Advanced Jacket Material Selection

William DeWitt, Swati Neogi, Brian G. Risch**, Pierre Coat, Danny Ammons,
George Karady* and Johnny Madrid*
Alcatel OFCCC, Claremont, NC
*Arizona State University, Department of Electrical Engineering, Tempe, AZ
**To whom correspondence should be addressed.

ABSTRACT

When assessing the long-term reliability of ADSS cables placed on high voltage power structures, environmental effects of EMF voltage, UV radiation, temperature extremes, humidity, salt and pollution need to be examined to determine which type of jacket material should be used. This paper examines results of extensive materials aging and dry band arc testing conducted on ADSS cables with varying jacket materials in order to determine the relative importance of these environmental factors, and how combinations and interactions of these effects influence the degradation of cable jacket materials.

This paper correlates climatological factors in addition to the EMF system configuration into reliability guidelines. World maps of climatological data and pollution levels are surveyed in order to estimate how these factors can lead to variability in cable lifetime and reliability. Finally, climatological data is combined with materials aging data and electrical test results to present improved guidelines for assessment of long term robustness of cable networks.

INTRODUCTION

All Dielectric self-supporting (ADSS) fiber optic cable offers a rapid and economical solution for utility and telecommunication companies to deploy optical fiber cables along existing electric and telephone utility pole rights of way assets. ADSS cables offer an alternative solution over other aerial application cables such as lashed or Figure-8 cables. All dielectric solutions are preferred and sometimes mandatory for installation in or near electric power lines on utility structures where cables containing metallic elements are not advised.

When ADSS optical fiber cables are installed in close proximity to high voltage power lines, two electrical phenomenons known as dry band arching and corona have caused premature failure of cables. Corona is caused by high electric field gradients at the tips of the suspension hardware and has been observed in both field and laboratory environments. While corona can be very damaging to the cable, mitigation devices exist. When properly installed at each attachment point, these devices

dissipate the electrical energy that causes the phenomenon.[1,2]

Dry band arcing is a completely different phenomenon that has proven to be a more elusive problem to solve and is the subject of this paper. Events leading to dry-band arcing can be described as follows. When first installed, the outer jacket of an ADSS cable is hydrophobic and non-conductive. As a result, its resistance is very high even when wet. Over time, however, it becomes hydrophilic and in some environments, significant contamination may accumulate. During wet conditions the contamination layer can become conductive and capacitively coupled currents from adjacent energized conductor's flow within this layer. As the contamination dries, narrow bands form. These bands can have high voltages across them, enough to cause arcs to occur across the dry band. If the current available to the arcs is high enough (i.e. the resistance of the contamination is small enough to allow pre dry-band currents in the milliampere range) arc heating can degrade the ADSS jacket and cause cable failure.[3]

Selection of the proper cable jacket material is very important to guarantee the long-term reliability of the cable. This selection depends upon the phase to phase voltage of the power utility system, the environment, and the position of the ADSS cable within the electrical field. In very low field voltage environments, a typical high-density polyethylene (HDPE) material is used. However, in higher field voltage special track resistant jacket material is required to prevent the dry band arcing caused by proximity to high voltage lines. Cross-linked or filled thermoplastic materials have shown the best resistance to electrical activity. Previous research has shown that filled thermoplastic jacket materials containing approximately 2.5% carbon black provide a superior combination of electrical and mechanical properties for protection of the cables.[4]

A thermoplastic track resistant jacket with acceptable carbon black content provides a three pronged solution to dry band arcing. First, the addition of carbon black ensures the ADSS will be resistant to UV aging, thus reducing collection of salt/pollution on cable sheath subsequently

lowering the cable resistance. Second, properly selected filled thermoplastic jacket materials minimize carbon surface tracking better than cross-linked materials. This assures a high electrical stability of the cable jacket. Finally, the filled thermoplastic track resistant jacket is resistant to heat damage by ablation (vaporization of material resulting in pitting), should arcing occur[5,6]. A filled thermoplastic also provides similar abrasion resistance to HDPE jacket material.

Some consider a Mid Span Space Potential of 12-25 kV as the standard threshold for specifying special jacket materials for ADSS cable[7,8], but a previous study "Continued investigations of ADSS designs and reliability considerations with respect to field voltage tracking, and cable installation practices," *IWCS Proceedings 1997*, concluded that without further protection, cable jackets prematurely failed at this threshold voltage.[3] Other factors also need to be considered such as climate, pollution level, wet/dry cycles etc.

EXPERIMENTAL

The cables tested were of a similar construction in which Polybutylene Terapthalate (PBT) tubes containing optical fibers were stranded around a central strength member. Superabsorbent waterblocking materials were used to make the interstices between the tubes watertight.[9] The inner core was surrounded by an inner sheath made of Medium Density Polyethylene (MDPE). Between the inner sheath and outer sheath aramid strength yarns were applied. The material of the outer sheath was varied in order to examine the effects of environmental exposure and electrical testing as a function of outer jacket material. Various outer jacket materials were investigated in this study as well as earlier studies[3,4,5,8] to get a complete representation of all common, commercially available jacket materials. A diagram of the cable construction is shown in Figure 1. Details of outer jacket material and are outlined in Table 1.

Figure 1. Schematic Representation of the Cross Section of Typical ADSS Cable.

- Ripcords
- PBT Tube
- Central Strength Member
- Optical Fibers
- Aramid Strength Yarns
- Water Blocking Material
- PE Jackets
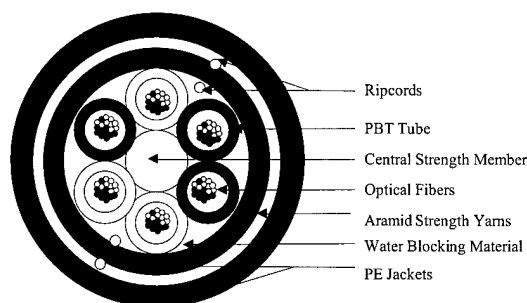
The track-resistant materials used in this study were specially formulated filled thermoplastic compounds. The performance of such compounds relative to crosslinked polyethylene PE has been compared in an earlier study.[3]

Effect of Aging on Mechanical Performance of the Outer Cable Jacket

Four cables with different outer jacket materials were subjected to heat and moisture aging and UV aging conditions. Heat aging had been done at 85°C and at 85% relative humidity for 30 days. Heat aged as well as virgin cables were subjected to UV aging according to the IEC standard 68-2-5. Procedure C of the standard has been followed and the duration of the test was 10 days. The total UV dose received during the 10 Day UV test was 220 KWh/m^2 or (792 MJ/m^2). The test temperature was kept constant at 50°C. Mechanical properties such as the tensile strength and the elongation of the outer cable jacket after aging were measured according to the method FOTP 89 and compared with that of the unaged outer cable jacket. An Instron model 4202 was used for tensile measurement.

Table 1: Composition of Cable Jacket Materials.

Cable A	HDPE
Cable B	Filled Thermoplastic/ High Filler
Cable C	Filled Thermoplastic/ Low Filler
Cable D	Unfilled Polyolefin Compound

Effect of Dry Band Arcing

Effects of dry band arcing on the performance of both dry and flooded ADSS cable jackets were studied by subjecting the cables to electrical field voltage before and after aging. Two test methods were compared in order to give correlation between different test methodologies. A standard salt-fog test as well as an alternative accelerated electrical test was performed on filled thermoplastic track-resistant jacketing compounds and HDPE. The accelerated test method was performed on all materials. The design of electrical experiments and details of the test methods are described below.

Salt-Fog Testing

Salt Fog testing was performed on unaged and aged cables according to IEEE P1222 Draft March 1997 - Annex A. Each cable sample was sealed at both ends and attached to a high voltage brass ferrule on one end and a grounded cable dead end on the other. The samples were then placed under tension and put into the salt fog chamber. A 1% NaCl (salt) solution was dispensed at a constant rate of 0.4 liters per cubic meter per hour. After the system was energized at 30 kV, the cables were inspected at 50 hours, 100 hours and then every 100 hours there after. Values of the parameters used in salt fog test are listed below.

Duration of the test:	1000 hours (42 days)
Test Voltage:	30 kV
Temperature:	15-25°C
Flow rate:	0.4 liters/hr/m^3
NaCl content:	10 kg/m^3
Particle size:	5-20 micron

It is important to note that the Salt Fog test is a constant flow test that simulates conditions that are not likely to occur in nature. This test method is currently under review by the IEEE Fiber Optics Standards Committee.

Accelerated Electrical Testing.

To simulate more realistic in-service environmental conditions on high voltage networks, an experimental setup subjected the cables to a series of wet and dry cycles, an extreme example of preconditions for dry band arcing. An experimental set-up was built indoors in Arizona State University's High Voltage Laboratory. This test setup is based on the theory of capacitive coupling and uses a Thevenin Equivalent circuit to model the electrical behavior of an ADSS cable installed near phase conductors.[10] Figure 2 shows the high voltage electrical connections and Figure 3 shows the experimental set-up. Similar to the Salt Fog test, the water reservoir contains water and NaCl (salt) to simulate the effects of precipitation and pollution. Table 2 shows the electrical and pollution levels each cable was subjected to.

Three levels of resistance of the cable representing a given pollution level have been suggested in previous research on the dry band arcing phenomenon:[11]

1. Light: 3.0 MΩ/m
2. Medium: 1.0 MΩ/m
3. Heavy: 0.1 MΩ/m

Table 2: Accelerated Electrical Test Key Parameters.

	Open Circuit Voltage (kV)	Pollution Level (MΩ/m)
Cable A	12	0.1
Cable B	20	0.1
Cable C	30	0.1
Cable D	30	0.1

-High Voltage Electrical Setup

The high voltage electrical setup is shown in Figure 2. High voltage is supplied through high voltage transformers. The high voltage is directly applied to the cables through a current limiting impedance.

Figure 2. Electrical setup.
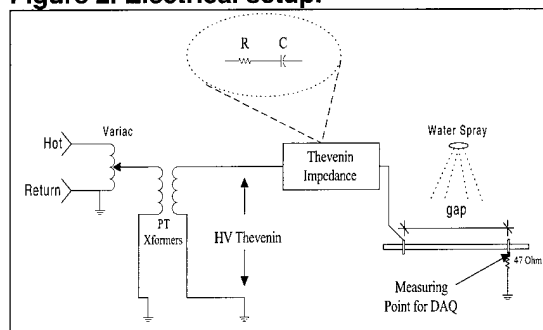
Figure 3. Test setup with electrodes.
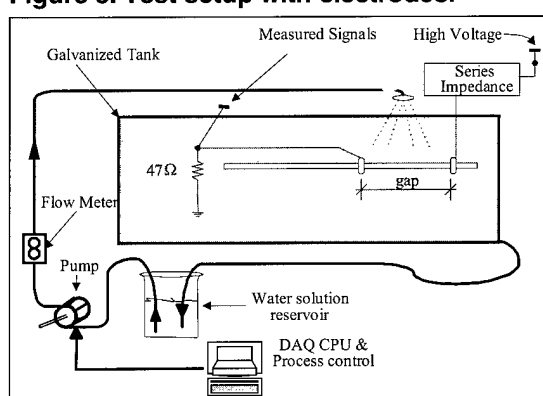
-Cable Setup

The cable samples tested had end plugs at both ends to prevent the interior of the fiber-optic cable from getting wet. The test cables were approximately 18 inches long. Two electrodes were attached to the fiber-optic cables, namely the high voltage and low voltage electrodes. The electrodes were spaced 2.5 in. 6.35 cm (± 0.5 cm) apart for all sets of experiments. The high voltage electrode was connected to the output side (high side) of the transformers and then to a series current limiting impedance and then to the cable's sheath. The cables were placed inside a galvanized metallic tank.

-Spray System

To simulate the environmental conditions of rain with pollution, a salt-water solution is sprayed onto the cable under test. The pump periodically cycles 2.0 minutes on and 13.0 minutes off. The spray system consists of five lateral-spread nozzles. The apparatus is pictured in Figure 5. The figure shows the top view of three spray nozzles. Two other nozzles are on the other side (not shown) and are equally spaced in between the three shown in the figure. The figure shows the water solution being sprayed.

Figure 5. Saltwater Spray Pattern
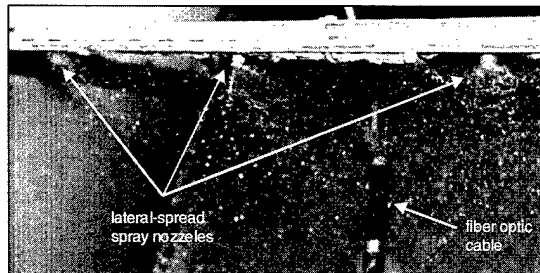
The spray nozzles were set up so that the region of electrical testing received the majority of the water. The flow rate of water was measured using an in-line flow meter. The water spray creates a wet conductive layer on the fiber optic cable sheath. The longitudinal field generated by the high voltage drives a current through this conductive layer. The current-limiting impedance limits the current. This current initiates the dry-band arcing process as the conductive layer dries.

Aging Effects

To simulate the worst case scenario for dry band arcing, the cables were aged at 85°C temperature and at 85 % relative humidity for 30 days before electrical testing. Additionally, cables were aged in a UV weatherometer to examine how UV aging would effect the electrical behavior of materials.

Surface Contact Angle Measurement

In order to determine the effects of aging on the hydrophobicity of the various jacket materials, a single drop of deionized water was carefully placed on the surface of each material. The shape of the drop and contact angle were then imaged with an optical microscopy system interfaced to a digital imaging system. Images of clean-virgin samples of each material were compared to aged and aged, polluted samples. Contact angle measurements were made from these images.

The adhesion tension between deionized water and the jacket material can be determined by multiplying the cosine of the contact angle by the surface energy of the air/water interface. The surface tension (energy) of the air/water interface is 72.5 dyn/cm at room temperature.[12]

AGING AND ENVIRONMENTAL EFFECTS

Performance of cables in electrical fields is highly dependent on the aging of the cable. On a newly installed dry cable, the surface sheath resistance is obviously quite high ($>10^9$ Ohm/m) so the induced currents are insignificant. Additionally, the cable surface is highly hydrophobic so moisture and contaminants are not prone to build up and thereby reduce surface resistivity. However, as a cable ages from thermal oxidation and exposure to ultraviolet rays from the sun, contaminants such as salt, pollutants, and moisture adsorb on the cable sheath. The

surface impurities can significantly reduce the electrical resistance to current flow on the surface of the cable.

Due to the inherent hydrophobic nature of polyethylene, the newly extruded ADSS jacket is not prone to collection of moisture on the cable jacket surface. As the cable surface begins degradation due to heat, UV-radiation, or exposure to ozone the cable sheath material may be wetted from rainfall. Additionally resistance may be lowered from salt or pollution. With a wetted and/or polluted cable surface, dry bands of high resistance surrounded by wetted sections of much lower resistance may develop. As these bands develop, the possibility exists for arcing across the dry band exists, which can damage an unprotected sheath by heat and ablation (vaporizing of jacket material causing pitting).

The rate of aging and the subsequent changes of surface properties of the cable are highly dependent on the region in which the cable is installed. In regions where UV exposure is low and climates are moderate such as northern Europe, aging effects will be minimal. However, in regions such as southern China where average temperatures are high, UV-exposure is high, and pollution levels are high the risk of dry-band arcing will be greater.

Global maps of average temperatures, rainfall, and sunshine are shown in figures 5-7.[13] Average UV dose was calculated and correlated to UV aging studies.[14] Depending on climatalogical region, mean temperatures can vary by 20°C or more, rainfall can vary by a factor of 100 or more, and annual UV dose can vary by a factor of 3 or more. The combined effects cause large variation on the aging of the cable surface, and therefore, the resulting changes in cable surface properties as a function of time. Consequently, cable lifetime and optimal installation configuration cannot be accurately determined unless climatological factors are included as part of the installation and service guideline scenario.

Similarly, other factors such as pollution, ozone, dust, or aerosols can influence the surface properties of cables and/or accelerate material degradation. Pollution levels can vary highly from nation-to-nation and from locality to locality. Seasonal variation in winds and other factors such as wildfires can also have effects on overall atmospheric particulate matter, and cables installed in coastal regions can experience the added risk of salt-spray. In areas of known high-risk levels of surface contamination, guidelines should be conservative to account for the effects of surface pollution on the electrical properties of the outer jacket.

Comparisons of industrial emissions and particulate pollution deposition data reveals large variation in pollution levels from region to region.[15,16,17,18] Total pollution levels and trends are highly variable and also dependent on seasonal weather patterns as well as natural events such as volcanic activity and wildfires. More specific details on trends and actual composition of surface pollution are

available from the references cited herein. Due to differences in national regulation, maximum pollution levels between the U.S., Europe, and Asia can vary by a factor of 10. Additionally, regional variation can be even greater.

RESULTS AND DISCUSSION

Effect of Aging on Mechanical Performance of the Outer Cable Jacket

Change in Tensile strength and Elongation of the cable outer jacket materials after heat aging, UV aging, and heat aging followed by UV aging are listed in Table 3 and Table 4.

Table 3 and Table 4 illustrates that the heat aging and UV aging conditions used for this study did not produce significant changes in ultimate material properties relative to the changes in surface properties. For jacket material D an annealing effect from aging appears to be increasing ultimate elongation. Jacket material C is the only material that shows measurable degradation in material properties after aging.

Table 3: Percentage change in tensile strength due to heat aging, UV aging, and heat followed by UV aging.

	% change in tensile strength			
	Cable A	Cable B	Cable C	Cable D
Heat	+2.6	+8.7	-24.9	-15.5
UV	-1.9	+3.4	-7.3	-4.6
Heat+UV	-8.0	-5.1		

Table 4: Percentage change in elongation due to heat aging, UV aging, and heat followed by UV aging.

	% change in ultimate elongation			
	Cable A	Cable B	Cable C	Cable D
Heat	+6.0	+15.0	-26.0	+32.0
UV	-12.9	+6.7	-33.0	+27.0
Heat+UV	-37.5	+8.7		

Figure 5. Global Map of Average Temperatures.
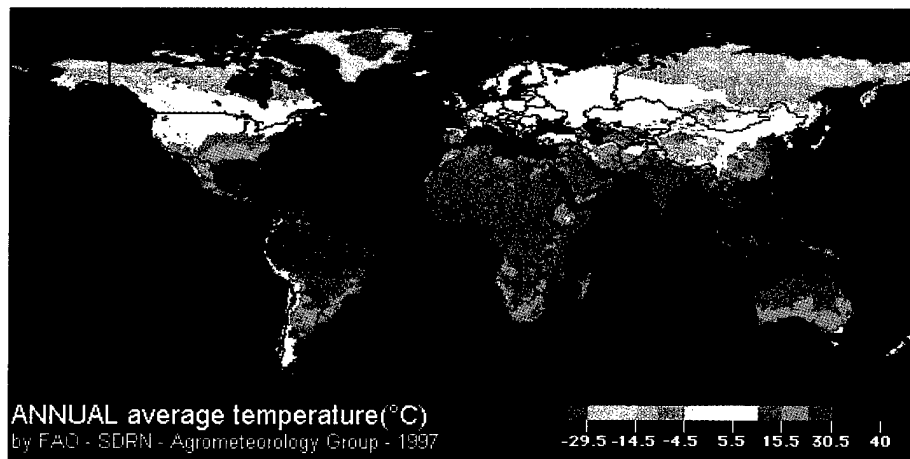
Figure 6. Global Map of Average Rainfall.
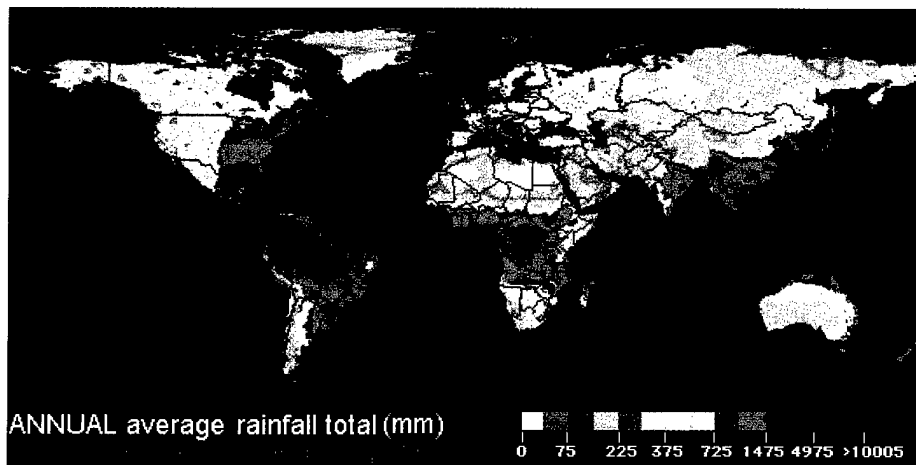
Figure 7. Global Map of Average Sunshine.

ANNUAL average sunshine fraction (%)
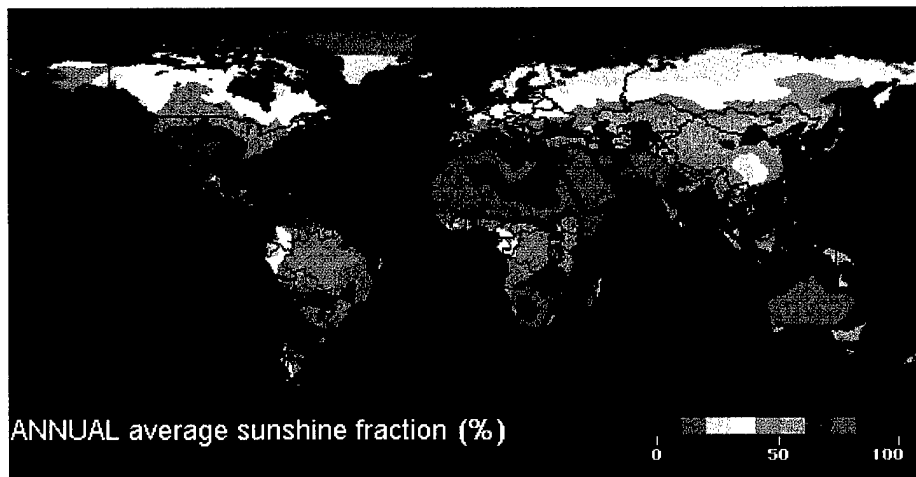
Effect of Aging and Pollution on Surface Properties

Figure 8 and Tables 5 & 6 summarize the results of contact angle measurements between deionized water droplets and jacket surfaces. From the figure it is obvious that both pollution and aging have a significant influence on the contact angle. The adhesion tension (A_{SLV}) between deionized water and the jacket material can be determined by the following equation:

$$A_{SLV} = \gamma_{LV} * \text{Cos } \theta = 72.5 \text{dyn/cm} * \text{Cos } \theta. \quad (1)$$

Where γ_{LV} ,72.5 dyn/cm, is the surface tension (energy) of the air/water interface at room temperature.[19] If the adhesion tension between water and the jacket material increases above 72.5 dyn/cm, wetting of the cable surface will occur.

After UV aging the adhesion tension increased substantially for all materials studied. The filled thermoplastic materials showed better UV damage resistance than the unfilled materials. The effects of UV aging on surface properties were far more significant than the effects of UV or heat aging on bulk mechanical properties. Relative changes in adhesion tension were up to several hundred percent, although, no significant aging effects were noted from tensile testing. These results indicate that, especially for UV aging, material damage is concentrated on the cable surface, where it is most likely to alter electrical properties.

Although there was substantial variation in the adhesion tension of the virgin materials, all of the polluted surfaces had nearly identical adhesion tension. This phenomenon indicates that once a certain level of cable pollution is present, pollutant type and concentration dominate the surface electrical properties. Pollution increased the adhesion tension by 12 to 28 dyne/cm and was equal in significance to UV effects.

The total U.V. dose received during the 10 Day U.V. test was 220 KWh/m^2 or (792 MJ/m^2). This U.V. dose is equivalent to direct exposure in southern Arizona for about 1 year, direct exposure in Miami for about 1.5 years, or direct exposure in Northern Europe for about 3 years.[11] The amount of damage accumulated during U.V. testing was compounded by the 50°C test temperature, which is almost 30°C hotter than the average temperature for southern Arizona and 40°C hotter than for northern Europe. Black surfaces, however, can easily reach this temperature in the southern U.S.

In comparison to heat aging, where physical changes occur more uniformly throughout the material, UV aging localizes most of the damage to the surface of the material. The effects of UV on the surface properties are far more significant than the effects of either heat or UV on the bulk properties of the jacket material. Since the surface properties of the material are far more important for determining the overall electrical properties of the cable, surface measurements are far more useful in determining material robustness relative to real-world weathering effects.

Table 5: Adhesion Tension Measurement Results.

	Adhesion Tension (dyne/cm)			
	Cable A	Cable B	Cable C	Cable D
Virgin	6.3	13.8	19.4	2.5
Heat Aged	12.6	20.7	25.9	9.5
UV aged	42.6	29.5	29.5	30.0
Polluted	29.5	31.8	31.8	30.6
Aged and Polluted	41.6	45.6	45.6	30.6

Table 6: Change in Adhesion Tension Due to UV Aging and Pollution.

	Change in Adhesion Tension			
	Cable A	Cable B	Cable C	Cable D
Heat aging	6.3	6.9	6.5	7.0
UV aging	36.3	15.7	10.1	27.5
Pollution	23.2	18.0	12.4	28.1
Heat aging + pollution	35.3	31.8	26.2	28.1

Results of Salt Fog Testing

Table 7 summarizes the results of the salt fog testing carried out in accordance with IEEE P1222 Draft 1997 Annex A. This is a pass/fail test method where very little can be drawn from the results, other than the fact that Cable A, a with a standard HDPE outer jacket fails in short order under the harsh conditions and 30 kV.

Table 7: IEEE P1222 Draft 1997 Annex A Salt Fog Test Results.

	Cable A	Cable B	Cable C	Cable D
Virgin	Fail (1.6 h)	Pass	Pass	N/A
Heat Aging	N/A	Pass	Pass	N/A

Results of Accelerated Electrical Testing

The accelerated electrical testing resulted in a ranking of the four cables that were tested. Cable B performed the best followed by Cables C, D and A respectfully.

Figure 8: Contact Angle Measurements of Virgin, Aged, and Polluted Cable Samples.

Cable A - Virgin
$\theta = 85°$
$A_{SLV} = 6.3$ dyne/cm

Cable A – UV aged.
$\theta = 54°$
$A_{SLV} = 42.6$ dyne/cm

Cable A – Aged and polluted
$\theta = 55°$
$A_{SLV} = 41.6$ dyne/cm

Cable B - Virgin
$\theta = 79°$
$A_{SLV} = 13.8$ dyne/cm

Cable B – UV aged.
$\theta = 66°$
$A_{SLV} = 29.5$ dyne/cm

Cable B – Aged and polluted
$\theta = 51°$
$A_{SLV} = 45.6$ dyne/cm

Cable C – Virgin.
$\theta = 75°$
$A_{SLV} = 19.4$ dyne/cm

Cable C – UV aged.
$\theta = 66°$
$A_{SLV} = 29.5$ dyne/cm

Cable C – Aged and polluted
$\theta = 51°$
$A_{SLV} = 45.6$ dyne/cm

Cable D – Virgin
$\theta = 88°$
$A_{SLV} = 2.5$ dyne/cm

Cable D – UV aged.
$\theta = 65°$
$A_{SLV} = 30.6$ dyne/cm

Cable D – Aged and polluted.
$\theta = 65°$
$A_{SLV} = 30.6$ dyne/cm

Figures 9, 10, and 11 are representative plots of IMSQ vs. Time of a wet and dry cycle from the accelerated electrical testing performed at the ASU Electrical Engineering Department laboratory. Figure 9 shows current on a virgin cable rising dramatically then stabilizing at a constant value that indicates the cable is fully saturated with water. The current then remains level afterward for a short period after the spray is turned off, then becomes somewhat erratic for a short period indicating dry band arcing activity. However, the current then quickly falls off indicating a cessation of the arcing. This is a key indication that the virgin cables indeed show a high level of hydrophobicity.
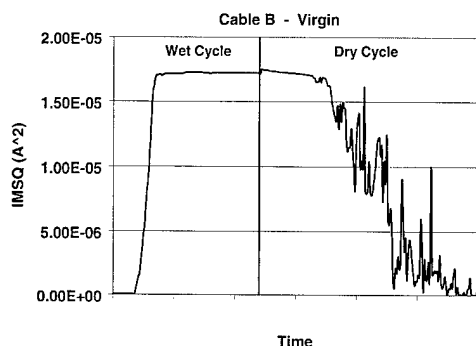
Figure 9: IMSQ vs. Time plot of Cable B – Virgin

In contrast, Figure 10 shows that in an aged cable, the current rises dramatically and somewhat sooner than the virgin cable, but then becomes erratic and never levels or drops off indicating a prolonged arcing period. This yields the conclusion that UV and Temperature / Humidity aging facilitates a more hydrophilic surface in which dry band arcing occurs sooner and lasts longer.
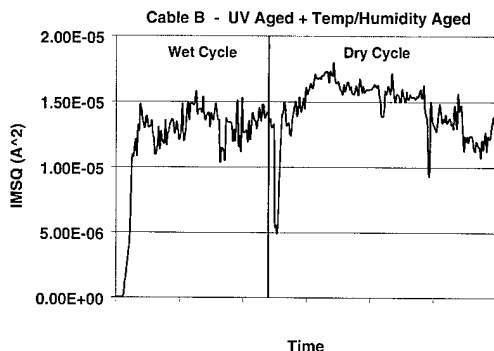
Figure 10: IMSQ plot of Cable B – UV Aged and Temp/Humidity Aged.

Figure 11 shows the complete IMSQ vs. Time plot for the virgin sample of Cable A. As indicated by the erratic behavior in the wet cycle, arcing began almost immediately and continued until this sample failed prior to completing the first wet/dry cycle. It is important to recall that this sample was tested at an equivalent space potential of 12

kV, a threshold value used by some cable manufacturers for their standard jacket material.
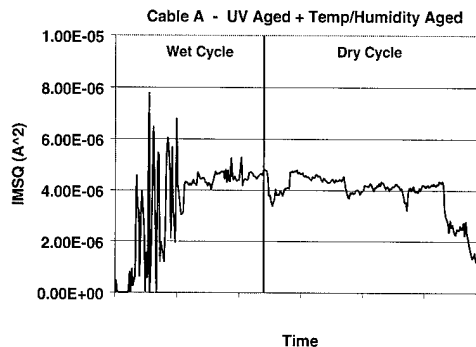
Figure 11: IMSQ plot of Cable A – Virgin.

CONCLUSIONS

Aging and pollution effects have been shown to significantly alter surface properties of ADSS cable jacket materials representative of a variety of materials used throughout the industry. These changes in surface properties have been correlated to significant differences in electrical test results simulating dry-band arcing. Based on a combination of surface property measurements and electrical test results on a variety of aged and unaged cable materials in this and previous studies, it is recommended that jacket material selection and installation guidelines be determined by electrical test data from aged cable samples. Installation guidelines using test data from aged cable samples will be more accurate for normal service life regardless of the type of jacketing material used. The use of aged cable data will ensure cable system robustness even if a combination of environmental and electrical factors act in combination. Guidelines for installation made without taking aging and pollution effects into account will not accurately assess the risk of system failure. Finally regional climatological factors should be an integral part of deciding where to place ADSS in the high voltage power system.

ACKNOWLEDGEMENTS

REFERENCES

[1] Besztercey, G., Karady, G., and Tuominen, M. W. "Corona Caused Deterieration of ADSS Fiber-optic Cables on High Voltage Lines." *IEEE Transactions on Power Delivery*, 14, No. 4 October 1999, 1438-47.

[2] Karady, G., *et. al.* "A Mitigation Method for Dry-band Arcing Caused Deterioration of ADSS Fiber-optic Cables",

Proceedings of The IEEE Power Engineering Society Winter Meeting, **4**, 2000, 2391-6.

[3] Tuominen, M.W., Bonneville Power Administration, private communications

[4] Keller, D.A, D.J. Benzel, J.P. Bonicel, C. Bastide, F. Davidson, "Continued Investigation of ADSS Designs and Reliability Considerations with respect to Field Voltage Tracking and Cable Installation Practices", *Proceedings of the 46th International Wire and Cable Symposium*, November 1997.

[5] Vaughan, A.S., S.G. Swingler, M. Lanfear, H. Weingandt, and H. White, "Laser Ablation and Thermal Decomposition Studies of Fiber Optic Cable Sheathing Materials", *IEEE proceedings*, October 1992, 501-510.

[6] Vaughn A.S., Robbie D A., Hosier I.L., Sutton S.J., "Simulations of Surface Discharge Damage on Self Supporting Fiber Optic Cables", *Plastics in Telecomm Proceedings*, 6E, September 1998, 87-96.

[7] Carter, C., *et al.*, "Mathematical Model of Dry Band Arcing on Self Supporting All Dielectric Optical Cables on Overhead Power lines", *IEE Proceedings-C*, **139**, No 3, May 1992, 185-96.

[8] Rowland S., et al. "Electrical Aging and Testing of Dielectric Self Supporting Cables for Overhead Power lines", *IEE Proceedings-A*, 140, No 5, September 1993, 351-56.

[9] Neogi, S, Risch, B.G., and Soltis, M., "Materials Reliability of Flooded and Dry-Core ADSS Cable", *Proceedings of the 48th International Wire and Cable Symposium,* November 1999, 795-806.

[10] R.G. Olsen, "An improved model for the electromagnetic compatibility of all-dielectric self-supporting fiber optic cable and high voltage poser lines," *IEEE Transactions on Electromagnetic Compatibility,* 41, No 3, August 1999.

[11] G.G. Karady, S. Devarajan, M. Tuominen, "Novel technique to predict dry band arcing failure of fiber optic cables installed on high voltage lines," *IEEE Power Tech '99 Conference*, Aug-Sept 1999, Paper PBT99-160-30, Budapest, Hungary.

[12] Kaser, V., *J. Colloid and Surface Sci.*, 56, 622 1972.; Adamson, A.W. *Physical Chemistry of Surfaces*, Wiley, New York, 1990.

[13] Data compiled by FAO-Environmental and Natural Resources Service (SRDN) Agrometerology Group, 1997.

[14] De Jong, B., *Net Radiation Received by a Horizontal Surface at the Earth*, Delft University Press, 1973.

[15] International Institute for Applied Systems Analysis, Laxenburg, Austria. Data complied from CORINAIR '90/94 and EMP/CLRTAP emission data.

[16] *1998 National Air Quality and Emission Trends Report,* EPA Office of Air Quality Planning and Standards. Research Triangle Park, NC, March 2000.

[17] *Clean Air Status and Trends Network (CASTNet) 1998 Annual Report*, U.S. Environmental Protection Agency Office of Air Quality Planning and Standards, Research Triangle Park, NC, August 1999.

[18] *RAINS – Asia*, International Institute for Applied Systems Analysis, Laxenburg, Austria.

[19] Kaser, V., *J. Colloid and Surface Sci.*, 56, 622 1972.; Adamson, A.W. *Physical Chemistry of Surfaces*, Wiley, New York, 1990.

AUTHORS

Swati NEOGI

OFCCC
Alcatel
Telecommunications
Cable

2512 Penny Rd.
P.O. Box 39
Claremont, NC 28610

Swati Neogi is a Senior Material Scientist and Project Manager at Alcatel's Optical Fiber Cable Competence Center. She received her Ph.D in Chemical Engineering from Ohio University. During her doctorate studies, she worked on modeling of simultaneous mass transfer and reaction of disc ring reactor used in the manufacturing process of polyethylene terepthalate. Before joining Alcatel in 1996, she worked in commissioning a PET plant.
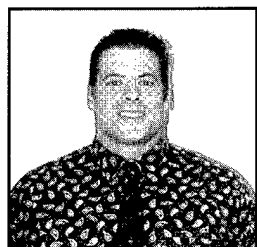
Brian G. RISCH

OFCCC
Alcatel
Telecommunications
Cable

2512 Penny Rd.
P.O. Box 39
Claremont, NC 28610

Brian G. Risch is the Materials Technology Manager at Alcatel Telecommunications Optical Fiber Cable Competence Center. He holds a B.A. degree in Physics from Carleton College and a Ph.D. in Materials Science and Engineering from Virginia Polytechnic Institute and State University. His Ph.D. research was in the area of polymer crystallization and structural property relationships in polymers. Directly after he finished his Ph.D. he worked for ORD laboratories in the area of optical polymers developing new polyurethane and polythiourethanes for high performance ophthalmic lens applications. Since 1996 Brian has worked for Alcatel's Optical Fiber Cable Competence Center (OFCCC) in the area of thermoplastic cable materials. His specialization has been in the area of and crystallization behavior and materials reliability for thermoplastic cable materials.

William F. DeWITT

OFCCC
Alcatel
Telecommunication
Cable

2512 Penny Rd.
P.O. Box 39
Claremont, NC 28610

William F. DeWitt is a Development Project Manager at Alcatel Telecommunications Optical Fiber Cable Competence Center. He holds a B.S. in Mechanical Engineering from Grove City College and a Masters in Business Administration from The Pennsylvania State University. Prior to joining Alcatel in 1999, William worked for AMP, Incorporated in a variety of positions ranging from Manufacturing Engineer to Plant Manager.

Pierre COAT

OFCCC
Alcatel
Telecommunications
Cable

2512 Penny Rd.
P.O. Box 39
Claremont, NC 28610

Pierre Coat joined Alcatel in 1992 after receiving his degree in Photonic and Optical Sciences in Lannion, France and completing a 2 months study program on optical fiber characterization at France Telecom. He is currently a microscopist and spectroscopist in the Material Development Laboratory at Alcatel Telecommunication Optical Fiber Cable Competence Center.
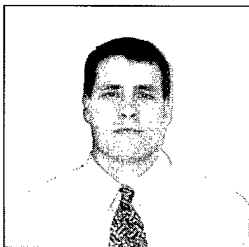
James D. AMMONS

OFCCC
Alcatel
Telecommunication

2512 Penny Rd.
P.O. Box 39
Claremont, NC 28610

James D. Ammons is a microscopist and material analyst at Alcatel Telecommunication Optical Fiber Cable Competence Center. He received his B.S. in Physics/ Mathematics from Lenoir-Rhyne College in Hickory, North Carolina. Before joining Alcatel, he served 5 years in the United States Navy and the U.S. Marine Corps.

George G. KARADY

Arizona State
University

Tempe, AZ
85287

George G. Karady received his BSEE and Doctor of Engineering Degrees in electrical engineering from Technical University of Budapest in 1952 and 1960 respectively. Dr. Karady was appointed to Salt River Chair Professor at Arizona State University in 1986. Previously he was with EBASCO Services where he served as a Chief Consulting Electrical Engineer, Manager of Electrical Systems, and Chief Engineer of Computer Technology. He was Electrical Task Supervisor for the Tokomak Fusion Test reactor project in Princeton. Dr Karady is a registered Professional Engineer in New York, New Jersey, and Quebec. He is the author of more than 100 technical papers.

Johnny A. MADRID

Arizona State
University

Tempe, AZ
85287

Johnny Madrid received his BS degree in Electrical Engineering from New Mexico State University in 1994 and a MS degree in EE from Arizona State in 2000. During his MS he worked on experimental test for correlating dry band arcing damage on ADSS cables to time to failure. Prior to attending school, Johnny worked for the Los Alamos National Laboratory on the Lunar Prospector Mission, part of NASA's discovery program, from 1996 to 1998. He also served in the United States Army during Desert Shield and Desert Storm in 1991.

Development of ECO-OPTICAL Fiber Cord

Toshinori Seki,   Tatsuo Yoshihara,   Yasuo Suzuki,
Masahiko Saegusa,   Kiyoshi Hiramoto

Showa Electric Wire & Cable Co. Ltd ., Miyagi, JAPAN

ABSTRACT

This paper summarizes the development of ECO-OPTICAL FIBER CORD (Ecological Optical Fiber Cord) by using polyamide compound with flame retardant additives for fiber jacket and halogen free, flame retardant poly-olefine (HF FR-PE) for cord jacket.

The comprehensive testing of the developed cord has revealed superior performance in mechanical and flame retardant characteristics as well as sufficient flexibility.

INTRODUCTION

In recent years, the prevalence of high-speed LAN systems in business and residential areas has been pushing the installation of various types of optical fiber cord in the office, home and inside the building.

PVC has been the most popular jacketing material for optical fiber cord, due to its frame retardant, flexibility, superior mechanical performance and easy coloring.

However, as harmful gas like dioxin generated from burnt PVC and lead compound included in PVC stabilizer turned lately out to affect adversely earth environments, social requirements arise to replace PVC with poly-olefin materials (PE).

We developed ECO-OPTICAL FIBER CORD (Ecological Optical Fiber Cord) by using polyamide compound with flame retardant additives and halogen free FR-PE (HF FR-PE), which revealed superior performance in mechanical and environmental characteristics.

Optical fiber cord structure
ECO-OPTICAL FIBER CORD

ECO-OPTICAL FIBER CORD is shown in Fig.1, Fig.2 and Table 1, respectively, for its view, sectional structure and specification.

ECO-OPTICAL FIBER CORD is featured by the combination of HF FR-PE cord jacket and flame retardant polyamide fiber jacket.

Fig1   ECO-OPTICAL FIBER CORD
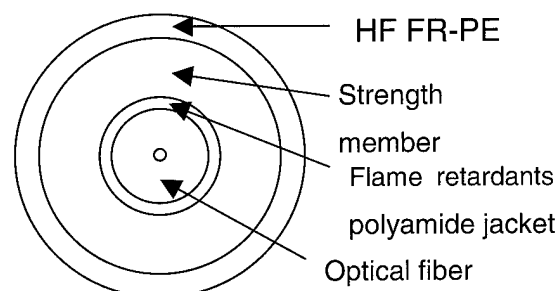
Fig2   Sectional structure
(ECO-OPTICAL FIBER CORD)

Table 1   ECO-OPTICAL FIBER CORD specifications

Contents			Specifications	
Poly amide jacket fiber	Optical fiber	Fiber type	SMF or GI	
		Coat resin	Heat cured silicone resin	
		Diameter	ϕ0.4mm	
	Fiber jacket	Material	Polyamide with frame retardants	
		Diameter	ϕ0.9mm	
Dielectric strength member		Material	Poly aramid fiber	
Cord jacket		Material	Halogen free FR-PE	
		Diameter	ϕ2.0mm	ϕ2.8mm

Design of ECO-OPTICAL FIBER CORD jacket

We have set the requirements for designing ECO-OPTICAL FIBER CORD as follows:

(a) Flame retardant : Self-extinction within 60 sec (According to JIS C 3005 INCLINED TEST)

(b) Smoking density : Ds = less than 150 (at only cord jacket) (According to JCS No.397A Section No.5)

(c) Generated gas acidity : PH = more than 3.5 (at only cord jacket) (According to JCS No.397A Section No.7)

(d) Materials to be used should be Halogen free and lead compound free.

(e) Superior performance in mechanical characteristics

(f) Good flexibility

(g) Easy coloring

(h) No dioxin should be generated from burnt PVC.

The flexibility of optical fiber cord is mainly affected by the hardness of the jacketing material so that we examined various types of HF FR-PE, which normally have trade-off relationships with flame retardant performance.

We chose one desirable material, which has sufficient softness close to that of PVC and rather high oxygen index, the specification of which is shown in Table 2.

Study of polyamide jacket with Frame Retardant

The use of this HF FR-PE as cord jacket, however, may cause the degradation of flame retardant performance of optical fiber cord, so that we considered its enhancement by adding flame retardant additives to polyamide fiber jacketing.

We chose amino-triazine compound as frame retardant additives for polyamide jacket, by putting it in the form of master batch (MB : 60 wt%) to polyamide resin.

Various types of trials were prepared by changing the ratio of flame retardant additives in the master batch ; 0, 20, 40, 60 wt%.

The outer diameter of the fiber jacket was 0.9 mm for all of the trials.

ECO-OPTICAL FIBER CORD test

Mechanical test

According to JIS C 6830, we examined mechanical test at wavelengh of 1310nm.

Table 3 shows mechanical performance of ECO-OPTICAL FIBER CORD , no optical transmission loss and no damage to the cord jacket in various mechanical tests.

Temperature cycling test

We examined optical transmission loss at wavelengh of 1310nm by 3 times cycling thetemperature in the range of between −10 degree C and +40 degree C.

Table 2　Material property of ECO-OPTICAL FIBER CORD jacket

Property		unit	HF FR-PE
Density		g/cm^3	1.55
MFR *1		g/10min	0.1
Tensile Strength		MPa	13.5
Elongation		%	210
Aging *2	TS	MPa	11.9
	EI	%	170
Oxygen index		-	39
Smoke density		Ds	120
Generated gas acidity		PH	4.2
Brittleness Temperature		Degree C	< 45

*1 : 230deg C　*2 : 100deg C – 48hours

Table 3　Mechanical performance of ECO-OPTICAL CORD

Contents	Test condition	Result
Tensile Loading	Tension:60N φ2.0mm Tension:80N φ2.8mm time : 5min	no loss variation (0.00dB) and no damage of Jacket
Compressive Loading	Term load : 5N/mm Time : 1min	
Repeated Impact Testing	Hammer weight :100g Hammer height : 1m Striking surface diameter : 25mm at 3cycle	
Cord Cyclic Flex test	Bend diameter : 50mm 1000cycles , Tension:20N	
Cord Bend test	Wind diameter : 50mm 6 turn , 10 cycle	
Twist Test	Sample length : 250mm Tensile load : 2kg , 20 cycle	

Fig 3 shows temperature performance of ECO-OPTICAL FIBER CORD , optical transmission loss variation less than 0.02 dB/km in the range of between −10 degree C and +40 degree C
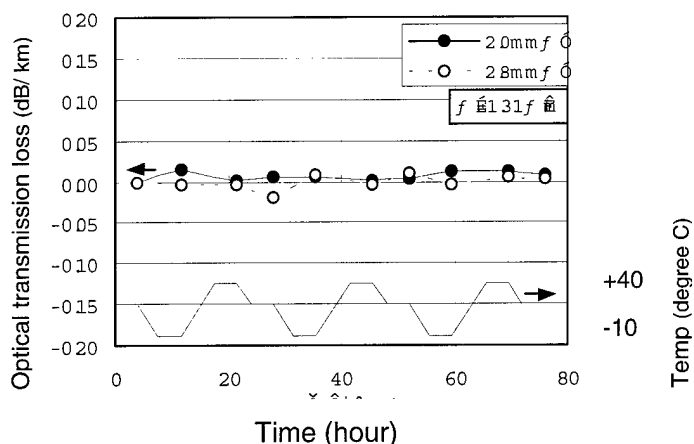
Fig 3   Temperature performance

Material property of ECO-OPTICAL FIBER CORD jacket

According to JIS C 6830 , we examined Material property of ECO-OPTICAL FIBER CORD jacket. We used cylindrical sample of the cord jacket.

Table 4 shows cord jacket , revealing high performance to satisfy specification to the cord jacket in various material tests.

Flame retardant test of ECO-OPTICAL FIBER CORD

We prepared two types of ECO-OPTICAL FIBER CORD, which have outer diameter of 2.0 mm and 2.8 mm

Table 4 Material property of ECO-OPTICAL FIBER CORD jacket

Contents		Specification	Result
Tensile strength		more than 10MPa	13.8MPa
Elongation		more than 200%	222%
Aging *1	TS	Retained more than 80%	102%
	EI	Retained more than 80%	83%
Shrink back *2		Within 10%	2.6%

*1 : 100deg C – 48hours   *2 : 100deg C – 1hours

respectively, both of which using jacket material as shown in Table 2 and flame retardant polyamide fiber jacket.

The tests were done in accordance with JIS C 3005 Incline Test , as shown in Fig 4.

Test results are shown in Table 5, together with the pictures of burning pattern for Samples A and D shown in Fig 6.

Table 5   JIS C 3005 incline test result

Sample	Fiber jacket (Concentration of flame retardants M.B)	Cord jacket : HF FR-PE	
		φ2.0 mm	φ2.8 mm
A	Polyamide (0 wt%)	Failure	Failure
B	Polyamide (20 wt%)	Failure	Failure
C	Polyamide (40 wt%)	Failure	Failure
D	Polyamide (60 wt%)	Pass	Pass
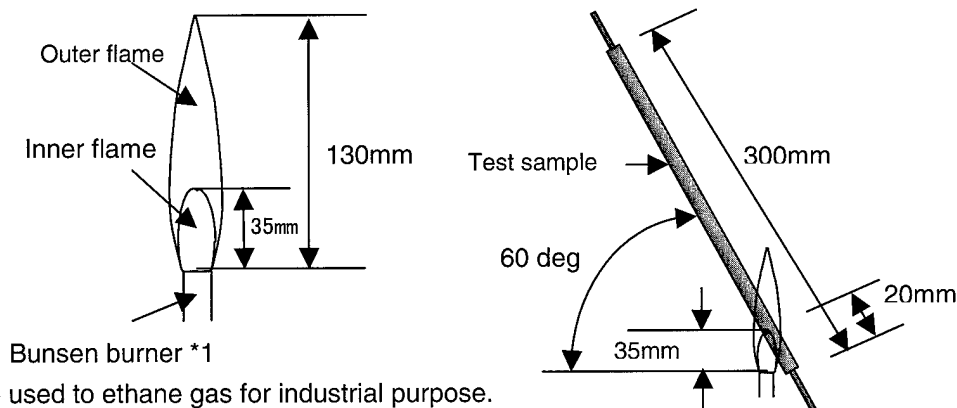
*1 : We used to ethane gas for industrial purpose.

*2 : We put out Bunsen burner after ignite for 10sec.

Fig 4   Test method (JIS C 3005 incline test)

Sample A : The flame, after ignition, gradually became smaller due to flame retardant effect of HF FR-PE, but, reached finally to the upper end.

Samples B and C : The flame reached to the upper end in both samples, but, the size of flame became smaller than Sample A.

Sample D : The flame self-extinguished within 60 seconds after ignition, passing the flame retardant test JIS C 3005 Incline Test.
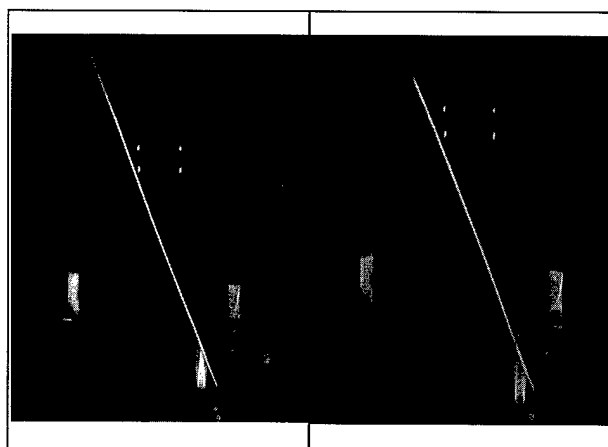
(a) Immediately after ignition

(d) 40 sec after ignition
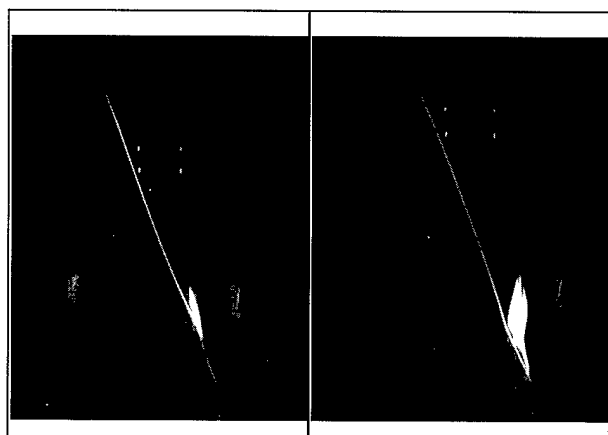
(b) 10 sec after ignition
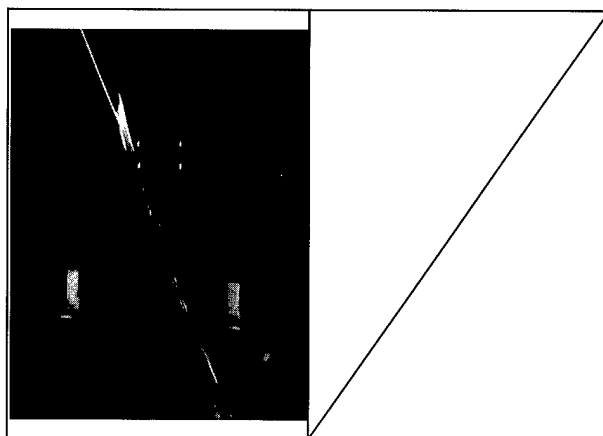
(e) 180 sec after ignition
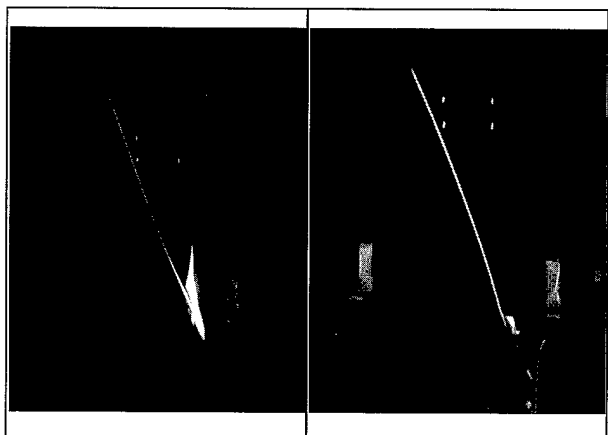
(c) 30 sec after ignition

Left side : Sample A
Right side : Sample D

Fig 6   Burning pattern of ECO-OPTICAL FIBER CORD

Discussion

We have found that the samples showed different burning patterns depending on the ratio of flame retardant additives in polyamide resin.

The heat decomposition process of amid-triazine, generally, is described as shown in Fig 7.
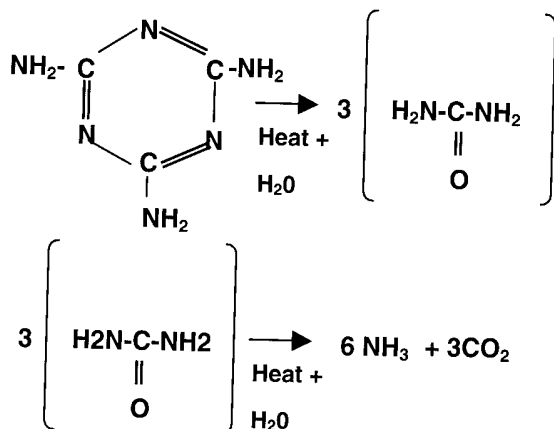
Fig 7 The heat decomposition process of amino-triazine

When amino-triazine compound is burnt, low hostile, nonflammable gas like carbon dioxide and ammonia will be generated by the heat decomposition. The more the compound, the more the amount of gas.

We consider that when the amount of these nonflammable gasses is sufficient enough, the gasses will fill the interstices inside the cord, keeping oxygen away from flame, so as to make the flame self-extinguished.

Conclusion

We have researched HF FR-PE, flame retardant polyamide and their combination, and examined them on its frame retardant performance (JIS C 3005 Incline Test).

That study has revealed that appropriate combination of type and contents of flame retardant additives in polyamide jacketing is important for the flame retardant performance of optical fiber cord with HF FR-PE jacket.

The newly developed ECO-OPTICAL FIBER CORD, which consists of halogen free and lead compound free materials, has shown not only high performance in flame retardant and mechanical characteristics but also sufficient flexibility similar to the conventional PVC jacketed optical fiber cord.

Toshinori Seki

Showa Electric Wire
& Cable Co., Ltd.
No.1 Nabekura
Funaoka Shibata-gun
Miyagi-ken , 989-1606
JAPAN

Toshinori Seki received his B.S degree from Science University of Tokyo in 1992. He joined Showa Electric Wire & Cable Co., Ltd. in 1992.

He is an engineer of the Fiber Optic Group Telecom. Engineering Dept.

Ultrasonic Inspection Of Central Strength Member for Fiber Optic Cable Applications

David L. Fecko[1], Curtis Carter[2], Dirk Heider[3], John W. Gillespie, Jr.[3]

1. Owens Corning Science and Technology Center, Granville, Ohio
2. Owens Corning Science and Technology, Duncan, South Carolina
3. Center for Composite Materials, University of Delaware, Newark, Delaware

Abstract

This paper describes ultrasonic, non-destructive evaluation (NDE) techniques for the inspection of composite rods, which are used as a central strength member in optical fiber cable constructions. Failure of a strength member can lead to loss in the signal carrying capability of the fiber optic cable. The purpose of this research is to use on-line, ultrasonic NDE to inspect the composite strength member for defects during the production process so that they can be repaired or removed. Two ultrasonic inspection techniques were evaluated: through-transmission immersion inspection and rolling contact bulk wave analysis. Both techniques were expected to be capable of discerning gross defects such as delaminations. However, the velocity measurements obtained in the bulk wave analysis were also able to detect changes in the materials' mechanical stiffness. The study includes work that was performed both off-line in a post-processing application, and in-line during simulated and actual composite rod production.

Keywords

Ultrasonics; non-destructive evaluation; central strength member; pultrusion; fiberglass composite; cable reinforcement

1. Introduction

Fiber optic cables are designed for many different applications, from trans-oceanic to plenum and breakout designs. There are myriad designs to address the specific needs of each application. The primary purpose of the cable is to house and protect the optical fiber from end to end. It must keep the fibers safe from environmental, physical, and chemical damage. In general, there are strength members built into the cable in order to protect the fiber from the damage associated with laying, cornering, and similar actions that can cause stress and strain. One of the most common elements used in this function is a Central Strength Member.

The Central Strength Member (CSM) is the backbone of a fiber optic cable. Central Strength Members can be made of many materials, including fiberglass composite rods. These products provide flexural stiffness to protect against buckling of the cable during installation. They also impart excellent dimensional stability owing to their consistent diameter and shape. High tensile modulus in the CSM carries the stresses that may be placed on the fiber optic cable if the cable is designed properly. Any failure of the CSM will lead to problems either in cable construction, or in the ability of the cable to transmit a signal.

Furthermore, the cost of the CSM is a very small portion of the total cable cost. It is very important to detect and correct any problems with the CSM before it reaches a cable manufacturer. The most common defect with this product is split rod. Split rod occurs when a point defect, such as a clump of broken glass filaments, is entrapped in the rod. The rod, being of unidirectional design, can only rely on the strength of the fiber to matrix bond strength to hold it together in the direction perpendicular to the fibers. When a defect causes a large enough stress concentration to overcome the fiber to matrix bond strength, the rod can split, as shown in Figure 1.
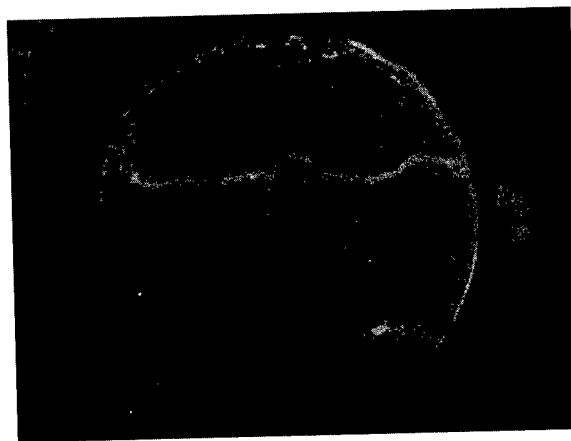
Figure 1. Micrograph of Split Rod Defect

The CSM is manufactured using the pultrusion process. In a typical pultrusion process, the fibers are supplied from several packages of material mounted on a creel. The fibers feed through a tensioning device and into a dip tank containing the polymer resin. The fibers, which are wet out with the resin, then go into a die where they are formed into the finished cross section. The forming die typically is heated to initiate the curing reaction in the polymer. The material that exits the die is then cut into sections or, in the case of CSM, wound onto spools for shipment. This process lends itself nicely to in-line inspection, because a correctly located inspection station can provide 100% inspection of the product on-line.

2. Ultrasonic Inspection

Ultrasonics offer an opportunity to examine the mechanical integrity and surface quality of the rod without mechanically straining the rod. The idea is to send an ultrasonic wave through

the rod in a pitch/catch type arrangement. The received signal can be analyzed for velocity to determine if there are any changes in modulus, and attenuation to determine if there are any defects or delamination present. This type of inspection is not completely new, but applications to inspect pultruded parts during the manufacturing cycle are rare.

Ultrasonic inspection techniques have been used to inspect pultruded parts successfully. In 1993, Fecko et al. [1] used an acousto-ultrasonic technique to detect porosity in a unidirectional pultruded rod of rectangular cross-section. The same pultrusion process was later inspected using the ultrasonic velocity of plate waves [2]. On-line inspection of pultruded composites for the aircraft industry has also been accomplished using more traditional pulse-echo techniques [3]. The primary goal of the aircraft inspection application was to find porosity and resin starved areas in the composite. In another recent application, bridge decks planned for the University of New Mexico were inspected off-line using the velocity of ultrasonic waves traveling in specific directions [4]. These velocities were used to determine the elastic modulus of the composite, which were then used to check the bridge design using a finite element code. These recent applications suggest that ultrasonic evaluation may be applicable to the in-process inspection of the CSM.

The velocity of an ultrasonic wave in a material is a function of its density and modulus. For homogeneous bulk materials, the speed of a longitudinal wave is given by Equation 1.

$$V = (E/\rho)^{0.5} \qquad (1)$$

Thus, a change in velocity signifies either a change in modulus, or in density, or both. This signal is very useful for process control, as it signifies the glass content in the composite. Varying glass content will effect both the density of the rod, and it's modulus.

The strength of an ultrasonic pulse in the pitch/catch arrangement is based on the power of the sending transducer, the sensitivity of the receiving transducer, the distance over which the pulse travels, and the number and type of boundaries that the pulse travels through. All of these variables, with the exception of the last one, are generally held fixed. A typical ultrasonic pulse travels through two boundaries in a pitch catch arrangement, one when the pulse enters the sample and one when it leaves the sample. The acoustical impedance of the materials determines the amount of transmission from one side of an interface to the other. The greater the difference in acoustic impedance, the more reflection will occur, and less transmission. Once again, if the sample is homogeneous, and the transducers are held in a fixed location, the signal intensity will not change. However, when there is a change in the sample, the intensity will change. For example, if there is a delamination, the sound will have 2 additional interfaces to travel through, one into, and one out of the delamination. Thus the amplitude of the transmitted signal contains information about the presence or absence of defects in the sample.

Another technique, acousto-ultrasound (AU), can be used to excite and detect Lamb waves in laminated composite materials. A unique feature of the Lamb wave is the dispersive nature of the wave propagation. The speed of sound depends not only on the material modulus but also on the propagation frequency.

Tang et al. [5] summarizes the results of the "higher order plate theory" for the flexural mode. The calculation of the dispersion dependency is based on plate stress-strain relationship in a laminate and thus, can be applied to any composite. Also the solution (often called the characteristic wave equation) is in not invertable, simple optimization schemes can enable the calculation of the material properties.

The characteristic wave equation for an orthotropic laminate (Equation 2) depends on wave number k=ω/v (frequency, velocity), material properties (extensional stiffness A_{55}, bending stiffness D_{11}, and density ρ) and the laminate thickness (h).

$$\left(D_{11}k^2 + A_{55} - \frac{4}{3}\rho\omega^2\right)\left(A_{55}k^2 - \rho h\omega^2\right) - A_{55}^2 k^2 = 0 \qquad (2)$$

Especially for the upper and lower bounds of the lamb wave frequency, Equation 2 simplifies to

$$\upsilon(\omega \to 0) = \sqrt{\omega\sqrt{\frac{D_{11}}{\rho h}}} \qquad (3)$$

$$\upsilon(\omega \to \infty) = \sqrt{\frac{A_{55}}{\rho h}} \qquad (4)$$

For the intermediate frequencies, the phase velocity v(f, D_{11},A_{55}) is a function of both D_{11} and A_{55}. Figure 2 shows the theoretical obtained dispersion curve for the composite rod with model input values of D_{11}=114 Nm, A_{55}=1.4x10^7 N/m, ρ=2100 kg/m^3, and h=3 mm.
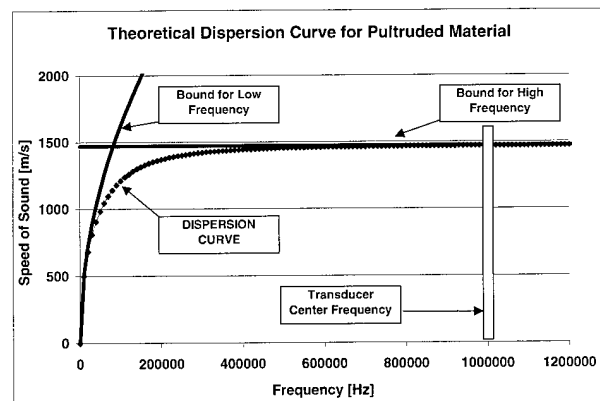
Figure 2: Theoretical obtained Dispersion Curve

2.1 Experimental

Two primary means of ultrasonic analysis were examined; immersion and rolling contact. The immersion system was designed to send an ultrasonic pulse through the rod in a direction perpendicular to the fiber. The rolling contact arrangement was designed to send an ultrasonic pulse along the length of the rod, parallel to the fiber direction. Each system had its advantages and weaknesses, and these will be discussed next.

2.1.1 Immersion testing

Ultrasonic inspection using two immersed transducers was investigated. Two Krautkramer 5 MHz unfocussed immersion transducers were mounted on either side of a stainless steel test fixture (Figure 3). There was a hole in the center of the test fixture for the composite rod to go through. The test fixture was flooded with water, and an ultrasonic pulse was sent. The pulse was generated using a Krautkramer USPC 2100 Ultrasonic Instrument. The signal was generated with a 250-volt spike pulse at a repetition rate of 10 kHz. The receiving signal sensitivity was set between 40 and 60 dB gain. A gate was set at an appropriate level to detect the split rod defect.
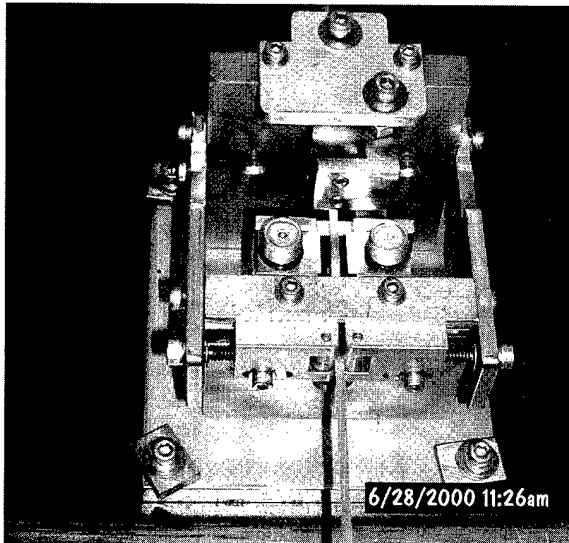
Figure 3. Ultrasonic Immersion Test Fixture

The split rod defect is a form of delamination of the composite rod. It causes the ultrasonic signal to travel through more interfaces, thus decreasing the signal amplitude. When the signal dropped below the gate level, an alarm was triggered.

A small 2.3mm rod was used for the trial, as it was expected to be more difficult to inspect the smallest diameter rods using this technique. Defects were induced using a utility knife, slitting the rod at various angles and lengths to simulate the split rod defect. The only time that the splits were not detected were when they were positioned in the same plane as the transducers. For this reason, a second set of transducers was positioned at 90 degrees from the first set. These initial attempts at performing this inspection on-line were very successful at slow speeds, but as the line increased to production speeds, the signal intensity became varied. The variation was a result of several causes. One cause was slight movement of the sample up or down, which changed the path of the ultrasonic wave from going through the rod, to traveling around the rod. This would cause a large increase in the amplitude. To correct for the movement of the rod, focussed paintbrush type transducers were used. These transducers focus the ultrasonic beam onto the rod and do not allow the signal to bypass the sample (Figure 4).

Figure 4. Focussed Paintbrush Transducer

When this type of transducer was used in a through-transmission mode, the system was quite capable of picking up defects at both the low and high speeds. However, this method does not give any information about the modulus or density of the composite.

2.1.2 Rolling Contact Testing

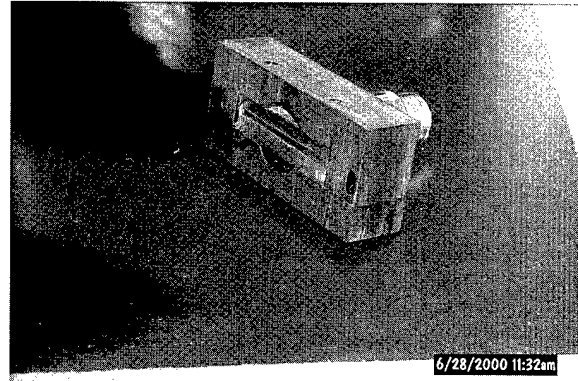A second type of ultrasonic testing was evaluated using transducers that coupled to the CSM via a rolling elastomeric layer. These transducers were positioned 50mm (approximately 2 inches) apart in the fiber direction, so that the ultrasonic wave traveled along the fiber direction, as opposed to the immersion testing where the ultrasonic wave traveled perpendicular to the fiber direction. The reason for this arrangement was two-fold. First, by sending the wave through a longer distance in the CSM, more material can be inspected with a single pulse. Secondly, this type of arrangement allows one to measure the ultrasonic velocity in addition to the attenuation. The attenuation will yield information about the presence or absence of defects between the transducers. And the velocity will yield information about the physical properties (modulus and density) of the composite.

A photograph of the test fixture is shown below in Figure 5. In this figure, the transducers are fixed in-between two guide wheels. The guide wheels help keep the CSM in the center of the rolling contact transducers, and allow a fixed pressure to be applied for consistent coupling.
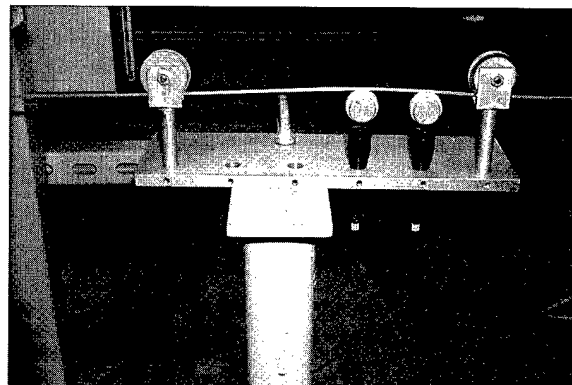
Figure 5. Rolling Contact Test Fixture.

The ultrasonic wave propagated in this arrangement is similar to a Lamb wave that travels in a plate. It will have coupled shear and longitudinal components. The rolling contact arrangement was used to inspect a 3.0mm diameter sample of CSM. The rod was first examined off-line after production. However, in subsequent trials the inspection was applied on-line during the manufacture of the CSM. A typical signal trace of the ultrasonic pulse after traveling through the composite is shown in Figure 6.
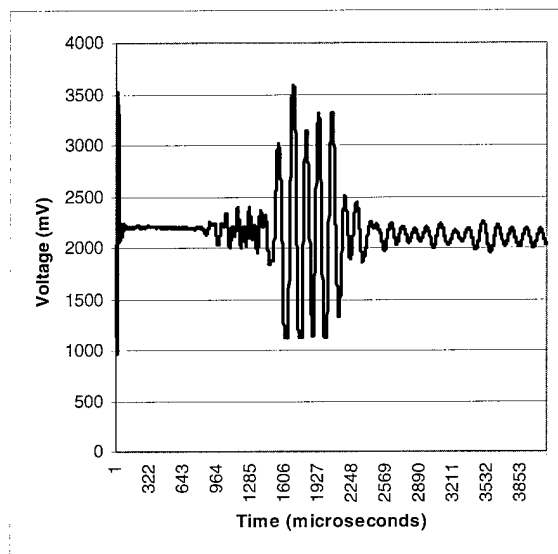
Figure 6. Typical Ultrasonic Signal

In this trace, one can see three distinct portions; first a fast traveling low amplitude signal, followed by a slower, high amplitude portion, and finally a low amplitude "ringing" portion. The fast signal appears to have the most longitudinal character. A longitudinal wave is the fastest wave in this case. It's speed and amplitude are influenced by the glass content in the composite, and it is expected to be relatively insulated from defects such as splits oriented along the fiber direction in the rod. The higher amplitude middle section is the portion of the signal that appears to hold the most promise as an inspection signal for split rod. When the rod is damped in-between the transducers by pinching it with one's fingers, this signal is eliminated.

The high amplitude signal was analyzed for velocity on a set of 18 samples tested off-line. The velocity of each sample was measured using the arrival time of the largest peak and the distance separating the two transducers as a fixed distance. These samples were then examined to determine the glass content. Recall from Equation 2 that the velocity of an AU ultrasonic wave is related to its physical properties. The velocities as a function of glass content are given below in Figure 7. The correlation between ultrasonic velocity and glass content is a direct result of an increase in the elastic modulus and density as the glass content of the composite rises.

To calculate the theoretical effect of density and modulus change, Equation 2 was used to calculate the speed of sound variation at a frequency of 1 MHz, the approximate center frequency of the contact transducers. The speed of propagation as a function of the modulus and density is shown in Figure 8.
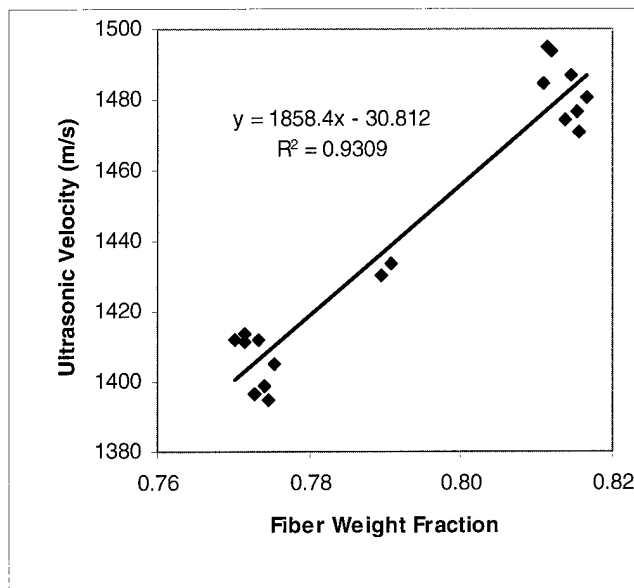
Figure 7. Ultrasonic Velocities vs. Glass Content
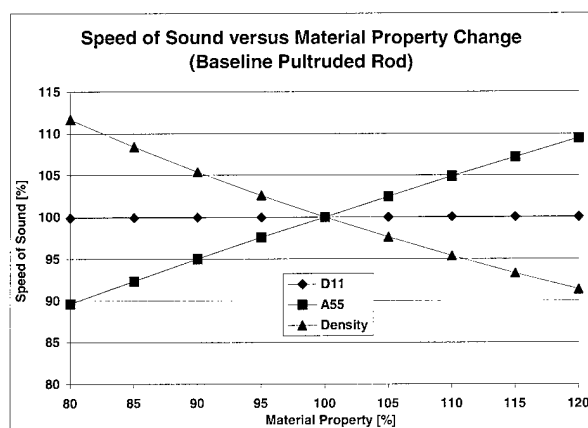
Figure 8: Sensitivity Analysis of AU-Velocity

It can be clearly seen that the speed of sound is not sensitive to a D_{11} stiffness shift. This is due to the high transducer center frequency of 1MHz which is near the upper frequency bound (Figure 3) and thus Equation 4 can be applied. Density and A_{55} have an inverse effect on velocity change, an increase in density decreases the speed of sound whereas an increase in A_{55} increases the speed of sound. Overall the decrease in experimentally obtained AU-velocity from the highest material density to the lowest given in Figure 7 (3% change) is approximately 5%. The density reduction for lower fiber volume fractions increases the AU-speed by approximately 2%. Thus, the dominating effect must be associated with a decrease in stiffness. Applying Equation 4 to a 5% velocity decrease (incorporating the decrease in material density), the stiffness reduction in A55 can be calculated to be

24% from the highest fiber weight fraction to the lowest fiber weight fraction in Figure 7.

To examine the effect of more severe defects on the propagation of the bulk waves, several "split rod" type defects were induced using a utility knife and bending the sample. These defects caused the signal amplitude to decrease and often to shift to a later arrival time, i.e. slow down. This is to be expected, as damage in the composite will add transition layers that cause reflection, and also will decrease the composite's modulus. This system was also tried on the production line during the production of several reels of CSM product. For the production trial, the system was set up using a 'gate' to alarm if the signal intensity dropped below a predetermined value of approximately 50% of the original signal. The ultrasonic pulser/receiver alarm output was hooked up to a data logger that recorded all alarms. Alarm status is indicated by a –5V signal for 3 seconds. The device was sampled every 2 seconds, ensuring that every alarm was captured. There were 3 reels of material that were produced using this inspection method. Of the 3 reels, only one had any problems associated with it. In that case, a contact point became clogged with a small amount of fuzz, resulting in a slightly rough surface on the rod. The ultrasonic inspection immediately signaled that there was a problem, and the operator performed an in-depth inspection of the line and found the source of the problem, which was a clogged forming die. The run was allowed to continue to observe the capability of the ultrasonic inspection system. The output (Figure 9) shows how the alarms became more frequent as the problem intensified.
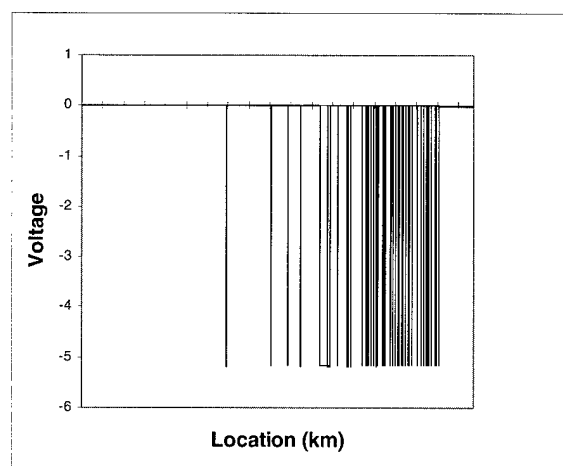
Figure 9. Rolling Contact Production Trial

3. Conclusions

The pultrusion manufacturing process is easily adapted to an in-line inspection that checks 100% of the product. This paper focussed on the use of ultrasonics to inspect the composite rod. Immersion testing and Rolling Contact testing were examined. Of the two techniques, the rolling contact testing yielded the most information about the quality of the rod. Defects such as split rod

were easily detected by examining the signal amplitude. Observing the velocity of the ultrasonic signal can also monitor physical properties such as modulus and density of the composite. These techniques will be refined until they are suitable for use in the production environment to help continue to meet or exceed customer expectations and product quality.

4. Acknowledgments

5. References

[1] D. L. Fecko, K. V. Steiner, and J. W. Gillespie, Jr. "Acousto-Ultrasonic Inspection of Pultruded Composites," in 1993 SAMPE Technical Conference

[2] D. L. Fecko, "In-situ Ultrasonic Porosity Monitoring for the Thermoplastic Matrix Pultrusion Process," Ph.D. Dissertation, University of Delaware, 1996

[3] R. W. Englebart, M. L. VanDernoot, D. D. Coppens, C. Koppernaes, "On-Line NDE of Pultruded Airframe Stiffeners," in 43rd International SAMPE Symposium, 1998

[4] A. K. Maji, K. Donnelly, M. Salas, "Terrestrial Applications of a Composite Lattice Space Structure," in International SAMPE Symposium and Exhibition (Proceedings) v 43 n 1, 1998.

[5] B. Tang, E.G. Henneke, II and R.C. Stiffler, " Low frequency flexural wave propagation in laminated composite plates", Proceedings on a Workshop on AU: Theory and Applications, Blacksburg, Virginia, pp.45-65, 1987.

David L. Fecko is a Senior Scientist in the Owens Corning Electrical and Telecommunications group. He holds a Bachelor and Masters degree in Polymer Science from The Pennsylvania State University, and a Doctor of Philosophy degree in Materials Science from The University of Delaware's Center for Composite Materials. Please send correspondences to:
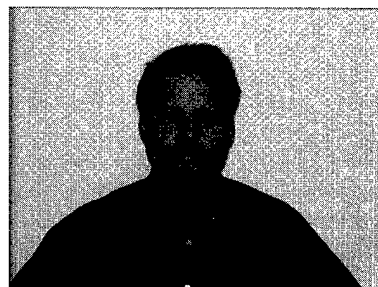
Dr. David L. Fecko
Owens Corning Science and Technology Center
2790 Columbus Road, Route 16
Granville, OH 43023

Thermal and Mechanical Optimization of Easy-Access Flexible Buffering Materials

George Dallas Ph.D., Geoff Witt, Brian G. Risch Ph.D., Melissa Stouffer,
Vincent Bourget, and Nelly Drabczyk

O F C C C
Alcatel Telecommunications Cable & Alcatel Cable France
2512 Penny Rd, Claremont, NC

ABSTRACT

Over 40 polymer blends were investigated for flexible buffer tube applications for fiber optic cable. A variety of compounds based on copolymers of polypropylene, polyethylene, and/or EVA were investigated in terms of mechanical characteristics, melting behavior, and processibility. Optimal material properties based on melting point, energy to break, yield behavior, and ultimate elongation were developed and related to functional requirements. Buffer tube access using a variety of techniques was related to energy to break, yield behavior, and ultimate elongation.

Varying the volume percent of high melting point polyolefin had a systematic effect on buffer tube melting behavior. Additionally, small changes in composition had significant effects on modulus (flexibility), yield behavior, as well as elongation and energy to break. Processing conditions effected residual buffer tube shrinkage, crystallinity, and mechanical properties. Additionally, the combination of buffer tube material and geometry effected accessibility. Finally, the requirements developed in the study are combined in order to produce a flexible buffer tube possessing enhanced handle-ability and accessibility. With the improvements in mechanical properties, a ripthread access system was designed. This resulted in easier access of active fibers without significant attenuation increases.

INTRODUCTION

Due to increased demand for high capacity telecommunications systems, access and distribution sections of networks are facing greater space and cost constraints. In order to fit a higher fiber density into existing cable rights of way, new, higher fiber density cables are being developed.[1,2] With these new cable designs comes a need for new flexible buffering materials.[3]

Efficient design of the cable structure requires high fiber counts per cross-sectional area and easy access to the fiber bundle. This paper focuses on tailoring the buffer tube material in a semi-tight buffered cable so that it protects the fibers and allows for easy mid-span access. A rip thread in the buffer tube enhances the ease of access[4], but requires optimized buffer tube material properties to ensure that fibers are not placed under excessive stress during access. The buffer tube and rip thread mechanical properties are intentionally selected so that a mid-span access can be performed with minimal attenuation increases in the fibers. The advantage of the rip thread system is that there is low risk of damage to the fibers and there are no special tools required.

The present materials used for buffer tubes include impact modified polypropylene, (i-PP), polyvinylchloride, (PVC), and polybutyleneterephthalate, (PBT). PVC and PBT work for certain cable designs and applications, but have some weaknesses for a semi-tight buffered application which include:

- Shrinkage
- Plasticizer migration, some PVC compounds
- Hydrolytic Stability
- Mechanical changes with aging
- Thermal Stability

Although the current generation of i-PP materials does not have the above problems, it is too tough for a rip thread application. Therefore, a customized polyolefin compound tailored to meet specific mechanical and thermal requirements for access was developed. This polyolefin compound was formulated to have optimized mechanical properties for easy access along with elevated thermal stability to maintain dimensional stability during jacketing and use. This paper reviews how composition, processing and design were customized and how mechanical properties related to ripthread access and attenuation of the fibers.

EXPERIMENTAL

A wide variety of characterization techniques were used to determine the thermal and mechanical properties of the buffer tube variants. They included tensile, thermomechanical, differential scanning calorimetry, and dynamic mechanical thermal analysis. The tensile properties were determined on an Instron 4202 with an XL extensiometer at room temperature and 100 mm/min.

The thermomechanical, dynamic mechanical, and differential scanning calorimetry were conducted on TA models 2940, 2980 and 2920 respectively. Thermal tests were performed in a temperature range from −125°C to 200°C at 10°C/min. under nitrogen. The cooling was done on a GCA cooler for the dynamic mechanical tester and a LNCA cooler for the differential scanning calorimetry.

Crease diameter measurements were done by looping a buffer tube on itself and pulling on one end to make the loop smaller. The point where tube buckled was called the crease diameter.

Attenuation measurements were made on an EG&G model CPM 500 power meter. The attenuation was measured at 100 msec intervals at a wavelength of 1550 nm.

Materials

Four polyolefin based materials were blended together to optimize the buffer tubes mechanical properties. These materials included two grades of hard impact polypropylene (H-i-PP) and a soft grade of impact polypropylene (S-i-PP). A soft polyethylvinylacetate (EVA) copolymer was also used in some formulations. These materials were blended in combinations of two or three polymers to manipulate modulus, yield stress and strain, and energy to break.

RESULTS AND DISCUSSION:

The benefit of a polyolefin blend is that one can tailor the mechanical properties of the finished product with the strengths of each component. Requirements of the material were that it have a melt point above 155°C, a yield strength between 5 to 15 MPa and an elongation to break between 500 and 900 % elongation. Also, the yield strain must be above 5%. The material must also be compliant and dimensionally stable from –40°C to 85°C.

Initially, a discussion of the range of material strengths should be reviewed. Figure 1 is a plot of stress vs strain for the H-i-PP, PVC, and the S-i-PP. The first two are presently used as buffer tube materials. The H-i-PP has high modulus and high stress at yield compared to PVC. This is due to the semicrystalline nature of the polymer. The PVC, an amorphous plasticized polymer, has lower modulus and high strength, but no distinct yield point, because it is not semi crystalline like the H-i-PP.

The S-i-PP material has a lower stiffness than H-i-PP and it has a lower yield stress. Also, the S-i-PP has higher elongation to break. The critical region of the stress strain curve is the energy to break for and PVC, and the energy to yield for the S-i-PP the H-i-PP. Essentially, the stress and energy needed to start deformation is higher for the H-i-PP and PVC than the S-i-PP. This is related to the energy needed to start a tear in the buffer tube with the rip thread. Once the material has yielded, it will continue to deform and fracture with continued tearing from the rip thread.

Figure 2 is a plot of breaking strength and elongation for all of the compositions tested. Composition is listed on the x-axis in terms of volume percent H-i-PP/S-i-PP/EVA and cooling conditions (low and high cooling rate).
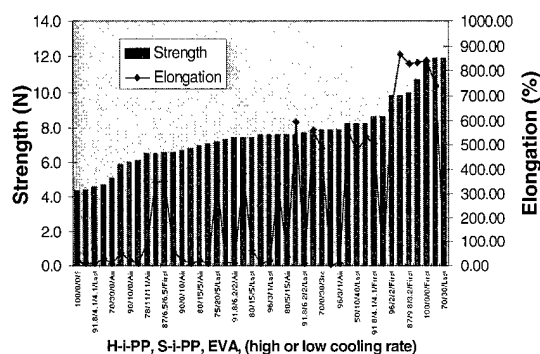
Figure 2: Strength and Elongation for the Materials Tested

Creasing of the buffer tube while being looped over a small diameter is an undesirable characteristic. This creasing was determined for all of the materials and plotted in Figure 3. This creasing was determined to be related to yield strain. Thus materials with yield strains greater then 6% had very low probability of creasing under normal handling conditions. The observed stains coincide well with the calculated ones, where the surface strain is equal to the radius of the tube divided by the radius of diameter of the buffer tube loop.

Figure 1: Stress vs Strain for Flexible Buffering Materials
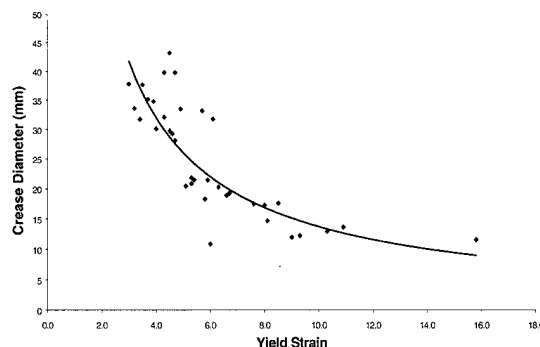
Figure 3: A Plot of Crease Diameter vs. Yield Strain

Changing the buffer tube wall thickness was also used tochange the ease of rip thread access. Figure 4 shows the influence of buffer tube wall thickness on the load required to open the buffer tube. Reducing the load to tear, by increasing the wall thickness from 1x mm to 2x mm doubled the required load to yield the material. All three of these loads were found to be at an acceptable level to propagate a tear. Although, reducing the load makes the rip thread easier to use and can reduce the load on the fiber bundle.
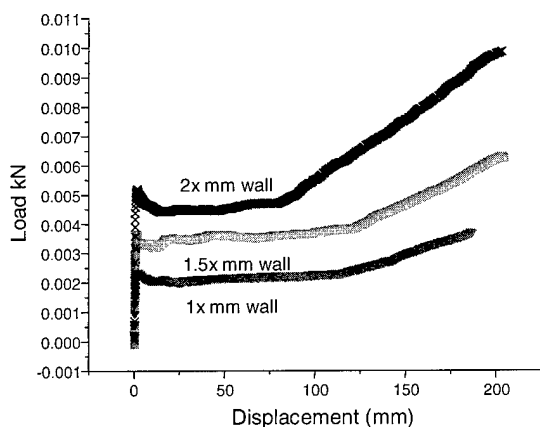
Figure 4: Load vs Displacement as a Function of Buffer Tube Wall Thickness

Besides understanding the effect of design and mechanical properties, it was also necessary to explore the effects of processing and composition on the thermal properties. Figure 5 shows the effect of either quench cooling or slow cooling the polypropylene buffer tubes. The slow cooled sample shows very little dimensional change as a function of temperature, while the quench cooled tube has much more thermal expansion after 50°C. The stability of the air cooled sample is attributed to the increased crystallinity and increased thermodynamic stability of the crystalline phase due to slower cooling. More time at optimal crystallization conditions is possible with air cooling. The processing change resulted in energies to melt of 66 J/g for the quench cooled materials and 72 J/g for the slow cooled materials. This corresponds to a 9% difference in melting energy and crystallinity. The elongation to break for these materials also varied between high and low cooling rates. This variation allows for tailoring the buffer tubes mechanical properties by process changes.
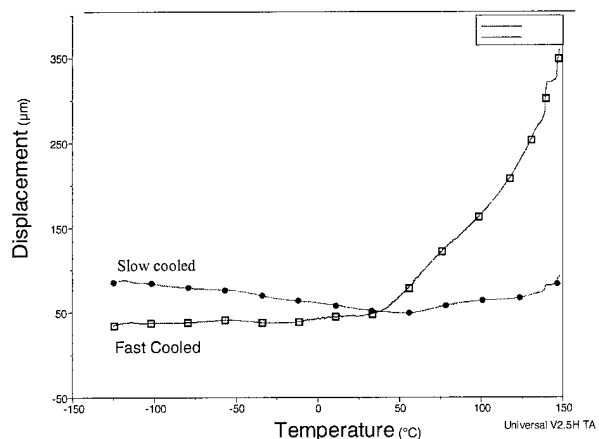
Figure 5: Displacement vs Temperature as a Function of Processing Conditions

Differential Scanning Calorimetry

Incorporating increasing amounts of the higher melting point materials increased the overall melting points of the blends, Figure 6. High melting points are necessary to insure thermal stability of the buffer tubes during jacketing and end use. The compounds tested varied from 100% S-i-PP to 100% H-i-PP. The most pronounced variation in crystalline melting point was seen when amounts between 1 and 25% of the H-i-PP were incorporated into the blend. When greater than 25% of H-i-PP was added, little additional effect on melting point was noted. Therefore, 25% of H-i-PP is the minimum amount necessary to insure ensure dimensional stability through processing.
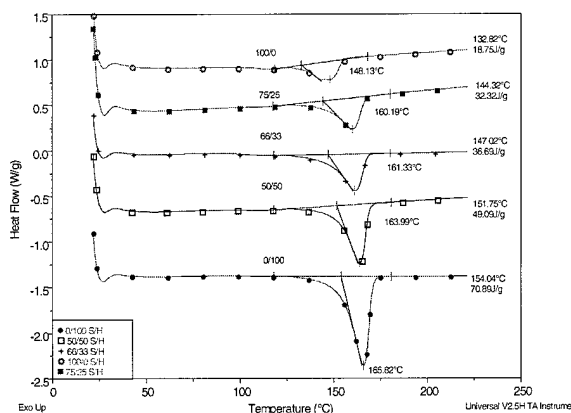
Figure 6: Differential Scanning Calorimetry vs Blend Composition
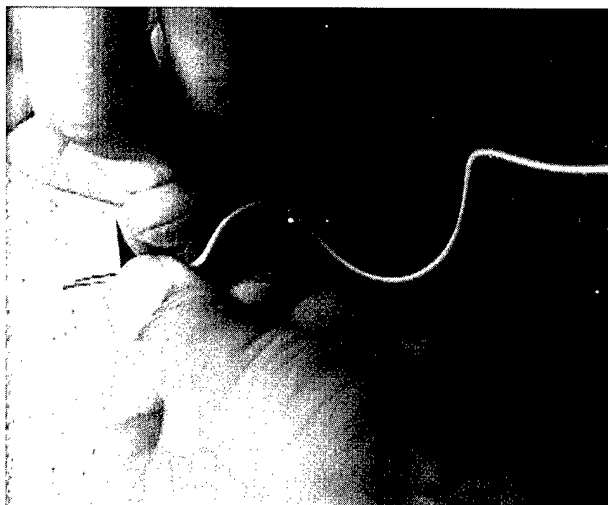
Figure 7a: Buckling of PVC Buffer Tube During Initiation of Tear with Rip Thread

Figure 7b: Spreading of PVC Buffer Tube from Pulling by Rip Thread

Access

Attenuation as a function of access was performed during all access steps for ripcord and tool access to determine which step(s) caused the most significant attenuation increases. The various steps for ripcord access were: 1) ring cut, 2) access of the rip thread, 3) initiating the tear and 4) continuation of the tear. The tool access method for PVC varied only in that instead of using a ripcord, the tube was split with a tool. Attenuation measurements during rip thread was performed with both the PVC and polypropylene blend buffer tubes. Typical attenuation increases are shown in Table 1 for ripcord access of PVC and the polyolefin blend as well as for PVC with tool access. PVC access with the tool and ripcord access with the polyolefin blend both result in negligible attenuation. Low attenuation during access is best accomplished by using a rip thread and an optimized poly-olefin blend.

Figures 7a and 7b show that initiating the tear in the rip thread with a PVC compound caused the fiber bundle to buckle resulting in macrobending loss. The resulting peaks were up to several dB for PVC during rip thread access. Negligible attenuation increase occurred during the other midspan access steps. Figure 7b shows that the PVC could not easily be torn and deformed instead. This illustration shows that the key to low loss mid-span access with a rip thread is to reduce the energy to initiate a tear.

Figures 8a and b show access and attenuation for the polypropylene buffer tube. The initiation of the tear with the rip thread took much less energy and the rip thread could be easily torn through long spans of buffer tube, without damaging the fibers. The resulting attenuation increases was typically less then 0.1 dB, which was a significant improvement compared to PVC ripcord access. These long tears in the buffer tube resulted in the buffer tube being easily removed from the fiber bundle, with very low loss.

Figure 8a: The Rip Thread Initiating a Tear in Polypropylene Buffer Tube

Figure 8b: Removal of the Buffer Tube from the Fiber Bundle

Table 1. Typical Attenuation (dB) vs Access Step for PVC and i-PP Buffer Tubes

	Ring Cut	Initiate Tear	Pulling Thread	Remove Tube
Ripcord Access				
PVC	< 0.1	1-120	~ 0	0
i-PP	0.1- 0.5	< 0.1	~ 0	0
Tool Slitting Access		Slitting		
PVC	< 0.1	n.a	< 0.5	0

CONCLUSIONS

The new generation of semi-tight cable designs carry with them the benefit of significantly simplifying the access to the optical fibers within the buffer tube. To maximize this benefit, improved polyolefinic blends, product geometry and process control are required. These not only permit easy access into the optical fiber cable, but reduce the risk of damage or service interruption in the optical network.

The rip thread accessibility of a semi-tight buffer unit is directly related to the composition and processing of the material. Materials with optimized yield energies or lower energies to break than conventional materials must be used. The mechanical properties that are required have been successfully identified and a material has been developed to meet these requirements. A new easy access technique has been developed that allows access on live fibers with reduced risk to signal attenuation.

ACKNOWLEDGEMENTS

We would like to thank Will Thomas, Stefan Richter and Stephen Schmidt for making the buffer tube samples. We would also like to thank the OFCCC modeling group for their insightful discussion on material bending mechanics.

REFERENCES

[1] Garcia, M., *et. al., Proc. 47th International Wire and Cable Symposium,* 1998, 57-65.

[2] Pastruska, S., et al., *Proc. 48th International Wire and Cable Symposium,* 1999, 106-111.

[3] Risch, B., et al., *Proc. 48th International Wire and Cable Symposium,* 1999, 199-203.

[4] Harbort, H., et al., *U. S. Patent,* 4,909,593, Mar. 20, 1990.

Author Information
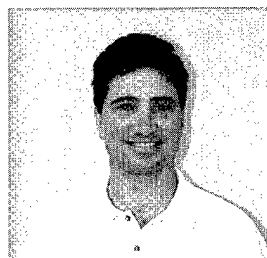
George Dallas
Alcatel OFCCC
2512 Penny Rd.
P.O. Box 39
Claremont, NC 28610

George Dallas is a scientist in the Materials Group at Alcatel Telecommunications Optical Fiber Cable Competence Center. He holds a B.S. degree in Chemistry from Hartwick College, an M. S. in Chemistry from San Jose State and a Ph.D. in Materials Science and Engineering from Virginia Polytechnic Institute and State University. His Ph.D. research was a fundamental study of materials response in the GHz frequency region and the effects of water and aging on high temperature poly(amide-imides). Directly after he finished his Ph.D. he worked for Beloit Manhattan in the area of failure analysis and materials development for roll covers used in paper machines. Since 1999 George has worked for Alcatel's Optical Fiber Cable Competence Center (OFCCC) in the area of thermoplastic cable materials. His specialization has been in the area of compounding filled semi-crystalline thermoplastics for optimized processing, properties and reliability in cable applications.

Armored Flame Retardant Sheaths For Indoor/Outdoor Cable

Felix Achille & Kenneth E. Bow

Engineered Laminates, The Dow Chemical Company
Midland, Michigan
517-636-6417 · fachille@dow.com
517-638-3759 · kebow@dow.com

Abstract

Cables with an armored flame retardant sheath can be used indoors where flame retardancy is required and outdoors where mechanical strength and rodent protection are needed. The use of dual purpose armored cable can reduce the costs of terminations in buildings and increase the overall reliability of the system by protection from environmental hazards. A new coated steel with a polyolefin based coating has been developed for bonded sheaths for either optical fiber or metallic cable that has the ability to bond to either polyvinyl chloride (PVC) or halogen-free polyolefins (HFPO) jackets. This coating has a lower melting point versus the standard coatings used for bonding to polyethylene jackets. As a result the bonding to PVC and HFPO jackets is facilitated at the lower melt temperatures associated with the extrusion of these jackets.

Keywords

Flame Retardant, Armored, Indoor, Outdoor, Cable, & Steel

1. Introduction

The use of an armored cable with a flame retardant sheath results in a single cable design that can be used in both indoor and outdoor applications. This cable sheath can be used indoors where flame retardancy is required and outdoors where mechanical strength and rodent protection are desired. Without a flame retardant sheath, it is often required that the cable design be switched from a non-flame retardant outdoor design to a flame retardant indoor design. Alternatively, the outdoor cable must be run in conduit to its termination point. Such procedures increase the cost of installation both from material and labor points of view.

The construction of local area networks (LAN's) or so called "campus networks" also favors the use of dual-purpose indoor/outdoor cable. A campus environment typically consists of multiple buildings that require both indoor and outdoor rated cables. The use of dual rated cable greatly facilitates the installation of such networks. It is possible to further reduce costs by having the flexibility to locate electronic components at distances greater than the 50 ft. (15 m) necessitated if conduit and standard outdoor cables were used. This allows the electronics to be placed conveniently for system operation.

There is also a new class of cable called "powered broadband" [1]. This cable contains fibers and low voltage power conductors. This, in turn, allows the electronics to be placed where needed in the system and to be conveniently powered by the communications cable. The use of an armored flame retardant cable sheath essentially packages the fibers and conductors in its own conduit. This facilitates the installation of the cable and the steel provides a certain level of shielding for the power conductors. The use of dual purpose armored cable reduces the costs of terminations and increases the convenience of installation saving labor costs as well.

The benefits of using armored cable in the outdoor environment have been documented elsewhere [2,3]. These benefits are rodent and other wildlife protection, mechanical protection, especially crush and impact resistance, moisture and chemical resistance and waterblocking of the jacket armor interface. Some additional benefits are the ability to use the coated steel armor as a means to monitor the sheath for intrusion and long distance locating from a central point [4,5].

2. Materials for Armored Flame Retardant Sheaths

2.1 Coated Steel

Typically, a bonded sheath is used with the coated steel armor. A bonded sheath is one in which the plastic coated steel is adhesively bonded to the outer jacket (plastic oversheath) of the cable. In the case of outdoor cable, various types of polyethylene are used. As mentioned previously, polyethylene is not suitable where flame retardancy is required. For indoor/outdoor (I/O) cable, a flame retardant jacket such as polyvinyl chloride (PVC) or halogen-free polyolefin (HFPO) based compound must be used. The standard copolymer coating used on the steel for polyethylene jackets is not compatible with PVC. A special coating is required on the steel to be adhesively compatible with the polar nature of the PVC. A new coating system with a unique copolymer was developed to be compatible with PVC jackets. In the process of working with this PVC compatible steel, it was discovered that it is also compatible with HFPO jackets. There were advantages to using this steel with HFPO compounds as well as the PVC jackets. The first is that a single armor can be used for flame retardant sheath applications calling for either a halogenated or halogen-free jacket. The second is that this coating can form a high level of bond strength to these jackets at significantly lower melt temperatures.

The properties of the coated steel with the PVC compatible coating are shown in Table 1. These properties are compared to the standard copolymer coated steel used for outdoor applications with polyethylene jackets. The more elastic nature of the PVC compatible coating results in an apparently lower peel strength (coating-metal bond). The heat seal property (coating-coating bond) is comparable. This product meets the requirements of ASTM B736 for a Type I, Class 1 coated metal.

Table 1. Comparison of the Properties of I/O Coated Steel to Standard Coated Steel

Coated Steel	Compatibility	Minimum Adhesion* in N/m (lb/in)	
		Peel	Heat Seal
Indoor/Outdoor	PVC, HFPO	350 (2.0)	1750 (10.0)
Standard	PE, HFPO	610 (3.5)	1750 (10.0)

*Specification Values

The PVC compatible coating does not contain any PVC or other halogenated components. It is not inherently flame retardant. (Obviously, the bonded sheath system relies on the jacket to provide the flame retardancy). Since the coatings are polyolefinic in nature, they can also provide high levels of corrosion protection to the steel.

It should be pointed out that the standard coating is also compatible with the HFPO jackets. However, the breakthrough is to use the PVC compatible coating with HFPO jackets and gain the advantage of higher levels of bond at lower melt temperatures. Also note that various HFPO, PVC and LSPVC jackets were used for these studies.

2.2 Polyvinyl Chloride (PVC) Jackets

General purpose PVC jackets are normally designed to meet the flame test requirements for the vertical tray type of cable test such as UL1581, IEEE 383 or 1202, or IEC 332-3C or the specimen tests, such as VW-1 or IEC 332-1. These jacket compounds contain plasticizers, which may compromise smoke properties. PVC compounds are regarded as inherently flame retardant due to their halogen (chlorine) content but various additives are often added to increase flame test performance.

A new class of low smoke (LS) PVC compounds have been specially formulated to meet the smoke and propagation requirements of the UL910 plenum fire test [6]. These compounds differ from the general purpose compounds because they contain special additives for smoke suppression, special polymeric plasticizers and char formers. The key properties they offer are low smoke and extremely low levels of flame propagation.

2.3 Halogen Free Polyolefins (HFPO)

The development of halogen free materials was driven primarily by the defense and transportation industries [7]. In particular, the lessons learned from shipboard and subway fires led to the development of halogen-free materials with properties of low smoke and fume to improve serviceability of equipment and safety of personnel. These materials received acceptance in the communications industry because the low fume characteristic was very important in preventing collateral damage to electronic equipment from the smoke generated during a fire situation. The smoke from halogenated materials, in particular, could cause high levels of corrosion of the electronics resulting in costly failures of equipment remote to the actual fire [8].

2.4 Adhesion

A jacket bond test developed in the laboratory was used to evaluate the adhesive compatibility of the coated steel with the HFPO and PVC compounds. A plaque or sheet of the jacketing material is first prepared in a heated press. The plaque is 152 x 152 mm (6 in x 6 in) in dimensions and 1.9 mm (0.075 inches)

thick. After the plaque is prepared, a layer of steel is placed on the plaque with a strip of polyester film at one end. The sandwich construction is then reinserted into a press heated to 182°C (360°F). The bonding time is 2.5 minutes with 25 tons platten pressure. The laminate is then cooled to 15.5°C (60°F) in 2.5 minutes under the 25 tons of platten pressure. The laminate is then cut into test samples having the dimensions of 25 x 152 mm. The test samples now have the structure of a laminate sheath from a cable.

Adhesive strength is then determined on a tensile testing machine using a test speed of 50 mm/min (2 inches/min) and a 180° angle of separation. The use of the polyester film to prepare the sample allows a tab to be formed which is inserted in one jaw of the tensile tester while the jacket is inserted into the other jaw. A steel bar is inserted with the jacket to keep the peel angle at 180°.

The adhesion results are shown in Table 2.

Table 2. Jacket Bond Strength of I/O Coated Steel to PVC and HFPO Jacket Compounds

Jacket	Adhesion in N/m (lb/in)	
PVC	1402	(8.0)
LSPVC-1	2979	(17.0)
HFPO-3	3435	(19.6)

The number after the compound is only an identifying code.

3. Manufacture of Armored Flame Retardant Sheath

3.1 Cable Sheath Preparation

An experimental sheathing line was used for the preparation of cable samples for testing. This line uses commercial forming and extrusion equipment. Cable samples were prepared using a corrugator in line with a cone former to corrugate and shape the steel armor. A commercially available core was enclosed within the armor. A jacket was applied over the longitudinally formed steel with a 63.5 mm (2.5 inch) 24:1 L/D ratio extruder. A 10 turn metering screw with a 3:1 compression ratio was used with the PVC compound and a 2:1 compression ratio screw was used with the HFPO compound. Melt temperature was set according to guidelines recommended by the compound manufacturer.

3.2 Corrugation Profile

The depth of the corrugations and the number of corrugations per unit length are the most important parameters for the performance of the bonded sheath in mechanical tests [9]. Performance in the bend (FOTP-37) and flexibility (FOTP-104) tests, in particular, depends on the corrugation parameters. The simple rule is that if the number of corrugations per unit length is increased, then less depth may be required to obtain the same relative performance in the mechanical tests. The obvious advantage to use more corrugations and less depth with the HFPO and PVC compounds is that it should be easier to fill the corrugations with polymer. Filling the corrugations is another key parameter for performance of a bonded sheath. Filling the corrugations results in the highest levels of bond strength and acceptable performance in the mechanical tests.

For the cable samples prepared for testing the corrugation number was 14 corrugations/inch (25.4 mm) and the depth was 0.032 inches (0.84 mm). These are the standard conditions for the cable diameter

chosen for tests. Cable diameter is also a factor in choice of corrugation parameters. For diameters less than 15 mm, for example, 20 corrugation per inch could be used. The depth could be reduced to 0.35 mm and the cable may still achieve the required mechanical performance.

3.3 Preheat

The use of preheat on the coated steel may also help facilitate corrugation fill. Typically, there are four ways to preheat the coated steel after it has been formed around the cable core and before it reaches the cross-head of the extruder. These are 1) induction; 2) quartz lamps; 3) hot air guns; and 4) gas flame. The induction method is the preferred method. It heats the steel exclusively by using radio frequencies to generate eddy currents in the steel. The quartz lamps are normally assembled into a tunnel configuration and rely on infra-red radiation to heat the steel. Generally, two or more hot air guns are required. They rely on convection to heat the steel. With both the lamps and the hot air guns, a lot of heat is lost to the environment. The oldest method is the gas flame. The gas flame can oxidize the surface of the coatings and actually prevent a bond at the overlap and to the jacket. There is a high level of inefficiency with the gas flame.

3.4 Bonded Sheaths with HFPO Compounds

Processability of HFPO's are reduced over polyethylenes because of their high filler loadings. This creates the situation where they have a higher melt viscosity and, therefore, are more difficult to run through an extruder. The high melt viscosity raises pressures in the extruder to levels that, in turn, limit rpm, line speed and output. This is illustrated in Table 3 for two commercially available HFPO compounds. For the particular extruder and polyethylene screw used in these trials of processability, the limits on extruder pressure were reached long before the capacity of the extruder was exceeded.

Table 3. Processability of HFPO Jacketing Compounds

Jacket	Extruder Speed, (rpm)	Melt Temp., °C	Output, kg/hr	Cross-head Pressure, MPa
HFPO-2	25	160	54.5	30.5
	50	-	-	>34.5
HFPO-3	25	154	49.5	26.8
	50	155	102.2	30.8

There have been attempts to improve the processability of the HFPO compounds [10]. As Table 3 shows the third generation product is more extrudable than the second generation product, which could not be run at 50 rpm. However, it was not possible to run over 50 rpm on the laboratory extruder with the third generation product due to pressure limitations.

The basic issues with obtaining good adhesion to coated steel with HFPO compounds are the relatively low melt temperatures they require and their high melt viscosities due to their high filler loading. This is illustrated in Table 4 for the coated steel with the standard copolymer coating and an HFPO compound. The bond strength is very low compared to that obtained with a polyethylene jacket using the standard extruder conditions for polyethylene. The high melt viscosity of the HFPO compound limits the ability of the HFPO to flow into the valleys of the corrugations. Basically, the extrudate wants to rest on the crests of the corrugations. Typically the crests only represent about 10 to 20% of the surface area

available for bonding. Bond strength to this limited area is not enough to give a functional sheath.

Table 4. Adhesion of HFPO and LLDPE to Corrugated Coated Steel with Standard Coating

Jacket	Adhesion in N/m (lb/in)	
LLDPE	2454	(14.0)
HFPO-1	584	(3.33)

In a subsequent extrusion trial melt temperature on HFPO-3 was increased and the die and tip configuration was changed to force flow of the compound directly onto the coated steel armor. The "pressure extrusion" configuration is obtained by moving the tip forward relative to the position of the die. This allows the extrudate to flow radially into the corrugations of the coated steel as it exits the die. As a consequence, the corrugations are filled with polymer and the bond strength is substantially increased. These data are shown in Table 5.

Table 5. Adhesion of HFPO-3 to Corrugated I/O Coated Steel

Extrusion Condition		
Melt Temp. °C (°F)	165	(329)
Pressure MPa (psi)	22.7	(3280)
Adhesion N/m (lb/in)	3399	(19.0)

3.5 Bonded Sheaths with PVC Compounds

A LSPVC compound was used in one set of trials to make a bonded sheath. A PVC screw was used to extrude this resin. It was found that the LSPVC compound offered more flexibility during processing than the HFPO compounds. As the data of Table 6 show the HFPO compound was approaching the limit on cross-head pressure for the extrusion line while even at 100 rpm the LSPVC compound was showing a relatively low pressure of 12.3 MPa which is well below the operating pressure of the extruder. There was a significant difference in output, however, with the LSPVC having about half the output of HFPO at 50 rpm. However, the LSPVC had more flexibility from a process standpoint than the HFPO compound. This flexibility allows pressure extrusion to be used with the LSPVC compounds to achieve corrugation fill without adversely affecting extruder pressures.

Table 6. Processability of Halogen Free (HF) and Low Smoke Polyvinyl Chloride (LSPVC) Cable Compounds

Compound	Extruder Speed, (rpm)	Melt Temp., °C	Output, kg/hr	Cross-head Pressure, MPa
HFPO-3	50	155	102	30.7
LSPVC-2	50	159	52	12.3
	100	160	111	12.2

3.6 Mechanical Performance

A new category of cable, Network-Powered Broadband Communications Cable, was created for use in accordance with Article 830 of the National Electrical Code. The requirements for these cables are covered in Subject 2261 of the Underwriters Laboratories and are in accordance with UL 13 and UL 444.

For indoor cable, UL 444 and Telecordia TA-NWT-00131 are applicable. For outdoor cable, the REA/RUS PE-90, ANSI/ICEA S-87-640 and Telecordia GR-20-CORE Issue 2 are applicable.

Previous work has shown that the bonded sheath with a HFPO or LSPVC jacket can meet the mechanical requirements for indoor and outdoor cable according to the UL and Telecordia standards [11]. Other work has shown that an armored bonded sheath cable with a PVC jacket can meet the requirements for powered broadband cable [12].

3.7 Flame Performance

Flame testing was conducted using the IEEE 383 vertical tray flame test. This is a general purpose test similar to UL 1581 and IEC 332-3. It uses a 70,000 BTU/hr (20.5 kW) flame source. Cable samples 8 ft (2.7 m) long are mounted in a vertical tray. The test duration is 20 minutes and the test requirement is that the flame not propagate the length of the tray.

A cable sample was prepared on the experimental jacketing line for the flame test. For this particular cable the core consisted of 4 number 10 AWG copper conductors enclosed in an overall jacket of PVC. The coated steel was corrugated then formed over this core and jacketed with the HFPO-1 compound. The armored cable and PVC jacketed core were tested separately for the sake of comparison. The results are shown in Table 7. The armored cable had a slightly greater char height versus the PVC jacketed conductors. The explanation for the difference is that the armor may act to conduct some of the heat away from the burn area, which, in turn, increases the char height.

Table 7. Results of IEEE 383 Vertical Tray Flame Test* for Armored Bonded Sheath Cable

Sheath	Armor	Char Height, m (ft)	Pass?
PVC Core	No	0.9 (3.0)	Yes
HFPO Steel	Yes	1.0 (3.3)	Yes

* IEEE 383 is a small scale test to provide a laboratory rating of the relative flammability for cable under controlled conditions. Results of this test are not intended to reflect behavior of the cable or materials in an actual fire situation.

There was an interesting result with respect to the smoke generated. A smoke density light obscuration test was used to quantify the smoke generated in the tests. A smoke detector measures the amount of light blocked due to smoke from the test cable. The concept behind this test is to be able to view an "EXIT" sign throughout the test. For the armored cable, the "EXIT" sign was clearly visible during the test. The amount of light that was blocked was 43%. For the PVC jacketed core, there was a large quantity of smoke. It appeared that the armor and HFPO jacket acted as a fire and smoke barrier thereby providing additional protection to the core.

A similar observation was made in the UL 910 horizontal cable tests of shielded cable with an HFPO jacket. The test was not passed using the HFPO jacket. However, there was evidence that the shield was acting as a fire barrier. There was a reduction in the rate of flame propagation throughout the test when the metallic shield was part of the sheath construction.

It has been previously reported that the armored cable with the PVC jacket would pass the UL 1666 riser test [13].

4. Conclusions

A unique coated steel product has been developed for indoor/outdoor cable applications. This coated steel is adhesively compatible with both PVC and HFPO jacketing compounds. It allows the fabrication of flame retardant sheaths for use indoors while providing the mechanical, rodent and moisture resistance needed for outdoor applications. This coated steel facilitates the manufacture of bonded sheath because it has a coating with a lower melting temperature. This is an aid to the bonding process since most PVC and HFPO compounds are extruded at relatively low melt temperatures.

The key processing limitation with PVC and HFPO jacketing compounds is their relatively high melt viscosities which, in turn, are related to relatively high filler loadings. This makes it difficult for these compounds to flow into the corrugations of the coated steel. It was demonstrated that the use of pressure extrusion could aid in corrugation fill and the fabrication of an acceptable bonded sheath.

The armored cable with a flame retardant jacket can meet the flame requirements for indoor cable and provides the mechanical, rodent and moisture resistance required for outdoor cable. The use of a single cable for both environments results in considerable cost savings for the cable user by eliminating the need for splicing different cable designs together at the entrance point to the building. The flame retardant, armored sheath design is especially suitable for construction of local area networks, "campus networks," and applications calling for powered broadband cable.

4. Acknowledgements

5. References

[1] UL Subject 2261, Network-Powered Broadband Communications Cable, Underwriters Laboratory, 1285 Walt Whitman Road, Melville, NY, 11747-3081, USA (Feb. 8, 1999).

[2] K. E. Bow, "Comparison of Armored and All-Dielectric Fiber Optical Cable Designs," *Wire and Cable Technology International*, 46-48 (November 1998).

[3] K. E. Bow and W. F. Busch, "Armored Fiber Optical Cable for Subscriber Use," *Wire Journal International* (February 1988).

[4] J. Chamberlain and D. Vokey, "Fiber Optic Preventative Maintenance: Increasing Reliability and Plant Longevity," *Proceedings of the EuroCable Conference 1998*, 304-312 (EC'98).

[5] J. Chamberlain and D. Vokey, "Going Where No Tone Has Gone Before," *Outside Plant*, 58-63, (May 1999).

[6] C. Glew and J. Kotak, "Improved Low Smoke Fire Retardant Compounds for Plenum Cable Applications," *Wire and Cable Technology International*, 58-61 (November 1998).

[7] P. Watmore, "Today's Cable Considerations," Wire Industry, 444 (June 1990).

[8] V. Babrauskas, R. D. Peacock, E. Braun, R. W. Bukowski and W. W. Jones, "Fire Performance of Wire and Cable: Reaction-to-Fire Tests – A Critical Review of the Existing Methods and New Concepts," *Technical Note 1291, U.S. Department of Commerce* (October 1991).

[9] W. F. Busch, K. E. Bow and D. G. Pikula, "Effect of Sheath Processing Parameters on Cable Performance," *Proc. International Wire and Cable Symposium*, 427-433 (November 1989).

[10] J. Preston, D. Sawyer and L. P. Artingstall, "The Use of Halogen Free, Fire Retardant Materials in LAN and Communication Cables, and a Look Towards the Next Generation," *Wire Industry*, 403-408 (May 1998).

[11] K. E. Bow, "Armored Flame Retardant Fiber Optical Cable for Indoor/Outdoor Applications," *Proceedings of the EuroCable Conference 1999*, 61-68 (EC'99).

[12] J. Heevey, M. Gimblet, J. Register, "Development and Application of a Composite Fiber/Copper Cable with Remote Powering Capabilities," Proceedings of the 48th International Wire and Cable Symposium, 755-763 (November 1999).

[13] Ibid, Heevey, et. al.

6. Biographies

Felix Achille received a B.S. degree in Chemistry in 1977 from Illinois State University. He joined The Dow Chemical Company in 1978 as a chemist and is now a Research Leader for the Dow Fabricated Products Business, Engineered Films & Laminates group. Since 1994, he has been active in the development and implementation of new plastic coated metals for use in fiber optic telecommunication cables.

The Dow Chemical Company, 200 Larkin Center, 1605 Joseph Drive, Midland, MI 48674.
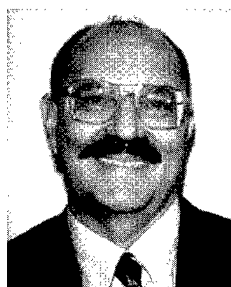
Kenneth E. Bow received the B.S. degree in electrical engineering from Michigan State University in 1962. Following graduation, he joined The Dow Chemical Company, Midland, MI, where he has been involved in the research and development of materials for the wire and cable industry for more than 30 years. He is currently the Chief Scientist for the development of polymer and coated metal products for wire and cable applications. His primary responsibilities are for the global development of applications and cable technology associated with cables using plastic-coated metallic shielding and armoring tapes. Ken is a former member of the IWCS Committee. He is active in the standards process of IEEE and the Electronics Industry Association (EIA).

The Dow Chemical Company, 200 Larkin Center, 1605 Joseph Drive, Midland, MI 48674.

Bluetooth™, A Cable Replacement Overview — A Perspective from the IEEE 802.15 Working Group for Wireless Personal Area Networks™

Ian C. Gifford

M/A-COM, Inc.
Lowell, MA 01853-3295 USA
+1-978-442-4650 · giffordi@tycoelectronics.com

Abstract

Wireless personal area networks will proliferate early in the millennium and the IEEE 802.15 Working Group for Wireless Personal Area Networks™ (WPAN's™) [1] will provide the leadership in the IEEE 802 Standards Committees to establish open standards for these WPAN's™. The IEEE 802.15 Working Group for WPANs™ is developing Wireless Personal Area Network standards for short-range wireless networks. A primary goal for WPANs™ is to replace all the cables the mobile worker has today i.e., cell phone to laptop/PDA, cell phone to headset, etc. The Working Group is cognizant of emerging industry specifications, viz., Bluetooth™ [2], HomeRF™ [3], Firefly-RF [4], etc. and realizes that it is important to build on the work of these groups as they enjoy significant market interest and industry participation. One of the primary motivations for this Working Group is to ensure the best use of a shared medium.

Keywords

"Bluetooth; Wireless; PAN; WPAN; Wireless Personal Area Network; Telecommunications; Data Communications; Radio Frequency (RF); Spread Spectrum (FHSS); IEEE; 802; 802.15"

1. Introduction

The group currently has six activities underway. The first under Task Group 1 is drafting a standard derived from the Bluetooth™ Specification Version 1.0. Task Group 2 will develop a Recommended Practice for PHY Layer Coexistence. The third activity under Task Group 3 is reviewing candidates to choose from to begin drafting a High Rate WPAN™ standard. The fourth activity is the Radio 2 Study Group and it is tracking the activities of the Bluetooth™ Radio2 Working Group (next generation). The fifth activity is the Low Rate Study Group and is chartered to investigate a Low Rate WPAN™ standard with multi-month to multi-year battery life and very low complexity. The sixth and final activity is a marketing effort aimed at promoting understanding of the issues and activities of 802.15

2. Conclusions

The Bluetooth™ Overview will be short and from the point of view of the IEEE. The Author is an Officer and Voting Member of the IEEE 802.15 Working Group for Wireless Personal Area Networks™ as well as an Early Adopter of the Bluetooth™ SIG.

3. Acknowledgments

Special thanks to the members of the IEEE 802.15 Working Group for Wireless Personal Area Networks™ for their continued support of the WPAN™ initiative in the IEEE.

4. References

[1] IEEE 802.15 Working Group for Wireless Personal Area Networks™: http://ieee802.org/15/index.html

[2] Bluetooth SIG™: http://www.bluetooth.com/

[3] HomeRF™ Working Group: http://www.homerf.org

[4] Firefly-RF: http://www.firefly-rf.org/

5. Biography

Ian Gifford was born in Framingham, Massachusetts, USA. He received a Bachelors in Economics from Boston University, Boston Massachusetts, USA, in 1981. He is Director of Standards at M/A-COM, Inc., a Tyco Electronics Company, in Lowell, Massachusetts, USA. For the past 15 years he has worked on wireless solutions for wide area, local area and personal area networks. Additionally, he is an active member in a number of Standards Development Organization's e.g., ITU-R, TIA, and Committee T1 as well as a few Industry Special Interest Groups and Alliances e.g., Bluetooth™ Special Interest Group, etc. He is also currently Vice Chair of the IEEE 802.15 Working Group for WPANs™.

HDR (High Data Rate): A Wireless Solution for Internet Access

Michael A. Lapadula
QUALCOMM
San Diego, CA USA
+1-858-658-2722 · mlapadula@qualcomm.com

Abstract

HDR is a high performance and cost effective Internet solution for consumers and businesses. It is a spectrally efficient CDMA technology optimized for packet data services providing up to a forward link throughput of 2.4 Mbps in a standard CDMA 1.25 MHz frequency carrier. HDR will offer carriers and consumers next generation 3G performance today with unprecedented speed, capacity and mobility. This talk will discuss the status of the technology, the benefits, the relationship to future 3G, similarities to existing IS95 CDMA and the various market rollout options. HDR will unleash the internet to portable, mobile and fixed wireless users.

Keywords

High Data Rate (HDR); internet; wireless

Biography

Mr Lapadula has been with Qualcomm in San Diego for six years and is responsible for marketing, business development and sales of all Qualcomm products for government customers. Previously he was Vice President of marketing for 12 years for Loral Corporation's Terracom Communications Division. Prior to that he was with Rockwell International's Collins Transmission Systems Division in Dallas Texas. He has worked on several occasions as a consultant to various US Government groups and spent over 35 years in the telecommunications business on a worldwide basis.

Mr. Lapadula attended Catholic University of America in Washington D.C. from 1962-1967 majoring in Space Sciences and Applied Physics, Aerospace Engineering.
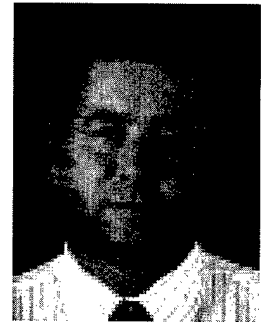
The "Hows and Whys" of Broadband Fixed Wireless

Chris Leising
Telcordia Technologies
Red Bank, NJ 07701
+1-732-758-5218   cleising@telcordia.com

Abstract

This talk will provide an overview of the role of Broadband Fixed Wireless in the evolving telecom-munications landscape. Fixed wireless capabilities will be considered from the perspective of history, technology, regulatory considerations, and market impact. A glimpse of the Broadband Wireless future will also be posed.

Keywords

"Broadband Fixed Wireless; LMDS; MMDS; WLL; Broadband Wireless Access; point-multipoint"

1. Introduction

Traditional Wireless Local Loop (WLL) provides a wireless tether in support of basic POTS capabilities; Broadband Fixed Wireless provides real capacity (256 kbps - 155 Mbps) for the 'last mile". By using roof-top or tower mounted base stations, a relatively narrow RF beam can be transmitted to roof or wall mounted subscriber antennas. Dynamic bandwidth allocation air interfaces provide flexible capacities to individual subscribers, while bandwidth is delivered to customers inside the building via wireline (e.g., DSL) or wireless solutions.

So what's the place of Broadband Fixed Wireless in the marketplace? In areas with underdeveloped infrastructure, Broadband Fixed Wireless provides a way to get rapid deployment. In areas with substantial embedded infrastructure (e.g., incumbent carriers), it provides an economic alternative access technology. While it provides opportunities in nearly all segments, the small to medium business market in densely populated areas is a primary target.

2. Conclusions

Broadband Fixed Wireless offers the ability to be quickly deployed, with a high level of scalability. It can typically be shown that Broadband Fixed Wireless is a clear winner over wireline access technologies, particularly in markets where the "take rate", or penetration, is moderate.

3. Biography

With twenty-three years of telecommunications experience, Chris Leising has a broad background in Wireless, Wireline Broadband, ISDN, CLASS, and Public Telephone Service technologies and feature capabilities. His work has been split evenly between Systems Engineering/Planning and the laboratory environment. Chris has also worked extensively with Wireless Service Providers and Equipment Suppliers, RBOC Client groups, industry task forces and forums, and the ISDN Equipment Supplier community in capacities ranging from Consultant to Project Manager. In his current role as Director of LMDS Systems Engineering, Chris manages a group of RF Engineers and Software Developers, and has responsibility for Telcordia's Broadband Fixed Wireless consulting and RF planning tool offerings. Chris received his BSEE from Monmouth College, and performed his MSEE work at the Rutgers University Graduate School of Engineering. He is an accredited Project Management Professional from the Project Management Institute. He is a member of Eta Kappa Nu.

Strategic Wireless Analysis: When and Where to Deploy Wireless Services or Technology

Howard Sherry

Telcordia Technologies, Inc.
Red Bank, NJ 07701 USA
+1-732-758-2208 · hsherry@telcordia.com

Abstract

Over the past five years, there has been an explosion in the opportunities accessible to incumbent and emerging wireless service providers. Fueled by large amounts of new spectrum, the availability of financing and a strong demand for service offerings that can be effectively served with wireless technology, carriers have installed wireless access networks to provide both narrowband and broadband services to residential and business customers. While the business prospects for these carriers remain quite positive, the challenges of competition and technology evolution is beginning to play a more and more important role. For example, with multiple competitors serving many service areas and coverage no longer a significant differentiator, mobility wireless carriers are wrestling with multiple complex business decisions dealing in large part with service deployment and technology modernization. This talk will provide an overview of the wireless services, technologies, and serving arrangements being considered followed by a description and demonstration of a software-based technology/business analysis tool used by carriers to address this area.

Keywords

"Wireless; Mobile Wireless, Cellular, Personal Communication Services or PCS, 3G, MMDS, LMDS, Strategic Wireless Analysis Tool (SWAT) "

1. Introduction

The emergence of a truly competitive market in telecommunications brings with it new headaches and opportunities. This is particularly true for the mobile sector, where 3-6 operators often have viable networks – and ready access – to desirable subscribers. Carriers have come to the realisation that services and the new technology necessary to deploy these services are critical factors in the path to business success. Wireless carriers can no longer just focus on gaining market share. They need to address questions such as:

- What are desirable new technology, service, or architecture approaches? When and where should they be deployed?

- How can we get more from an existing system or license?

- What is the best way to migrate to 2G+ or 3G?

- Which strategy will be profitable for us?

- What might our competitors do?

- Which solutions are profitable <u>and</u> minimize risk?

- What happens when assumptions change?

Given the large capital requirements involved, carriers are finding that a closer link between business/financial planning and engineering is needed to make sound decisions. The talk will use SWAT (Strategic Wireless Analysis System), a software based planning tool developed by Telcordia, to discuss the complex nature of the problems being addressed and the methodology being used to solve them.

2. Conclusions

Competition and an increased focus on new services are forcing changes in how many wireless carriers are planning their future investments. Carriers are finding that an understanding of the complex interactions among traffic, capacity, propagation, equipment costs and operations costs are needed to ensure that economically sound decisions are being made and that they are not blindsided by competition.

3. Biography

Dr. Howard Sherry has over 27 years of experience in managing, leading and participating in research, planning, standardization, and consulting efforts for both wireless and wireline networks. Howard joined Bell Labs in 1972 and transferred to Bellcore (now called Telcordia Technologies) with the 1984 AT&T Divestiture, holding positions as Member of Technical Staff, Supervisor, District Manager, Division Manger, Director and Chief Scientist in network planning and research organizations. For the last twelve years, Howard has been responsible for managing and participating in projects on network architecture, mobility management, economic assessment, planning tool algorithms, and protocol definition associated with cellular, PCS and wireless local loop solutions. He is currently serving as the Chief Technology Officer of the Telcordia Mobility Wireless business unit. He received a Ph.D. and MS in Electrical Engineering from the University of Pennsylvania and BS in Electrical Engineering from Worcester Polytechnic Institute.

Effect of Cabling Process and Installation on Polarization Mode Dispersion

Li Li , Chen Wei

Siemens Optical Fibre Cables Ltd.,Chengdu PR China

+86 28 5182968 lili@sofc.siemens.com.cn wei.chen@sofc.siemens.com.cn

Risheng Yang

Corning Incorporated

Abstract

In this paper we examine the influence of cabling processes (coloring, tubing, stranding and jacketing) on Polarization Mode Dispersion (PMD) in loose tube and ribbon cables. Both G652 and G655 fibers have been studied to observe any significant differences between them.

Moreover, the relationships between the PMD coefficients of un-cabled and cabled fibers have been determined by comparing values for cabled fibers to initial fiber values.

Finally, PMD measurements have been performed on several routes installed in different areas with quite different environments to investigate the influences of both installation and environment. The values measured on installed cable routes are compared to the calculated link design value, (PMDq) based on the distribution of PMD measured on fiber in uninstalled cable. The results show that the PMD link value reasonably represents practical installed performance.

Keywords

PMD, G655, G652, Cabling, Installation, Effect

1. Introduction

With the wide application of 10 Gbit/s communication systems, (PMD) has become an important issue in both high-quality analog systems and high-speed digital systems, as high PMD values may significantly degrade transmission quality. Over the past few years, many papers have been published on PMD effects on standard single mode fiber (G652) in loose tube cables. However, there have been only a few studies on the effect of cabling processes in ribbon cables and on non zero dispersion shifted fibers (G655) in loose tube cables. There are also few studies on the effect of installation on PMD.

The phenomenon of PMD is caused by birefringence, which may be the result of either intrinsic or extrinsic stress. This paper will concentrate on the effect of extrinsic stress on PMD.

For fiber and cable manufacturers, it is important to estimate the PMD coefficient of the fiber link. Using the Monte Carlo numeric method [1], the distribution of measured PMD for cabled fibers has been used to calculate the PMD link value. The theoretical link-value PMDq gives a statistical upper bound at a probability level of 10^{-4} for the PMD coefficient of the concatenated fibers comprising an optical cable link .

2. Experiment

2.1 Cable Design

The results of this study were obtained from fibers and cables supplied to commercial networks. The loose tube cable structures are common designs employing a PC/PP double layer tube (see Figure1).
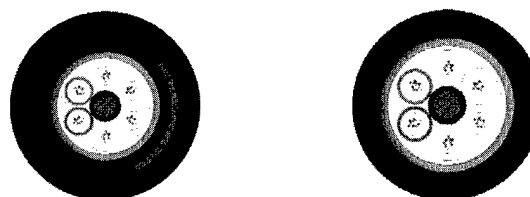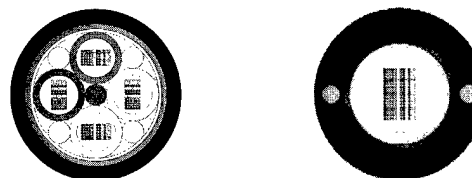

Direct Buried Cable   Duct Installed Cable

Figure 1. Structures of loose tube cables in this study

The structure of the ribbon cables is loose tube type. This study exclusively concerns 12-fiber ribbons, which are the most commonly used design in China. Typical ribbon cable designs are provided in Figure 2.

Figure 2. Structures of ribbon cables in this study

2.2 Measurement Method

Several PMD measurement techniques have been standardized. The interferometric technique was chosen for this study for the following reasons:

- Measurement is quick and simple
- Wide dynamic range
- Does not require communication between the input and output ends of the fiber
- Portable and resistant to vibration

In this study, we made measurements both in the factory and in the field. This method is well suited to our application. An EXFO FTB-300 (5500 analyzer) test set was employed in our test. Initial PMD measurements were made on natural fiber.

Normally there are 4 key steps in cable manufacturing: coloring, tubing, stranding and jacketing. PMD measurements were performed following the tubing process and following the jacketing process (finished cable). This is because the fiber is deployed under tension after coloring (which would generate misleading PMD values) and is essentially in an unchanged deployment after both stranding and jacketing.

3. Result and Analysis

3.1 Effect of Cabling Process on PMD

3.1.1 G655 Fiber

As G655 ribbon cables are rarely used in China, only loose tube cables are investigated in this part of the study. Two different fiber sources are used, denoted A and B. Fiber A and B are both G655 fiber with large effective area. Sample A was supplied from United States The same cable design and manufacturing process were applied to each fiber type.

As shown in Figure 3 and 4.

1. The intrinsic PMD for sample A is lower than for sample B.

2. During and after cabling the PMD is lower and more consistent for sample A which has lower intrinsic PMD..

3. Fiber with an intrinsic PMD above or around 0.1ps/km^1/2 is more sensitive to extrinsic stress (Similar result was reported previously [2].
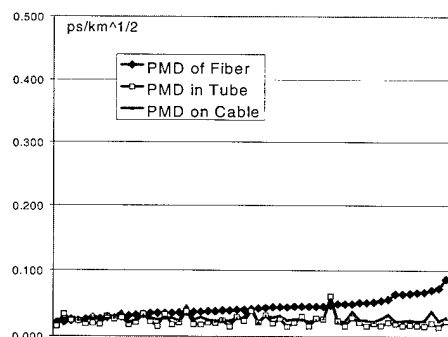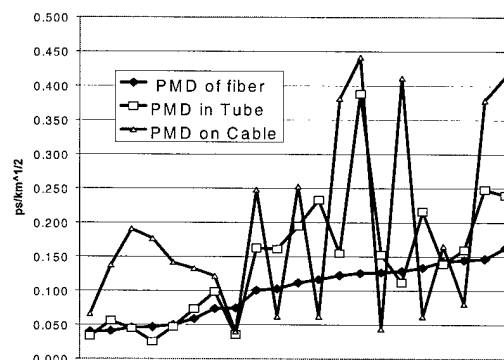
Figure 4. PMD change of G655 (Sample B) fiber in cable

3.1.2 G652 Fiber

Loose tube cable

All G652 fiber was manufactured by the same source as sample A of G655 fiber.

Figure 5 shows PMD change during the loose tube cable manufacturing process. The average PMD (geometric mean) of fiber, tube and cable is 0.034, 0.025, 0.041ps/√km respectively. As with the G655 fiber, PMD remained stable after buffering, the stage at which PMD is lowest. Some samples with higher fiber PMD values increased more dramatically in the final cable but even these results are well within widely accepted industry limits.
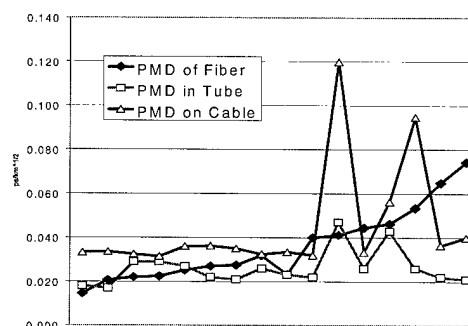
Figure 5. PMD change of G652 fiber in cabling process of loose tube cable

Ribbon cable

In ribbon cable, the result is a little different. PMD increased after tubing, then typically decreased slightly when cabled (although tube and cable values are relatively similar). See Figure 6. The cabled fiber PMD values are still well within generally accepted industry limits of 0.5 ps/√km for 10 Gbit/s operation

The different PMD relationship between the tube and finished cable for loose tube and ribbon cables is explained by the different strain experienced by the fibers in the ribbon. As the ribbon is helical stranded in the buffering tube, and once the tube is stranded around the central element, the strain on the ribbon decreases, resulting in decreased PMD. See Figure 7.
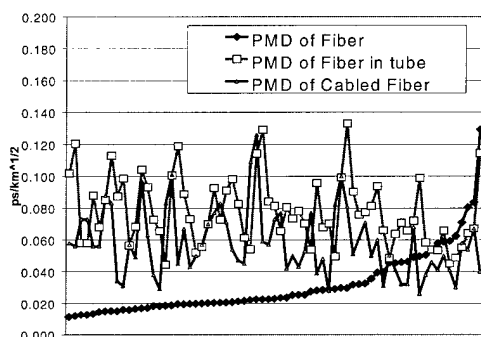
Figure 3. PMD change of G655 (Sample A) fiber in cable

Figure 6. PMD change of G652 fiber in cabling process of ribbon cable
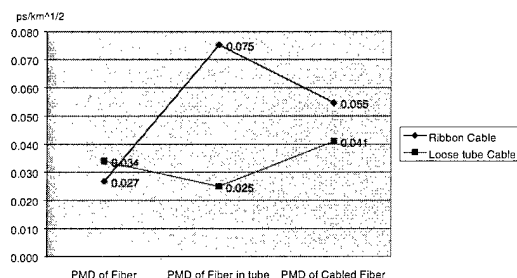

Figure 7. Different change trending of the cabling process on loose tube cable and ribbon cable

3.2 PMD on installed cables

3.2.1 G655 cables

The cable route for this experiment is located in northeast of China, crossing mountains, plains and rivers. The cables are 64-fibre hybrid loose tube structure consisting of 48 G655 fiber and 16 G652 fibers. There are 8 tubes with 8 fibers per tube. Installation is both in duct and direct buried. Five cable sections were tested, each ~40km in length (individual cables were typically 2km) leading to 240 data points for the installed G655 fiber. Figure 8 shows the PMD on uninstalled cables and installed cables. There is no significant change in PMD after installation.
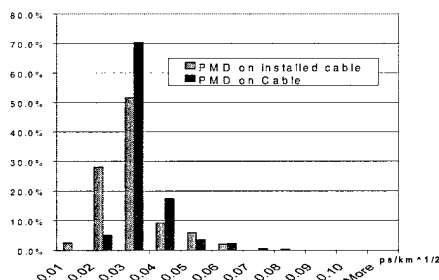

Figure 8. PMD of G655 cable before and after installation

Using the PMD data on uninstalled cable, calculating by the Monte Carlo Method (IEC/86C/265/CD), the PMD link value (PMDq) was obtained. Figure 9 shows the comparison between the Monte Carlo distribution and measured data on installed links. The Monte-Carlo distribution is somewhat tighter than the actual installed distribution. PMDq is in reasonable agreement with the upper limit of the bulk of the installed PMD values although the actual maximum measured is greater as this value lies outside the bulk of the distribution.

Figure 9. Comparison of PMD between Monte Carlo distribution and measured values on installed links

3.2.2 G652 loose tube cables

PMD was measured on installed cables on three routes. The results are shown in Table 1. The typical cable length is ~2km.

Route No.	Installatio n method	Cable Designe	Total Length	Max. PMD (ps/km^1/2)	Average PMD (ps/km^1/2)
1	Duct	32f	70km	0.173	0.033
2	Duct and bury	64f (24f G652)	200km	0.149	0.035
3	Duct and bury	64f	70km	0.150	0.020

Table 1. Route information of G652 fiber experiment

After installation, the PMD of some fibers increased slightly. However, the average PMD level dropped, as shown in Figure 10. This may be due to additional strain inducing birefringence on the fibers when the cable is wrapped around the shipping drum.

Figure 10. PMD of G652 cable before and after installation

As with the G655 fiber, the Monte Carlo distribution was calculated from the PMD data on the shipping spools and compared with the measured PMD of installed links, see Figure 11. As with the G.655 data, PMDq is in reasonable agreement with the upper limit of the bulk of the distribution of installed PMD measurements but the presence of some outlying data makes it lower than the actual maximum measured value.
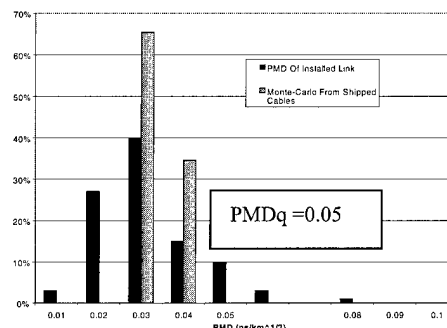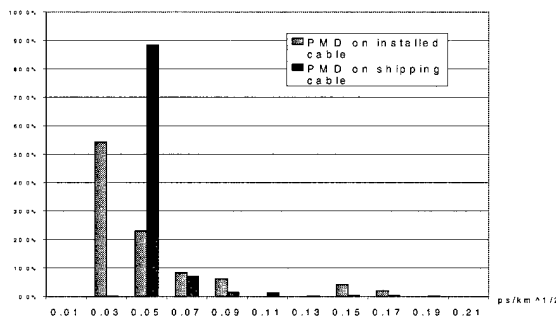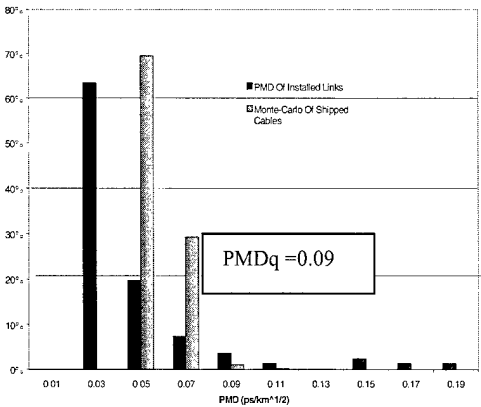

Figure 11. Comparison of PMD between Monte Carlo distribution and measured values on installed links

3.2.3 G652 Ribbon Cable

Ribbon cable was not installed in time to be included in this study. Instead, a single 2km 144 fiber-ribbon cable was used to simulate installation by laying the cable out loosely on the ground and splicing the ribbons to each other to generate 12 effective links of 24km. The PMD of the spliced fibers was determined and the results are in Figure 12. The PMD of the simulated link is dramatically less than the PMD of the individual sections on the shipping drum. Clearly Monte Carlo method would significantly overestimate the upper installed PMD in this situation.
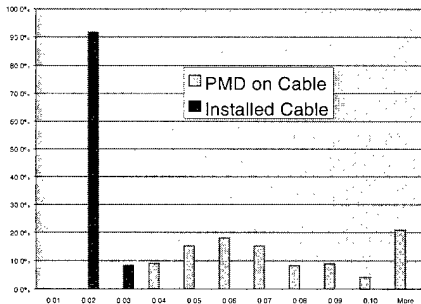

Figure 12. The PMD of ribbon cable before and after installation

3.3 Additional Experimentation

From above tests we can see that the fiber of Sample A is quite resistant to the cable manufacturing process and installation, process, particularly the G655 fiber. To further prove its resistance to adverse deployment, we performed two additional experiments. The first was temperature cycling, the second was to induce the bending that may occur at a splicing box.

• **Temperature test**

A 24-fiber loose tube G655 cable of sample A fiber was placed in a temperature chamber. The cable length was 2km. All the fibers of each cable was spliced together to get a 48km link.

The chamber was set up with a temperature sequence of 20°C, -40°C, +70°C and 20°C. The PMD of the spliced fiber link at these temperatures is shown in Table 2 with the additional attenuation induced.

	20°C	-40°C	+70°C	20°C
Sample A PMD (Ps/km^1/2)	0.020	0.024	0.026	0.027
Additional Attenuation (dB)	0.0	0.0	0.0	0.0

Table 2: G655 fiber performance under temperature change

• **Bending test**

This experiment was carried out on the same cable as the previous temperature test. The fiber was bent in a progressively smaller circle from 5cm to 3cm diameter at the side of each splicing point. Although the attenuation increased, the PMD was not significantly changed. See Table 3.

Diameter	PMD	Attenuation increase	
	(ps/km^1/2)	1310nm	1550nm
Initial	0.055	0	0
φ5cm	0.053	0.001	0.000
φ4cm	0.051	0.000	0.002
φ3cm	0.047	0.002	0.05

Table 3: The change of PMD and attenuation while bending

As previously demonstrated, sample A exhibited good resistance to PMD increases from environmental changes.

4. Conclusions

G655 fiber with a low intrinsic PMD has good resistance to external change. PMD of G655 fibers with a higher intrinsic PMD will be less resistant to external influences.

The PMD of deployed G652 fiber is typically less than cable shipping spool PMD although some may be higher.

Monte Carlo method is a reliable way to predict PMD properties of an installed link of loose tubed cable although some links may fall outside the normal range of the distribution and exceed PMDq. PMDq may be overly conservative in the installation of ribbon cable.

5. Acknowledgments

Mr. Ian Davis of Corning Optical Fibres for technical and editorial assistance in writing this paper.

6. Reference

[1] 86C/265/CD-IEC 61282-3: Guidelines for the calculation of PMD in fiber optic systems. 09,09,1999

[2] Scott Grindstaff, Joseph Hill, Omid Daneshvar, "EXTRISIC STRESS ON POLARIZATION MODE DISPERSION IN OPTICAL FIBER CABLES," IWCS, 1993, PP.647-653.

Authors:
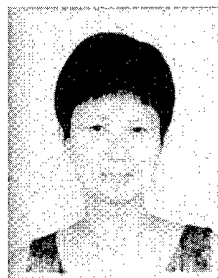
Li Li

Siemens Road No.1

Hi-Tech Development Zone

Chengdu 610042, P. R. China

Ms. Li Li is a test engineer at Siemens Optical Fibre Cables Ltd.. She holds a Master of Science degree from Chengdu Electronic Scientific & Technology University and a B.S. degree in Physics from the University of Defense Science and Technology.
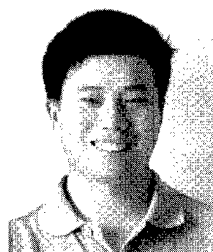
Chen Wei

Siemens Road No.1

Hi-Tech Development Zone

Chengdu 610042, P.R. China

Mr. Chen Wei was born in 1970. He joined Siemens Optical Fibre Cables Ltd. in 1995, and now is the manager of testing department. He graduated from Shanghai JiaoTong University in 1992 with a B.S. in Polymer Engineering. From 1992-1995, he was engaged in material development at Chengdu Tele-communications Cable Ltd. Co.

Risheng Yang

Corning Incorporated

Biography not available.

Study on PMD of Large Effective Area G655 Fiber

Tiejun Wang, Mu Zhang

Yangtze Optical Fiber and Cable Co. Ltd. Wuhan, CHINA 430073
+8627-87802541-3115 · yofcfibe@public.wh.hb.cn

Abstract

The PMD performance of fiber is very critical for high speed DWDM system. To take the advantage of PCVD, we studied and optimized the preform, fiber and cable fabricating process, and achieved low PMD for G655 fiber by PCVD process.

Keywords

PMD; G655 Fiber; PCVD Process

1. Introduction

In DWDM telecommunication and analogue system, PMD performance is a very difficulty issue because it is random and very difficulty to compensate. PMD is the synthetic result of fiber birefringence and fiber mode coupling. It's sensitive to the environment. Outside pressure brought from cabling, installing and temperature varying can make the asymmetric core worse. Therefore, to reduce PMD during fiber fabrication is the key solution.
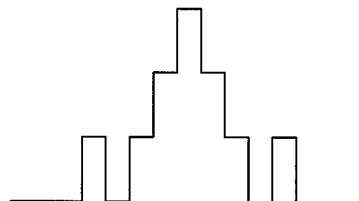
2. Fiber preparing

2.1 PCVD process

Plasma-active Chemical Vapor Deposition (PCVD) is known as its high deposition efficiency of doped silica together with the precise control of the refractive index profile in preform making. During the process, the desired gas mixtures, a combination of $SiCL_4$, $GeCL_4$, C_2F_6 and O_2 are fed into the substrate tubes at a special low pressure. A moving non-isothermal plasma area is generated inside the tube by a microwave (2.45GHz). Reactions are stimulated and deposition of the desired glass components on the inner wall of the substrate tubes occurs in this plasma area. During deposition the substrate temperature is kept constant at a temperature at about 1200°C by a stationary furnace over the whole unit. In the PCVD process, the microwave energy required to maintain the plasma and to stimulate the reactions is coupled directly into the gasphase without influenced by heat transfer problem. So the transverse speed of the resonator can be high, and the deposition layer is very thin (micron thickness), which makes the profile accurate and precise.

2.2 Refractive Index Profile of LEA-NZDF

The RI profile of LEA-NZDF is usually parabola with multi claddings to present characters for high rate and big capacity transmission (Figure1). The refractive index and diameter of the core and ring are fixed to give a reasonable character. The higher refractive index on the core and complex RI profile distribution increase the difficulty of making circular and homogeneous

tension preform, therefore, PMD of LEA-NZDF is relatively harder to decrease.

Figure 1. RI profile of LEA-NZDF(preform)

2.3 Preform Preparing by PCVD

The most directly way to reduce PMD is to manufacture fiber with its core as circular as possible and stress in both redial and axial directions as homogeneous as possible. The core circularity includes geometrical circularity and optical circularity, and they are mostly determined by the even deposition. During deposition, gas pressure inside deposition tube is kept low to guarantee the uniform distribution of gas mixture concentration. The gasflow is carefully controlled by MFC to keep the residence time of the reactive gas in the plasma zone, constant to get the same deposition yield of SiO_2 and GeO_2. Different MFC are also used to maintain the same materials structure in the reactive zone. The applied plasma power is kept stable and proportional to the deposition rate, no any power varying available. The deposition is also strongly related to the inner wall temperature of the substrate tube, so beside the plasma power, the stationary furnace temperature should also be kept constant. The even deposition is also guaranteed by the resonator transverse speed. We maintain it to make it stable and proportional to the deposition rate.

Another main reason causing PMD is inner stress. It is well known that preparation of preform is always associated with the generation of stress because that different doped regions forming the core and the cladding usually have different thermal expansion coefficients. To reduce the stress to a low level can benefit PMD at the following process steps. Considering this, we make full use of the advantages of PCVD to design and fabricate preform of LEA_NZDF. Refractive index profile is specially designed and dope at the interface of core and cladding is controlled by more accurate deposition to make the profile smoother, therefore, inner stress is decreased.

At the collapse step, in order to prevent tube deforming we adjust the pressure inside and outside the deposited tube to get a balanced state. If there is tube deformed at previous process,

flame is used to reshape that deformed part and inner stress is also released at the same time. Table 1 is the parameters of LEA_NZDF preforms prepared by PCVD. The result show both geometrical and optical parameters are improved to give an even waveguide, so is low PMD.

Table 1. Preform parameters in three directions

	Φ clad	Φ core	Δ
0°	10.655	5.037	0.356
120°	10.653	5.031	0.354
240°	10.654	5.028	0.354
Avg.	10.654	5.032	0.354
Std.	0.001	0.006	0.002

2.4 Fiber Drawing

During the drawing process, main reason causing core ellipticity and asymmetric lateral stress in the fiber are analyzed. We focused on furnace heat zone for it contributes more in PMD reduction. A wide heat zone can provide a stable and homogeneous temperature distribution, so the dope can defuse equally in radial direction in the melt state. A long heat zone to the neckdown region is helpful releasing asymmetric tension. Figure 2-1,2-2 are PMD distribution verse furnace diameter (80mm, 60mm).

High drawing temperature is helpful for PMD, but it can make attenuation worse. So the temperature and drawing tension should be balanced to get both reasonable PMD and attenuation.

3. Cabling Process Analyzing

LEA_NZDF with low PMD fabrication is one aspect to reduce the link PMD, the stability of PMD performance for further process such as cabling process up to installation is also a key point. We investigated statistically PMD performance on drum with no tension, coloring process, stranding process and inner sheathing process. The results are shown on Figure 3~Figure 6. During the cabling process, side pressure on the fiber and bending can be created to the fiber. Thus, birefringence and mode coupling vary and so is PMD. The figures show that the PMD sensitivity is low and therefore PMD keeps stable after cabling.

4. Transmission Experiment

The 16×10Gb/s WDM transmission was successfully conducted through 400km LEA_NZDF prepared by PCVD. The experiment setup is shown in Figure 7.

The parameters of the experiment system are: transmission rate: 9.95328Gb/s; signal pattern: 2^{31}-1 stochastic pseudocode; BER<10^{-12}; wavelength range: 1548.51nm~1560.61nm with equal space channels. The eye diagrams after transmitting 400km fiber is shown in Figure 8. The BER performance curve at 1550.92nm is shown in Figure 9.

When BER=10^{-10}, all of the channel penalty is less than 1.0dB. No impact induced by PMD was observed in the transmission.

5. Conclusions

We fabricated LEA-NZDF fiber with low PMD by PCVD method. Preform, fiber and cable processes are analyzed and optimized. As a result, we obtained low PMD LEA-NZDF fiber and cable and the link value of PMD is low (less than 0.1ps/ $\sqrt{}$ km).

6. Acknowledgments

7. References

[1] Andries H.Van Bergen, Ton Breuls, "PCVD: The Ultimate Technology for Production of High Bandwidth Multimode Fibers", IWCS 47, 66-71(1998).

[2] P.K. Bachmann, W.Hermann, etc., "Stress in optical waveguides. 1: Preform", Applied Optics, Vol. 25, No.7, 1093-1098 (April, 1986).

[3] Tiejun Wang, Shuqiang Zhang and Donglan Chen, "Study on PMD of Fibers Prepared by PCVD", China OFC Technical Conference, 1999.

SPEAKER BIOGRAPHY
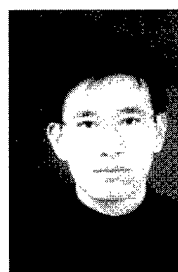
Tiejun Wang
Yangtze optical fiber & Cable co.Ltd.(YOFC)
Wuhan, 430073 P.R. CHINA
Yofcfibe@public.wh.hb.cn

Tiejun Wang was born in 1969. He received his B.S. degree in optical engineering from Huazhong university of science and technology(HUST) in 1992 and M.S. degree in opticalelectronics in 1998 from HUST. Since 1998, he works in YOFC as a chief engineer in R&D group. His responsibilities focus on new fiber product and process optimizing.

Figure 2-1 PMD distribution of 80mm furnace
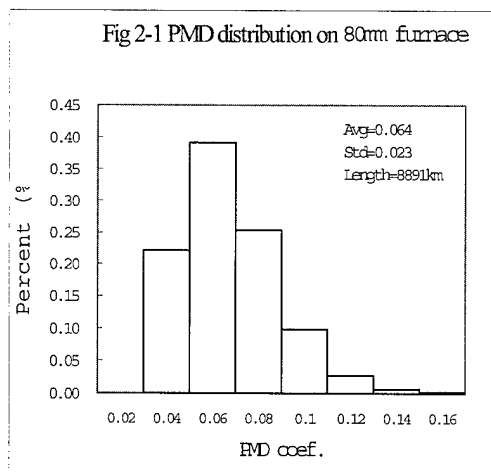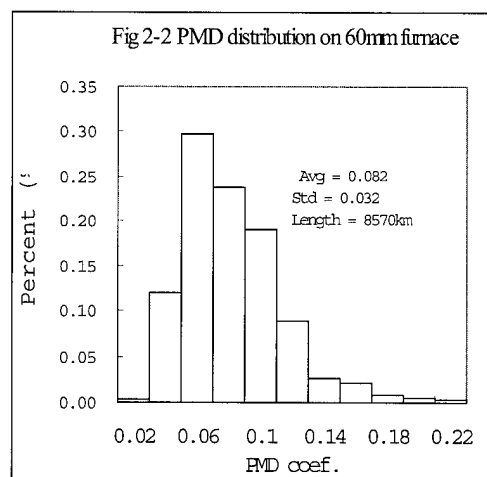

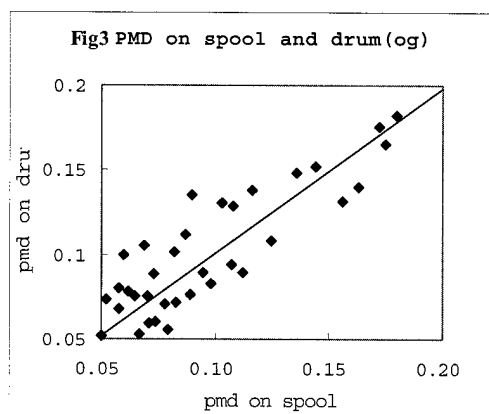**Figure 2-2 PMD distribution of 60mm furnace**

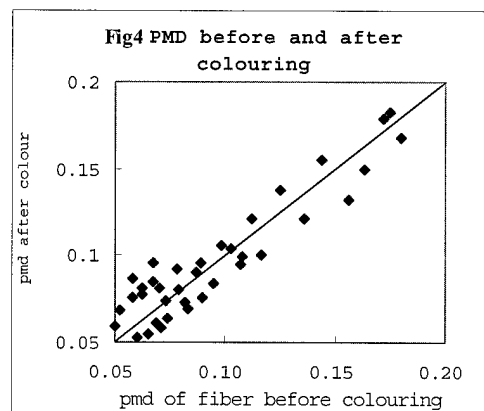**Figure 3 PMD on spool and on drum(0g)**

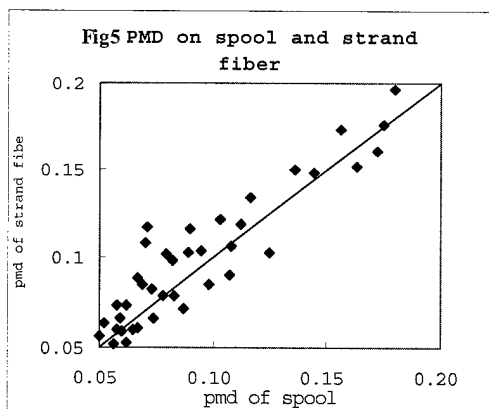
Figure 4 PMD before and after coloring

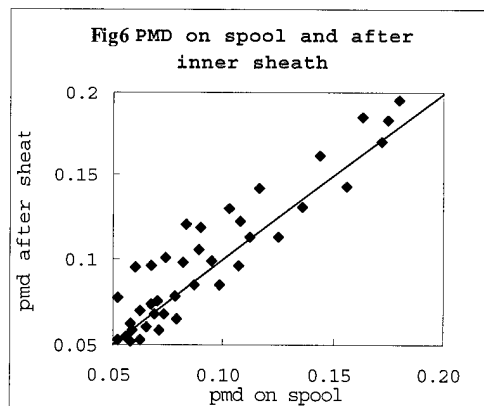**Figure 5 PMD on spool and of strand fiber**

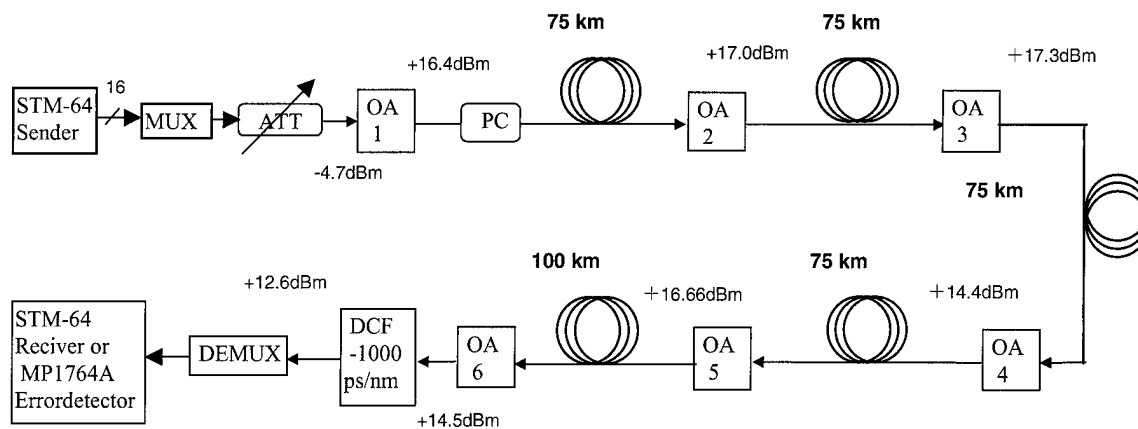**Figure 6 PMD on spool and after inner sheath**

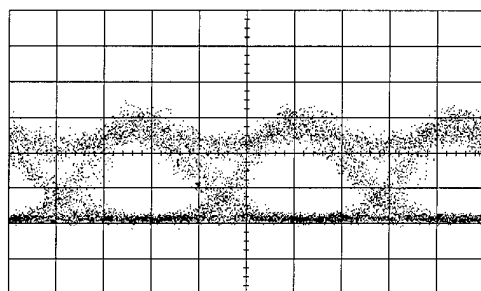**Figure 7 Scheme of the 160Gb/s system**

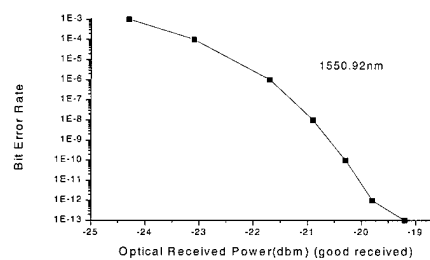**Figure 8 Eye diagram after 400km (1550.92nm)**

Figure 9 BER performance curve

Computer Assisted Optimisation of Cable Design

Hugh G. Sasse*, Mohammed M. Al-Asadi*, Alistair P. Duffy*;
Kenneth G. Hodge# & Arthur J. Willis#

*Department of Electronic and Electrical
Engineering, De Montfort University, Leicester,
England LE1 9BH

#Brand-Rex Ltd, Viewfield Industrial Estate,
Glenrothes, Fife, Scotland KY6 2RS

Principle Contact: email hgs@dmu.ac.uk

Abstract

The design of communication cable systems requires that the best solution be found for several competing parameters. Often, a single ideal solution is not obtainable and a trade-off must be found. A means of visualising the solution space can assist in this search, as can computationally efficient search methods. This paper presents two such techniques: evolutionary computing (concentrating specifically on genetic algorithms); and "colour mapping" for visualising the space by mapping independent parameters into a colour space. These two techniques are complementary. Genetic algorithms are computationally intensive, simple to implement and can cope with a large number of variables. They have shown their utility in other fields, but seem to under utilised in cable design. Colour maps are novel, computationally simple and require careful selection of the mapping functions. They are suitable for a limited number of independent variables but provide an output that is particularly intuitive.

1 Introduction

A Genetic Algorithm is a means of solving a broad class of optimisation problems. For example finding sets of input parameters to an equation or numerical model that give rise to a desired set of outputs. This is an approach based on responding to the statement: "We will know the answers are correct when we see them, but we are not sure what mix of input variables will give us these answers". The Genetic Algorithm is loosely based on Darwin's Theory of Evolution, and specifically how this evolution takes place in the cells of living things. The algorithms themselves have been well researched and applied to other areas of the engineering field[1,2], and they have features wich make them attractive to the cable design community. This paper aims to explain the functioning of the genetic algorithm and suggests its role in cable design and manufacture.

There are a number of ways of solving optimisation problems: problems in which the best value(s) must be found for some variable(s). In many cases there may be a system of n equations with m unknown variables, such that $m > n$, therefore a unique solution may not exist; the purpose of the Genetic Algorithm is then to find the one or more families of variables that satisfy the equations. In this way this optimisation is a process of searching. Examples of other methods available for the solution of such problems include linear programming, hill climbing, simulated annealing, and purely random searches[3]. All of these methods including genetic algorithms have their own benefits and disadvantages. In order to present a balnced picture, the next section will review some of these techniques before concentrating on the Genetic Algorithm.

2. Optimisation Techniques

This section outlines some of the techniques used in optimising solutions to equations, or optimising numerical models all these cases there is some measure of quality of the proposed solution, and this may be considered to be the solution's fitness: fitness for the purpose to which the equation or model is put in fact.

2.1 Random Searches

Random searches are simple to implement, but they are an inefficient way of finding a solution to a given problem. Basically, this search method involves taking a series of guesses at the solution, until a satisfactory solution is found. Clearly there is no intelligence used in the search; results from one attempt provide no "seed" information for the next attempt at a solution. However, random perturbation can be helpful in other searching strategies, and random stimulation is even advocated in the discipline of lateral thinking, to provoke another train of thought that may yield a solution to the problem[4]. Randomness is an important part of other searching methods such as Genetic Algorithms where it is used in the mutation of genes and often in the selection of breeders, and, of course, in the creation of the initial population. An example would be finding values of inductance (L) and capacitance (C) in a tuned circuit, to give a desired resonant frequency. A random search would simply take a guess at L and C independently until two values were found to give the correct answer.

2.2 Linear Programming

Linear programming is basically a graphical method for use in problems where the equations that specify the problem are known and are linear for example in simple mixing problems. The equations are expressed as lines bounding a 2-dimensional area and some point in this area must be chosen to maximise some property such as profit. So the best solution lies on the boundary, usually at a vertex of an enclosing polygon.[5,6,7,8].

For this class of problem it can be very effective, and the concept has been extended to nonlinear programming, but there are many problems whose nature is very hard to express mathematically where the relationships governing performance are unknown, and then an appropriate heuristic approach is needed.

2.3 Hill Climbing

Hill climbing introduces the idea of a solution surface, which covers a solution space. If there are only two dimensions to the solution space this is like a hilly landscape where the "height" of a point on the surface is a measure of how good the solution is, i.e.

its fitness. The computer can only examine one point at a time, and cannot "see" the whole space. So the hill-climbing algorithm is to move to another, better, solution from the current one by only going in a direction that takes you "higher". Higher is fitter. This moving higher would involve testing points in the immediate neighbourhood of the current position to determine the best direction of travel. In practice the number of dimensions of the solution space is determined by the number of unknowns in the problem.

This technique does not need the problem to be specified purely as equations, and so can be used where the nature of the problem is not clear, but a solution's quality can be measured. For simple cases where the surface is convex such as the tuned circuit example in section 2.1, this method is adequate, but if there is more than one hill and valley in the landscape, then the climber may only reach the top of a small hill, and not find the mountain across the valley, even if the valley is shallow. If the tuned circuit is modelled so as to include third resonances, it is possible that one of these may be found, completely missing the fundamental resonance actually required.

To overcome the problem of finding a local maximum, or minimum (the climber would just keep going downhill to find a minimum), random stimulation can be used. In this case you tolerate moving away from a good solution in the hope that you will find a better solution by re-starting the search elsewhere. This leads naturally to the idea of simulated annealing.

2.4 Simulated annealing

When metal is heated and allowed to cool, the crystal structure of the metal changes. As the metal cools, the vibrating atoms in it tend to reach a configuration with minimal energy as they continually realign themselves with their neighbours. Simulated annealing regards the solution space as being at a given temperature, and a point is allowed to move about in this space (vibrate) due to this temperature. A movement towards a better solution is always accespted, but a move away from a good solution is only accespted peobabbalistically. The probability of accepting such a move increases with temperature.[8,9] In this analogy, energy is related to the inverse of fitness, so that minimal energy means maximal fitness. As the system "cools" (the vibration decreases) so the points move towards the minimal "energy" states, which represent the best quality solutions. This technique has been successfully applied in many areas, such as coding theory [10] and PCB design [11,12].

3 The Genetic Algorithm
3.1 Operation

The genetic algorithm is different from the search strategies discussed above because it is not based on a model of motion in a solution space, but it is based on a biological model. Competing individuals express their own solution to the problem within their "genetic makeup", and they are allowed to breed to create new offspring, which will hopefully benefit from the mix of solutions (genes) from their parents. Less fit individuals may have less chance of breeding, and their genetic lines will die off relatively quickly.

The makeup of an individual is a (proposed) solution to the problem. This is expressed in a chromosome, the genes of which hold the parameters subject to variation which may yield a

solution. This chromosome is represented in the computer as a string of bits. What this string represents depends on the problem being tackled: binary strings can represent anything in a computer so it may be representing several integers or floating point numbers, or complex numbers, parts of a parse tree (where the solution is a program) or even a series of characters to be fed to an application. The manipulation of this chromosome as a genetic entity takes place entirely at a bitwise level, only the testing of proposed solutions extracts the parameters from it and applies them to the problem.

Individuals have associated with their chromosome a fitness. How this fitness is determined is problem specific. It is usual for the fitness to relate to the breeding chances of the individual. This reflects the cases in nature where only the fittest dominant animals, best adapted for their environment, get to select mates.

The process of breeding is where two individuals copy their chromosomes and align the copies. They then exchange parts of these chromosomes with each other, so that the two resulting child chromosomes have components from each parent. This is called crossover. Therefore one child may have the first part of its chromosome before the crossover point from one parent, and the rest from the other parent. The second child is the other way around. The location of the crossover point, is selected at random, and in some genetic algorithms there may be more than one crossover point.

If the string of bits is now regarded as a collection of variables, then some variables will be received intact from one parent (those before the crossover point), and some will be received intact from the other parent Therefore most of the variables will be received intact from the parents. The crossover point may land in the middle of a variable, so that will get some bits from one parent and some from the other, and thus will be a new value (if the variable is not an identical value in both parents). Hence, the location of the child's position in the solution space jumps relative to that of the parents. This overcomes the local maximum problem of hill climbing by avoiding the adherence to a local solution only, and is in some ways similar to a random search, but with *a priori* information from previous searches (the parents).

In biological systems, occasionally a mutation will occur; sometimes this can be beneficial for the species, particularly when the species is under evolutionary stress. In genetic algorithms mutation is achieved by altering the value of a bit (or bits) at random, with a very low probability. This mutation is done when the new individual is created. Mutation thus performs a jump to a random position in the solution space, reaping the benefits of random stimulation whilst holding on to the directed search of the genetic algorithm. It is important to realise that mutation is not the main agent of change in genetic algorithms or in nature, but that crossover is. That is why mutation rates are kept reasonably low. Allowing the mutation rate to vary when more change is necessary can be useful particularly when the diversity of the population is small, but change in the environment provides an evolutionary stressor.

Computationally, and practically, the population can only be finite, and there must be some means of imposing this limit. Commonly the least fit individuals are replaced by the children, so that even if the breeding parents are selected at random the later generations should, overall, be fitter than those before. Clearly the population must be large enough to ensure genetic diversity is maintained, whilst being small enough to permit timely evolution.

The fitness may be determined on a one-by-one basis, each

chromosome expressing a solution to the problem. Alternatively, if, for example, the problem being tackled is in the area of games, such as a chess playing program, then the individuals may measure their fitness against the whole of the current population. This is sometimes known as tournament selection [1]. As stated before, the fitness may be used to select which individuals breed. There are various schools of thought on this, one is that only the fittest should breed [13,14], and one is that a random selection biased towards the fittest should be used. Alternatively, an entirely random selection procedure could be used and the weakest weeded out by replacing them with the children of the breeders. If a strong "selectionist" strategy is used, so that only the fittest and no others are chosen as breeders, then the population can be saturated with one type of individual. This will usually result in a less than satisfactory solution, and the lack of genetic diversity with result in stagnation. The fitness of the population will not improve. This can be worked around by making the mutation rate a function of the diversity of the population, so that if the population is "saturated" then the mutation rate increases. If a less selectionist strategy is used convergence will take longer.

3.2 Factors affecting Performance of the GA

Variables in the genetic algorithm which can be modified to tune its performance are:

- The population size, where a small population may saturate with one chromosome type, or take many generations to find a solution. A large one may take too long for each generation.
- The chromosome implementation: how the problem space isexpressed in the implementation. Here, a poor design of chromosome may lead to mutations taking individuals outside the solution space. Also, if the chromosome doesn't cover the solution space properly, the answer will be less than adequate; for example if the chromosome only represents a real when a complex number is needed then a G.A. could not find the square root of -1.
- The number of breeders per generation, where too few breeders may mean the convergence to a good solution takes too long. Having too many may mean that good solutions in a generation may only get one "breeding season" before they are overwritten.
- The mutation rate, if too high will result in damage to the offspring, too low and the diversity will not be maintained.
- How the mutation is implemented
- How the breeders are selected (The fittest, Monte Carlo, etc).Too much opportunity given to only the best individuals will result in the population saturating with the current best, so the GA reaches only a local maximum, and does not pick up valuable traits from the others in the population. Too weak a selection criterion will result in slow convergence.
- How the fitness is determined (tournament, etc). Tournament selection can be slow, but not re-adjusting a chromosome's relative fitness could lead to a weak population.

All of these factors have no clear solution and, therefore, experience and some trialing is beneficial. It may indeed be possible to optimise the performance using another genetic algorithm to find values for these parameters.

3.3 Colour maps

To obtain an intuitive grasp of the solution space, some means of representing it is necessary. If there is only one variable then the quality of the solutions may be represented by a graph. If there are two dimensions there a surface plot may be adequate. Often there will be more variables that can be considered. For example, the diameter of conductors in a cable, and also their separation will affect the impedance of the cable Z, the attenuation α, and also the return loss rl. Other parameters may also be affected, such as the manufacturing cost, the minimum bend diameter, and the weight.

If one considers the first three electrical characteristics above (Z, α, rl), it is clear that they will all be altered simultaneously as the conductor dimensions and spacing change. To represent three quantities on a surface plot is difficult, but since the human eye can respond to three different colour stimuli at once it seems intuitive to assign primary colours to each of these properties.

There is a large body of work on colour theory[16,17], and there are a number of computationally intense methods of representing colour. For the purposes of interpreting the results it was clear that an additive form of colour was needed, so that components that together contributed to the fitness could be seen to be adding up to give that fitness. Whilst the HSV colour system is more intuitive, the colour system supported by our printing language and by the visual display, is the RGB (Red, Green and Blue) colour space. This is computationally simpler though it is device dependent, but as can be seen from the results, this is not a significant problem.

It can be seen that the way these colours mix give identifiable regions within the soluution space, which are immediately apprehended by the eye, since segmeting space into coloured regions is a natural operation for the eye. It is immediately obvious where the best performance (denoted by the whiter regions) lies, and the distribution of the primary colours gives an intuitve feel to how the cable's performance is affected by the variation of the diameter and separation parameters.

4 Results.

This section illustrates the implementation of a relatively simple GA to illustrate its application in a problem in the field of cable design.

4.1 Shielded Transmission Line

The first example chosen was to determine suitable dimensions for a shielded lossless transmission line so that it would have a given high frequency impedance.

The cable has 2 inner conductors, of radius d, the centres of which are separated by a distance s. The internal diameter of the outer screen is D and the dielectric thickness is τ.The impedance is given by [15]:

$$Z_0 = \frac{\eta}{\pi}\left(\ln\left(2p\left(\frac{1-q^2}{1+q^2} \right) \right) - \frac{\left(1+4p^2\right)}{16p^4}\left(1-q^2\right) \right)$$

where

$$p = \frac{S}{d}, \qquad q = \frac{S}{D}, \qquad \frac{\eta}{\pi} = 120 \ \Omega$$

The GA predicted results for $Z_0 = 100\Omega$ for a cable with air dielectric. Figure 1 illustrates results for varying the number of

breeders for various population sizes, and shows the cumulative number of successful convergences for the given population size. An ideal situation would be where there was successful convergence for every number of breeders (a gradient of 1 on the graph). It can be seen that this situation is approached as the population size increases. It is also clear that smaller populations provide fewer convergent solutions in general, due to the limited potention of the smaller gene pool.
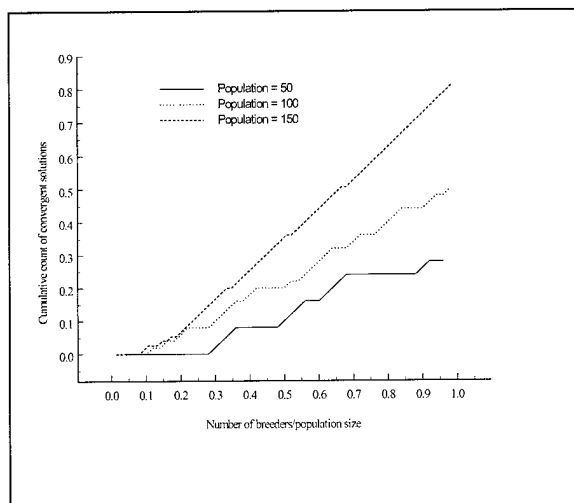

Figure 1 Proportional cumulative count of convergent solutions as a function of the number of breeder/population size for three values of population size.

Figure 2 shows *p* versus *q* for all solutions (including the non-convergent solutions, most of which were within a few milliohms of 100Ω and Figure 3 shows *p* versus *q* for only the convergent solutions. The resulting curve is clear, as are the non-convergent solutions.
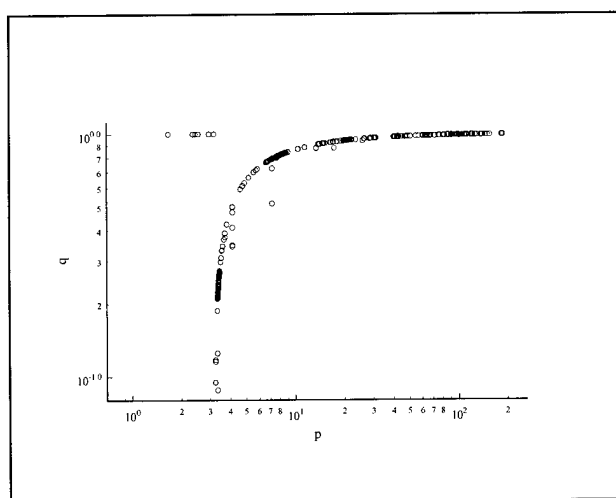
Figure 2. Solutions for a shielded cable (including non-convergent solutions) for 100Ω operation showing the design variables 'p' and 'q'.

A genetic algorithm was developed in C++ with a number of assumptions built into it which, while actually weakening it, provided further evidence to the robustness of the method, because the technique works even in sub-optimal circumstances. In particular the random number generator used in the GA was not initialised to a random value upon startup. This allowed repeatable trials, but meant that there was some inherent bias in the tests. Also the mutation function would only alter the value of one bit in the chromosome at any time, not each bit with equal probability (in which case more than one could be mutated at one time). Despite this the algorithm with mutation converged successfull in many cases. This demonstrates that although the impedance equation was one equation in two unknowns (p, q, to give the desired Z_0) a solution was still found.
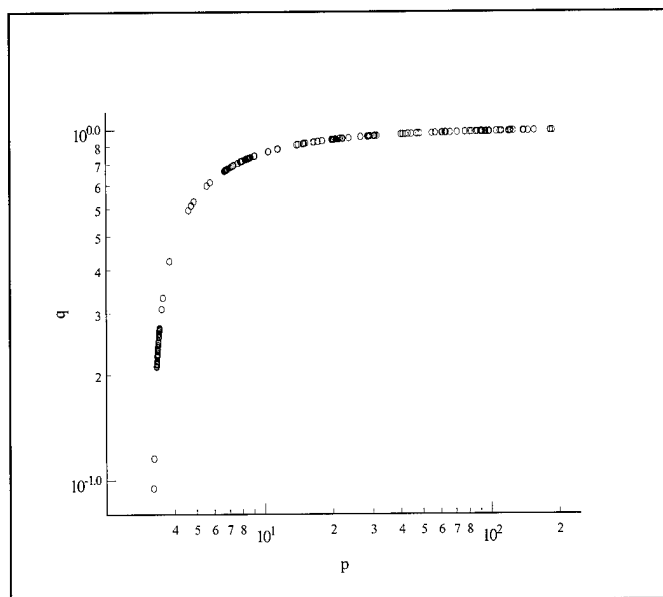
Figure 3. Reproduction of figure 2 (including only convergent solutions).

The problems of how to design the chromosome are well illustrated here. If q > 1 then an attempt will be made to take natural logarithm of a negative number. if p < 1 then the two inner conductors will touch. Therefore it was necessary to ensure that the binary representations in the chromosome could not produce these values of p and q. This was achieved by a linear mapping from p to p' such that $p' = (m\, p + c)$, choosing m and c so that p' is in the correct domain; similarly for q.

Tests were run for this equation with different population sizes and number of breeders per generation. The results broadly support the view that more breeders speeds up convergence, that large populations converge more quickly than small populations, and that even when convergence took more than the expected time, the fitness of the fittest variable was still fair (less than one milliohm out in most cases).

The fitness functions for impdance, return loss and attenuation are displayed using a colour map in Figure 4.

5 Other Possible Applications

Genetic algorithms are robust, and they do not need an exact

description of how to solve the problem. Provided that a solution can be recognised when it is found, they lend themselves to areas where analysis is difficult.

- Simultaneous Equations with N equations in $N + k$ unknowns. The equation for impedance in the shielded cable example above was for $N = 1$, $k = 2$.
- In numerical modelling if the GA is to evolve a model being simulated, then the fitness of the simulation could be tested at intervals. If this fitness is less that satisfactory, then the simulation could cease, otherwise it could continue for a more accurate result.

6 Discussion and Conclusion

This paper has introduced Genetic Algorithms in the context of other techniques to solve problems where a "good" solution may be identified but the input variables cannot be clearly identified. Many of the aspects which make GAs difficult to implement successfully have been introduced. A specific set of results were presented which identified the design ratios for the familiar problem of a shielded transmission line. Additional results for varying population sizes and numbers of breeding pairs in each generation showed how the effectiveness of the GA generally increases as these two increase, however there is a clear observation about the marginal gains of constantly increasing these.

Providing they are well thought out, and properly implemented, Genetic Algorithms are an additional powerful weapon in the armoury of the cable designer.

A technique for giving an overview of the problem space has also been demonstrated, using colour maps. This has been shown to be an intuitive means of grasping the interaction of a number of facets of the problem.
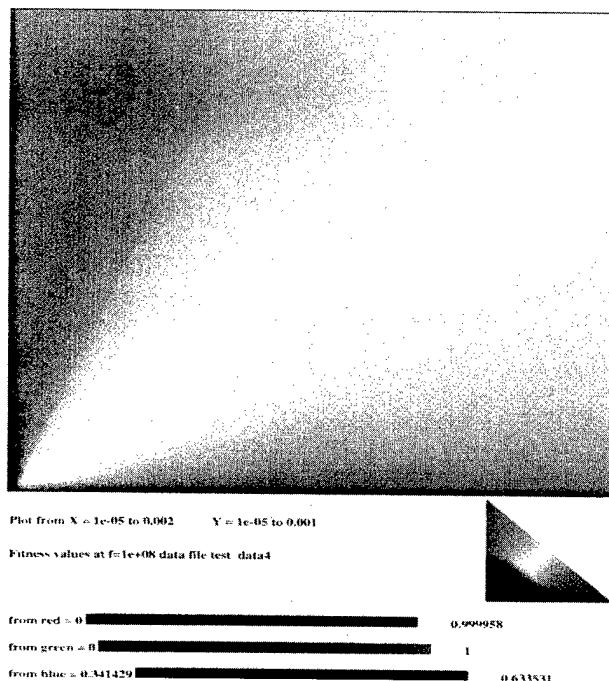
Figure 4 Colour map for fitness functions, red = Z_o, green = RL, blue = α. Fitness is proportional to colour intensity where. X axis is τ and Y-is S.

7 References

[1] Heitkoetter, Joerg and Beasley, David, eds. (1998) "The Hitch-Hiker's Guide to Evolutionary Computation: A list of Frequently Asked Questions (FAQ)", USENET: comp.ai.genetic. Available via anonymous FTP from rtfm.mit.edu:/pub/usenet/news.answers/ai-faq/genetic/

[2] Clive Davidson,"Creatures from Primordial Silicon" New Scientist, 15 November 1997, pp 30-34

[3] Peter Coveney and Roger Highfield "Frontiers of Complexity" Faber and Faber (England), Ballantine Books (USA) 1995

[4] Edward de Bono, "Po -- Beyond Yes and No", Harmondsworth Penguin, 1973

[5] Gass, S. L. "Linear Programming" 4th Edition McGraw Hill 1975

[6] Danzig, G.B."Linear Programming and Extensions" Princeton Universtiy Press 1963

[7] Ralston, Anthony (Ed) "Encyclopedia of Science and Engineering" Van Norstrand Reinhold 1983

[8] Casti, John L. "Five Golden Rules: Great Theories of 20th Century Mathematics" J. Wiley and Sons 1996

[9] Gershenfeld, Neil "The nature of Mathematical Modelling" Cambridge University Press 1999

[10] M. C. Forman, A. Aggoun and M. McCormick; "Simulated Annealing for Optimisation and Characterisation of Quantisation Parameters in Integral 3D Image Compression" Second IMA Conference on Image Processing: Mathematical Methods, Algorithms and Applications (forthcoming publication). 1998

[11] Kirkpatrick, S. Gerlatt Jr, C.D., Vecchi, M.P. "Optimization by Simulated Annealing" Science 220 671-680 1983

[12] Kirkpatric, S. "Simulated Annealing: Quantitative Studies" 1984

[13] John H Holland, "Genetic Algotithms" Scientific American, July 1992, pp. 44-50

[14] Rick L. Riolo, "The Amateur Scientist: Survival of the Fittest Bits" Scientific American, July 1992, pp 89-91

[15] S. Ramo, J. R. Whinney and T. Van Duzer "Fields and Waves in Communication Electronics", Third Edition, J. Wiley and Sons, New York, 1994.

[16] J.D. Foley, A. van Dam, "Fundamentals of Interactive Computer Graphics" Addison-Wesley, 1982

[17] Poynton, Charles "Frequently-Asked Questions about Color" http://www.inforamp.net/%7epoynton/ColorFAQ.html

Authors Biographies

Hugh Sasse graduated from The University of York in 1985, and since then has been working in the Machine Vision Group and later the Applied Electromagnetics Group at De Montfort University, Leicester. He embarked on part-time study for MPhil/PhD in 1999. His main research interests are computer modelling of novel antenna structures and other communication channel components, with an emphasis on optimisation of such structures.

Mohammed M. Al-Asadi, Alistair P. Duffy, Kenneth G. Hodge and Arthur J. Willis. For photos and biographies see "Return Loss Prediction For Cascaded Systems",paper 17-04 in these proceedings.

Optimized Process to Splice Dispersion Compensation Fibres with Standard Single-Mode Fibres

Ming Cheng

Yangtze Optical Fibre and Cable Company Ltd., Wuhan, China

0086-27-87802541   mcheng@public.wh.hb.cn

Abstract

Dispersion compensating fibre module (DCM) is widely used to upgrade the existing G.652 fibres to DWDM long distance transmission system. The figure of merit (FOM) of DCM becomes very important for transmission system performance. An efficient way to improve the FOM of DCM is to decrease the splice loss between DCF and SMF. If we use normal splicing parameters to splice them, the splice loss will be high (about 0.5 dB). Many experiments have been done in order to make clear the relations between splice loss with different splice parameters on a commercial splicer. Splicing parameters were optimized after analyzing the test data. Using the optimized parameters to splice DCF and SMF, the splice loss can be decreased to just above 0.1 dB. For the optimized splicing process is of simple and fast, so it can be easily applied in DCM production.

Keywords

Dispersion compensation fibre; single-mode fibre; splice; diffusion;

1. Introduction

The mode field diameter (MFD) and refractive index profile (RIP) of DCF are much different from that of SMF. Generally, the MFD of DCF and SMF are around 5.5 μm and 10.5 μm respectively at 1550 nm window. The intrinsic splice loss between two fibres with different MFD's can be calculated with the butt-joint approximation [1].

$$\alpha_s = 20 \log \frac{1}{2}(\frac{w_1}{w_2} + \frac{w_2}{w_1}) \qquad (1)$$

Where w_1 and w_2 are mode field radii for the two fibres being mechanically spliced. The calculated splice loss between DCF and SMF can be as high as 1.0~2.0 dB. If we use normal splicing parameters to splice them, the splice loss will be around 0.5 dB. The large splice loss will degrades the FOM of DCM.

In order to reduce the MFD's mismatch of two fibres or fibre with components, many works have been reported. The first way is to use intermediate fibres (IMF) between two different fibres [2,3,4]. Using an IMF between DCF and SMF to reduce the splice loss was also reported [2,4]. The splice losses after using IMF between DCF and SMF were still about 0.4 dB. Preparing IMF will take additional time in production. The second way is to use core material diffusion technology to decrease the mismatch between two components or fibres [1,5,6,7,8,9]. Some of these works

focused on producing a taper using microtorch and electrical furnace. It is not easy to control and it will take extra time if we use this technology in DCM production. Directly using commercial splicer to do the core material diffusion in the splicing process between DCF and SMF has not been reported, so we decided to do some research on this aspect.

2. Principle of material diffusion

According to thermodynamics theory, material diffusion depends on material concentration gradient and temperature. We can describe it using the following formula.

$$dn = -D \frac{dC}{dr} dSdt \qquad (2)$$

The formula indicates that the number of particles (dn) diffused through surface (dS) within time (dt) is proportional to the material concentration gradient (dC/dr). Where the diffusion coefficient D is defined as:

$$D = D_0 e^{-\frac{Q}{RT}} \qquad (3)$$

From formula (3) we know that diffusion coefficient D increases exponentially with temperature T. That means increasing diffusion temperature can greatly shorten diffusion time in order to reach at same diffusion effect. When we use a commercial splicer, we can increase discharge current or lengthen discharge duration to increase diffusion temperature.

It is well known that most single-mode optical fibre, except pure silica core fibres, consist of a pure silica cladding and germanium-doped silica core. Besides germanium, other materials can also be doped in-or in the surrounding of the core region, such as fluorine for depressing the refractive index profile within core or in cladding. Different dopant materials and different levels of dopant concentration result in different refractive index profiles of the fibres. If a fibre core is doped including fluorine, the diffusion speed of the core will be higher. Generally speaking, a high concentration between the core dopant leads to high refractive index differences between the core and cladding, to a larger numerical aperture, and to a smaller mode field diameter. With heat treatment (by microtorch, closed electrical furnace, electrical arc etc.), the dopant material of the core tends to diffuse into the cladding. Given the same temperature and time of heating, different fibre designs result in different diffusion speeds of the core. For example, the higher the dopant concentration, the higher

the diffusion speed that can be obtained. Thus a fusion process of some duration is often used to minimize the mode field mismatch of two fibres, especially when DCF with high dopant concentration and small mode field diameter are to be spliced.

The germanium concentration in the fibre core of DCF is higher than that of SMF, but the MFD of DCF is smaller than that of SMF. If we splice these two fibres, then at a definite discharging time, these two MFD's will become nearly same as the theory predict.

From the above analysis, the MFD mismatch can be decreased through core material diffusion. The different splice parameters can reach a nearly same material diffusion effect. This gives us a theoretical feasibility to optimize the splice parameters appropriate to DCM production.

3. Experiments and results
3.1 Experiment set-up and splice loss measurement
We used a commercial optical fibre splicer to do the investigation. In those splicing experiments the preheating conditions were same. The preheating time is 180 ms. The pre-fusion discharge current strength is 70 units. The forward time is 40 ms.

We designed an on-line monitoring method. It can be used to monitor the output power variation in the whole splicing process [10]. The splice loss measurement accuracy is 0.005 dB.

3.2 Experiments results:
3.2.1 The relation between splice loss with the product of discharge current and discharge duration:
We have done experiments to investigate the relation between the splice loss and the products of discharge current and discharge duration in order to find some rules. The results are shown in Figure 1. Here we set E= the product of discharge current and duration.

- We can divide the curve into three parts: down part (A~B section), bottom (B~C section) and up part (C~D section).

- A~B section: When E < Eb, the splice loss between DCF and SMF decreases exponentially with E increasing. This accords with the theory prediction. For the material diffusion speed increases exponentially with the temperature. The diffusion temperature is determined by the function of discharge current and the discharge duration.

- B~C section: When E arrives at value Eb the splice loss will reach at its bottom (B ~ C section). This means the MFD matches each other at this section. In B~C section, all of the splice loss can be accepted for production, this gives us a great margin to optimize the parameters.

- C~D section: If E value becomes larger than Ec, the splice loss will increase again. The slope of C~D section is smaller than that of A~B section. This can be explained with that with E value increase, the concentration gradient will become small and the diffusion speed will decrease. If the E value continue to increase, the new MFD mismatch will emerge due to the inappropriate discharge condition.

- The curve in Figure 1 is a typical curve. Different discharge current will correspond to different curve, but the shape of the curve is similar, only the minimum splice loss and its corresponding E values are different. At the same time the slopes are different too.
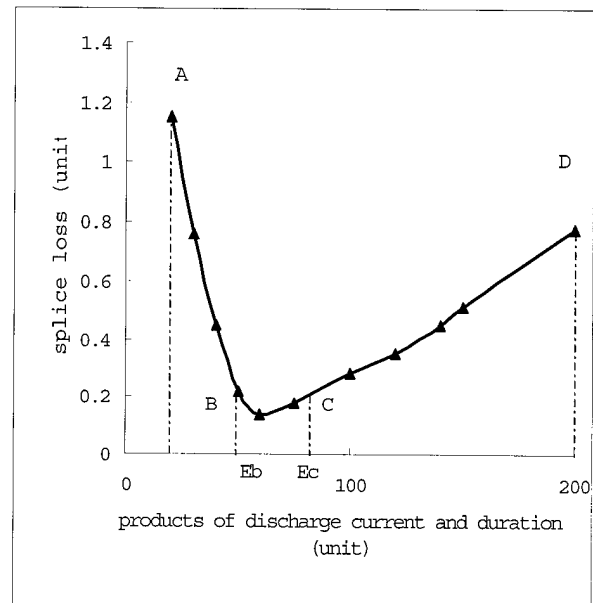

Figure 1. Relation between splice loss and products of discharge current with discharge duration (typical)
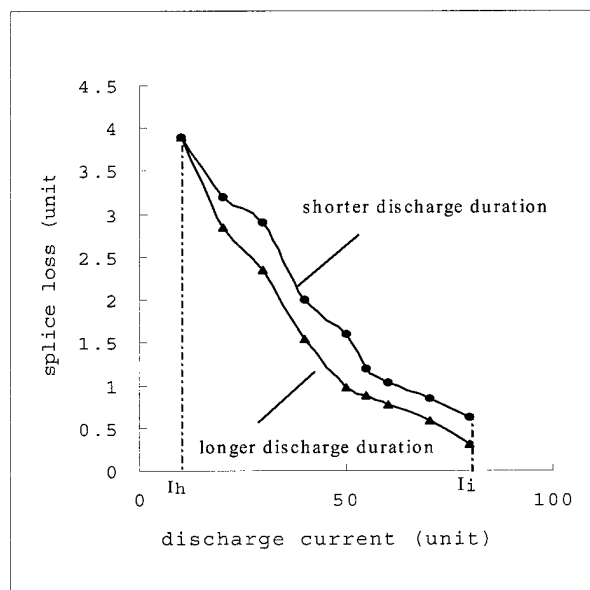
3.2.2 The relation between the splice loss with the discharge current (I)
From Figure 2 we see that in a certain range (Ih~Ii) of the discharge current, the splicing loss decrease with discharge current increase under same discharge duration.

- If I ≤ Ih (less than 10 units), no matter how long the discharge duration is, the fibres can not be spliced together (of course this is an extreme situation). For this reason the splice loss at a small discharge current are nearly same because the two fibres have not been spliced together.

- If I ≥ Ii (larger than 80 units), even the discharge duration be short, the large current discharge will generally fuse the fibres ends apart. Despite at sometimes the fibres can be splice together at the condition I ≥ Ii, the tensile strength of the fibre splice will be ruined. From the LCD monitor on the

splicer we can see that the fibre joint have been deformed by the strong current.

- If Th ≤ I ≤ Ii, the mechanical strength of the fibre splice will be fine. It is suitable for our parameter selection. From the figure we can see that using stronger discharge current can shorten the MFD mating time and is easy to arrive low splice loss.

- We can reach the same splice loss through two ways: one is using stronger discharge current (such as around 70 units) and shorter discharge duration. The other way is using lower discharge current and longer discharge duration. For the two ways have nearly same effect on the splice loss, this give us a space to accommodate the spicing parameters to different situation.

Figure 2. The relation between splice loss and discharge current (typical)

3.2.3 The relation between the splice loss and the discharge duration

We investigated the relation between the splice loss and the discharge duration under the same discharge current. For different fibres with different MFD's the results are little different, the typical result is as follows.

- The splice loss decreases fast with the discharge duration increase. If the discharge duration increase further the splice loss will stay at its bottom. With the discharge duration increase continuously, the splice loss will increase again. (it looks like that shown in Figure 1)

- If the current is relatively high (> 70 units), the long time discharge will negatively influence the splice in two aspects:

one is decreasing the splice tensile strength, the other is deforming the splice that result in the new mismatch of fibre.

- The unit of time is determined by the fusion temperature and by the dopant material surrounding the core. It may be seconds, minutes. Even if only arc fusion is used, different values of the discharge current can lead to variations in the discharge duration, up to a tenfold increase for reaching the minimum splice loss point.

- If the splice has been finished with suitable splicing parameters then we use additional discharge to anneal the fibre splice and the discharge current is not strong (below 20 units), it will have no evident effect on splice loss. The heat absorbed from the discharge is not enough to introduce the additional core enlargement. This means the splice is stable when the splicing process is finished.

3.2.4 The splice parameters change with the different MFD's differences (Δ MFD).

We chose the DCF samples with different MFD to splice with SMF in order to investigate the influence of ΔMFD on the splice loss. The results are as follows.

- According to the theory, the MFD's can become same due to the core material diffusion. This means for different DCF with different MFD, the minimum splice loss will be nearly same, but in practice, different ΔMFD will yield different minimum splice loss. This implies that core material diffusion can not solve the problem completely; the splice loss between two different fibres is also decided by other factors.

- Different ΔMFD related to different product of discharge current and discharge duration. The bigger the ΔMFD, the bigger the product E should be applied. That is, the product E increases proportionally to the ΔMFD.

- The bigger the ΔMFD is, the bigger the minimum splice loss is. The lower discharge current is more suitable for DCF with smaller MFD in order to reach its lowest splice loss. For example if 70 units discharge current is suitable for splice DCF with MFD about 5.3 μm, then normally 60 units discharge current is suitable for splicing DCF with MFD about 5.0 μm.

4. Conclusion

A splicing technique is developed and implemented in a commercial fibre splicer in order to splice DCF and SMF. The MFD mismatch can be decreased directly by the discharge in the splicer. The splicing parameters are optimized for different situations. Using it we spliced SMF and DCF and the splice loss reached just above 0.1 dB. For the optimized splicing program parameters have the advantage of practical and convenient, so it is suitable for DCM production.

5. Acknowledgement

6. References

[1] W. Zheng et al, Erbium-doped fibre splicing and splice loss estimation, Journal of Lightwave Technology, Vol.12 No.3, 1994

[2] K.Shireishi et al, Spot size reducer for standard single-mode fibres utilizing a graded-index fibre tip, pp50-53, ECOC97

[3] M.J,Holmes,et al, Matching fibres for low loss coupling into fibre amplifiers, Electronics Letters, Vol.26 No.25, 1999

[4] B.Edvold et al, New technique for reducing the splice loss to dispersion compensating fibre, TuP.07, 245-248, ECOC'96, Oslo

[5] M.N.McLandrich, Core dopant profiles in weakly fused single-mode fibres, Electronics Letters,1988 Vol.24 No.1

[6] J.S.Harper et al, Tapers in Single-mode optical fibre by controlled core diffusion, Electronics Letters,1988 Vol.24 No.4

[7] K.Shiraishi et al, Beam expanding fibre using thermal diffusion of the dopant, Journal of Lightwave Technology, Vol.8 No.8, 1990

[8] H.Y.TAM, Simple fusion splicing technique for reducing splicing loss between standard single-mode fibres and erbium-doped fibre, Electronics Letters,1991 Vol.27, No.17

[9] K.Himeno, et al, Splice loss of large effective area fibre and its reduction by mode field conversion, ECOC'97

[10] M. Cheng et al, Loss measuring and process monitoring in splicing of two different fibres, Vol. 4077-19, pp97-100, ICSC2000, SPIE

Ming Cheng
Yangtze Optical Fibre and Cable Co.
Ltd. (YOFC)
Wuhan 430073
P. R. China

Ming Cheng was born in 1962. He received BSc. degree in physics in 1983 at Wuhan University and MSc degree in solid-state physics in 1990 at Huazhong University of Science and Technology (HUST) in China. Since 1994 he has been with Yangtze Optical Fibre and Cable Co. Ltd. (YOFC), responsible for R & D related to optical fibre, fibre optics and optical fibre telecommunications.

Geometric and Mechanical Characteristics of Newly Developed SM-NSP (Single Mode Non-Strippable Primary Coated) Fiber

Keiko Shiraishi, Tomotaka Murase and Haruhito Noro

R & D Sec. of Opto-Electronics

Showa Electric Wire & Cable Co., Ltd.

4-1-1 Minami-Hashimoto Sagamihara Kanagawa 229-1133,Japan

+81-42-774-8208   E-mail:k930258@snt1.swcc.co.jp

Abstract

The handling of optical fibers has become an important issue for the construction of optical communication networks. There is a strong requirement for the mechanical reliability of a fiber to be maintained even if the coatings have been removed.

SM-NSP (Single Mode Non-Strippable Primary coated) fiber has been successfully developed as a new type of fiber, whose glass cladding is covered with a thin hard-polymer. The NSP layer protects the cladding surface from unexpected damage and enhances the mechanical reliability of the fiber. The SM-NSP fiber is designed so that its geometrical accuracy and optical properties are equivalent to those of conventional SM fibers in order to have interchangeablity with SM fibers. The results indicate that the mechanical reliability of an SM-NSP fiber is superior to that of an SM fiber, especially when the coatings have been removed. The results also indicate that an NSP layer remains intact throughout a fiber termination process.

Keyword: NSP, fiber, reliability, dynamic tensile

Introduction

Recently, there has been a rapid spread of optical fiber networks throughout the world, and most communication wires have been replaced by optical fibers in the long-distance communication field. Furthermore, in order to obtain a high capacity and high-speed data communication, many optical communication systems have been developed for short distance transmission such as wiring in a building, wiring among buildings, connecting communication units and connecting optical inboard units. With these developments in optical communication systems, new optical connectors (a fiber physical contact connector [1,2], a crimp-type connector) and new techniques of optical inboard wiring [3] have been proposed. These new methods are aimed at making the optical connecting process simple and inexpensive.

However, these improvements in connection methods have let to increase in fiber density around a transmission unit. Since a bare fiber whose outer coatings have been stripped off has greatly reduced mechanical strength due to a physical contact and to the stripping process itself, great care should be taken when handling a bare fiber during a termination operation process in order to maintain the reliability of a communication system with high fiber density.

In order to preserve the mechanical strength of a fiber during and after a termination process, we have developed a new type of optical fiber called SM-NSP (Single Mode Non-Strippable Primary coated) fiber, whose cladding surface is covered with a thin polymer (NSP) layer. As the NSP layer consists of a hard polymer that is not easily removed, the mechanical reliability of an optical fiber can be maintained during a stripping process by the protective effect of the NSP layer.

In this report, we describe the structure and the size accuracy of an SM-NSP fiber. The mechanical reliability and optical properties under various environmental conditions are also described.
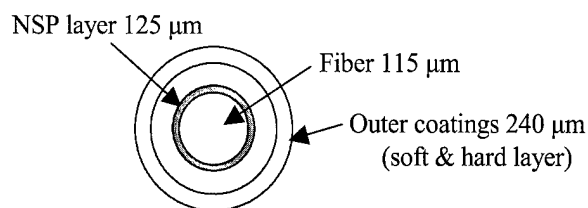
Design of SM-NSP Fiber

A schematic cross-section view of an SM-NSP fiber is shown in Figure 1. The SM-NSP fiber is coated with a thin polymer of 5 μm in thickness directly on cladding glass of 115 μm in diameter. An epoxy ultraviolet-curable resin that has firm adhesion to the glass cladding is used as the NSP layer.
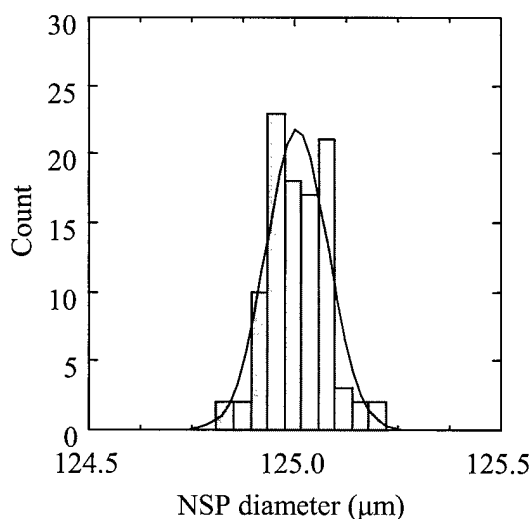
The NSP diameter (125 μm) is the same as that of a conventional SM fiber. Since the NSP layer is very thin, it has little effect on fiber structures such as concentricity and non-circularity. Furthermore, the mechanical strength of SM-NSP fiber is similar to that of a conventional SM

fiber because the mechanical strength depends on the cross-section of glass fiber.
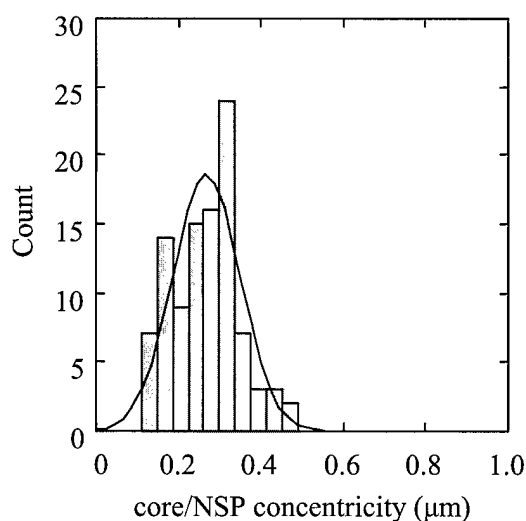
The SM-NSP fiber is also designed so that the MFD (mode field diameter), the core/NSP concentricity and the NSP non-circularity are equivalent to those of an SM fiber. The reason for designing the structure of the SM-NSP fiber to be the same as that of an SM fiber is due to consideration of an interchangeability for connection and splicing with an SM fiber. As in the case of an SM fiber, a soft layer and a hard layer are coated on the NSP layer, making the outer diameter 240μm.

NSP layer 125 μm
Fiber 115 μm
Outer coatings 240 μm
(soft & hard layer)

Figure1 Schematic cross-section of an NSP fiber

Experiment

Size Accuracy of SM-NSP Fiber Geometry

The size accuracy of the geometry of a prepared SM-NSP fiber is described in this section [4]. Histograms of the NSP diameter and the core/NSP concentricity are shown in Figures 2 and 3, respectively. As shown in Figure 2, the median value and standard deviation of the NSP diameter were 125.0 μm and 0.08 μm, respectively. These values can be considered to be of the same accuracy as those of an SM fiber. The maximum value of the core/NSP concentricity shown Figure 3 was less than 0.5 μm. These measurement results suggest that the NSP fiber can be prepared with high geometric accuracy.

Data on SM-NSP fiber geometry are summarized in Table 1 together with data on MFD and NSP non-circularity. The reference data in Table 1 are general specifications of an SM fiber. As can be seen Table 1, the MFD and the NSP non-circularity of prepared NSP fiber also satisfy the general specifications.

Figure 2 Histogram of NSP diameter

Figure 3 Histogram of core/NSP concentricity

Table 1   SM-NSP fiber geometry

Parameter	Unit	Reference*1	Median	Standard deviation
MFD at 1.31μm	μm	9.3 ± 0.5	9.2	0.02
NSP diameter	μm	125.0 ± 1.0	125.0	0.08
Core/NSP concentricity	μm	≤ 0.8	0.3	0.08
NSP non-circularity	%	≤ 1.0	0.2	0.10

*1 These are general specifications for an SM fiber

Dynamic Tensile Properties
of an SM-NSP Fiber

Dynamic tensile tests were performed to investigate the protective effect of the NSP layer on the cladding surface of SM-NSP fiber and SM fiber. Test samples of 125 μm in diameter were prepared [5]. These bare samples were prepared by mechanically stripping outer coatings of 40 mm in length off the middle part in sample fibers. The mechanical stripping was performed with a newly developed fiber stripper, which is described in the next section.

Fiber Stripper

Since a conventional fiber stripper consists of a metal blade, the NSP layer would be easily damaged during a stripping process using a conventional fiber stripper, and the NSP may no longer have a protective effect. In order to avoid such damage, a new fiber stripper consisting of a pair of polymer blades has been developed. A diagram of this tool is shown in Figure 4. The outer coatings of the NSP fiber are crushed between the plastic blades and can be removed by sliding the tool along the fiber. The NSP layer is not transformed during a stripping process because the polymer blade is softer than the NSP layer. This fiber stripper can also be used for a conventional SM fiber.
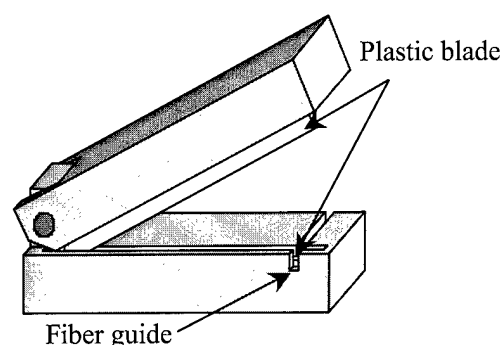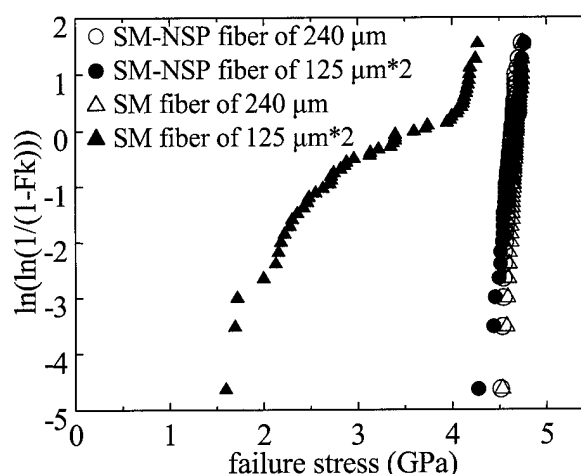
Dynamic tensile test

The dynamic tensile tests were carried out in an environment of 23°C and 50%RH. The strain rate and gauge length used in these tests were 10%/min and 200 mm, respectively.

The Weibull plots for the dynamic tensile tests are shown in Figure 5. The median value and the m_d value for each test are also shown in Table 2. In the case of fibers of 240 μm in diameter with outer coatings, the median value of failure stress was about 4.6 GPa for both the SM-NSP fiber and SM fiber, as shown Table 2. The m_d values of these fibers were also similar (about 100). These results indicate that the addition of an NSP layer to the optical fiber does not cause degradation of fiber strength.

On the other hand, in the case of fibers of 125 μm in diameter without outer coatings, there were remarkable differences between the SM-NSP fiber and SM fiber, as shown in Figure 5. The failure stress of the SM-NSP fiber of 125 μm in diameter was similar to that of the SM-NSP fiber with outer coatings. In addition, it is reasonable to assume that there was no degradation of mechanical strength of the SM-NSP fiber due to the high value of m_d (60). On the other hand, in the case of the SM fiber of 125 μm in diameter without outer coatings, the failure stress

Figure 4 Fiber stripper

Figure 5 Weibull plots of SM-NSP and SM fiber

Table 2   Weibull parameter

Samples	Median (GPa)	m_d
SM-NSP fiber of 240 μm	4.62	105
SM-NSP fiber of 125 μm*2	4.63	60
SM fiber of 240 μm	4.67	99
SM fiber of 125 μm*2	3.18	4

*2: Mechanical stripping of outer coatings of 40 mm in length off the middle part in samples of 240 μm

was widely dispersed and the mechanical strength was obviously degraded.

As mentioned above, Figure 5 and Table 2 clearly show that the SM-NSP fiber maintains its mechanical reliability because the NSP layer remains intact throughout the stripping process and protects the glass cladding even after the stripping.

Heat-resistance tests

In the termination process of an optical fiber, a bare fiber stripped of its outer coatings is adhered to a connector with a heating-curable adhesive. When an SM-NSP fiber is used as an optical communication wire instead of a conventional SM fiber, the NSP layer might be heated during this process. Heat-resistance tests were therefore performed on SM-NSP fibers.

Heat-resistance test

Figures 6 (a) and (b) show changes in the NSP diameter and core/NSP concentricity, respectively, at temperatures of 85, 100 and 125°C. Test samples of NSP fiber of 125 μm in diameter without coatings were heated in a constant-temperature oven, and the structure of the fiber was checked at one-hour intervals.

As can be clearly seen in Figures 6 (a) and (b), the NSP geometry did not change significantly even after heating to 125°C for 3 hours. Since an optical adhesive is usually cured by heating up to 125°C for a few 10 minutes, it is concluded that an NSP fiber can be terminated by a conventional process without any damage to the NSP layer.

Use of a hot stripper

In a fiber ribbon stripping process, which is one of the indispensable processes for constructing an optical transmission unit, the outer coatings of the fibers are heated and pulled out along the fiber by applying side pressure. When a fiber ribbon constructed of NSP fibers is terminated, the NSP layer would be deformed by this heating and side-pressing process. Thus, deformation of an NSP layer during a ribbon strip process is discussed in this section.

Samples of 8-fiber ribbon constructed of NSP fibers were experimentally prepared. These fiber ribbons were stripped of their outer coatings using a conventional ribbon stripper at temperatures of 100 and 150°C. The operation time was 20 seconds.

Figures 7 (a) and (b) show the NSP diameter and core/NSP concentricity after stripping, respectively. These figures clearly show that the distributions and averages of the NSP diameter and core/NSP concentricity after heated stripping are equivalent to those of NSP fibers shown in Table 1. These results therefore indicate that the NSP layer was not deformed by using a fiber ribbon stripper.
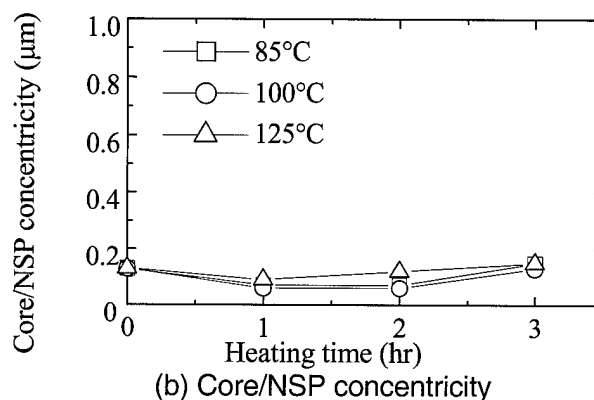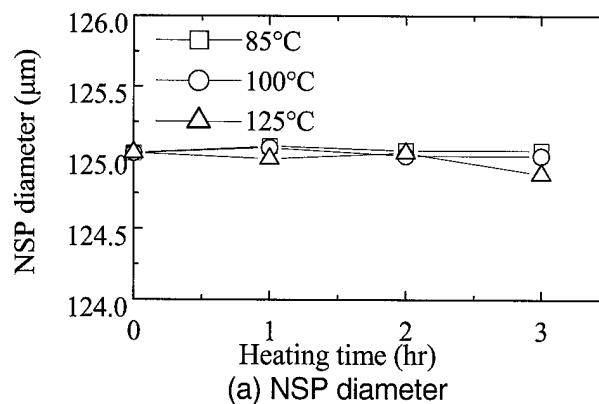

(a) NSP diameter

(b) Core/NSP concentricity

Figure 6 Results of Heat resistance test

(a) NSP diameter

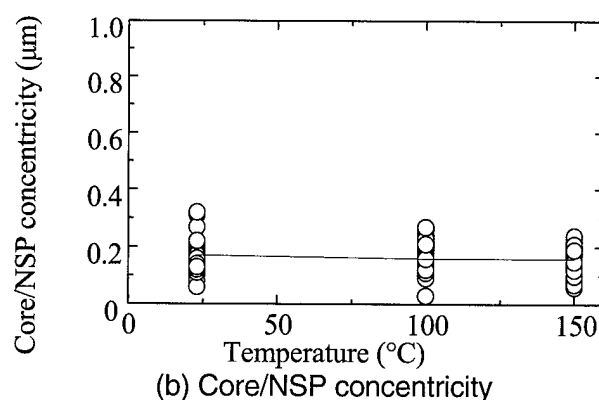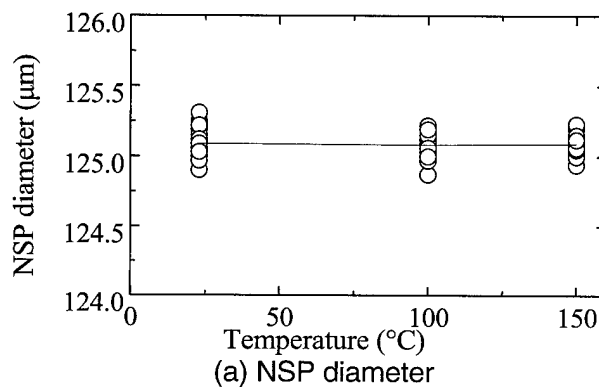(b) Core/NSP concentricity

Figure 7 Results of Hot Stripper test

Environmental Properties of SM-NSP Fiber

We also investigated the effect of the NSP layer on the optical properties of the fiber. The test conditions and measurement results are shown in Table 3. The fluctuations at a wavelength of 1.55 μm were measured with OTDR continuously during the tests.

The fluctuations in transmission loss were less than 0.02 dB/km in all of the tests. In addition, no difference in transmission loss was observed between the SM-NSP fiber and SM fiber. These results suggest that an NSP layer does not influence the transmission loss due to its small thickness.

Table 3 Environmental properties   (@1.55 μm)

Test conditions	Fluctuations of transmission loss (dB/km)	
	SM-NSP fiber	SM fiber
Temperature cycling (-40 to 80°C, 30 cycle)	0.02	0.02
Temperature and humidity cycling (-10 to 65°C -93%RH × 20 cycle)	0.02	0.02
Temperature and humidity (+80°C -95% RH × 300 hr)	0.01	0.01

Conclusion

We have developed a new type of fiber (SM-NSP fiber) that is thinly coated with a polymer of 5 μm in thickness on glass cladding. The geometry of the NSP diameter, core/NSP concentricity, MFD and NSP non-circularity for the SM-NSP fiber were accurately prepared. Therefore, the geometry of the SM-NSP fiber sufficiently satisfies the general specifications of an SM fiber.

The NSP layer plays an important role in maintenance of the mechanical reliability of the fiber by protecting the glass cladding even after the outer coatings have been stripped off. The results of dynamic tensile tests showed that there was almost no degradation of the mechanical strength of the SM-NSP fiber. Comparison with the mechanical properties of an SM fiber showed that the SM-NSP fiber had much better mechanical reliability due to the effect of the NSP layer. The results also showed that the SM-NSP fiber is stable in various environmental conditions as is an SM fiber.

Furthermore, the NSP layer was not deformed by heating and side pressure, operations used in fiber termination and in the hot-stripping process of a fiber ribbon. These results suggest that the SM-NSP fiber can be used in a conventional optical boarding process.

Acknowledgements

References

[1] M.Kobayashi, et al., "Fiber management technique for optical device integration on a circuit board", Journal of NTT Technology, vol.12, No.2, pp42-55 (2000)

[2] T.Yoshida, et al., "Reliability test results of FPC optical connector with PSC-SM optical fiber", The 1999 IEICE General Conference, C-3-61, pp215 (1999)

[3] I.Arishima, et al., "Processing and Structure of Optical Wiring for Optical Circuit Board", The 1998 Society Conference of IEICE, C-3-11, pp145 (1998)

[4] T.Murase, et al., "Development of Single Mode Non-Strippable Primary Coating Fiber -Study of SM-NSP Fiber Geometry and Characteristics-", The 2000 IEICE General Conference, B-10-38, pp413 (2000)

[5] K.Shiraishi, et al., "Estimation Concerning Mechanical Properties of Single Mode Non-Strippable Coating Fiber", The 2000 IEICE General Conference, B-10-39, pp414 (2000)

Speaker Biography

K.Shiraishi received her B.E. degree form Tokai University in 1993. She joined Showa Electric Wire & Cable Co., Ltd. in 1993. She is an engineer working with R&D Sec. of Opto-Electronics.

Development of 48-core Optical Fiber Cable
of Stainless Steel Pipe Structure With 4-Fiber Ribbons

Hiroshi Keruma, Norihumi Kimura, Yasushi Sudo,

Yuji Tezuka, Katuich Saito, Kazumasa Nemoto

OCC Corporation
Engineering Development Department Kaminokawa Plant
Tochigi, Japan
+81-285-56-3314· email: keruma@occ.ne.jp

Abstract

The multimedia field, as typified by the Internet, is presently undergoing remarkable growth in terms of information volume and optical fiber networks are being rapidly set up throughout the world. With this rapid establishment of networks, optical fiber cables are being increasingly laid directly in fields, in sewerage systems, and in adverse environments such as mountainous areas. The requirements for using optical fiber cables under such circumstances include water resistance, corrosion resistance, reliability, and strength for protection from wildlife such as rodents as well as from trees. We have developed a 48-core optical fiber cable consisting of twelve 4-fiber ribbons in a stainless pipe with an outside diameter of 5 mm, for application under such adverse environments. In this paper, we describe the optical characteristics, mechanical characteristics, and environmental characteristics of the developed cable, and also demonstrate that the cable is more advantageous than the slotted type and plastic loose tube type cable through comparison in terms of cost effectiveness. With regard to rodent-proofing, we conducted experiments using real rats to verify that the stainless pipe itself has sufficient strength.

Keywords

Optical fiber cable; stainless pipe; rodent proof; optical characteristics; mechanical characteristics; environmental characteristics.

1. Introduction

With the swift popularization of the Internet, more optical fiber cable networks are now being rapidly constructed throughout the world. Accompanying this progress, optical fiber cables are being laid more frequently under a variety of severe environments and higher strength is therefore required as a cable characteristic. On the other hand, reduction of the overall costs of cable network construction is also a major issue. In terms of reducing not only the cost of cable but also that of cable construction, various aspects such as higher density installation space and shorter installation time have been discussed so far and there have been increasing demands such as for the use of smaller diameter cables and weight reduction. In most cases where such a high-strength

cable characteristic is required, slotted type or loose tube type cables have been used up to now with a wrapping of metal tape or the application of a corrugated structure to them for reinforcement. However, these cables have resulted in an increase in overall costs because of their higher prices, larger outside diameters, and greater weight. To solve these problems, we evaluated a prototype 48-core optical fiber cable that employs a high-density packaging technique in which the optical fibers are directly inserted into a high-strength stainless pipe, and verified that the cable has superior characteristics and cost effectiveness.

2. Cable Structure

Figure 1 and Table 1 show the structure of the newly developed cable, and Table 2 lists the characteristics of the packaged optical fiber. SM type 250 μ m optical fiber is used, and machined as a 4-core fiber ribbon of 0.3 mm in thickness and 1.1 mm in width to reduce the splicing cost. The stainless pipe has an outside diameter of 5.0 mm and a thickness of 0.3 mm. It is internally treated with waterproofing jelly and is equipped with twelve 4-fiber ribbons (48 fibers in total). In addition, two strength members with a diameter of 1.0 mm are set diagonally to increase the allowable tension, and the structure is covered with an anticorrosive polyethylene sheath. This structure provides a high ratio of the cross-sectional area of the 4-fiber ribbons to the area of the stainless pipe, accounting for 30%
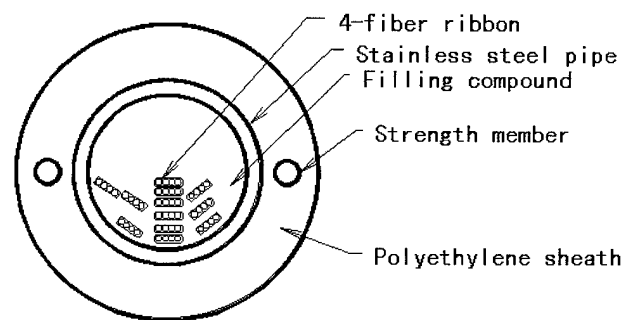
Figure 1. Cross-section of the 48-core optical fiber cable of stainless pipe structure

Table 1. Cable structure

| Number of Fiber	48
Fiber ribbon	4-fiber ribbon × 8
Stainless pipe diameter (Inner/Outer)	4.4mm/5.0mm
Strength member	1.0mm steed rod × 2
Cable diameter	9mm
Cable weight	100kg/km

Table 2. Fiber construction

Fiber type	SMF (ITU-T G652)
Mode-field diameter	$9.3 \pm 0.5 \mu$ m
Cladding diameter	$125 \pm 1 \mu$ m
Primary coating diameter	$250 \pm 15 \mu$ m
Proof	1%, 1sec
4-fiber ribbon dimension	0.3mm × 1.1mm

3. Optical Performance

3.1 Change in optical attenuation during manufacturing process

Figure 2 shows the change in optical attenuation during the manufacturing process. As seen from the figure, there is no significant increase in optical attenuation during the process from the fiber through cable manufacturing. The value is satisfactory and remains stable.
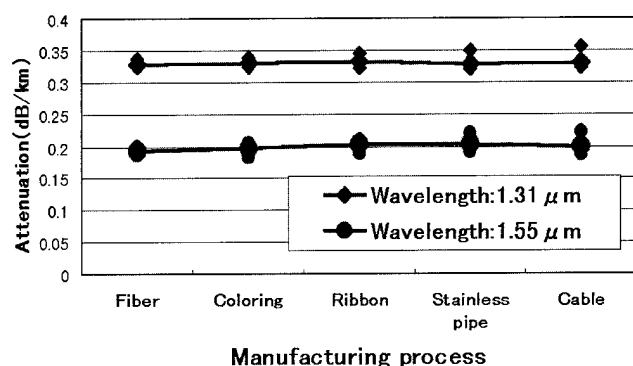
Figure 2. Change in optical attenuation during the manufacturing process

3.2 Fiber strain

Table 3 show the results of measuring the strain of manufactured optical fibers using BOTDR(Billion Optical time Domain Reflect Meter). All of the test fibers (24 fibers in total) at both ends of each 4-fiber ribbon were measured. The results of the measurements confirmed that the strain remaining in the optical fiber is very small and that the newly developed cable structure provides high reliability in optical fiber life.

Table 3. Fiber strain (%) of the cable

(Wound on drum, diameter=400mm)

Strain (max)	Strain (min)
0.015%	0%

3.3 Temperature characteristics

Figure 3 shows the results of a temperature cycling test after cable manufacturing. The test was conducted with a cable wound around a drum of 400 mm in diameter, within a test temperature range of -30℃ to +70℃ in two cycles. As in the case of the optical fiber strain measurements, all of the optical fibers at both ends of the installed 4-fiber ribbon were loop-connected for measurement. Good test results were obtained, confirming that each fiber had a very small change in optical loss of less than 0.05 dB/km.
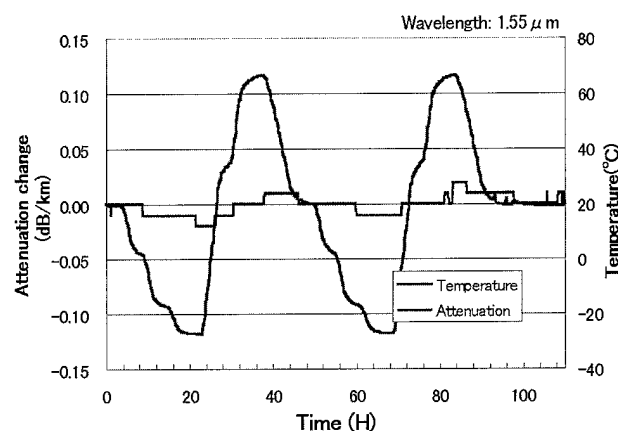

Figure 3. Temperature cycling test

4. Mechanical Characteristics

Table 4 shows the results of mechanical characteristics tests such as tensile strength, bending, crush, impact, squeezing, torsion, and water penetration. The results of these tests confirmed that the newly developed cable meets the general requirements for all mechanical characteristics of optical fiber cables in Japan. Figures 4 and 5 show the results of the crush test and impact test. With regard to the allowable limits in these tests, we confirmed that the mechanical strength of the cable was about 3 times higher in the crush test and about five times higher in the impact test than the general requirements listed in Table 4. We also conducted a rodent-proofness test for one week using eight rats. Figure 6 shows the test results. We found that the polyethylene sheath was considerably damaged but the stainless pipe was somewhat scratched on its surface only. There was little deterioration in mechanical strength.

Table 4. Result of mechanical test

| Test item	Test methods	Result
Tensile strength	2670N	No loss increase
Bending	Bending diameter 10D	No loss increase
Crush	Length: 100mm Load :1960N	No loss increase
Squeezing	Wheel: R250mm Angle :120° Load : 1470N	No loss increase
Impact	Weight: 1kg Height: 1m	No loss increase
Torsion	Angle:±90°/m Length: 1m	No loss increase
Water penetration	Height of water: 1m Length :3m Time :24H	No water flow
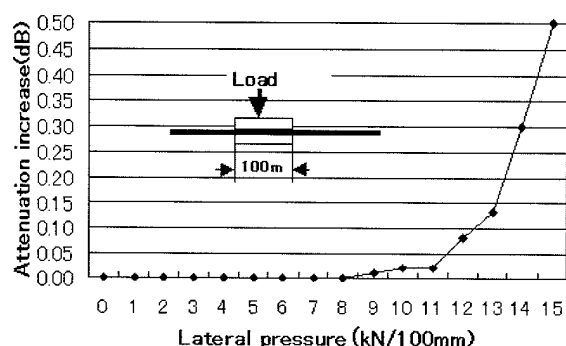
**Figure 4. Crush test**
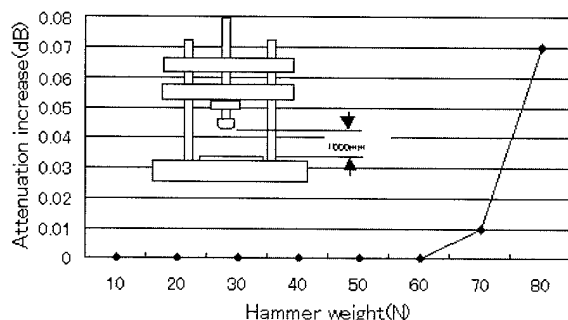
Figure 5. Impact test
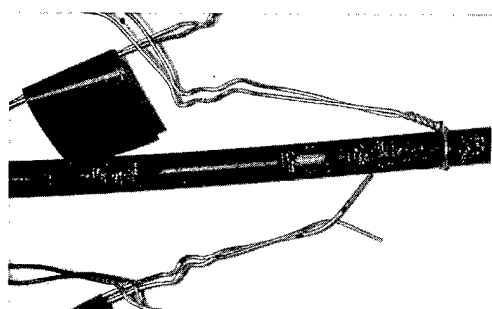
Figure 6. Rodent-proofness

5. Dimensional and Cost Comparison with Other Optical Cables

Figure 7 shows a comparison of outside diameter, weight, and manufacturing cost between the high-strength slotted core optical fiber cable and loose tube type optical fiber cable with steel tape armoring, and the developed cable. Figures 8 and 9 show structural diagrams of the compared cables. As a result of the comparison, we found that the cable outside diameter could be reduced by about 25% and the cable weight by 40% compared to the slotted and loose tube type cables, and that the manufacturing cost was almost the same as the loose tube type and 20% less than the slotted structure.
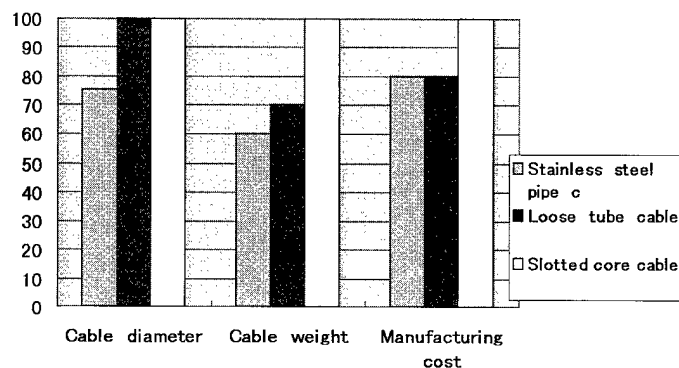
Figure 7. Dimensional and Cost Comparison with Other Optical Cables
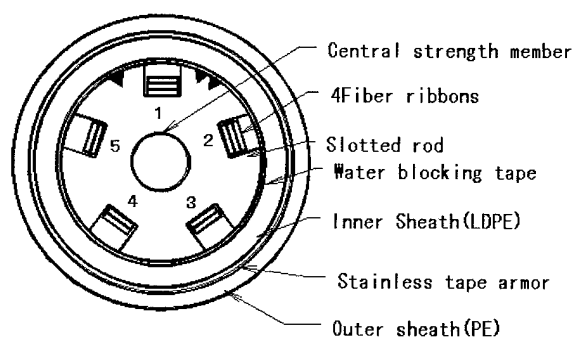
Figure 8. Cross-section of the 48-core slotted optical fiber cable with tape armor type
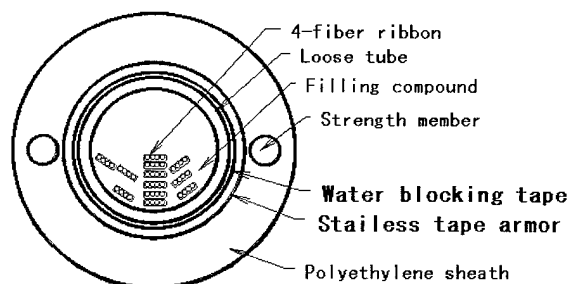
Figure 9. Cross-section of the 48-core loose tube optical fiber cable with tape armor type

6. Conclusions

We developed a 48-core optical fiber cable consisting of twelve 4-fiber ribbons in a stainless pipe of 5 mm in outer diameter, clarified its optical, mechanical, and environmental characteristics, and made economic comparisons with slotted type cables and plastic loose tube type cables to verify its advantages. We will conduct various field tests of the developed cable to further confirm its reliability.

7. References

[1] Y.Sudo et al, "Development and environment testing of optical fiber cable with small diameter stainless pipe" OCC corporation., IWCS (1997).
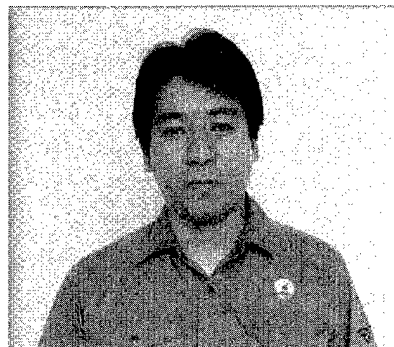
Hiroshi Keruma
+81-285-56-3314· email: keruma@occ.ne.jp
OCC Corporation Engineering Development Department
Kaminokawa Plant Tochigi, Japan

Hiroshi Keruma was born in 1961. He joined OCC Corporation after his graduation from Utsunomiya University with a B.E in 1984,and has been engaged in engineering department cable division. He is an engineer of the KAMINOKAWA PLANT.

A Study on the Structure of Strain Sensing Cable
Using Multi-Pointed Fiber Bragg Gratings

Kazuhiko Terasawa, Haruo Ooizumi, Katsuaki Kondo, Yoshiki Yamakawa,
Takeshi Genji, Kazuo Imamura, Hiroshi Ubukata
Mitsubishi Cable Industries, LTD.
4-3,Ikejiri,Itami-city,Hyogo-Prefecture,664-0027,Japan
TEL:+81-727-81-8793／Email: Kazuhiko_Terasawa @mitsubishi-cable.co.jp

Abstract

Optical distortion distribution was evaluated using an optical fiber having fiber gratings (FBG: Fiber Bragg Grating) incorporated in an optical fiber cable. The cable has an oval structure allowing the cable to bend only in one way. The fiber for a distortion measuring have FBGs with different wavelengths fabricated periodically on a single fiber. The slotted rod incorporating FBG fabricated optical fiber is an oval structure having an X-Y stiffness ratio of 5:1. Linear slots incorporate the fibers to be in one direction. Using this as the core, a covering tape layer is wound and a polyethylene sheath is covered over to be made into an oval structure. The bending distortion can be controlled by the placements of FBGs and also by the way the fiber is secured. We were successful in locating the place of distortion.

Keywords

Fiber Bragg Grating (FBG) ; optical fiber cable ; strain sensing ; unsymmetrical ; bending

1. Introduction

Recently, longitudinal distortion sensing is being studied using communication optical fiber cables or optical fibers. These sensing methods use various scattering light from the optical fiber. For example, when using the Raleigh scattering, distortion is detected by the loss value from strain applied to the optical fiber. This method enables a qualitative evaluation but it is not quantitative. On the other hand, when using the Bourillian scattering, a quantitative evaluation is possible by evaluating the Bourillian shift when strain is applied to the optical fiber, but a distance resolution of a few meters exists which is restricted by the pulse width of the light source used for the evaluation. In comparison, with a cable incorporating an optical fiber with FBGs, strain is measured with the resolution of spaces between FBGs and allows distortion sensing according to various usage. [1] This method also allows high speed distortion measurements by simultaneous observation of each FBG reflection. In this paper we introduce a distortion sensing cable using FBGs and the observations of distortion when the cable was bent.

2. Cable design

For distribution measurement of strain applied in minute areas, the sensing cable structure must be uniform lengthwise. In optical fiber cables for communication the optical fibers are placed symmetrically in the cable with the cable core in the center to prevent as much strain as possible. It is also designed to enable smooth core movement. On the other hand, the distortion sensing cable requires a different design as its purpose is to sense the strain applied on the outside as it is, at the optical fiber. For the cable design, the cable cross section was made oval so that the cable would bend in only one direction. A difference was made in the stiffness in the X,Y direction. The strength member was a small sized stranded steel wire to maintain the flexibility of the cable. To the cable center, it is an unsymmetrical tight structure without stranding. As a result of this design, the cable can bend easily in one direction allowing the distortion to the cable to be transmitted directly to the optical fiber.

3. Cable structure

Figure 1 shows the cross-section of the cable. FBGs with different reflecting wavelengths were placed evenly on an optical fiber. The fiber was incorporated linearly in a slot of the oval slotted rod. The covering tape was wound over and the polyethylene sheath was applied evenly. The longer
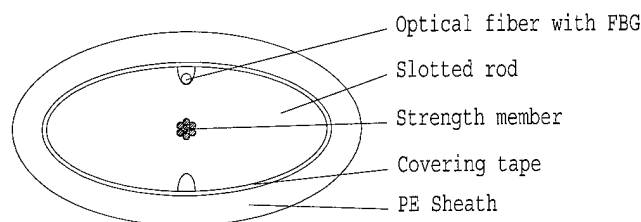
Fig.1 The cross-section of the cable
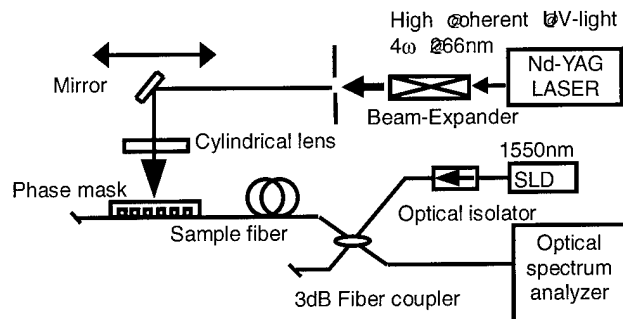
**Fig.2 Structure of fiber grating fabrication system**

outer diameter of the cable was 20mm, the shorter was 10mm. For flexibility an 1.2mm stranded steel wire was placed in the center as the tension member. The optical fiber for FBG was put under the hydrogen treatment and irradiated from above the coating with a Nd-YAG laser fourfold harmonic wave which swept over a phase mask.(see Fig.2) [2]. This fabrication method prevents strength deterioration in the fiber.[3] Figure 3 shows the reflected spectrum of the optical fiber with FBGs. In approximately 1.5nm wavelength, ten FBGs having a different reflected wavelength were placed. The fiber had δ λ = 11.5 nm/% of reflected wavelength shift under
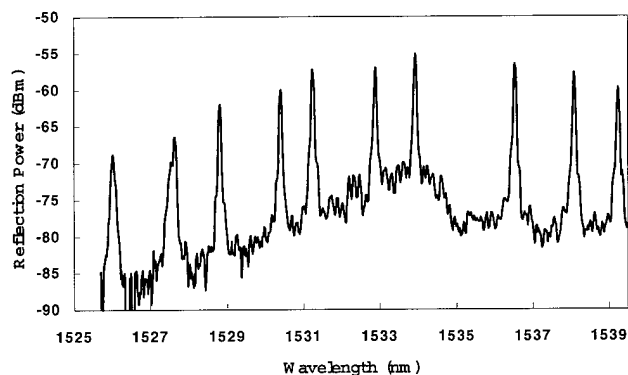
Fig.3 Reflection spectrum

strain. The relation of distortion under such strain and the wavelength shift is shown in Figure 4. The slotted rod was an oval structure with X-Y stiffness ratio of 5 . Table 1 shows the bending stiffness of the slotted rod.

As samples we prepared a cable with an optical fiber core having ten FBGs placed evenly on a 50cm length which was completely fixed in a slotted rod (sample 1), and a cable with an optical fiber having ten FBGs placed in a ten meter length which was fixed at several points (sample 2).
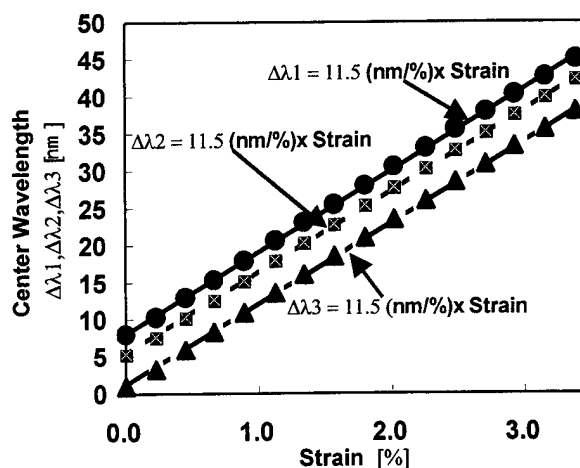
Fig.4 Strain dependence of shift in peak wavelength

Table 1   Bending stiffness of the slotted-rod

Axial	Radius (mm)	Bending stiffness $(N \cdot m^2)$
X	1 6	1 .
Y	7	0

4. Distortion observation system

The distortion observation system is shown in Figure 5. Light is transmitted into the cable through a 3dB coupler from an ASE light source. The reflected light from the FBG was observed by a optical spectrum analyzer. The cable before bending is regarded as the initial state and each reflected peak wavelength of the FBG is also regarded so. The distortion by bending was obtained from the variation of each reflected peak wavelength and the distortion applied to each FBG.
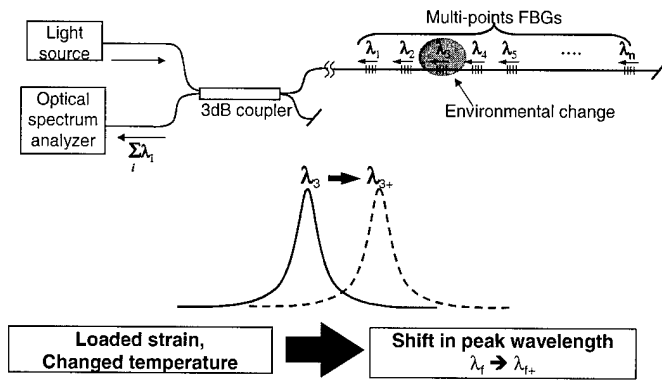
Fig.5 Distortion observation system

5. Cable characteristics

With the sample 1 cable, distortion was measured using a mandrel to make a 550 mm ϕ bend. In Figure 6 and Table 2, the reflected wavelength shift and the distortion caused by the bend of each FBG is shown. The distortion is distributed evenly and in a stable amount. A maximum distortion of 0.9%, a minimum 0.6%, an average of 0.8% was observed. Because the fiber is completely fixed in the cable, the fiber hardly moved. The distortion is largely thought to be due to the strain of the fiber, caused by the length from the cable center to the center of optical fiber. As the bending distortion when the fiber is not moving, the calculated value was 0.9% when the strain,which is caused by the length from the cable center to the center of optical fiber, was taken into account. This value matches well with actual measurements.

With the sample 2 cable, one point in the cable was lifted to make the bends for testing. The lifted height was 0.5m and 1m. The locus of the cable bend made by the lift formed almost a sine wave. The distortion peak was the lifted point of the cable, its distribution becoming smaller as it became farther from the peak. Figure 7 shows the relation between the spaces of fixed points of the FBGs, the center of the bend and a point that is 1 meter apart from the center of the bend. The bending distortion when the center of the bend was lifted up one meter was 0.059% when there was one meter between fixed points. As the spaces between fixed points was made larger, the distortion tended to become smaller. The same trend could be observed when 0.5 m was lifted and a maximum 0.039% was obtained. Furthermore, at pointsthat were one meter apart from the center of the bend, the same

trends were observed though the distortion was smaller. From these results, we believe that it is possible to detect the center of the bends and by optimizing the FBG fixes , it is possible to locate the center of the bends and its distortion .

Table. 2 Strain on FBGs

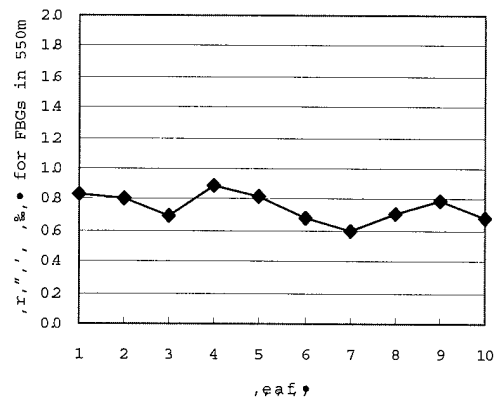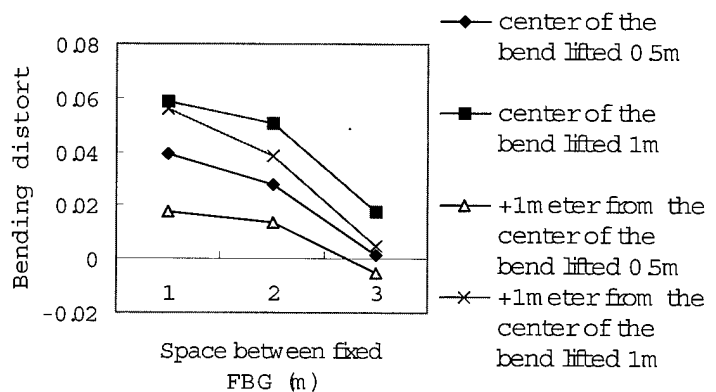| FBGs	Wavelength Shift of FBGs（n	Strain （%
FBG1	9	0. 8
FBG2	9. 3 2	0. 8 1
FBG3	7. 9 4	0. 6 9
FBG4	1 0. 2 4	0. 8 9
FBG5	9. 4 3	0. 8 2
FBG6	7. 8 2	0. 6 8
FBG7	6. 7 9	0. 5 9
FBG8	8. 1 7	0. 7 1
FBG9	9. 0 9	0. 7 9
FBG10	7. 8 2	0. 6 8

Fig.6 Strain for FBGs

**Fig.7 Bending distortion of the optical sensor cable**

6. Conclusion

Using an optical fiber with FBGs placed every 1.5 nm wavelength, an optical fiber cable with an oval cross section which could be bent in only one direction measured the optic distortion distribution. The FBGs were fabricated on high-strength distortion distribution measuring fiber from above the coating, and incorporated linearly in slotted rods with an oval structure having an X-Y stiffness ratio of 5 . When the fiber was fixed and unable to move, the observed bending distortion was a large 0.9% effected by the strain of the fiber. In an cable that was not entirely secured, only the distortion

of the fiber was observed which was below 0.1%. Furthermore we observed that the distortion differed according to the bending point of the cable, and found that that the center of the bend could be located. The bending distortion measurements using this cable depends on how the fiber is fixed. Though further examination is necessary for a quantitative analysis, it is useful for locating the bending place.

We believe that an optimum distorting sensing cable is possible by changing the FBG placements and how it is fixed to the cable according to usage.

7. References

[1] K. Kondo, T. Genji, T. Nakai, K. Imamura and Y. Imada : "Sensor application of germanosilicate fiber Bragg gratings fabricated by direct writing method", OFS13, pp. 208-211 (1999).

[2] D. Vares, D. M. Cstantini, H. G. Limberger and R. P. Salathe, "Fabrication of high-mechanical-resistance Bragg gratings in single-mode optical fibers with continuous-wave ultraviolet laser side exposure", Opt.Lett., 5, pp. 397-399 (1998).

[3] K. Imamura, T. Nakai, K. Moriura, Y. Sudo and Y. Imada : "Mechanical strength characteristics of tin-codoped germanosilicate fiber Bragg gratings by writing through a UV-transparent coating", Electron.Lett., 10, pp. 1016-1017 (1998).

Authors
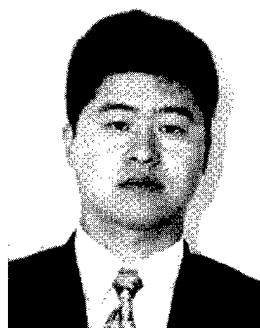
Kazuhiko Terasawa
Mitsubishi Cable
Industries, Ltd.
4-3, Ikejiri, Itami,
Hyogo, 664-0027,
Japan

Mr. Terasawa, engineer of Telecommunication Engineering Dept., is engaged in design and development of optical cable. He received his M.S. degree in Electrical Engineering from Osaka Prefecture University in 1994.
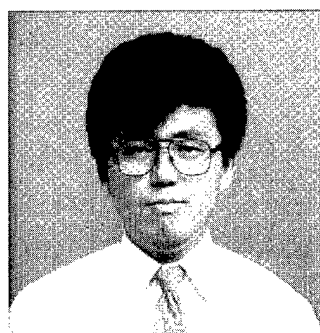
Haruo Ooizumi
Mitsubishi Cable
Industries, Ltd.
4-3, Ikejiri, Itami,
Hyogo, 664-0027,
Japan

Mr. Ooizumi, engineer of Telecommunication Engineering Dept., is engaged in design and development of optical cable. He received his B.S. degree in Applied Pysics from Tohoku University in 1988.

Katsuaki Kondo
Mitsubishi Cable
Industries, Ltd.
4-3, Ikejiri, Itami,
Hyogo, 664-0027,
Japan

Mr. Kondo, staff research engineer of Photonics Research Laboratory, is engaged in design and development of optical components. He received his M.S. degree in Electromagnetic Energy Engineering from Osaka University in 1996.

Yoshiki Yamakawa
Mitsubishi Cable
Industries, Ltd.
8-30, Tenmabashi 1-
Chome,
Kita-ku, Osaka
530-6025, Japan

Mr. Yamakawa, engineer of Telecommunication Engineering Dept., is engaged in development of optical cable. He received his M.S. degree in Electrical Engineering from Kinki University in 1995.

Kazuo Imamura
Mitsubishi Cable
Industries, Ltd.
4-3, Ikejiri, Itami,
Hyogo, 664-0027,
Japan

Mr. Imamura, senior research engineer of Photonics Research Laboratory, is engaged in design and development of optical subscriber systems and optical components. He received his M.S. degree in Electrical Engineering from Osaka University in 1983. He is a member of The Institute of Electrical Engineers of Japan and The Japan Society of Applied Physics.

Takeshi Genji
Mitsubishi Cable
Industries, Ltd.
4-3, Ikejiri, Itami,
Hyogo, 664-0027,
Japan

Mr. Genji, research engineer of Photonics Research Laboratory, is engaged in design and development of optical communication components. He received his M.S. degree in Electrical Engineering from Kyoto Institute of Technology in 1994. He is a member of the Japan Society of Applied Physics.
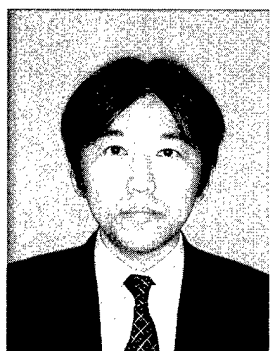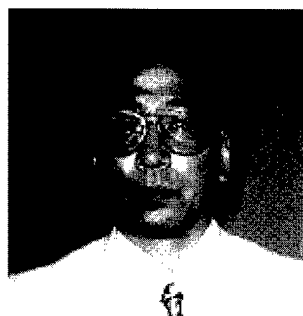
Hiroshi Ubukata
Mitsubishi Cable
Industries, Ltd.
4-3, Ikejiri, Itami,
Hyogo, 664-0027,
Japan

Mr. Ubukata, chief of Telecommunication Engineering Dept., has been engaged in design and development of Telecommunication cable. He received his B.S. degree in Electrical Engineering from Hokkaido University in 1972.

Downsized Dry and Non-Slotted Core Cable with Fiber Ribbons

Tomoyuki Yokokawa, Itaru Sakabe, Toyoaki Kimura,
Hiroki Ishikawa, Wataru Katsurashima and Nobuhiro Akasaka

Sumitomo Electric Industries, Ltd.
1 Taya-cho, Sakae-ku, Yokohama, 244-8588 Japan
Phone : +81-45-853-7164
e-mail: yokokawa@yklab.sei.co.jp

Abstract

Downsized dry and non-slotted core cable with fiber ribbons for distribution network has been developed. The cable realized downsizing by 36% in height and weight reduction by 57% compared with the conventional cable by a grooved plastic spacer. The manufactured cable has been taken various tests and confirmed its high performance on various requirements.

Keywords

Aerial, Distribution, Dry and Non-Slotted Core, Fiber Ribbons and Self-support

1. Introduction

The booming demand for the Internet service has been spread all over the world for last decade. For realization of FTTH (Fiber To The Home) to meet it, low cost and easy handling aerial cable has been required [1]. Therefore, we reconsidered the structure of conventional self-supported aerial cable, and developed downsized dry and non-slotted core cable using fiber ribbons. In this paper, the cable design and various test results of our manufactured cable are described.

2. Cable design

Fig. 1 and Fig. 2 show the cross section of our newly developed 40-fiber and 48-fiber self-supported cable, respectively. They have dry and non-slotted core using ten 4-fiber ribbons, four 12-fiber ribbons, respectively. Each cable jacket contains preventive elements against the after-shrinkage of extruded plastic and to control the vast linear coefficient of the jacket. Ripcords are also held in each cable jacket to make it easy and safe in sheath entry, even in a mid-span of the jacket as well as at the terminal. Cable core has an excess length (XSL) against the messenger wire (MW) shown in Fig.3. Cable height is 17 mm and weight is 0.15 kg/m, so downsizing by 36% in height and weight reduction by 57% compared with the conventional cable with slotted rod could be realized.

Fig.1 Newly developed 40-fiber cable

Self-supporting Wires
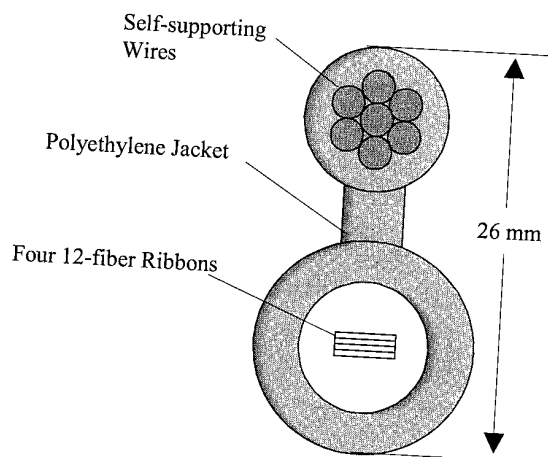Polyethylene Jacket
Ten 4-fiber Ribbons
17mm
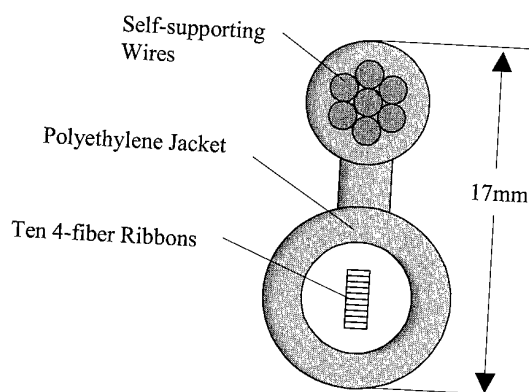
Fig.2 Newly developed 48-fiber cable

Self-supporting Wires
Polyethylene Jacket
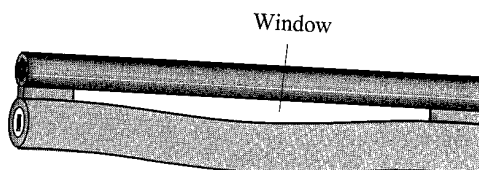Four 12-fiber Ribbons
26 mm

Window

Fig.3 Excess length of the cable core against the messenger wire

3. Cable performance

The following evaluation tests have been conducted on the manufactured 40-fiber cable such as attenuation change in manufacturing process, temperature cycling test, vibration test, mid-span entry test and various mechanical tests.

3.1 Attenuation change in manufacturing processes

Attenuation of each process was monitored and traced both at 1310 nm and 1550 nm. The results are shown in Fig.4. As you can see from that, stable attenuation was confirmed throughout the processes with the average attenuation of 0.35 dB/km at 1310 nm and 0.20 dB/km at 1550 nm.

corresponding to the temperature profile shown in Fig.5. This figure also shows the transmission loss change at 1550 nm of the cable sample for cyclic temperature. Attenuation change during the temperature cycling test was small enough to serve for a distribution purpose. This test result indicate that our manufactured cable provides stable transmission property ranging from –30C to 70C.

Fig.4 Attenuation change in manufacturing process
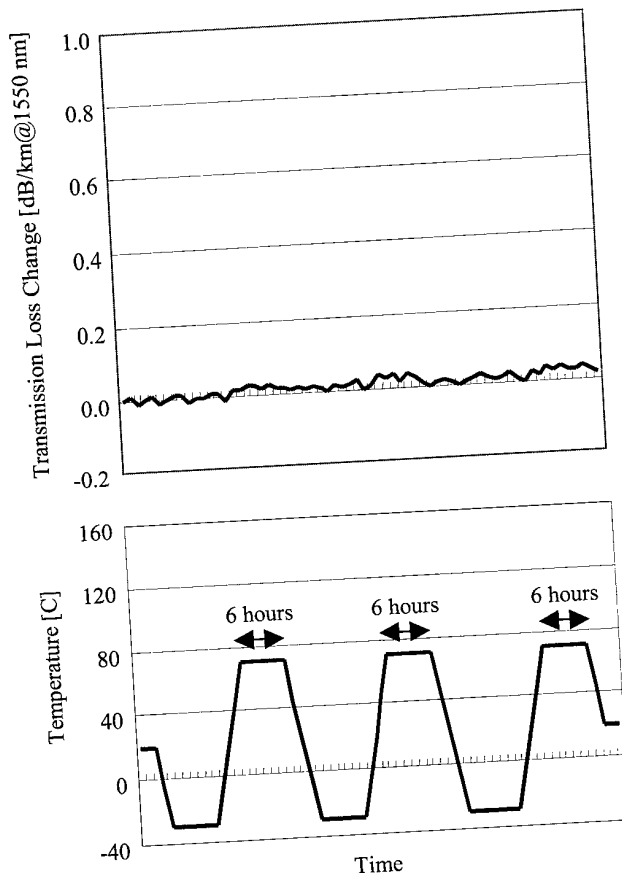
Fig.5 Profiles of temperature cycles used in Temperature cycling test and transmission loss change at 1550 nm

3.2 Temperature cycling test

Temperature property was also investigated between –30C and +70C. The cable was wound on 800 mm in diameter drum. Transmission loss variation due to temperature cycling was continuously monitored at a wavelength 1550 nm. For the accuracy of the measurement, the eight fibers in a 500 m cable sample were fusion spliced to result in a 4.0 km long test sample loop. This sample loop was then subjected to heat cycle

3.3 Vibration test

Vibration test was conducted on our cable sample. The setup is shown in Fig. 6. The cable sample was installed between poles and then vibrated with the severe condition as described in Table 1. Very little movement of fiber ribbons was measured after one-day vibration (10^5cycles), but it was not increased after ten-day vibration (10^6 cycles).
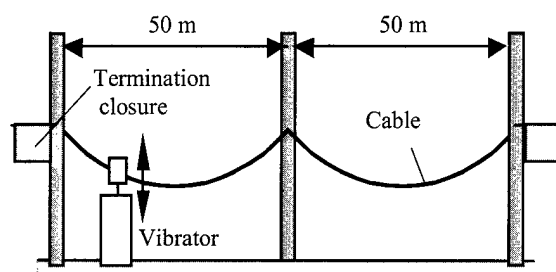
Fig.6 Setup of Vibration test

Table 1. Vibration test conditions

Items	Conditions
Span length	50m*2
Stringing tension (Strain of messenger wire)	764N (0.04%)
Frequency	3 Hz
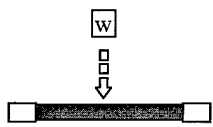
3.4 Mid-span entry

The work of mid-span entry was investigated by monitoring of attenuation change at a wavelength of 1550 nm. It was easy to pick up any ribbons after dividing the cable jacket into two pieces with ripcords. It took only two minutes to complete the work and no attenuation change was observed (<0.1dB) during the process.

3.5 Mechanical properties

Stable properties were confirmed on various mechanical tests on the manufactured cable such as tensile load, torsion, repeated bending, squeezing, crush and impact. Test methods were based on IEC60794-1-2. For this test, the eight fibers in the manufactured cable sample were fusion spliced. The change in attenuation was continuously monitored at 1550 nm. From these tests, it can be seen that our developed cable has excellent properties also for those mechanical requirements.

Table 2. Mechanical properties

Items	Conditions	Results
Tensile load	Sample length: 100 m Tensile load: 3720 N	<0.01dB
Torsion	Sample length: 1 m Stringing tension: 98 N FIX	<0.01dB
Repeated Bending	Sample length: 5 m Bending diameter: 320 mm, 160 mm Bending angle: 180 degrees The number of times: 10 cycles	<0.01dB
Squeezing	Sample length: 100 m Stringing tension: 1960 N Pulley: a diameter of 500 mm Bending angle: 90 degrees Pulley	<0.01dB
Crush.	Plate width: 100 mm Crushing force: 1960 N	<0.05dB
Impact	Mass of the weight: 1 kg Height: 1 m w	<0.01dB

3.6 Water penetration

A 1-meter static head was applied at one end of a 1-meter length of the manufactured 48-fiber cable for 24 hours. We confirmed that no water leaked through the open cable end.

4. Conclusion

Downsized dry and non-slotted core aerial cable with fiber ribbons has been developed. The cable realized downsizing by 36% in height and weight reduction by 57% compared with the conventional cable by a grooved plastic spacer. We confirmed that it was easy to access to fibers inside even in a mid-span of the jacket and that the cable had high performance and high reliability on various requirements for distribution purpose. We believe the cable will be helpful to realization of FTTH with increasing speed.

Reference

[1] H. Iwata, "Novel Optical Fiber Cable for Distribution Use in Access Network, " in Proc. 48th IWCS, pp.20-24, (1999).

Authors

Tomoyuki Yokokawa

Sumitomo Electric Industries, Ltd. Yokohama Research Laboratories

1, Taya-cho, Sakae-ku, Yokohama, 244 Japan

Tomoyuki Yokokawa received his M.E. degree in electrical engineering from Waseda University in 1994. He joined Sumitomo Electric Industries, Ltd. in 1994 and he has been engaged in research and development of fiber optic cable. Mr. Yokokawa is a member of the Optical Network R&D Department in Yokohama Research Laboratories and a member of the IEICE Japan.

Itaru Sakabe

Sumitomo Electric Industries, Ltd. Yokohama Research Laboratories

1, Taya-cho, Sakae-ku, Yokohama, 244 Japan

Itaru Sakabe received his M.E. degree in electronic engineering from Electro Communication University in 1993. He joined Sumitomo Electric Industries, Ltd. and he has been engaged in research and development of fiber optic cable. Mr. Sakabe is a member of the Optical Network R&D Department in Yokohama Research Laboratories and a member of the IEICE Japan.

Toyoaki Kimura

Sumitomo Electric Industries, Ltd. Communications Division

1, Taya-cho, Sakae-ku, Yokohama, 244 Japan

Toyoaki Kimura received his B.E. degree in electrical engineering from Keio University in 1998. He joined Sumitomo Electric Industries, Ltd. and he has been engaged in design and development of communication cables. Mr. Kimura is a member of the Communications Division.
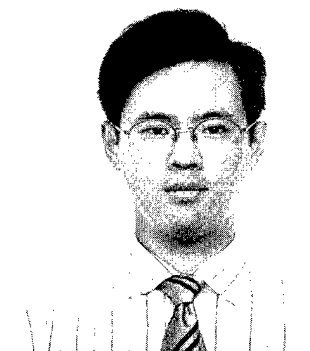
Hiroki Ishikawa

Sumitomo Electric Industries, Ltd. Yokohama Research Laboratories

1, Taya-cho, Sakae-ku, Yokohama, 244 Japan

Hiroki Ishikawa received his M.E. degree in applied physics from Tohoku University in 1990. He joined Sumitomo Electric Industries, Ltd. and he has been engaged in research and development of fiber optic cable. Mr. Ishikawa is a senior engineer of the Optical Network R&D Department in Yokohama Research Laboratories and a member of the IEICE Japan.

Wataru Katsurashima

Sumitomo Electric
Industries, Ltd.
Communications Division

1, Taya-cho, Sakae-ku,
Yokohama, 244 Japan

Wataru Katsurashima received his B.E. degree in applied physics from Tokyo University in 1987. He joined Sumitomo Electric Industries, Ltd. and he has been engaged in research and development of fiber optic cable. Mr. Katsurashima is a senior engineer of the Communications Division and a member of the IEICE Japan.

Nobuhiro Akasaka

Sumitomo Electric
Industries, Ltd.
Yokohama Research
Laboratories

1, Taya-cho, Sakae-ku,
Yokohama, 244 Japan

Nobuhiro Akasaka received his M.E. degree in chemical engineering from Tokyo University in 1983. He joined Sumitomo Electric Industries, Ltd. and he has been engaged in research and development of fiber optic cable. Mr. Akasaka is a Chief Research Associate of the Optical Network R&D Department in Yokohama Research Laboratories and a member of the IEICE Japan and the Material Life Society of Japan.

Fiber Strain On Field-Deployed Aerial Optical Cables

T.-C. Chang, C.-M. Hsiao, H.-J. Chen, H.-P. Hsu, Y.-c. Lin, Y.-K. Tu

OSP, Telecommunication Labs, Chunghwa Telecom Co., Ltd R.O.C.

Tel: 001-886-3-424-5767   **E-mail**: CCT752440@CHTTL.COM.TW

Abstract

In this study, two self-supporting modified loose-tube type optical cables were manufactured and deployed in seasonal windy and seashore mountain humid areas. After the completion of field deployment, attenuation changes of the cables were monitored by Power Meter and OTDR, and the strain distribution of the fibers were measured by a Brillouin OTDR. The results showed that the overall degradation that result from environmental degradation and mechanical strain-stress induced degradation did not or not yet appear on these two cables, at least, under one-half year of field service.

Keywords

Self-supporting optical cable; BOTDR; strain

1. Introduction

In the case of aerial optical cable, stresses due to installation stretching, temperature change, and gusty winds especially Typhoon, are added to the optical fibers in the cable. These stresses degrade the reliability of the optical fibers and cause attenuation increase. Therefore, many papers dealing with the structure related stress release, and mostly focusing on the cable design and theoretical tension analysis [1-4] has reported. Yet, practical measurement and evaluation of the field-in-service cable fiber strain or stress were fewer presented. It is of interest to understand the strain-stress property on an aerial optical fiber cable after field installed. Recently, aerial optical fiber installation has increased vastly here in Taiwan partially due to the local requirements for broadband access and the push of fiber to the last mile by telecommunication company. The need of Internet access in the remote areas also prompt up the use of aerial optical cables since those areas are either lacking of constructed conduits or difficult to dig the conduits.   Although Cable TV companies have

a large installed base of this type of aerial cables, under the severe wind load environment here in Taiwan, they need to replace the aerial cable every 5-6 years. Obviously, cost and maintenance consideration requires that the reliability issues, especially the stress-strain degradation behaviors on the aerial cables should be addressed.

2. Cable structure and performance

The tested cable structure is a self-support jelly-filled LAP sheath, 12-48 fibers loose tube type optical cable that consists of a messenger wire combined together with the PE sheath. The suspension wire is made of 18 mm^2 stranded steel wires with a diameter of 5.4 mm and a minimum break force of 2040 kgw.

There are two major concepts for protecting the optical fiber from tensile forces. One is enlarging the cable modulus, the other is introducing excessive fiber length into the cable design. From our field experience, the loose tube cables with a longer stranding pitch and large { Excess Fiber Length } / { Inner Tube Diameter } ratio were capable of surviving from a heavy wind loads. This time, we modified the duct cable parameter and manufactured two sections of self-support cables and deployed in the field to study the fiber strain that may exercise in the cable.

Table 1 shows measurements of optical and mechanical properties of the two self-support aerial cables after manufacture and before field deployment. The fiber attenuation is measured using an OTDR at 1550 nm. Mechanical characteristics measurements of the two aerial optical cables were carried out according to TR-NWT-001121. Measurement results show that no optical loss increased larger than 0.1 dB during and after the tests of every mechanical test item. The fiber strain measurement using Brillouin Optical Time Domain Reflectometer showed that all the fibers stress were all smaller than 0.02%.

Table 1. Self-support aerial cable performance

| Test item	Cable 1	Cable 2
Attenuation at 1550 nm	< 0.3 dB/km	< 0.3 dB/km
Fiber strain	< 0.02%	< 0.02%
Tensile loading and bending	< 0.1 dB	< 0.1 dB
Compressive loading	< 0.1 dB	< 0.1 dB
Impact	< 0.1 dB	< 0.1 dB
Twist	< 0.1dB	< 0.1 dB
Cyclic flexing	< 0.1 dB	< 0.1 dB

3. Fiber strain after field deployment

In this study, the two manufactured self-supporting modified loose-tube type optical cables were deployed at two areas. Route 1 is a typical seasonal windy area with a deployed length of about 1 km. The cable has a fusion splice point and joints with a slot ribbon cable. Route 2 is a seashore mountain humid area with a deployed length of 5.1 km and has 4 fusion points. These cables were pulled along the pole by a tensile gauge to keep the tension applied to the cables was under specified safe region. At the pore around a corner and every 5 pore, the cable was left with a Ω-shape to keep the excessive cable length. The span length of this cable is smaller than 50 m. After the completion of field deployment, attenuation changes of the cables were monitored by a Power Meter and an OTDR, and the strain distribution of the fibers were measured by a Brillouin OTDR. Data were cumulated and analyzed for one-half year.

Figure 1 and 2 shows the typical fiber attenuation loss characteristic during 17 months period. Based on the measurement, these cables were proved to be in good condition since no particular increases in optical loss were found.
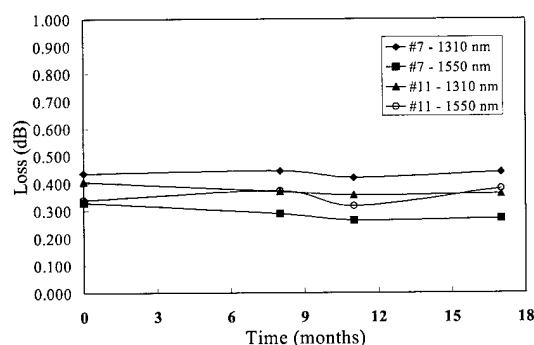
Fig.1 Attenuation changes of route 1 cable after deployment
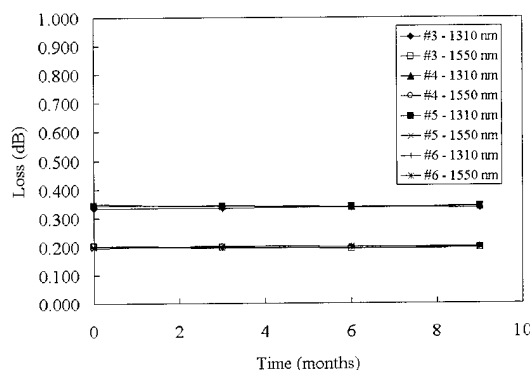
Fig.2 Attenuation changes of route2 cable after deployment

Figure3 and 4 shows the results of fiber strain in the longitudinal direction using the BOTDR. There was no significantly fiber strain occurred and the maximum fiber strain were less than 0.05% during the test period. We also found that the fiber strain in aerial optical cable can release to a constant value by the relaxation of cable length.

All of the measurements indicates that the overall degradation that result from environmental degradation and mechanical strain-stress induced degradation did not or not yet appear on these two cables, at least, under one-half year of field service. On the other hand, when examining some of the individual measurement, occasional abnormal higher attenuation and sometimes strains higher than the original 0.01% was observed. However, such results usually disappeared when a repeated measurement was conducted. This means that some sudden strain rise likely due to a gusty wind may occur, but due to the excellent loose tube design, the tentative strain was self-adjusted by the fibers on their own, and the strain was released. Nevertheless, it is expected that the continuous strain-rise-then-strain-release process may attribute to a fatigue effect on the fiber, and it will be interesting to see how long a fiber fatigue will appear, and how is the performance of the cable will be affected. Continuous measurement and performance monitoring will be conducted on these two field-service cables. Long-term reliability of the aerial optical cable therefore, may be able to evaluate if substantial strain-stress induced fatigue appears to affect the performance of the cables. The strain-stress measurement by a Brillouin Optical Time Domain Reflectometer may provide a good indication of the aerial cable reliability.
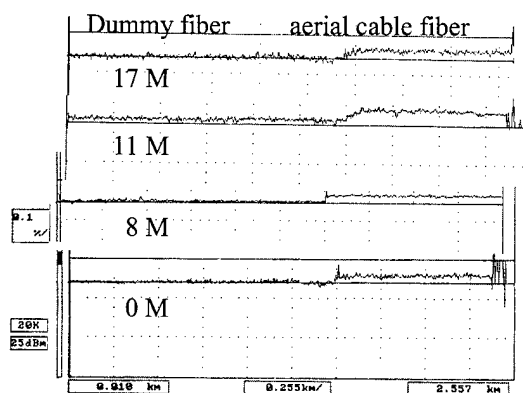
Fig.3 Fiber strain distribution of route 1 cable after deployment
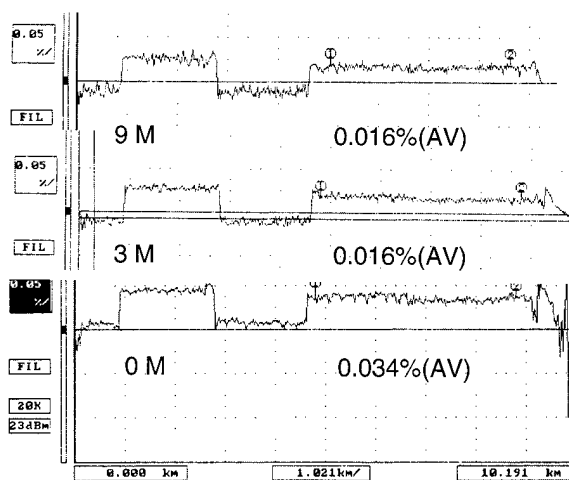
Fig.4 Fiber strain distribution of route 2 cable after deployment

Change of fiber loss at 1300 and 1550 nm after tensile force was applied to fiber are shown in fig. 5. No significantly attenuation increasing was found when fiber was strained to 0.3%. It meant that fiber strain did not increase attenuation. From this result, we can conclude that we can not evaluate the optical cable just from OTDR data. Fibers have small attenuation loss change does not mean fiber is strain free. It is necessary to measurement fiber strain in evaluation the cable performance.
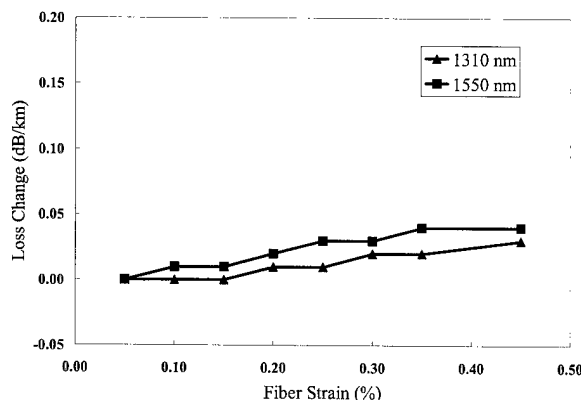
Fig.5 Relation of fiber strain and attenuation change

4. Conclusion

We investigated the fiber strain of field-deployed modified loose tube type self-supporting aerial optical cable. The results showed that the overall degradation that result from environmental degradations did not inflence the performance of these cables within one and half year of field service. Obivious, the proper desingn allow the cable exercise its strain relaxation from length release. Although, the cables showed ignorable optical loss after one and half year service does not mean its long term performace will be the same since there is still a strain contantly applied on the cables. Strain applied on cable may cause static fatigue to influce the long-term reliability of the cable instead of the observable short-term increasing in attenuation. It is of interesting to see how long the fatigue induce performace degradation will begin to occur and that will be the service life of the cable under that enviroments.

5. References

1. Ulrich Oestreich, Gunter Zeidler, 29th IWCS, pp 394-401, 1980
2. A.S. Dodd, H.R. Mcdowell, R.S. Wagman, 39th IWCS, pp 166-175, 1990
3. P.S. Keith, E.L. Buckland, 36th IWCS, pp 419-425, 1987
4. M.Iwazaki, K. Katagiri, 29th IWCS, pp 432-437, 1980

Biographies

Ting-Chung Chang
OSP, T.L.
Chunghwa Telecom
P.O. Box 6-48, Yang Mei
Taoyuan, Taiwan 326,
R.O.C.

Ting-Chung Chang received his M.S. degree in Applied Chemistry in 1984 from Tsing Hua University and then directly joined T.L.. He is now a research scientist and a member of outside plant laboratory in T.L.

Chieh-Mei Hsiao
OSP, T.L.
Chunghwa Telecom
P.O. Box 6-48, Yang Mei
Taoyuan, Taiwan 326,
R.O.C.

Chieh-Mei Hsiao received her M.S. degree in Chemical Engineering from Tsing Hua University. She joined T.L. in 1981 and presently worked as a research scientist and a member of outside plant laboratory in T.L.
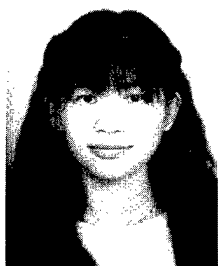
Huei-Jen Chen
OSP, T.L.
Chunghwa Telecom
P.O. Box 6-48, Yang Mei
Taoyuan, Taiwan 326,
R.O.C.

Whei-Jen Chen received her M.S. degree in Applied Chemistry in 1991 from Tsing Hua University and then directly joined T.L.. She is now a research scientist and a member of outside plant laboratory in T.L.

Hsi-Pai Hsu
OSP, T.L.
Chunghwa Telecom
P.O. Box 6-48, Yang Mei
Taoyuan, Taiwan 326,
R.O.C.

Hsi-Pai Hsu is currently a project manager of the material group of Loop and Outside Plant Laboratory, Telecommunication Labs. He received his Ph.D. degree in Chemistry in 1983 and has engaged in industrial materials research since then.

Yih-chyuan Lin
OSP, T.L.
Chunghwa Telecom
P.O. Box 6-48, Yang Mei
Taoyuan, Taiwan 326, R.O.C.

Yih-chyuan Lin received his Ph.D. degree in Photochemistry from Georgetown University. After working as a postdoctoral Fellow in the Institute of Materials Science at the University of Connecticut, he joined Telecommunication Laboratories in 1989 and presently is the project manager of O.S.P. materials and construction project.

Yuan- kuang Tu
OSP, T.L.
Chunghwa Telecom
OP4423, 12, Lane 551,
Min-Tsu Road Sec. 5,
YangMei,Taoyuan, Taiwan
326, R.O.C.

Yuan-Kuang Tu received his BS, MS and Ph.D degrees in EE from National Taiwan University in 1977, 1979, and 1988. He joined T.L. in 1981 and worked for integrated optics, optoelectronic devices, and optical fiber communications. From 1990 to 1996, he was the project manager of Photonic Technology Research in Applied Research Lab. Now he is the Managing Director of the Outside Plant Technology Lab., and is in charge of the technology developments for access network. He is a member of IEEE/LEOS, IEEE COMSOC, ISHM ROC Chapter, Chinese Institute of Engineering, Optical Engineering Society of ROC, and Electronic Devices and Materials Association.

Improvements on Damping Techniques for Fiber Optic Cables

David C. Sunkle, John J. Olenik, Matthew D. Fullerman
Preformed Line Products, Cleveland, Ohio

ABSTRACT

With the steady increase in fiber optic cable spans in the world, more and more problems are arising from dynamic cable motion. Cable motion affects virtually every aerial cable that is installed today. In some instances, the hardware developed to control cable motion has given rise to new challenges and complications. This has increased the importance of the research and testing involving this phenomenon and has necessitated the development of new products to meet the ever-changing needs of the industry.

This increased awareness and research has given rise to many advances in the products used to minimize fiber optic cable motion.

The rise in ADSS installations in high voltage fields has given new focus to issues such as corona, tracking, and dry band arcing. Inherent in these phenomena is the cable hardware. New products are required to minimize the electrical stress on the cable, allowing it to resist the effects of being installed in the high electrical stress applications. Again, testing and verification are essential in the development of products for these issues.

This paper will discuss the development of testing methods to ensure that these new products meet the needs of their environment. Data will be presented that shows the effectiveness of the products in the laboratory. Past testing indicates that there is a good correlation between laboratory findings and field studies.

BACKGROUND

Previous work has shown that the Spiral Vibration Damper (SVD) is effective in reducing vibration on ADSS cables.[1,2,3] In addition, it has been found that there is an acceptable correlation between the laboratory performance of an SVD and its performance in the field. In other words, a damper that performs well in the laboratory will perform adequately on an operating line. Newer applications of ADSS cable place the damper in a highly stressed electrical environment. After detailed analysis, this high electrical stress was found to deteriorate the plastic material of the damper over time. This deterioration of the material was overcome by placing the damper further out into the span where the electrical stress was greatly reduced, Figure 1. While this solved the material problem, it greatly increased application difficulty, Figure 2. Therefore a program was undertaken to develop a testing program to evaluate a different material which can withstand the high electrical stress field.
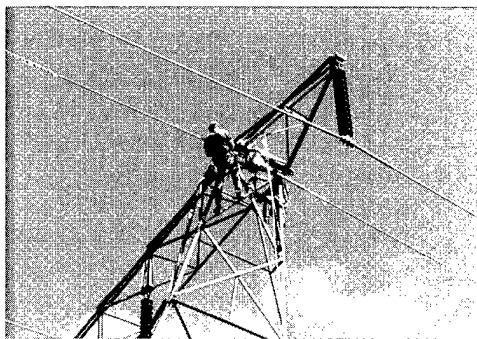
Figure 1 - ADSS with SVD's Applied

Note: SVD Distance from Structure – 3.5 m
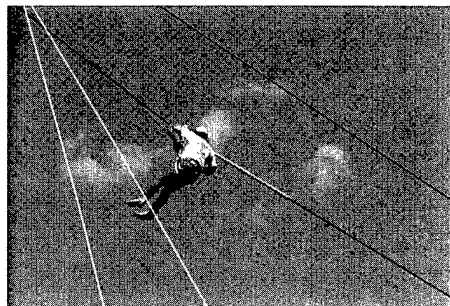
Figure 2 - Lineman Installing SVD

DEVELOPMENT OF THE TEST PROGRAM

The first objective was to determine a testing program which can simulate the environment in which this product would be placed. Several performance requirements were identified, including the ability to withstand the outdoor environment in a high electrical stress field and the ability to withstand fatigue. In addition, the product must effectively damp vibration similar to the standard SVD. To examine product performance, the following tests were developed:

1. Damper energy dissipation testing
2. Ultra-violet testing

3. Fatigue vibration testing
4. Electrical testing

Damper Energy Dissipation Testing

As mentioned above, from previous testing it has been shown that impact damper field performance can be predicted by conducting a laboratory energy dissipation test. It has been further shown that the standard SVD has acceptable performance in the laboratory and has an acceptable correlation to field performance. Therefore if the new impact damper has similar performance to the standard damper, then it can be assumed that the new impact damper will perform satisfactorily on an operating line.

To determine the energy dissipation characteristics of the new impact damper, a vibration test was conducted per the IEEE 664-1993. Laboratory damper efficiency testing of an SVD was performed by the power method. A length of ADSS was installed in a laboratory vibration span at a constant tension equal to the installation tension of the ADSS cable and maintained by a pivoting balance beam. Square faced, rigid clamps were installed at each end of the cable to minimize energy losses in the terminations, resulting in a test span of 30 m. An SVD was installed on the ADSS approximately 130 mm from a rigid clamp, Figure 3. A vibration shaker was installed to excite the ADSS. An impedance transducer, a combination load cell and accelerometer, was installed between the shaker armature and the test cable to measure the force and acceleration imparted to the test cable. Figure 4 is a schematic of the test setup.
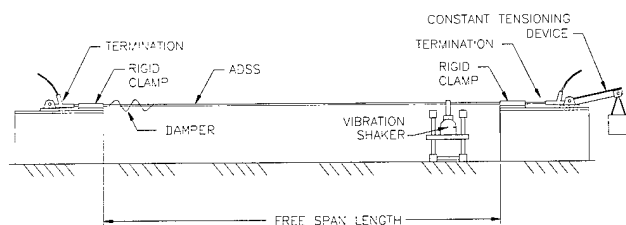
Figure 3
SVD Installed on Laboratory Test Span

The signals from the amplifiers were sent through a tracking filter, which removed all frequency components other than the driving frequency, and then viewed with an oscilloscope. The force and acceleration signals from the impedance transducer were sent to an FFT analyzer, which displayed the frequency spectrum of each signal and the phase angle between the two signals.
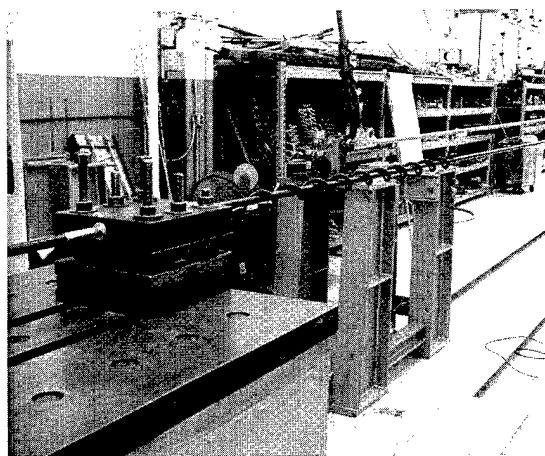
Figure 4 – Laboratory Test Setup

Measurements to determine the dissipated power were taken at tunable harmonics within the specified frequency range of .185/D to 1.295/D, where D is the conductor diameter in meters. At each frequency, the shaker input was adjusted to a specific level in order to obtain an antinode loop velocity of 200mm/s. To measure the antinode amplitude of the first free vibration loop from the damper, a miniature accelerometer was installed on the conductor and the signal sent to the FFT analyzer. The force, acceleration and conductor amplitude were then obtained from the FFT analyzer display. The dissipated power was then calculated and plotted.

This was conducted for the standard impact damper and the new impact damper. For the complete test procedure, refer to previous publications.[1,2]

Test Results. The results are given in Figure 5. The performance is extremely similar and therefore it can be concluded that the new impact damper will perform at acceptable levels.
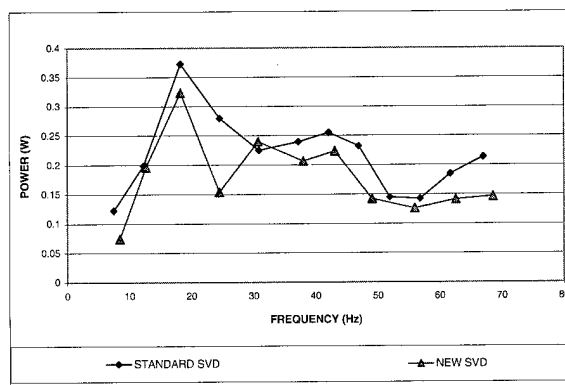
Figure 5 – Energy Dissipation Test on SVD's

Ultraviolet Testing

To verify a material will properly function when it is exposed to sunlight, it is necessary to conduct ultraviolet testing. In the case of the impact damper, samples of the rod were placed in a UV chamber and tested per ASTM-G 53-94. The samples were exposed to 4000 hours of ultraviolet testing. Samples were removed every 1000 hours and an impact test was conducted to determine impact performance.

Test Results. There was no visible change in the material after 4000 hours. There was no reduction in the impact performance over the exposure period. Refer to Figure 6.

Figure 7 –
New Material Formed Into a Distribution Tie

Figure 8
Test Setup for Fatigue Testing

Test Results. After 50,000,000 cycles of vibration, there was no failure of the product.

Electrical Testing

Plastic materials which are placed in a high electrical stress environment may deteriorate due to a phenomenon called tracking. In this phenomenon, the electrical discharges burn or track the material. This, if severe enough, can eventually fail the product.

Various companies have proposed electrical evaluation tests for ADSS cables and hardware in a high voltage environment.[5] To date, there is not an internationally accepted test method. IEEE has presently established a Working Group to look into this. Laboratory attempts were made to replicate the testing done at other laboratories but were unsuccessful at obtaining any meaningful data.

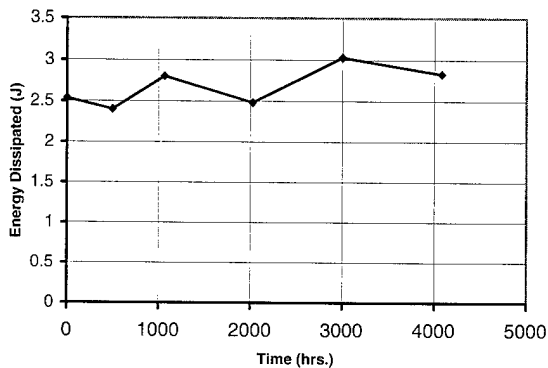Therefore, a previous test method which was utilized to determine the electrical performance of plastic ties was referenced. For this test, a plastic tie was exposed to leakage currents by placing a 25 kV line to ground potential across a conductor to an insulator pin. A plastic tie attached the insulator to the conductor, Figure 9. The assembly was now exposed to alternating wet mist/dry cycles. One cycle consisted of 5 minutes of mist and 25 minutes of air-drying. This cycle continued until tracking occurred or 400 hours (800 cycles). The standard material used for SVD's and the new material were evaluated.

Figure 6 – Energy Dissipated During Impact Testing

Fatigue Testing

Previous testing has been conducted to verify that the impact type damper will not wear out when properly used.[4] A more severe test of a material consists of a fatigue test where the material is tested with regard to bending stresses. This will help determine if there is any notch/fatigue sensitivity of this material. To conduct this test program, the rod was formed in the shape of a typical distribution tie, Figure 7. The tie was then installed on a 13-mm diameter cable and a pin insulator and vibration fatigue tested for 50,000,000 cycles of aeolian vibration. The amplitude of vibration was 1mm and the frequency was 53 Hz. See Figure 8 for the test setup.

Figure 9 - Electrical Test Chamber

Test Results. After 19 hours (38 cycles), the standard material began to show signs of tracking. After 158 hours, the tie was severely tracked, Figure 10. The new material showed no signs of tracking after 400 hours (800 cycles).
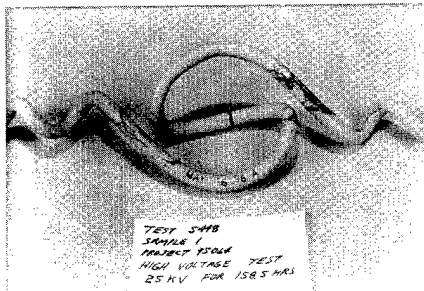
Figure 10 - Severe Tracking on Standard Material
After 158 Hours of Exposure

FIELD EVALUATION

At present, an SVD made from this new material has not been installed on an ADSS cable in a high electrical stress environment. However, field evaluations of this material have been made on other products used in high electrical stress applications. The products include the Air Flow Spoiler and the ADSS-CORONA™ coil. Air Flow Spoilers, a device to reduce galloping, made from this material, have been installed on operating transmissions lines over 700 kV in excess of two years with no signs of degradation of the material. ADSS-CORONA Coils made from this material have been installed at the ends of dead-ends and suspensions for ADSS to reduce electrical stress. These products have been installed for over two years with no signs of deterioration of the material.
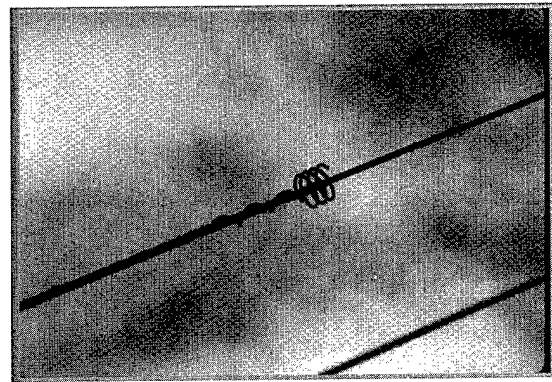
Figure 11 – ADSS-CORONA™ Coil
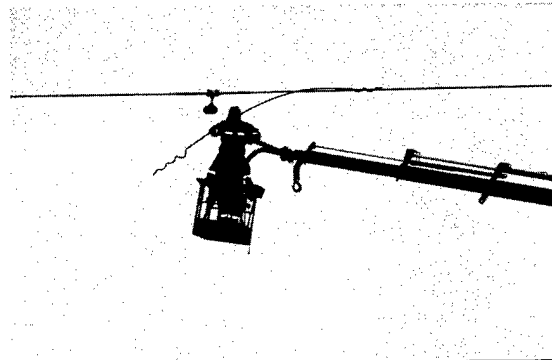
Figure 12 – Air Flow Spoiler

CONCLUSION AND FUTURE WORK

A preliminary test method was developed to determine if a new plastic material can survive in the high electrical stress environment in which ADSS cables and hardware are placed. This method needs to be further improved once the IEEE determines the proper test technique. In addition, vibration testing was used to verify the new material was as effective at reducing vibration as the standard material.

Further work needs to be done by conducting field evaluations of the new impact dampers on operating ADSS lines in high electrical stress environments to verify there is no degradation of the SVD or ADSS cable. Plans are in place to set up various field test sites. In addition, attempts will be made to conduct some further electrical testing on the impact damper at an outside laboratory, even before the IEEE establishes their standard.

REFERENCES
[1] Sunkle, David C., McKenna, Dennis F., and Olenik, John J. "Evaluation of Damping Effectiveness of Impact Dampers on ADSS Cable" presented at 48th International Wire and Cable Symposium, November 15-18, 1999.

[2] Sunkle, David C., Olenik, John J., and Fullerman, Matthew D. "Determination of Damping Effectiveness

on ADSS," to be presented at ESMO 2000 October 8-12, 2000 Paper #25C-TPC-13

[3] Sunkle, David C and Christian, David F. "The Effects of Tension on Vibration of All-Dielectric Self-Supporting Fiber Optic Cable," presented at the Seventh International Conference on Transmission and Distribution Construction and Live Line Maintenance (ESMO-95 CP-23), Columbus, Ohio, October 29 – November 3, 1995

[4] Champa, Raymond J. "Aeolian Vibration Test to Evaluate Wear Characteristics of Spiral Vibration Dampers (SVD's) on All Dielectric Fiber Optic Cable (ADSS)," TR-696-E Preformed Line Products, July 26, 1991

[5] Militaru, Cristian, "ADSS Cables Electrical Corrosion Tests," Alcoa Fujikura Ltd., Spartanburg, SC. Presented at the 48th International Wire and Cable Symposium Proceedings, November 15-18,1999.

AUTHORS

David C. Sunkle, P.E., Preformed Line Products, 660 Beta Drive, Mayfield Village, Ohio 44143

David is a degreed Mechanical Engineer and a Registered Professional Engineer. He has been with Preformed Line Products for 22 years and is presently the Product Engineering Manager. His responsibilities include development, evaluation, and approval of all products developed by PLP-U.S. Dave is an active member of IEEE and is chairman of TFG3 in CIGRE WG 11, Subcommittee 22.

John J. Olenik, Preformed Line Products, Mayfield Village, OH 44143

John attained his Mechanical Engineering Degree in 1994. He has been with Preformed Line Products for 3 years, and is presently the Technical Support Engineer for both the Domestic and International Power Products. He is an active member of IEEE, and is involved in several working groups dealing with the Power Industry.

Matthew D. Fullerman, Preformed Line Products Mayfield Village, OH 44143

Matt received his Bachelor's Degree in Mechanical Engineering in 1998. He has been employed at Preformed Line Products as a Technical Support Engineer in the International Operations Department since 1999. He is responsible for both Power and Telecommunications products. Matt is an active member of IEEE.

Cost Saving Optical Fibre Aerial Cable System
For Distribution and Access Networks

Carsten M. Gregor, Ulrich Jansen, Heribert Mühlen, Reinhard Girbig

Alcatel Kabel AG & Co
Mönchengladbach, Germany
+49 (0)2166 27 0 · carsten.gregor@wrh.acab.alcatel.de

Abstract

This contribution describes a new economical aerial cable link technology. The necessary components for the erection of a complete optical fibre Sinfony™ link shall be reported in detail.

Particular the small and compact cable design, consisting of a jelly filled laser welded stainless steel tube, stranded around a catenary wire, including its mechanical and environmental characteristics will be presented. For instance the tensile strength and temperature dependence of the fibre attenuation will be shown.

Additionally it shall be considered that the installation of this highly reliable Sinfony-concept can be performed in a time saving procedure, resulting in a most favourable economy.

Primary conclusion or result: A complete new economical aerial cable link technology. including cables, accessories and installations for the distribution and access network will be described.

Background: Due to the increased request of new operators for own distribution and access networks it is necessary to provide appropriate economical solutions.

The following details will be described:

- Sinfony™ cable design and performance for distribution and access network applications
- Accessories
- Link tests and installation methods

Keywords

Optical aerial cable; access network; distribution network; alternative installation technique; right-of way solution; steel-tube; short span; medium span; loose tube;

Introduction

Due to the deregulation of the telecommunication market new carriers install own fibre optic cable networks in order to be competitive and independent to the incumbents. The costs of such necessary huge networks are extremely high, unfortunately. And thus a most economical concept for a total cable network is highly important, particular for the distribution and access level.

It has widely been proven that the dominating portion of the passive network costs are caused by the conventional cable installation measures. Therefore the desired cost reduction activities are focused mainly on optimizing these laying methods. Among various technologies optical fibre cable links are integrated into existing infrastructures for gas [1], drinking water [2], railway-track-application [3] and sewer [4].

In addition to such established alternative solutions for the distribution links a new generation of a metallic aerial cable design shall be introduced.

Cable Design

The cable construction of Sinfony™ was derived from the well known and introduced OPGW with stranded stainless steel tube [5, 6]. The optical unit is a laser welded stainless steel tube in which the fibres are loosely housed, embedded in filling jelly. This tube is stranded around a central wire. An OPGW has to cover the functions of an usual earth wire which are carrying short time currents and lightning protection. A minimum strength has to be achieved because of mechanical loads given by long spans and additional loads like ice and wind. Now the Sinfony™ does not have to cover this functions and is only made for short span applications it can be reduced to the minimum. This is the central wire and the steel tube with the optical fibres (see Figure 1).

To be able to create standardised fittings the central wire has always a diameter of 3,5 mm. Depending on the mechanical requirements it can be made of aluminium alloy (AA), galvanised steel (St) or aluminium clad steel (ACS).

To cover different fibre demands two sizes of steel tubes are available. Up to 36 fibres the tube dimensions are 3,0/ 3,5 mm (inner/ outer ∅), for up to 60 fibres the diameters are 3,4/ 4,0 mm.

Figure 1. Sinfony™-Cable
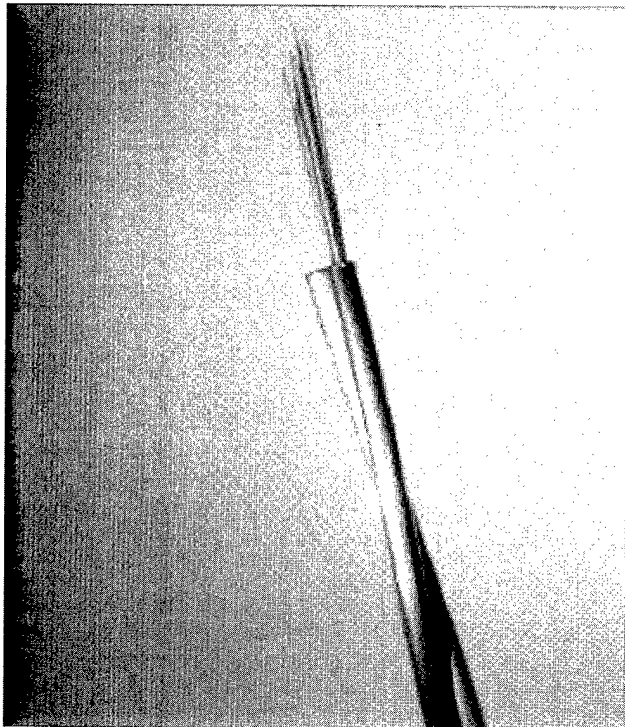
Cable Characteristics

The characteristics according to IEC Standards of different Sinfony™ cables are shown within the following table:

Wire ∅: 3,5mm	AA	St	ACS
Rated Tensile Strength [kN]	2,8	12,6	12,5
Maximum Fibre Count	36 / 60	36 / 60	36 / 60
Cable Diameter [mm]	7 / 8	7 / 8	7 / 8
Weight [kg/km]	55 / 65	105 / 114	94 / 104
Modulus of Elasticity [kN/mm^2]	60	180	162
Thermal Elongation Coefficient [10^{-6}/K]	23	11	13
Permissible Maximum Working Stress [N/mm^2]	123	550	546
Everyday Stress (16 % RTS) [N/mm^2]	47	209	208
Ultimate Exceptional Stress [N/mm^2]	211	943	936
Maximum Permissible Installation Force [kN]	1,2	5,3	5,3
Minimum Bending Radius [mm]	53	53	53
Temperature Range for Installation Temperature Range for Operation	-10 to +50 °C −40 to +80 °C		

Cable Installation

The cable can be installed in different ways similar to the installation of other aerial cables like e.g. a figure-8 cable. The easiest way is to unroll the cable from the drum and lay it alongside the line. In a second operation the wire will be cut at tension locations, approximately every 500 m, and the cable will be hoisted to the fixing points. The fixing at the tension points is done by small helical dead ends (See Figure 2) commercially available as well as the suspension rods. For sag adjustment a self clamping grip on the wire in addition to a lever hoist is used. If it is not possible to attach the cable to the tower outside the installation is done like for ADSS or OPGW using sheaves, pulling rope and a winch.

At branching, connecting or termination points the steel tube is leaded down to joint boxes housing single fibre management modules (Figure 3) and fixed at the tower with clamps. At termination points the steel tube can be even led into stations or buildings without additional joint box and cable as long as it is protected against crush and sufficiently grounded. Eventually lighting protection measures have to be foreseen.

Figure 2. Sinfony™-Cable at tension point
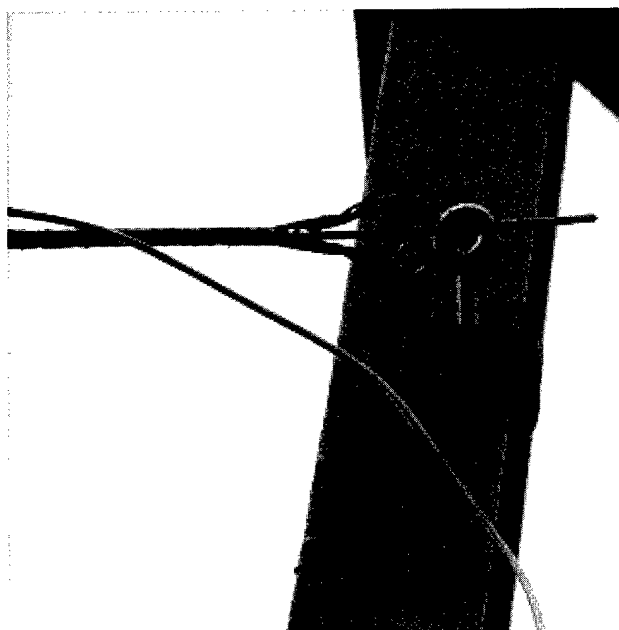
Figure 3. Sinfony™-Cable at termination point
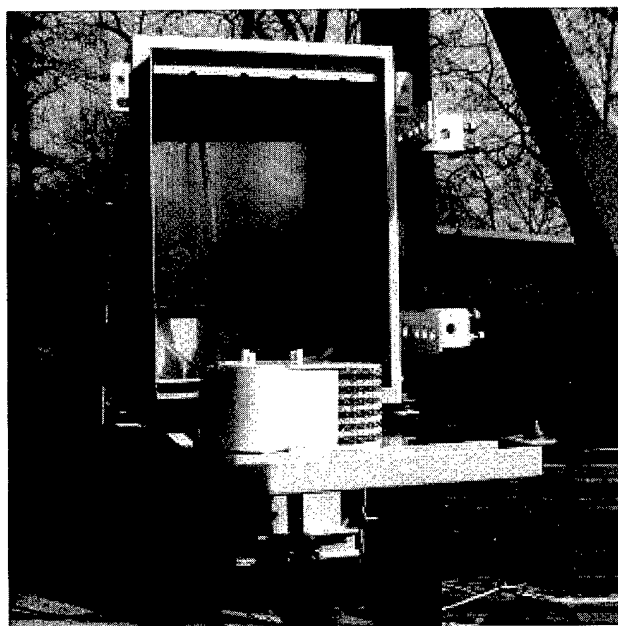
Measurements

The functionality and cable performance with respect to the transmission characeristics must be verified by different test procedures.

The requirements on the cables optical, mechanical and environmental properties must take into account general tests procedures as given in IEC 60793 / IEC 60794 and specifications from the customer.

These tests include optical, mechanical and environmental properties of the cable and fibers.

Parameters that are not influenced by cabling procedures or mechanical and environmental stress on the cable

(e.g. fiber geometry, mode field diameter, chromatic dispersion) can be controlled by an appropriate quality control of the fiber manufacturer.

In order to simulate the impact of mechanical and environmental stress on the cable transmission, especially attenuation performance, it must be tested on the cable itself.

For the Sinfony™ – cable, used as an self supporting outdoor arial cable, the following test should be done to control the behaviour on mechanical and environmental stress:

- temperature cycle test within the operating temperature range

- aeolian vibration test

- bending test

- tensile test

- corrossion test

Table 1. Test results / proposals

Parameter	limit (proposal)
Temperature cycle test (-40°C/+70°C) $\Delta\alpha$ (1550nm)	See Figure 5 $\leq 0,10$ dB/km
resistance to aeolian vibration (15% RTS; 107 cycles) mechanical behaviour $\Delta\alpha$ (1550nm)	no mechnical damage; $\leq 0,10$ dB/test length
Bending (r= 15xdiameter of cable) $\Delta\alpha$ (1550nm)	$\leq 0,10$ dB
tensile strength (14 kN) fiber strain $\Delta\alpha$ (1550nm)	See Figure 4 no fiber strain at operating load no change ($\leq 0,05$ dB)
corrosion test (salt fog test)	no degradation of strength

The verification of these requirements should be checked within a type test approval. Other requirements may be added due to specific applications.

Figure 4. Tensile Strength Test
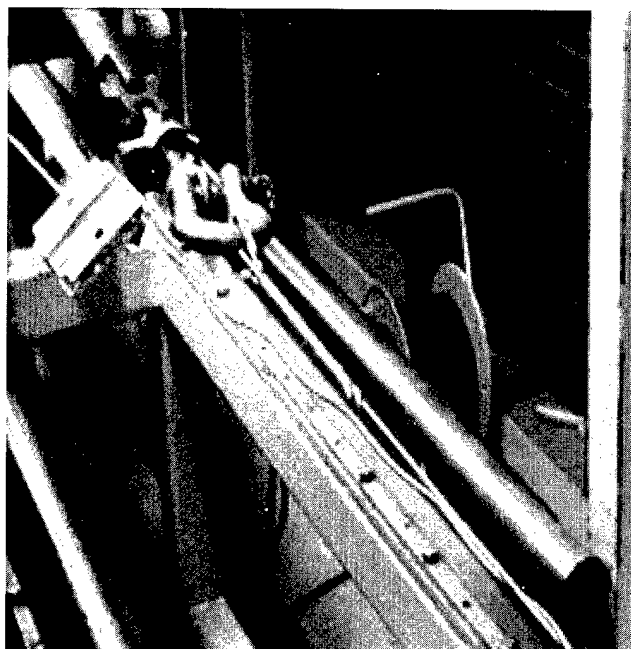
Figure 5. Temperature Cycle Test Results
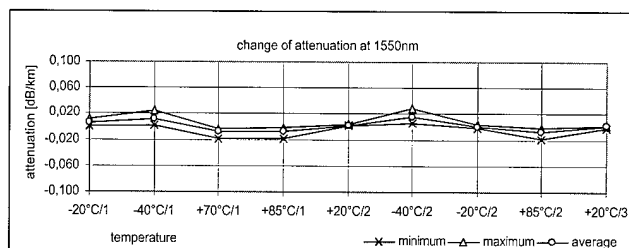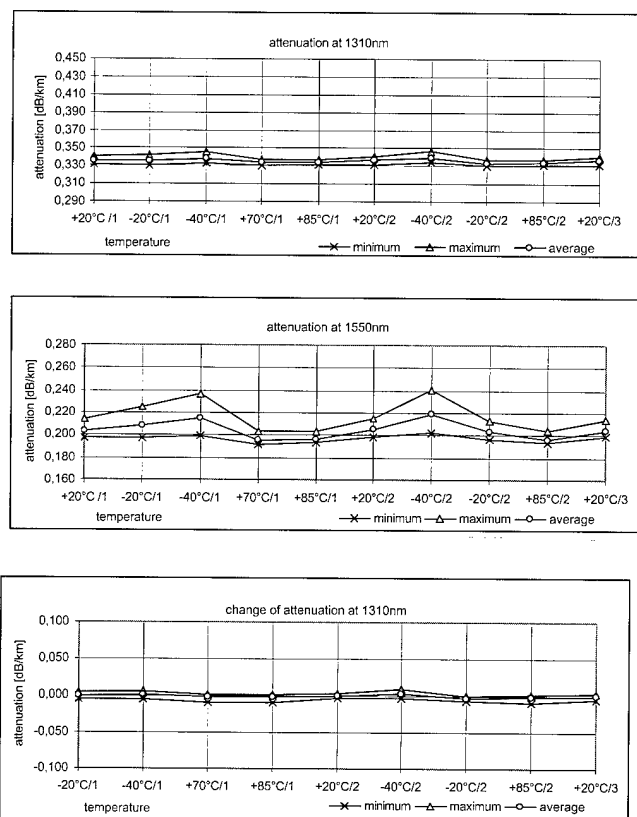
Conclusions

The sinfony™ concept is based on a complete metallic cable design with small dimensions, reduced weight, high fibre counts and a very fast installation technique. Due to it´s metallic design the lifetime expectance is comparable with OPGW and so at least double of the lifetime expectance of dielectric optical aerial cables. Contrary to complete dielectric cables the Sinfony™ cable is rodent protected, flame retardent and resistant against bird picking, industrial and traffic air contamination and saltfog-atmosphere. First trials have shown, that a cost reduction of 40 % compared to conventional concepts can be obtained as well under certain conditions as the installation time for a complete sinfony™ link can be dropped down remarkable.

References

[1] Paul E. Gregor, Lothar Kuhn, Dr. Alexander Weiss, "Optical Fibre Cable Links Within Gas Pipelines as an Alternative Telecommunications Route Technology", *International Wire & Cable Symposium Proceedings 1999.*

[2] Paul E. Gregor, Helmut G. Haag, Werner Braun, "Optical Fibre Cable Links within Drink Water Pipes as an Alternative Telecommunications Route Technology", *International Wire & Cable Symposium Proceedings 1998.*

[3] Paul E. Gregor, Heribert Mühlen, Gerhard Knopp, "Experiences and development trends for railway track cable technologies", *Signal + Draht Nr. 12/1999.*

[4] Helmut G. Haag, Wolfgang Liese, Klaus Nothofer, Wolfgang Teschner, Alexander Weiss, Wolfgang Stapel, "Experiences from Construction and Operation of Fibre Optic Cable Plants in Sewer Systems", *International Wire & Cable Symposium Proceedings 1999.*

[5] Helmut G. Haag, Georg Hög, Ulrich Jansen, Johann Schulte, Peter E. Zamzow, "Optical Ground Wire and All Dielectric Self-Supporting Cable –A Technical Comparison-", *International Wire & Cable Symposium Proceedings 1994.*

[6] Helmut G. Haag, Georg Hög, "Self-supporting optical fibre aerial cable constructions and related fibre

parameters for the transmission at 1550 nm", *International Wire & Cable Symposium Proceedings 1991.*

Authors:
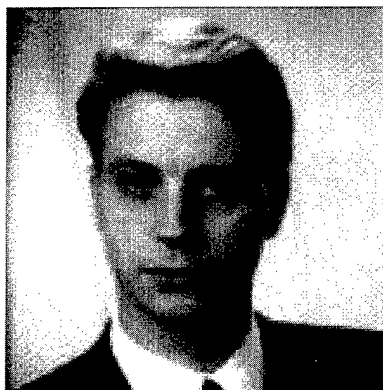
Casten M. Gregor was born in 1970. He received his Dipl. - Phys. degree from the Gerhard-Mercator-University Duisburg in 1995. After reaching his business referent degree due to the additional study of business administration at the Rheinisch-Westfälische Universität Aachen and Technische Akademie Wuppertal he joined Alcatel Kabel in 1997 for a trainee as young-high-potential.

Belonging to the product management team he joined the optical aerial development group in November 1998.

In April 2000 he became the head of the City Carrier Department within Alcatel Cable.

E-mail: Carsten.Gregor@wrh.acab.alcatel.de
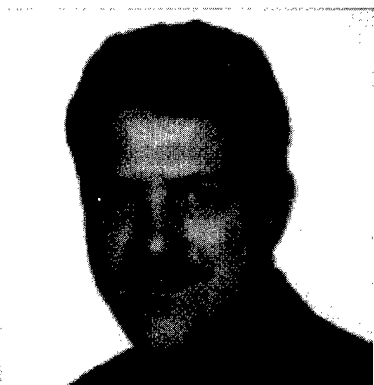
Ulrich Jansen was born in 1963. He received his Dipl.-Ing. degree from the Rheinisch-Westfälische Technische Hochschule Aachen in 1990 and joined the company in the same year. As a member of the development department for optical fibre cables he was responsible for the development of optical ground wires (OPGW) until end of 1996. Since 1997 he is Product Manager for aerial cables in the product group OAC.

E-mail: Ulrich.Jansen@wrh.acab.alcatel.de
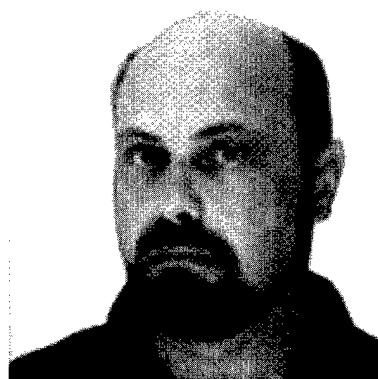
Reinhard Girbig was born in 1954, received his Dipl.-Ing. Degree from the Ruhr University Bochum in 1982 and joined AEG Kabel in 1987 as a development engineer in the fibre optics area, responsible for the technical aspects of OTDR measurement. In 1991 he became head of the Optical Fibre Cable Installation Technique Group. Between May 93 and April 1996 he was working as a project engineer and responsible for the Transmission and Characterization Group in the Alcatel Optical Fiber Cable Competence Center in Bezons, France. He is now responsible for the engineering department in the Product Group Optical Aerial Cables within Alcatel Cable.

E-mail: Reinhard.Girbig@wrh.acab.alcatel.de

Heribert Mühlen (39) is head of the Optical fibre cable measurement group.

He reached his Dipl.-Ing. degree from the Technical University of Aachen and joined Alcatel Kabel in 1987.

He is engaged in the field of Optical fibre cable measurement technique, quality control of Optical fibre cables and standardization of measurement procedures.

E-mail: Heribert.Mühlen@wrh.acab.alcatel.de

Halogen-Free Flame Retardant Cable Materials :
Improvement of Flame Retardancy and Suppression of Smoke Density

Do Hyun Park, Sangcheol Kim, Gun Joo Lee

Insulation materials Technology Group, LG Cable Research & Development Center,
555, Hogye-dong, Dongan-gu, Anyang-shi, Kyungki-do, Korea

+82-31-450-8333   ·   dhpark@cable.lg.co.kr

Abstract

In this work, halogen-free flame retarded polyethylene was investigated to study the effect of inorganic fillers on the improvement of flame retardancy and the suppression of smoke density. Through the analyses on thermal stability and smoke density, it is found that the flame retardancy developed by MDH could be effectively increased by the additional incorporation of zinc borate and mistron vapor. This result is confirmed by the observation of fire performance with cone calorimetry. Morphological study supports that the improvement of flame retardancy and the suppression of smoke density is due to hard and compact charred layer which is formed by the interactions between polymer and inorganic fillers. This charred layer provides a good thermal and flame barrier. .

Keywords

Wire; cable; Flame retardant; :smoke.

1. Introduction

Polyethylene polymers are used in many fields such as housing, transport or electrical engineering applications. Due to their chemical constitution, these p[polymers are easily flammable and so flame retardancy becomes an important requirement. This property can be achieved in several ways, especially by incorporation of additives. Until now, halogen compounds have been widely used and exhibited the greatest effect for this purpose. However, such problems as the corrosiveness, the smoke emission and the toxicity of combustion products have been an important issue continuously [1]. Finally, the usage of halogen compounds begins to be limited and the alternative halogen-free flame retardants such as aluminum or magnesium hydroxides and phosphorous-containing materials have attracted much attention of aerospace, microelectronic, cable and wire manufacturers [2-9]. The inorganic flame retardants decompose endothermally with the release water around the temperature at which polymers themselves decompose and do not induce the smoke and corrosive gas problems. Nevertheless, they must be used in large amounts (usually 60 wt%) and this lead to the loss of mechanical properties of the polymer matrix.

The aim of this work is to study the effect of inorganic fillers on the improvement of flame retardancy and the suppression of smoke

density. Ternary polymer blends consisting of ethylene-ethyl acrylate (EEA), polyethylene (PE), maleic anhydride-grafted polyethylene (m-PE) are prepared as a matrix to increase the loading of inorganic fillers. The effect of inorganic fillers on thermal stability and fire performance is quantitatively analyzed by DSC, TGA, smoke box and cone calorimetry. To identify the flame-retardant mechanism of this halogen-free system, the surface morphology after combustion was investigated.

2. EXPERIMENTAL

2.1 Materials

The polymers used in this study are ethylene-ethyl acrylate copolymer (15 wt% ethyl acrylate, EEA), polyethylene (PE), maleic anhydride-grafted polyethylene (m-PE). Magnesium hydroxide ($Mg(OH)_2$, MDH), zinc borate ($2ZnO \cdot 3B_2O_3 \cdot 3.5H_2O$, ZB), and mistron vapor ($3MgO$, $4SiO_2$ and H_2O, MV) are used as the additive to increase the flame retardancy and reduce the evolution of smoke during the combustion of materials. The surface of MDH was treated with stearic acid ($CH_3(CH_2)_{16}COOH$).

The composition of ternary polymer blend (EEA/PE/m-PE) as a matrix was fixed at 65/35/5 by weight. The total content of inorganic fillers is 55 wt %. The polymer blends were modified in four ways: (1) 55 wt % MDH, (2) 45 wt % MDH and 10 wt % talc, (3) 45 wt % MDH and 10 wt % ZB and (4) 45 wt % MDH, 5 wt % ZB and 5 wt % MV. The mixtures of polymers and inorganic fillers were processed in a double roll plasticator at 120°C for 30 minutes. To get the Sheets (200 x 200 x 1 mm^3), the mixtures were pressed at 185 °C for 10 minutes.

2.2 Thermal analysis and mechanical properties

The thermal properties of polymers were measured by using differential scanning calorimeter (DSC2910, Dupont TA instruments Co.) and thermogravimetric analyses were also carried out at heating rate of 10oC/min using TGA2950 (Dupont TA instruments Co.). A dumbbell type specimen with the width of 5.6 mm and the gauge length of 20 mm were tested at 200 mm/min by using Instron 6022 and the number of specimens are at least 5.

2.3 Fire test

The smoke generated from burning samples was measured as the specific optical density (Ds) by Smoke box (Rheometric Scientific Co.). Under non-flaming mode, the heat flux of furnace was fixed at 2.5 W/cm^2 and then the smoke density caused by the thermal

degradation of specimen were measured. Cone calorimeter (Atlas Co.) was used to obtain heat release rate (HRR) and the analyses were carried out according to ASTM 1356-90 under a heat flux of 35 kW/m^2. This heat flux has been chosen because it corresponds to the evolved heat during a fire.

2.4 Morphology

The shape of inorganic fillers and the surface morphology of burned samples were observed using a scanning electron microscopy (Hitachi Co. S-2500C). The samples were coated with gold-palladium and the accelerating voltage was 25 kV.

3. RESULTS AND DISCUSSION

3.1 Thermal and mechanical properties

In this study, three kinds of polymers, ethylene ethyl acrylate (EEA), polyethylene (PE), maleic anhydride-grafted polyethylene (m-PE) were blended. The homogeneity of polymer matrix was investigated by the thermal analyses with DSC. As listed in table 1, the melting temperatures of EEA, PE and m-PE are 98.0, 130.0 and 128.3°C, respectively.

Table 1 Thermal properties of polymers

	T_m (°C)	Δ H (J/g)	Tm of EEA/PE/m-PE blend (°C)	Tm of MDH-filled EEA/PE/ m-PE blend (°C)
EEA	98.0	39	95.2	87.8
PE	130.0	133	125.7	124.9
m-PE	128.3	151	-	-

In ternary blend systems, the melting temperatures fall down slightly for all polymers even though the peak of m-PE is not observed separately from the peak of PE due to the small amount. However, the behavior of the glass transition temperature cannot be observed. Thus, this phenomenon does not indicate that the polymer chains in the amorphous are miscible.

When the polymer blends are modified with inorganic filler, MDH, the drop of melting temperatures increases and especially the larger drop occurs for EEA. This drop is induced because the crystallization is more interrupted by the interaction between polymer and inorganic filler. In fact, the drop of melting temperature increases for EEA, which has a greater affinity with MDH due to the polar functional group. The interactions between polymer and MDH are illustrated in figure 1. -OH groups existing in the surface of MDH interacts with ethyl acrylate branches of EEA and gives adhesion to polymer matrix. This adhesion is also enhanced by coating filler with stearic acid. The non-polar group of stearic acid bounded in MDH increase the interaction with nonpolar matrix, PE. In this system, the third component of m-PE were also used to increase the adhesion.
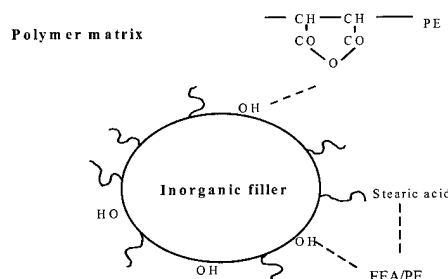
Figure 1   Schematic drawing showing the interactions between MDH and polymer matrix.

As shown in figure 1, grafted maleic anhydride group of PE has hydrogen bonding with MDH and the main chains of polyethylene are tightly imbedded in matrix, resulting in better incorporation of inorganic fillers. In the aging experiments (121°C x 168 hr), this strong adhesion plays an important role and thus the residual tensile strength and elongation is over 90% as listed in table 2.

Table 2   Mechanical properties of MDH-filled EEA/PE/m-PE blend before and after aging

	Before aging	After aging
Tensile strength (kgf/mm2)	1.38	1.37 (99 %)
Elongation (%)	584	531 (91 %)

3.2 Fire performance

3.2.1 Thermogravimetric Analysis

To maintain burning in polymer systems, three ingredients need to be supplied, such as heat, fuel and oxygen. Thus, to effectively prohibit polymer from burning, the flame retardant must remove one or more of these three ingredients. According to several studies, magnesium hydroxide (Mg(OH)$_2$, MDH) is used as an acid- and halogen-free flame retardant for various plastics. When heated, MDH decomposes according to the endothermic reaction as follows:

$$Mg(OH)_2 \rightarrow MgO + H_2O - 1,316 \text{ (J/g)}$$
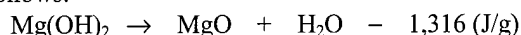
In the course of this reaction, 30 ~ 35 wt% of the substance is released in the form of water vapor, which displaces the oxygen necessary for combustion, acting as an inert protective gas. In addition to the energy consumption above described, the oxides and other decomposition products of the polymer formulation are deposited as a mineral coating on the surface of the material and this also significantly retard further advancement of the combustion process. This coating and the surface-active magnesium oxides that are formed as intermediate products, adsorb combustion products such as tar and soot particles. Therefore, only a limited amount of them manage to make the transition to the gas phase, thus effectively reducing smoke density.

Figure 2 shows the TGA curves of polymer blends modified with various flame retardants. The thermal degradation of ternary polymer blend begins at 400°C, proceeds steeply and the decomposition step of each polymer is not separated. Around 500oC, the polymers are completely decomposed without no residues. When modified with inorganic fillers, the decomposition proceeds in two steps (330 ~ 420°C, 420 ~ 500°C). The first step corresponds to the degradation of inorganic fillers including MDH, ZB, and MV. The second step is assigned to the degradation of polymers, especially polyethylene chains. Even if the onset of degradation of modified polymer blends begins at lower temperature, the weight loss is slowed down in the second step and the amount of residues also becomes high. In other words, over 420°C, the degradation of polymers is effectively retarded by MDH and thus the residues increases up to 28%. Furthermore, the amount of residues increases by the additional incorporation of ZB and MV.
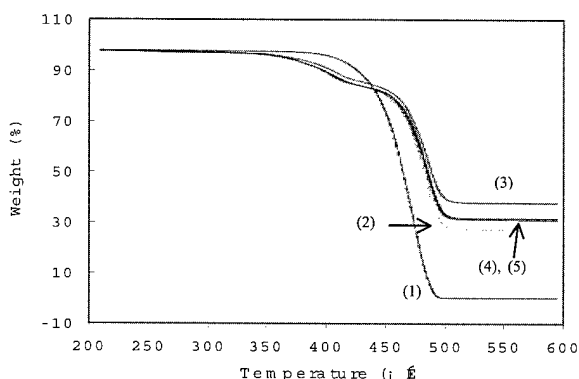
Figure 2   TGA curves of polymer blends filled with various flame retardant: (1) none, (2) MDH, (3) MDH/ZB, (4)MDH/MV, and (5) MDH/ZB/MV.

3.2.2 Smoke Emission

One way to measure the smoke generated from burning polymers is to test in the NBS Smoke Density Chamber.

Figure 3 shows the typical results of smoke emission testing (ASTM E662, under non-flaming condition) on ternary polymer blends modified with various inorganic fillers. As mentioned above, magnesium hydroxide causes a considerable delay in the onset of smoke evolution and significantly lowers the overall level of smoke produced about to 300. Furthermore, the additional incorporation of ZB and MV markedly slows the rate of smoke evolution and reduces the maximum smoke density. When both ZB and MV are used with MDH, the onset of smoke evolution is effectively retarded and over 15 min the smoke becomes saturated, resulting in the minimum smoke density. Therefore, it can be speculated that, in the blends exposed to heat and flame, both ZB and MV interact with MDH and

exhibit a synergistic effect for the depression of smoke evolution.
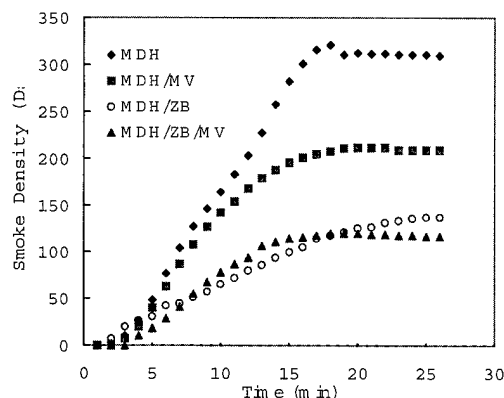
Figure 3   The evolution of smoke density of polymer blends filled with various flame retardants.

Figure 4 shows the scanning electron micrographs of inorganic fillers. The size of MDH is in the range of 1 ~ 2 μm and, above mentioned, this particle plays a role as a flame retardant giving off the water vapor which displaces the oxygen and functions as protective gas. This is confirmed by the micrograph in figure 5 showing the surface morphology before the catastrophic degradation. The irregular holes with submicron size indicate the generation and the emission of water vapor during the combustion. ZB has a typical median particle size of 3 μm and the chemical composition is $2ZnO·3B_2O_3·3.5H_2O$. The borate component (B_2O_3) forms a glassy layer on the char to protect the char from being further oxidized. Also, the water given off can cool the flame and promote the formation of a highly foamy and heat-insulating char. This behavior can make ZB to effectively act as a smoke suppressant, which is confirmed by the large drop of smoke density in figure 3. The shape of mistron vapor, which is composed of $3MgO$, $4SiO_2$ and H_2O, is platelet and the particles are polydisperse. During the combustion, the inert components of MgO and SiO_2 of mistron vapor form thin film on the surface, which can slow down heat transfer between the gaseous phase and the condensed phase.

Figure 6 shows scanning electron micrographs of the residues after combustion. Compared with MDH-filled polymer blends, the surface of blends modified with both MDH and ZB is covered with more compact charred layer. In other words, ZB acts as a sintering agent to produce a hard and porous residue, which is a good thermal barrier. Furthermore, in the presence of silicone polymer or SiO2, zinc borate can form borosilicate glass around the combustion temperature of polymers. In other words, the interactions between ZB and MV reinforce the protective shield under flame stress and thus the evolution of smoke is effectively suppressed. Also, the effect of flame retardancy is increased. The behavior of inorganic filler as a smoke suppressant and flame retardant is discussed in more detail in the next section.

(1)   (2)   (3)
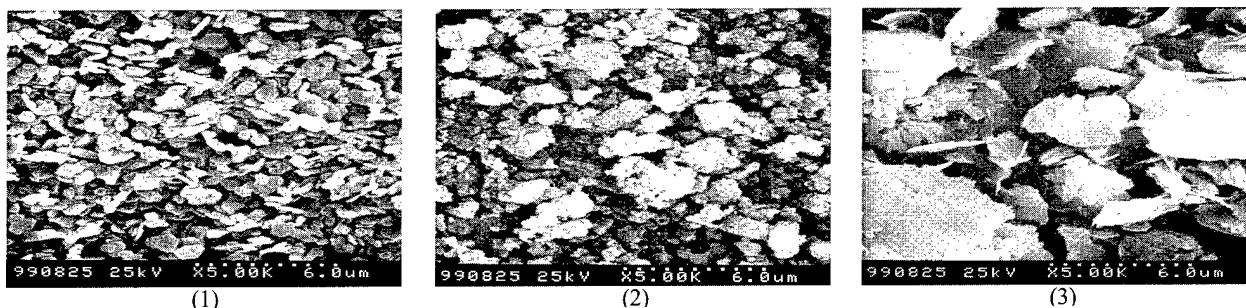
Figure 4   Scanning electron micrographs of various inorganic fillers: (1) MDH, (2) ZB, and (3) MV.

(1)   (2)   (3)
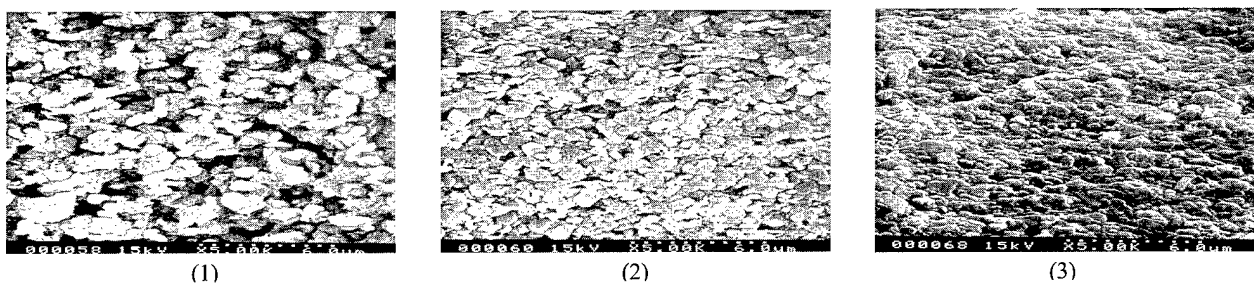
Figure 6   Scanning electron micrographs of the surfaces of polymer blends modified with various flame retardant (after combustion):   (1) MDH, (2) MDH/ZB, (3) MDH/MV, and (4) MDH/MV/ZB.

Figure 5   Scanning electron micrographs of the surfaces of polymer blends modified with MDH.

However, the HRR is effectively suppressed by the endothermic reaction of MDH and decreases by the formation of an expanded protective shield, which is induced by inorganic fillers.   Thus, over a long time (600 sec) the heat is continuously released.   Finally, the HRR increases again over 500 sec, which indicates the degradation of heat-protective shield formed on the surface.   This second peak is lowered by the additional incorporation of ZB or MV.   Furthermore, when both ZB and MV are added together, the synergistic effect is observed.   The HRR decreases over an entire range and the second peak, which is more delayed, is lowest.   This behavior is consistent with the results from TGA and smoke density and confirms the synergistic interaction between ZB and MV as a flame retardant or smoke suppressant.

3.2.3 Cone Calorimeter by Oxygen Consumption

Figure 7 shows the curves of heat release rate (HRR), which is calculated using the oxygen consumed during the combustion.   For polymer blend without inorganic fillers, the HRR peak is high, 1224 kW/m^2 at 147 sec.   Since thermal degradation proceeds rapidly, all the energy is released fast within 200 sec.   Before ignition, the carbonization of polymeric material and the evolution of gases without oxygen consumption are observed.   After ignition, the HRR increase very steeply by the contribution of the external heat source energy and the combustion of polymer.   By the addition of inorganic fillers, the HRR is dramatically reduced to about 200 kW/m^2 and the second peak is also observed over 500 sec.   The curves proceed through three steps: after ignition, the degradation of polymeric materials initiates and the values of HRR increases.

Figure 7   The curves of HRR   versus time (heat flux of 35 kW/m^2).

The total heat evolved (THE) curves confirm the HRR change as shown in figure 8. For all blends, the total heat evolved has not changed so much, but the time at which THE of polymer blends modified with inorganic fillers reaches the equilibrium value is significantly retarded. This time is more delayed by the additional incorporation of ZB or MV than by the addition of only MDH.

Figure 8   The curves of   THE   versus time (heat flux of 35 kW/m^2).

A cone calorimeter also allows the measurement of the weight loss during the combustion of the materials as illustrated in figure 9. The weight loss of pure polymer blends occurs steeply and then decreases slowly over 200 sec, which corresponds to the HRR peak. By the addition of inorganic fillers, the weight loss is significantly slo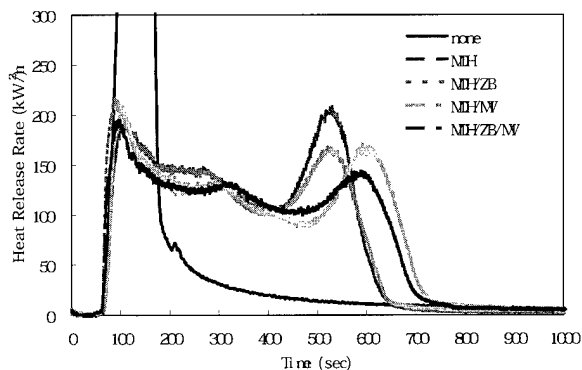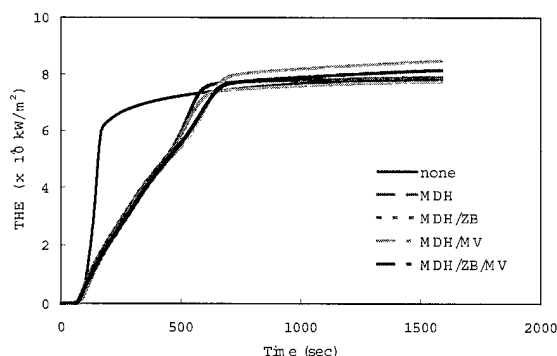wed down and reaches an equilibrium over 600 sec, which corresponds to the second HRR peak. In other words, the weight loss of the blend proceeds until an expanded protective shield is completely decomposed. The residues increase over 30wt% by the addition of inorganic fillers. When MDH-modified polymer blend is additionally incorporated with both ZB and MV, the amount of residue is highest and the weight loss is most delayed. These results confirm again the synergistic effect of ZB and MV in the flame retardancy.
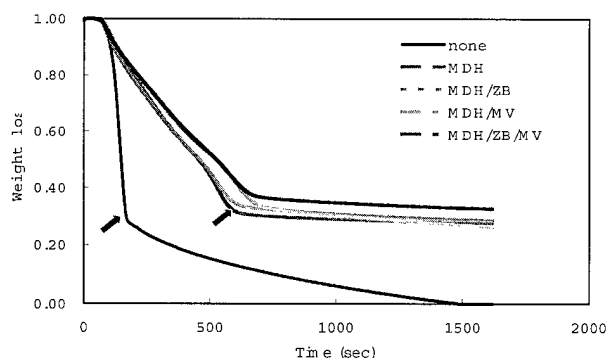
Figure 9   The weight loss curves versus time (heat flux of 35 kW/m2)

4. Conclusions

In this work, we have investigated halogen-free flame retarded polyethylene to study the effect of inorganic fillers on the improvement of flame retardancy and the suppression of smoke density. It is revealed that the flame retardancy developed by MDH could be effectively enhanced by the additional incorporation of zinc borate and mistron vapor. The interaction between zinc borate and mistron vapor aids in developing a hard and compact charred layer, which increases the resistance under flame stress and reduces the combustion rate. Thus, due to this additional protective glassy barrier the flame retardancy is improved and the evolution of smoke density is also effectively suppressed.

5. Reference

[1]   Hirscher M. M., In Fire and Polymers, edited by Nelson, American Chemical Society pp. 462 (1990).

[2]   Hornsby P. R. and Watson C. L., Plastic and Rubber Processing and Applications, 6 169 (1986).

[3]   Halloway L. R., Rubber Chem Technol., 61 186 (1988).

[4]   Miyata S., Imahashi T., and Anabuki H., J. Appl. Polymer Sci., 25 415 (1980).

[5]   Shen K. K., Plastics Compounding, (1988).

[6]   Rothon R. N., Paticulate-Filled Polymer Composites, Chap. 6 Paticulate Fillers used as Flam Retarant, edited by Rothon R. N., Harlow Longman, (1995).

[7]   Hornsby P. R. and Watson C. L., Polymer Degradation and Stability, 30 74 (1990).

[8]   Stinson J. M., J. Vinyl Addit. Tech., 2 94 (1995).

[9]   Molesky F., Schultz R., Midgett S., and Green D., J. Vinyl Addit. Tech., 2 159 (1995) (2000)

Development of Halogen-Free Flame-Retardant Optical Fiber Cables

Fumiki Hosoi, Fuminori Nakajima, Hiroshi Ono,
Nobuhisa Ishii, Ichiro Kobayashi
The Furukawa Electric Co., Ltd
Ichihara Chiba Japan
Phone: +81-436-42-1771   E-mail: fumiki@ch.furukawa.co.jp

Abstract

In consideration of the environmental effects of optical drop cables, indoor cables, and termination cables which are used near subscribers, we developed cables that employ jackets composed of halogen-free material. We developed some halogen-free materials for cable jacket of the three cable types, to suit both the environmental conditions and the cable characteristics. Because halogen-free materials have different chracteristics from conventional PVC, we investigated how to maintain cable performance. For lateral pressure performance of indoor cables and for transmission losses of optical cord at low temperatures, we particularly investigated the cross- sectional shape of the indoor cable and the shrinking force of optical cord jacket materials at low temperatures. Obtaining satisfactory mechanical characteristics for each of these types of cables, we succeeded in developing halogen-free, flame-retardant optical fiber cables.

Keywords

Halogen-free; Flame retardant; Drop cable; Indoor cable; Termination cable

1. Introduction

With the rapid growth of optical network systems, optical fibers have become increasingly used inside office buildings and homes. The cables used near subscribers in office buildings or homes include optical drop cables for fiber dropping to homes, indoor cables for wiring in homes, and termination cables for connection to optical modules. These cables are shown in figures 1-3. The cables must be small because they are installed in narrow spaces, such as inside the walls or floors of homes and inside small- diameter pipes. The cable sizes are therefore minimized by using 0.25-mm optical fiber and thinner-than-usual cable jacketing. These cables conventionally employed a jacket made of PVC. PVC, however, contains halogen, which emits harmful gases upon combustion, producing negative effects on the environment. In view of this problem, we developed an optical drop cable, indoor cable, and termination cable of halogen-free material.

Halogen-free flame-retardant cable jacket
0.25mm dia. SM optical fiber
Steel member
Cable Size:1.6 X 3.0mm
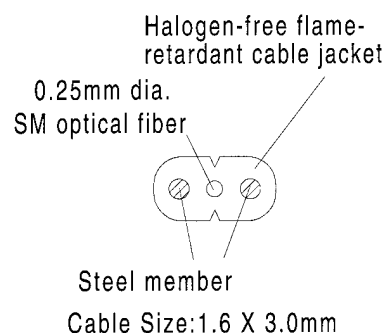
Fig.1 Structure of the indoor cable

Halogen-free flame-retardant cable jacket
Halogen-free flame-retardant Optical cord
Steel member
Cable Size: 2.6 X 3.8 mm

Fig.2 Structure of the termination cable

0.25mm dia. SM optical fiber
Steel member
Halogen-free flame- retardant cable jacket
Steel member
Cable Size: 2.0 X 4.5 mm
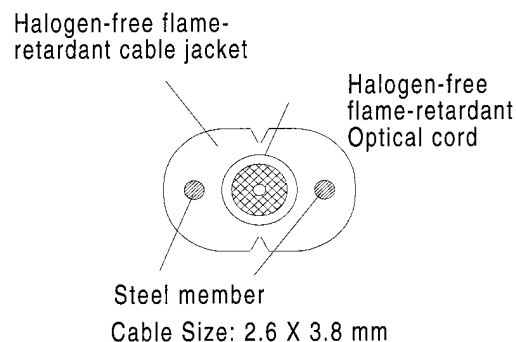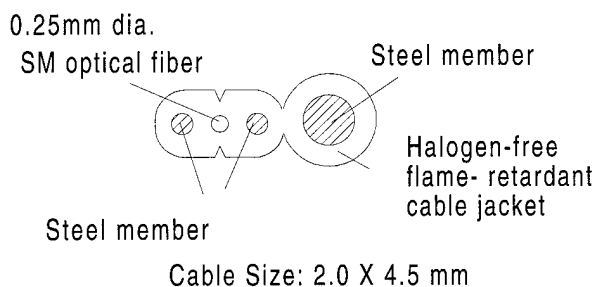
Fig.3 Structure of the optical drop cable

2. Requirements for the halogen-free, flame-retardant cables

The criteria for the development of all halogen-free cables used near subscribers were as follows:

• To have adequate flame retardation

• Use of halogen- free materials

The other criteria varied, depending on the environments in which the cables are to be used.

2.1 Requirements for outdoor use (for an optical drop cable)

• Low degradation by ultraviolet rays

• Durability below –30°C

• Resistance to acids and basis

2.2 Requirements for indoor use (for indoor cable and termination cable)

• Cream or other light color for cable jacket to harmonize with interiors

3. Cable design

An optical fiber is composed of glass and UV resin, so flame-retardation of an optical fiber cable is achieved by applying a flame-retardant jacket material around the fiber. The cables used near subscribers have thin cable jackets for minimized structure, so that adequate flame-retardation must be obtained by using a higher-performance flame-retardant agent or by incorporating more of the flame-retardant agent. When more flame-retardant agent is compounded into a cable jacket material, the original properties of the jacket material deteriorate and cable performance characteristics also deteriorate. It is therefore important to balance flame-retardation with cable performance in developing halogen-free flame-retardant cables used near subscribers.

3.1 Design of the optical drop cable

3.1.1 Investigation of cable jacket material
In designing the halogen-free optical drop cable, we regarded long-term reliability as more-than-usually important because this cable is used outdoors. We chose polyolefin as the cable jacket material and selected a flame-retardant agent with a high enough level of flame retardation that it could be used in small quantity. We maintained the original properties of polyolefin by using this high-performance flame-retardant agent in decreased quantity. This resulted in a cable jacket material having sufficient mechanical strength, resistance to ultraviolet radiation and to acids, and durability below –30°C.

3.2 Design of the indoor and the termination cables

3.2.1 Investigation of cable jacket material
In designing the halogen-free indoor and termination cables, which are both used indoors, we regarded harmony with interiors as more important than in the case of the outdoor drop cable. We therefore developed cable jacket materials with cream or other light colors. We chose polyolefin as the cable jacket material and selected a flame-retardant agent with light color to match the cable jacket color. This flame-retardant agent has a lower level of flame-retardation than that of the optical drop cable, so we obtained sufficient flame-retardation by compounding a larger quantity of the agent into the cable jacket material.

3.2.2 Improvement of lateral pressure characteristics in an indoor cable.
In the halogen-free cable jacket material for indoor use, a larger proportion of flame-retardant agent was incorporated, so the properties of the polyolefin were affected. The Young's modulus of the polyolefin became smaller than that of conventional PVC, and this induced deterioration of the lateral pressure characteristics of the cable.

(a) Cause of transmission loss increase under lateral pressure
Figure 4 shows the mechanism of transmission loss increases in the indoor cable. It is assumed that the indoor cable installed on a floor may receive pressure from the base of a desk or from a human foot. In this case, a bend in the cable jacket is created by the edge of the base of the desk or the human foot. That bend also occurs in an optical fiber. The bend in the optical fiber causes increased transmission losses. The halogen-free material we developed has a smaller Young's modulus than does conventional PVC, so flexural rigidity of the halogen-free material is lower than that of PVC. It is therefore easy for the bend to be created by a desk or a foot pressing on the cable jacket, increasing the transmission losses caused by lateral pressure to levels greater than those of PVC.

(b) Improvement of lateral pressure characteristics
We investigated the cross-sectional shape of the indoor cable. To prevent an increase in transmission losses caused by lateral pressure, we designed an almost-rectangular cable cross-section, as shown in figure 5. The nearly rectangular shape of the cable cross section increases the flexural rigidity of the cable. A simple explanation is given below. An elliptic shape, as shown in figure 6(a), approximates the conventional cross-sectional shape of the indoor cable, and a rectangular shape, as shown in figure 6(b),

approximates that of the newly designed one. Flexural rigidity of these two shapes is expressed as

Elliptic shape: $(\pi/64) \times A^3B$

Rectangular shape: $(1/12) \times A^3B$

and because $(\pi/64)$ is less than 1/12,

$(\pi/64) \times A^3B < (1/12) \times A^3B$

This relationship shows that the rectangular shape has greater flexural rigidity than does the elliptic shape. The flexural rigidity of the cable jacket thus can be increased by using the shape similar to a rectangle, in other words by widening the straight part α, as shown in figure5. To confirm this effect, we manufactured halogen-free indoor cables with varying the straight part α.

(c) Design of the cross-sectional shape of the cable

The wider the straight part α, the more the cross-sectional shape of the cable resembles a rectangle. Conversely, the more the shape resembles the conventional ellipse, the closer the condition approaches to α=0. Figure 7 shows the relationship between length of the straight part α and the increase in transmission loss under lateral pressure. Length of the straight part α is expressed by a relative value normalized at the thickness of the cable. This figure shows that transmission loss increase is suppressed at α = 0.19 and is almost perfectly suppressed at α = 0.74. (The shape becomes a rectangle when α = 1.) Based on these results, we designed the cross-sectional shape of the cable for α≥0.41, which adequately suppresses any increase in transmission loss under lateral pressure.
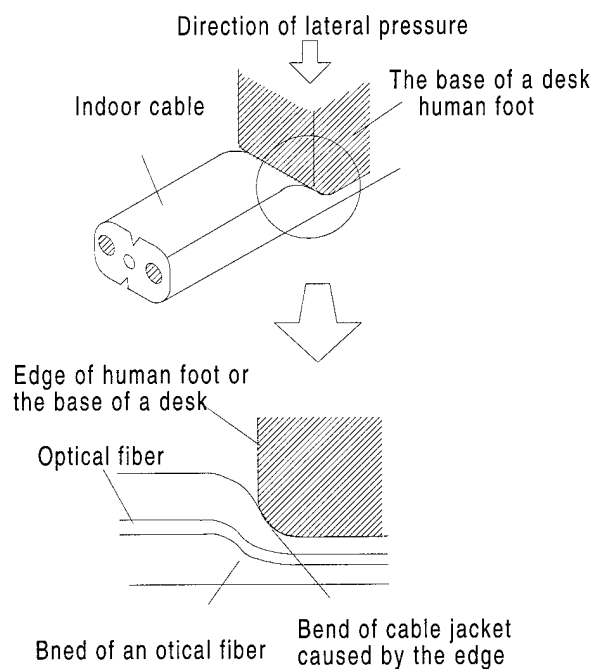
Fig.4 Mechanism of transmission loss increase in the indoor cable under lateral pressure
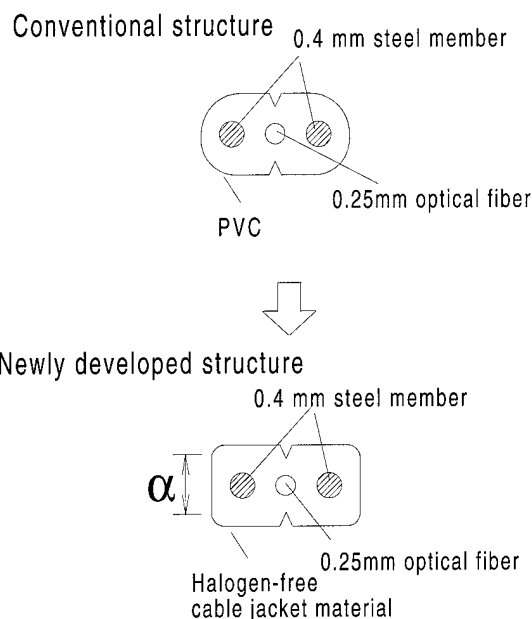
Fig.5 Cross-sectional shapes of the conventional and newly developed indoor cables
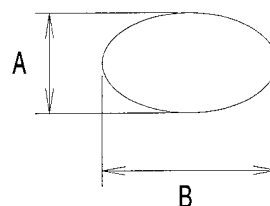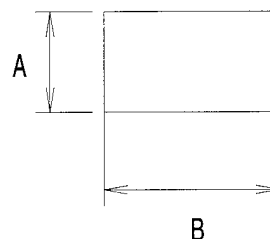
Fig.6 Figures approximating the cable cross-sectional shapes
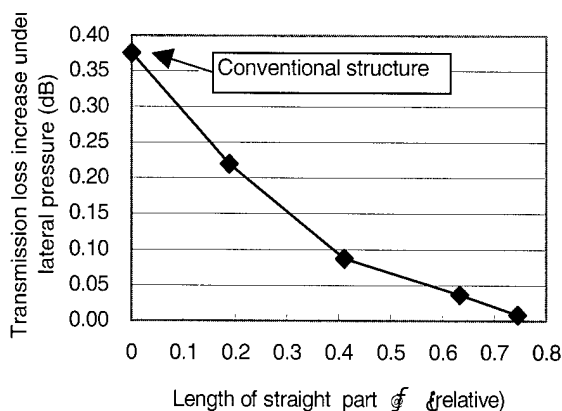
Fig.7 Improvement of lateral pressure performance by use of a cable cross-sectional shape closer to a rectangle

3.2.3. Investigation of the optical cord for the termination cable

When the optical cord jacket for the termination cable shrinks at low temperatures, the shrinking force is applied directly to the optical fiber because aramid yarn of strength member have durability not to compressive force but to elongation force. This causes bending of the optical fiber, so transmission losses increase. We developed several halogen-free materials for optical cord and determined that these materials have different properties from each other. In particular, the shrinking force at low temperature differs greatly among materials. Transmission loss increases at low temperatures are thus a matter of concern. We manufactured five optical cords using materials 1 through 5 and evaluated the changes in transmission loss at low temperature. Figure 8 shows the relationship between shrinking force of the cord jacket material and increased transmission loss. Shrinking force of the cord jacket at -10 °C is expressed by a relative value normalized at PVC's shrinking force. As shown in figure 8, we found that

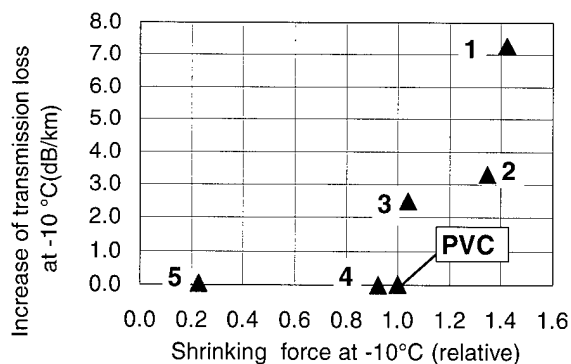transmission loss increase at low temperature is significant for materials 1, 2, and 3, all with shrinking forces exceeding that of PVC. Generally shrinking force at low temperatures is proportional to the Young's modulus of the material, and it is therefore desirable to select a material with a small Young's modulus to decrease the shrinking force. The Young's modulus that is too small, however, decreases flexural rigidity of the optical cord and causes deterioration of the lateral pressure characteristics of the cord. In figure 8, material 5 shows a problem in its lateral pressure characteristic, because its Young's modulus is too small. (In material 5, transmission loss was more than 0.1 dB at 4.9 N/mm.) We chose material 4 as the cord jacket material because it demonstrated a good balance of the two characteristics.

4. Characteristics of cables

4.1 Characteristics of halogen free cable and cord jacket materials

Table 1 shows the characteristics of halogen-free, flame-retardant materials for the cables used near subscribers. Table 2 shows results of reliability evaluations of cable jacket materials for outdoor use. As shown in these tables, the materials chosen for both indoor and outdoor use revealed good characteristics with using in their intended environments.

4.2. Characteristics of cables

Table 3 shows the mechanical characteristics of the cables we developed. Excellent mechanical characteristics were obtained for all the cables. Each cable satisfies the flame-retardation test specified by Japanese Industrial Standard C3005[1]. We have developed cables having higher level of flame-retardation equivalent to that of the conventional PVC jacketing.

Table.1 Characteristics of halogen-free, flame-retardant cable jacket materials

Test Item	Material A	Material B	Material C
Tensile strength (Mpa)	13.0	9.6	12.3
Elongation at break (%)	620	210	240
Brittle temperature (°C)	-41	-23	-54
Smoke density at NBS test	94	77	150
Degree of acidity of gases during combustion (pH)	4.1	4.1	3.5

Table.2 Characteristics of reliability of cable jacket material for outdoor use

Item	Elongation retention (%)
	Material A
Thermal aging 100°C×48hr	94
Durability at 10%H$_2$SO$_4$ 50°C×50days	102
Durability at 10%HCl 50°C×50days	105
Durability at 3%NaOH 50°C×50days	103
Oil resistance specified in ASTM 50°C×50days	102
Degradation by ultraviolet rays 4000hr	90

Material A: Cable jacket material for the optical drop cable

Material B: Cable jacket material for the indoor and the termination cables

Material C: Cable jacket material for the optical cord with the termination cable

Table3. Mechanical test for halogen-free flame-retardant cables (@1.55μm)

Item	Condition	Result of cables	Optical cord for termination cable
Transmission loss	Measured by OTDR	≤0.22dB/km	≤0.22dB/km
Temperature cycling	Indoor -10~40°C Outdoor -30~70°C	≤ 0.1dB/km	≤ 0.1dB/km
Bending	R=30mm	≤ 0.02dB	≤ 0.02dB
Lateral pressure	Cable: 1200N/25mm Cord: 4.9 N/mm	≤ 0.02dB	≤ 0.02dB
Torsion	±180°	≤ 0.02dB	—
Impact	300g×1m	≤ 0.02dB	—
Flame retardation	JIS C 3005	Passed (Inclined test)	Passed (Horizontal test)

5. Conclusion

We developed halogen-free, flame-retardant cables for use near subscribers, giving consideration to environmental effects. Our works are summarized as below.

(a) In designing the halogen-free cable jacket material for an optical drop cable, we regarded long-term reliability as especially important because this cable is used outdoors.

(b) In designing the halogen-free cable jacket materials for indoor and termination cables, we regarded harmony with interiors as having importance for indoor usage, so we developed cable jacket materials in cream or other light colors. In the cable jacket materials for indoor use, the original properties of the jacket material was changed by incorporating a large quantity of a flame-retardant agent, degrading the cable's ability to withstand lateral pressure. We therefore selected an almost-rectangular shape for the cable cross section to restore the lateral pressure performance.

(c) In the jacket material of the optical cord for a termination cable, we suppressed transmission loss increases at low temperatures and restored resistance to lateral pressure by finding the optimum balance between shrinking force of the cord jacket at low temperatures and the Young's modulus of the cable.

(d) Test results confirmed that each cable had good material and mechanical characteristics and had a higher level of flame-retardation equivalent to that of conventional PVC.

We were able to develop halogen-free flame-retardant cables for use near subscribers and demonstrated that these cables have characteristics at least as good as those of conventional PVC cables.

6. References

[1] Japanese Standards Association, " Test methods for rubber or plastic insulated wires and cables JIS C 3005", pp24-25, 1993

[2] F. Hosoi, et al. "Halogen-free, flame-retardant optical fiber cable for the MT- RJ optical connector", Proc. of EC 2000, pp236 – 242, 2000

Fumiki Hosoi

The Furukawa
Electric Co., Ltd
6,Yawata
Kaigandori,Ichihar,
Chiba,290-8555,
Japan

Fumiki Hosoi received his M.E. degree in Physics engineering from Tokyo University in 1995. He joined The Furukawa Electric Co., Ltd and has been engaged in research and development of the optical fiber cables.

Ichiro Kobayashi

The Furukawa
Electric Co.,Ltd
6,Yawata
Kaigandori, Ichihara,
Chiba, 290-8555,
Japan

Ichiro Kobayashi received his B.E. degree in Physics from Chuo University in 1986. He joined The Furukawa Electric Co., Ltd and has been engaged in research and development of the optical fiber cable. He is now a senior research engineer of Fitel Photonics Laboratory.

Fuminori Nakajima

The Furukawa
Electric Co., Ltd.
6, Yawata Kaigandori
Ichihara, Chiba 290-
8555, Japan

Fuminori Nakajima received his M.E. degree in Material Engineering from Nagaoka University of Technology in 1992. He joined The Furukawa Electric Co.,Ltd. in 1992 and has been engaged in research and development of the materials for optical fiber cables.

Nobuhisa Ishii

The Furukawa
Electric Co.,Ltd
6,Yawata Kaigandori,
Ichihara, Chiba,
290-8555, Japan

Nobuhisa Ishii received his M.E. degree in Applied Chemistry from Waseda University in 1987. He joined the Furukawa Electric co., ltd. in 1975 and has been engaged in the development of the materials for optical fiber cables. He is now a senior research engineer of Fitel Photonics Laboratory.
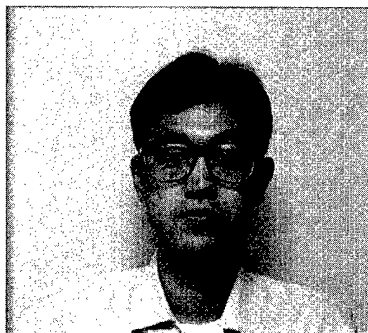
Hiroshi Ono
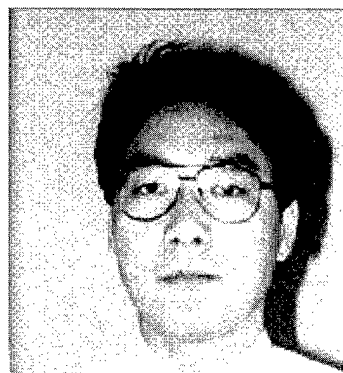
The Furukawa
Electric Co.,Ltd
6,Yawata Kaigandori,
Ichihara, Chiba,
290-8555, Japan

Hiroshi Ono received his M.E. degree in Applied Chemistry from Tokai University in 1992. He joined The Furukawa Electric Co., Ltd and has been engaged in production engineering of optical fiber cable. He is now an engineer of the Assembly Production Engineering Section of Optical communication Division.

An Innovative Breakthrough in the Fire Retardancy of Halogen Free Cable Sheathing Materials

Lai Ping Artingstall, Joe Preston, Peter Salthouse, and Dudley Sawyer

Scapa Polymerics Limited
Columbine Street
Openshaw
Manchester
United Kingdom
+44-161-223-2688
scapa.polymerics@scapapolymerics.com

1. ABSTRACT

Over the past 15 years, halogen free, fire retardant systems have progressed sufficiently in Europe to become an acceptable part of the cable maker's technology[1,2,3]. This is not so in the USA, use of these products generally being confined to cables being imported back into Europe. Both fire regulations and cable fire test differences have severely restricted growth in North America, with criteria such as UL 1666 Riser vertical fire test[4] requiring a higher level of fire retardancy compared to the European norms IEC 60332 parts 3A and 3C[5]. Previously with power cables there has not been a problem with meeting UL 1666 requirements in view of the specified constructional methods used for these cables. However, where data and telephone cables are concerned, the jacketing is usually of a much-reduced radial thickness leading to an overall reduction in the flame-retardant content of the cable. This is reflected in turn by the large scale fire test performance of such cables, making the achievement of UL 1666 and IEC 60332 part 3A performance a much more difficult prospect. Compound D36 will now allow the cable maker to produce such constructions that will meet UL 1666 with a high degree of comfort whilst maintaining acceptable levels of processability and meeting all other needs and requirements of halogen free, low smoke, fire retardant sheathing compounds. The paper outlines the development and technical benefits of compound D36.

One of the key attributes necessary to improve fire performance of cables is to enhance the char stability of the sheath. This property alone aids the protection of the inner construction of the cable. This new compound exhibits excellent char cohesion and hence is a key factor in the cable's performance during large-scale fire tests. Other fire properties illustrating significant improvements are reduced heat release and smoke generation with cone calorimetry being the chosen method of analysis for determining the predicted fire performance of the sheathing material.

2. INTRODUCTION

Although there have been no recent major changes within North America in terms of cable fire testing, the Construction Products Directive (CPD) has proposed new modified fire test criteria for Europe. Initially it was believed fire testing in European countries may include similar methods to UL 910 (Steiner Tunnel)[6], HIFT systems. Currently the legislation is moving more towards a modified IEC 60332 part 3 test, including heat release and smoke generation as well as the existing height of burn criteria. Table 1 summaries the proposed Euro-classes in broad terms.

Table 1 – CPD Euro-classes.

Class	Test Method	Main Criteria	Additional Criteria	Cable Types
Ac	Undecided but main test thought to be 332-3, modified to include heat release and smoke. (Ref FIPEC)	Not applicable to polymer insulated/sheathed cables.		M. I.
Bc		Fire propagation; Total heat release; Rate of heat release; Increasing levels of fire performance, Ec to Bc	Flaming droplets, smoke production	Mainly LSOH power & data
Cc				
Dc				
Ec			Flaming droplets	PVC power & data
Fc	No performance specified			

Halogen free system are generally well specified in terms of low smoke emission; therefore, logically, all efforts were directed towards improving both fire retardance and reducing the levels of heat release.

The cone calorimeter was an ideal method of analysis for the development of compound D36 in terms of the improved fire properties required. Throughout the development, all trial formulations were analysed in terms of peak heat release, total heat release, average heat release and time to ignition via the cone calorimeter. All data will be illustrated within the paper. Additional fire test data has also been assessed in terms of smoke generation, oxygen index, temperature index and cable fire testing. All additional technical performance data for compound D36 will be discussed and illustrated within the paper and compared to data normal expected from high performance

halogen free, fire retardant, low smoke sheathing compounds.

Several comparisons will made throughout the paper against international specifications illustrating that compound D36 is not only excellent in terms of its fire performance but is also capable of complying with all physical requirements listed for applications within the wire and cable markets.

3. PHYSICAL PROPERTIES

Mechanical and physical test requirements for halogen free, fire retardant compounds are now well established in many parts of the world, especially in Europe. Here, specifications covering sheathing compounds for use on power cables were established early, a typical example being BS 7655 type LTS 1[7]. Compound D36 more than exceeds these requirements as is shown in Table 1.

More recently, the European countries have agreed a common specification covering sheathing requirements for telecommunication and data cables. The requirements of this specification, HD 624 part 7[8] are also shown in Table 1.

Table 1 – D36 vs BS 7655 type LTS1 and HD 624 part 7

Properties	BS 7655 Type LTS1	HD 624 Part 7	Comp'd D36
Tensile Strength	10 MPa (min)	9 MPa (min)	12 MPa
Elongation at Break	100% (min)	125 % (min)	165 %
After ageing for 7 days at 100ºC			
T.S. variation	±40 % (max)	±30 % (max)	+24 %
E@B value	100 % (min)	100 % (min)	140 %
E@B variation	±40 % (max)	±30 % (max)	-15 %
Heat Shock for 1 hour	Pass @ 150ºC	Pass @ 130ºC	Pass - no cracks
Cold Bend At –15ºC	Pass - no cracks	Pass - no cracks	Pass - no cracks
Cold Elongation At –15ºC	20 % (min)	20 % (min)	85%
Hot Pressure 80ºC for 4 hours	50 % (max)	50 % (max)	25 %

Requirements in the USA however are not so clear. Here, the preference is to measure the halogen free, fire retardant compound against the requirements of the more standard material that it displaces e.g. PVC. A typical example is shown in Table 2.

Table 2 – D36 v UL Class 43 PVC

Properties	UL Class 43 PVC	Compound D36
Tensile Strength	10.3 MPa (minimum)	12 MPa
Elongation at Break	100 % (minimum)	165 %
After ageing for 10 days at 100ºC :		
T.S. variation	> 70 % retention	125 % retention
E@B variation	> 65 % retention	75 % retention
Heat Shock 121ºC for 1 hour	Pass (no cracks)	Pass (no cracks)
Cold Bend At –25ºC	Pass (no cracks)	Pass (no cracks)

A more important difference between these groups however has been the fire test requirements for the relevant cables. Ever since their introduction, European power cable compounds have been required to perform well in the various IEC 60332 part 3 category fire tests. This has never been a problem for this class of cable with their naturally flame retardant compound rich constructions. More difficult has been the performance of the telecom/data with initially a high reliance on the use of flame retardant tapes and over-size sheath radial thicknesses in the cable constructions. However, later compounds, e.g. Compound S540[9] have overcome these difficulties allowing thin radial sheath constructions with minimal use of tapes.

Now we have been able to extend these compound design techniques to develop the new Compound D36 which is suitable for the demanding UL 1666 applications and also for the new higher specification CPD Euro-classes.

4. FIRE PERFORMANCE
4.1 Cone Calorimeter
A Fire Testing Technology Cone Calorimeter was used to conduct experiments according to ASTM 1354-90. The method is based on oxygen consumption calorimetry. All samples tested were in the form of plaques (100 x 100 x 5mm) and were wrapped in aluminium foil (0.3mm thickness). These were exposed in a horizontal orientation to an external heat flux of either 50 kW/m² or 75kW/m². The lower heat flux was used to compare Compound D36 to other standard, but less flame retardant, halogen free compounds. The higher heat flux was used when comparing different D36 formulations. This was used so that differences not seen at the lower flux were shown; also this heat flux is nearer that used in the UL 910 (Steiner Tunnel) test of 88 kW. The fire behaviour of the samples was evaluated using the cone calorimeter, which allowed a quantification of the combustion behaviour of the polymers under well-ventilated,

controlled radiant heat transfer conditions simulating real fire conditions. The most important parameters determined are the heat release rate (HRR, kW/m^2) and maximum HRR (Peak HRR) because they define the fire size[10]. Since the shape of the HRR curve varies for different samples the average HRR is also reported for the duration of flaming combustion. Other important parameters determined were time to ignition (TTI, s), flameout time (s), and mass loss rate (MLR, g/s) as well as the smoke production and the formation of toxic gases. The volume of smoke production was determined as the specific extinction area (SEA, m^2/kg) and the toxicity of the gases characterised by the CO yield (kg/kg).

4.2 Heat Release and Smoke Data

The following figures show how Compound D36 was formulated to improve the overall flame retardant properties compared to standard production compounds - the second generation S300 and the third generation S540. All three compounds were exposed to a heat flux of $50kW/m^2$; when $36kW/m^2$ was used, the formulations self extinguished in the early stages of the burning process leading to less than 10% mass loss.

The results obtained from the heat release rate (HRR) and specific extinction area (SEA–smoke) are shown in graphical form in Figures 1 and 2.
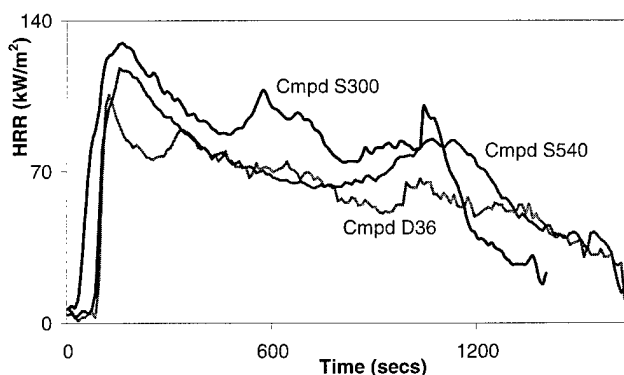
Figure 1 - Heat Release Rate Comparison at 50kW

As shown from both graphs there is a decrease in both the peak HRR and SEA from our second generation Compound S300 to our proposed fourth generation Compound D36.

This overall improvement trend of flame properties is also confirmed in the increase of time to ignition (TTI) from 60secs for S300, 85secs for S540, to 96secs for D36. The improvement in properties for Compound D36 is attributable to formulation changes but mainly to the addition of a char-promoting additive, all of which are halogen free. The benefits of Compound D36 derive from the insulating properties conferred by the formation of an intumescent char.
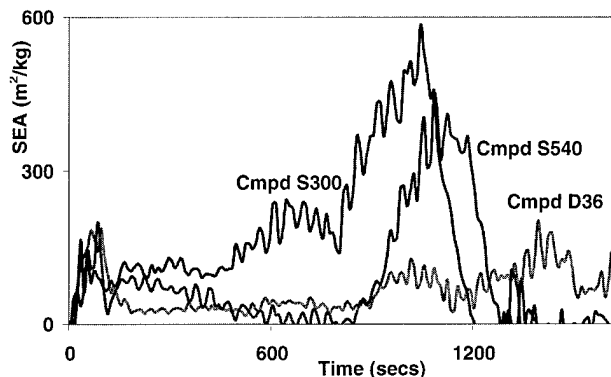
Figure 2 - Specific Extinction Area Comparison at 50kW

In order to show further improvements, all subsequent D36 formulations were tested on the cone calorimeter at a heat flux of $75kW/m^2$. For comparative reasons D36 was tested at both heat fluxes. The peak HRR increased from 111 to $137kW/m^2$. The resulting peaks have also increased due to the increase in heat flux.

In order to make further improvements, synergistic char promoters and other additives, all of which are halogen free, have been investigated. These possess different modes of action as flame-retardants, all of which result in an accumulative benefit. The HRR of two of the most recent development formulations together with D36 are shown in Figure 3.
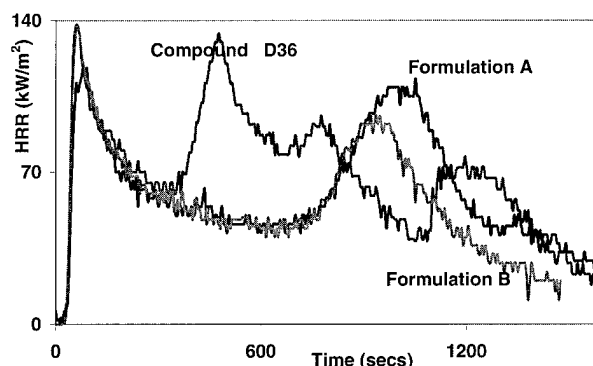
Figure 3 - Heat Release Rate Comparison at 75kW

This figure shows that the second peak in D36 can be eliminated together with a reduction in the peak HRR for formulation A.

4.3 ASTM E662

The ASTM E662 test method[11] was used to assess the smoke emission of Compound D36. Figure 4 shows the results for the flaming mode and Figure 5 those for the non-flaming mode. Tests in both modes were carried out on 1.5mm thick plaque samples.

Figure 4 – Smoke (Flaming Mode)

Figure 5 – Smoke (Non-flaming Mode)

Both figures clearly show the improvements in smoke evolution that have been achieved with Compound D36 when compared to second and third generation halogen free, fire retardant compounds.

4.4 Material Fire Tests

There are two tests generally used by the cable industry to assess the degree of fire retardance of materials. These are the Critical Temperature Index and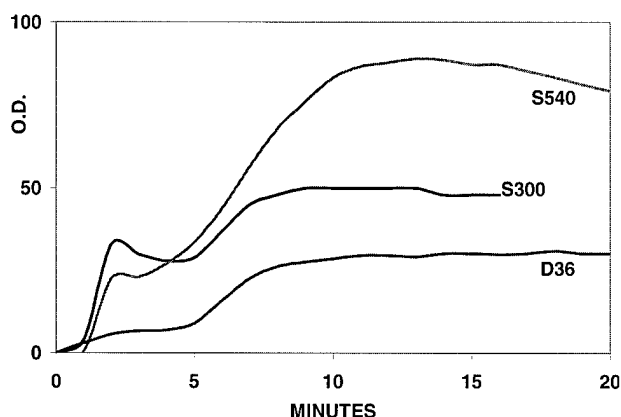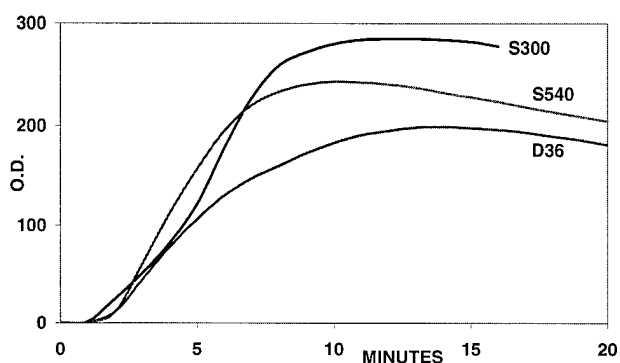 the Oxygen Index, both of which are detailed in ISO 4589[12]. The results for Compound D36 are given in the following table together with those for the second and third generation products for comparison.

Table 3 – Combustion Gases Analysis

Properties	S300	S540	D36
Oxygen index	35%	45%	49%
Critical Temperature index	270ºC	330ºC	335ºC

4.5 Combustion Gases and Toxicity Index

The most common methods of test for the quantities of acid and corrosive gases evolved during combustion are now grouped together in IEC 60754[13]. The toxicity of the gases is evaluated using the NES 713 method[14]. The index produced is computed by measuring the concentrations of 12 selected gases evolved under the specified fire conditions. Table 4 shows the results of these tests ranged against the generally accepted cable industry standard. Again these demonstrate the superior level of performance of Compound D36.

Table 4 – Combustion Gases Analysis

Properties	D36	Standard
Acid gas emission (%)	zero	0.5 maximum
pH	5	4.3 minimum
Conductivity (μS/cm)	10	100 maximum
Toxicity Index	1	5 maximum

5. CABLE FIRE TESTS

Category 5 data cables both FTP and UTP versions were sheathed with compound D36 and subjected a variety of cable fire tests: -

IEC 60332-1 single wire, vertical flame test[15] - **the maximum height of the cable charred or affected as measured from the point of flame application was < 6 cms for both constructions.**

IEC 60332-3 (category C, designation F) large scale vertical fire test for bunched wires or cables - **the maximum height of the cable charred or affected as measured from the bottom of the burner was < 70 cms for both cable types (in front of the cable group).**

IEC 60754-1 acid gas evolution - **the average gas yield expressed as hydrogen chloride was < 5 mg/g.**

IEC 61034 smoke density test (3 metre cube)[16] - **the minimum light transmission recorded was > 85% for both cable constructions.**

The Category 5 FTP cable sheathed with compound D36 was also subjected to a second IEC 60332 part C cable fire test. Heat release and smoke generation has been included in a modified version of this vertical fire test as developed by the FIPEC research project[17]. The values achieved are listed in table 5. All data achieved is expected to comfortably meet the proposed new requirements as defined by category B of the new European CPD legislation.

Table 5 – Modified 60332 (FIPEC) data.

Criteria	Value
Peak Heat Release of cable. 0 to 10 minutes. (kW)	13.3
Peak Heat Release Rate of cable. 10 to 20 minutes. (kW)	16.24
Total Heat Released at 10 minutes. (MJ)	4.63
Total Heat Released at 20 minutes. (MJ)	9.77
Peak Smoke Release Rate of cable. (m^2/s)	0.33
Total Smoke Released at 10 minutes. (m^2)	67.8
Total Smoke Released at 20 minutes. (m^2)	145.5
Maximum extent of charred portion measured on the cable. (m)	0.97

6. CONCLUSION

A halogen free, flame retardant, low smoke sheathing material has been developed to support cable constructions in meeting cable fire test requirements both in USA and in Europe. This material is suitable for all areas of cable sheathing manufacture, power/energy, telecommunication, data and fibre optic applications.

Compound D36 will now allow the cable maker to produce such constructions that will meet UL 1666 and the higher Euro-class categories as outlined in the newly proposed CPD fire test requirements with a high degree of comfort and maintain acceptable levels of processability.

This new compound exhibits excellent char cohesion and hence is a key factor in the cable's performance during large-scale fire tests. Overall, D36 represents an innovative breakthrough in halogen free, low smoke, fire retardant sheathing materials.

7. ACKNOWLEDGEMENT

Scapa Polymerics Ltd. wish to acknowledge the assistance and facilities made available to them by the Chemistry Department of the University of Salford in the furtherance of this work.

8. REFERENCES

1. Dr J. Taylor, et al. : Recent advances in zero halogen, low smoke, fire retardant compounds, IWCS, November 1987.

2. Dr J. Taylor, et al. : Sheathing power and telecom cables, IWCS, November 1992.

3. J. Preston, et al. : Further new developments in halogen free, fire retardant, low smoke materials, INSULEC-97, November 1997.

4. UL1666 : Test for Flame Propagation Height of Electrical and Optical-Fiber Cables Installed Vertically in Shafts.

5. IEC 60332-3:1992, Tests on electric cables under fire conditions. Tests on bunched wires or cables.

6. UL910 : Test for Flame Propagation and Smoke Density Values for Electrical and Optical-Fiber Cables used in Spaces Transporting Environmental Air.

7. BS 7655:Section 6.1:1997, Specification for Insulating and sheathing materials for cables, Part 6.

8. CENELEC HD 624.7 S1, Materials used in communication cables. Part 7: Halogen free flame retardant thermoplastic sheathing compound.

9. J. Preston, et al. : A new fire retardant sheathing concept for UTP data cables and fire retardant cables, EUROCABLE, June 1999.

10. V. Babrauskas : Fire Mater., 1984; 8:81

11. ASTM E 662-83, standard test method for Specific Optical Density of Smoke generated by solid materials.

12. ISO 4589, Plastics - Determination of burning behaviour by oxygen index, part 2 - Ambient temperature test and part 3 - Elevated temperature test.

13. IEC 60754-1:1982 and IEC 60754-2:1991, Test on gases evolved during combustion of electric cables.

14. Naval Engineering Standard 713, Determination of the Toxicity Index of the products of combustion from small specimen of materials.

15. IEC 60332-1:1993, Tests on electric cables under fire conditions. Method of test on a single vertical insulated wire or cable.

16. IEC 61034-2:1991, Measurement of smoke density of electric cables burning under defined conditions. Part 2: Test procedure and requirements.

17. FIPEC, Fire Performance of Electric Cables, Final Summary Report, FIPEC Consortium 1999.
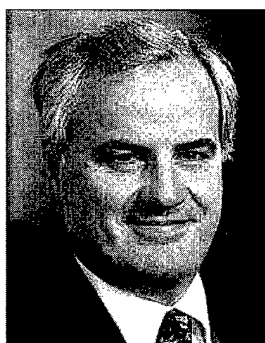
Lai Ping Artingstall
Scapa Polymerics Ltd
Manchester, M11 2LH
England

Lai Ping Artingstall studied "A" levels in both mathematics and chemistry at Central Manchester Colleges prior to joining Scapa Polymerics Ltd in 1990 as a Quality Control Inspector. In 1991 she transferred to the Product Development Section where she has been instrumental to the development of the latest range of low smoke, halogen free, fire retardant compounds. Recently qualified to BSc (Hons) in Polymer Technology she is now continuing her studies at Salford University with a view to attaining MPhil.

Joe Preston
Scapa Polymerics Ltd
Manchester, M11 2LH
England

Joe Preston joined Scapa Polymerics Ltd in 1970 as a Laboratory Assistant following 2½ years' experience in the Plastics Industry. He studied chemistry at the North Trafford College of Technology. In 1977 he became responsible for the Quality Control function at Scapa Polymerics. He transferred his efforts in 1982 to Development, working on specialised cable tapes, and in more recent years, the Megolon range of low smoke, halogen free, fire retardant compounds. In 1991 he was appointed Technical Manager of Scapa Polymerics, responsible for all development and quality control functions.

Dudley Sawyer
Scapa Polymerics Ltd
Manchester, M11 2LH
England

Dudley Sawyer joined Scapa Polymerics Ltd in January 1991 to work on the development of new zero halogen, flame-retardant extrusion compounds for the electrical cable industry. He gained BSc (Hons) in Chemistry at the University of Manchester and he has extensive experience of the cable industry having previously spent 21 years with BICC Cables in a variety of technical roles. He is currently Head of the Technical Service team where his responsibilities include guidance and help to customers on the use of our compounds.

Dr Peter Salthouse
Scapa Polymerics Ltd
Columbine Street
Manchester, M11 2LH
England

Peter Salthouse joined Scapa Polymerics in 1998 having spent 5 years with sister company, Scapa Tapes. He gained a BSc in Chemistry at Bath University and a PhD at Strathclyde University in Physical Chemistry. He has extensive experience in R&D in the polymer field and is currently Head of the New Product Development team.

Thermal Effect on Material Properties and Transmission Performance of Coaxial Drop Cables

S.-H. Chou, J.-C. Lin, H.-F. Lin, Y.-H. Hwang, C.-H. Hsieh, H.-P. Hsu, Y.-c. Lin, Y.-K. Tu

OSP, Telecommunication Laboratories, Chunghwa Telecom, Taiwan, R.O.C.
Tel: 001-886-34245761   E-mail: shc@chttl.com.tw

ABSTRACT

Thermal effect on material properties and transmission performance of coaxial drop cables has been studied in this study. Transmission performance studied includes characteristic impedance, attenuation, structural return loss, velocity of propagation and capacitance. The material properties of insulation can be qualified by the changes in transmission characteristics. Cable material property discussed is the dielectric constant of insulation. Changes in attenuation, capacitance and velocity of propagation are very appropriate to be considered as a quality of insulation material property. Structural return loss is not a good property to qualify the insulation material property, but is an important performance to further study the foam structure of PE dielectrics. Furthermore, degradation of PE dielectrics and migration of plasticizer from PVC jacket were studied by FTIR.

INTRODUCTION

Coaxial cable has been used in video and broadband applications for a long time. Coaxial drop cables are designed to carry high frequency radio waves (5 MHz to 1 GHz) from some distribution point to the user [1].

Coaxial drop cable typically consists of two concentric conductors separated by an insulation material. The center conductor consists of a copper-clad steel, whereas outer conductor is made up of a combination of a laminated aluminum tape and aluminum braid wire. Otherwise, PE (polyethylene) and PVC (polyvinyl chloride) are usually used as cable insulation material and cable jacket material, respectively.

PE is chosen as the cable insulation polymer since it can provide coaxial cable with favorable electrical characteristics. Furthermore, the PE is usually foamed to reduce the dielectric constant and then provide high performance coaxial cable. However, mechanical strengths of PE dielectrics and PVC jacket significantly dropped that may be attributed to degradation of PE dielectrics and migration of plasticizer from PVC jacket.

Chen et al. studied the processing of foamed PE for high performance coaxial cable applications and suggested that if the foam maintains a consistent and uniform cell structure, then it is capable of superior electrical performance, such as stability of structural return loss, characteristic impedance and capacitance [2].

Thermal aging effect on high frequency transmission characteristics of coaxial drop cables has been studied in our study group [3]. It has concluded that the changes in electrical characteristics were attributed to insulation properties changed. Based upon the previous study, this study continues to further study the thermal effect on the material properties of coaxial drop cable and to provide the relationship between cable electrical properties and cable material properties.

Cable material property discussed is the dielectric constant of the insulation. During the aging process, material properties of center conductor, PE dielectrics and PVC jacket were studied by Auger Electron Spectroscopy (AES) and Fourier Transform Spectrometer (FTIR). Furthermore, there will be five electrical properties, including four high frequency properties, characteristic impedance, structural return loss, velocity of propagation and attenuation, and one low frequency property, capacitance, examined. It is well known that these five electrical parameters are related to the dielectric constant of the insulation material. For clearly explaining each parameter, the relation between dielectric constant and each electrical property will be described below.

EXPERIMENTAL SECTION

Six samples used in this work were from three manufacturers (identified as C, T and W), including RG-59 and RG-11 coaxial drop cables for each manufacturer, and referred as C-59, C-11, T-59, T-11, W-59 and W-11. All samples have 75 ohm impedance and are with standard shield.

The samples cut into 100 meters in length were prepared to be aged at three different temperatures, 55, 85 and 100°C in the ovens, and then removed from the aging environments after 1, 4, 8, 16, 25, 39 and 52 weeks for electrical tests. On the other hand, the samples cut into

30 cm in length were prepared at the same aging conditions for material property tests.

Cable electrical measurements were performed by DCM CMS-COAX system, which has been described in previous paper [3]. All data were stated as the average of values at three individual measurements to ensure the accuracy of measurements. Material identification analysis were performed by AES (VG, Microlab 310D) and FTIR (Bruker, IFS-48).

RESULTS AND DISCUSSION

AES study and FTIR study. The presence of oxidized copper on the conductor surface is observed by AES study. When the samples were aged at 100°C, the results from depth profiling analysis show that oxidation layer was observed only at the beginning of aging process. Furthermore, the thickness of oxidation layer did not increase over the aging time. It suggests that Al foil provides an efficient method to isolate center conductor from oxygen and no further oxidation occurs.

FTIR spectra are mainly used to study the migration of plasticizer from PVC jacket. The spectra of PVC jacket and PE dielectrics for W-11 jacket samples as an example are shown in Figure 1 and 2, respectively. Three spectra in these two figures labeled as A, B and C are the spectra before aging and after aged at 100°C for 26 weeks and 39 weeks aging periods, respectively.

In Figure 1, the absorption bands at 2950, 1725, 1290, 1125 and 1071 cm^{-1} belong to the characteristic absorption of DOP (dioctyl phthalate), which is the plasticizer of PVC. However, the intensities of these bands decrease with the aging time. It indicates that a part of DOP is lost from PVC during the aging periods.

On the other hand, in Figure 2, no extra absorption bands (for example, the absorption band of DOP) are observed when the samples were aged at 100°C for 26 weeks and 39 weeks aging periods. It means that DOP does not migrate from PVC jacket to PE dielectrics. Furthermore, the absorption band around 1740 cm^{-1} is the characteristic absorption of C=O group, which is attributed to thermal degradation of PE dielectrics. Based upon FTIR spectra for the PE dielectrics of all six samples, the PE dielectrics of C-11 provides the best resistance to thermal effect, whereas the PE dielectrics of C-59 is the worst one.

Furthermore, Al foil located between PVC jacket and PE dielectrics are also studied by FTIR. The spectra of the inside of Al foil (i.e., face to PE dielectrics) and the outside of Al foil (i.e., face to PVC jacket) are shown in Figure 3. The spectrum of the surface faced to PVC jacket clearly shows several characteristic absorption bands of DOP, whereas the spectrum of the surface faced to PE dielectrics doesn't. The result ensures that DOP

does not penetrate Al foil to interact with PE dielectrics. Furthermore, PE degradation can not be considered as a quality of plasticized PVC because no DOP characteristic absorption band was observed in PE spectrum.
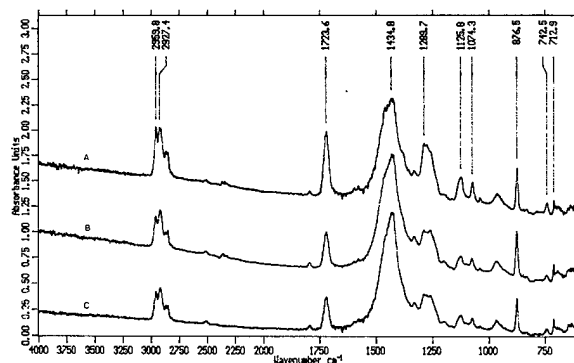
Figure 1. FTIR spectra for the PVC jacket of W-11 before aging (A), after aged at 100°C for 26 weeks (B) and 39 weeks (C).
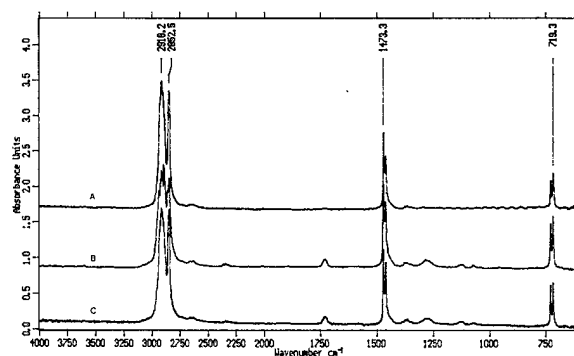

Figure 2. FTIR spectra for the PE dielectrics of W-11 before aging (A), after aged at 100°C for 26 weeks (B) and 39 weeks (C).
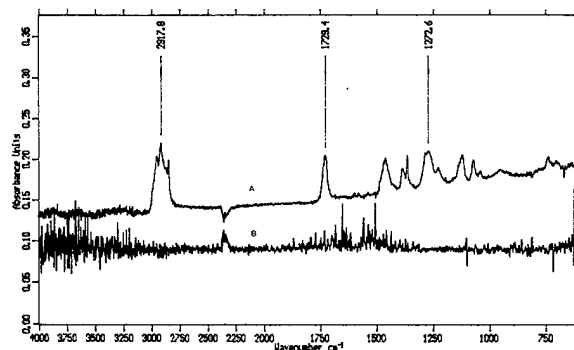

Figure 3. FTIR spectra for Al foil faced to PVC jacket (A) and to PE dielectrics (B)

Characteristic impedance measurement. In order to reduce signal energy loss, impedance matched

for whole transmission system is a very important issue for various applications. In general, the characteristic impedance of the cable varies as a function of the frequency of the applied signal, but is not related to length.

It is well know that, at very high frequencies, the value of characteristic impedance approaches to a fixed value (for example, 75 ohm). The values of this parameter at 450 MHz were chosen for further discussion to find out the thermal aging effect.

The standard deviation of characteristic impedance values at three individual measurements is between 0.00 to 0.25.

The characteristic impedance, no matter what the sample is, remains almost unchanged when the samples were aged at 55 and $85^{\circ}C$ over 52 weeks, whereas it definitely decreases with aging time when the samples were aged at $100^{\circ}C$.

Upon transmission theory, the characteristic impedance of the cable can be determined by primary constants. However, at high frequency, it can be determined by inductance and capacitance only [4,5]. On the other hand, it can be calculated from the outside diameter of center conductor (d), the inside diameter of outer conductor (D) and the dielectric constant of the insulation (ε) as expressed in Equation (1) [4].

$$Z_{0,\infty}(ohm) = \frac{60}{\sqrt{\varepsilon}} \cdot \ln\frac{D}{d} \qquad (1)$$

The outer diameter of center conductor and the inside diameter of outer conductor measured directly from the samples are listed in Table 1. In this study, it is simply assumed that cable dimension is unchanged during the aging process.

Based upon characteristic impedance data and d and D data shown in Table 1, the dielectric constants of the insulation can be calculated by Equation 1.

Table 1. Measured diameters from the samples

Sample	Outer diameter of center conductor (d, mm)	Inside diameter of outer conductor (D, mm)
C-59	0.81	3.60
T-59	0.81	3.57
W-59	0.81	3.69
C-11	1.63	7.05
T-11	1.62	7.00
W-11	1.62	6.91

The dielectric constant data for the samples aged at $85^{\circ}C$ and $100^{\circ}C$ were calculated by Equation 1. Over the aging time up to 52 weeks, the dielectric constant changes are between 0.00 and 0.03 for all six samples aged at $85^{\circ}C$, whereas they are between 0.08 and 0.25

aged at $100^{\circ}C$. It suggests that they are small enough to be negligible when the samples were aged at $85^{\circ}C$.

Figure 4 is a plot of dielectric constant changes vs. aging time for all six samples aged at $100^{\circ}C$ over 52 weeks. During the aging process, T-59 has the largest dielectric constant changes up to 0.25 and C-11 is the smallest one only 0.08. On the whole, RG-11 samples can provide better insulation material property than RG-59 ones, which is probably attributed to larger cable dimension and thicker cable insulation. Furthermore, the insulation material for T-59 sample displays the worst resistance to thermal aging effect.
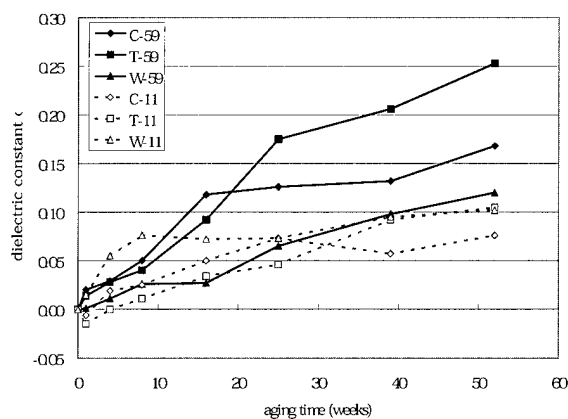
Figure 4. Dielectric constant changes for six samples calculated from characteristic impedance data with aging time up to 52 weeks.

Structural Return Loss (SRL) measurement.
SRL is utilized to describe the portion of the total return loss, which is due to these structural changes along the cable [6]. Structural variations of the cable in a periodic and random manner produce reflections of signals within the cable and reduce the signal strength.

It has to be noted that SRL measurements exhibit high inaccuracy and fluctuation. Although there is no equation to describe the relation between SRL data and dielectric constant of insulation reported, a very interesting result has already been observed in the SRL data for T-59.

Except the sample T-59 aged at $100^{\circ}C$, all other samples have no valuable observations, even aged for a period up to 52 weeks. However, as defined, SRL is used to measure the uniformity of cable impedance along the cable. During the aging process, if a decrease in cable impedance is uniform along the cable, then the cable still has good SRL performance. It therefore indicates that the other five samples have stable SRL performance and the foamed PE still has a consistent and uniform cell structure for the samples aged at $100^{\circ}C$ over 52 weeks.
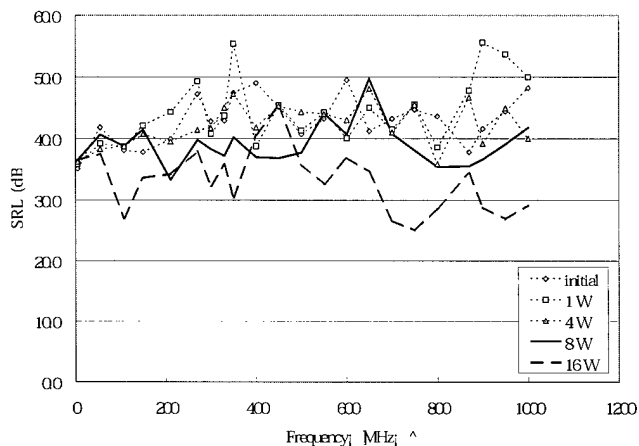
Figure 5a. SRL data for T-59 before aging and aged at 100°C up to 16 weeks.
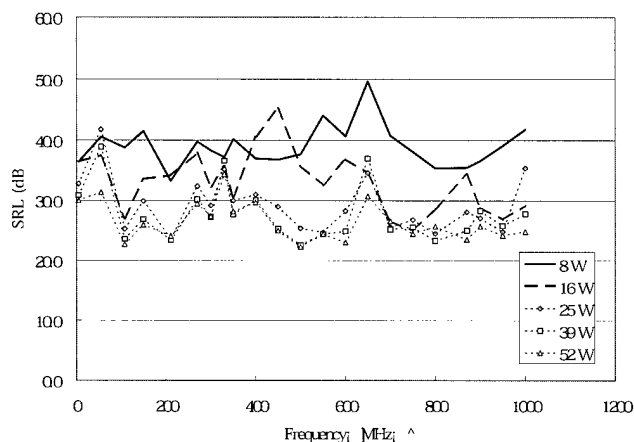
Figure 5b. SRL data for T-59 aged at 100°C up to 52 weeks.

The SRL data for T-59 are illustrated graphically in Figure 5a and 5b. Figure 5a includes the data before aging and after aged for 1, 4, 8 and 16 weeks, whereas Figure 5b shows the data after aged for 8, 16, 25, 39 and 52 weeks. The data are separated into two parts intentionally to easily describe the features.

At first, the SRL data remain unchanged during the first 4 weeks. Sequentially, the data start to have slightly changes at 8 weeks, and then have a fairly rapid change from 8 weeks, 16 weeks to 25 weeks. Finally, from 25 weeks to 52 weeks, the data have a gradually slow change with time.

It seems difficult to draw conclusions from SRL data. However, It is clear from the SRL result that, during the process aged at 100°C, the foam structure of PE in T-59

sample can not provide a consistent and uniform cell structure any more.

Velocity of propagation (VP) measurement. VP is the speed of an electrical signal down a length of cable compared to the speed of light in a vacuum, expressed as a percentage (%). At high frequencies, VP asymptotes towards a constant value [7]. The data of VP were measured at center frequency of 200 MHz in this study. The standard deviation of VP values at three individual measurements is always zero; VP therefore is a reliable parameter.

In the thermal effect study, the VP data remain constant when the samples were aged at 55°C, whereas ones slightly decrease with a maximum of 0.2% for W-11 aged at 85°C. However, when the samples were aged at 100°C, the VP data significantly decrease with time. For C-59 samples, the VP data decrease with a maximum of 2.5%.

For practical cables, VP depends on the properties of the insulation material surrounding the conductor simply expressed in Equation (2) [7].

$$VP = \frac{1}{\sqrt{\varepsilon}} \tag{2}$$

Based upon Equation (2) and the VP data, the dielectric constants of the insulation can be calculated. Figure 6 is a plot of dielectric constant changes vs. aging time for six samples aged at 100°C. It needs to be noted that there are completely different scales in Figure 4 and Figure 6. The difference between two figures is probably due to the equations derived from different theory. However, except T-59, the trend of dielectric constant changes for the other five samples is not similar for the same sample in these two figures at all.

On the other hand, the relationship between SRL data and dielectric constant of insulation for T-59 can be discussed. The trend of SRL data (shown in Figure 5a and 5b) is very similar with that of dielectric constant changes based upon VP data (shown in Figure 6). The data remain almost constant during the first 4 weeks, and then start to have slightly changes at 8 weeks. Sequentially, the data have a significantly rapid change from 8 weeks, 16 weeks to 25 weeks. Finally, ones have a gradually slow change from 25 weeks, 39 weeks to 52 weeks.

It means that, for T-59 sample, the SRL data is consistent with the dielectric constants calculated from VP data. On the other hand, C-59 sample continues to be the same SRL performance but very poor insulation property from VP data.

**Figure 6. Dielectric constant changes for six samples calculated from VP data with aging time up to 52 weeks.**

Figure 7. Dielectric constant changes for six samples calculated from capacitance data with aging time up to 52 weeks.
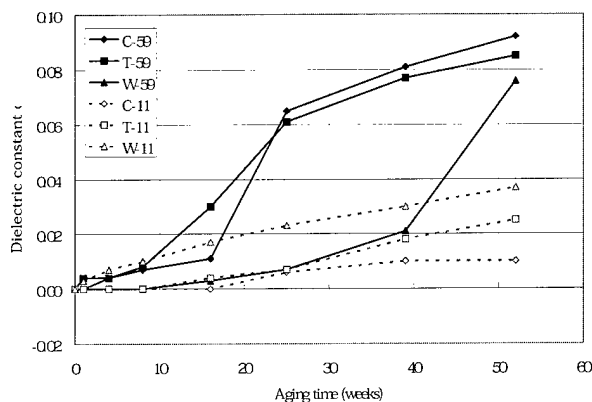
Capacitance (C) measurements. Based upon the structure of coaxial cable, there is capacitance between center conductor and outer conductor. Cable capacitance is the only discussed parameter defined low frequency parameter, measured at a test frequency of 1 kHz. The standard deviation of capacitance values at three individual measurements is below 0.10 nF/km; capacitance therefore is also a reliable parameter.

Capacitance only increases with a maximum of 1.00 nF/km when the samples were aged at 85°C. Therefore, there is no thermal effect on capacitance when the samples were aged at 55 and 85°C for the aging time up to 52 weeks. Furthermore, when the samples were aged at 100°C, the capacitance data significantly increase with time. The data for T-59 and C-59 exhibit the worst cases due to an increase near to 10.00 nF/km.

The relation between capacitance and dielectric constant of the cable insulation can be expressed as Equation (3) [5].

$$C(nF / km) = \frac{55.67 \cdot \varepsilon}{\ln \dfrac{D}{d}} \qquad (3)$$

Based upon this equation, an increase in capacitance states clearly a decrease in dielectric constant of the insulation. Figure 7 is a plot of dielectric constant changes vs. aging time for six samples aged at 100°C. Again, Figure 7 displays the same scale as Figure 4, but different scale from Figure 6.

Comparing Figure 6 with Figure 7, these figures show that both exhibit almost the same tendency for the curves represented the same sample, especially for three RG-59 samples.
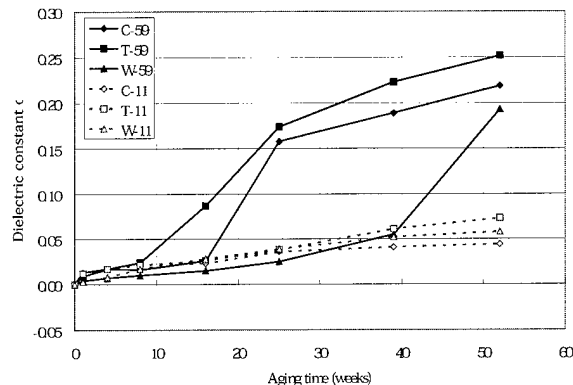
Attenuation measurement. It is well known that attenuation is an expression of how much signal energy is lost due to conductor and dielectric losses, which have been described in the literature [2,8]. Generally, lower transmission loss of coaxial cable can be obtained through the increase in the conductor size, the reduction of the dielectric constant of the insulation, the increase in the insulation diameter and so forth. Simply, attenuation, including conductor and dielectric losses, is directly proportional to the square root of dielectric constant of insulation.

The standard deviation of attenuation data at three individual measurements is between 0.00 and 0.03 dB. Based upon the previous study and this study, concerning the combination effect of aging temperature and aging time on attenuation performance, no effect was observed when the sample was experienced at 55°C up to 52 weeks, whereas thermal effect was clearly shown at 85°C and 100°C.

Although attenuation changes increase as increasing the operating frequency, attenuation changes show just a somewhat monotonous increase with the frequency as higher than 100 MHz. Therefore, as discussed for characteristic impedance, the values of attenuation at 450 MHz were chosen for further discussion.

Figure 8 and 9 show plots of dielectric constant changes (in arbitrary unit) vs. aging time for six samples aged at 85 and 100°C, respectively. These two figures have the same units, but not the real unit of dielectric constant. However, comparing to the data for the samples aged at 100°C, the samples aged at 85°C have very stable performance due to less changes of dielectric constant.
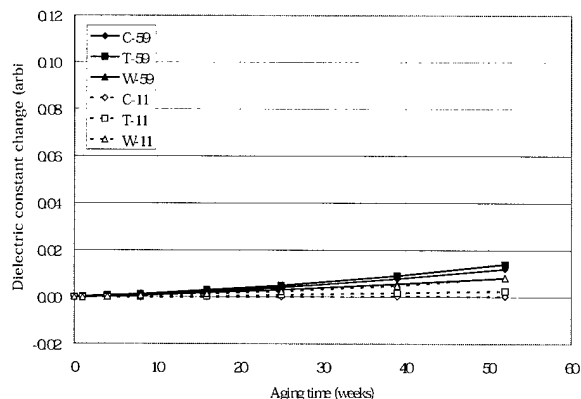
Figure 8. Dielectric constant changes for six samples calculated from attenuation data aged at 100°C.
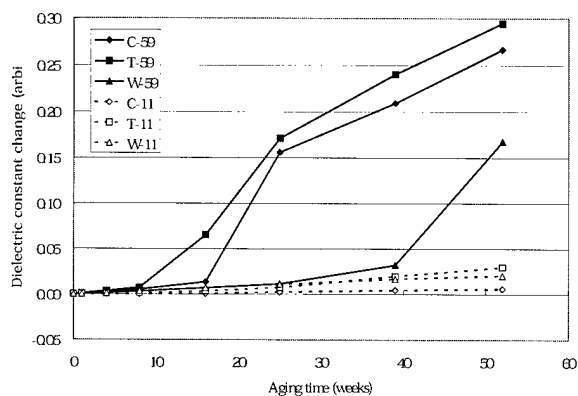
Figure 9. Dielectric constant changes for six samples calculated from attenuation data aged at 85°C.

Furthermore, comparing Figure 9 with Figure 6 and Figure 7, these figures exhibit almost the same tendency for the curves represented the same sample.

In summary, the T-59 sample has similar trend of dielectric constant changes as a function of aging time, regardless of the dielectric constants calculated from the data of characteristic impedance, VP, capacitance and attenuation. If the T-59 sample was aged at 100°C for 8 weeks, then the characteristic impedance was decreased by 1.0 ohms, VP was dropped by 0.2%, capacitance was increased by 0.9 nF/km, and attenuation

was increased by 3.64 dB/100 m at 450 MHz. Furthermore, comparing to the standard deviation for each parameter mentioned above, it is clear based on the discussion, the attenuation datum is very appropriate to be considered as a quality of insulation material property.

CONCLUSION

During the thermal aging process, cable transmission characteristics exhibit the increase in attenuation and capacitance, and the decrease in characteristic impedance, structural return loss and velocity of propagation. The data of attenuation, velocity of propagation and capacitance are very appropriate to be considered as a quality of insulation material property. On the other hand, structural return loss is not a good property to qualify the insulation material property, but is an important performance to further study the foam structure of PE dielectrics. Furthermore, the tendency of characteristic impedance is not consistent to that of velocity of propagation, capacitance and attenuation, it may be due to the other contribution. Otherwise, based upon FTIR study, PE degradation can not be considered as a quality of plasticized PVC because the plasticizer of PVC does not penetrate Al foil to interact with PE dielectrics.

REFERENCE

1. J.N. D'Amico and G.F. Apger, *Proc. 45th IWCS*, 977, 1996.

2. S.-H. Chou, J.-C. Lin, H.-F. Lin, Y.-H. Hwang, C.-H. Hsieh, H.-P. Hsu, Y.-c. Lin and Y.-K. Tu, *Proc. 47th IWCS*, 325, 1998.

3. T. Chen, R.E. Ginger, J.R. Leech and S.G. Maki, *Proc. 48th IWCS*, 476, 1999.

4. J. Weir, *Outside Plant*, 70, August 1996.

5. "Communications Cable and Transmission System", Seimen, 1976.

6. GR-1398-CORE, *Bell Communications Research, Generic Requirements*, Revision 1, 1996.

7. DCM Technical Paper.

8. L.M. Hore, V.J. Ferraro, O.G. Chavez and J.N. D'Amico, *Proc. 45th IWCS*, 946, 1996.

High Speed Polypropylene Buffering

Mikko I. Lahti

Nextrom Oy
P.O Box 44, Vantaa FIN-01511, Finland
+358-9-50251 · mikko.lahti@nextrom.com

Abstract

The telecommunication cable industry has very tough requirements for polymer stability. In harsh environments polypropylene impact copolymers (i-PP) can offer good alternative to poly(butulene-terephtalate) (PBT) which has been traditionally used for fiber optic buffer tube applications. i-PP has another properties such as low cost, flexibility and good processability, which make it attractive material for secondary coating. The location of the middle capstan, jelly type and PP compound are the most critical process parameters in PP buffering. If the material selection is done correctly then it is possible to reach almost the same excess fiber length (EFL) criteria with PP than with PBT. Several PP grades and different process conditions were investigated for secondary coating in order to meet PP process requirements. Cooling trough construction and tube tension, as well as the capstan position was of great interest.

Keywords

Polypropylene; Secondary coating; Buffering; Excess length; Shrink back, Cable cooling

1. Introduction

Despite the benefits which polypropylene can offer against PBT it has not been world wide used in secondary coating applications because of the difficult EFL control. The main difference between PBT and PP is the shrinkage behavior of the material after extrusion. This arises from the difference in crystallization kinetics of the two materials. In the case of PBT crystallization is very rapid and occurs almost instantly once the melt is cooled below the melting point of the polymer. The crystallization will be completed by the time the tube reaches the capstan wheel. So in the case of PBT the tube will only shrink after it has left the capstan wheel due to the cooling. This shrinkage is used to generate and control the EFL and it is controlled by the difference in temperature of the cooling baths. With PP the kinetic of crystallization is much slower, and the material can still crystallize after it leaves the capstan wheel. This can lead to a high EFL. The crystallization behavior of polypropylenes will vary dramatically from grade to grade and will depend upon polymer chemical structure and the inclusion of a nucleating agent in the material. When targeting high line speeds with PP it is important to keep the tube tension as low as possible. When the line speeds are increased the friction between the tube and the water batch will

increase exponentially. When PP tubes are cooled down under tension the post extrusion shrinkage will be extremely high. The internal stresses, which are created during the cooling process, will ruin the final performance of the final product. Therefore the construction based on middle capstan can lower the shrink back tendency because the capstan is equipped with driven wheel which reduces the tension build-up in the cooling trough.

There have been several studies on the use of nucleated PP grades in secondary coating applications [1-3]. Studies have shown that nucleated PP grades can improve the ultimate use temperature, dimensional stability and mechanical properties. The present work focuses on the investigation of the PP process needs in order to control EFL.

Table 1. The effect of the material selection on the EFL. Line speed 200 m/min; 2/3 mm tube

Test	PP	PP grade	Jelly	Jelly type	EFL/%
1	A	homopolymer	A	PBT	0.6
2	B	copolymer	A	PBT	0.54
3	C	nucleated	A	PBT	0.32
4	A	homopolymer	B	PP	0.55
5	B	copolymer	B	PP	0.34
6	C	nucleated	B	PP	0.05

1.1 Materials

The polypropylene grades investigated in this study are shown in Table 1. Grades A and B have been used in copper cable applications. Grade C is nucleated i-PP, which is obviously the most suitable grade for secondary coating applications. Two kinds of jellies were tested. Type A is widely used in PBT applications. Type B is PP compatible jelly. The preliminary EFL results are shown in Table 1. It clearly shows the importance of the correct material selection in PP buffering. The following studies were carried out with C type PP and B type jelly.

2. Results

High-speed secondary coating line was used in this study. Figure 1 presents the line configuration. It consists fiber pay-off, continuous jelly filling system, 60-mm extruder, cooling trough and automatic dual take-up. The cooling system is equipped with new middle

---

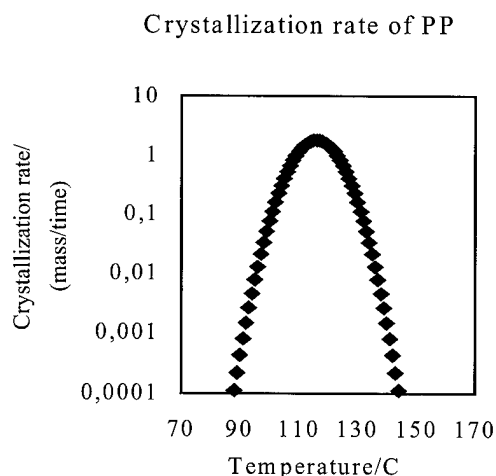capstan that is placed over the cooling trough. The location of the middle capstan can be optimized according to the process needs.
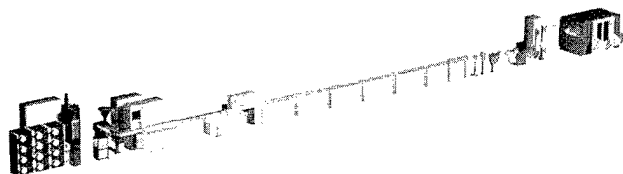
Figure 1. Secondary coating line OFC 40

The test line is equipped with modular cooling trough. The automatically adjustable telescopic section is based on immersed water-cooling. The other modules can utilize the traditional water cooling methods or new low friction cooling (LFC) system.

$$G = A \cdot exp\text{-}((T_{max}\text{-}T)/\tau)^2 \qquad (1)$$

where G is the crystal growth rate with units mass/time, T_{max} is the temperature of maximum growth rate, and A and τ are constants that adjust the height and width of the curve. Figure 2 presents the crystallization rate of non-nucleated PP. The maximum crystallization rate for PP is slightly over 120 °C. The crystallization kinetics of PP materials can vary dramatically according to the molecular structure and the addition of the nucleating agent.

The cooling behavior of PP tube was studied with infrared imaging camera. The surface temperature of the tube was measured at several locations in the cooling trough: 3, 5, 7, 9 and 15 meters. These measurements were then implemented to the cooling calculation program, which calculates the heat penetration to the tube.

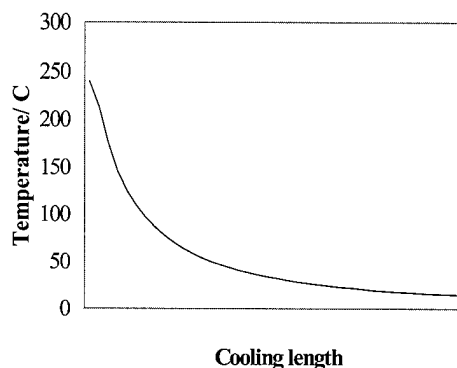**Figure 2. Crystallization kinetics of Polypropylene**

The crystallization kinetics was studied in order to optimize the secondary coating for process for PP needs. In this study only macro scale crystallization was investigated. The basic idea was to characterize the crystallization process in secondary coating application. When these semi-crystal polymers crystallize the density of the material will change dramatically. For PP this density change is roughly 5 % depending on the crystallinity level of the polymer. If the tube crystallizes on the middle capstan it will lead to uncontrolled EFL and high shrink back characteristics. The EFL can only be compensated by fiber tension and cooling water temperature if most of the crystallization takes place before the middle capstan. Therefore it is very important to adjust the capstan position according to the material characteristics.

The growth rate of the polymer crystals was investigated with the following equation [4]:


Figure 3. The maximum plastic temperature vs. the length of the cooling trough

Figure 3 shows that the PP grade needs rather high temperature profile (high initial temperature). The crystallization kinetics and cooling rate are combined in Figure 4. The slow crystal growth rate of the PP occurred rather far away from cross head at 10 meters. The shape of the PP crystallization curve could be adjusted with the addition of the nucleating agent. The crystallization of the PP compound takes place at low temperature (< 130 °C). The capstan position should be tailored according to the material characteristics and process speeds.

The optimum capstan position for PP can be based on the Figure 4. The capstan position seemed to play an important role in PP buffering. It was obvious that when the middle capstan is too close to the cross head then the crystallization will dramatically effect on EFL. If the tube crystallizes on the middle capstan it will lead to uncontrolled EFL and high shrink back characteristics. The EFL can only be compensated by fiber tension and cooling water temperature if most of the crystallization takes place before the middle capstan.

Figure 5 shows how drastically the EFL depends on the middle capstan position. Tests were made at 200 m/min and the product size was 2.00/3.00 mm. Actually the capstan position is having stronger effect on the EFL than fiber tension. The EFL range can be controlled from 0.05 to 0.30% by only changing the capstan position. This method is based on the gliding of the fibers to the capstan. If the jelly properties are not optimized to the PP buffering then EFL is not dependent on the capstan location.

Crystallization in cooling trough
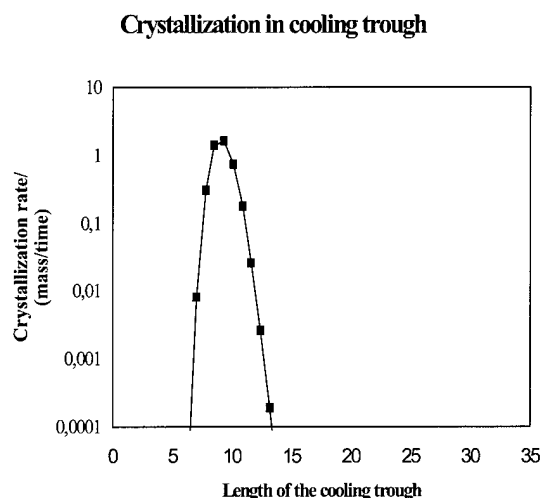
Figure 4. Crystallization rate vs. length of the cooling trough

It is possible to achieve low (< 0.05%) EFL with careful material selection and correct capstan positioning even at high speed (200 m/min). The stability of the products was characterized with EFL measurement taken from the sample, which was freely on floor. Polyolefins have high shrink back characteristics. Jacketing applications have been using very low draw down ratios in order to avoid shrink back. Buffering speeds are so much faster that the effect of the tooling can be neclegted as a source for internal stress. Tooling is, of course, playing important role in jelly feeding.

Table 3. The effect of the process parameters on the shrink back

Cooling trough tension	Tooling DDR	Speed	EFL/ % initial	EFL/ % (24h) Off reel
Low	Low	Low	0.02	0.08
High	Low	Low	0.01	0.15
Low	High	High	0.00	0.07
High	High	High	0.02	0.29

Table 3 sets out that the shrink back tendency is mainly dependent on the line speed and the cooling process. When line speeds are above 200 m/min then the friction between the water and the tube will increase dramatically. If the target line speed is 400 m/min then the tension that is applied to the hot tube can reach 10 Newton's. Rapid cooling under tension will certainly create internal stress, which will relax and increase EFL remarkably.
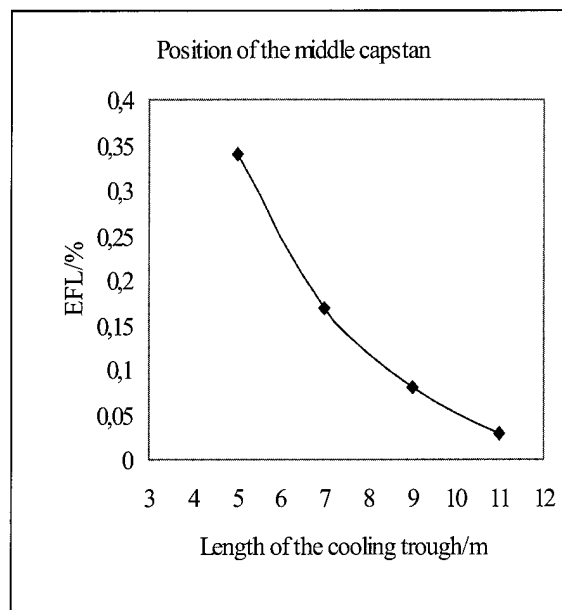
Figure 5. The effect of the DWC position on the EFL

When targeting high line speeds with PP it is important demand to keep the tube tension as low as possible. When the line speeds are increased the friction between the tube and the water batch will increase exponentially. When PP tubes are cooled down under tension the post extrusion shrinkage will be extremely high.

Therefore the construction based on middle capstan can lower the shrink back tendency because the capstan is equipped with driven wheel which reduces the tension build-up in the cooling trough. Further improvements are based on LFC, which minimizes the tension build up during the cooling process. Figure 6 presents 3 different tests, which are made at 200 and 300 m/min. LFC technology was tested at 300 m/min. It is marked as LT in Figure 6. The initial EFL values were all below 0.1 %. The sample made at 300 m/min with traditional cooling trough had EFL above 0.35% after one day. It was possible to lower the friction between the tube and the heat transfer media with LFC and decrease the amount of the internal stress in the tube.

3. Conclusion

Polypropylene can offer good alternative to PBT, which has been traditionally used for fiber optic buffer tube applications. PP has another properties such as low cost, flexibility and good processability, which make it attractive material for secondary

coating. Despite the benefits which polypropylene can offer it has not been world wide used in secondary coating applications because of the difficult EFL control.
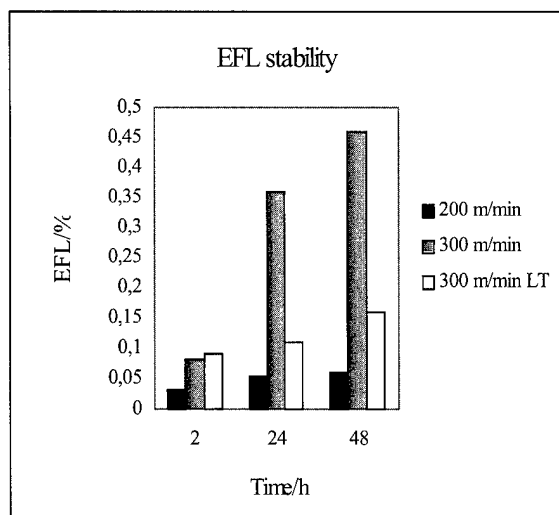
Figure 6. The EFL stability

The different polymer characteristics have to be taken into account when secondary-coating process is tailored for different buffering materials. If the tube crystallizes on the middle capstan it will lead to uncontrolled EFL and high shrink back characteristics. The EFL can only be compensated by fiber tension and cooling water temperature if most of the crystallization takes place before the middle capstan. Therefore it is very important to adjust the capstan position according to the material characteristics. For high speed PP buffering the cooling process should be based on low friction technology in order to guarantee stabile products.

The cooling process, jelly type and PP compound are the most critical process parameters in PP buffering. If the material selection is done correctly then it is possible to reach almost the same EFL criteria with PP than with PBT.

4. Acknowledgments
Special thanks to my colleagues Jussi Korolainen, Jorma Kuivila and Mikko Saikkonen for their valuable assistance, comments and commitment.

5. References

[1] M. Adams, J. Holder, C. McNutt, O. Tatat and H. Yang, "Buffer Tubes – Next Generation", Proceedings IWCS 1995, pp. 16-21.

[2] H.M.Yang, J.D. Holder and C.W. McNutt, "Polypropylene-polyethylene Copolymer Buffer Tubes for Optical Fiber Cables and Method for Making the Same", U.S Patent 5 574816, November 12, 1996.

[3] B. G. Risch, "Influence of Nucleating Agent and Melt Flow Index on Impact Polypropylene Fiber Optic Buffer Tubes", 56th Annual SPE ANTEC Conf. Proceedings, 1998, pp. 1016-1020

[4] M. E. Nichols and R. E. Robertson, "The Multiple Melting Endotherms from PBT", *J. Polym Sci.* 30, 755 (1992).

Author

Dr. Mikko Lahti

Nextrom Oy

P.O. Box 44

Fin-01511 Vantaa

Finland

Mikko Lahti received the degree of M. Sc. in Chemical Engineering in 1991 and the degree of Dr. Tech. in Polymer Technology in 1996. Before joining Nextrom in 1997 he worked as Research Scientist in European Joint Research Center in Milan. Currently, as R&D Manager at Nextrom, he is responsible for the development of the extrusion processes for fiber optic cables.

Combined Optical Fiber Draw Process and Proof Testing:
A Unique Method to Increase Productivity

Harri Turunen, Timo Mattila, Jari Sinkko
Nextrom Oy, Vantaa, Finland

ABSTRACT

This paper introduces a new method of combining the optical fiber draw process with proof testing. A random fiber break does not disturb the draw process in on-line proof testing because the changeover can be performed at full line speed. Firstly, we discuss proof testing theory and the latest research results. Secondly, we simulate the on-line proof testing process using dynamic modeling. Finally, we describe the principles and functions of the machine as well as the type tests and their results.

INTRODUCTION
Background and Research Problem

One consequence of steady growth in the optical fiber market is that fiber manufacturers are seeking more efficient processes. Combining the draw process with proof testing provides distinct economic advantages.

We claim that on-line proof testing eliminates one process step in the optical fiber production chain, as proof tested fiber can be wound onto shipping spools at preplanned lengths. We further claim that on-line proof testing saves expensive floor space, since an on-line proof tester is actually a combination of a proof testing machine and a dual take-up

The problem we set out to solve is how to keep the tension of the fiber within specified limits in all situations - i.e., constant speed, planned cut and random fiber break. We also addressed methods of leading the free fiber end through different machine elements after a fiber break.

Aim of the Study, Boundaries and Methods

The aim was to develop a model to describe the behavior of the fiber in a dynamic situation. The basic idea was for the model to incorporate those process elements that are identical to all fiber processes.

A simulation model of on-line proof testing was developed. Another target was to evaluate experimentally how fiber can be conveyed in different kinds of tubes at different running modes. The development of the on-line proof-testing machine is based on the results of this study. This study focuses on the area downstream from the coating unit of the draw tower.

THEORETICAL BACKGROUND
Proof Testing Theory

There have been significant developments in the general understanding of fiber reliability, and especially the role of proof testing, over the last two decades. New models have been introduced that provide a better understanding of the reliability of fiber in the long run. The long-term physical data [1] seems to support the two-region power law model best. The definition and requirements for proof testing have been developed to respond better to the requirements of these new models. The leading standards with respect to proof testing requirements have also changed during the past decade. The latest theory and standards highlight the following aspects:

- The dwell time of the proof testing cycle has no effect on the final strength of proof tested fiber.
- There is always a decrease in strength during the proof testing cycle in a non-ideal environment. This is a concern because the fiber might not break even though its strength decreases below the proof stress.
- The operation of the proof tester must be designed to minimize the decrease in strength. This can be achieved by arranging a high unloading rate in a proof test cycle.
- Since a decrease in strength does in fact occur, it must be monitored and reported. The proof test level itself is not pertinent, whereas the minimum strength after the proof testing cycle is of far more importance.

As long as the decrease in strength cannot be calculated or approximated with any degree of accuracy, the minimum strength is unknown.

The decrease in the strength of optical fiber for a given stress history can be expressed by the damage equation for sub-critical crack growth in brittle materials [2].

$$S_f^{n-2} - S_i^{n-2} = -\frac{1}{B}\int \sigma(t)^n dt \ , \qquad (1)$$

where
σ = stress applied to fiber, static or dynamic
S_i = initial strength at the beginning of the test
S_f = final strength for the stress history
$t = 0$ when the test begins
B and n are crack growth parameters for the fiber

This equation can be applied to components of the proof testing cycle by integration over the corresponding times.

Failure during Loading. Loading is similar to dynamic fatigue testing. The stress during loading is given by $\dot{\sigma}_l t$ and the upper limit of the integral is $t = \sigma_f / \dot{\sigma}_l$, where $\dot{\sigma}_l$ is the loading rate. This integration gives the equation for final strength of $S_f = \sigma_f$. [3].

$$\sigma_f^{n-2} = S_i^{n-2} - \frac{\sigma_f^{n+1}}{B(n+1)\dot{\sigma}_1}. \qquad (2)$$

It can been seen from equation (2) that the decrease in strength during unloading can be limited by a faster loading rate. When the loading rate increases, the upper limit of the integral decreases, and consequently the last term of equation (2), which describes the decrease in strength, also diminishes.

Failure during Dwell. In this case, the fiber passes the loading portion, but fails at the proof stress $S_f = \sigma_p$. The upper limit of integration is now $t = \sigma_f / \dot{\sigma}_l + t_*$ when failure occurs at moment t_*, starting when dwell commences. Integration gives the following equation. [3].

$$\sigma_p^{n-2} = S_i^{n-2} - \frac{1}{B}\left[\frac{\sigma_p^{n+1}}{(n+1)\dot{\sigma}_1} + \sigma_p^n t_*\right]. \qquad (3)$$
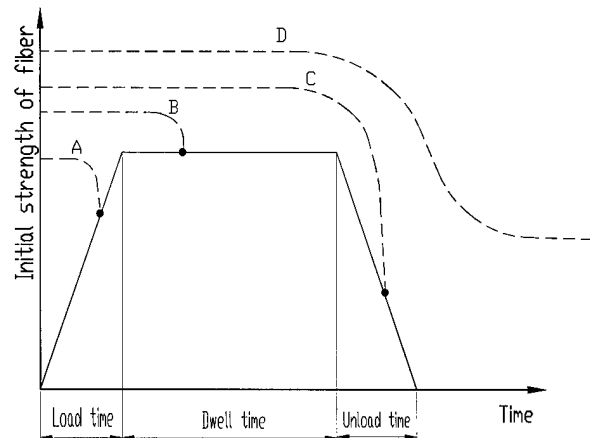
Failure during Unloading. Unloading cannot be ignored in proof testing since it is an opportunity for crack growth. The strength at failure is a culmination of crack growth during loading, dwell and unloading. The upper limit of the integral is now $t = \sigma_f / \dot{\sigma}_l + t_d + (\sigma_p - \sigma_*) / \dot{\sigma}_u$, where σ_* is the failure strength during unloading. Integration over time t gives an equation describing the failure strength during unloading. [3].

$$\sigma_*^{n-2} - \frac{\sigma_*^{n+1}}{B(n+1)\dot{\sigma}_{ul}} = S_i^{n-2} - \frac{1}{B}\left[\frac{\sigma_p^{n+1}}{(n+1)\dot{\sigma}_1} + \sigma_p^n t_d + \frac{\sigma_p^{n+1}}{(n+1)\dot{\sigma}_u}\right]. \qquad (4)$$

Passing the Test. The flaws that pass the proof test have a final strength, which is affected by all three components of the proof test cycle. The upper limit of integration is now $t = \sigma_f / \dot{\sigma}_l + t_d + \sigma_p / \dot{\sigma}_u$. Integration over the entire proof test cycle gives the final strength of fibers surviving the test. [3].

$$\sigma_{f*}^{n-2} = S_i^{n-2} - \frac{1}{B}\left[\frac{\sigma_p^{n+1}}{(n+1)\dot{\sigma}_1} + \sigma_p^n t_d + \frac{\sigma_p^{n+1}}{(n+1)\dot{\sigma}_u}\right]. \qquad (5)$$

The dotted line in figure 1 describes the strength of the fiber during a proof testing cycle. The continuous line describes the proof stress during the cycle. Failure occurs when the two lines cross each other (marked with dots).

Fig. 1. Strength decrease during proof testing

(A) Fiber break during loading
(B) Fiber break during dwell
(C) Fiber break during unloading
(D) Test pass despite a strength decrease. [2].

With respect to loading, failures occur in stress below the proof stress (curve A). During dwell time, those flaws with an initial strength greater than proof stress grow and subsequently fail. Note that flaws do not grow to a final strength below the proof stress during dwell time and that the minimum final strength is exactly equal to the proof stress. The dwell time has no effect on the minimum strength after the test. The minimum strength is independent of exactly when the failure occurred in dwell time.

The dwell time does, however, cause crack growth. Therefore a higher initial strength S_i is needed to survive a longer dwell time (curve B). Failures during unloading are of special interest because the strength at failure is at that point below the proof stress. The strength at failure is a culmination of crack growth during loading, dwell and unloading (curve C). The flaws that pass the proof test have a final strength that is affected by all three components of the proof test cycle. The most concerning fact is that these flaws can grow during unloading to below the proof stress and still pass the test (curve D).

Longer dwell time, therefore, does not produce stronger fiber. This is an important finding for the on-line proof testing concept introduced later [4]. It is also interesting to note that the requirement for a high unloading rate can be met in the on-line proof tester concept. In an optimized proof tester, the proof test level and the minimum strength after the test do not differ significantly.

Proof Testing Standards

TIA/EIA FOTP-31-C is probably the most accurate of all the standards on the effect of a decrease in strength during the proof testing cycle. This U.S. standard provides

formulas for calculating the necessary proof stress (σ_p) when the permitted minimum final strength (S_{min}) and the fiber fatigue parameters are known. The unload time of the proof testing cycle is designated t_u. The determination of σ_p is an iterative process using equation (7) when equation (6) is true.

$$\sigma_p^2 t_u \leq (n-2)B \qquad (6)$$

$$S_{min} = \sigma_p \left[1 - \frac{\sigma_p^2 t_u}{(n+1)B} \right]^{1/(n-2)} \qquad (7)$$

When equation (8) is true, σ_p is determined by equation (9).

$$\sigma_p^2 t_u \geq (n-2)B \qquad (8)$$

$$\sigma_p = S_{min}^3 \left(\frac{n+1}{3} \right)^{3/(n-2)} \left(\frac{t_u}{(n-2)B} \right) \qquad (9)$$

When equations (6) and (8) are both valid, equations (7) and (9) will both give the same result.

The target has been defined as the minimum final strength after the proof test, instead of the proof stress level. This illustrates the widely accepted modern understanding of fiber reliability. [5].

The European IEC standardization committee has taken a different approach. It has not provided detailed formulas for calculating the minimum final strength. This may be because the determination of crack growth parameter B is still under discussion. Detailed mathematical analyses can be found in the technical reports of the IEC standardization committee [6]. These mathematical analyses produce the same result as that presented in the FOTP-31-C standard. The approach of the IEC standardization committee also acknowledges the influence of the unload rate in proof testing by stating that the load time and the unload time in the proof testing cycle should be as short as possible. [7].

In line with the FOTP-31-C standard, the IEC standard also acknowledges the fact that the fiber coating can share a part of the load experienced during the proof test cycle.

Both leading U.S. and European standards agree on the basics of proof testing. A high unload rate should be arranged in order to minimize the difference between the proof stress and the final minimum strength. Diverging from past practice, no requirements are now set for the dwell time in the proof testing cycle since a longer dwell time does not produce any increase in the strength of the fiber.

Dynamic Modeling

The purpose of the dynamic modeling was to describe the tension behavior of the fiber after the fiber is drawn. The modeling is based on the fact that several process elements are similar throughout all finishing processes. Combining these elements, therefore, makes it possible to model the behavior of fiber tension in a complete process. [8].

In this case we modeled only the end part of the combined fiber draw and proof testing process. A computer simulation based on the modeling work was then generated. The input parameters for the simulation include line speed, reel dimensions, and the eccentricity of rotating parts. The outputs of the simulation are graphical and numerical presentations of fiber tension (see figure 2).

We focused on tension behavior and simulation downstream from the draw tower coater but upstream from the auxiliary capstan. This eliminated the draw coater and all parts upstream as well as the fiber cutter and the suction fan downstream from the auxiliary capstan.

The first step was to model the fiber tension in a normal run and in ramps. The elements that affect tension during a normal run and ramps are the capstans, dancer, idle wheels and take-ups. The mathematical formulas are as follows [9]:
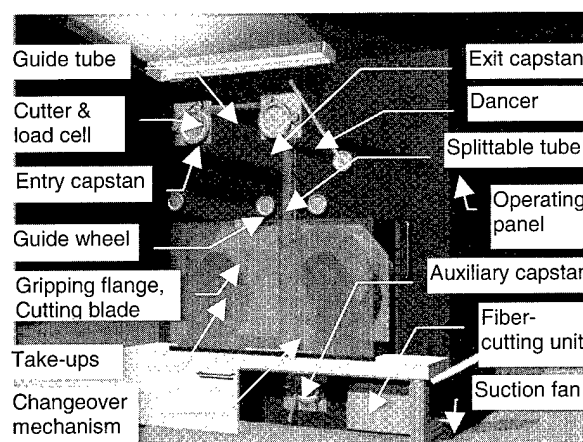

Guide tube
Cutter & load cell
Entry capstan
Guide wheel
Gripping flange, Cutting blade
Take-ups
Changeover mechanism
Exit capstan
Dancer
Splittable tube
Operating panel
Auxiliary capstan
Fiber-cutting unit
Suction fan

Fig. 2. On-line proof testing in principle

Idle Wheel. The phenomena that affect the rotational movement of the idle wheel and the tensile load of the fiber are included in equation (10) in the following order: idle wheel inertia, bearing friction, out-coming fiber tension, in-going fiber tension, air resistance and idle wheel geometry. The torque equilibrium of the idle wheel is given as

$$-J\alpha - K_b\omega + (F_o - F_i)r - K_a\omega^2 + \sqrt{x_c^2 + y_c^2}\, mg(\omega t + \phi_0) = 0 \cdot \quad (10)$$

Dancer. The dancer modeled here is a pivot-type dancer. A pivot joint and dancer wheel is modeled separately. The phenomena that affect the dancer wheels and must therefore be evaluated are included in equation (10).

Equation (11) shows the pivot joint model. The model incorporates the moment of inertia of the polar mass of the idle wheel, pivot joint friction, external force, out-coming fiber tension and in-going fiber tension. It was assumed that there is little displacement of the dancer wheel and that the change in the wrap angle of the fiber around the dancer is negligible.

$$J_p\alpha_p + K_p\omega_p - F_E l_e + F_o l_o + F_i l_i = 0 . \quad (11)$$

Capstan. The modeling of the capstan is based on the phenomena that affect the rotational movement of the capstan, and thus also the tensile load of the fiber going through it. These are included in equation (12) in the following order: motor torque, capstan wheel inertia, bearing friction, belt pulley bearing friction, out-coming fiber tension, in-going fiber tension, and capstan wheel geometry. The torque equilibrium of the capstan is given as

$$M - J\alpha - (K_b + K_B)\omega + (F_o - F_i)r + \sqrt{x_c^2 + y_c^2}\,mg\sin(\omega t + \phi_0) = 0 . \quad (12)$$

Take-up. The tension is affected by a take-up rotating according to equation (13), which includes the terms for motor torque, reel inertia, bearing friction, winding tension, air resistance and reel geometry. The torque equilibrium of the take-up is given as

$$M - J\alpha - K_b\omega - F_i r - K_a\omega^2 + \sqrt{x_c^2 + y_c^2}\,mg\sin(\omega t + \phi_0) = 0 . \quad (13)$$

The on-line proof testing process was modeled by using these elements. The simulation included disturbances traveling in both directions - i.e., from the coater to the take-up and from the take-up to the coater. The reflection from the coater and from the take-up was ignored. The speeds of the rotating parts formed an essential part of the simulation. The speed differences between rotating parts create elongation, which can be seen as tension.

It was assumed that the angular speed of the motor-driven shafts remains constant regardless of fiber tension. The eccentricity of the rotating parts than creates a variation in tension because the circumferential speed varies.

The circumferential speed of the idle wheels varies with the tension because the tension is comparable to the speed difference between the wheels. In this case, the fiber is the driving force. The program interface is shown in figure 3.

FUNCTIONAL DESCRIPTION
The proof testing is performed by addressing the speed difference between two servo-driven capstans; the entry and exit capstans. The entry capstan includes a load cell for proof tension measurement. Between these capstans the fiber runs through a tube that guides the fiber during threading and after a fiber break. A cutting blade is installed at the entrance of the guide tube for use in planned fiber cutting (see figure 2).
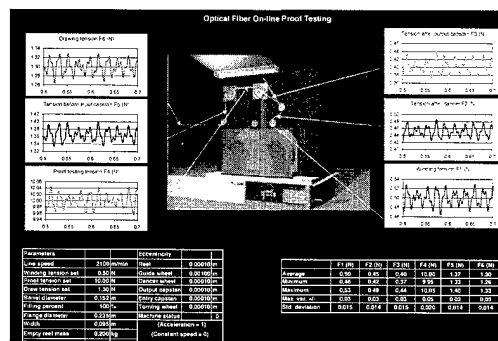

Fig. 3. Simulation program

The dancer unit consists of a dancer arm, a splittable tube and wheels for both take-up modules. During a normal run, the dancer arm is on the same side as the spooling take-up. When a random fiber break occurs and during planned cutting, a new incoming fiber runs through the tube to the auxiliary capstan. After tightening the fiber, the tube opens and the dancer-arm moves the fiber to the guide wheel of the other take-up.

At the same time the changeover mechanism moves the fiber in between the gripping flange of the take-up. A new reel is accelerated to process speed and the gripping flange is closed, simultaneously cutting the fiber with an integrated cutting blade. Spooling onto a new reel commences and the tube is closed to wait for the next fiber break. During the changeover the fiber runs from the auxiliary capstan to the fiber-cutting unit, and from there into the suction fan.
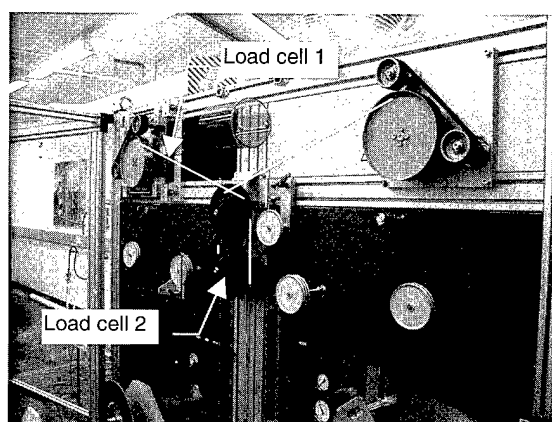

**Fig. 4 Test rig for proof tension test**

TESTS AND RESULTS
Proof Tension Variation
This test was performed to confirm that it is possible to measure the force on the capstan caused by the fiber. This signal is then used as feedback for controlling proof tension. The test rig is shown in figure 4. Load cell 1 measured the force on the capstan, which was installed on linear bearings.

The fiber tension was simultaneously measured by load cell 2, which was mounted inside a wheel. The purpose was to demonstrate that the actual fiber tension was still within the specifications stipulated in the standards even though the capstan was installed on linear bearings. The results of this test are shown in table 1 and in figure 5.

Fig. 5. Proof tension variation

Fig. 5. Proof tension variation
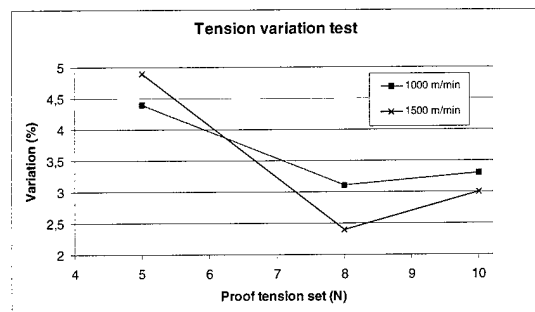
Table 1. Proof tension variation

| Line speed (m/min)	Proof tension (N)	Tension variation (±N)	Tension variation (±%)
1000	5	0,22	4,4
1000	8	0,25	3,1
1000	10	0,33	3,3
1500	5	0,25	4,9
1500	8	0,19	2,4
1500	10	0,30	3,0

The results show that this new method for measuring tension does not cause additional variation in fiber tension. However, there is greater variation in the signal (load cell 1), but this is only a measurement error caused by vibration of the capstan unit. Since the error is not detectable in the tension of the fiber, the signal can be suitably filtered for the needs of the control system.

Fiber Conveying Tests
The test plan is shown in table 2 and the test rig in figure 6. The first stage of testing consisted of threading tests through a tube.

Table 2. Fiber conveying test matrix

| Tube material	Tube diameter	Running mode	Air flow
Material A	10 mm	Threading	None
Material B	30 mm	Fiber break	Low
Material C	50 mm	Planned cut	High
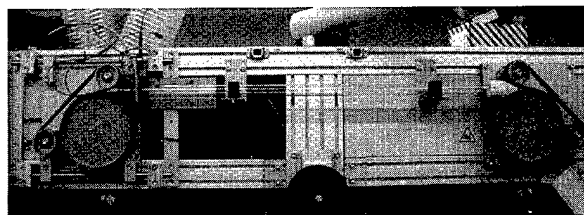
Fig. 6. Test rig for fiber conveying test

All the parameters for threading the fiber through the capstans and the tube were found as a result of this testing. Fiber conveyance inside the tubes at 1600 m/min was also successfully tested. The next step is to test higher speeds while simultaneously cutting the fiber.

Change-over Mechanism
The reliability of the changeover mechanism and the whipping protection were also tested. The same principle is used with a new dual take-up (see figure 7). The test rig differs from the final solution, but the results are fully comparable.
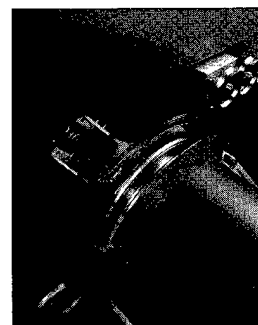
Fig. 7. Change-over and whipping protection

Proper operation of the changeover mechanism and whipping protection was confirmed in trials at 1600 - 2100 m/min.

SUMMARY AND DISCUSSION
A new method for combining the process for drawing optical fiber with proof testing was introduced. We claimed that on-line proof testing removes one process step in the optical fiber production chain. We further claimed that on-line proof testing saves expensive floor space.

The most important findings in proof testing theory were that the dwell time in the proof testing cycle has no effect on the final strength of proof tested fiber. The operation of the proof tester must be designed to minimize the decrease in strength. This can be achieved by arranging a high unloading rate in the proof test cycle. Both leading U.S. and European standards agree on these basics of proof testing. Thus a longer dwell time does not produce stronger fiber. This is an important finding for the on-line proof testing

concept. In an optimized proof tester, the proof test level and the minimum post-test strength do not differ significantly.

A simulation model of on-line proof testing was developed. An on-line proof testing process was modeled by using process elements. The simulation included disturbances traveling in both directions - i.e., from the coater to the take-up and from the take-up to the coater. The speeds of the rotating parts formed an essential part of the simulation.

A tension variation test was conducted to confirm that it is possible to measure the force on the capstan caused by the fiber. The results showed that this new method for measuring tension does not cause additional variation in fiber tension.

The parameters for threading the fiber through the capstans and tube were found as a result of the fiber conveying tests. Fiber conveyance inside the tubes at 1600 m/min was also successfully tested. Proper operation of the changeover mechanism and whipping protection was confirmed in trials at 1600 - 2100 m/min.

Development of the on-line proof-testing machine is based on the results of this study. The on-line proof tester is an independent unit, which can be installed in different draw towers.
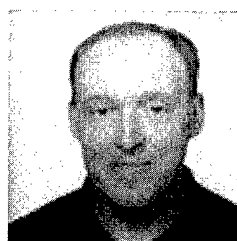
REFERENCES

1. Linda K. Baker, Corning Incorporated, Mechanical reliability modeling of optical fibers, Wire & Cable Technology International, November 1999, pp. 40-41

2. Y. Mitsunaga, Y. Katsuyama, H.Kobayashi, Y. Ishida, Failure prediction for long length optical fiber based on proof testing, Journal of Applied Physics 53 (7), July 1982, pp. 4847-4853

3. G.S. Glaesemann, The effect of proof testing on the minimum strength of optical fiber, Corning Incorporated, International Wire & Cable Symposium proceedings 1991, pp. 582-586

4. T. Mattila, "Reliable high speed proof testing of optical fiber", Interwire proceedings 1997, pp. 166-172.

5. TIA/EIA standard FOTP-31-C, Proof Testing Optical Fibers by Tension, 1995

6. Technical report on the power law theory of optical fiber reliability, IEC SC 86A/WG1, Phoenix meeting, February 1996

7. IEC standard 793-1-B1 Optical fiber proof test, 1996

8. Reid, K. N Shelton, J. J. Shin, K-H. Distributed control of tension in a web handling system. Oklahoma: Web Handling Research Center, 1989. 34 p. (Project Report April 1989).

9. Turunen, H. K. Mechanical behavior of fiber during finishing processes. Espoo, Finland: Helsinki University of Technology, 1997. 104 p. (Faculty of Mech. Eng., Licentiate Thesis).

Harri Turunen received his M.Sc. degree in Mechatronics and Space Technology in 1993. He joined Nextrom in 1992, where he was first involved in the R & D of heavy take-ups. In 1995 he joined the fiber optic group where he now works as an R&D Manager. He received his Licentiate of Technology degree in 1999.

Timo Mattila joined Nextrom in early 1996 as a research engineer for developing optical fiber finishing processes. Today he holds the position of product manager for fiber coloring systems. Mattila completed his M.Sc. degree in mechanical engineering at Helsinki University of Technology in 1997 and his B.Sc. degree at the Institute of Technology in Helsinki in 1991.

Jari Sinkko joined Nextrom in 1997. He is currently a senior mechanical engineer, working mainly with draw towers and tower components. Mr. Sinkko completed a B.Sc. degree in mechanical engineering at the Insitute of Technology in Pori in 1987.

Mailing address for all the authors:

Nextrom Oy
B.O.Box 44
FIN-01511 Vantaa, Finland

Numerical Modeling of the MCVD Process for the Manufacture of Glass Preforms

Muralidharan, Ravi O. Prasad, Eric W. Grald

Fluent Inc., Lebanon, New Hampshire

ABSTRACT
A numerical simulation of heat and mass transport in the modified chemical vapor deposition (MCVD) process with application to manufacture of high quality optical fibers is performed. Quasi-steady and transient simulations are carried out for the multiple-species and conjugate heat transfer problem and the results are compared with experimental data. The computed temperature and thermophoretic particle deposition profiles are compared with experimental results and show excellent agreement. The effect of the inlet gas flow rate on the deposition efficiency of silica particles is also studied.

INTRODUCTION
The modified chemical vapor deposition process is currently used to manufacture glass preforms for high quality optical fiber fabrication. In this process, a silica tube is rotated on a lathe and is heated by a slowly traversing oxy-hydrogen torch. A mixture of gases, such as $SiCl_4$ and O_2, flow into the rotating tube and are heated to high temperatures. Kim, et al.[1] carried out a study of the chemical kinetics of $SiCl_4$ oxidation. This process creates very fine particles of silicon oxide. These particles move with the gases to the relatively cold zone downstream of the torch and deposit on the inner wall of the tube due to thermophoresis. Thermophoresis is a phenomenon by which suspended particles experience a force in the direction of decreasing temperature[2]. These deposited particles consolidate into a thin glassy layer by sintering as the torch traverses along the tube. After 10-40 layers are deposited, the tube is collapsed into a solid preform rod and is then drawn into a long thin fiber. Cho, et al.[3] carried out an experimental study of the MVCD process in a fused-silica tube. They used a tube rotational speed of 60 rpm. It was analytically shown that tube rotation speeds larger than 30 rpm result in almost uniform wall temperatures in the circumferential direction. So, the circumferential variations are negligible.

In the MCVD process, it is important to study the effects of various process parameters on the particle deposition rate and efficiency to reduce the production cost. The deposition is determined by thermophoresis, which depends on the temperature field, which in turn requires the knowledge of the velocity field in the tube. In most of the previous studies, the tube wall temperatures were specified *a priori*. It should be noted that different operating conditions result in different tube wall temperatures, which reduces the flexibility of these previous models for studying the effect of various parameters on the MCVD process. To alleviate this drawback, the tube wall temperatures are computed as part of the model in the present study.

In this work, the commercial computational fluid dynamics (CFD) package, FLUENT, based on the finite volume method, is used to solve the conservation equations of mass, momentum, energy and species concentrations. The effects of chemical reactions and temperature-dependent fluid properties are included. The localized heating of the moving torch is modeled using a heat flux boundary condition varying with space and time.[4,5]

MATHEMATICAL MODEL
A configuration similar to the one used in the experimental setup of Cho and Choi[3] is used in the present analysis (see Fig. 1). As the circumferential variations are negligible, an axi-symmetric case is studied. The oxy-hydrogen torch moves along the length of the tube.

Fig. 1 Schematic diagram of MCVD process

A gas stream consisting of 60% silixon tetarchloride and 40% oxygen is introduced from one end of the tube. The gases are heated to the reaction temperature near the torch where the silica particles are formed. The following chemical reaction takes place in the tube:

$$SiCl_4(g) + O_2(g) \longrightarrow SiO_2(s) + Cl_2(g)$$

The silica particles are then directed to the cold zone downstream of the torch by the thermophoretic force and are deposited on the inside the tube wall. The particle velocity due to thermophoresis is given by:

$$V_{th} = K_{th} \nu \frac{\nabla T}{T} \qquad (1)$$

The conservation equations of mass, momentum, and energy are:

$$\frac{\partial \rho}{\partial t} + \frac{\partial \rho u_i}{\partial x_i} = 0 \qquad (2)$$

$$\rho \frac{\partial u_i}{\partial t} + \rho u_j \frac{\partial u_i}{\partial x_j} = -\frac{\partial p}{\partial x_i} + \frac{\partial \tau_{ij}}{\partial x_i} \qquad (3)$$

$$\rho C_p \frac{\partial T}{\partial t} + \rho C_p u_i \frac{\partial T}{\partial x_i} = \frac{\partial}{\partial x_i}\left(k \frac{\partial T}{\partial x_i}\right) + r_{sc} \Delta H_{sc} \qquad (4)$$

The species mass fractions are tracked by separate conservation equations. The thermophoretic motion of the silica particles is modeled using a sink term in the silica conservation equation. This sink term is calculated using the silica particle velocity given by Eqn. (1). The species conservation equations are:

$$\rho u_i \frac{\partial Y_{sc}}{\partial x_i} = \frac{\partial}{\partial x_i}\left(\rho D_{sc} \frac{\partial Y_{sc}}{\partial x_i}\right) - r_{sc} \qquad (5)$$

$$\rho u_i \frac{\partial Y_{so}}{\partial x_i} = \frac{\partial}{\partial x_i}\left(\rho D_{so} \frac{\partial Y_{so}}{\partial x_i}\right) - \frac{\partial}{\partial x_i}\left(\rho Y_{so} V_{th}\right) + r_{so}\left(\frac{M_{so}}{M_{sc}}\right) \qquad (6)$$

$$\rho u_i \frac{\partial Y_{cl}}{\partial x_i} = \frac{\partial}{\partial x_i}\left(\rho D_{cl} \frac{\partial Y_{cl}}{\partial x_i}\right) \qquad (7)$$

where r_{sc} is the first-order reaction rate. The subscripts sc, so and cl refer to the silicon chloride, oxide and chlorine, respectively. The reaction rate is computed as:

$$r_{sc} = \rho \, Y_{sc} \, k_0 \exp(-E_a/RT) \qquad (8)$$

The mass fraction of oxygen is calculated from the following expression:

$$Y_o = 1 - (Y_{sc} + Y_{so} + Y_{cl}) \qquad (9)$$

For the conditions encountered in the present MCVD process, the flow is laminar. A parabolic velocity profile is given at the inlet and the walls are treated as no-slip boundaries. The heat flux due to the moving torch is expressed as:[5]

$$q = q_{max} \exp(-\lambda^2(x - x_{torch})^2) \qquad (10)$$

where x_{torch} is the torch location at a particular time. So, the heat flux decreases exponentially both upstream and downstream of the torch. The radiative dissipation from the tube walls is simulated using the band-approximation.[5,6]

A quasi-steady analysis, as suggested by Choi, et al.[4], is carried out. Here, the simulation is carried out in the reference frame attached to the torch. The repeated sweeps of the torch are taken into account by the two-torch model.

The properties of the fluid are mass-weighted averages of the properties of the individual gases and are temperature-dependent.[7,8] The properties of the quartz tube are also temperature-dependent. The radiation in the solid is modeled using an effective thermal conductivity for the quartz:

$$k_{effective} = k_{solid} + \frac{16n^2 \sigma T^3}{3\alpha} \qquad (11)$$

The deposition efficiency of the silica particles is defined as the mass fraction of the silicon chloride entering the tube that is deposited as silica particles. Mathematically, this is:

$$E(x) = 1 - \left(\frac{\int_0^R (\rho u Y_{sc}) r dr + \int_0^R \rho u Y_{so} r dr \frac{M_{sc}}{M_{so}}}{\int_0^R (\rho u Y_{sc} r dr)_{x=0}}\right) \qquad (12)$$

SOLUTION PROCEDURE

The model as described in the previous section was solved using the latest version of the general purpose commercial computational fluid dynamics program FLUENT 5. A detailed description of the numerical method and several validation studies of this software are given by Mathur and Murthy.[9]

A computational mesh encompassing the silica tube wall and gas space inside was created – the governing equations described earlier are solved in each of the resulting control volumes or cells. The typical mesh consisted of 800 by 13 cells. Calculation time on a typical engineering workstation computer was around three hours for the quasi-steady case.

RESULTS AND DISCUSSION

The silica species mass fraction and fluid velocity plots from a quasi-steady simulation in the region near the torch are shown in Fig. 2. The high temperature near the torch initiates the reaction and silica particles are formed. The parabolic velocity profile before the torch is disturbed near the torch region because of the large change in gas density that occurs due to heating. More of the flow is displaced towards the centerline resulting in a higher velocity there.

The temperature profiles on the outer wall of the tube predicted by the quasi-steady simulation are shown in the Fig. 3. The maximum calculated temperature is 2052 K. The experimental results of Cho and Choi[3] are also shown for comparison. The computed temperature field compares well with the experimental measurements both for the regions close to, and farther away from, the torch.
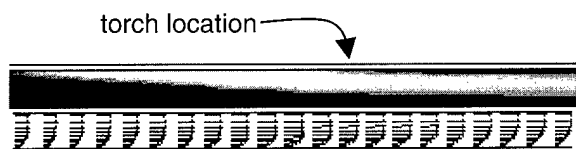
Fig. 2 Silica mass fraction contours (top) and velocity vectors (bottom) near the torch. The mass fraction range is (0, 0.21) and velocity range is (0.017, 1.55 m/s).
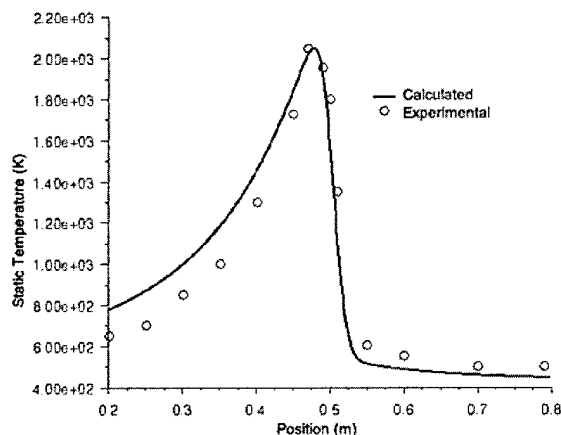
Fig. 3 Comparison of calculated wall temperatures with the experimental data (V_{torch} = 20 cm/min, inlet gas velocity = 0.187 m/s)

The temperature profiles from the unsteady simulation at a few instances in time are shown in Fig. 4. The temperature profiles from the unsteady simulation are very similar to the one from the quasi-steady case. So, for many practical applications, the quasi-steady simulation is

sufficient to obtain insight into the flow, temperature and species fields. The temperature drops to a minimum value ahead of the torch before rising again due to the effect of the previous sweep of the torch. The formation of the relatively cold region ahead of the torch is a favorable condition for the MCVD process. Thermophoresis forces the newly formed silica particles from the reaction zone to this relatively cold zone where they are deposited. The deposited particles consolidate into a thin glassy layer by the sintering process as the torch traverses. Most of the deposition occurs in the cold region.
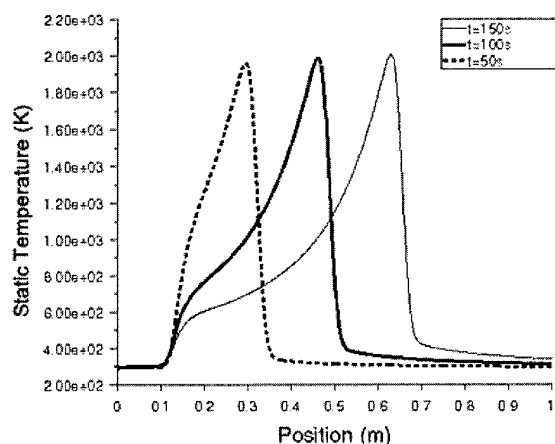
Fig. 4 Temperature profiles at several times from the unsteady simulation. The torch traverses one sweep in 225 s
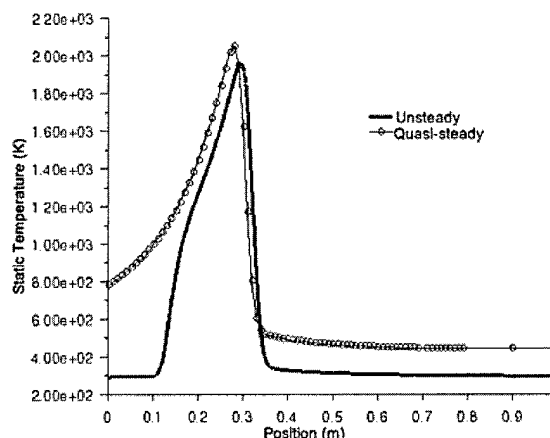
Fig. 5 Comparison of wall temperatures when the torch is near the inlet

The only difference between the quasi-steady and unsteady cases is noticed when the torch is near the inlet. Fig. 5 compares the temperature profiles from the unsteady case when the torch is near the inlet (time = 50

s) with those obtained in the quasi-steady case. The quasi-steady case predicts higher temperatures when the torch is near the inlet. Near the inlet, the gases do not heat up before entering the reaction zone in the unsteady analysis, compared to the times when the torch is away from the inlet (in that case, the gases travel through the hot regions before entering the reaction zone. This is implicitly assumed in the quasi-steady case). The unsteady simulation takes the entrance effects into account and predicts the temperatures more accurately.

Fig. 6 shows the deposition efficiency of the silica particles as a function of axial distance from the torch. Again, the agreement between the model result and experimental data is very good. Most of the particle deposition occurs within a distance of 0.3 m downstream of the torch.
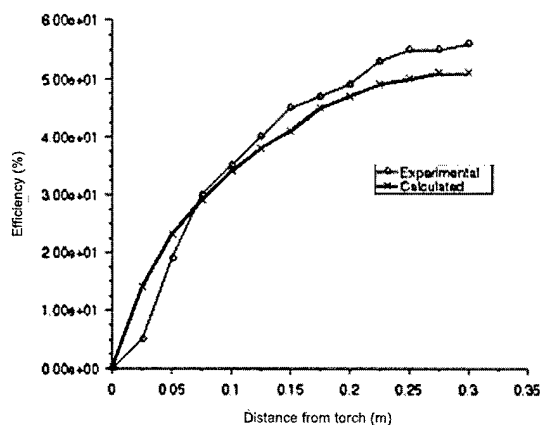
Fig. 6 Comparison of the calculated deposition efficiency with the experimental values. The experimental efficiency is 55.8% while the calculated value is 51%
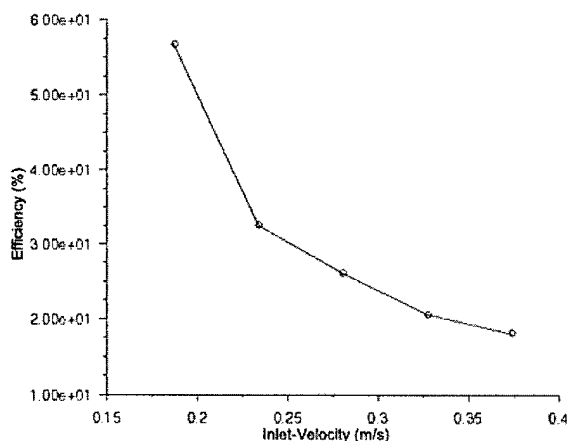
Fig. 7 Variation of silica particle deposition efficiency with the flow rate of inlet gases

The variation of the deposition efficiency with the flow rate of the inlet gases is depicted in Fig. 7. The deposition efficiency decreases as the inlet velocity is increased. The decrease in efficiency is due to two factors:

• The silica particles formed in the reaction zone are carried away axially with higher velocity when the flow rate is increased. So, the convective transport dominates over thermophoretic transport. This is unfavorable for deposition.
• As the flow rate is increased, the residence time of the gases in the tube decreases. This results in less reaction and hence lower amounts of silica being formed.

CONCLUSIONS

In this paper, a model is developed for the computer simulation of the MCVD process. The governing equations for fluid flow, heat and mass transfer are solved using a commercial CFD program and the results are validated against published experimental data. Because the silica tube wall temperatures are computed based on the torch heat input, the present model has a distinct advantage over previous studies where the wall temperatures were specified *a priori*. The model has been implemented in a very general form that allows process parameters to be easily modified. Thus the model can be used to quickly determine the effect of process changes (such as inlet flow rate, torch speed, inlet concentrations, torch heating profile and repeated sweeps of the torch) on the temperature field and particle deposition efficiency.

NOMENCLATURE

C_p = specific heat at constant of the gas
D = diffusion coefficients of the individual species in the mixture
E = deposition efficiency
E_a = activation energy
ΔH = reaction enthalpy
K_{th} = thermophoretic coefficient
k = thermal conductivity
M_i = molecular weight of species i
n = refractive index of quartz
p = pressure
q_{max} = maximum heat flux of the torch
R = Universal gas constant
r = reaction rate
t = time
T = temperature
u = axial velocity
v = radial velocity
V_{th} = thermophoretic velocity
x = axial coordinate
y = radial coordinate

Y_I = mass-fraction of the species i

$\propto$ = Rosseland mean absorption coefficient

λ = coefficient of heat flux distribution

τ = stress tensor

ν = kinematic viscosity

σ = Stefan-Boltzmann constant

The subscripts sc, so, o and cl refer to the corresponding values for $SiCl_4$, SiO_2, O_2 and Cl_2, respectively.

REFERENCES

1. Kim, K. S., and Pratsinis, S. E., 1988, "Manufacture of Optical Waveguide Preforms by Modified Chemical Vapor Deposition," *AIChE Journal*, Vol. 34

2. Walker, K. L., Geyling, F. T., and Nagel, S. R., 1980, "Thermophoretic Deposition of Small Particles in the Modified Chemical Vapor Deposition (MCVD) Process," *Journal of American Ceramic Society*, Vol. 63

3. Cho, J., and Choi, M., 1995, "An Experimental Study of Heat Transfer and Particle Deposition for Modified Chemical Vapor Deposition," *ASME Journal of Heat Transfer*, Vol. 117

4. Choi, M., Park, K. S., and Cho, J., 1995, "Modeling of Chemical Vapor Deposition for Optical Fiber Manufacture," *Optical and Quantum Electronics*, Vol. 27

5. Park, K. S., and Choi, M., 1994, "Analysis of Unsteady Heat and Mass Transfer during the Modified Chemical Vapor Deposition Process," *Journal of Heat Transfer*.

6. Siegel, R., and Howell, J. R., 1992, *Thermal Radiation Heat Transfer*, Hemisphere, Washington, DC

7. Weast, R. C., and Arstle, M. J., 1981, *CRC Handbook of Chemistry and Physics*, CRC Press, Boca Raton, FL

8. Perry, R. H., and Green, D., 1973, *Perry's Chemical Engineer's Handbook,* McGraw-Hill International Edition

9. Mathur, S. R., and Murthy, J. Y., 1997, "A Pressure Based Method for Unstructured Meshes", *Numerical Heat Transfer*, Vol. 31

Muralidharan received his B.Tech. degree in Chemical Engineering from the Indian Institute of Technology, Madras, India, in July 1997. He has worked for Fluent Inc. since then, specializing in the modeling of optical glass fiber and other materials processing applications.

Fluent Inc.
10 Cavendish Court
Lebanon, NH 03766 USA
(603) 643-2600

In-Situ Measurement of Primary Coating Modulus on Optical Fiber by Pull-Out-Modulus Technique

Tetsuo Katsuta, Hirofumi Uchida, Yuji Naito, Zen Komiya, Takashi Ukachi

JSR Corporation Tsukuba Research Laboratories

Tsukuba, Ibaraki, Japan

+81-298-56-1218 · tetsuo_katsuta@jsr.co.jp

Abstract

A direct measurement method of primary coating modulus on an optical fiber was developed. The glass of the coated fiber was pulled at constant speed and the resultant stress was measured. For accurate measurement, a new equipment was designed and manufactured. The share stress was converted to Young's modulus to evaluate the cure degree of the coating. It was confirmed that the measurements were carried out in elastic region. The specimen showed no hysteresis. Relaxation during the measurement was confirmed to be negligible. By using this new equipment, some sample fibers were evaluated. It revealed that the primary coating has an optimum curing condition to achieve the highest cure degree. Comparing to other methods to evaluate cure degree of the primary coating, such as gel fraction or IR technique, the pull-out-modulus provides more direct information relating to performance as an optical fiber.

Keywords

Optical fiber; primary coating; UV cure; pull-out-modulus; in-situ; Young's modulus.

1. Introduction

UV curable polyurethane acrylates have been used as protective coatings of the optical fiber. Recent high demand for optical fiber is driving the drawing speed faster. UV curable coatings need to be cured constantly at elevated drawing speed. To secure satisfactory cure of the coating, several methods to evaluate the cure degree of the coatings have been employed. Gel fraction of the coating layer is one method. However, because the separation of primary and secondary layers is difficult, the gel fraction represents combined cure degree of the two layers. Microscopic attenuated total reflection infra red (ATR-IR) spectroscopy provides direct measurement of IR spectra of primary and secondary layers. Since the IR spectra indicate the consumption of acrylic double bond, it is not a direct indication of physical properties of each layer as a protective coating. Modulus of the secondary coating can be measured by preparing "macaroni" sample or scraping off the coating layer without removing primary layer [1]. Because the modulus of the primary layer is smaller in two orders of magnitude than the secondary layer, the contribution of the primary layer can be neglected. Several direct measurement methods for primary coating modulus have been suggested. The first report by C. R. Taylor appeared in 1985 [2]. It described a measuring method by pulling out the glass from a cramped coated fiber. Thus it is called "pull-out-modulus test". Following the Taylor report, we developed a new method to measure viscoelastic properties of coating on optical glass fiber using torsion pendulum method [3]. This method also enables us to measure properties of coatings on fiber directly. However, the obtained data were a combination of primary and secondary coatings. In 1994, K. Oishi reported "push-in-modulus test" saying that it is easier to prepare test samples than "pull-out-modulus test" [4]. K. Mitsuhashi filed a patent claiming an accurate method for measuring "pull-out-modulus" by using a certain equipment [5]. Unfortunately, regarding pull-out-modulus measurement method, non of these reports described details of the measuring equipment nor accuracy of the data. In this paper, we describe a design of newly developed "pull-out-modulus" tensile machine and some results obtained by using this machine.

2. Experiments
2.1 Preparation of "Pull-Out-Modulus" Tensile Machine

Design and fabrication of "pull-out-modulus" tensile machine will be discussed in the results and discussion section.

2.2 Preparation of Coated Optical Fiber

Doubly coated optical fiber was prepared using conventional primary and secondary coating and a drawing tower. Representative characteristics of the coatings are summarized in Table 1.

The glass diameter was 125 μm. The thicknesses of the primary and secondary layers were 35 and 25 μm respectively. The diameter of the resultant coated fiber was about 250 μm. The drawing speed was changed from 100 m/min to 500 m/min in a 100 m/min step. The application and curing of the coatings were done by tandem manner. One 6 kW UV lamp for each coating was used. The input power of the UV lamp for primary coating was varied to 35 % or 100 % input. The input power of the lamp for the secondary coating was kept 35 % throughout the experiments.

2.2 Evaluation of Coated Fiber

Young's modulus of the primary layer on the fiber was measured by using "pull-out-modulus" tensile machine described in the following section.

Gel fraction of the coated fiber was measured by using methyl ethyl ketone (MEK) as solvent. The coated fiber was extracted with boiling MEK using Soxhlet apparatus for 12 hours. The resultant

fiber was dried under vacuum and then conditioned. Weight change after the extraction was recorded. The fiber was burned in a furnace to remove the coating layer. The weight of the remaining glass was measured to calculate the gel fraction of the coating layer. Gel fraction of primary layer on the fiber was assumed by subtracting secondary gel fraction obtained by single coating experiments under the same drawing conditions from the gel fraction of the whole coating layers of the fiber.

Consumption of acrylic double bond was measured by microscopic ATR-IR. By scraping off the coating layer from the fiber, the surface of the primary layer was put on a Zn-Se prism. Decrease of IR absorption peak at 810 cm^{-1} assigned to terminal hydrogen on acrylic double bond was measured as adjacent 780 cm^{-1} peak as an internal standard. The peak ratio of unreaced primary coating was defined as 0 % cure. Complete consumption of acrylic double bond (100 % cure) was defined as no peak at 810 cm^{-1}.

Table 1. Properties of primary and secondary coatings

	Primary coating	Secondary coating
Liquid*		
Viscosity (Pa •s)	3.4	3.8
Density (g/cm³)	1.04	1.10
Cured**		
Young's modulus (MPa)	1.2	840
Tensile strength (MPa)	3.0	40
Tensile elongation(%)	200	55
Water absorption (%)	1.5	2.6

* Viscosity and density were measured at 25 C.

** Properties of cured film were measured at 23 C.

3. Results and Discussion

3.1 Development of "Pull-Out-Modulus" Tensile Machine

The picture and schematic drawing of the tensile machine for "pull-out-modulus" is given in Figure 1. The machine has a

micrometer screw to control the movement of the hook. Slow and precise movement of the hook is realized by a motor with a reduction gear head and the micrometer screw, that are connected through timing belts. These hooks are designed to avoid cramping of a specimen different from conventional tensile machines, which sometimes results in break of fiber. The upper hook simply hang the specimen and the lower one pulls it without fixation. By hanging the specimen, it is easy to put a fiber specimen precisely vertical, which is often difficult by cramping.

A specimen is prepared as shown in Figure 2. Two metallic cylinders, which have a hole with 0.26 or 0.28 mm diameter in their center are put on the both ends of a coated fiber with 10 mm distance. The fiber is fixed by a minimum amount of cyanoacrylate adhesive to the cylinder. The coating layer is cut at the surface of each cylinder by using a razor. This specimen is put on the hooks. Since the surface of each end of the cylinder and hooks are prepared to have accurately right angle, the fiber is suspended vertically.

Actual displacement is around 20 μm and load range is around 10 g. Displacement rate (3 μm/min) was adjusted to be similar to that of Young's modulus measurement of cured film (1 mm/min for 25 mm sample length). It takes about three minutes to pull out 20 μm, which corresponds to 45 % deformation. Modulus of the primary coating is calculated according to the formula shown as equation (1). By using this new machine some samples were measured. An example of stress and strain curve (S-S curve) chart is shown in Figure 3. In the range of 10 ~ 20 μm displacement, S-S response gave linear relationship. When the specimen was left at constant displacement in the midst of the measurement for about one minutes, the load did not change, which indicates that there is no slipping, no plasticization by adhesive, and no obvious relaxation in this time scale. To confirm there is no adverse effect from the adhesive, a fiber specimens prepared by metallic cylinders with wider hole (0.28 mm) and smaller hole (0.26 mm) were compared. The modulus obtained did not change by the width of the cylinder hole. Hysteresis was also evaluated. S-S lines for pulling out and the return at the same rate had the same slope, which again confirmed the measurement is in elastic range.

$$E = \frac{(1 + n) \, W}{\pi LZ} \, \ln(D_p/D_f)$$

(1)

E: Young's modulus   n: Poison's ratio   W: Load
L: Length of metallic pipe   Z: Displacment of glass fiber
Dp: Diameter of primary coating layer   Df: Diameter of glass fiber
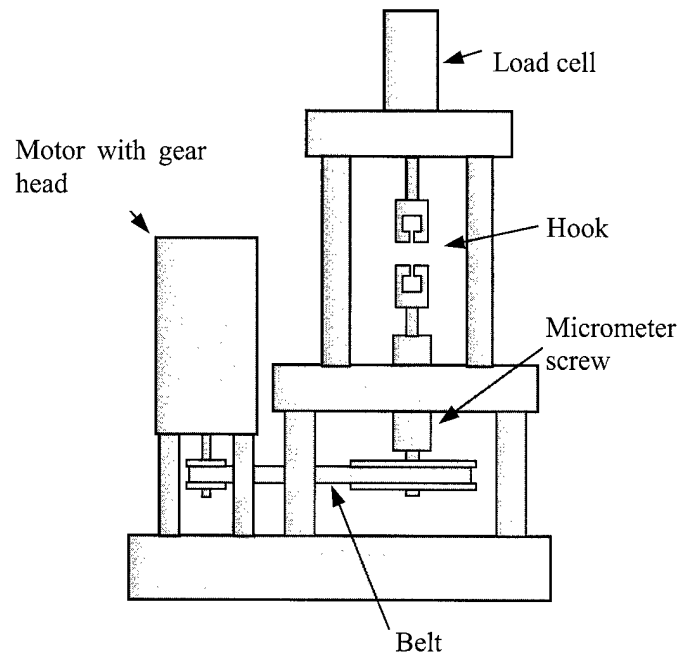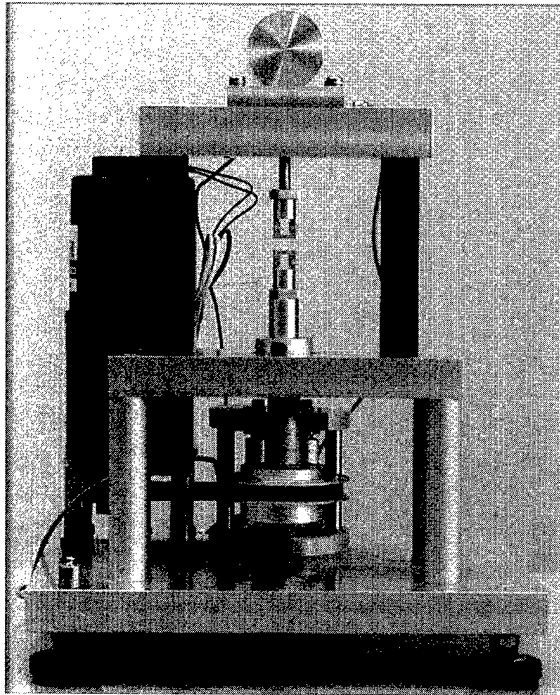
Figure 1. Picture and schematic drawing of "pull-out-modulus" tensile machine.
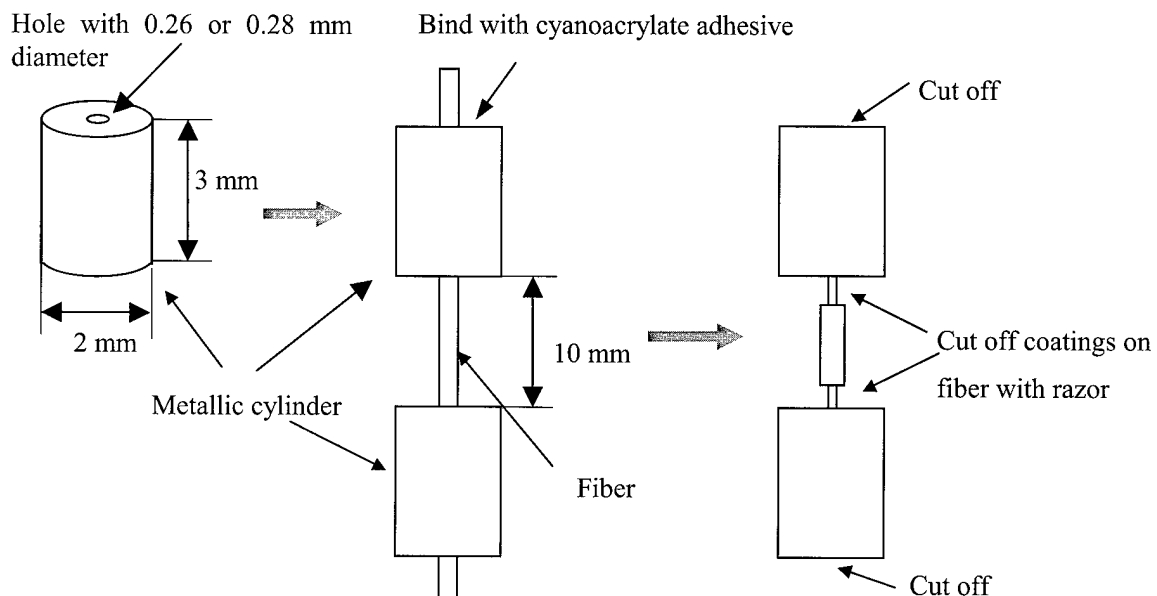
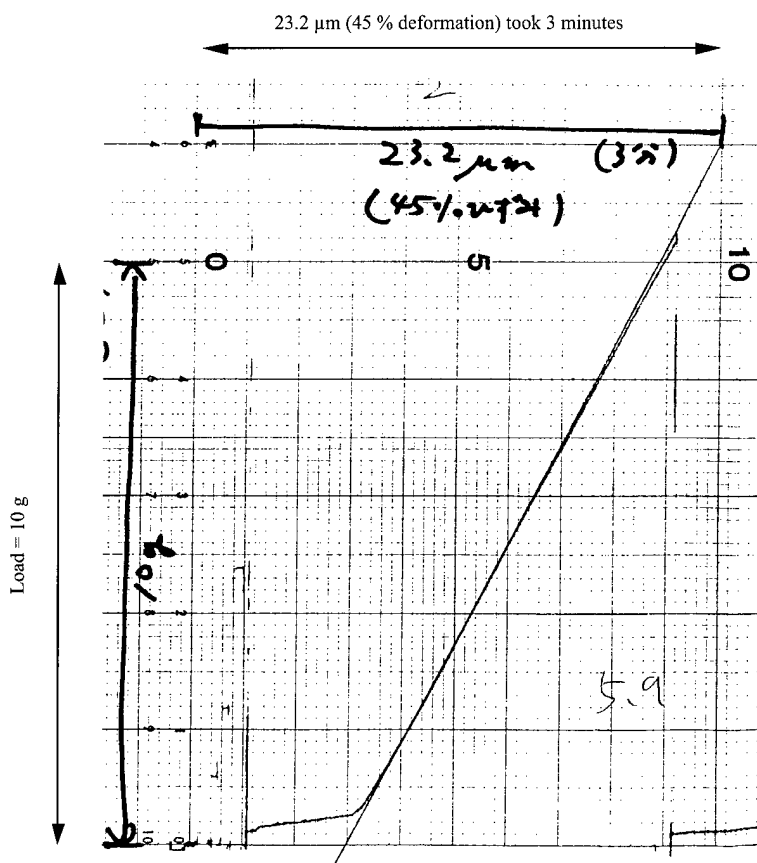**Figure 2. Preparation of a fiber specimen for measurement of "pull-out-modulus".**

23.2 µm (45 % deformation) took 3 minutes

Figure 3. An example of S-S curve chart. Displacement was 23.2 µm and load was around 10 g. It took 3 minutes to "pull-out" the glass.

3.2 "Pull-Out-Modulus" and Gel Fraction of Primary Coating on Optical Fiber

Figure 4 includes plots of pull-out-modulus and gel fraction of the primary layer on fiber against drawing speed. When the input power of the UV lamp for primary coating was set 35 %, gel fraction started decreasing at around 200 m/min of drawing speed. Whereas the pull-out-modulus of the primary layer on the fiber seemed to have maximum value at 200 m/min of drawing speed.

When the UV lamp power was increased to 100 %, the values of the gel fraction and modulus decreased at slower drawing speed. However, the gel fraction and modulus gradually increased as the increase of the drawing speed and reached maximum value at 300 ~400 m/min of draw speed. At faster drawing speed range, primary coating cured with 100 % input power indicated higher gel fraction and higher Young's modulus than those cured with 35 % input power. This behavior is in good accordance with the results we reported in the previous IWCS [6]. Namely, the increase of UV lamp power for primary coating does not simply increase the cure

degree but shows optimum points. In this case, drawing speeds at 200 m/min for 35 % input and 400 m/min for 100 % input are considered to be the optimum points.

3.3 "Pull-Out-Modulus" and ATR-IR of Primary Coating on Optical Fber

The ATR-IR spectra of the primary coatings on the fiber were measured. The consumption of acrylic double bond was calculated and listed in Table 2 along with the pull-out-modulus data. Figure 5 shows the relationship between pull-out-modulus and the ATR-IR data. It is interesting that the relationships are different when the primary coating was cured by 35 % input power lamp or 100 % power lamp. The primary coating cured by 35 % input power reaches higher modulus at the same consumption of acrylic double bond, and hence it reaches higher modulus at high double bond consumption. This observation suggests that the formation of urethane acrylate network is affected by the intensity of the UV lamp. This result is again in good accordance with our previous observation [6].
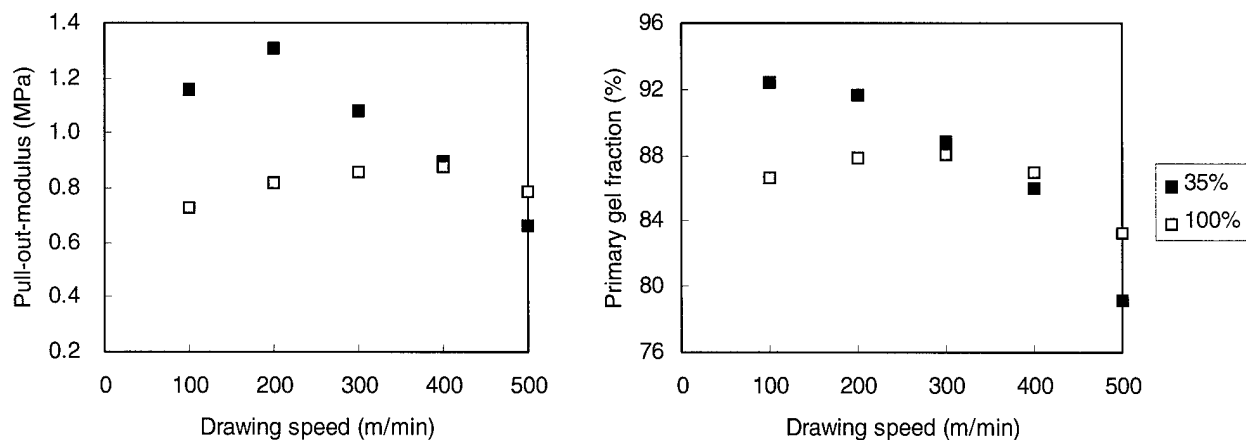
Figure 4. Pull-out modulus and gel fraction of primary coating layer at 35 % and 100 % input power of UV lamp for primary coating.

Table 2. Pull-out-modulus and acrylic double bond consumption measured by ATR-IR

	Pull-out-modulus (MPa)		Consumption of acrylic double bond (%)	
	UV lamp power		UV lamp power	
Drawing speed (m/min)	35 % (6 kW)	100 % (6 kW)	35 % (6 kW)	100 % (6 kW)
100	1.16	0.74	99	95
200	1.31	0.83	98	95
300	1.08	0.87	91	93
400	0.90	0.77	88	90
500	0.66	0.70	81	85
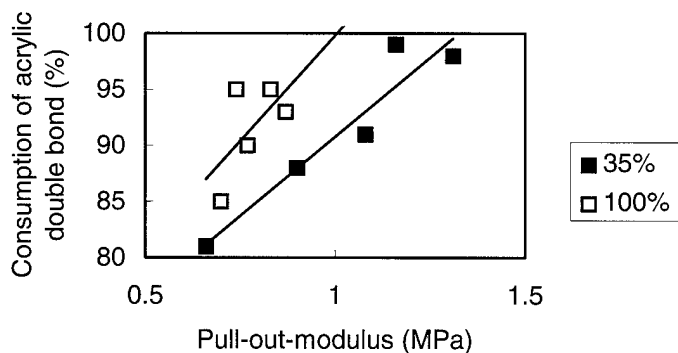
Figure 5. Relationship between pull-out-modulus and consumption of acrylic double bond measured by ATR-IR.

4. Conclusions

We have developed a new method to evaluate the modulus of the primary coating on the fiber directly. It was confirmed that the measurements were carried out in elastic region and relaxation during measurement was negligible. By using the new method, several optical fibers prepared at different drawing speed and UV lamp power for primary coating were evaluated.

Dependence of the pull-out-modulus of the primary coating showed maximum values against drawing speed indicating the presence of optimum curing condition for primary coating.

Comparison was made with other methods to evaluate the cure degree of primary coating.

Gel fraction showed good correlation with pull-out-modulus, although the gel fraction of the primary coating was tedious to obtain because the gel fraction of the secondary coating needs to be measured in separate experiments to subtract it from the gel fraction of primary and secondary combined layers.

Acrylic double bond consumption data by ATR-IR were also compared with pull-out-modulus data. The modulus data and IR data were not in a complete one-by-one correlation. The relationship was affected by the power of UV lamp for primary coating. These results indicate that the cure behavior of the primary coating is affected not only by drawing speed but intensity of the UV light. Therefore, ATR-IR method should not be used as a sole analytical method to evaluate the cure behavior of the primary coating.

5. References

[1] T. Ukachi, A. Aoyama, Y. Naito, K. Igarashi, *Proceedings of 41st IWCS*, page 261, 1992.

[2] C. R. Taylor, "In situ mechanical measurements of optical fiber coatings", *Meeting Digest of OFC '85*, page 20, 1985.

[3] K. Igarashi, Y. Naito, C. Tosaki, Y. Matsumura. *OFC/IOOC '89 Technical Digest, TUQ9*, 1987.

[4] K. Oishi, N. Akasaka, T. Hattori, *Proceedings of 43rd IWCS*, page 553, 1994.

[5] JP H0742169.

[6] J. Yoshizawa, Y. Naito, H. Takase, Z. Komiya, T. Ukachi, *Proceedings of 48th IWCS*, page 680, 1999.
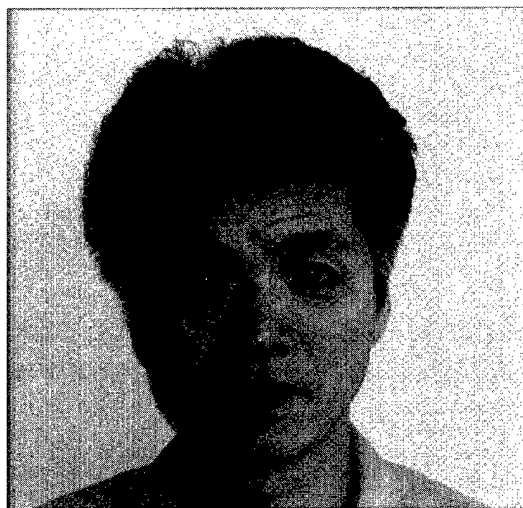
Tetsuo Katsuta
Tsukuba Research Laboratories
JSR Corporation
25 Miyukigaoka Tsukuba, 305-0841 Japan

Testuo Katsuta graduated from Industrial Chemical course of Chemical Industry High School in Tokyo in 1970 and joined JSR Corporation. He has been engaged in research and development work of surface morphology analysis technique by mainly using electron microscopy. He is now a chief engineer of radiation curable materials group.

Development of a High Lightning-Resistant Optical Ground Wire (OPGW)

Edvaldo C. Mendes, Marco A. Scocco

Pirelli Cabos S.A.
Sorocaba, SP, Brazil
+55-15-225-1616 · edvaldo.mendes@pirelli.com.br, marco.scocco@pirelli.com.br

Maria G. Alvim, Mauro A. Gomes, Armando I. Nigri, Afonso O. Silva, Claudia F. Oliveira

Furnas Centrais Elétricas S.A.
Rio de Janeiro, RJ, Brazil
+55-21-528-4602 · alvimmg@furnas.com.br, mauroag@furnas.com.br, cmfo@furnas.com.br

Abstract

This paper presents the development of a high lightning-resistant OPGW cable in partnership with Furnas Centrais Elétricas, one of the most important Brazilian Energy Utilities. The main goal of this work was to design a cable that withstand the harmful effect of the long duration stroke known as the continuity component of the natural lightning current, at high protection level.

The use of high class galvanized steel wires and aluminum tube protection of the optical core, with a low increase in weight and diameter of the cable, lead this OPGW cable to be an enhanced lightning-resistant and cost-effective solution, when compared with other design alternatives.

Other aspects involved in developing the OPGW cable as lightning arc test methodology, maintenance criteria and field evaluation are also discussed.

Keywords

Optical fibers; ground wire; overhead line; OPGW; lightning strike.

1. Introduction

Ground wire cables are typically suspended between the spaced-apart support towers and above the base electrical conductors of the power transmission network to protect from the high current and voltage surges presented by direct or near-by lightning strikes.

In these electric power transmission lines each time more comes being applied composite overhead ground wires with optical fibers known as OPGW that, besides the specific function of protection of the power lines, have to provide an optical media, through the inward use of optical fibers. It should not be taken for granted that fiber optic cables will be trouble free on high voltage overhead lines.

The maintenance of the integrity of ground wires (GW/OPGW) endangered by the occurrence of environmental phenomena as lightning strikes is one of the basic aspects for reliability of the system and one important design parameter. In the case of OPGW, this aspect is more critical because the cable can transport a high digital bit-rate of a telecommunication network.

With the great expansion of the use of OPGW in overhead transmission lines in the last years in Brazil, thousands of kilometers of cables had been installed in all the regions of the country.

However, exposed to the most diverse keraulic levels (isokeraulic level: annual total days on which lightning occurs) of tropical or equatorial climate environments, these OPGW cables had suffered severe damages due to atmospheric strokes.

This paper describes the development stages of an enhanced lightning-resistant and cost-effective solution of OPGW cables, when compared with other design alternatives.

Results of OPGW performance for other type tests are presented, as well as the lightning arc tests performed at Cepel Electrical Energy Research Center - Rio de Janeiro/Brazil.

2. Lightning on OPGW
2.1 Lightning Phenomena

Several studies have been made in order to evaluate the damage levels on OPGW cables due to lightning strikes. Basically, natural lightning currents typically have different components:

- A first stroke of positive or negative polarity.

- Subsequent strokes of negative polarity.

- A continuing current (long duration stroke) of positive or negative polarity.

Of the different components of a lightning flash only the first return stroke and the continuing current contain remarkable charges. From laboratory experiments it is well known that the impulse currents of first return strokes do not cause severe damage to metal surface, when striking an OPGW [1].

Severe damages of the wire outer layer and even of optical fibers inside an inner tube may only be caused by long duration strokes. The total charge of a long duration stroke, having a long duration pulse length of about 0.1 s to 1 s, is the decisive quantity because it determines the melting energy flux at the striking point on the wires surface [2].

These continuing currents constitute a severe threat to OPGW, where also the second layer of strands may suffer damage.

The investigations performed showed that the overall damage of a ground wire depends closely with:

- Wire diameter of the strand.

- Wire material.

- Degree on the tensile force applied to the wire.

- Protection level (charge) desired to the cable.

These considerations are very important to select suitable armoring materials for the OPGW cable to withstand high lightning protection levels.

2.2 Test Methodology

As lightning arc tests were not considered by the current OPGW Brazilian Specification [3] this matter leaded the electric energy utilities to revise drastically their cable acceptance criteria, also forming a working group at Brazilian Standard Commission (ABNT) for evaluation of the phenomena and to review the Specification.

During the last year the ABNT Commission conducted a large number of continuing current tests on a variety of ground wires (conventional and optical) and have successfully improved the test techniques to best simulate in laboratory the effects of natural lightning. The developed test methodology [4] and acceptance criteria have been developed as summarized in the following.

2.2.1 Test Set-up [4]

The tests shall be performed on the mid-point of a sample of OPGW not less than 10 m long.

An iron rod shall be used as the electrode which shall be positioned above the OPGW. The electrode and OPGW shall be connected by a copper fuse wire. The distance between the electrode and OPGW shall be of 6 cm. The applied tensile load on the sample OPGW shall be 15% of RTS (rated tensile strength).

The lightning simulation tests (five times) are carried out on the same OPGW sample, but not at the same place on the OPGW. The level of the continuing current, which depends on the desired level protection, shall be applied during 0.5 s (pulse length).

After each current application the cable shall be tensioned until a predicted test limit load. This test limit load is the maximum allowable tension (maximum tension under expected worst case loading conditions) multiplied by a specified safety factor (usually between 1 and 3).

2.2.2 Acceptance Criteria

On completion of the test, the following acceptance criteria shall be considered:

- Damages in structural or protection elements that expose the optical unit or optical fibers to environmental agents (e.g. moisture) or affect the good performance of the optical fibers shall constitute a failure.

- Any permanent or temporary variation in optical attenuation, up to the maximum allowable tension, greater than the specified value (0.1 dB) shall constitute a failure.

- The cable shall withstand the test limit load by 3 minutes.

3. Cable Development

3.1 Furnas Requirements

Furnas required a 24 SM optical fibers OPGW cable for a 750 kV Transmission Line, with the total length of 273 km, between the cities of Ivaiporã and Itaberá, Paraná State, Brazil.

As this type of cable requires an extremely high reliability due to the complicated repair conditions, Furnas established a severe acceptance criteria for the lightning arc test: no broken armor wires occurrence are allowed due to the effect of lightning at the higher level protection (charge of 200 C). This condition provides the almost absence of repairing intervention.

3.2 Study on Armor Wire Materials

Usually, the armoring wires of OPGW cables are made of aluminum-clad steel, aluminum alloy or a mixed of them, mainly due their contribution to the short circuit capacity of the cable. However, laboratory tests showed that these materials are not likely to support high levels of lightning strikes without significant amount of wires broken. Only an excessive increase in wire diameter of these materials can avoid this effect.

To find a cost-effective solution with a low increase in weight and diameter of the cable, Pirelli and Furnas studied the use of high class galvanized steel wires as armoring layer of OPGW, because this material need much energy to fuse due to lightning strike incidence.

In fact, different to the behavior of aluminum, zinc needs little energy to dissolve. If zinc is clad on the surface of the steel wire, the arc is expected to act on this portion, causing the arc spot to spread widely along the surface of the wire. As a result, the thermal energy will be spread widely and reduced. In addition, thermal energy will be absorbed by vapor when the zinc layer is fused and vaporized [5].

Other important aspect considered was the field evaluation of the conventional ground wires (3/8" EHS) with class A galvanized steel wires (3.09 mm of wires diameter) installed in the same region for more than 15 years. As a result of this study, it was established a positively good long-term performance with respect to corrosiveness and lightning resistance.

Despite of this fact, it was decided to use for the OPGW cable the class B (520 g/m²) of galvanized steel wires to be applied as armor layer.

3.3 Cable Description

The OPGW cable consists basically of a dielectric optical core with loose tube construction, covered by an aluminum tube to provide the desired short-circuit capacity and mechanically protected by the use of one armoring layer of high class galvanized steel wires. A cross section of the cable is illustrated in Figure 1.
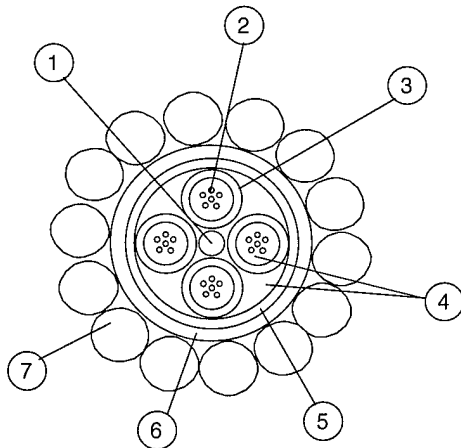

Figure 1. OPGW cable cross section

1) Central strength member

2) Optical fibers - 24 SM

3) Protection tube

4) Filling and flooding compounds

5) Tapes

6) Aluminum tube

7) Armoring (12 x 3.09 mm of high class galvanized steel wires)

The main characteristics of this cable are shown in Table 1:

Table 1. Main characteristics of OPGW cable

Overall diameter	15.5 mm
Unitary weight	8.2 N/m
Metallic section	125.7 mm^2
Linear thermal coefficient	13.3x10^{-6} 1/°C
Modulus of elasticity	132 kN/mm^2
Rated tensile strength	111 kN
Electrical resistance DC @ 20°C	0.539 Ω/km
Short circuit capacity (t=0.3 s; T$_i$=50°C)	70 kA^{2}s

4. Type Tests

4.1 Lightning arc tests

Several prototype tests have been performed at Cepel Electrical Energy Research Center - Rio de Janeiro/Brazil, and showed that galvanized steel wires have higher lightning resistance when compared with aluminum-clad steel and aluminum alloy ones of close diameters [6]. The proposed OPGW withstand successfully 5 tests at the maximum protection level (charge of 200 C = 100 A x 0.5 s) without any armor wire broken.

4.2 Other Type Tests

The following qualification tests were carried out according to Brazilian Standard [1] and Furnas requirements:

- Attenuation.

- Thermal cycling.

- Water penetration.

- Compression.

- Sheave.

- Minimum bending radius.

- Strain margin.

- Cut-off length.

- Aeolian vibration.

- Creep.

The obtained results demonstrate successfully an excellent performance of the proposed OPGW cable with high class galvanized steel wires as armoring.

5. Conclusions

The use of high class galvanized steel wires and aluminum tube protection of the optical core, with a low increase in weight and diameter of the cable, lead this OPGW cable to be an enhanced lightning-resistant and cost-effective solution, when compared with other design alternatives.

6. Acknowledgments

The authors acknowledge the support and permission of Furnas Centrais Elétricas and Pirelli Cabos to elaborate and present this paper.

7. References

[1] W. Zischank and J. Wiesinger, "Damages to Optical Ground Wires caused by Lightning", *10th International Symposium on High Voltage Engineering*, 3 pp. (August, 1997).

[2] M. Böhme and K. Möller, "Arc Motion during Lightning Test of Power Ground Wires with Optical Fibers (OPGW)", *ICLP-98*, 571-575 (1998).

[3] ABNT Standard NBR 14074, "Composite Overhead Ground Wire with Optical Fiber (OPGW) – Specification", under revision.

[4] ABNT Draft 03:086.02-081, "Composite Overhead Ground Wire with Optical Fiber (OPGW) – Lightning Strike Current – Method of Test", to be published.

[5] M. Yokoya at al., "Development of Lightning-resistant Overhead Ground Wire", *IEEE trans. On Power Delivery*, Vol. 9, No. 3, 1517-1523 (1994).

[6] CEPEL Report UNIAP-1008/99 (October, 1999).

Authors

Edvaldo Chaves Mendes (edvaldo.mendes@pirelli.com.br) was born in São Paulo-SP, Brazil in 1960. He received M.Sc. degree in Mechanical Engineering from Federal University of Santa Catarina in 1986 and joined Pirelli Cabos S.A. He has been engaged in development engineering of aerial optical cables and is responsible of Telecommunication Laboratory. He is a member of ABNT Standard Commission of aerial optical cables.

Maria das Graças Alvim (alvimmg@furnas.com.br) of Furnas Centrais Elétricas S.A.

Mauro Argento Gomes (mauroag@furnas.com.br) of Furnas Centrais Elétricas S.A.

Marco Antonio Scocco (marco.scocco@pirelli.com.br) was born in São Paulo-SP, Brazil in 1957. He received B.Sc. degree in Physics from University of São Paulo and M.Sc. in Electronic Engineering of the same University in 1990. He is currently the Telecommunication Engineering Manager of Pirelli Cabos S.A. He is a member of ABNT Standard Commission.

Armando Issac Nigri of Furnas Centrais Elétricas S.A.

Afonso de Oliveira e Silva of Furnas Centrais Elétricas S.A.

Claudia Fernandes de Oliveira (cmfo@furnas.com.br) of Furnas Centrais Elétricas S.A.

Lifetime Prediction of ADSS-Cables in High Voltage Lines

Reinhard Engel, Sabine Will
Corning Cable Systems, RD&E
96465 Neustadt, Germany

David Wartschinski
Technische Universität Ilmenau, Hochspannungstechnik
98684 Ilmenau, Germany

Abstract

Dielectric aerial cables are normally exposed to a combination of harsh environmental conditions, like humidity, dust, UV-sunlight and extreme temperatures. If they are installed between the support towers of high voltage power lines, surface currents flow on the cable sheath and considerably accelerate the natural cable aging by eroding and puncturing the cable jacket.

A variety of tests have been proposed to check the resistance of the cable sheath for erosion and tracking under combined stresses. These tests compare the properties of different materials or cable designs relative to each other and categorize them into more or less resistant.

In our study a test procedure for ADSS cables in high voltage lines has been developed that accelerates erosion considerably under environmental conditions without leaving the linear electrical aging model. The test results can, therefore, be used to forecast ADSS cable lifetime under given environmental conditions.

Keywords

ADSS; aerial cable; lifetime; lifetime forecast; sheath erosion; high voltage; tracking; dry band arcing.

1. Introduction

The fast completion of existing infrastructures with communication cables for data transmission has developed into a profitable business for power utility companies in the recent years. Driven by the rapid increase of demand for data transmission capacity, all possible manners of installing dielectric optical fiber cables have been utilized. They are lashed to ground wires or are suspended between the towers of overhead power lines under lifeline conditions. By that the telecommunicational meaningless power utility line becomes in addition an important data transmission line with similar high requirements regarding reliability and continuous traffic. In contrast to the high expectations for reliability of operation are the considerable stresses, these cables are exposed to in high voltage lines. Besides natural environmental factors like moisture, pollution, heat, cold and UV-sunlight, the destruction of the cable sheath by electrical surface currents is of great importance.

Most harmful for the long-term function of ADSS cables is the combination of several stress factors like moisture, pollution, strain and surface current. This results in an agressive and destructive effect to the cable sheath, which can cause the early breakdown of an aerial cable line by tearing apart a cable link.

Improved erosion resistant jacket materials and field control elements inside and outside of ADSS cables have resulted in a significant extension of cable lifetime that can be seen by comparing different cables under the same operating conditions. Local controlling in power lines is costly and time consuming and hinders a smooth spreading of ADSS cable applications particularly in high voltage lines with an operation voltage greater than 220 kV. For these lines, ADSS cabling is only occationally accepted due to the danger of strong electrical sheath erosion.

The urgent questions of cable operating companies for the safe operating lifespan can only satisfactory be answered, if there is a fast and reliable forecast, considering cable design and local environmental conditions. For the cable manufacturers, this forecast can be a tool for optimizing ADSS cables to local conditions and to the lifetime expectations of the cable operators.

2. Test Procedure

In the test procedure for determing the lifetime of ADSS cables, the local conditions in the power utility line have to be imitated as realistically as possible for valid results. In addition, the natural sheath erosion has to be accelerated considerably to be of advantage compared to test installations in high voltage lines. The following test conditions have to be considered:

Dry Band Arcing

On the sheath of ADSS cables in high voltage fields a special kind of surface discharges appeare, which often lead to ring-shaped erosion traces. To imitate the natural aging, these surface discharches, called dry band arcing [1], should also in a lifetime test be the dominant factor.

Driven by the voltage gradient along the cable, an electrical current flows on the cable surface from the center of the span toward the

grounded span ends at the towers. On a dry sheath surface the current is negligibly low. Depending on the potential difference it can reach up to a few mA in the vicinity of the tower if the cable surface is wet and polluted (Figure 1). If the surface is continuously wet and conductive, the surface current only generates some Joule heat that accelerates the drying, but does not cause any erosion (A). During evaporation of the water film, dry zones are formed that interrupt the current flow and are therefore bridged by electrical discharges. The discharges appear as small arcs that erode the cable surface by burning small particles (B). Becoming larger in area and number, the dry zones raise the average electrical surface resistance and by that reduce the number (C) and intensity (D) of discharges, until they are finally vanished.
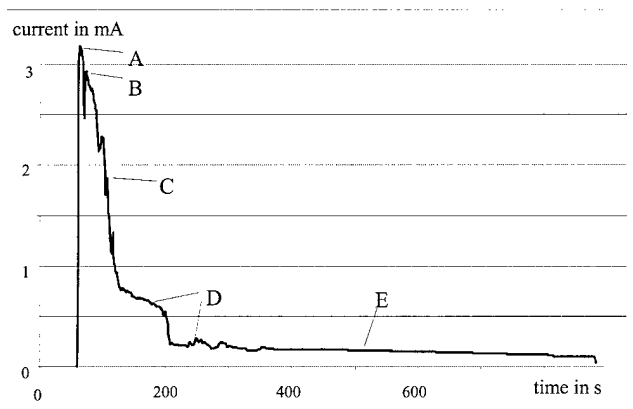
Figure 1. Typical dry band current

The most powerfull discharges with the strongest erosion effect appear during the first minutes of drying. Therefore, for an accelerated erosion during testing, this first phase should be generated as frequently as possible.

As a measure for the resistivity of the jacket material against degradation, the number of drying phases can be counted, which is required for generating clear erosion traces. Our experiments have shown an active electrical phase for up to ten minutes after two minutes of moisturizing the cable surface. Adding a safety margin of three more minutes, we could run a complete wet dry cycle within 15 minutes or 100 cycles per day.

Surface Wetting

ADSS cable sheaths are mainly manufactured from polyethylen whith a water repellent surface. This hyrophobic characteristic prevents the surface from wetting with a continuous waterfilm by forming drops with wide dry zones in between. Therefore, dry band arcing is suppressed on new made aerial cables. After installation, the surface tension is gradually diminished by environmental influences like UV sunlight and pollution, and the probability of surface arcing increases. This time-wasting preparation can be shortened, if a wetting agent and some mineral salt is added to the

water. The wetting agent produces the contiuous water layer and the salt improves the electrical conductivity.

These ingredients additionally enable the simulation of different grades of pollution. In test cycles with only weak moisturing and complete drying, a layer of salt will grow on the cable surface, which simulates the surface effects in dry areas at a high level of dust or sea water spraying. Cycles with intensive wetting represent the conditions in rainy areas, where the cable surface is washed regularly and kept clean most of the year.

Field strength distribution

For the imitation of the real electrical relations in the vicinity of the towers, both the electrical current along the sheath surface and the electrical field strength have to be simulated (Figure 2). The current on the test sample can be increased to the value of a half span length by adding a capacitor C between the high voltage source and the "hot" cable fitting. The level of the electrical space potential and its distribution around the tower fitting are generated in the test arrangement by a high voltage electrode HV.

Installed ADSS cables usually show the strongest erosions close to the tower, where they are attached by grounded clamps or spirals. Within the last millimeters, where the wires of the suspension spiral grip the jacket, the most severe deteriorations take place. Here we find the strongest surface currents and the greatest potential difference in the whole span. In addition, the spiral wire tips can concentrate the field strength to such high levels, that tip discharges may occur and intensify the destroying erosion in this
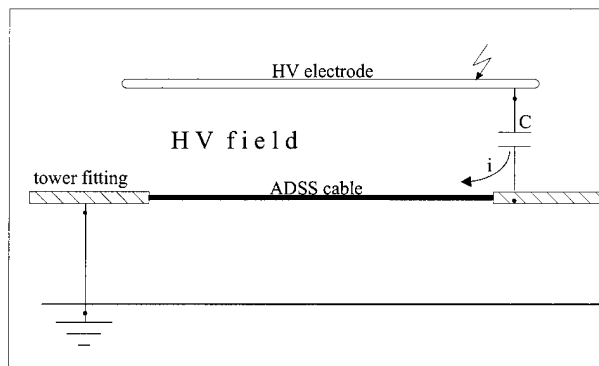
spot [2].

Figure 2. Realistic imitation of electrical field and current

Test voltage

The space potential, which is given by the voltage of the HV-electrode, controls the intensity of the surface discharges. Raising the voltage intensifies the electrical erosion and thus reduces the number of test cycles.

But the voltage level is limited, due to the dimensions and the dielectric strength of the test equipment. And even more important is the fact, that these test results supply the data for a lifetime forecast calculation.

During the test, the same kind of discharges should perform on the ADSS cable as can be seen in the high voltage line. In our experiments, we found that the typical ring-shaped erosion marks are produced at a voltage between 20kV and 40kV. Higher voltages result in accelerated aging. But if the voltage gets too high, effects can be noticed that cannot be seen on installed ADSS cables under normal conditions. These effects are electrical breakdowns along the cable sample, widespread erosions and fast burning of the cable sheath at the beginning of the suspension spiral. They are beyond the linear electrical aging model, diminish the evidence of the results and should be avoided in an ADSS cable lifetime test.

Mechanical Strain

Typically ADSS cables contain a layer of aramid yarns directly under the sheath for taking up the pulling forces of the installed cable under tension. Because of the cables' dead weight, the pulling forces in even lines are highest at the towers and lowest in the center of the span. At the end of the span, the pulling forces have to be transmitted through the cable sheath to the fittings which requires a non-slipping adhesion between the jacket and the aramid layer. In case of oscillations and high wind loads on the cable, there can be some slipping and elongation of the sheath at the cable ends. Already eroded pinholes and tracks can now be enlarged mechanically, accelerating the process of destruction.

For a better lifetime forecast, the mechanical strain has to be considered by applying the maximun allowed mechanical load to the cable sample within the test chamber.

Sample Positioning

On even ground there is a typical slope of about 3° at the span ends of the installed ADSS cable. The slope causes the water to flow toward the span center, facilitating dry zones in the tower area and dry band arcing next to the suspension spirals. This arrangement should also be provided in the test chamber, to be as close to reality as possible.

3. Test chamber

The comlete test arrangement is accommodated in a standard double length steel container and measures 13m x 2.5m x 2.5m (Figure 3). For the variation of the test conditions, the design of the chamber allows of a test voltage of up to 80kV. To prevent electrical breakdowns between the high voltage electrodes E and the grounded surroundings, this voltage cannot be exceeded.

The electrodes are located parallel to the container ceiling and simulate for the cable sample S, the electrical field distribution of the power utility line close to a tower. The required pulling force is applied to the sample by means of a hydraulic cylinder F.
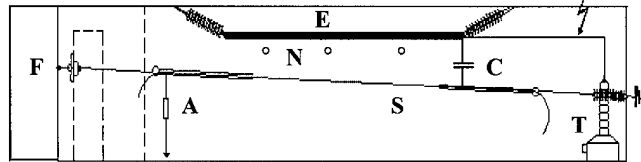
Figure 3. Test chamber

Even the high voltage transformer T and the current meter A are housed inside the container. In contrast to other test arrangements [3,4], there is no need to fill up the whole chamber with salt fog. Only the cable samples are moistured by nozzles N, spraying them directly with a mixture of water, salt and wetting agent. During spraying the high voltage is switched off. After two minutes of spraying, when the cable samples are completely wet, the water is stopped and the voltage is switched on again. Spraying to the samples directly and in cycles considerably reduces the amount of test water. In the following thirteen minutes the drying and dry band arcing takes place, which is very similar to the drying under natural circumstances.

To achieve a normal drying velocity, the container is ventilated and stabilized to room temperature.

4. Lifetime evaluation

Surface discharges with hot spots at the base are the driving force for ADSS cable sheath erosion. They mainly occur when the continuously wetted cable surface starts drying and small dry gaps between wet areas have to be bridged. These tight dry zones are preferably generated after rain falls, but can also be build up by dew or dense fog, especially when the cable surface is polluted. A higher test voltage effects stronger discharges, which generate more thermal energy and accelerate the surface erosion. On the other hand, the hot spots at base become more mobile and move around within a larger area and deminish the critical eroding effect in depth.

Two parameters are mainly responsible for the intensity of erosion of the ADSS cable surface:

- The number and duration of the drying phases per year

- The level of electrical room potential

For the test arrangement described here, all relevant aging conditions within a power utility line have extensivly been considered. The aging is accelerated by a fast sequence of realistic drying phases and by a moderate increase of the test voltage above the space potential in the utility line.

Under natural conditions in the open air, with a continuous line voltage, two erosive phases can be found with every shower of rain

and every dew: the moisturing and the drying phase, which have similar erosion impacts. In our test chamber we only have one erosive phase during drying, as we have to switch off the voltage during moisturing to avoid imprinting the spraying patterns of the nozzles on the cable sheath. To compensate this loss of erosion speed, the test voltage can be increased for faster erosion to a value above the real line space potential. The drying phase in the test now has the same impact to the cable surface as a shower of rain in the high voltage line.

In the test there can be run 100 drying cycles within 24 hours, which gives an acceleration factor of 300 to 500 for dry landscapes. This means that a cable within the test chamber is in one day exposed to the same erosion than within one year in the power utility line. For rainy landscapes with frequent dense fog and dew, the acceleration factor is reduced to values below 100.

5. Conclusions

The lifetime of ADSS cables in power utility lines strongly depends on the electrical space potential, on the local climatic and environmental conditions and -of cause- on the cable design. If the surroundings of the installed ADSS cable are well known, a lifetime forecast for the cable in the respective link can be made by means of the proposed test arrangement.

6. Acknowledgements

7. References

[1] S. M. Rowland, I. V. Nichols, "The effects of dry-band arc current on aging of self-supporting optical cables in high fields," IEE Proc.-Sci. Meas. Technol., 143, pp. 10-14, (1996)

[2] A. J. Peacock, J.G.C. Wheeler, "Development of aerial fibre optic cables for operation on 400 kV power lines," IEE Proc.-A, 139, pp 308-309, (1992)

[3] C. Militaru, "ADSS Cables Electrical Corrosion Tests," International Wire and Cable Proc., pp. 617-619, (1999)

[4] IEEE P1222 Draft , "Standard for All Dielectric Self-Supporting Fiber Optic Cables (ADSS) for Use on Overhead Utility Lines", (1995)
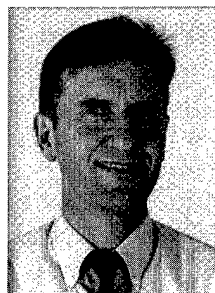
Reinhard M. Engel
Corning Cable Systems
Special Communication Cables
RD&E
Austraße 101
96465 Neustadt
Germany
reinhard.engel@corning.com

Reinhard Engel received his Ph.D. in 1985 from the University of Kaiserslautern. He has been developing optical cables and accessories for 20 years. Presently, he is managing the dielectric aerial cable development activities for Corning Cable Systems in Neustadt.

Sabine M. Will
Corning Cable Systems
Special Communication Cables
RD&E
Austraße 101
96465 Neustadt
Germany
sabine.will@corning.com

Sabine Will joined Siemens AG in 1970 and has been engaged in research and development of materials for copper and optical fiber cables. She is now project leader for dielectric aerial cables at Corning Cable Systems in Neustadt.

David Wartschinski

TU-Ilmenau
Fachgebiet Hochspannungstechnik
Kirchhoffstrasse 1
98684 Ilmenau/ Thür.
Germany

David.Wartschinski@E-Technik.TU-Ilmenau.DE

D. Wartschinsky received his degree as an Diplom-Ingenieur from the Technische Universität Ilmenau in 1993. He has been working since 1994 on several research projects in the High Voltage Engineering department and is now member of a joint research project with Corning Cable Systems on aerial cables lifetime.

Dynamic Menisci in a Pressurized Fiber Applicator

Sravan Ravinutala, Kunal Rattan, Constantine Polymeropoulos
and Yogesh Jaluria
Mechanical and Aerospace Engineering Department Rutgers, The State University of New Jersey
Piscataway, New Jersey
(732) 445-3650 · poly@jove.rutgers.edu

Abstract
The present work describes experimental measurements and numerical simulations relevant to the coating process of optical fibers in pressurized and unpressurized applicators. The experimental work focused on the influence of simulated entrance geometry using micropipettes tubes of different diameters, applicator pressures and fiber speeds on air entrapment and on the shape of the upstream coating meniscus. Computed results include the shape of the flow field, the pressure distribution and effect of tube length.

1. Introduction
Optical fibers require single or multiple layers of protective coating which is applied using a continuous process, where the vertically moving fiber is passed through a suitably designed applicator filled with liquid coating material. Upon entering the applicator, air entrained by the fiber is replaced by the coating liquid in the vicinity of an apparent dynamic contact surface between the air, the liquid and the moving fiber. At the applicator exit the fiber is drawn through a coating die, forming a downstream meniscus as the coating fluid is deposited on the fiber. The liquid coating is then cured before winding onto a drum.

Because of their practical importance, different types of coating processes for photographic film, magnetic tape, wire, etc., have been considered by numerous investigators. References 1 and 2 are reviews that can be consulted for discussion on the subject. Replacement flows with plunging fibers have included measurement of apparent contact angles [3-6], measurement of critical fiber speeds for air entrainment [4,6], air bubble stripping [7], prediction of coating thickness [8], and numerical simulation of the applicator flow field [9,10]. Recent visualization studies have shown that air entrapment by the moving fiber is accompanied by meniscus saw tooth shaped deformations [6] from where air bubbles are ejected by tip streaming from interface cusps near the fiber [11]. Examples of other experimental works on replacement flows appropriate to the present study are those with tapes or with rotating horizontal cylinders partially immersed in a pool of liquid [12-14]. It should be pointed out that air displacement by the wetting liquid depends on molecular interactions at the surface of the solid

substrate, which have not yet been resolved. Results from asymptotic analysis in the limit of small capillary numbers have been in good agreement with measurements of the liquid/air interface shape and the velocity field in the vicinity of a plunging relatively large diameter cylindrical surface [15,16]. However, because of the absence of a predictive general theory, most of the experimental data on the dependence of contact angle, meniscus depth, and incipient air entrainment have been correlated based on dimensionless correlations.

Production draw speeds for optical fiber for telecommunications can be in the range of 20-30 m/sec, exceeding by more than two orders of magnitude the critical air entrainment speed for a fiber plunging into a free liquid surface of coating fluid. Except for information in different coating process patents, the exact procedures used for minimizing the appearance of air bubbles in the final fiber coating are not well publicized. Fiber coating applicators are, however, operated at elevated pressures where the coating fluid is forced into the entrance die, forming a meniscus within the clearance region between the moving fiber and the die inner surface. The motivation of the present work was, therefore, to examine the influence of size on the upstream coating meniscus. The entrance die is substituted with a series of different small diameter transparent glass micropipettes, and the applicator is operated at pressures which are sufficiently high to force the free surface within the micropipette tube. This paper includes observations and measurements using different glass tube diameters, pressures and fiber speeds, as well as comparisons with previous results [6], obtained using an open, unpressurized applicator. Results from the numerical simulation of the flow field within the glass tubes were also compared with the experimental findings, indicating general good agreement.

2. Experimental
2.1 Apparatus
Figures 1 and 2 are schematic diagrams of the overall experimental apparatus and the test section, respectively. The fiber motion was controlled using a commercial optical fiber rewinder system with a speed range between approximately 0.02 and 17 m/sec. The test applicator was a stainless steel block with a machined cavity 2 cm x 2 cm in cross-section and overall effective height adjustable from approximately 2 cm to less than
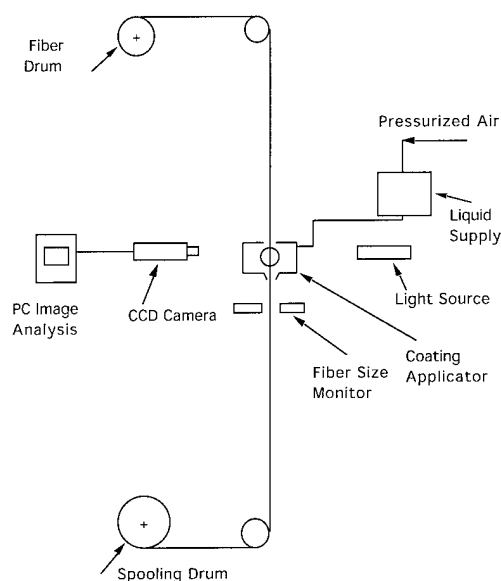
Figure 1. Schematic diagram of apparatus
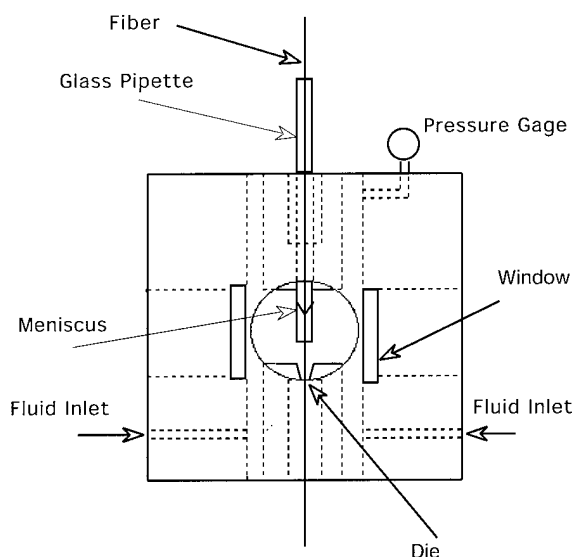
Figure 2 . Schematic diagram of test applicator

1 cm. Two pairs of 1cm diameter flat glass windows on each wall allowed visualization of the flow from two perpendicular directions. For open unpressurized meniscus tests the fiber entrance to the test section was through a 350 μm diameter coating die. For the pressurized tests the upstream die was substituted by a series borosilicate micropipette tubes of different diameters which permitted visualization of the position

and shape of the entrance meniscus as it was forced into the micropipette tube by pressurizing the test applicator. The exit was through a 300 μm coating die. The test liquid was glycerol and was supplied using two opposing inlet ports at the lower portion of the applicator. Clean dry air was used for pressurization of the liquid reservoir using a pressure regulator. The liquid flow rate and pressure within the test applicator were controlled using a parallel two-valve system. A bare 1.59 mm wire diameter, type K type thermocouple (not shown in fig. 2) was positioned near the fiber (at approximately one fiber diameter distance) to monitor temperature changes associated with viscous dissipation. Visualization of the meniscus employed diffuse back lighting from continuous incandescent light sources. Images of the menisci from two perpendicular directions were acquired using telescope equipped CCD cameras and video tape recorders. The taped images were analyzed using image processing and analysis software. The resolution of the optical system depended on the object distance, which ranged from 30 cm to 1 m resulting in magnification between 200 and 100 and pixel to pixel spacing between 5 μm and 10 μm depending on magnification. The edge of the meniscus and fiber were identified using Sobel edge detection.

The glass fibers used were coated with a single coat of UV curable polyacrylate. The coated fiber diameter was 256 μm and was measured using a fiber diameter monitor. Tests were carried out using borosilicate glass micropipettes approximately 2 cm long with internal diameters of 790 μm, 630 μm, and 556 μm, resulting in fiber to pipette diameter ratios of 3.08, 2.46, and 2.17, respectively. Of importance was to center the fiber within the glass micropipete tubes. Viewing from two perpendicular directions through the two window pairs was essential in this process. The pressures measured at the fluid inlet of the applicator used were up to approximately 180 KPa. Measurements were taken for a range of fiber speeds exceeding those for air entertainment. The test fluid used was glycerine (viscosity 0.88 Nsec/m^2 at 21 °C) and the capillary number was between approximately 2.8 and, 12.

2.2 Experimental Results and Discussion

Figures 3A,C show images of the meniscus formed with the fiber moving into an unpressurized open cup applicator, and figs 3B,D show the meniscus forced inside the 632 μm ID micropipette by pressurizing the applicator. The fiber speed in both figures was 20 m/min, (larger than the approximately 10 m/sec minimum speed for air entrainment [6]), the applicator pressure was 60.69 KPa, and both sets of images (A,B and C,D) were taken at the same electronic shutter speed (10^{-4} sec). In both cases the dynamic contact angle was near 180°. Figure 3A clearly shows the breakdown of the meniscus into saw tooth patterns and tip streaming as previously observed [6,11]. On the other hand, the pressurized applicator meniscus image, 3B, appears to be smooth suggesting suppression of large scale breakdown at the same fiber speed. Lack of symmetry in fig. 3C

is due to small eccentricity of the fiber within the micropipette. Figures 3C, and 3D are low magnification images clearly demonstrating that the unpressurized meniscus generates a large number of relatively large air bubbles compared to the pressurized meniscus in fig. 3D where air bubbles are probably too small to be detected. Comparison of the shape of the
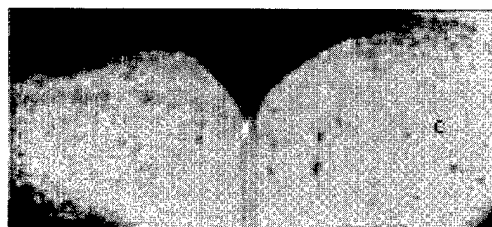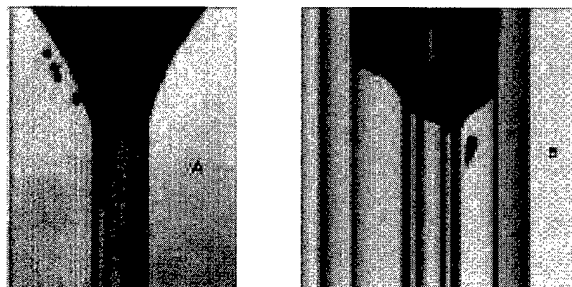
menisci in figs 3A and 3B shows that the effects of pressure and
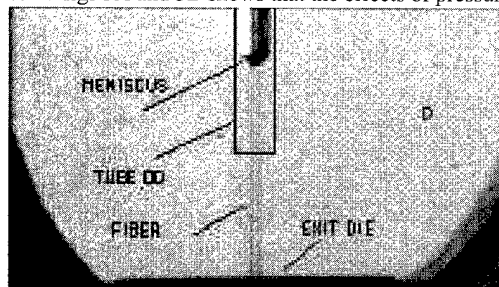
Figure 3. A, C, unpressurized test section. B, D, meniscus in 630 μm diameter tube, test section at . Fiber speed 20 m/min

geometry are to flatten the meniscus and to increase the slope of the liquid-air interface near the fiber compared to those for an unpressurized meniscus. This probably results in a smaller air volume available for entrainment accounting for the difference between figs. 3C and 3D. However, a clear understanding of the effect of pressure on air entrainment requires further investigation.

The thermocouple probe (not shown in fig. 3) registered a temperature increase of approximately 0.4 °C at a fiber speed of 20 m/min (corresponding to a Capillary number of 4.06)

when placed at an axial position of one pipette diameter from the tube mouth. The temperature increase was attributed to viscous dissipation within the pipette tube.

The equilibrium distance of the meniscus from the tube mouth is a consequence of a mass balance between liquid outflow due to viscous drag by the moving fiber and liquid inflow due to the pressure drop between the tube entrance and the meniscus. In addition, the meniscus geometry depends on a balance between forces due to the pressure difference across the free surface, surface tension forces and viscous fluid forces. Further investigation is needed to establish whether for given operating conditions the position and shape of the meniscus are unique. Experience with the present apparatus has shown that the for a sufficiently high pressure and fiber speed maintaining a stable meniscus requires careful adjustments to avoid catastrophic disruption of the free surface leading to loss of pressure. Measurements of the equilibrium distance, H, from the tube mouth and of the resulting meniscus height, h, were correlated using non-dimensional parameters obtained by dimensional analysis. The non-dimensional parameters used were the Capillary number, $V\Delta R/\sigma$, the parameter $P_t\Delta R/\sigma$, and the geometric ratios, $H/\Delta R$, h/R_f, and $R_f/\Delta R$ and where V was the fiber speed, P_t was the applicator pressure, R and R_f were the tube and fiber radii, respectively, $\Delta R = R-R_f$, and σ was the surface tension. The empirical correlation relation obtained was as follows:

$$\frac{H}{R_f} = A[\frac{V\Delta R}{\sigma}]^b [\frac{P_t\Delta R}{\sigma}]^c [\frac{h}{\Delta R}]^d [\frac{R_f}{\Delta R}]^e$$

Where A = 0.0293, b = -1.203, c = 1.240, d = 0.217, and e = -1.935. The square of the regression coefficient was 0.914.

A $[(V\Delta R/\sigma)^b (P_t\Delta R/\sigma)^c (h/\Delta R)^d (R_f/\Delta R)^e]$
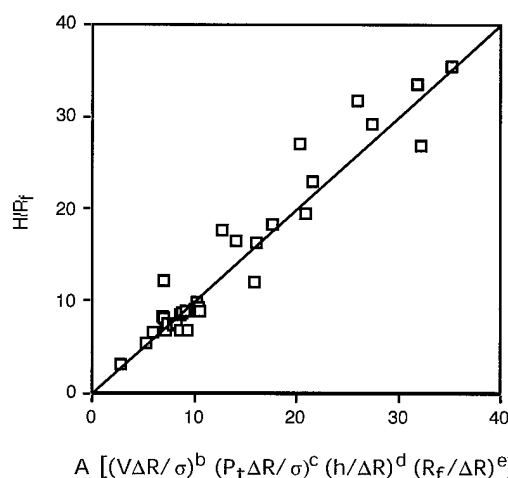
Figure 4. Experimental Correlation

3. Computation
3.1. Numerical Modeling

Numerical modeling of the flow within the micropipette tubes was carried out to study the effect of the meniscus shape on the overall flow, as well as the effect of pressurization on the applicator. The numerical study used the geometry employed in the experiment, the appropriate operating conditions and the shape of the meniscus obtained from the experiments. The flow at the exit of the glass tubes was assumed to be developed.

Simulation of the meniscus as the fiber enters the coating applicator required a coordinate transformation, which was applied to the axisymmetric cylindrical Navier-Stokes equations. The transformation technique followed was similar to that used by Rodi et al. [17], using the primitive variable technique to solve for the velocity (u, v), pressure (p) and involving contravariant velocity coefficients in the convective terms. The resulting non-linear coupled system of equations were solved using the Successive Over Relaxation (SOR) method for the pressure and the Alternating Direction Implicit (ADI) for the velocity equations. A finite volume method similar to the SIMPLER algorithm developed by Patankar [18] was employed. The second order conservation equations were approximated using the central differencing scheme for the convective and diffusion terms.

3.2 Numerical Results and Discussion

A fiber speed of 10m/min is considered in the following section. The coating material used was glycerol (ρ =1250kg/m^3, μ = 0.832 Ns/m^2), as employed in the experiments. The distance of the meniscus from the exit of the tube was 0.00428m, the fiber diameter was 254μm and the tube diameter was 800μm. The fiber was positioned axisymmetrically at the center of the tube, and the fluid entered and exited from the bottom of the tube.

Calculated velocity vector plots are shown in Fig 5. The fluid entered at the bottom and rose to the top curving along the meniscus, where it was then pulled down along with the fiber back to the bottom of the tube. The figure also shows close-ups of the vector plots near the meniscus. Results for higher fiber speeds showed a recirculation region near the meniscus similar to that observed experimentally. The calculated velocity field was found to be in general agreement with the visualization of the flow in the experiments.

A pressure decrease along the length of the tube is required to force the coating fluid inside the tube. For the results shown the pressure at the bottom of the tube was set at 18 kPa. which, because of fluid motion, was lower and not directly comparable to the measured at the applicator wall.

The effect of pressure on the meniscus distance, H, from the bottom of the tube was considered for the same fiber speed of 10m/min. For this calculation the meniscus shape was kept

unchanged along with all other operating conditions. The pressures for four different distances are shown in Fig 6. The pressure difference between the top and bottom of the tube was found to increase almost linearly with the length of the tube, as illustrated in the figure.

The fluid entered the tube at the bottom and also exited at the bottom along with the fiber. The mass flow rate entering the tube was found to increase linearly as the length of the tube was decreased. This resulted in a stronger flow in the tube as the length of the tube is decreased. The calculated temperature rise due to viscous dissipation was of the order of 1*C, which was similar to that observed experimentally.
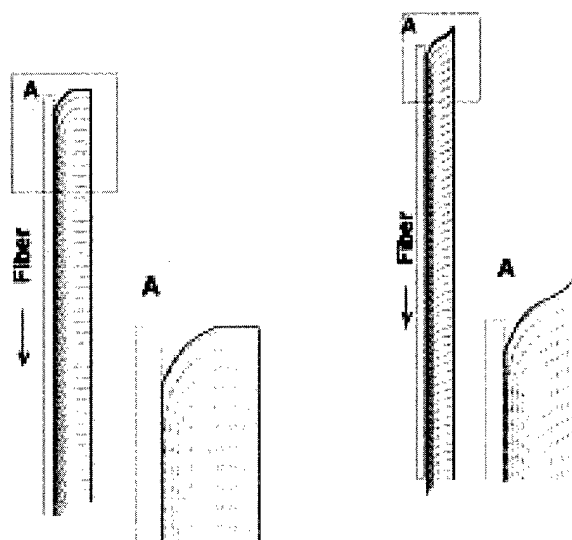
Figure 5. Computed velocity fields for two different meniscus shapes
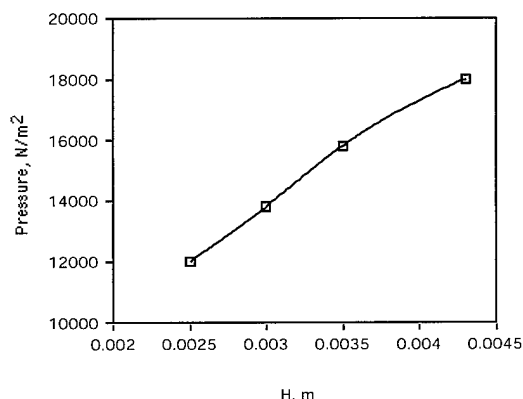
Figure 6. Variation of meniscus distance with pressure. Fiber speed: 10 m/min

4. Conclusions

The effect of entrance geometry on the entrance meniscus in a pressurized fiber coating applicator was experimentally simulated using micropipettes of different sizes. Using pure glycerine as the test fluid the amount of air entrapped decreased from the open meniscus to that of the pressurized case. The meniscus shape appeared to flatten with increasing fiber speed and applicator pressure. Experimental data and dimensional analysis were used to generate an empirical correlation for the meniscus position within a micropipette tube. The stability of the meniscus required careful control of the pressure and fiber speed. The calculated flow field was found to be similar to the observed flow. The results so far show the basic nature of the flow in the applicator and indicate means to curb air entrapment and control meniscus stability.

5. Acknowledgment

6. References

1. Blake, T.E., (1993), "Dynamic Contact Angles and Wetting Kinetics", Ch. 5, *Wettability*, Berg, J.C. ed., Marcell Dekker, New York.
2. Kistler, S.F., and Schweizer, P.M., (1997), "Liquid Film Coating", Chapman and Hall, London.
3   Inverarity, G., (1969), "Dynamic Wetting of Glass Fibre and Polymer Fibre", *Br. Polym. J.*, v. 1, pp. 245-251.
4   Ghannam, M., T.,and Esmail, M.N., (1993), "Experimental Study of the Wetting of Fibers", *AIChE J.*, v. 39, pp. 361-365.
5. Ghannam, M., T., and Esmail, M.N., (1997) "Experimental Study on Wetting of Fibers with Non-Newtonian Fluids", *AIChE J.*, v. 43, pp 1579-1588.
6. Abraham, A., and Polymeropoulos, C.E., (1999), "Dynamic Menisci on Moving Fibers", 48th IWCS, Atlantic City, N.J.
7. Aloisio, C.J., (1984), "Coating Optical Fibers with Dual Dies Separated by a Pressurize Chamber", *Fiber and Integrated Optics*, v. 5 pp.81-97.
8. Panoliaskos, A., Hallett, W.L.H., and Garis, I.,(1985), "Prediction of Optical Fiber Coating Thickness", *App. Opt.*, v. 24, pp. 2309 –2312.
9. Abott, J.S., and Francis, D.C., (1989), "Analysis of the Optical Fiber Coating Process Using FIDAP: Flow, Heat Transfer, and 3D Calculation of Centering Forces", Proc. 3rd FIDAP Users Conf.
10. Rattan, K, and Jaluria, Y., (1999),"Simulation of Flow in Die and Applicator For Optical Fiber Manufacturing", 48th IWCS, Atlantic City, N.J.
11. Simpkins, P., and Kuck, V., (2000), "Air Entrapment in Coatings Via Tip Streaming Meniscus", *Nature*, v. 403 pp. 641-643.
12. Burley, R., and Kennedy, B.S., (1976), "An Experimental Study of Air Entrainment at a Solid/Liquid/Gas Interface", *Ch. Eng. Sc.*, v. 31, pp. 901-911.
13. Burley, E., and Jolly, R.P.S., (1984), " Entrainment of Air into Liquids by a High Speed Continuous Solid Surface", *Ch. Eng. Sc.*, V 39, pp. 1357-1372.
14. Gutoff, E.B., and Kendrick, C.E., (1982), "Dynamic Contact Angles", *AIChE J.*, v. 28 pp. 459-466.
15. Dussan, E. B., Rame, E., and Garoff, S., (1991), "On Identifying the Appropriate Boundary Conditions at a Moving Contact Line: an Experimental Investigation", *J. Fluid Mech.*, v. 230, pp. 97-116.
16. Marsh, J.A., and Garoff, S., (1993), "Dynamic Contact Angles and Hydrodynamcs near a Moving Contact Line", *Phys. Rev. Let.*, v. 70, pp. 2778-2781.
17. Rodi, W. , Majumdar, S., and Schonung, B. (1989), "Finite Volume Methods for Two-Dimensional Incompressible Flows with Complex Boundaries.", Computer Methods in Applied Mechanics and Engineering, vol. 75, pp. 36-392.
18. Patankar, S.V., (1980) " Numerical Heat Transfer and Fluid Flow ", Hemisphere, Washington, D.C.

C.E. Polymeropoulos
Department of Mechanical and Aerospace Engineering
Rutgers University
97 Brett Road, Piscataway, NJ 08854-8058

Dr. Polymeropoulos is a Professor of Mechanical Engineering at Rutgers and has been teaching and doing research in the general area of thermal processes.
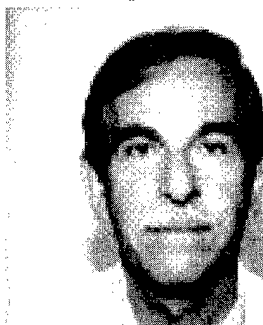
Effect of Furnace Design on High Speed Optical Fiber Drawing

Xu Cheng and Yogesh Jaluria

Dept. of Mechanical and Aerospace Engineering
Rutgers, The State University of New Jersey
New Brunswick, NJ 08903
+1-732-445-3652 · jaluria@jove.rutgers.edu

Abstract

The drawing speeds employed in the manufacturing of optical fibers have been increasing in recent years due to growing worldwide demand. This places stringent demands on the manufacturing process, mainly because of large temperature gradients that can generate thermally induced defects and variations in fiber characteristics. Glass flow in drawing fibers of 125 μm diameter from cylindrical silica preforms of diameters ranging from 10 to 20 cm plays a critical role in the feasibility of the process and in the maintenance of fiber quality. This paper presents an analytical and numerical study of the optical fiber drawing process for such large diameter preforms and draw speeds as high as 25 m/s. The neck-down profile is determined by using a balance of forces acting at the surface. The transport in the glass is calculated to obtain the temperature, velocity, tension and defect distributions. Because of the large reduction ratio in the diameter, a coordinate transformation is used to convert the complex domains to cylindrical ones. The numerical results are validated by comparisons with experimental and numerical results in the literature for lower draw speeds. The focus of the study is on the furnace dimensions, particular its length, and on the wall temperature distribution. The effects on the defects generated in the fiber, on the neck-down profile, and on the feasible domain for the process are determined.

Keywords

Optical fiber; draw furnace; fiber drawing; draw process simulation.

1. Introduction

One of the widely used methods to draw optical fibers involves continuously feeding a silica glass preform into a cylindrical heating furnace, heating the glass above its softening point of around 1900 K, and pulling it into a fiber of diameter around 125 μm[1]. As the preform proceeds through the heating zone, it narrows down sharply and yields the "neckdown" region. The neckdown profile strongly depends on the fiber drawing conditions and significantly impacts the diameter uniformity[2], strength, and transmission loss[3] of optical fibers.

The drawing speeds employed in the manufacturing of optical fibers have been increasing in recent years due to the increase in demand. Economical fabrication of optical fibers requires large preforms drawn into fiber at very high speed. However, the high drawing speed requires advances in furnace design to meet the required specifications and to ensure the correct draw tension[4][5]. An optimal design of the draw furnace is becoming an urgent and highly challenging task to achieve high-volume production of optical fibers.

The furnace dimensions have to be increased as larger diameter preforms are being employed[4][6]. In addition, a strong connection exists between the heating furnace design and the fiber quality. Draw-induced defects are determined by the history of the thermal process undergone by the silica glass and are thus affected by the preform/fiber size, draw speed, configuration of draw furnace and temperature distribution[7]. To satisfy the continuous fiber drawing operation, draw tension ought to be kept under specified limit[8][6]. However, draw tension is very sensitive to the thermal as well as geometric configuration of the heating furnace[6]. Since minimizing the furnace temperature is desirable to increase its lifespan[4], an extension of the heat zone length is usually an efficient and inevitable approach. An attempt to optimize the furnace geometry was implemented in [9] by considering the power supply efficiency of the draw furnace.

This paper presents an analytical and numerical study of the optical fiber drawing process in a cylindrical furnace. A resistance graphite furnace, configured with low-speed aiding argon flow, is chosen. The inert gas flow introduced into the furnace cavity keeps the graphite heating element from oxidation. A conjugate problem with a free surface of glass is considered. A complex thermal analysis, involving conduction, convection and radiation heat transfer, is necessary to analyze and design draw furnaces which can produce low-signal-loss and high-strength fibers at high draw speeds. The transport in the two regions is solved to obtain the temperature, velocity, tension and defect distribution in the glass. The zonal method is used to model the radiative heat transfer in the glass[10]. The neckdown profile of the preform is iteratively determined by a force balance.

The effect of the length and heating conditions on the neck-down profile, on the temperature and velocity distribution, on the defects generated, and on the draw tension in the fiber during the drawing process are determined. A feasible domain is obtained. Interest also lies in the determination of an optimal length or wall temperature that minimizes the defects, while keeping the productivity high. The diameters of the preform and the fiber are kept fixed at 5 cm and 125 μm, respectively. The numerical results are validated by comparisons with experimental and numerical results in the literature for smaller draw speeds[11][12][13][14].

2. Analysis

The transport phenomena in a cylindrical graphite furnace are investigated for high-speed optical fiber drawing. A conjugate problem involving the glass and the purge gases is considered. Laminar flow is assumed due to the high-viscosity and low-velocity, respectively, in the glass and in the gas flow. The transport in the two regions is coupled through the boundary conditions at the free surface. Conduction, convection and radiation are coupled in the heat transfer analysis.

The governing equations for axisymmetric conditions, developed in cylindrical coordinates for both the glass and the purge gas, are given in [14]. The viscous dissipation and the radiative source terms are only kept for the glass due to their importance. For the convenient implementation of the finite difference method, the free-surface domains for the glass and purge gas are transformed into cylindrical ones[13]. The boundary conditions for a free surface, arising from a force balance, are employed here at the interface between the glass and the purge gas. A more detailed discussion about the governing equations and the boundary conditions can be found in [13] and [14].

Point defects generated at high temperature during the fiber drawing process will cause transmission loss and mechanical strength degration in the fiber[7]. One of the most important point defects, E' defect, is found to be drawing-induced, depending on the draw temperature, draw speed and fiber diameter[7]. Basically, E' defects in silica glass are generated from the breaking of Si-O bond of a potential precursor. However, the Si-O bond can be formed again due to recombination. Therefore, the concentration of E' defects is the net effect of generation and recombination. Hanafusa et al.[7] formulated E' defect behavior during the fiber drawing process based on the theory of the thermodynamics of lattice vacancies in crystal. In this study, Hanafusa's equation is applied to a mass point moving along the streamline in order to compute the E' defect concentration. This equation is:

$$u\frac{dn_d}{dz} = n_{p0}\nu\exp(-\frac{E_p}{kT}) - n_d\nu[\exp(-\frac{E_p}{kT}) + \exp(-\frac{E_d}{kT})] \quad (1)$$

Where, n_d and n_{p0} represent the concentrations of E' defects and initial precursors respectively, while E_d and E_p are corresponding activation energy of these. All values needed are taken from [7]. For pure silica, the initial concentration of E' defect is assumed to be zero.

Draw tension is determined by considering the contribution of the viscous force, surface tension, inertia force and gravity, resulting in the equation:

$$F_T = 3\pi\mu R^2\frac{\partial u}{\partial z} + \pi R^2\varsigma H + \pi\rho\int_z^L R^2 u\frac{\partial u}{\partial z}dz - \pi\rho g\int_z^L R^2 dz \quad (2)$$

The finite difference method based on the Alternating Direction Implicit (ADI) algorithm is employed. Two non-uniform discretization schemes, a finer one for the transport equations and a coarser one for the radiation analysis, are adopted to capture the dramatic changes in the physical variables, particularly viscosity.

The radiation transfer is a volume phenomenon in the semi-transparent glass and a very time-consuming method, the zonal model[10], is used to accurately compute the radiative source term. Numerical experiments are necessary to obtain the optimum discretization schemes. Successive Under-Relaxation (SUR) is needed to resolve the strong non-linearity caused by the temperature and vorticity changes.

3. Results and Discussion

The effect of draw furnace dimensions is first investigated. The heat zone length is varied from 25 to 50 cm, while the furnace diameter is kept as 7 cm. A parabolic temperature profile with maximum of 2500 K in the middle and minimum of 2000 K at the two ends is prescribed at the furnace wall. The dimensionless temperature profile is kept exactly same for all the furnace lengths. Two draw speeds, 15 m/s to 25 m/s, are considered. Constant properties are assumed for the aiding Argon flow moving at 0.1 m/s. Both the preform and the purge gas enter the furnace at 300 K.

Figure 1 shows the neckdown profiles corresponding to different furnace lengths. It is seen that the furnace length affects the starting point of the neckdown section and its shape. A longer heating zone starts the deformation of the glass rod much later due to relatively lower temperature upstream. The profile also varies more gradually according to the milder change in heat flux. A high draw speed can delay the process of preform deformation as well. A longer heating distance is needed at higher draw speeds for the process to be feasible.

The temperature lag between the surface and centerline temperature, defined as $T_{lag}=(T_s-T_c)/T_c$, describes the thermal response process in the glass. Figure 2 shows the variation of maximum lag in the drawing process. It is seen that the heating zone length affects the lag level only slightly. However, the influence of draw speed is significant. The temperature difference between the surface and centerline temperature increases about 30% when the draw speed goes up from 15 m/s to 25 m/s. This result suggests that the residence time of the glass rod inside the heating furnace is the dominating factor to control the radial temperature difference, since a longer residence time causes the preform to be more uniformly heated.

The radial non-uniformity in the temperature in the perform noticeably affects the velocity field, because glass viscosity is an exponential function of the temperature. This can cause the redistribution of the material dopants and impurities, and therefore impact the fiber quality[7]. Similarly, the axial velocity lag between the centerline and the surface in the neck-down region is defined as $v_{lag}=(v_s-v_c)/v_c$ and the variation of the maximum lag is shown in Figure 3. Clearly, the velocity lag is very sensitive to the furnace dimensions. The lag decreases significantly with an increase in the furnace length. The lag difference at two draw speeds is obvious only for shorter furnaces. However, it diminishes as long as the heating zone is above 40 cm.

Figure 4 shows the fiber's average concentration of E' defects at the furnace exit. The defect concentration monotonically increases with an increase in the heating zone length and with a decrease of the draw speed. It is because a longer residence time of fibers inside the heating furnace will cause more frequent occurrences of Si-O bond breaking in the precursors.

The draw tension is of particular interest in fiber drawing, because a high tension affects optical and mechanical properties of the fiber in terms of index of refraction, residual stresses, and transmission losses, ultimately influencing the fiber strength and optical quality. A draw tension kept under a certain threshold is also critical to achieving continuous pulling of optical fibers without breakage[15]. Figure 5 shows the dependence of draw tension on the furnace length and draw speed. It is found that the draw tension decreases dramatically with an increase in the furnace length for a given temperature profile. The reason is that a longer heating zone gives rise to relatively smaller rate of change of radius with distance and the viscosity also changes more gradually. Therefore, the draw tension is reduced. This result also indicates that a moderate furnace length is desirable to achieve low fiber tension particularly for high-speed fiber drawing. From the figure, it is found that a high draw speed can cause a high draw tension. In general, draw tension varies linearly with the draw speed[1][4][11].

For a given temperature profile, furnace length and draw speed can be considered to determine a feasible domain of fiber drawing. Figure 6 shows the maximum draw speeds possible for various heat zone geometries. In practice, the fiber drawing may never reach the boundaries due to the unacceptable draw tension.

The dependence of the preform/fiber characteristics on the draw temperature are investigated for a typical draw speed of 15 m/s. A fixed furnace length of 30 cm is employed. The imposed temperature profile is still parabolic while only the maximum temperatures at the mid-point of the furnace are changed, ranging from 2200 K to 3000 K.

As expected, the sensitivity of most physical variables to the draw temperature variation is very strong. Figure 7 shows the neckdown profiles for different draw temperatures. Increasing draw temperature causes the neck-down deformation much earlier and more sharply. It is because the preform is heated up to the softening point faster at a higher temperature.

The maximum temperature and velocity lag in the glass are shown in Fig. 8 and Fig. 9. It is seen that the temperature lag slightly decreases when the draw temperature increases. Simultaneously, the velocity lag varies parabolically with the draw temperature. The lag levels are all above 30% at two extreme draw temperatures, i.e. 2200 K and 3000 K respectively. However, the reasons for this are a little different. The former temperature almost reaches the lower temperature boundary of the feasible drawing domain for the given furnace, and, therefore, a weak heat input at the glass surface extends the thermal response at the center. On the contrary, the temperature as high as 3000 K causes a rapid change of velocity at the glass surface by applying a very intense heat flux on it. However, the effect can not propagate to the center immediately due to thermal inertia.

Figure 10 shows the generation of the E' defect in the fiber. E' defects in the fiber are very sensitive to the drawing temperature and its average concentration at the furnace exit increases by almost two orders in magnitude when the draw temperature goes up from 2200 K to 3000 K. This result suggests that minimizing the drawing temperature is not only desired for increasing the lifespan of draw furnace, but also for decreasing the point defects in the optical fiber to an acceptable level. The variation of draw tension with the draw temperature is shown in Fig. 11. Due to the exponential dependence of the glass viscosity on the temperature, the draw tension decreases dramatically with the increase of the furnace temperature. Thus, increasing the draw temperature becomes important for tension control. Obviously, the optimum design of draw furnace is possible by considering a trade-off of these characteristics.

4. Conclusions

This paper presents an analytical and numerical study of the high-speed optical fiber drawing process within a cylindrical furnace cavity. The effects of geometric and thermal design of the draw furnace on various physical variables are investigated. A conjugate problem, involving the glass and the purge gas, is solved with the finite difference method. The zonal model is used for the radiation analysis in the glass.

The results show that most physical variables characterizing the quality of drawing fibers strongly depend on the dimensions and the draw temperature of the heating furnace. Generally, the heating length dominates the neckdown, velocity lag, point-defect concentration and draw tension. Defects increase and draw tension decreases for a given temperature profile when the heating furnace gets longer. The draw temperature also significantly affects these variables. The temperature lag demonstrates a parabolic relationship with the draw speed. A high temperature causes a low level of draw tension, but a dramatic jump in defect concentration. Among these variables, the temperature lag is not very sensitive to the change in furnace design. All these observations suggest that optimal design of draw furnace for high-speed fiber drawing can be achieved by constructing an objective function from the velocity lag, defect concentration and draw tension.

5. Acknowledgments

6. References

[1] Paek, U.C. and Runk, R.B., *Journal of Applied Physics*, 49, 4417-4422(1978).

[2] Smithgall, D.H., *The Bell System Technical Journal*, 58, 1425(1979).

[3] Blyler, L.L., Jr. and Williams, J.C., *AIChE Symposium Series*, 83(258), 27-28(1987).

[4] Rajala M., Asikkala K., Makinen M., Tuurnala T., and Peltoluhta E., *International Wire & Cable Symposium Proceedings 1998*, 483-488(1998).

[5] Paek, U.C., *AICHE Symposium Series*, 83(258),32-37(1987).

[6] Paek, U.C., *Transactions of the ASME*, 121, 774—788(1999).

[7] Hanafusa, H. Hibino, Y. and Yamamoto, F., *J. Applied Physics*, 58(3), 1356-1361(1985).

[8] Sakaguchi, S., and Kimura, T., *Technical Digest of OFC'85*, San Diego, CA, Paper MG2(1985).

[9] Nicolardot, M. and Orcel, G., *International Wire & Cable Symposium Proceedings 1999*, 369-376(1999).

[10] Yin, Z. and Jaluria Y., *Journal of Heat Transfer*, 119, 597-603(1997).

[11] Choudhury, S.R., Jaluria, Y. and Lee S. H.-K., *Numerical Heat Transfer(Part A)*, 35, 1-24(1999).

[12] Choudhury, S.R. and Jaluria, Y., *J. Mater. Res.*, 13(2), 483-493(1998).

[13] Choudhury, S.R., and Jaluria, Y., *J. Mater. Res.*, 13(2), 494-503(1998).

[14] Yin, Z. and Jaluria Y., *Transactions of ASME*, 120, 916—930(1998).

[15] Sakaguchi, S., *IEEE Journal of Lightwave Technology*, LT-2(6), 808-815(1984).
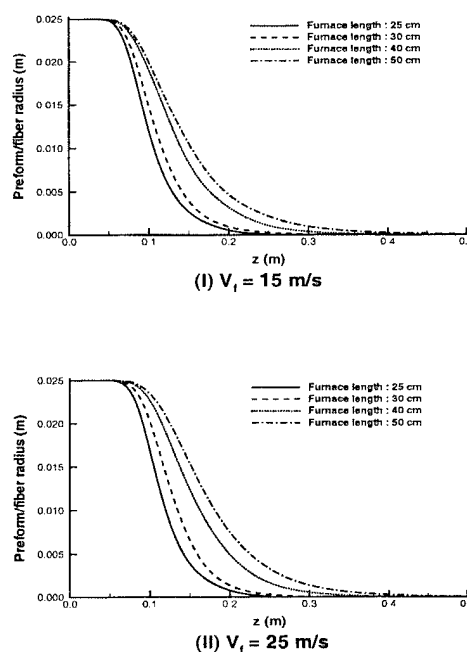
Figure 1. Neckdown shapes for different draw speeds.
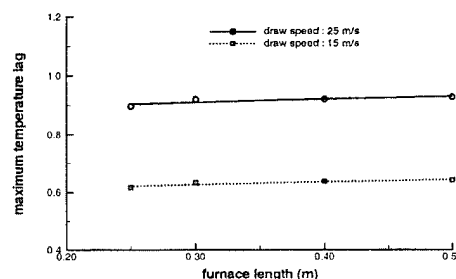
Figure 2. Maximum temperature lag between glass surface and centerline.
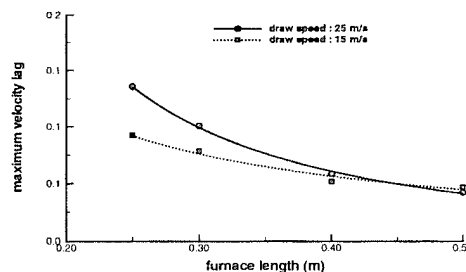
Figure 3. Maximum velocity lag between glass surface and centerline.
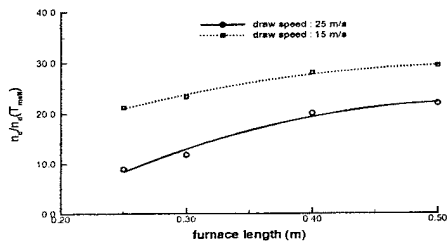
Figure 4. Average concentration of E' defects at the furnace exit.
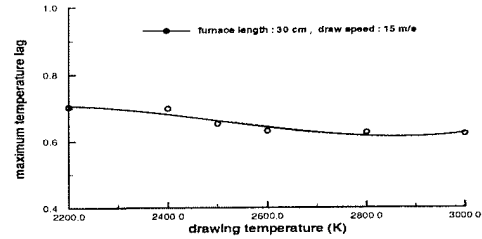
Figure 8. Dependence of maximum temperature lag on furnace wall temperature.
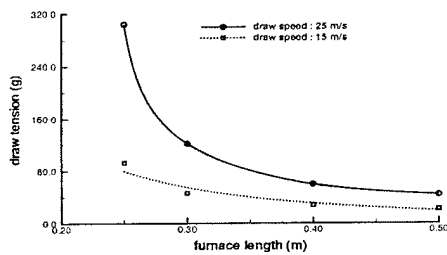
Figure 5. Dependence of draw tension on furnace length.
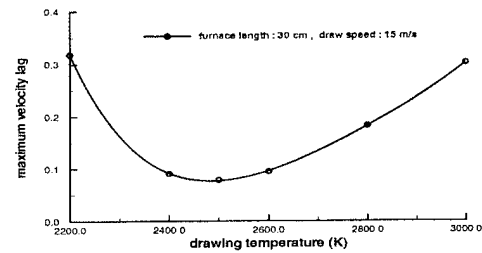
Figure 9. Dependence of maximum velocity lag on furnace wall temperature.
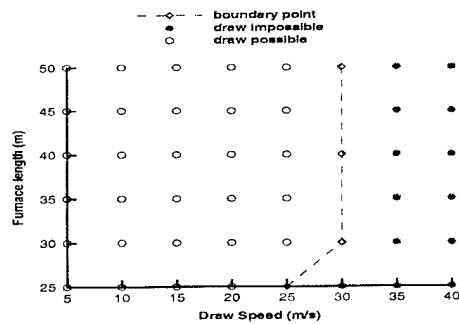
Figure 6. Feasible domain of draw speed.
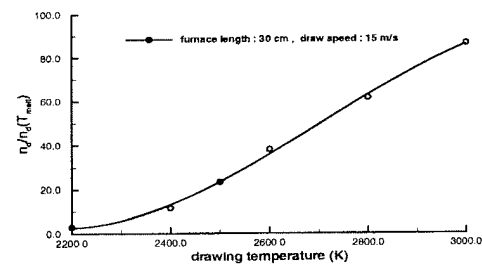
Figure 10. Dependence of average concentration of E' defect on furnace wall temperature.
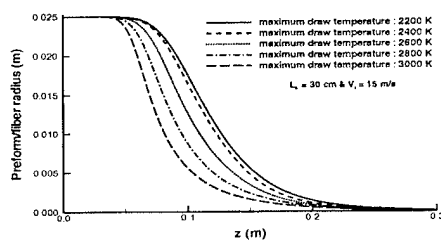
Figure 7. Dependence of neckdown shape on furnace wall temperature.
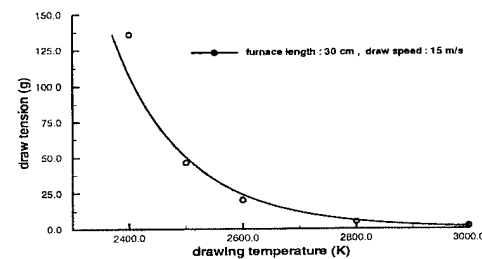
Figure11. Dependence of draw tension on furnace wall temperature.
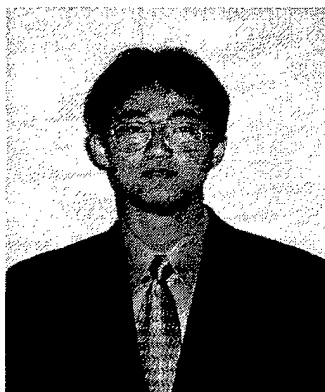
Mr. Xu Cheng is a graduate student of Mechanical and Aerospace Engineering at Rutgers University. He received his Bachelor's degree from the Thermal Engineering Department at Tsinghua University, Beijing, China. He is currently involved with the numerical simulation, design and optimization of the optical fiber drawing system for his Ph.D. thesis.

Dr. Yogesh Jaluria is Professor of Mechanical and Aerospace Engineering at Rutgers University. He worked at A T & T Bell Laboratories, Princeton, and at the Indian Institute of Technology, Kanpur, India, before joining Rutgers University. He has been an active researcher in fluids and thermal engineering. Much of his recent research has been in materials processing, particularly in optical fiber manufacture, polymer processing, and thin film deposition. He has contributed more than 320 technical articles, including over 130 in archival journals, five books, and 14 chapters in books. He has two patents in materials processing. He has received several national and international awards for his research, which has been largely funded by the National Science Foundation, the State of New Jersey and industry.

Development of new aerial access cable with 4-fiber ribbons

Tetsuya YASUTOMI, Masato KOHSAKA, Eiji KONDA, Ichiro KOBAYASHI,
and Akio HASEMI

FITEL Photonics Laboratory, The Furukawa Electric Co., Ltd.
6 Yawatakaigan-dori, Ichihara, Chiba, Japan
+81-436-42-1771   tomy@ch.furukawa.co.jp

Abstract

We developed a new type of aerial distribution optical fiber cable, which is small in size and light in weight. The new cable offers various advantages: only a single process in manufacturing process because of the simple structure; easy mid-span branching with ordinary tools; and easy handling of the fiber ribbons because of the absence of jelly around the fiber ribbons.

Successful test results were obtained for the new cables regarding transmission loss, temperature and mechanical characteristics, mid-span branching, and long-term reliability. We confirmed from these results that the new cable is suitable for aerial distribution cable.

Keywords

Fiber; cable.

1. Introduction

Expansion of the use of optical fiber cables for access networks requires an optical fiber cable that is small in size, light in weight, and easy to handle [1]. The conventional types of optical fiber cables for access networks typically include single tube cables and loose tube cables; these, however, have the disadvantage of difficult handling of the ribbons because of the use of jelly.
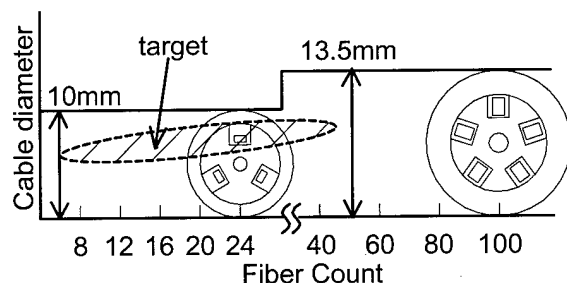
Figure 1. Development Target

An aerial distribution optical fiber cable with the SZ-slotted rod, shown in figure 1, was developed and put in use in Japan [2] [3]. The slotted rod with three grooves is used in low-fiber-count cable of up to 24 fibers, and that with five grooves is used in high-fiber-count cable of more than 24 fibers. In order to expand the use of optical fiber cables for access networks, it is increasingly necessary to miniaturize cables for a low-fiber-count range of up to 40 fibers. We therefore developed a new type of aerial optical fiber cable in the low-fiber-count range (four to forty).

2. Requirements for the aerial distribution cables

2.1 Cable structure using fiber ribbons

The cable structure should be composed of fiber ribbons, which reduce the jointing time for feeder cables or other distribution cables and make jointing easy.

2.2 Long-term reliability in aerial installation environment

The aerial cables are installed between poles. The suspension member of such a cable becomes elongated because of suspending tension, thermal expansion, and wind pressures. The fibers of the aerial distribution cables must not suffer influence of the elongation of the suspension member.

2.3 Mid-span access

The distribution cables need to branch in mid-span of the cables, in order to drop to customers. The structure must therefore provide easy access to the fiber ribbons at any position along the cable.

2.4 Economical structure

Expansion of the use of optical fiber cables for access networks requires the economical construction of access networks. The cable should be small in size and light in weight so that the installation time can be reduced, and that should has simple structure so that the cable can be manufactured by only a single process.

3. Cable design

We designed the new cable structure that satisfies the requirements for aerial distribution cables described above.

3.1 Self-supporting structure with excess cable length

We selected a self-supporting structure with excess cable length, so the cable core is longer than the suspension member, in order to prevent elongation of the fibers when the suspension member is elongated as a result of suspension tension, thermal expansion, and winds. Two strength members are provided to reinforce the cable.

3.2 Optimum of cable size

We designed two types of the cables that consisted of a stack of optical fiber ribbons and two strength members; one has a cable core in which the stack of ribbons cannot rotate (Type 1), and the other has a cable core in which the stack of ribbons can rotate (Type 2). The cross section of the stack of ribbons is expressed as follows.

$$S1 = W \times H \tag{1}$$

$$S2 = \pi \left(W^2 + H^2 \right) / 4 \tag{2}$$

$$W = 0.25 \times n + 0.1 \tag{3}$$

$$H = 0.3 \times N \tag{4}$$

S1: Cross section of stack of optical fiber ribbons (Type 1)
S2: Cross section of stack of optical fiber ribbons (Type 2)
n: Number of fibers in a fiber ribbon
N: Number of stacks of fiber ribbons

The calculated results of the cross section of a stack in the fiber-count range up to 40 fibers are shown in figure 2. The type 1 design provides such a small stack occupation area over the whole range that the cable clearly can be miniaturized. On the other hand, the curves demonstrate that a 4-fiber ribbon type can be used to miniaturize a cable in the fiber-count range up to 28 fibers, and an 8-fiber ribbon type can be used to miniaturize in the fiber count range over 28 fibers in the type 2 design.
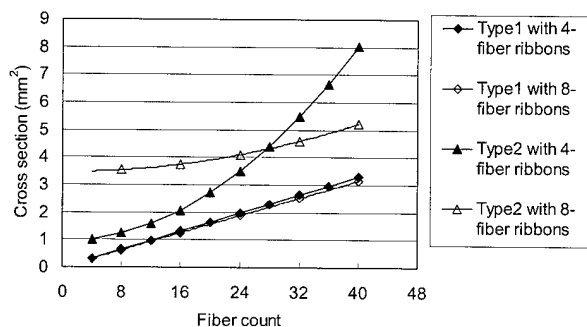
Figure 2. Cross section of ribbon stack

3.3 Fiber strain and transmission loss increase at cable bend

In type 1 cable, the fiber strain of outer layer of the ribbon stack when the cable is bent is expressed as follows.

$$\varepsilon = \left(0.3 \times \frac{N-2}{2} + 0.15 \right) / R \tag{5}$$

R: Radius of the cable bend

The strain of fibers when the cable is bent with a radius of 150 mm is shown in figure 3. When the number of layers of fiber

ribbons increases, the fiber strain increases and so the rotation force of ribbon stack, to release the fiber strain, increases. The buffer layer cannot bind the stack, and the fibers are bent. The trial cable with 4-fiber ribbons was bent with a radius of 150 mm over a temperature range of −30 to +70°C, and the transmission loss change was investigated. Results are shown in figure 3. An increase in transmission loss, caused by the fiber bending, was seen in cables having more than five layers of fiber ribbons.

The type 1 structure can best be used for miniaturization and is most suitable for practical use in the fiber-count range up to 16 fibers; in the fiber count range over 16 fibers, it found that the type 2 structure is more suitable.
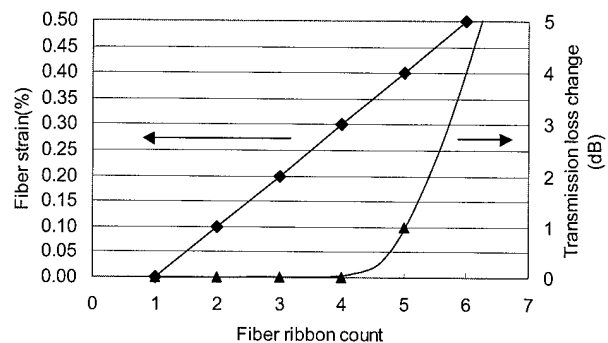
Figure 3. Fiber strain (Type1)

4. Cable structure

We manufactured the two types of cables as follows, based on the cable design described above.

4.1 Type 1 cable design

A cross-sectional view of the type 1 cable is shown in figure 4. The 4-fiber ribbons are stacked and ribbon stack, buffer layer, and two strength members are jacketed with polyethylene. The cable core is intermittently connected to the suspension member with excess cable length.
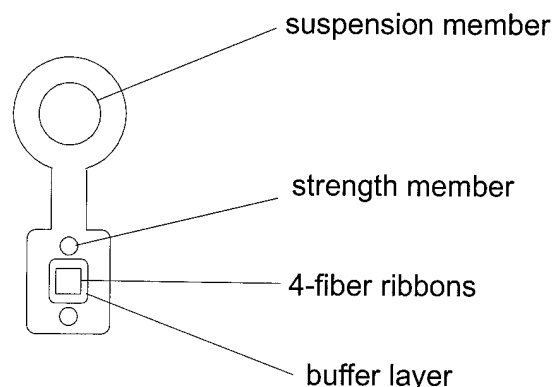
Cable height: 11.0mm, Cable weight: 0.10kg/m

Figure 4. Type 1 cable design

4.2 Type 2 cable design

A cross-sectional view of the type 2 cable is shown in figure 5. The 4-fiber ribbons are stacked and ribbon stack, buffer layer, and two strength members are jacketed with polyethylene. The cable core is intermittently connected to the suspension member with excess cable length.
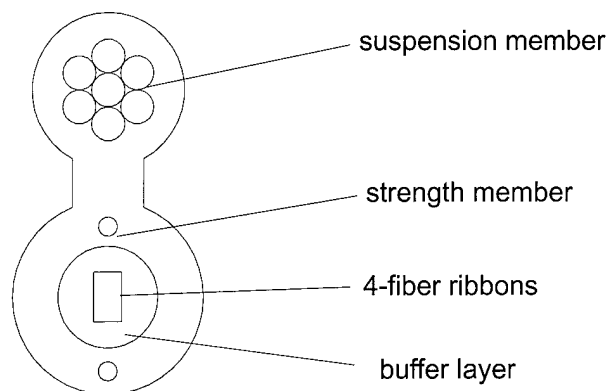
Cable height: 17.0mm, Cable weight: 0.15kg/m

Figure 5. Type 2 cable design

5. Cable performance

Results of an evaluation of the two types of cables are summarized below.

5.1 Transmission loss in manufacturing process

The transmission loss characteristic of the trial cable is shown in figure 6. No significant loss change was observed in the manufacturing process.
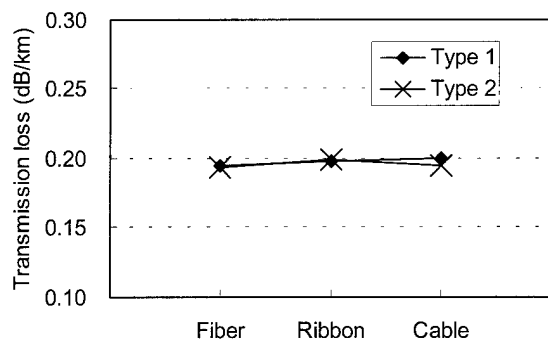
Figure 6. Transmission loss change in manufacturing process (@1.55μm)

5.2 Temperature characteristics

Transmission loss changes were investigated over a temperature range from -30 through +70°C. Results are given in figure 7. No significant loss change was observed over this range.
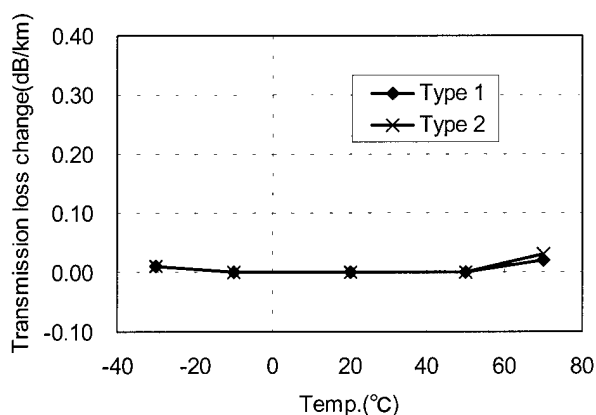
Figure 7. Transmission loss change in temperature cycling (@1.55μm)

5.3 Tensile characteristics

Fiber strain was investigated when an elongation strain equal to 0.35 percent was applied to the suspension member of the trial cable. The results are shown in figure 8. No increase in fiber strain was observed up to an elongation strain of 0.3 percent. This confirmed the trial cable has sufficient excess length for more than 0.3 percent elongation of the suspension member
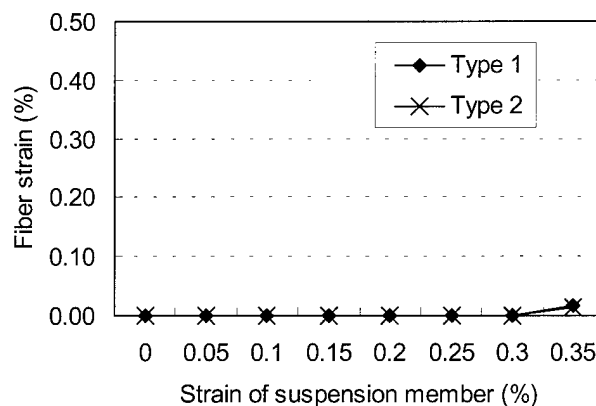
Figure 8. Tensile test

5.4 Other mechanical characteristics

The results of the mechanical tests are summarized in table 1. Each trial cable was evaluated for bending, lateral pressure, squeezing, twisting, and impact. These tests all yielded satisfactory results.

Table 1. Results of mechanical test (@1.55μm)

Item	Condition	Result
Bending	6D	< 0.01 dB
Lateral pressure	1960 N/ 100 mm	< 0.01 dB
Squeezing	R = 250 mm 1960 N	< 0.01 dB
Twist	±360°/m	< 0.01 dB
Impact	1 kg × 1 m	< 0.01 dB

5.5 Mid-span access

The transmission loss change was investigated when the sheath was removed at a length of 500 mm and the ribbons are picked up, and the excess length of the fiber ribbons was measured after the operation. Results are shown in table 2. No significant loss change was observed, and sufficient excess length of the fiber was measured.

Table 2. Results of mid-span access

Type	Transmission loss change	Excess fiber length
Type 1	< 0.01 dB	> 40 mm
Type 2	< 0.01 dB	> 40 mm

5.6 Vibration test

The trial cable was installed between poles with a span of 35 meters, and a million repetitions of 250-mm-amplitude vibration was imposed. The general view of this test is shown in figure 9. The transmission loss change in this test is shown in figure 10. There was almost no significant change in loss, and movement of the fiber.
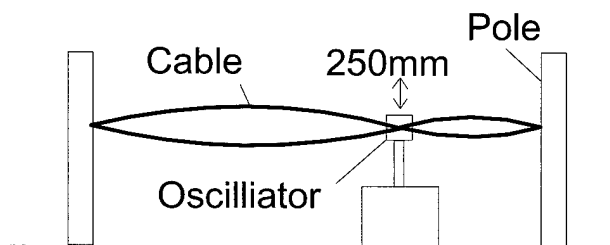
Figure 9. Vibration test
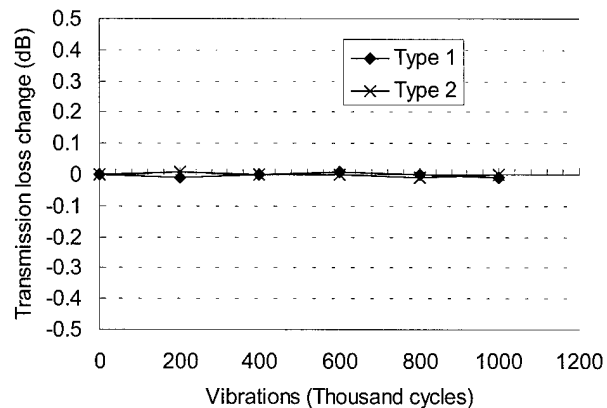
Figure 10. Transmission loss change under vibration (@1.55μm)

5.7 Installation test

The trial cables were installed between poles, and long-term transmission loss change was investigated. Results are given in figure 11. There was almost no significant change in loss, and movement of the fiber.
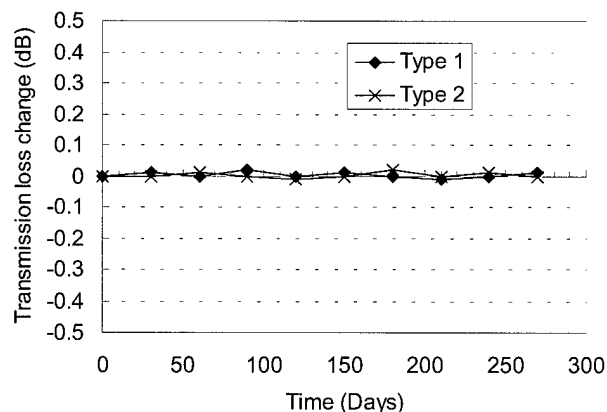
Figure 11. Transmission loss change while Installed (@1.55μm)

6. Conclusions

We developed new types of optical fiber cables. The advantages of this cable are summarized as follows:

- Only a single process in manufacturing process is need because the simple structure.
- It is small in size and light in weight, so economical construction of access networks is possible.
- It is easy to handle the fiber ribbons because of the absence of jelly around the fiber ribbons.
- The successful results obtained in evaluation testing for various characteristics

We hope that the use of optical fiber cables for access networks expands with this new cable.

7. References

[1] H.Iwata *et al.*, "Novel Optical Cable for Distribution Use in Access Network", 48th IWCS, pp.20-24 (1999)

[2] Kobayashi *et al.*, "Development of aerial distribution cables with 4-fiber ribbons", 46th IWCS, pp.166-175 (1997)

[3] D.Iwakura *et al.*, "Development of new aerial self-supporting cable with excess fiber ribbon length in SZ-slot", 48th IWCS, pp.578-584 (1999)

Authors
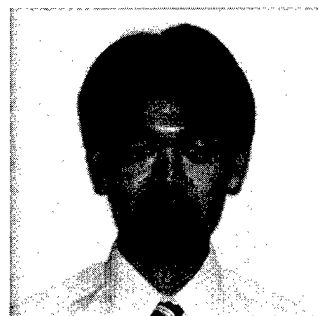
Tetsuya Yasutomi

The Furukawa Electric
Co., Ltd.

6 Yawatakaigan-dori,
Ichihara, Chiba, Japan
tomy@ch.furukawa.co.jp

Tetsuya yasutomi received his M.E. degree in Metallurgy Engineering from Tokyo University in 1998. He joined The Furukawa Electric co., ltd. in 1998 and has been engaged in research and development of optical fiber cables. He is now a research engineer of FITEL Photonics Laboratory.

Masato Kohsaka

The Furukawa Electric
Co., Ltd.

6 Yawatakaigan-dori,
Ichihara, Chiba, Japan
kosaka@ch.furukawa.co.jp

Masato Kohsaka received his B.E. degree in Electric Engineering from Ryukyu University in 1989. He joined The Furukawa Electric co., ltd. in 1989 and has been engaged in research and development of optical fiber cables. He is now a senior research engineer of FITEL Photonics Laboratory.
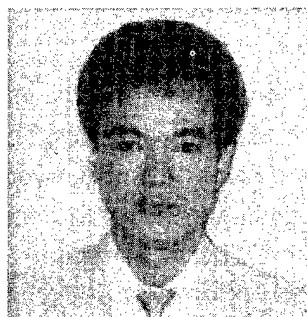
Eiji Konda

The Furukawa Electric
Co., Ltd.

6 Yawatakaigan-dori,
Ichihara, Chiba, Japan
konda@ch.furukawa.co.jp

Eiji Konda joined The Furukawa Electric co., ltd. in 1977 and has been engaged in research and development of optical fiber cables. He is now a research engineer of FITEL Photonics Laboratory.

Ichiro Kobayashi

The Furukawa Electric
Co., Ltd.

6 Yawatakaigan-dori,
Ichihara, Chiba, Japan
Ichiro@ch.furukawa.co.jp

Ichiro Kobayashi received his B.S. degree in Physics from Chuou University in 1986. He joined The Furukawa Electric co., ltd. in 1986 and has been engaged in research and development of optical fiber cables. He is now a manager of FITEL Photonics Laboratory.

Akio Hasemi

The Furukawa Electric
Co., Ltd.

6 Yawatakaigan-dori,
Ichihara, Chiba, Japan
hasemi@ch.furukawa.co.jp

Akio Hasemi received his B.S. degree in chemistry from Chiba University in 1979. He joined The Furukawa Electric co., ltd. in 1992 and has been engaged in research and development of optical fiber cables. He is now a general manager of FITEL Photonics Laboratory.

Development of the New Downsized Aerial Optical Cables with SZ-Slotted Rod and without Slotted Core

Masayoshi Yamanaka, Hirohito Watanabe, Akimi Yamasaki, Naoki Okada,

Koichiro Watanabe, Matsuhiro Miyamoto

Fujikura Ltd.
Research and development department
Telecommunication cable division
1440, Mutsuzaki, Sakura-shi, Chiba, Japan
+81-43-484-3945   masayoshi@s.fujikura.co.jp

Abstract

In order to construct the optical access networks economically, new downsized aerial cables have been developed. We have successfully achieved small and lightweight self-supporting aerial cables with high advantage of easy mid-span access operation.

The SZ-slotted core structure was redesigned in order to reduce diameter and weight compared with ordinary slotted core cable, on the basis of improvement of manufacturing technology and design concept. Moreover, new cable core structure without slotted has been developed for low fiber count cable. We confirmed that this structure was better than SZ-slotted core with respect to small diameter, lightweight, and low cabling cost. Based on these designs, the aerodynamic drags of the cable decrease, so that the size of stranded steel messenger are reduced. Therefore, the small and lightweight self-supporting aerial cables are designed.

The newly designed self-supporting aerial cables provide mid-span access operation as easy as that of ordinary self-supporting cable.

These aerial optical cables are expected to be suitable for construction of the FTTH networks in the future.

Keywords

Self-supporting aerial optical cable; mid-span access; SZ-slotted rod; new structure without slotted core

1. Introduction

In recent years, the optical access networks are under construction to achieve the Fiber To The Home (FTTH) networks in the future. In Japan, the aerial cable networks are general. Therefore, the self-supporting cable is the suitable structure from the viewpoint of the easy installation.

In the access networks, the cables should be designed in consideration of easy mid-span access operation. Ease of mid-span access is considered to be one of the key technologies in the FTTH applications. The SZ-stranded structure is suitable for mid-span access, because any optical fiber can be picked out from the installed cable at any point for distributed subscribers. The self-supporting aerial SZ-slotted core cables with 4-fiber ribbons was already developed and commercialized.

Considering the future optical access networks, the small diameter and lightweight cables with easy branching performance may be effective to reduce material and installation cost. Therefore, we have tried to decrease the SZ-slotted core cable diameter without degradation of easy mid-span access operation. And the new simple cables without slotted core for lower count structure have been designed with easy mid-span access operation.

2. New self-supporting aerial cable with 4-fiber ribbons

We have designed the new downsized self-supporting aerial cables in consideration of easy mid-span access operation and small diameter and lightweight in order to decrease the cost. The key points of the cable design are as following.

1) Mid-span access operation

The availability of mid-span access is indispensable for construction of the optical access networks for distributed subscribers. Ease of mid-span access is considered to be a key of aerial cable design

2) Downsizing and lightweight

For easy installation of the aerial cable, it should be self-supporting structure, small diameter, and lightweight cable.

3) Cost reduction

The stranded steel messenger applied to new aerial cables can be downsized due to the reduction of size and weight of optical cable portion [1]. Downsizing the optical cables and the stranded steel messengers save the material cost. Moreover, new cable structure except for the slotted core structure for low fiber count cable should be introduced to reduce cable cost.

3. Structure of new self-supporting aerial cable

3.1 Downsized SZ-slotted rod type

As mentioned above, the self-supporting cables are desirable in access aerial networks. The mid-span accessibility is most important factor. The SZ-slotted core cable is favorable structure for mid-span access operation. The optical fiber can be picked out from the SZ-slotted core cable at the any point, because the slots of the SZ-slotted rod are made to reverse alternately [2]. The schema of the optical fiber picked out from the SZ-slotted core aerial cable is shown in Fig.1. We had developed the self-supporting aerial cables with the SZ-slotted rod. And the cables have the sag to steel messenger. These conventional SZ structures have disadvantage of larger diameter than that of helical slotted core cable.
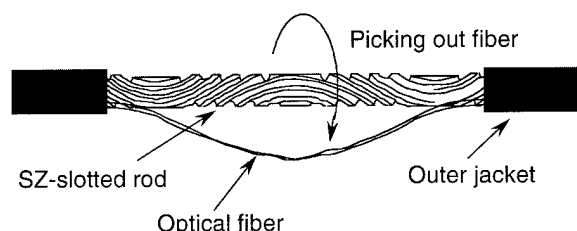
Fig.1. Schema of optical fiber picked out from SZ-slotted core cable

So far, we need to design the SZ-slotted rod to have enough large gap in a slot. In order to get the stable transmission characteristics, it was necessary to reduce the unexpected force to the fiber ribbons by sufficiently large gap [3]. And insertion of the fiber ribbons into the slots of the SZ-slotted rod with stable condition is an important process technique.

In this study, we have found out that the good transmission characteristics of thinner SZ-slotted rod could be obtained with small gap in a slot by new design. And we have improved manufacturing techniques enabling that the optical fiber ribbons can be inserted securely into the narrow SZ-slots. We have successfully developed the small SZ-slotted rod of which diameter almost equal to that of the conventional helical core cables [4].

It has been reported that the most important structural parameter to get the good transmission characteristics and small fiber strain is the reverse lay angle [3], [4]. And it has been known that the reverse lay angle of 275degree is optimum value. However, that optimum value was obtained on the assumption that the locus of the slots on the SZ-slotted rod is sinusoidal wave.

We have paid attenuation to locus of a slot on an SZ-slotted rod, and studied the strain of locus of a slot on an SZ-slotted rod by using the Fourier transformation method. The optimum locus of a slot on an SZ-slotted rod became clear through the Fourier

analysis of a locus data obtained from rotary encoder moving along a locus.

In has been reported that the stacked fiber ribbons are rotated inside each slot for back twisting. However, we have made it clear that back-twisting the ribbons should not be uniform along the longitudinal direction of the SZ-slotted rod. The ideal back twisting condition is shown in Fi.2. In the rotated part range that is defined as the center between reverse points, the fiber ribbons should not be back twisted. Then, near the reverse point, the ribbons should be back twisted about 90 degree.
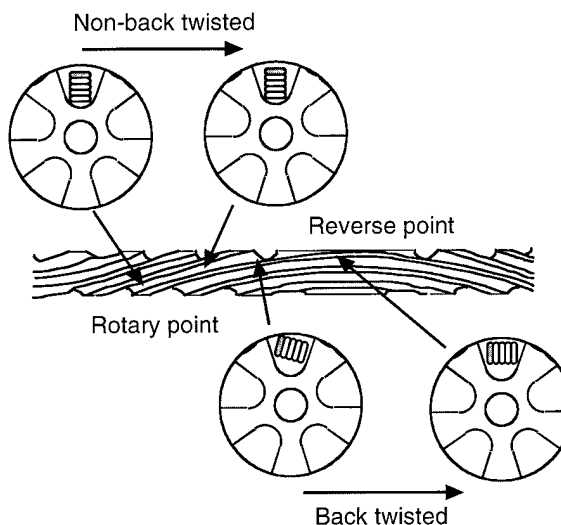
Fig.2 Condition of ideal back twisting

We have established the technique so that the stacked ribbons are inserted into each slot with the ideal back twisting in order to manufacture the downsized SZ-slotted core cable that has stable characteristics. Moreover, the technique helps increase the manufacturing speed.

The downsizing the SZ-slotted rod resulted in the downsizing the aerial cables. The new downsized self-supporting aerial cables are shown in Fig.3 and the comparison between the new cables and the conventional cable is shown in Table.1. About 12~13% decrease in height and about 22~27% decrease in weight are achieved in new cables.

3.2 Slotted rod less type

The material cost of the cable core has more significant effect on cable cost per fiber count for lower fiber count. We have adopted new cable core structure without slotted rod for less than 40-fiber count aerial cable. These cables provide the advantages of the easy installation because they have lightweight and small diameter as shown in Fig.3 and Table.1. About 31% decrease in height and about 51% decrease in weight are achieved in new cables.

This new cable structure is very simple and it consists of sheath with strength member, stacked 4-fiber ribbons and dry core. This

structure enables to be easy sheath entry and quick ribbons preparation by eliminating the wiping out process of filling compound from ribbons. And this cable can be fabricated by one process. Conventional self-supporting sheath process is applied.
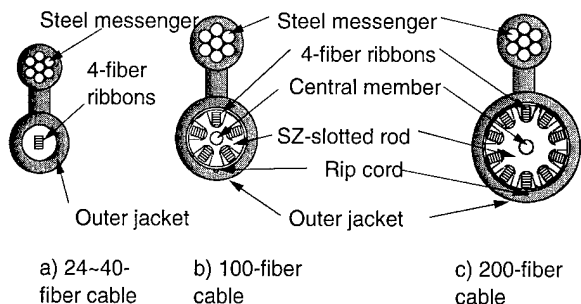
Fig.3-1. New optical access cables
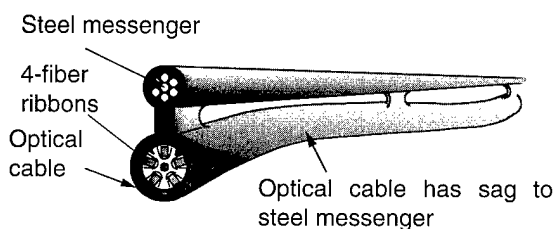
Fig.3-2. Self-supporting cable structure

Table.1 Structure of new aerial cables

Cable Structure		Height	Weight
40-fiber	New cable	18mm	0.17kg/m
	Reduction ratio	-31%	-51%
100-fiber	New cable	23mm	0.28kg/m
	Reduction ratio	-12%	-22%
200-fiber	New cable	27mm	0.36kg/m
	Reduction ratio	-13%	-27%

4. Performance of trial cables

The trial cables were manufactured and tested in order to evaluate cable performance. Both environmental and mechanical testing were performed on the trial cables. And mid-span access operation was also evaluated.

4.1 Mechanical characteristics

The trial cables were tested to ensure acceptable mechanical resistance during installation and operating conditions. During these tests, the attenuation changes were not observed at 1.55 μm wavelength. Test procedures and the results are summarized in Table 2.

4.2 Environmental test

To test the environmental performance of the cable, we subjected the trial cables to a temperature-cycle test. The temperature-cycle pattern for this test and the obtained results are given in Fig 3. During the test, the change in attenuation was less than 0.15 dB/km at both wavelengths of 1.55 μm and 1.3 μm.
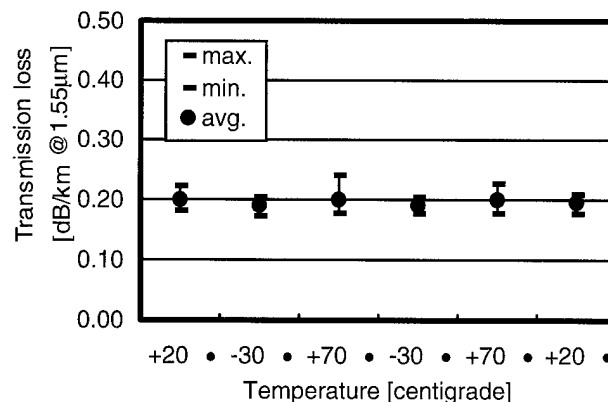
Fig.4-1. Temperature-cycle characteristics of 40-fiber aerial cable
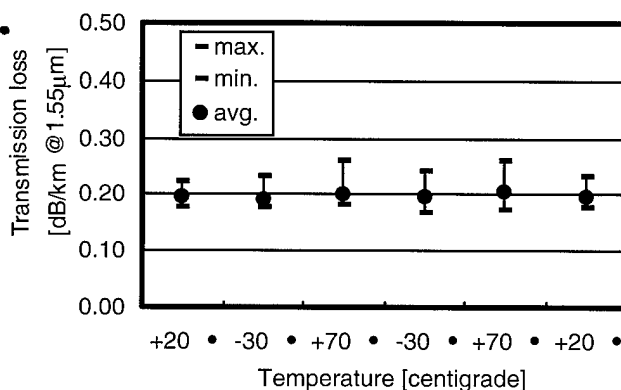
Fig.4-2. Temperature-cycle characteristics of 200-fiber aerial cable

4.3 Mid-span access operation

Fiber sag of 20mm is at least required for using the conventional identification tool [1]. When the 500 mm length of sheath is removed, the fiber sag is measured picked out from new aerial optical cable. It was confirmed that the fiber sag was more than 20 mm for mid-span access operation.

The mid-span access performance was evaluated using installed trial cables with the SZ-slotted rod and without slotted core. Fig.5 shows the operating processes and time during each process. It was clarified that the mid-span access performance of the new aerial cables was equal to that of the conventional aerial cables. Especially, mid-span operating time of the new aerial cable without slotted core take less than that of the SZ-slotted core cable.

Table.2. Mechanical characteristics

Test performed	Test procedure	Cable performance
Tensile test	Tensile load: 0.2%	No attenuation change observed
Installation test	Allowable tension Bending radius:250mmR	No attenuation change observed
Bending test	Bending radius:160mmR	No attenuation change observed No visual damage observed
Crush test	1960N/100mm	No attenuation change observed No visual damage observed
Torsion test	90 ˚CW&CCW twist	No attenuation change observed No visual damage observed
Impact test	9.8N/m	No attenuation change observed No visual damage observed

Attenuation changes was measured by 1.55μm wave length

Mid-span access procedure
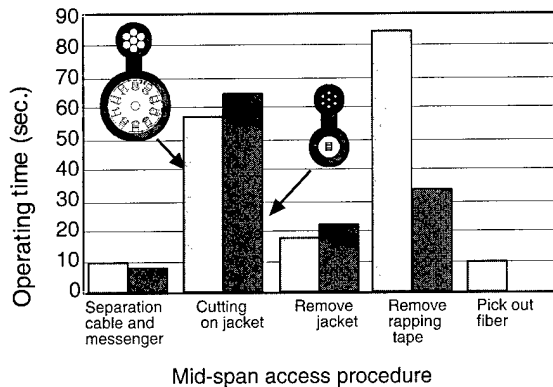
* When rapping tape of non slotted core cable is removed, fiber is picked out.

Fig.5. Operating time of mid-span access

5. Conclusions

We have developed the new aerial optical cables with downsized SZ-slotted core and without slotted rod. Downsizing SZ-slotted core cable was obtained by means of advanced process and design technologies. Moreover, for less than 40-fiber cables, the new structure without slotted core has been developed in order to get lighter weight and smaller diameter with a good mid-span access performance.

The trial cables were manufactured and tested. These trial cables showed an excellent performance.

The downsized aerial cables have advantageous points to the conventional types as follows.

1) The downsizing the cables decreases a weight and a diameter.

2) These provide with the decreasing of the cost of the material and installation.

These aerial cables are expected to be suitable for construction of the FTTH in the future.

6. References

[1] H. Iwata, et al.: IWCS Proceedings, pp.20 (1999)

[2] H. Iwata, et al.: IWCS Proceedings, pp.4(1997)

[3] N. Okada, et al.:IWCS Proceedings, pp.122(1999)

[4] M. Yamanaka, et al.: NFOEC Technical Proceedings, Vol.1 pp.230 (1999)

Authors

Masayoshi Yamanaka

Research and development department

Telecommunication cable division

Fujikura Ltd.

1440, Mutsuzakki, Sakura-shi, Chiba, 285, Japan

masayoshi@s.fujikura.co.jp

Masayoshi Yamanaka was born in 1966. He joined Fujikura Ltd after his graduation from Tohoku University with M.E. degree in 1992 and has been engaged in research and development of optical fiber cables. He is now an engineer in the Telecommunication Cable Department and a member of the IEICE of Japan.
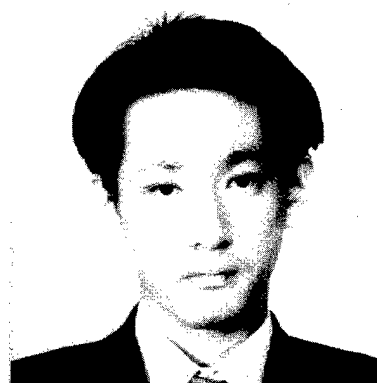
Akimi Yamazaki

Research and development department

Telecommunication cable division

Fujikura Ltd.

1440, Mutsuzakki, Sakura-shi, Chiba, 285, Japan

yamazaki@s.fujikura.co.jp

Akimi Yamazaki was born in 1971. He joined Fujikura Ltd after his graduation from Osaka University with M.E. degree in 1997 and has been engaged in research and development of optical fiber cables. He is now an engineer in the Telecommunication Cable Department and a member of the IEICE of Japan.
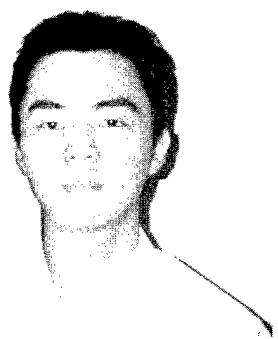
Hirohito Watanabe

Research and development department

Telecommunication cable division

Fujikura Ltd.

1440, Mutsuzakki, Sakura-shi, Chiba, 285, Japan

hiro@s.fujikura.co.jp

Hirohito Watanabe was born in 1971. He joined Fujikura Ltd after his graduation from Yokohama National University with M.E. degree in 1996 and has been engaged in research and development of optical fiber cables. He is now an engineer in the Telecommunication Cable Department and a member of the IEICE of Japan.
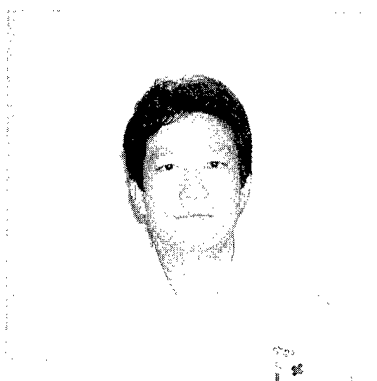
Naoki Okada

Research and development department

Telecommunication cable division

Fujikura Ltd.

1440, Mutsuzakki, Sakura-shi, Chiba, 285, Japan

naookada@s.fujikura.co.jp

Naoki Okada was born in 1964. He joined Fujikura Ltd after his graduation from Chiba University with B.E. degree in 1986 and has been engaged in research and development of optical fiber cables. He is now an engineer in the Telecommunication Cable Department and a member of the IEICE of Japan.

Koichro Watanabe

Research and development department

Telecommunication cable division

Fujikura Ltd.

1440, Mutsuzakki, Sakura-shi, Chiba, 285, Japan

kwatanabe@s.fujikura.co.jp

Koichro Watanabe was born in 1959. He joined Fujikura Ltd after his graduation from Tohoku University with B.E. degree in 1988 and has been engaged in research and development of optical fiber cables. He is now a manager in the Telecommunication Cable Department and a member of the IEICE of Japan.
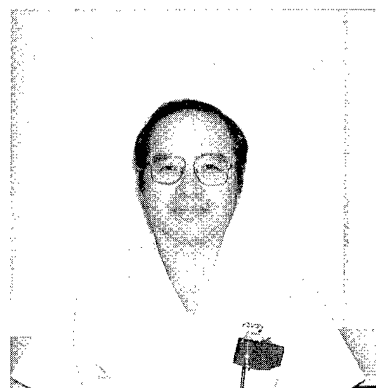
Matsuhiro Miyamoto

Research and development department

Telecommunication cable division

Fujikura Ltd.

1440, Mutsuzakki, Sakura-shi, Chiba, 285, Japan

mmiya@s.fujikura.co.jp

Matsuhiro Miyamoto was born in 1953. He graduated from Nagoya Institute of Technology with a B.E degree of electrical engineering. He joined Fujikura Ltd. after his graduation from Tokyo Institute of Technology with M.S. degree in 1978 and has been engaged in research and development of optical fibers and optical fiber cables. He is now a general manger of the Telecommunication Cable Department and a member of IEICE of Japan.

Design of Compact Size Aerial Cable
for Easy Mid-Access Network

H.T. Choi, S.C. Park, Y.I. Lee, H.J. Kang

Taihan Electric Wire Co., Ltd.
Anyang-City, Kyungki-do, Korea
+82-31-420-9350
htchoi2@taihan.com, scpark@taihan.com, yilee@taihan.com, hjkang@taihan.com

Abstract

We have designed a compact size ribbon aerial cable for easy mid-access network and branching. The designed cable have a dual structure consisted in SZ slotted rod for internal layer and ribbon tubes for external layer. We have investigated the amount of fiber excess length for branching and optimum structures taken into account clearance and strain caused by cable bending. This cable had good mid-access characteristic for suitable aerial applications and also showed excellent mechanical and environmental performances.

Keywords

SZ slotted rod; ribbon tubes; mid-access; slack length.

1. Introduction

As the demand of optical fiber is rapidly increased for worldwide Internet, we designed a ribbon aerial cable with compact size for easy mid-access network. It is very important to design the optical cable structure to access fibers in mid-point on the aerial environments. Also, we should consider high-count fiber cable for feasibility of expanding to the end users. Thus, we try to design a dual structure cable with combination of SZ slotted rod and ribbon tubes. The manufacturing method and characteristics between SZ slotted cable and ribbon tube cable is different from each other. The SZ slotted core shall be designed with structurally sufficient clearance into groove, proper lay length and reverse lay angle of slot, and the residual strain must be technically controlled by applying tension for long-term fiber compatibility. On the other hand, in case of ribbon tube construction, it shall be considered adequate clearance in tube as well as lay length to control minimum fiber bending radius. In order to accommodate larger fiber excess length, we theoretically investigate optimum structures and lay lengths for SZ slotted rod and ribbon tube according to each fiber strain. In this paper, we will describe this type of cable show the suitable structure as well as excellent properties to use long haul networks.

2. Theory and Cable Design
2.1 Theory

In order to prevent the unexpected force to the fiber, it is important to control fiber excess length in accordance with SZ reverse lay length. Especially in case of SZ slotted rod, the fiber strain is the most considerable factor during cable bending. From the above-mentioned problems, we theoretically investigated optimum structures and lay lengths each type.
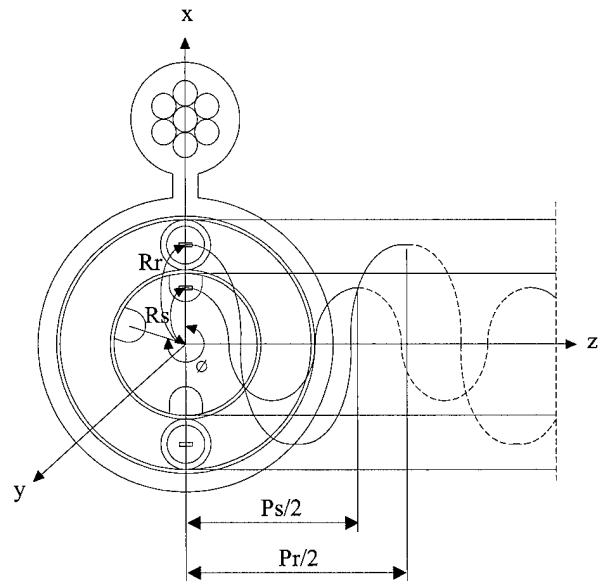
Figure 1. Set-up for SZ path length analysis

Figure 1 shows the calculation model of fiber excess length for internal SZ slotted rod and external ribbon tube. The fiber slack length can be expressed by using cylindrical coordinate system, and the fiber path length is expressed as following equation (1);

$$x = Rs \cos \theta$$

$$y = Rs \sin \theta$$

$$z = \frac{Ps}{2} + \frac{Ps}{2\pi} \sin^{-1} \frac{2\theta}{\phi}$$

$$F(l) = \int_C f(x, y, z)dl$$

$$= 2 \int_{-\phi/2}^{\phi/2} \sqrt{(\frac{dx}{d\theta})^2 + (\frac{dy}{d\theta})^2 + (\frac{dz}{d\theta})^2} \, d\theta \qquad (1)$$

Where, by substituting $t = \sin^{-1} \frac{2\theta}{\phi}$

The fiber path length is calculated by equation (2);

$$F(l) = 2 \int_{-\pi/2}^{\pi/2} \sqrt{(\frac{dx}{dt})^2 + (\frac{dy}{dt})^2 + (\frac{dz}{dt})^2} \, dt$$

$$= 2 \int_{-\pi/2}^{\pi/2} \sqrt{\left(\frac{Rs\phi}{2}\right)^2 \cos^2 t + \left(\frac{Ps}{2\pi}\right)^2} \, dt$$

$$\approx Ps \left[1 + (\frac{\pi Rs\phi}{2Ps})^2 \right] \tag{2}$$

When the cable jacket is removed at the reverse point, the slack length is simply obtained as equation (3).

$$S(l) = \sqrt{(\frac{F(l)}{2})^2 - (\frac{L}{2})^2} \tag{3}$$

Where,

ϕ	: SZ reverse angle
Ps or Pr	: SZ reverse pitch
L	: Removed jacket length for each type
Rs or Rr	: Fiber bending radius for each type

The slack length depends on different reverse pitches and the point where SZ reverse pitch is located at removed jacket length. The theoretical evaluation programs and several experiments have successfully led to optimum conditions as reverse pitch and angle of SZ slotted rod is 500mm and 275 degrees respectively. To satisfy the mid-access properties, the slack length was investigated in line with the variation of SZ reverse pitch and removed jacket length.
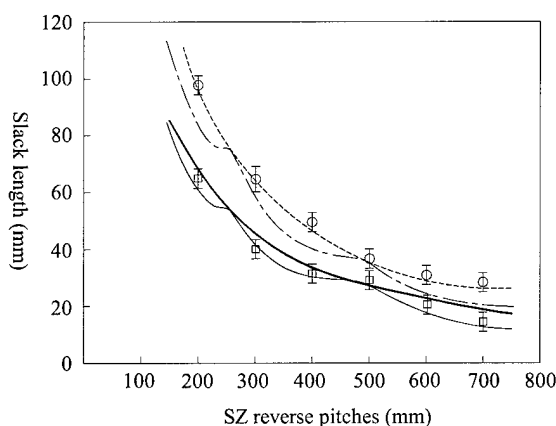
	———	Theoretical value
SZ slotted rod	——	Simplified value
	田	Experimental value
	—·—·—	Theoretical value
Ribbon tube	------	Simplified value
	Φ	Experimental value

Figure 2. Fiber slack length in SZ slotted rod and ribbon tube

Figure 2 is shown a schematic representation of relationship between slack length and SZ reverse pitches when the center of removed jacket length is located in mid-point of SZ reverse pitch. The slack length was expected to obtain according to the SZ reverse pitch when the bending radius is 5.2mm and jacket removal length is 500mm. In order to get more than 20mm slack length, it was necessary to remove the cable jacket more than 500mm.On the other hand, in case of external ribbon tube, SZ reverse pitch should be minimum 400mm to meet the minimum bending radius condition. Also as the bending radius of ribbon tube is larger than that of SZ slotted rod, we can easily get longer slack length. By using same equation and method of SZ slotted rod, more than 30mm slack length can be obtained from 500mm removal of cable jacket. The trial cable of ribbon tube was manufactured with the 600mm SZ reverse pitch in order to get the stable slack length as the margin of minimum stranding pitch for ribbon tube is enough.

2.2 Cable Design

The SZ slotted cable has a strong construction against external force such as impact, compression and etc.. But, ribbon tube cable is more flexible and accessible with easy handling per tube. To exploit above-mentioned both advantages, the criteria to be considered when we design aerial cable are based on the following points;

1) Use of 4-fiber ribbon for easy branching

2) SZ structure for easy mid-access

3) Composite cable with SZ slotted rod and ribbon tubes

2.2.1 SZ slotted rod for internal layer. The SZ slotted rod shall be taken mid-access performance as well as minimized residual strain into consideration. This rod has ten grooves and each groove contains five 4-fiber ribbons with 0.3mm thickness. From the theoretical and experimental analysis, the SZ pitch and reverse angle is adapted 500mm and 275 degrees respectively. Especially, the 4-fiber ribbon is inserted in slot by back-twisting method to reduce the twist and lateral force for long-term reliability.

2.2.2 Ribbon Tubes for external layer. The clearance and reverse lay length of tubes are the most important parameters as these factors generate the fiber strain due to bending or stranding. These factors can be calculated considering minimum bending radius of fiber caused by pitch circle radius. But, the actual strain may be decreased compared to theoretical value because of its loose tube construction. The ribbon tube has additional fiber excess length itself as the stacked ribbons are helically twisted during the tube extrusion process. This excess length of fiber in tube shall be served as an absorption factor against stress although lateral force such as tensile loading or bending is applied. The ribbon tubes also withstand the cable contraction or expansion without excessively bending of ribbon in tube, which is resulted in strain or attenuation increase of ribbon fiber. Because of the different thermal expansion coefficient of cable components,

bending of ribbons and strain increase may occur from extreme temperature change. To adjust this thermal expansion and contraction, the clearance of inner diameter of ribbon tube is one of the critical components. The sufficient excess length and stable thermal properties of ribbon tube can be produced with proper clearance. The several kinds of ribbon tubes, which have different clearance, were made and tested to find out the ideal clearance for aerial application as shown in Figure 3. The inner diameter of tube should be more than Rt*N(mm), and is calculated by equation (4).

$$T \, id \geq \sqrt{(Rt \cdot N)^2 + Rw^2} + 2\Delta C \qquad (4)$$
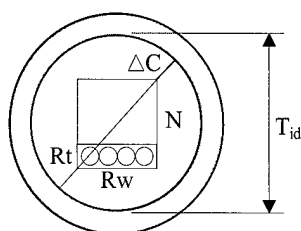
Rt   : Ribbon thickness
Rw   : Ribbon width
N   : Number of stacked ribbon
△C   : Clearance

Figure 3. Clearance of ribbon tube

Accordingly based on experimental analysis, the clearance is determined minimum 0.6mm when strain is less than 0.1% and added loss is not more than 0.05dB/km. The tube is made of thermoplastic resin with high Young's modulus, and the jelly is filled into loose tube as water blocking. The eleven loose tubes are stranded by reverse lay method around SZ slotted rod in order to obtain easy mid-access.

We manufactured several trial cables with various twisting pitches and investigated its performance by several tests. Table 1 and Figure 4 demonstrates the cross-section and characteristics of 420-fiber aerial cable with dual layers, which have slot and ribbon tube. The both layers are designed dry types to ensure craft friendly accessibility and 8-figure construction with 7/2.0mm suspension strand wire.

Table 1. Other mechanical tests

Items	Construction
Diameter	24.8mm(width), 35.8 mm(height)
Weight	0.63 g/m
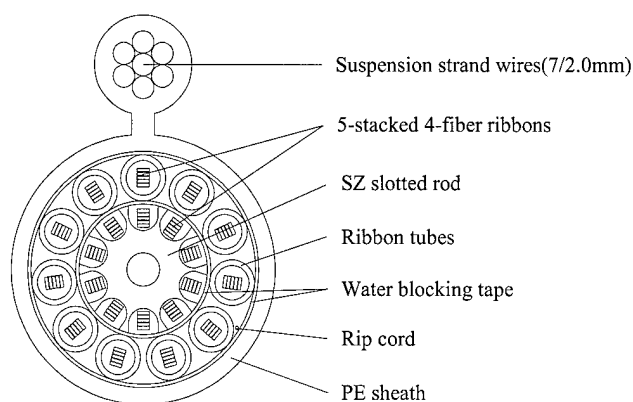
Figure 4. Cross-section for 420-fiber aerial cable

3. Cable Performance Tests

3.1 Tensile Loading Test

The installation tension in the aerial environments was applied to the trial cable, then the fiber strain and transmission loss was checked. Figure 5 shows the relationship between tensile force versus fiber strain of ribbon in slot and tube respectively for aerial cable. When the tensile force is applied to aerial cable up to 12kN, there was no change in optical attenuation, and the fiber strain was observed less than 0.05%. The fiber strain of ribbon tube is shown less than that of fiber in slot. The reason came from lower strain in ribbon tube is that the ribbon tube type has some more fiber excess length, and loose construction provides hydrostatic component of resistance to fiber core structure during tensile loading.

○	Cable strain
□	Fiber strain in SZ slotted rod
△	Fiber strain in ribbon tube
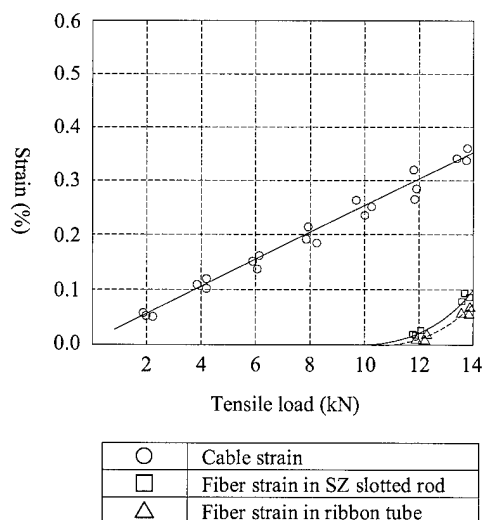
Figure 5. Relationship of strain versus tensile loading

3.2 Galloping Test

The 8-figure self-supporting cable, assuming that it is installed under wind condition, is investigated to assess the fatigue performance for fiber long-term compatibility. Figure 6 is shown a facility configuration for galloping test. The cable was tensioned to a minimum 50% of the maximum rated installation tension and excited by shaker in the vertical plane. The attenuation was continuously monitored and recorded. The change in attenuation at 1550nm was stable not more than 0.05dB during the test.
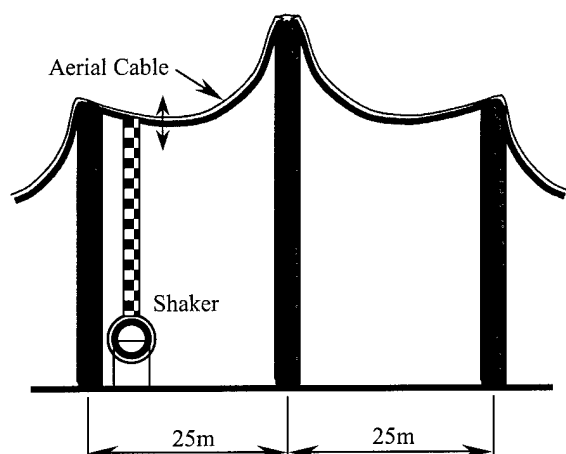
Figure 6. Set-up for galloping test

3.3 Aeolian Vibration Test

The aeolian vibration test was performed as similar as galloping test facility. The cable was tensioned to 100% of the rated maximum installation tension. The optical fiber was concatenated one fiber from each slot and tube. And then, the shaker excited the cable in the span to allow for vibration loops. The cable was subjected to a minimum of 100 million vibration cycles. The attenuation was continuously monitored and recorded. No significant attenuation increase and mechanical damage was observed.

3.4 Temperature Cycling Test

The behavior of transmission loss at extreme temperature range was experimentally investigated for each type. The 1-km cable length is wound onto a reel and placed in an environmental chamber. The concatenated fiber was mostly chosen by edge fibers of ribbon from each slot and tube as these are positioned in the weakest condition. And then, the range of temperature test from – 30 degree to +70 degree was applied. The maximum attenuation increase of each layer was not greater than 0.05dB/km at 1550nm as shown in Figure 7. Especially, the ribbon tubes exhibited a stable characteristic regardless of extreme temperature change.
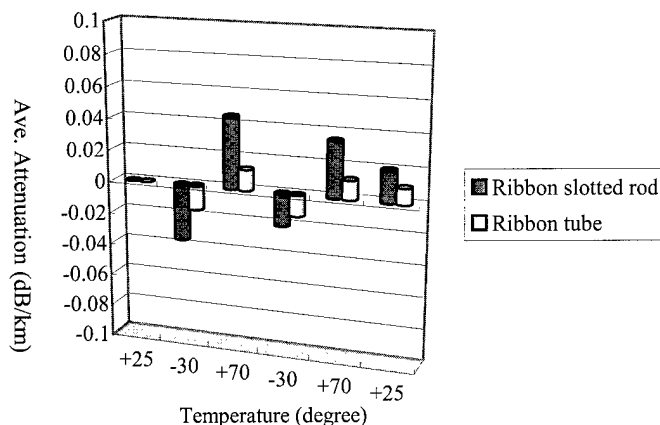
Figure 7. Temperature cycling test

3.5 Other Mechanical Test

The cable was evaluated for other mechanical and environmental tests such as crush, impact, bending and twisting according to international standards. The results are shown in Table 2 and presented good characteristics.

Table 2. Other mechanical tests

Items	Test procedure	Conditions
Crush	EIA/TIA-455-41 or IEC 794-1-E3	2000N/100mm 10 minutes duration No damage observed Change = less than 0.05dB
Impact	EIA/TIA-455-25 or IEC 794-1-E4	1kg weight, 1m height 10 different points with 100mm interval No damage observed Change = less than 0.05dB
Bending	EIA/TIA-455-104 or IEC 794-1-E6	10 times (cable OD) 25 cycles No damage observed Change = less than 0.05dB
Twisting	EIA/TIA-455-85 or IEC 794-1-E7	2m length clock & counterclockwise 180 degrees, 10 times No damage observed Change = less than 0.05dB

4. Conclusion

In order to realize the FTTH for easy mid-access performance, we have evaluated a aerial cable that is consisted in SZ slotted rod for internal layer and ribbon tubes for external layer. Based on theoretical analysis and actual cable design, the optimum lay length of SZ slotted core and ribbon tube was studied and at that time we found that this cable has proper slack length, which is more than 20mm at branching point. We have demonstrated that the new aerial cable has not only the excellent transmission

characteristics but also suitable aerial applications. And also, this cable structure will lead to a solution for composite cable with combination of slot and tube to make effective use of advantages such as more flexible and accessible.

5. Acknowledgments

The authors wish to thank J.C. Jo and N.E. Kwack for assistance in manufacturing cable including tests and gathering data, and their valuable contributions to this paper.

6. References

[1] Hiroki Ishikawa, Yoshiyuki Suetsugu and Gen Morikawa, "A study on mid-span accessibility for ultra high count SZ-type optical fiber cable" Proceedings of the 47th International Wire and Cable Symposium, 1998. pp. 542~ 547

[2] Naoki Okada, Yoshiyasu Sato, Akimi Yamasaki and Matsuhiro Miyamoto, "Study of the SZ-stranded 2000-fiber cable with 8-fiber ribbons for underground access networks" Proceedings of the 47th International Wire and Cable Symposium, 1998. pp. 220~ 226

[3] Naoki Okada, Masayoshi Yamanaka, Koichiro Watanabe and Matsuhiro Miyamoto, "Study on bending strain of SZ slotted core cable with fiber ribbons" Proceedings of the 48th International Wire and Cable Symposium, 1999. pp. 112~ 117

7. Biographies

Hee-tea, Choi

Taihan Electric Wire
Co., Ltd. Korea
htchoi2@taiham.com

H.T. Choi received his B.A. degree from Hanyang University in 1994. He joined Taihan Electric Wire Co., Ltd. and has been engaged in Fiber Optics Engineering Team. Now he is an assistant manager of Fiber Optics Engineering Team and has worked a variety of design and development projects in cables and materials.
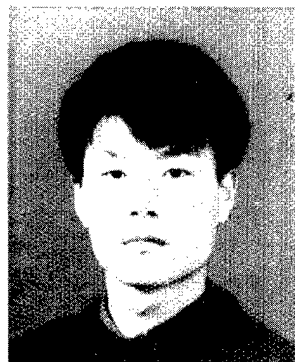
Sang-cheol, Park

Taihan Electric Wire
Co., Ltd. Korea
scpark@taihan.com

S.C. Park received his B.A. degree from Ajou University in 1994. He joined Taihan Electric Wire Co., Ltd. and has been engaged in Fiber Optics Engineering Team. Now he is an assistant manager of Fiber Optics Engineering Team. He has been involved with ribbon and slotted cable products since 1996.
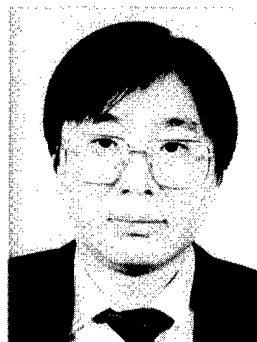
Young-ik, Lee

Taihan Electric Wire
Co., Ltd. Korea
yilee@taihan.com

Y.I. LEE received his B.A. and M.S. degree from Yonsei University in 1981. He joined Taihan Electric Wire Co., Ltd. and has been engaged in Fiber Optics Engineering Team. Now, he is a general manager and he is a member of SG. 6 CCITT sub-committee of Korea and the Korea Institute of Communication Sciences. His current work focuses on product development and application of fiber optic and cable design.

Hee-jeon, Kang

Taihan Electric Wire
Co., Ltd. Korea
hjkang@taihan.com

H.J. Kang received his B.A. degree from Hanyang University in 1979. He joined Taihan Electric Wire Co., Ltd. and has been engaged in Fiber Optics Engineering Team. He has worked in development and research of optical fiber and cable during 20 years. Now he is a managing director in Anyang communication factory.

Self-Damping Characteristics of the Transmission Lines with Attached Optic Cable

Zhan Gao, Alois Weiß

Corning Cable Systems RD&E,
D-96465 Neustadt Germany
+49 9568-932307, alois.weiss@corning.com

ABSTRACT

This paper deals with the influence of attached fiber optic cable on aeolian vibration of ground wire. To study the self-damping characteristics, the power dissipation of a vibrating ground wire has been measured for three cases:

- bare ground wire
- ground wire with a lashed cable
- ground wire with a wrapped cable

Both lashed and wrapped cable increase the self-damping of ground wire.

Keywords

AD-Lash; aeolian vibration; ground wire; lashed cable; optical attached cables; self-damping characteristic; wrapped cable;

1. INTRODUCTION

As the demand of industry and consumers for voice, video and data becomes ever more voracious, telecommunication firms are scrambling to satisfy it. With overhead power line networks already in place, OPtical Attached Cables (OPAC) are an economical and fast way to install end-to-end optical aerial cable network.

1.1 AD-Lash cable system

The AD-Lash system is one of the concepts for optical attached cables. The AD-Lash cable is fixed with a special lash band either to the ground wire or phase wire (Figure1).
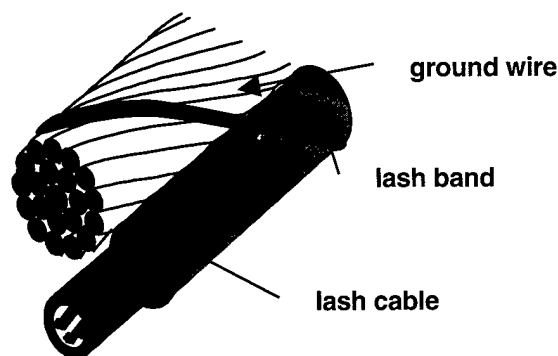
Figure 1: AD-Lash cable system

The AD-Lash system solution consists of dielectric fiber optic cable, special lash band and optimized installation procedure using special machinery. This system has been developed to be installed along overhead power lines.

The standard AD-Lash cable is a central buffer tube design with up to 48 fibers (Figure 2). The lash band is completely weatherproof and reinforced by glass yarns .
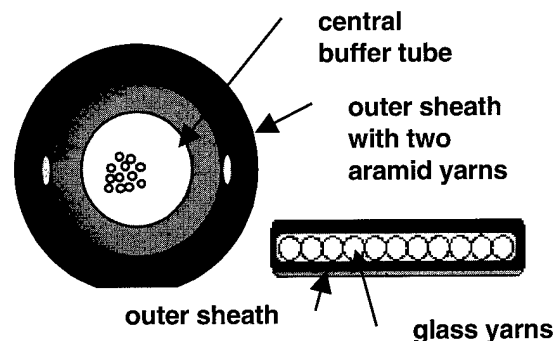
**Figure 2:   AD-Lash cable and
lash band design**

A radio-controlled (or manual) lashing machine (Figures 3 and 4) winds the band around the messenger wire and the AD-Lash cable so that the cable is permanently fixed underneath the phase wire or the ground wire.
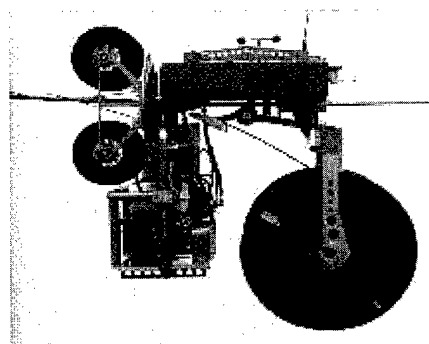
Figure 3:   radio controlled lashing machine
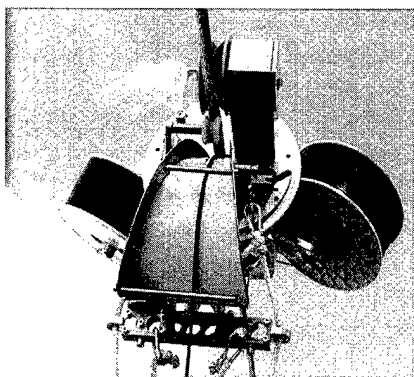
Figure 4: manual lashing machine

With the AD-Lash system it is possible to install up to 25 km per day.

1.2 Wrapped cable
The wrap is an alternative OPAC-solution. With this system the optical cable, typically a stranded loose tube design, is directly wound around the messenger wire.

loose tube

central member

filler

outer sheath
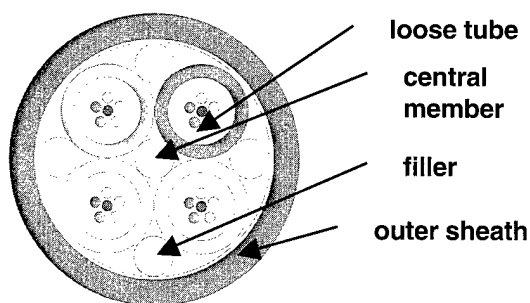
Figure 5: wrap cable

1.3 Aeolian Vibration
The phenomenon of aeolian vibration is well known from transmission lines. The cause is vortex shedding at the ground wire/conductor (Figure 7) in a low turbulent air that appears especially at wind velocities between 0.5 m/s and 7 m/s.

Figure 6: Wrap cable wound around a messenger wire

Figure 7: vortex shedding

The vibration of wire is perpendicular to the direction of the wind. Aeolian vibration may give rise to fatigue failure of ground wire and conductor.

The frequency of aeolian vibrations depends on the wind velocity and wire diameter and is given by

$$f = S\frac{V}{d} \tag{1}$$

where f is the frequency of the vibration, S the Strouhal-number (0.185), V the wind velocity and
d the diameter of the wire.

For the critical range of the wind velocity between 0.5m/s and 7m/s, the frequency of the vibration is shown in the Figure 8 for two wires with different diameters.
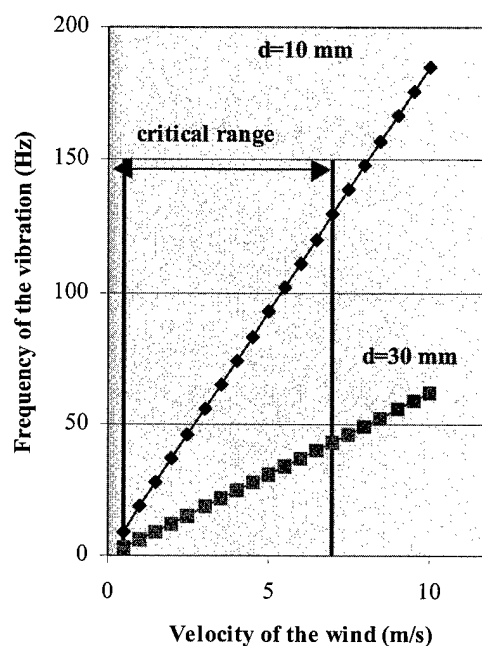
Figure 8: critical range of aeolian vibration

2. Measurement of aeolian vibration
To study self-damping characteristics of ground wire with and without an attached cable, the power dissipation has been measured in three cases:

- bare ground wire
- ground wire with a lashed cable
- ground wire with a wrapped cable

The ground wire used in the experiment has a diameter of 9.0 mm (7 stranded single wires each 3.0 mm in diameter) and the lashed optical cable has a diameter of 5.9 mm. The manual lashing machine (Figure 4) was used to install cable over the whole length of the ground wire sample.

The lashing machine fastened the cable underneath the ground wire by means of two lash bands that were wound helically around the ground wire and cable. The two ends of the cable were secured to the ground wire by clamps (Figure 9) and the cable part beyond the clamps was cut.
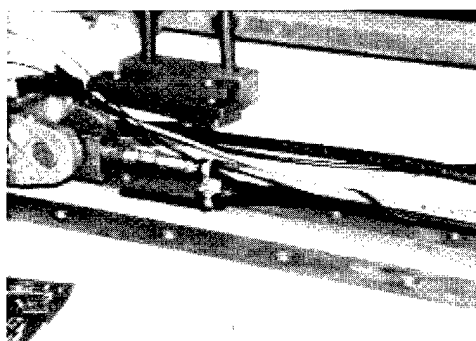
Figure 9: Clamps at the end of the ground wire

The wrapped cable with an outer diameter of 8.4 mm was manually wound around the ground wire over its entire length with a pitch of 0.5 m. During the wrapping procedure the cable was pulled by a tension of about 80 N in order to achieve a tight wrap. (Figure 10) The end of the wrapped cable was secured to the ground wire by using clamps.
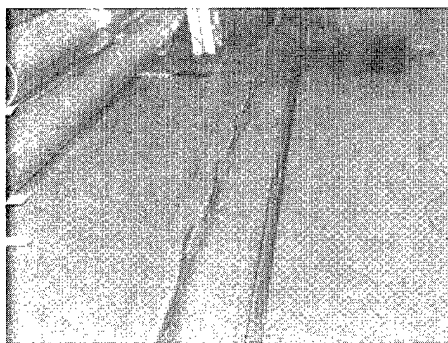
Figure 10: wrapped cable on a ground wire

The decay method was used for the measurement of the self-damping characteristics. The ground wire was tensioned during the tests to a nominal 6.8 kN between two terminations with a span length of 29.2 m. An electrodynamic shaker was connected to the specimen at one end of the span to provide a driving force. In the decay testing the span was brought into the resonance at tunable frequencies. Different measurements have been taken at the frequency range between 6 and 100 Hz at three vibration angles 5′10′ and 20′.

A good method to describe the damping characteristics is the damping ratio h which gives the ratio between the energy E_{diss} dissipated per cycle and unit length and the maximum kinetic energy $E_{c,max}$ per unit length.

$$h = \frac{1}{4\pi} \cdot \frac{E_{diss}}{E_{c,max}}$$

with

$$E_{diss} = \frac{P_{diss}}{f}$$

$$E_{c,max} = \mu\pi^2 f^2 A^2$$

(2)

3. Measurement results

Measurements of the self-damping characteristics of ground wire with OPAC show that OPAC increase the self-damping capacity of ground wire. The damping ratio of a ground wire with AD-Lash is 10 times higher than bare ground wire or ground wire with wrapped cable.
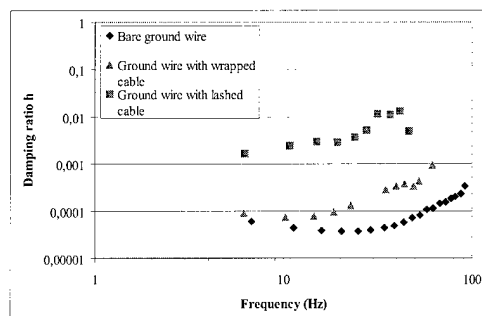
Figure 11a: Influence of attached cables on the self-damping characteristic of the ground wire at the vibration angles 5'
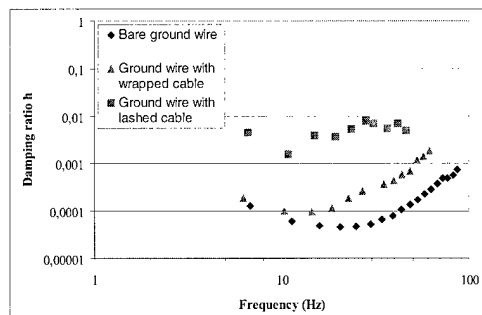
Figure 11b: Influence of attached cables on the self-damping characteristic of the ground wire at the vibration angles 10'
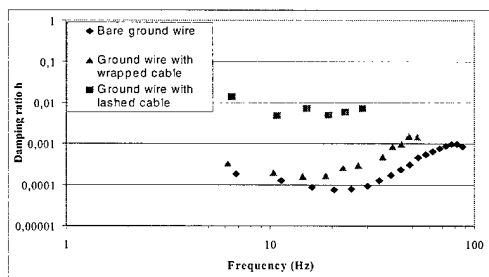
Figure 11c: Influence of attached cables on the self-damping-characteristic of the ground wire at the vibration angles 20'

4. Discussion

If two objects are continously connected and one of both will be induced to osscilate, there will be no phase difference between the oscillations of both objects. If the connection is not so rigid and one of the two objects is induced to oscillate, the phase of the oscillation of one is different to the other one. This occurs when the two objects have different masses and dimensions. The difference causes a faster dissipation of the oscillation energy of the entire system. During the measurement lash cable and messenger wire beat against each other. This beating causes friction between both and the self-damping capacity is increasing. This means that the ground wire with AD-Lash has higher self-damping capacity than a bare ground wire. The difference of the self-damping characteristics between AD-Lash system and wrapping system is based on the better connection between wrap cable and messenger wire.

5. Conclusions

- Attached cables improve the self-damping capacity of ground wire.
- Self-damping of ground wire with AD-Lash is about 10 times higher compared to the self-damping of ground wire with wrapped cable.
- Vibration damping systems are not necessary for ground wire with an AD-Lash system.
- The additional load on the tower due to the weight of the AD-Lash cable can be ignored because of the better self-damping characteristic of the ground wire with OPAC especially with AD-Lash.
- The critical range of aeolian vibrations is reduced by installing an attached cable, especially the AD-Lash system.

6. Acknowledgments

We want to thank the following individuals for their technical advice: Mr. Buchwald and Mr. Krispin.

7. Authors

Mailing address
Corning Cable Systems
Special Communication Cables GmbH & Co KG SCC RD&E 2
Austr. 101
D-96465 Neustadt bei Coburg

Alois Weiß

Alois Weiß received his Dipl.-Ing. (FH) in Elektrotechnik from Fachhochschule Coburg in 1997. He joined Corning Cable Systems (formerly Siemens) in Neustadt in 1997. He is now engaged in cable installation technology.

Zhan Gao

Zhan Gao received his B.S. and M.S. degrees in Material Science and Engineering at the University Tongji, Shanghai, China in 1985 and 1988, respectively. In 1994, he received his Ph.D. from the University Erlangen-Nuremberg in Germany. In 1991, he joined Corning Cable Systems (formerly Siemens) in Neustadt, Germany. After working on material and cable testing, he was responsible for the cable modeling. He left Corning Cable Systems in June 2000 and is now working for Infineon.

8. References

[1] E.S.Doocy, A.R. Hard, C.B. Rawlins, R. Ikegami, "Wind-Induced Conductor Motion" *Electric Power Research Institute.*, (1979).

[2] Guide on Conductor Self-damping Measurements. IEEE Std 563-1978

[3] Guide on Conductor Self-damping Measurements. CIGRE SC22 WG01, Electra No. 62

Shot Resistance Analysis of Self-Supported Metallic Armored Aerial Optical Cable

João G. Aguiar [1], Paulo J. P. Curado [1], Carlos E. Salla [1],
Edvaldo C. Mendes [2], Marco A. Scocco [2]

[1]Fundação CPqD, Campinas, São Paulo, Brazil
[2] Pirelli Cables S.A., Sorocaba, São Paulo, Brazil

Summary

The performance evaluation and study of fiber optical cables exposed to ballistics tests will be shown in this work. Toward this end, various ballistics tests were done on three types of aerial fiber optical cables- all dielectric self-supported (ADSS), optical ground wire (OPGW) and metal armor protected (OPMA). 12 gauge guns were used with different pellet types at different distances, and after the shots, optical fiber continuity was verified and cable damage observed. The results allowed a comparative performance evaluation, and verified that the OPMA cable performance was far superior to that of the dielectric cable while similar to that of the OPGW cable, thus establishing a minimum technical requirement for proving cable resistance at the same degree of protection as offered by the OPMA cable. An analysis of the employed tests methodology will also be presented, determining the aggressive parameter influence and the influence related to the alternative cables' performance in the test.

1. Introduction

The aerial optical plant in Brazil have many optical cable applications where it is necessary for the cable to be fire proof, fire setting being a common practice in the country's agriculture, and at the same time bullet proof, whether from the hunter's bullet or acts of vandalism.

To deal with these situations a metal armor protected cable (OPMA) was developed, as shown in a previous work [2] that described the product development and field testing.

During the product development, in order to more thoroughly analyze this cable model, a study aimed at analyzing in detail the degree of aerial cable's resistance to ballistics, test conditions necessary to evaluate that resistance, establishing an evaluation requirement and comparing the OPMA cable's resistance to other aerial cables available in Brazil was done.

The cables used in this study are shown in figures 1, 2 and 3.
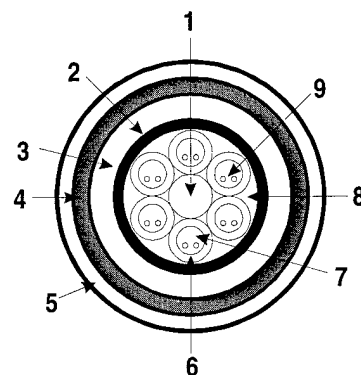
1- Central member	6- Loose tube
2- Waterblocking tape	7- Jelly
3- Inner jacket	8- Jelly
4- Strength member	9- Optical fiber
5- Outer jacket	

Figure 1- ADSS Cable
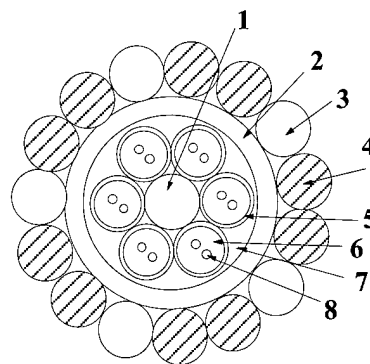
1- Central member	5- Loose tube
2- Inner jacket	6- Jelly
3- Steel wire	7- Jelly
4- Aluminum wire	8- Optical fiber

Figure 2 –OPMA Cable
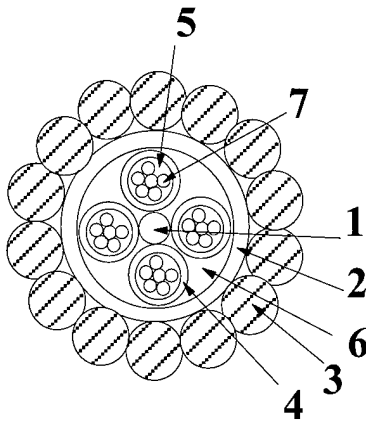
1- Central member   5- Jelly
2- Aluminum inner jacket   6- Jelly
3- Steel wire   7- Optical fiber
4- Loose tube

Figure 3 –OPGW Cable

2. Evaluation Strategy

The existing international standard IEC 60794-1 Optical Fiber Cables – Generic Specification [3] that describes the test method IEC 60794-1-E13 – "Shot-gun Damage [1] was used as the reference in the optical cable gunshot resistance analysis.

This method was adopted as the reference for establishing test methodology. It contains the method for performing the test, recommending a distance of 20 meters and the use of number 4 and 7 pellets, leaving other values open depending on the cable specification. Besides this, it defines attenuation increase as a requirement in the cable evaluation.

To establish the starting point of the tests the existing bibliographies were analyzed [4, 5 and 6], in which 12 and 20 gauge arms were used with number 3, 4, 6, 7 and 8 pellets at distances of 5, 10, 15 and 20 meters.

It was shown that increasing the distance of the gunshot caused a greater dispersion of the pellets, decreasing the number of pellets that hit the cable as well as the force of each pellet's impact. Thus, shots fired from a smaller distance cause greater damage to optical cable. The pellet mass also influences the impact energy, with larger mass pellets causing greater damage to the cable.

With these facts as a basis, it was decided to perform a series of discharges using a 12 gauge shotgun, commonly found in Brazil, with number 3 pellets (ϕ 3,5 mm) and number 6 pellets (ϕ 2,75 mm) at distances of 5, 10 and 15 meters to study the effects of the gunshots on aerial cables.

The test specimens were taken from three types of aerial optical cables; all dielectric self supported (ADSS), optical ground wire (OPGW) and metallic armor protected (OPMA).

3. Tests performed

In the gunshot tests the same methodology was used with the following specific setup characteristics:

3.1. Test specimens

For each of the cable types three 35 meter test specimens were prepared, taken from their spools, and the optical fibers then joined to form one continuous segment. The two free ends were terminated in pigtails as shown in figure 4.
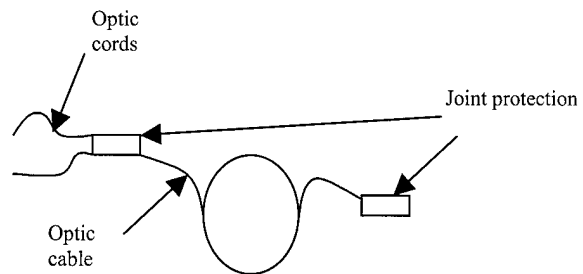
Figure 4. Test specimen prepared for the gunshot test

3.2. Test preparation

Each test specimen was laid on the ground and then fixed to the metal structure in a vertical position with a 15 kgf weight on the lower end to keep the specimen straight up and down. The optical cords were connected to an optical power measuring device and a light source. The ballistics test person positioned himself at a distance "L" from the cable, as shown in figure 5.
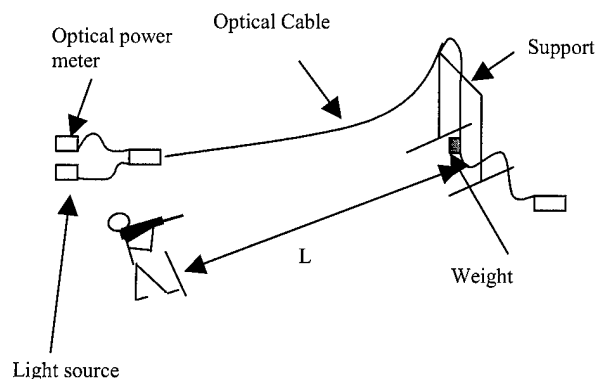
Figure 5. Test Setup

3.3. Test plan

As previously stated, a series of shots varying in distance and pellet type was planned for each type of cable. After each shot the optical continuity was verified and a visual inspection performed to characterize the cable damage caused by each situation.

3.4 Results

The results are shown in tables 1, 2 and 3.

Table 1 shows the results obtained after discharges of 12 gauge shotgun using #6 pellets at 5, 10 and 15 meters.

Table 1. 12 Gauge #6 pellet shots

Cable	L (m)	# Hits	Fiber damage	Optical Cable damage
ADSS	15	Few	No	Sheath perforated without optical fibers hit.
ADSS	10	Several	No	Sheath perforated without optical fibers hit.
ADSS	5	Various	Yes	Sheath perforated, totally destroying the cable, attenuation increase without optical fiber rupture.
OPMA	15	Few	No	No significant armor damage.
OPMA	10	Several	No	Armor marked, no wire destruction or polymer sheath exposure.
OPMA	5	Various	No	Damage and deformation to the aluminum wires, but cable not compromised.
OPGW	15	Few	No	No significant armor damage. Similar to the OPMA cable.
OPGW	10	Several	No	Armor marked without wire destruction or core exposure.
OPGW	5	Various	No	Superficial wire damage without cable compromise. Less damage than the OPMA.

Table 2 shows the results obtained after discharges of 12 gauge shotgun using #3 pellets at 5, 10 and 15 meters.

Table 2. 12 Gauge #3 pellet shots

Cable	L (m)	# Hits	Fiber damage	Optical Cable damage
ADSS	15	Few	No	Sheath perforated without optical fibers hit.
ADSS	10	Several	Yes	Sheath perforated and ruptured on the posterior part of the cable, optical fibers ruptured.
ADSS	5	-	-	Not done.
OPMA	15	Few	No	More damage to the armor than seen with the #6 pellet.
OPMA	10	Several	No	Armor marked, no wire destruction or polymer sheath exposure.
OPMA	5	Various	No	Significant damage to the wires hit (more to the aluminum wires). External Sheath not hit.
OPGW	15	Few	No	No significant armor damage. Less damage than on the OPMA cable.
OPGW	10	Several	No	Armor marked without wire destruction or core exposure. Less damage than on the OPMA cable.
OPGW	5	Various	No	Concentrated impact markings with significant damage to the wires hit. Cable core not hit. Less damage than the OPMA.

After executing the planned tests another ballistic sequence was performed with the ADSS cable using number 3 pellets. The results are shown in table 3.

Table 3. 12 Gauge #3 pellet shots on the ADSS Cable

Cable	L (m)	# Hits	Fiber damage	Optical Cable damage
ADSS	15	Few	No	Sheath perforated without optical fibers hit.
ADSS	10	Several	No	Sheath perforated without optical fibers hit.
ADSS	5	Various	**Yes**	Significant damage with optical fiber rupture.

Photos 1 through 11 show some visual test results.

4. Result analysis

The principle factors that influence the impact energy on the cable are:

- pellet size
- mass of used pellets
- the distance from which the arm is fired

The arm caliber and the quantity of gunpowder in each cartridge also influences impact intensity, but this was considered to be a constant since a 12 gauge shotgun and factory loaded ammunition was set as the standard.

The results demonstrate that at a distance of 15 meters using the two pellet type all the cables tested show good performance in regards to optical fiber rupture, although the pellets did penetrate the outer ADSS cable jacketing. The increase in the number of optical fibers in the aerial cable could change this result, because the probability of damage to one of the fibers increases. In other words, optical continuity should be complemented by visual analysis of the damage to the cable.

At the distance of 10 meters using #6 pellets none of the cables demonstrated optical fiber rupture. With the #3 pellet one of the ADSS cable test specimens already showed optical fiber rupture.

Firing at 5 meters using #6 pellets the OPGW and OPMA cables showed only small armor imperfections. The ADSS cable presented with total sheath perforation by several pellets and fiber attenuation increase, suggesting that the pellets lodged in the cable body pressing upon the optical fibers.

Firing at 5 meters using the #3 pellet caused a significant deformation of the OPGW and OPMA cable armor, but without optical fiber breakage. On its turn the ADSS cable showed optical fiber breakage, demonstrating that this test condition is very severe.

Based on this we conclude that the OPMA cable possesses ballistic resistance much greater than that of the ADSS cable. In relation to the OPGW cable, we observe that the OPMA cable suffered more deformations, although the pellets did not hit its core or cause optical fiber damage.

Although the initial studies had indicated an ideal distance of 15 meters for ballistic tests, the experiments performed show that at this distance even the ADSS cable, having no special protection, provides good optical fiber protection even though its mechanical structure is impacted by aramid filament rupturing.

5. Conclusions

Dielectric and armored aerial optical cables ballistic resistance was shown in this work. Various test results including cable performance analysis under diverse test parameters were presented.

As a result, it was possible to determine the condition under which the real behavior of cables submitted to ballistics tests can be evaluated. The resistance of these cables should be greater than that of the ADSS cable, which when originated, did not take into account this characteristic. Thus, it is proved that the requirement that demands the most ballistic resistance is that in which 12 gauge, #3 pellet shots are fired at 5 meters, observing then the optical continuity of the cable and the damages inflicted on its structure.

6. Acknowledgements

7. References

[1] IEC 794-1-E13 – "Shot-gun damage" – 4th edition – 1996

[2] Scocco, M. A. et al – "OPMA – A high mechanical and heat performance alternative optical cable for aerial application" IWCS 1999, pp 471-475.

[3] Bonicel, J.P.; et.alli; "Aerial Fiber Optic Cable for Railway Applications Metallic or Dielectric Solutions"; IWCS Proceedings 1994; pg. 368

[4] Hogari, K.; Hibi, T.; "Non-metallic Optical Fiber Cable with High Impact Resistant Sheath"; IEICE Trans. Commun. Vol. E76-B; 1993; pg. 32

[5] Akzo Nobel; "Twaron aramid tapes as ballistic protection for Aerial Optical Fiber Cables"

Authors

João Guilherme Dias de Aguiar
R&D Center Foundation (CPqD)
Campinas, Brazil

João Guilherme Dias de Aguiar, born in 1960. Degree in Mechanical Engineering from Campinas State University (UNICAMP) –1982, specialized in Materials and Manufacturing Processes- UNICAMP – 1986. Worked in the UNICAMP Physics Institute in laser development from 1984 to 1986. Has worked at CPqD since 1986 in the area of outside plant products, where he has been involved in projects, specification, tests, implementation and maintenance outside plant, both optical and metal. He has also worked in training for the area. Currently de is part of the Optic Networks Elements Area team .

Paulo José Pereira Curado
R&D Center Foundation (CPqD)
Campinas, Brazil

Paulo José Pereira Curado was born in 1962. Degree in Mechanical Engineering from Campinas State University (UNICAMP) in 1985, joined Telebrás Research and Development Center in the Outside Plant Department. Has been engaged in research and development of optical fiber cables for trunk lines and Optical Subscriber Networks in Outside Plant area. Manager of Optical Outside Plant Area of CPqD Foundation. Coordinator of Fiber Optic and Optical Fiber Cable Study Commission of Brazilian Standardization Association (ABNT).

Carlos Eduardo Salla
R&D Center Foundation (CPqD)
Campinas, Brazil

Carlos Eduardo Salla, born in 1964. Electronic technician, BA in Mathematics from Pontifícia Universidade Católica de Campinas (PUCC) in 1984; specialization in optical interferometry at France Telecom. Has worked at CPqD Foundation since 1984 in the following areas: electric component failure, Erbio fiber Optical amplifier development and optical supervision systems development. Was optic network elements division manager and is currently Optical Communication Area and Network Infrastructure Manager for the CPqD Foundation.

Edvaldo Chaves Mendes
Pirelli Cables S.A.
Sorocaba, Brasil
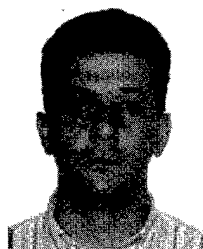
Edvaldo Chaves Mendes was born in São Paulo-SP, Brazil in 1960. He received M.Sc. degree in Mechanical Engineering from Federal University of Santa Catarina in 1986 and joined Pirelli Cabos S.A. He has been engaged in development engineering of aerial optical cables and is responsible of Telecommunication Laboratory. He is a member of ABNT Standard Commission of aerial optical cables.

Marco Antonio Scocco
Pirelli Cables S.A.
Sorocaba, Brasil

Marco Antonio Scocco was born in São Paulo-SP, Brazil in 1957. He received B.Sc. degree in Physics from University of São Paulo and M.Sc. in Electronic Engineering of the same University in 1990. He is currently the Telecommunication Engineering Manager of Pirelli Cabos S.A. He is a member of ABNT Standard Commission.
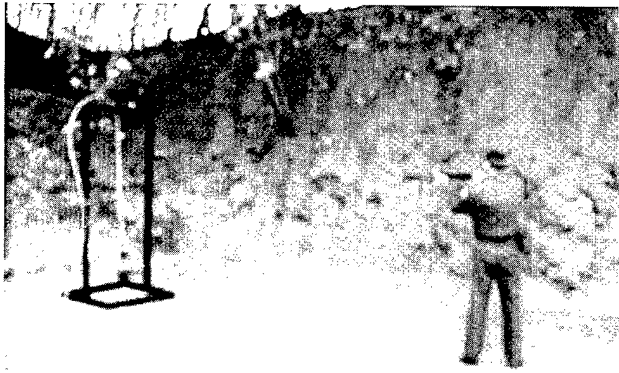
Photograph 1. Shot fired from 5 m
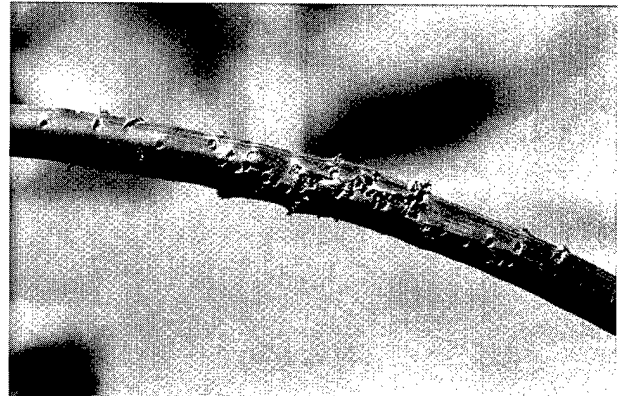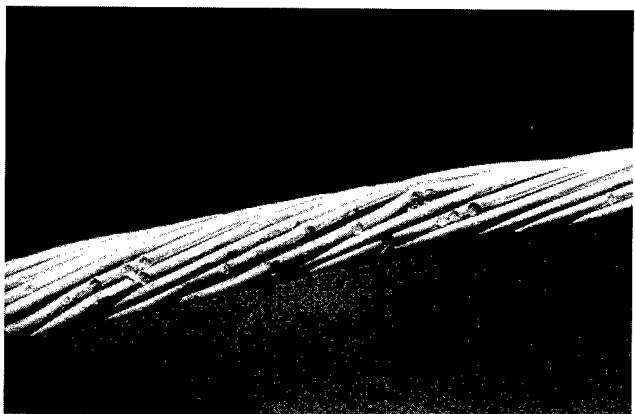

Photograph 4. ADSS Cable, #6 pellet, from 5 m
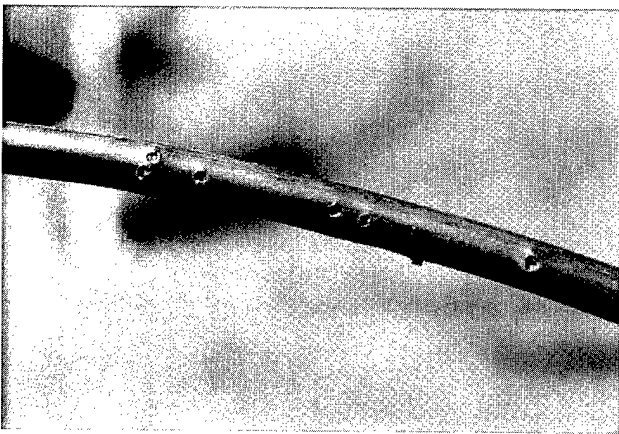
Photograph 2. ADSS Cable, #3 pellet, from 10 m
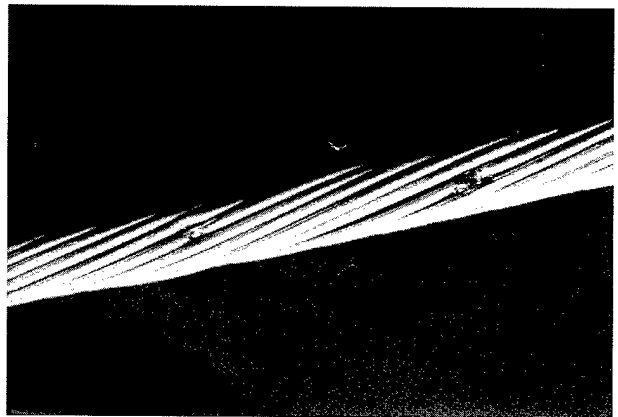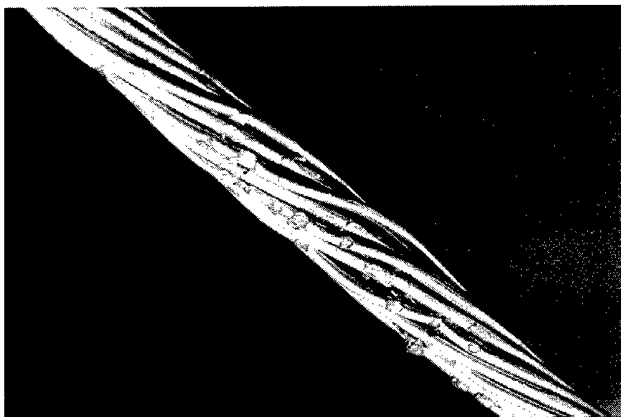

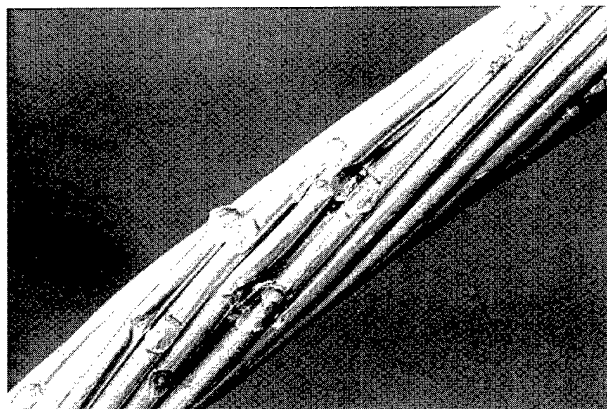**Photograph 5. OPMA Cable, #3 pellet, from 10 m**
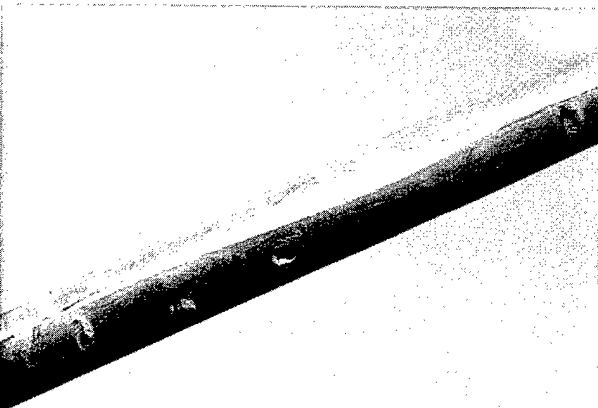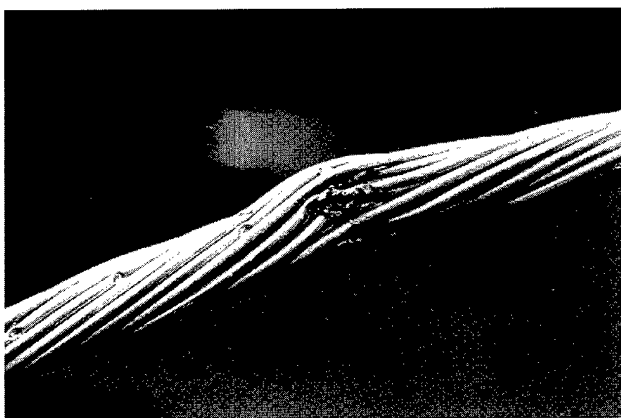

Photograph 3. ADSS Cable, #3 pellet, from 10 m
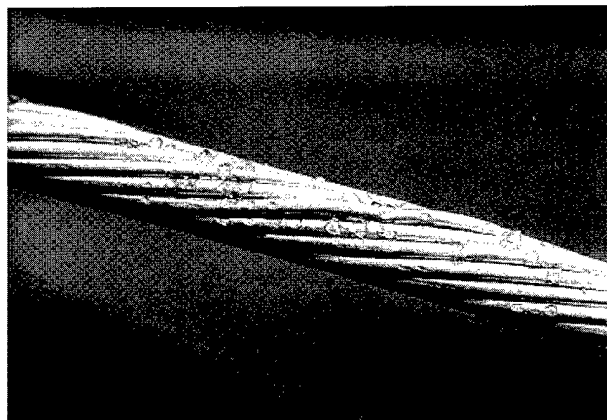

Photograph 6. OPMA Cable, #6 pellet, from 5 m
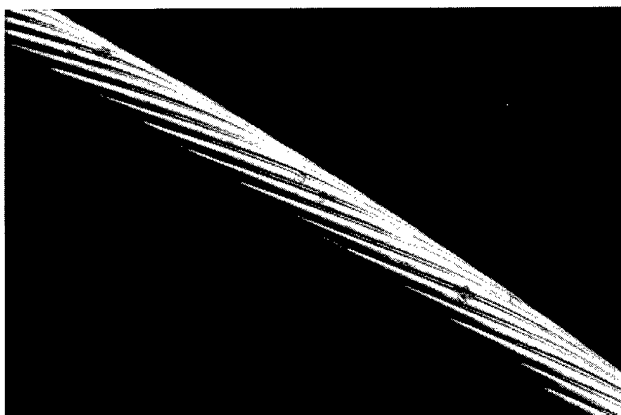
Photograph 7. OPMA Cable, #6 pellet, from 5 m

Photograph 10. OPGW Cable, #3 pellet, from 5 m

Photograph 8. OPMA Cable, pellet 3, from 5 m

Photograph 11 - OPGW Cable, #6 pellet, from 5 m

Photograph 9. OPGW Cable, #6 pellet, from 10 m

Comparison of Installation Techniques and Cable Designs Commonly Used in the United States and Japan

Timothy F. Summers

Product Line Manager, Loose Tube Cable, Cable Operations
Corning Cable Systems, Hickory, North Carolina
828-327-5374, tim.summers@corning.com

Abstract
The two largest telecommunications markets are the United States and Japan. These two markets lead the world in the amount of optical cable installed annually. Given these factors, it is important to understand the cable and installation technologies used in these dominant nations. However, these two markets have very different cable designs and installation techniques. The purpose of this paper is to compare and contrast the outside plant optical cable designs and installation techniques used in the United States and Japan.

1. Introduction
As the optical cable industry enters its fourth decade, outside plant cable designs and installation options abound. However, the cable designs can be grouped into a few basic categories such as stranded loose tube, single tube and slotted rod.[1] Likewise, installations can be categorized into three groups: duct, direct buried, and aerial. This paper will examine the outside plant cable designs and installation methods used in the two largest telecommunications markets in the world, namely the United States and Japan. It is not the intent of this paper to provide a comprehensive or esoteric analysis of every cable design and installation technique used in these two countries but rather to give an overview of the most common outside plant cables and installation methods.

2. Common Cable Designs in the United States
The most popular outside plant optical cable design in the world is stranded loose tube cable. This cable was originally developed in Europe but has gained acceptance throughout the world. Loose tube is the predominant optical cable design in the United States. Loose tube acceptance in Japan has been limited due to the inclination of Japanese customers for slotted rod cables.
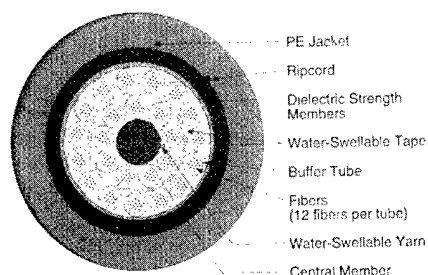
Loose tube cables are constructed with a central member at the center of the cable. The central member is typically made of glass-reinforced plastic (GRP) or similar dielectric material. The central member may provide some tensile strength for the cable but more importantly, it provides resistance to the contraction of the cable components at low temperatures. Around the central member are the buffer tubes, stranded in an "SZ" pattern. The hollow, color-coded buffer tubes have an inside diameter that is much larger than the outside diameter of the fiber. This provides a relatively strain-free environment for the optical fibers, decoupling the fibers from the remainder of the cable. A jelly-like substance fills the remaining space in the tube, preventing moisture from getting near the fibers and eliminating the possibility of this water freezing and leading to an increase in attenuation or fiber breakage. The fibers typically have some excess fiber length inside the tube to allow them to remain in a strain-free condition during installation and long term operation. The standard number of fibers per tube is six or twelve but other counts are possible to meet customer needs.
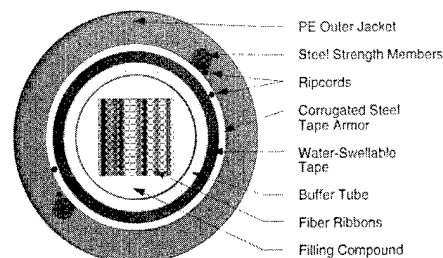
"SZ" stranding of the buffer tubes facilitates mid-span access of the cable. In a mid-span access, the buffer tubes can be easily unwrapped at the "SZ" reversal point allowing easy access to individual buffer tubes. The number of buffer tubes stranded around the central member depends on total fiber count but typically the minimum is five to ensure a round cable. For higher fiber count cables, typically above 120 fibers, the buffer tubes may be stranded in two layers. Stranded loose tube cables are commonly available up to 288 fibers, but higher fiber counts are possible.

After stranding the buffer tubes around the central member, the buffer tubes are typically bound together with binder tapes to maintain the integrity of the core. At this point, most loose tube manufacturers apply a waterblocking tape to prevent water migration in the cable. A few years ago, dry waterblocking tape technology replaced the "flooding" gel that was the common waterblocking technique in the eighties and early nineties.[2] In a flooded design, the core of the cable was flooded with a jelly-like material to provide a physical barrier and prevent water migration. With the advent of economically feasible dry waterblocking technology, the jelly was replaced with the tape thus making cable end preparation much faster and easier.
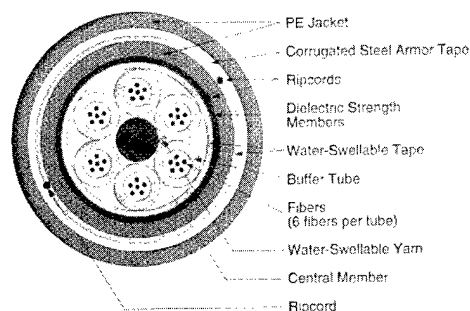
After stranding and the application of waterblocking tapes, high tensile strength yarns are added and a jacket is extruded around the cable. The yarns, typically aramid and fiberglass, provide the majority of the cable's axial tensile strength required for installation and long term operation. On top of the tensile yarns, a jacket, typically made of black polyethylene, is extruded around the cable. The use of polyethylene as a jacketing material is common worldwide and facilitates easy installation and a long lifetime. As a sheath option, a plastic-coated, corrugated steel tape armor can be applied underneath the outer jacket to provide additional mechanical protection, particularly for cables buried directly in the earth. Figures 1 and 2 show typical cross-sections of non-armored and armored stranded loose tube cables with various fiber counts.
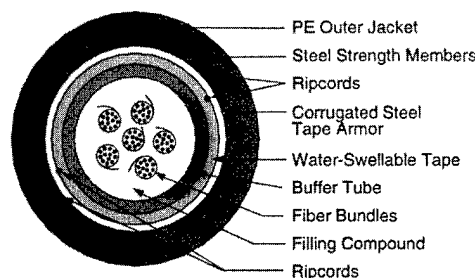
Figure 1. Non-Armored Loose Tube Cable

PE Jacket
Ripcord
Dielectric Strength Members
Water-Swellable Tape
Buffer Tube
Fibers (12 fibers per tube)
Water-Swellable Yarn
Central Member

Figure 2. Armored Loose Tube Cable

PE Jacket
Corrugated Steel Armor Tape
Ripcords
Dielectric Strength Members
Water-Swellable Tape
Buffer Tube
Fibers (6 fibers per tube)
Water-Swellable Yarn
Central Member
Ripcord

Figure 3. Armored Single Tube Ribbon Cable

PE Outer Jacket
Steel Strength Members
Ripcords
Corrugated Steel Tape Armor
Water-Swellable Tape
Buffer Tube
Fiber Ribbons
Filling Compound

Figure 4. Armored Single Tube Cable

PE Outer Jacket
Steel Strength Members
Ripcords
Corrugated Steel Tape Armor
Water-Swellable Tape
Buffer Tube
Fiber Bundles
Filling Compound
Ripcords

Another cable design common in the United States is the single tube cable. Instead of multiple tubes stranded around a central member, a single tube is located at the center of the cable with tensile elements surrounding the tube. The central tube is extruded around the fibers with some excess fiber length. The fibers are organized in the central tube in one of three ways: single, color-coded fibers; fibers bundled together with a color-coded yarn; or fibers in ribbon form. Fiber bundles are typically bundled in groups of six or twelve color-coded fibers while ribbon constructions typically have twelve or twenty-four color coded fibers.

After buffering the fibers in the central tube, the tube is jacketed but in a different configuration from loose tube cables. Since there is no central member nor tensile yarns, there must be some other mechanism to mitigate the contraction of the cable's components at low temperatures and provide tensile strength for the cable. To achieve these functions in single tube cables, GRP or steel rods are placed outside of the central tube and embedded in the jacket. As with stranded loose tube cables, single tube cables typically use polyethylene as the jacket material and armored versions are also available. Figures 3 and 4 show some typical single tube cable cross-sections.

3. Common Cable Designs In Japan

In Japan, the predominant cable design is the slotted rod design, sometimes called the slotted core ribbon (SCR) design or the star design. Slotted rod cables are constructed with a plastic slotted rod surrounding a steel or dielectric central member. The central member performs the same contraction mitigation function as in stranded loose tube cables and it also provides the cable's tensile strength. In Japan, a steel central member is the standard versus a GRP central member, which is standard in the USA. The slotted rod is extruded around the central member in a star shape. The slots are typically in a helical pattern but the "SZ" slot pattern is growing in popularity. The number of slots depends on fiber count and ribbon configuration. Each slot contains a specified number of ribbons with each ribbon having two-, four- or eight-fibers. The total fiber count in the cable and customer preference are the primary determinants of ribbon type. Two- fiber ribbons are typically used in cables with fiber counts of 12 - 128 and four-fiber ribbons are common in cables with 20 - 300 fibers. Above 300 fibers, nearly all designs use eight-fiber ribbons. See Figures 5 and 6 for some typical slotted rod cross-sections.
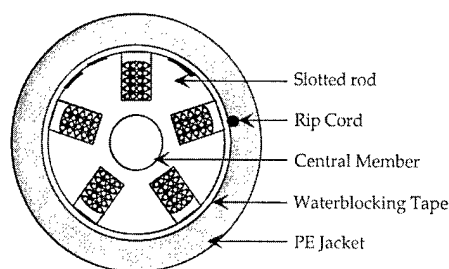
Figure 5. Slotted Rod Cable
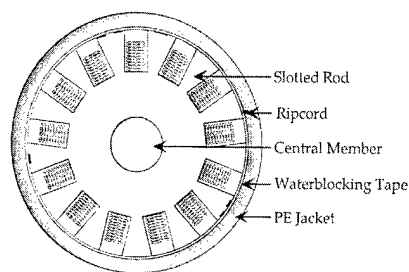
Figure 6. Slotted Rod Cable

SZ slotted rod cables are growing in popularity in Japan. Unlike their helical slot cousins, SZ slots make mid-span access very easy. In Japan's drive toward fiber-to-the-home, service providers are finding mid-span access a necessity and want to make it as quick and easy as possible[3].

Two sheath options are common in Japan for outside plant cables. Some customers prefer waterblocking tapes followed by a polyethylene jacket. Others prefer a laminated aluminum tape followed by polyethylene (LAP sheath). The waterblocking tapes perform the same function as in loose tube and single tube cables described above, that is to prevent water migration. In cables with a LAP sheath, there is no mechanism to prevent water from migrating down the cable.

4. Comparison of the Predominant Cables

The slotted rod design, though standard in Japan, has not gained acceptance in the USA. Likewise the stranded loose tube and single tube designs standard in the USA have gained only limited acceptance in Japan. Much of this has to do with the origin of the development of these cables and customer preference in the two countries driven in part by those who manufacture and market the cables in the respective countries. The differences between the cable designs are significant and in some cases fundamentally incompatible such that trying to use both cable designs in a single network becomes impracticable. The primary differences discussed below are base unit of fiber groupings, fiber identification, intra-cable fiber protection, tensile strength elements, waterblocking technology, and

mechanical protection. Some of these differences impact the installation techniques common in the two countries.

4.1 Base Unit Of Fiber Groupings

The base unit of fiber groupings in a network determines much of the hardware selection and configuration for the system. In the United States, the standard fiber grouping is in multiples of six. For loose tube cables, this means that the tubes contain either six fibers or twelve fibers. In USA ribbon cables, twelve or twenty-four fiber ribbons are used. Typically the twenty-four fiber ribbons can be easily split into two twelve-fiber ribbons. In Japan, where slotted rod ribbon cables dominate, the fibers are typically grouped in ribbons of four or eight, with one exception. The one exception is the two-fiber ribbon found in some SZ slotted rod cables. This two-fiber ribbon cable can be easily integrated into a network with four and eight fiber ribbon cables.

The selection of the base unit of fiber groupings is an important one. Once a service provider begins building a network with one or the other base unit, 6/12 or 4/8, it is difficult to integrate the other base unit grouping without special accommodations. These accommodations include special splicing and routing adaptations that are not routine and make system documentation difficult. In the USA, most termination hardware is designed for groups of six or twelve. This applies to fiber organizers in splice trays, connector panels in cross-connect hardware, distribution frames, etc. In Japan, the four- and eight-fiber ribbons drive the configuration of the hardware.

4.2 Fiber Identification

Of obvious importance is the ability to uniquely identify each fiber in a cable. Stranded loose tube cables achieve this by color coding each buffer tube and each fiber within each buffer tube. Single tube cables use color coded fibers along with a colored binder thread or printing on the ribbon matrix.[4] In slotted rod cables, each ribbon is comprised of colored fibers. The fiber color sequence in each ribbon uniquely identifies each ribbon and fiber in a slot. Each slot is uniquely identified by means of stripes on the rod itself. The fiber identification in the USA and Japan cable designs are basically dictated by the cable design.

4.3 Intra-Cable Fiber Protection

The fundamental means by which the fiber is protected inside a cable differs among the cable designs used in the USA and Japan. In the USA where stranded loose tube and single tube cables dominate, the intra-cable fiber protection is achieved by means of a buffer tube. The tube surrounds the fibers or ribbons and decouples them from the rest of the cable. In Japan where slotted rod cables dominate, the intra-cable fiber protection is achieved by the slotted rod. The ribbons are placed in the slot below the circumferential surface of the rod.

When an outside plant cable is terminated, the fibers must transition from the end of the cable into a splice tray or connector housing. The buffer tubes in a stranded loose tube cable are typically routed into the splice tray or connector housing affording some level of protection for the fibers inside a closure or other termination hardware. In single tube cables, the tube is typically cut off just inside the hardware outer panel and the fibers or ribbons transition to the splice tray either

unprotected, or they can be fed through transition tubing. Likewise the rod of a slotted rod cable is cut off just inside the hardware outer panel and the ribbons transition to the splice tray either unprotected or through transition tubing. Any of these ways are acceptable but the end user must determine the level of fiber protection with which he is comfortable.

4.4 Termination of Tensile Strength Elements in Hardware

Most cable manufacturers and cable installers recommend that the tensile strength elements be secured when the cable is terminated in hardware. The primary tensile strength elements in loose tube cables are the aramid and fiberglass yarns stranded around the cable core. These yarns are completely separate from the cable jacket and can be easily secured inside a closure or other termination hardware. In single tube cables, the tensile elements are often embedded in the jacket and must be separated from the jacket and secured in the termination hardware. In slotted rod cables, the central member is the tensile member. To secure the tensile member, the polyethylene rod must be removed to expose the tensile member. Comparing these three cable designs, the tensile elements in single tube cables are the easiest to secure in termination hardware.

4.5 Waterblocking Technology

One area where loose tube, single tube and slotted rod cables share technology is in how they prevent water migration. All three cable designs typically use waterblocking tapes and yarns to prevent water migration in the cable if the cable jacket is breached. Loose tube and single tube cables have to deal with blocking water inside the tubes. Today this is most commonly achieved by means of a suitable jelly, which provides a physical barrier to water migration. This jelly must be removed during cable termination requiring extra time. Slotted rod cables do not require a jelly because the tapes and yarns alone provide water penetration performance to meet customer specifications. This makes cable end preparation easier in slotted rod cables when compared to loose tube or single tube cables.

4.6 Mechanical Protection

In loose tube cables and to a certain degree in single tube cables, the operating temperature window and mechanical performance characteristics are determined by the free space inside the tubes, excess fiber/ribbon length, the lay length of the stranded tubes and the dimensions of the cable components. In slotted rod cables, the combination of ribbon tension, slot lay length, slot dimensions, and ribbon stack height determines the operating temperature range and mechanical performance characteristics.

The outer sheath is a cable's first line of mechanical protection. As mentioned before, the jacket is typically made of black polyethylene. Additional mechanical protection can be achieved by adding a metallic armor tape. In the USA, a corrugated steel tape armor under the jacket is common for cables to be directly buried in the ground. The armor provides additional protection against rodents and other underground hazards. Corrugated steel tape is not commonly used with slotted rod cables because, as discussed below, direct buried installations are very rare in Japan.

4.7 Comparison of Cable Specifications

One primary industry standard cable specification in the USA is "ANSI/ICEA Standard for Optical Fiber Outside Plant Communications Cable, ANSI/ICEA S-87-640-1999" (ICEA-640).[5] "ICEA-640" has gained acceptance among many USA end users. In Japan, one cable standard is "Ribbon Type Optical Fiber Cables, D-106."[6] "D-106" was created and is referenced by many of the Japanese electric power companies and their telecommunications subsidiaries. Table 1 summarizes the cable mechanical and environmental performance from these two specifications.

Table 1. Sample Mechanical Performance

	ICEA-640	D-106*
Attenuation Coefficient	≤ 0.5/0.4 dB/km at 1310/1550 nm	≤ 0.50 dB/km at 1310 nm
Operating Temperature Range	-40°C to +70°C	-20°C to +60°C
Installation Tensile Strength	2670 N	2060 - 3720 N**
Crush	220 N/cm	196 N/cm
Impact	4.4 N•m, 2 impacts at three different points	4.9 N•m, 1 impact at ten different points
Cycle Flex (Bending)	25 cycles, ±90°, 20X cable OD mandrel diameter	5 cycles, ±180°, 20X cable OD mandrel diameter
Twist	45–70 N***, ±180°, 2 m cable length, 10 cycles	245 N, ±90°, 1 m cable length, 3 cycles
Water Penetration	1 m cable, 1 m head of water, 1 hour	Not specified

* Mechanical and environmental performance may differ depending on cable design and fiber count.
** Specified tensile strength depends on fiber count.
*** Tensile load during twist test depends on cable iameter.

The most significant differences noted in Table 1 are operating temperature range and water penetration performance. ICEA-640 is used primarily in North America covering a vast land region and therefore a wide temperature range. Japan is smaller in size with a more limited temperature range though cables deployed in Hokkaido, Japan's northernmost island, often require performance down to -30°C, as acknowledged in D-106. The ICEA-640 water penetration specification is common for outdoor cables in the USA. D-106 does not require water penetration performance of its cable designs. Water penetration is an important parameter in long term outside plant cable performance.[7,8] Some Japanese end users specify cable designs with a water penetration requirement, but D-106 does not. The differences in performance summarized in Table 1 are also a result of fundamental design differences between the two types of cables. The design of the cable will impact the mechanical and environmental performance exhibited by a particular type of cable.

5. Common Installation Methods in the United States

Cable installations in the United States can be grouped into three categories: duct, direct buried and aerial. Deciding which installation to use is dictated primarily by customer preference, cost, availability of facilities (such as a duct system or utility poles), and local restrictions. Of the 1998 USA local exchange carrier installations, 38% were duct installations, 36% were buried and 26% were aerial installations.[9] Duct installations are common in urban areas and campus environments where duct systems are already in place. In recent years, some customers have been burying multiple ducts on long haul routes to provide the flexibility of easily pulling in additional cables. Direct buried installations are common where it is desirable to have the cable out of sight and there is no duct system present. It is used in many residential areas as well as many long haul routes. Aerial installations are common in urban areas where utility poles are present or where a customer has access to aerial rights-of-way. In some areas, particularly new housing developments, local regulations prohibit aerial installations because of the perceived "unsightliness" of the aerial plant.

Duct installations involve pulling or "pushing" a cable into semi-rigid plastic tubing commonly called innerduct. Historically cables have been pulled into the duct by means of a pull line either by hand or with the assistance of a winch. This is a straightforward installation and is very common (see Figure 7). The limiting factors are friction and forces resulting from sidewall pressure in bends. In long installations, a mid-assist device is often used, commonly a winch-driven wheel around which the cable wraps to provide pulling assistance.
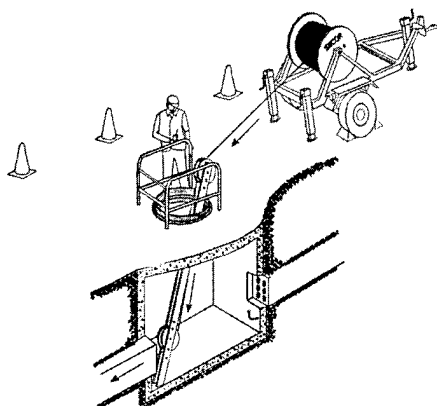
Figure 7. Duct Installation

In recent years, another duct installation method has emerged, namely air-assisted cable installations, or more commonly referred to as "jetting" or "blowing."[10] In an air-assisted installation, the cable is "pushed" by a tractor mechanism while blowing compressed air into a pre-installed duct. This technique allows the cable to "float" inside the duct during installation and can result in a near tension-free installation. Key advantages to jetting are reduced installation labor and lower material expense. In both pulled and air-assisted duct

installations, lubricants are commonly used to reduce friction and increase installation lengths.

In a direct buried installation, the cable is plowed or trenched directly in the ground. Two types of plowing are common. In a static plow, a blade slices through the earth and places the cable in the ground. In a vibratory plow the blade vibrates as it slices through the earth and places the cable in the ground (see Figure 8). Trenching involves digging a trench then placing the cable in the trench and backfilling the dirt to fill the trench (see Figure 9). The use of trenching or plowing is dependent on terrain, soil conditions, equipment availability, environmental impact, location of other utility lines, etc. Direct buried installations can be combined with duct installations to negotiate obstacles, particularly roadways and railroads, by direct burying up to the obstacle then installing duct around the obstacle.
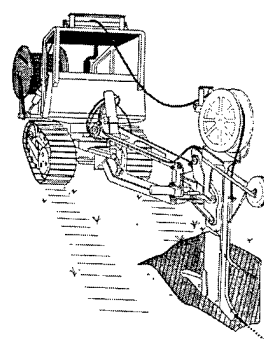

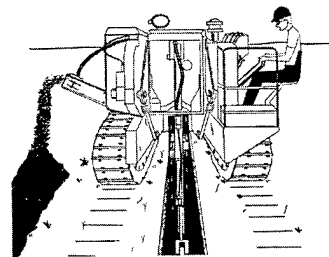**Figure 8. Direct Buried Installation – Plow-In Method**

Figure 9. Direct Buried Installation – Trenching Method

Aerial installations are less popular for fiber optic cable in the USA and are used in areas where the terrain is unsuitable for underground installations or where a customer has access to aerial rights-of-way. Two types of aerial installations are common in the USA: lashed and self-supporting. The lashed aerial method is a two-step process. The first step is to install a supporting wire strand, or the load bearing wire for the optical cable. This strand is sometimes referred to as the messenger. The second step is to place the optical cable next to the supporting strand by one of two basic methods, dictated by the terrain and access to the poles and supporting strand. The

drive-off, or moving reel, method is used when the entire route can be traversed by reel carrying vehicles. The cable is raised to the strand and lashed in one operation as the reel is moved along underneath the strand in a vehicle (see Figure 10). The second method, stationary reel or pull-in method, is used for cable routes that are inaccessible to vehicles. The cable is pulled in beneath the strand along a series of pulleys, or cable blocks. Once the cable is in place, it is lashed to the strand (see Figure 11). The lashing machine secures the cable to the strand by wrapping a small continuous lashing wire around both the strand and the cable in a spiral pattern. One or two wires are typically employed. The wires are typically steel but dielectric ones are also available.
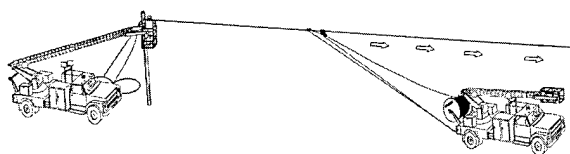
Figure 10. Aerial Installation – Drive-Off Method
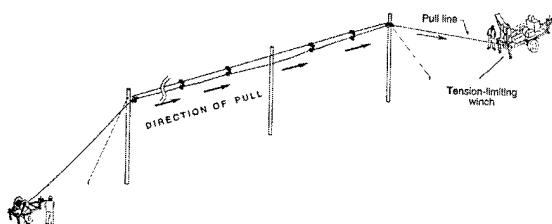
Figure 11. Aerial Installation – Stationary Reel Method

In other aerial installations, self-supporting cables are used. These cables are installed in one step since the supporting strand is integral to the cable. They come in two basic types. The first is the "Figure-8" self-supporting cable whereby a steel strand is joined to the optical cable by a web extruded along with the jacket. The strand provides the aerial support for the optical cable. Figure-8 cables use pole hardware similar to that used in lashed aerial installations. The other type of self-supporting aerial cable is a concentric design, typically all-dielectric. This design typically uses additional aramid yarns to increase the tensile load bearing capability for the cable. Its concentric design makes it less susceptible to aerial effects such as galloping

6. Common Installation Methods in Japan

As mentioned previously, the predominant installations in Japan are aerial and duct. Aerial plant is ubiquitous as are duct systems, particularly in urban areas. The discussion below reveals that Japanese duct and aerial installation techniques have some significant differences compared to those used in the USA.

Figure-8 slotted rod cables are common in Japan with constructions similar to those used in the USA, with a few variations. The variations in some Japanese Figure-8 cables include a "window" in the web and an optical cable overlength relative to the strand[11] (see Figure 12). The basic purpose of the window is to allow air to flow through the web to minimize the effects of galloping. The overlength keeps the optical cable in a relatively strain-free condition as the supporting strand is tensioned. The windowed web has been used for many years and is not always combined with the optical cable overlength.
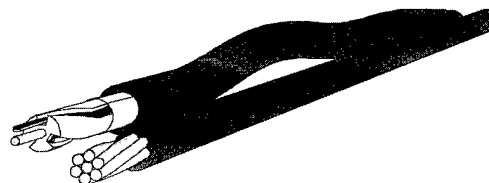
Figure 12. Windowed Web With Cable Overlength

Lashing is used on aerial cables in Japan but other techniques for attaching the optical cable to the strand are also popular. One such method is the "hangered" design. In this type of installation method, the supporting strand is first installed but then instead of lashing the cable to the strand, hangers are clipped to the strand with the cable resting in the hangers. The hangers are spaced about every half meter (see Figure 13). As a hybrid between lashing and hangers, some Japanese installers use a spiral preform rod wrapped around both the cable and the strand. This method has also seen some use in the USA (see Figure 14). Japanese manufacturers also attach the cable to the strand in the factory using lashing wires or molded plastic. Figure 15 depicts the molded plastic piece connecting the cable to the supporting strand. Though less popular than Figure-8 and hangered installations, these other methods have been in use since the 1980s and continue today.
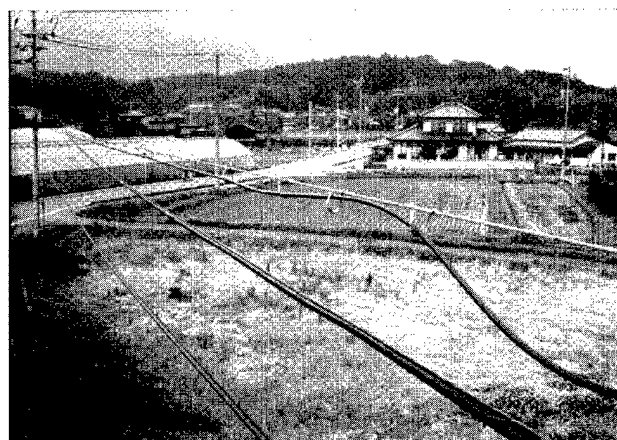

Figure 13. Aerial Installation - Hangers
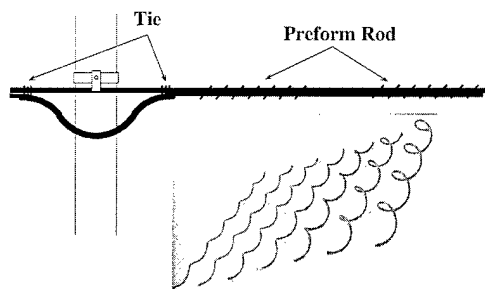
Figure 14. Spiral Preform Rod

Figure 15. Molded Plastic Hanger

Japanese duct installations, like installations in the USA, typically use a pull tape or rope attached to the end of the optical cable. Depending on the customer in Japan, a tractor pulling system may be used for mid-assistance in the middle of the run and pulling at the end of the run versus a winch-assisted wheel. See Figure 16 for a picture of this device. The device squeezes the cable between the two belts, pulling it along. Jetting and the use of lubricants are not widely accepted in Japan.
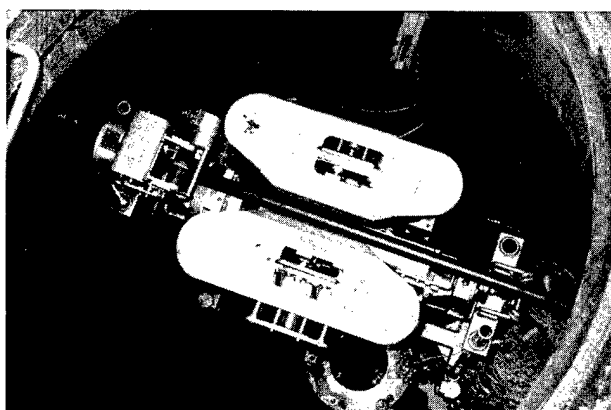
Figure 16. Tractor Pulling Device

7. Comparison of Installation Techniques

In many respects, installation methods in the USA and Japan are very similar. Differences have grown out of customer preference, technology and the urbanization of the two countries. One obvious installation difference caused by the urbanization of Japan is the lack of direct buried installations.

Direct buried installations are rare in Japan because of extensive underground utilities, lack of open area, and lack of rights-of-way that can tolerate direct buried installations. Other differences include methods for attaching the optical cable to the supporting strand, techniques of through splicing in the aerial plant, installation lengths, use of lubricants, and duct installation methods.

7.1 Methods for Attaching the Cable to the Supporting Strand

For those installations where the optical cable is attached to the strand (cables other than self-supporting) distinct differences exist between Japan and the USA. In the USA, lashing the cable to the supporting strand in the field is the predominant aerial installation method and is typically achieved by pulling a lashing machine along the cable and supporting strand to lash them together. Not so in Japan, where the cable is attached to the messenger in many different fashions including pre-lashing in the factory, hangering in the factory, manual lashing with a spiral preform rod in the field and manual hangering in the field. The choice of method is largely guided by customer preference, cost, available craftsmanship and available equipment.

7.2 Techniques of Through Splicing in the Aerial Plant

In Japan, the aerial plant is very crowded. Wires and cables run in every direction and at every level possible. This makes storing any cable slack on the supported strand difficult. This is one of the primary reasons that through splicing is used rather than butt splicing. In a through splice, one cable enters one end of the closure and the other cable enters the opposite end of the closure. In the USA a butt splice is common whereby both cables enter the same end of the closure requiring one cable to change directions on the strand creating a loop-back on the strand. Due to the crowded aerial plant, butt splicing is not done in Japan but rather a through splice is performed. The butt splice makes the splicing configuration inside the closure a little simpler. Through splicing makes hanging the closure and cable slack storage on the supporting strand more difficult.

7.3 Installation Lengths

The urbanization of an area can greatly impact the accessibility to the installation area. The more crowded the installation area, the more difficult the installation. In Japan, the congested urban areas and small, narrow streets make cable installations difficult thus limiting the cable lengths that can be installed. It is very difficult to negotiate a nine foot reel in the narrow streets of Tokyo! The estimated average optical cable length in Japan is about 750 meters while the estimated average length in the USA is about 3500 meters. This significance difference reveals the fact that installations in Japan are more difficult and time consuming and the distances between urban areas in Japan are significantly shorter.

7.4 Use of Lubricants

The friction encountered in duct installations can be greatly reduced by using a quality pulling lubricant. Lubricants have been specially designed for optical cables, both for pulling as well as jetting and are commonly used for duct installations in

the USA to make the installation process quicker and easier. In Japan, the use of pulling lubricants is infrequent due in part to the relatively short installations, but those who do use lubricants may have an advantage.

7.5 Duct Installation Methods

The difference in duct installation methods between the USA and Japan arise from differences in end pulls and mid-assist techniques. In the USA, winch driven wheels are used to pull cables from the end and at mid-assist points. In Japan, tractor pulling devices are sometimes used for this purpose, which may be one of the reasons pulling lubricants are not more widely used. Equipment availability and customer preference are the primary dictates of choosing one method over the other.

8. Conclusions

Both countries, Japan and the United States, have well established networks of outside plant cables. Stranded loose and single tube cables are predominant in the USA while slotted rod cables are the mainstay in Japan. Key differences among these cable designs include how the fibers are identified, grouped, and protected within the cable as well as cable mechanical and environmental performance and cable termination. Key differences in installation techniques include methods for attaching the optical cable to the supporting strand, equipment for duct installations, cable installation lengths, techniques for through splicing in aerial installations, and the frequency of direct buried installations. End users and installers in both countries could learn from one another to improve their own installation methods and techniques.

9. Acknowledgements

10. References

1. J. Englebert, S. Hassett, T. Summers, "Optical Fiber and Cable for Telecommunications," The Electronics Handbook, p. 864-894, Boca Raton, USA 1996
2. C. E. Clyburn III, A. G. Bringuier, "A Dry Core Loose Tube Cable for Outside Environments," Proceedings of the Forty-Fourth International Wire & Cable Symposium, p. 29-36, 1995
3. H. Iwata, M. Okada, S. Tomita, N. Kashima, T. Hoshijima, M. Kama, K. Nishizawa, "Design of Aerial Optical Fiber Cable System Suitable For Easy Branching," Proceedings of the Forty-Sixth International Wire & Cable Symposium, p. 4-11, 1997
4. "Optical Fiber Cable Color Coding," TIA/EIA-598-A, Telecommunications Industry Association, 1995
5. "Outside Plant Communications Cable," ICEA S-87-640-1999, Insulated Cable Engineers Association, Inc., 1995
6. "Ribbon Type Optical Fiber Cables," D-106, Japanese Power Utilities Standard – Unified Specification, 1996
7. O. Bresser, A. Leenen, "Waterblocking In Optical Cables," Proceedings of the 29th International Wire &Cable Symposium, p. 290-298, 1980
8. M. Fukuma, N. Akasaka, S. Suzuki, "Dry Type Waterblocking Optical Fiber Tape Cable with Slotted Rod," Proceedings of the Thirty-Sixth International Wire & Cable Symposium, p.350-356, 1987
9. "Statistics of Communications Common Carriers," Federal Communications Commission, 1999
10. W. Griffioen, G. Plumettaz, "Current Developments in Cable-In-Duct Blowing Techniques," Proceedings of the Forty-Sixth International Wire & Cable Symposium, p. 363-367, 1997
11. See Note 3 above.
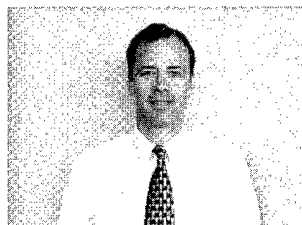
Timothy F. Summers
Product Line Manager
Loose Tube Cable
Corning Cable Systems
PO Box 489
Hickory, NC 28603

Tim started with Siecor, now Corning Cable Systems, in 1990, as an applications engineer after spending seven years in the United States Army. He has eight years of experience with the Japanese telecommunications market both as Applications Engineer and Product Line Manager - Slotted Core Ribbon Cable and moved to his current position earlier this year. He received a BS in 1983 and an MBA in 1997, both from Wake Forest University.

Air-Blown Fiber Application Issues in Korea Telecom For Optical Access Networks

Joungyoung Ha, Youngtak Lee, Soondeok Baek*

Korea Telecom Access Network Laboratory   *Access Network Technologies Ltd.
Daejon, Korea   Daejon, Korea
+82-42-866-3149 jyha@kt.co.kr   +82-42-864-1580
+82-42-866-3029 lyt63@kt.co.kr   bsd@antec.co.kr

Abstract

Korea Telecom(KT), the biggest general opertor in Korea is widening the bandwidth of the access networks based on fiber optics. Air-blown fiber technology that blows fiber bundle into small diameter tubes was taken into account as a candidate for fiber link construction. Many application issues like compatibility with conventional cables, network design, cost and more were studied. Series of tests and studies showed nice results and led to the conclusion that the technology can be introduced into exsiting access networks without conflict.

Keywords

Air; Blown; Fiber; Access

1. Introduction

To provide high speed internet connection and leased line service to customers, KT has been upgraded existing copper networks to fiber based ones. However, optical access network construction costs very high, finding right way of investment has very important meaning.

Air-blown fiber, originated from UK and spreading into building, campus and access network was studied for adoption into KT's networks.

Laboratory performed several tests including maximum blow length for both straight and curved route, temperature cycling and cable joint into existing loose tube closures. The center and cascade blowing method provided was proved very effcient way for minimizing fiber splice.

In the aspect of network design, we checked economical benefits of the technology application through simulation with various design criteria. For the analysis, we divided customer areas into 2 regions based on the distance from central office and applied different service demand. Both full Air-blown fiber networks and hybrid structure with conventional cable were considered.

The results were very promising because the application not only saves installation costs at present but guarantees easy network upgrade in the future.

2. Tests for Compatibility and Performance

2.1 Closure Accomodation

Cable joint into existing closure is important because feeder network construction in metropolitan area will be finished by the end of year 2000. Mostly they were constructed with loose tube cables. In this area, Air-blown fiber can take the role of distribution and drop branches.

We checked connectablilty with several major closures in KT. Most splice trays in closures hold tubes by cable ties. Some trays do not have enough seat space for 5mm outer diameter tube, but it can be bypassed using extra tube of 3.5mm diameter. This kind of extra tube is prevalent in most closures for preparing loose tubes onto trays. In this case, the tube is inserted into the blown fiber tubes and it's opposite concept to conventional loose tube preparation.
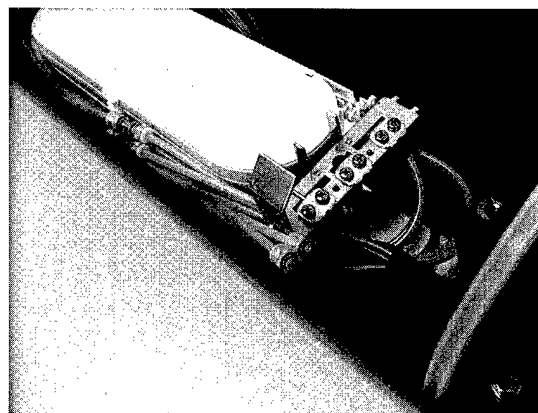

Figure 1. Closure with blown fiber tube

Air-blown fiber cable does not require excess length at installation and maintenance because fiber splicing is not necessary. Normally, blowing head can go into manhole or tube end can go out from closure for operation.

Excess cable length for future joint and fiber splice is main cause of manhole congestion. Tube jointing is simple compared to fiber splicing that requires elaborate fiber preparation and equipment operation, so tube route can be simply managed in manhole. So, blown fiber closure can be seated inline without excess length and does not cause additional complexity in manholes.

2.2 Installation at Straight

For reference of the performance, we measured blowing length of fiber bundles in straight route. Finding nice place with over 2km straight and even surface is not easy in city area. We selected cement-paved bank of river with total length of 2.3km. The course has some curves but they are very slow and total angle is below 45 degrees.
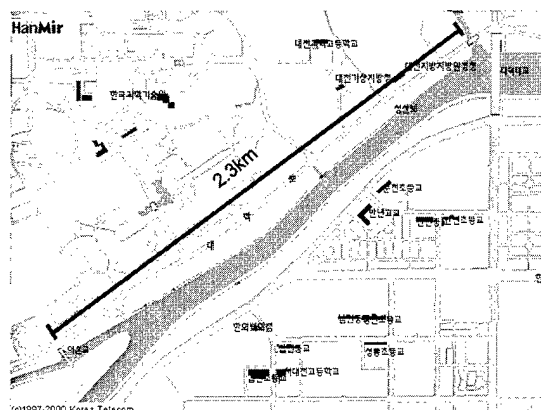

Figure 2. Test route for straight installation

20 segments of 100m length tubes were layed and connected. Air flow meter was used to check the flow rate at the supply of 10 bar pressure.

4, 8 and 12 fiber bundles were blowed into different length of tube. 4 fiber was tested at 1900m and 8 fiber was at 1600m. During the installation, bucking was occurred several times and as a consequence, the blowing speed was dropped. Both bundles reached to the end with the minimum speed of 10m/min. It seemed that fibers could go farther but it would take more installation time due to slower speed.

According to the other tests we've done, fibers can travel with the speed of 30m/min at 1600m for 4 fiber and 1200m for 8 fiber. 12
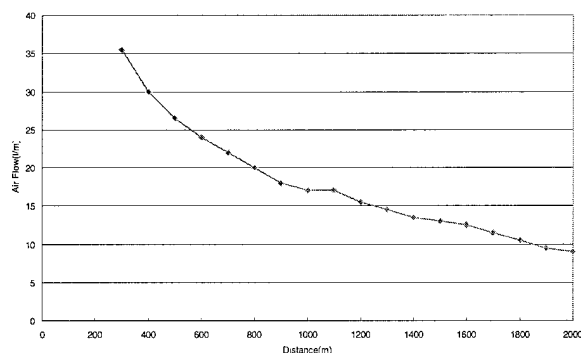
Figure 3. Air flow through 3.5mm inner diameter

fiber was tested at 1300m length and minimum speed was 17m/min.

The straight course we've tested is not a normal access environment, but the results can be a guide for such cable route as along railroad or highway.

2.3 Installation with Bend

For this test, a reference route was devised. The path has 1000m length and total 1800 degrees bend angle. A 180 degrees bend with 11cm diameter was included and it is for reflection of loop branch. All other bends have 60cm diameter.
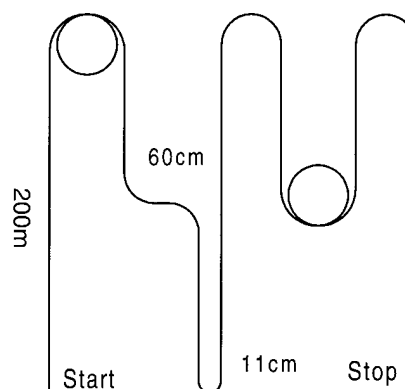
Figure 4. Test route with bend

4 fiber bundle traveled well as expected and suffered no speed drop. For 8 fiber, it took 42 minutes and speed was dropped from over half distance.

12 fiber showed better performance than 8. It can be explained as that the more symmetrically flexible structure of 12 fiber bundle would undergo less friction in tube while installation.

3. Network Design Consideration

3.1 Service Penetration

For qualitative analysis of the economical benefits, three patterns of service demand were considered.

Table 1. Supply Model

Model	Service Demand(%)				
	1 yr	2 yr	3 yr	4 yr	5 yr
A	50	70	79	83	85
B	25	40	55	70	85
C	10	15	25	45	85

The pattern A, representing metropolitan or central commercial area, has high initial demand and gradual increase as shown in Table 1. Based on the demand ratio, we calculated necessary number of ONUs, installation and products cost for both conventional cable
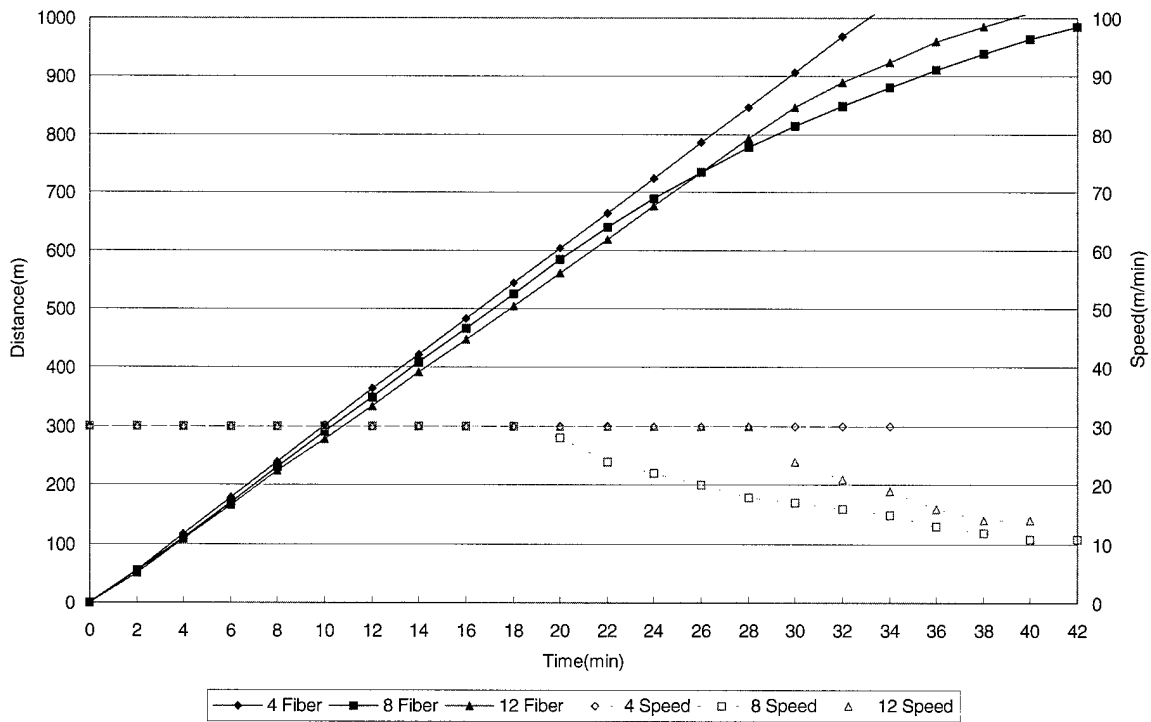
Figure 5. Performance in a curved route

and air-blown fiber. The underdeveloped or reconstructing area will normally have low initial demand and in the final stage of development, it will have steep demand increase. This is pattern C. Mid-scale city that has linear increase was marked as pattern B.
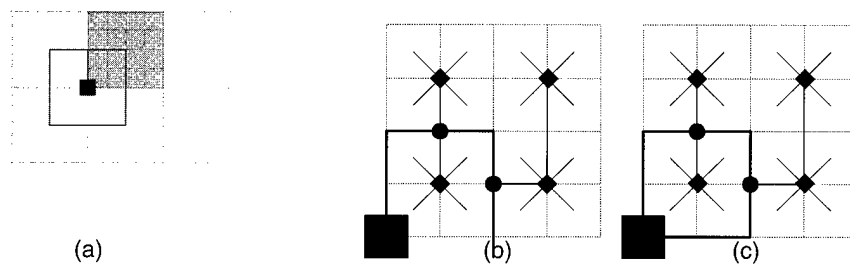
3.2 Core Region

We devided a central office coverage in city area into 2 regions. One is core region where most important customers locate densely and the other is the outer where service demand is relatively low compared to core.

For typical 4 x 4km square area, the core occupies one fourth as shown in Fig. 6. There are one or more feeder and many branch

cables to connect customers. Looped feeder connects all the ONUs with 2 directions for network stability and this same concept applied to the blown fiber network.

The conventional cable network has fiber splices at every cable branch but blown fiber network can have only tube joints in this region. This is very import point in network design and costruction considering the installation time and cost.

The cost analsis for this region are listed below. The cost savings obtainable from 5 year application of air-blown fiber ranges from 18% to 65%. In the calculations, we expected that those demands at

Figure 6. Central office coverage with
(a) shaded core region (b) conventional cable route (c) air-blown route
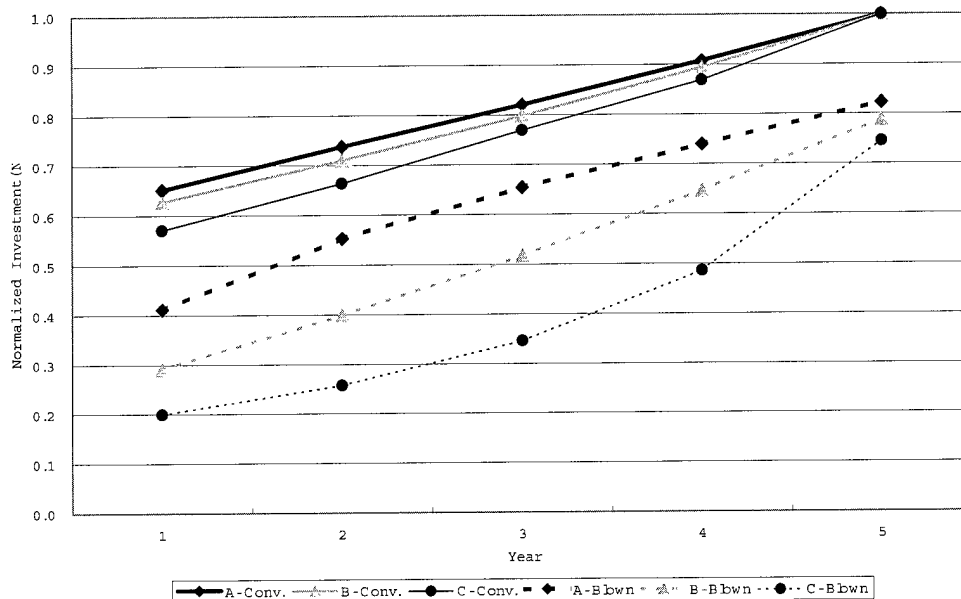
Figure 7. Investment for core region

every year will surely occur, but sometimes it is totally unpredictable in the real world. When predicted demand is not come true, pre-installed conventional cable networks will be just a kind of over-investment.

3.3 Outer Region

For outer region, we devised 2 stages network because ONU locates far from the central office because the longer blowing distance, the higher installation cost.

Inner route acts as a kind of feeder and outer router connects with distribution and drop cables. When a demand arises, maximum possible fiber-count bundle is installed through inner route to the splice point that connects inner and outer route. This method need fiber splice but can reduce the total blowing distance.

3.4 Hybrid Construction for Outer Region

It is true that applying air-blown fiber into the situation with fixed fiber demand is not so competitive. As indicated in the results of Figure 9, high initial demand can be regraded as a kind of fixed one and in this case, cost effect is relatively low compared to other cases.

Hybrid construction, only inner route was replaced with conventional cable was considered. When compared to core area, economical benefits decrease was mainly caused by long distance blowing to ONUs, so installing feeder with conventional cable can be an altanative.

In this case, all supply patterns go similar and cost more at first year compared to all blown fiber construction but total costs of 5 years are less than that. Figure 10 shows that his type can bring

(a)   (b)
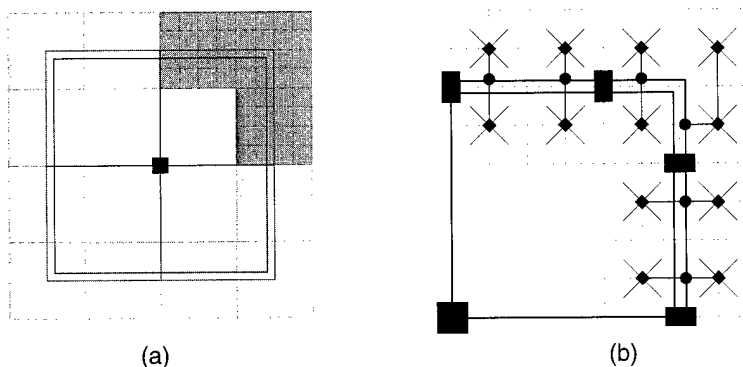
Figure 8. Central office coverage with
(a) shaded outer region (b) air-blown fiber route(conventional not shown)
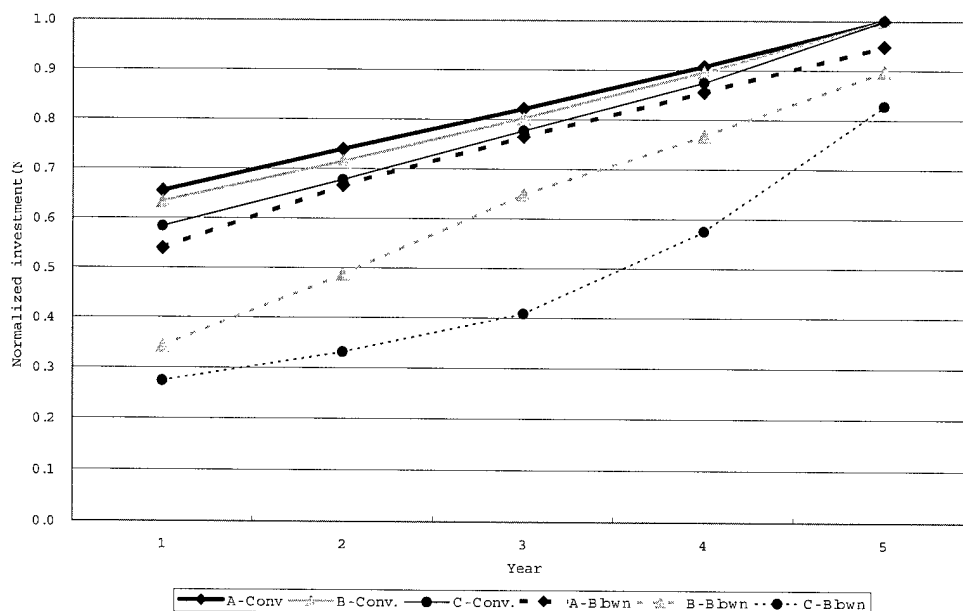
Figure 9. Investment for outer region
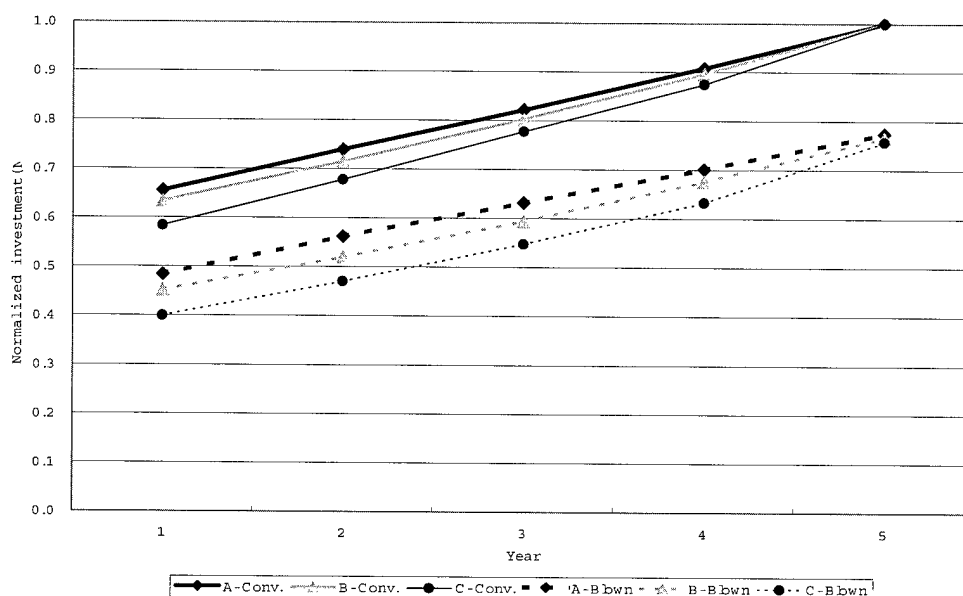
Figure 10. Investment for outer region with hybrid construction

additional 7~13% of cost savings compared to all blown fiber networks.

4. Field Tests

In the back yard of laboratory, where various kinds of outside plant facilities are tested, several kilometers of tube cables and fiber bundles were installed. Its purpose is for performance evaluation of the cables, fibers and installation equipments in the aspects of outside operation. Aerial route construction will be added for tests, too.

Beside these tests, some field trials in the access networks that transmit commercial signals will be carried on at a few selected sites.

5. Conclusions

From a network operator's point of view, air-blowing fiber technology was studied and tested. Many test and simulation results showed its promising aspects coming from the property of supplying just today's fiber demand.

Economical benefits of network design and many other operational merits including inline cable joint, minimum chance of fiber splice, fiber upgradability accroding to future technology development and more will surely make the technology a competitive candidate for KT's access network construction.

6. References

[1] Andy Mayhew, John Mellis, "Blown Fibre as a Reduced Cost Network Planning Solution", *ANCIT Workshop* (1998).

[2] S.A. Cassidy, M.H. Reeve, "A radically new approach to the installation of optical fibre using the viscous flow of air", *International Wire and Cable Symposium* (1983).

[3] Itaru Sakabe, et al., "A study of Air Blown Fiber for a Long Distance Tube", *International Wire and Cable Symposium* (1997).

[4] Keith Cockrill, et al., "Blown fibre – a reference test blowing route", *International Wire and Cable Symposium* (1997).

Bibliography

Joungyoung Ha
jyha@kt.co.kr

Korea Telecom Access Network Laboratory
62-1, Whaam-dong, Yusung-gu, Daejon, Korea

Joungyoung Ha graduated from Kyoungpook National University and received his M.E degree in Electronic Engineering in 1989. He joined Korea Telecom Research and Development Group in 1992 and performed series of outside plant research projects including development of reusable single and multi-fiber mechanical splices, optical component measurement technology and their applications. His recent interest is development of the construction technology for optical subscriber networks.

Youngtak Lee
lyt63@kt.co.kr

Korea Telecom Access Network Laboratory
62-1, Whaam-dong, Yusung-gu, Daejon, Korea

Youngtak Lee received M.S. and Ph.D. degrees in Electronic Engineering from the Sung Kyun Kwan University in Korea, in 1988 and 1999, respectively. Since 1989, he has been with the R&D group at the Korea Telecom, where he is currently a director of Optical Outside Plant Engineering Division. His research interests include optical access network engineering, specialty optical fibers and optical fiber Bragg grating applications.

Soondeok Baek
bsd@antec.co.kr

Access Network Technologies Ltd.
62-1, Whaam-dong, Yusung-gu, Daejon, Korea

Soondeok Baek graduated from Kyoungpook National University and received his M.E degree in Electronic Engineering in 1988. He joined Korea Telecom in 1991 and performed series of outside plant research projects including development of ribbon fiber cables, aerial cables and access network design technologies. Recently He retired temporarily from Korea Telecom and established an optical network engineering company named Access Network Technologies Ltd.

Field Measurement Results for Pan European Non Zero Dispersion Fiber Network

Stephen C. Mettler, Lawrence R. Dunn & William J. Shinnick
Lucent Technologies
Norcross, Georgia
770-798-2728 smettler@lucent.com

Jean Marie Naulot
Lucent Technologies
Paris, France
jnaulot@lucent.com

David P. Tanis
Lucent Technologies
Dublin, Ireland
dtanis@lucent.com

Ispran Kandasamy & Mark G. Graveston
Lucent Technologies
London, England

Derek Foxwell
Viatel UK Ltd.
London, England

Abstract

At no other time in the history of communications has the race to satisfy the global demand for bandwidth been more aggressively pursued by service providers, and equipment suppliers. Accordingly, the development of products for information transport has progressed rapidly with new application based fibers leading in fiber network deployments around the globe. In this article, we will discuss the field installation practices, procedures and results from installing an extensive Non-Zero Dispersion Fiber telecommunication system in Europe. The use of this new fiber type required that correct field practices and procedures be observed to guarantee that the system design performance requirements were fully met. The field data from the first phase of Viatel's Pan-European Network confirm that low splice losses and excellent end-to-end losses were achieved using conventional installation methods and standard fusion splicing equipment updated to current programs.

1. Introduction

Worldwide demand for more bandwidth in communications systems has driven the development of optical transmission products with more wavelengths and higher bit rates. These new products place greater requirements on the transmission medium – optical fiber. The development of new fiber types designed to operate in these systems requires consideration in system design and field installation methods. As these new systems are deployed, product manufacturers, system operators and installation companies are learning that they must cooperate and learn together to provide these new services economically and efficiently.

Viatel's entry into Europe began with a challenge; to construct a Pan European, facilities-based fiber network, using the very latest optical technologies, in a matter of months. Among the many choices reviewed was the selection of optical fiber. It was recognized that once the cable was installed, it would have to support customers well into the new millennium. Because of technology and system advances, Dense Wavelength Division Multiplexing (DWDM) and 10/40 Gb/s bit rates, low loss and optimal dispersion characteristics in the C and L transmission bands are critical requirements for system design. Viatel selected TrueWave® fiber from Lucent Technologies, and became the first Pan European carrier to deploy Non Zero Dispersion Fiber (ITU-T G.655 fiber) in their backbone network.

To meet their investor's commitments and internal corporate plans, Viatel planned a very aggressive time schedule to install and turn up the network. To meet the tight construction deadlines, the project management team used local firms that were familiar with fiber placing to install and splice the cable. And, while each of the teams that built the initial phase was experienced, Viatel required the very best network installation. Accordingly, updated classroom training on splicing G.655 fiber was provided to all teams.

After installation, verification of the quality of the Phase 1 installation was important to Viatel, both to confirm that they received what they paid for and for their marketing campaign when they present their fiber network specifications to their end customers. To accomplish this, a comprehensive test plan was developed and an extensive program consisting of end-to-end Optical Time Domain Reflectometer (OTDR) readings and power meter measurements were undertaken. Each type of test measurement had specific purposes. The OTDR measurements provided both the end-to-end span loss budget information for the

fiber and all splices for a cable segment that went from optical amplifier to optical amplifier and the individual splice losses. The power meter measurement, made on a completed regenerator section containing multiple cable spans, provided all fiber and joining losses from the transmitter to the receiver. The purpose of the plan was twofold: first, to establish the

Figure 1: Pan-European Route Map
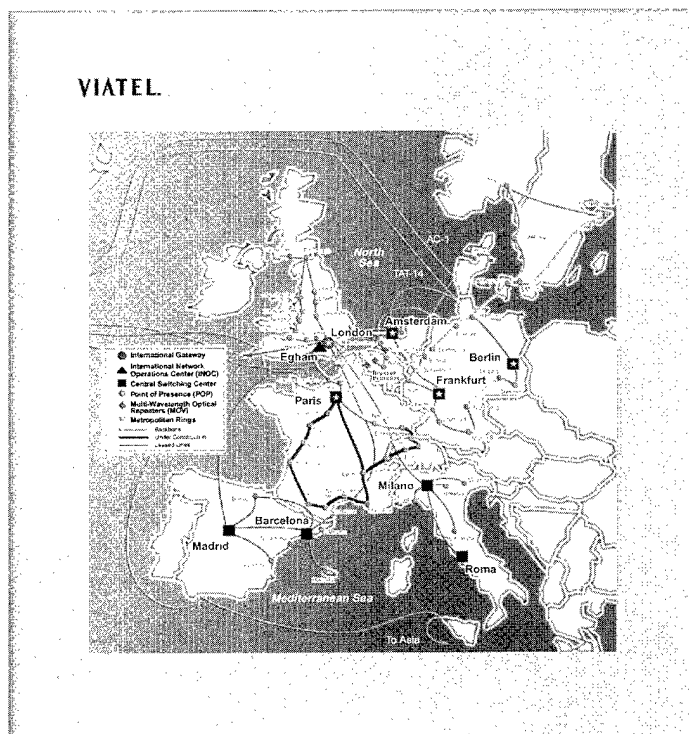
end-to-end installed loss of the optical fibre, and second, to confirm the quality of the splicing.

The testing results are important because they provide critical base line information for the design, operation and maintenance of the network and give the marketing group information on the quality of the fiber system when they are preparing to offer clients a fiber lease program.

The measurement results from the test plan were excellent. In the end, nearly 24,000 TrueWave fiber splices were tested, with an average splice loss of 0.04 dB per splice. More significant to Viatel's customers, the average installed and spliced path-loss of the 70,000 km of NZDF fiber that was tested, was 0.21 dB/km. This finding is significant for several reasons. First, generic fiber loss values in the 1550 nm (DWDM operating range) band are usually 0.20 dB/Km - 0.25 dB/Km. The test results show that TrueWave fiber in the Viatel network, in full network spans with splicing included, is at the low end of the range. Second, splicing does not add significant loss to the loss values found in unspliced fiber. Third, installed fiber with splices falls within the system design parameters for DWDM systems.

2. Why Non Zero Dispersion Fiber?

Prior to the Viatel network, all Pan-European networks were built with conventional or "standard singlemode" fiber – which is a part of the G.652 specification. It was first introduced into the global market in 1983 and initially optimized for long distance systems operating in the 1310 nm transmission band. However, in the early 1990's increased demand for transmission capacity by system operators required advanced technologies. In addition to increasing the line speeds by going to higher bit rates, systems were being upgraded by adding carrier wavelengths using wavelength division multiplexing. Recently, DWDM systems, initially capable of supporting eight wavelengths, have been refined to operate at eighty or more wavelengths over the C and L transmission bands providing terabit capacity.

While standard singlemode fiber is capable of supporting 1550 nm signals at speeds of 2.5 Gb/s and greater, it can prove expensive to upgrade to higher bit rates and additional wavelengths in DWDM systems because of the dispersion compensation management required to reform the optical pulse. As transmission speeds increase, even more dispersion management is required and it may be both technically difficult and cost-prohibitive to run 40 Gb/s signals over G.652 fibers.

Given the tremendous advances being made in expanding system bandwidth using DWDM and higher bit-rate transmitters, fiber type has emerged as one of the key parameters in network optimization. This shows in global purchasing patterns. Presently, G.655 fiber designed and optimized for high capacity networks utilizing today's and tomorrow's new transmission technologies is the choice of network providers. Ensuring Viatel's future is meeting and exceeding their customers' expectations in providing the best network possible today and tomorrow. Continuing advances in technology make this a never-ending task, however, using the best possible technology in today's systems provides insurance for tomorrow.

3. Splicing Issues

Since its introduction in the mid-1990s, NZDF fiber has emerged as the new standard for long-haul networks. The reasons for the strong market acceptance of this new fiber type lie in the optimization of several key characteristics, such as chromatic dispersion and dispersion slope, for supporting ultra high capacity DWDM systems, resulting ultimately in superior cost per bit comparisons. Additionally, in achieving this optimization, certain fiber parameters, such as index profile, are typically more complex for NZDF fibers than for standard G.652 fibers. [1] This complexity can affect the fusion splicing characteristics of NZDF fibers. Since splice-loss expectations affect system design, typical splice loss distributions must be determined. [2] In addition, fusion machines must be updated using appropriate programs developed by the fusion machine manufacturers in cooperation with the fiber manufacturer, to provide low loss splicing of these new fiber types. [3]

Figure 2: Phase 1 Splice Loss Data - TrueWave Fiber

Mean = 0.04 dB
Median = 0.03 dB
Sigma = 0.04 dB
N = 23800

Figure 3: A to B - One-Way OTDR

Mean = 0.22 dB/Km
Median = 0.22 dB/Km
Sigma = 0.02 dB/Km
N = 227
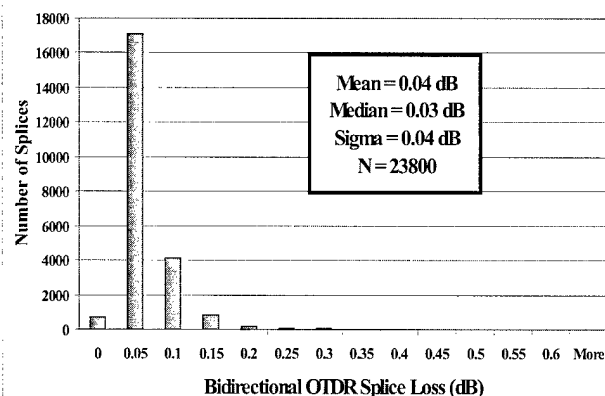
In the case of the Viatel network, the complexity of the construction project was increased by the fact that Phase 1 was installed by different sub-contractors using different splicing machines and having varying degrees of experience and skill level and operating in various countries. Despite all these factors, the completed Phase 1 system met or exceeded all design goals

4. Training

It is important to pay particular attention to whole life cost issues when any new or revised technology is introduced to the field. Accordingly, improvements in splicing and placing can improve system performance and network profitability. Phase 1 of Viatel's Pan-European project represented the first major deployment of NZDF fiber in Europe. Although the differences between G.652, used within traditional networks, and G.655 fiber are relatively small from a craft perspective, it was considered advisable to provide upgrade training on splicing and cable installation to the country based installation companies.

To be as effective as possible in transferring G.655 technology from source experts to the field, relevant fiber courses were reviewed and revised along with an update of course instructors. To introduce G.655 to the craft, a rolling pan-European training program was implemented to the installation groups on the key differences in fiber handling and splicing via classroom training and field assistance. Results from craft training and field assistance resulted in a well deployed and installed physical network with excellent splice losses and very good end-to-end fiber measurements

5. Splice Loss Results

Local contractors in each country used their standard single-fiber splicing equipment and procedures to perform installation and splicing. This means that each contractor used the fusion-splicing machine that they had on hand and with which they were familiar. The splicing software programs were updated to the latest version recommended by the machine manufacturer for G.655 fiber.
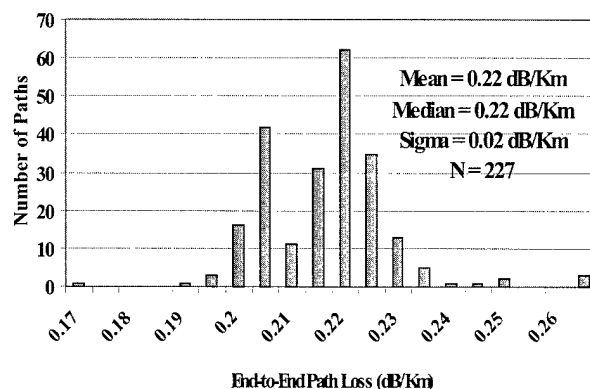
Splicing machine estimates were initially used to remake splices. Actual splice losses were confirmed using OTDR and unacceptable splices were remade. Even though splicing machines from several different manufacturers were used the splice losses were very uniform over the entire system. The splice loss distribution, Figure 2, was measured using bidirectional OTDR measurements at 1550 nm. A mean splice loss of 0.04 dB was achieved for almost 24,000 splices with an acceptable number of remakes. As fiber and splicing machine manufacturers continue to improve their respective products, we expect that field splicing will continue to improve in loss and productivity as it has for conventional fiber over the years.

6. System End-to-End loss

The Figures 3, 4 and 5 show the OTDR measured end-to-end (two-point) loss for several typical sections of the Phase 1 system (60 to 80 Kms). Figures 3 and 4 show the loss in each of the two directions and Figure 5 shows the bidirectional average end-to-end loss in dB/Km. The range of one-way readings is very consistent with a few exceptions. Three paths in the data shown had end-to-end loss greater than 0.26 dB/Km. Examination of the OTDR traces
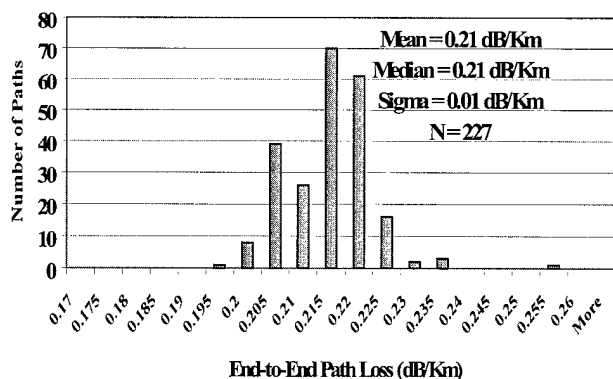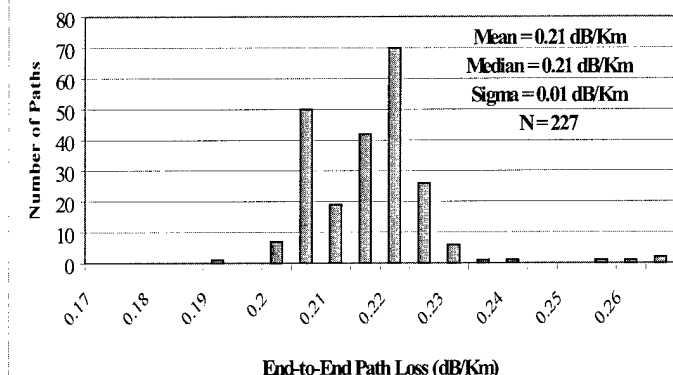

Figure 4: B to A - One-Way OTDR

Mean = 0.21 dB/Km
Median = 0.21 dB/Km
Sigma = 0.01 dB/Km
N = 227

Figure 5: A/B OTDR Average

Mean = 0.21 dB/Km
Median = 0.21 dB/Km
Sigma = 0.01 dB/Km
N = 227

End-to-End Path Loss (dB/Km)

on these paths showed that these were in error due to improper handling of the up front reflection. Maximum loss was 0.22 dB/Km for the 76.55 Km leg for example.

The average measurements are even more uniform, as would be expected. Two paths had total loss slightly above 0.25 dB/Km, however, these paths were well within the loss budget since allowance for splice loss is included. All end-to-end path losses include all splicing and are well within the design budget. Over 99% are below the loss budget for the fiber only before splicing, of 0.25 dB/Km. This shows that, even with additional loss due to splicing, the span losses are very low.

7. Conclusion

NZDF fiber networks are no more difficult to install than conventional single-mode fiber networks. There are differences in the fiber design and geometry between G.652 and G.655 fiber; however, with use of NZDF-specific splicing machine programs and appropriate training of installation crew members and supervisory personnel, high-tech application-specific fiber networks are easy to install and excellent results are readily achievable.

Optical fiber type has emerged as a critical component in the overall design of ultra-high capacity DWDM optical networks. Selecting the right fiber type for specific network functionality is now made easier because of advancements in splicing techniques. Key fiber parameters, which affect system performance, can be measured at the manufacturing location. However, splice loss and installed end-to-end loss must obviously be tested in the field. Entire fiber spans must be measured for span performance parameters -- and the splicing must be the best it can be.

The extensive testing that Viatel undertook upon completion of Phase 1 of their network verified the excellent splicing and installed loss results for their TrueWave NZDF fiber network. These results provide a baseline for planning loss budgets, and for performance assurances for dark fiber customers who are constructing high capacity DWDM networks across Europe.

8. References

[1] S. C. Mettler, L. R. Dunn, A. L. Ingles & H. C. Chandon, "Splicing Considerations for Non-Zero Dispersion Fiber," Proc. of NFOEC '99, Chicago, IL, p. 51, (September, 1999).

[2] P. Lindskog, B. Sundstrom, J. Tyrcha & R. Sundberg, "Minimize Network Installation Costs by Setting Appropriate Maximum Splice Loss Values," Proc. of 47th IWCS, Philadelphia, PA, p. 522 (November, 1998).

[3] D. Duke, C. Henderson, G. Karl and G. Mackie, "Migration of Core-Alignment Fusion Splicing from the Splicing Van to Outdoor/FTTH Applications," Proc. of NFOEC 2000, Denver CO, (August, 2000).

AUTHORS

Stephen C. Mettler is a Distinguished Member of Technical Staff in the Ribbon Technology group at Bell Laboratories in Atlanta, Georgia. He received the B.S. in Engineering from the U.S. Air Force Academy in 1962. He received M.S. (Physics, 1972) and Ph.D. (Mechanical Engineering, 1976) degrees from Purdue University. He has published over thirty papers, is co-author of a book and a book chapter on optical fiber splices and connectors and holds eight patents in fiber optics.

Lawrence Dunn is a Member of Technical Staff in the Global Customer Technical Support at Lucent Technologies. He joined Bell Laboratories in 1972 and has worked in various assignments in fiber optic splicing, apparatus, testing, cable and systems engineering. He is a graduate of the State University of New York in Mechanical Engineering and holds three patents in fiber optics.

William Shinnick is the Technical Director for the Lucent OFS Customer Care Organization. He joined the company in 1970 and has held a wide range of assignments in Product Management, Project Development, Business Development and Engineering, supporting both copper and fiber network solutions for global applications. He is located at the Lucent Technologies Norcross facility after recently returning from a six-year assignment in Asia Pacific and Europe. Bill has a Bachelor of Science from University of Maryland, a Masters in Project management from George Washington University.

Derek Foxwell is Viatel's Vice President for Infrastructure. He is responsible for the successful completion of the firm's network build in the UK, Netherlands, Belgium, Germany and France. Prior to joining Viatel, Mr. Foxwell served as a consultant to major submarine cable system operators -- including NYNEX Network Services, known today as FLAG, Ltd.; Esprit Telecom UK Ltd.; and Sprint International. He was also employed with British Telecom. Mr. Foxwell is a chartered engineer, a member of the Institution of Electrical Engineers and the Institute of Directors.

New Concept For Fibre Optic Systems Using Rivers And Lakes As Right Of Way

Gunnar Berthelsen

Alcatel, Oslo, Norway

+47 22 63 83 06 – gunnar.berthelsen@alcatel.no

Abstract

A complete portfolio of products and services has been developed to carry out installations in rivers and lakes in many different conditions.

1. Introduction

In the last few years rivers and lakes (R&L) have increasingly been used as rights of way (RoW), and to meet this a number of cable and components, as well as installation methods have been developed and tested.

The main feature of R&L as an RoW is that it provides a quick and inexpensive means of cable deployment for new operators who do not have access to the "normal" RoW's. R&L also provides an opportunity to reduce significantely the time to market for high capacity fibre optic cables.

The main countries where the developed products and methods have been used are France, Norway and Switzerland:

France
- 700 km in rivers
- Marinised terrestrial cable
- Cable trenched into riverbed

Norway
- 1500 km in rivers and lakes
- Submarine type cable
- Cable laid on river and lakebed

Switzerland
- 250 km in lakes
- Marinised terrestrial cable
- Cable laid on lakebed

An R&L project can be point - point systems up to 400 km without intermediate amplification, or Festoons with multi-cable landings.. In figure 1 is shown an example of a Festoon installed in Lake Geneva totalling 100 km of cable.
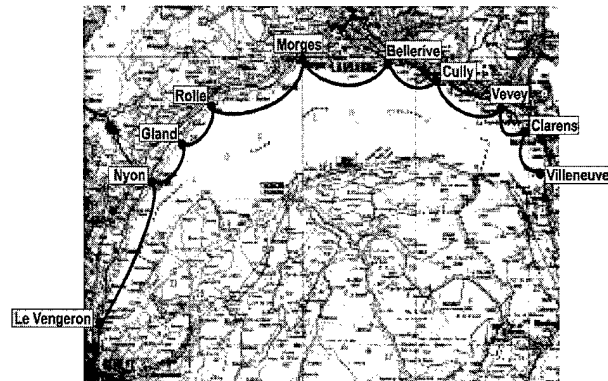
Figure 1. Lake Geneva Festoon

R&L is a symbiosis of submarine and terrestrial technology, and the total solution takes parts from each area. Each project is different from the previous and thus, each one must be engineered individually.

A total R&L project may therefore involve a number of "Work Packages", depending on the nature of each project:
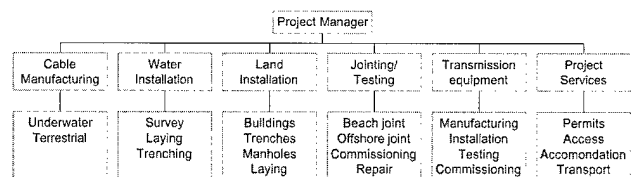
Figure 2. R&L project organisation

An R&L project will therefore be made up of a combination of different elements from the total R&L product portfoilo:

Cable
• Steel tube design
• Plastic tube design
• Duct cables
• Direct burial cables

Componenets
• Landline
• Marinised landline
• Submarine

Installation
• On river or lake bed
• Buried in river or lake bed
• Installation in river bank
• Local concepts
• Combinations of special and local concepts

Transmission equipment
• SDH
• IP

2. Cable Solutions

In addition to "normal" duct and direct burial cables for use in dry sections of an R&L project, it is developed two principaly different families of submarine- and underwater cables where fibres are contained in steel- and plastic tubes respectively, with the following main characteristics:

Steel tube
• Fibres in steel tube
• Derived from submarine
• Modularity 48 or 96
• Lengths up to 200 km
• Low weight/small diameter
• Underwater, in-line joints
• Underwater branching units

Plastic tube
• Fibres in plastic tube
• Terrestrial cable core in Al-tube
• Modularity 6, 12, 24
• Lengths up to 20 km
• Shallow water joint

Tensile strength is an important parameter that must be chosen as a compromise between high strength (heavy armour) to meet the installtion and operation strains, and the need for lighter cables (light armour) to be able to use light installation methods.

As a guideline the following can be used in selecting tensile strengths:
• buried cables in rivers 10-30 kN
• unburied cables in a river or lake with little possibility for anchour damages 30-100 kN
• unburied cables in a river with strong rapids or possibilities for anchor damages 150-400 kN

2.1 Steel Tube Cables

The steel tube family is a complete range with cables in tensile strengths from 10 kN up to 400 kN, with fibre counts up to 384, and is a combination of the URC-1 (submarine) cable family, and the RLC-1 (special R&L) cable family.

Both these steel tube families are based on the same technology, and use the same accessories. Thus, this range should meet all requirements that might arise in an R&L project.
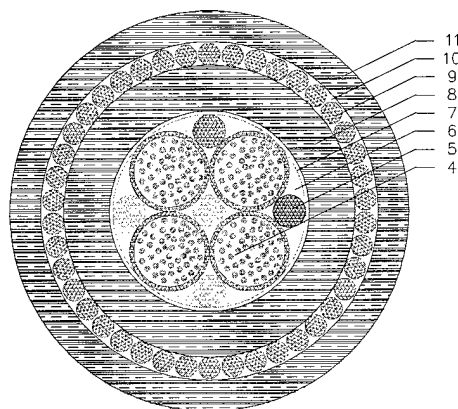
Figure 3. 192 fibre RLC-1 type cable

The 192 fibre RLC-1 cable has 48 fibres in each of four steel tubes (4), an inner sheath (8), one layer of armouring (9) and an outer sheath (11). The diameter is 20 mm, the weight is 0.7 kg/km,and the NTTS is 30 kN.
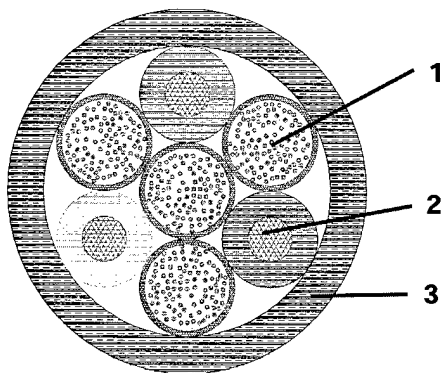
Figure 4. 384 fibre RLC-1 type cable

The 384 fibre RLC-1 cable has 96 fibres in each of four steel tubes (1), Insulated armour wires (2) and and outer sheath (3). The diameter is 22 mm, the weight is 0.6 kg/m and the NTTS is 20 kN.

2.2 Plastic tube cables

The plastic tube cables are low tensile strength cables (10 kN) with fibre counts up to 584 developed for R&L applications, and consists of two separate families of marinised land cables called RLC-2 and RLC-3.
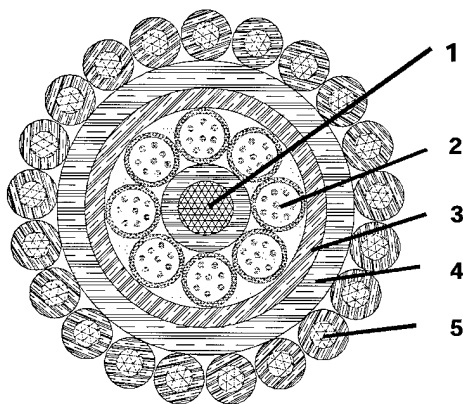
Figure 5. 192 fibre RLC-2 type cable

The 192 fibre RLC-2 cable has a sheathed central steel strength member (1), eight plastic tubes with 24 fibres in each (2), a welded aluminium tape (3), an inner sheath (4), and insulated armour wires (5). The diameter is 20 mm, the weight is 0.6 kg/m, and the NTTS is 10 kN.
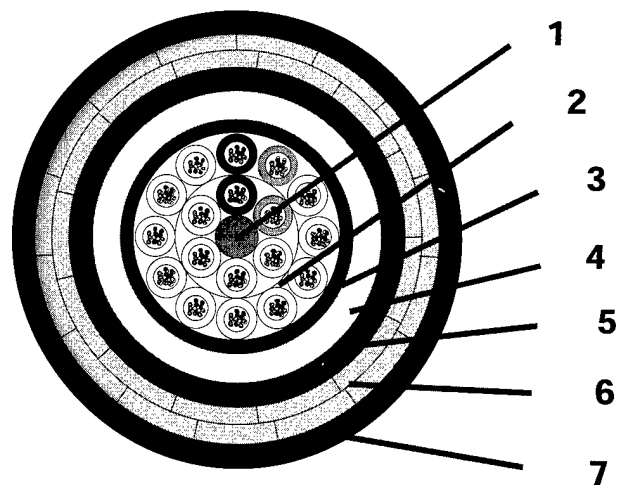
Figure 6. 216 fibre RLC-3 type cable

The 216 fibre RLC-3 cable has an FRP central strength member (1), 12 fibres in each of 18 plastic tubes (2), an inner sheath (3), an extruded aluminium sheath (4), an intermediate sheath (5), two layers of flat steel armour (6), and an outer sheath. The diameter is 32 mm, the weight is 2.2 kg/m and the NTTS is 9 kN.

3 Installation

A cable in an R&L project may be laid in a number of different ways, depending on the bed of the river or lake, requirements for protection, crossings of other cables or pipelines, landing conditions, etc. However, these may be summarised as:

- Lay cable on the river- or lakebed with trenching only at landings and crossings
- Trench cable completely
- Lay ducts on the river- or lakebed with limited trenching, and pull in cables when needed
- Trench ducts completely and pull in cable when needed

These installations can be carried out in either of several ways

- Transported solution, where the complete equipment is shipped to installation site, and carry out the complete installation with own personnel.
- Combined solution, where only specialised equipment (drum pay-offs, caterpillars, trenchers, etc) are shipped out to be operated by own personnel, but use local barges,

boats, tugs, etc to be operated by local personnel.

- Local solution, where only local equipment and personnel are used.

3.1 Transported solution

A completely self contained concept for laying cable on a river- or lake bed has been developed in Norway. The boat and an equipment container is transported on one truck, and floats for storing cable on another truck. This equipment has been transported all over Norway (4000 km long) and has been used to install about 1500 km of cable. Impressions of this concept is shown below.
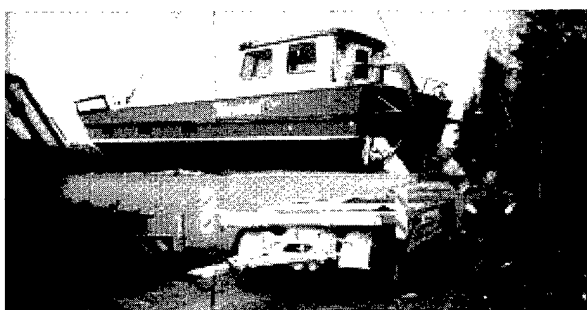
Figure 7. Road transport of the boat

Figure 8. Laying cable directely from the boat

With the drum on the boat 10 km continous lengths can be laid, and with the drum on a barge 30 km continous lengths can be laid (cable with 20 mm OD and weight 0.5 kg/m). The laying speed is >1 km/hour, and the maximum laid depth is 400 m. The draft of the boat is1 m.
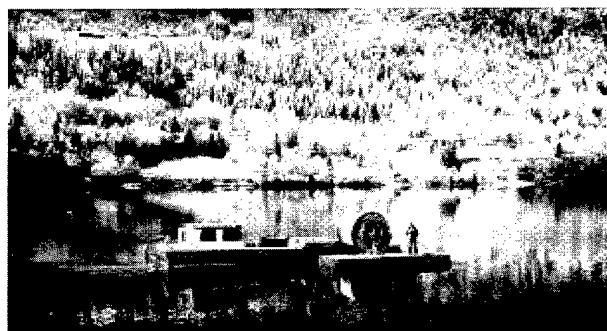
Figure 9. Laying cable from a drum on a barge

As can be seen from figure 9 the operation can also be carried out during the winter, as long as the river or lake does not freeze up.

3.2 Combined operation

In a combined operation specialised equipment has to be transported, and some general equipment should be chartered locally. The split will vary from project to project, but a general view may be:

Transportable equipment
- Cable pay-offs
- Caterpillars
- Sheaves
- Cableways
- Trenchers

Local equipment
- Cranes
- Barges
- Tugs

Below are shown some examples. In figure 10 is shown a large barge (which could be locally chartered) equipped with drum payoffs, cableways and sheaves that could be transported as special equipment. The necessary tugs or other barges used for propulsion, should also be chartered locally.

In figure 11 is shown a large plough (it is more than 2 m tall), which would in most cases be a special piece of equipment that has to be brought to the installation site.
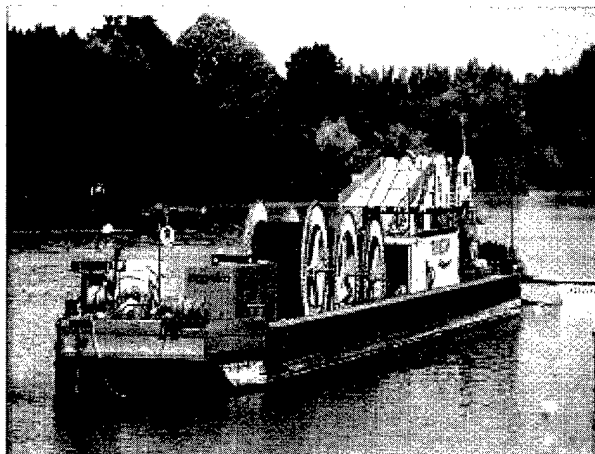
Figure 10. Installing 3 cables simultaneously
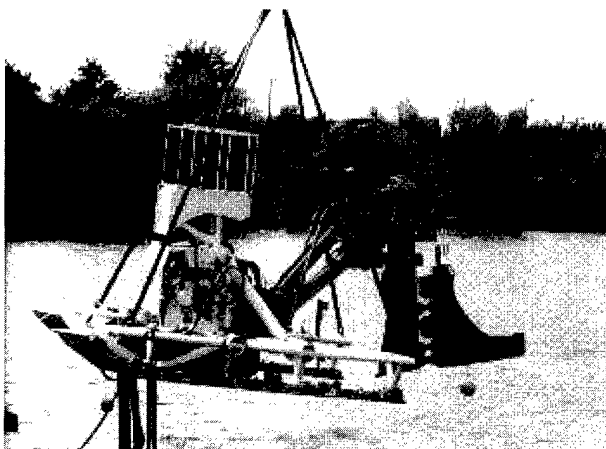
Figure 11. River bed plough

The equipment shown in figures 10 and 11 have been used in French rivers.

3.3 Cable landings
Cable landings normally need special protections, as this is where the danger of damage is largest, and cables are therefore buried in this section even if they are only laid on the river or lake bed on the rest of the route.

In "jettable" soils the cable is protected by a heavy PE pipe which is then trenched by water jetting, as shown in figure 12.
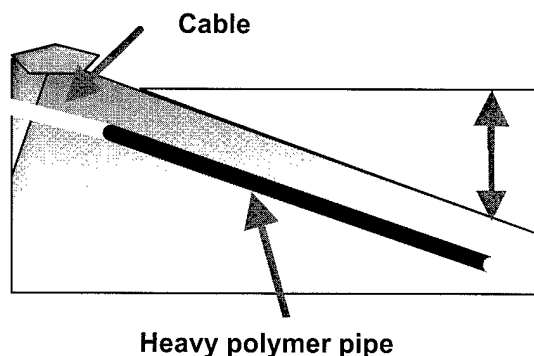
Heavy polymer pipe

Figure 12. Cable landing principle

In a lake landing a polymer pipe should be used down to a water depth of about 10 m, and it should be trenched to a depth into the soil of more than 0.5 m. In figure 13 is shown two cables entering heavy polymer pipes.

Figure 13. Cable laid on the lakebed entering a heavy polymer pipe at landing.

If the lakebed is not trenchable (rock), the heavy polymer pipes should be bolted to the landing rock as shown in figure 14:

Figure 14. Heavy polymer pipe bolted to landing rock.

4. Jointing

In order to make up a complete R&L system various jointing technologies are required:

- Beach joint between "wet" and "dry" cable
- Planned joints during manufacturing or installation to achieve a long cable length
- Repair of damaged cable during installation
- Branch off to a landing from a long main cable
- Deep (>10 m) and shallow water solutions (<10 m)

Figure 15. Beach joint manhole

A beach joint is normally made in manholes similar to the one shown in figure 15, and as can be seen, it is basically similar to a terrestrial joint manhole.

The joint closure that has been used as a beach joint is a terrestrial closure similar to the one shown in figure 16.
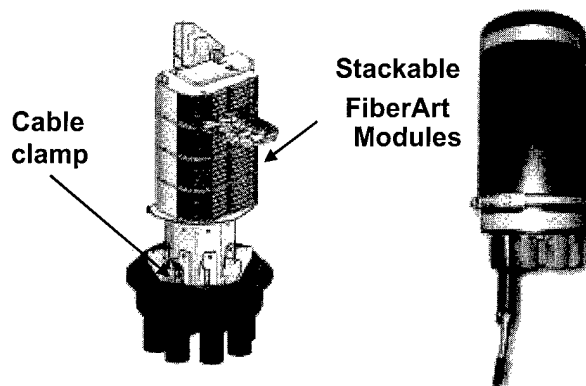
Figure 16. Beach joint closure

For submarine joints at depths greater than about 10 m, a submarine joint closure with bend restrictors has been developed. This is the same as is used for submarine cables, and an outline of this joint is shown in figure 17.

Bend restrictors are use for heavy armoured cables at depths greater than about 200 m. Thus, in most river and lake cables a bend restrictor is not found to be necessary.
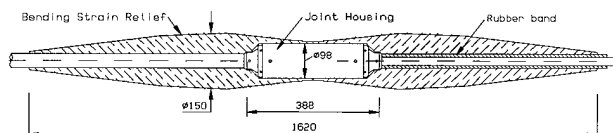
Figure 17. Deep water joint with bend restrictor.

Without the bend restrictor, the diameter of the joint closure is 10 cm and the length is 40 cm.

Two versions of the deep water joint closure have been developed, one for up to 48 fibres and a longer housing for up to 192 fibres. More than 200 of these joints are in use worldwide, and they are rated for depths down to 3000 m.

In shallow rivers, where the joint box do not have to support the cable during laying and possible retrieval, a simpler jointing box has been developed. This is shown in figure 18.
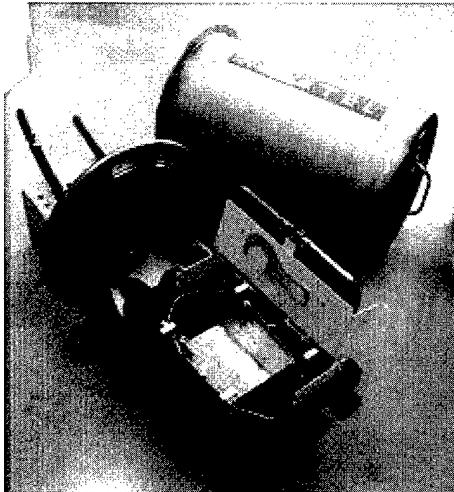
Figure 18. Shallow water joint

In cases where two or more cable ends are to be taken ashore from a long Festoon, an off shore branching unit has been developed. The principle and an actual branching unit is shown in figure 19. The branching unit is completely passive, and distributes fibres from one arm into the other two arms.
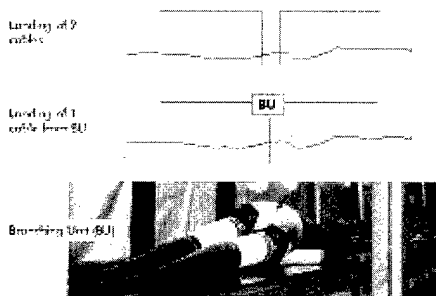
Figure 19. Branching Unit

5. Cost Considerations

Different methods of installation and cables and components used will have different costs intitially, and also over time. For example will

- a cable laid cable on a river or lake bed involve a light (and low cost) installation method, but a heavy (and more expensive) cable.
- a cable trenched into the riverbed involve heavier installation equipment, but lighter cable
- a cable pulled into a pipe that has been prelaid and pretrenched involve the heaviest installation equipment, but the lightest cable

On the other hand
- Installing all possible fibres initially gives the highest financial risk (since all fibres may not give a return initially)
- Installing cable when needed is less financially risky.

Thus, an evaluation of the the life cycle costs of R&L projects in different configurations has been carried out, based on a 10 year period, taking into account cable and component costs, installation cost, required repairs over the 10 years, etc.

In many cases an R&L project also involves use of the river or lake bank (instead of installing the cable in the water), and calculations have been carried out also for this solution, for comparison.

The life cycle cost results according to these calculations are shown in figures 20 and 21 (relative to untrenched cable with all fibres installed initially):

Un-trenched cable 192 fibres installed initially	100 %
Un-trenched cable 48 fibres/year in 4 years	350 %
Trenched cable 192 fibres installed initially	370 %
Trenched ducts 48 fibres/year in 4 years	870 %

Figure 20. Relative installation cost in River & Lake bed

Trenched cable 192 fibres installed initially	310 %
Trenched ducts 48 fibres/year in 4 years	550 %

Figure 21. Relative installation cost in River & Lake bank

Thus for any project it is necessary to evaluate the risk for damage, but it is clear that laying cable on the bed of a river or lake is far less expensive than burying the cable. A risk for damage may be compensated by an even heavier armouring, and still give a less expensive system than if the cable is buried into the river or lake bed.

6. Conclusion

A complete concept for using rivers and lakes as right of way for installing telecom cables has been developed.

7. Acknowledegement

The author wishes to thank Mr. Gunnar Skau, Bravida, Norway, Mr Antoine Veyrat, LDCable, France, Mr. Jean Fehlbaum, Alcatel, Switzerland and Mr Christophe Chaussecourte, Alcatel, France for valuable contributions in preparing this material.

Author

Mr. Gunnar Berthelsen was born Oslo, Norway in 1947, and graduated from Heriot-Watt University, Edinburgh, Scotland with a B.Sc Hon in 1971. He has worked with fibre optics since 1976. He is employed by the Cable Networks Product Line in Alcatel where he has held positions as Technical Manager in Norway, Technical Manager in Europe, and is now Manager of Business Development in Norway.

Gunnar Berthelsen
Alcatel
P.O. box 130, Økern
0509 Oslo
Norway

gunnar.berthelsen@alcatel.no

Innovative Solutions for Access Networks

W. Griffioen, A. van Wingerden, C. van 't Hul, P. Lock, A. van der Tuuk

NKF KABEL BV
Delft, The Netherlands
+31-152605721 · willem.griffioen@dlf1.nkf.nl

Abstract

Optical fiber is on its way to conquer, after the long haul network, also the access network. The specific needs for optical access networks has lead to innovative solutions. An overview and current state of art is given of such solutions, all based on small-size guide-tube systems: copper twisted-pair and coaxial networks which can migrate to optical fiber, "grow-with-market" optical networks for greenfield situations and shared access networks where telecom operators can rent optical connections.

Keywords

Access network; cable; outside plant; optical fiber; copper twisted-pair; coax; migration; small-size guide-tube system; air-blowing.

1. Introduction

Deregulation of the telecommunications market has caused a rapid growth of existing networks and many new networks are being built now. Most of the investments until now were in the backbone network. But the big boom has still to come: reconstruction of the access network. The requirements needed for optical access networks has lead to innovative solutions, based on small-size (7 or 10 mm) guide-tube systems. They allow growth in a competitive environment. Migration of current networks, both traditional telecommunications and CATV, to optical networks is also addressed. An overview and current state of art is given of those solutions, all of them based on said guide-tube systems.

2. Small-size Guide-tube Systems

The guide-tube system is a new concept for optical access networks which takes away the limitations of traditional technology [1,2]. It consists of bundles of individual guide-tubes running through a protective HDPE duct network. A trunk duct runs through the streets and smaller ducts branch to the subscribers. Low-cost splittable "clip-on" branching connections are used which can be placed at any place and any time (see Figure 1). After connection of the chosen guide-tubes to each other individual paths are created. Here miniaturized cables can be installed without splice, e.g. by simply pushing or using compressed air. These cables are copper twisted-pair (1 quad) or optical (2-48 fibers) cables. Also coaxial cables can be blown in the guide-tube systems. All cable constructions offer excellent resistance to outside plant conditions and handling. The bundle of guide-tubes does not entirely fill up the protective duct to offer sufficient mechanical protection [3], to make all tubes accessible at any place and for ease of installation of the bundle.
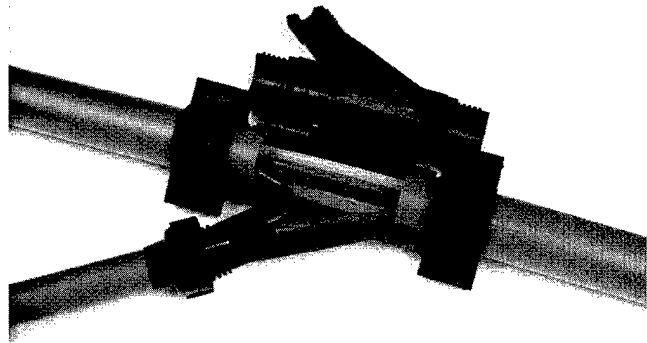
Figure 1. Clip-on Y-connector for branching a guide-tube. A mini-cable passes here without splice.

The concept can be completed with optional joint boxes to connect cables from feeder-, distribution- and drop-part of the access network. Separate protective ducts may be used for these parts of the network but integrated solutions are also possible. The new concept is less costly than traditional techniques for optical access networks. It solves today's problems connecting business customers and brings FTTH within reach.

3. Copper Twisted-pair to Optical Fiber

In the Flashnet project newly built copper twisted-pair access networks were prepared for future migration to Fiber To The Home. It started with the JetNet project [1]. A solution was found for migrating that part of the access network that is the most difficult: the outermost offshoots with their numerous branches. Protective HDPE ducts are loosely filled with bundles of (7 mm) guide-tubes in which individual single quad (1x4) cables can be blown. By using simple clip-on Y-connectors for the tubes, branches in the network can be made at any place and time, without the need to splice. In the future optical fibers can replace the copper quads. The first trial was carried out in December 1996, the first operational pilot in September 1997.

Next, the concept was further developed for the area more close to the local exchange. Here larger copper cables are used. From the central office armored 450x4 feeder cables are direct-buried into the ground (see Figure 2). They are spliced to 3 unarmored 150x4 feeder cables which are blown into 63/51 mm HDPE ducts (see

Figure 3). Next splice is to 3 (or 4) 50x4 (or 25x4) distribution cables which are blown into 40/32 mm ducts. The distribution cables follow the streets in the residential areas, each serving 80 subscribers (20% stock capacity). Finally the drop cables, single quads installed in bundles of 7 mm guide-tubes in 40/32 mm ducts, are spliced to the distribution cables by means of up to 6 joint boxes. They branch to the houses.
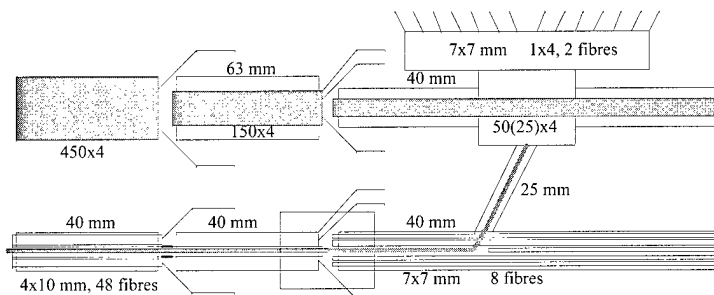
Figure 2. Schematic view Flashnet network structure.

Figure 3. Air-blowing 3.8 tons (world record) of 35 mm diameter 150x4 cable into a 63/51 mm duct over 2 km using 2 cascaded air-blowing units.

Extra HDPE ducts are lead parallel for future optical cables (see Figure 2). From the central office a 40/32 mm duct with 10 mm guide-tubes follows the 450x4 cable. A connection is made to 3 different 40/32 mm ducts with 10 mm guide-tubes following the 150x4 cables. Cables with 48 fibers are blown through said guide-tubes without a splice. They can be spliced to 8-fiber cables which are installed in bundles with 7 mm guide-tubes in 40/32 mm ducts following the 50 (or 25) x4 cables. The 8-fiber cables can be connected to the joint boxes for the drop cables by means of Y-

connectors (see Figure 2) and by replacing the lid of these boxes by an optical joint box. An optical home-connection is obtained by replacing the copper quad-cable by a 2-fiber cable. Half of the fiber capacity is used for point-point links, the rest is reserved for FTTH for all houses using 1:8 and 1:4 splitters in the first and second splice point, respectively. Several operational pilots were completed, from September 1999, including installation in high-rise buildings. The technique has been chosen in The Netherlands, after a European tendering procedure, as the new standard for new installations, renovation and repair.

4. Coax to Optical Fiber

A comparable situation is met in CATV networks. In the same guide-tube system miniature coaxial cables can be installed. Cables with attenuation in the range from 18 dB/100 m to 9 dB/100 m at 230 MHz can be blown in 7 and 10 mm guide-tubes, respectively. Migration to optical fiber is again possible. Empty guide-tube systems parallel to conventional hybrid fiber-coax networks are an alternative. A pilot project is expected in The Netherlands at the end of the year 2000.

5. Greenfield Optical Access Networks

Above networks finally migrate to all-optical access networks. So, if you skip the copper a solution is already there for optical access networks. For FTTH this is true. However, business customers connected on glass required further development of the system. Extreme flexibility is needed. Moreover fiber-counts and distances are larger here. The technique has been further optimized to cope with these requirements [2]. Cables with from 2 up to 48 fibers can be blown in over lengths of up to 6 km. Typical configurations of guide tubes and cables are shown in Figure 4. The fully outside-plant resistant system (cables with hermetic steel barrier, same construction as used in Optical Power Ground Wire, OPGW cables) offers a flexibility which was not offered by traditional technology: costs grow with market, low-cost branching, any place any time, save on duct space and fast installation technology.
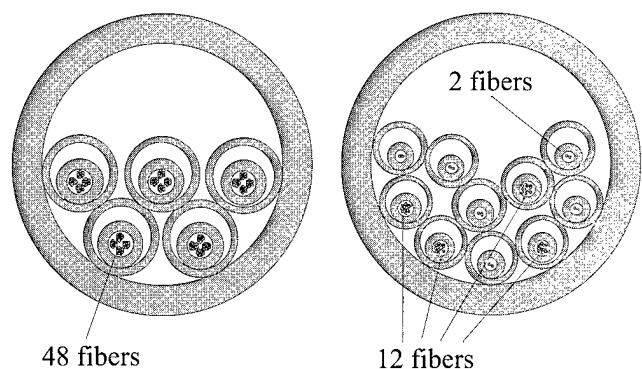
Figure 4. Typical example of guide-tubes and cables used, in this case in a 40/32 mm protective duct.
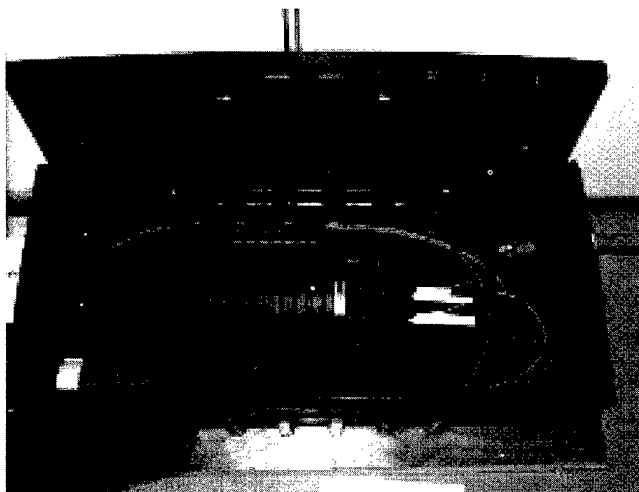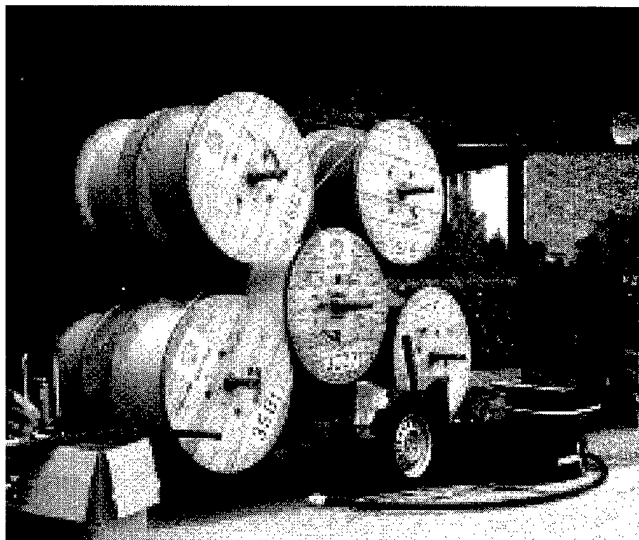
Figure 5. Example of joint box with splice closure. All cables are fed watertight in the splice closure.

Figure 6. Blowing a bundle of guide-tubes into a protective duct (pilot example).

Installation is like other techniques used in the outside plant (but now with flexibility as needed for access networks). Existing duct-routes, manholes and splicing technology (see Figure 5) can be used. This has made the technique so universal that it is also used in backbone networks. A clear advantage here is the possibility to install only the fibers needed and to postpone the choice of fiber types until they are really used. The system has been demonstrated in many pilot projects, from FTTH to long haul networks, in different countries, first in September 1999.

6. Installation Techniques

Installation of a bundle of guide-tubes is done in the field, by blowing (see Figure 6). This is done using traditional equipment with some accessories to feed the bundle. Typical length per blow is 1.5 km, a little less in extremely tortuous trajectories. Longer guide-tube lengths are easily obtained by just connecting tubes to a next length.

The cable is blown in using a miniature blowing device [4]. Also a small compressor will suffice. Typical length per blow is 1.5 km, a little less in tortuous trajectories. Cables up to this length, e.g. the cables to the customer, can be installed quickly. For longer cable-lengths the same cascading techniques are used as in traditional technology: tandem blowing with multiple blowing equipment or using a buffer device where the cable is coiled. This passive device, which is a miniaturized version of a commonly used device, is fed by the blowing equipment (see Figure 7).

Figure 7. Passive buffer coil, driven by blowing equipment, for extending cable blowing length.

7. Shared Optical Access networks

The technique of the guide-tubes is also used for shared optical access networks in business areas. A third party exploits these networks and different telecom operators can rent dark fibers, which connect their subscribers inside such areas. The areas are surrounded by a "circular road" (see Figure 8) which serves as a border: cables from outside, feeding the shared network, may not cross internal cables to avoid single points of failure. The circular road consists of 40 mm protective ducts, filled with 5 guide-tubes of 10 mm with place for 48-fiber cables each.
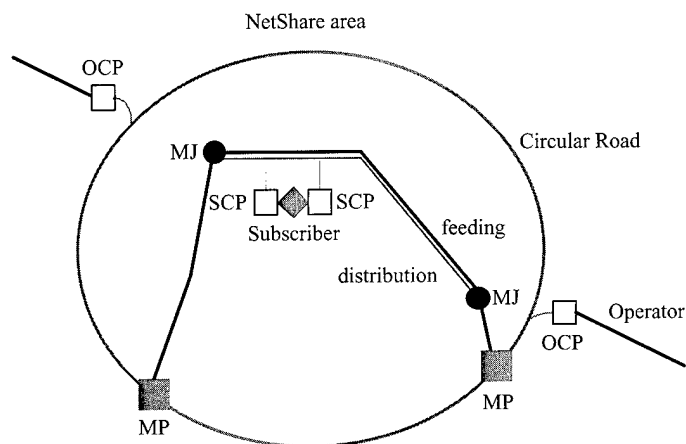
Figure 8. Schematic view of shared access network.

Telecom operators enter the shared network at Operator Connection Points (OCP). Here a splice is made to a dedicated 48-fiber cable that is fed into one of the five guide-tubes from the circular road by means of a Y-connector. To make the connection redundant this is done at two points. The 48-fiber cables from the OCPs are patched in Manipulation Points (MPs) to fibers with subscriber destination inside the shared area. As an option active equipment can be placed in MPs when Telecom Operators ask for this.

The internal network consists of double-routed 40 mm ducts with 5 guide-tubes for 48-fiber cables. These feeder cables are spliced in MJs to 12-fiber distribution cables that drop to the subscribers via Y-connectors. The distribution cables are installed in 7 mm guide-tubes in bundles of 10 in 40 mm ducts. Splicing distribution cables to feeder cables is done in elements of 4 fibres. At the Subscriber Connection Point (SCP) the connection is made to the subscribers. This is done in units of 2 fibers. A SCP can have multiple outlets for different subscribers and/or Telecom Operators.

Two pilot projects with shared network are presently under construction in The Netherlands. The potential number of double-connected subscribers per pilot is about 300 to 800. The actual number of first subscribers will be much less. Traditional technology would not be economical. But, with the system with

guide-tubes initial investments can be kept low. Future expansion of the network is possible without digging again.

8. Conclusions

The outside plant solution based on small-size guide-tubes offers the flexibility which is required for copper and optical access networks. It also offers the possibility to migrate from copper to glass. The technique has been proven in many field trials and pilots. The possibility to install only those fibers which are paid for and to postpone the choice of fiber types has made the system also attractive for use in long-distance backbone networks. Finally the same technique can also be used in shared access networks where different telecom operators rent links to their subscribers.

9. Acknowledgments

10. References

[1] W. Griffioen, H. Nijstad, A.T.M. Grooten, A. van Wingerden, G. Brown, D.F. Hawkins, G. Plumettaz, "A new, extremely versatile, access network cabling concept for migration to optical fiber", *Proc. 45th IWCS* (1996), 485-489.

[2] W. Griffioen, A. van Wingerden, C. van 't Hul, "Versatile outside plant solution for optical access networks", *Proc. 48th IWCS* (1999), 152-156.

[3] K. Nygård Skalman, E. Siönäs, S. Edman, G. Danielsson, "The equipment and cables used in the optical fibre network at Banverket, Sweden", *Proceedings Interwire*, Atlanta (USA), November 1992.

[4] G. Plumettaz, "A new universal tool for the placement of microcables in the local and business access network", *Proc. EC'99* (1999) 76-80.

11. Biographies

Willem Griffioen received a MS degree in Physics and Mathematics from Leiden University (Netherlands) in 1980 and worked there until 1984. He joined KPN Research, St. Paulusstraat 4, 2264 XZ Leidschendam, The Netherlands. Responsibilities R&D of Outside-Plant and Installation Techniques. He worked at Ericsson Cables, Hudiksvall (Sweden) and at Telia Research, Haninge (Sweden) in the scope of exchange/joint projects with KPN Research. He received his Ph.D. (Reliability of Optical Fibers) in 1995 from the Technical University of Eindhoven (Netherlands). Currently, since

1998, he is product manager at NKF KABEL, Schieweg 9, 2627 AN Delft, The Netherlands.

Arie van Wingerden received his B.Sc. degree in Electrical Engineering in 1971. In the same year he joined NKF KABEL BV, Schieweg 9, 2627 AN Delft. Worked in the R&D department and was involved in various cable development projects and high frequency measuring methods. In 1984 he became Engineering Manager of the Project Department and responsible for engineering of Outside-Plant and Telecommunication Systems. Today responsible for Technology and active in advanced network concepts.

Cees van't Hul received a BS degree as Electrical Engineer at Technical High School in Arnhem in 1975. He jointed ELGAWA, a contracting company in Surinam and was responsible for the Medical and Electrical Department. From 1982 he jointed BATCO Surinam as Manager Technical Department until 1985. Since then he jointed NKF Kabel, Schieweg 9, 2627 AN Delft (Netherlands), first as Project Manager in the contracting of High Voltage systems, later as Manager Quality Department. Since 1995 he is involved in the developing of Telcom Cable systems.

Pieter Lock received his MS degree in Electronic Engineering from the Technical University Delft (The Netherlands) in 1981. In the same year he joined NKF KABEL BV in the R&D department and was involved in various development projects for optical video transmission systems. From 1989 he was responsible for production and later for sales in the NKF Electronics division. He currently, since 1999, is involved as product manager for infrastructure and Outside-Plant architectures at the NKF Communication Networks division.

Albert van der Tuuk, born 1 November 1951, having achieved his Bsc EE at the Technical Academy in Zwolle, is at NKF KABEL B.V. since 1982. After a short period of working in the R&D of optical fibre, he joined the marketing department for optical applications. From 1985 –1988, he was involved in the establishment of Yangtze joint venture in Wuhan, PRC. Back in Holland, he founded the NKF Electronics division. Since 1994, he is marketing director, during the last years mainly responsible for the worldwide introduction of new flexible network architectures.

Application of Cross-Connection Series on Optical Fiber Access Network

Kil-Lye Kang, Do-Hyun Nam, Sok-Ho Kim, Geun-Ha Chin, and Woon-Ha Kim

Access Network Laboratory, Korea Telecom
TaeJon, South Korea
+82-42-866-3166 · klkang@kt.co.kr

Abstract

As the subscriber's demands of high speed and broadband service are increasing, the needs to construct the optical fiber access network are increasing. In FTTH/C, the network design of optical access network becomes diverse by the types of subscriber and service. In the process of designing optical access network, the function of cross-connection at the positions where the connections are accomplished with distribution and access cable is needed. Therefore, for the high flexibility and cost-effectiveness in the optical access network, the three types of cross-connection products that could be used in the serious environmental conditions are developed.

Keywords

Optical Fiber Access Network, Optical Cross-Connection, Optical Distribution Network, FTTH, Rotating plate

1. Introduction

Among the access technologies of high speed and broadband service, the DSL technology that deploys the existing copper line has been developed. However the DSL technology is considered as the intermediate solution to offer broadband service to subscribers due to the difficulties in supplying broadband service in terms of the transmission rate and quality, adverse effects on existing services, and causing complicated management in MDF to adapt new services.

Therefore, it is taken into account as the request to replace the copper line with optical fiber, and the attention is increasing. Optical access network is divided into 3 evolution stages of FTTO, FTTC, and FTTH depending on how much the existing copper lines are replaced with optical fiber, and where the ONUs are.

In this paper, the usage strategies for the developed products in optical access network of Korea Telecom, especially for the FTTC in regarding the adaptability and performance are discussed.

2. Cross-Connection Products in Optical Access Network

As seen in Figure 1, it must be considered to make solutions of application with cross-connection series, in regarding the positions and the number of splices. In order to figure out the appropriate number of optical distribution points per a loop, we consider the cost of access and distribution cable, installation of those cables, and products of distribution should be considered. By comparing the cost per distribution point with the constant loop length (6km) and constant the number of fibers(200cores), it is determined that the number of cost-effective distribution points is 16. For example, the proper number of the distribution point is 16 for less than 600 fibers, and 32 for more than 600 fibers feeder cable. Also the proper numbers of distribution cables that are branched from feeder cable should be 16 to 72.

If the cross-connection products are applied in distribution point, it is possible for any cross-connection products on the same loop to use all feeder cables. Therefore, the efficiency of optical fiber feeder network can be increased by at least more than 20 percent if optical fiber cross-connection products are applied. If the supplied rate of optical fiber distribution cable is increased by about 2 times, we can deal with the change of demand more flexibility at the distribution point. Thus the number of optical fiber terminated in a cross-connection product should be 32 to 144.

2.1 Application of the Optical Fiber Cross-Connection Products in Optical Distribution Point

The application of cross-connection products at the point of optical distributions is beneficial to the supply of optical fiber access cables per an ONU. Consequently in case of building or apartment area, the above and under-ground type in MDF of apartment and building, on green area of land, or in manhole can be installed.

In case of residential area, the type of pole-mountable, under-ground can be applied in pole or manhole for the reason of not-enough space.

As we mentioned before, optical fiber cross-connection product increases the efficiency of optical fiber feeder network, and it also distinguish the separation point between optical fiber distribution cables and optical fiber access cables. Therefore it is easy to maintain and beneficial to improve optical fiber distribution network and access network separately.

Figure 1 shows the schematic diagram of our optical fiber access network applied with the optical fiber cross-connection products.

3. Optical Fiber Cross-Connection Products

3.1 Above-Ground Optical Fiber Cross-Connection Cabinet (AGOC)

The AGOC product is a cabinet type installed on street and green area of land for the large optical feeder cable. The cabinet has water-proof property to protect optical fiber and splices from environment.
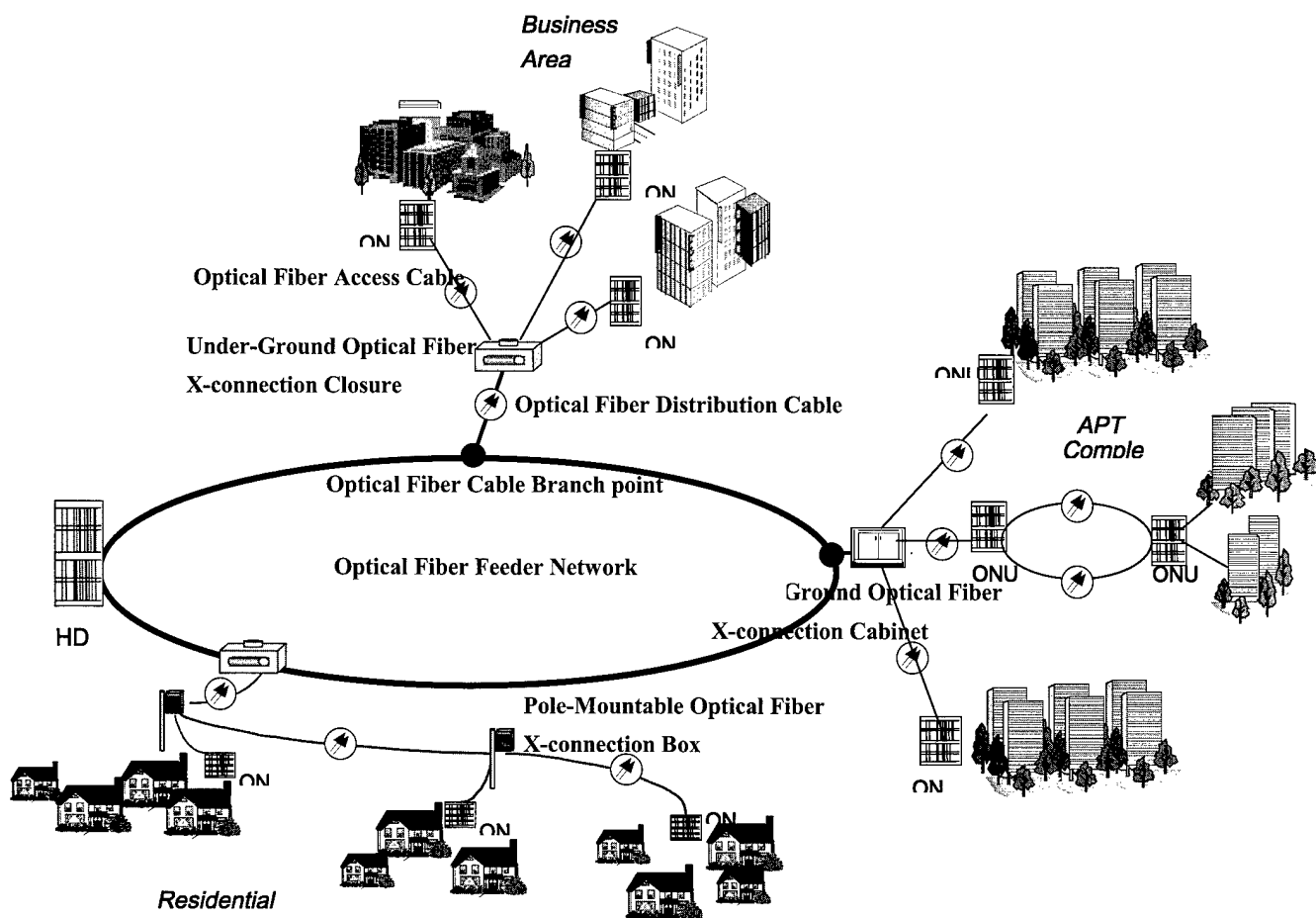
Figure 1. The Schematic Diagram of Optical Access Network in FTTC

The inner module consists of connector shelf and splice shelf and it can be installed on 19' rack. The connector shelf has a patch panel which has 72 SC type adapter. A total of 144 fibers can be accommodated in cabinet. The front and the rear side of patch panel are interconnected with distribution cable from feeder and access cable to ONU. Figure 2 shows a cabinet and inner module of the above-ground optical cross-connection cabinet.

The splice shelf is composed of 6 hinged-tray which include 12 –fiber splice of loose tube(16-fiber splice of ribbon fiber). One side of cabinet has cable entrances of 2 lines, each cable entrance has apparatus which fix main strength member in cable. We make front and rear door in cabinet for the purpose of providing two accessing points according to cable type, distribution cables and access cables.

Thus we should install the distribution cables to rear door side because the cable has few opportunity for maintenance after the

first installation, but access cables should be installed to front door side for the frequent splicings and cross-connections .

3.2 Under-Ground Optical Fiber Cross-Connection Closure(UGOC)

The UGOC can be installed in manhole for small size apartments, buildings, and in residential area, because of limited space to install the products.

Manhole has small space and high humidity environment. Therefore the closure requires properties of small-size, high density and water-proof. The UGOC consists of square-shape dome type cover, end cap, and sealing materials. In the inner module, there are optical fiber splice tray, jumper storage tray and patch panel for connector. The end cap is equipped with apparatus for fixing main strength member of optical cable and for assembling of the inner module.
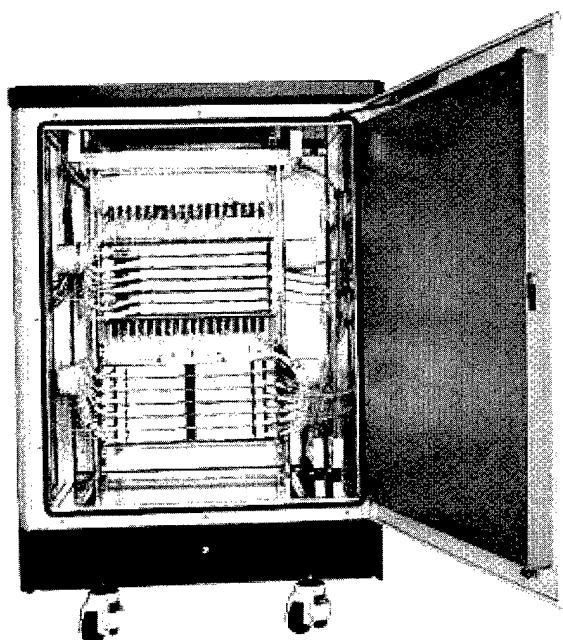
Figure 2. Cabinet and inner module of above-ground optical fiber cross-connection cabinet

Figure 3 shows a under-ground optical fiber cross-connection closure.

The inner module consists of a patch panel on the center and both side with rotating plate which can be swung in the opposite direction each other, and the patch panel has the 36 SC adapters. Also jumper storage tray is jointed with rotating plate longitudinally and can be folded to patch panel. And the bottom
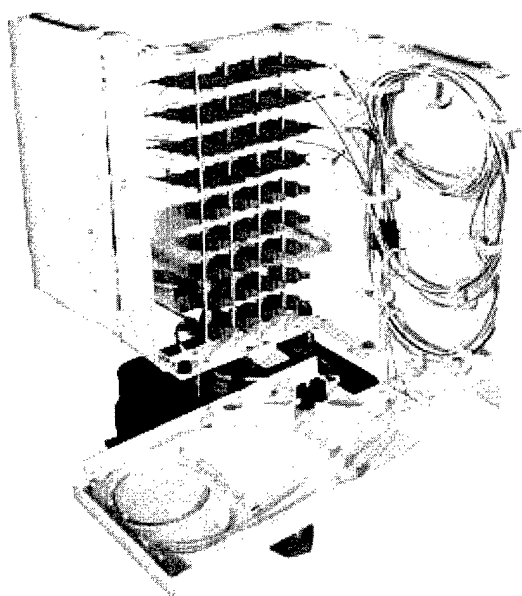
(a) Inner Module
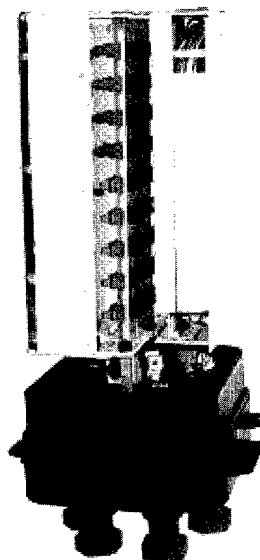
(b) Folded inner Module   (c) closure
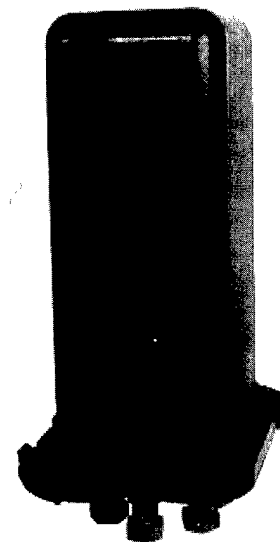
Figure 3. The Inner Module and closure of under-ground optical fiber cross-connection closure

of this jumper storage tray is hinged with splice tray which can be unfolded or folded to jumper storage tray. Cable entrance in end-cap is sealed with screw-type plug that has hole in center.

In the case of installation and maintenance, we can make S-shaped inner module by unfolding the two parts of the jumper storage tray and the fiber splice tray in order, and thus we can get enough working space. After the splice and connection ended, we fold each tray in the reverse order, and then inner module becomes square-shape finally. Consequently, we achieve easy operation, small size and high capacity closure.

3.3 Pole-Mountable Optical fiber Cross-Connection Box(PMOCB)

This product connects distribution cable of small fiber from feeder cable to access cable for ONU in residential area. In case of limited spaces for installing both the above-ground and under-ground products in residential area, pole-mountable box can be applied. The box design has the concepts long shape in length similar to pole.

The rotating plate in the center of box, which has patch panel that is assembled with 24 SC type adapter, and has the apparatus for fixing splice tray and jumper storage tray. There are two horizontal plates for sealing function for rain. The upper one is installed below the top of rotating plate, and the other is the bottom plate for the entrance of 8 cables. Especially, the one side of rotating plate is hinged with box longitudinally.
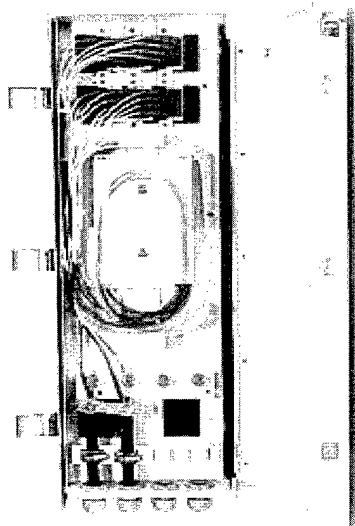
(a) Rotating Plate Closed
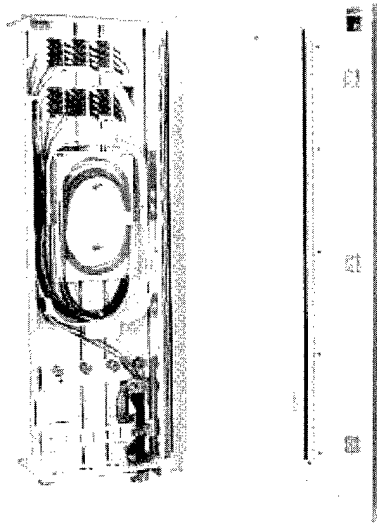
(b) Rotating Plate Opened

Figure 4. A pole-mountable optical fiber cross-connection box

Therefore, it is possible to splice distribution cable from feeder cable on rear side and access cable on front side of the rotating plate. Each cable is interconnected to both side of rotating plate. After the splicing and connection of distribution cable on the rear side of rotating plate have done, the rotating plate

can be closed in the right wall of the box. With the swing function of rotating plate, there is no interruption by distribution cable for entrance and splice of access cable. We achieved easy operation, efficient management and high capacity structure by using the rotating plate. Also we used thin, transparent window for inspecting of optical fiber radius in optical jumper cord storage tray. Figure 4 Shows a pole-mountable optical fiber cross-connection box.

4. Performance Test
Table 1 shows the results of functional, optical, mechanical and environmental tests for optical cross-connection products by using the JDS FITEL 3170 loss meter and switch for optical loss.

5. Conclusion
The range of the capacity and the application cases are examined such as the applications of optical cross-connection products in FTTC, the structural characteristics for three types of products, performance test results, and the efficiency of applications in FTTC.

In FTTH architecture, it is expected to apply the variety of capacity and type of optical cross-connection products that was developed in KT for diverse optical distribution network architecture. Under the limited space for the installation, the flexibility by the rotating structures of modules in the pole-mountable and under-ground products give easy installations and maintenance in optical access network operations.

Now we investigate the efficient applications of optical cross-connection products in distribution network design, especially the requirements for FTTH, and continue to effort for developing of equipment and technology in relation to ATM-PON.

6. Acknowledgments
Thanks to the persons who involved in the co-research of "Development of Outside Plant Products for Ribbon Fiber Cable', and special thanks to Chang Woong Jung, Chan Sul Park and Woo Sin Jo.

7. References

[1] Bellcore TR-TSY-000949 Issue 1, June 1990 "Generic Requirements for Service Terminal Closures used with Optical Cable'

[2] Bellcore TA-NWT-000326 Issue 4, December 1993. "Generic Requirements for Optical Fiber Connectors"

[3] Bellcore GR-771-core Issue 1, July 1994. "Generic Requirements for Fiber Optics Splice Closures. Splice Closure Features and Functions"

Table 1. The results of functional, optical, mechanical and environmental test for optical fiber cross-connection products [1][2][3]

Test	Conditions	X-connection cabinet/closure/box		
		Above-ground	Under-ground	Pole-mountable
Cable Pullout	F=Dx1000N/45, 30min	No cable out	〈 1PSI	No cable out
Cable Bending	10kgf, 15min at each 90°angle 90°~ 360°, 2 cycle		〈 1PSI Not exhibit any bubbling	No cable out
Cable Torsion	Retained 2hr at each -20±2°C, 40± 2°C Cable twist in 90°→ -180°→ 90° 2cycle/min, 10cycle		Not exhibit any bubbling Not exhibit any fracture	No mechanical Damage
Impact Resistance	Retained 2hr at each -20±2°C, 40± 2°C 6PSI, 2.4kg, 2.54cm. 1m height	not air, 7.2kg, 16cm height No mechanical damage	〈 1PSI Not exhibit any bubbling	
High Temp	75±2°C, 24hr	〈0.2dB		〈0.2dB
Temp Cycling	-40±2°C~ 60±2°C, 8hr/cycle. 20cycle	〈0.2dB	-30±2°C~ 60±2°C 〈 0.2dB, 〈 1PSI	〈0.2dB
High Humidity	40±2°C, 95±2%RH, 96hr	〈0.2dB		〈0.2dB
Rain Intrusion	3.8ı /min, 0.5m, 60min	〈0.2dB No sign of water Intrusion		No sign of water Intrusion
Salt Fog	40±2°C, 5% salt spray, 96hr	No sign of Corrosion		No sign of Corrosion
Water Immersion	Depth 1.5m, 20days		No sign of water Intrusion	
Vibration	10-50-10Hz/2min, amplitude 0.75mm Vibration time 1hr. each axis	〈0.2dB	5-55-5Hz/2min, 1mm, Vibration time 2hr. 〈0.2dB, 〈 1PSI	〈0.2dB No mechanical Damage

Authors

Kil-Lye Kang

Korea Telecom Access Network Laboratory

62-1, Whaam-dong,

Yusong-gu, Taejon, Korea

305-348

Kil-lye Kang graduate from KAIST in 1993 with a M.S. Degree on Chemistry. Then, joined in Korea Telecom and is engaged in development of outside plant devices.
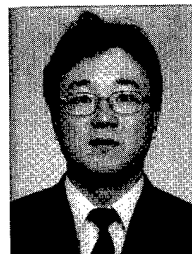
Do-Hyun Nam

Korea Telecom Access Network Laboratory

62-1, Whaam-dong,

Yusong-gu, Taejon, Korea

305-348

Do-Hyun Nam graduate from HanYang University in 1987 with a M.S. Degree on Mechanical Engineering. Then, joined in Korea Telecom and is engaged in development of outside plant devices.
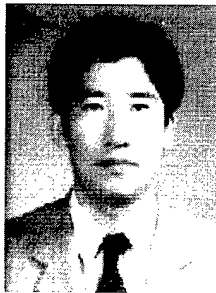
Sok-Ho Kim

Korea Telecom Access
Network Laboratory
62-1, Whaam-dong,
Yusong-gu, Taejon, Korea
305-348

Keun-Ha Chin

Korea Telecom Access
Network Laboratory
62-1, Whaam-dong,
Yusong-gu, Taejon, Korea
305-348

Sok-Ho Kim graduate from HanYang University in 1988 with a M.S. Degree on Material Engineering. After 3yrs developing electronic materials in KIST, he joined in Korea Telecom and is engaged in development of outside plant devices.

Keun-ha Chin graduate from Seoul National University in 1993 with a M.S. Degree on Mechanical Engineering. He then joined in Korea Telecom and is engaged in development of outside plant devices.
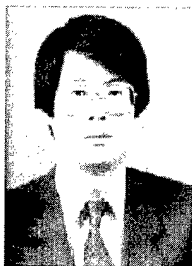
Woon-Ha Kim

Korea Telecom Access
Network Laboratory
62-1, Whaam-dong,
Yusong-gu, Taejon, Korea
305-348

Woon-Ha Kim graduate from KyungBuk University in 1980 with a B.S. Degree and Hanyang University in 1991 with a M.S. Degree on Electronic Engineering. He is engaged in research of access technology.

Prospect a Reconstruction of the Future Central Office in Korea Telecom

Do-Hyun Nam, Kil-Iye Kang, Keun-Young Kim, Sang-Wan Na, and Jae-Jin Lee

Access Network Laboratory, Korea Telecom
TaeJon, South Korea
+82-42-866-3064 · namdh@kt.co.kr

Abstract

Preparing the future broadband network services, there are some movements to prepare new faces of central office. In Korea Telecom, providing a more space which for the new systems with limited floor space problems has been seriously considered. In this paper, making a new plan for providing a space under serious conditions and applying a new scheme of optimizations with systems in transmission and MDF rooms are discussed. In addition, making the basic schemes for the optimizing are presented, which need to consider the future evolution of access and backbone network. The future CO rearrangement and replacement should be as flexible as possible in accommodating the high capacity systems for increasing traffics on the internet.

Keywords

Central office, optimization, transmission room, MDF room, access network, network evolution.

1. Introduction

To prepare the new millenium's internet demands of data traffics concerning from the dial-up services to mobile internet services, there must be new strategies to set up the schematic of the future central office's reconstruction for the purpose of stable services. In this paper, reconstruction of central office that means the providing a successful plan to the future network for accommodating the diverse systems such as the switches, transmissions, MDF, cabling systems and the other things. In addition, the space problems should also considered for new systems. In order to serve more subscribers per a switch, there have been replacements and improvements with increasing the geometrical coverage, and applying the IDLC with the loop carrier that induces the transformation of transmissions in the access network. In this paper, replacements and rearrangement of the systems in transmission room, cabling systems, and MDF rooms will be discussed mainly, and the scheme of central office future trend in accordance with network evolution is discussed.

2. Main issues

Korea Telecom has some difficulties in providing data services(xDSL, OLC, etc) like the other companies, so reviewing the future network trends and making a solution for field conditions are needed. In order to support the floor space for new systems in limited conditions and to prepare the solution for reshaping the scheme of reconstructing the CO, the following can be issued, such as

In transmission room ;

- Repositioning and replacement for the PCM, DCS, and access network systems.
- Cabling for fiber optics in CO.
- Reasonable methods for providing a space for future systems

In MDF room ;

- What to do when switches are upgraded.
- How to control the "Vacancies" in the MDF when IDLC is applied with ONU.
- How to optimize the MDF environment for the future.

For network evolution ;

- With the trends of future network in the system transitions in central office.
- How to control the access network transmission systems in central office.

3. Strategies of optimization in CO
3.1 Define CO types

It is impossible to adapt a unique solution to all kind of CO which has the many different environmental conditions such as the scalability, the number of subscriber line and geographical conditions. For optimal solutions, the dividing and grouping are needed. CO can be divided as four groups.

- Core in switching, transmission and enlarged CO.
- Non-core in switching, transmission and enlarged CO.
- Non-core in switching, transmission and conventional CO.
- Small CO that will be enclosed in enlarged CO.

Where enlarged CO has the characteristics of increased spans and switching capacity and small CO that has only function of transmission

With analysis of those group's common features in the view of network planning, plus particular characteristics which concern the floor space problems, the system types in transmission room, cabling systems and MDF, and more adaptive strategies can be built for CO one by one.

3.2 Solution for the space of transmissions

The reasonable way to provide the space in transmission room is the combination of the replacement, rearrangement, and utilizing the

uninstalled space, which yields the efficiency 30~40% in average. The methods can be expressed as follows:

3.2.1 Replacements. In the transmission room, there are many kinds of systems from the PCM to the optical fiber transmission systems. There are some antique systems for the traditional services which for the leased line services, DID, and DOD on the basis of copper cables. Now for the purpose of the systematic organizing, the out-dated systems must be replaced by new systems. In order to make proper solutions for the replacement, the following can be considered.

- Analyzing the basic elements such as the plans of switches improvement and the transmission system upgrade between the Com, and the scale for leased line.

- The present conditions of transmission systems and future plan of network.

- The arrangement diagram and cabling of copper/fiber optics.

- The economic analysis of the replacements for many cases.

3.2.2 Rearrangements. The schematic block diagram of the transmissions must be provided at first and to make a space plan for the future transmission systems that will be installed according to the system characteristics. Like the same case with replacements, the following can be considered as reasonable in the same case with the replacements.

- The relationships of transmission room position which must make a accordance with the switch and MDF room with the basis of cabling path.

- The analysis of efficient managing in the manpower.

- The plan of the unused floor space is required.

- The definition of path and architecture with copper/fiber optic cables.

- The economics of rearrangement from the PCM to fiber optic transmissions.

In addition, the other important thing is utilizing the unused floor space with the replacement schemes discussed and rearrangement in accordance to given floor space conditions in CO.

3.2.3 Comparison and comments. Among the methods discussed above, the best can not be chosen as only one solution in practice, thus comparison the methods and how to make solutions for common case should be considered.

Table 1. Comparison the upper methods

Item	Replacements	Rearrangement	Utilizing the unused space
Merit	•Can be used for the basic plan of upgrading systems •Possible to make best efficiency with rearrangement	•Easy application of new systems with level of functions •Cabling upon the	•Low cost

	•Reusability of systems is possible	grid panel can be rearranged.	
De-merit	•Must considering the rearrangement	•High cost •Low effectiveness	•Unusual in practice
Com-ment	•After making a proper analysis for respective CO style, the detailed plan for the floor space which includes rearrangement and replacement that pertinent to the network planning, and at the same time verification of the empty space, must meet the requirements of it's own demands		

3.3 Effectiveness in managing the CO space

The schematic of ideal diagram for an optimized transmission room is shown as Figure 1 and in order to supply floor space for new systems, grouping with the level of signals, and cabling conditions must be considered also.
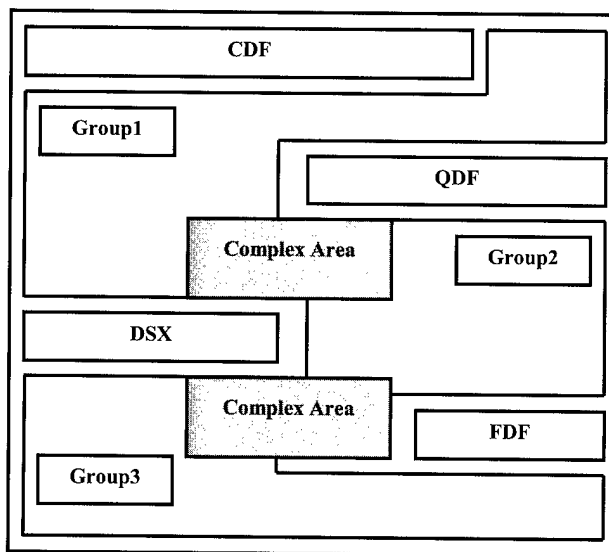
Figure 1. Ideal schematic diagram of transmission room

3.3.1 Common requirements of cabling system. The path selections of cabling are different case by case. However, the definitions of common requirement are necessary to perform the stable cable management.

- No cross over in routing the copper and fiber optics from the basement to maintenance room and both cables must have their own different paths.

- Copper termination cables to be connected with MDF must be rearranged to meet the reasonable replacement of protection magazines and the acceptability of MDF transformation due to the IDLC function in switch system.

- The shortest path(the basement inlet position of fiber optic cables must be oriented by the FDF position in transmission

room) and bending radius of that must be kept correctly all over the path.

- The cable path should be determined prior to define the function of systems in MDF room, and the transmission room must meets the requirement of cable management.

- The path of copper cable should follows the far-end wall side between MDF and transmission room, and as centered as possible.

3.3.2 Grouping the transmission systems.
Under the conditions of limited space and the unclear work responsibility of access network management, the reasonable solutions are reconstructing the responsibility for transmission and MDF maintenance, and making a proper policy, long term plan for how to install and replace is just value added procedure. A proper solution will be established in the near future in Korea Telecom. The classification of the transmissions in detail is given in Table 2.

Table 2. Grouping the transmissions

Group1	PCMs, DSU, FDSU(DS0~DS1)
Group2	MX13, DXC13(DS1~DS3)
Group3	SMOT1, SMOT4, NT-2.5G, WDM
Access transmissions	ADSL, FLC(Fiber Loop Carrier), SLCS

There must be a plan for those access transmission systems for installation and management.

3.4 MDF room
The evolutions of MDF are evident and the main reason is the demands of explosive data services which invoked the applying the IDC connector that has more stable quality than binding post type in connector block of switch side. The other reasons are

- The necessity for the cabling and space due to unbundling for CLEC.

- The improvement of the effectiveness in space management with IDLC and new data services will make a vacancy in the MDF(V side of protection magazine).

3.4.1 Optimizing the MDF.
In the near future, Korea Telecom will faces the common phenomena in MDF which have no subscriber line with the protection magazine for the applying the IDLC and FTTH in access network. Therefore, how to rearrange the MDF and when to replace the binding post block related to switches will be important issues in the MDF room. There are some methods for such as:

- Using vaults closures for copper termination cables.

- Determining the time for improving in regarding MDF condition.

- After making a two-dimension map of magazines which covers the subscriber area and analyzing the pattern of that magazines.

- In addition, the smallest and good quality MDF must be selected, making strategies of the replace the magazine depend on the cable rout of outside plant and the characteristics of subscriber, including the rearrangement of outside copper cables.

- If there is a improvement with switch systems, described steps for MDF must be considered as soon as possible.

3.4.1 Future environments of MDF room.
For the purpose of performing the quality of data services and for one stop services, the MDF room needs to be changed to put up with the main function of subscriber's total management. Of course, the management system of subscriber line should be installed and versatile access transmission systems should also be operated in MDF room. Thus the elementary control of air and power must be considered, the skilled work responsibility will be required for the diverse requests from the customers.

4. Network evolutions
It is still not clear what the future transport network will be. On the basis of the SDH architecture, the trends will be concentrated on the IP traffic of internet, and it is very easy to anticipate the future aspect in explosive IP services. Profoundly, as the same cases in access network, the structure and architecture of transmission will be focused on IP/WDM in the future. There have been many researches and have looked upon the future network of IP/ATM/WDM[1].

In the long run, the change of the network will be reflected on the systems in CO. Upon the present SDH systems, the new WDM systems will be installed together and DCS will be replaced by OXC. Central offices can be divided into core and tributary offices. Tributary segments are just like the same as baseline architecture, and traffic from tributary offices is routed to the nearest core offices [2]. Hence the type definition of CO for the feature is very important procedure to prospect the future network evolution.

Applying the routers and metro WDM is in the rapid progressing[3], so at first there'll be complicated features in the system level. However, after the maturity of IP services and system developments, which are pertinent to the future trends, there may be some gentle but firm pattern in CO.

Access networks are in the process of changing to the fully optical which would be accomplished with ATM-PON/WDM-PON. In many practical cases, the combination of copper and fiber technologies is used. As we see, there are multiplicity of solutions, the cost-effective technology will be distinctive features in access network. Therefore, the appearance of home network with leased copper line or fiber optic line is growing very fast in the SOHO and cyber apartment. Under those conditions, if the OLT(optical line terminal) will be a platform in access network, we must analyze the economics of the pure IP(IP/WDM) architecture comparing the effects of ethernet in OLT(IP/SDH/WDM or IP/ATM/SDH/WDM).

As the network technologies evolving, things will happen and the future aspects of maintenance room in CO are like these;
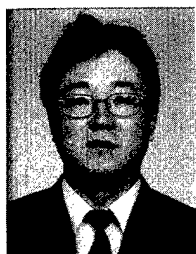
- Replacing the low level of PCM very quickly for old leased line services in case of changing to the large capacity switches.

- Analysis for the transformation of transport network core/access technologies will be clear through the defining the function of OLT.

- Defining the concepts, markets, and technologies of broadband services in addition to the demanded bandwidth of per a customer will be needed[4].

- MDF room will be a core part in managing the subscriber's line.

- Upon the switch improvements, many access transmission systems will be converged to OLT.

- In core CO that covers OLXC layer, the BDCS will be replaced by OXC quickly.

- ATM switches will carry out the connection between the core and tributary offices.

5. Conclusions

- The replacement of systems must be planned adequately with the evolutions of access network and with improving the efficiency of floor space usability by the means of system rearrangement.

- From the low level of CO to high level, sophisticated reconstruction planning is required on the basis of the optimization schemes according to inner status.

- Upon the optimization of CO systems, reshaping the related work responsibility between the transmission and MDF room.

- For cable management of fiber optic from underground to transmissions, there must be the different route via the copper cable.

- For the purpose of providing reasonable solutions for optimizing the central office, there are some important factors. Forecasting the future plan from the switches to MDF, researching for the trends of broadband services and policies, considering the most important problems under the present situation with maintenance flow, and preparing the integration of MDF for maintenance with subscriber line are the important aspects in prospecting the future CO evolution.

6. Acknowledgments

7. References

[1] Andrzej Jajszczyk, "What is the Future of Telecommunications Networking?," *IEEE Communication Magazine.*, p. 15 (June, 1999).

[2] Robert D. Doverspike, Steven Phillips and Jeffery R. Westbrook , "Future Transport Network Architectures ,"*IEEE communication Magazine*, p. 96 (August 1999).

[3] Satoru Okamoto, Masafumi Koga, Hiro Suzuki, and Kenji Kawai, "Robust Photonic Transport Network Implementation with Optical Cross-Connect System," *IEEE Communication Magazine*, p. 94 (March, 2000).

[4] Geng-Sheng Kuo, " Broadband service Concepts, Markets, Technologies, and Trials," *IEEE Communication Magazine*, p.54(october,1999)

Authors

Do-Hyun Nam
Korea Telecom Access Network Laboratory
62-1, Whaam-dong,
Yusong-gu, Taejon, Korea
305-348

Do-Hyun Nam graduate from HanYang University in 1989 with a M.S. Degree on Mechanical Engineering. Then, joined in Korea Telecom and now he is engaged in development of outside plant devices and in optimization of CO.

Kil-Lye Kang
Korea Telecom Access Network Laboratory
62-1, Whaam-dong,
Yusong-gu, Taejon, Korea
305-348

Kil-lye Kang graduate from KAIST in 1993 with a M.S. Degree on Chemistry. Then, joined in Korea Telecom and now she is engaged in development of outside plant devices and in optimization of CO.

Keun-Young Kim

Korea Telecom Access
Network Laboratory
62-1, Whaam-dong,
Yusong-gu, Taejon, Korea
305-348

Keun-Young Kim graduate from HanYang University in 1991 with a M.S Degree on Materials Engineering. Then, joined in Korea Telecom and now he is engaged the planning & coordination team.

Jae-Jin Lee

Korea Telecom Access
Network Laboratory
62-1, Whaam-dong,
Yusong-gu, Taejon, Korea
305-348

Jae-Jin Lee graduate from KyungBuk University in 1997 with a M.S. Degree on Electronics Engineering and Ph. D on Computer Engineering from Korea University in 1997 Then, now he is a director of xDSL technologies and outside plant devices.
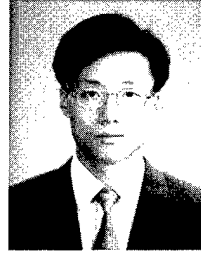
Sang-Wan Na

Korea Telecom Access
Network Laboratory
62-1, Whaam-dong,
Yusong-gu, Taejon, Korea
305-348

Sang-Wan Na graduate from HanNam University in 1995with a B.S. Degree on Electronic Engineering. Then, joined in Korea Telecom and now he is engaged in the planning & coordination team.

A Concrete Optical Fiber Network Deployment Featuring New Fiber Management Technology

Hans G. Naumann
Wingas/Winterstall A.G
Kassel, Germany
+49 561 301 1379

Bertrand P. Joly, Véronique Stappers
Alcatel Cable Interface
Bezons, FRANCE
+ 33 1 39 96 56 56

Abstract

As many other competitive Telecom Service providers, the pipeline Operators such as gas Distributors have opened the access to their own Telecom distribution network.

In these circumstances, a main concern is the individualization of the subscriber management which requires :

- Access to the individual fibre or circuit within an otherwise mass interconnection environment ;

- Maximum intercircuit (interfibre) transmission immunity during installation and operation.

In the actual implementation presented, we describe the characteristics of the technical solution which we developed, installed and controlled to fulfill the technical objectives.

To that aim, specific new single fibre/ single subscriber management technology has been implemented at the interconnection points of the network i.e.

- Cable jointing closures

- Optical distribution frame (ODF)

The technical choices are aiming at allocation flexibility, low implementation cost, ease of installation together with high fibre mechanical protection including during installation and operation.

1. Introduction

Wingas is a joint venture of the BASF subsidiary Winterstall A.G and the Russian natural gas producer RAO Gazprom. Wingas operates a 1,850 Km gas pipeline network across the German territory.

Wingas operates its own telecommunication network since 1992; this network has been upgraded through fiber optic cables since 1998.

This network being rented to National and International Operators, Wingas has to offer an access to optical fiber at any point of the network without disturbing transmission on the other fibers.

In order to ensure the required transmission integrity all the interconnect equipments have to offer 2 main technical features :

- Maintain fiber and patchcable length preservation in all moving parts

- Provide Operator with individual fiber /circuit/ patchcord access during installation and intervention phases.

These principles have been applied by Wingas at the straight cable jointing points and the optical distribution access nodes.

2. Cable jointing closures

The optical fiber transport network is built up using 288 fiber cables made of 24x12-fiber-loose-tube bundles.
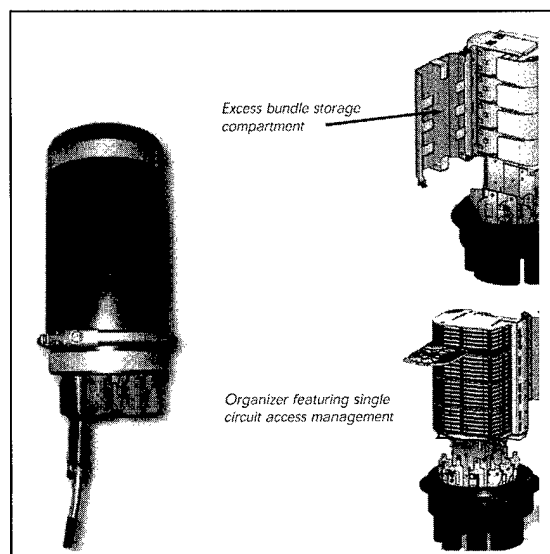
Figure 2-1

As shown in Figure 2-1, the selected cable jointing closure is a dome shape structure providing :

- Single side (base) cable entry on a flat surface especially dedicated to cable sealing (whether heatshrink or mechanical) and cable clamping

- 360° splice access when the cover is withdrawn which facilitates cable integration functions such as cable clamping, bundle routing, overlength bundle management and splice tray access

The jointing closure incorporates 4 single subscriber (circuit) management fiber organizers providing the required transmission integrity in case of reintervention.

At the outcome of the cable clamping breakout, the 12-fiber bundles go through the overlength storage compartiment and are led to the appropriate organizer level (see figure 2.2)
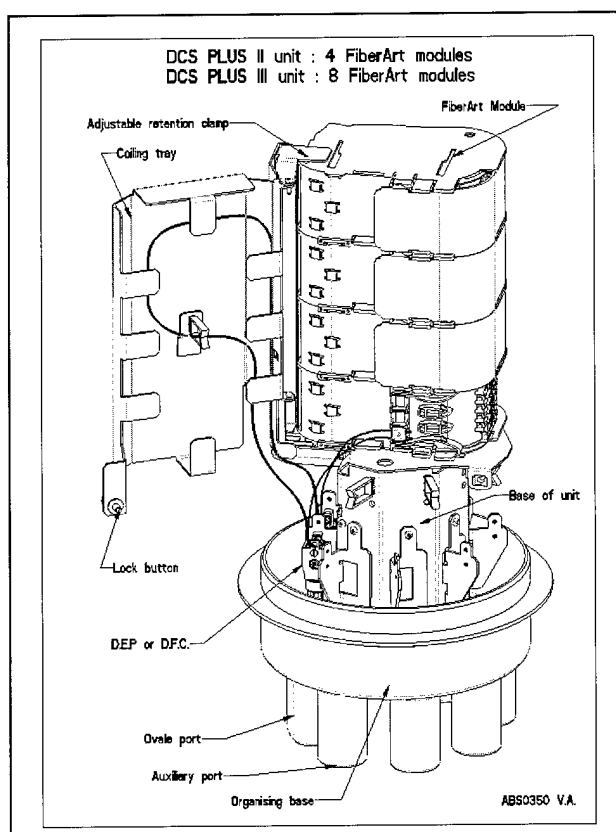
Figure 2-2

Each 12-fiber bundle is splitted into two 6-fiber cores in the organizer fan-out entry; each one of these 6-fiber cores is routed to each tray where 6 incoming fibers are spliced with 6 outgoing fibers.

The 4 organizer modules containing 12 trays each provide splicing for 72 fibers; each splice is protected with a heatshrink cover.

The straightforward cable bundle management inside the closure eliminates the necessity to retube the fibers. The fan-out system being part of the single subscriber management organizers induce efficiency and simplification of the installation work; considerable savings of implementation time and cost have been experienced using this technique.

3. Optical Distribution Frames
3.1 The principles
Let us recall first the principles of a cross connect interface which is the aim of the optical distribution frame (ODF).

We can define the ODF as a structured biunivocal interface between 2 random spacial sets of extremities (cable-in and cable-out).

This is illustrated in Figure 3-1.
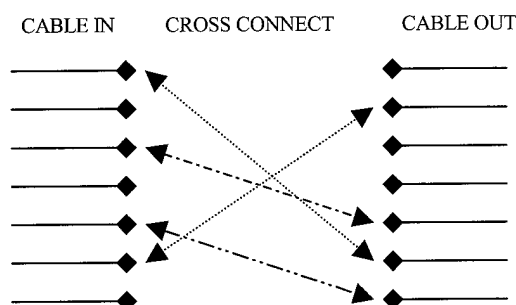
Figure 3-1 : Cross-connect

If we go one step from this straightforward description, we can add that :

■ The 2 cables may not be installed at the same time

■ The cross connect flexibility may be provided using 2 techniques : the patchcord technique as represented in Figure 3-2 and the pigtail technique as represented Figure 3-3
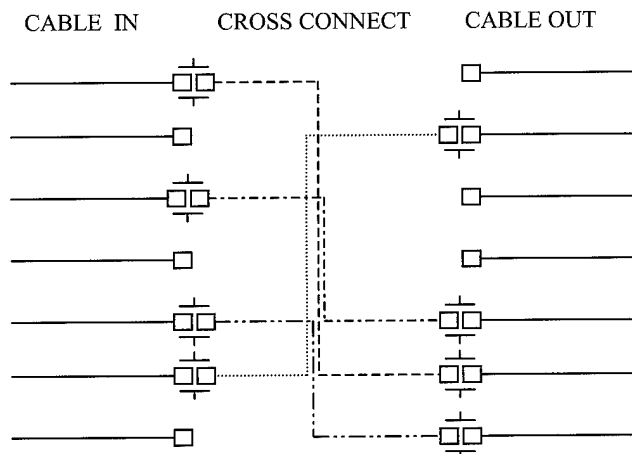
Figure 3-2 : Cross-connect with patchcords

These diagrams illustrate 2 additional issues, namely patchcord routing and patchcord storage management. The routing has to be organized, in particular if the user wants to be able to reintervene in the patchcord flow. On the other hand a storage provision is mandatory for obvious security reasons, and because as is usually the case, the patchcord is manufactured in standard length at the factory.

CABLE IN   CROSS CONNECT   CABLE OUT
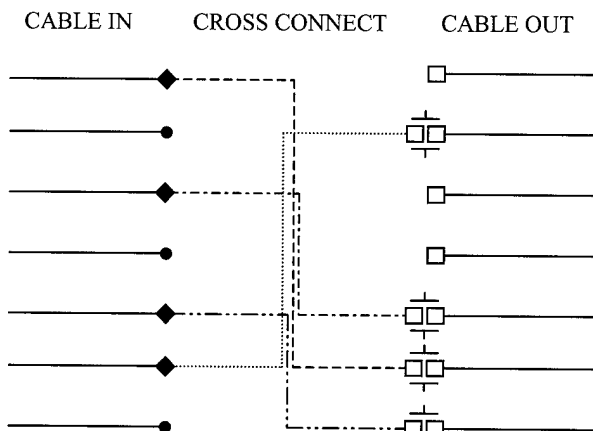
Figure 3-3 : Cross-connect with pigtails

3.2 The application : Splicing

The fiber distribution applied in the present application is based on a 2 fiber ring; hence the interconnection cabinet is the place where incoming and outgoing cables are cross connected by means of 2-fibers elements. The topology here is cross-connect through pigtails as illustrated in Figure 3-3.

The network distribution cable is a 144 optical fiber cable to be managed as 72 duplex fibers.
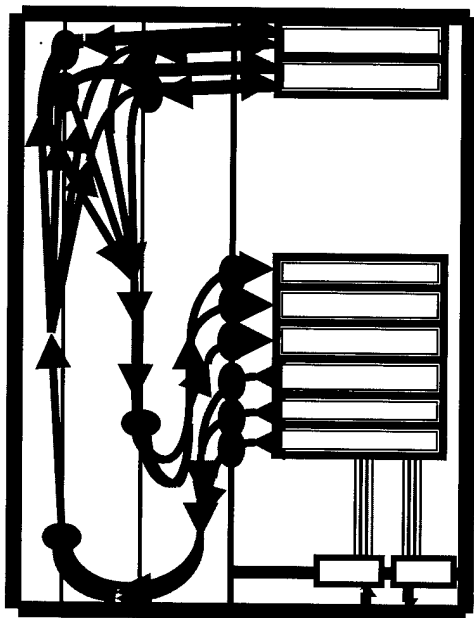
Figure 3-4

As described in Figure 3-4, the 144 optical fiber core of the incoming and outgoing cables are splitted into sub-element of 48 fibers. Each one of these is routed to a splicing modular rack incorporating 2 organizers receiving 2x12 fibers each. The outcome of this splicing rack is 24 duplex pigtails which are elegantly recognizable using different colours for the incoming and outgoing cables.

Splicing module with individual management of the fibres.

Patching module by level.

Splicing module with individual management of the fibres.
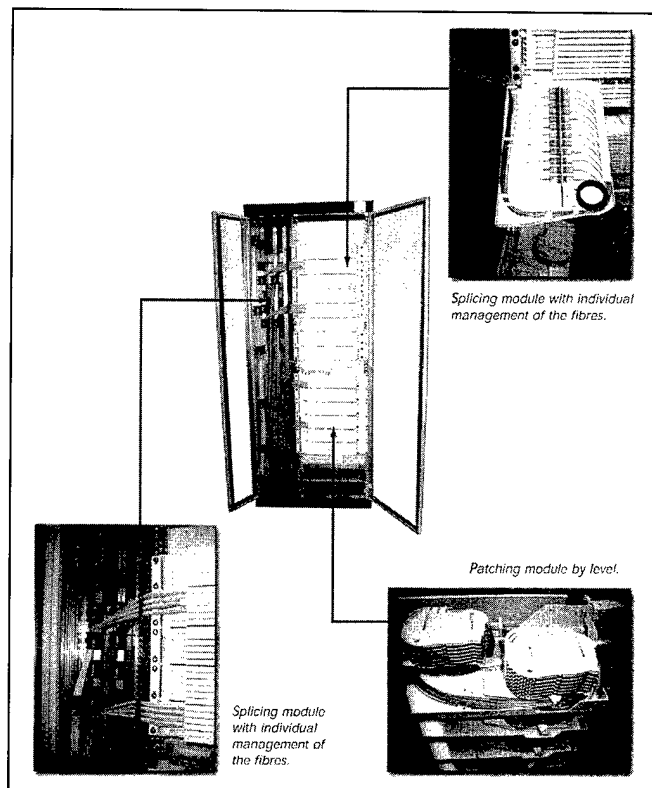
Figure 3-5

An actual view of the realization can be seen on Figure 3-5 where we show a global view of the ODF cabinet, the splicing rack featuring single subscriber access management (the same component as the one appearing in the jointing closure), the pigtail wiring management and the cross-connect rack basic 12-connector tray.

Since our FiberArt organizer did not offer the full individualization of the pigtail management (see Figure 3-6),
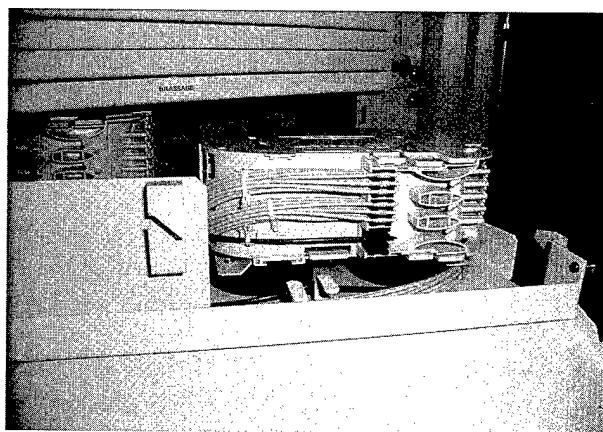
Figure 3-6

Wingas asked for a complementary feature, allowing to intervene on duplex pigtail without any risk of interaction with other pigtails.

This was realized as shown on Figure 3-7.
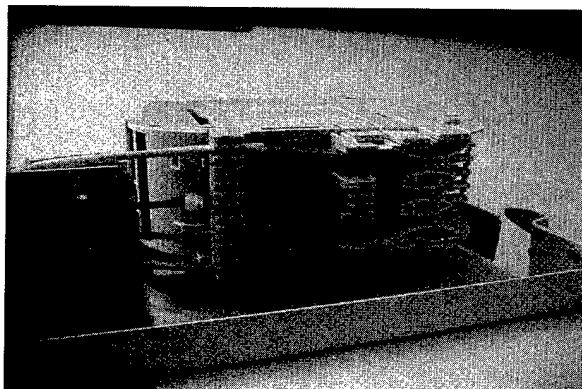
Figure 3-7: Dual pigtail management

3.3 Patchcord routing

The left hand side of the cabinet is devoted to pigtail routing and overlength storage managements. Each pigtail is a 2.4 mm loose tube protected fiber. Openable Diabolo-shaped drums adjustable in position provide attachment and guiding of the pigtails. Overlength is managed at the bottom part of this flow.

As an illustration of the problems one may face in the field, the original wiring method we had conceived i.e the routing of all incoming pigtails in the same drum (see Figure 3-8) had to be modified to the routing through the same drum of incoming and outgoing pigtails linking to one cross-connect sub-module (see Figure 3-9). In the first case we could not insure the principle of length preservation on moving parts.
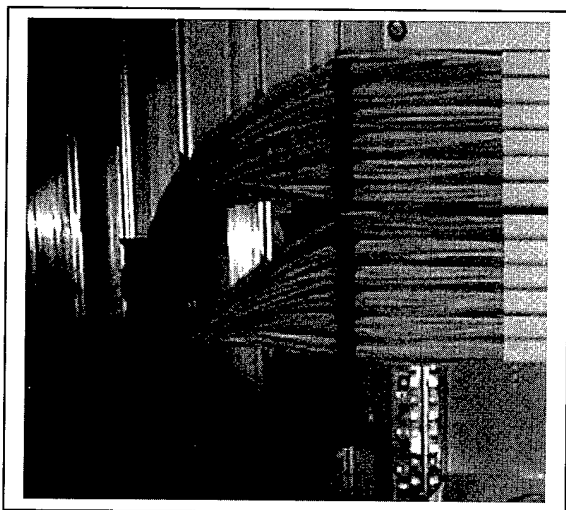
Figure 3-8
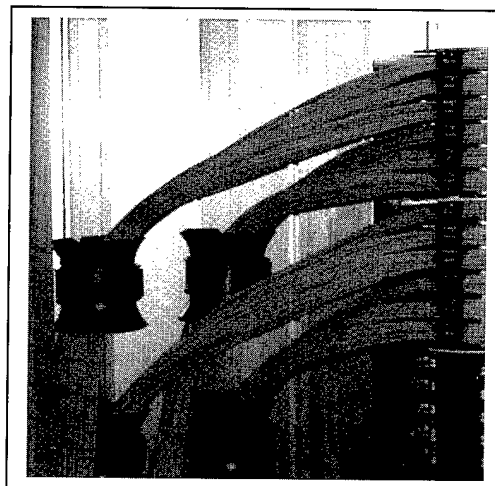
Figure 3-9

As seen in Figure 3-5, the cross-connect (patching) is a straight forward function accomplished in slim 12 SC connectors trays compiled in 72 SC-connector assembled racks.

4. Transmission integrity

Together with single subscriber management, transmission integrity during installation and operation is of course a must in such interconnect equipments.

In order to make sure that pertubations occurring during such phases were limited to an acceptable level, we have set up a specific beta-test. Atttenuation measurements of normalized inputs, 1,550 nm were performed at a sampling frequency of 100 KHz (much higher that the pertubing action around 1 Hz); 4 lines could be tested simultaneously with this high speed detection system.

A cabinet is equipped with a full capacity of 192 interconnected G655 fibers, i.e 192 patchcords equipped with 2 connectors SC/APC (see Figure 4-1).
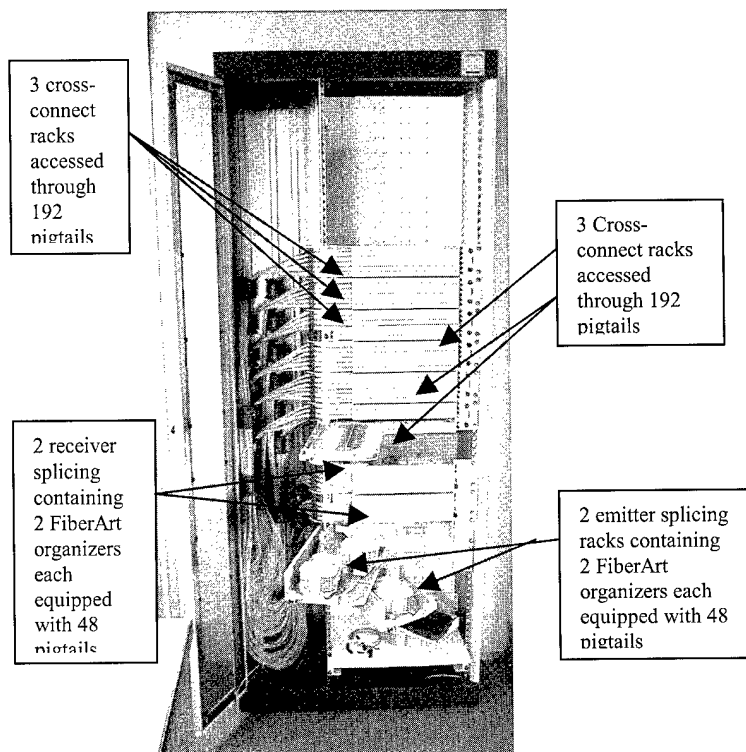
Figure 4-1: Integrity test set up

FOCS/S mechanical splices are used to make all the temporary connections for source power adjustment and output measurements.

The experimental set up is shown in Figure 4-2.
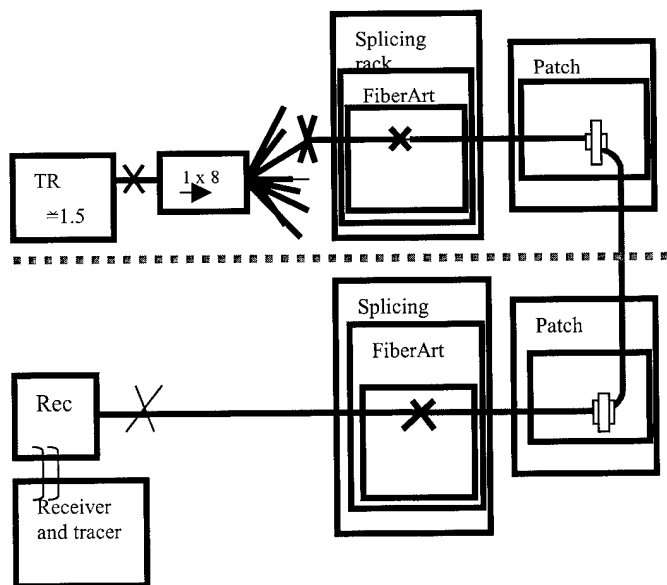
Figure 4-2

Among the incoming pigtails, 8 units are connected to a 1.55 µ EXFO emitter FOT 150 through a 1x8 coupler. These incoming pigtails are distributed in 4 FiberArt organizer modules, this allows to test the interaction within this organizer when opening and closing the splice tray.

Interaction with the Operator appears when one manipulates the trays of the FiberArt emitter (or receiver) organizer modules; when one acts on the splicing or the cross-connect racks and/or when one acts on the patchcord linking emitter and receiver cross-connect racks.

The first thing we want to ascertain is the acceptable pertubation level induced by the manipulation of the organizer splice tray.

When opening and closing several times the elementary organizer tray containing 4 fiber splices, the maximum attenuation variations obtained are shown in Figure 4-3 and listed in Table 1. We can infer from these results that the organizer does not induce any sizable pertubation and is up to the user requirement.

Table 1: Opening and closing the elementary organizer tray

Test line ref

Max atten db	1	2	3	4
Transient atten var	0.02	0.02	0.02	0.02
Static atten var	0	0	0	0
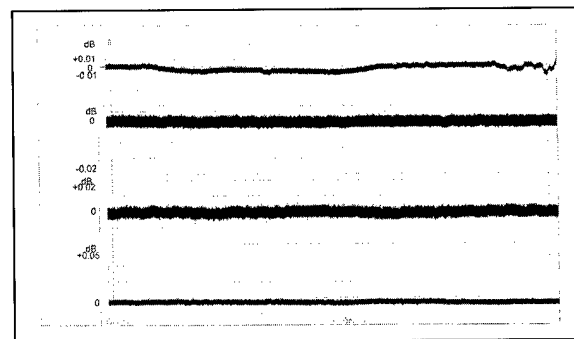
Figure 4-3

When opening and closing the swiveling cross connect and splicing racks the maximum attenuation variations obtained are shown on Figure 4-4 and listed in Table 2.

Table 2: Opening and closing the racks

Test line ref

Max atten db	1	2	3	4
Transient atten var	0.04	0.02	0.005	0.005
Static atten var	0	0	0	0
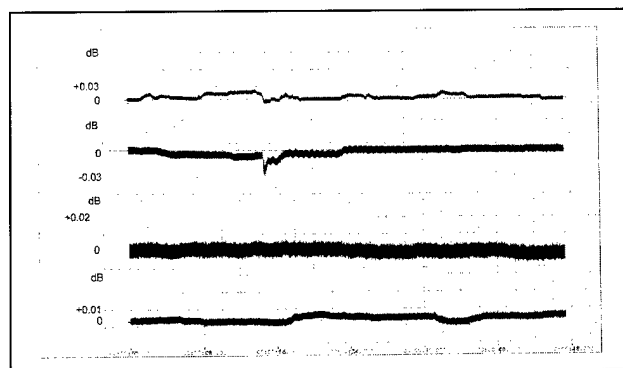
Figure 4-4

The permanent and transient attenuation variations appear very limited.

When we remove and reinstall a patchcord completely in the cross connect rack and the patchcord wire management zone we get the results shown in Figure 4-5 and compiled in Table 3.

Table 3: Complete removal of a patchcord

Test line ref

Max atten db	1	2	3	4
Transient atten var	0.11	0.02	0.02	0.03
Static atten var	0	0.005	0	0.005
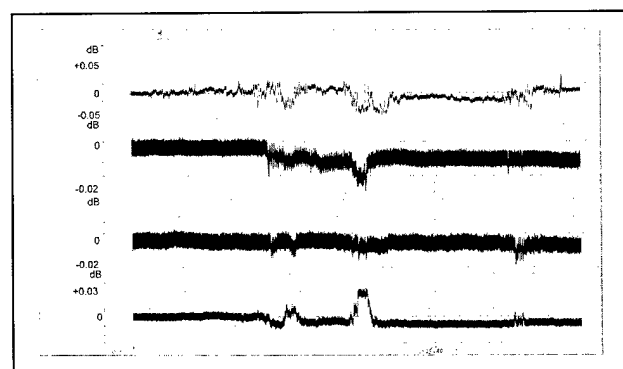
Figure 4-5

We can of course confirm that this operation has the larger pertubation transient effect but does not induce any sizable permanent attenuation variation.

5. Conclusions

The present concrete network deployment of interconnect equipments incorporating new technology has proven that the principles of network transmission integrity preservation during implementation and operation can readily be combined with ease and competitive installation features.

6. Acknowledgements

Philippe Laurency is deeply acknowledged for assistance during field installation trials and transmission integrity testing.

7. Authors
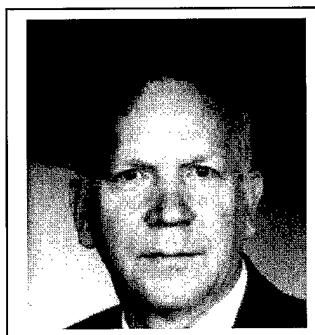
Hans G. Naumann –
Wingas/Winstershall AG

Friedrich Ebert Strasse 160 – 34119 Kassel - Germany

Hans G. Naumann is the head of the Telecom Department of Wingas.
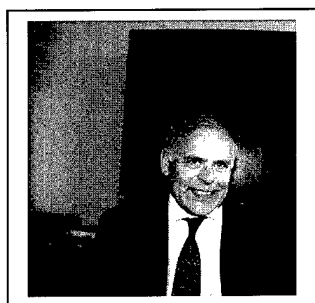
Bertrand P. Joly –
Alcatel cable Interface

35 rue Jean Jaurès – 95872 Bezons Cedex – France

Bertrand P. Joly has been Deputy General Manager of Alcatel Cable Interface since 1991. He was appointed head of the Telecommunications Components Competence Center of Alcatel Cable in 1992.

Véronique Stappers –
Alcatel Cable Interface

35 rue Jean Jaurès – 95872 Bezons Cedex – France

Véronique Stappers has been with Compagnie Deutsch in the Fiber Optic Connector activity and is with Alcatel Cable Interface since 1998 as marketing Manager.

Investigations on Different Approaches for Multimedia Home Wiring Systems

Dr. Christian Pfeiler, Andreas Waßmuth

Draka Multimedia Cable GmbH

90475 Nuremberg, Germany

+49-911-8337-176 · christian.pfeiler@drakamc.com

Abstract

Structured cabling systems (according to e. g. ISO 11801, EIA/TIA 568 A or EN 50173) are since a long time a standard communication infrastructure for office buildings. They have nearly totally replaced application specific solutions due to their flexibility and the fact that an open system supports competition among suppliers of active and passive network components. Development of new systems will be based on the transmission parameters of the different cabling classes. This finally leads to economical benefits for the user.

It is expected that a similar development will take place for cabling of private homes. Several approaches for structured home wiring systems are presently put on the market and considered in several standardisation bodies (e. g. ISO/IEC JTC 1/SC 25/WG 1, /1/). They all are based on a star cabling topology and support usually voice, data and video/television applications.

Main differences are found referring to the construction of the used cables, the design of the central cable distribution units and adapted communication outlets. While the design of the cable distribution units mainly influences the clearness of functional possibilities and installation practice, the cable characteristics are decisive for the performance of the total system.

As too low cable performance is crucial for special applications the following criteria are emphasised and investigated in more detail:

- length limitations due to attenuation and minimum necessary signal levels for video and television applications

- frequency ranges available for specific applications

- crosstalk phenomena and the resulting interference to specific applications

- EMC–requirements e. g. screening efficiency, transfer impedance

The investigation show restrictions for the usage of twisted pair cables and coaxial cables with small conductor diameter for television purpose due to attenuation and — in case of twisted pair cables — frequency limitations. Crosstalk between the different elements and cable-sharing has also to be taken into account. High screening effectiveness of coaxial cables becomes more important. Therefore a figure eight cable consisting of an overall shielded

twisted pair cable and a coaxial element appears to be the most suitable solution.

Keywords

home wiring; home cabling; coaxial cable; data cable; multi–core cable;

1. Approaches to Home Wiring Systems

For the areas of interest — distribution devices, cables and outlets — the following approaches can be found:

1.1 Central distribution units

- modular elements for each coaxial and symmetrical cable

- small units from office cabling area (e. g. 10" patch panels)

- specific developed distribution units for all supported services (figure 1)
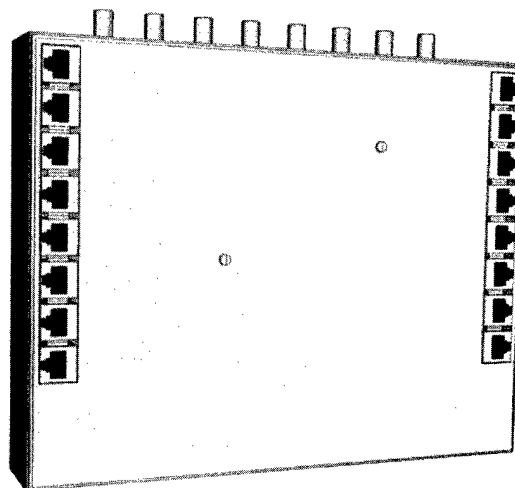

Figure 1: Example of a home wiring distribution unit; services are each led to a specific side

While down–sized modules from office cabling are mainly designated for small office applications, modular approaches offer scaleable solutions but do not give clear arrangement inside the distributing housing. Focussing on the private home special designed home wiring distribution units are preferred to ensure that the owner is able to manage his home wiring by himself.

1.2 Cables

- multi–core (figure 2) or figure eight cables (figure 3) with coaxial and twisted pair elements
- pair shielded twisted pair data cables (S/STP)
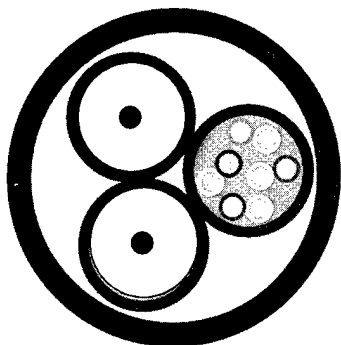
Figure 2: Example of a multi–core home wiring cable; two coaxial and one UTP element
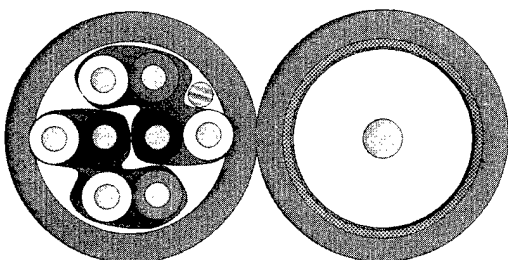
Figure 3: Example of a figure eight home wiring cable; one coaxial and one FTP element

When multi–core cables are used the twisted pair elements carry voice and data applications. The four transmission pairs can be divided into two pairs for data and two pairs for digital or analogue telephone application. The coaxial elements transmit video or television signals.

In case of the application of pair shielded cables video or television signals have to be converted by a balun to be transmitted. Besides the video application the remaining three pairs have to carry the voice and data signals.
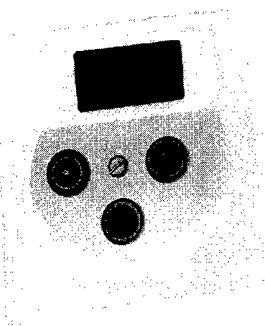
Figure 4: Example of a multimedia socket with outlets for data, telephone, radio, terrestrial and satellite television

1.3 Outlets

In most cases usual sockets for data, telephone and television services can be used. Special outlets which sum up these functions are available (figure 4). In the case that pair shielded data cables are used socket which keep the pair shielding are preferred. Selecting proven connector technologies (e. g. F–, IEC–typ for coaxial and RJ45 for data/telephone plugs) ensures compatibility to all end user devices. Usage of data cables with individually shielded pairs requires specially developed connectors, balun's and patch cords.

2. Cable Performance Requirements

2.1 Attenuation

The channel length is mainly determined by the attenuation of the used cable. For symmetrical cables the use of a standard category cable according to ISO 11801 or EIA/TIA 568 A leads to 90 m installation cable plus 10 m patch cable possible for data and voice application. The ability to transmit TV–signals over the same distance is investigated for three cable typ's.

For a symmetrical cable with individual pair shields with performance beyond Category 7 ("Category 8", 1200 MHz) the attenuation can be calculated by formula 1 /2/. The attenuation of patch cables is assumed to 1.5 times higher.

$$\frac{\alpha}{dB/100m} = 1.645\sqrt{\frac{f}{MHz}} + 0.01\frac{f}{MHz} \qquad (1)$$

Furthermore two common CATV drop cable typ's are chosen with the following dimensions and properties (table 1).

Table 1: Coaxial cables used for calculation

cable type	0.8/3.5 AF	1.0/4.8 AF
Cu wire diameter	0.8 mm	1.0 mm
insulation diameter (foamed PE)	3.5 mm	4.8 mm
outer conductor	Al–foil + tinned Cu–braid	
attenuation	dB/100m	dB/100m
450 MHz	17	14
862 MHz	25	19
2150 MHz	40	31

Coaxial connecting cords are assumed to be of the same type as installation cables. For pairs of balun's and CATV–outlet sockets the calculation is done with 2 dB attenuation. The considered frequencies are maximum for CATV systems (450 and 862 MHz) respectively for satellite aerials (2150 MHz). The results of the calculation are shown in table 2.

The maximum allowable attenuation for a CATV–channel is approximately 45 dB (approximately 105 dBμV output level, minimum 60 dBμV receiver input level) respectively 40 dB (approximately 90 dBμV output level, minimum 50 dBμV receiver input level) for satellite aerial systems. So it can be seen that the channel length has to be reduced for transmission over 0.8/3.5 AF

for 2.15 GHz. Using Category 8 cables leads to length restrictions at 862 MHz /3/. Therefore current draft standards propose 50 m of installation cable /2/. 2.15 GHz is far beyond the capabilities of today's twisted pair cables.

Table 2: Attenuation budget for different coaxial channels

	450 MHz	862 MHz	2.15 GHz
90 m Cat. 8	35.5 dB	51.2 dB	
10 m Patchc.	3.9 dB	5.7 dB	
2xBalun	2 dB	2 dB	
total att.	41.4 dB	58.9 dB	
100 m 0.8/3.5	17 dB	25 dB	40 dB
socket	2 dB	2 dB	2 dB
total att.	19 dB	27 dB	42 dB
100m 1.0/4.8	14 dB	19 dB	31 dB
socket	2 dB	2 dB	2 dB
total att.	16 dB	21 dB	33 dB

2.2 Crosstalk

Signal quality is possibly affected by crosstalk between the several cable elements. While measuring crosstalk between symmetrical and coaxial elements in cables as show in fig. 2 and 3 no significant interference is detected when highly screened coaxial elements (e. g. Class A of table 3) are used (values better than the dynamic of 100 dB). The shielding of the coaxial element is sufficient to achieve such values also for UTP/coaxial cables. Therefore also crosstalk between several coaxial elements will not lead to problems in video and TV transmission.

When the system is designed to use cable sharing for the different applications (e. g. data and telephone) an additional crosstalk margin of 3 dB has to be added /4/.

If all services use one single symmetrical data cable with individually shielded pairs only cables of at least the highest category considered in standardisation should be installed due to crosstalk problems of cable constructions of inferior quality /5/. But also cables of capabilities beyond Category 7 show interference of TV signals due to data transmission /6/. This is the reason that proposals of new standardisation work items demand for even higher NEXT limits referring to "Category 8" /7/.

A further effect that can not be neglected when using unshielded cables is "alien–crosstalk". That means an interference between two or more unshielded cables laid in parallel. Measurements indicate that alien–crosstalk can reach a level comparable to crosstalk inside an unshielded cable in worst case /8/. Figure 5 shows a comparison of alien–crosstalk for two parallel unshielded respectively foil–shielded data cables. Alien–crosstalk adds to crosstalk inside the cable and therefore the crosstalk power–sum may exceed limits.
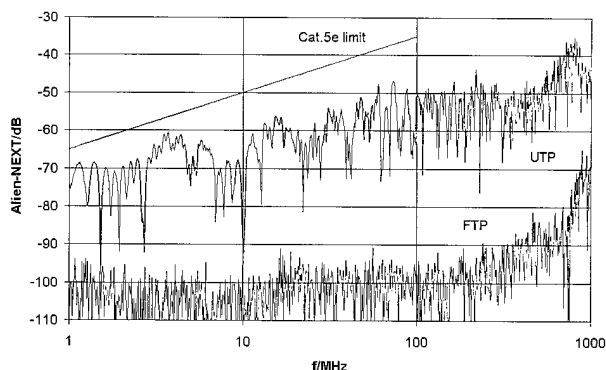
Figure 5: Measurement of alien–crosstalk for two unshielded respectively foil–shielded data cables

2.3 Screening Effectiveness

The proposal for new screening classes of CATV–cables by IEC TC46 (table 3) indicates the need for well shielded cables especially for CATV–networks. As by the distribution of signals in cable–TV networks phase–correllated emission from multiple leakage's is possible this can be a serious source of interference.

Table 3: Limit Values for CATV–Cables (proposal of IEC TC46/WG5)

Transfer Impedance	Class A: 5 mΩ/m @ 5 MHz
	Class B: under consideration
Screening attenuation	Class A: 85 dB; 30 to 1000 MHz
	Class B: 75 dB; 30 to 1000 MHz

For frequencies below 30 MHz transfer impedance instead of screening attenuation is used to characterise screening effectiveness. This frequency range is important for return path signals e. g. of cable modems. The proposal of 5 mΩ/m at 5 MHz for Class A cables and somewhat higher for Class B appears to be plausible by assuming the following model.

For an estimation of the interference field strength at frequencies between 5 and 30 MHz a plane arrangement of one cable with the impedance and propagation constants of the inner and outer system Z_1, Z_2, γ_1 and γ_2 is considered. Both systems are coupled by the transfer impedance Z'_k. At the place x appears in the outer system for an element of the length dx an interference voltage of

$$U_1(x) = U_{10} e^{-\gamma_1 x} Z'_k \, dx \, / \, Z_1 \qquad (2)$$

according to /9/. Where U_{10} is the voltage at the beginning of the inner system (e. g. the output of a cable modem). This voltage causes two partial waves travelling in positive and negative x–direction with halve of the amplitude. The part travelling towards the beginning of the cable is:

$$I_2(x) = -\frac{1}{2} \int_0^l \frac{U_{10} e^{-\gamma_1 x} Z'_k \, dx \cdot e^{-\gamma_2 x}}{Z_1 Z_2} \qquad (3)$$

For an infinite long arrangement and with the simplification $\gamma_1 \approx \gamma_2$ this leads to:

$$I_{20} = -\frac{U_{10}Z'_{k}}{4\gamma_1 Z_1 Z_2} \qquad (4)$$

Furthermore it is supposed that the magnetic field strength can be calculated by $I_{20}/2\pi r$. If an often used value for the impedance of the outer system $Z_2 \approx 150\,\Omega$ is supposed the equivalent electrical field strength is:

$$\frac{E}{dB\mu V/m} = 20\log\left|\frac{U_{10}Z'_{k}Z_0}{8\pi\gamma_1 Z_1 Z_2 r} \cdot \frac{1}{\mu V/m}\right| \qquad (5)$$

Where $E/H = Z_0 = 377\Omega$ and as a further simplification it can be assumed that $|\gamma_1| \approx \omega/v_p$.

According to German authorities in a distance of 3 m the disturbing field strength at the worst case frequency (5 MHz) has to be lower than 34 dBµV/m. Together with some safety margin for degradation of the transfer impedance of connecting cords by mechanical stress and for connectors this leads to a demand in the range of the proposal shown in table 3. When a data cable with individually shielded pairs is used the symmetry of the pair together with the transfer impedance according to ISO 11801 ensures keeping this requirement.

3. Conclusions

Future demand for structured home cabling rises needs for appropriate cables. Currently available constructions are examined under consideration of attenuation, crosstalk and screening performance.

Attenuation budgets for typical TV signal transmission show restrictions for the use of coaxial cables with too small inner conductor and for transmission over symmetrical data cables. Cable length has to be reduced. Crosstalk is a critical parameter for symmetrical data cables in multimedia application. Performance beyond Category 7 is needed. For unshielded data cables crosstalk between adjacent cables ("alien crosstalk") can degrade channel performance. Cable sharing application can request additional crosstalk margin. Latest standardisation activities show that enhanced screening effectiveness of coaxial cables is needed to ensure low interference for new services like the return path of cable modems.

A combination of shielded data cables and well screened coaxial cables appears to be the most suitable solution for home cabling. Together with special home adapted distribution devices structured home wiring systems are able to support all domestic multimedia applications.

4. References

/1/ ISO/IEC JTC1 SC25 WG1 N797: Integrated Cabling for all Services other than Mains Power in Homes, SOHO and Building, revision 12; http://www.metrolink.com/sc25wg1/documents/n797.zip

/2/ CLC SC 46 XC: Multi–Element Metallic Cables used in Multimedia Application as Video Analogue and Digital Communication and Control, Specification for Screened Cables Characterised up to to 1200 MHz; June 1999

/3/ Engles, Y.: Cabling for Multimedia, Does copper solve it all? EuroCable 2000, pp. 117—-120

/4/ ISO/IEC 11801 2nd edition; ISO/IEC JTC 1/SC 25/WG 3 N598, 2000-05-08

/5/ Backmann, M.; Pfeiler, C.; Waßmuth, A.: Crosstalk model for pair–shielded data cables. International Wire and Cable Symposium 1997, pp. 238—243

/6/ Haag, H; Gregor, P.; Voigt, M.: High Grade Data Cables and Connecting Hardware for Generic Cabling; 5. ITG–Fachtagung Kommunikationskabelnetze 1998, pp. 153—-162

/7/ 3P Newsletter No. 1/2000; http://www.3Ptest.dk/newsletters/3Pne1_00.pdf

/8/ Fehr. C.; Pfeiler, C.; Waßmuth, A.: Alien–Crosstalk oder: Der Nachbar spricht mit. LANLine Spezial Verkabelung V/1999, pp. 52—55

/9/ Kaden, H.: Wirbelströme und Schirmung in der Nachrichtentechnik. Springer–Verlag 1958

Authors

Christian Pfeiler (35) received his diploma in electrical engineering in 1990 at the University of Dortmund. In 1995 he obtained a doctor's degree (Dr.–Ing.) at the same university. He joined the product development department of Draka Multimedia Cable GmbH in 1995.

Andreas Waßmuth (38) joined the company after his studies in electrical engineering at Ruhr Universität Bochum in 1986. After positions in development and support for local area networks he took over responsibility for R&D–activities and engineering of copper telecommunication cables

Mailing address
Draka Multimedia Cable GmbH
Wohlauer Str. 15
D-90475 Nuremberg
Phone: +49 911 8337 176
Fax: +49 911 8337 206
Email: christian.pfeiler@drakamc.de

Generic Home Cabling Concepts
Universal Integration of Cable, Connecting Hardware & Active Components

Bernd Babelotzky and Stefan Mohr

Corning Cable Systems
Munich, Germany
+49-89-5111-3167 · Bernd.Babelotzky@corning.com

Abstract

The paper describes in a technical and economic point of view the advantages of different structures and types of generic home cabling systems to provide the universal infrastructure for all kind of communications in telephony, television and data. The main discussion topic are systems for the European market, but all systems could easily be adapted to the US or world market.

Keywords

home cabling; television; SOHO; twisted pair; coax; balanced cable; BALUN; multimedia

1. Introduction

In business and industry environment the past has shown that the earlier unstructured 'cabling as needed' could lead to a strong increase of costs and investing in blind alleys. Triggered by the rapid development of the world wide web, the experience gained by business is now to be applied in private homes dwellings and flats. So the most important cornerstones are well thought-out overall concepts, good planning and high-performance products.

For the benefits of flexible connection of all multimedia equipment into any room, anywhere in our private houses, a "Generic Home Cabling System" should be part of the house planned in the same way as the power cabling already is. Modern life means continuous changes. The point is to have a "Home Cabling System" (HCS) which can be freely adapted to our requirements and makes us being able to rearrange the rooms of our house as often as we want, without reinstallation – no drilling, no milling, no cable threading.

Up to now coaxial cable has been used almost exclusively for television transmission systems over short distances. As a result, the sending and receiving equipment as well as the test equipment used in TV technology is designed for coaxial connection. In order to take the next step toward a multimedia cabling system after the integration of data and voice signals, today the transmission of television signals should be possible over the same universal cabling system as data and voice.

Three concepts for generic home cabling systems integrating the requirements for TV transmission, telephony and data will be discussed in this paper:

- one based on balanced cables shielded in pairs with application-specific connecting cords, pure star structure;

- one based on hybrid coax/data cables with interchangeable modules, hybrid star/bus structure;

- one based on coax, data and fiber optic cables, pure star structure.

2. Basics

People want to share information in form of data, voice and picture files, they want to share devices like printer, video recorder or satellite receiver and they want to share simultaneously the access to external networks like telephone or internet. For this we need the integration of voice, video and data applications and even home automation on one powerful HCS.

People who are willing to invest for good communications want a cabling system with all modern conveniences. That means a cabling system that is easy structured, easy to install and easy to use. Also this cabling system has to be future proofed, since the lifetime of home cabling systems must be much longer than in business or industry.

Analog to generic cabling systems in business or industry a cabling system in private homes will consist of patch panels, cables and wall outlets and the architecture will be close to a star structure. However in private homes rooms are more often rearranged and they change their intended purpose during the years, e.g. from study to sleeping room. Therefor the HCS has to be very flexible and should provide in most rooms higher performance than actually needed. Different to business or industry cabling are also the installation conditions. In private homes there is less room for cable routing and outlets must be small and inconspicuous since beauty is much more important.

But the highest challenge for the development of a good HCS is the variety of applications demanded in private life. This means many different applications need to be supported, applications not only for information, communication and home automation but also for bandwidth intensive entertainment and multimedia.

2.1 Planning

Whereas in the past planning of the cabling as a function of the type of rooms' use was perfectly sensible, in view of the separate cabling for telephone and TV, today planning a cabling independently of the future use of the individual rooms should preferably be considered for a application-independent home cabling system.

Broadly speaking the situation with regard to the installation of information and communication technology was hitherto as follows:

1. For the implementation of the building TV, telephone and data networks separate planning was necessary in each case and in the past this was as a rule carried out and implemented by different companies.

2. There is no information on the quality of the application-specific cabling, alone the functionality of the currently desired applications was crucial for the acceptance.

In contrast, the basis for the planning of an application-independent cabling system is knowledge of the high frequency characteristic of the cabling, or rather of each individual link. If the high frequency characteristic is known, the level values for the active distribution systems (TV, telephone, data, etc.) can be suitably determined. If the building administrator or owner is in possession of the acceptance report for the building internal, application-independent cabling, the administrator or an installer can plan any new application and its distribution in the building on the basis of the electrical parameters given there.

The acceptance of the application-independent cabling and the cutover of the active units and distribution systems for TV, telephone, data, etc. can be performed separately.

2.2 Structure

Well-structured generic cabling is the basis for a future-oriented, application-independent and economical network. This is the experience gained by business and industry which should now to be applied in our private homes and dwellings. Therefor the design of HCS and above all the cabling structure will be very much the same as in the European standard EN 50173: "Application-independent cabling systems" and the almost identical international standard ISO/IEC 11801: "Information technology - Generic cabling for customer premises".

Modern information and communication cabling has a star-shaped structure. These point-to-point connections allow individual switching, and flexible logical topologies can be set up. On such a star-shaped cabling system it is possible to operate both networks with a tree topology (ISDN), bus topology (Ethernet) as well as with ring topology (Token Ring) without restriction. The simple overview makes rapid trouble-shooting and flexible servicing possible.

Whereas in the past coaxial cabling systems for TV distribution have been set up in tree topology, today star structure is the state of the art. Only star structure provides the possibility to independently distribute all programs, received by one or more satellite antennas, to every individual TV set and monitor.

A problem in the case of star structure is the fact that with many ports many cables also have to be laid in parallel. This can lead to difficulties in the case of cable laying in confined physical conditions. A space problem can also arise in the central node of the star-shaped cabling in the case of a large number of incoming cables. However, in general the wish is to have as many ports as possible available within a room, in order to be flexible in the event of subsequent rearrangement or of a change in the use of the room. Anyone who does not allow enough space for the cabling and therefore tends to be sparing with the quantity of cable laid may later have to make recourse to more expensive and less satisfactory solutions.

2.3 Central Cabling Node

In HCS the node of the star-shaped cabling should be located in a central distribution location. In the case of a purely star structure, there is access from here to each individual socket. Equipments which are located in different rooms can be linked together in the central node by simply bridging with connecting cables. The

electronic switching of connections is of course additionally feasible.

The central distribution box is the place for the provision of all desired control, information and communication services. Here there is space for the accommodation of systems for telephony, data and TV. Examples of this are the telephone system, the distribution system for satellite television, ISDN router for a shared Internet access line, heating and light control, etc.

3. Home Cabling Concepts

In the following three concepts for generic home cabling systems integrating the requirements for TV transmission, telephony and data will be briefly presented.

3.1 Balanced Cabling Concept

Basis of the balanced cabling concept is a high performance 4-pair PiMF cable (PiMF – Pairs in Metal Foil), in which every wire pair has a separate foil shield. These type of cable fulfil the most severe requirements of the international cabling standards for customer premises (ISO/IEC 11801).

The structure of the cabling system is purely star-shaped. Starting from a central node, all network ports are interconnected with each other on a star-shaped basis. As a result the system offers maximum flexibility for the connection of the most diverse terminals to the most varied points, whether between ports of different rooms or between ports within the same room.

This cabling system is a well thought out overall concept, consisting of a double-shielded, balanced copper cable and a modern terminating technology with a connector face plan divisible in pairs. Application-specific connecting cords make possible the connection of any type of data, telephone or video application, including future ones. A TV adapter cord provides the ideal solution of integrating all types of video applications into the same cabling as for data and voice applications. It performs the transformation of the unbalanced television signals of the 75Ω coaxial cable into the balanced signals of the 100Ω twisted pair (TP) cabling. Therefor a matching transformer (BALUN – Balanced-unbalanced) is integrated into the TV connector housing. Very low cable resources are occupied since the multimedia connector on the other side of the cord permits the tapping of one single wire pair.
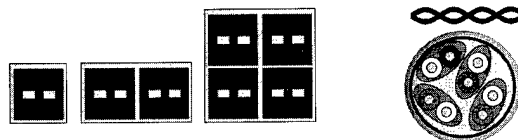
Fig.1: Multimedia Connector with optional tapping of 1, 2 or 4 pairs

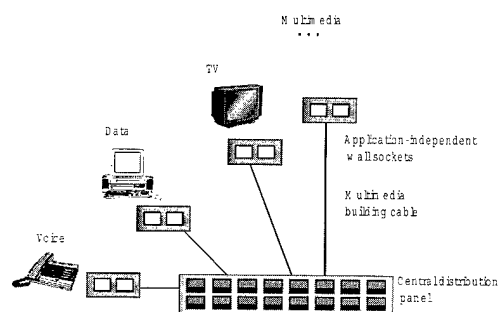Fig.2: Multimedia Cable – Pairs in Metal Foil

Fig. 3: Balanced Cabling Concept

The overall shield of the cabling system provides high protection against the effect of electromagnetic interference fields and overvoltages at ports of active components. With this a save operation is ensured.

Such an overall concept with components carefully matched to each other offers:

- High transmission reliability,

- Compliance with most severe EMC regulations of European TV standards,

- Flexibility through the tapping of optionally 1, 2 or 4 pairs,

- Universality and future-orientation through application-specific connecting cords and system reserves.

3.2 Hybrid Cabling Concept

This concept is based on a hybrid coax/data cable and a hybrid star/bus structure. It combines the advantages of star structure and bus structure.

In bus structure the wall outlets are lined up along one cable. This leads to considerable saving of cable and space, especially in the central distribution box, since there must not be installed a separate access jack for every wall outlet.

The hybrid concept is a combination of star and bus structure. Not every single wall outlet but the wall outlets of one room together are separately connected over one cable with the central node. With help of a feed-through technique the applications can be fed through from socket to socket within one room.

In this concept a 75Ω coaxial cable and a category 5 S/UTP cable (100Ω) are fixed together in a separable cable compound. The coaxial cable is preferably meant to be used for broadband applications as CATV or satellite TV and the S/UTP cable is meant for all the other applications as data and telephone. Both cable types have a separate universal access. This means the outlet socket is build up two times modular. It consists of a basic component with two application independent interfaces, one adapter inserts for two coax connectors and one adapter inserts for two TP connectors.

Such a modular concept with adapter inserts for all kind of applications offers:

- Cable and space efficiency through the feed-through technique,

- Compliance with EMC regulations,

- Openness for low cost TV distribution systems,

- Future-orientation through the application independent interfaces.
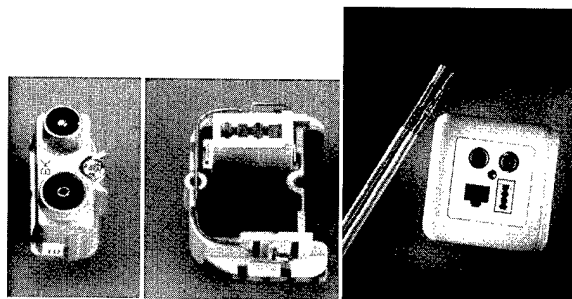
Fig. 4: Adapter Insert for two Coax Connectors

Fig. 5: Adapter Insert for two UTP Connectors

Fig. 6: Hybrid Cable and Modular Socket

3.3 All Media Cabling Concept

Nobody really knows how the future will look. So one who believes that pure fiber optic cable systems will be the near future should install coax, S/STP and fiber optic cables in pure star structure and in additional some vacant pipes. This may be very cost intensive but it provides the highest flexibility.

Fiber optics is always seen as the generic transmission medium of the near future because of large bandwidth, low length restriction and no EMC problems. But near future doesn't seem to come closer since all equipment still work electronically and optoelectronic converter are still to expensive especially for telephone. At the same time copper cables and connectors, modulation techniques and source coding are getting more and more powerful. So "fiber to the desk" may be a solution for business and industry if one will exclusively employ high data rate transmission systems up to the desktop of the user and using voice-over-IP for phoning and video-conferencing, but for HCS fiber optics as a cost-effective solution seems to be far away.

So one may use S/STP for data and voice, coax for video and fiber optics for future applications or to span large distances.

Such an all cable concept with standard termination techniques offers:

- Compliance with EMC regulations,

- Openness for low cost TV distribution systems,

- Future-orientation through the use of all cable types.

4. TV Distribution Concepts

Since the highest challenge for the development of a good HCS is the integration of TV, TV distribution concepts will be discussed before we will compare the different HCS concepts.

There are many possibilities for TV distribution over an application-independent cabling system. Two will be presented in this paper. The TV signals originating from broadband cable, satellite or from terrestrial reception are fed over low-loss coaxial cable to the central distribution point. After possible processing, splitting up and amplification, they are here fed to the input receptacle which is connected to the desired output socket via the multimedia cabling.

Starting from the output level of the head end unit or the antenna system, the level appearing at the output socket can be calculated as a function of the attenuation characteristic of the intervening cable link. From this the extent to which additional amplifiers must be used can be seen.

In the following we will concentrate on Sat TV distribution since there the largest bandwidth is in use. In order to obtain more transmission capacity, the satellite programs are radiated in two planes of polarization (vertical and horizontal). Thus without additional conversion only the programs of one or the other of the planes of polarization can be parallel transmitted over a single broadband cable.

4.1 Remote-controlled Sat Receiver

This concept places the Sat receivers in the central distribution box. This means there are several remote-controlled Sat receiver modules, each module alone supplying a single customer with a standard amplitude modulated TV signal. Each customer is assigned a different TV channel (frequency range) for the transmission of the TV signal from the receiver module to the TV set. With a remote-control unit the customers can control their respective receiver modules and select their desired programs from the complete spectrum of received satellite programs. The remote-control unit uses an extra wire pair for transmission of the control signals. The remote control of the head end is thus independent of the type of TV distribution network (bus, tree or star topology).

4.2 Remote-controlled Transponder Conversion

The bandwidth over which the individual program packages can be transmitted via satellite is limited by the satellite transponders to approximately 40 MHz. Thus 1 analog and up to 8 digital television programs can be transmitted via a transponder. If, in accordance with program selection, only one 40 MHz frequency band of a transponder is always converted from the 1st Sat IF range to the standard TV frequency range, the demands made on the distribution network are considerably simplified. With the aid of such a transponder converter any desired television program can be transmitted over the star-shaped building cabling with the lowest possible attenuation. At the other end in turn the conversion back into the IF range suitable for the Sat receiver takes place.

The transponder conversion is independent of whether the signals are in digital or in analog form and whether it is a case of radio or television signals, or arbitrary digital data signals.

It is controllable via the normal remote-control unit of the Sat receiver. This allows to switch through any program to the television set that is received by the satellite dish.
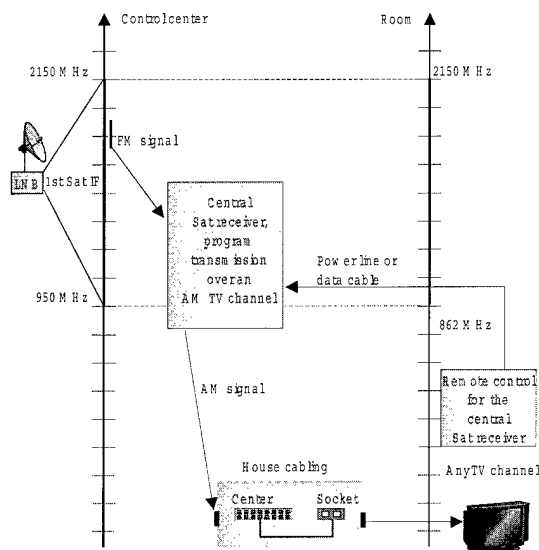
Fig. 7: Remote-controlled Sat receiver
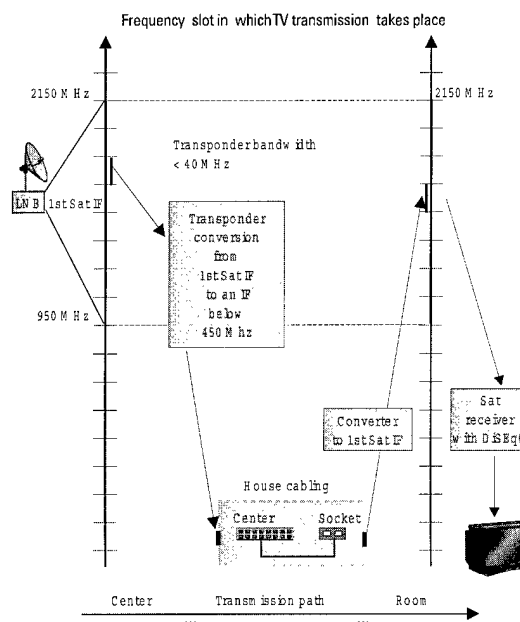
Fig. 8: Transponder conversion

Tab.1.Comparison Home Cabling Concepts

	HCC	BCC
TV channels up to 450 MHz		
CATV German Telekom	√	√
transmission of a complete transponder packet remote controlled by the Sat receiver	√	√
Internet TV, MPEG-2	√	√
TV channels up to 860 MHz		
Terrestrial TV and private CATV	√	—
SAT-IF distribution 950 – 2150 MHz		
transmission of 1 polarization plane of 1 Sat position	√	—
Telephone, Data, Multimedia		
ISDN, ADSL, POTS	√	√
10BASE-T, 100BASE-T	√	√
Gigabit Ethernet	—	√

BCC – balanced cabling concept

HCC – hybrid cabling concept as well as all media cabling concept

5. Comparison

In table 1 the balanced cable concept and the hybrid cable concept are compared in their capability relating to the most important applications. One can see that with high performance balanced cable systems not all standard amplitude modulated TV channels can be transmitted at the same time over one cable. The reasons for this are that attenuation increases steeply with higher frequencies and that even specially developed BALUNs do not work in a very high quality over the whole frequency range up to 860MHz. But nevertheless all actual Telekom CATV channels can be fed through and for transmission of more TV channels new distribution techniques as the "customer-controlled transponder conversion" can be used.

As far as Sat TV is concerned even with a good coaxial cable there are strong difficulties to transmit all programs at once that can be received by one satellite position. But this is necessary to be able to use a TV set and a video recorder independently at one link. If we look further in the future we should rise the question whether in 5 or 10 years video on demand, pay per few, internet TV and a private video hub will not play a much bigger role than channel hopping between hundreds of TV programs. And to

transmit 1,2 or 3 TV channels at once, the 2 GigaHz frequency bandwidth of a coaxial cable is not necessary. However, the actual TV distribution hardware is developed for coaxial cables and therefor it is still cheaper to use coaxial cable for TV transmission. Also the link length for balanced cable systems is limited to about 50 meters in case of CATV transmission up to 450MHz but even with a good common coax cable the SAT-IF transmission will end at 65 m due to the high frequency of 2 GHz.

As we said earlier simplicity is important for the acceptance. The feed-through technique which comes together with the hybrid cable concept presented in this paper is more complicate to handle than a pure star structured system. For this system detailed documentation is important to assure easy future servicing, whereas for a point to point connection a special documentation is not necessary since assignment is evident.

As far as only the passive cabling system is concerned a balanced cabling system is the most cost-effective one since product and installation costs are the lowest. But taking also active components into account the hybrid coax/data cable system brings savings by using cheaper TV distribution hardware.

6. Market Situation

The question is how HCS will become a part of the houses planning in the same way as the power cabling already is? Selling HCS without applications will convince not any customer. It is absolutely necessary to provide turn key solutions including active components. This solutions must be easy to handle and to install since nobody else than conventional electrician have to do the work at the end. Relating to benefits and costs HCS must win the comparison with wireless solutions. This does not mean that both could not go together, but it must be shown that pure wireless solutions are less powerful, more cost intensive and more susceptible to interferences. Wireless applications as Bluetooth, DECT, DAB, infrared, etc. must be seen as good completion to HCS. As far as the important internet access is concerned xDSL is a very cost effective way of upgrading the copper infrastructure and competing against fiber and wireless competitors.

7. Conclusions

Today the transmission of television signals over the same universal cabling system as data and voice is already reality. Cabling systems, composed of a high-performance terminating technology and balanced cables shielded in pairs are fully capable for the transmission of television signals and thus multimedia-capable. The conversion of the unbalanced television signals to the balanced signals of the TP cabling is performed by a BALUN integrated in special connecting cords. As things are getting more and more complicated: the simpler the cable system is to handle, the faster it will be accepted. Star-shaped TP cabling systems are most flexible and simple. But as TV equipment is designed for coaxial connection hybrid coax/TP cabling systems are still the most cost-effective ones.

With the integrate of different cable systems for different applications in one generic cabling we have to bring the knowledge and the language of different professions together under one roof. Therefor the role of the facility manager as the integrator of varied disciplines and planning processes will be more and more important.

8. Abbreviations

BALUN – <u>Ba</u>lanced-<u>un</u>balanced

CATV – Cable Television

EMC – Electromagnetic Compatibility

HCS – Home Cabling System

PiMF – Pairs in Metal Foil

POTS – Plain Old Telephone Service

S/STP – Screened Shielded Twisted Pair

9. References

[1] EN 50173: Information Technology - Generic Cabling Systems, 1995.

[2] Draft EN 50173 (2000), CLC TC 215, Dec. 1998.

[3] ISO/IEC IS 11801: Generic Cabling for Customer Premises, 1995.

[4] ISO/IEC 11801, Updated Draft Specifications for Class E and Class F, Cancun/WG3, Jan. 1999.

[5] EN 50083-2:1995/A1:1997 Part2: Electromagnetic Compatibility of Devices

[6] ISO/IEC JTC 1/SC 25 N564 Updated Draft: Integrated cabling for all Services other than Mains Power in Homes, SOHO (Small Office, Home Office), and Buildings, Cancun/WG3, Jan. 1999.

[7] 622 Mbps ATM transmission in balanced cabling networks, *S. Mohr et al.,* Proceedings of NOC'96, Heidelberg.

[8] 1 Gbps Data Transmission via Balanced Cabling: Measurement Results and Trends, *D. Schicketanz, A. Oehler,* Proceedings of NOC'98, Manchester.

[9] ITG Conference on Information Technology: "Multimedia Cabling for SOHO and Homes", *D. Schicketanz, B.Babelotzky,* Köln Dez.1998.

Authors

Bernd Babelotzky received his Diploma in Electrical Engineering in 1995 at the University of Kaiserslautern working on data and noise characterization of a 16QAM digital transmission link in the laboratories of "Institut Supérieur d'Electronique de Paris". In the same year he joined SIEMENS AG in the research and development department for the communication cables business unit. There he worked on system development for generic cabling. January 2000 he changed to Corning Cable Systems where he is working on system development for home cabling systems.

Bernd.Babelotzky@corning.com

Stefan Mohr received his Diploma in Electrical Engineering in 1989 at the University of Kaiserslautern working on coding schemes for noisy transmissions. In 1993 he obtained a Doctor's degree at the same university. He work on the characterization of optical fibers. He joined SIEMENS AG in the research and development department for the communication cables business unit in 1993. There he was responsible for generic cabling and hardware design. January 2000 he changed to Corning Cable Systems where he is working as Product Line Manager for customer premises cabling.

Stefan.Mohr@corning.com

Power Line Telecommunications for Residential Home Network

Authors: O. Bouffant, D. Le Bras, H. Le Cozic, P. Gay, M. Le Dizès, P. Legaud, J-M. Auzizeau, G. Térol

France Télécom R&D / DTD
22300 Lannion, France
+33296052803 - olivier.bouffant@francetelecom.fr

Abstract

This paper deals with preliminary France Télécom R&D studies in the field of "in-door" low voltage networks, called "PowerLine Technology" (PLT).

Its relates the tests defined and realized by FTR&D for the evaluation of PLT. The goal of our research is to re-use the existing low voltage network inside residential houses for broadband services.

Preliminary studies on both infrastructure and PLT systems show that it is possible to provide a good connection to Internet services (web) and to transfer data between two home PC's.

Initially, a reference infrastructure is defined in order to recreate the characterization of the low voltage network in terms of attenuation and characteristic impedance.

Subsequently, tests performed on equipment such as indoor modems are carried out for transmission (tests on IP services) and Electro-Magnetic Compatibility (EMC) which are an important aspect of these studies.

Finally, a point is made on the domain of the standardization of the PLT.

Keywords

Powerline; Low voltage network; Home network; Characterization; EMC; IP transmission; Standardization

1. Introduction

More and more households are equipped with electronic devices such as TV sets, VCRs, PCs, phones, video cameras, etc.

The aim of telecommunications operators is to distribute all kind of services (home automation, phone, multimedia, video, etc.) behind different types of broadband access networks like ISDN, xDSL, FTTx, cable, satellite, etc.

These services have to be available in each room creating a small local area network (mini-LAN) in the house.

Different media can be used: wired media (copper pairs, optical fibers, etc.) and wireless (radio, infra-red, etc.). For wired solutions, a major question is the use of new cabling, with problems of installation, cost, etc.

The use of the existing low voltage network (or Powerline) offers one main advantage: it is provided in every room!

2. Characterization of "INDOOR" low voltage network (or Powerline)

2.1 Introduction

To carry out the characterization of powerlines, medium used in PLT, a reference infrastructure is defined with the following parameters: topology, cable length, outlets, etc.

So characterization is achieved in two ways: with and without voltage on the lines.

The most significant parameters for good quality transmission are attenuation and characteristic impedance.

This chapter describes in detail the measurements of characteristic impedance and attenuation in the following two ways

2.2 Evaluation of Powerline infrastructure

2.2.1 Definition of the infrastructure under test

The infrastructure is made up of a low voltage network called "house no.1" with two rooms 70 metres apart.

The network installed in "house No.1, room No.1" is shown in figure 1.

The caption on the outlets means: (line number, outlet number on the line) and length of the line from the repartition tab and the outlet in metres.

This network is typical of residential customers with one single-phase electrical meter, one 500mA differential circuit breaker, a repartition tab equipped with fuse for each line in the room (see figure 2).
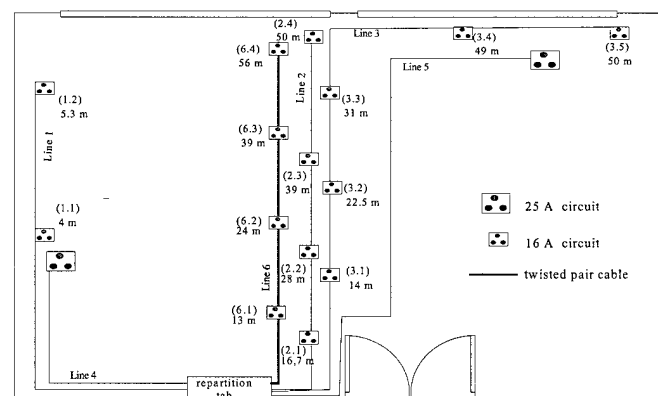
Figure 1: "house no.1, room no.1" low voltage network diagram

These lines are made with traditional cable ("H07 type") as used in residential houses.

In our network, one line is made with both traditional cable (line 2) and a new twisted pair cable with 70mm lay (line 6) in order to compare the characteristic performances of PLT.
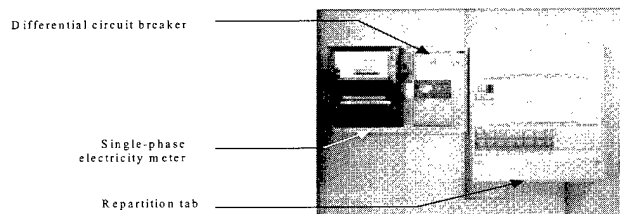
Figure 2: installation of the indoor powerline infrastructure

2.2.2 Measurement devices

The measurement method used for powerline is the same as for the characterization of telecommunications cables. All the powerline measurements are carried out with a network analyzer.

The test set up is composed of a network analyzer connected to the network via an adaptation box and two baluns for the measurements under voltage.

The attenuation measurement is shown in figure 3 and the characteristic impedance one in figure 4.

The network analyzer does not allow high voltage (few volts only), so adaptation boxes have to be used between powerline and the device used to carry out the measurement under voltage.
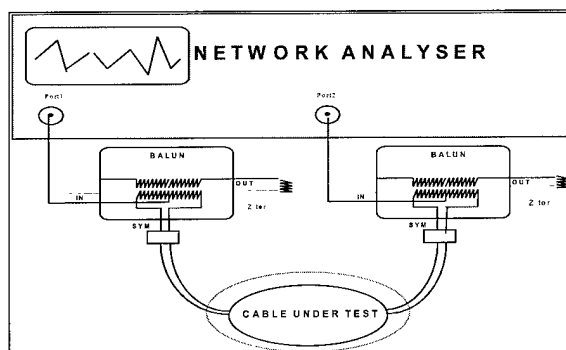
Figure 3: attenuation measurement
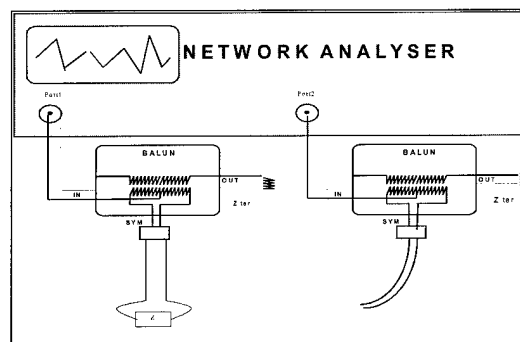
Figure 4: characteristic impedance measurement

2.2.3 Attenuation measurement without voltage

Figures 5 and 6 show the attenuation curves of the powerlines in a frequency band up to 100MHz for 50 metres lines with 4 outlets. Since the line is disconnected from the repartition tab, this one is not taken into account in the measurement.
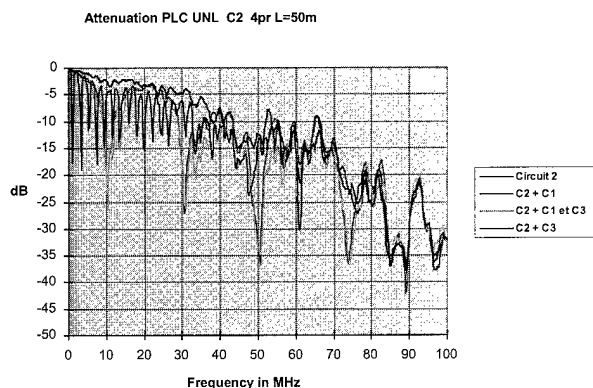
Figure 5: attenuation measurement of traditional cable
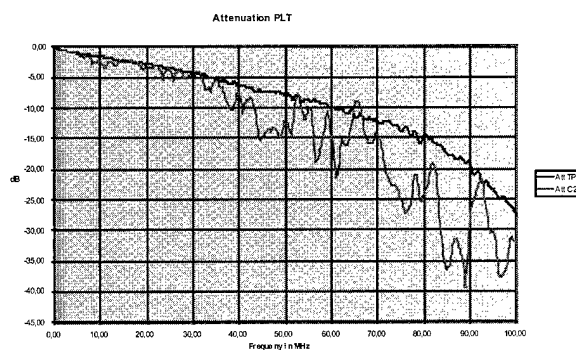
Figure 6: comparison of attenuation for traditional cable and twisted pair cable

The average attenuation is approximately the same for the two types of cable, with better regularity for the twisted pair cable.

2.2.4 Characteristic impedance without voltage

Figure 7 shows the characteristic impedance curve of the powerlines (classical cable and TP cable) in a frequency band up to 100MHz for the same line (50 metres, 4 outlets).

Since the line is disconnected from the repartition tab, it is not taken into account in the measurement.

CHARACTERISTIC IMPEDANCE PLC
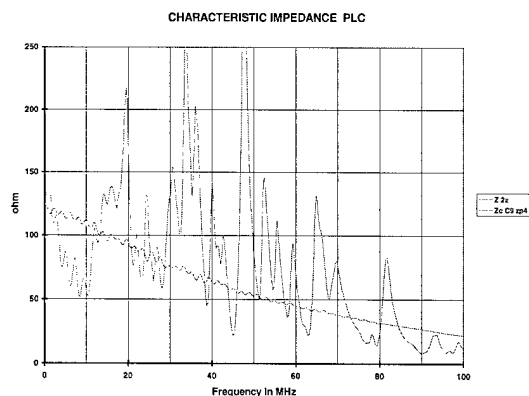
Figure 7: comparison of characteristic impedance for traditional cable and twisted pair cable

For traditional cable, the impedance fluctuations are high and depend on several parameters (cable length, number of outlets, number of connected devices, etc.).

For the twisted pair cable, the curve is more stable and the average value fluctuates slightly around 50 and 100 Ohm.

2.2.5 S-Parameters (cables under voltage)

The measurements taken are the impulse responses of the transmission channel and the S21 parameter.

The equation of the S21 parameter is as follows:

$$S_{21} = \frac{1}{\cosh(\gamma L) + \frac{1}{2}\left(\frac{Zc}{Zref} + \frac{Zref}{Zc}\right)\sinh(\gamma L)}$$

The attenuation (or insertion loss) is calculated with the S21 parameter as following:

$$\text{Insertion Loss[dB]} = -20\log(|S_{21}|)$$

As previously stated, these measurements are made with adaptation boxes to de-couple the 50Hz so as not to destroy the measuring equipment and to be able to inject and recover the signal on the powerline. These coupling/de-coupling elements are constructed on the basis of figure 8.
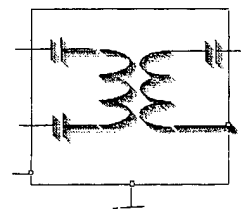
Figure 8: RF/electrical line coupler

The coupler characteristics are: 5dB transmission loss and - 10dB return loss in a frequency band from 1 to 30MHz, sufficient performances to simulate the future device implemented in the final modems.

A serious limitation for the time domain measurement concerns the choice of the pulse width and shape. The chosen parameters are as follows:

Frequency band	1 to 100MHz
Time domain	0 to 500ns

The main parameters analyzed are:
- several line lengths, up to 100 metres, which are representative of most of the lines in a house,
- with and without interference (TV-set, hair-drier, heater, etc.)

Figures 9 and 10 show the measurement results for the same line as previously used (50 metres, 4 outlets).
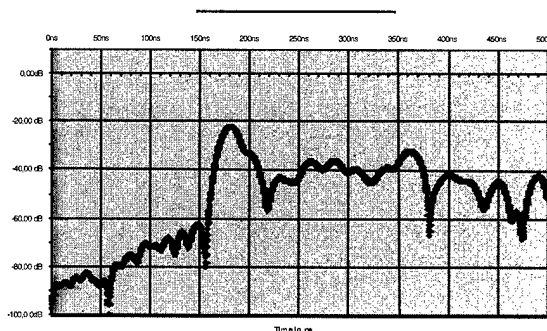
Figure 9: impulse response
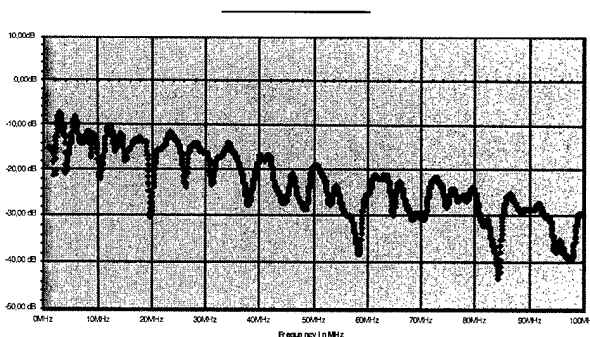
Figure 10: (s$_{21}$) parameter module

2.3 Conclusion

The first results in low voltage network characterization show a small difference in parameters between the measurements with and without voltage. This needs to be confirmed with further measurements.

The characterization under voltage is interesting because it is representative of a real environment. The next step is to carry out these same measurements in customers' houses during future field trials.

The characteristics of the twisted pair cable are better than the traditional cable and the use of such a cable would allow powerline transmissions to be optimized.

3. Equipment tests

3.1 Introduction

PLT systems, as other communications broadband systems such as ADSL, have the same constraints: reliable transmitted data with advanced modulation technologies (OFDM or GMSK) and error controls with the feature of not producing emission and conduction noises that pollute the electromagnetic environment.

Following the example of xDSL technologies, the main application for the PLT is to provide Internet access with average and high bit rates.

3.2 Transmission tests with IP server

The first goal is to verify that services offered to future ADSL customers can be transported on low voltage networks using PLT modems.

The second goal is to analyze the transmission quality of one or several of these services according to several parameters such as simulated services, channel quality, electrical perturbation.

3.2.1 Test configuration

The test configuration is as follows (see figure 11):
- the modems are placed at the end of the lines in order to have the maximum length
- modems and PC IP addresses are chosen to operate under a sub-network specified in the ADSL modem/router
- the bit rates are:
- downstream: 1.20 Mbit/s max.
- upstream: 0.76 Mbit/s max.
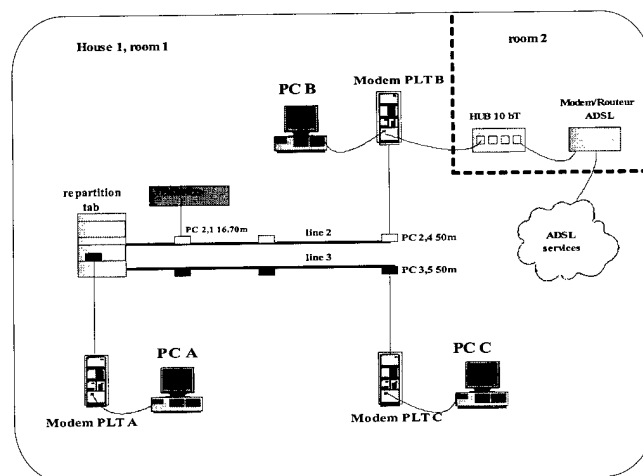
Figure 11: test set up with PLT modems connected to an IP server

3.2.2 Quality of transmission with IP services on Powerline

Firstly, PLT modems are tested with IP services simulated using simulation software.
Secondly, the access to real services is verified.
Thirdly, other services are added with the simulation software.
Then, several parameters are analyzed (number of applications required, frequencies, power).

3.2.2.1 Tests with simulated IP services

• **Without interference**
With file transfer tests, the minimum power for satisfactory running without interference is calculated.
The results show:

Frequency	minimum power	IP Test	FEC Led
5 to 25 MHz	-37dBm	OK	no error

The configuration used without perturbation shows a good transmission with minimum power (- 37 dBm) and a bit rate of 1.27 Mbit/s.

• **Interference due to a hair-drier**
The use of a hair-drier (for interference), connected as shown in the figure 11, produces transmission stops and even modem de-synchronization, with the previous minimum power (- 37dBm).
The emitted power Pe= -25dBm is then chosen to measure the effect of interference on transmission.

The goal is to monitor the behavior of the PLT modems with a large demand in services.

- **Without interference**

The superposition of video services and file transfers can be carried out correctly in these conditions:
- the number of file transfers is quite low (two with voice over IP)
- these transfers have to avoid the modems used for video services

If these conditions are not met, the following faults occur:
- the video bit rate fluctuates and decreases
- then the image becomes fixed
- file transfer bit rates increase (see figure 12)
- the global bit rate stays about 1.3Mbit/s.

There is no obvious synchronization between the fluctuation of the image quality and the bit rate: resulting in a shift of a few 1/10 second.
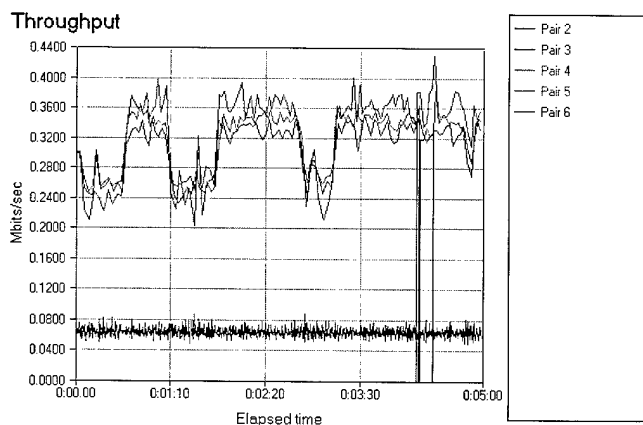
Figure 12: bit rates variation with several service applications

- **With interference**

Same previous remarks can be made.
New remarks are (see figure 13):
- the use of the hair-drier reduces the bit rate which decreases from 1.3Mbit/s to 1.1Mbit/s with a power level of −25dBm
- again, the use of the hair-drier creates interference at all the frequencies.
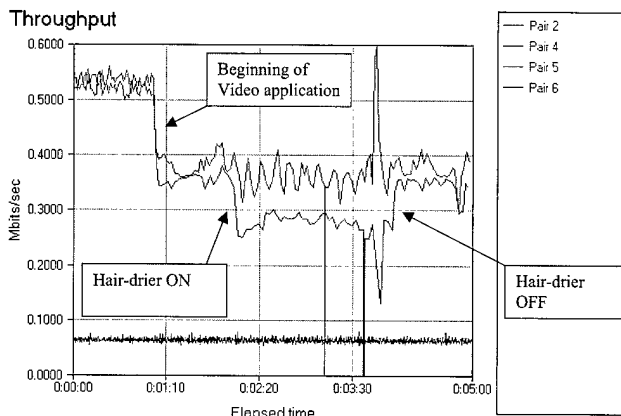
Figure 13: bit rates variation

3.2.3 Conclusion

The test results are generally very interesting:

- The IP configuration of PLT modems is correctly designed for the adaptation at the connection to the IP services.
- The behavior of the services and bit rates in regard to different constraints such as several service demands is normal.

3.3 EMC

3.3.1 Test configuration

A point-to-point link is made between two PCs (with an Ethernet interface) via the PLT modems and the low voltage network.
For conduction measurements, the modulation used by the modems is GMSK which allows a good spectral efficiency.
For emission measurements, the modulation used by the modems is OFDM.

3.3.2 Conduction measurements

- *Measurements of the signal and direct noise on low voltage network*

The principle is to have the frequency spectrum with and without PLT signal on the line between 10kHz and 30MHz (see figure 14).
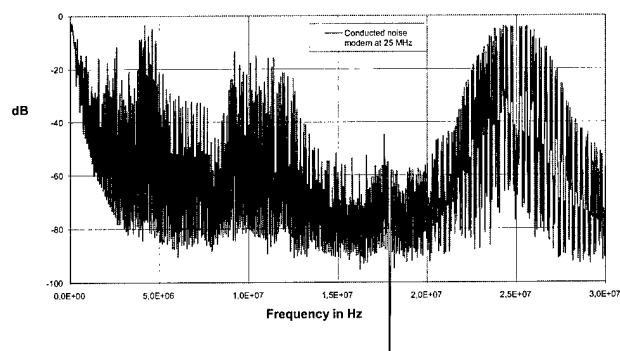
Figure 14: EMC measurements on the low voltage network

The noise is recorded instantaneously. A PLT carrier is seen at 25MHz with a level of −5dBm and noise can be seen up to about 15MHz.

The relatively high noise on the low voltage network around 5MHz and 10MHz shows the small margin available in these frequency bands to operate the PLT. The question is to decide whether this noise is intrinsic to the line or related to the environment.

- **Measurements of conducted emissions with LISN according to the EN55022 standard**

The Line Impedance Stabilization Network (LISN) is placed in series with the line and allows the conducted HF interference to be measured according to the EN 55022 standard.

This is a common mode measurement, between phase-earth and neutral-earth.

The PLT signal being emitted between phase and neutral (differential mode), this measurement is taken to evaluate the way in which this test should be applied (according to the standard) to the PLT (see figure 15).
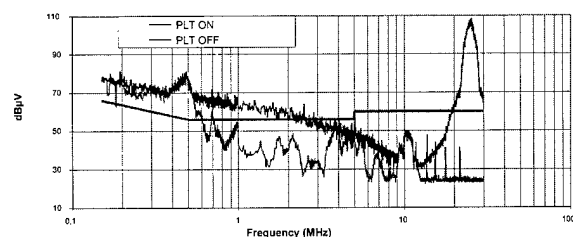
Figure 15: measurements with LISN

The PLT carrier, at its maximum level, exceeds the limit of the EN 55022 standard by about 40 dB.

Taking into account the measurement conditions, the results must be relativized and the actual value is below 40dB.

The result shows that:

- generally, PLT has more interference than xDSL systems (in particular ADSL).

- The intrinsic noise of the low voltage network is a serious problem for the efficient running of PLT because even with modems shut down, the limit of the standard is exceeded at some frequencies (around 500kHz).

This initial research on the measurements of conducted noise with different interfaces show the difficulty of interpreting the results due to the measurement conditions which differ greatly for each situation.

For future characterizations and in order to compare the results, it is very important to define a single precise measurement condition and respect this condition.

3.3.3 Conducted emission measurements

These measurements are made with and without interference.

On an electrical outlet, the PLT signal spectrum is measured on the one hand with the stationary noise on the line and on the other with hair-drier noise (see figures 16 and 17).
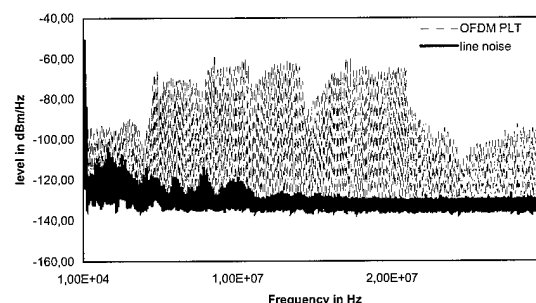
Figure 16: conducted emission on a low voltage network with modems and without interference
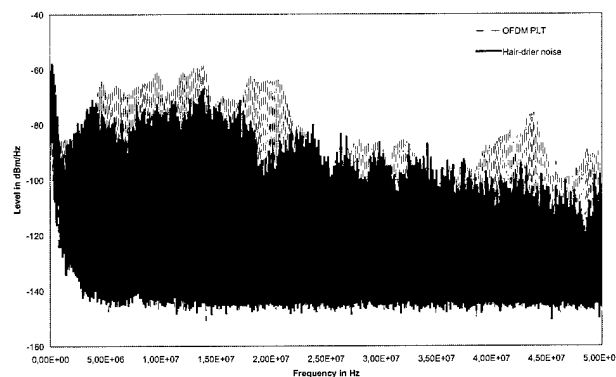
Figure 17: conducted emission on a low voltage network with modems and with interference

The result shows a high Signal/Noise Ratio (SNR) margin in the presence of stationary noise (this means that the OFDM carriers should probably be reduced).

But when the hair-drier is in use the margin is very small.

3.3.4 Conclusion

This initial research in EMC on indoor PLT shows the real problems to be solved for the development of the PLT.

Concerning interference, the standardization defined only for conducted emission below 30MHz is not sufficient for PLT. The measurements in conducted emission must be stabilized.
The use of LISN (standardized according to EN 55022) is not realistic with the use of PLT modems because the link is not bi-directional.
In terms of immunity and radiated emission, measurements have to be made on PLT.

Modulation techniques and error correction codes should allow the low voltage network to be used as a medium for broadband transmission.
The aim is to find an acceptable compromise between a sufficient emission power level (good transmission quality) and a low emission power level so as not to perturb the environment.

4. Standardization

There is only one standard in this area, called EN 50065 [1], taking into account frequencies from 3kHz to 148.5kHz, created by the CENELEC and part of harmonized standards concerning the European EMC directive.

One of the hindrances to the development of PLT is the uncertainty surrounding the regulations (standard, limit values, etc.) to be applied in terms of EMC.
It is easily understandable that high bit rate transmission over an unshielded untwisted pair can generate high levels of electromagnetic interference.
Thus, current work in standardization for defining specific limits for these systems is advancing slowly because of the divergence of points of view and interests (on the one hand development of PLT transmission systems and on the other, protection of radio-electric services used under 30 MHz).
Several standardization bodies are working on the domain: CENELEC TC 205, 210 and 215, ETSI and CEPT.
A common project including these bodies began at the beginning of the year 2000 under the following name: ETSI Project PLT.
Fora are working in parallel and are now co-operating in the PLT forum.
In terms of EMC, two major approaches being studied, with both advantages and disadvantages:
- The "chimneys" approach
- the "flat" approach.

5. Conclusion

Preliminary FTR&D research in the power line technologies field is very interesting.
Concerning the characterization of the low voltage network, measurement can be made when voltage is present on the line with good results that represent a real situation. The use of twisted pair cable can generate a new way to transmit the PLT. The characterization in real customers houses will be carried out soon during future field trials.
The EMC measurements reveal the problems to be solved for the development of PLT in terms of conducted and emitted

interference. The goal of the subsequent research is to find an acceptable compromise between good transmission and low interference in terms of emission power, with the possibility of accelerating the PLT standardization process.
Finally, the initial tests on IP transmission with real Internet services and a bit rate in the Mbit/s range point the way to future field trials with real customers in a real environment, which will be the next step for FTR&D in the domain of PLT.

6. Reference

[1] CENELEC EN 50065-1 "Signaling on low-voltage electrical installations in the frequency range 3kHz to 148.5kHz, Part 1: general requirements, frequency bands and electromagnetic disturbances", 1991+A1:1992+A2:1995+A3:1996

7. Authors

Olivier Bouffant graduated from the University of Toulon in Electronics in 1992. He joined France Telecom R&D center in 1994. Working in the Access Network Infrastructure Laboratory, he is project manager on in-house Network for residential and business customers

Daniel Le Bras began his career with France Telecom R&D in 1984.
Working in the Access Network Infrastructure Laboratory, he is in charge of residential home network tests, specializing in the powerline infrastructure.

Herve Le Cozic began his career with France Telecom R&D in 1981. After six years in a Physical-Chemical Laboratory, he joined the Access Network Infrastructure Laboratory in 1987. Working on standardization for data cables, he is in charge of telecom cables, connectics and home wiring tests.

Philippe Gay began his career with France Telecom R&D in 1982. Working on the Access network Architecture, Studies & Evaluation Laboratory, he is in charge of all the activities around Powerline in France Telecom R&D.

Jean-Marc Auzizeau began his career with France Telecom R&D in 1986. After working on CATV networks, he joined the Security, reliability & Environment Laboratory in 1999 and is in charge of the EMC studies for powerline.

Michel Le Dizès began his career with France Telecom R&D in 1986. Working on the Access network Architecture, Studies & Evaluation Laboratory, he is in charge of the residential home network tests, specializing in powerline systems.

Gérard Térol began his career with France Telecom R&D in 1974. After working on the evaluation of opto-electronics components, he joined the Security, reliability & Environment Laboratory in 1998 and is in charge of EMC tests and trials.

Pierre Legaud began his career with France Telecom R&D in 1983. Working on the Access network Architecture, Studies & Evaluation Laboratory, he is in charge of the residential home network studies, specializing in powerline and wireless systems.

Return Loss Prediction for Cascaded Systems

Mohammed M Al-Asadi[1] , Alistair P Duffy[1] , Kenneth G Hodge[*] and Arthur J Willis[*]

[1]Department of Engineering and Technology, De
Montfort University, Leicester, LE1 9BH UK.

[*]Brand-Rex Ltd, Glenrothes, Fife, Scotland,KY6 2RS
UK.

Principle contact: email alasadi@dmu.ac.uk

Abstract
The paper presents an analytical approach to the calculation of the
return loss from a cascaded system of '*n*' discrete components,
such as cables and connectors, based on knowledge of the
impedance and the propagation constant of each element. The
impedance and the propagation constant may be obtained
analytically or experimentally. The return loss prediction also takes
into account variations in the termination impedance and in length
of cables. Results are compared with those obtained using other
analytical methods and are also compared with simulations of the
communication channel based on the Transmission Line Matrix
(TLM) method and with measurements. These comparisons
confirm the validity of the derived equation.

1. Background
In the development of Category 5e, and latterly Category 6
cabling, a deeper understanding of a wider range of transmission
line characteristics of the cabling system has been required.
Particularly with respect to the new emerging protocols, e.g.
1000baseT. One such characteristic is Return Loss (*RL*), which
has proved problematic with respect to development of certain
components, in particular patchcords. The theory in this particular
field is not well developed and has, consequently, presented
standardisation bodies and the industry in general with challenges
in definition of component performance levels and in setting
requirements.

The performance of twisted pair copper cables can not be fully
predicted unless the secondary parameters of the cable, such as
return loss, propagation constant and characteristic impedance can
be determined. Calculations frequently used to determine the
return loss, only take into account the mismatching between the
characteristic impedance of the cable and the load impedance [1].
They generally, do not take into account the mismatching between
the impedance of the cable and the source impedance.

Return Loss, *RL*, and Structural Return Loss, *SRL*, are measures
of the reflected signal at the sending (near) end. They represent
the combination of the structural effects (irregularity and handling
effects) and the effects of the departure from the nominal
characteristic impedance of the cable. The importance of the *SRL*
is that it increases the losses that transmitted signals suffer along
the cable in addition to the attenuation losses. For a system of a
uniform twisted pair cable connected between a matched source
and a matched load, the amount of the reflected signal represents
the return loss of the system. However, if the cable is not uniform,
or suffers from irregularity for any reason, then the amount of
reflected signal represents the structural return loss.

Generally, both return loss and structural return loss of a simple
channel are calculated using equations that rely on characteristic
impedance and the impedance of the termination only [1]. The
aim of this paper is to develop a general formula to be used for the
calculation of both return loss (*RL*) and structural return loss
(*SRL*) of simple channels and multi-stage cascaded channels. The
formula developed in this paper takes into account the effects of
the termination of the transmission channel, the effects of source
output impedance and the effects of impedance mismatching
between the cascaded stages. It also relates length and the periodic
and random structural variation of cables to the return loss
calculation [2]. The equation also relates the structural return loss
of the cable to the attenuation deviation of the cable or
transmission channel [3] by including the propagation constant of
all channel components in the equation. The next section
describes the development procedure of the equation.

2. Equation Development
To understand the development of the return loss equation of a
cascaded channel, the development of a simple transmission
channel return loss equation is described in the following
subsection.

2.1 Simple Channel Equation
Using 2-port network principles, a mathematical equation for the
calculations of the return loss of a twisted pair cable as a function
of cable propagation constant, γ, the characteristic impedance of
the cable, Z_o, source output impedance, Z_s, and load impedance,
Z_L, is developed. Return loss can be calculated as:

$$RL = -20\log(S_{11}) \tag{1}$$

A single pair cable of length *l* and characteristic impedance Z_o
connected between a source of output impedance Z_s and a load
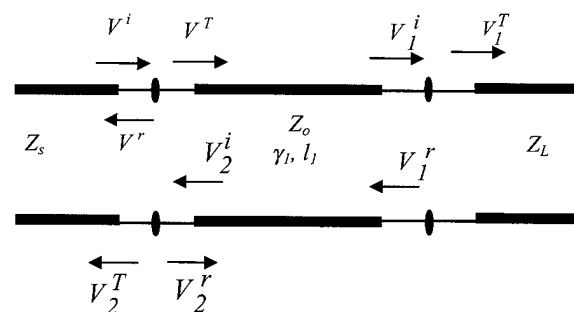termination of impedance Z_L can be illustrated as in figure 1.

**Figure 1 Two ports network representation of a
simple channel**

The transmitted voltage to the far end of the cable does not represent the whole signal injected from the source to the near end. Part of the injected voltage will dissipate as a result of attenuation and return losses. Phase changes will also be experienced due to the phase constant of the transmission line. Hence, for accurate calculations, the incident parts of the voltages into any end of the cable should be calculated taking into account the complex propagation constant. For the cable represented in figure 1:

$$V_1^i = V^T \cdot e^{-\gamma_l l_l} \tag{2}$$

where l_l is the length of the cable segment and γ_l is the propagation constant of the same cable which is given as:

$$\gamma_l = \sqrt{(R + j\omega\ L) \cdot (G + j\omega\ C)} \tag{3}$$

where R, L, G and C are the primary parameters of the cable and ω is the angular frequency. Using the same principle, we also have:

$$V_2^i = V_1^r \cdot e^{-\gamma_l l_l} \tag{4}$$

Using reflection and transmission coefficients at the connections between the cable and both the source and the load of figure 1, it can be seen that:

$$V^r = V^i \frac{Z_o - Z_S}{Z_o + Z_S} \tag{5}$$

$$V^T = V^i \frac{2 \cdot Z_o}{Z_o + Z_S} \tag{6}$$

$$V_1^r = V_1^i \frac{Z_L - Z_o}{Z_L + Z_o} \tag{7}$$

$$V_1^T = V_1^i \frac{2 \cdot Z_L}{Z_L + Z_o} \tag{8}$$

$$V_2^r = V_2^i \frac{Z_S - Z_o}{Z_S + Z_o} \tag{9}$$

$$V_2^T = V_2^i \frac{2 \cdot Z_S}{Z_S + Z_o} \tag{10}$$

The overall reflected voltage at the source end of the cable, can then be calculated as:

$$V_{total}^r = V^r + V_2^T = V^i \frac{Z_o - Z_S}{Z_o + Z_S} + V_2^i \frac{2 \cdot Z_S}{Z_S + Z_o} \tag{11}$$

Using equations 2, 4 and 8 the above equation, 11 can then be written as:

$$V_{total}^r = V^i \frac{Z_o - Z_S}{Z_o + Z_S} + \frac{2 \cdot Z_S}{Z_S + Z_o} \cdot e^{-\gamma_l l_l} \cdot \frac{Z_L - Z_o}{Z_L + Z_o} \cdot e^{-\gamma_l l_l} \cdot V^T$$

Using equation 6, this equation can be simplified and rewritten as:

$$V_{total}^r = V^i \left[\frac{Z_o - Z_S}{Z_o + Z_S} + \frac{2 \cdot Z_S}{Z_S + Z_o} \cdot \frac{Z_L - Z_o}{Z_L + Z_o} \cdot \right.$$
$$\left. \frac{2 \cdot Z_o}{Z_S + Z_o} \cdot e^{-2\gamma_l l_l} \right] \tag{12}$$

The S_{11} parameter can then be obtained as:

$$S_{11} = \frac{V_{total}^r}{V^i} = \left[\frac{Z_o - Z_S}{Z_o + Z_S} + \frac{2 \cdot Z_S}{Z_S + Z_o} \cdot \frac{Z_L - Z_o}{Z_L + Z_o} \right.$$
$$\left. \cdot \frac{2 \cdot Z_o}{Z_S + Z_o} \cdot e^{-2\gamma_l l_l} \right] \tag{13}$$

Assuming that

$$m_1 = \left(\frac{Z_o - Z_S}{Z_o + Z_S} \right) \tag{14}$$

$$m_2 = \left(\frac{2 \cdot Z_S}{Z_S + Z_o} \right) \tag{15}$$

$$m_3 = \left(\frac{2 \cdot Z_o}{Z_S + Z_o} \right) \tag{16}$$

$$m_4 = \left(\frac{Z_L - Z_o}{Z_L + Z_o} \right) \tag{17}$$

$$m_5 = \left(e^{-2\gamma_l l_l} \right) \tag{18}$$

Equation 13 can then be simplified to:

$$S_{11} = m_1 + m_2 \cdot m_3 \cdot m_4 \cdot m_5 \tag{19}$$

Substituting the last equation in equation 1, the return loss RL, can then be obtained as:

$$RL = -20\log(m_1 + m_2 \cdot m_3 \cdot m_4 \cdot m_5) \tag{20}$$

Since m_5 is a function of the propagation constant (i.e. attenuation and phase) and both the propagation constant and the characteristic impedance are functions of the frequency and the cable dimensions, therefore the return loss is a function of the frequency and the cable dimensions. Due to the fact that the propagation constant is also a function of the cable length and the lay length, the return loss will also be a function of them. Any

changes in the values of the source impedance or the termination, the return loss will be changed.

Having introduced the concept on which further analysis is based, a more complicated transmission channel is discussed in the following subsection.

2.2 A General Cascaded Channel Equation

Following is the development of more general transmission channel, where there are several cables and connectors cascaded between a source and a load. The characteristic impedance of the source end connector is Z_{o1}, its propagation constant is γ_1 and its length is l_1 while the characteristic impedance of the load end connector is Z_{o3}, its propagation constant is γ_3 and its length is l_3. The overall transmission channel is illustrated as in figure 2.

From the above circuit, the total incident voltage from the source and the total reflected voltage from the transmission channel are given respectively as:

$$a_1 = {}_0V_L^i \tag{21}$$

$$b_1 = {}_0V_L^r + {}_0V_L^T \tag{22}$$

S_{11} of the circuit can be obtained as:

$$S_{11} = \frac{b_1}{a_1} \tag{23}$$

Following the procedure described in the previous sub-section, S_{11} of the circuit illustrated in figure 2 and given in the above equation can now be obtained as:

$$S_{11} = m_1 + m_2 \cdot m_3 \cdot m_4 \cdot m_5 + m_2 \cdot m_3 \cdot m_6 \cdot m_7 \cdot \\ m_8 \cdot m_9 + m_2 \cdot m_3 \cdot m_6 \cdot m_7 \cdot m_{10} \cdot m_{11} \cdot m_{12} \cdot m_{13} \tag{24}$$

where the parameters m_1 to m_{13} are given as:

$$m_1 = \left(\frac{Z_{o1} - Z_S}{Z_{o1} + Z_S} \right), \qquad m_2 = \left(\frac{2 \cdot Z_S}{Z_S + Z_{o1}} \right)$$

$$m_3 = \left(\frac{2 \cdot Z_{o1}}{Z_S + Z_{o1}} \right), \qquad m_4 = \left(\frac{Z_{o2} - Z_{o1}}{Z_{o2} + Z_{o1}} \right)$$

$$m_5 = e^{-2(\gamma_1 l_1)}, \qquad m_6 = \left(\frac{2 \cdot Z_{o1}}{Z_{o1} + Z_{o2}} \right)$$

$$m_7 = \left(\frac{2 \cdot Z_{o2}}{Z_{o1} + Z_{o2}} \right), \qquad m_8 = \left(\frac{Z_{o3} - Z_{o2}}{Z_{o3} + Z_{o2}} \right)$$

$$m_9 = \left(e^{-2(\gamma_1 l_1 + \gamma_2 l_2)} \right), \qquad m_{10} = \left(\frac{2 \cdot Z_{o2}}{Z_{o2} + Z_{o3}} \right)$$

$$m_{11} = \left(\frac{2 \cdot Z_{o3}}{Z_{o2} + Z_{o3}} \right), \qquad m_{12} = \left(\frac{Z_L - Z_{o3}}{Z_L + Z_{o3}} \right)$$

$$m_{13} = \left(e^{-2(\gamma_1 l_1 + \gamma_2 l_2 + \gamma_3 l_3)} \right)$$

By induction, S_{11} of equation 24 can now be rewritten in the following general form, 25, which is substituted in equation 1 to give the return loss of a multi-cascaded transmission channel as in equation 26. In equation 26, Z_s is source impedance, Z_{n+1} is the load impedance and n is the number of the cascaded elements of the transmission channel, where the source connection is given number 0. For the channel shown in figure 2, we have $n = 3$. Using equation 26, the return loss of the cascaded transmission channel of figure 2 can be obtained. If the stages between the source and the load represent a transmission channel with irregularity and its impedance is variable along the length of the cable, then the above equation can be used for the calculation of the structural return loss generated by the structure effects. In this case, each of the segments represents different impedance. The advantage of the developed equation that it can handle a more practical transmission channel.
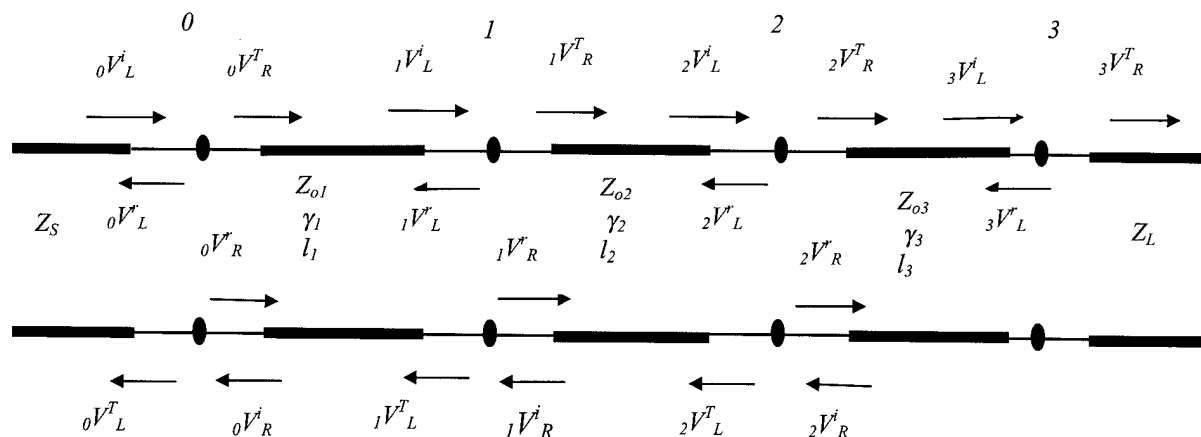
Figure 2 A source-connector-cable-connector-load transmission channel.

$$S_{11} = \frac{Z_1 - Z_s}{Z_1 + Z_s} + \left[\sum_{k=1}^{k=n} \left\{ \left[\prod_{i=1}^{i=k} \left(\frac{2 \cdot Z_i}{Z_i + Z_{i-1}} \cdot \frac{2 \cdot Z_{i-1}}{Z_i + Z_{i-1}} \right) \right] \right\} \cdot e^{-2\left\{ \sum_{j=1}^{j=k} \gamma_j l_j \right\}} \cdot \frac{Z_{k+1} - Z_k}{Z_{k+1} + Z_k} \right] \tag{25}$$

$$RL = -20 \log \left[\frac{Z_1 - Z_s}{Z_1 + Z_s} + \left[\sum_{k=1}^{k=n} \left\{ \left[\prod_{i=1}^{i=k} \left(\frac{2 \cdot Z_i}{Z_i + Z_{i-1}} \cdot \frac{2 \cdot Z_{i-1}}{Z_i + Z_{i-1}} \right) \right] \right\} \cdot e^{-2\left\{ \sum_{j=1}^{j=k} \gamma_j l_j \right\}} \cdot \frac{Z_{k+1} - Z_k}{Z_{k+1} + Z_k} \right] \right] \tag{26}$$

3. TLM Model

Another tool for computing the return loss and the structural return loss is the application of Transmission Line Matrix (TLM) modelling method of a single twisted pair cable [4]. The model allows the computation of the secondary parameters of cables under different conditions of operation. The computation of the return loss of a twisted pair cable using the TLM model is obtained from the knowledge of both incident and reflected voltages at both near and far ends [5]. Since the TLM model represents a time domain approach, the frequency domain response of the cable can be obtained by Fourier Transformation. Secondary parameters of the cable can then be obtained.

Return Loss can then be obtained as:

$$RL = 20 \log \left(\left| \frac{VL_N^r}{VL_N^i} \right| \right) \tag{27}$$

where VL_1^r is the reflected voltage from the near end of the transmission channel and VL_1^i is the incident voltage into the near end of the channel. The validation of equation 26 is presented in the next section.

4. Equation Validation

Equation, 26, is used for the calculation of the return loss of a simple channel comprising a source of impedance Z_s, a 1 m length of Category 5 cable of impedance Z_o and a load of impedance Z_L. The dimensions of the cable are:

$D = 0.94 \; mm$, $r = 0.265 \; mm$, $ll = 20 \; mm$.

Where D is the distance between the centres of the conductors, r is the radius of each conductor and ll is the lay length of the cable.

The new equation is validated against a standard equation obtained from reference [6].

$$RL = -20 \log \left(\frac{Z_i - Z_s}{Z_i + Z_s} \right) \tag{28}$$

where Z_i is the input impedance of the transmission channel looking from the source end and is given as:

$$Z_i = Z_o \left(\frac{Z_L \cosh(\gamma \; l) + Z_o \sinh(\gamma \; l)}{Z_o \cosh(\gamma \; l) + Z_L \sinh(\gamma \; l)} \right) \tag{29}$$

γ is the propagation constant of the cable and l is the length of the cable. For a matching condition where the source and the load impedance have the same value as the characteristic impedance of the cable, return loss results are plotted as in figure 3. It should be mentioned here that Z_s and Z_L represent amplitudes only while Z_o represents a complex quantity (amplitude and phase).

Figure 3 shows an excellent agreement between both sets of results. The advantage of using the new equation is reported in the discussion section. Further, the equation and the TLM approach are used for the calculation of RL as is presented in the following section.
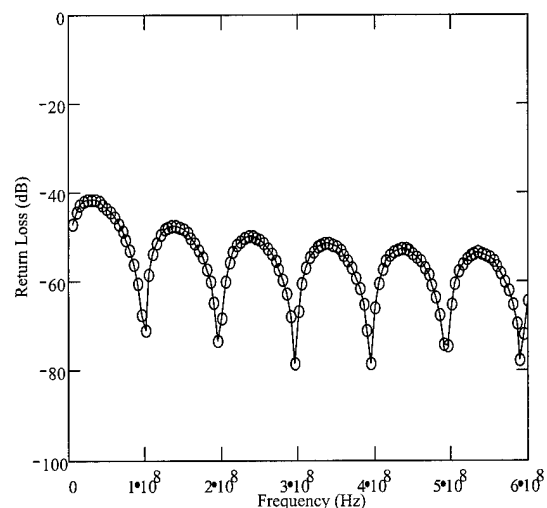
Figure 3 Return loss of a simple channel calculated using equation 28 ('o' samples) and the new equation, 26, (solid line) up to 600 MHz.

The same system, when modelled using TLM, gives the results of figure 4. It is clear that there is a high level of correlation between figures 3 and 4, further verifying the behaviour of equation 26 and the accuracy of TLM.
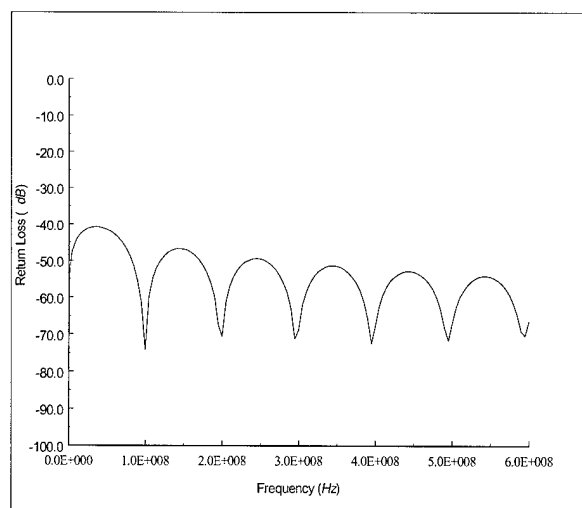
Figure 4 Return loss of a simple channel calculated using the TLM approach (equation 27).

5. Implementation and Results

The proposed analytical equation 26 was validated in the previous section. This section applies this equation for the calculation of the return loss of cascaded channels. Two configurations of channels are investigated as follows:

1. A transmission channel of three segments compromising a near-end connector, single pair cable and a far-end connector connected between a source and a load. The dimensions of the cable were as those mentioned earlier. Both connectors are assumed ideal by being considered so that they are circular and have the r and D as those of the cable. The length of the cable was $1m$ and the length of each connector was $1cm$. Results were obtained for a matching condition where both source and load impedance values equal the nominal characteristic impedance of the cable. As the connectors had the same dimensions as the cable, the characteristic impedance of both connectors matches that of the cable, as does the propagation constant. The return loss is calculated and plotted in the figure 5. The figure also includes the return loss calculated for the same channel where the load end was terminated with a resistance of 85Ω. It also includes results obtained for a mis-matching condition where the load end is terminated with a resistance of 115Ω. Results obtained here illustrate that both cases of mis-matching between the transmission channel and the load would obviously lead to the increase in the return loss of the channel.

2. A more complicated channel consisting of 7 segments connected between the source and the load comprises a near end short link, a far end short link and a long twisted pair cable connected between the, each segment is joined by a connector, the length of each connector is $1cm$. The

length of each cable of the two links is $1m$ and the length of the long cable is $10m$. Such a channel is practically used for communication between computers in a computer network. Again, the connectors are assumed circular with the same cross-sectional dimensions of all cables. Using the analytical equation 26, the return loss of such a channel where n=7 is calculated for different termination. Figure 6 illustrates results of matching conditions and those obtained for a mis-matching condition when the channel is terminated with a load of 85Ω. For a termination of 15Ω, results are plotted as in figure 7.
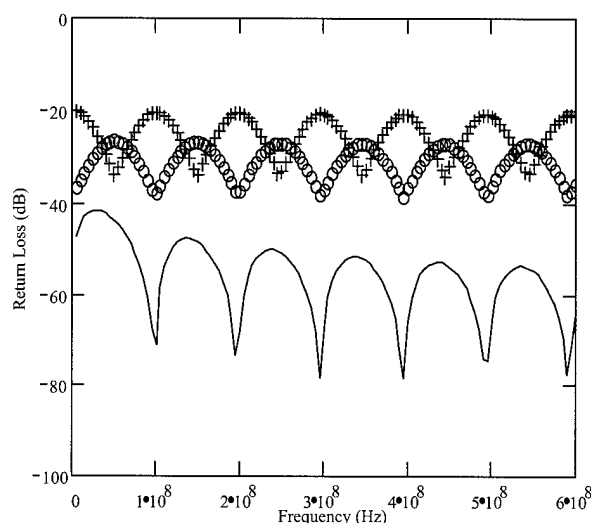
Figure 5. Return loss of a 3-segment channel. $Z_L=Z_o$ (solid line), $Z_L=85\Omega$ (o samples) and $Z_L=115\Omega$ (+ samples).
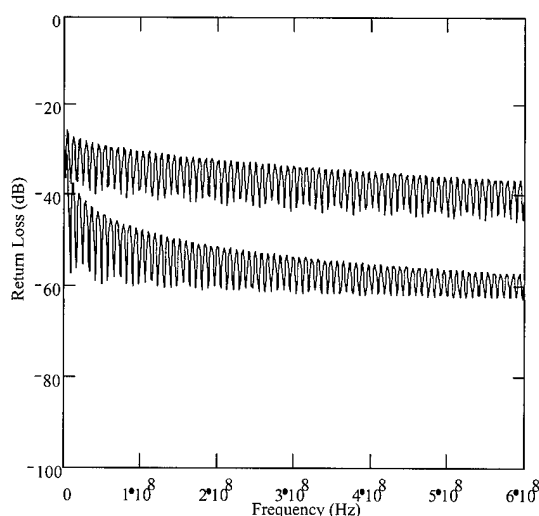
Figure 6. Return loss of a 7-segment channel where a 10m cable is used. Lower plot ($Z_L=Z_o$), and Upper plot ($Z_L=85\Omega$).

Comparing figures 5 and 6 illustrates that increasing the length of the cable leads to the reduction of the phase effect on the overall value of the return loss. It also shows that variations in the return loss value are less at higher frequencies than those at lower frequencies. In order to validate this point, a longer channel was investigated.
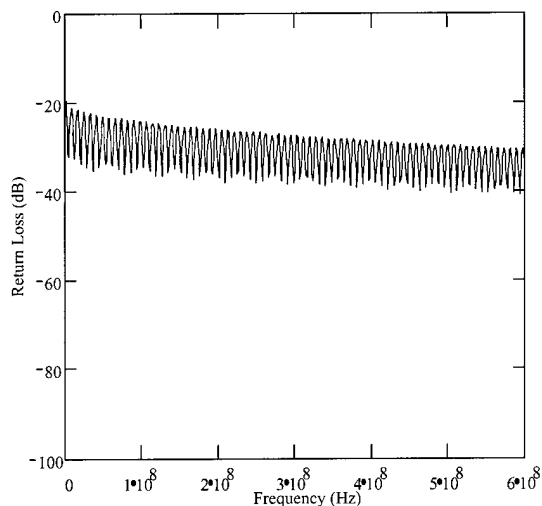
Figure 7. Return loss of a 7-segment channel where a 10m cable is used and Z_L=115Ω.

3. A similar channel to that investigated in 2 is investigated here where a 100m cable is used. Again the return loss was calculated using the equation 26, For matching condition, for a termination of 85 and for a termination of 115, results are plotted as in figure 8, 9 and 10 respectively.
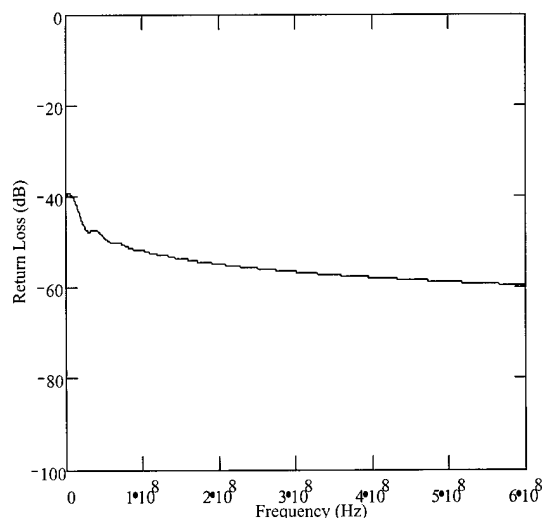
Figure 8. Return loss of a 7-segment channel where a 100m cable is used where Z_L=Z_o.
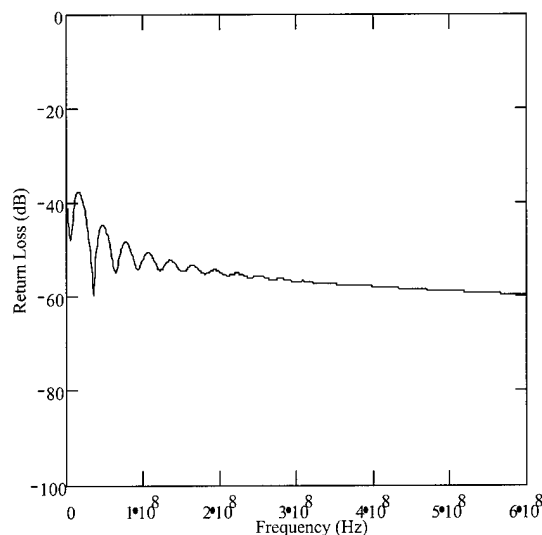
Figure 9. Return loss of a 7-segment channel where a 100m cable is used where Z_L=85Ω.
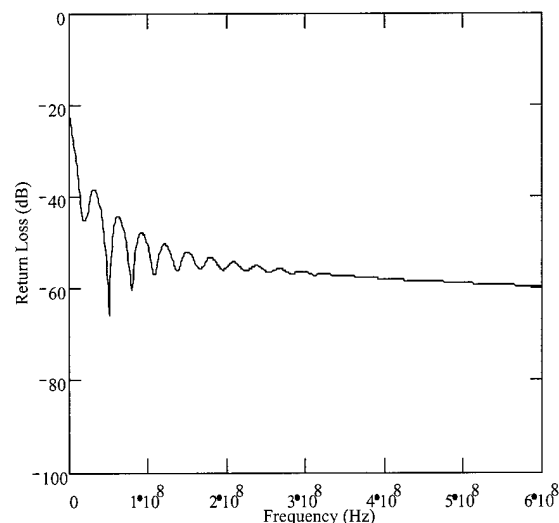
Figure 10. Return loss of a 7-segment channel where a 100m cable is used where Z_L=115Ω.

Figure 8, 9 and 10 illustrate that for long channels, load termination within the impedance limits would not affect return loss values at high frequencies. All sets of results demonstrate the advantage of using such equation in the calculation of the return loss of any communication channel

6. Discussion and Conclusion

A simple and flexible equation has been developed for the calculation of the return loss of communication channels and compared against existing equations for simple channels.

Another approach for the calculation of the return loss of a cascaded channel was presented using the TLM method. It was also used for the calculation of the return loss of the same channel investigated using the developed analytical equation. Results obtained using both approaches show excellent agreement. The analytical equation was then used for the calculation of different communication channels containing a number of connector and cable elements. Return loss for all channels and under different conditions of termination was presented. Again studying all sets of results leads to the conclusion that many factors such as channel length, mis-matching and may be impedance discontinuity play a big role in controlling the return loss vale of the channel.

The disadvantages of equation 28 is that, for a cascaded channel where n cables and connectors are present, equation 28 should be used n times to obtain the input impedance of the channel. The 1st time is to calculate the input impedance of the last stage of the channel, containing the load and the last segment (which could be the far end connector) of the channel. The resulting impedance can then used as load for the rest of the channel, where equation 28 should be used again to compute the input impedance of this load and the next stage of the channel, etc. The last value of the input impedance can be used in equation 27 for the calculation of the return loss of such a channel.

Using equation 26, any number of cascaded elements in the communication channel can be accounted for.

Similarly, the TLM approach discussed here also provides a second tool for the calculation of the return loss of both simple and more complicated channels.

It is proposed that the equation presented in this paper will have application in the prediction of performance of cascaded communication links.

As the equation was developed using a two-port network principles and it relies on impedance values, propagation constant and physical length of each component of the transmission channel, it can also be used for the calculation of the return loss of a shielded twisted pair channels.

7. References

[1] IEC/TC 46C, project number: IEC 61156-1 titled 'Test procedures for determining characteristic impedance (Z_o) and Return Loss (RL)', March 1996 and its amendment, 10/10/1997.

[2] L. M. Hore: 'Return loss of metallic telecommunication cables due to periodic and random structural variation and temperature', International Wire and Cable Symp. Proc., 1992, pp. 757-664.

[3] H. W. Friesen: "Relating the structural return loss of cable pairs to the associated attenuation deviation and delay jitter", International wire and cable symposium proceedings 1995, pp. 261-268.

[4] Mohammed M. Al-Asadi, Alistair P. Duffy, Kenneth G Hodge and Arthur J. Willis: 'Twisted pair cable design analysis and simulation', Accepted for publication in the 49th IWCS conference to be held in Atlantic City, USA, 13-16 November 2000.

[5] M. M. Al-Asadi, A. J. Willis, K. Hodge and A. P. Duffy: 'Modelling as a Tool for Analysing Handling Effects in Structured Wire Cabling', 1oth IEE Int. Conf. on EMC, 1-3 Sept 1997, pp. 131-136.

[6] S. Ramo, J.R. Whinnery and T. Van Douzer: 'Fields and waves in communication electronics', 2nd edition, 1984, Wiley.

Authors Biographies

Dr Mohammed Al-Asadi received his BSc degree from the University of Basra, Iraq and an MPhil degree from the University of Nottingham, UK both in Electronic and Electrical Engineering in 1988 and 1992 respectively. Between 1993 and 1996 he was working on a research project at the University of Nottingham, developing a program to incorporate charge particle motion in electromagnetic fields with transmission line modelling method. In 1996, he joined De Montfort University in Leicester, UK, where he is working as a Research Fellow and obtained his PhD degree. His research involves the investigation of high frequency performance of structured wire cabling in communication systems. He is the author and co-author of many journal and conference papers. His research interests include EMC, communication cables, electron beam, field-particle interaction devices, numerical methods and simulation of electromagnetic fields.
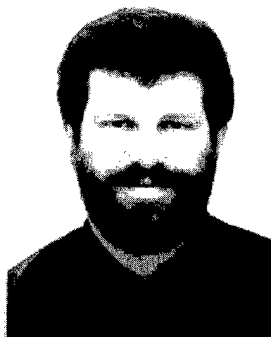

Dr Alistair Duffy was born in Yorkshire, UK, in 1966. He graduated with a 1st class BEng degree in 1988 and an MEng in 1989 from the University College, Cardiff. After a period working for Oyster Terminals in Newport, Gwent, as inter alia buyer, development engineer and sales support engineer, he read

for a PhD at Nottingham University with professors Christopoulos and Benson. He gained his Doctorate in 1993 and after post-doctoral work took up a post as a Lecturer in Communication Engineering at De Montfort University, Leicester, UK, where he is now a Principal Lecturer. His responsibilities include being Head of the Applied Electromagnetics Group and lecturing on various communication systems topics. He is currently vice-Chairman of the Institution of Electrical Engineers' Professional Group on Electromagnetics, and a member of the Professional Group on EMC. Topics of particular interest include the design and analysis of components for the physical layer of a communication system, techniques for the comparison of complex data sets, numerical modelling, EMC (particularly novel test methods), bio-electromagnetic effects and high frequency heating.

Mr Ken Hodge holds a BEng from Liverpool University, UK, and an MSc from Warwick University, UK. He is currently a representative to BSI and CENELEC committees working on LAN cabling. Ken has been working in the cable industry since 1982. He was initially involved with the development of optical and copper data communication and

telecommunication cables, then transferred to the R&D facility as Design Manager Optical Cables. He is now Technical Manager at Brand-Rex (A Caradon Company).
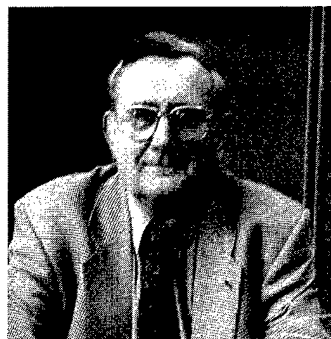
Mr Arthur J Willis has been involved in the design and development of cables since joining BICC in 1957, and as Chief Engineer was responsible for the early development of communication cables for information technology. He is currently Technical Consultant to Brand-Rex Limited.

The Calculation Method of Wind Pressure Load for a Bundle of Aerial Cables

Hideya KUWAHATA, Ryoichi KANEKO, Hironori TANADA
Hirotsugu KATO, Tetsuo SHINOHARA and Toshiyuki HIRAHARA
NTT Access Network Service Systems Laboratories
1-7-1 Hanabatake, Tsukuba, Ibaraki, 305-0805 Japan
+81-298-52-2533 · kuwahata@ansl.ntt.co.jp

Abstract

When designing outside aerial plant, it is important to calculate the wind pressure load so that the appropriate telecommunication pole or messenger wire can be selected. The wind pressure load is calculated by simply adding together the diameters of each cable and using the existing method. When several optical fiber cables are bundled with a spiral hanger, it is unclear how they will behave under windy conditions as a result of bundling and not fixed in the hanger. This means it impossible to calculate the appropriate wind pressure load.

To resolve these problems, we observed the behavior of the spiral hanger and bundled cables in a wind tunnel experiment, and undertook an investigation to determine whether the theoretical value calculated by our proposed wind pressure load method was correct by comparison with experimental values.

Keywords

Cable bundling, Spiral hanger, Wind pressure load, Summation of diameter, Cross-section for wind pressure load.

1. Introduction

The increase in the provision of optical access services has led to the installation of aerial optical fiber cable. The number of cables that can be fixed on a telecommunication pole is limited because NTT and another company use poles in common. This also means that aerial facilities can be something of an eyesore. So a method is needed by which several cables can be bundled thus resolving the above problems. A spiral hanger is one possible solution. The use of cable bundling has some merits. One is that an additional new optical cable can be easily installed, and the other is that existing bundled cable can be simply removed. When cable is bundled, however, it is impossible to calculate the appropriate wind pressure load under windy conditions because several cables are installed within the space enclosed by the spiral hanger. (Henceforth we refer to this as "hanger space"). This means we need an appropriate method for calculating the wind pressure load for bundled cables so that we can design efficient

outside plant. In this paper, we describe a method for calculating the wind pressure load for aerial cables bundled in a spiral hanger.

2. Cable bundling

With the existing cable installation method only one cable is installed and it corresponds to one supporting object (messenger wire). With the cable installation method using the spiral hanger (as shown in cross-section in Fig.1) several cables are installed in the hanger space and correspond to only one supporting object.
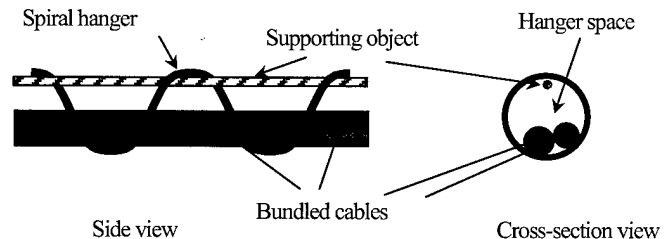
Figure 1. A bundle of aerial cables

This makes it possible to add more aerial cables efficiently and speedily. With bundled cable installation, it is unclear how cables will behave under windy conditions because several cables are unfixed in the hanger space. So we have to confirm the cables' behavior, and develop a method for calculating the wind pressure load so that we can obtain an accurate value for bundled cables.

3. Wind pressure load

The load acting on aerial cables is shown in Fig.2.
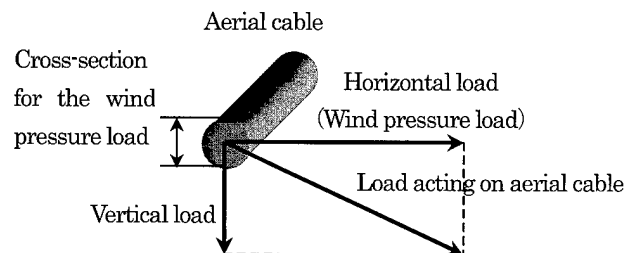
Figure 2. Load acting on aerial cable

---

[1] Ginza-Build. 4-26, Matsubara, Kagoshima, 892-0833, Japan

The wind pressure load is equal to the horizontal component of the load acting on the cables. The value depends on the wind speed and the aerial cables' cross-section. In outside aerial plant, two types of wind pressure load are applied corresponding to each area. They are;

[Type A] Wind pressure load per unit area: 100 [kgf/m²]
       (Equal to wind speed of 40 [m/s])
[Type B] Wind pressure load per unit area: 50 [kgf/m²]
       (Equal to wind speed of 28 [m/s])

Wind pressure load is calculated by timing it and from the cross-section of the aerial cables. The cross-section of each cable is different, and the cross-section of bundled cables is particularly unclear. This makes it necessary to determine the behavior of each cable at different wind speeds by wind tunnel experiments.

4. Experiment and analysis method
4.1 Experiment systems

As shown Fig.3, we constructed a simulated outside plant in a wind tunnel, and measured the tension that acts on a supporting object under wind speeds of 0 to 50 [m/s]. We also recorded the behavior of aerial cables using a video camera.
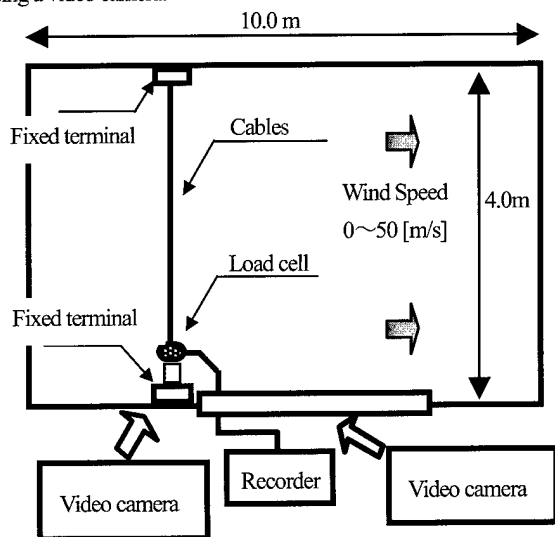
Figure 3. Experimental systems in wind tunnel

4.2 Analysis method
We converted the measured tension to wind pressure load by using following equation

$$\left(\frac{W_1 S^2}{8T_1}\right)^3 + \left[\frac{3}{8}S^2\left\{\frac{T}{EA} - \alpha(\theta_1 - \theta)\right\} - \left(\frac{W S^2}{8T}\right)^2\right] \times \left(\frac{W_1 S^2}{8T_1}\right) = \frac{3W_1 S^4}{64EA} \quad (1)$$

    W_1: Initial Load [kg/m]
    T_1: Initial Tension [kN/m]
    θ_1: Initial Temperature [°C]

W: Load of Windy condition Load [kg/m]
T: Tension of Windy condition Tension [kN/m]
θ : Temperature of windy condition [°C]
S: Span length between poles [m]
A: Cross-section area of supporting object [m²]
E: Young rate [kN/ m²]

We then compared it with the theoretical equation (2)

$$p = 1/2\, \rho\, cv^2 d \quad (2)$$

    p : pressure load per meter [kgf/m²]
    ρ : density of air [kg · s²/m⁴]
    c : constant for object shape (c=1)
    v : wind speed [m/s]
    d : cross-section for wind pressure load [m]

5. Experimental result and discussion
5.1 Relation between cross-section and wind pressure
We converted the experimental tension data to wind pressure load by using equations (1) and (2), and plotted it in Fig.4.
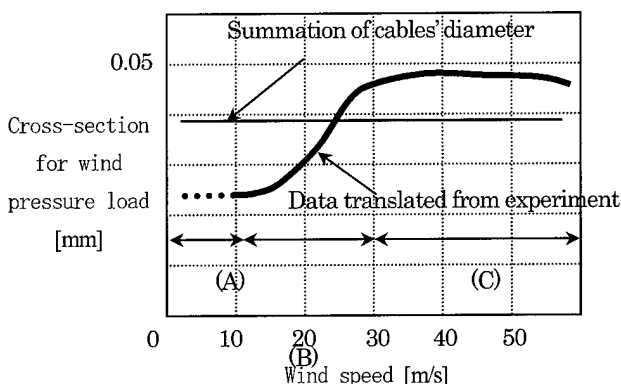
Figure 4. Change in cross-section by wind speed

The following are obtained from figure 4.
i)In range A(0 [m/s] < wind speed < 10 [m/s])
Cross-section is small; therefore wind pressure load is also small. Then cables remain at the bottom of the hanger space, (Video evidence).
ii) In range B(10 [m/s] < wind speed < 30 [m/s])
The higher wind speed is, the higher wind pressure load becomes. Then cables begin to be pushed toward the hanger wire and stacked vertically along it. Therefore cross-section increase and pressure load become higher.
iii) In range C(wind speed > 30 [m/s])
The cables are almost completely vertically stacked along the hanger wore as a result of the wind pressure load, which becomes higher than the summation of the cables' diameters. From this point on, the cross-section reaches an almost constant value.
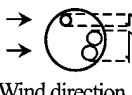
Table 1. Effect of wind speed on cables

The behavior of the cables in range C is important because the wind pressure load for Type A (40 [m/s] wind speed) or Type B (28 [m/s] wind speed) is calculated when aerial outside plant is designed as described above. Table 1 shows that light optical cables are stacked vertically along the hanger wire in the hanger space.

The cross-section converted from the experimental value is greater than the summation of the aerial cables' diameters, so we must consider the cross-section of the hanger as regards wind pressure load.

5.2 Cross-section considering hanger of spiral shape

The cross-section for the wind pressure load of the hanger is assumed to be the thickness of the hanger wire, and we investigated thus as follows using three samples in a wind tunnel experiment.

ⅰ)Sample 1.

Here the sample consisted of a messenger wire and a spiral hanger.
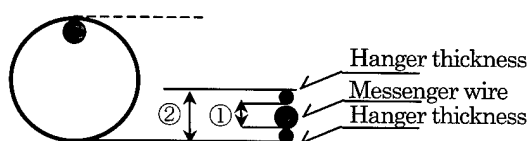
Figure 5. Cross-section for wind pressure load (Sample1)

As shown Fig.5, the cross-section for the wind pressure load is regarded as being

①:only the diameter of messenger wire

②a summation of the thickness of hanger and ①

ⅱ) Sample 2.

Here optical aerial cables are installed into a hanger space and the diameter summation of the cables is smaller than the inside diameter of the hanger. As shown in Fig. 6, the cross-section for wind pressure load is regarded as being

①: diameter of messenger wire and cables

②: a summation of the thickness of hanger and ①
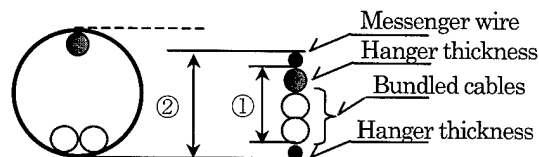
Figure 6. Cross-section for wind pressure load (Sample2)

ⅲ)Sample 3.

In this case the optical aerial cables are installed in the hanger space and summation of cable diameters is larger than the inside diameter of the hanger.
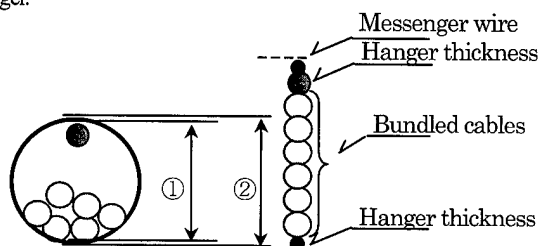
Figure 7. Cross-section for wind pressure load (Sample3)

As shown in Fig. 7, the cross-section for wind pressure load is regarded as being

①:the outside diameter of the hanger

②:the inside diameter of the hanger

The wind pressure load is calculated using equation (2) based on above assumed cross-section for wind pressure load. We obtained the following three graphs as shown Fig. 8 to 10.
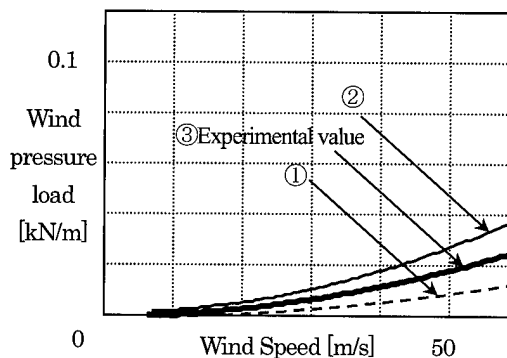
Figure 8. Wind pressure load
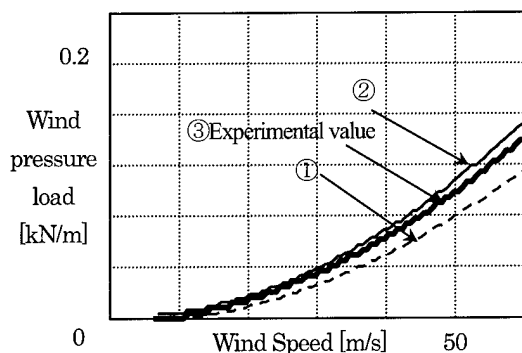
Figure 9. Wind pressure load
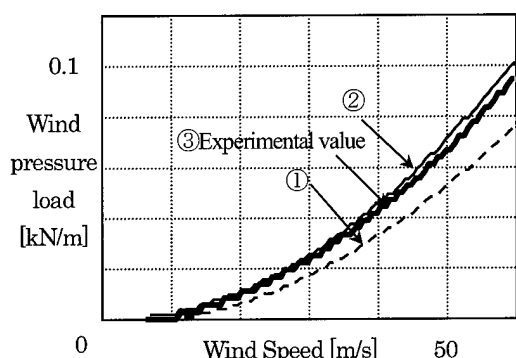
Figure 10. Wind pressure load

According to Fig. 8 to 10, the value obtained in experiment ③ is higher than that of obtained when the messenger wire diameter is considered the cross-section for the wind pressure load ①. Moreover, the value obtained in experiment ③ is smaller than that obtained when we consider the diameter summation of the hanger thickness to be the cross-section for the wind pressure load. Therefore, in terms of the easy design of safe aerial outside plant, it is necessary to calculate the wind pressure load on the basis of the thickness of the hanger wore being added to the messenger wire diameter.

According to figure 8 to 10, The value of experiment ③ is higher than that of messenger wire diameter treated as cross-section for wind pressure load ①. And, the value of experiment ③ is smaller than that of considering diameter summation of hanger thickness as cross-section for wind pressure load . Therefore at the point of easy and safe design of aerial outside plant, it is necessary to calculate wind pressure load which thickness of hanger wire is added to messenger wire diameter.

6. Conclusion

We undertook an experiment in a wind tunnel to confirm the behavior of optical cables under windy conditions and to calculate the appropriate wind pressure load.

We proved that the cables stay at the bottom of the hanger space at low wind speed but that they stack vertically in the hanger space as the wind speed increases. This shows that the wind pressure load increases as the cross-section increases.

With a bundle of cables, and taking the cables' behavior in the hanger space into consideration, we can decide the cross-section for the wind pressure load by appropriately following the flow shown in Fig. 11.
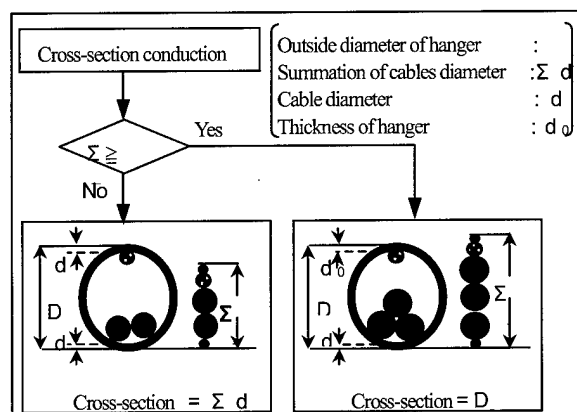
Figure 11. Flow of cross-section conduction

Acknowledgements

Reference

[1] R.Kaneko et al "Development of cable bundling technology for optical fiber cable" Raisers (2000)
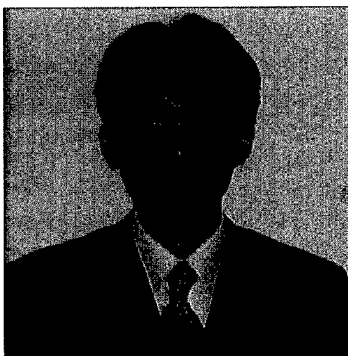
Hideya KUWAHATA

NTT Access Network
Service Systems Laboratories

1-7-1 Hanabatake, Tsukuba,
Ibaraki, 305-0805, JAPAN

Hideya KUWAHATA was born in 1974 and received B.E. and M.E. degrees in engineering from Kyushu University in 1997 and 1999 respectively. He joined NTT in 1999. Since then he has been engaged in research on aerial outside plant.

Successful Deployment of ADSS Cables in EHV Environments

Amitabha Mukhopadhyay[1], Karthik Krishnamurthy[2], Mark Boxer[2]

1 - Engineering Dept, Con Edison
New York, NY
+1-212-460-3685 · Mukhopadhyaya@coned.com

2 - Aerial Cable Systems, Alcoa Fujikura Ltd.
Spartanburg, SC
+1-864-433-5331 · karthik.krishnamurthy@alcoa.com
+1-864-433-5388 · mark.boxer@alcoa.com

Abstract

Alcoa Fujikura Ltd. has worked with customers to deploy well over 10,000 km of ADSS cables with "tracking-resistant" outer sheaths in EHV environments, on transmission systems with line voltages of 115 kV and higher. There have been no failures due to damage to the outer jacket caused by dry band arcing on this type of outer jacket. This paper will discuss the various modes of failure in ADSS fiber optic cables deployed in high voltage power lines, and will discuss the methods that Alcoa Fujikura Ltd. has used in order to successfully deploy cables in these situations. Finally, the paper will provide two case studies for cables deployed in EHV environments, one of which has been deployed on a 345 kV line, in a 40+ kV space potential, for over 10 years.

Keywords

ADSS; EHV; electrical stress; tracking; tracking-resistant; corona.

1. Introduction

With the introduction and acceptance of fiber optics as a preferred method for communications, power utilities are deploying more and more cables on the transmission and distribution rights of way (ROW). Many studies have addressed the topics of problems that may be seen if cables are improperly deployed on extra high voltage (EHV) transmission line right of way; however, not much public information is available about successful deployments of cables in these environments. There are several reasons for this discrepancy: First, overall, there is very little understanding of the techniques needed to successfully deploy ADSS cables in EHV environments. The phenomena of dry band arcing, tracking, and corona, all of which may contribute to degradation of cable jackets, and subsequent cable failure, are not well understood by fiber optic cable manufacturers. Many of these manufacturers have little experience in aerial cables in general and ADSS cables in EHV environments specifically, having provided the majority of cables for underground applications. Only a limited number of companies have a successful long-term (> 3 years) track record for placing cables in EHV environments. Second, the materials used to combat tracking and dry band arcing in ADSS cables in EHV environments are often proprietary formulations of specially processed materials. Manufacturers are not typically forthcoming with information about these materials, leading to difficulty in developing standards for materials. Finally, to this point, there has been no agreement amongst industry participants regarding standards to properly test materials and resulting material performance in order to ensure a 40 year lifetime.

2. ADSS Degradation Mechanisms

Two mechanisms are the cause for the problems that have been seen on ADSS cables in high voltage systems. They are erosion due to tracking of the outer jacket, and damage to the outer jacket caused by corona. The two mechanisms of tracking and corona are different, and must be approached differently and separately in order to ensure long-term reliability of the system. Both of these mechanisms become problematic when they damage the outer sheath of the cable to the point that the underlying aramid strength yarns of the cable are exposed to UV light and the water of the surrounding environment. Once this occurs, the aramid yarn can lose strength, and ultimately the cable will break into two pieces, destroying the optical fibers in the process.
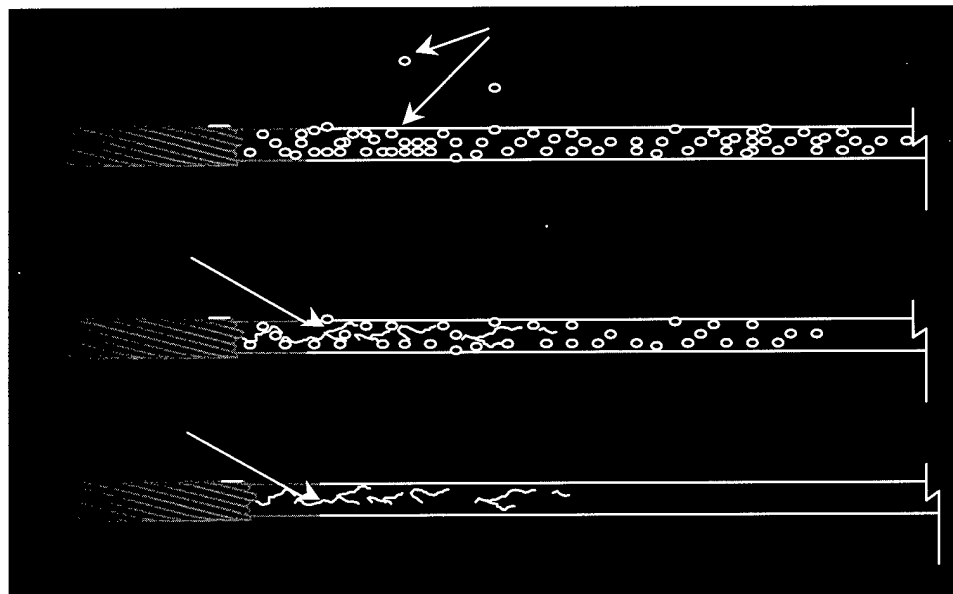
2.1 Tracking

Tracking erosion is defined as the formation of a conductive path of localized deterioration of the surface of the insulating material. The tracking process of the cable jacket results when a cable is placed in an extra high voltage environment. The towers that the cables are placed upon are grounded, resulting in a strong voltage gradient very near the structures. This voltage gradient serves as the catalyst for scintillation from the span to the structure during repeated wetting and drying of the cable's jacket. If the cable material cannot withstand the effects of this scintillation, degradation of the jacket will result, leading to the tracking process described above. Figure 1 illustrates the concept of the space potential vs. span length.
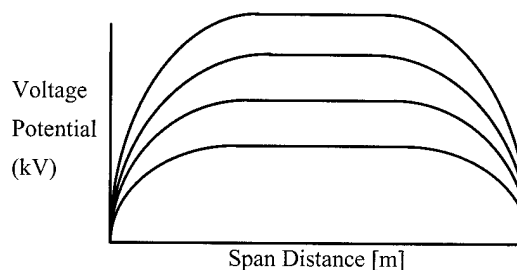
Figure 1. Space Potential Vs. Span Length

As the cable's jacket is subjected to repeated wet - dry cycles, if the jacket cannot resist the electrical stresses imposed by the scintillation, tracks may form on the cable. This process of wet – dry cycles and the onset of tracks is shown in Figure 2.

generated. It is well-documented that polymers which are exposed to large concentrations of ozone will ultimately become more brittle. Since ADSS cables are required to stretch during ice and wind loads, brittle polymers will ultimately split during the

Figure 2. ADSS Cable Tracking Mechanism

2.2 Tracking Mechanisms

Four different mechanisms are present during the tracking process. Each of these mechanisms will be discussed further.

First, the tracking process results in an actual mechanical etch of the cable's outer jacket. This mechanical etch results in a "chipping" away of the material, caused by the power of the arc. This process has been compared to the process that occurs during electrical discharge machining (EDM). EDM uses electrical arcs to remove metal during manufacturing of various metal and carbide parts. Clearly, any material considered for use as a "Tracking Resistant" type jacket must be able to withstand the energy in the arcs in order to resist this chipping effect.

The second mechanism that occurs during the tracking process is the generation of heat. Current flow across the cable surface results in increased heating of the jacket material. If the material used for the outer jacket cannot withstand the level of heat produced by the tracking mechanism, the polymer will flow and yield, ultimately causing the jacket to separate. This will in turn expose the aramid yarns. The majority of ADSS failures that have been described in literature can be attributed to jackets extruded with thermoplastic materials that cannot withstand the heat of the arc, and the subsequent melting and displacement of the material.

The third mechanism that occurs during the tracking process is the production of ozone as a by-product of the electrical arcs that are

elongation that occurs during these loads, exposing the aramid yarns. Therefore, the jacket material chosen must be able to withstand the effects of ozone.

Finally, carbonization of the sheath material could occur during the tracking process. This carbonization produces a lower - resistance preferential path for subsequent arcs. Future arcs will follow these lower resistance paths, continually eroding and melting the jacket of the cable until it is breached. A cable which has experienced tracking is shown in Figure 3 below.

Figure 3. Tracking Damage on ADSS jacket

2.3 Methods to prevent Tracking - Related Damage

In order to prevent tracking-related damage, each of the four mechanisms listed in the previous section must be addressed. A fully integrated solution incorporating both advanced materials and advanced applications engineering is essential. This portion of the paper will discuss the ways to avoid tracking-related damage.

The first mechanism mentioned above is the mechanical etch of the cable's outer jacket. Fortunately, mechanical etching only occurs in cables which are able to withstand the effects of the other mechanisms, meaning that it is seen as the dominant mechanism only at very high space potentials. Clear understanding of the ROW's electrical characteristics is essential in order to accurately map the space potential at the location of the ADSS. The main way to avoid this mechanical etching is by placing cables in relatively low space potentials through effective applications engineering.

The second mechanism mentioned is the heat generated by the arcs. The way to avoid damage by heat is by having cable jackets which are thermoset materials instead of thermoplastic. Thermoplastic materials are materials which have "glass transition" temperatures and which will ultimately soften in the presence of heat. Thermoset materials are materials which will not soften, but may burn in the presence of extreme heat. . If a cross-linked cable is used, the heat mechanism is neutralized, because the temperatures seen even in extremely high space potentials are usually cool enough such that a cross-linked cable will not burn. Cross-linking of the polymers is the method which is most commonly used to produce a thermoset material. Cross-linking often occurs naturally in polymers over time, but must be performed in cable manufacturing in order to ensure appropriate properties. Unfortunately, the cross-linking process during manufacturing is slow and often expensive. As a result, very few cable manufacturers offer cross-linked products for tracking-resistant jackets.

The third mechanism to address is ozone resistance. Cable manufacturers often include special compounds in the cables to offset the effects of ozone.

The fourth mechanism to address is specific tracking-resistance. Once again, cable manufacturers often include special, and proprietary compounds, to provide resistance to the tracking process.

To summarize, the compounds used by successful ADSS cable manufacturers will be cross-linked polymers with special additives to control tracking and provide ozone resistance. Also, in addition to material requirements, cables must be located in the appropriate environments. Alcoa Fujikura, and other cable manufacturers, use computer programs to specify the location where cables can be safely deployed. These computer programs are used to identify the space potential that exists at the proposed cable location. Space potential is a surrogate measurement for the overall amount of energy in the dry band arcs that are produced. As one might expect, the closer that a cable is placed to a conductor, the higher the space potential. Other factors which influence the space potential calculation include the type and diameter of the conductors and ground wires, the geometric configuration of all conductors, and the phasing of the conductors. Space potential calculation is a relatively common calculation, and the methods that are used by Alcoa Fujikura Ltd. have been validated by the calculations performed by numerous other organizations. Tracking-resistant cables from Alcoa Fujikura are typically specified for a maximum space potential of 25 kV.

Finally, in addition to proper applications engineering, cables must be installed properly, with no sheath damage, in order for them to withstand the effects of tracking. If the cable's jacket is damaged during installation, liquid water can enter the cable and eventually cause damage to the aramid, resulting in eventual cable failure.

As was stated in the opening paragraphs of this paper, Alcoa Fujikura has well over 10,000 km of cable with tracking-resistant outer jackets deployed in EHV environments, with many examples of cables on 220, 230, 345, and 500 kV lines. A full customer list is available from representatives of Alcoa Fujikura Ltd. As was also stated earlier in the paper, there have been **zero failures** of AFL's ADSS cables caused by tracking of the outer jacket with cables that have the tracking-resistant outer jacket.

2.4 Corona Mechanism

Corona is defined as "the audible and luminous discharge of metallic elements when electric field intensity exceeds the dielectric breakdown strength of air." Essentially, corona occurs when the electric field is high enough to ionize the air. Corona is well understood as it applies to power cables, and some of the same rules apply. The surrogate measurement that is used to predict when corona will occur is electrical field strength, typically measured in units of kV/cm. Please note that this measure is different than the space potential unit of kV.
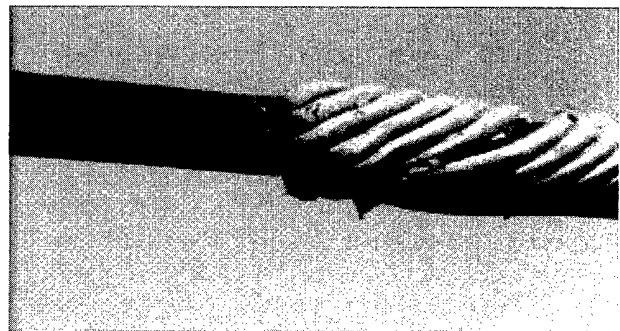

Figure 4. Corona Damage on ADSS jacket

Corona damage is most likely to occur at the end of a rod tip that sticks out the farthest from the group of the several Structural Reinforcing Layer rods. The end of the rod tip serves as an electrical stress concentrator, and therefore is the place where corona is seen. Corona damage is relatively easy to identify, as corona activity strips off the galvanization from the ends of the armor rods. Also, due to the electrical activity, pitting of the cable jacket is seen right at the tips of the rods. Corona damage is illustrated in Figure 4.

Corona damage is easy to prevent by using specially designed corona protection devices for fiber optic cable. These devices come in several shapes and styles, and are effective at reducing the electrical stress at the location, thereby eliminating the source of corona. The devices are placed to cover the tips of the rods, and lessen the electric field strength, and thereby possibility for corona, at the interface between the cable and the hardware. A picture of a corona ring is shown in Figure 5.

It is very important to know that corona is a different mechanism than dry band arcing or tracking, and must be addressed during the network design stage as a different mechanism. Solutions to prevent tracking damage will not work against corona, and solutions to stop corona damage will not prevent tracking from occurring. Once again, proper engineering of the network is needed to guarantee success.
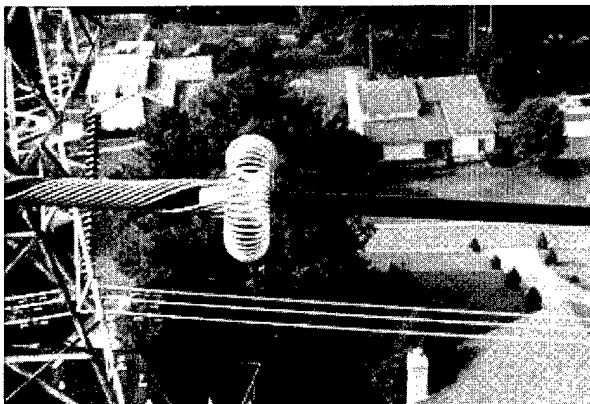
Figure 5. Corona Ring on ADSS cable

3. AFL's High Voltage Experience - Examples of Success

As was mentioned previously in the report, well over 10,000 km of AFL ADSS cable with tracking-resistant outer jackets have been installed in various environments around the world. There have been zero reported cases of problems due to tracking of the outer jacket with these installations. Of the hundreds of installations, two specific ones are discussed below. They are interesting primarily because of the aggressive electrical environment in which the cables are installed.

3.1 Case Study Number 1, Con Edison, New York City

One of the first installations performed by Alcoa Fujikura with tracking-resistant jacket technology was at Consolidated Edison in Staten Island in New York City. The installation occurred in the late 1980s, and the cable has now been operational for over 11 years. The location of the installation is shown in Figure 6 below.

Figure 6. Location of ADSS installation

The installation is interesting for several reasons: This cable is installed on a 345 kV, double circuit line. And, the area is a very high pollution area, close to the Freshkills landfill, the landfill for New York City. Petroleum and concrete factories are also located within 1 km of the route. As can be seen from the location, the cable is also located very near the salt water environment of the Atlantic Ocean. However, the closest water to the cable is brackish water, a mixture of salt and fresh water. The installation was a live line installation. The reason for this is because, Con Edison could not have power outages as they supply the power for New York City. Figure 7 shows the installation site.


Figure 7. Installation site for ADSS

As was mentioned earlier in this presentation, the cable is located in a 40+ kV space potential. The cable is an Alcoa Fujikura Ltd. tracking-resistant cable, originally manufactured by Superior Optics (which was eventually bought by Alcoa Fujikura Ltd.). Corona rings were not originally placed at all locations, but were added on the line upon the recommendation of Alcoa Fujikura Ltd. This is the oldest installation of ADSS cable in EHV environments that we know of, and is also by far the most aggressive. The 40+ kV space potential number has been calculated and confirmed by several sources. The cable is inspected frequently by Con Edison and Alcoa Fujikura, and no signs of tracking of the outer jacket are present. Figure 8 shows a site where corona was seen and caused a limited amount of damage during the first few months after the cable was installed. The corona was easily arrested by the use of corona rings. Corona-induced damage was seen at other sites without corona rings, but was arrested by the use of corona rings. Since no new signs of damage or degradation have been seen, it is expected that this cable will continue to perform well in the future.
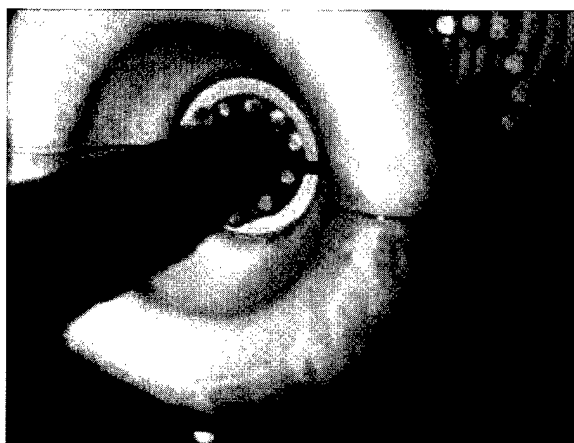
Figure 8. Corona Ring on ADSS cable

3.2 Case Study Number 2, Southeastern U.S.

This cable is on a 500 kV route from Rome, Georgia to the outskirts of Atlanta, Georgia, for a total of approximately 120 km. Part of the line is single-circuit, part of the line is double-circuit. The cable was installed in 1995, with inspections occurring every three years. A tracking-resistant outer jacket was used in combination with corona rings. The maximum space potential for this installation was 25 kV. The single-circuit portion of the installation was installed with the line energized using land-based crews. The double-circuit portion was installed with the line energized using a helicopter-based crew. In this case, the ADSS was installed under the static wire. As expected, no degradation due to either tracking or corona has been seen on this line, and it is expected that this cable will continue to perform well in the future. Figures 9 and 10 show pictures of this installation.
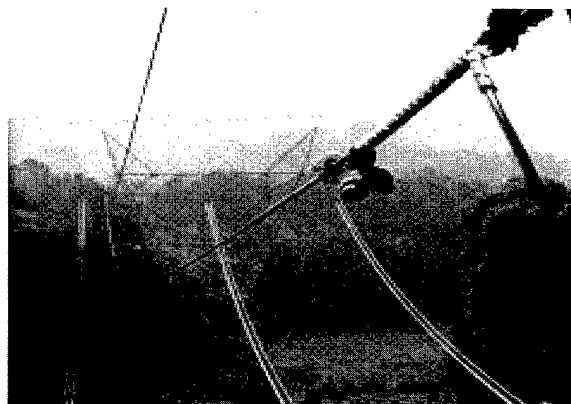
Figure 9. ADSS installed below the static wire
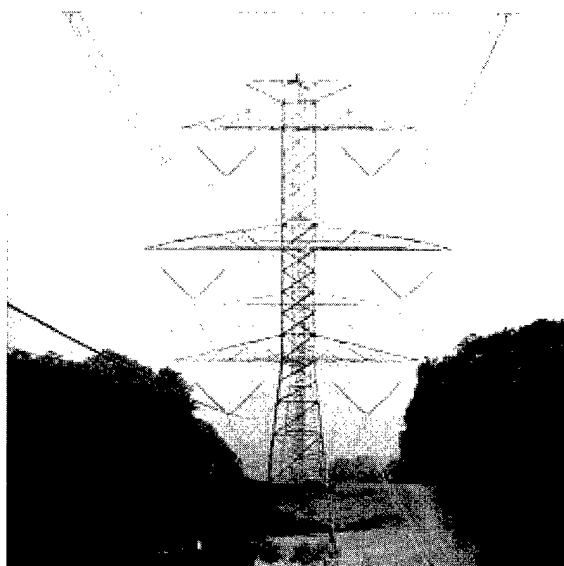
Figure 10. ADSS is in the center of 500 kV circuit

4. Conclusions

As has been shown in this paper, it is possible to successfully and reliably install ADSS cable in EHV environments. Installations have been performed with fine results since the late 1980s. However, it is very important that proper materials and proper engineering be performed in order to ensure success.

As many of the published papers have shown, if the manufacturers and users of ADSS cables on high voltage lines do not fully understand the phenomena associated with HV environments, then problems may result. However, if customers work with knowledgeable manufacturers and take proper care during the engineering and installation of the cables, then the installations will be successful.

5. References

[1] C. Militaru, "ADSS Cables Electrical Corrosion Tests," *Proceedings of the 48th IWCS*, p. 614 – 620 (November, 1999).

[2] C.N. Carter, M.A. Waldron "Mathematical model of dry-band arcing on self-supporting, all-dielectric optical cables strung on overhead power lines," *IEEE Proceedings – C, Vol. 139, No. 3*, (May, 1992).

Authors

Mark Boxer received a Bachelor's Degree in Mechanical Engineering from Georgia Tech in 1988. He has worked in the Applications Engineering Group for Aerial Cable Systems as an Aerial Cable Systems Applications Engineer for the past 6 years, and currently serves as the Applications Engineering Manager for Alcoa Fujikura Ltd.'s Aerial Cable System's Business Unit.

Mailing Address: Alcoa Fujikura Ltd., Ridgview Center, Highway 290, Duncan, SC 29334
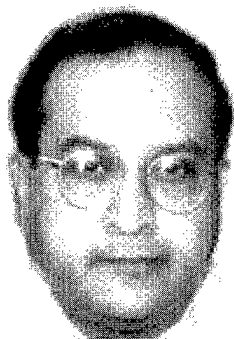
Amitabha Mukhopadhyay received a B.S.E.E degree from the University of Calcutta,India and a M.S.E.E from the Polytechnic Institute of New York. Between 1974 and 1987 he was with Gibbs & Hill, Inc., New York, involved in Design and Engineering of Substations, Transmission and Transportation Systems. In 1987 he joined Con Edison as Electrical Engineer.
He is currently involved with Substation and Transmission Projects as well as E.M.F issues.

He is a member of I.E.E.E. / E.E.I SCC 28 Committee, and is a registered Professional Engineer in New York State.

Mailing Address: Consolidated Edison Co. of New York, Inc. 4 Irving Place, New York, NY 10003-3598
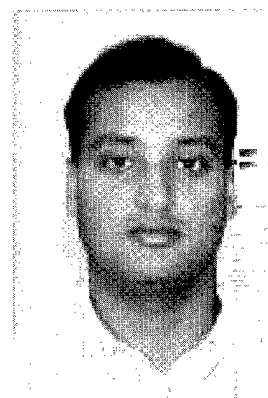
Karthik Krishnamurthy received a Bachelor's degree in Mechanical Engineering from the University of Madras in 1994 and an MS degree in Mechanical Engineering from Virginia Polytechnic Institute and State University in 1996. He then worked for three years in Development and Product Engineering in the fiber optic cable industry. Since 1999, he has been employed with Alcoa Fujikura Ltd. as an Applications Engineer in the Aerial Cable Systems Department.

Mailing Address: Alcoa Fujikura Ltd., Ridgview Center, Highway 290, Duncan, SC 29334

Development of a Dispersion Equalizing Submarine Cable Unit with Pure Silica Clad Fiber

Kenichi Mizoguchi, Hideya Moridaira, Shinji Asao

FURUKAWA ELECTRIC CO., LTD.
Chiba Telecommunication Cable Plant,
Ichihara, Chiba 290-8555 Japan
+81-436-42-1642   k-mizo@ch.furukawa.co.jp

Abstract

The recent optical submarine transmission system with large capacity was based on a combination, primarily consisting of non-zero dispersion shifted fiber (NZ-DSF) with negative chromatic dispersion, and dispersion-equalizing fiber with positive chromatic dispersion, which cancelled accumulated negative dispersion. In generally, pure SiO_2 core fiber had been used as a dispersion-equalizing fiber, because of with high positive chromatic dispersion and ultra low attenuation. (0.175dB/km at 1.55 μ m) Since manufacturing pure SiO_2 core fiber required using fluorine to reduce reflective index at cladding part, the product cost was too expensive, compared to manufacturing conventional Ge-doped core/pure SiO_2 clad fiber. In order to utilize the conventional fiber as dispersion equalizing fiber, it was necessary to solve the problem of optical attenuation, which had a more than 10% higher value than pure SiO_2 core fiber. However this attenuation problem was solved, because of improving attenuation and growing attenuation margin due to introduced amplification system. And this unit, which stranded Ge-doped core/pure SiO_2 clad fiber, confirmed to possess superior unit property, resistance property of water pressure, and temperature cycle property, and few attenuation change in the cabling process.

Keywords

Dispersion equalize, Submarine Cable, Pure silica clad.

1.   Introduction

There were several kinds of structures of optical submarine cable. Example structure was shown in Figure 1. After stranding optical fibers on tension member and consolidation with UV curable resin, the outer surface was covered with three pieces of divided steel tube, some steel wires, and copper layer coating.

Growing capacity of optical submarine cable in recent wavelength division multiplex technology, the optical fiber was using NZ-DSF with so negative chromatic dispersion as to avoid non-linearity effect. And dispersion-equalizing fiber was needed to cancel accumulated negative dispersion of NZ-DSF. General properties, which were required for dispersion-equalizing fiber, were shown in Table 1.
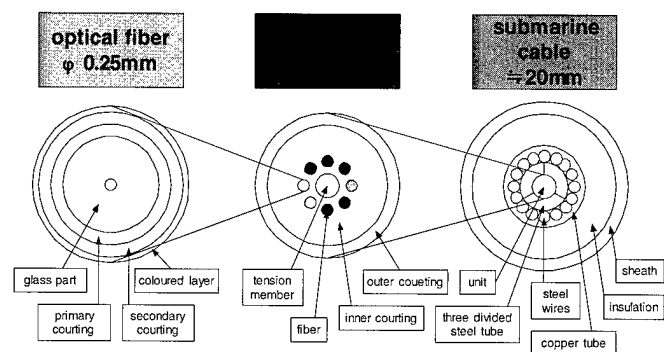
Figure 1. Structure of submarine cable

Table 1. Specification of dispersion-equalizing fiber with positive dispersion

Item *1	Specification
Average attenuation	$\leqq$ 0.190dB/km
Average chromatic dispersion	$\fallingdotseq$ 18.5ps/(nm·km)
PMD *2	$\leqq$ 0.10ps/rkm
Aeff	$\geqq$ 70μ m^2
Macro-bending loss *3	$\leqq$ 1.0dB/m

*1 All property was measured at 1.55 μ m.
*2 PMD was measured on reel.
*3 Bending diameter was ϕ 20mm.

Until now, dispersion-equalizing fiber with positive chromatic dispersion had been used pure SiO_2 core fiber of simple step index profile. This fiber was known to have properties of ultra low attenuation and high chromatic dispersion. However, pure SiO_2 core fiber had a disadvantage. Manufacturing cost was high, as it required utilizing expensive fluorine gas, in order to reduce the reflective index in the cladding part.

The use of 1.3 μ m general-purpose SMF, which was made out of Ge-doped core/pure SiO_2 clad fibers, was theoretically possible as dispersion equalizing fiber on the fiber profile. In order to use it for optical submarine cable, it had to manage to be low attenuation and low macro-bending loss at the same time. To improve macro-bending loss, it was effective to heighten reflective index of core part by higher germanium concentration. But higher germanium concentration might cause fiber attenuation to deteriorate.

This study achieved development in Ge-doped core/pure SiO_2 clad fibers met the specification shown in Table 1. The optical fiber unit using this fiber showed few attenuation change of cabling process. In addition, good long-term-reliability performance of unit was also confirmed, the resistance property of water pressure and temperature cycle property.

2. Improved properties of Ge-doped core / pure SiO_2 clad fiber

2.1 Pure SiO_2 core fiber compared with conventional Ge-doped core / pure SiO_2 clad fiber

The properties required for dispersion equalizing fiber of a submarine transmission system met the following strict criteria: ultra low attenuation (less than 0.180dB/km), high positive chromatic dispersion (more than 18ps/(nm · km)) and good macro-bending property (less than 1dB/m). (All properties were measured at 1.55 μ m, and bending diameter was ϕ 20mm.) These properties were the most appropriate for pure SiO_2 core fiber. Pure SiO_2 core fiber could achieve proper property, including ultra low attenuation. However, on the other hand, from the distribution of reflective indexes as shown in Figure 2, it was necessary to add expensive fluorine gas to the clad, in order to reduce reflective index, resulting in a great disadvantage, a several-fold increase in the manufacturing cost.
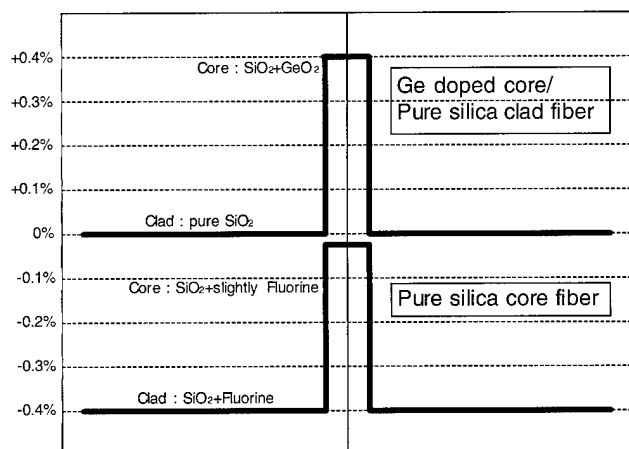
Figure 2. Refractive index profile compared

When the conventional SMF applied to dispersion-equalizing fiber, two problems were attenuation (average, 0.191dB/km at 1.55 μ m) and macro-bending loss (average, more than 10dB/m at 1.55 μ m, ϕ 20mm bending). If higher core germanium concentration and higher reflective index was, it's effective to improve macro-bending loss. However, higher core germanium concentration caused increasing attenuation, it did not result in low attenuation.

2.2 Improved attenuation of pure SiO_2 clad fiber

For achievement of low attenuation of Ge-doped core/pure SiO_2 clad fiber, it was necessary to reduce contamination in the glass, example for OH absorption. And reflective index of core part was so higher as to avoid increase of macro-bending loss. Since viscosity in the glass changed with lower contamination in pre-form glass, furnace temperature on the fiber-drawing was optimized. The result of optimized were shown in Figure 3 using 4 pre-form drawing. As deviation from best temperature was increasing, it was showed attenuation was higher.
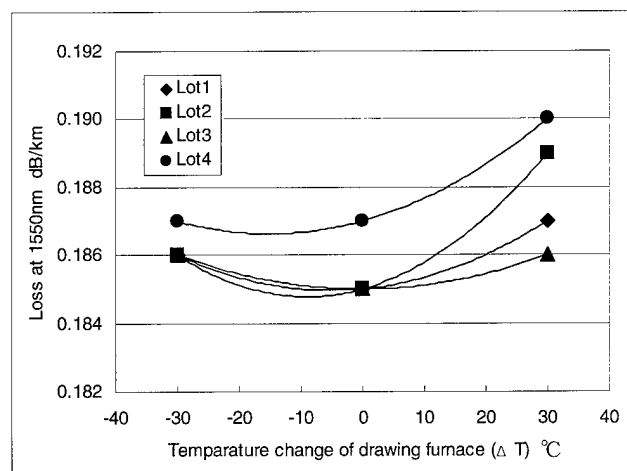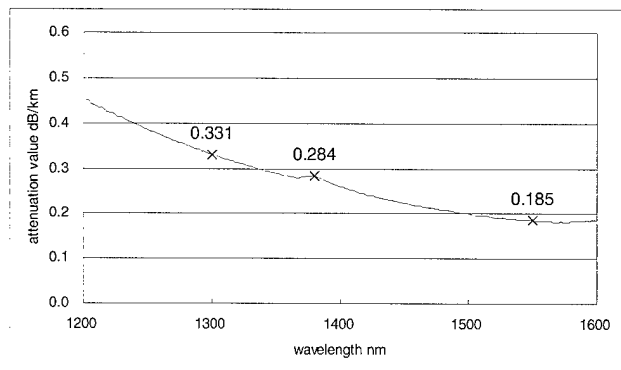

Figure 3. Relationship between temperature of drawing furnace

After optimizing drawing-furnace, average attenuation was 0.187dB/km and minimum attenuation was 0.185dB/km at 1.55 μ m. It was also clear from loss spectra that the effect of removing contamination, near the -1.38 μ m OH absorption peak was observed to be small. (Refer to Figure 4.)

Figure 4. Loss spectra of Ge-doped core / pure SiO₂ clad fiber

2.3 Other properties of pure SiO₂ clad fiber

2.3.1 Macro-bending loss

Since fibers for submarine cable were used under high lateral force, good macro-bending loss was required. The core germanium concentration was so higher as to heighten reflective index, thus macro-bending loss was good value less than 0.1dB/m. The value of macro-bending loss, chromatic dispersion value, Polarization Mode Dispersion (PMD) and effective Area (Aeff) is shown in Table 2.

Table 2. The table of Property Compared

Item *1	Pure silica core fiber	Ge-doped core fiber
Average attenuation	0.176dB/km	0.187dB/km
Average chromatic dispersion	18.6ps/(nm·km)	18.4ps/(nm·km)
PMD *2	0.06 ps/rkm	0.04 ps/rkm
Aeff	75μ m²	85μ m²
Bending loss *3	0.2dB/km	0.1dB/km

*1 All property was measured at 1.55 μ m.

*2 PMD was measured on reel.

*3 Bending diameter was φ 20mm.

2.3.2 Chromatic dispersion

Ge-doped core/pure SiO₂ clad fiber included germanium with higher concentration, it was possible to be influenced by material dispersion of germanium. So it was afraid to be smaller chromatic dispersion value. But chromatic dispersion value of Ge-doped core/pure SiO₂ clad fiber was 18.4 ps/(nm·km), it was similar value of for pure SiO₂ core fiber, 18.6ps/(nm·km).

2.3.3 PMD (polarization mode dispersion)

The measurement with fiber on reel found no difference, and good values.

2.3.4 Aeff (effective area)

The value was larger than pure SiO₂ core fiber. It was possible to change profile to with larger Aeff, because the shape of reflective index profile was simply step shape. Ge-doped core/pure SiO₂ clad fiber was made using VAD method, which had the advantage of good profile controllability over other method.

2.3.5 Fiber proof and splice

For submarine cable, high proof test was required to be loading of 2% strain, for more than 1 second, and for the entire length. The weibull's plot obtained by the dynamic tensile strength test under
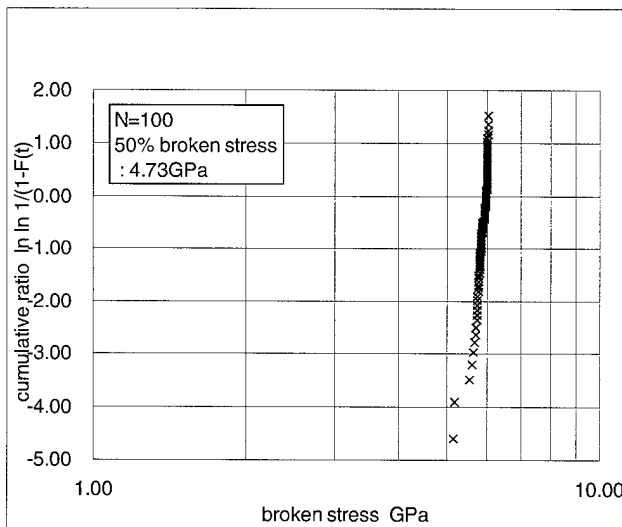
Figure.5 Weibull plot of Ge-doped core / pure silica clad fiber

the condition of non-proof, is shown in Figure 5. No problems were observed regarding its strength.

3. Unit Property of Pure Silica Clad Fiber

3.1 Loss transition of the assembling process

#### 3.1.1 Attenuation of fiber splice

After 2% fiber proof test, fibers with shorter length than unit standard length were taken fiber splice. This process was melting splice, re-coating UV resin, and finally 2.5% proof test for more than one second. The distribution of splice attenuation after this high strength spice process is shown in Figure 6. It indicates good splice attenuation of 0.04dB/km.
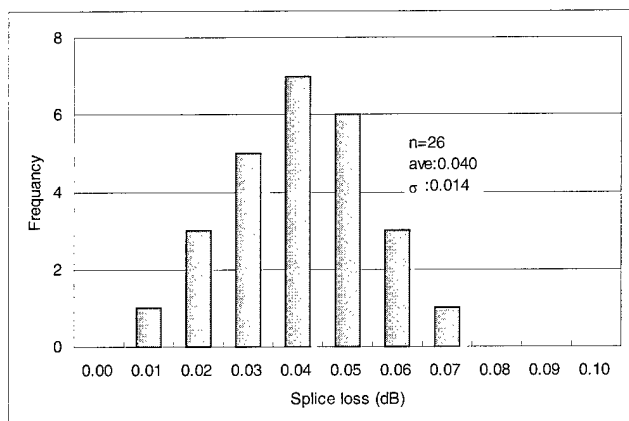
Figure 6. Splice loss value distribution

Attenuation value distribution before and after the assembling process

The process of unit assembling was to consolidate same length fibers and strength member by UV curable resin. These fibers were stranded in a constant direction around strength member with less than 1mm diameter, and consolidated using UV curable resin. If fibers had weak macro-bending property, it caused high increasing attenuation for fibers coated by hard UV curable resin. The distribution of attenuation before and after the assembling process was shown in Figure 7. Using fibers with good macro-bending properties, best loss values were less than 0.19dB/km after assembling, creating no problems.
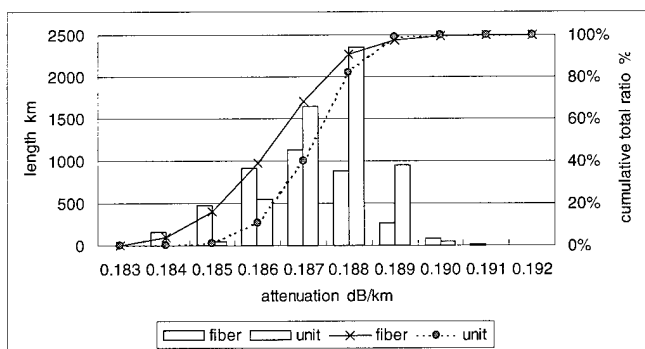
Figure 7. Attenuation value distribution before and after assembling process

3.2 Loss transition of the Cabling process

The attenuation change of product process from optical fiber, optical fiber unit, and cable was shown in Figure 8. It was not confirmed much increasing attenuation as cabling process.
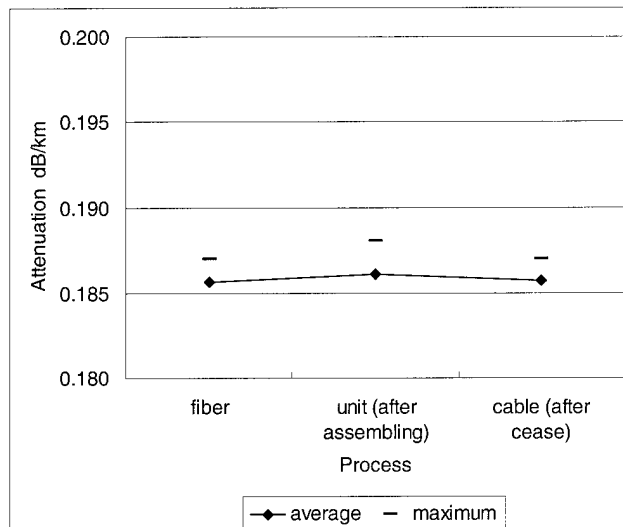
Figure 8. Attenuation change of cabling process

*Fiber attenuation value was measured on reel. Unit attenuation value was measured on ϕ 1600mm drum.

3.3 Unit reliability performance

Unit reliability performance as an optical fiber unit for submarine cable, was estimated to apply high water pressure and temperature cycle change. Water pressure was applied at 9.81Mpa, while monitoring the undersea cable construction. Since attenuation was stable when adding or releasing pressure, no problems were confirmed.(Refer to Figure 9.)
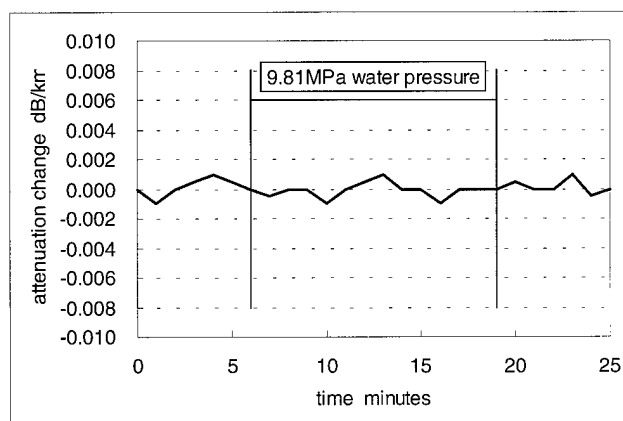
Figure 9. Water pressure performance of unit

*Sample length was 100m

Unit attenuation with temperature change from –20 to 50℃ was shown in Figure 10. It was not confirmed any problems such as increased attenuation at low temperature.
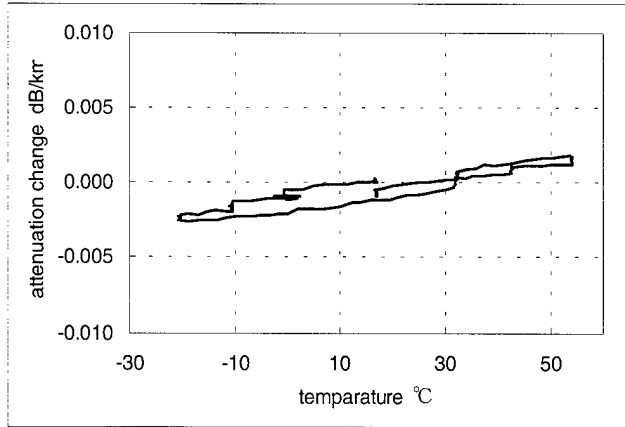
Figure 10. Temperature cycle performance of unit

4.   Conclusion

Ge-doped core/pure SiO_2 clad fiber was able to put into special use as for dispersion-equalizing fiber, for improvement property of attenuation and macro-bending loss. It was important point of development, to reduce attenuation and macro-bending loss of conventional SMF. An average attenuation less than 0.19dB/km were achieved, on the result of this development. But loss value of Ge-doped core/pure SiO_2 clad fiber was still higher than the value of pure SiO_2 clad fiber, it was more than 0.01dB/km of difference. However the margin of attenuation was so growing as to introduce of Erbium Doped Fiber Amplification (EDFA), cost merit of Ge-doped core/pure SiO_2 clad fiber was more appropriated. Therefore, practical application was realized.

In future optical submarine transmission system, the system composition was to compensate both chromatic dispersion value and dispersion slope. Generally, it was combined Reverse Dispersion Fiber (RDF) and high performance SMF, which modified Ge-doped core/pure SiO_2 clad fiber of this study to enlarge Aeff.

This Ge-doped core/pure SiO_2 clad fiber had some merit, low cost, and fine productivity. Thus, the demand of this fiber for optical submarine cable would expect greatly to increase.

A Novel Undersea Cable Design with Plastic Loose Tube, Low Excess Fiber Length, and Fixed Fiber Termination for Bend Sensitive Fibers

C. S. Ma, S. Bernstein, Q. Zhong, T. V. Kutt, R. J. Rue, C. E. Murphy, G. Gullo

TyCom Ltd.

Eatontown, New Jersey; Newington, New Hampshire

(732)578-7830, cma@tycomltd.com

Abstract

This paper presents a design for an undersea optical cable that successfully resolves the attenuation issues of highly bend sensitive fibers with large mode field diameter used in ultra-high speed broadband transmission. To meet the requirements of the rigorous environment of an undersea cable system, this new design combines a loose tube with low fiber excess length, and uses a new technique of fiber termination in a cable splice box. The result of this approach minimizes the microbending of the fiber in the cable and reduces local accumulation of fiber along the cable and near a splice box. Plastic loose tube is utilized in this design, which provides an economical protection to the fibers in a traditional cable structure. The design of the fiber termination in the splice box demonstrates that the fibers can be terminated firmly without significant attenuation change.

Keywords

Large mode field fiber, microbend sensitivity, undersea cable.

1. Introduction

An undersea optical fiber cable traditionally accommodates either tight-buffer (tight-fit) or loose tube design. Due to the increased demand for ultra-high speed broad band transmission, fibers with larger mode field diameter (or effective area) are needed. These fibers are usually highly bend sensitive. To resolve this issue, some have proposed coating traditional fibers with a layer of larger diameter UV acrylate [1], while others have moved away from the loose tube design and utilized a tight buffer [2] to control the loss in the cable. According to our experience, the cabling process usually generates some degree of microbending within the fibers in a tight buffer structure. A large mode field diameter fiber with high bend sensitivity is more vulnerable to increased loss in the tight buffer design. Figure 1 shows the fiber attenuation results comparison between a loose tube cable and a traditional tight buffer cable.

This development work demonstrated that the loose tube design, with appropriate fiber excess length control, provides a benign environment for the fibers and produces low loss during and after cabling. In addition, the design of the fiber termination in the cable joint constrains the fibers to avoid any local loss increase and makes cable handling, such as deployment and recovery, identical to that of a cable with tight buffer design.

In the following sections, details of the design, properties and cable performance are discussed.
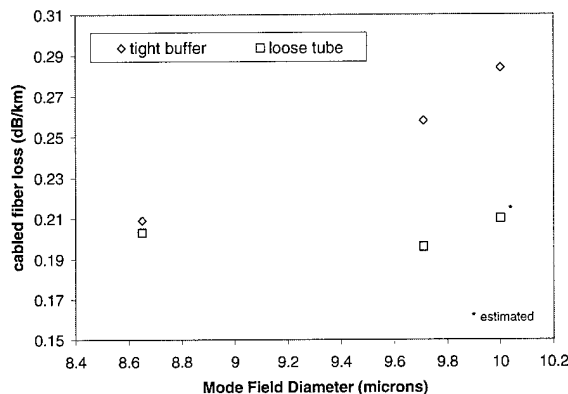

Figure 1 Fiber attenuation with different MFD in different cable designs

2. Cable

2.1 Core Structure

The core of the undersea optical fiber cable is a loose tube using a traditional thermoplastic tube material. Gel is used in the tube which serves as a filling compound to prevent water ingress and to gently support the fibers to reduce the impact of microbending. The fill ratio of the gel is designed to be as high as possible to reduce voids and increase the waterblocking effectiveness. The fiber count varies and is being pursued up to 16 for a 17-mm size cable and 24 for a 21-mm cable. Fibers are laid in the tube straight without helix.

2.2 Cable Structure

The basic design of the cable structure remains the same as a tight-buffer cable but the core is replaced by a loose tube. Outside the tube, twenty-four stranded wires form a tight package surrounding the loose tube as shown in Figure 2. Next, copper tape is welded and swaged down on the wires to serve as an electrical conductor and a protective sheath. Then a polyethylene jacket is extruded over the copper to serve as insulation. This structure is designated as "Light Weight" (LW) cable. For additional strength and abrasion capability, armor wires can be added to the outside of the LW cable to create different types of protected cable.
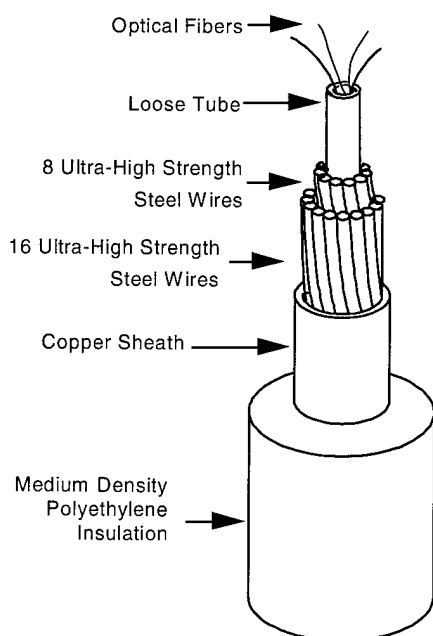
Figure 2. Loose Tube Cable (LW) Structure

2.3 Material

2.3.1 **Loose Tube** There are several important advantages in the use of a thermoplastic material such as Polybutylene Terephthalate (PBT) in an undersea loose tube construction. (1) A plastic tube is more economical than a metallic tube in both raw material cost and the capital costs of the processing equipment. (2) Unlike a metallic tube construction which requires a longitudinal jointing technique (consequently introducing seams), plastic can be extruded, thus eliminating concerns about seam reliability. (3) PBT affords excellent dimensional stability and surface morphology to minimize optical impact on enclosed fibers. (4) PBT has proven to be very stable for the operating environment of undersea cables, has no corrosion issues and is thus unlikely to generate hydrogen in the presence of seawater. (5) In addition to the material stability, the shrinkback characteristics of PBT are utilized to effectively control the excess fiber length in the loose tube.

An extensive material qualification program was carried out to evaluate PBT, including its physical and chemical properties. Specific qualification items included hydrolytic stability, melt flow characteristics before and after processing, water content, degree of crystallization, and compatibility with other cable construction materials.

2.3.2 **Filling Compound** The cable filling compound, or gel, must also be chosen carefully. In evaluating different sources of gels, emphasis was placed on the rheological properties, specifically, the viscosity and critical yield stress. Based upon analytical modeling and cable attenuation testing, a range of a

critical shear stress of 0.003 to 0.010 psi and a cone/plate viscosity of 20,000 to 40,000 cps were established to be the optimum value ranges for loose tube construction. The choice of such rheological property ranges allows us to control the coupling of fibers to the loose tube in such a way that sufficient excess fiber length (EFL) is maintained to allow fiber movement during the loading and unloading of tensile strain, while preventing water ingress in the event of a cable cut.

The characterization of gels involves an assessment of both static and dynamic rheological properties, which are related to both tube processing and the resultant fiber properties. In addition, extensive chemical and physical evaluations of the gel properties, such as volatilization of gaseous species (including hydrogen) and gel compatibility with tube and fiber coating materials, were carried out.

3. Cable Properties, Performance, And Qualification

3.1 Excess Fiber Length (EFL)

To minimize the interaction of fibers in a loose tube, the excess length of fibers must be tightly controlled, especially at the last stage of the manufacture process. During tube manufacture, the fiber excess length is controlled to be less than 0.20%. In the process, which adds the steel strand wires and copper sheath, the tube strain is controlled to make the EFL in the strand wire package 0.05% or less. During the polyethylene extrusion process, the fiber strain in the cable is generally unchanged. Figure 3 shows the change of fiber attenuation after various process steps. The fiber attenuation is significantly improved from loose tube to cable, which correlates to a significant reduction of excess fiber length. In the final cable stage, the fiber is almost straight in the tube.
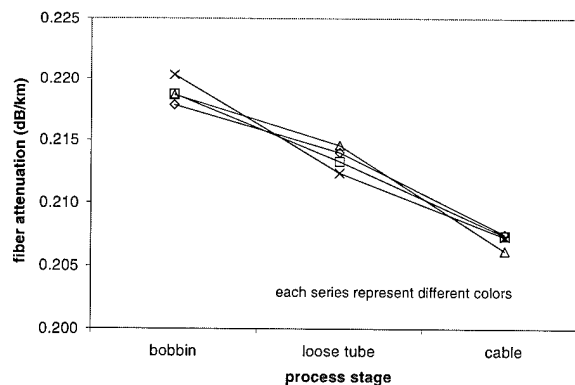

Figure 3. Fiber EFL and Attenuation Relationship

3.2 Fiber Count

The fiber count for 17-mm cable, with tube inner diameter of 1.88 mm, was tested for up to 16 fibers. The average attenuation of fiber relative to fiber count is shown Figure 4. The slightly higher

cabled fiber losses for the 4 and 6 fiber counts are believed to be the result of unstable EFL during the early stage of production. The results show that the fiber count does not significantly affect the fiber attenuation in a 17-mm loose tube cable up to 16, which gives a packing density of 29%.
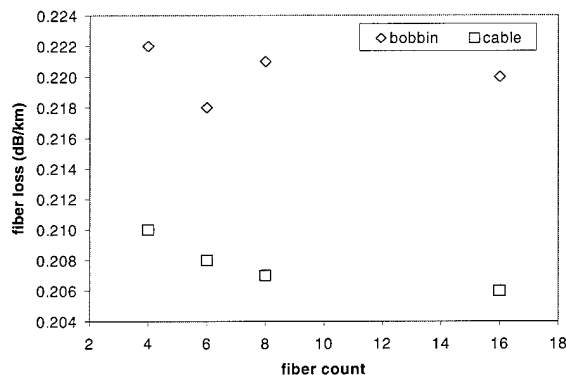

Figure 4. Cabled fiber loss versus fiber count

3.3 Gel Fill

The gel fill is a critical parameter affecting water ingress. This value is defined as the average ratio of actual gel volume in the tube to the total volume available. The gel fill is controlled to approximately 95%. It was found in water ingress tests with cable sample lengths of 250 meters that the gel fill could be as low as 87% and still pass the test. For a 1-km test length, the cable must withstand a pressure of 8000 psi for two weeks without water leak. In fact, the actual water penetration in this test was less than 10 meters. From the gel fill, the critical shear stress of the gel, and the length of the cable sample, it was calculated that a 1-km cable could withstand well more than 8000 psi without water ingress through the full length.

3.4 Qualification

A series of qualification tests was conducted which subjected the cable to the most severe in-service environmental conditions of tension, bending, temperature, and pressure expected in the field. This design has met the requirements without any issues. A primary area of focus was the coupling and the interaction between the fibers and the loose tube gel medium. Test procedures were developed to permit measurement of the EFL on 100-meter long test specimens after the tube manufacturing stage and in the finished cable stage. Other testing focused on the shear interaction between fiber and gel. A number of trial lengths of loose tube with different gel types were manufactured and tested. Figure 5 shows a comparison of the shear adhesion properties of different gels in cabled loose tube with the fiber unrestrained at the specimen ends. Gel A was chosen due to its better coupling with the fibers. Once this most favorable gel material was characterized, cable manufacturing parameters could be specified to provide the tight control of EFL desired in the finished cable.
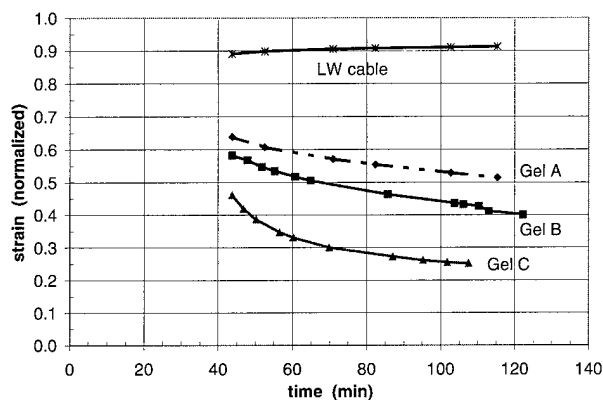
Figure 5. Shear adhesion of fiber in different gels

Using optical phase delay test methodology for fiber strain measurement, testing on finished cable lengths was conducted to determine the final EFL for the product. Figure 6 shows fiber slack measured during tensile testing on a LW cable specimen.
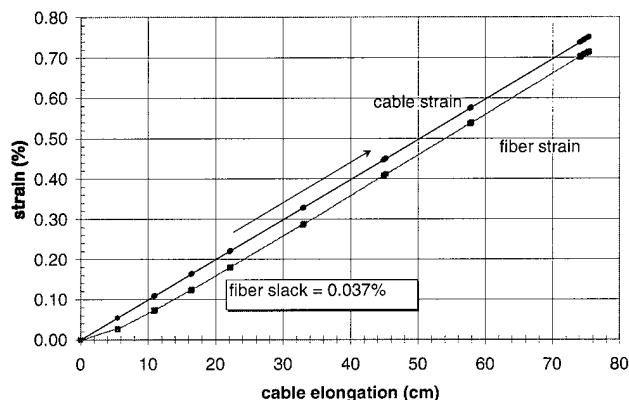

Figure 6. EFL test of a 17 mm LW cable

4. Joint Design, Performance And Qualification

4.1 Joint Design

The cable-to-cable joint and cable-to-repeater coupling anchor assembly are required to withstand the forces of deployment and recovery and to withstand ocean environments including pressure of up to nearly 15,000 psi. They must provide reliable connections for fibers which transition from the cable structure and for splicing. Joints and couplings must also be capable of withstanding full system voltage for the system lifetime requirement of 27 years.

When the cable core design was changed from one using an extruded elastomer with a central wire to the loose tube, a new method for preventing the fibers from moving into the cable structure from the joints became necessary. A ferrule and holder were developed. The fibers are splinted and potted within the ferrule. A commercial product originally designed as a mass fusion splice holder provides adequate strength and shows low loss under tension, which recovers when the tension is removed. The ferrule does not damage the fiber coating during severe load and temperature exposure tests. The ferrule retainer assembly has a trough that contains and restrains the ferrule. Tension forces applied to the fibers are transferred to the joint through the retainer assembly. The PBT tube is reliably fixed to the cable structure and does not require restraint at the joint. Other features of the joint required slight modification to accommodate the new fiber trajectory and placement in the joint. The details of the joint are shown in Figure 7 below.
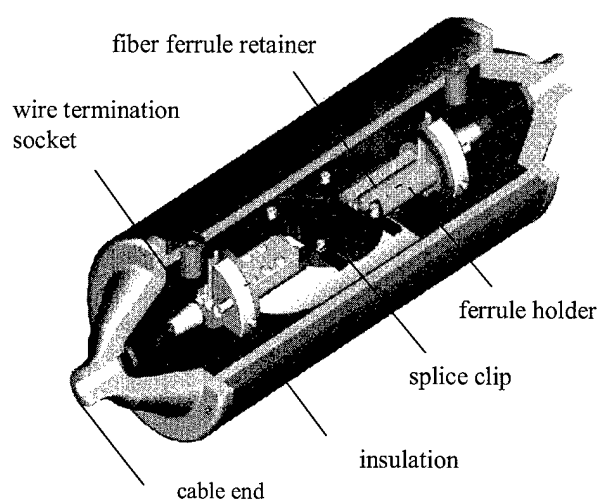
Figure 7. Cable-to-cable joint

4.2 Qualification

A standard set of qualification tests is performed whenever joint designs are altered significantly. For the loose tube joint, bench tests were done to verify the fiber retention and optical loss characteristics of the ferrules. These included temperature cycles and simulated loading during cable tension with a design factor (multiplier). Then joints within 100-meter cable samples completed the listed tests. Criteria included no visible damage or excursive or residual loss greater than .05 dB times the number of splices in the joint.

Tests:

Storage Temperature Test
Shock and Vibration
Applied Torsion
Sheave Laying and Recovery
Tensile with and without Swivel

Cyclic Tension
Hydrostatic Pressure
High Voltage

Figure 8 shows a tension test result for the joint. The fibers show slightly higher but stable loss during peak load holding, and the losses come back to normal after loading.
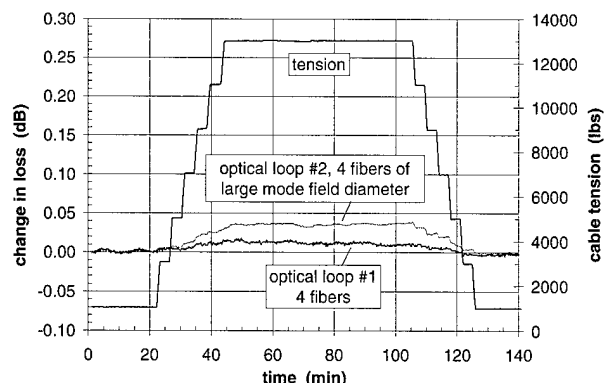
Figure 8. Tensile test results of cable to cable joint

Separate tests were done to qualify the insulation molding process. The optical loss was monitored during the molding process.

5. Sea Trial

The purpose of the sea trial was to study the performance of the fiber in the loose tube cable and in the cable-to-cable joints during deployment and recovery. The sea trial was conducted in November, 1998 in the western Atlantic at an ocean depth of 5000 meters. Three different cable joints and cable joint designs were integrated into the cable. The designs that were studied employed various methods of fiber restraint: an unrestrained fiber, fiber restrained with a drum, and fiber restrained with heat-shrink ferrule. A cable repair operation was simulated and a shipboard cable joint with unrestrained fibers was constructed. The shipboard joint was then deployed and recovered.

5.1 Deployment and Recovery

The sea trial cable system was deployed at an average payout speed of 2 knots. During deployment, the behavior of the fibers was quite stable. No significant attenuation changes were observed in all of the fibers with the attenuation in most of the fibers showing no change. The maximum increase in attenuation in one of the fibers was less than .01 dB/km.

Cable recovery tensions are greater than tensions during deployment and larger changes in measured optical attenuation were seen during recovery. The average loss increase in the fibers ranged from 0.0047 to 0.016 dB/km. After complete recovery, the residual average loss increase was 0.005 dB/km of all the cables.

5.2 Cable Repair Operations

The cable-to-cable joint deployment and recovery cycle was followed by cable redeployment, cutting of the cable midspan, grappling of the two ends, and a shipboard cable-to-cable joint. The shipboard joint was then deployed and recovered. The cable was grappled and although the grappling hooks secured the fibers and prevented any fiber movement, slight movement of the fiber was observed after the cable end had been brought to the jointing area.

5.3 Repair Joint

The change in fiber attenuation in the cable joints with restrained fibers was insignificant. The optical attenuation measurements at the cable joint with unrestrained fibers indicated unstable fiber pull-in and loss increase. After dissection of the cable joint, the fiber pull-in was measured to be in the range of 5.5 to 6.4 inches from deployment to complete recovery. Due to this fiber pull-in, two fibers showed a higher local loss increase in the range of 1.3 to 5 dB. This confirmed that the unrestrained fiber joint design was inappropriate for this cable design.

6. Conclusion

This cable design is now in steady production. Several systems have been successfully deployed and their excellent performance demonstrates that this design is adequately benign to the bend sensitive fibers with larger mode field diameter. In addition, this simple but robust design with economical yet reliable materials makes this cable system easy to manufacture, handle, and repair.

7. Acknowledgement

The authors would like to acknowledge the valuable suggestions made by S. Shapiro and R. F. Gleason of the Department of Undersea Cable Development & Implementation during the preparation of this paper.

8. References

[1] K. Mitsuhashi, T. Hayano, T. Shimomichi, T. Abiru, K. Oohashi and M. Miyamoto, "Development of Submarine Optical Cable Unit Using a Large Effective Area Fiber", IWCS 48th Symposium, p. 312 (1999).

[2] O. Nagatomi, K. Yamamoto, H. Wakamatsu, R. Kanda, R. Morikawa, "Development of New Tight-Fit-Type Submarine Cable with Large Core Fibers for WDM System, IWCS 48th Symposium, p. 317 (1999).

AUTHORS

Chung-Shin Ma

TyCom Laboratories
Rm. 1E208
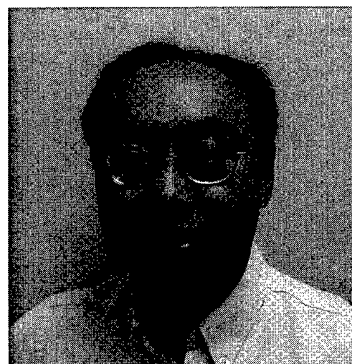250 Industrial Way West
Eatontown, NJ 07724

Chung-Shin Ma is a Distinguished Member of Technical Staff of TyCom Laboratories. His current work includes new cable design and development, process study and improvement, and project management. He joined TyCom (previously TSSL) in 1997. He obtained his Ph.D. from the Engineering Mechanics of Iowa State University.

Steve Bernstein

TyCom Laboratories
Rm. 2F209
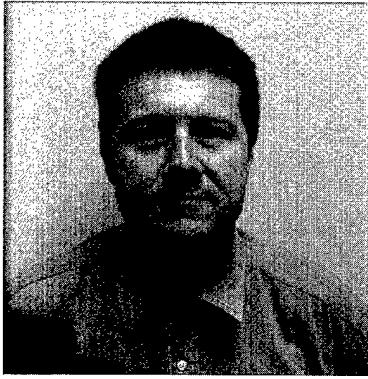250 Industrial Way West
Eatontown, NJ 07724

Steve Bernstein has been employed by AT&T Undersea Systems and then Tyco since 1982. He has worked on joint and coupling development as well as insulating processes. Steve has a BSME from Fairleigh Dickinson U. and an MSE-ME from the University of Michigan.

Qian Zhong

TyCom Laboratories
Rm. 1F213
250 Industrial Way West
Eatontown, NJ 07724

Qian Zhong is a Distinguished Member of Technical Staff at TyCom Laboratories. He joined AT&T Bell Labs in 1992 after receiving his Ph.D. from the University of Pennsylvania. He is responsible for materials design, development, and reliability issues in the undersea systems.

Ralph J. Rue

TyCom Laboratories
Rm. 1E215
250 Industrial Way West
Eatontown, NJ 07724

R.J. Rue received his AAE-MET degree from Vermont Technical College, and his BS-MET degree from Trenton State College. He joined the Undersea Systems Cable Development & Implementation Department at AT&T Bell Laboratories in 1984. His work has been focused on the development testing and analysis of fiber optic undersea cable designs and related hardware. He is currently a Senior Member of Technical Staff with the Cable Development Division of TyCom Laboratories and is responsible for development and qualification testing of new cable, joint, and coupling designs.

Tiiu V. Kutt

TyCom Laboratories
Rm. 1E206
250 Industrial Way West
Eatontown, NJ 07724

Tiiu received her doctorate in civil engineering and engineering mechanics from Columbia University in 1985. Since then, she has worked in several organizations at AT&T on a broad range of problems involving telecommunications cable and repeater installation and recovery as well as tow cables. She is currently part of TyCom, Ltd.

C. E. Murphy

TyCom Integrated
 Cable Systems
2073 Woodbury Ave.
Newington, NH 03801

C. E. Murphy is the Manager of Product Engineering at TyCom Integrated Cable Systems. He joined TyCom in 1985. He has held a few positions at TyCom including Development Engineer and Product Engineer. His major contributions to fiber optic ocean cable are in the areas of cable and joint design and development. He is a member of IEEE and holds an A.S.E.T. from New Hampshire Technical College, and a B.S. in Management and an M.B.A. from New Hampshire College.

Gary Gullo

TyCom Integrated
 Cable Systems
2073 Woodbury Ave.
Newington, NH 03801

Gary Gullo joined Simplex Technologies in 1999 as a Product engineer after working in polymer cross-linking R&D field. He is currently involved with jointing development and testing, quality integrity issues, chemical / polymer compatibility, and fiber coating issues. Gary attended the University of Massachusetts at Lowell where he obtained his B.S. in Plastics Engineering in 1996 and is near completing his M.S. in Plastics Engineering.

Development of High-Count Tight Type Fiber Unit for Submarine Cables

Juan C. Aquino, Kazuto Yamamoto, Osamu Nagatomi, Hirofumi Wakamatsu, Ryo Kanda,
Rokuro Morikawa

Engineering Development Department, Submarine Systems Division, OCC Corporation
Kitakyushu, JAPAN
carlos@occ.ne.jp

Abstract

In this paper we describe the development of high-count tight type fiber unit for repeatered submarine cable systems. This highly reliable tight type 16 fibers unit design, based on OCC's 12 fibers unit for repeatered and 24 fibers unit for repeaterless systems, has been optimized for its use with newly developed fibers that are micro and macro bend sensible. This new unit design combined with fibers for dense wavelength division multiplexing (DWDM) communication systems applications was aimed to respond to the growing demand of trans-oceanic ultra high capacity links and at the same time conform the reliability requirements for submarine cables. The developed fiber unit was cabled and evaluated applying it to the OCC-22S LW cable, considering the power feeding requirements of 8 fiber pairs and that it is one of our most reliable cable designs with a well known performance. As the result of field evaluation during a sea trial we confirmed that the new fiber unit is fully applicable to our current cable design.

Keywords

High-Count; tight type fiber unit; submarine cable; DWDM.

1. Introduction

The trend toward ultra high speed optical communication systems impulsed by the fast growing information technology, e-commerce and internet traffic have created new needs in the submarine cable network field. High channel capacity, highly reliable and short development/evaluation period are the requirements of nowadays planned optical submarine cable networks that are to be linking major points in Europe and North America to Asia and South American countries. Trans-oceanic submarine cable system's construction expenses represent a big portion of the system budget, therefore technology that allows ultra high capacity under the same construction costs has become the most attractive option. As methods to achieve high channel capacity in submarine cable systems (1) enhanced wavelength multiplexing on a limited bandwidth, (2) cable with high fiber count design and (3) extended bandwidth (L-Band deployment) approaches has been done.

To achieve (1) the combination of large core effective area fiber and reversed chromatic dispersion (CD) slope fiber has been proposed as an alternative to reduce fiber's non-linearity effects. Also fibers with reduced CD slope that mitigate the effects of chromatic dispersion in DWDM systems can be mentioned. However these fibers designs were optimized to reduce non-linear effects due to launch power as well as CD effects in long-haul systems and allow fairly good

channel increment, compared to nowadays fibers for WDM applications they are more micro and macro bend sensible [2]. This represents a big obstacle when trying to cable the fiber with out affecting its optical attributes. To achieve (2), supposing that we keep the same fiber density, applying same design as actual units will lead us to a very large unit, which may not be affordable nor applicable to our current cable design. Therefore to realize an enhanced fiber density we must optimize the unit design taking in to account that micro and macro bend sensibility as well as cost represents very tight design constraints.

These needs made us analyze the design of our highly reliable fiber unit for repeatered and repeaterless system applications[1] so as to obtain a high count tight type fiber unit for repeatered submarine systems, capable of holding newly developed optical fibers for DWDM applications as well as to be applicable to current cable design. This time we succeed at cabling newly developed fibers for DWDM applications using optimized high-count fiber unit design. Results of unit's optimization and evaluation as well as manufactured LW cable's field evaluation are presented.

2. Fiber Unit Design

To achieve highly reliable fiber unit design that can be manufactured with our existent machinery we decided to analyze the thigh type design applied in repeatered and repeaterless cable systems. Moreover, we decided that new fiber unit is to be deployed with one of our actual well known cables design in order to obtain enhanced reliability and operability of final cable. Here the unit's outer diameter was fixed. The next step and most difficult one was to decide the fiber layer structure and fiber spacing so that optical attributes of unitized fibers are not affected. In order to evaluated the performance of each possible design we manufactured several short length sample units and conducted some test on each one of them. Evaluation results regarding four of those samples, referred to as design type A ~ D, are introduced.

3. Unit Evaluation

The fiber applied to each of the manufactured samples was a common well-known single mode fiber for submarine applications. The effect of unitizing the fiber is evaluated by comparing the optical characteristics of the fiber before and after the process. Finally the best design is selected and applied to manufacture a long length cable.
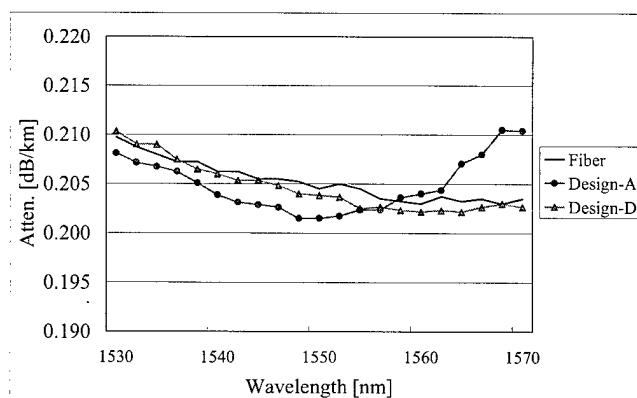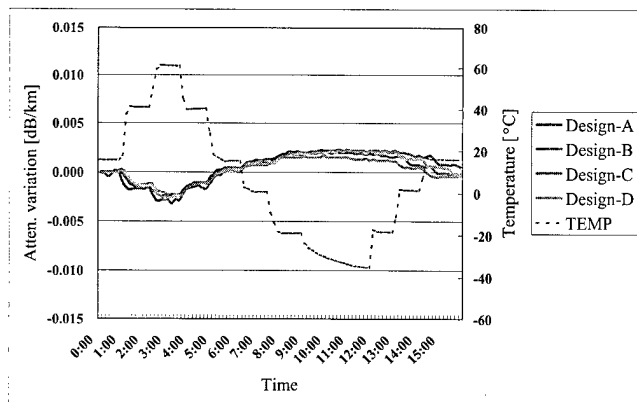
3.1 Spectral Characteristic

Each manufactured sample was evaluated by comparing the fiber's attenuation spectral characteristic before and after unitizing process. Figure 1 shows characteristics of original fiber and unitized fiber for the most representative cases, it can be noted that spectral characteristic of fiber unitized using Design-A shows almost the same tendency of original one until a point around wavelength 1550 nm where the characteristic curve has a turning point. Beyond this point attenuation increases with wavelength. For Design-D case, spectral characteristic of fiber agrees with original fiber's one over the all measurement range, showing that unitizing with this design does not affect fiber's optical attributes.

3.2 Temperature Stability

Figure 2 shows temperature stability test results for four different unit designs. The samples are temperature cycled between -40 °C and +60 °C around a reference temperature of +15 °C, while variation on attenuation characteristic is monitored continuously. Based on previous results, we confirmed that temperature stability of each design is at the same level of conventional 8-fiber unit applying the same single mode fiber and that also residual variations are in the range of actual in-service products.

Figure 1. Spectral attenuation characteristic of unitized fiber

Figure 2. Temperature stability characteristic of various unit design

3.3 Mechanical Characteristics

In Table 1, results of repetitively bending the fiber unit are shown. This test is conducted as part of the unit's mechanical characteristic evaluation program. It can be seen that Design-C is more bend sensible than Design-D. After the test, residual variation is very small for both unit designs so confirming that attenuation increase during Design-C evaluation has direct relation to unit structure.

Table 1. Mechanical Characteristic evaluation (Bending test results)

Test Item		Design-C	Design-D
Repetitive Bending Test	Attenuation increase	-0.010 dB	0.000 dB
	Attenuation decrease	0.000 dB	0.001 dB
	Residual variation	0.000 dB	0.001 dB

3.4 Design Selection

Based on evaluation results described here, selection of the optimum fiber unit design is analyzed. Concerned about spectral attenuation characteristic of fiber unitized with Design-A in the wavelength range ≥1550 nm we decided to avoid applying this structure considering that enhanced bandwidth must to be achieved. Regarding mechanical performance of Design-C, we considered that cable applying this fiber unit might have some issues regarding mechanical performance during evaluation process after cabling. Finally, we have to decide between Design-B and Design-D units, which showed almost the same performance during evaluation tests so confirming that they might be cabled without problem. Considering that the only difference between those two designs is unit outer diameter and material resources expenses to unitize fiber, we choose Design-D as the design to be used to manufacture a long length unit that is applied to OCC-22S LW cable.

4. Long Length Sample Manufacturing

The selected fiber unit design introduced above is applied to manufacture a long length unit sample utilizing newly developed fibers for DWDM. Then, unit is cabled and thoroughly evaluated.

4.1 Applied Fibers

In order to respond to the fast grow in the demand of ultra high capacity submarine cables applying DWDM technology, we consider the utilization of following fibers to be applied to the newly developed 16 fibers unit design. (1)Hybrid fiber constituted by newly developed large core effective area fiber and reverse chromatic dispersion slope fiber and (2) single constituted fiber with lowered chromatic dispersion slope. Both fibers are optimized to obtain low non-linear effects and low chromatic dispersion slope characteristic.

Also other standard fibers for submarine cable applications are selected so as to evaluate the design for future systems applications as well as actual ones. Table 2 shows typical characteristics of 8 types of fiber. 2 fibers of each type are applied to manufacture long length unit sample.

As introduced above, some of the utilized fibers are combined to obtain better performance. Table 3 shows an example of such a hybrid combination and the expected optical characteristics.

Manufacture unit sample's cross section diagram is illustrated in Figure 3.

Table 2. Characteristics of applied fibers

Fiber Type	Clad Diam.	Aeff @1550 [nm]	Optical Atten. @1550 [nm]	Chrom. Disper. @1560 [nm]	Disper. Slope @1560 [nm]
	μm	μm²	dB/km	ps/nm/km	ps/nm²/km
A	125	69	0.206	-2.5	0.117
B	125	52	0.200	-1.7	0.070
C	125	50	0.202	-2.8	0.054
D	125	101	0.193	18.3	0.063
E	125	23	0.251	-24.1	-0.065
F	125	115	0.187	20.7	0.062
G	125	105	0.168	21.1	0.057
H	125	20	0.274	-47.2	-0.055

Table 3. Characteristics of hybrid fiber

Fiber Combination	Aeff @1550 [nm]	Optical Atten. @1550 [nm]	Chrom. Disper. @1550 [nm]	Disper. Slope @1550 [nm]
	μm²	dB/km	ps/nm/km	ps/nm²/km
D+E	60	0.222	-2.3	-0.002
G+H	60	0.217	-2.0	0.020

4.2 Unit characteristic

Manufactured 16 fibers unit is sampled to perform some evaluation test in addition to those performed during the design

optimization process. Figure 4 shows the temperature stability characteristic measured at the most representative 2 fiber loops. Although we might suppose from the results in Figure 4 that fibers constituting Loop-2 are more sensible to external forces compared to Loop-1 constituting fibers, the amount of attenuation variation in Loop-2 is in the range of values obtained when performing the same evaluation test on 8 fibers unit.
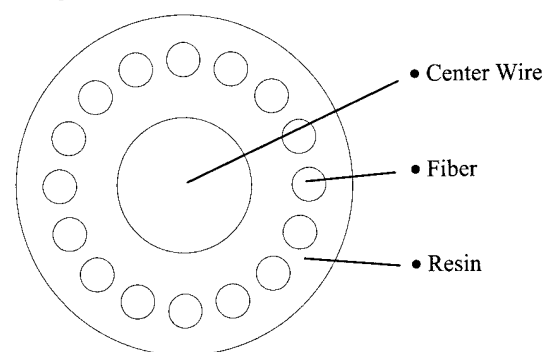
Figure 3. Cross-section diagram of developed fiber unit
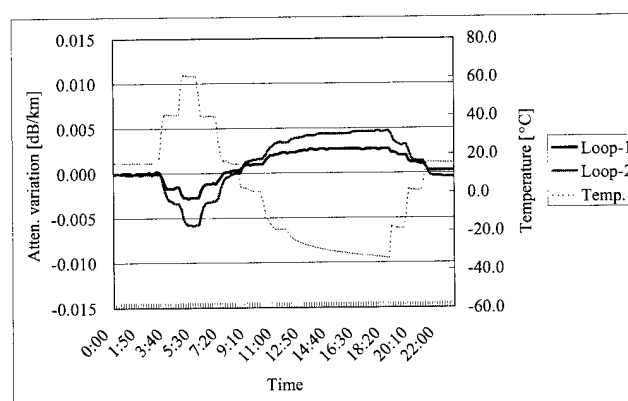
Figure-4 Temperature stability characteristic

Regarding the unit's mechanical characteristics, evaluation conducted on the same loops as above revealed that performance on those fibers are in the same level of nowadays available 8 fibers unit for submarine cable application utilizing fiber for WDM applications. With the obtained results we can be confident that this unit might be cabled without problem.

4.3 LW Cable's Characteristics

Figure 5 shows the structure of manufactured LW cable applying newly developed 16 fibers unit. Cable's characterized dimension and mechanical attributes are described in Table 4. Our experience manufacturing this cable as well as the highly reliable performance that can be obtained with this cable becomes the most important factors when selecting the cable design.

4.3.1 Attenuation Variation At Cabling. Figure 6 shows attenuation measurement results at each step of cabling process. Measurements are performed in accordance to the cut-back technique utilizing a wavelength variable laser source and optical power meter in wavelength around 1550 nm. Results in Figure 6

represent the average of the obtained values for each fiber type at 1550 nm wavelength. Attenuation variations indicate that cabling process does not affect optical attribute of fiber.
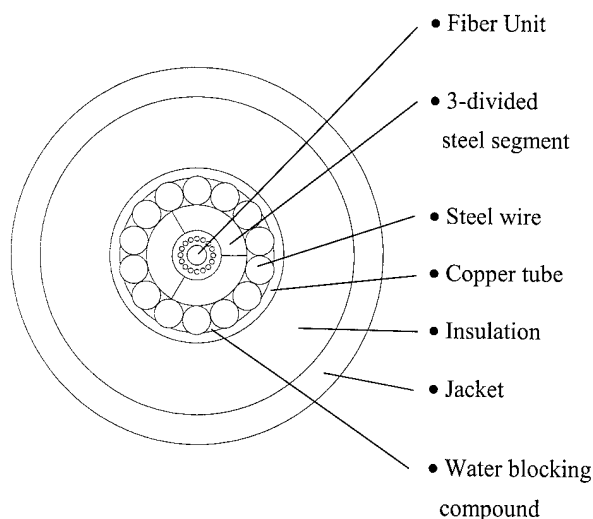
Figure 5. Structure of LW Cable with high-count fiber unit

**Table 4. Cable's typical characteristics**

Cable nominal diameter	22.5 mm
Cable weight in air	9.0 kN/km
Cable weight in water	5.0 kN/km
Minimum breaking load	98 kN
Storage factor	0.54 m³/km
Minimum bending radius	900 mm
Maximum deployment depth	8000 m
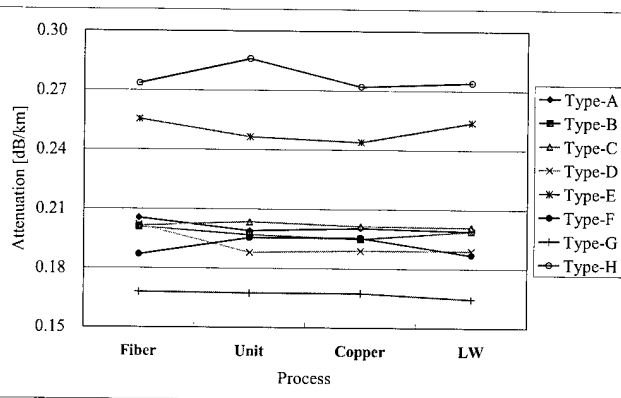
Figure 6. Attenuation variation during cabling

4.3.2   Spectral Characteristic. Attenuation-wavelength relation over the range from 1100 nm to 1600 nm of each fiber type measured before unitizing and after LW cable process are compared. Figure 7 describes the most explanative result among the obtained ones. In Figure 7 we can see that attenuation characteristic of bare fiber over wavelength range from 1550 nm to 1600 nm tends to increase. We can observe that after cabling this tendency is mitigated and that attenuation decreases as wavelength increases over the range ≥1400 nm. We suppose that this effect is directly related to bare fiber winding condition during acceptance inspection, after cabling fiber bending is released and such condition causing attenuation increase in the long wavelength region is mitigated.

4.3.3   PMD Variation At Cabling. Figure 8 shows average PMD of each fiber type measured after each step during cabling process. From Figure 8, we can see that PMD increases during unit process, this is caused by an small amount of tension applied on fiber unit during winding. Also, it is understood that variation in PMD during unit process is completely reversed during Copper tube process for all fiber types except for types E and H. PMD of these two fibers are believed to be very sensible to external stress. This might become an issue to be mitigated during cable mass production.
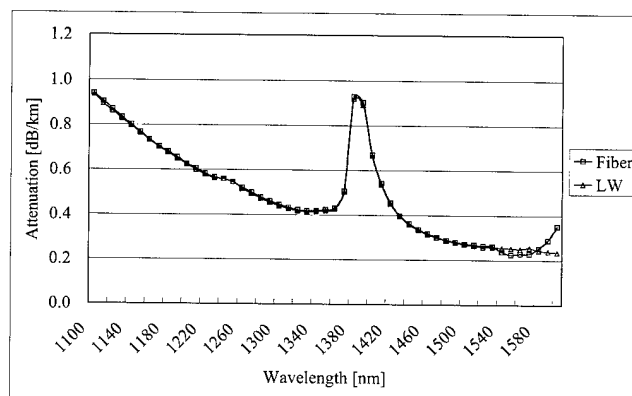
Figure 7. Variation of attenuation spectral characteristic during cabling process
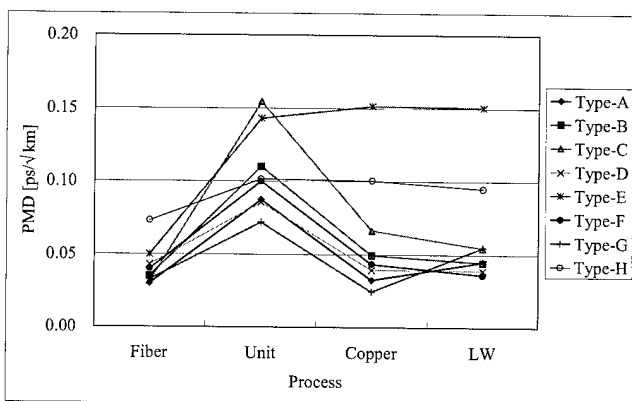
Figure 8. PMD variation during cabling

4.3.4 Operational Temperature Characteristic. Figure 9 shows the variation on optical attenuation characteristic of each fiber type when is temperature cycled between +30 °C and +3 °C and the reference attenuation is measured at +15 °C. This is to evaluate the variations that might be measured during an imminent installation of the cable. In Figure 9 the left ordinates axes was arranged so that separation between channels is equal to 0.005 dB/km (one division). From Figure 9, we can confirm that temperature stability of all fibers is of the same level of nowadays products and that LW cabling new developed 16 fibers unit does not affect the attributes of applied fibers.
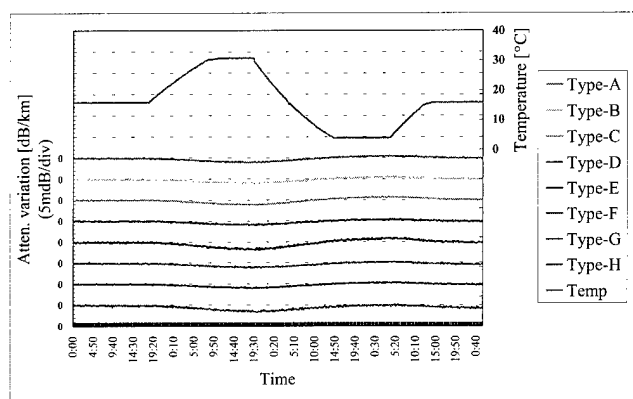
Figure 9. Temperature stability measurement results

5. Sea Trial

As a part of the evaluation of new developed 16 fibers unit, manufactured long length cables were tested in a sea trial. During the sea trial, cable laying, holding and recovery operations are performed to confirm the cable's mechanical performance and its capability to undergo such operations with no effects to optical attributes of deployed fibers. The sea trial was carried out in the sea area Eastern Okinawa, JAPAN, where the average depth is 6000 m.

5.1 Sea Trial Lay Out

Figure 10 shows an explanative lay out of the sea trial. The evaluated cable was arranged with 2 pieces (5 km and 15 km long) of OCC-22S LW type cable applying 16 fibers unit connected through a Joint Box (JB). A total of eight measurement loops were arranged by loop splicing fibers at the End Box (EB). Figure 11 illustrates JB laid operation during sea trial.

5.2 Continuous optical attenuation monitoring

During sea trial variation of optical attenuation on each loop was measured continuously. Figure 12 shows optical attenuation variation measured during each operation of the sea trial (positive variation indicates attenuation decrease). Figure 12 also indicates the start and end point of each operation. We can see that as the cable was laid a decrease in optical attenuation equivalent to the fiber's temperature characteristic variation can be confirmed at each loop. During hold operation the variation amount at each loop is negligible thus confirming that total attenuation variation until the

start of hold operation were mainly caused by temperature variation that cable experienced when was laid. Finally, optical attenuation variation reversed as cable recovery operation went on. After the cable was completely recovered, we confirmed that residual variation at each loop was almost negligible (≤0.001 dB/km) and of the same level of that obtained with 8-fiber unit application.
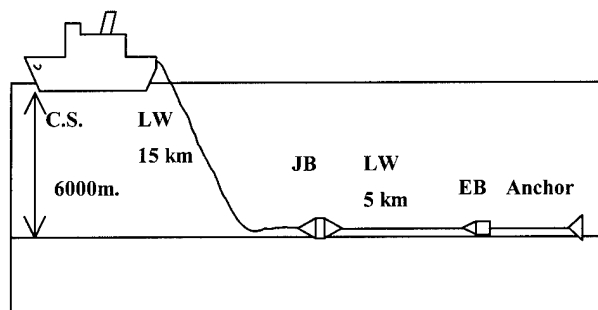
**Figure 10. Sea trial lay out**
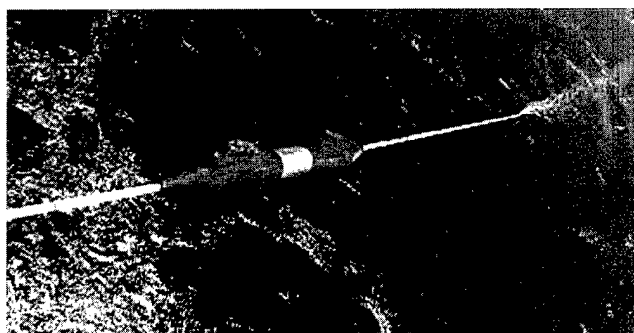
**Figure 11. JB being laid during sea trial**
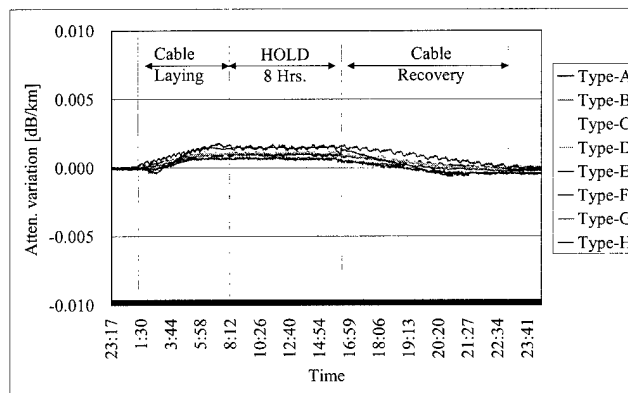
Figure 12. Optical attenuation continuous monitoring results

5.3 Optical Characteristic Variation

Traces of OTDR measurements performed on one fiber loop before laying operation and after recovery operation are shown in Figure 13 and Figure 14 respectively. Each measurement was performed with the same test equipment and under the same conditions. From this results we confirmed that JB and EB performance together with cable's performance applying 16-fiber unit can be deployed in actual submarine systems.
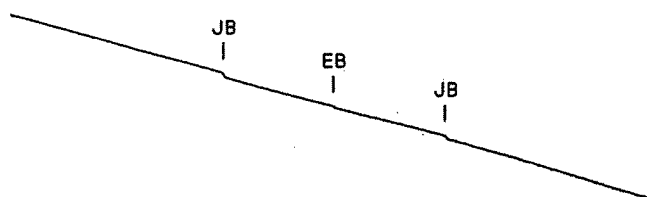
Figure 13. OTDR trace before cable's lay operation
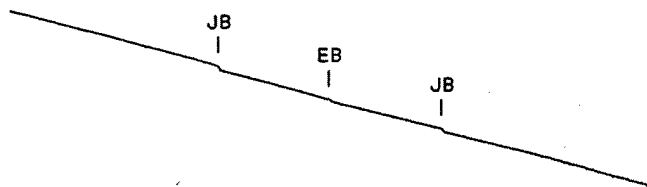
Figure 14. OTDR trace after cable's recovery operation

6. Conclusions

~ In response to the growing demand for ultra high capacity, utilizing dense wavelength division multiplexing technology we studied the structure and design of a 16-fiber unit for repeatered submarine cable systems applications.

~ Evaluation results of tests performed on short length LW submarine cable sample manufactured applying optimized fiber unit design confirmed that excellent optical and mechanical performance could be obtained.

~ Long length fiber unit utilizing new developed fibers with enhanced performance for DWDM applications was manufactured and cabled. On-land evaluation of cable as well as a sea trial was performed with excellent results confirming that optimized high-count fiber unit design is applicable for its deployment in submarine cables.

~ Variation on attenuation characteristics measured during the sea trial was mostly caused by the fiber's temperature characteristic. This confirmed the highly reliable performance that can be obtained with the tight type fiber unit applied to our current cable design.

7. Acknowledgments

Our special thanks to all the people who worked and collaborated at manufacturing and evaluating the unit samples and cables.

8. References

[1] Osamu Nagatomi, "Development of New Tight-Fit-Type Submarine Cable with Large Core Fibers for WDM Systems" 48th IWCS, p.317-323 (1999).

[2] Takato Nishida, "Developtment of Repeaterless Optical Fiber Submarine Cable System for Extensive Application" 45th IWCS, p.527-531 (1996)

About the Authors
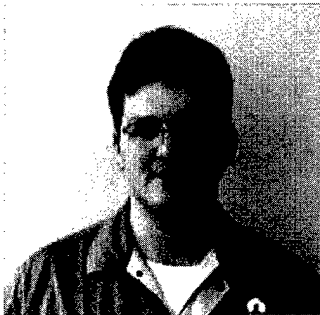
JUAN CARLOS AQUINO
OCC Corporation
1-105-2 Hibiki-Machi
Wakamatsu-ku Kitakyushu
808-0021 JAPAN

Juan Carlos Aquino was born in 1971. He received his M.E. degree in Electronics from the Kyushu Institute of Technology. He joined OCC in 1999 and has been engaged in the research and development of optical fiber submarine cables. Actually, he is an engineer at the Engineering Development Department, Submarine Systems Division and member of the IEICE of Japan.
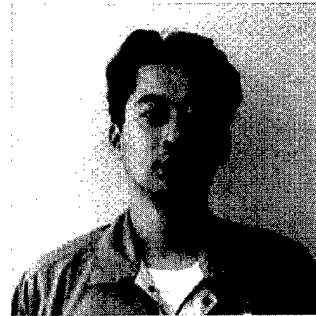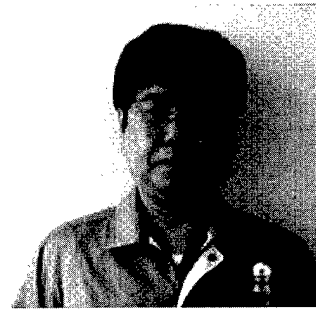
HIROFUMI WAKAMATSU
OCC Corporation
1-105-2 Hibiki-Machi
Wakamatsu-ku Kitakyushu
808-0021 JAPAN

Hirofumi Wakamatsu was born in 1965. He graduated from Kyushu Sangyou University with B.E. degree in Chemistry. Since he joined OCC, he has been engaged in the research and development of optical submarine cables. Actually, he is an engineer at the Engineering Development Department, Submarine Systems Division.

KAZUTO YAMAMOTO
OCC Corporation
1-105-2 Hibiki-Machi
Wakamatsu-ku Kitakyushu
808-0021 JAPAN

Kazuto Yamamoto was born in 1967. He graduated from Tokai University with B.E. degree in Mechanics in 1990. Since he joined OCC, he has been engaged in the research and development of optical submarine cables. Actually, he is a senior engineer at the Engineering Development Department, Submarine Systems Division.

RYO KANDA
OCC Corporation
1-105-2 Hibiki-Machi
Wakamatsu-ku Kitakyushu
808-0021 JAPAN

Ryo Kanda was born in 1973. He graduated form the Kyushu Institute of Technology with B.E. degree in Electrical Engineering. Since he joined OCC, he has been engaged in the research and development of optical submarine cables. Actually, he is an engineer at the Engineering Development Department, Submarine Systems Division.

OSAMU NAGATOMI
OCC Corporation
1-105-2 Hibiki-Machi
Wakamatsu-ku Kitakyushu
808-0021 JAPAN

Osamu Nagatomi was born in 1969. He received his B.E. and M.E. degree in Mechanics from the Kyushu University. Since he joined OCC, he has been engaged in the research and development of optical fiber submarine cables. Actually, he is an engineer at the Engineering Development Department, Submarine Systems Division and member of the SNAJ of Japan.

ROKURO MORIKAWA
OCC Corporation
1-105-2 Hibiki-Machi
Wakamatsu-ku Kitakyushu
808-0021 JAPAN

Rokuro Morikawa was born in 1957. He graduated form the Housei University with B.E. degree in Mechanical Engineering. Since he joined OCC, he has been engaged in the research and development of optical submarine cables. Actually, he is a Deputy General Manager at the Engineering Development Department, Submarine Systems Division.

High Performance Nearly Dispersion-Flattened Hybrid Optical Transmission Lines for Ultra-Large Capacity Transoceanic Systems

M. Tsukitani[1], Y. Nagao[2], E. Yanada[1], T. Kato[1],
E. Sasaoka[1], Y. Makio[1], M. Nishimura[1], and T. Oshima[2]

(1) Yokohama Research Laboratories, Sumitomo Electric Industries, Ltd.
(2) Fiber Optics Engineering Department, Sumitomo Electric Industries, Ltd.
1 Taya-cho, Sakae-ku, Yokohama, 244-8588, Japan
+81-45-853-7171 · email address : tukitan@yklab.sei.co.jp

Abstract

This paper describes design optimization and performances of hybrid optical transmission lines consisting of effective area (A_{eff}) enlarged pure-silica-core fiber (PSCF) and dispersion compensating fiber (DCF). We have fabricated tight structure type optical units for submarine cables and excellent performances have been confirmed. Furthermore, we have fabricated the optical unit containing splices between PSCF and DCF, and it has been confirmed that no loss increase caused by unit structure between before and after the unit fabrication has been observed and good environmental test results have been obtained.

Keywords

pure-silica-core fiber ; dispersion compensating fiber ; hybrid transmission line ; splice loss ; submarine cable

1. Introduction

For the next generation long haul ultra-large capacity Wavelength Division Multiplexed (WDM) submarine transmission systems, optical transmission lines with low nonlinearity and low dispersion slope are indispensable. Recent investigation has shown that the hybrid optical line consisting of dispersion-unshifted single mode fiber and dispersion compensating fiber (DCF) is one of the most promising candidates to fulfill those requirements [1]-[8]. It has already been successfully demonstrated that the hybrid optical transmission line enables transmission of more than 1Tbit/s capacity over 10,000km [4].

This paper describes design optimization and performances of hybrid optical transmission lines consisting of A_{eff} (effective area) enlarged pure-silica-core-fiber (PSCF) [9] and design-optimized DCF. Successful fabrication of tight structure type units for submarine cables with and without splices between PSCF and DCF is also described. Excellent performances have been confirmed.

2. Design and performances of hybrid optical transmission line

2.1 Design of hybrid optical transmission line

The configuration of the hybrid line (PureCouple[TM]) is illustrated in Fig. 1. The first part of the line is A_{eff} enlarged PSCF (Z-PLUS

Fiber[TM]), which employs the depressed cladding structure in order to expand A_{eff} while maintaining good bending characteristics [9]. Table 1 shows the typical characteristics of the PSCF. Its A_{eff} is as large as 110μm², and the nonlinear coefficient (n_2/A_{eff}) [10] is 30% lower than that of the conventional PSCF (Z Fiber[®]).
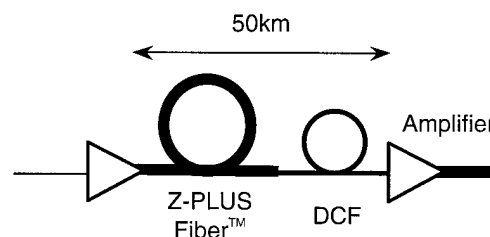
Figure 1. Configuration of hybrid optical transmission line (PureCouple[TM])

Table 1. Typical characteristics of PSCF (Z-PLUS Fiber[TM]) (@1550nm)

Loss [dB/km]	0.170
Dispersion [ps/nm/km]	20.4
Disp. Slope [ps/nm²/km]	0.059
A_{eff} [μm²]	110.0
n_2 [×10⁻²⁰m²/W]	2.8

As for the DCF, the W-type refractive index profile has been employed. In the design of DCF, the refractive index difference of the depressed cladding Δ^- is fixed to –0.36% and, by adjusting the core index difference Δ^+ within a range from 1.0% to 2.0%, we optimize the DCF structure with maintaining macrobending loss of 3dB/m for a diameter of 20mm.

In the design optimization of the hybrid optical transmission line and DCF, we assume the repeater span is 50km and the average span dispersion is set to 0ps/nm/km at 1550nm. For nonlinearity evaluation, we use the equivalent A_{eff}, which is defined by the cumulative phase shift due to the self-phase-modulation under the condition that the signal power at the output end of the line is constant. Figure 2 shows the averaged span loss and Fig. 3 shows

the equivalent A_{eff}, both of which are calculated as a function of the DCF length ratio with varying the average dispersion slope (Save.). It has been found that the hybrid optical transmission line gives the minimum value of the span loss when the DCF length ratio is about 40%, and that the equivalent A_{eff} is maximized when the DCF length ratio is approximately 30%. In addition, it has been confirmed that there is a tradeoff relationship between the average dispersion slope and the equivalent A_{eff}.
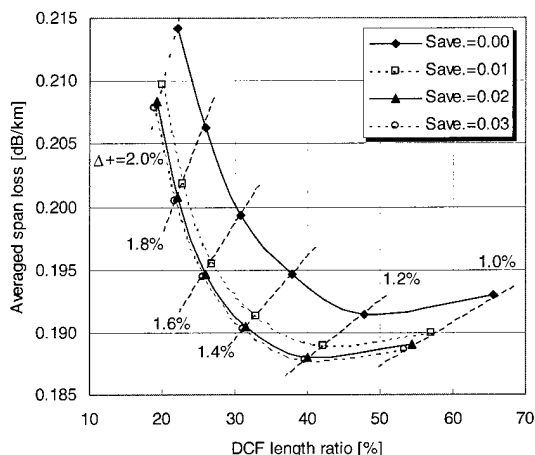
Figure 2. DCF length ratio VS. averaged span loss
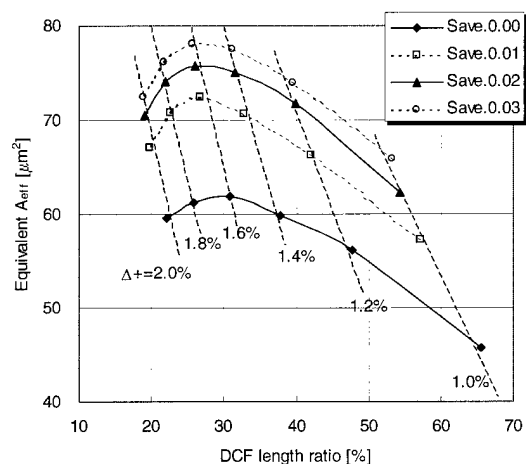
Figure 3. DCF length ratio VS. equivalent A_{eff}

2.2 Performances of hybrid optical transmission line

Based on the design optimization, we have fabricated the hybrid optical transmission lines with the DCF length ratio of about 35% and the average dispersion slope of 0.02 ps/nm²/km considering the span averaged loss and nonlinearity. Table 2 summarizes the typical values of the characteristics of the PSCFs, the DCFs and the hybrid lines with the line length of about 50km. The equivalent A_{eff} is a little smaller than the calculation results. This is because the span average dispersion is set to −2 ps/nm/km

(0ps/nm/km in the calculation) and design of the fabricated fibers is slightly off the calculation, which results in macrobending loss considerably better than predicted. Figures 4 and 5 show typical attenuation spectra of PSCF, DCF and a hybrid line including splice loss, which indicate no bending-induced loss increase even in L-band for both fiber types. Figure 6 shows spectral dispersion curves. It is clear that the dispersion slopes of the hybrid lines are significantly smaller than that of the conventional NZ-DSF (Non-Zero Dispersion Shifted Fiber).

Table 2. Characteristics of hybrid line (@1550 nm)

	PSCF	DCF	PSCF+DCF
Dispersion [ps/nm/km]	20.4	-46.7	-2.1
Disp. Slope [ps/nm²/km]	0.059	-0.059	0.020
Loss [dB/km]	0.170	0.264	0.205[*]
A_{eff} [μm²]	106.0	20.4	60.0[**]
Macrobending loss (20φ) [dB/m]	0.5	0.8	-

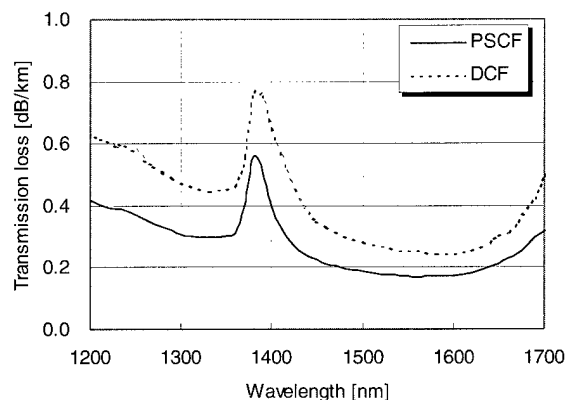[*] : including a splice loss between PSCF and DCF
[**] : equivalent A_{eff}

Figure 4. Spectral attenuation of PSCF and DCF

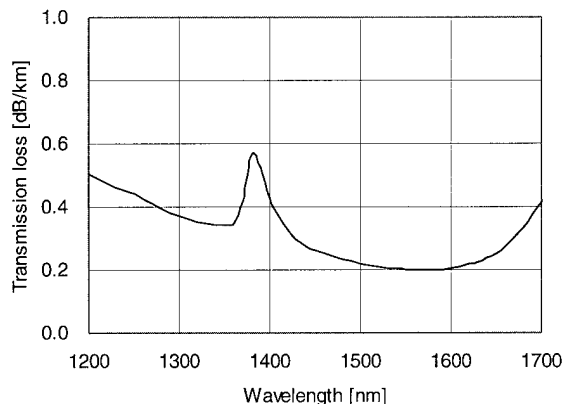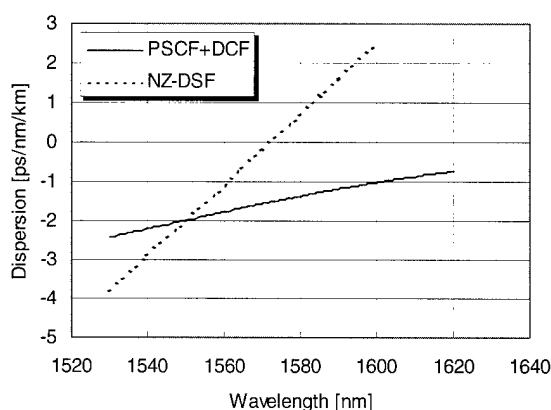
Figure 5. Spectral attenuation of hybrid line with splice

**Figure 6. Chromatic dispersion of hybrid line and NZ-DSF**

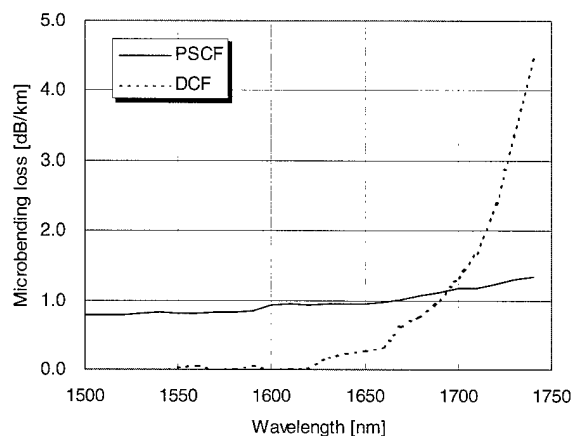## 2.3 Microbending loss characteristics of PSCF and DCF

In general, DCFs exhibit steep loss increase in the long wavelength region. In order to examine the cause of the loss increase in DCF, firstly we have measured the spectral attenuation difference between spooled and loosely coiled DCFs. Figure 7 shows the attenuation spectrum of DCF with a winding diameter of 280mm. In spite of the same winding diameter, loss increase is smaller in the loose coil. From this result, the main cause of the loss increase on the bobbin has been believed to be microbending loss caused by lateral pressure coming from the bobbin and/or adjacent fibers, rather than macrobending loss.
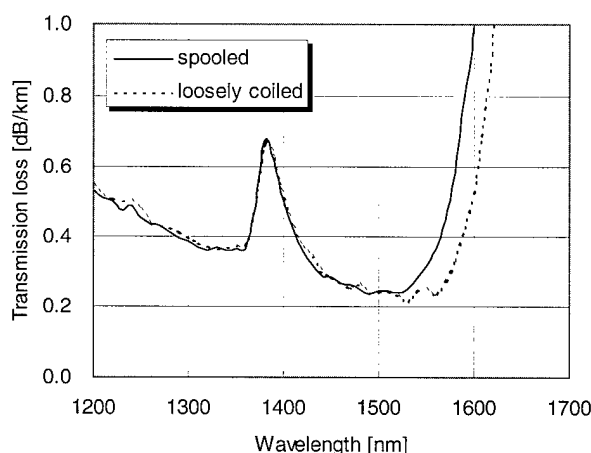
Figure 7. Spectral attenuation on spooled and loosely coiled DCF

We have examined the microbending loss behavior by winding test for both PSCF and DCF. The loss increase is measured after winding the test fiber with a constant tension of 80g on a 400mm

diameter bobbin whose surface is covered with wiremesh [11]. Figure 8 shows test results for PSCF and DCF. DCF's loss increase is steeper than that of PSCF in the long wavelength region [12]. It has been known that microbending loss is closely related to the mode field diameter based on the Petermann's first definition (MFD1) [13]. Figure 9 shows the MFD1 calculated for PSCF and DCF. The difference in behavior of loss increase between PSCF and DCF may be attributed to the difference in the wavelength dependence of MFD1.

Figure 8. Microbending loss of PSCF and DCF measured by the wiremesh method
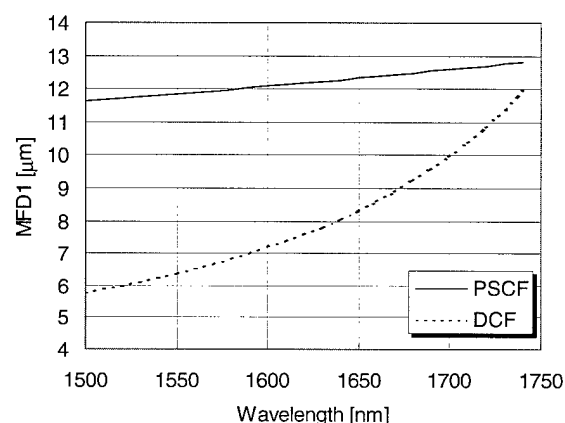
Figure 9. Wavelength dependence of MFD1 for PSCF and DCF

3. Characteristics of optical unit for submarine cable

3.1 Optical unit

We have fabricated optical units for submarine cables containing the PSCFs and the DCFs. Table 3 shows characteristics of the fibers used in trial units. The DCFs exhibiting different levels of macrobending loss (for the bending diameter of 20 mm) have been chosen to examine the allowable limit of the macrobending.

Table 3. Characteristics of fibers used in trial unit (@1550 nm)

	PSCF1	PSCF2	DCF1	DCF2	DCF3
Dispersion [ps/nm/km]	20.7	20.7	-44.5	-52.8	-69.5
Disp. Slope [ps/nm^2/km]	0.059	0.059	-0.080	-0.039	-0.038
Loss [dB/km]	0.170	0.170	0.269	0.261	0.371
MFD [μm]	11.6	11.5	5.1	5.4	5.7
A$_{eff}$ [μm^2]	110.1	107.7	19.6	21.9	25.5
Macrobending loss (20φ) [dB/m]	0.2	0.2	2	12	63

3.2 Spectral attenuation

Figures 10, 11, 12 and 13 show attenuation spectra of spooled fibers and optical unit for PSCF1, DCF1 (typical), DCF2 (slightly bend-sensitive) and DCF3 (the worst). Optical unit lengths are about 3km. It has been confirmed that for all PSCFs no bending-induced loss increase is observed up to 1700 nm. On the other hand, for all DCFs loss decrease is observed after the unit fabrication. So long as macrobending loss is less than about 10dB/m (for 20mm diameter), it should be possible to maintain low attenuation even in L-band.
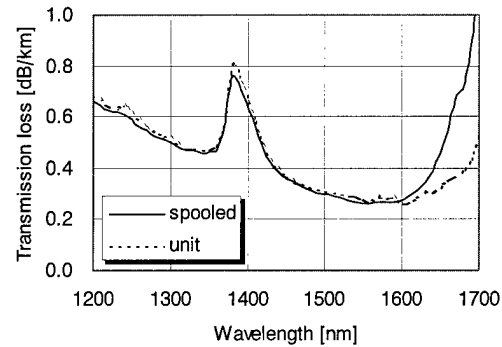
The main cause of the loss reduction in DCF during the optical unit fabrication is believed to be microbend relaxation.
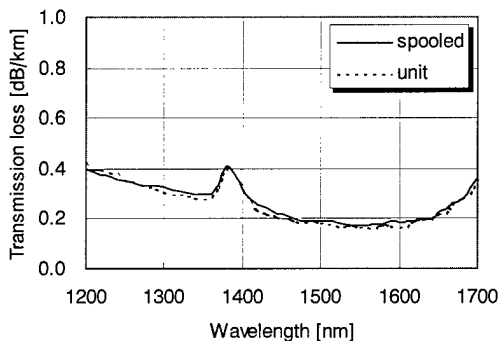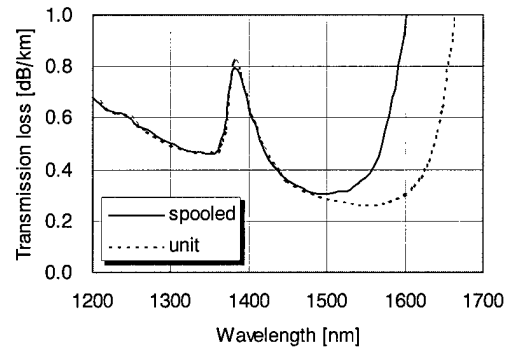

Figure 10. Spectral attenuation for PSCF1
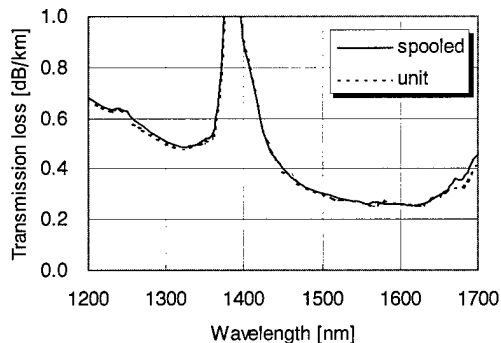
Figure 11. Spectral attenuation for DCF1

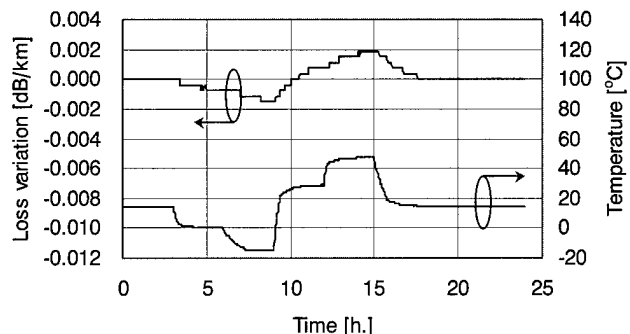**Figure 12. Spectral attenuation for DCF2**

Figure 13. Spectral attenuation for DCF3

3.3 Environmental tests for optical unit

Figures 14, 15 and 16 show results of the temperature cycling test between -15℃ and 50℃ observed at 1550nm for PSCF1, DCF1 and DCF3. Table 4 summarizes the loss variation at -15℃ and 50 ℃. These values coincide well with the intrinsic temperature dependent loss variation of silica glass, indicating that there is no additional loss variation caused by the unit structure.
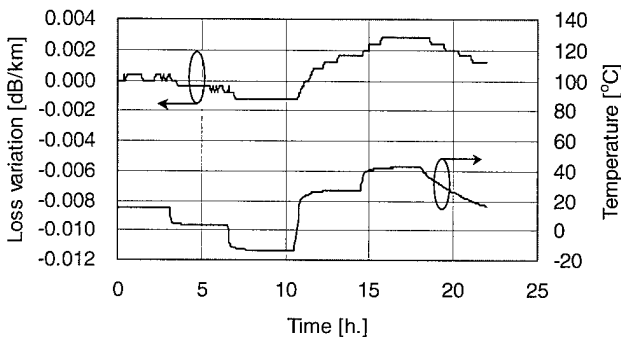
Table 4. Results of temperature cycling test (@1550 nm)

	PSCF1 [dB/km]	PSCF2 [dB/km]	DCF1 [dB/km]	DCF2 [dB/km]	DCF3 [dB/km]
-15℃	-0.0015	-0.0011	-0.0015	-0.0024	-0.0012
50℃	+0.0019	+0.0019	+0.0026	+0.0056	+0.0028

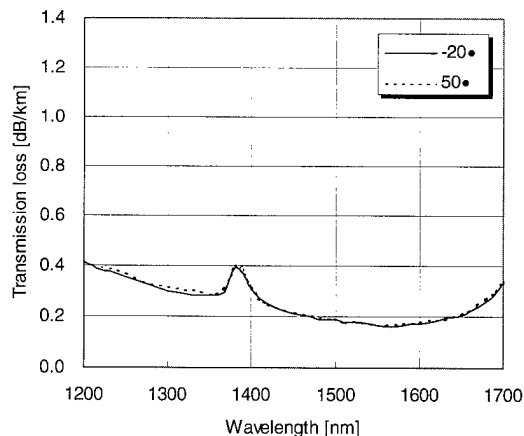**Figure 14. Temperature characteristic for PSCF1**
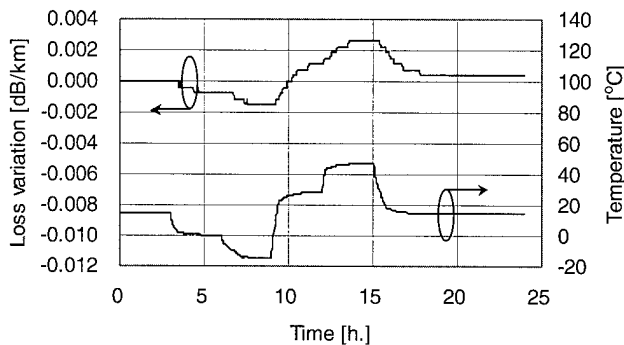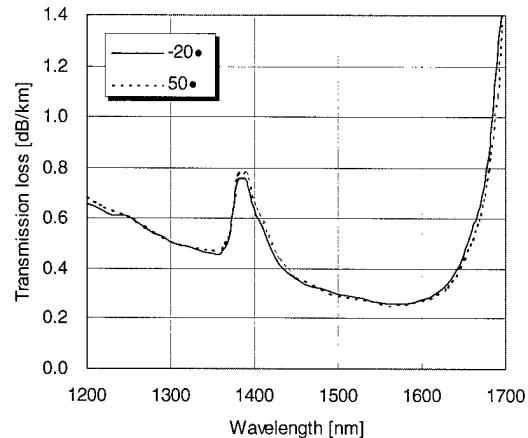
Figure 15. Temperature characteristic for DCF1

Figure 16. Temperature characteristic for DCF3

Figures 17 and 18 show attenuation spectra measured at –20℃ and 50℃ for PSCF1 and DCF3 in the unit. It has been confirmed that no change in spectra attenuation is observed.

Figure 17. Temperature dependence of spectrum attenuation for PSCF1

Figure 18. Temperature dependence of spectrum attenuation for DCF3

Table 5 shows results of the hydrostatic pressure test with pressure up to 20 MPa. The length of a test unit is 500 m. Loss increase for 10 MPa is less than 0.002 dB/km, which is as low as those of the non-zero DSFs in optical units of the same type.

Table 5. Result of hydrostatic pressure test (@1550nm)

|	PSCF1 [dB/km]	PSCF2 [dB/km]	DCF1 [dB/km]	DCF2 [dB/km]	DCF3 [dB/km]
10MPa	0.0006	0.0010	0.0000	0.0000	0.0004
20MPa	0.0022	0.0013	0.0000	0.0002	0.0008

3.4 Splice loss

Splice loss is very important in the hybrid lines. It is essential to realize not only low splice loss, but also high stability. Table 6 shows characteristics of the fiber used in an optical unit containing splice. This trial optical unit whose length is 2.2 km has been composed of PSCF, DCF and a splice. Figure 19 shows the spectral attenuation of the splice measured on the bobbin and in the optical unit. It has been confirmed that the splice loss between PSCF and DCF is about 0.2dB and exhibit a slight decrease from 1530 nm to 1620 nm in both cases, indicating no bending-induced loss. Furthermore, any splice loss variation during the optical unit fabrication has not been observed.

Figure 20 shows results of the temperature cycling test for the optical unit with the splice between –20℃ and 50℃ at 1550nm. Only loss variation observed is the intrinsic temperature dependent loss variation of PSCF and DCF. From this result, it has been confirmed that the loss variation at the splice is negligible.
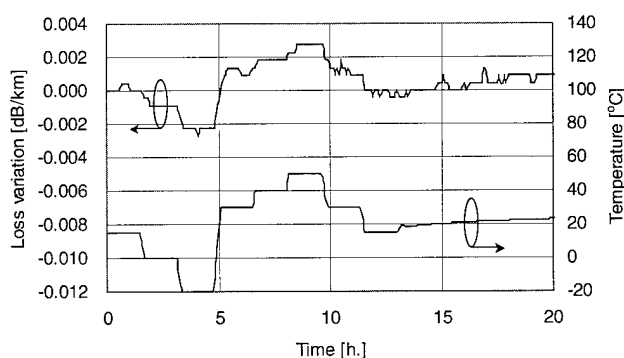
Table 7 shows results of the hydrostatic pressure test for the 500 m unit consisting of 250 m PSCF, 250 m DCF and a splice. It can be concluded that the loss variation is sufficiently small even in the optical unit containing the splice.

Table 6. Characteristics of fibers used in trial optical unit with splice (@1550nm)

	PSCF3	DCF4
Loss [dB/km]	0.169	0.279
Dispersion [ps/nm/km]	20.5	-47.7
Disp. Slope [ps/nm²/km]	0.059	-0.075
A_{eff} [µm²]	110.3	18.8
Macrobending loss (20φ) [dB/m]	0.2	0.0
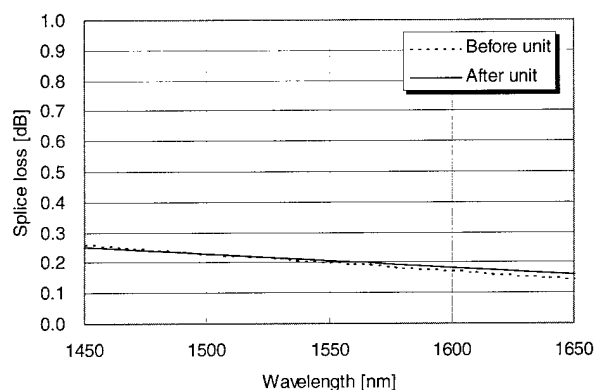
Figure 19. Spectral splice loss between PSCF and DCF

Figure 20. Results of temperature cycling test of optical unit with splice

Table 7. Results of hydrostatic pressure test (@1550 nm)

	Loss variation [dB/km]
10MPa	0.0028
20MPa	0.0040

4. Conclusions

We have successfully developed high performance nearly dispersion-flattened hybrid transmission lines consisting of A_{eff} enlarged pure-silica-core fiber and dispersion compensating fiber. They exhibit the span loss as low as 0.205 dB/km, the span dispersion slope of 0.020 ps/nm²/km and low nonlinearity with the equivalent effective area of 60 µm².

We have also successfully fabricated tight structure type optical units using the fibers which compose the hybrid optical transmission line. It has been confirmed that the transmission loss decreases in the long wavelength region by microbend relaxation. Through environmental tests, it has also been confirmed that loss variations in both fiber types are as low as those in the conventional fibers in the units of the same type.

Furthermore, we have fabricated an optical unit with splice between the A_{eff} enlarged pure-silica-core fiber and the dispersion compensating fiber. Splice loss is as low as 0.2 dB at 1550nm and exhibits no bending-induced additional loss in L-band. It has been found that no loss variation is observed before and after the optical unit fabrication, and that through environmental tests splice loss variation on splice is negligible.

5. Acknowledgments

The authors wish to thank Dr. Shigeru Tanaka for continuous encouragement and discussion.

6. References

[1] K. Mukasa, Y. Akasaka, Y. Suzuki, and T. Kamiya : 'Novel network fibre to manage dispersion at 1.55µm with combination of 1.3µm zero dispersion single mode fibre', Proc. ECOC '97, 1, pp.127-130, 1997

[2] K. Kashiwada, M. Onishi, S. Ishikawa, T. Kato, T. Okuno, and M. Nishimura : 'Ultra-low chromatic and polarization mode dispersion hybrid fibre links for ultra-high speed transmission systems', Proc. OECC '98, Paper 15C1-3, pp.364-365, 1998

[3] M. Murakami, T. Matsuda, and T. Imai : 'Quarter terabit (25 × 10Gb/s) over 9288km WDM transmission experiment using nonlinear supported RZ pulse in higher order fiber dispersion managed line', Proc. ECOC '98, PD, pp.79-81, 1998

[4] T. Naito, N. Shimojoh, T. Tanaka, H. Nakamoto, M. Doi, T. Ueki, and M. Suyama : '1 Terabit/s WDM Transmission over 10,000km' ,Proc. ECOC'99, PD2-1, pp.24-25, 1999

[5] M. Tsukitani. T. Kato, E. Yanada, M. Hirano, M. Nakamura, Y. Ohga, M. Onishi, E. Sasaoke, Y. Makio, and M. Nishimura : 'Low-loss dispersion-flattened hybrid transmission lines consisting of low-nonlinearity pure silica core fibers and dispersion compensating fibers', Elec.Lett., Vol.36, No.1, pp.64-66, 2000

[6] C. R. Davidson, C. J. Chen, M. Nissov, A. Pilipetskii, N. Ramanujam, H. D. Kidorf, B. Pedersen, M. A. Mills, C. Lin, M. I. Hayee, J. X. Cai, A. B. Puc, P. C. Corbett, R. Menges, H. Li, A. Elyamani, C. Rivers, and Neal S. Bergano : '1800 Gb/s transmission of one hundred and eighty 10 Gb/s WDM channels over 7,000 km using the full EDFA C-band', OFC'2000, PD25, 2000

[7] T. Tsuritani, N. Takeda, K. Imai, K.Tanaka, A. Agata, I. Morita, H. Yamauchi, N. Edagawa and M. Suzuki ; '1 Tbit/s (100 × 10.7 Gbit/s) transoceanic transmission using 30nm-wide broadband optical repeaters with Aeff-enlarged positive dispersion fibre and slope-compensating DCF', Proc. ECOC'99, PD2-8, 1999

[8] R. Kurebayashi, S. Ono, T. Ogata and H. Okamura ; '10 Gb/s, 64 ch, 10,000-km transmission capability of ha hybrid-fiber transmission line', Proc. OECC, Paper 11A1-3, pp. 12-13, 2000

[9] T. Kato, M. Hirano, M. Onishi, and M. Nishimura : 'Ultra-low nonlinearity low-loss pure silica core fibre for long-haul WDM transmission' , Elec. Lett., 35, pp.1615-1617, 1999

[10] T. Kato, Y. Suetsugu, M. Takagi, E. Sasaoka and M. NishimuraNishimura : 'Measurement of the nonlinear refractive index in optical fiber by the cross-phase-modulation method using depolarized pump light', Opt. Lett., Vol. 20, pp.988-991 , 1995

[11] JF. Libert, JL. Land, J. Chesnoy : 'The new 160 Gigabit WDM challenge for submarine cable systems', IWCS'98, pp. 375-384, 1998

[12] Lars Grüner-Nielsen and Stig Nissen Knudsen : 'Cabling of dispersion compensating fibres', IWCS'99, pp483-487, 1999

[13] K. Petermann, 'Theory of microbending loss in monomode fibers with arbitrary refractive index profile', Arch. Elek. Übertragung. Vol. 30, pp.337-342, 1976.
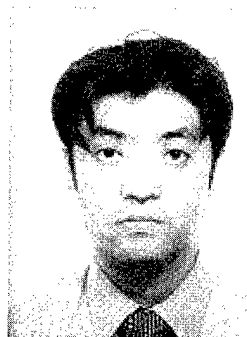
AUTHORS

Masao Tsukitani

Sumitomo Electric Industries Ltd.

1 Taya-cho, Sakae-ku, Yokohama, 244-8588, Japan

Masao Tsukitani received the B.S. and M.S. degrees in physics from the University of Keio, Japan, in 1996 and 1998, respectively. He joined Sumitomo Electric Industries, Ltd. in 1998, and has been engaged in research and development of dispersion compensating fiber. Mr. Tsukitani is a member of the Institute of Electronics, Information and Communication Engineers.

Yoshiaki Nagao

Sumitomo Electric Industries Ltd.

1 Taya-cho, Sakae-ku, Yokohama, 244-8588, Japan

Yoshiaki Nagao received the B.S. and M.S. degrees in material science from Electro Communication University, Japan, in 1991 and 1993, respectively. He joined Sumitomo Electric Industries, Ltd. in 1981, and has been engaged in research and development of optical fibers, optical cables and related technologies.

Eiji Yanada

Sumitomo Electric
Industries Ltd.
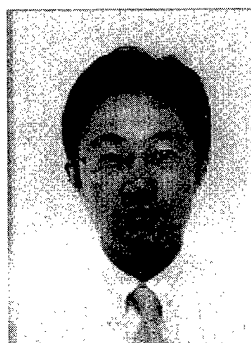
1 Taya-cho, Sakae-ku,
Yokohama, 244-8588, Japan

Eiji Yanada received the B.S. and M.S. degrees in physics from the University of Kyusyu, Japan, in 1990 and 1992, respectively. He joined Sumitomo Electric Industries, Ltd. in 1992, and has been engaged in research and development of dispersion compensating fiber. Mr. Yanada is a member of the Institute of Electronics, Information and Communication Engineers.

Takatoshi Kato

Sumitomo Electric
Industries Ltd.

1 Taya-cho, Sakae-ku,
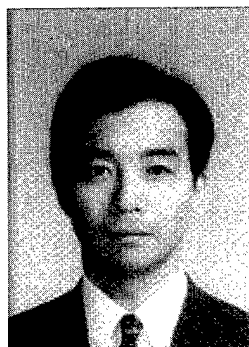Yokohama, 244-8588, Japan

Takatoshi Kato received the B.S. and M.S. degrees in electronic engineering from the University of Tokyo, Japan, in 1991 and 1993, respectively. He joined Sumitomo Electric Industries, Ltd. in 1993, and has been engaged in research and development of optical fibers for long-haul transmission. Mr. Kato is a member of the Institute of Electronics, Information and Communication Engineers of Japan.

Eisuke Sasaoka

Sumitomo Electric
Industries Ltd.

1 Taya-cho, Sakae-ku,
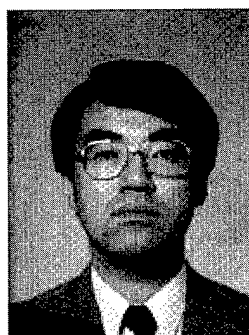Yokohama, 244-8588, Japan

Eisuke Sasaoka received the B.S. degree in physics from the University of Tsukuba, Japan, in 1986. He joined Sumitomo Electric Industries Ltd. in 1986 and engages in research work on optical fibers. Mr. Sasaoka is a member of the Institute of Electronics, Information and Communication Engineers of Japan.

Yoshinori Makio

Sumitomo Electric
Industries Ltd.

1 Taya-cho, Sakae-ku,
Yokohama, 244-8588, Japan

Yoshinori Makio received the M.S. degree in Information Engineering from Tokyo Institute of Technology, Japan, in 1982 He joined Sumitomo Electric Industries, Ltd. in 1982 and has been engaged in research and development of optical fibers. He is a member of Institute of Electronics, Information and Communication Engineers of Japan.

Masayuki Nishimura

Sumitomo Electric
Industries Ltd.

1 Taya-cho, Sakae-ku,
Yokohama, 244-8588, Japan

Masayuki Nishimura received the B.S. and M.S. degrees in electronic engineering from the University of Tokyo, Japan, in 1979 and 1981, respectively. He joined Sumitomo Electric Industries, Ltd. in 1981, and has been engaged in research and development of optical fibers, optical cables and related technologies. Mr. Nishimura is a member of the Institute of Electronics, Information and Communication Engineers of Japan.

Toshio Oshima

Sumitomo Electric
Industries Ltd.

1 Taya-cho, Sakae-ku,
Yokohama, 244-8588,
Japan

Toshio Oshima received the M.S. degrees in applied physics from the Tokyo University of Education, Japan, in 1976. He joined Sumitomo Electric Industries, Ltd. in 1979, and has been engaged in designing and developing optical fiber cable and in quality assurance for optical fiber and cable.

Using Twist to Evaluate Fiber Optic Ribbon Properties

Mahmood Tabaddor and Charles Aloisio
Bell Labs, Lucent Technologies, Norcross, Georgia
+1-770-798-3368 mtabaddor@lucent.com

Abstract

In assessing the quality of a fiber optic ribbon prior to full-scale manufacturing, the ribbon is subjected to a twist test. The purpose of the test is to ensure that ribbons will not fail under twisting conditions that exist in cabling or handling operations. In this paper, we will outline the requirements and the possibilities for using the ribbon twist test equipped with sensors. For this study, we demonstrate the viability of twist loading using the RDS-II rheometer. The RDS has the advantage of being equipped with sensitive sensors. The purpose of this investigation was to determine the potential of using twist data (torque versus twist angle collected by sensors) in characterizing ribbon quality. In this paper, we present some early experimental results on the twist response of fiber optic ribbons.

Keywords

Twist, Optical Fiber, Ribbon, Torque, Composite

1. Introduction

First, we begin with a brief description of the ribbon twist test setup. Next, we describe the experimental setup with the RDS. In the results section, we display plots of torque versus angle of twist for various ribbon samples. Coupling the results with some observations, we identify characteristics of the torque versus angle of twist curve, measure mechanical properties of the ribbon, and discuss possible failure modes.

2. Ribbon Twist Test

A schematic of the ribbon twist tester is shown in Figure 1. The purpose of the ribbon twist test is to twist a short sample of ribbon until catastrophic failure is observed. This test is a variation of a twist test meant to measure resistance to twist [1]. The bottom clamp imposes a rotation along the longitudinal axis of the ribbon. The upper end constrains the ribbon against rotations about the longitudinal axis but allows for longitudinal extension (or shortening). A dead weight places the ribbon under tension during the twist test. An earlier version of this test set-up contained no sensors and relied on the visual identification of the onset of catastrophic failure of the ribbon. Once failure was observed, the test operator stopped the test. The number of turns to failure was then recorded as a measure of ribbon quality.

Since this was an offline test, during the initial startup of a ribbon manufacturing line, a sample was subjected to the ribbon twist test. If its output - number of turns to failure - was below a certain value, the process components were examined to identify and correct the culprit.

However, an understanding of the complex mechanics of failure point to the fact that the ribbon twist tester was not a very reliable tool for ribbon quality checks. We found that the deficiency of the old setup was due to two factors: (i) The ribbon twist test set-up relied on visual detection of failure by the test operator and (ii) that catastrophic failure was the criteria. We will expound on both these points in later sections.
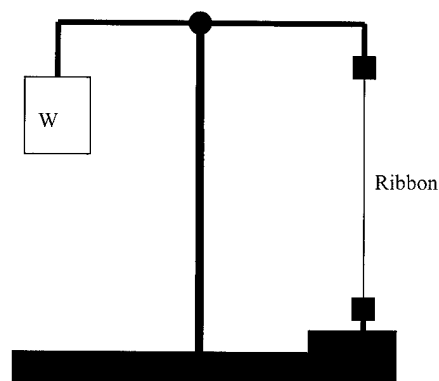
Figure 1 Schematic of Ribbon twist tester

3. RDS Setup

The set-up of the RDS-II rheometer is shown in Figure 2. The RDS is an instrument whose primary function is to determine rheological properties of materials. However, we have chosen this instrument because it can twist a sample at specified rates while recording parameters such as torque (g-cm) and angle of twist (degrees). The RDS did have a limitation on sample size. We had to test lengths much smaller than the nominal length for the ribbon twist tester. For our tests, ribbon sample lengths were approximately 49 mm. The ribbon was cut and placed into special clamps. These clamps, in turn, were placed into inserts. For the top position, the clamp was allowed to slide against the insert. The boundary conditions were such that the bottom was constrained to a specific rotation rate while the top was constrained from rotation but free to translate along the axis of the ribbon. We chose a rotation rate of 0.06 rad/s, slower than the typical ribbon twist tester (2 rad/s). All samples were subjected to at least one full rotation. Beyond a twist angle of 400 degrees, ribbons (both 12 and 24 fiber) would completely slip out of the top holder. Also, with the RDS, no axial load could be applied to the ribbon except for the dead weight of the ribbon and the top clamp.

4. Results

For our samples, we chose both 12-fiber and 24-fiber ribbons. However, most of our results were collected from 24-fiber ribbon samples since the structural response and data were more informative. The 12-fiber ribbon is likely to exhibit the same qualitative behavior at higher angles of twist. For the 24-fiber ribbon, we tested samples produced under two different processing conditions and then chose one condition where we purposely instigated a defect. The nominal dimensions of the ribbons were 0.3 mm x 3.0 mm for the 12-fiber ribbon and 0.3 mm x 6.1 mm for the 24-fiber ribbon.

4.1 24-Fiber Ribbons

Figure 3 shows the results of torque and angle of twist for four, 24-fiber ribbon samples manufactured under condition 1.

An examination of the data in more detail reveals that the early portion of the plot is linear but only for very small angles (approximately 5 degrees). After this relatively short linear section, the curve begins to slope upward in a nonlinear fashion. At about an angle of twist of 80-95 degrees, a slight hump in the curve is obvious. This hump is identified as a bifurcation point, a point of structural instability. Visually, the ribbon appeared to buckle slightly along the length (Figure 4) at the same time as this hump appeared in the data set. For a unidirectional composite (ribbon) subjected to torque, both tensile and compressive stresses develop with increasing rotation [2]. This buckle could be a result of compressive stresses that develop within the central portion of the ribbon. The buckle is not an indication of material or interface failure but can be a good
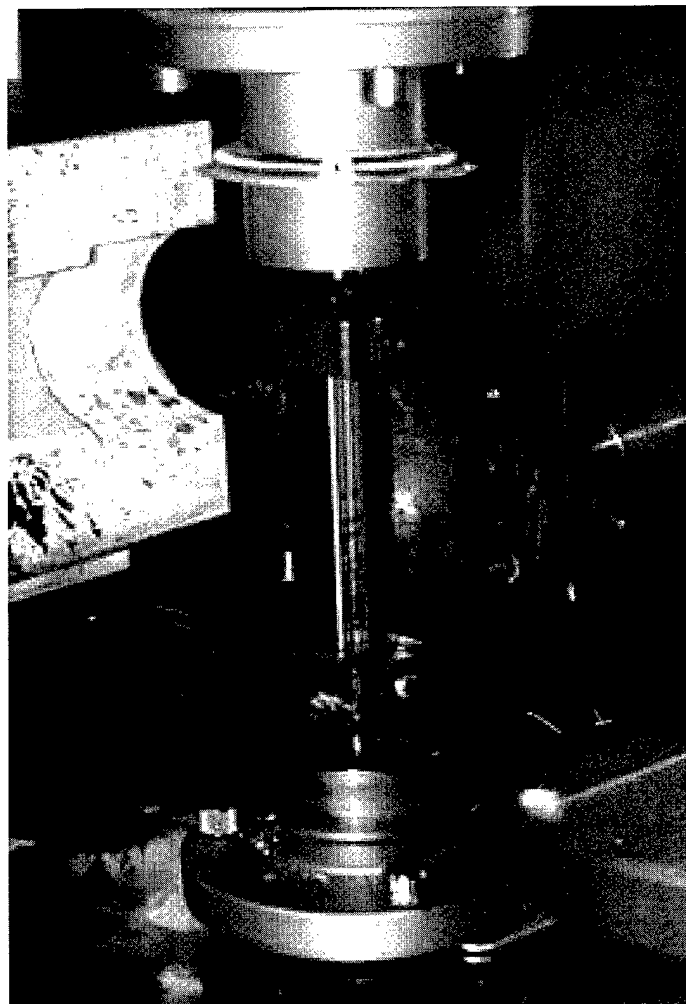
Figure 2 Photograph of an untwisted ribbon sample in the RDS-II rheometer

guidepost to small structural defects that affect ribbon stiffness.

Subsequent to the hump, which we call the post-buckled region (100 – 280 degrees), the slope rises monotonically and steadily but is less than the pre-buckled slope. However, the post-buckled slopes show greater variation now. This may point to the quality differences associated with condition 1 ribbons. One possible difference was the variation in planarity.

The next noted occurrence, in the post-buckled region, was small undulations in the data. Sometimes, these undulations were accompanied by acoustic events, audible cracking noises. Since the testing environment was relatively noisy, some acoustic events were probably undetected. We believe that the undulations are signatures of debondings occurring between the colored fiber and the matrix as revealed by post-mortem visual examination of the ribbon samples. The

undulations have variability in magnitude and location but all occur after 200 degrees of twist. The variability of these markers may point to the effect of processing and material variability. The debondings are a primary measure of interface strength but are likely to have random distributions as they are sensitive to imperfections and stress risers (such as local cure, planarity, voids in matrix, etc.).
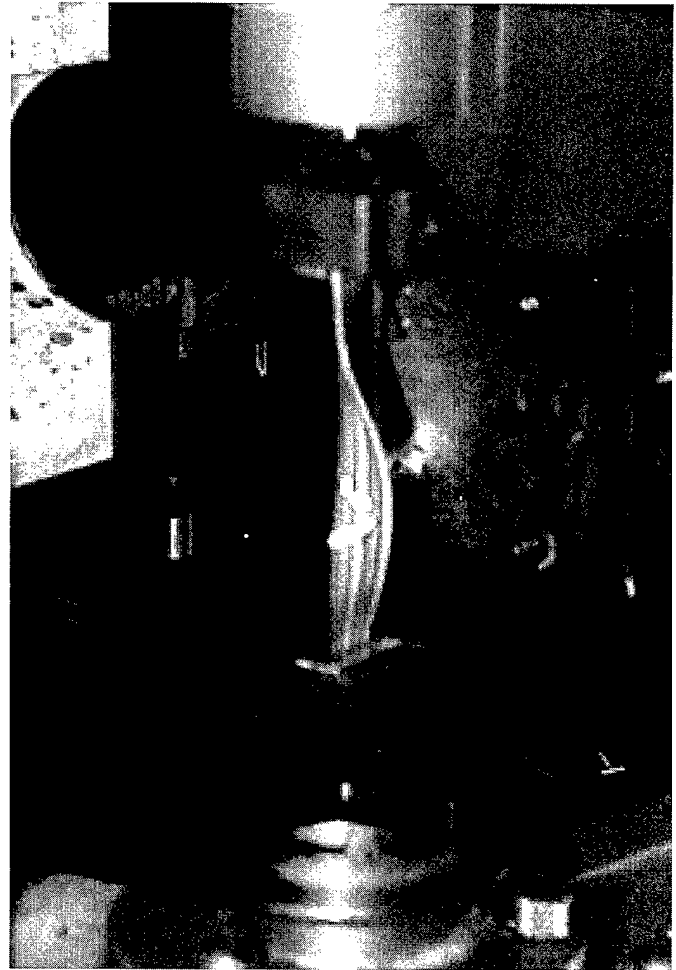
For an angle of twist greater than 300 degrees, the response variations are even more marked. We believe that at this stage, both process variability and imperfections in test setup and boundary conditions[1] are intermingled. For instance, one sample remained in its original configuration while another sample experienced a secondary instability and took a very complex three-dimensional shape (Figure 5).

For all samples shown in the plot, the test can be considered nondestructive. Despite the appearance of debondings, the structural integrity of the fibers within the matrix was maintained. Repeatability of the twist test for angles of twist less than 100 degrees was examined and found to be acceptable. No data on unloading or creep effects was collected.
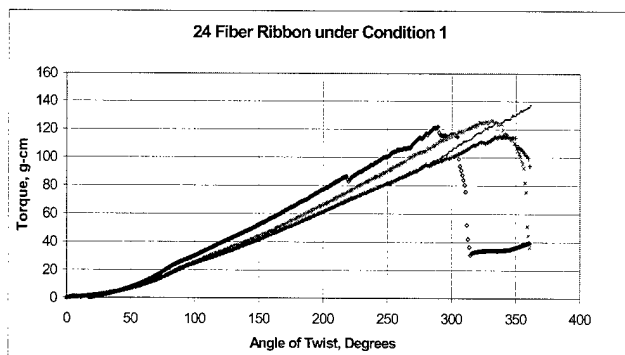
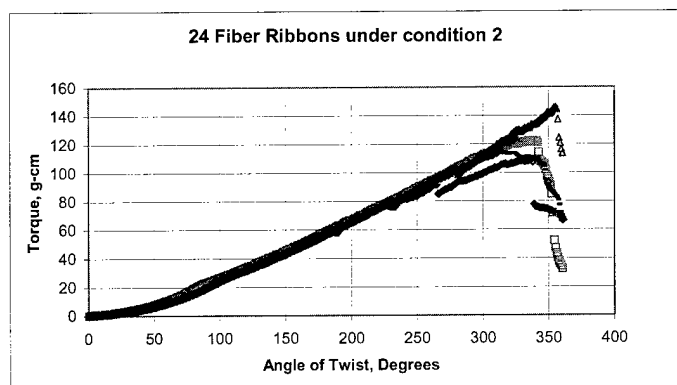Figure 3 Torque versus angle of twist for 24-fiber ribbons manufactured under condition 1

Figure 4 Photograph of twisted sample in the early post-buckled region

For the samples manufactured under condition 2, Figure 6 shows the data of torque and angle of twist. Again, the same general features are prominent: a short linear section followed by an upward sloping section that culminates in a gentle hump (80-100 degrees). Once more, the data for the post-buckled portion rises monotonically and steadily. A comparison of the slopes for both conditions 1 and 2 samples shows that the initial linear slope gradually increases until a buckle appears. After the buckle, the slope is steady but higher than that of the initial linear portion. There is one noticeable difference between conditions 1 and 2 samples[2]. For condition 2 samples, the post-buckled curves match well for a large angular range (up to 260 degrees). This may point to the improved uniformity of the ribbon under condition 2 processing parameters. However, for condition 2 samples, undulations were found to occur slightly below 200 degrees in 3 out of 4 samples.

---

[1] For instance, stick-slip between clamp and insert could affect results.

[2] Numerical results of error analysis of data are omitted.

Figure 7 Photograph of defective 24-fiber ribbon

Figure 8 shows data for the defective ribbons. The nature of the defect is shown in Figure 7. This particular defect consists of an asymmetric deficiency of matrix localized between two fibers (2nd green and 2nd brown). Looking at the torque versus angle of twist data, the one obvious difference is the nature of the initial buckle. The instability occurs over a wider range, 80-110 degrees, and instead of a smooth hump, it appears as a short but sharp drop (Figure 9). The change in the nature of the instability can be attributed to the defect. The defect can affect the stiffness of the structure while also creating an asymmetry or imperfection that leads to such a drop. Of course, the nature of the drop will depend upon the location and size of this particular defect. For the defective ribbons, 3 out of 4 samples split (along the entire length of the sample) during the test at the location of the defect. Though for one sample, the split occurred at a twist angle of 200 degrees while in another sample, it split at a twist angle of approximately 300 degrees. In one instance, the green fiber was clearly separated. And for another sample, it split during removal from the clamps. It is likely that this sample had a split, which had not traversed the entire length of the ribbon.

Figure 5 Photograph of twisted ribbon sample during secondary instability

Figure 6 Torque versus angle of twist for 24-fiber ribbons manufactured under condition 2
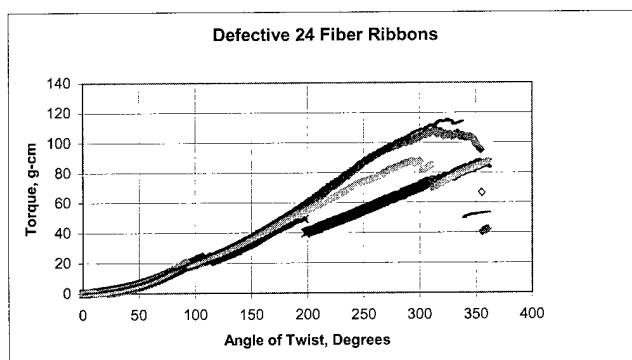
Figure 8 Torque versus angle of twist for defective 24-fiber ribbons manufactured under condition 2

Similar to the undefective condition 2 samples, the post-buckled curves match quite well in the range of 100-200 degrees of twist.

Finally, all curves appear to reach a maximum torque value before the end of one full rotation. However, at this point, the variability in the maximum torque value and twist angle masks any attempts to use it as an indicator of ribbon quality.

4.2 12-Fiber Ribbon

Figure 10 shows the twist data for the 12-fiber ribbons. The equivalent point of instability, or buckling, was determined to occur around 320 degrees. Examination of samples after removal revealed no debondings. Condition 1 sample reached a maximum torque around 420 degrees and then proceeded to decrease. During this decrease, the sample was experiencing significant shortening due to a very complex three-dimensional distortion similar to Figure 5. We would expect that if sufficiently large rotations could be imposed without boundary problems, that the qualitative nature of the torque versus angle of twist plot would match, in general, that of the 24-fiber ribbon.
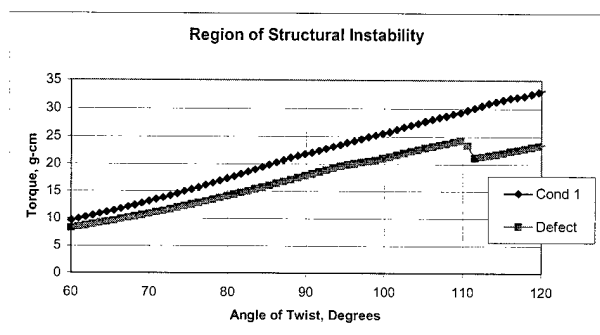

Figure 9 Zoom of torque versus angle of twist data in the buckling region

4.3 Material Properties

In this section, we calculate certain mechanical properties of the ribbon from the torque versus angle of twist data. Specifically, we calculated the inplane shear modulus and the longitudinal Young's modulus of the ribbon. To obtain the ribbon shear modulus, we employed the following relation [3]

$$T = \frac{1}{3}bc^3 G\theta + \frac{1}{360}Ebc^5\theta^3 \qquad (1)$$

where T is the applied torque, G is the ribbon shear modulus, b is the width of the ribbon, c is the thickness of the ribbon, E is ribbon longitudinal tensile modulus, and θ is the angle of twist per unit length. To calculate the shear modulus from the twist data, we take the first term on the right hand side of the equation and curve fit the linear portion of the data set. This term provides only a first order approximation to the shear modulus ([4],[5]). Using a least-squares fit of the data in a range of 0-6 degrees of twist [6], we calculated a shear modulus of 4.5 x 10^9 dynes/cm^2 for 24-fiber ribbon condition 1 sample, 5 x 10^9 dynes/cm^2 for 24-fiber ribbon condition 2

sample, and 4.4 x 10^9 dynes/cm^2 for 12-fiber ribbon condition 1 sample. There was some difficulty in obtaining accurate curve fits for the defective ribbon samples. The shear moduli for the defective ribbons ranged from 2 to 8 x 10^9 dynes/cm^2. As a point of comparison, an oscillatory test was used to determine the shear modulus of 24-fiber ribbon. The test predicted a ribbon shear modulus value of 10^{10} dynes/cm^2 for a condition 2 sample without a defect and a ribbon shear modulus value of 5 x 10^9 dynes/cm^2 for a condition 2 sample with a defect.

Looking at Equation (1), we see that the contribution from the ribbon longitudinal modulus term grows at a fast rate as the angle of twist increases. This modulus includes the influence of the fibers, matrix, and coatings (contribution dependent upon volume fraction). Of these components, the modulus of the fiber is significantly higher and so its contribution to the overall longitudinal modulus of the ribbon is most important. So any decrease or increase in the volume fraction of the optical fiber will have an influence on the twist strength of the ribbon. Curve fitting of the data to obtain ribbon longitudinal modulus values was performed but that data is not presented here.
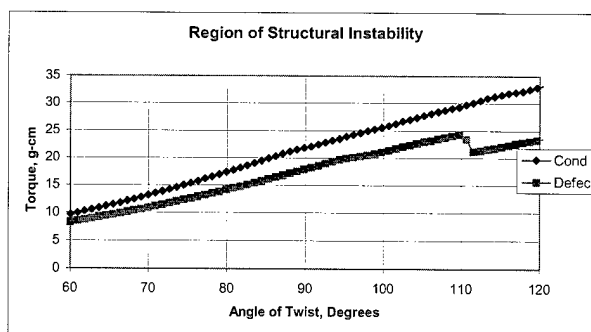

Figure 10 Torque versus angle of twist for 12-fiber ribbons manufactured under condition 1

5. Debondings

Examination of samples upon removal revealed debonding sites. For the jog samples, the area of debondings appeared to be larger than the samples for the line speed. However, since the number of samples were small and the technique to evaluate the debonding area rather crude, a microscopic evaluation of debonding areas may provide a more meaningful measure of interface strength between the colored fiber and matrix. These debondings are believed to be a result of the shear stresses or normal radial stresses that develop along the interface.

6. Discussion

From the twist data for 24-fiber ribbon, some common characteristics have been discerned: short linear portion

followed by an upward sloping nonlinear section that culminates in an instability.

After the instability point, identified as a buckling mode, the torque increases monotonically and steadily with angle of twist. In this post-buckled region, the behavior begins to diverge amongst the various ribbon samples as the angle of twist approaches a full turn. In the post-buckled region, small variations in the curve have been attributed to debondings at the matrix/colored fiber interface. Sudden large changes in the torque values at the higher angles of twist are indicative of more complex three-dimensional responses.

In studying the twist data, there is some confidence that such data can provide insightful, if not quantitative, information about the quality of a ribbon. For instance, the existence of a defect was apparent in the signature of the instability point. Also, only defective ribbon samples were split. The difference in ribbon quality between the two different processing conditions was apparent in the variation of the post-buckled curves. Of course, to increase confidence in such a test, a database of responses of typical and defective ribbons must be compiled.

Looking forward, these results point to the possibility of developing a non-destructive ribbon twist test, one that would detect or fail only defective ribbons. With a nondestructive test, the possibility of its presence on the line, evaluating ribbon as it is being manufactured, is more likely. Also, such a test may be able to distinguish between various grades of quality.

7. References

[1]   Generic Requirements for Optical Fiber and Fiber Optic Cable, Bell Core, September 1994.

[2]   Gong, X.L., Laksimi, A., Lai, D.W., and Benzeggagh, M.L., Stress Analysis in Unidirectional Composite Plates under Torque Loadings: Experimental Observation, *Journal of Reinforced Plastics and Composites*, Vol. 14, pp. 29-44, 1995.

[3]   Timoshenko, S., *Strength of Materials: Part II*, Van Nostrand Company, New York, 1947.

[4]   Timoshenko, S., and Goodier, J.N., *Theory of Elasticity*, McGraw-Hill Book Co., New York. 1970.

[5]   Tsai, C.L., Daniel, I.M., and Yaniv, G., Torsional Response of Rectangular Composite Laminates, *Journal of Applied Mechanics*, Vol. 57, pp. 383-387, 1990.

[6]   MATHCAD, Version 7.0, User's Guide, Mathsoft Inc., 1997.

8. Biography

Mahmood Tabaddor has been a Member of Technical Staff at Bell Laboratories since 1996. He has his graduate degrees in Engineering Mechanics from University of Michigan and Virginia Tech. He has had brief stints at Georgia Tech and Goodyear Tire & Rubber Co.

Charles Aloisio began his career with Bell Labs in 1952. He worked in the Materials Group with Bell Labs in Indianapolis from 1967 to 1972, while obtaining his MS and PhD from Purdue University. He is currently a Distinguished Member of Technical Staff in the Material Technology Group and has worked on applying rheology and viscoelasticity to a variety of materials such as polypropylene and polyethylene for cable sheathing and DEPIC insulation, copper and optical fiber coatings.

Operative Lifetime of Commercial Fibers

Torbjörn Svensson

Telia Research AB, Farsta, Sweden
+46-8-713-8159 · torbjorn.k.svensson@telia.se

Jan Björkman

Telia Carrier & Networks, Farsta, Sweden
+46-8-713-2027 · jan.b.bjorkman @telia.se

Abstract

Experiments presented here on commercial fibers during 5 years accelerated aging have shown that, depending on environment, vendor, and external conditions, the estimated lifetime of regular G.652 fiber may be considerably less than the usual expectations on fiber cable. Environmental influence may cause excessive transmission losses and also makes the fibers increasingly vulnerable to mechanical stress with time.

The operative lifetime of terrestrial cable expectedly will include temporary events as rearrangement and splicing, when discoloring, embrittlement and coating delamination affects the handling of aged fiber. Such events will cause the end of life of severely aged fiber.

The estimation here of operative lifetime in case of aging requires an approach different to the classic usage of n-values applied on stress cracking. A method suitable for calculating the operative lifetime of aged fiber was thus elaborated. A physical foundation of underlying mechanisms of degradation was also sought for by AFM studies.

Keywords

Optical fiber; G.652; lifetime; aging; strength; ribbon; delamination; discoloring.

1. Introduction

Today, a million miles of fibers is in service at Telia in Sweden. The steadily increasing amount of fiber, and the variations in environmental resistance of fibers housed by the same G.652 family, some years ago motivated a long-term study of aging [1], which now has concluded with the prediction of in-field lifetime of the fibers.

The estimation of threats due to aging required an approach different to the classic usage of so called n- and B-values applied on stress corrosion [2, 3]. A method suitable for estimating the operative lifetime of aged fiber was thus elaborated. The method is based on two-point bending of aged fibers, extrapolation of Weibull- and Arrhenius data to the relevant fiber lengths and temperature, and the mechanical stresses involved in the in-field conditions for a number of cases.

Some results from the aging studies such as strength degradation will be presented here, along with AFM studies on underlying mechanisms of degradation, and briefly commented. Finally, based on the test data from 5 years of aging, the operative lifetimes of the tested commercial fibers will be shown, calculated for cases of water-immersion at 10 °C.

2. Trends During Aging
2.1 Findings in Brief

An exhaustive embrittlement of commercial optical fibers soaked in water was found at 80°C, but also at ambient temperature, 23°C, a significant reduction of strength was observed after five years of aging. Aging of fiber in pure gel, and of gel-coated fiber in water lead to a somewhat complex behavior, although gel has a protective influence, in general. Filling gel also increases the n-value, which is advantageous for stressed fibers. Generally, the fibers tested should perform well during a long period, but water ingress and high temperature may drastically shorten their operative life.

Severe problems may arise from aged fiber. Some of these are triggered by handling, e.g during the repair of water soaked cables. This procedure demands convenient stripping and splicing of fibers. Changes in fiber strength, strippability or color identification may aggravate or interrupt the work. Other problems stem from permanent stress causing intrinsic failures, e.g due to fiber excess in a ribbon. Finally, well-known problems are transmission losses originating from the swelling and delamination of coating.

The calculations made here indicate that mechanically related problems from aging may arise after quite a short period, just a few years in water.

2.2 Degradation of fiber

The degradation of 5 fibers from different vendors has been measured in varying environments during a 5-year period. On the following pages is shown the strength of aged fibers from the vendors A, B and C. Their n-values will also be briefly commented, although graphs are not presented.

Data are median values of strength from two-point bending at 23°C 50% RH after aging in three environments: water, gel, and gel-coated fiber in water, at two temperatures: 23°C and 80°C. The time-axis is logarithmic, given as the number of weeks of aging. The strength is given for a strain rate of 30 % per minute, and was measured after one week of reconditioning at 23°C 50% RH. Strength of the 4-fiber ribbon is calculated per strand, i.e. that of glass. More details can be found in Ref [1].

2.2.1 Strength

During the last years of aging, there has been an obvious tendency of decrease of strength of all the tested fibers, from all the vendors. All fibers (strands, and ribbon) being immersed in water, with clean surface or covered with a layer of gel, have lost at least a portion of their strength after 5 years of aging, Figures 1- 6.
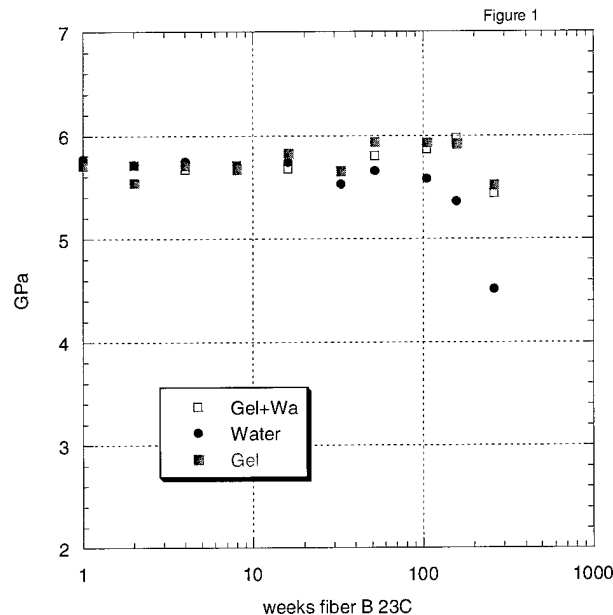
has to assume that handling of the fiber in field will be adversely affected after sufficient time in water.

Aging of fibers in pure gel causes irregular changes of strength with time. The strength is preserved under considerable time of aging, though. See Figure 2 for fiber B at 80 °C. It is a well-

Figure 1. Fiber B 23°C
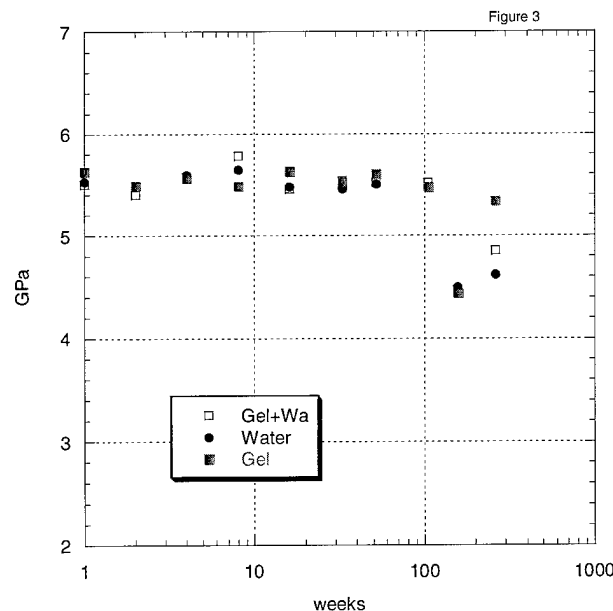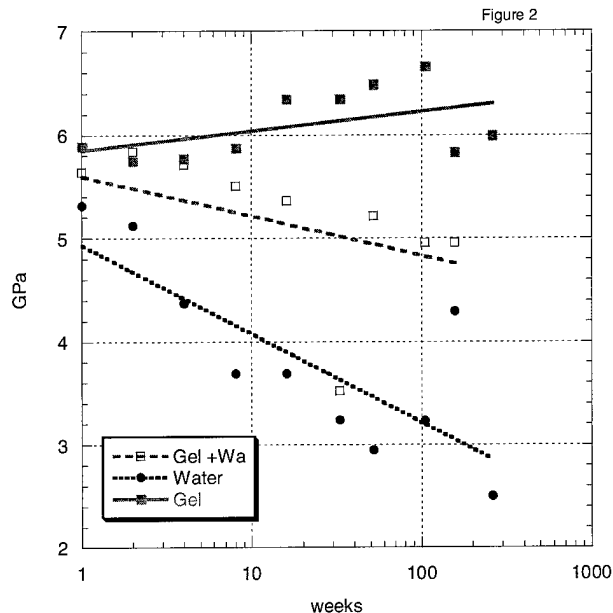

Figure 2. Fiber B 80°C

Figure 3. A-ribbon 23°C

Figure 4. A-ribbon 80°C

Some of them have been severely embrittled since the start of testing. This is the case both at 23 °C and at 80 °C. Data bears no evidence of any permanent level of strength to be reached after long time of aging in water, but very low strengths have been reached, out of handleability in bending tests. Conservatively, one
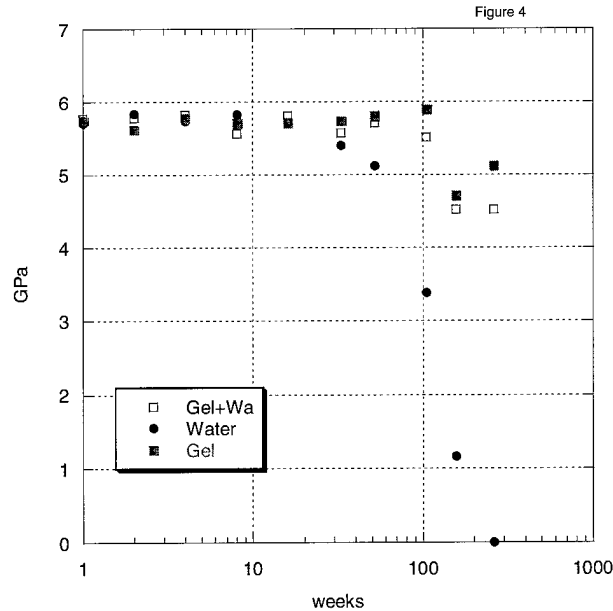
known fact that the strength can increase markedly after a short period in gel. Keller reports on a 10 % increase after 4 weeks in gel at 85°C [4]. A longer period of observation shows that the change in gel may not be permanent, however. An example is C-ribbon, which continually degrades in gel at 23 °C (Figure 5). To

various extents, the very last samples taken of the fibers all show a tendency to weaken even in gel.

Gel will keep the strength essentially constant with time for the A-fiber, while the initial increase is significant in Vendor C fibers in gel. The reason might be sought in the used gel formulas: their abilities of glass reactions, buffering, pH-value etc., or of the coating: absorption of gel components, swelling or dissolution. The gels were specific for each vendor, and the physical mechanism behind strength increase can not be easily derived. Certain observations bound to the vendor will follow below.

Vendor A fiber. All environments, also pure gel causes a strength decrease of 15% or more, at 156 weeks. The worst decrease at that time was found in water at 80 °C, in ribbon which was embrittled by a factor of 5. After 260 weeks in this environment, the fiber could not even be handled in a bending test. See Figure 4. Also water at ambient temperature degraded the fiber, but after considerably longer time, Figure 3. A drastic decrease of strength thus occurs after about 30 - 100 weeks in water, depending on the temperature. The fiber strands appear to have resisted aging better than the ribbon did, in all environments. Even a small increase from a minimum of 2.5 GPa was noted from the final years' of aging. (No graphs)

Vendor B fiber in water at 80 °C shows a significant minimum of strength at 50 weeks, about 3 GPa, thereafter it increases to about 4.2 GPa at 156 weeks, followed by a new minimum of 2.5 GPa at 260 weeks. Figure 2. The occasional increase of strength may be caused by a change of geometry of growing notches during corrosion of the fiber glass. Visually, the smoothest surface of glass was also observed to occur at 156 weeks, by AFM measurements on fiber aged during 16, 52, 156 and 256 weeks, respectively.

Vendor C fiber. A tendency for C-fiber (and for A-fiber) is that the strength after aging in gel is lower for ribbon than for strands. However, the strength of C-fibers at 80 °C is markedly higher in pure gel than in water, or as gel coated in water. Figure 6.

2.2.2 n-values

This parameter (stress corrosions susceptibility parameter, *n*) indicates the fiber's resistance to fatigue, and the n-value should be high. Generally was found that the value increases with the time of aging, especially in gel combined with water. The observed effects of aging on *n* can not be presented here in detail, but will be briefly summarized by the conclusion: filling gel increases the value of *n*, and preserves or increases the fiber strength.

The latter effect may be due to an improved n-value as well as to a reduced corrosion. Also water alone increases the n-value, *but* essentially in fibers of significantly reduced strength, which models for stress-induced crack propagation can explain. A reduced strength is found conjunct with increasing value of n found after sufficient time of aging.
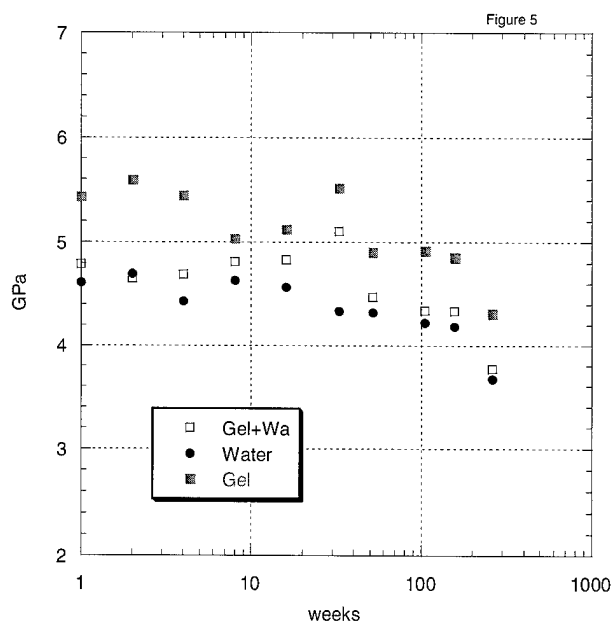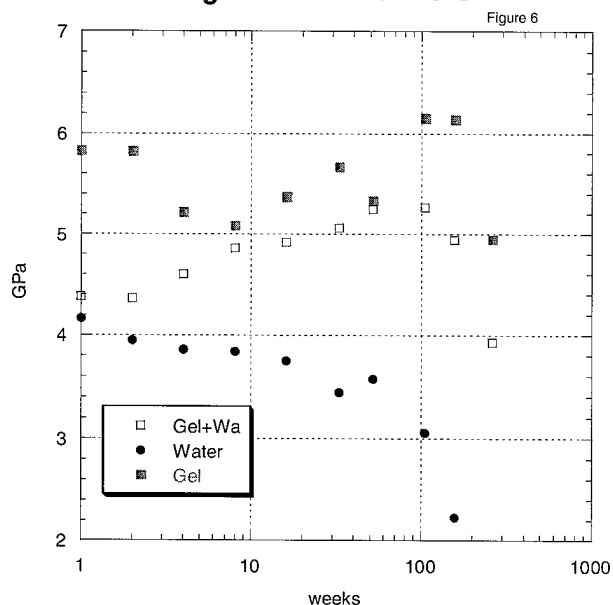

Figure 5. C-ribbon 23°C

Figure 6. C-ribbon 80°C

2.3 Coating Influences

2.3.1 General

The ribbonizing of strands appears to little influence the aging of the tested fibers. Generally, the strength is *lower for ribbon than for strands in filling gel*. This effect may be a bending test artifact caused by the swelling of coating, which could not be measured by direct means. In the *presence of water* the strength of Vendor C-ribbon (only) was *higher* than for the strand. Although the interpretation of effects may vary, figures and measurements indicated dimensional changes in all the environments, which continued throughout the period of aging.

The curing of coatings (primary layers and ribbon) influences the aging resistance [5]. The irradiation dose must be carefully adjusted. A 100 % cure is not striven for, since e.g strippability is adversely affected, and too little UV leads to sticky fibers which degrade faster. The chemical degradation of polyurethane acrylate has been described by e.g Per-Anders Högström [6]. The exact degree of cure of the tested fibers was not known, and may have varied between strands and fiber ribbon.

2.3.2 Delamination

Splicing and termination of delaminated fibers may end in a catastrophe. If the coating tends to slip on the glass it may be easily peeled off, leaving large portions of the fiber naked. Such a fiber can be handled, in principle, but it must be immediately protected which is out of reach using conventional tools. The adhesion of coating to the glass may be tailored to the application by a chemical primer. A firm adhesion must be weighed against the ability to mechanically strip the fiber, not leaving residuals on the glass. The ribbon must also be possible to cleave into strands.

During 1996 some measurements at Telia had shown that water ingress lead to changes in attenuation after only one day in this environment, water and 80 °C. Further studies of the attenuation of Vendor A and -C ribbons showed a gradual change, up to a hundred hours. Thereafter the attenuation was fairly constant, about 1.25 - 2.0 dB per km, until the experiment was interrupted after 2,000 hours of soaking.

Delamination of fiber coating and ribbon was later found to be the reason for transmission losses, originating from microbending. Observations showed that A-ribbon would swell after 4 weeks of soaking in water at 80 °C during which the thickness can vary between 0.4 and 0.6 mm. Microscopy of the cross section of a ribbon showed that glass fibers were misaligned, leading to bends along the fiber. Similar observations were made for Vendor C-ribbon, after 16 weeks of soaking.

2.3.3 Discoloring

The color of coating must be preserved as it is essential for the identification of fibers during cable repair and termination. Due to the small dimensions, a slight discoloring may aggravate identification. The problem has been treated in literature [7]. A standard test would simplify comparisons, here the grade of discoloring is determined subjectively in Table 1.

Only the highest temperature, 80 °C affected discernibility, of Fiber B and Vendor C fibers. For technical reasons Vendor A fibers may not be shown in Table 1. On C-ribbon the color of the fiber strand began to change in gel at 104 weeks, water caused a

slight change after 16 weeks, while gel coated fiber in water ("Mix" in Table 1) changed after 33 weeks.

A similar, but delayed dependence of environment was observed on fiber ribbon. Rating of the discernibility is from 0 (original appearance) to 5 (severely discolored, usually dark brown). Discernibility below 3 would be fully acceptable.

| Table 1. Discoloring at 80 °C								
	B-fiber strand			C-fiber, strand			C-fiber, Ribbon		
weeks	Mix	Wat	Gel	Mix	Wat	Gel	Mix	Wat	Gel
16	1	1	0	0	1	0			
33	2	1	1	1	1	0			
52	3	2	2	2	1	0	1	0	0
104	3	3	2	3	2	2	3	2	2
156	4	4	3	4	3	3	5	4	4
260	4**	4*	4	5*	4*	4	5	5	4
Peeling-off (*) or glass fracture (**) unabled stripping								

3. AFM Studies

A number of models of chemical attack, nucleation of flaws, and of microstructural development were matched against data from measurements. Identical models cannot be used for all fibers, since they do not react consistently to the same environment. Using AFM, atomic force microscopy, showed that the surface morphology of glass sometimes varies between fibers treated the same way. At least one of the fibers studied had a pattern of rot, shown in Figure 7, in which the width and height of the small spots develops irregularly with time. (The technique used in this picture has transformed shallow mesas into steep mountains).

In these AFM studies, the limited number of scanned surfaces and two-point bending could not be used to reveal the earliest flaws which may occur during aging. Extrapolation techniques and more data are necessary to find an application in lifetime estimation according to the Section 4. There is no doubt that an increased knowledge of surface morphology of fibers could help in developing models, which quantitatively relates to macroscopic measures as the strength. Some examples will be given below.

3.1 Structural relations

Two measures are coveniently accessible from the AFM instrument: the RMS-value of surface roughness, and the average diameter, D of surface irregularities. The value of D was estimated from the micrographs by linear intersection.
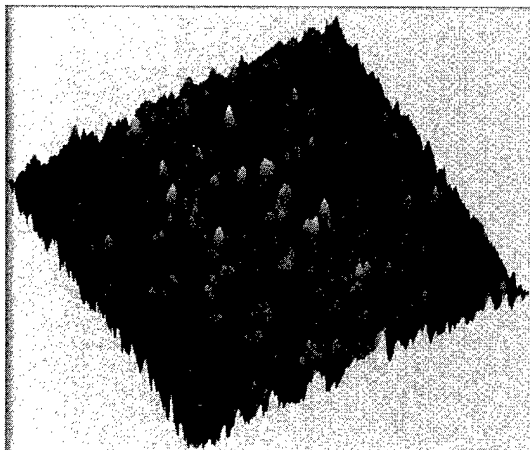
Figure 7. A-ribbon after 156 weeks at 80°C in water. Topography of 3x3 µm²surface.

The observed fiber strength could be well related to calculated strength by either of two different approaches: 1) use fracture mechanics on RMS values only, or 2) use the ratio RMS/D, which is jusified by the notch effect imposed by soft spots, when observed. These features have a limited size and equiaxial shape reminding of rot, i.e., they form a protruding layer assumedly being soft and extending into the bulk of glass. The corresponding strength relations are presented here without derivation.

Approach (1) assumes a notch depth proportional to RMS, which combined with the fracture toughness of glass gives the relation with strength, S according to

$$S = 12/(a_0 + 4RMS)^{1/2} \text{ Gpa}$$

where $a_0 \approx 4.5$ nm, at a strain rate of 30% per minute.

Approach (2) assumes a shape factor due to the softer portion extending into stiffer bulk glass. The spots have an average value of lateral extension, D. The notch effect on stress acting on the deeper portion of glass is proportional to the ratio RMS/D, and leads to a calculated value of strength, S according to

$$S = So/[1 + 8.5(RMS/D)] \text{ Gpa}$$

where So is the strength of fresh fiber, before aging. The average strength of Vendor A ribbon was initially 5.5 GPa, and 1.16 GPa in the degraded state shown in Figure 7. The data from AFM was RMS= 10.9 nm, and D= 53.6 nm. Applying the last equation gives a calculated value of 2.0 GPa, which is 1.74 times higher than the real strength. A conservative estimation of strength is approached by choosing the lowest value calculated from the two

expressions. In this case the approach (1) would give 1.73 GPa, or 1.5 times the real strength. The choosen example is occasionally not very significant, probably because of a scattered strength. On the other hand, good estimates were found in all other AFM specimens where the calculated strength was within 0.83 and 1.06 times that of real strength. The two expressions are empirical, physically founded approaches, and based on structural causes of stress amplification. They might be useful in cases, when there is a need for an interpretation of failures and the amount of fiber is sparse.

4. Operative Lifetime of Aged Fibers

A number of cases are believed to impose an augmented risk for failure of transmission. The ones presented are all due to the mechanical failure of fiber in 96-fiber cable: resplicing (assuming two levels of strip force, 8.9 N according to an IEC TC 86A proposal of peak force, and to 1/3 of the initial bending strength), handling (0.3 m radius bends along 10 m cable), cable pitch (radius 0.243 m). Fiber bends in manholes and ducts, and ground displacements due to excavations or creep of soil and rocks, depend on local conditions that were not calculated here. Other cases are ribbon strain due to internal fiber excess (0.1%), and bends in splice boxes (radius 35 mm). Also, the effective radius from allowed cable bends and pitch, and finally a calculation being harmonized with Telia's lifetime requirements based on stress cracking and 1/3 of proof stress.

The procedure for determination of lifetime is described in Section 6.4. In Table 2 below are shown the results from applying this procedure on one fiber strand and on two ribbons, using aging parameters in water at 10°C, for each fiber type. Fixed variables, L, F and the load at failure, were estimated according to the respective case.

Lifetimes for fiber in filling gel are considerably longer, and will not be presented. It is interesting to compare the lifetimes with the lifetime usually required for cables, 40 years or 2 080 weeks. The lifetimes are based on eq (3), and on two values of $m_d = 20$ and 10, respectively, since an exact value of the Weilbull modulus is difficult to determine. For other parameters see Section 6.2, Table 3.

Table 2 shows, that stripping during cable repair, and residual stresses due to fiber excess within ribbon, may be crucial for lifetime. The calculated values are not very reliable, since values of activation energy and Weibull modulus could not be very accurately determined. Qualitatively, the ranking of risks will not be altered by these circumstances, though.

Table 2. Lifetimes in water at 10 °C

Case	Description	L, km	F, %	Load, GPa	Lifetime, weeks $m = 20$			Lifetime, weeks $m = 10$		
					Vendor A ribbon	B-fiber, strand	Vendor C ribbon	Vendor A ribbon	B-fiber, strand	Vendor C ribbon
1.1	resplicing 8.9 N	0.096	10	0.73 dynamic	604	1 635	3 393	311	110	30
1.2	resplicing 1/3 init	0.096	10	1.89 dynamic	304	105	(13)	(270)	(91)	(13)
2.1	handling	0.96	1.0	0.015 dynamic	$2.1 \cdot 10^4$	$6.2 \cdot 10^6$	$3.8 \cdot 10^5$	7 651	$7.7 \cdot 10^5$	$1.2 \cdot 10^5$
2.2.1	cable pitch	100	0.1	0.018 static	$1.4 \cdot 10^4$	$2.7 \cdot 10^6$	$2.4 \cdot 10^5$	4 062	$2.0 \cdot 10^5$	$5.7 \cdot 10^4$
2.2.2	man hole/ canal.	1-100	0.1	--- static						
2.2.3	ground displ.			--- static						
2.2.4	ribbon strain	10	0.1	0.26 static	1 203	$(1.2 \cdot 10^4)^1$	$1.1 \cdot 10^4$	460	580	1 618
2.2.5	splice boxes	0.192	0.1	0.125 static	2 872	$9.5 \cdot 10^4$	$3.7 \cdot 10^4$	1 178	$1.2 \cdot 10^4$	$1.1 \cdot 10^4$
2.2.6	allowed bends + cable pitch.	10	0.1	0.035 static	8 081	$8.6 \cdot 10^5$	$1.3 \cdot 10^5$	2 634	$7.9 \cdot 10^4$	$3.3 \cdot 10^4$
Harm.	1056-A215	100	0.1	0.23 static	1 211	$1.2 \cdot 10^4$	$1.2 \cdot 10^4$	424	413	1 211

Dynamic loading condition is 30%/min. [1]B-fiber only available as fiber strand
Lifetimes is based on eq (3), eq (4) and Table 3. Values within brackets () are minimum times limited by the parameter k_2, which is: fiber B: 0.25 w @ 80° C/ 91 w @ 10 °C, C-ribbon: 0.01w @ 80 °C / 13 w @ 10 °C, A-ribbon: 50 w @ 80 °C / 270 w @ 10 °C.

5. Conclusions

In this study have been predicted the operative lifetimes of aged fiber cables, under the assumption that lifetime is limited by events as failing attempts to handle and repair the cable, but also by intrinsic failures of fiber. These lifetimes may be considerably less than the usual requirements, 25 - 40 years.

The risk for problems is enhanced by harsh environment, and is further increased by events involving handling of the fiber. A most annoying situation is the splicing of fiber necessitated by e.g cable cuts during excavation, after long time water ingress into cable. The life of a large cable length may then come to an end with a single cable cut. Eventually all of a span must be replaced, significantly increasing the cost of repair. Besides such local events, the risks may be diffusely scattered in the network, such as aging embrittlement combined with external stresses, or internally due to e.g fiber pitch and excess length of fiber in ribbon.

However, thanks to the filling gel used in many cables, the embrittlement caused by water and time can be avoided, or delayed. The risks can be minimized by applying filling gel, by installing in well drained ground and dry tubes, and by carefully controlling the manufacturing processes, especially of fiber ribbon.

The facts and arguments presented in this paper should motivate operators to perform their own analysis of environmental effects on the reliability of proprietary networks in order to assure future assets. Such research and analysis will certainly always be legitimate when going to introduce new or modified fibers, vendors, cable constructions and installation procedures.

6. Appendices

6.1 Strength distribution

The probable strength, S_L of an arbitrary length of fiber, L is assumedly related to the effective length and strength of a two-point bending test specimen, L_{ref} and S_{ref} respectively, through the Weibull parameter m according to

$$\frac{S_L}{S_{ref}} = \left(-\frac{L_{ref}}{L} \ln(1-F) \right)^{1/m} \quad\quad\quad (1)$$

6.2 Degradation in water

Empirically, the time-variable reduction of strength of fiber during a two-point bending test aged in water at 80°C can be expressed by a 3-parameter relation as:

$$S_{ref} = S_{ref}^0 / (1 + k_1 \cdot (t - k_2)^p) \quad\quad\quad (2)$$

where the time of aging, $t > k_2$ and S_{ref}^0 is the strength of fresh specimens at $t = 0$. S_{ref} is thereby the strength during two-point bend testing of an aged specimen.

While eq (2) is a degradation function, f, which varies with time, the eq (1) describes the failure distribution g(L, F, m), at a specific time. At arbitrary time, t the varying strength will be given by

$S_L=f(t)\cdot g(L,\ F,\ m)$, or $S_L(t) = S_{ref}\ (t)\ \cdot\ (S_L/\ S_{ref})$, since m is assumedly time-invariant. From this follows the complete expression for the time-dependent strength of arbitrary long fibers at a certain probability F:

$$S_L(t)= \frac{S_{ref}^0}{1+k_1(t-k_2)^p} \cdot \left(-\frac{L_{ref}}{L}\ln(1-F)\right)^{1/m}$$

The time-to-failure is explicitly solved as:

$$t = k_2 + \left(\frac{1}{k_1}\left(\frac{S_{ref}^0\cdot\left(-(L_{ref}/L)\ln(1-F)\right)^{1/m}}{S_L}-1\right)\right)^{1/p}$$

$$= \{F \ll 1\} =$$

$$t = k_2 + \left(\frac{1}{k_1}\left(\frac{S_{ref}^0\cdot\left(F\cdot L_{ref}/L\right)^{1/m}}{S_L}-1\right)\right)^{1/p} \quad\text{.................(3)}$$

required that

$$\frac{S_{ref}^0}{S_L}\left(F\cdot L_{ref}/L\right)^{1/m}>1.$$

By fitting of the parameters k_2, k_1, and p to the measured data from fibers in this study according to Table 3 below, their degradation in water is quite well described, for longer periods. One should keep in mind that values of activation energy, Q and Weibull modulus could not be very accurately determined.

Table 3. Aging parameters of fibers

Fiber	k_2, weeks	k_1, weeks^{-p}	p	Q, kJ
Fiber B	0.25	0.102	0.5	70
A-ribbon	50	0.035	1.0	20
C-ribbon	0.01	1.0	0.9	30

The values of activation energy are determined from the onset of degradation, being adjusted by a few steps of iteration. An example of a measured and calculated degradation in water is shown in the Figure 8 below. Although the very first week of strength may not be accurately modeled - Figure 5 and 6 hints at a temperature-dependent, transient drop - the residual time of operative life will be.

6.3 Temperature dependence

From the Arrhenius relation between reaction rates at different temperatures T_1 and T_2 follows that the time, t to reach a certain degree of completion can be expressed by the equation:

$$\frac{t_1}{t_2} = \exp\left[\frac{Q}{R}(\frac{1}{T_1}-\frac{1}{T_2})\right] \quad\text{.................(4)}$$

where $R = 8{,}3143$ J/K. The expression is valid under the assumption that the reaction process is not modified by temperature. Alternatively, the activation energy, Q, can be evaluated from the two values of time necessary to reach the same, say, strength according to

$$Q = R\cdot\ln(\frac{t_1}{t_2})\Big/(\frac{1}{T_1}-\frac{1}{T_2})$$

As an example, the strength of Vendor B fiber in water at 23 °C (296 K) and at 80 °C (353 K), shows a small but significant decrease after approximately 200 and 2 weeks, respectively. The above expression yields an activation energy of 70 kJ/mole. The value is comparable with 80 kJ/mole reported [8]. In other cases treated here, the evaluation yields significantly lower values of Q, 20 - 30 kJ/mole. See Table 3. Similar low energies are also observed during static fatigue, values about 55-65 kJ/mole at 3 GPa are recently reported [9].
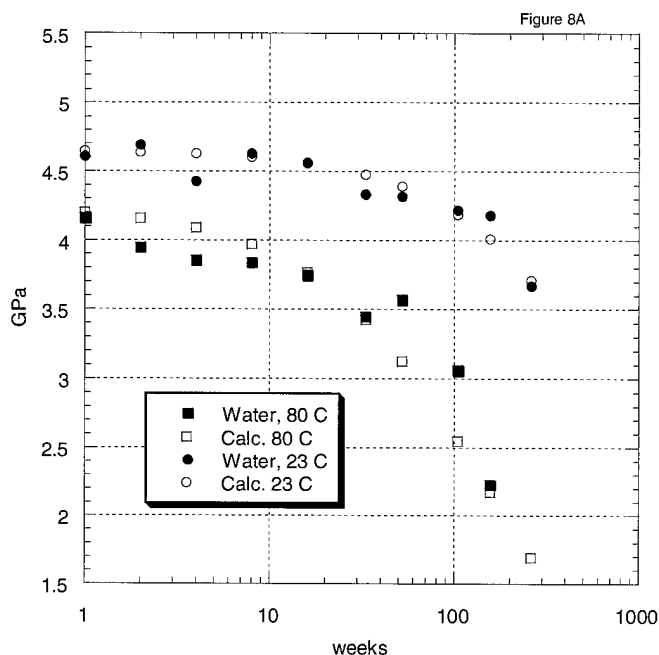
Figure 8. Calculated and measured strength of C-ribbon at 23°C and 80°C in water.

Extrapolation of time according to eq (4) down to a ground temperature of 10 °C will shift the strength decrease to 738 weeks, or 3 times longer than at 23 °C.

6.4 Lifetime of exposed portions

Below is the procedure used to determine the lifetime of aged cable portions assumedly prone to mechanical damage. The first two steps are useful when experimental facilities do not allow the determination of times-to-failure of long fiber lengths:

1. Try to estimate the *m*-value of the lower failure mode in a bending test of fiber aged at e.g 80°C.

2. Extrapolate bending strength to long lengths, under the assumption of a unimodal strength distribution.

3. Apply some model, e.g equation (2), such that the degradation of fiber with time can be calculated. Use the model to determine the value of the activation energy Q from two sets of temperature data, using eq (4). The temperature must not be such that wrong mechanisms interfere.

4. For each case of augmented risk, a suitable failure criterion in the operative environment is stated. The criterion used here is the allowable level of probability, F that strength approaches a certain load. Assign fixed values of the variables, L, F and the load at failure of the exposed portion.

5. Finally, make an Arrhenius extrapolation of time-to-failure at operating temperature, by multiplying with eq (4). The result will be the requested time of life.

A number of cases and criteria of failure exists, depending on networks and needs. Some examples are given in Table 2.

7. References

[1] J. Björkman and T. Svensson, "Ageing of fibres and ribbon in water and filling compound", *Proc. 45th IWCS*, 547-553 (1996).

[2] Y. Mitsunaga, K. Katsuyama and Y. Ishida, "Reliability assurance for long-length optical fibre based on proof testing", *Electronics Letters* 17, 567-568 (1981)

[3] T. Svensson, "Evaluation of B-values of Telecom Fibers. Objectives and Methods", *Proc. Materials Research Society*, Vol 531, 47-52 (1998).

[4] A. Keller et al., "Continued development of the plenum-outdoor totally dry optical fiber cable designs", *Proc. 48th IWCS*, 409-415 (1999).

[5] H. H. Yuce et al., "The mechanical performance of aged dual-coated fibers with varying extents of coating cure", *Proc. 42nd IWCS*, 857 (1993)

[6] P.-A. Högström, S. Karlsson and U. W. Gedde, "Structural changes in polyacrylate coatings exposed to degrading environments", *Proc. 45th IWCS*, 464 (1996)

[7] R. Frantz, and I. Plitz, "The effects of aging on the discernibility of the color identification of optical fibers", *Proc. 42nd IWCS*, 850 (1993)

[8] Volotinen, Griffioen, Gadonna, and Limberger, eds., *Reliability of Optical Fibres and Components, Final Report of COST246*, Springer-Verlag, p 97 and 141, (1998)

[9] N. Evanno, M. Poulain an A. Gouronnec, "Optical fiber lifetime in harsh conditions", *Proc. SPIE*, Vol 3848, 70 (1999)

The Authors

Torbjörn Svensson received his M.Sc. and Ph. D. from the Royal Institute of Technology, in Stockholm, Sweden. He joined Telia 1985 as a materials specialist. His engagement has flourished between quality assurance, testing- and measurement techniques for fibers and cables, splicing technology, fiber access networks and systems reliability, holding some patents on test methods. Internationally, he has contributed some of his findings to the IWCS, SPIE, MRS, COST, ECOC, NFOEC, and other fora. Torbjörn is project manager at Telia Research.

Jan Björkman holds a degree in chemical engineering from Malmö Technical School. He joined Telia 1977 as a specialist in polymer materials. He is responsible for optical fibers and cables. Being engaged in quality assurance and environmental issues, once he initiated, and encouraged this study. Jan is senior engineer at Telia Carrier & Networks. Internationally, he participates in the IEC SC 86B and the CENELEC TC 86B.

Measurement of Discrete Strain Change in a High-Fiber Count Slotted-Core Ribbon Cable Using Bragg Gratings

Frederick M. Sears, Shami S. Sodhi, Hani M. Nassar,
Robert J. Whitman* and Allen C. Gregory
Research, Development & Engineering
Corning Cable Systems LLC, Hickory, North Carolina
*Corning Incorporated, Corning, New York

Abstract

Discrete fiber strain measurements using fiber Bragg gratings (FBGs) with a spatial resolution of 50 mm were made for an experimental 600-fiber Slotted-Core Ribbon (SCR) cable. The partially filled SCR cable was made with FBGs in the top, middle and bottom ribbons in two slots. Discrete strain measurements were made with the cable on 0.75, 1.4 and 2.1 meter drum diameters. Measurements were made relative to a straight cable configuration to examine the effect of pure cable bending on strain.

Near-sinusoidal strain behavior was observed for edge fibers as the fibers in the ribbon oscillated from being in tension to being in compression. The variation of fiber strain (peak-to-peak) along the laylength is much larger in the edge fibers (maximum of 0.21 % peak-to-peak strain on the 0.75 meter drum diameter) than in the middle fibers (maximum of 0.113 % peak-to-peak strain on the 0.75 meter drum diameter). Maximum discrete fiber tension (0.098 %) and compression (0.083 %) were observed for the 0.75 m cable drum diameter relative to a straight cable configuration. Maximum strains are used to predict lifetimes of optical fiber cable on a small diameter reel.

Keywords

Optical fiber sensors; fiber Bragg grating; discrete strain measurement; Slotted-core ribbon cable; 8-fiber ribbon; ribbon-to-ribbon friction; cable bending stress.

1. Introduction

Non-discrete strain measurement methods in optical fiber ribbons and cables include measuring change in average strain for a test sample from a reference condition using the phase-shift technique and measuring distributed fiber strain along the length of a fiber using a Brillouin Optical Time Domain Reflectometer (BOTDR). Resolution of the BOTDR is limited to two meters and consequently cannot distinguish localized short-length variation in fiber strain along the laylength in a stranded cable. Using a BOTDR, it is only possible to measure fiber strain averaged across a few laylengths at this time. From a fiber reliability standpoint, the fiber strain at any point along the fiber is important.

With the emergence of fiber Bragg gratings being used as strain sensors in optical fiber cables, it is now possible to measure strain at discrete locations along the length of an optical fiber cable. Fiber Bragg gratings act as filters reflecting light at specific wavelengths [1,2]. The wavelength reflected by a given Bragg grating varies linearly with applied strain. As a result, strain at a discrete location in an optical fiber can be measured by monitoring the wavelength of light reflected by a grating written along the fiber's length.

Previous work using fiber Bragg gratings to measure discrete strain in ribbons measured strain in only one fiber position in the ribbon stack [3] or examined strain across the fibers in one ribbon of a stack [4]. This work measures discrete strain in an eight-fiber ribbon stack mapped as a function of fiber position in the top, middle and bottom ribbons along the length of the fibers.

In this study, discrete strain with a spatial resolution of 50 mm was measured on fibers in an experimental 600-fiber Slotted-Core Ribbon (SCR) cable. By strategically placing Bragg gratings in nine different fibers in a stack of 10, eight-fiber ribbons, discrete fiber strain was measured. Discrete strain measurements were made on 0.75, 1.4 and 2.1 meter cable drum diameters relative to a straight cable configuration. The various cable drum diameter measurements show the effect of radius of curvature on cable strain. All measurements are relative to a straight cable configuration to examine the effect of pure cable bending on strain.

2. Fiber Bragg Grating Properties

Exposure of a fiber core to intense optical interference creates a periodic perturbation of the refractive index along the fiber length, which is known as a fiber Bragg grating. The index perturbations in the fiber core cause a narrow band of incident light in the fiber to be reflected by successive coherent scattering from the index variations. Transmission reflection spectra for a series of fiber Bragg gratings are shown in Figure 1. Seventeen fiber Bragg gratings are written into the fiber for this spectra.
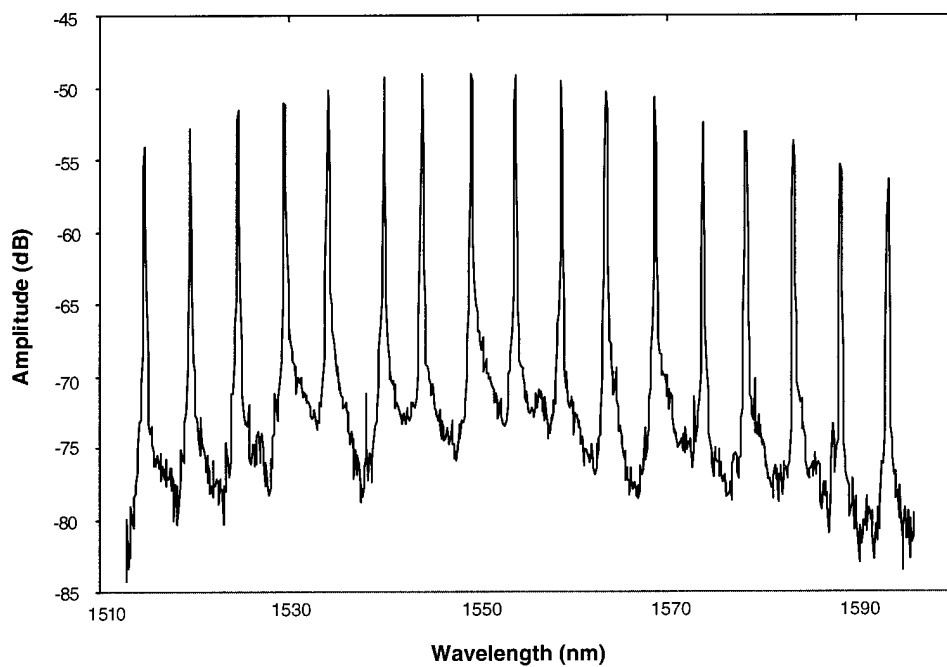
Figure 1. Transmission reflection spectra for grating series 17-2 (17 fiber Bragg gratings written into the fiber).
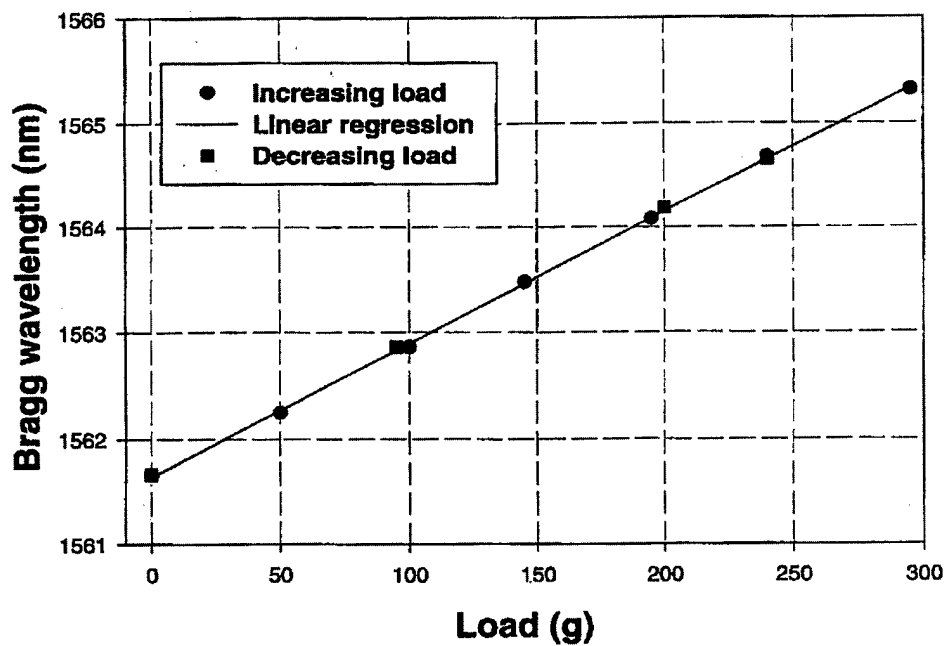

Figure 2. Bragg wavelength as a function of the applied load.

This filter has high rejection filtering of about 25 dB. Any change in fiber properties, such as strain which varies the modal index or grating pitch, will change the Bragg wavelength. The grating sensitivity is governed by the fiber's elastic and elasto-optic properties. The amount of wavelength shift is given by [5]

$$\frac{\delta\lambda_B}{\lambda_B} = \varepsilon\,[1 - 0.5\,n^2(p_{12} - \mu(p_{11} - p_{12}))] + \xi\Delta T\ . \qquad (1)$$

Where ε is the axial strain, n the effective index of refraction, p_{ij} the strain optic or Pockel's coefficients, μ Poisson's ratio, and ξ the thermo-optic coefficient. For $n = 1.468$ at 1550 nm, $p_{11} = 0.113$, $p_{12} = 0.252$ and $\mu = 0.17$, then equation (1) becomes

$$\frac{\delta\lambda_B}{\lambda_B} = 0.79\,\varepsilon + \xi\Delta T\ . \qquad (2)$$

Typical values for the sensitivity to an applied axial strain are 1 nm/millistrain [1] at 1300 nm. For measurements conducted in this study around 1550 nm, a 1.2 nm/0.1 % wavelength/strain relationship was used.

The measured Bragg wavelength as a function of the applied load is shown in Figure 2. To determine if the grating had any hysteresis, the load was slowly reduced for the Bragg grating from 300 g as can be seen in Figure 2. No hysteresis was evident.

3. Discrete Strain Measurement Using Fiber Bragg Gratings

In this study, strain is measured at discrete points along approximately two laylengths (1 laylength = 425 mm) of a 600-fiber SCR cable (cable OD = 23.3 mm) using fiber Bragg gratings. Measurements were made during the various stages of manufacturing the cable and on various diameter cable drums. Figure 3 shows a cross-section of the 600-fiber SCR cable with slots 1, 3, 5 and 7 filled. Two of these slots (Slot 1 and Slot 5) had Bragg gratings in the top, middle and bottom ribbons as shown by the shaded fibers in Figure 3. Each 8-fiber ribbon had 3 fibers with Bragg gratings, typically Fiber 1, Fiber 4 or 5 and Fiber 8. In each fiber with Bragg gratings, the gratings were uniformly spaced over 800 mm (approximately two laylengths). Grating locations within the 3 ribbons with gratings in each slot are aligned within ± 1.5 meters of each other. Slot 1 had "9-unit gratings" (9 gratings spaced approximately 100 mm apart) and slot 5 had "17-unit gratings" (17 gratings spaced approximately 50 mm apart). For this paper, primarily strain measurements for Slot 5 are presented and discussed. The data is similar for Slot 1, but with less resolution, i.e., 9 gratings per fiber vs. 17 gratings per fiber.
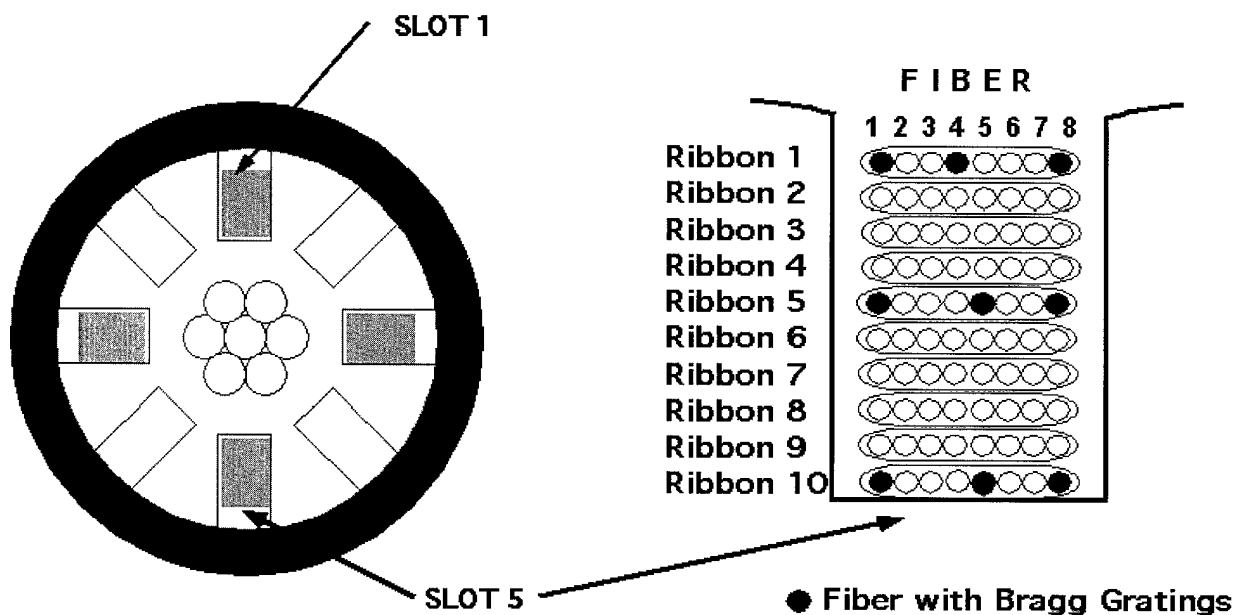

Figure 3. 600-fiber SCR cable cross-section. Cable OD is 23.3 mm. Slots 1 and 5 contain fibers with Bragg gratings. Bragg grating positions in Slot 5 are indicated by shaded fibers in the stack of 10, eight-fiber ribbons.

The reflected light spectra from the gratings was measured during various cable configurations which included (1) Straight cable section containing the gratings, and (2) Cable wound on a 0.75, 1.4 and 2.1 meter diameter drums. Using the measurements for the straight cable as a reference (zero strain), the fiber strain at each cable diameter was calculated for the different Bragg gratings. It is important to measure the effect of the cable bend radius relative to the straight cable to isolate the "pure bending" results in order to evaluate the cable drum's effect on cable lifetimes. These bending strains are mostly eliminated once the cable is installed.

The fiber strain is proportional to the shift in wavelength of light reflected from each grating relative to the straight cable configuration. The measurement repeatability is typically about 0.01 %. All measurements were made at least 24 hours after re-reeling in order to allow for strain stabilization after ribbon movement in the cable.

4. Strain Measurement Results and Discussion

4.1 Discrete Fiber Strain

Figure 4 shows cross-sectional views of the bent 600-fiber cable with only one ribbon for illustrative purposes. Optical fibers in the 8-fiber ribbon are in tension above the cable neutral axis and in compression below the cable neutral axis. This same evolution from tension to compression repeats itself through each laylength as the fiber ribbon is helically stranded around the central member. Figure 4 shows four cross-sections of the bent 600-fiber cable rotated through 90° for 1 laylength. Each cross-section shows how the 8-fiber ribbon rotates relative to the cable neutral axis.

Measurements of discrete strain change along the fiber lengths for various cable drum diameters relative to a straight cable configuration are shown in Figure 5. The edge fiber illustrated in Figure 5 is Fiber 8 from Slot 5, Ribbon 1, which is the top ribbon. The letters A, B, C and D indicate the positions of the 8-fiber ribbon in the cable cross-sections shown in Figure 4. Each of the 17 gratings in Figure 5 are equally spaced 50 mm. Maximum discrete tension (maximum of 0.098 %) and compression (maximum of 0.083 %) are observed for the 0.75 m diameter cable drum. Strain increases due to decreasing cable drum diameter is seen in the edge fibers as well as the middle ribbon fibers. Figure 6 shows the discrete strain change vs. distance along the middle fiber in the top ribbon (Slot 5, Ribbon 1, Fiber 4). Each of the 3 cable drum diameters in Figure 6 is plotted relative to a straight cable configuration. The strain measurements show that the edge fibers in the ribbons exhibited higher maximum strain as compared to the middle fibers. The variation of fiber strain (peak-to-peak) along the laylength is much larger in the edge fibers (maximum of 0.21 % strain on the 0.75 m drum for Ribbon 10, Fiber 8, Slot 5) than in the middle fibers (maximum of 0.113 % strain on the 0.75 meter drum for Ribbon 1, Fiber 4, Slot 5).
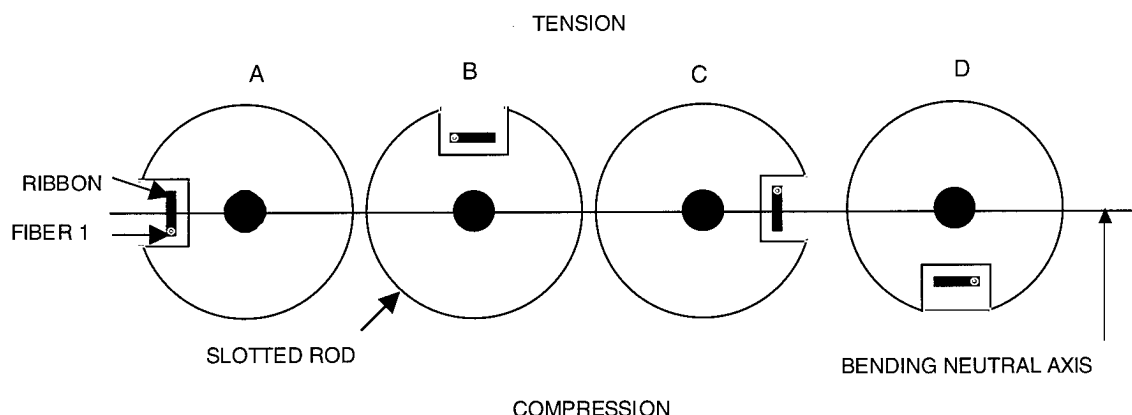
Figure 4. Cross-sectional views of a bent 600-fiber cable. Optical fibers in the 8-fiber ribbon are in tension above the cable neutral axis and in compression below the cable neutral axis. Cross-sections of a bent 600-fiber cable are rotated through 90° for 1 laylength. The 8-fiber ribbons are rotated relative to the neutral axis. The letters A, B, C and D are used to indicate the positions of the 8-fiber ribbon for the strain data in Figure 5.
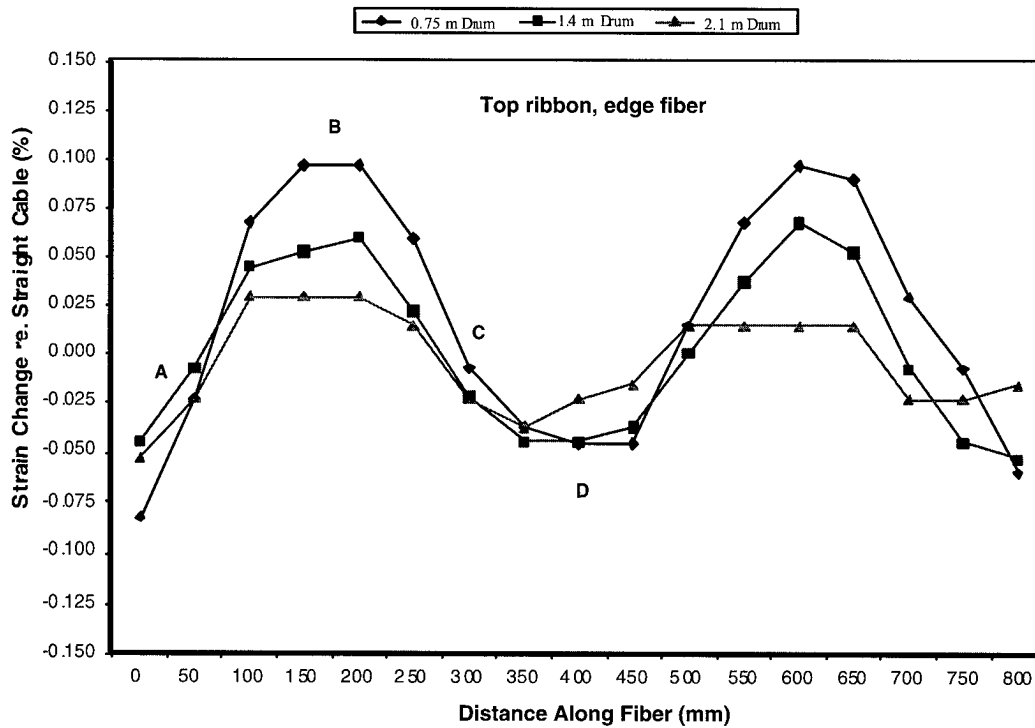
Figure 5. Edge fiber, top ribbon (Slot 5, Ribbon 1, Fiber 8) discrete strain change vs. distance for 3 cable drum diameters relative to a straight cable configuration. Grating spatial separation is 50 mm. The letters A, B, C and D indicate the positions of the 8-fiber ribbon in the cable cross-sections in Figure 4.
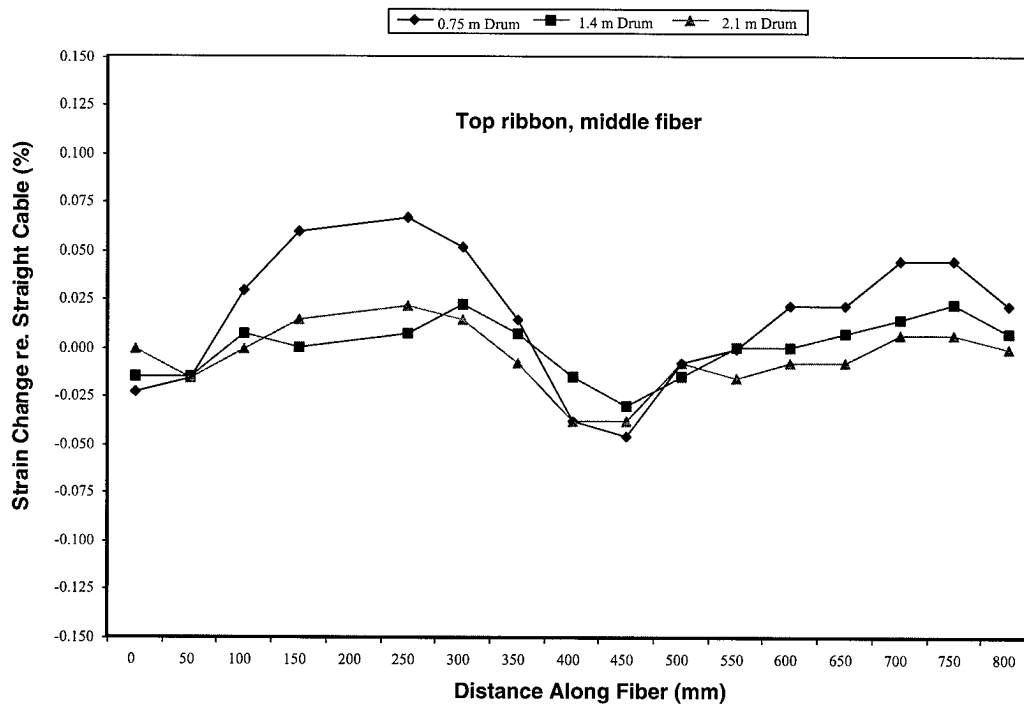

Figure 6. Middle fiber, top ribbon (Slot 5, Ribbon 1, Fiber 4) discrete strain change vs. distance for 3 cable drum diameters relative to a straight cable configuration. Grating spatial separation is 50 mm.

Near-sinusoidal behavior is observed in Figure 5 and to some extent in Figure 6 as the ribbon oscillates from being in tension to being in compression. Such near-sinusoidal strain behavior can be observed particularly for the edge fibers over the approximately 2 laylengths containing Bragg gratings. Data for the other edge ribbon fibers is very similar to that in Figure 5. The locations for the maximum strains for all three-cable drum diameters indicate laylengths on the order of 425 mm in Figure 5.

Figure 7 shows discrete strain change vs. distance for edge fibers (Slot 5, Fiber 1) in Ribbons 1, 5 and 10 for the 0.75 m cable drum diameter relative to a straight cable configuration. The peak maximum and minimum strains do not overlap since the gratings do not begin at exactly the same point along the cable length. The locations of the gratings in each ribbon are within ± 1.5 meters of each other. Figure 8 illustrates discrete strain change for the middle ribbon (Slot 5, Ribbon 5) vs. distance for Fibers 1, 5 and 8 for the 2.1 m cable drum diameter relative to a straight cable configuration. As in Figure 7, the peak maximum and minimum strains do not overlap since the gratings do not begin at exactly the same point along the cable length. The maximum discrete tension is 0.083 % while the maximum compression is 0.052 % for Fiber 1 in Figure 8. Both Figures 7 and 8 exhibit near-sinusoidal behavior as observed in Figures 5 and 6 as the ribbon oscillates from being in tension to being in compression along the fiber length.

4.2 Average Fiber Strain

An alternative method to analyze the discrete strain measurements in the 9 different fibers in Slot 5 is to calculate the average strain in all 17 Bragg gratings similar to what would be measured using a BOTDR or a phase-shift strain measurement. Table 1 lists the average discrete strain relative to a straight cable configuration for the Bragg grating fibers contained in Ribbons 1, 5 and 10 as a function of cable drum diameter. The standard deviations are shown in parenthesis and are much larger than the averages since there is a large excursion between the maximum and minimum strain values over 2 laylengths. It should be noted that the averages would be more statistically significant if the strain was averaged over many more than 2 laylengths. However, these data can still show trends. The positive strain averages represent tension while the negative strain averages represent compression measured for the fibers with Bragg gratings. Only ribbon 1 (top ribbon) has average strain in tension for the 0.75 meter drum diameter while ribbons 5 and 10 are completely in compression.
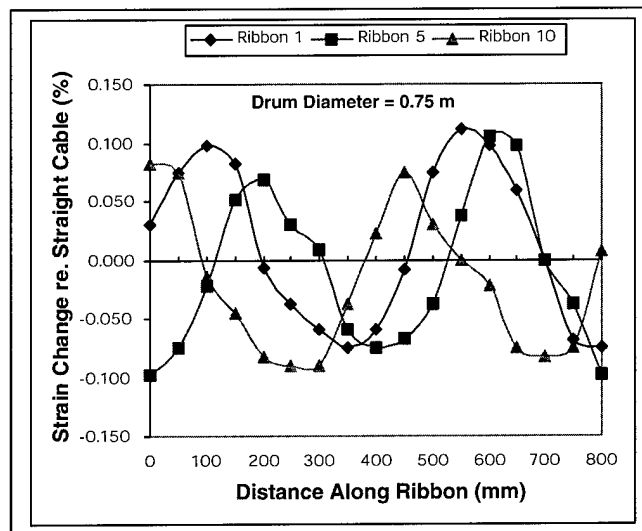

Figure 7. Edge fiber (Slot 5, Fiber 1) discrete strain change vs. distance for Ribbons 1, 5 and 10 for the 0.75 m cable drum diameter relative to a straight cable configuration.
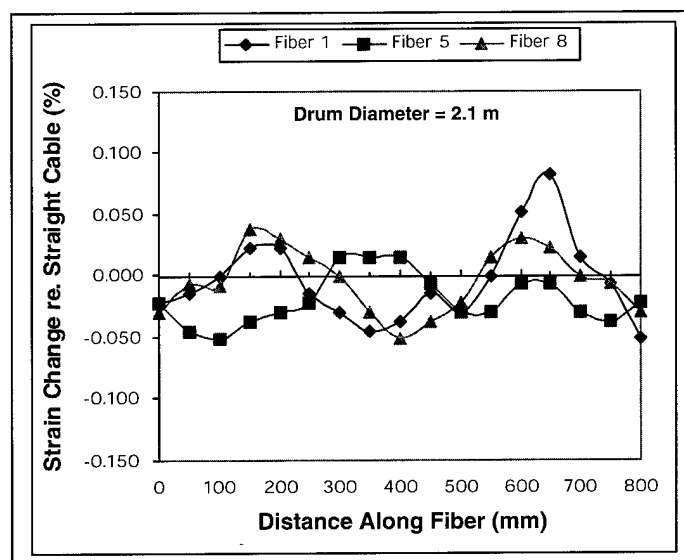

Figure 8. Middle ribbon (Slot 5, Ribbon 5) discrete strain change vs. distance for Fibers 1, 5 and 8 for the 2.1 m cable drum diameter relative to a straight cable configuration.

Table 1. Average strain vs. cable diameter relative to a straight cable configuration (standard deviations are in parenthesis)

Ribbon Number	Cable Drum Diameter (m)	Fiber 1 Average Strain (%)	Fiber 4 or Fiber 5 Average Strain (%)	Fiber 8 Average Strain (%)
Ribbon 1	0.75	0.014 (0.069)	0.015 (0.034)	0.019 (0.062)
	1.4	-0.004 (0.045)	0.001 (0.014)	0.002 (0.044)
	2.1	-0.005 (0.035)	-0.004 (0.016)	-0.004 (0.026)
Ribbon 5	0.75	-0.010 (0.066)	-0.009 (0.018)	-0.004 (0.064)
	1.4	-0.011 (0.048)	-0.013 (0.015)	-0.008 (0.049)
	2.1	-0.004 (0.035)	-0.020 (0.021)	-0.004 (0.027)
Ribbon 10	0.75	-0.019 (0.061)	-0.015 (0.025)	-0.017 (0.068)
	1.4	-0.015 (0.049)	-0.007 (0.016)	-0.012 (0.056)
	2.1	-0.005 (0.020)	-0.011 (0.014)	-0.012 (0.035)

Figure 9 shows the average strain change for Ribbon 1 (top ribbon, Slot 5) relative to a straight cable as a function of inverse cable drum radius for Fibers 1, 4 and 8, respectively. The average strain is shown graphically as a function of the inverse of the cable drum radius since the longitudinal strain in the plane of symmetry for the circular cable is inversely proportional to the radius of curvature (or the cable bend radius). Ribbon 1 (Figure 9) shows all fibers with approximately linearly increasing strain as the inverse of the cable drum radius increases. It is understood that reducing the bend diameter of an optical fiber cable increases the strain, so this behavior is expected. Similarly, for Slot 1, Figure 10 shows the average strain change for Ribbon 1 (top ribbon) relative to a straight cable as a function of inverse cable drum radius for Fibers 1, 4 and 8, respectively. Slot 1 is averaged over 9-Bragg gratings instead of 17 gratings as in Slot 5. Similar to Figure 9, all fibers show approximately linearly increasing strain as the inverse of the cable drum radius increases.

Strain trends for the middle and bottom ribbons in Table 1 are not as clear as for the top ribbon. For example, Ribbon 1 is the only ribbon in the stack with a constantly free surface which allows room for free movement and accordingly, is primarily in pure bending as exemplified by the approximately linearly increasing

strain with the inverse of cable drum radius. During cable bending, the ribbons will rotate until they contact another ribbon or the slot walls. Ribbon adhesion will minimize individual ribbon movement and increase bending stresses. Ribbon 5 (middle ribbon) is constrained (ribbons adhered to each other) from movement in the ribbon stack due to processing tensions and friction between the ribbons on each of it's sides. Ribbon 5 probably also undergoes some bending on its edge (ribbon edge parallel to the bending axis) at some point along the length of the fiber Bragg gratings. Ribbon 10 (bottom ribbon) is probably being partially constrained from movement in the ribbon stack due to processing tensions and friction between the ribbon above it and the bottom of the slot. Overall strain in Ribbon 10 is probably affected by the ribbon-to-ribbon and/or ribbon-to-slot bottom surface adhesion which may be broken as the cable bend diameter is reduced and consequently the strain is reduced.

Varying strain behavior in a ribbon stack and the interactions between the ribbons in the stack is not well understood, but it is probably due to a combination of stresses such as pure bending, the ribbon being bent on its edge, ribbon slip-stick forces due to friction and the in-process ribbon tensions. These different causes of stress combine at different levels depending on the location of the ribbon in the stack.

4.3 Maximum Fiber Strain and Cable Lifetime

Table 2 lists the maximum discrete tensile strains and the locations of those strains due to the cable drum diameters for Slot 5. One can observe that the maximum tension is always on an edge fiber, which is expected since they are "unprotected" relative to the interior fibers in a ribbon. It should also be noted that the location of the maximum tension on the 1.4 meter drum diameter actually occurs in four other fiber locations, namely Ribbon 1, Fiber 8; Ribbon 5, Fiber 1; Ribbon 5, Fiber 8; and Ribbon 10, Fiber 8.

Table 2. Maximum discrete tensile strains and locations due to cable bend diameter (relative to a straight cable configuration)

Cable Drum Diameter (m)	Tension (%)	Ribbon	Fiber
0.75	0.112	1	1
1.4	0.068*	1	1
2.1	0.083	5	1

*Also the maximum tension for Ribbon 1, Fiber 8; Ribbon 5, Fiber 1; Ribbon 5, Fiber 8; and Ribbon 10, Fiber 8.
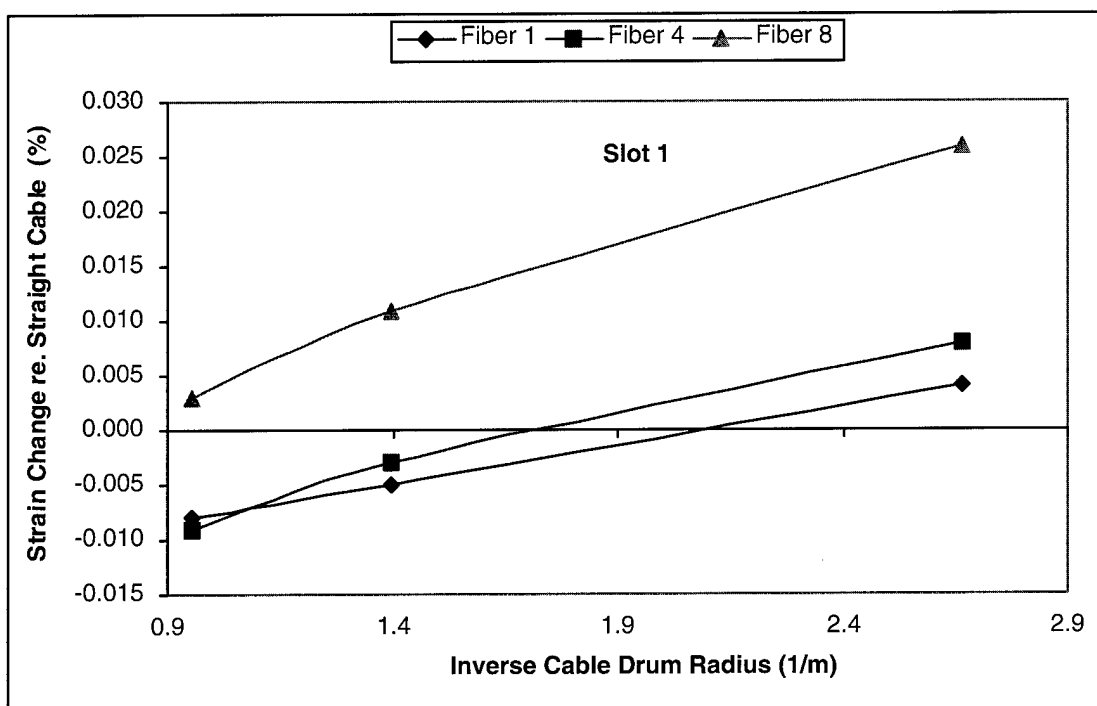
Figure 9. Top ribbon (Slot 5, Ribbon 1) average strain change relative to a straight cable configuration vs. inverse cable drum radius for Fibers 1, 4 and 8.
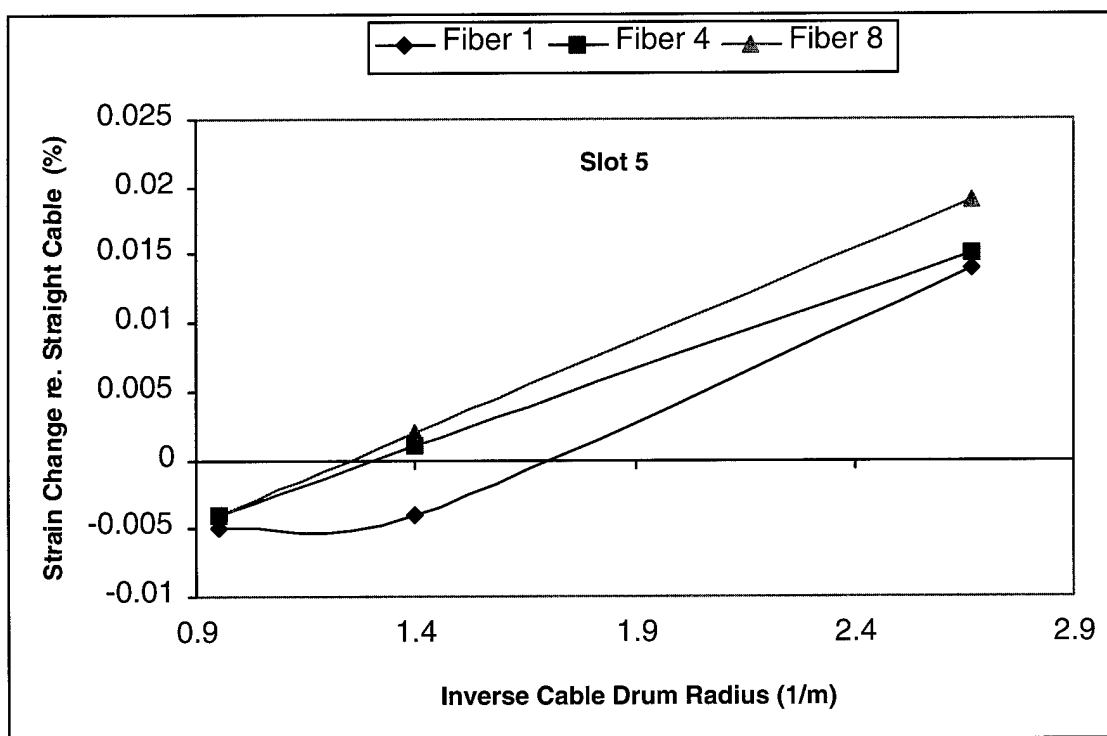

Figure 10. Top ribbon (Slot 1, Ribbon 1) average strain change relative to a straight cable configuration vs. inverse cable drum radius for Fibers 1, 4 and 8.

Table 3 lists the maximum discrete compressive strains and the locations of those strains due to the cable drum diameters for Slot 5. Similar to the maximum tensile strains, the maximum compression is always on an edge fiber and in particular, always on the same bottom ribbon edge fiber. This fiber position is obviously susceptible to higher strains due to its location in the ribbon stack.

Table 3. Maximum discrete compressive strains and locations due to cable bend diameter (relative to a straight cable configuration)

Cable Drum Diameter (m)	Compression (%)	Ribbon	Fiber
0.75	-0.127	10	8
1.4	-0.105	10	8
2.1	-0.090	10	8

Maximum strains are important for predicting lifetimes of optical fiber cables. Methodologies have been developed to make long-term failure probability predictions provided the fiber *n* value and strength distributions are appropriate for the application [6, 7]. Therefore, for a 25 year lifetime, fiber strain may be as high as 0.2 %, even for a small bend radius. Consequently, the strains generated on a cable drum diameter as small as 0.75 meters will not reduce the lifetime of the cable under most conditions.

5. Conclusions

Discrete fiber strain measurements were made using fiber Bragg gratings with a spatial resolution of 50 mm along the laylength of an SCR cable. The partially filled experimental 600-fiber SCR cable was made with fiber Bragg gratings in the top, middle and bottom ribbons of two slots. Discrete strain measurements were made on 0.75, 1.4 and 2.1 meter cable drum diameters relative to a straight cable configuration to examine the effect of pure bending on strain.

The following conclusions can be made:

- Edge fibers in the ribbons exhibited higher maximum strain as compared to the middle fibers.
- Maximum discrete tension (0.098 %) and compression (0.083 %) were observed for the 0.75 m diameter cable drum for a straight cable configuration.
- The variation of fiber strain (peak-to-peak) along the laylength is much larger in the edge fibers (max. of 0.21 % strain on the 0.75 m drum) than in the middle fibers (max. of 0.113 % strain on the 0.75 m drum).
- Near-sinusoidal strain behavior was observed for the measured fibers as the ribbon oscillates from being in tension to being in compression.

- The top ribbon in both slots measured, showed all fibers with approximately linearly increasing average strain as the inverse of the cable drum radius.

Strain behavior variation observed in a ribbon stack and the interactions between the ribbons in the stack is probably due to a combination of stresses such as pure bending, the ribbon being bent on its edge, ribbon slip-stick forces due to friction and the in-process ribbon tensions. These different causes of stress combine at different magnitudes depending on the location of the ribbon in the stack.

For a 25 year lifetime, fiber strain on a cable drum may be as high as 0.2 %, even for a small bend radius. The maximum strains generated on a cable drum diameter as small as 0.75 meters will not reduce the lifetime of the cable.

6. Acknowledgments

7. References

[1] K. Hill and G. Meltz, "Fiber Bragg Grating Technology Fundamentals and Overview," Journ. Light. Tech., Vol. 15, No. 8, August 1997.

[2] Bennion et al., "Tutorial Review: UV-written in-fibre Bragg gratings," Opt. & Quant. Elect. Vol. 28, 1996.

[3] T. Genji et al., "Strain Distribution Measurement in Bent Optical Cables Using a Fiber Ribbon with Multi-pointed Fiber Bragg Gratings," International Wire & Cable Symposium Proceedings, pp. 775-779, 1999.

[4] Z. Gao et al., "A Study of the Fiber Strains in Central Tube Ribbon Cables," International Wire & Cable Symposium Proceedings, pp. 61-65, 1999.

[5] J. Guemes et al., "Measurement of strain distribution in bonded joints by fiber Bragg gratings," SPIE Vol. 3330, March 1998.

[6] K. Hodge et al., "Predicting the Lifetime of Optical Fibre Cables Using Applied Stress Histories and Reliability Models," International Wire & Cable Symposium Proceedings, pp. 713-724, 1992.

[7] G. Glaesemann and S. Gulati, "Design methodology for the mechanical reliability of optical fiber," Optical Eng., Vol. 30, No. 6, pp. 709-715, June 1991.

Frederick M. Sears received the SB and SM degrees from MIT in 1975, in the five year honors program, and a Ph.D. degree from the University of California at Berkeley in 1980, all in Mechanical Engineering. Since 1990, Dr. Sears has been with S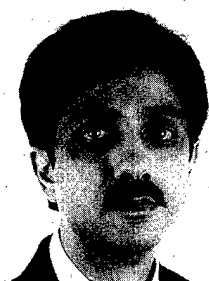iecor, now Corning Cable Systems in Hickory, NC, where from 1991 to 1995 he managed the Ultra-High Fiber Count Cable development program. He is presently Manager of the Technical Staff in the Research, Development & Engineering Department. Previously, Dr. Sears worked at Bell Laboratories from 1980 to 1990 (now Lucent Technologies), first in Murray Hill, NJ, as a Member of Technical Staff, where he pursued research and development on optical fiber characterization techniques. In 1984, he transferred to the Atlanta Bell Laboratories location, pursuing optical fiber research and development on modal noise in single-mode lightguide systems, cutoff wavelength, characterization of polarization-maintaining fibers, interconnection of polarization-maintaining fibers, Fabry-Perot fiber interferometry and fiber optic cable design. Dr. Sears is a member of the Optical Society of America and Pi Tau Sigma.

Authors' Address:
Corning Cable Systems
P. O. Box 489 - RH
Hickory, NC 28603-0489

Bob Whitman, as the Market Manager for Growth Markets at Corning Incorporated, is responsible for end-user customer support for CLEC, ISP and ITS markets. Bob started with Corning as an Applications Engineer in June 1997. Prior to joining Corning, Bob served eight years in the United States Navy as a Nuclear Power Engineering Officer. Bob holds a BS degree in Industrial Engineering from Hofstra University and is a member of the Optical Society of America.
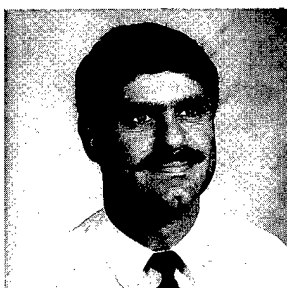
Hani M. Nassar received an MS degree in Mechanical Engineering from the Georgia Institute of Technology in 1981. He is currently manager of the Japan cable development group in the Research, Development & Engineering department of Corning Cable Systems, formerly Siecor. Since joining RD&E in 1982, his major emphasis has been on the development of hybrid cables, feeder cable systems, OPGW, submarine cables and the whole family of slotted core products for the Japan market.

Shami S. Sodhi was born in India in 1964. He received his MS in Electrical Engineering from Virginia Polytechnic Institute and State University in 1989. Since 1989, he has been with Siecor, now Corning Cable Systems in Hickory, N.C. and is presently Manager of Product Evaluation in the Research, Development and Engineering Department. He has authored and co-authored several papers and is a member of the IEEE.

Allen C. Gregory was born in Valdese, NC in 1958. He received an AAS degree in Electronics Technology from Catawba Valley Technical Institute in 1978. He joined Superior Cable Corporation in 1978, later known as Siecor and today as Corning Cable Systems. Since 1993, he has been a Senior Technician in the Research, Development and Engineering Department at Corning Cable Systems.

In Situ Analysis of the Glass Transition of UV Curable Inks on Optical Fiber Using Micro-Thermomechanical Analysis

Rolando Domingo, Keqi Gan, _Tonya McKay_, Ed Zahora

DSM Desotech, Inc., 1122 St. Charles Street, Elgin IL 60120, USA

Abstract

The glass transition of UV curable inks on optical fiber was determined using the new technique of micro-thermomechanical analysis (μ-TMA). This analytical technique combines a miniature heating system with an atomic force microscope, allowing simultaneous surface imaging and thermal characterization of the material. A clear ink base and a series of pigmented systems were investigated using both this technique and traditional flat film thermomechanical analysis in order to determine the effect of different pigments on the T_g of the coating. Results from both techniques were compared in order to evaluate the efficacy of the microscopic method for the determination of coating properties on fiber. Depth profiling of the T_g was also performed on a cross-section of each fiber to examine gradient effects on the coating layers from the curing process.

1. Introduction

Thermal methods such as differential scanning calorimetry (DSC), dynamic mechanical analysis (DMA), and thermomechanical analysis (TMA) have long been standard analytical tools for the characterization of polymer physical properties. Generally, fairly large samples are required for analysis by these traditional thermal methods. In the case of DSC, several milligrams of sample are required for measurements, and for DMA and TMA, films of reasonable size are required. These techniques probe the bulk properties of the material, generally not being capable of resolving any microscopic heterogeneities within the sample. Results from these types of experiments are sometimes referred to as being specimen-averaged.

In the field of optical fiber coatings, these types of methods have been relied upon to determine the thermal properties of flat films of the coating formulation of interest. This is considered to be a less than ideal procedure, because the properties of the coatings on fiber may differ from those of flat films due to significant processing differences. Thus, it is desirable to develop techniques which will allow for the elucidation of the properties of coatings on the fiber. In this paper, we explore the potential utilization of micro-thermal analysis for the in-situ determination of the glass transition of UV-curable inks on optical fiber.

The technique of micro-thermal analysis is a relatively new one. It incorporates the elements of thermal analysis and atomic force microscopy into one instrument.[1] In this instrument, the AFM probe is replaced with a silver-coated platinum wire, known as a

Wollaston wire. The wire is then bent into a v-shape, and the silver is etched off of the wire, exposing the sub-micron diameter platinum wire. When current is passed through the Wollaston wire, it acts as a miniature heating and thermal sensing device. This probe can then be scanned across a sample surface, while the temperature is ramped up at very high rates. This combination of features allows for simultaneous imaging of surface topography and thermal characterization of the material of interest.

The instrument operates with two separate feedback loops, force control (constant force between the sample and the probe) for topography determination and current control (constant flow of current through the Wollaston wire) for thermal information. The use of the current control technique imparts the ability to perform various thermal analysis experiments on very small samples or on very small locations on a sample simply by monitoring the current flow through the wire probe. This provides the scientist with the capability to examine materials that may not normally be practical or even possible to analyze with traditional bulk thermal analysis tools.

There are two main modes of operation of the instrument. In the first, the probe is scanned across the surface of the material while it is maintained at a constant, elevated temperature. The current control system can measure the rate of heat dissipation into the sample, making it possible to spatially resolve or "map" regions of a sample with varying thermal conductivity.

The second mode of operation is localized thermal analysis. In this type of experiment, a particular region of interest is selected on the sample surface. The temperature of the probe is then ramped up at very fast rates (25°C/sec or 1500°/min), and the differential thermal response is monitored, as well as the vertical position of the probe. As the material heats up, it begins to soften at a particular temperature, and the probe begins to sink into it. This softening point correlates with the glass transition of amorphous materials and the melting point for crystalline or semi-crystalline materials.

This second technique has been used to study the phase miscibility of polymer blends, to study the softening temperatures of multilaminate polymer films, to aid in the identification of constituents in printed materials, and to characterize interphases found at interfaces between multicomponent systems.[2,3] Our group has also done some preliminary work where the technique was used to determine the glass transition of inks coated onto optical fiber.[4] This paper will summarize and discuss the results of additional

experiments performed on fiber optic materials utilizing this technique.

One of the main items of interest in this study, in additional to the evaluation of a new analytical technique, was to study the variation in the glass transition behavior across the whole series of inks. Each ink color is obtained by mixing a colorant (pigment dispersion) into the ink base resin. The colorant contains dry pigment, dispersing agents, and multi-functional acrylates. In order to achieve the proper shade, different quantities of dry pigment are mixed into the various pigment dispersions. Thus, each different pigment dispersion will usually contain a different quantity of multi-functional acrylate.[5] Additionally, the weight percentage of pigment dispersion used in the ink formulations varies for every final ink color. The result is that there may be significant variation in the amount of multi-functional acrylate contained in each of the ink colors. This could affect the degree of crosslinking in the material upon cure, subsequently causing variations in the glass transition range, depending upon the color.

Another variable worthy of consideration is the density of the dry pigment itself. One theory which has been proposed is that the higher the volume of pigment contained in the ink, the higher the free volume in the cured material. Some of the colors, such as blue, red, violet, green, and yellow, contain organic pigments that have lower density, will potentially have a higher volume occupied by pigment. Titanium dioxide, the pigment used to provide opacity to inks and to achieve white and lighter shades of other colors, has a relatively high density, and thus, occupies less volume inside the final product. Thus, depending upon the amount and type of dry pigment present in the formulation, significant differences in free volume may exist from color to color, impacting the glass transition behavior of the final cured material.

Organic pigments may also absorb UV radiation at various wavelengths, depending upon the pigment color, effectively competing with the photoinitiators in the coating system. They can also scatter and block energy due to their particulate nature, contributing to uneven or incomplete cure. Both of these phenomenon challenge the formulator's job of providing the maximum homogeneity of properties within all of the colors of an ink line.[6]

2. Materials and Methods:

In these experiments, we analyzed a series of twelve different colors of UV-cured ink, all based upon the same resin formulation. The objectives of the project were to study the capability of the micro-thermal analyzer to measure the glass transition of these inks on fiber, to compare these results to those obtained using traditional thermomechanical analysis (TMA) on flat films, and to study the effects, if any, that pigment color has on the glass transition temperature of the product.

Two different sets of flat film samples were prepared for the TMA experiments. One set of drawdowns was prepared with a thickness of 75 microns and another with a film thickness of 25 microns. These were cured on a Fusion UV curing unit at 1.0 J/cm^2 using a "D" lamp. The inked fibers were prepared using CPC-6 fiber on a Nextrom OFC 52 inking machine at 1000 m/min, with one 600-watt power D-type lamp. The system was purged with nitrogen at a rate of 40 liters per minute.

The flat film samples were analyzed by thermomechanical analysis on a TA Instruments' 2940 TMA using a heating rate of 5°C/min and an expansion-type probe. The data obtained was analyzed using the Universal Analysis software from TA Instruments.

The fiber samples were analyzed with the μ-TA 2990 in the localized thermal analysis mode. Prior to fiber analysis, instrument calibration was performed by using a series of polymer standards. Once this was completed, the selected fiber was mounted onto the sample wafer, and the instrument was cooled via liquid nitrogen to -70°C. Using the video monitor, a suitable location on the sample surface was selected and the probe was engaged to the surface. The probe was then heated at a rate of 25°C/sec and the vertical position of the probe was monitored by the instrument. In this manner, the softening point could be easily detected, which in these amorphous samples, correlated with the glass transition. Several replicates were performed for each sample.

3. Micro-thermal Analysis Results:

Once the surface of the sample was examined via optical microscopy and a suitable location for analysis was selected, and the sample was cryogenically cooled, each temperature ramp took less than 30 seconds, so it was possible to run several replicates for each sample. Care had to be taken when engaging the probe that it was not grazing the side of the fiber or on a point of too great curvature. It was observed that the thermograms had a very bumpy appearance and the transitions were not extremely reproducible. On several occasions, the curves displayed what appeared to be multiple transitions.
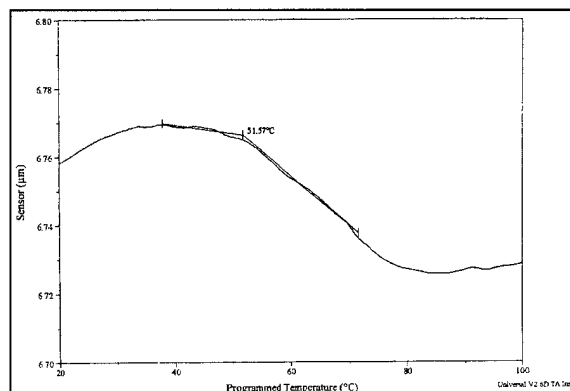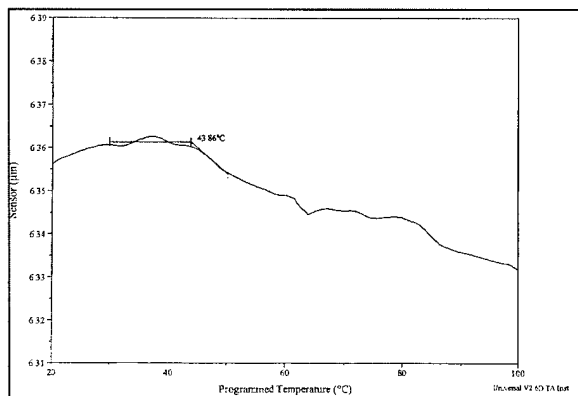

Figure 1. Localized thermal analysis of violet ink on fiber.

Figure 2. Localized thermal analysis of red ink on fiber.

The reason for this type of behavior is believed to lie in the nature of pigmented systems. Inks are inherently heterogeneous materials, with pigment particles dispersed throughout the bulk of the material. The size of these particles ranges from 0.1 microns to as much as 3 microns, yet the tip of the probe used for the microscopic thermal analysis is sub-micron in size. Hence, it is likely that the probe may come to rest upon a pigment particle, which could influence the shape of the curve, as well as the temperatures at which transitions are observed.

It is also possible that the small relative size of the probe to the material makes it possible to detect microscopic heterogeneity in the cured film. If the pigment is interfering with the photoinitiator and leading to inhomogeneous cure, then perhaps small variations in cross-link density are being detected by the micro-thermal analyzer. This could lead to the bumpy appearance of the thermograms or to the appearance of multiple transitions.

Another hypothesis presented is related to the localized nature of the heating by the probe. It is possible that the small probe is heating such a thin layer (< 0.1 µm) of the coating film, that once it penetrates the first layer, it is essentially beginning with a new layer, which could give rise to the appearance of multiple transitions.

The thermograms selected for this study were those which displayed the smoothest profiles and most obvious transitions. The glass transition temperature was determined by finding the point at which the slope of the curve changed.

Seven of the twelve colors display a softening point at or around 50°C by this technique. The other colors show some variation in the surface T_g in the range of 40-60°C. This seems to be indicative that pigment type and/or colorant is indeed having some impact on the physical properties of the material.

4. Comparison between the two techniques:

The thermograms generated on the flat films by traditional thermomechanical analysis were generally much smoother and more predictable than those generated by micro-thermal analysis. The probes used for this type of analysis have such a large contact area, that they essentially averages out any sort of microscopic variations in properties of the material. Thus, the softening point observed by the probe would be that for the bulk of the sample. Of course, this technique also requires a sample much larger than the diameter of an optical fiber.
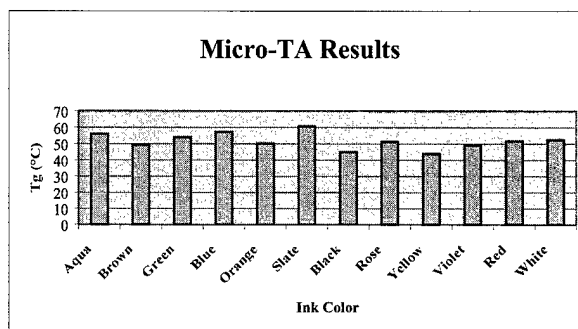
Figure 3. Glass transition of inks on fiber as determined by micro-thermal analysis

The results obtained with TMA on flat films showed a similar range of glass transition values for the series of inks, from 38-62°C. The numbers found by TMA on flat films did not always correlate with the numbers found by micro-thermal analysis on inked fibers. This demonstrates the importance of the capability of measuring physical properties on fiber as opposed to flat films.
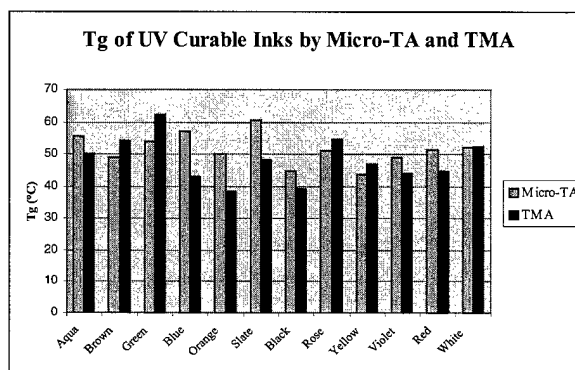
Figure 4. Graphical comparison of glass transition values for each ink color, as determined by the two techniques

Table 1. Glass Transitions Temperatures

Color	T_g by μ-TA (°C)	T_g by TMA (°C)
Aqua	56	50
Brown	49	54
Green	54	62
Blue	57	43
Orange	50	39
Slate	61	48
Black	45	39
Rose	51	55
Yellow	44	47
Violet	49	44
Red	52	45
White	52	52
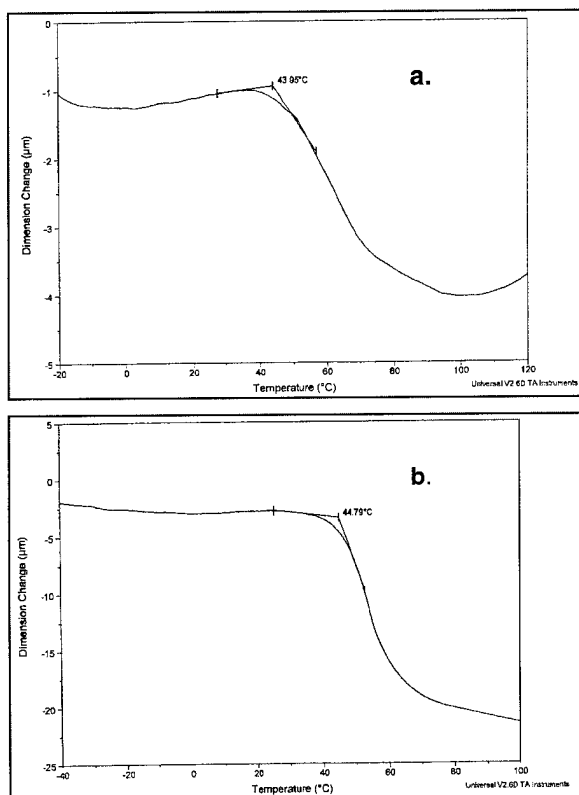
Figure 5. Traditional thermomechanical analysis of a film made of a. Violet ink and b. Red ink

5. Conclusions:

The use of a microthermal analyzer for the determination of ink T_g on optical fiber is a novel application of the technique. The data showed that the thermal probe is capable of detecting microscopic heterogeneities within the pigmented material. This can sometimes prove to be problematic if the purpose of the experiment is to determine an average value for the glass transition of the material. However, if several replicates are performed on various locations of the ink surface, it can be possible to determine an average value for the material.

The results obtained with both the micro-thermal analysis on the fibers and the macro-TMA on the flat films showed variation in the glass transition values for the different colors. The range was the same for both techniques, from approximately 40-60°C. However, the data between the TMA and the μ-TA did not always correlate. This is attributed to two different factors. The first is the fact that the size of the thermal probe relative to the sample is much larger in the TMA than in the μ-TA. Thus, the bulk behavior of the material is detected with the TMA, while more microscopic behavior is observed with the μ-TA. The second factor to consider when observing the data differences between the techniques is that the samples analyzed were processed differently. It is possible that under the very fast cure conditions of the inking line that the material properties develop differently. This emphasizes the importance of developing techniques to reliably examine the physical properties of the inks in situ rather than with flat films.

Acknowledgements:

References:

[1] Levor, T.J., Price, D.M., *American Laboratory*, August 1998

[2] Price, D.M, Reading, M., Caswell, A., Hammiche A., Pollock, H.M., *Microscopy and Analysis*, May 1998

[3] Pollock, H.M., Hammiche, A., Song, M., Hourston, D.J., Reading, M., *J. Adhesion*, Vol. 67, 217-234, 1998

[4] Domingo, R., Gan, K., McKay, T., Zahora, E., *EuroCable 2000*, IOS Press, 2000

[5] Gan, K., Internal communication, November 1999

[6] Legneti, P., Devive, E., Radtech Report, September/October 1995

Relation Between the Fictive Temperature and Mechanical Strength of Optical Fibers vs. their Drawing Conditions

D.-L. Kim[a], Minoru Tomozawa[a], Sophie Dubois[b], Gérard Orcel[b]

[a]Rensselaer Polytechnic Institute
Troy, New-York
+1-518-276-6659 tomozm@rpi.edu

[b]Alcatel Cable
Conflans, 78700, France
+33-1-39-19-12-32 sophie.dubois@alcatel.fr

Abstract

Relationships between fictive temperature, defined as the temperature at which the glass would be at equilibrium if brought to that temperature, and many glass properties such as mechanical properties are reported in the literature. Such relationships are of great interest for optical fibers.

Fibers were drawn under different conditions of diameter, speed, tension and overclad viscosity. Their fictive temperatures and mechanical strength were measured to relate the draw condition to the fiber characteristics. The surface fictive temperatures of silica glass optical fibers were measured using IR reflection spectroscopy with a microscope attachment. A new relation between IR peak wavenumber of the silica structural band and the fictive temperature is derived. The fiber surface fictive temperature depends strongly on fiber diameter, draw tension and overclad viscosity. It is demonstrated that the surface fictive temperature and hence the surface structure is set before the fiber exits the draw furnace. The dynamic fatigue behavior of the fiber was also found to depend on its surface fictive temperature.

Keywords

Fiber; mechanical properties

1. Introduction

A glass can have different structure and properties depending upon its thermal history. This is attributed to a different fictive temperature[1], i.e. the temperature at which the liquid structure froze to turn into a glass. Usually a glass cooled rapidly has a higher fictive temperature than a glass cooled slowly. Also impurities change the structural relaxation of silica glass. A few ppm of Al impurities increase the fictive temperature of the glass[2]. A silica glass with a higher fictive temperature has higher mechanical strength[3], greater mechanical fatigue resistance[3], lower viscosity[4], and higher light scattering intensity[5] due to greater density fluctuation and greater HF etching rate[6]. Often the fictive temperature of a glass surface is different from that of the bulk[7]. Since glass properties such as chemical durability and mechanical properties are greatly influenced by the surface conditions of the glass, it is important to determine the surface fictive temperature separately from the bulk fictive temperature.

Recently, we found a simple IR method to determine the fictive temperature of silica glass[8]. In this method, we use an empirical relation that exists between the IR peak position of the silica structural band and the glass fictive temperature. The IR structural band peak position reflects the Si-O-Si bond angle[9]. IR absorption can determine the bulk fictive temperature, while IR reflection can determine the fictive temperature of a surface layer of ~0.5μm. In this paper effect of fiber drawing conditions on the surface fictive temperature and mechanical strength of the resulting optical fibers were investigated. In general, a faster cooling rate results in a higher fictive temperature of the glasses. In the commercial optical fibers, however, the diameter of the fiber has to be fixed at 125 μm, and cooling rate cannot be varied without changing other parameters such as temperature of fiber drawing and the fiber drawing tension. Therefore, in the present research, the design of experiment (DOE) method was used to isolate the effect of the individual parameter of fiber drawing conditions.

2. Experimental Procedure

2.1 Fiber Drawing

A design of experiment was built to determine the effect of the fiber thermal history on fictive temperature and mechanical strength. Three draw parameters were included into the design of experiment: draw speed, draw tension and fiber diameter since they affect greatly the fiber cooling rate. A fourth parameter, the concentration in Al impurities in the preform overclad was also considered since it varies the glass viscosity and hence the draw temperature of the fiber. The whole design of experiment is presented in Table 1. The fiber were draw in random order to exclude any order effect. Five preforms were used to achieve all the conditions of the design of experiment. However, during the statistical analysis, it was confirmed that no preform effect skewed the results.

Table 1. Table of experimental conditions.

sample #	Draw speed (m/min)	Draw tension (g)	Fiber diameter (μm)	ppm Al in overclad
1-27	400	30	80	0
2-26	400	120	80	0
3	1000	120	80	0
6-24	700	75	125	0
7-25	400	120	170	0
8	1000	30	170	50
9-18	400	120	80	50
10-17	700	75	125	50
11	400	30	80	50
12	1000	45	85	50
13	1000	120	170	50
14-20	400	30	170	50
19	400	120	170	50
22	400	30	170	0

2.2 Mechanical Strength Testing

The fiber strength was measured using a Fiber Sigma two point bending apparatus. The fiber were tested at five different stress rates (0.3, 3, 30, 300, 3000 MPa/s) in a controlled atmosphere (humidity 50% ± 5%, temperature 23°C ± 2). Thirty samples were measured at each stress rate. The dynamic stress corrosion susceptibility factor is determined for each fiber using the following equation:

$$\log(\sigma_f) = \frac{\log(\dot{\sigma}_a)}{n_d + 1} + \text{intercept} \qquad (1)$$

A measurement example is shown in Figure 1.
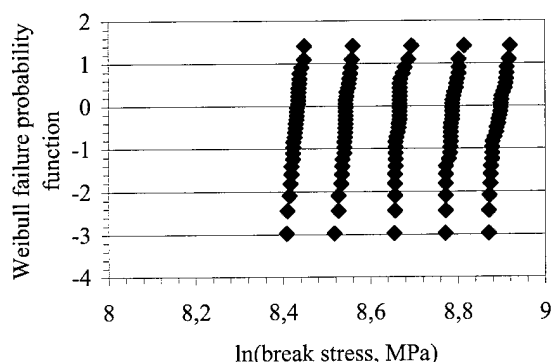
Figure 1. Dynamic fatigue results for fiber 13. The n-value is 18.7.

2.3 Fictive Temperature Measurement

First, the fictive temperature vs. IR reflection peak wavenumbers relation was obtained in order to use it as the calibration curve. The fibers coating was removed by immersing the fiber in hot sulfuric acid-nitric acid (98% H_2SO_4 –2% HNO_3) solution at 200°C for 30 seconds. The bare fibers produced in this manner was heat-treated at selected temperature; 1300°C, 1 hrs; 1200°C, 6 hrs; 1100°C, 66 hrs and 1000°C, 200 hrs and quenched to fix the structure at the heat-treatment temperatures. These heat-treatment conditions are known to be sufficient to establish metastable equilibrium states at each temperature. The IR reflection spectrum of the fiber was obtained using a Nicolet FTIR with SpectraTech microscope attachment. The beam size employed was 20μm x 120 μm with the longer dimension being parallel to the fiber axis. Figure 2 shows a typical IR reflection spectrum where a reflection angle of 28° was used and 1000 scans were taken.
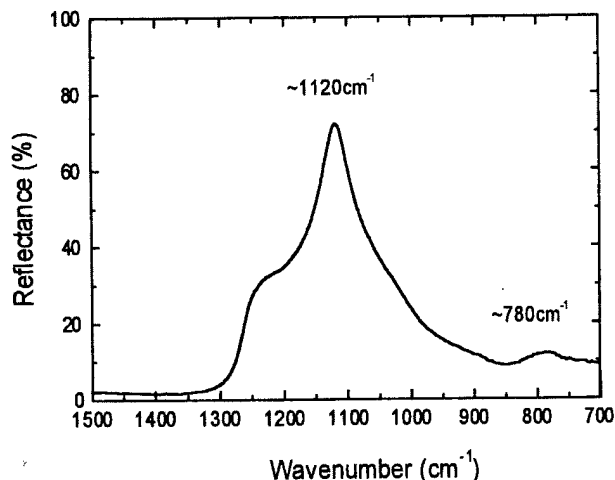
Figure 2. An example of IR reflection spectrum of a silica glass optical fiber surface. Reflection angle 28 degree and an aperture size of 20μm x 120 μm with the 120 μm side parallel to the fiber axis were used.

It has been shown[9,10] that the IR structural band near ~1120 cm^{-1} is due to asymmetric stretching vibration of the Si-O-Si bond and that the peak position reflects the Si-O-Si bond angle[10]. Also, it was shown earlier that the peak position of this band correlates with the fictive temperature of silica glass[8]. The IR reflection peak shifts to a larger wavenumber as the fictive temperature decreases. This indicates that the Si-O-Si bond angle increases with decreasing fictive temperature. The data is usually analyzed using an empirical relationship such as in Figure 3.
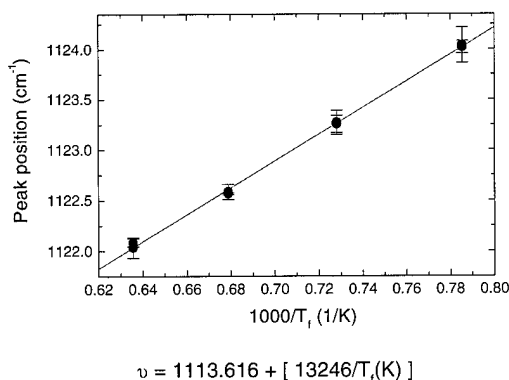
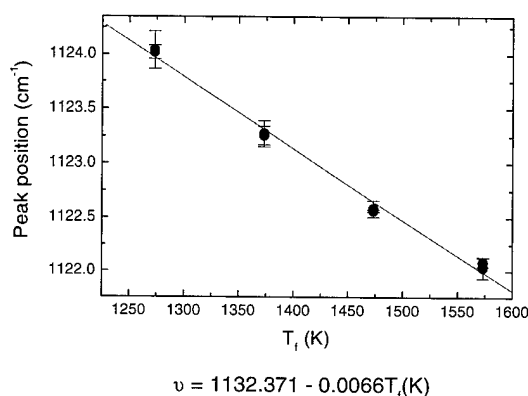$$\upsilon = 1113.616 + [\ 13246/T_f(K)\ ]$$

Figure 3. IR reflection peak wavenumber vs. the reciprocal of the absolute surface fictive temperature of silica glass optical fibers.

The straight line, which is the least square fit to the data can be expressed as

$$\nu \ (cm^{-1}) = 1113.616 + [13246/T_f(K)] \qquad (2)$$

where $\nu \ (cm^{-1})$ is the IR reflection peak wavenumber and T_f is the corresponding fictive temperature in the absolute temperature scale. However, Devine and Marchand[13] found that the IR wavenumber and silica glass density is linearly related. Since the density is likely to change linearly with the fictive temperature rather than with the reciprocal of temperature, the same data are plotted in the linear temperature scale in Figure 4.

$$\upsilon = 1132.371 - 0.0066T_f(K)$$

Figure 4. The IR reflection peak wavenumber vs. the absolute surface fictive temperature of silica glass optical fibers.

The straight line, which is the least square fit to the data can be expressed as

$$\nu \ (cm^{-1}) = 1132.371 - 0.00660 \ T_f(K) \qquad (3)$$

The fictive temperature of a glass is known to be dependent on the cooling rate of the glass[21, 22] with the higher cooling rate resulting in a higher fictive temperature, by

$$d \ln |q|/d \ (1/T_f) = A - \Delta H/R \qquad (4)$$

where q is the cooling rate, A is a constant, ΔH is activation energy and R is the gas constant. Using this relation, the fictive temperature of silica optical fiber can be estimated. The fictive temperature of an annealed silica glass, which is cooled at a rate of a few °C/min., would be close to its glass transition temperature, 1200°C. The cooling rate of the silica optical fiber with a diameter of 125 µm at its softening point, 1750°C, is estimated to be ~ 6.5x10³ °C/s using an equation derived by Paek and Kurkjian[16]. Using the activation energy, ΔH, for the viscous flow, 170 kcal/mol [4], the fictive temperature of the glass fiber is

estimated to be ~ 1600°C. This value is closer to the fictive temperature estimated by the linear extrapolation. Consequently, equation (3) will be used in the remainder of the present paper.

The IR reflection peak wavenumbers of the as-drawn silica optical fiber prepared under various drawing conditions were measured at 5 different locations for each fiber and the average and the standard deviation were calculated. The obtained average IR reflection peak wavenumbers were converted to the fictive temperatures using equation (3) assuming that the linear relationship extends to higher temperatures.

3. Results

3.1 Mechanical Strength

The measured n_d values range from 18 to 30 with an error bar of ± 1.

The mechanical strengths were analyzed in terms of n_d and intercept. The statistical analysis only showed an effect of the fiber diameter on n_d and intercept; the noise on the experimental values being too high to extract the other parameters impact.

3.2 Surface Fictive Temperature

The present method of fictive temperature determination assumes the linear extrapolation of the IR peak wavenumber-fictive temperature relationship to higher temperatures. The fictive temperature obtained using equation (3) was approximately 1650°C ~1750°C.

The statistical analysis of the design of experiment gave good results: there is no aberrant value and the standard deviation of the design is 95%. From this analysis Equation 5 is derived to predict fictive temperature. The error on the fictive temperature predicted by this equation is of ± 17°C.

$$T_f = 1765.5 - 0.91 \ \emptyset + 0.14 \ \sigma + 0.29 \ a \qquad (5)$$

where T_f is the predicted surface fictive temperature in °C, Ø is the fiber diameter in µm, σ is the draw tension in g and a is the Al content in ppm. The draw speed is not included in the equation since there was no significant effect on the fiber surface fictive temperature.

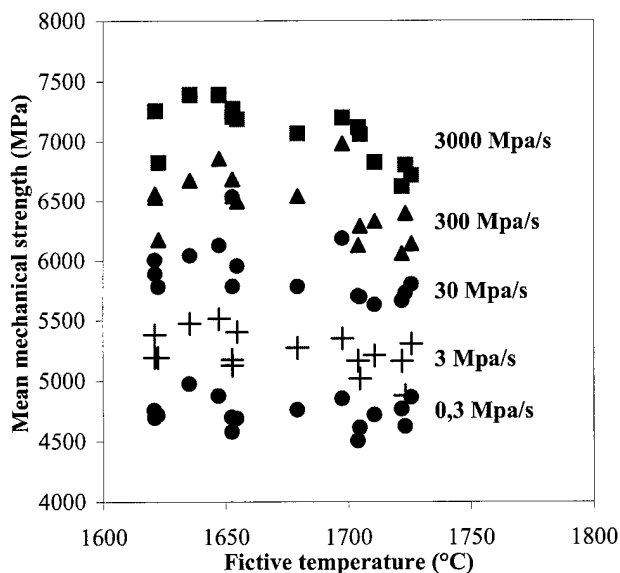## 3.3 Relation Between Mechanical Strength and Surface Fictive Temperature

The dynamic stress corrosion susceptibility factor values were plotted against fictive temperature (Figure 5). n_d appears to increase with fictive temperature with a significant change of slope for a temperature around 1650°C. Statistically significant relation could be found between n_d and fictive temperature:

$$n_d = 3788 - 4.532 \times Tf + 1.362 \times 10^{-3} \times Tf^2 \qquad (6)$$
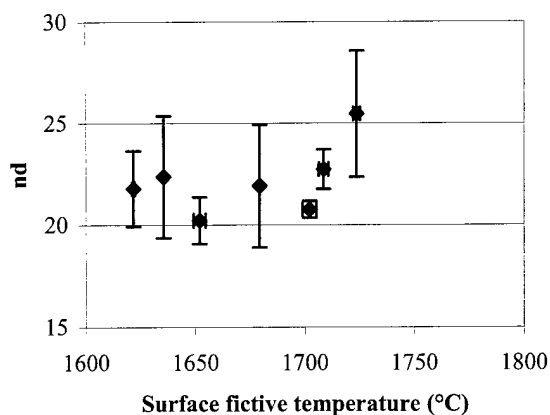
Figure 5. Dynamic stress corrosion susceptibility factor, nd versus fictive temperature.

The strength of the fibers was plotted versus the surface fictive temperature (see Figure 6). For high stress rate, the strength of the fiber decreases with the surface fictive temperature in the high fictive temperature range. As for n_d a change of slope is observed around 1650°C. Below this temperature, the mechanical strength is almost constant. However for lower stress rate, the strength remains constant on the whole fictive temperature range studied here.

Figure 6. Mechanical strength of fibers versus measured fictive temperature.

4. Discussion

The fictive temperatures of the silica optical fibers were estimated using the relation between the IR reflection peak wavenumber and fictive temperature obtained in the glass transition temperature range shown in Figure 4 and extrapolating the straight line to

higher temperatures. The extrapolation assumes that with increasing fictive temperature, the IR structural band wavenumber continues to decrease and correspondingly the Si-O-Si bond angle continues to decrease. Since the extrapolation is extensive, there can be a substantial error in the absolute magnitude of the estimated high fictive temperature. Furthermore, since silica glasses exhibit a peculiar relation between the specific volume and fictive temperature[11], with the volume becoming a minimum at around 1500°C, even the extrapolated trend of the relation itself may be in doubt. However, there are supporting evidences for the present analysis. First, molecular dynamic calculation[12] showed that the Si-O-Si bond angles continue to decrease with increasing fictive temperature, consistent with the present assumption. Second, a structural study by Devine and Marchand[13] also showed, again consistent with the current analysis, that chemically vapor deposited silica, which is expected to have a very high fictive temperature, had an extremely small IR peak wavenumber and a corresponding small Si-O-Si bond angle. They estimated that the fictive temperature of the silica made by chemical vapor deposition is in excess of 2400°C. Furthermore, Lee et al's finding[14] of a high defect concentration in the optical fiber especially near the surface appears consistent with the high fictive temperatures obtained by the present analysis.

The other concern is the effect of the residual stress on the IR measurement. Since the stress can cause the shift of the IR peak[15], it could influence the fictive temperature determination from the IR peak position. According to Paek and Kurkjian[16] and Kurkjian and Paek[17], residual stress in the fiber cladding can be generated either from the difference in thermal expansion coefficient (thermal effect) of the core and cladding or from the difference in viscosity (mechanical effect) of the core and cladding. The magnitude of the former is independent of the fiber draw tension while the magnitude of the latter increases with increasing draw tension. The measured axial stress in the cladding of an optical fiber with GeO_2-doped core-SiO_2 cladding was found to be a few Kg/mm^2 [18,19] consistent with the theory. The amount of wavenumber shift of the IR peak of silica glass by uniaxial stress was found[15]to be ~ 0.5 cm^{-1}/GPa. Consequently, the peak shift which can be caused by the expected range of the residual stress in the optical fiber is estimated to be ~0.02 cm^{-1}, which is within the experimental error. Therefore, the magnitude of the residual stress commonly found in the optical fiber is expected to have no measurable influence on the present measurements. Furthermore, similar IR wavenumber was obtained for pure silica glass fiber without core, which cannot have the type of the residual stress discussed above. When silica glass fibers with a thinner diameter of 6-25μm are produced at a higher temperature such as 2200~2400°C, birefringence was observed[20] but the corresponding stress, again, is too small to influence the IR peak positions measurably. Thus, the observed low IR peak wavenumber cannot be attributed to the residual stress and is likely due to the high fictive temperature of the fiber.

The relationship between the drawing parameters and the fictive temperature is clearly established by Equation 5. In this equation, it seems peculiar that the draw speed which in general affects greatly the cooling rate of the fiber would have no impact on fictive temperature. The draw speed changes the glass temperature most noticeably when the glass moving speed is close to fiber draw speed, that is when the fiber diameter is about stabilized at 125 μm. The fiber diameter reaches its nominal value at a

Special Concerns of In-building Radiating Cable Systems

James H. Scelsi, James W. Denson
Trilogy Communications, Inc.
Pearl, Mississippi
+1-601-933-7615 · Trilogyjhs@aol.com

Abstract

In-building radiating cable systems have unique concerns not encountered in other applications. Not only are common concerns such as the electrical and mechanical aspects of the cable to be considered but the fire ratings are to be addressed as well. A cable has been developed that eliminates the need for mica tape, as well as Teflon, both of which would add considerably to the cable's cost. This new cable differs from conventional plenum radiating cables in two respects; the inner conductor is fitted with discs and the outer conductor consists of annularly corrugated aluminum.

This paper discusses a new, low-cost plenum-rated radiating cable, which does not sacrifice electrical performance or mechanical integrity.

Keywords

Radiating, Leaky, in-building, Plenum, coax cable.

1. Introduction

Radiating cables used for in-building applications must conform to strict fire codes as well as perform adequately both electrically and mechanically. In-building cables are specially constructed to conform to the National Electric Code's definition of a V-rated, riser rated or the more stringent plenum rating. Because of these requirements, simply applying a low-smoke polyvinylchloride jacket to a cable is not normally sufficient to obtain a plenum rating. Usually some other approach to cable design is needed such as incorporating a layer of mica tape or using Teflon.

In addition to mica tape or Teflon, plenum rated radiating cables are typically constructed of a copper-clad center conductor with a spiral polyethylene material formed over it to serve as the dielectric. Because of the tight bending radii typically encountered in building installations, a corrugated outer conductor is chosen to provide flexibility. For this new cable, a corrugated aluminum outer conductor was chosen, however the traditional spiral dielectric commonly seen in plenum radiated cables was abandoned in favor of another construction.

The center conductor of this new cable is fitted with discs made of polyethylene injection molded onto the center conductor. This construction substantially reduced the amount of plastic in the cable. A corrugated aluminum outer conductor is then formed over this disc/center conductor assembly. Next, slots were cut into the cable by milling off the peaks of corrugation on opposite sides of the outer conductor. Lastly, a low-smoke PVC jacket is extruded over the construction.

2. Mechanical Concerns

In-building systems are typically designed using half-inch radiating cable. This diameter of cable is chosen because of the electrical requirements of the cable and the tight bending demands commonly seen in buildings. Because of the confined spaces the mechanical integrity of the cable is important making smaller diameter, lighter, and easily bendable cable a requirement.

Cable weights are also a concern because the area in which the cable is routed such as false ceilings is usually not made to support additional weight. Larger diameter cables can weigh as much as 1.07 lbs./ft. A competitor's ½"-radiating cable is rated at .16 lbs./ft, where this new cable weighs .125 lbs./ft. This is some 30% lighter.

The ability of a cable to bend readily into the tight spaces commonly encountered in buildings is a major concern. This new cable has a minimum-bending radius of five inches, which is small enough to bend around the most restrictive spaces.

A cable's bending moment, the amount of force needed to start the cable to bend, is a measure of how readily a cable can be maneuvered into tight spaces. This new cable will bend when a force of 25 ft.*Lbs. is applied, slightly lower than the 3 ft.*Lbs needed to bend a competitor's model.

3. Fire Rating Concerns

The National Electric Code defines three fire-rating classifications in which coaxial cable used for in-door applications must conform. They are V (UL1581/CATV), riser (UL1666/CATVR), and plenum ratings (UL910/CATVP). The (UL1666/CATVR) riser rating allows cables, which achieve this rating to be routed between floors in such areas as elevator shafts, and stairwells. Cables of this variety consist of non-halogenated fire-retardant jackets and meet low toxicity and smoke requirements.

The more stringent plenum rating is required for cable installations in air ducts, plenums, or other air-handling spaces. Plenum rated cables are required to meet flame propagation restrictions, and low smoke and toxicity requirements. This new cable is manufactured with discs consisting of a polyethylene material suitable for plenum applications.

4. Electrical Concerns

The main electrical concerns of any radiating cable system are insertion loss, and coupling loss. A cable's insertion loss is the attenuation in a cable due to the losses in the conductors and dielectric. The coupling loss refers to the difference in signal levels from what is received by a portable radio to what is inputted into a system. Typically, this quantity is specified in some median value for some specified distance from the cable. Because of the limitations imposed by space and bending restrictions, only smaller diameter cables are practical for in-building applications. Therefore, a ½" diameter cable is commonly used. A cable of this size can be expected to provide a usable signal up to sixty feet away from the cable. This is usually enough to illuminate an entire room.

4.1 Electrical Measurements

Attenuation measurements of the cable taken while the cable was suspended two inches from a concrete floor show a loss in the

order of 3.9 dB/100' at 800 MHz. Figure 1 shows a plot of the attenuation values at various frequencies.
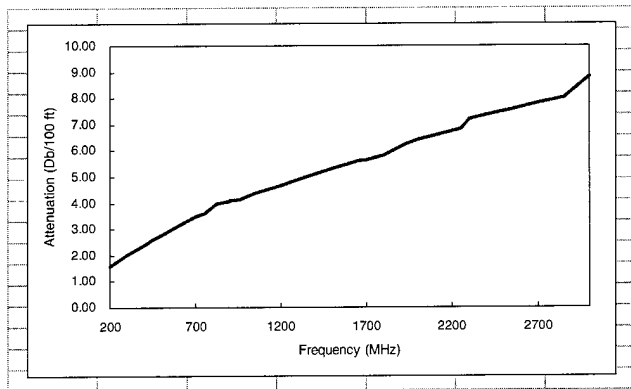
Figure 1. Plot of attenuation values per 100 feet of new model of radiating plenum cable

Median coupling loss measured 64 db at 800 MHz. Figure 2 shows a plot of how the measured coupling loss varied for frequencies adjacent to 800 MHz. Because of the extremely low value of plastic in the cable, its velocity of propagation measures 93% of C.
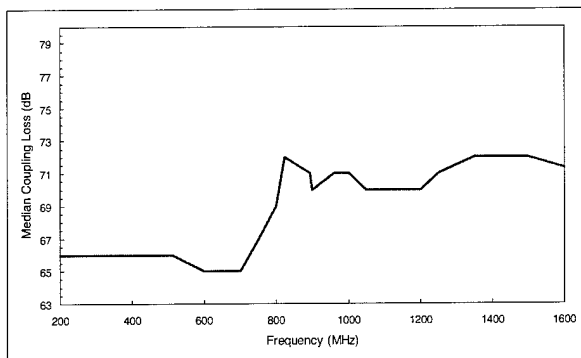

Figure 2. Median coupling loss values measured at a distance of 20 feet from the cable.

5. System Design Concerns

5.1 Hardware & Equipment

In-building radiating systems typically consist of an external antenna, bi-directional amplifier, and radiating cable, connectors, hangers, and terminations. Notice in figure 3; cable ties are used to support a radiating cable above a false ceiling. These ties are spaced three to four feet apart. If the cable is to be mounted to concrete or plaster walls, a self-locking hanger is suggested, along with a stand off.
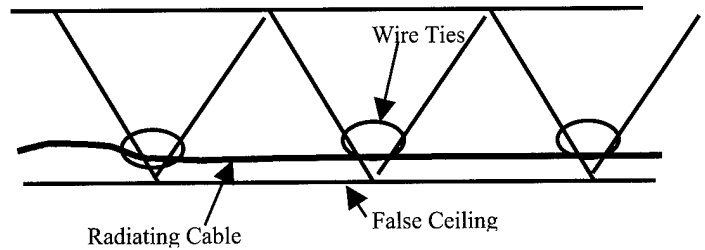
Figure 3. Drawing showing a method of mounting radiating cable above a false ceiling

Most designs employ an external antenna mounted on top of the structure feeding the radiating system. From there, a jumper is attached connecting the bi-directional amplifier to a length of riser-rated non-radiating coax routed between the floors. At each floor the radiating cable is attached to the riser cable by means of a power splitter. At the end of the radiating cable a fifty-Ohm terminating load is attached. Should a cable run end in a larger room, a small antenna may be substituted. Both examples are shown in figure 4.
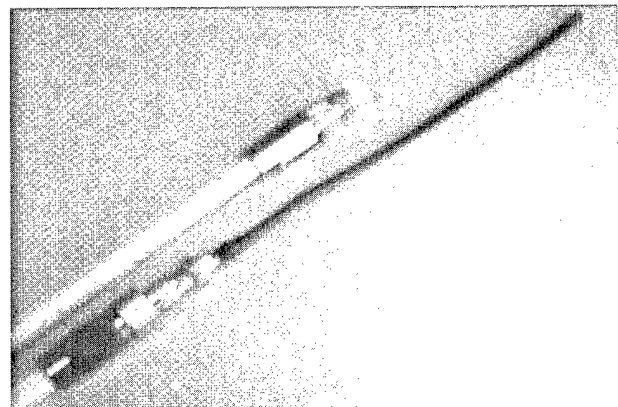
Figure 4. Radiating Cable using terminating antenna and load

5.2 Mounting Concerns

Focusing our attention at the top of the configuration with the external antenna, the mounting concerns are the same as with any roof-mounted installation. The antenna should be securely mounted to the building and away from potential interferers. From there, a jumper is attached connecting a bi-directional amplifier located near by. On the output side of the amplifier is attached a length of riser-rated cable. This cable is routed through the floors by way of an elevator shaft or stair well. This span can be mounted to the wall by means of self-locking clamps. The radiating cable is then attached to this cable at each floor by means of a cable tap.

Since the mounting configuration of the radiating cable will affect its performance, some thought should be put into its routing. Materials such as concrete, metal, etc., change the radiation characteristics of the cable. The cable may be mounted above the false ceiling and secured to the tile beams by means of cable ties as shown in figure 4. At the end of the cable run, a fifty-Ohm termination or low gain antenna is needed to properly terminate the cable.

5.3 Design Example

Buildings are complex structures requiring coverage in relatively open spaces, narrow corridors, staircases, and elevator shafts. Because of the common construction materials, and the affect these materials have on a propagating RF signal, the propagation loss in such an environment is higher than in an open environment. However, a relatively uniform and reliable coverage may be achieved by properly designing the system.

In this example, a four-story building is to be fitted with a radiating cable system. We will incorporate the method previously discussed, which utilized existing coverage outside the structure and extending this coverage into the structure by means of a bi-directional amplifier and radiating cable. A rough lay out is shown in figure 5.
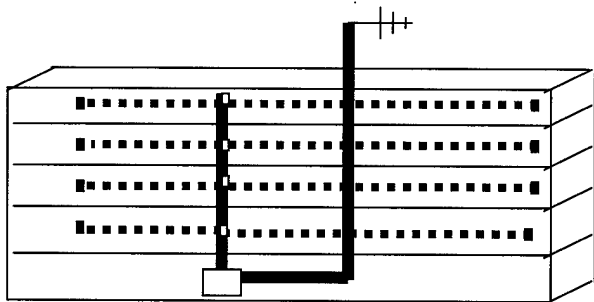
Figure 5. Four-story building radiating cable design example

To determine the estimated signal level seen by a hand held portable in the building we add the gains and losses of each element in the system.

Forward path (tower to building)

Input from transmitter	+10 db
Attenuation (200 feet of 7/8" coax at 894 MHz)	-2.4 dB
Gain of Bi-directional Amplifier	+30 dB
Attenuation (50 feet of ½" coax at 894 MHz)	-1.03 dB
Power Divider Loss (4 dividers @ loss of 4.75 dB ea.)	-19 dB
Attenuation (600 feet of ½" radiating cable at 894 MHz)	-24.54 dB
Coupling Loss (median value)	-66 dB
Body Masking Effect	-5 dB
Total	-77.97
Minimum receiver level	-95
System Margin	+17.03

Similarly for the case where the hand held is communicating with the donor site.

Reverse path (hand held to the donor site)

Input from transmitter	+25 dB
Attenuation (200 ft. of 7/8" coax @ 894 MHz)	-2.4 dB
Gain of Bi-directional Amplifier	+30 dB
Attenuation (50 ft. of ½" coax @ 894 MHz)	-1.03 dB
Power Divider Loss (4 @ loss of 4.75 dB each)	-19 dB
Attenuation (600 ft. of ½" plenum radiating @ 894 MHz)	-24.54 dB
Coupling Loss (median value)	-66 dB
Body Masking Effect	-5 dB
Total	-67.97
Minimum receiver level	-95
System Margin	+27.03

In this design we used a trunk and feeder configuration method to distribute the signal. A main (trunk) line is set up between the floors and a feeder line consisting of the radiating plenum cable is tapped off at each floor. Off-air measurements should be taken using a ½-wave dipole antenna attached to a spectrum analyzer. A map of field strength levels can then be made of all locations throughout the building showing the performance of the system.

6. Cable Design & Theory of Operation
6.1 Theory of Operation

Taking a slight departure from previous discussions, we now focus on the theoretical aspects of a corrugated aluminum disc-dielectric radiating cable. The basic cable structure is shown below in figure 6.
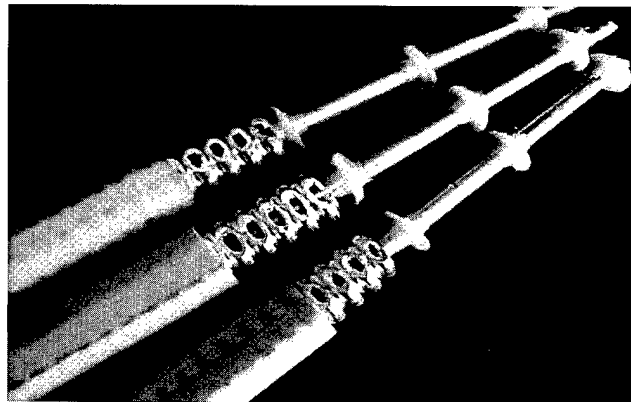

Figure 6. Radiating plenum cable Cut-away view

The inner and outer conductor are separated by dielectric discs injection molded on to the inner conductor. This configuration strengthens the cable against lateral pressure. The outer conductor is aluminum, and the inner conductor is comprised of copper-cladded aluminum.

The characteristic impedance of a cable is approximated by the formula given by (1).

$$Zo \cong \sqrt{L/C} \qquad (1).$$

Where L is the inductance per unit length and C is the capacitance per unit length of cable. The inductor can be calculated by formula (2).

$$L = \frac{\mu o}{2\pi}[\ln(\frac{b_{avg}}{a}) + \frac{1}{a\sqrt{4\pi f\sigma_{in}}} + \frac{q}{bavg\sqrt{4\pi f\sigma_{out}}}] \quad (2)$$

Where $bavg=b+\Delta b/2$ as shown in figure x, μ_o is the magnetic permeability, a is the inner conductor radius, f is the frequency, σ_{in} is the conductivity of the inner conductor, σ_{out} is the conductivity of the outer conductor, and q is the pitch of the corrugation.

The capacitance is therefore calculated by formula (3).

$$C = \frac{2\pi\varepsilon_{eff}}{\ln\frac{[b_{avg}]}{a}} \quad (3).$$

Where ε_{eff} is the equivalent dielectric constant of the space between the inner and outer conductors, including the conductors, discs, and the air contained in the cable, a is the outer diameter of the inner conductor, and b_{avg} is the average inner diameter of the outer conductor. A characteristic impedance of 50-Ohms can be achieved by properly selecting the disc size, inner conductor, and outer conductor.

The radiation from a leaky coax is caused by the holes cut into the outer conductor of the cable. In this new cable a portion of each corrugation is milled off to allow the RF energy to leak out. The radiation from this cable can be thought of as the vector sum of all the slots in the cable. The angle of radiation and position of each slot as shown in figure 7 affect the phase of the energy leaking from each of these slots.
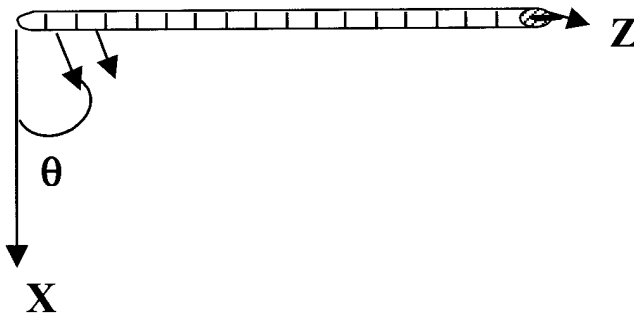
Figure 7. Assumed pattern of energy radiating from cable.

Let the cable propagation phase constant be defined as Φ.

$$\Phi = -\beta v Z \quad (4).$$

And the total phase change will be defined as

$$\Phi tot = (-\beta v + koSin\theta)Z \quad (5).$$

Where Z is the propagation in the Z direction, k_o is the free space wave number of the radiation, θ is the angle of observation, and βv the phase propagating constant.
Summing the contributions for the principle radiating polarization gives (6), (7).

$$Ez = (\sum_{m=0}^{m-1} b_m e^{jmx(-\beta v+k_oSin\theta)})\frac{1}{(1-e^{jp/2(-\beta_v+k_oSin\theta)})} \quad (6)$$

$$E\phi = (\sum_{m=0}^{m-1} a_m e^{jmx(-\beta v+k_oSin\theta)})\frac{1}{(1-e^{jp/2(-\beta_v+k_oSin\theta)})} \quad (7)$$

6.2 Cable Structure
A coax cable having a perfectly enclosed outer conductor does not radiate a measurable amount of energy. Consequently, an electric field outside the cable has neglectable effect on signal travelling inside the coax. Openings in the shield of the outer conductor cause electromagnetic coupling between the field inside the cable and the outside similar to a conventional antenna.

The size and arrangement of these openings determines the mechanism of the electromagnetic coupling. With this in mind, there are two families of leaky coax defined. One group has equidistantly-spaced holes in the outer conductor. This family is known as coupled mode or surface waveguide. The second variety, named radiating mode, is characterized by periodically spacing the slots. This new model of radiating coax belongs to the family known as 'coupled mode'.

The energy in a radiating cable can be described as a wave flowing through the cable and at all points where the energy "sees" a slot it induces a surface wave which spread forward and backward outside the cable.

As described in previous sections, an important electrical characteristic of a radiating cable is its attenuation. This is determined by losses encountered in the conductors and dielectrics. Another important factor is the cable's coupling loss. This is defined as the ratio of received power at an antenna to the power travelling inside the cable. Both coupling loss and attenuation is affected by the size of the hole cut into the outer conductor. For this cable, a slot size was chosen that showed adequate coupling loss without sacrificing attenuation.

7. Conclusions
In-building applications of radiating coaxial cable have to meet standards not imposed upon traditional outdoor cables. A coax's fire rating is of special concern along with its ability to bend in close quarters. In-building radiating cables must perform adequately electrically and mechanically as well as conform to fire codes. The new radiating cable presented here meets these requirements and does so by not using costlier materials such as mica and Teflon.

8. References
[1] K. Watanabe, J. Baldauf, Mmiyamoto, Y. Suzuki, K. Ogawa, "New Widebandwith Microwave Leaky Coaxial Cables" *International Wire & Cable Symposium Proceedings,* p.596-600 (1993).

[2] H.G. Haag, G. Thonneben, K. Schulze-Buxloh, "Leaky Coaxial Cables for Mobile Communication", *International Wire & Cable Symposium Proceedings*, p.596-600, 1993.

[3] J. Scelsi, "Radiating Coaxial Cables: How Design Affects Performance"," *Master's Thesis, University of Mississippi*, (December 1998).

9. Authors

James (Jim) H. Scelsi received a BS degree in Electrical Engineering from the University of South Alabama in 1992. He then attended the University of Mississippi where he received an MS degree in Computer Engineering. He joined Trilogy Communications in 1997 as a product development engineer. He frequently lectures and writes on the subject of radiating coaxial cable. He is a member of the Institute of Electrical and Electronic Engineers (IEEE), and the Society of Cable Telecommunications Engineers (SCTE).

James (Jim) W. Denson received a BS in Polymer Science from the University of Southern Mississippi in 1992. He joined Trilogy Communications in 1995 as a materials engineer. He is a member of the American Society for Testing and Materials (ASTM), the Society of Plastics Engineers (SPE), and the Society of Cable Telecommunications Engineers (SCTE).

Differential Skew within Symmetrical Transmission Lines

Dietmar Gleich[1], Mats Josefsson[1], Marcus Lindström[1] and Ratimira Šimundic[2]

[1]Ericsson Cables AB, Hudiksvall, Sweden
[2]Faculty of Electrical Engineering and Computing, Zagreb, Croatia
+46-650-36256   dietmar.gleich@eca.ericsson.se

Abstract

In this paper measurement and effects of differential skew within symmetrical transmission lines are discussed. Different measurement methods are described and compared using either symmetrical pulses of a fixed frequency and shape, symmetrical sine waves swept over a wide spectrum or single ended sine waves. The physical mechanisms such as effects of resistance unbalance and capacitance earth unbalance and dependence of skew on transmission line length are examined. The relationship between longitudinal conversion transmission loss (LCTL) and skew is described and a simple model is presented and tested. Finally, the effect of skew on eye patterns is discussed.

Keywords

Differential skew; symmetrical transmission line; longitudinal conversion transmission loss; eye-pattern

1. Introduction

Data rates are rapidly increasing both in stationary and in cellular switching systems. Often these systems use symmetrical cables for internal data exchange. With increasing clock frequency differential skew is becoming increasingly significant for signal integrity. It is therefore very important to have quick and generally useful skew measurement methods. Deeper understanding of the relationship between skew, LCTL and eye pattern quality can help find practical high speed cable characteristics.

2. Measurement Methods
2.1 With Pulses
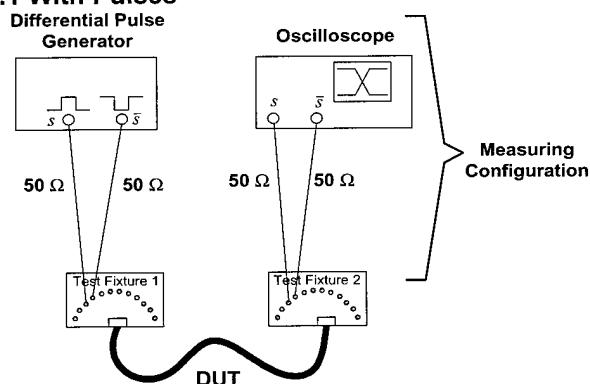
Figure 1. Measurement with pulses

One method for measuring skew is taking a differential pulse generator and a two-channel oscilloscope presented on figure 1. It

is very important that the skew generated in the differential pulse generator and detector (oscilloscope) is not too high.

Moreover, none of the connection lines should generate a significant high skew. This means that electrical lengths of those connection lines must be the same for each part of the differential signal. Calculations can be made to eradicate smaller differences.
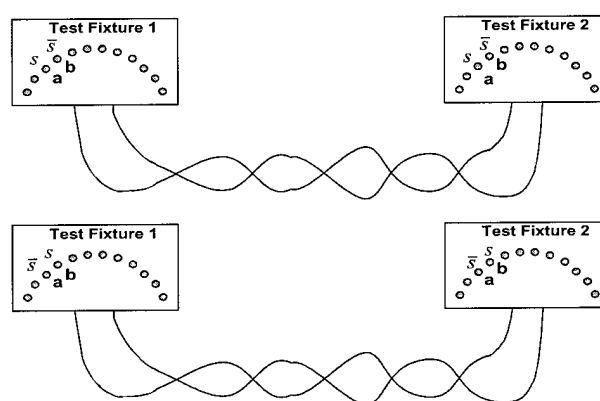
Figure 2. Branch swapping

One possibility is branch swapping. It means swapping *a* and *b* side of the device under test (DUT) on both test fixtures while all the remaining configuration stays the same as shown in figure 2.
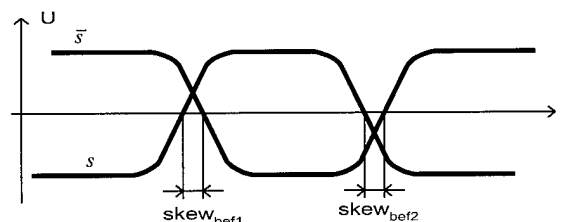
Figure 3a. Measurement before branch swapping
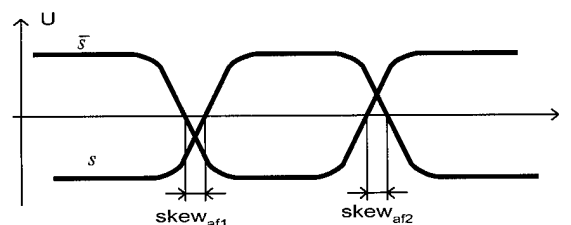
Figure 3b. Measurement after branch swapping

When the skew in the measuring configuration ($skew_{mc}$) is significantly lower than in DUT ($skew_{DUT}$), the results on

oscilloscope before and after the branch swapping will in principle look like those presented in figures 3a and 3b, respectively.

When measuring, one detects both the skew of the measuring configuration and DUT. Assuming the skew within the measurement configuration is constant, it can be eliminated. After branch swapping only the skew of DUT is inverted, but not the skew of the measuring configuration. So, when the results of the two measurements are subtracted, the skew$_{mc}$ is eliminated and the skew$_{DUT}$ is doubled, as presented in equation (1).

$$skew_{bef\,1,2} = skew_{mc} + skew_{DUT}$$
$$skew_{af\,1,2} = skew_{mc} - skew_{DUT} \qquad (1)$$
$$skew_{DUT} = \frac{skew_{bef\,1,2} - skew_{af\,1,2}}{2}$$

2.2 Sweeping with Sine Waves

Another method for skew measurement is using a network analyzer, generating a symmetric signal and detecting phase differences after passing DUT. To make sure that the unbalances in the measuring equipment do not exceed an acceptable level, it can be checked as shown in figure 4. Such unbalances might arise between input channels *Ain* and *Bin* in the network analyzer, between the connection lines *Cx1+Cx2* and *Cx1'+Cx2'* and inside the hybrid junction. Small deviations can be eliminated in the same way as described in 2.1.
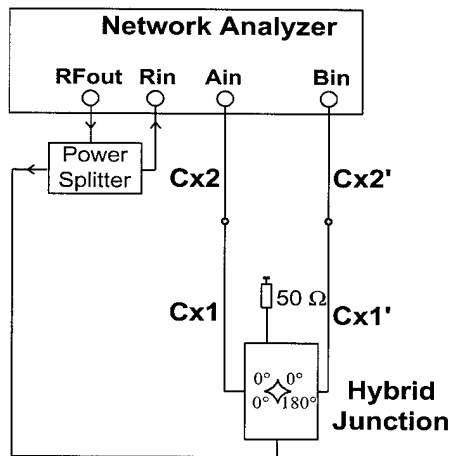
Figure 4. Accuracy test

Figure 5 shows the configuration for the measurement of differential skew in the frequency domain. The output signal from the network analyzer is transformed into a symmetrical signal in a hybrid junction. DUT is excited symmetrically. The relative phase difference between the input channels *Ain* and *Bin* can be measured directly. Branch swapping as already described in 2.1 can eliminate measurement discrepancies caused by the measurement equipment.
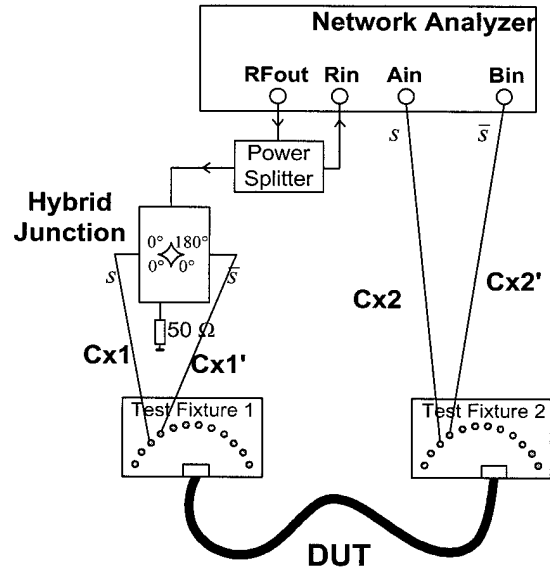
Figure 5. Measurement with sine waves
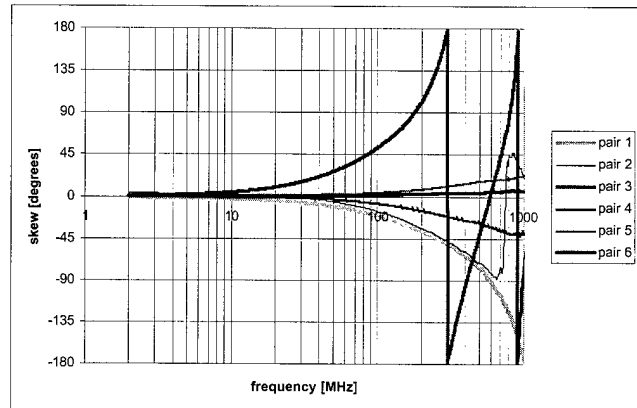
Figure 6. Skew (degrees) from sine measurements

Calculation of time skew from angular skew is made using:

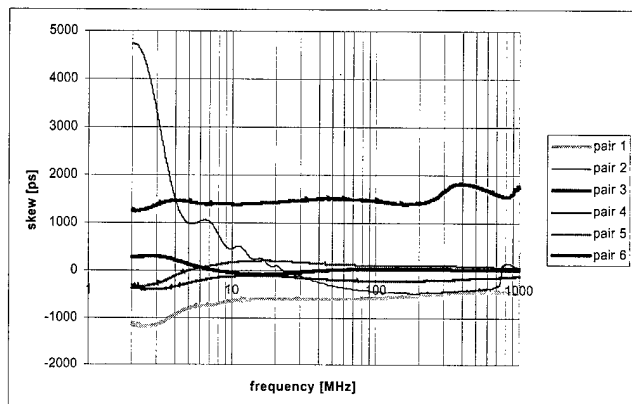$$skew(time) = \frac{skew(degrees)}{360} \cdot \frac{1}{f} \qquad (2)$$

Figure 7. Skew (ps) from sine measurements

Pair 3 in figure 6 shows a phase shift at about 300 MHz and 900 MHz. The reason is that the network analyzer only displays angles from −180° to +180°. At the points of phase shifts an angle of a multiple of 360° needs to be added (or subtracted) to get the real value. For the calculation of the skew in time this operation was carried out.

2.4 Comparison

The measurements with sine waves in frequency domain and with rectangular pulses show good agreement as presented in figures 8 a-d. The given frequency is for the pulses the inverse of the pulse period and the shape of the pulses is square (50% duty cycle). The transition time of the pulses seems not to be critical. Measurements with rise times between 50 ps and 1 ns did not show any difference outside measurement tolerances. DUT was here a separately screened pair cable with a length of 20 m.
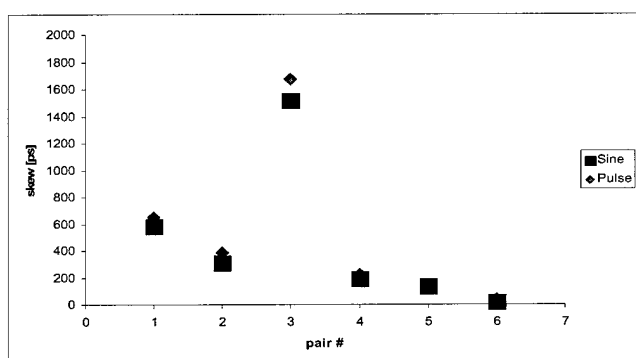
Figure 8a. Skew at 50 MHz
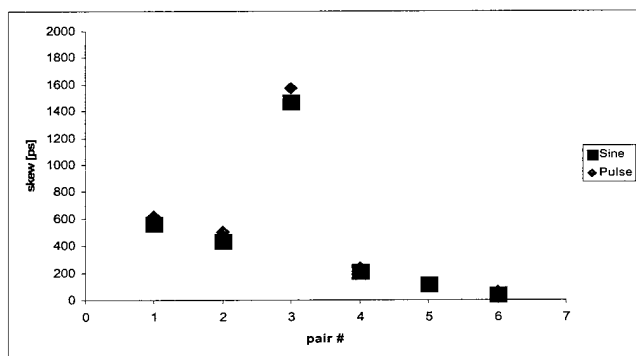
Figure 8b. Skew at 100 MHz
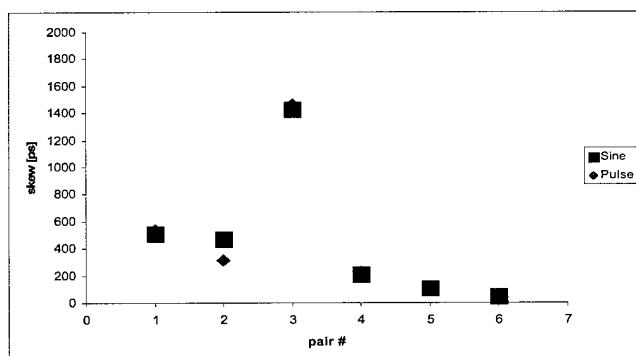
Figure 8c. Skew at 200 MHz
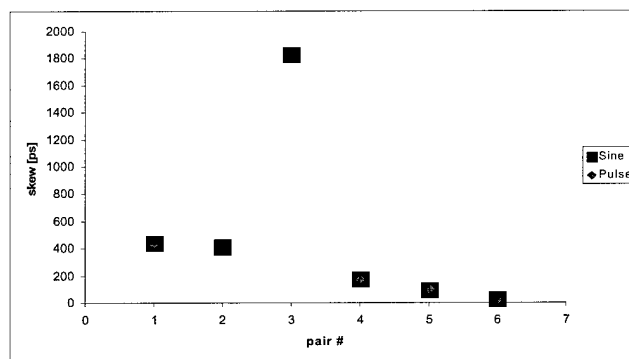
Figure 8d. Skew at 400 MHz

3. Physical Mechanisms
3.1 Unbalances Effects

The propagation velocity of the signal is determined by the primary parameters: resistance R, inductance L, capacitance C and conductance G as shown in equation (3) and figure 9. Any difference in primary parameters between the two wires of a transmission line causes differences in the propagation velocity as described in equation (4). Since the wires are coupled, this is not the only phenomenon observed. As a consequence of inductive and/or capacitive coupling between the two wires, the signal in one wire will induce a signal with the opposite polarity in the other wire, thus counteracting skew.
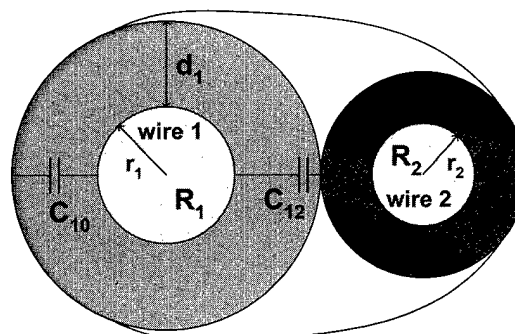

Figure 9. Resistance and capacitance in a pair

$$\beta = \mathrm{Im}\left\{\sqrt{(R' + j\omega L')(G' + j\omega C')}\right\} \tag{3}$$

$$v_{ph} = \frac{\omega}{\beta} \tag{4}$$

To find the LF-parameters that affect skew within a pair a simple test was made using a test set-up with possibilities to adjust resistance and capacitance while inductance is held constant.

The set-up was made using two 5-m L-shaped plastic profiles mounted together to a T-profile, as presented in figure 10. On each L-profile a copper tape was attached along the profiles. The T-profile was placed over a ground plane made of brass where the

height above the ground plane of each profile is adjusted using plastic screws. The differential impedance was set to 100 O and capacitance earth unbalance was minimised.

To produce resistance unbalance small stripes of copper tape were attached to the top of one strip-line. While the resistance of each strip-line was measured, the capacitance of each was checked to ensure that capacitance earth unbalance was minimised.

To achieve capacitance earth unbalance a dielectric material (polyethylene) was inserted between one strip-line and the ground plane. The dielectric was moved to cover part of, or the whole width of the strip-line. Capacitance between each strip-line and the ground plane was measured.
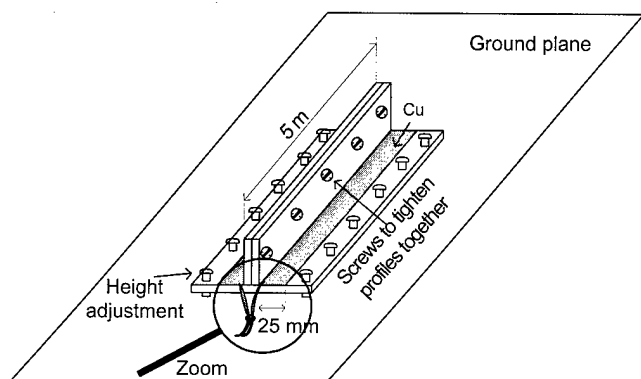
Figure 10. Measurement set-up

Figure 11 shows electrical scheme of this measurement set-up.
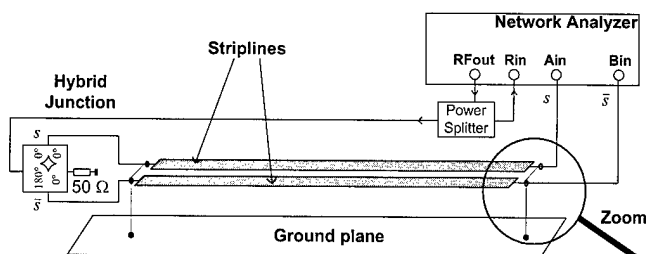
Figure 11. Electrical scheme

Figure 12 shows the measurement set-up zoom where the connections between the inner copper conductors of the coaxial cables and strip-lines are presented in detail. Skew is measured with network analyzer according to the method described in 2.2.
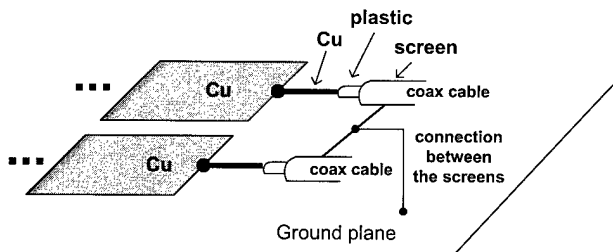
**Figure 12. Measurement set-up zoom**

Resistance unbalance is calculated from equation (5), where

$$R_{un} = \left| \frac{R_1 - R_2}{R_1 + R_2} \right| \tag{5}$$

the capacitance earth unbalance is calculated from equation (6):

$$C_{eun} = \left| \frac{C_{10} - C_{20}}{C_{10} + C_{20}} \right| \tag{6}$$

Definitions of capacitance and resistance can bee seen in figure 9. The figures 13 and 14 show that skew is much more influenced by capacitance earth unbalance than by resistance unbalance. The probable cause lies in the fact that jwC is much greater than R for higher frequencies.
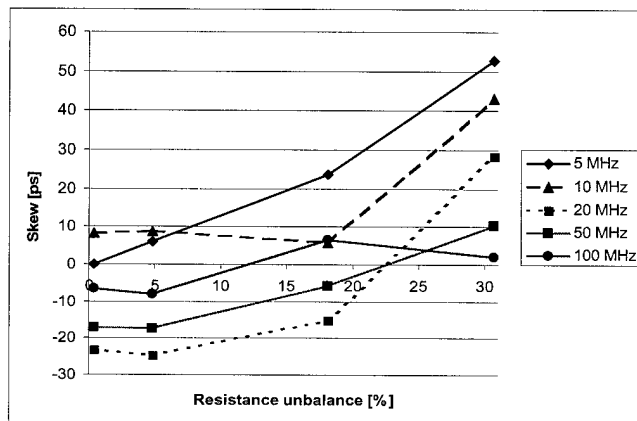
Figure 13. Skew dependence on different resistance unbalances
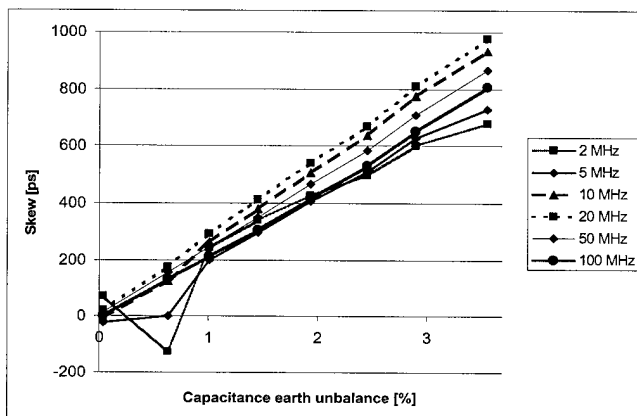
Figure 14. Skew dependence on different capacitance earth unbalances

3.2 Length and frequency dependence

Table 1 shows the skew for different lengths of the same type of cable, whereas the skew per length is calculated in table 2. It can be noticed that skew is not necessarily linear with the length. Skew can also vary with frequency as can be seen on pairs 2 and 3 on figure 7. This can be partly explained by the unequal properties of the cables along the length. Another mechanism is that highly

coupled pairs tend to reduce initial skew over length as it was observed in our measurements. This could even result in absolute higher skew for short lengths than for longer lengths.

Table 1. Skew (ps), f=333.3 MHz, Pulse method

	pair 1	pair 2	pair 3	pair 4	pair 5	pair 6
1 m	22	4	23	52	46	19
5 m	47	7	118	159	339	24
10 m	82	27	220	204	655	49
20 m	230	92	462	432	25	128

Table 2. Skew/length (ps/m) calculated from above

	pair 1	pair 2	pair 3	pair 4	pair 5	pair 6
1 m	22	4	23	52	46	19
5 m	9	1	24	32	68	5
10 m	8	3	22	20	66	5
20 m	12	5	23	22	1	6

4. Relationship between Skew and LCTL

4.1 LCTL measurement

We define longitudinal conversion transfer loss (LCTL) as:

$$LCTL\,[dB] = -10 \cdot \log\left(\frac{\text{common mode output power}}{\text{input power (differential)}}\right) \quad (7)$$

and equal level LCTL (EL-LCTL) as:

$$EL\text{-}LCTL = LCTL\,[dB] - \text{differential attenuation}\,[dB] \quad (8)$$
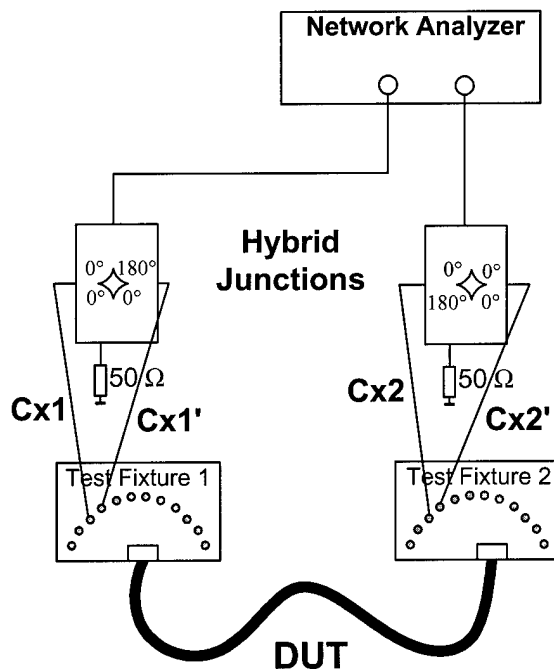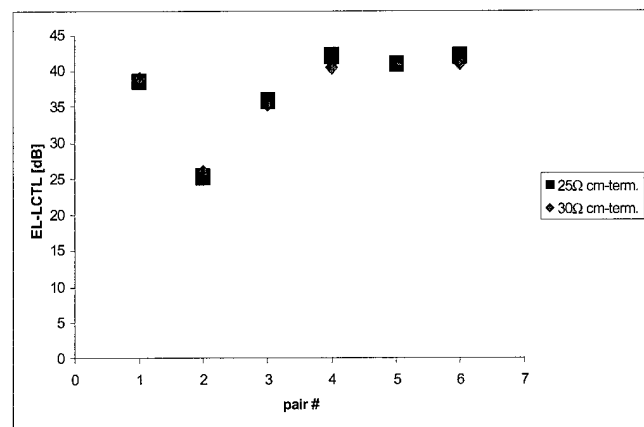
Figure 15. LCTL measurement

With the first hybrid junction a symmetrical signal is generated from the output signal of the network analyzer. At the far end of the DUT either the common mode or the differential mode power is detected through another hybrid junction (H). The two powers are compared and the difference [in dB] is the EL-LCTL. Table 3 shows the measurement results compared with those made with

baluns (B) which is a well documented method and described for example in [3] and [2]. The fit satisfies within the common frequency range allowing for different resonance frequencies.

Table 3. EL-LCTL measured with hybrid and balun

Method	f [MHz]	pair 1	pair 2	pair 3	pair 4	pair 5	pair 6
H	20	29.0	25.7	21.2	42.0	35.4	40.2
B	20	27.8	22.3	20.7	41.0	34.9	41.0
H	80	16.5	17.5	7.8	25.4	30.6	39.2
B	80	16.5	19.0	8.3	26.5	31.6	38.3

All in this paper otherwise shown skew and LCTL measurements were made with a common mode termination of 25 Ω. According to our measurements the common mode impedance of the DUT is about 30 Ω. In order to compare the effect of a slightly mismatched common mode termination on LCTL measurements a test was made. Baluns with 25 Ω (mismatched) and 30 Ω (matched) common mode termination were used for the measurement of EL-LCTL. Figure 16 shows that the differences are small, so common mode termination seems not to be critical here.

Figure 16. Comparison of EL-LCTL measurements with 25 Ω and 30 Ω common mode termination

The theoretical measurement deviation caused by impedance mismatch can be calculated from the reflection factor (r) at the point of impedance change:

$$r = \frac{Z_{DUT} - Z_{system}}{Z_{DUT} + Z_{system}} \quad (9)$$

With the impedance of the DUT at 30 Ω and the system impedance being 25 Ω the reflection factor is 9.1%. This corresponds to a fault of about 0.75 dB.

4.2 LCTL calculation from (time-) skew

Since skew means deviation from the ideal 180° phase difference between the wires in the pair, skew generates common mode currents and thus influence LCTL. There exist two forms of skew:

phase (time) skew and amplitude skew. The phase skew will be presented in detail, whereas the amplitude skew only in principle.
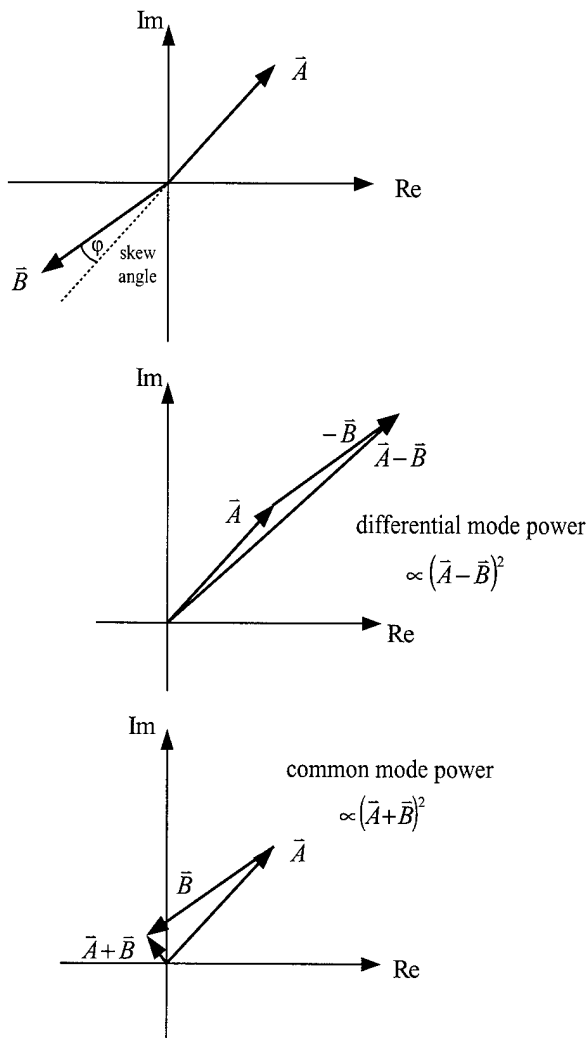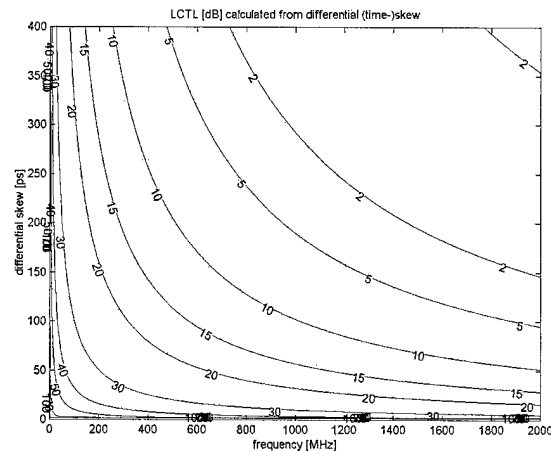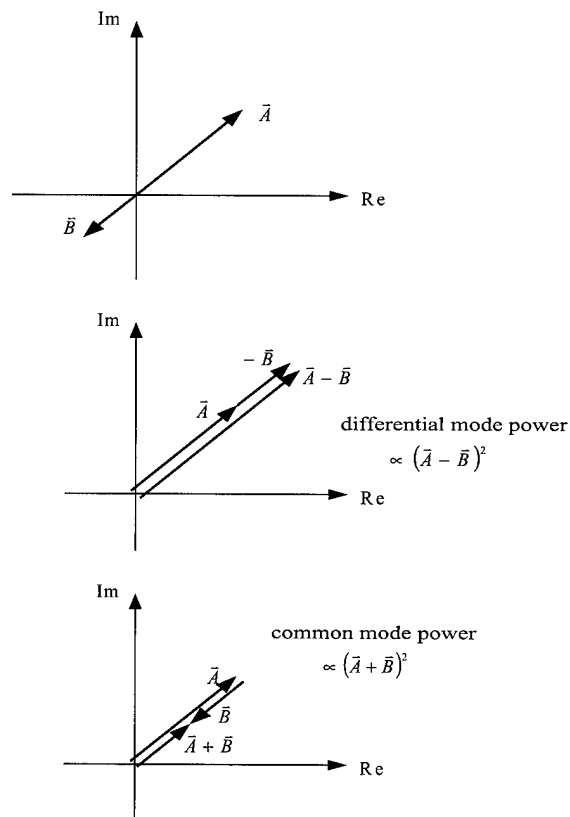

Figure 17. Phase skew

The signals in the wires of a pair are considered to have the same amplitude and frequency but a difference in phase (180° + skew angle). The differential voltage can be calculated by subtracting the vectors and the common mode voltage by adding the vectors, as shown in figure 17. The powers of the differential and common mode signals are obtained by squaring them, respectively.

LCTL is here defined as the ratio of the common mode power to the total power. Figure 18 shows the LCTL calculated from time skew (when neglecting amplitude skew). When only measuring phase attenuation has no influence, so LCTL is here the same as EL-LCTL.

The influence of amplitude skew can be calculated in an analogous way as shown in figure 19.

Figure 18. LCTL calculated from skew

Figure 19. Amplitude skew

4.3 Comparison of calculated and measured LCTL

Despite the fact that only phase skew was considered for the EL-LCTL calculation, the results and direct measurements differ only a few dB over a wide frequency span. The only major discrepancy is in pair 2 at frequencies of some 10 MHz, see figures 20-21. Pair 2 has much higher capacitance earth unbalance (cca 6%) than other pairs.
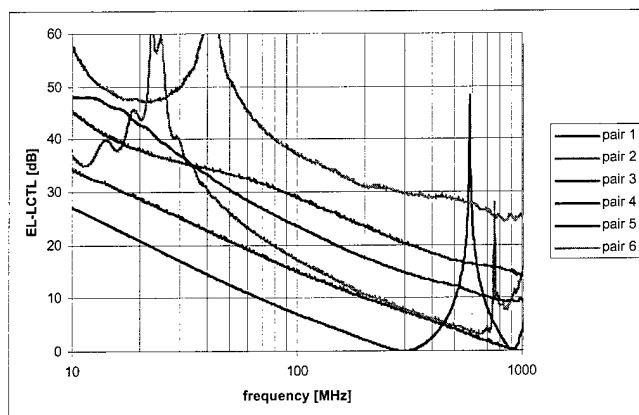
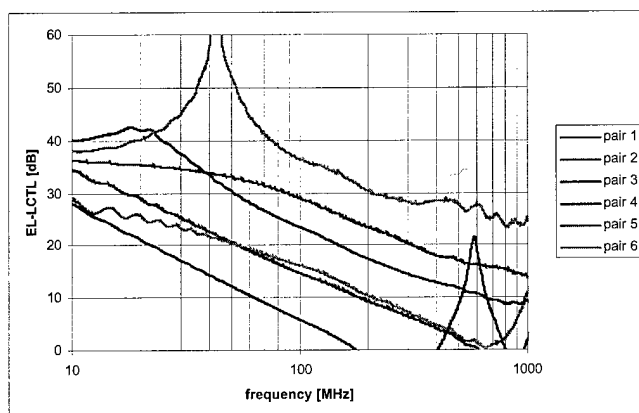**Figure 20. EL-LCTL calculated from skew**

Figure 21. EL-LCTL measured directly

Matching of the two measurements shows that it is often sufficient to consider phase skew only when calculating LCTL. If so, the equations (7)-(8) and figure 17 can also be applied reversibly, meaning calculating phase skew from EL-LCTL.

4.4 Mixed mode S-parameters

An alternative for performing a differential measurement on the DUT with symmetrical signals is to directly measure scattering parameters in single-ended conditions and calculate the mixed-mode S-parameters [1].

With the mixed-mode S-parameters (figure 22) the reflection and transmission characteristics of the DUT can be evaluated for combinations of differential and common mode stimuli and responses.

The big advantage is that no extra connection device is needed (e.g. balun or powersplitter) which might decrease the available bandwidth.

Figures 23 and 24 show comparison between pure symmetrical and mixed-mode measurements. Also in this case different impedance mismatch between the DUT and the 50 Ω measurement system has to be considered. For small reflection coefficients (less than 10 %) the result from the two different measurements are comparable. More work is in progress.

$$\begin{bmatrix} S_{11} & S_{12} \\ S_{21} & S_{22} \end{bmatrix}$$

Single ended S-Matrix

Figure 22. Definition of S-Matrices

Mode   Differential   Common

$$\begin{bmatrix} S_{DD\,11} & S_{DD\,12} & S_{DC\,11} & S_{DC\,12} \\ S_{DD\,21} & S_{DD\,22} & S_{DC\,21} & S_{DC\,22} \\ S_{CD\,11} & S_{CD\,12} & S_{CC\,11} & S_{CC\,12} \\ S_{CD\,21} & S_{CD\,22} & S_{CC\,21} & S_{CC\,22} \end{bmatrix}$$
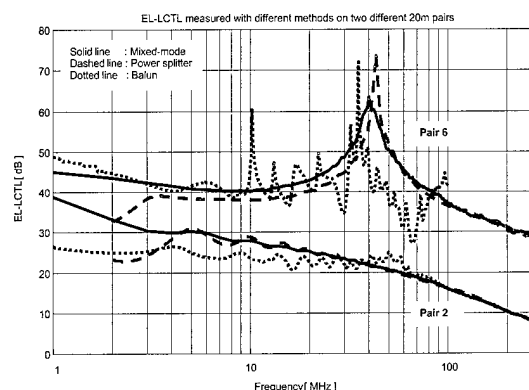
Mixed-mode S-Matrix

Figure 23. EL-LCTL measured with different methods on two different 20 m pairs
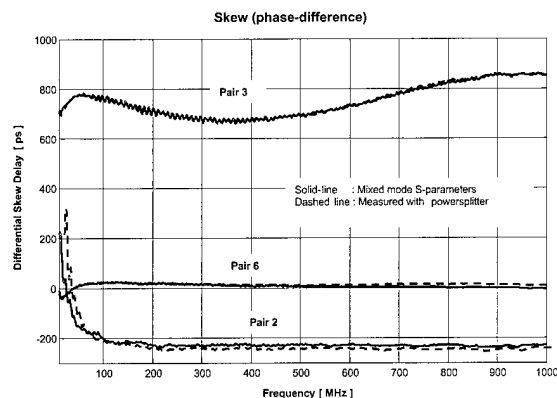

Figure 24. Skew measurement with hybrids respectively mixed mode S-parameters

5. Eye-patterns

5.1 Measurement set-up

Eye pattern measurements were done with a pulse generator delivering a pseudo-random NRZ code to a symmetrical output and an oscilloscope with two input channels. The same fixtures were used as for the skew measurements described in 2.1.

5.2 Results and discussion

Figures 25 a-b show eye-pattern measurements at different frequencies on a pair with high skew and on a pair with low skew. The differences can be seen at all frequencies but the impact on the eye opening is bigger for the higher frequencies. High skew results in two distinct pulse edges, best seen in figure 25a at 50 MHz and 100 MHz.
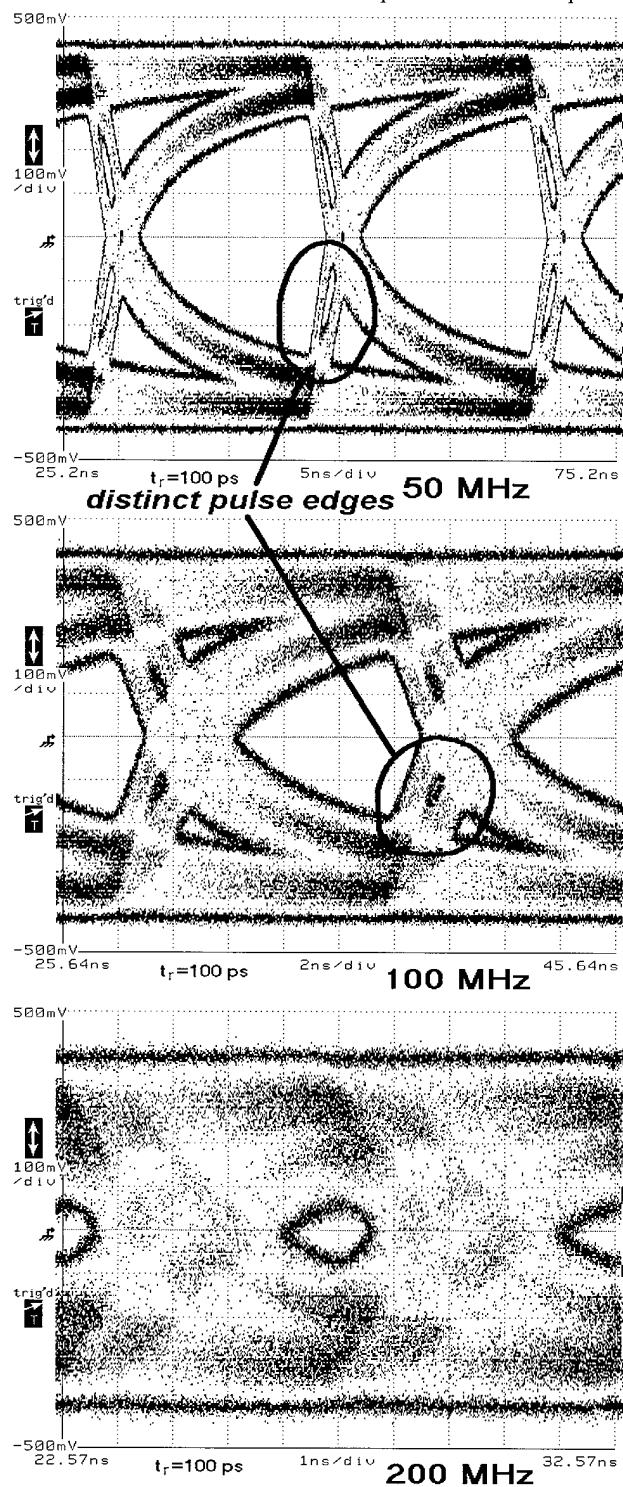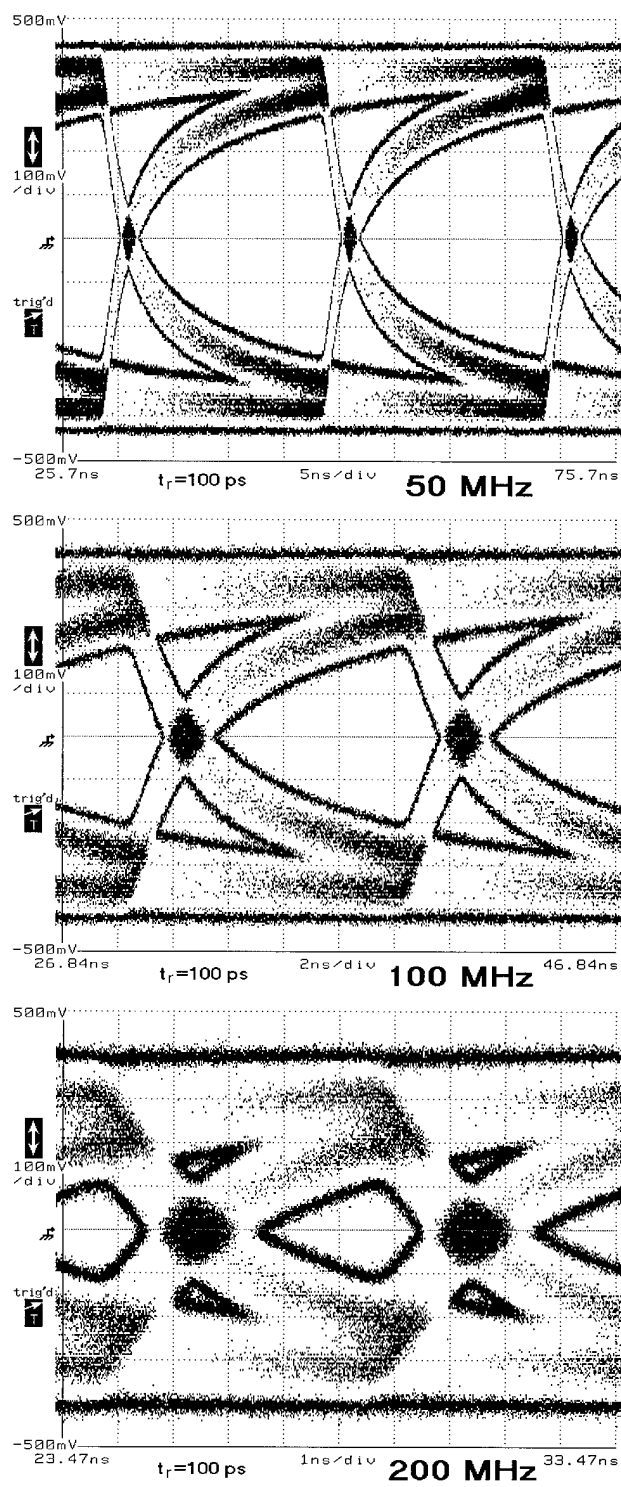

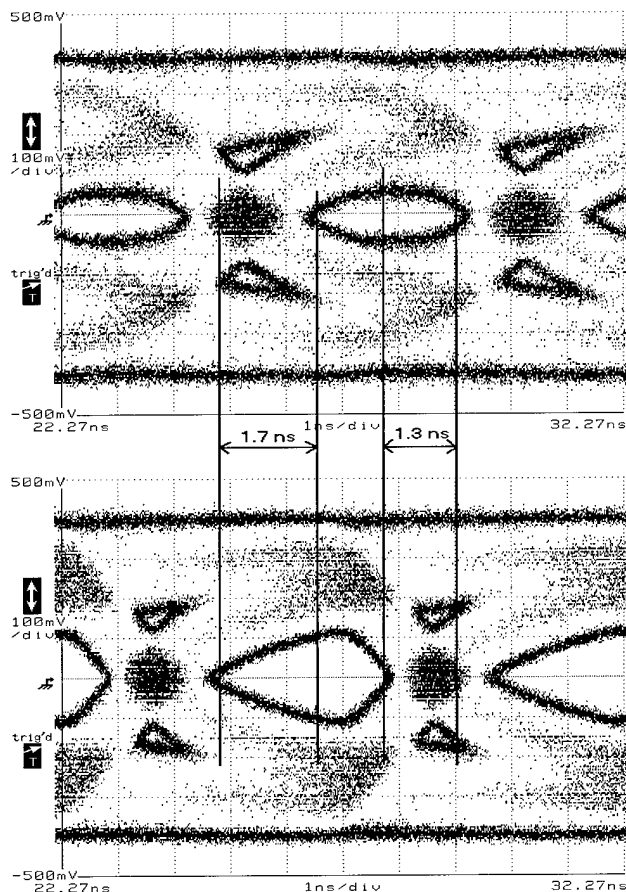**Figure 25a, high skew pair**

Figure 25b, low skew pair

Figure 26a. t$_r$=100 ps, high skew wires, 200 MHz

Figure 26b. t$_r$=100 ps, low skew wires, 200 MHz

In figures 26a-b the signals for each conductor in the pair are displayed separately. The eye opening for each wire in the high skew pair in figure 26a is similar to the one for the low skew pair. Only in the upper diagram of figure 26a the amplitude is somewhat lower (amplitude skew). But when added the eye opening is clearly reduced. Adding two signals for the low skew pair in figure 26b does not reduce eye opening significantly. The skew can be measured at approximately 1.5 ns (average between the time differences of the beginnings respective end of data eye), which is about the same as when measured with two methods earlier mentioned in 2.1-2.
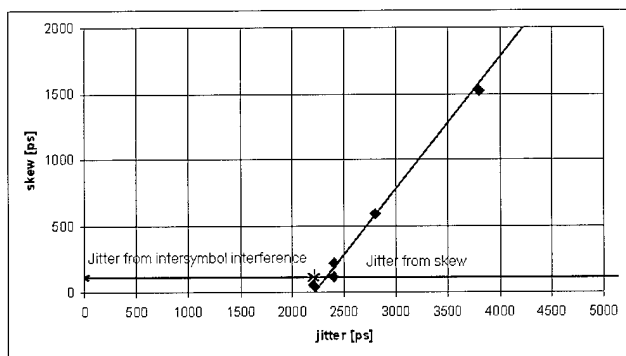

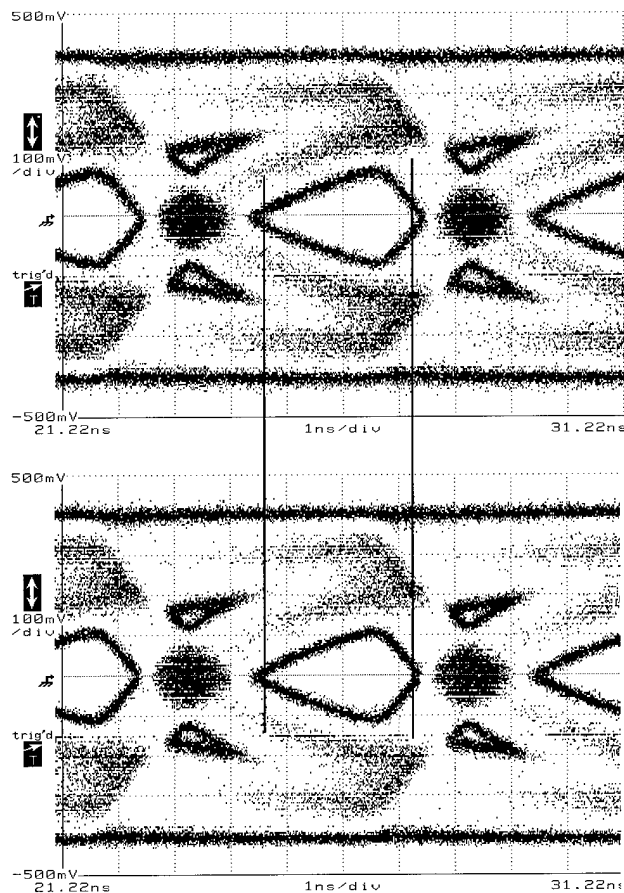
Figure 27. Skew versus jitter at 100 MHz

Figure 27 shows the jitter dependence on skew. Even for pairs with lower skew, jitter is not less than a threshold value that is determined by length of transmission line and encoding of data. The attenuation increases with frequency and for this reason the amplitude of the faster components of the signal is lower than that of the slower ones. This is one mechanism causing jitter even in the perfectly symmetrical cable.

When a pair has differential skew, the time value is added to the time value of the jitter from intersymbol interference. Therefore, the upward gradient of the line connecting skew jitter plots is constant and equals 1. However, this rule is no longer applicable when amplitude skew is significantly high.

6. Conclusions

It was shown that skew measurements with pulses, with differential power splitters and mixed mode S-parameters give comparable results. The advantage of the latter two is that when skew is not constant over frequency this can be detected easily. Skew for different data transmission speeds can be measured in one sweep. The importance of this parameter can be seen from the eye patterns in the last section.

Further a clear connection between skew and LCTL could be shown. This opens an additional way of characterizing the balance of symmetrical transmission lines.

Further theoretical work is necessary. The aim is to find relevant and easily applicable measurement methods to characterize symmetry.

7. References

[1] Bockelman, D.R., Eisenstadt, R. "Combined Differential and Common-Mode Scattering Parameters: Theory and Simulation", *IEEE Transactions on Microwave Theory and Techniques*, Vol. 43, No 7, July 1995.

[2] ITU-T Recommendation G.117, "Transmission Aspects of Unbalance about Earth" (1996).

[3] IEC 46C/415/CD, "Unbalance attenuation [in the near end (LCL) and far end (LCTL)]" (2000).
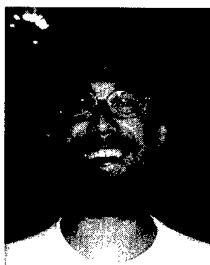
Dietmar Gleich received his Dipl. Ing. (FH) in 1995 from Fachhochschule Ulm, Ulm, Germany and his M.Sc.E.E. from Högskolan i Halmstad, Halmstad, Sweden in 1997. He joined Ericsson Cables in 1997 where he is working in the transmission technology department.
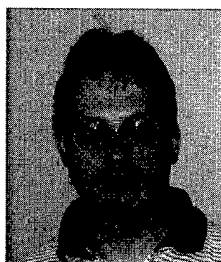
Marcus Lindström received his M.Sc.E.E. in 1993 from Linköping Institute of Technology, Linköping , Sweden. He joined Ericsson Cables in 1997 where he is working in the transmission technology department.
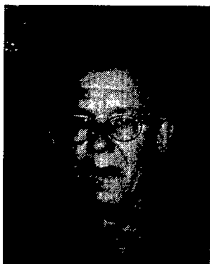
Mats Josefsson received his M.Sc.E.E. in 1980 from Chalmers tekniska högskola, Göteborg, Sweden. He joined Ericsson Cables in 1980 where he is presently leading the transmission technology department.
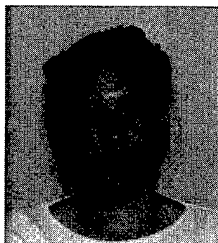
Ratimira Šimundic received her B.Sc.E.E. and M.Sc.E.E. from the Faculty of electrical engineering and computing, Zagreb, Croatia in 1996 and 1999, respectively. She has been working at the same faculty from 1997, as a research assistant and is presently enrolled in Ph.D. studies.

Variable Radiating Cables Operating at Frequencies up to 2200 MHz Measurements of the Prototypes in a Tunnel

A. Coraiola, E. Cottino, T. Pozzoli
Sirti S.p.A, Network Technologies Dept.
Via E. Fermi, 2 - 20060 Cassina dè Pecchi (MI) - Italy
+39-02-95885145 · E.Cottino@Sirti.it

E. Mahlandt
Radio Frequency Systems GmbH
D - 30179 Hannover - Germany
+49-511-6762366 · Erhard.Mahlandt@rfseurope.com

Abstract
Slotted cables of the "Vario" type, thanks to their property of distributing emitted power evenly along their lengths by compensating longitudinal losses, are optimized radiating structures for tunnels and offer significant advantages over conventional cables with increasing frequency.

This articles gives some highlights on the design of a tunnel plant employing variable cables and provides test results of two new "Vario" prototypes working at frequencies up to 2200 MHz.

1. Introduction
The decision of realizing new radiating cable types operating at the frequency bands of 1800 MHz and 2200 MHz, in addition to the traditional 900 MHz band, comes out from the necessity of assuring the DCS service in some tunnels, mostly located in urban areas, of the new high speed railway line in Italy.

Even if natural propagation in tunnels is usually good at high frequencies, the radiating cables for cellular services are still preferred to antennas when mobile stations are inside trains / vehicles. In these cases the supplementary attenuation of the vehicle body is usually much less if radiating cables rather than antennas are employed.

After some general considerations on tunnel systems employing variable cables, this article provides the main characteristics and some structural details of two new types of the Vario cable (which have lengths of 800 m and 500 m). It also gives the results of the measurements carried out in a tunnel on the prototypes.

The grading technique has been widely used to vary the emitted power with the cable length so limiting the dynamics to only about 20 dB.

The main parameters highlighted in the measurements are those traditionally evaluated for radiating cables and affecting downlink and uplink amplifier dimensioning: system loss and dynamics.

The two cable types are designed according to the safety requirements for confined space installations i.e.: flame retardancy (IEC 60332-1, 60332-3C), very reduced opaque smoke emission (IEC 61034), halogen and corrosive gas free (IEC 60754-1/2).

2. System Considerations
The variable leaky cable, proposed and described in [1], [2] has the property of compensating the longitudinal loss with variations of the coupling loss, starting from a particular cable extremity. The benefits, with respect to traditional cables, are linked to longer cable sections and lower diameter, with consequent reduced number of amplifiers, copper economy and easiness of installation.

For a given length and diameter a VARIO cable enables to obtain a reduced "system loss" (attenuation between cable input connector and mobile antenna connector) and a low "dynamics" (maximum attenuation variation).

These two favourable electrical properties, and particularly the reduction of dynamics, permit the design of tunnel communication systems, in the UHF range and in multicarrier operation, using amplifiers with very limited power.

This can be observed from the expression, already reported in [3], giving $n+i_M / p_m$ (received noise plus maximum intermodulation in the carrier band, over minimum carrier power) of a wideband tunnel communication system:

$$\frac{n+i_M}{p_m} = KT_0 b \cdot \sum_1^N \frac{f_j}{p_j} + c \cdot \left(\sum_1^N \frac{p_j}{i_{3j}} \right)^2$$

The above expression is valid for multicarrier operations both for the uplink and the downlink paths and the symbols (referred to either path) represent:

N   number of amplifiers (or generally active elements) of the tunnel system;

f_j , i_{3j} noise figure and 3rd order intercept point of the amplifier "j";

p_j carrier power referred to the same point where f_j and i_{3j} are given. If the carrier power is variable, because of signal dynamics, p_j represents the minimum power.

$k\,T_0\,b$ is the thermal noise power in the modulated carrier band. and:

$$c = c_{dw}{}^2 \qquad \text{for downlink path}$$

$$c = (c_{up} - 1)^2 \cdot h^3 \qquad \text{for uplink path.}$$

"c_{dw}" is the downlink carrier number ($c_{dw} \geq 5$) and "c_{up}" is a statistical parameter corresponding to the total uplink carrier number in the highest level range (we suppose that . c_{up}, < 5).

h ($h > 1$) is the signal variation (dynamics) corresponding to the attenuation differences between line amplifier and mobile unit. It strongly depends on the radiating cable characteristics.

Dynamics plays a very important effect in the degradation of the uplink signal as the above relations show.

Therefore it is the main aim of the "Vario" design to reduce this dynamics.

3. Design and characteristics of "Vario" cable

The intention of a VARIO design is to minimize the variation of system loss over the cable length. In order to reach this goal the coupling loss of the cable is decreased section wise from comparably high values at the beginning to a very low figures at the end. Therefore the longitudinal loss of the first sections is very close to the figure of a non-radiating cable and increases to the last sections. The system loss can be balanced perfectly for just one frequency. At higher frequencies the system loss increases towards the cable end while at lower frequencies the system loss decreases. If a VARIO cable shall be optimized for more than one frequency band a compromise has to be made. Anyway, due to this more even distribution of energy along the cable longer system lengths can be realised and the dynamic range of system loss can be reduced remarkably especially in the GSM 1800 and UMTS bands where the longitudinal loss of cables is comparably high.

Two prototypes of radiating cables with variable coupling loss have been designed and manufactured. Both cables operate in the so called radiating mode as from approximately 860 MHz with slot patterns that suppress unwanted higher modes up to the 3rd harmonic. The coupling loss of the cable sections are adjusted by variation of slot density and size.

A 1 5/8" cable has been manufactured with a length of 800 m and a maximum system loss of 100 dB, 95% reception probability figure in the GSM 1800 band. The second cable is made in a size of 1 1/4" and a length of 500 m. The maximum system loss 95% figure in free space at 1800 MHz is 95 dB.
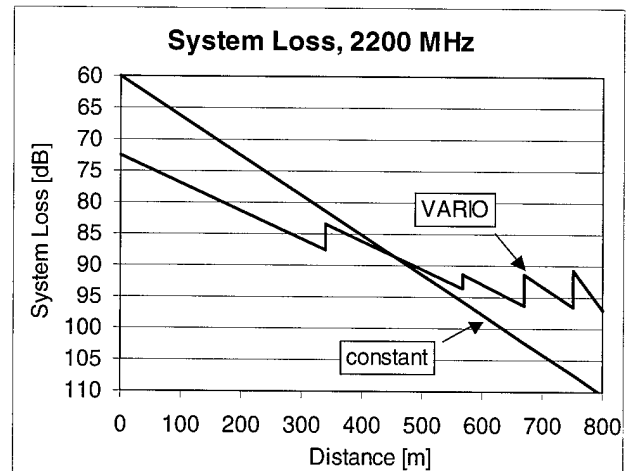

Figure 1: System loss of 1 5/8" VARIO and constant coupling loss cables at 2200 MHz

Figure 1 shows a system loss comparison of a 1 5/8" cable with constant coupling loss and a VARIO cable at 2200 MHz. As from a distance of about 450 m the VARIO cable provides a lower system loss while on the other hand the dynamic range of system loss is reduced from 50 dB to 25 dB.

At 900 MHz the VARIO cable provides a 8 dB lower maximum system loss and a 12 dB lower dynamic range (see figure 2). The values are based on free space measurements of the different cable sections according to IEC 61196-4.
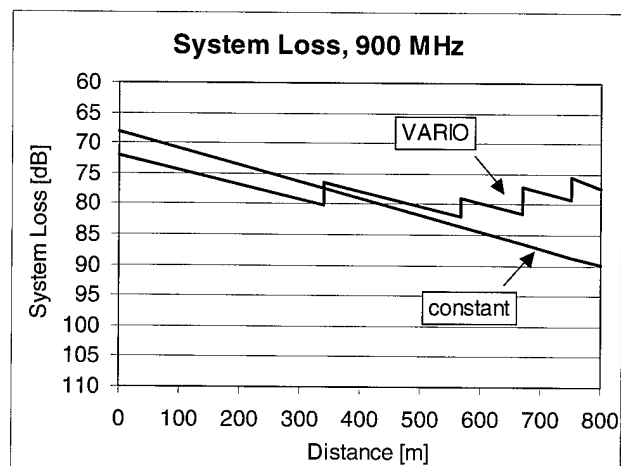

Figure 2: System loss of 1 5/8" VARIO and constant coupling loss cables at 900 MHz

4. Description of the tests

Two radiating cable prototypes were installed in a new rail tunnel not yet in service, without tracks, power lines and wall-brackets.

The first radiating cable prototype had a diameter (measured on the dielectric) of 1 5/8" and a length of 800 meters.

This cable was installed on the wall through suitable clamps, starting at 200 meters from the tunnel entrance at a height of 6 meters.

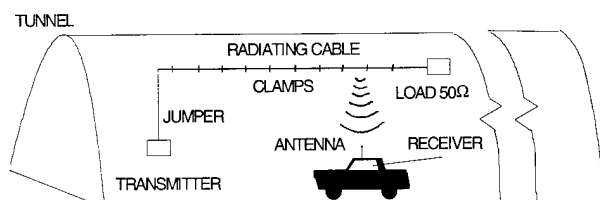The second radiating cable 1 1/4", 500 m. long, was installed in sequence, with the same modalities.

Both cables were of the "Vario" type.

A transmitter was connected through a jumper to the beginning of the cable. For Vario cables the beginning corresponds to the less slotted section, while the far end, corresponding to the more slotted section, was connected to a 50 ohm load.

System Loss values have been taken by an halfwave dipole connected to a receiver transported by a small van running in the tunnel. The receiver was interfaced with a PC to work out measured data.

The measurements were taken at distances of 3.5 meters (simulating the near track) and 7 meters from the cable (simulating the far track) at the frequencies of 150, 450, 900, 1800 and 2200 MHz both in vertical and horizontal polarizations. In order to assure a sufficient resolution approximately 33 measurements/meter with a measurement time of 1 msec were taken .

Figure 3 shows the test set up used in the tunnel of Aulla for the measurements of the two radiating cables prototypes.

UMTS frequency bands on the near track. As the coupling loss inside a tunnel varies only slightly with the antenna distance the results obtained on the far track are very similar.

At 921 MHz the system loss of the 800 m 1 5/8" cable is very even and the dynamic range is just 15 dB based on the local 50 % figures.

Figure 4: Test results of 800 m VARIO cable at 921 MHz

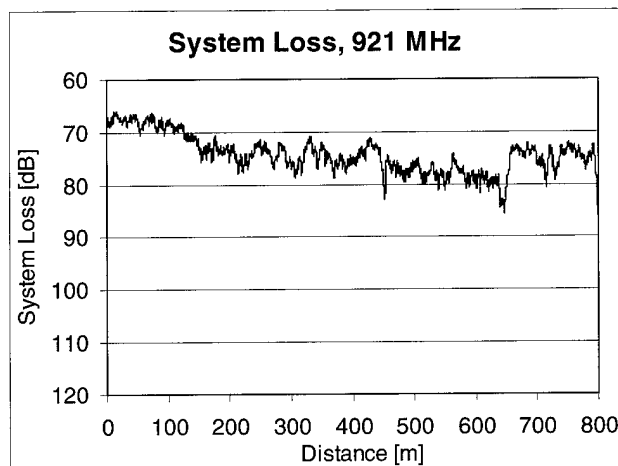**Figure 3. Test set up for radiating cable measurements**

5. Measurements and results

In contrary to normal leaky cables, where it is sufficient to test a short portion (approximately 100 m) of a cable to describe the total cable length, with VARIO cables the complete cable length must be measured in order to verify the efficiency of the compensation.
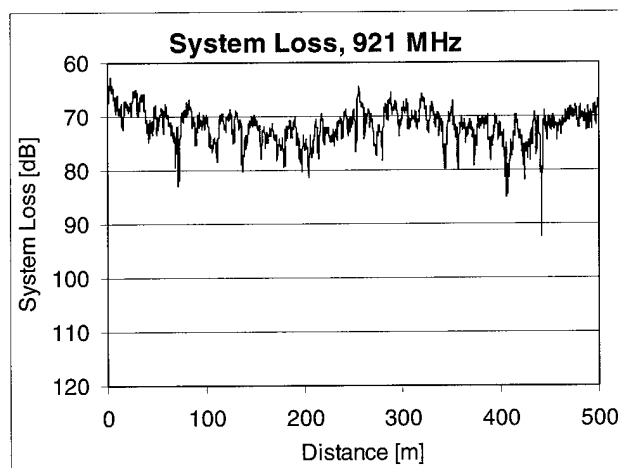
The figures contained in this paragraph show some typical results of the tests in the tunnel environment obtained in the GSM, DCS and
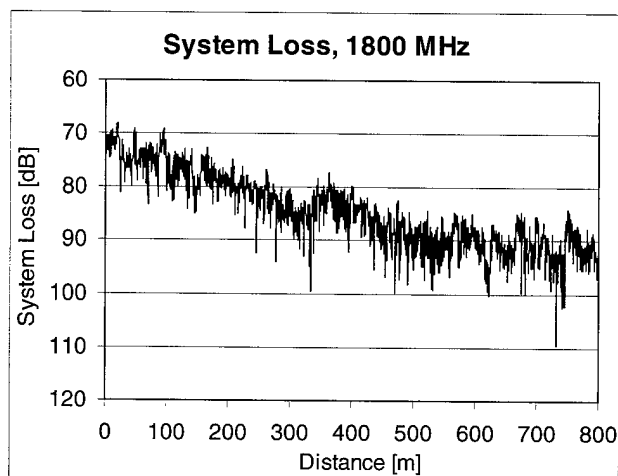

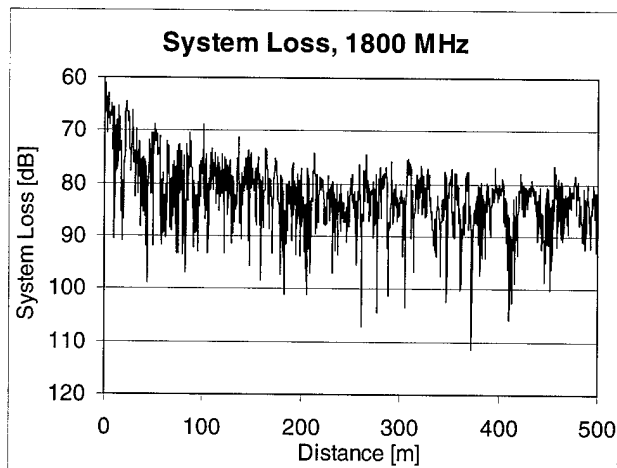**Figure 5: Test results of 500 m VARIO cable at 921 MHz**

The system loss with the 500 m long 1 1/4" cable is similar. Due to the shorter length the system loss is furthermore balanced (figure 5), the dynamic is 11 dB.

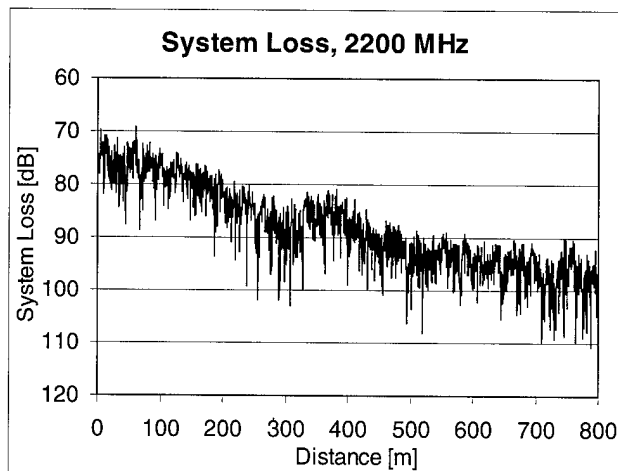The results in the upper bands of 1800 and 2200 MHz are shown in the diagrams of Figures 6 to 9.

Both cables provide good system loss values and dynamics not higher than approximately 30 dB.
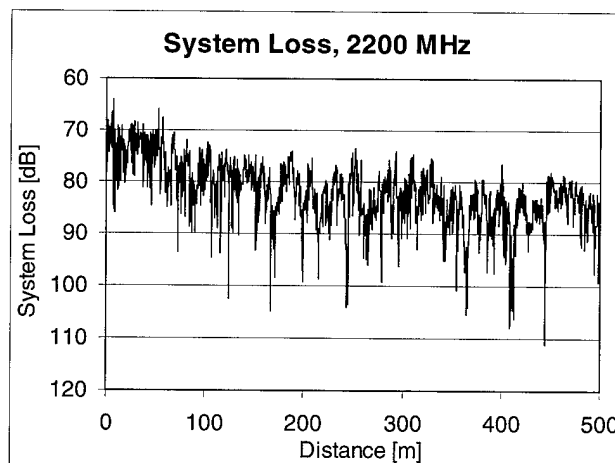
System Loss, 1800 MHz

Figure 6: Test results of 800 m VARIO cable at 1800 MHz

System Loss, 1800 MHz

Figure 7: Test results of 500 m VARIO cable at 1800 MHz

System Loss, 2200 MHz

Figure 8: Test results of 800 m VARIO cable at 2200 MHz

System Loss, 2200 MHz

Figure 9: Test results of 500 m VARIO cable at 2200 MHz

6. Conclusions

In the 900 MHz band both VARIO cables provide a low system loss and a very small dynamic range.

In the 1800 and 2200 MHz band the dynamic is increased but much less than it could be happened with a cable with constant coupling loss.

The measurements on the prototypes have demonstrated that radiating cables with length of up to 800 meters designed using the Vario concept enable to achieve good amplitude performances even in the DCS 1800 and UMTS bands.

7. Acknowledgments

We would like to thank Mr. Pezzati of Ferrovie dello Stato (national railway system) and Mr. Zanello of Società Italferr for allowing us to use the railway tunnel, which in turn permitted us to perform the test.

8. References

[1] A. Coraiola, K. Schulze Buxloh, "Variable Leaky Feeders for Cellular Radio Systems", *International Conference on Wireless Communications, IEEE*, Vancouver, Jiune 1992.

[2] A. Coraiola, H: G. Haag, K. Schulze Buxloh, G. Thönneßen, "Leaky Coaxial Cable with Length Independent Receiving Level", *International Wire and Cable Symposium*, Reno, November 1992.

[3] H. D. Hettstedt, A. Coraiola, M. Heddebaut, K.S.Buxloh, J. Boby, S. Baranowsky, M. Liénard, "Development and Applications of Radiating Cables in the ICAR Project: GSM Retransmission in Tunnels*", First World Congress on ATT and IVHS, ERTICO*, Paris, December 1994.

Authors
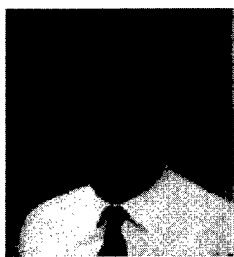
Edoardo Cottino

SIRTI Spa

Via E. Fermi 2

20060 Cassina dè Pecchi

Milan - Italy

e-mail: E.Cottino@sirti.it

Edoardo Cottino graduated in electronic engineering from Politecnico of Turin in 1982. After a small experience as avionic system design engineer, in 1985 move to AET Telecomunicazioni in the borning Optical Technology Laboratory following the plant activities. In 1989 has been leading of the Laboratory and in 1994 move to guide the entire Optical Technology Dept. of AET. In this period can follow the evolution the Italian optical fiber network focusing the activity in field of fiber, cables, accessory and trasmission system. With the merging of AET in SIRTI in 1995 he has called to Milan as head of Cables and Optical Technologies Dept., with the objective to study and analyse the evolution of the telecommunications network both in the access and in the core segment.

Currently, he is the head of Network Technologies Division of SIRTI in Cassina dè Pecchi.

He is member from 1990 of ITU/IEC Standardisation Sector and author of several publications on optical fiber system and optical networking.
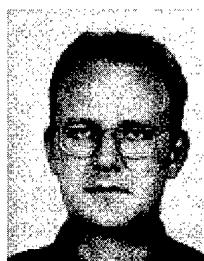
Erhard Mahlandt

RFS

Radio Frequency Systems GmbH

Kabelkamp 20

30179 Hannover - Germany

Erhard Mahlandt was born in 1963.He received hisDipl.-Ing. (FH) degree in 1990 and joined RFS in the same year. He is responsible for the development and measurement techniques of radiating cables and foam dielectric cables.

50 Ohm Smooth-Walled Outer Conductor Coaxial Cable and Connectors for Telecommunications Applications

Ronald A. Vaccaro
Engineering Manager
CommScope, Inc. of North Carolina
Newton, NC 28658

Abstract:
Wireless (PCS and Cellular) communications site construction schedules are being urgently compressed, pressuring system providers and engineers to demand new and innovative products which speed critical construction schedules while simultaneously providing increased operational longevity and reliability. Recent advances and developments in coaxial cable designs with smooth-walled outer conductors, along with innovations in connector design, cable preparation, assembly and performance, have addressed these issues. These new coaxial cable and connector products allow for rapid installations while exhibiting reduced connector assembly variability along with improved environmental and electrical performance of the system.

I.   INTRODUCTION
The typical construction discussed in this paper is coaxial cable. Coaxial cable is comprised of three main elements: 1) the center conductor (the signal travels along this) 2) the dielectric (a spacer used to separate the inner and outer conductors) 3) the outer conductor (a ring located around the dielectric – this is the electrical ground). These cables are used in telecommunications applications commonly at frequencies over 800 MHz. In particular, this paper reviews foam dielectric coaxial cable commonly used on cellular and PCS sites.

Coaxial cable is configured on a typical cell site is as follows:

Starting at the top, antennas are located on a tower (as high as practical). Connected to the antenna is coaxial cable. The coaxial cable runs to the radio, which is typically located on the ground. The radio itself is either located inside a cabinet (enclosure) or a small shelter. To minimize signal loss (attenuation), it is common for the coaxial cable to be as large as possible (1-5/8″ in diameter is a normal size) for most of it's length. At each end of the 1-5/8" cable (before it reaches the radio or antenna), it is common to use a short (2 m) length of small (1/2" in diameter) cable, for a more simplified installation (flexibility).

II.   HISTORY
Microwave and early cellular buildouts were taking place 10 to 20 years ago. Generally, the construction was done by highly skilled construction personnel and technicians. People in these businesses were very familiar with coaxial (corrugated outer conductor) cable. This coaxial cable had been around a very long time, and worked fairly well in this application. Sites were spaced far apart (especially microwave) so their density was low. This meant "few" sites were to be built (when compared to today's PCS buildout). Sites were planned to a much greater extent, and acquisition was much easier – no tower moratoriums, etc.

Transmission line products of the time included waveguide and coaxial cable. While a great many of the microwave sites were constructed using waveguide, this product will not be considered in this paper. Coaxial cable was available in many different constructions. Outer conductors generally available were corrugated solid copper and braided wire. The most common dielectrics were PTFE, air and foamed polyethylene. Defining the cable by its outer conductor, some generalities can be made:

Braided Construction:

- Small diameter
- Poor environmental resistance
- Low power handling
- High connector craftsmanship
- High electrical loss
- Low cost

Corrugated Construction:

- Available in large diameters
- Fair environmental resistance
- High power handling
- High connector craftsmanship
- Low electrical loss
- High cost
- Robust (foam construction only)

The cable often selected (at this time) was corrugated. The most important features of this cable were the low loss and fair environmental resistance. This was the best (and most economical) solution for the time. Probably the largest drawback to this solution was the labor intensive and highly particular connectors, which were assembled to each end of the cable. But remember, highly skilled technicians were available to tinker with the connectors and make them work.

III. TODAY AND TOMORROW

So what has changed between yesterday and today? Plenty! First, the shear number cellular and PCS sites to be constructed. Consider the total number of base stations to be deployed in the US (all technologies).

Table 1. Base Station Deployment – US

Year	Deployment
2000	17,500
2001	17,900
2002	22,400

Source: Allied Business Intelligence

Even if the same number of skilled technicians and construction personnel existed, they are spread-out over a greater number of sites. Further, (with) the economy at near full employment, the overall skill level available has generally declined. Coupled with this is the trend to outsource this type of labor. Cost and liability to the system providers have been the main drivers of this. This relationship has made it much more difficult for system providers to enforce quality standards on their systems.

Second, site acquisition is a much more difficult process. City planning and zoning boards have made it much more difficult to gain the needed approval to build sites. This approval process (of course), is being done after system providers have paid great sums of money for the licenses. Their financial backers need to be paid, so there is a great amount of stress to get the towers built, so the billing can commence. All of this means once the site is approved, system providers will go to extraordinary lengths to get the site built, and on the air. This puts great emphasis on construction personnel to complete the site and move on to the next. They simply do not have time to tinker with connectors and cable to improve performance and reliability.

IV. THE IDEAL TRANSMISSION SYSTEM

Let's consider the ideal transmission system required to fulfill the needs described in the previous section.

(1) Electrical Considerations:

Low VSWR – this will improve system sensitivity on the receive side (Rx).

Low Insertion Loss – Allows more power to reach the antennas, or allows for higher antennas to help increase coverage

RF Shielding – Protect from EMI & RFI

Low Passive Intermodulation Generation – reduce bit-error rates in digital, and noise in analog systems.

Electrical stability – consistent electrical performance when bent.

(2) Mechanical Considerations:

Robust design – withstand rough handling on construction sites.

Flexibility – ease cable handling for contractors.

(3) Environmental Considerations:

Outer Shield – Continuous (360°), solid shield.

Water Leak Paths – completely sealed through the cable.

UV – resistant, to withstand years of exposure to sunlight.

(4) Connectors:

Improve Mechanical robustness – withstand handling on site.

Improve weather resistance – mitigate water entry into the cable.

Ease assembly/reliability – improve chances that unskilled workers will assemble properly.

V. AREAS FOR IMPROVEMENT:

Standard corrugated cable (of the time) offered no specification or guarantee for VSWR. In many cases, this forced system providers to purchase band selected cable, at a premium price. The attenuation (or insertion loss) had not been improved in years.

While the tough polyethylene jacket and continuous (360°) solid copper (corrugated) shield provided an excellent environmental barrier, the connectors did not. Despite the presence of o-rings (supplied loose with the connector) and secondary weatherproofing used (installed over the cable and connectors), water still often managed to enter the cable. This is undesirable, because water is an absorber of RF energy (think microwave oven!). Further, The layered construction and hollow core of these designs also allowed water to "flow" within the cable assembly once it passed the weatherproofing and connector.

The reason the connectors did not consistently provide a reliable environmental seal was due to their complicated assembly process. Connectors often consisted of five to ten loose piece parts. The assembly process was long and complicated with much cutting, filing and measuring required. The success of a connector assembly depended very heavily upon the craftsmanship ability of the installer. Complicating this fact was the ultimate determination for a successful assembly was not known until after it rained! Poorly or incorrectly assembled (or missing) o-rings did not

make themselves known often for months after the completed install.

VI. HOW SMOOTH-WALLED CABLE ADDRESSES THESE ISSUES:

(1) Electrical Considerations: Lowest standard VSWR cable available (1.10 VSWR). Lowest insertion loss cable available (9-10% lower than previous corrugated product available @ 1000 MHz). Shielding is effected by a smooth-walled, solid copper conductor. Low passive intermodulation generation (better than – 115 dBm).

(2) Mechanical Considerations: Highest tensile and crush strength available. Maintains shape (cross-section) and position while being installed. One drawback of this cable is that it is stiffer than similarly sized corrugated cable.

(3) Environmental Considerations: Solid copper outer conductor coupled with tough polyethylene jacket, which is UV resistant, and completely seals out water. Internal leak paths are fully sealed. Adhesively bonded layers, closed microcell foam and a sealed tubular center conductor eliminate internal water migration paths.

(4) Connectors: TranSplice connectors eliminate the interface (the weakest part of a connector). Lubricated and preinstalled o-rings guarantee proper installation. Engineered tools, which reduce craftsmanship, assist in cable preparation, no measuring needed, two piece connector.

VII. CONCLUSION

The aggressive deployment schedule of base stations is planned to continue for the foreseeable future. Uncertainties relating to the schedule of site implementations, coupled with the need to bring these sites on-line quickly, will probably not improve anytime soon. This means construction personnel will continue to be pressured to complete sites quickly and correctly. Having innovative products and tools, which allow them to fulfill this requirement, is paramount.

Recent advances in coaxial cable designs, which utilize smooth-walled copper outer conductors, adhesively bonded layers, sealed water paths (closed microcell foam, etc), along with simplified connector designs, allow construction personnel to meet this objective.

Market response to this innovative technology has been very strong. Installers have praised the ease of connectorization, reduced installation times and the durability of the product. Electrical sweep results almost always exceed requirements – sometimes by so much the functionality of the test equipment is challenged. The service providers benefit from improved system performance (quicker installations resulting in faster site turn-on, better coverage area, more reliable system performance and cost savings from the ability to downsize cable requirements). Even more importantly, the waterproof design of the cable, connectors and their interface has virtually eliminated many maintenance budgets.

VIII. ACKNOWLEDGEMENTS

IX. REFERENCES

Larry Swasey, "Wireless Base Stations, Markets Technologies and Building Blocks", 2Q 2000 Allied Business Intelligence Inc. Oyster Bay, NY.

Extrusion Process and Equipment for High Foamed RF Cable and Microwave Manufacturing

Siegfried Altmann

ROSENDAHL Maschinen GmbH; a company of KNILL Gruppe
8112 Pischelsdorf, Schachen 57; Austria
+43-3113-5100-0 · s.altmann@rosendahl-frisch.com · http://www.rosendahl-frisch.com

Abstract

The demand for both quality and capacity of wireless digital telephone systems is rapidly increasing. The target is to improve mechanical and electrical parameters of cables used in this systems. By using new production methods to increase the performance of RF cable manufacturing plants this higher levels can be achieved.

The properties of coaxial cables are mostly defined by three production steps: The corrugation copper tubing process of the inner conductor, the physical foaming process to apply the dielectric to the inner conductor and the corrugation process of the outer conductor. The sheathing process is less important for the quality and productivity of RF cable manufacturing. The production of thick wall, high foamed RF cables creates specific demands on the material properties and insulation lines.

Keywords

RF and microwave cable manufacturing equipment; gas injection system; bubble growth; nucleating agent; cell structure; SRL; Attenuation; Velocity of prorogation; aging; cell structure; cell growth control; Water penetration; Diffusion; Solubility; physical foaming; viscosity; nitrogen; partial pressure; density; bonding;

Introduction

RF cable manufacturing lines are known in the industry over several years. The increased demand of RF and microwave cables pushes the producer to increase the output as well as to improve the mechanical and electrical properties of the cables to support the end users' demands of the performance of the system.

This paper describes the background (processing of physical foamed insulation) for RF and microwave lines for ½' to 2 ¼' cables. The study shows the impact of

- properties of the materials
- processing of the materials
- parameters and design criteria for the processing equipment,

to built a basis for improvements of electrical and mechanical properties of RF cables as well as productivity combined with reduction of material costs.

Production Targets

Improve Product Quality

- ➤ {1} get Impedance to narrow tolerance
- ➤ {2} increase velocity of propagation
- ➤ {3} reduce attenuation
- ➤ {4} increase SRL levels
- ➤ {5} increase electrical resistance of insulation
- ➤ {6} increase the maximum operating voltage of the cable
- ➤ {7} reduce frequency shift properties
- ➤ {8} reduce temperature shift of electrical properties
- ➤ {9} avoid water penetration
- ➤ {10} take care to get flexible product style
- ➤ {11} improve tension resistance
- ➤ {12} reduce weight of the cable
- ➤ {13} increase crush resistance
- ➤ {14} increase ageing time of cable
- ➤ {15} improve optical outfit
  - ➤ {16} small regular cell structure
  - ➤ {17} closed cell surface and smooth surface

Increase Productivity

- ➤ {18} increase production speeds
- ➤ {19} keep the line continues running
- ➤ {20} reduce start up scrap
- ➤ {21} get the process to an easy reproducible status
- ➤ {22} reduce material costs
- ➤ {23} change the cable design
  - ➤ {24} reduce volume of copper
  - ➤ {25} reduce the amount of dielectric materials
  - ➤ {26} choose cheaper dielectric

Reduce Labour cost's

- ➤ {27} target low manufacturing energy consumption
- ➤ {28} optimise handling to run with low man hours

Keep Connector Assembly Easy

- ➤ {29} small mechanical tolerances
- ➤ {30} prepare tools for semi-automatic assembly

Reduce Flammability of Cable

Most of these targets are related to the cable design, organizational improvements combined with well done line configurations, materials characteristics and process parameters of the manufacturing process.

Process Determining Properties with Impact on Production Targets

There is a limited area to achieve the wished targets by changing the process setup. The main action is to increase the foam rate {2, 3, 5, 6, 7, 8, 10, 12, 22, 23, 24, 25} while using materials with low loss factor and low amount of nucleating agents { 3, 5, 6, 7, 8, 22, 26}. The processing behavior of materials combined with the known processing equipment results in narrow operating windows.

The extrusion system provides the following process defining tasks for this purpose:

➤ pulsation free draw in of the premixed compounds

➤ increase of pressure

➤ melting and homogenizing of the polymer

➤ providing a well done melt homogeneity before gas injection of the physical foaming additive

➤ homogeneous mix of gas under influence of pressure and temperature to achieve 100% solvability of the gas in the melt flow

➤ continues feeding cooling and homogenizing of the mixture of polymer with solved gas

➤ transport of the melt with higher pressure then the pressure of foaming agent

{1, 2, 3, 4, 9, 15, 16, 17, 18, 20, 21, 27, 29}

Influence of Melt Viscosity

Good foaming behaviour of the polymer is guaranteed if the melt viscosity drops slow and continues while the temperature increases during the softening.

Figure 1 points out that thermoplastic with a high amount of crystalline parts (like HDPE types) have worse processing behaviour compared to amorphe or partly crystalline Polymers with low crystalline parts (like LDPE types).

Solvability of Gas in Polymer

The solvability of gas in the polymer melt flow is an important limit when increasing the foam rate. For stable processing conditions 100% of the injected gas needs to be solved. Improvements may be achieved by the increase of the processing parameters, temperature and pressure. It is of great importance to use optimal geometry for the gas

injection system and the screw. This avoids process variations grounded by the growth of gas bubbles before solving the gas in the melt. The gas needs to be solved immediately after injection and not along the mixing part of the screw. {1, 4, 9, 15, 16, 17, 18, 20, 21, 29}
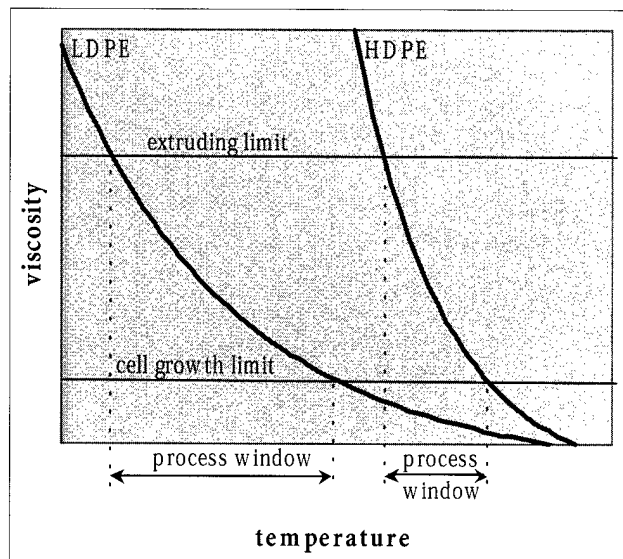

Figure 1: Processing windows of HDPE and LDPE

Amount of Nucleating Agent

The cell size is highly impacted by the amount of the nucleating agent.
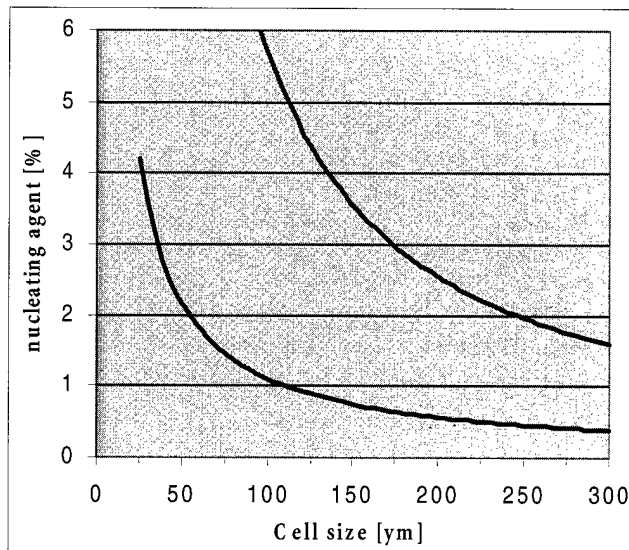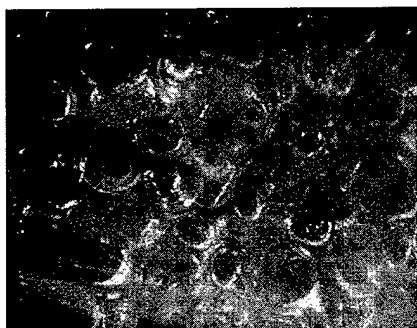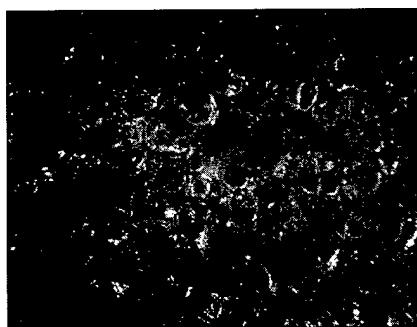

Figure 3: Influence of cell size by amount of nucleating agent.

Figure 4: Cell structure with 2770 ppm of nucleating agent when foaming in free air pressure


Figure 5: Cell structure with 5400 ppm of nucleating agent when foaming in free air pressure

The targets to reduce to loss factor and to reduce cell size by increasing the amount of nucleating agent built a conflict by itself. An additional aspect is the fact, that foamed insulation ages faster due to the degradation products from the nucleating agent. They consume and deactivate antioxidants during processing. Further more there is an impact by the energy given during decomposition process when using exothermic additives. For example 40 kcal/mol are released when using Azodicarbonamide which influences the melt temperature followed by the change of viscosity. Additionally a chance of viscosity happens by solving gas which is generated in the decomposing process and by gas injection.

Control of Cell Growth

Once the gas is solved in the melt it is important to achieve best homogenizing before the extrusion head will distribute the melt mechanical symmetric around the conductor. There are additional design targets compared to a classical extrusion head for RF cables.

To avoid differences of melt temperature with an impact on viscosity and cell growth one needs to achieve shear symmetry of the distributor.
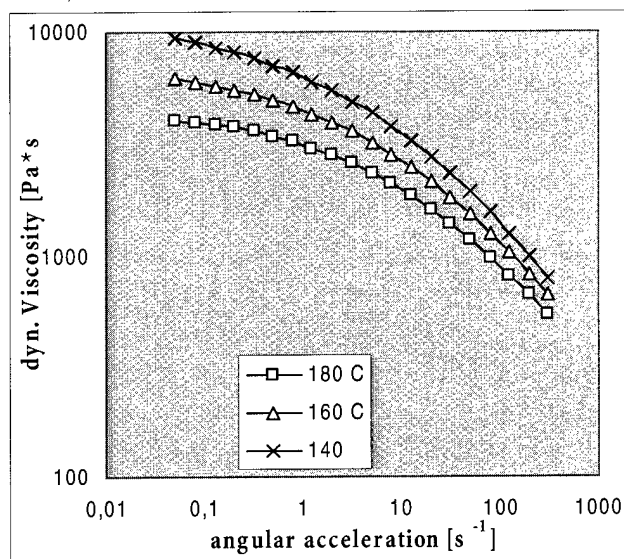
Figure 6: Dynamic viscosity of gasified melt in relationship to angular acceleration.

The foam will collapse without control of the cell growth at a higher foam rate. The cell size needs to be controlled in time domain as well as over the cross section. The increase of skin thickness avoids the collapse at the border of the conductor and the cooling water, but the internal cell structure in the cross section is still not homogeneous. This will result in higher shrinkage behavior of the product in the cooling trough and will also effect the mechanical properties like roundness, centricity and cell size. Water penetration may occur.

Therefor, it is a must to limit the cell size. The foaming process after the extrusion unit is influenced by:

➢ the operating parameters pressure and temperature
  ➢ in the extrusion head,
  ➢ in the tools,
  ➢ while leafing the process unit
  ➢ and in the cooling trough
➢ the viscosity and elasticity of the melt
➢ the gas-permeability of the polymer as well as the steam pressure.

The main starting conditions for homogeneous cell growth are:

➢ the gas needs to be totally solved in the visco-elastic melt (it is not essential how this gas came into the melt, whether chemical reaction or physical injection)
➢ the nucleating agent needs to be homogenized in the polymer melt
➢ the melt is thermal and visceral homogeneous along the bubble growing and freezing process.

By using classic extrusion head and tool design a over saturation of the gas in the melt occurs at the time of pressure drop when the melt leaves the die. As a result the separation process of gas and melt starts. The gas bubbles start to grow at the inhomogeneous points of the nucleating agent and its degradation products. The number of bubbles increases as long as an oversaturation of gas exists.

Gas starts to move from small bubbles into big bubbles parallel to the growth of new bubbles. This process may be evaluated by following the energy status of the gas bubbles according to the law of Schleith [11].

$$\sigma * dO = p * dV \qquad (1)$$

σ...Surfacetension O...bubblesurface

at the bubble surface

$$p_i = \frac{2 * \sigma}{r} \qquad (2)$$

p_i...partialpressure   r...bubbleradius

As a result the pressure in small bubbles is higher than in big bubbles when foaming in free air pressure and at constant surface tension. The gas will diffuse from smaller bubbles to bigger bubbles. The law of Stokesschen shows the speed of diffusion.

$$w = \frac{g * D^2}{18 * \eta} \Delta \rho \qquad (3)$$

w...speedofdiffusion g...gravity

D...diameterofbubbles η...dyn.vis$\cos ity$

ρ...density

Therefor the size of bubbles is essentially influenced by the diffusion process.

New Control System for Cell Growth

To surmount the need to use a relatively high amount of nucleating agent and to reduce the impact of gas diffusion between bubbles a new extrusion head and tool design was developed. This allows to

get control on
> temperature
> pressure

during bubble growth.

With the newly developed units it is possible to set the temperature and to influence the pressure during foaming.

With this parameters the partial pressure and the viscosity (related to temperature) may be adjusted. This allows to:

> reduce the amount of nucleating agents {3, 5, 6, 7, 8, 14}

> give controlled influence on the number of growing bubbles {1, 2, 3, 4, 5, 6, 7, 8, 9, 10, 12, 14, 15, 16, 17, 18, 20, 21, 22, 23, 24, 25, 26}

> give controlled influence on the size of growing bubbles {1, 2, 3, 4, 5, 6, 7, 8, 9, 10, 12, 14, 15, 16, 17, 18, 20, 21, 22, 23, 24, 25, 26}

> allow to run the process without inner and outer skin

> allow to increase the foam rate before collapse of insulation {1, 2, 3, 4, 5, 6, 7, 8, 9, 10, 12, 14, 15, 16, 17, 18, 20, 21, 22, 23, 24, 25, 26}

In practice the inner and outer skin is still used to guarantee the bonding properties of the insulation. {1, 4, 9, 13, 14, 15, 17, 18, 20} The thickness may be reduced to a minimum thickness at about 50ym for this issue. This gives a positive impact to attenuation due to the reduced amount of solid material in the insulation. Additionally the relative high amount of polar additives which are normally used in the skin material to guarantee bonding to the copper is reduced due to the smaller skin thickness.

The main parameters for the theoretical evaluation of the mentioned process of controlled and reproducible foam quality are the solve pressure of the gas and the viscosity of the melt. It is really difficult to estimate this parameters along the foaming and cell growth process. Therefor a feedback for each product type is needed from practical test runs. The relation of the process behaviour may be deducted from the law of Henry:

$$p_l * S = c \qquad (4)$$

p_l...Solvepressure= partialpressure = Pr essureadjusted

S...Solvability

c...Gasconcentration int hemelt

This known relationship helps to tune the parameters in the correct direction.

Conclusions

A new way to control the process parameters during bubbles growth was found. This allows to improve the properties of physical foamed RF and microwave cables.

It is possible to run the process in a smaller operating window with improvements by using digital closed loop systems for all the process related parameters.

This system is a support to get award of product quality produced with traditional materials and equipment.

The targets are a reduction of attenuation, a new quality standard of the SRL level and the reduction of the needed material amount.

The system is proven in a laboratory development surrounding and will be tested under mass production conditions soon.

Acknowledgments

References

[1] Hensen, Knappe, Potente: Kunststoff-Extrusionstechnik München: Carl Hanser Verlag 1986.

[2] Mund, B: Videokabel. Sitzung des Fachausschusses für optische Registrier- und Überwachungsanlagen, Düsseldorf, Mai 1988

[3] Klane, B: Physikalisches Aufschäumen von Kunststoffen mit Inertgasen. Draht 45 (1994) 3, S 197ff

[4] Henzler, W: Alternativen der PE-Isolierschaumerzeugung. Plastverarbeiter 54 (1994) 12, S 86ff

[5] Chang, Villamizar: Studies on Structural Processing. Polymer Engineering and Science 18 (1978) 9, S 687ff

[6] Ast, W: Der Extruder als Plastifiziereinheit. Düsseldorf, VDI-Verlag, 1977

[7] BASF, Ludwigshafen: Modellierung der Zellstruktur bei der Herstellung von Schaumstoffen. 75 Jahre Verfahrenstechnik

[8] Yoo,H.J. and Han, C.D.: A.I.CH.E.J 28, S 1002 (1982)

[9] Collias, D.I. and Baird, D.G.: Does a Microcellular Structure Improve the Modulus of Toughness of a Polymer Matrix, Antec 92, S 1532ff

[10] Kweeder, J.A., Ramesh, N.S., Campbell, G.A. and Rasmussen D.H.: The Nucleation of Microcellular Polystyrene Foam , Antec 91, S1398ff

[11] Schleith, O.: Schäume aus der thermoplastischen Schmelze. Düsseldorf, VDI-Verlag, 1981, S17ff

[12] Yoo, H.J. and Han, C.D.: Studies on Structural Foam Processing III. Polymer Engineering and Science 21 (1981) 2, S 69ff

[13] Altmann, S., Altmayr J., Wolf S. .: Physikalisches Schäumen. Firmenschrift der Firma ROSENDAHL Maschinen GmbH, Pischelsdorf 1995, 1999

[14] Iawa, M., Suzuki, Y., Ito, Y., Kawabata, S. and Takai, S.: New Nitrogen Gas Extrusion Process for highly expanded Polyethylen insulated coaxial cables, International Wire & Cable Symposium Proceedings, 1989, S 549ff

[15] Fogg, Peter G. T.polymeric material systems, Journal ISSN:0191-5622

[16] Kolmacka, Jan; Smilek, Pavel Methods and problems in measurement of gas solubility in polymer melts, Journal ISSN0322-7340

[17] Atkinson, E. B. The solubility of nitrogen in molten polyethylen, Journal JPLPAY

Biography

Siegfried Altmann, born in 1966, graduated from the "Engineering school of Electronics and Control Systems" in Pinkafeld. He joined Rosendahl in 1984 and started in the field of computer based control systems for cable manufacturing equipment. After various developments for the wire and cable industry he became the Technical Director of Rosendahl in 1997.

Siegfried Altmann
Rosendahl Maschinen Gesm.b.H
Schachen 57
8112 Pischelsdorf, Austria

s.altmann@rosendahl-frisch.com

http:// www.rosendahl-frisch.com

Author Index

A

Achille, F. 362
Aguiar, J. G. 505
Akasaka, N. 403
Al-Asadi, M. M. 111, 380, 578
Aloisio, C. 622
Altmann, S. 679
Altmayr, J. 149
Alvim, M. G. 466
Amato, A. J. 141
Ammons, D. 337
Anderson, M. 207
Andou, K. 298
Aquino, J. C. 607
Araki, E. 298
Arikawa, T. 187
Artingstall, L. P. 433
Arvidsson, B. 21
Asao, S. 596
Auzizeau, J.-M. 570

B

Babelotzky, B. 564
Baek, S. 520
Beggs, R. D. 309
Bernstein, S. 601
Bertaina, A. 38
Berthelsen, G. 530
Bigo, S. 38
Björk, A. 21
Björkman, J. 628
Blazer, B. J. 317
Bocanegra, L. M. 1
Borke, J. 220
Bouffant, O. 271, 570
Bourget, V. 357
Bow, K. E. 362
Boxer, M. 590
Brunhara, C. 169
Bush, H. M. 65

C

Caetano, M. A. 169
Cámara, S. 279
Carter, C. 352
Chang, T.-C. 408
Chariot, J.-F. 38
Chen, H.-J. 408
Cheng, M. 385
Cheng, X. 479
Chin, G.-H. 543
Chippada, S. 74, 89
Choi, H. T. 496
Chou, S.-H. 439
Coat, P. 337
Cocchini, F. 49

C (cont.)

Coraiola, A. 671
Cortines, C. G. 13, 279
Cottino, E. 671
Cressan, E. 271
Curado, P. J. P. 505

D

Dallas, G. 357
Davis, C. S. 1
de Montmorillon, L.-A. 38
Debban, Jr., H. P. 1
Denson, J. W. 656
DeWitt, W. 337
Dimitropoulos, C. D. 89
Dioh, N. 220
Dixon, L. A. 309
Dole, C. W. 135
Domingo, R. 646
Drabczyk, N. 357
Dubois, S. 650
Duffy, A. P. 111, 380, 578
Dunn, L. R. 526

E

Engel, R. 470
Embo, A. 255

F

Fecko, D. L. 352
Fleury, L. 38
Foxwell, D. 526
Fullerman, M. D. 412
Furtado, J. M. 225
Furukawa, H. 214

G

Galli, S. 248
Gallo, E. 261
Gan, K. 646
Gao, Z. 501
García, M. 13
Gay, P. 570
Genji, T. 398
Gifford, I. C. 367
Gillespie, Jr., J. W. 352
Girbig, R. 417
Gleich, D. 121, 661
Gomes, M. A. 466
Grald, E. W. 74, 89, 455
Graveston, M. G. 526
Gregor, C. M. 417
Griffioen, W. 538
Gregory, A. C. 636
Guillas, P. 271
Gullo, G. 601